

PREFACE

Karl A. GSCHNEIDNER, Jr., and LeRoy EYRING

These elements perplex us in our rearches [sic], baffle us in our speculations, and haunt us in our very dreams. They stretch like an unknown sea before us – mocking, mystifying, and murmuring strange revelations and possibilities.

Sir William Crookes (February 16, 1887)

Today, about a decade short of two centuries after Lt. C.A. Arrhenius discovered the rare earths, we are witnessing a rapid growth in our knowledge of this family of 17 elements. In the five years, 1971 through 1975, we have learned as much about the rare earths as in the previous 25 years. In an attempt to assess the current state of the art (1976) the editors, with the encouragement of the publishers and other fellow scientists, have invited experts in various areas to write comprehensive, broad, up-to-date, and critical reviews. Some of the subjects were chosen because they are mature and still quite active; others because they are essential as background information and for reference; and some topics because they are relatively new and exciting areas of research. Unfortunately there are a few areas which have not been included in the four volumes either because they could not be covered adequately at present or because the appropriate authors were unavailable. Perhaps a future volume could remedy this and bring other rapidly expanding topics up-to-date.

A goal of these volumes is to attempt to combine and integrate as far as practical the physics and the chemistry of these elements. The strategy has been to divide the work into four volumes, the first two dealing primarily with metallic materials and the other two with non-metallic substances. The interaction of these disciplines is important if our knowledge and understanding is to advance quickly and broadly. Historically there are several important instances where one discipline had a great influence on the advancement of the science of rare earths. From the time of Arrhenius' discovery in Ytterby, Sweden until the last naturally occurring rare earth was discovered (lutetium in 1907) the chemistry of the rare earths was hopelessly confused, but the theoretical work of Niels Bohr and the experimental studies of H.G.J. Moseley (both physicists) in 1913–1914 showed that there were 15 lanthanide elements to be expected plus the two closely related metals scandium and yttrium. The discovery of ferromagnetism in gadolinium by G. Urbain,

P. Weiss and F. Trombe in 1935 stirred much excitement and was a foreshadow of the activities of the past twenty years. All of this, however, might not have been were it not for the efforts of two groups of chemists headed by G.E. Boyd at the Oak Ridge National Laboratory and F.H. Spedding at the Ames Laboratory who in the late 1940's developed the ion exchange techniques for separating rare earths. The method developed by the latter group is still being utilized by many industrial firms for preparing high purity rare earth materials. In the 1960's and 1970's several important discoveries—rare earth phosphors, cracking catalysts, rare earth-cobalt permanent magnets, etc. have made significant practical impacts and stimulated much research, but the extent of these are difficult to judge and put into their proper perspective at this time. Hopefully, these four volumes, and any which may follow will make a major contribution to our progress in understanding these exotic and fascinating elements.

In writing these chapters the authors have been asked to use the term "rare earths" to include Sc, Y and the elements La through Lu, and the term "lanthanides" when referring to only the elements La through Lu. The editors have attempted to enforce this usage rigorously when editing the various chapters. Furthermore, we have encouraged the authors to use the SI units as far as practicable to bring the subject matter into accord with current scientific and technical practice.

CONTENTS

Preface	v
Contents	vii
List of Contributors	xi

VOLUME 1: METALS

1. Z.B. Goldschmidt	
<i>Atomic properties (free atom)</i>	1
2. B.J. Beaudry and K.A. Gschneidner, Jr.	
<i>Preparation and basic properties of the rare earth metals</i>	173
3. S.H. Liu	
<i>Electronic structure of rare earth metals</i>	233
4. D.C. Koskenmaki and K.A. Gschneidner, Jr.	
<i>Cerium</i>	337
5. L.J. Sundström	
<i>Low temperature heat capacity of the rare earth metals</i>	379
6. K.A. McEwen	
<i>Magnetic and transport properties of the rare earths</i>	411
7. S.K. Sinha	
<i>Magnetic structures and inelastic neutron scattering: metals, alloys and compounds</i>	489
8. T.E. Scott	
<i>Elastic and mechanical properties</i>	591
9. A. Jayaraman	
<i>High pressure studies: metals, alloys and compounds</i>	707
10. C. Probst and J. Wittig	
<i>Superconductivity: metals, alloys and compounds</i>	749
11. M.B. Maple, L.E. DeLong and B.C. Sales	
<i>Kondo effect: alloys and compounds</i>	797
12. M.P. Dariel	
<i>Diffusion in rare earth metals</i>	847
<i>Subject index</i>	877

VOLUME 2: ALLOYS AND INTERMETALLICS

13. A. Iandelli and A. Palenzona
Crystal chemistry of intermetallic compounds 1
14. H.R. Kirchmayr and C.A. Poldy
Magnetic properties of intermetallic compounds of rare earth metals 55
15. A.E. Clark
Magnetostrictive RFe_2 intermetallic compounds 231
16. J.J. Rhyne
Amorphous magnetic rare earth alloys 259
17. P. Fulde
Crystal fields 295
18. R.G. Barnes
NMR, EPR and Mössbauer effect: metals, alloys and compounds 387
19. P. Wachter
Europium chalcogenides: EuO, EuS, EuSe and EuTe 507
20. A. Jayaraman
Valence changes in compounds 575
Subject index 613

VOLUME 3: NON-METALLIC COMPOUNDS - I

21. L.A. Haskin and T.P. Paster
Geochemistry and mineralogy of the rare earths 1
22. J.E. Powell
Separation chemistry 81
23. C.K. Jørgensen
Theoretical chemistry of rare earths 111
24. W.T. Carnall
The absorption and fluorescence spectra of rare earth ions in solution 171
25. L.C. Thompson
Complexes 209
26. G.G. Libowitz and A.J. Maeland
Hydrides 299
27. L. Eyring
The binary rare earth oxides 337
28. D.J.M. Bevan and E. Summerville
Mixed rare earth oxides 401
29. C.P. Khattak and F.F.Y. Wang
Perovskites and garnets 525

30. L.H. Brixner, J.R. Barkley and W. Jeitschko
Rare earth molybdates (VI) 609
Subject index 655

VOLUME 4: NON-METALLIC COMPOUNDS – II

31. J. Flahaut
Sulfides, selenides and tellurides 1
32. J.M. Haschke
Halides 89
33. F. Hulliger
Rare earth pnictides 153
34. G. Blasse
Chemistry and physics of R-activated phosphors 237
35. M.J. Weber
Rare earth lasers 275
36. F.K. Fong
Nonradiative processes of rare-earth ions in crystals 317
- 37A. J.W. O'Laughlin
Chemical spectrophotometric and polarographic methods 341
- 37B. S.R. Taylor
Trace element analysis of rare earth elements by spark source mass spectrometry 359
- 37C. R.J. Conzemius
Analysis of rare earth matrices by spark source mass spectrometry 377
- 37D. E.L. DeKalb and V.A. Fassel
Optical atomic emission and absorption methods 405
- 37E. A.P. D'Silva and V.A. Fassel
X-ray excited optical luminescence of the rare earths 441
- 37F. W.V. Boynton
Neutron activation analysis 457
- 37G. S. Schuhmann and J.A. Philpotts
Mass-spectrometric stable-isotope dilution analysis for lanthanides in geochemical materials 471
38. J. Reuben and G.A. Elgavish
Shift reagents and NMR of paramagnetic lanthanide complexes 483
39. J. Reuben
Bioinorganic chemistry: lanthanides as probes in systems of biological interest 515
40. T.J. Haley
Toxicity 553
Subject index 587

Chapter 21

GEOCHEMISTRY AND MINERALOGY OF THE RARE EARTHS

Larry A. HASKIN*

*Lunar and Planetary Sciences Division, NASA Johnson Space Center,
Houston, Texas 77058, USA*

and

T.P. PASTER**

Molybdenum Corporation of America, Louviers, Colorado 80131, USA

Contents			
1. Introduction	2	5.5. Vulcanism on the continents	26
2. Formation and abundances of the lanthanides and yttrium	3	5.6. Lunar highland volcanics; KREEP	30
3. Evidence for lanthanide group fractionation during planet formation	5	5.7. Continental igneous-metamorphic complex	31
4. Lanthanides and yttrium in common sedimentary rocks	8	5.8. Anorthosite and early crust formation	34
4.1. The lanthanide-yttrium distribution of the NASC is common	9	6. Lanthanides in Earth's interior	36
4.2. Movements of the Earth's lithosphere	10	6.1. Possible large fragments of mantle	37
4.3. Rare-earth behavior during sediment formation	12	6.2. Ultramafic inclusions	40
4.4. Average crustal abundances of the lanthanides and yttrium	14	6.3. Eclogites	42
4.5. Secular changes in relative lanthanide abundances	15	7. Toward a quantitative understanding	43
4.6. Lanthanides in the oceanic environment	16	7.1. Mathematical models	44
5. Lanthanides in igneous rocks	19	7.2. Distribution coefficients	47
5.1. Volcanic lavas	19	7.3. Eu anomaly	52
5.2. Ocean floor igneous rocks	21	7.4. Developing, testing, and applying the models	55
5.3. Lunar mare basalts	22	7.5. Sm-Nd age measurements	64
5.4. Ocean island volcanic rocks	23	8. Lanthanide mineral resources	65
		8.1. Formation of lanthanide ores	65
		8.2. Commercially important lanthanide minerals	66
		8.3. Uses of lanthanides	71
		8.4. Assessment of lanthanide resources	74
		References	76

*Present address: Department of Earth and Planetary Sciences, Washington University, St. Louis, Missouri 63130, USA.

**Present address: Houston Oil and Minerals Corporation, Denver, Colorado 80206, USA.

Symbols

$C_{L,m}$ = concentration of trace element m in residual liquid L from fractional crystallization
 $C_{A,m}$ = concentration of the trace element in the liquid prior to onset of crystallization

X = fraction of system that has crystallized
 D = distribution coefficient; $D_{w,m}$ for solid w and element m ; i/j between phases i and j
 $C_{S,m}$ = average concentration of trace element in solid from fractional crystallization
 $C_{j,3}$ = concentration of Eu(III) in phase j (or k)

1. Introduction

Rare earth abundances in natural materials have become an important geochemical tool. The rare earth elements comprise a uniquely coherent group; wherever one rare earth appears, all others are present as well. The group is coherent because under most natural conditions all members share a common (3+) oxidation state, with anomalous behavior occurring under some conditions for Ce (4+) and Eu (2+). Natural materials differ substantially from each other in concentrations of the rare earths as a group and in abundances of individual rare earths relative to each other. In most natural situations, chemical separations within the rare earth group occur as a smooth function of atomic number. This makes it possible to find genetic relationships among diverse natural materials and to determine by what processes some natural materials formed.

From the geochemical point of view, the rare earths are "dispersed" elements, i.e., spread around among many common materials rather than concentrated into a select few. They are "lithophile," i.e., when allowed to distribute themselves among common silicate, metal, and sulfide phases, they overwhelmingly enter the silicates. Geochemically, the term "rare earth" is best restricted to mean lanthanides plus yttrium. Yttrium behaves like the heavier lanthanides, although just which heavier lanthanide is dependent on the particular chemical environment. The geochemical behavior of scandium is substantially different from that of the rare earths and is less well characterized and understood. For these reasons, scandium is not further discussed here.

The use of the rare earths as a geochemical tool began in the early 1960's with the development of techniques for their analysis by neutron activation, followed by methods of isotope dilution mass spectrometry. These techniques provided measurements of sufficient accuracy on common (but chemically complex) natural materials that the potential use of rare earth distributions could be recognized and put to use. Summaries of early work are given by Haskin and Frey (1966), Haskin et al. (1966a), and Herrmann (1968).

The story of the rare earths as presented here begins on a grand scale with the formation of those elements from simpler matter. It examines rare earth abundances in the solar system. It traces our knowledge of the behavior of the rare earths during condensation of primitive solar matter into planets and through major stages of planetary differentiation. It shows how rare earth abundances are used in studying rock-forming processes. It ends with a discussion of rare earth bearing minerals.

2. Formation and abundances of the lanthanides and yttrium

No one knows just how everything began, but it appears that, near the beginning, there was mostly hydrogen, perhaps some helium, but no rare earths or other heavy elements. Then stars began to form from those gases. In the cores of stars, nuclear reactions synthesize heavier elements. Sufficiently massive stars have relatively short lives, which they end by exploding their substance into space, to mix with primordial gas. New stars form from the mixtures.

The building of heavier elements from hydrogen is the source of energy for stars. Such fusion reactions are exoergic only through iron, however. Yttrium and the lanthanides are products of nuclear reactions incidental to stellar evolution, e.g., explosions of supernovae. They are the products of the stepwise capture of many neutrons by nuclei of iron or by heavier nuclei already synthesized from iron. Some lanthanide isotopes are produced when successive neutrons are captured on a slow time scale. Under those conditions, each nucleus produced by the capture of a neutron, if radioactive, had time to convert the extra neutron to a proton by beta decay before the next neutron was absorbed. Other isotopes resulted from neutron capture on an incredibly rapid time scale. Parent nuclei were exposed briefly to a flux of neutrons so intense that they absorbed all the neutrons that could be contained in energetically bound states. Afterwards, a series of beta decays ensued until a stable ratio of neutrons to protons was reached. The most proton-rich (and relatively rare) lanthanide isotopes were produced by nuclear reactions that absorbed protons. Detailed descriptions of nucleosynthetic processes are given by Clayton (1968) and in the more recent literature of astrophysics.

By the time our sun had formed, countless stars had already completed their life cycles. The clot of gas that produced the sun was a mixture of primordial hydrogen and heavier elements. These heavier elements were essential to producing the inner planets, satellites, asteroids, and other objects in the solar system which cannot be constructed from hydrogen and helium. The bulk of the heavy elements in the solar system is in the outer portions of the sun itself, which contains more than 99.87 percent of all the mass of the solar system. (The outer portions of the sun do not mix with the core, where nuclear reactions destroy heavy elements.) The abundances of yttrium and the lanthanides in the sun's atmosphere have been determined spectroscopically and are believed known with medium accuracy (Ross and Aller, 1976). Pieces of the Earth, the Moon, and meteorites, all of which condensed from the same batch of material as the sun, have been analyzed chemically to determine their abundances.

Of all the materials sampled in the laboratory, the class of meteorites called chondrites is believed to come the closest to retaining the nonvolatile elements of the solar system in their primitive relative abundances. If the processes that formed those meteorites did not appreciably fractionate the nonvolatile elements, then surely they did not separate yttrium and the members of the lanthanide series from each other. Thus, from analyses of chondritic meteorites, the relative elemental abundances of Y and the lanthanides in the solar system are known to a high degree of confidence.

Special (and somewhat rare) classes of stars have much higher abundances of the lanthanides in their atmospheres than does the sun, evidence of unusual stellar processes. On the whole, most stellar matter appears to have relative abundances of heavy elements similar to those of the sun (e.g., Unsöld, 1969). This suggests that statistical aspects have overcome the contributions of individual stars to the overall evolution of interstellar gas composition. Alternatively, current ideas about the origin of matter may be incorrect; the universe

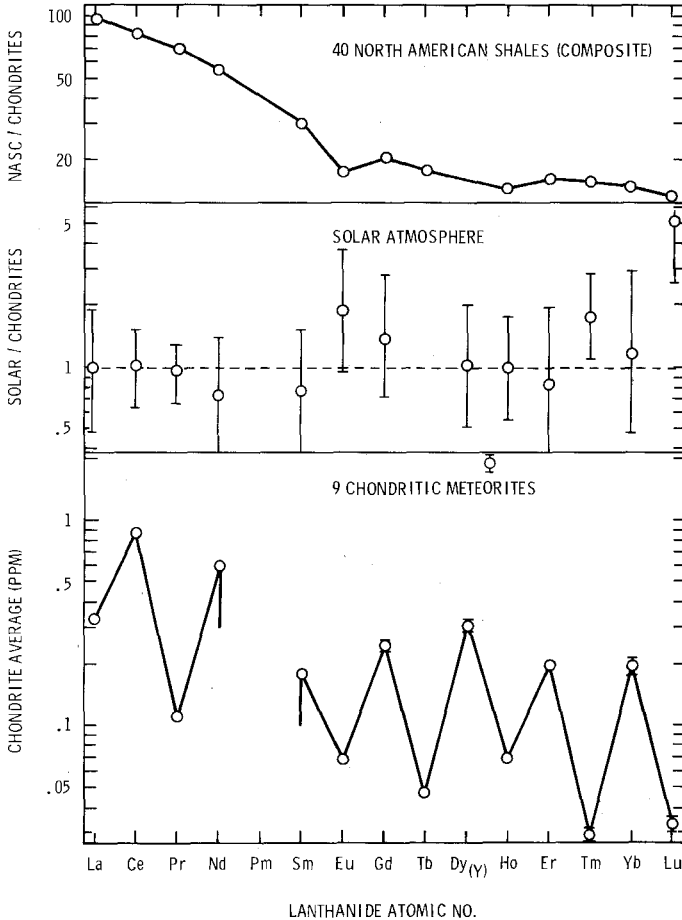


Fig. 21.1: Concentrations of lanthanides and yttrium in a composite sample of 9 chondritic meteorites (Haskin et al., 1968) are plotted against lanthanide atomic number in the lowest part of the figure. Relative lanthanide abundances for the solar atmosphere (Ross and Aller, 1976) and lanthanide concentrations for a composite of 40 North American shales (Haskin et al., 1968) are compared with the chondritic abundances in the middle and upper parts of the figure by plotting ratios of their lanthanide concentrations to those of the chondrites. Such comparison diagrams are used throughout this chapter.

may have begun with essentially the present abundances of lanthanides, or developed them very early.

Concentrations of the lanthanides and yttrium in a composite of nine chondrites (Haskin et al., 1968) are given in table 21.1.

Figure 21.1 shows the concentrations of the lanthanides in the chondrite composite plotted on a logarithmic ordinate against atomic number. The zigzag pattern reflects effects of nuclear stability. Stability is enhanced by pairing of all protons with other protons, all neutrons with other neutrons, or both. Elements of odd atomic number cannot have all their protons paired. For purposes of demonstrating chemical fractionation among the lanthanides it is common practice, in comparing the distribution of lanthanides in one substance with that of another, to eliminate the obfuscating zigzag effect. This is done by dividing one lanthanide distribution, element by element, by the other. The resulting ratios are plotted on a logarithmic ordinate against lanthanide atomic number. In the middle part of fig. 21.1, abundances for the sun's atmosphere, taken from Ross and Aller (1976), but converted from relative numbers of atoms to relative masses and arbitrarily normalized to La = 0.33, are plotted relative to the chondritic ones. It is easily seen that the solar abundances are the same as the chondritic ones except for Lu, for which the solar value must somehow be in error. Uncertainties are substantial for all the lanthanides.

3. Evidence for lanthanide group fractionation during planet formation

The lanthanide distribution at the Earth's surface does not match that of the chondrites. It is approximated by the abundances in a composite sample of North American shales (table 21.1) (Haskin et al., 1968). In the shales, the heavier lanthanides (Gd–Lu) and Y are uniformly enriched to about 15 times their chondritic concentrations. The lighter lanthanides are increasingly enriched from Gd (~20 times the chondritic value) to La (~100 times). The concentration

TABLE 21.1

Lanthanide and yttrium concentrations in parts-per-million in a composite of 9 chondritic meteorites and of 40 North American shales.

	Chondrites	Shales		Chondrites	Shales
Y	1.96 ± 0.09	27	Tb	0.047 ± 0.001	0.85
La	0.330 ± 0.013	32	Dy	0.317 ± 0.005	5.8
Ce	0.88 ± 0.01	73	Ho	0.070 ± 0.001	1.04
Pr	0.112 ± 0.005	7.9	Er	0.200 ± 0.005	3.4
Nd	0.60 ± 0.01	33	Tm	0.030 ± 0.002	0.50
Sm	0.181 ± 0.006	5.7	Yb	0.200 ± 0.007	3.1
Eu	0.069 ± 0.001	1.24	Lu	0.034 ± 0.002	0.48
Gd	0.249 ± 0.011	5.2			

Data from Haskin et al. (1968).

of Eu is anomalously low, ~ 0.67 times the interpolated value in fig. 21.1. Presumably, both the general increase in concentrations and the changes in relative abundances of the lanthanides are the result of processes of formation of planets.

Opportunities abound for chemical separations during formation and evolution of planets. To a first approximation the early solar system was a compositionally homogeneous nebula of gas and minor (but important) particulate matter. Presumably the nebula was disk-shaped, with a substantial temperature gradient decreasing outward from the central mass, or proto-sun. As it cooled, elements in gaseous form condensed to solid matter that coalesced somehow into ever larger chunks, finally resulting in accretion of planets. The inner planets (Mercury, Venus, Earth, Mars) formed too close to the sun for any appreciable amounts of the most volatile elements to condense. Thus, there was chemical separation according to volatility, beginning during formation of small grains and continuing through development of entire planets.

Present evidence from the inner planets indicates that substantial melting occurred during or soon after planetary accretion. This resulted in extensive chemical zoning, at least for Earth and Moon. Further chemical separation occurs even after planetary exteriors are solidified. Some is internal, yielding near-surface differentiated bodies to be exposed later by erosion, or as lavas extruded directly onto the surface. Some is external, results of planetary weathering or accumulation of solar debris (material left over from the principal stages of accretion, tumbling in as meteoroids).

Most work on the geochemistry of the rare earths has been concentrated on determining the understanding the lanthanide distributions in terrestrial and meteoritic matter and, most recently, lunar matter. Relatively little attention has been given to internal separations within the lanthanide group during condensation of the solar nebula. So far, no observational evidence requires that any planet, overall, have average relative lanthanide-Y abundances different from the average for the solar system. Recent evidence suggests, however, that the lanthanide group can fractionate during condensation of a gas of solar composition.

Some general models for equilibrium condensation of chemical elements from the solar nebula have been advanced (e.g., Grossman, 1972; Boynton, 1975). To a first approximation, they show yttrium and the lanthanides, which are among the most refractory of the chemical elements, as condensing at very high temperatures with calcium and aluminum. Numerous fragments of meteorites have been analyzed and nearly all of them show variation in relative abundance more or less similar in magnitude and type to variations found among terrestrial materials. (Even individual fragments of chondrites differ from the chondritic values, in ways not understood in detail, but not seeming to require extraordinary mechanisms for producing the variations.) In 1969 a large meteorite of very primitive nature (a carbonaceous chondrite) fell in northern Mexico. Overall, the rare earth abundances in that meteorite (called Allende) are the same as found in other chondrites. Found within that meteorite are small pink or

white inclusions with bulk compositions similar to those expected for early condensates from the solar nebula (Grossman and Clark, 1973). The lanthanides and yttrium are concentrated in them by some 20 times compared with chondritic meteorites as a whole (Grossman, 1973). By careful mass spectrometric analysis, some have been shown to have abundance distributions that cannot be rationalized as resulting from chemical separations accompanying ordinary geologic processes (e.g., Tanaka and Masuda, 1973) (fig. 21.2).

Boynton (1975) has offered a model based on thermodynamic equilibrium between a gas of solar composition and condensing solids to account for the results. In his model, Y_2O_3 condenses, beginning at about 1700 K and selectively removing the least volatile lanthanides. The resulting solid then serves as a buffering reservoir for yttrium and the lanthanides during condensation of the mineral perovskite ($CaTiO_3$) which, through a combination of vapor pressure and crystal site control, selectively removes certain lanthanides (e.g., Y and the heavier lanthanides, except Yb), leaving others (e.g., La, Ce, Nd, Eu, Yb) mostly behind in the gas. This solid perovskite becomes separated from the residual gas, and the gas further condenses to produce a solid with a lanthanide distribution like that found in the Allende inclusion. This solid is separated from the gas while the gas still contains substantial La, Ce, Nd, Eu, and Yb, which condense later in the mineral enstatite ($MgSiO_3$).

The Allende meteorite has also yielded materials with anomalous isotopic ratios for oxygen and magnesium. These are the first materials analyzed whose

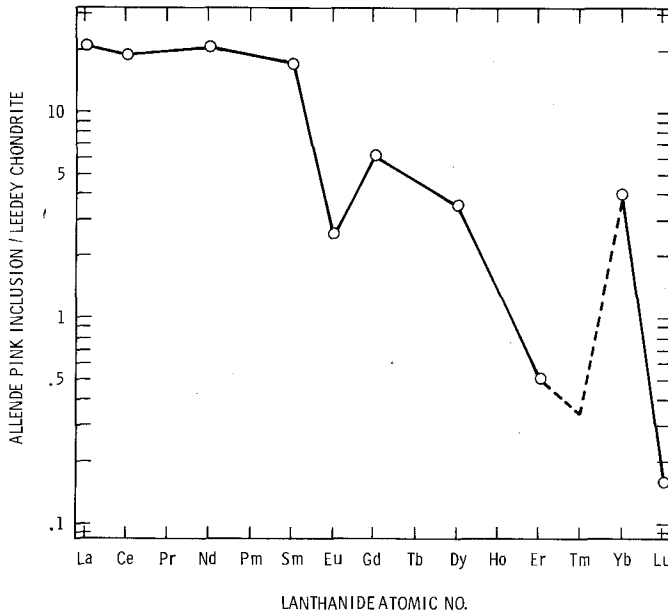


Fig. 21.2. Comparison diagram for lanthanide concentrations in a refractory inclusion in the Allende meteorite (Tanaka and Masuda, 1973).

isotopic compositions could not be explained as results of chemical isotope effects or bombardment by cosmic radiation and, therefore, seem to be relict inhomogeneities of the solar nebula. They may be, in part, residual grains of interstellar matter not destroyed when the solar nebula formed. Anomalous lanthanide distributions have recently been found in other meteorites as well (e.g., Nakamura and Masuda, 1973; Nakamura, 1974; Tanaka et al., 1975).

It is clear from table 21.1 and fig. 21.1 that the lanthanide distribution in the composite of North American shales (NASC) is different from that of the chondrites and the sun's atmosphere. Since the differences are a smooth function of atomic number (except for Eu), they are probably a result of processes of internal planetary differentiation. Differential condensation from a gas does not produce such smooth distributions (Boynnton, 1975). What, then, does the NASC distribution represent, or tell us about the history of Earth?

The NASC distribution (Haskin et al., 1968) had been found in a variety of sedimentary rocks. On comparing distributions found in several sedimentary rocks with abundances recently determined for meteorites by Schmitt and co-workers (1960), Haskin and Gehl (1962) noted that the relative lanthanide abundances in the sediments were clearly different from the presumed solar average. They suggested that the average terrestrial relative lanthanide abundances were the same as the chondritic, and that the high concentrations of lanthanides and yttrium and selective light lanthanide enrichment at the Earth's surface were a consequence of the differentiation of the planet into a crust, a mantle, and a core. Qualitatively, this idea can be rationalized as follows. Earth's core (the innermost 3 470 km in radius, 32.4% of the mass) consists mainly of metallic iron and nickel, plus perhaps some silicon and sulfur. The chemically active lanthanides would not be present in metallic form and therefore would not be dissolved in the core. Surrounding the core is the mantle (2 880 km thickness, 67.2% of the mass), believed to consist mainly of silicates of magnesium and iron (II). The structural sites in the corresponding minerals are too small for lanthanide ions, so the lanthanides, especially the larger, lighter ones, would be preferentially excluded from the mantle. Thus, a high proportion of Earth's lanthanides would end up in the crust (outermost layer, ~35 km thick for continents, ~5 km thick for oceans, ~0.45% of Earth's mass), a sort of scum consisting of lower density materials that have been excluded from both core and mantle. All evidence found so far is compatible with this rather general explanation, but no useful quantitative description of the process has been developed.

The lanthanide-yttrium distribution in the NASC is surprisingly common in sedimentary rocks. The explanation and significance bear on our understanding of crustal evolution and processes of formation of sedimentary rocks.

4. Lanthanides and yttrium in common sedimentary rocks

Shales are a common form of sedimentary rock. Sedimentary rocks are depositional products of weathering and erosion of other rocks. Those rocks

may be igneous (crystallized directly from a melt), older sediments, or metamorphic rocks (igneous or sedimentary rocks altered in mineralogy and usually in composition by the action of heat and pressure). Sedimentary rocks are highly variable in composition, structure, and type. Here they are classified in three categories: carbonates (mainly CaCO_3 and MgCO_3) deposited from solution, by inorganic or biogenic (biological) processes or both, such as limestones and dolomites; shales, comprised mainly of clay minerals that are insoluble weathering products of many common rock-forming minerals; and sands, which consist of small grains of mineral residues from weathering. If weathering has been extensive, over multiple cycles of sedimentation, the sands may be nearly pure quartz (SiO_2). If weathering has been rapid, sands may contain abundant mica, feldspar, and other silicates in addition to quartz. Sediments classed as carbonates frequently contain substantial clay or sand, sands often contain clays or carbonates, etc. Pure end-member sediments are very rare.

4.1. *The lanthanide–yttrium distribution of the NASC is common*

Composites of shales from three localities were analyzed by Minami (1935) and all found to have similar lanthanide distributions. Goldschmidt (1938), having observed that minerals rich in lanthanides had varied distributions, inferred that sedimentary processes remixed lanthanides from different igneous minerals back into their average, perhaps, primordial abundances. Haskin and Gehl (1962) analyzed ten samples of carbonates, sands, and shales and found in them distributions that resembled those found by Minami. Haskin et al. (1966b) reported lanthanide concentrations for 38 individual sedimentary rocks. The average relative abundances (but not the average absolute concentrations) for the 38 sediments were the same as those of the NASC. The average distribution for sediments from the Russian Platform (Balashov et al., 1964) was the same. A redetermination of one of the shale composites originally analyzed by Minami gave the same distribution (Haskin and Haskin, 1966). The average relative abundances of just a few sediments of each general type also matched the NASC distribution (9 carbonates, 7 sandstones, 5 greywacke sandstones, 8 ocean sediments, 9 shales; Haskin et al., 1966b). Only 14 of the 38 individual rocks had distributions like that of the NASC to within ± 15 percent, but only 15 percent of the rocks deviated from that distribution by as much as a factor of 1.5. Thus, whereas the lanthanide distributions in most samples of sedimentary rock differ measurably from the NASC distribution, the strong resemblance to that distribution is clear. An average for sedimentary rocks from any general locality produces it within a few percent.

The uniformity in this distribution is surprising. Most rocks are heterogeneous, complex chemical systems with complicated histories. There was no reason to presume that two samples of rock from the same rock formation, or even adjacent fragments from a single sample would show such similar lanthanide distributions, let alone rocks of different ages, from different places, and with different bulk compositions and mineralogies!

In most carbonates and sandstones, clay minerals are abundant. These

minerals have much higher lanthanide and yttrium concentrations than carbonate or quartz, and thus may contain the bulk of the lanthanides in the entire rock (e.g., Cullers et al., 1975). Roaldset (1975) showed that the phyllosilicate minerals (clay, mica group) do not concentrate the lanthanides in igneous rocks, but adsorb them as clays develop during weathering. The uniformity of lanthanide distributions among sediments is thus not a consequence of a preferred distribution for clay minerals. The clay minerals are products of weathering of igneous minerals and tend to inherit and average the lanthanide distributions of their sources. In order to discuss the effects of sedimentary processes on lanthanide distributions and further assess the uniformity of the distributions for common types of sedimentary rocks, it is necessary to outline the nature of large-scale geological processes at the Earth's surface.

4.2. *Movements of the Earth's lithosphere*

Modern geoscience (e.g., Press and Siever, 1974) recognizes large-scale movement of major segments of the Earth's crust and upper mantle. Continents are no longer viewed as inviolable centers of growth resting in fixed position on the Earth's surface. They are dragged about at rates of a few centimeters per year. They have all been parts of a single supercontinent (Pangaea) at least once, and have repeatedly collided, fused together, and parted along new fractures. The extent to which the original continents might have been chemically distinct from each other is not known. Certainly, their isolation from each other as chemical systems has been less than complete and mixing of materials at least along their edges has occurred. Their most stable central areas (shields) have not necessarily indulged in mixing, but are geochemically rather similar in any event.

Ocean floors move, too, spreading outward from ocean ridges. At ocean ridges, molten material from the Earth's interior wells up to the surface, providing fresh ocean floor. Portions of the ocean floor farthest from the ridges are drawn downward (subducted) into the Earth's interior. Continental matter, being less dense on the average than the rocks of the ocean floors, does not so readily sink.

These giant motions are not accomplished without stress, so earthquakes, volcanos, general uplifting of some areas, and downwarping of others occur. The unifying concept that brings these many aspects of Earth's surface behavior into coherence is known as Plate Tectonics. In this concept, the uppermost ~100 km of the Earth's surface is solid and rigid and called the "lithosphere." The lithosphere is broken into large segments called "plates," which float on a plastically deformable portion of the upper mantle known as the "asthenosphere." The plates move about in response to forces causing motion in the asthenosphere beneath. The exact nature of these forces and the extent to which convective motions of the deep mantle are involved are obscure.

The details of the chemical processes that accompany the machinations of plate movements are largely unknown but are a topic of vigorous pursuit. Any general description of geochemistry should be written and read in an aura of

awareness of the powerful concept of plate tectonics in order to nurture our understanding of both plate tectonics and the geochemical topic. This chapter is written in such awareness, but without an effort to contrive detailed explanations of rare earth geochemistry in terms of plate tectonics.

The production of sedimentary rocks is influenced by motions of crustal plates. Highest rates of sediment formation occur in regions where mountains are forming, typically at the edges of continents. In an over-simplified view, when the edge of an oceanic plate collides with the edge of a continental plate, the more dense oceanic crust is forced down, and the edge of the continental plate somewhat raised. The uplift of the continental plate makes mountains. On the oceanic side of the mountains, where the oceanic crust is subducted, a deep depression (eugeosyncline) develops. The mountains may form contiguous with the exposed land surface of the continent or, if the continental plate extends outward for a ways below sea level, the mountains may form some distance from shore. Nor must the mountains consist entirely of uplifted continental material. A major portion may arise from volcanic activity related to the subduction of oceanic crust. A relatively shallow sea may exist between shore and mountains; such a depression is called a miogeosyncline.

Sediments form as materials erode from the mountains or the major portion of the continent and are carried into the geosynclines. On the oceanic side, materials from the mountains fall into the eugeosyncline. The weight of these sediments further depresses the eugeosynclinal trough while the removal of material from the mountains tends to unload the continental plate so that it further rises.

The sediments falling into the eugeosyncline are quickly buried. A high proportion are sandstones that retain the mineralogical characteristics of their parents to a high degree. If those parents were igneous or high-grade metamorphic rocks, then only the most rapidly weathered minerals (e.g. olivines-orthosilicates of Fe, Mg, pyroxenes-metasilicates of Fe, Mg, Ca) are converted to clays, while feldspars (aluminosilicates of Ca, Na, K), micas (hydrated aluminosilicates), and quartz, along with many minor minerals remain intact. Such sediments are complex varieties of sandstone (e.g., greywacke). Many mountains are composed of material deposited in an earlier geosyncline; thus, geosynclinal sediments may be second, third, or later generation.

The same mountains erode into the miogeosyncline. There, slopes are somewhat shallower and more opportunity exists for weathering to alter the mineralogy. Also feeding into the miogeosyncline are sediments from the major portion of the adjacent continent. Such sediments tend to be several generations old. Most of the minerals of their precursors have been converted to clays. Sand grains are mostly quartz, a common igneous mineral highly resistant to weathering. Along the edge of the sea nearest the continent (the continental shelf) conditions may be rather quiet tectonically, and relatively pure end-member sediments can then accumulate (sandstones of nearly pure quartz, shales of nearly pure clay, and carbonates precipitated from the shallow seas).

To what extent are the lanthanides and yttrium from different sources mixed

together during sediment formation? To what extent are they mobilized and the group fractionated? To what extent do lanthanide distributions in sedimentary rocks reflect the distributions of their parent sources?

4.3. Rare earth behavior during sediment formation

Ronov, Balashov, and co-workers have extensively studied rare earths in a geologic setting such as that described in the previous section. Balashov et al. (1964) examined the chemical separations among the lanthanides brought about by weathering and sedimentary differentiation. They studied a series of sediments formed under tectonically rather quiet conditions on the Russian Platform. During early stages of sedimentation the climate was arid, and little differentiation occurred. Concentrations and relative abundances of the lanthanides and yttrium were relatively constant, and concentrations in sandstones exceeded those in shales. In the succeeding stages of sedimentation, a hot, humid climate prevailed and extensive weathering occurred. Lanthanide concentrations and relative abundances were more variable. There was a tendency for heavier lanthanides to mobilize and travel somewhat farther from their source regions than did the lighter lanthanides. Lanthanide concentrations decreased in the order shales, sands, carbonates. Relative abundances of light to heavy lanthanides decreased in the same order.

Ronov et al. (1972, 1974) broadened the study to include the Russian and Scythian platforms (representative of stable, continental regions), the miogeosyncline of the high Caucasus mountains, the mountains themselves, and the seaward eugeosyncline. The lanthanide concentrations in clays (shales) increased in a regular manner from the eugeosynclinal sediments to the Russian Platform; a similar trend was observed for carbonates (fig. 21.3). The opposite

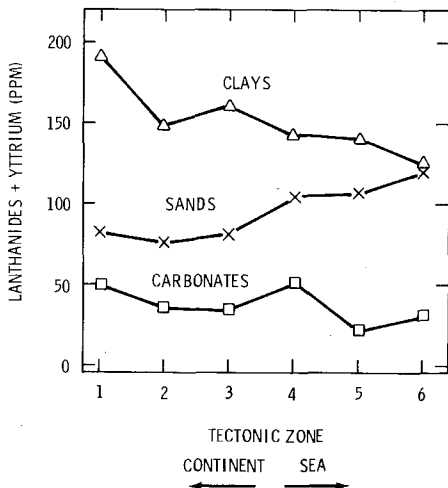


Fig. 21.3. Trends of total lanthanide abundance in sediments with location relative to the Russian Platform and adjacent eugeosyncline are shown (Ronov et al., 1972, 1974). Zone 1 is the farthest inland and represents the Russian Platform, zone 2 the Scythian Platform, zone 3 the northern miogeosyncline of the high Caucasus mountains, zone 4 the southern miogeosyncline, zone 5 the transcaucasian central massif, and zone 6 the seaward low Caucasus eugeosyncline.

trend was observed for sandstones, so that sandstones in the eugeosynclinal sediments had concentrations of lanthanides about the same as in the clays, decreasing inland to an extent that platform sands had lanthanide concentrations only about 5 percent as high as clays. Relative amounts of lighter to heavier lanthanides decreased from the platforms to the central mountains, then increased strongly seaward for clays and carbonates, but not for sandstones. The extent of relative enrichment in lighter lanthanides was greatest in the sandstones, with clays next, except in the eugeosynclinal sediments, where sandstones were the least enriched. The extent of the decrease in the ratio of light to heavy lanthanides was similar for all three classes of rocks over most of the traverse, except for the sandstones in the eugeosyncline (as noted previously) and a strong, light lanthanide enrichment in clays of the Russian platform. These trends were explained as the mixing of two main effects.

First, in tectonically quiet settings where differentiation is extensive, the bulk of the lanthanides ends up in the clays. The silicate minerals that are the main carriers of rare earths in igneous rocks are destroyed by weathering, and the resulting clays readily accept the lanthanide ions. Weather-resistant quartz does not accept lanthanides in significant quantities under igneous or sedimentary conditions. Thus the lanthanides concentrated mainly in the clays in well-differentiated sediments of the stable platform and relatively quiet geosynclinal regions, but remained with the mineralogically complex sandstones of the eugeosynclines.

Second, the source regions of the platform sediments, being typical stable continental areas, consisted mostly of siliceous rocks (granite-like igneous materials and their weathered products). Such igneous materials, on the average, have lanthanide distributions like that of the NASC. The eugeosynclinal region and, to a lesser extent, the miogeosynclinal region, had substantial contributions from local submarine and subaerial volcanos. The earliest, and most extensive, volcanics had lanthanide distributions characteristic of island arcs and ocean floors, relatively depleted in light lanthanides. That distribution appeared almost unaltered in the sandstones developed from the earlier volcanic rocks; there was some effect on the clays, as well. Later volcanism yielded igneous products with higher lanthanide concentrations and higher relative abundances of the lighter lanthanides, an effect transferred to the resulting sediments.

The mixing of the two effects is at most slightly modified by any mobilization of lanthanides over long distances. The lanthanide distributions of local regions appeared in the carbonate sediments of those regions. To a first approximation, lanthanide ions enter the aqueous phase during weathering, but only briefly. They are immobilized near their sources.

The common occurrence of the NASC lanthanide distribution attests to the thoroughness of mixing of lanthanides from different igneous sources over multiple cycles of weathering and sedimentation. It also attests to the uniformity of composition of different continental areas. To what extent does the NASC distribution represent the average for the Earth's crust?

4.4. *Average crustal abundances of the lanthanides and yttrium*

Ronov et al. (1972, 1974) give average concentrations for lanthanides in sediments. The concentrations are some 20 percent lower for the middle and heavy lanthanides and yttrium than those given for the NASC, which is reasonable since their estimates include sands and carbonates. Concentrations for the lightest lanthanides given by Ronov et al. are 40 to 50 percent lower than in the NASC because the eugeosynclinal sands are relatively deficient in those elements. The accuracy of their average for the sediments depends on the relative amounts of each type of sediment estimated to be in the region under consideration.

Ronov et al. also give estimates of the average lanthanide concentrations for the Earth's crust. Those values are very similar to their average for all sediments. Their estimates are probably as good as any in the literature. Such estimates are quite dependent on assumptions about types and compositions of materials in the middle and lower crust, and such assumptions are model dependent. All major segments of the Earth's crust are not similar; for example, the composition of the accessible igneous oceanic crust is strikingly different from that of the exposed continental crust; its volume is much less than that of continental crust.

It is not certain that the average crustal relative abundances given by Ronov et al. are better than those of the NASC, which are found on all continents and in the sediments covering the igneous ocean floors. In any event, the value of average crustal abundances is limited mainly to placing limits on the bulk composition of the Earth and considering the extent to which various elements have been excluded from the core and crust.

All present evidence indicates that the crust and uppermost mantle have higher lanthanide and yttrium concentrations than primitive, nonvolatile solar matter (i.e., chondritic meteorites). Prevailing opinion is that these segments of Earth are also relatively enriched in the lighter lanthanides, but such a conclusion presumes that the entire crust has the same compositional characteristics as the crustal surface. There is no reason so far to suspect that the relative lanthanide and yttrium abundances for the Earth as a whole differ from the chondritic distribution. The average lanthanide concentrations for the Earth may not be the same as the chondritic ones, but there is no compelling reason to believe that they are markedly different; i.e., a model crust of uniform composition does not contain a larger mass of lanthanides than would be available from a whole Earth, or even a mantle plus crust, of chondritic composition (e.g., Haskin et al., 1966a). For an alternative model of bulk planetary compositions, see Ganapathy and Anders (1974).

If the crust and upper mantle are indeed relatively enriched in the lighter lanthanides, did they attain that enrichment suddenly, e.g., in a catastrophic zoning of Earth into core, mantle, and crust, or gradually throughout geologic time?

4.5. *Secular changes in relative lanthanide abundances*

The tendency for sediments to average the individual lanthanide distributions of their precursors was put to use by Wildeman and Haskin (1973) to look for evidence of any gradual change from a chondritic distribution to that now characteristic of the crust. They analyzed 36 samples of the oldest available sedimentary rocks from 16 rock formations in the Baltic, North American, and South African shields. The samples were relatively undisturbed by metamorphism and ranged in age from ~ 1.7 to >3.0 billion years. They found no evidence that the abundances of the lighter lanthanides relative to the heavier ones had changed between >3.0 billion years ago and the present. The Earth, however, is some 4.5 billion years old. The oldest (igneous) rocks with carefully measured ages are only 3.7 billion years old. Thus, the record of the earliest development of the Earth's crust has been obscured.

The abundance of Eu relative to neighboring Sm and Gd was higher, on the average, in the Precambrian (older than 0.6 billion year) sediments, in comparison with those of the NASC and other sediments of younger age. Only two of the Precambrian sediments had relative Eu abundances lower than those of the NASC; the rest had abundances that were significantly higher. Wildeman and Haskin were unable to offer a convincing reason for this observation. High relative Eu abundances were found by Wildeman and Condie (1973) in Precambrian sediments from Wyoming and South Africa, by Nance and Taylor (mentioned by Jakeš and Taylor, 1974) in Precambrian Australian sediments, and by Tugarinov et al. (1973) in rocks of the Krivoy Rog series. Moorbath et al. (1975) show relatively high Eu values for sediments of ~ 3.7 billion years age from Isua, Greenland.

Jakeš and Taylor (1974) concluded that the relatively high Eu abundances in the Precambrian sediments reflected the abundances in the igneous rocks of their source regions. They suggested that the sediments might have derived from sources with high proportions of island-arc volcanic rocks. Those volcanics do not have relative Eu deficiencies as compared with chondrites. The younger sediments as represented by the NASC would have derived mainly from upper continental crust. Such average upper crustal material was suggested to be relatively deficient in Eu because the igneous processes that produced it would have retained that element selectively in the lower crust. In this model, the crust is compositionally stratified. Ronov et al. (1972, 1974) also suggested that the Precambrian sediments analyzed by Wildeman and Haskin (1973) were derived from island arc volcanics, which are not depleted in Eu.

There are substantial difficulties with this explanation. The island arc volcanics in question are relatively deficient in light lanthanides compared with the NASC and the Precambrian sediments. No combination of their distribution and that of Eu-deficient crustal material can produce the NASC-like distribution with increased Eu. Also, the sediments showing Eu anomalies include well differentiated shales, sands, and carbonates, probably not of eugeosynclinal origin. Finally, several of the Precambrian sediments had relative Eu abundances greater than that of the chondrites and, therefore, the island arc basalts.

Secular compositional changes in geochemistry are rare. The apparent trend in the relative abundances of Eu merits more attention.

4.6. Lanthanides in the oceanic environment

The moving ocean floors accumulate sediments, but not in great thicknesses like those near continental margins. Most igneous rocks of the ocean floor are strongly deficient in light lanthanides relative to the NASC but are not depleted in Eu. The ocean floors account for most of the surface area of the Earth. What lanthanide distributions are found in ocean sediments?

Wildeman and Haskin (1965) analyzed six samples of the most common types of deep-ocean sediment—clays and clays mixed with carbonate and siliceous tests of one-celled oceanic organisms (radiolaria, Globigerina, diatoms)—and two near-shelf sediments of known terrigenous origin (fig. 21.4). Within experimental uncertainty, the lanthanide relative abundances were the same as those of the NASC, consistent with other evidence that the principal source for ocean sediments is the continents, not the igneous ocean floors. This general result has been confirmed by Spirn (1965) and by Shimokawa et al. (1972). As the sea floors spread, they sweep the terrigenous lanthanides back toward the continents for recycling. This further serves to mix lanthanides from different continental sources.

Shimokawa et al. suggested that Eu was relatively depleted in their samples of ocean sediment relative to the NASC. More recent values for the NASC (Haskin et al., 1968) than those used by Shimokawa show that Eu is 0.67 times the

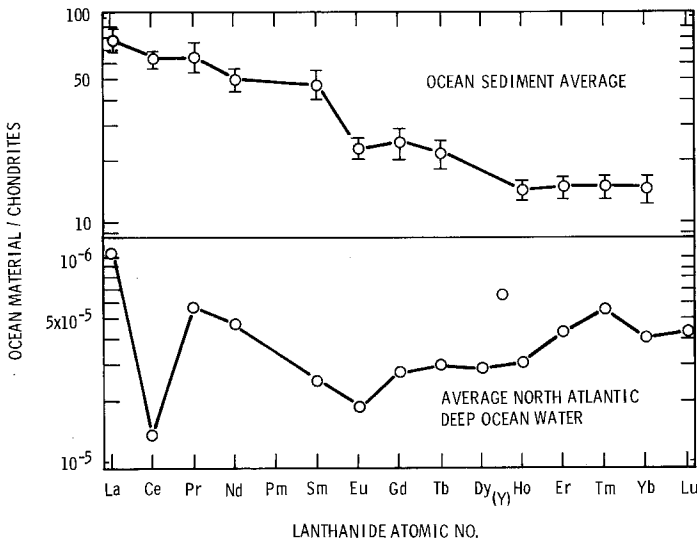


Fig. 21.4. Comparison diagram for ocean sediments (Wildeman and Haskin, 1965) and ocean water (Høgdahl, 1965–68).

interpolated value on a chondrite comparison diagram (fig. 21.1), in agreement with 0.69 for the sediments analyzed by Shimokawa et al.

Most of the lanthanides found in ocean sediments are of terrigenous (land) origin, but there are exceptions. Bender et al. (1971) analyzed a core from the slope of a mid-ocean ridge (the East Pacific Rise) that consisted mainly of calcite (CaCO_3) and had a lanthanide distribution similar to that of sea water, its apparent source. Piper (1974) reviewed available information on lanthanides in biogenic (of biological origin) and authigenic (of inorganic origin within the sea) materials separated from ocean sediments. Biogenic materials (carbonate tests from foraminifera and shells of pteropods, siliceous remains of diatoms, opaline silica) clearly derived their lanthanides from sea water. Authigenic barite (BaSO_4) phillipsite (a zeolite), montmorillonite (a clay), and metalliferous sediment from the crest of the East Pacific rise also reflected the influence of sea water. Robertson and Fleet (1976) reported on several iron and iron-manganese sediments from the Troodos massif that have negative Ce anomalies. Some are rather rich in lanthanides, with Sm concentrations ~ 100 times the chondritic value. The barite and the metalliferous sediments appear to be direct precipitates with sea water the lanthanide source. Sea water may have been the source for the montmorillonite and phillipsite also, but phillipsite especially has substantial ion-exchange capability and might well equilibrate with the lanthanides in sea water whatever its origin.

A main feature of the lanthanide distribution in these materials is a substantial depletion in Ce. Excess Ce is found in authigenic ferromanganese nodules (e.g., Goldberg et al., 1963; Ehrlich, 1968; Glasby, 1972-73). Presumably, the selective uptake of Ce by these common oceanic materials accounts for the relative deficiency of that element in ocean water. Concentrations of lanthanides in most biogenic and authigenic oceanic materials are relatively low, and the proportions of those materials in common ocean sediments are low, so their relative abundance distributions do not appreciably affect the overall abundances for the sediments that contain them.

Copeland et al. (1971) describe clays from the mid-Atlantic ridge that are derived from local igneous material and whose lanthanide distribution therefore matches that of the ocean floor basalts. The lanthanides must have been released from the minerals of the parent igneous rock into solution, but they did not equilibrate in any general way with ocean water before being captured by the clays.

The relative lanthanide and yttrium abundances in sea water (fig. 21.4) differ significantly from those of the NASC, as first shown by Goldberg et al. (1963) for water from the Pacific Ocean. Relative to the NASC, the ocean water was strongly depleted in Ce and increasingly enriched in the heavier lanthanides and yttrium. Spirn (1965) and Hayes et al. (1965) reported similar distributions for waters from the Atlantic Ocean and the Gulf of Mexico. Extensive analyses of ocean water from a wide variety of locations (Atlantic, Pacific, and Indian Oceans; Antarctic; Caribbean and Barents seas) were made by Høgdahl (1965-68; see also Høgdahl et al., 1968). Høgdahl set out to determine whether there

was sufficient variability in lanthanide concentrations and distributions in ocean waters that lanthanide analysis could be used to trace large scale movements of different water masses. Variations were present, but relatively small, thus requiring very painstaking analysis for their characterization and use. The average lanthanide concentrations for 11 samples of North Atlantic deep water illustrate the baseline distribution for ocean water, except for a few samples taken near surface and near land which showed relative abundances very similar to those of the NASC. The range of concentration of Sm for the samples of North Atlantic deep water was 2.6 to 5.7 parts per trillion (parts per 10^{12}) and the average was 4.5 pptr. The range in Sm concentration for all samples except those few obviously contaminated with terrigenous matter was 6 pptr, and values for 26 of 40 samples were between 3 and 6 pptr. Samples from the north Pacific ocean and the Caribbean sea had lanthanide concentrations approximately twice those characteristic of the other regions sampled, and Ce concentrations that were normal relative to La and Pr, compared with the NASC.

Høgdahl's measurements were made on unfiltered ocean water. Content of particulate material was several milligrams per 10 liter sample. Particulates were analyzed separately for several samples and found not to contain a high fraction of the total lanthanides present. Thus little, if any, unaltered terrigenous residue was present.

As discussed above, most ocean sediments have lanthanide distributions similar to those of the NASC. There is no net selective transport of certain lanthanides relative to others from the terrigenous sources to the oceans. The relative Ce deficiency in most ocean water is apparently a result of selective uptake of that element by authigenic ferromanganese nodules. The reasons for the other differences between the ocean water distribution and that of the NASC are not known. The lanthanide distributions for ocean water and authigenic materials demonstrate clearly that internal fractionation of the lanthanide group does occur in the oceanic environment. The concentrations of the lanthanides in ocean water are so low, however, that no large reservoir of material with a lanthanide distribution complementary to that of ocean water is to be expected. As Wildeman and Haskin (1965) indicated, the total amount of lanthanides in ocean water is less than the amount present in the upper 0.2 mm of ocean floor sediment. Thus, preferential extraction of some lanthanides from a few millimeters of sediment would not measurably alter the distribution in that sediment.

The low concentrations of lanthanides in ocean water reflect the rapid rate at which they are scavenged or swept out as terrigenous detritus. Mean residence times in the ocean are very short, ~50 to 600 years (Goldberg et al., 1963; Wildeman and Haskin, 1965), based on a model for mean residence time $t_A = A/(dA/dt)$ in which A is the total amount of a lanthanide present in ocean water at steady state and dA/dt is the amount introduced into (or precipitated from) the ocean per year.

Possibly, the lanthanide concentrations in ocean water are buffered by the sediments. If so, the Ce deficiency and the variations in concentration are not

easily understood. Possibly, most of the lanthanide in the sediments arrives there without any equilibration with ocean water, and the ocean water distribution is a kinetic steady state one dependent on dissolution of terrigenous material and precipitation of ferromanganese nodules and other authigenic and biogenic phases. Much of the lanthanide found in ocean water may be adsorbed on tiny bits of hydrated Fe or Mn oxides rather than in true solution.

5. Lanthanides in igneous rocks

In the discussion of sedimentary rocks it was concluded that the relative lanthanide abundances in those rocks represented the average distributions of their igneous precursors. What are the distributions in igneous rocks? Igneous rocks are those that form from high-temperature melts.

5.1. *Volcanic lavas*

Perhaps the most obviously igneous of all rocks are the volcanic lavas. Lavas are produced when material of the lower crust and mantle, down to depths exceeding ~ 100 km, melts and the resulting liquids are extruded onto the surface. These lavas contribute substantially to the composition of Earth's crust. They also serve as probes to the chemical composition of the mantle. Source materials for lavas (or magmas, i.e., molten material in general, whether it reaches the surface or not) usually melt only partially, leaving behind a refractory residue. The compositions of source materials and residues cannot be measured directly but must be inferred from the nature of the lavas, from knowledge of overall elemental abundances, from experimental determinations of phase diagrams, and from seismic and other geophysical evidence. Lanthanide concentrations and distributions in lavas are important indicators of source materials and melting processes.

The most common types of lavas are basalts. Basalts are composed principally of pyroxenes (Mg, Fe, Ca metasilicates) and feldspar (Ca, Na, K aluminosilicates). The general class of basalts known as tholeiites has two types of pyroxene, one with substantial Ca and one poor in that element, any may contain some olivine (Mg, Fe orthosilicate). The other general class, known as alkali-olivine basalts, has only the Ca-rich pyroxene, plus olivine (Mg, Fe orthosilicate). A basalt belongs to one class or the other according to whether it has enough SiO_2 that its ideal equilibrium ("normative") mineralogy has orthosilicate (olivine) as the only Ca-poor, Fe and Mg-rich silicate phase, or whether there is also, or instead, a Ca-poor, Fe and Mg-rich metasilicate (pyroxene). This is not a trivial difference since only under special conditions of composition, temperature, and pressure can a source provide lavas of both classes, or can a magma of one class be converted into a liquid of the other.

Many major volcanoes of picturesque character yield basaltic lavas. The Hawaiian islands, very young geologically, are tall accumulations of successive

outpourings of lavas most of which were tholeiites. The major portions of basalts found on land, however, have not extruded from such majestic cinder cones but come from cracks and fissures in continental crust. Tholeiitic plateau or flood basalts cover the Columbia River province, the Deccan plateau of India, and the Paraná basin of South America, all fairly young geologically. Alkali-olivine basalts are quantitatively much less abundant; examples are those of the Basin-Range province of Nevada and Utah, or of the Rhine province in Germany. The greatest volumes of basalts are the surprisingly uniform tholeiites that pave the floors of the oceans and which are extruded at the ocean ridges. Many of the lavas that pile up to produce oceanic islands are alkali-olivine basalts (e.g., Gough island in the Atlantic Ocean).

In comparison with the average composition of the continental crust, basalts are rich in the constituents of "mafic" minerals (Mg, Fe-rich ortho and metasilicates) and range in concentration from ~45 to ~52% SiO₂. A common type of lava that approaches basalt in composition but is closer to average continental crustal composition is andesite. Andesites average ~60% SiO₂ in composition. They are the most common lava of the island arcs that surround ocean basins (e.g., the Aleutians) but may occur in continental areas (e.g., the Cascades of Washington and Oregon). Their appearance is commonly associated with subducting oceanic floor.

Rhyolite is an example of even more siliceous (as much as 70% SiO₂), or acidic, volcanic material. Rhyolite is a product of rather extreme chemical fractionation relative to the average composition of Earth. It is a common material, but hardly abundant in comparison with basalt, or even andesite. Rhyolitic lavas mainly appear in regions where less extreme types of lavas predominate. Such silica- and alkali-rich materials as rhyolites melt at lower temperatures than basalts or andesites and produce viscous liquids. On cooling, many fail to crystallize, but produce obsidian glass. Some are so forcibly ejected that they erupt as shards of glass, producing widespread falls of volcanic ash and pumice.

There are no sharp boundaries separating various lava types from each other except those of definition. There is a more or less continuous gradation from one type to another over a range of silica concentrations extending from <45% to >70% SiO₂. Associated with the many varieties that result from different source compositions and conditions of origin is a plethora of names that usefully connote compositional and kinship relations only to experienced geologists. The three types described above are sufficient for this discussion of lanthanide distributions.

Lanthanide distributions in common lavas range from somewhat depleted to tremendously enriched in light lanthanides, relative to chondrites. Concentrations of heavier lanthanides are not as variable as those of light lanthanides. Positive, negative, or no Eu anomalies may be present. There is no systematic variation in lanthanide distributions with rock type as a whole, but there are somewhat systematic variations among volcanic rocks that are genetically related. It is convenient to consider two classes of lanthanide distributions for

volcanic rocks. One class is associated with ocean floor igneous rocks such as those found in mid-ocean ridge basalts and some island arc basalts and andesites. The magmas in this class have lanthanide distributions very similar to those of chondrites but are somewhat depleted in light lanthanides (La-Nd). The other class is typical of continental and ocean island volcanics and relates to magmas that are slightly to strongly enriched in the light lanthanides relative to chondrites.

5.2. Ocean floor igneous rocks

Ocean ridge basalts and associated igneous rocks were discovered to have distinct lanthanide abundances when dredge samples became available from the mid-Atlantic ridge (Frey and Haskin, 1964). They have been studied intensively ever since because of further oceanographic sampling and the Deep Sea Drilling Project (e.g., Kay et al., 1970; Philpotts et al., 1969; Schilling, 1975a; Hubbard, 1969; Frey et al., 1968, 1974). Typical lanthanide concentrations, relative to the averages for chondrites, are shown in fig. 21.5. Tholeiitic basalts with this distribution are remarkably common and widespread beneath the oceans.

Basalts, basaltic andesites, and andesites with this distribution are common in some island arcs (e.g., Jakeš and Gill, 1970; Ewart et al., 1973; Taylor et al., 1969). Their presence is believed to result from melting of subducted oceanic crust. By and large, the sediment layers which lie above the ocean floor tholeiites and are derived mainly from continental material are not subducted but piled up against continental margins in some manner that prevents their modifying significantly the trace element and isotopic abundances of oceanic crustal matter in the production of this class of island arc volcanics. Nor does ocean water severely modify the lanthanide distributions in volcanics that are extruded under

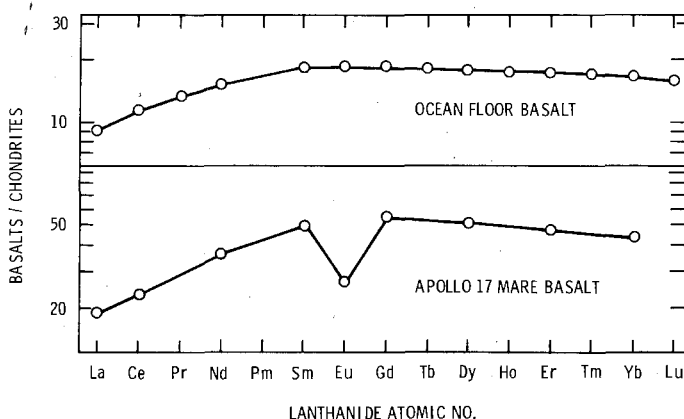


Fig. 21.5. Comparison diagram for typical ocean floor tholeiitic basalt (estimated from Frey et al., 1974) and average of 16 Apollo 17, high-titanium mare basalts (Shih et al., 1975).

water, either at the time of extrusion or on slow weathering (e.g., Herrmann et al., 1974; Philpotts et al., 1969; Frey et al., 1974).

The close similarity of the lanthanide distributions in ocean floor volcanics to that of the chondrites is further evidence that Earth has the same overall average relative lanthanide abundances as the chondrites. Otherwise, the uniformity of these melt products of the mantle found in all the oceans of the world would seem to be fortuitous. The distribution is not unmodified from that of the chondrites, and the lavas are not primitive or first-generation melting products of a primitive terrestrial mantle. Variations in lanthanide concentrations and relative abundances among ocean floor basalts are mainly the result of minor inhomogeneities in the mantle source regions, small differences in conditions of partial melting, and crystal fractionation of the lavas prior to eruption.

The light-lanthanide depleted distribution is so characteristic of ocean floor volcanics that its very rare appearance in materials of continental origin appears to be an accident of some complex combination of separation and mixing processes and events. Most occurrences of the light-lanthanide depleted distribution in materials found on continents is evidence that those materials actually derived from ocean floor or island arc volcanics, or at least, from the same type of mantle source.

Not all basalts or other igneous materials dredged or drilled from the ocean floors or found in island arcs have the characteristic light lanthanide depleted distribution (e.g., Frey et al., 1968; Nicholls and Islam, 1971; Kay et al., 1970; Jakeš and Gill, 1970; Balashov et al., 1970a; Jibiki and Masuda, 1974; Masuda et al., 1974; Schubert, 1972; Masuda and Jibiki, 1973; Schilling, 1971; Blanchard et al., 1976; Fleet et al., 1976; Bryan et al., 1976). Strong enrichments in light lanthanides are absent, except in some island arc volcanics, but mild enrichments are not uncommon. Qualitatively, all materials analyzed appear to be consistent with derivation from light-lanthanide depleted mantle sources.

5.3. *Lunar mare basalts*

It is interesting that those areas of the Moon dubbed lunar seas (maria) by the ancients have their floors paved with basalts. These basalts have lanthanide distributions (fig. 21.5) that range from slightly to strongly depleted in light lanthanides and somewhat depleted in heavy lanthanides (e.g., Shih et al., 1975; Philpotts et al., 1974). Their most striking feature is the substantial relative depletion in Eu. Anomalous concentrations of Eu are quite marked in lunar materials because the lunar regime was devoid of free oxygen ($\sim 10^{-13}$ atm compared with $\sim 10^{-6}$ atm for Earth's mantle). This caused most of the Eu in Moon to be in the 2+ oxidation state during differentiation of that planet.

Lanthanide concentrations are quite high in many lunar basalts in comparison with the range for terrestrial ocean floor basalts. This has been attributed to a general enrichment of Moon in refractory elements as compared with Earth. However, there is at present no requirement based on a mass balance for its

different segments that requires Moon to have higher average lanthanide concentrations than has Earth or, for that matter, the chondrites.

Our best understanding of why the terrestrial ocean floor basalts are relatively deficient in light lanthanides (and a number of other incompatible elements) is that these elements were in part separated away from the mantle in earlier geologic times (e.g., Gast, 1968; Philpotts and Schnetzler, 1970). Thus, the ocean floor materials were produced by further melting of an already partially depleted residue. Our best understanding of the origin of lunar mare basalts is that they, too, are products of remelting of material already partly depleted in light lanthanides during earlier formation of the lunar highlands (terrae) (e.g., Hubbard and Minear, 1975; Shih et al., 1975). Perhaps we do not give the ancients enough credit. Seas on Earth consist of water over sediments over basalts, all moving about, whereas seas on Moon are a vacuum over crushed basalt mixed with terra material over basalt. The mechanism for formation of terrestrial ocean basins is sea floor spreading whereas that for lunar mare basins is excavation by meteoroid impact. Nevertheless, the lanthanide distributions of the basalts in terrestrial and lunar seas are very roughly similar, and for roughly similar reasons. Both the terrestrial continents and the lunar highlands (e.g., Taylor, 1975) have average distributions that are relatively enriched in the lighter lanthanides.

5.4. *Ocean island volcanic rocks*

Basalts of oceanic islands have strikingly different lanthanide distributions from those of ocean floor basalts. Most are alkali-olivine basalts or olivine tholeiites with lanthanide distributions showing strong relative enrichment with decreasing atomic number. More acidic products of vulcanism are commonly found and show even stronger light lanthanide enrichments. Typical trends in distribution for related lavas from oceanic islands have been given for Gough and Reunion, islands (Zielinski and Frey, 1970; Zielinski, 1975), for Hawaiian basalts (Schilling and Winchester, 1969; Kay and Gast, 1973), for Cape Verdes and Fernando de Noronha (Kay and Gast, 1973), for Grenada, Lesser Antilles (Shimizu and Arculus, 1975), and for Ross Island (Sun and Hanson, 1975a). The observed trends (e.g., fig. 21.6) have been ascribed to results of fractional crystallization (e.g., Gough and Reunion islands) by varying extents of partial melting (e.g., Antilles) or by both (or either) (e.g., Hawaii). The source regions and partial melts, however, are not the same as those that produce the ocean floor suite of volcanics. This has been carefully demonstrated for the Azores (Schilling, 1975b) and for Iceland (e.g., Schilling, 1973; Schilling and Noe-Nygaard, 1974; O'Nions and Grönvold, 1973; Shimokawa and Masuda, 1972). Schilling (1975) showed that lanthanide distributions in the mid-Atlantic ridge changed progressively from the typical light-lanthanide depleted distribution of normal ridge basalts to light-lanthanide enriched patterns on approaching the Azores. Similar changes were observed along the Reykjanes ridge on approaching Iceland. The observed changes cannot be readily explained on the basis of a

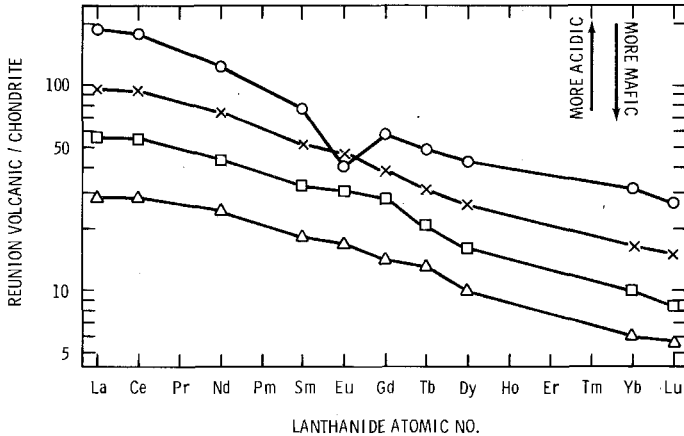


Fig. 21.6. Comparison diagram for volcanic rocks from Reunion island (Zielinski, 1975). The rock with lowest lanthanide concentrations is olivine-rich alkali basalt. Rocks with higher lanthanide concentrations are increasingly acidic in nature. The sequence is believed to be successive products of fractional crystallization.

single mantle source for both types of distribution but are consistent with mixing of lavas from the usual sources of ocean floor basalt with plumes or blobs of magma from deeper sources not depleted in incompatible elements. Similar arguments have been set forth by Sun and Hanson (1975b).

Masuda (1966, 1968) analyzed several basalts from Japan and found three groups, based on general petrographic characteristics and lanthanide distributions. Those groups, tholeiitic, high-alumina (also tholeiitic), and alkali basalts (fig. 21.7), were confirmed by Philpotts et al. (1971). The tholeiites are indistinguishable in lanthanide distributions from ocean floor basalts. The other basalt classes are enriched in light lanthanides, e.g., Fujimaka, 1975. Yajima et al. (1972) argued that the tholeiite type and high-alumina type basalts derived from separate magma sources. (Some of the "basalts" in both groups were actually andesites.) Tanaka and Sugisaki (1973) analyzed a series of basalts from a single Japanese geosyncline. The basalts were of the alkali class and those highest in stratigraphic sequence were the richest in lanthanides and the most strongly enriched in the light lanthanides, relative to chondrites. Nagasawa (1973) analyzed a series of basalts and more acidic lavas from the Oki islands, which lie between Japan and Korea. The lanthanide distributions were similar to those described earlier for Gough and Reunion islands.

The tholeiitic basalts of Japan that have light-lanthanide depleted distributions were collected on the eastern (Pacific Ocean) side. These islands, like the Caucasus geosyncline region discussed earlier (Ronov et al., 1974) show how lavas with ocean floor affinities and lavas with continental or oceanic island affinities both appear in island arcs. The basalts of the Crescent formation (northwestern Washington) are a good example of welding of materials partly of ocean floor affinity onto a continent (Glassley, 1974). The lower basalts of the

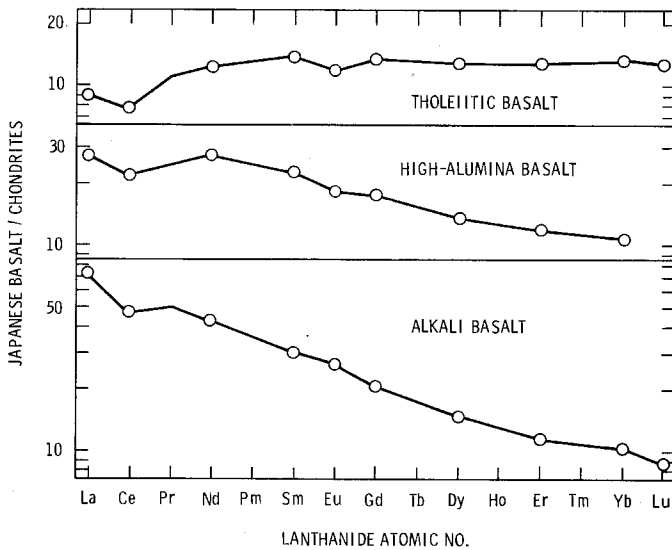


Fig. 21.7. Comparison diagram for lanthanide distributions in three classes of Japanese basalt (Masuda, 1968).

Crescent formation are tholeiites, with light lanthanide depleted distributions, and appear to be ocean floor basalts thrust against the western edge of the continent. The upper basalts are tholeiites also, but with lanthanide distributions mildly enriched in light lanthanides, similar to Hawaiian tholeiites or continental tholeiites and flood basalts.

Another occurrence of continental material that originated at least in part as oceanic crust is the Barberton Mountain terrain of southern Africa. Herrmann et al. (1976) found that basalts from the Komati formation had lanthanide distributions quite similar to those of ocean floor basalts, consistent with other types of evidence for an oceanic origin. Shih and Jahn (unpublished) found similar lanthanide distributions in other basalts from the same general region. The Barberton rocks are some 3.5 billion years old, far older than any present ocean floor material because of loss by subduction. That the source for these 3.5 billion year old lavas was already depleted in light lanthanides is consistent with the idea that loss of incompatible elements from the upper mantle occurred very early in Earth's history. Some of the lavas of the Komati formation contain far higher proportions of the constituents of olivine and pyroxene than do basalts. These lavas (peridotitic Komatiites) must represent very extensive (60–80%) melting of their source regions.

Metamorphosed volcanic rocks of great (Archean) age in northeastern Minnesota with light lanthanide depleted distributions were reported by Jahn et al. (1974) and by Arth and Hanson (1972). Jahn et al. suggested that those rocks were once part of an island arc volcanic system. Koljonen and Rosenberg (1974) noted the similarity in lanthanide distributions of several rocks of the Karelian

zone of Finland to those of ocean floor volcanics. Condie and Baragar (1974) found ocean floor type lanthanide distributions in the Archean Yellowknife greenstone belt of northwestern Canada.

Various rock suites found at the edges of continents or large islands and known as ophiolite complexes are considered by some geologists to be uplifted segments of ocean floor igneous strata. These suites include basalts plus igneous materials from beneath. Kay and Senechal (1972) show that the lanthanide distributions in the basalts from one such suite (Troodos, Cyprus) are those found in ocean floor volcanics. Menzies (1976) shows that associated materials, possibly residues of the production of such basalts, are even more depleted in light lanthanides. Montigny et al. (1973) found light lanthanide depleted distributions in several rocks from the Pindos (Greece) ophiolite suite and emphasized their oceanic origin.

5.5. *Vulcanism on the continents*

Lavas that are poured out onto the continents range from slightly to strongly enriched in light lanthanides, relative to the distribution in chondrites. The distributions in the basalts of the upper members of the Crescent volcanics of the Olympic peninsula (discussed above) are mildly enriched in the light lanthanides (Glassley, 1974). Whether these volcanics are properly considered part of an island arc, typical of oceanic island tholeiites, or typical continental tholeiites cannot be determined on the basis of lanthanide distribution. Volcanic rocks with small light lanthanide enrichments are found among suites of ocean floor volcanics and, in some cases, might come from essentially the same source regions, without contribution from deep mantle plumes. All volcanics of clearly terrigenous origin reported so far have light-lanthanide enriched distributions, approaching or exceeding the average for sediments of continental origin. It might be suspected that this results from contamination of lavas with typical continental crust during their ascent through it. Although a case for such contamination can be made in a few instances, it cannot account for this general trend, which is also observed in oceanic islands, which have no continental crust and which require a separate mantle source as discussed previously. It therefore seems probable that the sources of ocean floor volcanics simply do not contribute to terrigenous vulcanism or oceanic islands. Nevertheless, the occurrence of vulcanism on continents is associated with collisions of crustal plates and subduction. Along the coast of Western North America, subduction of oceanic plates is believed to be responsible for at least part of the vulcanism within the confines of the North American landmass. The greatest volumes of such volcanics are the flows of the Columbia river plateau. Some lanthanide distributions of mafic volcanics show fairly strong enrichment in light lanthanides (Osawa and Goles, 1970; Ragland et al., 1971; Brannon, Haskin, and McBirney, unpublished) (fig. 21.8). These are compared with the distribution in a composite of 282 basalts from all over the world but mostly from the United States (Haskin

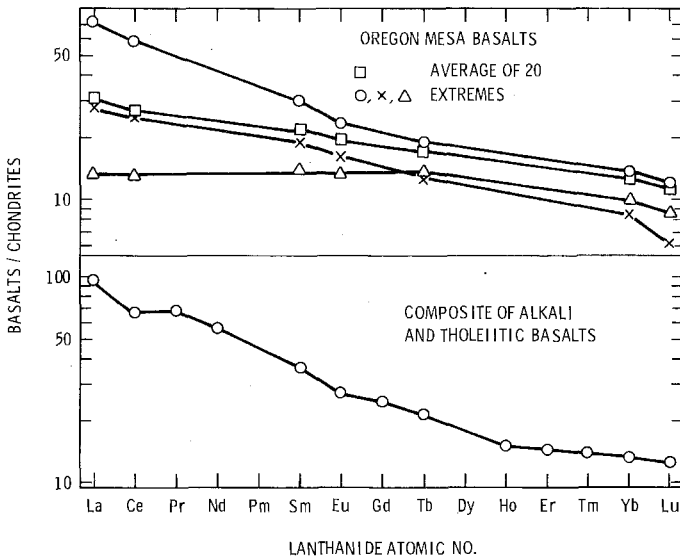


Fig. 21.8. Comparison diagram for continental basalts; average and extremes for 20 Oregon basalts (Brannon, Haskin, and McBirney, unpublished) and a composite of 282 mainly continental basalts (Haskin et al., 1968).

et al., 1968), which is very similar to that of the NASC except for the absence of a Eu anomaly.

Interpreting the lanthanide distributions (and other information) in volcanics from even a single volcano can illustrate the complexity of processes operating at a continental boundary. Condie and Hayslip (1975) have studied lanthanides in the younger lavas of the Medicine Lake, California shield volcano. This volcano first formed as much as half a million years ago and produced abundant basaltic andesite and andesite lavas, the youngest of which are at least 10 thousand years old. Then relatively small amounts of more acidic (siliceous) lavas were produced.

The lanthanide distributions (fig. 21.9) are reminiscent of those found on oceanic islands. However, Condie and Hayslip conclude that no simple model for progressive fractional crystallization or melting can account for the observed compositions. Different extents of partial melting of a common source, followed by fractional crystallization and perhaps mixing of magmas seemed to be required. Data on Pb and Sr isotopes permit no more than a few percent contamination of the basaltic or andesitic lavas with sediments or continental rocks. More siliceous (rhyolitic) lavas could well have derived by partial melting of continental material. Lavas of intermediate compositions were taken to be mixtures. It is not trivial to relate this complex set of processes to plate tectonics beyond noting that a subducting oceanic plate can serve as a heat source and a reservoir for some trace elements and isotopes.

Condie and Swenson (1973) found substantial light lanthanide enrichment in

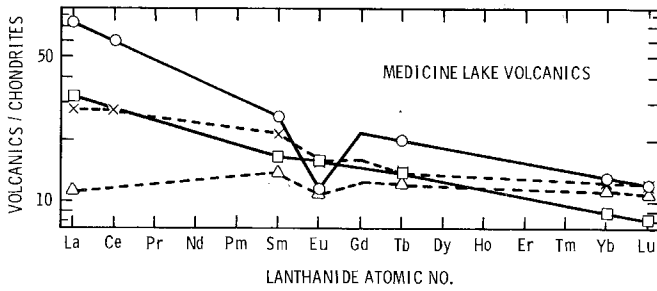


Fig. 21.9. Comparison diagram for lavas from a single (Medicine Lake, California) shield volcano (Condie and Hayslip, 1975).

andesites and more siliceous volcanic suites from Cascade range stratovolcanos of Washington and Oregon. Other siliceous lavas from the Cascades show variable, but light-lanthanide enriched distributions (Borchardt et al., 1971; Randle et al., 1971). Obsidian glasses are of particular archaeological interest because spear points and many other tools were made from them and their trace element compositions turn out to be specific to a given volcanic source (e.g., Griffin et al., 1969). Lanthanides are particularly useful “fingerprints” (Brown, Haskin, and Cook, unpublished).

Herrmann and co-workers (Herrmann, 1968; Herrmann and Wedepohl, 1970; Herrmann and Jung, 1970; Herrmann et al., 1974) have studied a wide variety of central European basalts and other volcanic rocks. All show light lanthanide enriched distributions. This includes basalts from Tholey in the Saar region, from which the term tholeiite is derived. Herrmann regards a shallow enrichment in light lanthanides as typical for continental tholeiites. This appears to be the case for most continental tholeiites (e.g., Columbia river plateau, Osawa and Goles, 1970, Brannon, Haskin, and McBirney, unpublished; Siberian platform, Balashov and Nesterenko, 1966; Deccan plateau, Nakamura and Masuda, 1971) but there is substantial overlap between strongly light-lanthanide enriched tholeiites and many alkali olivine basalts.

Kay and Gast (1973) reported analyses for strongly differentiated volcanics of the alkali basalt class from Arizona and Wyoming, several of which show extreme enrichment in light lanthanides (fig. 21.10). Capaldi et al. (1972) give data for a suite of siliceous volcanic rocks of alkali basalt kinship from Ischia, Italy that are very similar to those found on oceanic islands. Price and Taylor (1973) found strongly differentiated lanthanide distributions in alkali basalt related volcanics in New Zealand. Gerasimovskiy et al. (1972) analyzed many samples of highly-differentiated, alkalic lavas from volcanoes of the east African rift zone. Many of the lavas showed very strong enrichment in the light lanthanides, as well as relatively high concentrations of all the lanthanides (fig. 21.10).

The cause of very strong relative enrichment in light lanthanides for volcanic liquids, as will be discussed later, is often ascribed to the presence of the mineral garnet in the source region. Garnet has a high affinity for heavy lanthanides but a

low affinity for light lanthanides. In some cases of very high lanthanide concentrations and very strong light-lanthanide enrichment, some of the fractionation may result from selective gas phase transport. The class of carbonate rocks of igneous origin known as carbonatites is highly enriched in lanthanides and especially in light lanthanides (e.g., Eby, 1975; Loubet et al., 1972) (fig. 21.10). As pointed out by Loubet et al., there is no discontinuity in trend of lanthanide distributions in going from strongly fractionated alkali basalts to carbonatites. Another type of rock strongly enriched in lanthanides and fractionated in favor of light lanthanides is kimberlite (fig. 21.10). Lanthanide distributions in kimberlites have been reviewed and discussed by Paul et al. (1975). New data have been supplied by Fesq et al. (1975) and by Mitchell and Brunfelt (1975). Those authors show how liquid-crystal equilibria may be important in such strong fractionation of the lanthanides.

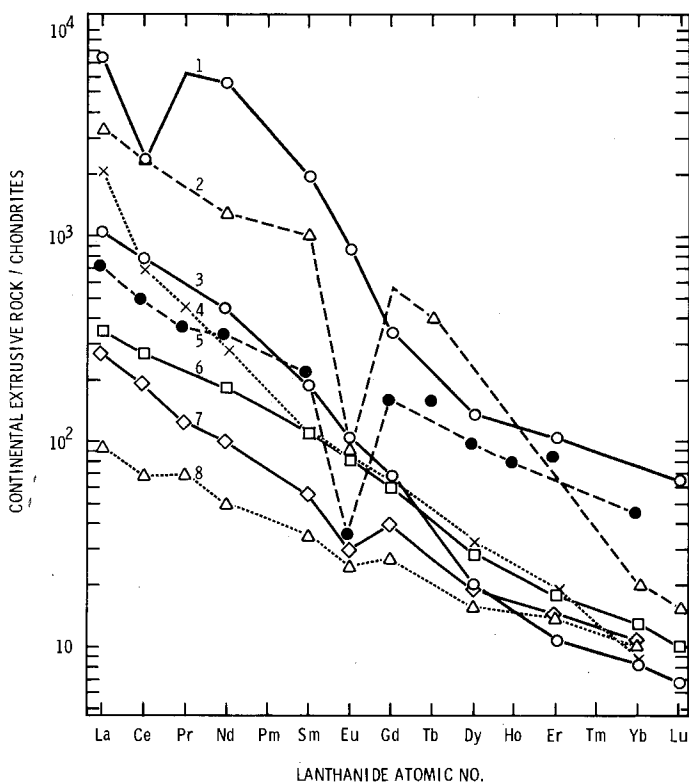


Fig. 21.10. Comparison diagram for highly differentiated, continental, alkali-rich rocks. No. 1 is a Norwegian carbonatite (Loubet et al., 1972), 2 an African kimberlite (Fesq et al., 1975), 3 and 6 alkali-rich American basalts (Kay and Gast, 1973), 4 an alkali carbonate, and 5, 6, and 8 alkali-rich lavas from Africa (Gerasimovskiy et al., 1972). These examples were chosen for their extremely differentiated lanthanide distributions and are richer in lanthanides than more average materials of their rock classes.

Kimberlites and carbonatites rise to the crustal surface from great depths, often with unusually explosive violence. It has been suggested that alkali basalts come from depths intermediate to those of kimberlites and continental or island tholeiites. Thus, there appears to be a trend of increasing light lanthanide enrichment of lavas with increasing depth of source. This apparent trend cannot yet be interpreted in terms of mantle composition in any general way. The relative importance of hypothesized gas extraction of lanthanides and crystal-liquid equilibria for producing severely fractionated lanthanide distributions is unknown.

5.6. *Lunar highland volcanics; KREEP*

Unlike Earth's lithosphere, Moon's lithosphere does not consist of plates that move about. Moon being a relatively small planet, it has cooled more rapidly than Earth so that its present lithosphere is equal in thickness to at least half the lunar radius. The lunar lithosphere thickened before the planets had swept up most of the interplanetary debris. Thus, the principal morphological features of the lunar highlands are impact craters. The last great impacts formed the basins of the lunar seas, which flooded with basalts. As a consequence of the heavy bombardment, all rocks collected from the lunar highlands are breccias, i.e., rocks constructed of fragments of previous rocks (which may be breccias of similar origin also). Many of these are confused mixtures of very small fragments from numerous precursors. Many have been partly converted to glass, or melted and recrystallized. The original igneous characteristics of most highland rocks have been obliterated by meteoroid impacts to the extent that the rocks cannot be classified petrographically by igneous type. Thus, there are no clear-cut examples of highland volcanic rocks equivalent to the well-preserved mare basalts. (The mare basalts formed late and were not as badly disturbed by impacts.)

The chemical compositions of some glasses and fragments indicate that those materials are strongly fractionated with respect to average lunar crustal matter. Such materials are probably partial melts or residues of extreme extents of fractional crystallization and, thus, volcanics. One of the most interesting is the material dubbed "KREEP" (e.g., Hubbard and Gast, 1971). KREEP was first found as fragments of glass in the soils from Apollo 12 (Oceanus Procellarum) and its name was coined in reference to its high concentrations of potassium, rare earths, and phosphorus. KREEP is a material of lunar highland, not mare, origin and has been found at all sampled Apollo and Luna sites. Lanthanides are abundant in KREEP. Their distribution is shown in fig. 21.11; compared to the chondritic distribution, KREEP is enriched in light lanthanides and strongly depleted in Eu. A few small samples of KREEP with igneous petrographic texture have been found, but that texture may result from impact remelting of KREEP breccia.

Hubbard et al. (1973) also present a case for a "very high alumina" lunar basalt. Blanchard et al. (1975a) identify a highland "pigeonite basalt." Blanchard

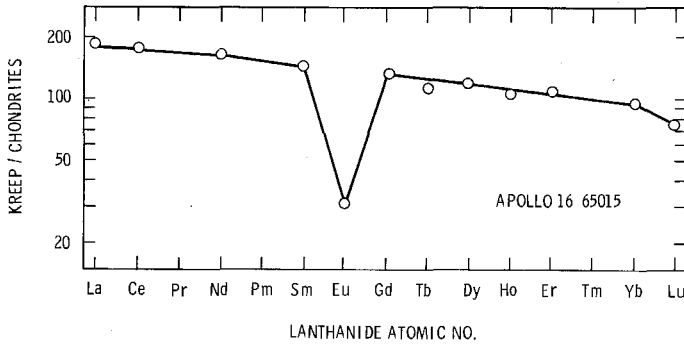


Fig. 21.11. Comparison diagram for KREEP-rich lunar rock 65015 (the "viper").

et al. (1975b) also argue that, although breccia formation may have obliterated the petrologic characteristics of most highland rocks, numerous small fragments have retained the chemical characteristics of their precursors. Undoubtedly other varieties will be identified.

The general shape of the KREEP lanthanide distribution is found in nearly all highland soils and many highland rocks of the Apollo collection. It is hard to reconcile that distribution as representative of the entire highland crust (e.g., Taylor, 1975). The region around Oceanus Procellarum has been surveyed by an orbiting gamma-ray spectrometer and shown to be rich in Th and U, elements associated with the lanthanides in KREEP. It is easiest to imagine that the distribution is that of volcanic products at the highland surface (e.g., Haskin et al., 1973).

5.7. Continental igneous-metamorphic complex

What, again, is the source of the lanthanide distribution found in sediments such as the shales (NASC) described earlier? That distribution does not come from rocks of the ocean floor volcanic suite, which are essentially its complement in relative lanthanide abundances, as compared with the chondritic distribution. It must come ultimately from continental igneous rocks separated early from the mantle and leaving behind the present source regions for the ocean floor volcanics. Just how long ago the stuff of the continents separated is difficult to determine, but both continental shields and ocean floor volcanics existed at least 3.5 billion years ago. A better approach might be to consider the rate at which new material from the mantle over geologic time may have contributed to the growth of the continents. In any event, the lanthanide distributions of common sediments, taken to average the distributions of their igneous continental precursors, have not evolved noticeably for 3.5 billion years, except perhaps for their Eu contents. How are lanthanides distributed in the materials that constitute the continents?

The average composition of continental material is often referred to as granitic

or as intermediate. The term "granitic" as used in this sense is a catchall for rocks with relatively high concentrations of SiO_2 , K_2O , and Na_2O , and relatively low concentrations of MgO and FeO , compared with basalts. True granites consist of feldspar (mostly K_2O -rich varieties), quartz (crystalline SiO_2), and subordinate amounts of a dark silicate mineral such as biotite mica. Granite-related rocks have lower densities than basalts or mantle residues; thus, continental materials float on top of the mantle and are not tectonically subducted in significant quantities. The granitic continental shields have remained stable for at least 3.5 billion years and probably for 4 billion years or more.

Granite itself is too siliceous to be representative in composition of the average continental crust. A mixture of half granite and half basalt is sometimes used to approximate the composition. There are rocks of intermediate acidity (e.g., diorites, andesites) whose compositions approach the average of continental crust, but they are not overwhelmingly abundant. The crust is a complicated mixture of many rock types, mostly metamorphosed substantially from their original igneous or sedimentary textures.

Three composite samples of granite-related rocks were analyzed for lanthanides by Haskin et al. (1968). The results, for 85 intermediate rocks (<60% SiO_2), 191 medium acidity "granites" (60–70% SiO_2), and 221 more acidic "granites" (>70% SiO_2), are shown in fig. 21.12. The lanthanide distributions for these rocks, as averaged by the composites, are very similar to the sediment distribution (NASC). There is a systematic, increasing relative depletion in Eu, as small increase in extent of light lanthanide enrichment, and an increase in heavy lanthanide concentrations with increasing SiO_2 contents. The composite of mainly continental basalts discussed earlier (fig. 21.8) more or less extends these trends except, like the intermediate rocks, has a noticeable negative Eu anomaly. Thus, the lanthanide distribution in the NASC can be understood, as presumed, as an average for its igneous precursors.

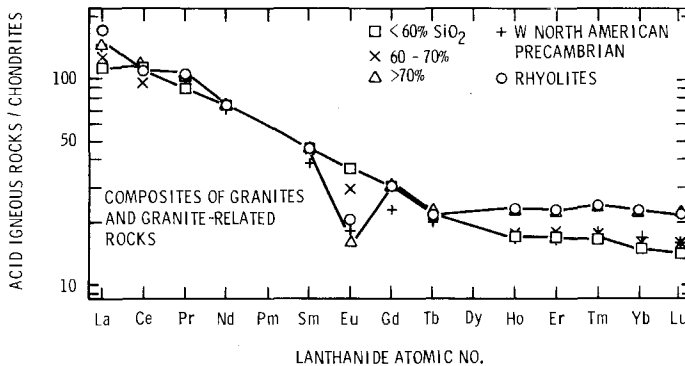


Fig. 21.12. Comparison diagram for composites of granite-related rocks. Three composites were constructed according to SiO_2 concentrations, one according to age and locality (western North American Precambrian), and one is of volcanic (rhyolites) rather than intrusive rocks.

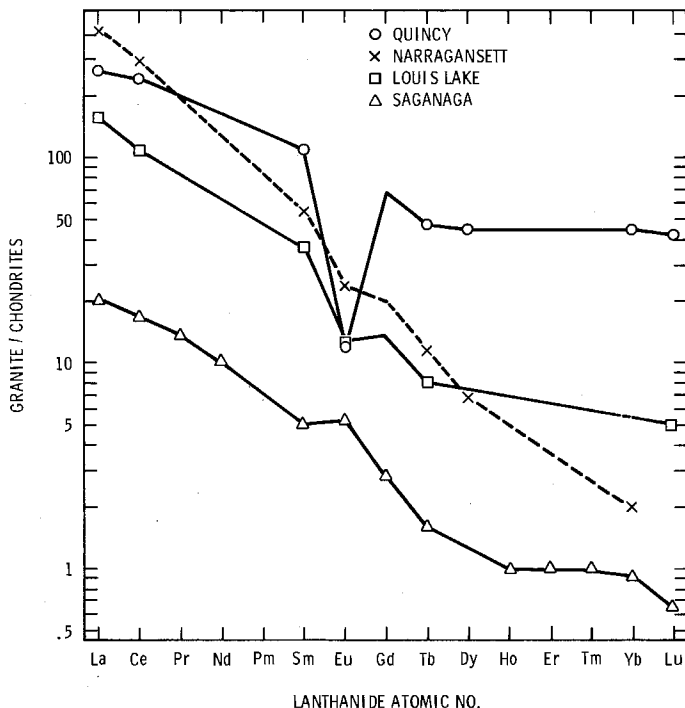


Fig. 21.13. Comparison diagrams for individual granites; Quincy and Narragansett (Buma et al., 1971), Louis Lake (Condie and Lo, 1971), and Saganaga (granite-related, Haskin et al., 1968).

Lanthanide distributions in individual specimens of granite-like rocks can vary markedly from the NASC distribution. Several examples are shown in fig. 21.13. Others are discussed in the reviews of Haskin et al. (1966a), and Herrmann (1968). Most, individual granites are relatively enriched in light lanthanides relative to chondrites, some not as much as the NASC, some more. Many show systematic enrichment with decreasing lanthanide atomic number extending from the heaviest lanthanides to La.

In some locations, series of rocks grading in composition from basaltic to granitic, with members possibly related genetically to a common parent are found. Such a case is the southern California batholith (Towell et al., 1965), for which a systematic trend of increasing lanthanide concentrations, increasing light-lanthanide enrichment, and increasing relative depletion in Eu were observed with increasing rock acidity (SiO_2 contents). This parallels the trends found for the composite samples discussed above.

Within large bodies of granitic materials systematic variations in lanthanide distribution are observed. Buma et al. (1971) found that subalkaline granites (approximately equal amounts of K_2O -rich and K_2O -poor feldspar) from Rhode Island had lanthanide distributions similar to those of the NASC, but had higher lanthanide concentrations, strong Eu depletions, and were less relatively

enriched in light lanthanides. Granites from Massachusetts with higher proportions of K_2O -rich feldspar were strongly enriched in lanthanides with decreasing atomic number from Yb to La and had very small Eu anomalies. Koljonen and Rosenberg (1974) show a variety of similar distributions for siliceous rocks from Finland. Taylor et al. (1968) found granites from the Snowy Mountains of Australia with somewhat less light-lanthanide enriched distributions than the NASC.

Granite magmas are often rich in volatile compounds (e.g., water, halides, carbonates, alkalis) that tend to accumulate as residual fluids as these magmas solidify. Some granites show steep increases in heaviest lanthanide abundances as a result of interactions with hydrothermal fluids, either associated with their formation or as a result of later interactions (e.g., Kazakhstan massif, Mineyev, 1963; Nigeria, Alekseyev, 1970 and Bowden and Whitley, 1974).

Systematic variations of lanthanide distribution with granitic rock type (based on mineralogy and bulk composition) are sometimes observed within rocks from a single granitic body or among granitic bodies from a given region and possibly related genetically to each other. Balashov et al. (1969) discussed general trends of increase in lanthanide concentration and relative light lanthanide enrichment with increasing magma alkalinity. Nagasawa and Schnetzler (1971) point out that sometimes the final products of fractional crystallization of magmas have lower lanthanide concentrations and less light lanthanide enrichment than intermediate products of magma differentiation. Condie and Lo (1971) found such trends in a differentiated granitic body in Wyoming (Louis Lake batholith). Anderson and Cullers (1976) show that two granite bodies (plutons) in the Wolf River, Wisconsin batholith are probably related to each other as product and residues of fractional crystallization processes. The residues are more SiO_2 rich, have higher lanthanide concentrations, and are relatively more depleted in Eu than the starting material. The most strongly differentiated residual material, however, shows a decrease in La and Ce compared with intermediate residues, all consistent with the general trends discussed above. Rocks regarded as early crystallized products of the fractionation had lanthanide distributions complementary to those of the residues.

While it is clear that granite-like rocks or mixtures of granite-like rocks and basalts can account for the lanthanide distribution of the NASC, the origin of continental material is still obscure. Some granites seem clearly to be products of extreme metamorphism of previously existing sediments. Others seem to be products of partial melting of material deep within the crust, or even the upper mantle, possibly of older volcanics. If volcanic, onto what sort of crust did the precursors to the granites extrude?

5.8. *Anorthosite and early crust formation*

The nature of the first solid materials to form at Earth's surface either as crust or precursor to crust is not known. The oldest rocks for which convincing ages

have been measured are not older than 4.0 billion years. From studies of lunar rocks we know that a crust formed on the Moon very soon after the birth of the solar system 4.5–4.6 billion years ago. The lunar crust appears to have formed after melting of at least the outer few hundred km of the Moon (approximately half or more of the entire mass of the moon). This crust was severely battered by infalling meteoroids, presumably the materials from which the Earth and Moon accreted. The severest part of the bombardment had ended before the mare basalts of the seas of Tranquillity and Serenity were extruded some 3.9 billion years ago. Presumably, Earth was subjected to a similar bombardment. That, plus erosion and tectonic movements, have surely obliterated Earth's earliest crust, taking the determination of its nature beyond the possibility of direct observation.

The nature of the lunar crust is imperfectly known. It is on a firm basis inasmuch as it was derived mainly from studies of samples. The samples, however, were collected from eight locations in a region on the lunar frontside that is not characteristic of the lunar highlands. An important characteristic of the lunar crust is its enrichment, relative to the remainder of the moon, in the constituents of Ca-rich feldspar ($\text{CaAl}_2\text{Si}_2\text{O}_8$). Presumably, feldspar-rich materials crystallized from the molten lunar exterior along with more mafic (Fe, Mg rich) minerals and collected selectively at the lunar surface. Samples of nearly pure feldspar rock, called anorthosite, were included with the lunar samples. Lanthanide distributions (fig. 21.14) in these rocks reflect the strong affinity of feldspar for Eu(II) and the relative preference for lighter members of the lanthanide series.

Anorthosites are found on the terrestrial continents, but only in relatively old (Precambrian) terranes. Unlike the other rocks discussed, anorthosites are not still being produced today. Might their appearance in terrestrial Precambrian terrains indicate that crust forming processes analogous to those on Moon occurred also on Earth?

Terrestrial anorthosites do indeed show the lanthanide distribution typical of feldspars (e.g., Philpotts et al., 1966; Green et al., 1969, 1972; O'Nions and Pankhurst, 1974; Duchesne et al., 1974) (fig. 21.14). The processes by which massive anorthosites form on Earth are unclear. Massive anorthosites tend to be associated with rocks of intermediate to acidic character, to which they may be genetically related. Pure feldspars from anorthosites reflect the lanthanide preferences of that mineral even more strongly than the anorthosites themselves, which contain small amounts of Fe, Mg-rich minerals (e.g., Griffin et al., 1974; Henderson et al., 1976). Although feldspar tends to concentrate lighter lanthanides relative to heavier ones, it does not concentrate any lanthanide except Eu relative to its starting material. Thus, concentration of feldspar at Earth's surface cannot explain the presence of the lanthanide distribution of continental material. Nevertheless, early crystallization of feldspar and its concentration at the lunar and terrestrial surfaces is indicative of the kinds of mechanisms by which certain lanthanides can be selectively concentrated in planetary crusts.

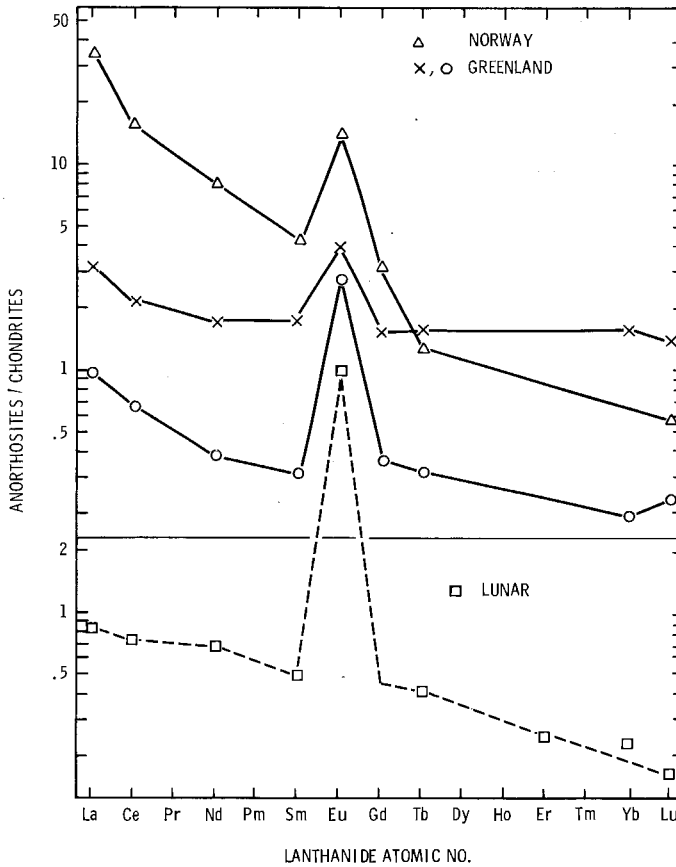


Fig. 21.14. Comparison diagram for terrestrial and lunar anorthosites (nearly pure feldspar rocks); Norwegian specimen (Green et al., 1972), Greenland samples (Henderson et al., 1976), and lunar rock 60025 (Haskin et al., 1973).

6. Lanthanides in Earth's interior

The higher lanthanide concentrations and the light-lanthanide enrichment of average continental material relative to chondrites has been attributed to extraction of these elements from the mantle. A residue is left behind, whose average lanthanide distribution must complement that of the continental crust, assuming that the overall relative lanthanide abundances for the Earth are the same as those in the chondrites. The ocean floor igneous suite appears to be derived from that residue. Are there rocks that can plausibly be considered samples of that residue, and which have distributions deficient in light lanthanides relative to the chondrites? Are there rocks that represent primitive terrestrial mantle from which the lanthanides and other incompatible elements have not yet been extracted?

Partial melting has been mentioned as a process by which materials are extracted from Earth's mantle to produce liquids that rise to the surface. Earth's mantle is large (~67% of Earth's mass) and deep (between ~5 and 2900 km). It is not known whether it was ever entirely molten or just how its formation relates to that of Earth's core. Its original lanthanide concentrations are not known nor is the extent to which it may have purged itself of incompatible elements.

Constraints on the bulk composition of the mantle are mainly density, solar elemental abundances, and compatibility with compositions of lavas derived from the mantle and extruded onto the surface. Lavas come from the upper few hundred km only. Phase changes because of increasing temperature and pressure with depth strongly affect the mineralogy of the mantle.

Experimental petrologists have determined the most likely suites of stable major minerals in source regions of lavas (e.g., Green and Ringwood, 1963). The principal minerals are olivine (Fe, Mg orthosilicate), low-Ca pyroxene (mainly Fe, Mg metasilicate), high-Ca pyroxene (mainly Ca, Mg metasilicate), garnet (Mg, Fe aluminosilicates), spinel (mainly Mg aluminosilicate), plagioclase feldspar (Ca, Na aluminosilicate), and amphibole (complex hydroaluminosilicates); additional minor phases can be present. As the temperature of assemblages of some of these minerals is raised, combinations of minerals begin to melt, according to the phase diagram for that system. As melting proceeds, some minerals of the combination are entirely liquefied, leaving behind residues of much simpler mineralogy. For example, the residue may be nearly pure olivine or low-Ca pyroxene, or a mixture, perhaps with some garnet, or high Ca-pyroxene, or plagioclase, depending on conditions of temperature and pressure, but usually with only 1-3 major minerals, most minor minerals having melted early.

6.1. Possible large fragments of mantle

Rocks consisting of the minerals discussed above, in combinations expected for mantle sources or residues, are found at Earth's surface. These rocks have high densities, high Mg and low silica concentrations, are rich in dark colored olivines and pyroxenes, and are referred to as ultramafic. Frey et al. (1971) and Philpotts et al. (1972) analyzed a variety of such rocks for lanthanides to determine whether their distributions would be like those in chondrites or deficient in light lanthanides relative to chondrites. Such a deficiency would be consistent with origin of those rocks in the mantle as well as with the complementarity of distributions for crust and mantle as described above. Very few of the ultramafic rocks analyzed had those characteristics; some typical distributions are shown in figs. 21.15-17.

The class of ultramafic rocks known as high-temperature alpine peridotites (fig. 21.15) does show the characteristics expected for mantle residues, for major elements as well as for lanthanides. Alpine peridotites occur in mountain-forming regions under conditions such that, in some cases, they could represent pieces of upper mantle that was wrinkled and thrust into the crust. Examples

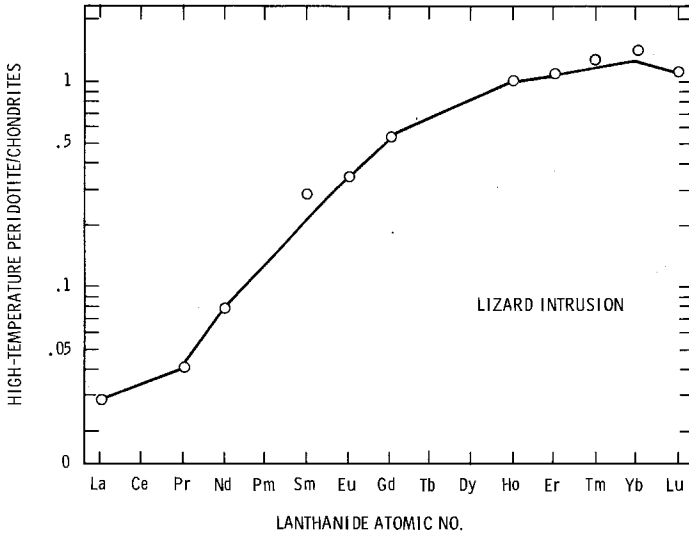


Fig. 21.15. Comparison diagram for a high-temperature, alpine-type peridotite, Lizard intrusion, Cornwall, England (Frey, 1969).

similar to those shown in fig. 21.15 have been given by Frey et al. (1971); Philpotts et al. (1972); Alekseyev and Zhelyazkova-Panayotova (1972); and Garmann et al. (1975). The most extensive study of a high-temperature, alpine-type ultramafic suite was that of the Lizard peridotite intrusion of Cornwall, England (Frey, 1969). The Lizard peridotite consists mainly of magnesian olivine and low-Ca pyroxene, plus some high-Ca pyroxene and spinel. Frey concluded that the peridotite had once been in equilibrium with a basaltic liquid and was therefore either a residue of partial melting or, possibly, an accumulation of mafic minerals precipitated from such a liquid at depth. He also showed that, assuming NASC sediment average concentrations for Earth's crust, and chondritic concentrations for the bulk Earth, only a quarter of Earth's mantle would need to be depleted in light lanthanides to the same extent as the Lizard peridotite to account for the lanthanide concentrations of the crust. He found that the mantle parent of the peridotite, in order to undergo a reasonable fraction of melting (~30%) to yield a liquid with lanthanide concentrations typical of those in basalts, would need to have lanthanide concentrations some 4 times the chondrite average, consistent with conclusions from studies of basalts (e.g., Gast, 1968; Frey et al., 1968). Frey also analyzed metamorphosed basaltic materials possibly derived from the Lizard peridotite. Their lanthanide distributions are those of ocean floor volcanics. Medaris, Cullers, and Helmke (unpublished) found light-lanthanide depleted distributions in alpine-type peridotites that are clearly portions of ophiolite suites, i.e., segments of ocean floor igneous strata incorporated into continents. This implies that alpine peridotites may be mantle residues from sources of ocean floor volcanics.

St. Paul's rocks near the axis of the mid-Atlantic ridge are another example of

ultramafic rocks (peridotites) that might have been uplifted from the suboceanic crust. They are not regarded as portions of ophiolite suites, however. Several were analyzed by Frey (1970) and by Frey et al. (1971); with one exception, their lanthanide distributions are considerably enriched in light lanthanides relative to chondrites or to typical ocean floor igneous materials (fig. 21.16). Frey (1970) noted the similarity in lanthanide distribution of St. Paul's rocks to those of island-type alkali basalt dredged from the same region (consistent with the rather general occurrence of oceanic rocks that are anomalous with respect to the typical ocean floor igneous suite). Contamination by continental crustal materials could be ruled out. The light lanthanide enrichment appears to be a primary characteristic of St. Paul's peridotite. Frey offered several explanations for the origin of the peridotite; the simplest was crystal accumulation at depth within the mantle from a liquid of basaltic composition. He emphasized the uncertainty of this explanation, as well as the evident complexity of processes and compositional heterogeneity within the mantle.

Ultramafic rocks are known to accumulate at relatively shallow depths in some instances when liquids of basaltic composition intrude into the crust or upper mantle, are trapped there, and solidify or partially solidify before further crustal movement allows the residual liquid to escape to the surface. Subsequent erosion and crustal uplift expose these solidified intrusions at the surface. Depending on composition and conditions of crystallization, the rocks near the bottom of such an intrusion may be mafic or ultramafic. An example of

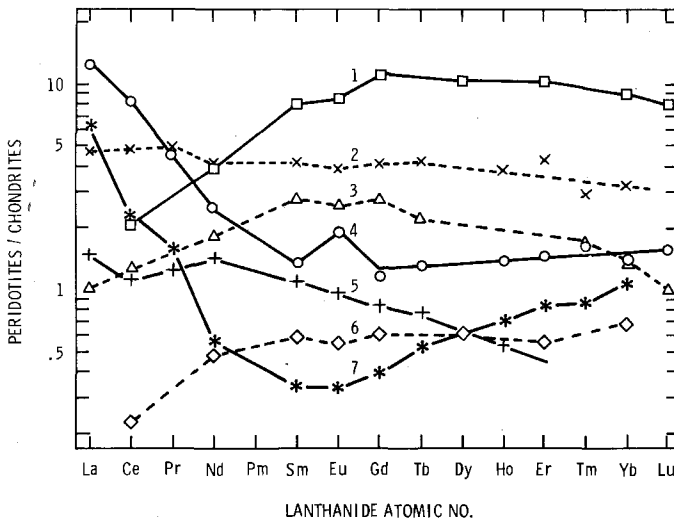


Fig. 21.16. Comparison diagram for peridotites; No. 1, inclusion in basalt, Kakanui, New Zealand, and No. 6, Webster peridotite body, North Carolina (Philpotts et al., 1972); 2, garnet-pyroxene rock and 5, spinel peridotite, portions of a single inclusion in basalt, (Reid and Frey, 1971); 3, peridotite from ultramafic layered intrusion, Preacher Creek, Wyoming (Potts and Condie, 1971); 4, St. Pauls rock (Frey, 1970); 7, inclusion in basalt, Dreiser Weiher, Eifel district, Germany (Frey et al., 1971).

lanthanide behavior in the Skaergaard intrusion, which produced mainly mafic rocks, will be discussed later. Potts and Condie (1971) analyzed several rocks of ultramafic composition from the Preacher Creek, Wyoming intrusion. The rocks consist mainly of olivine and high-Ca pyroxene. Their distributions showed increases in lanthanide abundances (fig. 21.16), relative to the chondritic distribution, from Lu to Sm or Eu, where a broad maximum occurred, followed by a decrease from Sm–Nd to La. Similar distributions have been observed for other intrusive rocks (compositionally similar to basalts) (e.g., Frey et al., 1968; Haskin et al., 1966a). Frey et al. (1971) reported lanthanide analyses from ultramafic rocks from other layered intrusions, the Stillwater, Bushveld, Muskox, and Matheson. The distributions ranged from approximately chondritic to light-lanthanide enriched; lanthanide concentrations ranged from ~ 0.3 to 2 times those of chondrites. These rocks cannot be considered primitive mantle sources of partial melts to produce basaltic liquids; they are clearly products of fractional crystallization of mafic liquids intruded near the Earth's surface.

The differences in lanthanide distributions between such ultramafic accumulates and their parent liquids emphasize the difficulties in inferring genetic relationships between some types of related materials just from lanthanide distributions alone. Frey et al. (1971) noted that monomineralic ultramafic rocks (e.g., nearly pure olivine or pyroxene) seemed to have more fractionated relative abundances than rocks with several minerals, for which mineral selectivities for certain lanthanides in many cases tend to balance each other. Garmann et al. (1975) reported lanthanide concentrations for three dunites (nearly pure olivine rocks); all three had distributions somewhat enriched in lighter lanthanides, similar to that from the Muskox intrusion (Frey et al., 1971).

6.2. *Ultramafic inclusions*

The most promising samples for providing information on mantle sources and residues are probably the nodules brought to the surface in basalts and kimberlites (fig. 21.16). Most nodules are peridotitic in composition. Mineral phases are those stable at the high pressure and temperature of the upper mantle; they survive when emplaced in the crust because solid-state phase transitions are so slow. The nodules are coated with frozen host matrix, but their hosts as liquids have not dissolved or reacted appreciably with their interiors. In one view they are considered to represent fragments of the mantle, either primitive source or residue, torn off during the vigorous intrusion of the host liquid and swept to the surface. In another view, they are clots of crystalline material that precipitated from the host liquid at great depth before the liquid rose. In either case they could have been contaminated with trace elements by host matrix; only a small amount of contamination by incompatible element-rich host matrix would be required to mask their intrinsic lanthanide distributions. Frey et al. (1971) reported a distribution for a garnet peridotite from New Zealand that was slightly depleted in light lanthanides, similar to some ocean floor volcanics, but with lanthanide concentrations only about twice those of chondrites. Similar

results were obtained by Flower (1971) for three peridotite nodules from alkali basalt from the Comores Archipelago, Indian Ocean. A peridotite nodule from alkali basalt in Germany had a V-shaped distribution (fig. 21.16) with a La concentration some 5 times and Sm less than 0.5 times the chondritic value. An Australian dunite (olivine) nodule showed light lanthanide enrichment very similar to that typical of crustal matter, but ranging in concentration from ~ 0.3 to 3 times the chondritic values; less than 2 percent contamination with host matrix would contribute the observed lanthanides. However, there was no direct evidence for contamination (Frey et al., 1971). Philpotts et al. (1972) analyzed peridotite nodules from basalt and kimberlite. Two nodules, from New Zealand (fig. 21.16), were even more depleted in light lanthanides than that reported by Frey et al. (1971). The rest were relatively enriched in light lanthanides, and ranged in lanthanide concentrations between ~ 0.1 and 10 times the chondritic values. The upper and lower limits were for the same specimen, which came from kimberlite of the Roberts Victor mine, South Africa. Herrmann and Wedepohl (1966) found low concentrations of light lanthanides (< 5 times those of chondrites) in peridotites from the Eifel district of Germany. Ridley and Dawson (1975) found light lanthanide enrichment in three African peridotites and mild lanthanide depletion in one. Nagasawa et al. (1969) found mild light lanthanide enrichment in two peridotite nodules, fairly strong enrichment in one, and a peak at Sm-Gd for another.

Shimizu (1975) and Varne and Graham (1971) analyzed garnets and Ca-rich pyroxenes from peridotite nodules but reported no whole-rock values. Mitchell and Carswell (1976) analyzed South African peridotite nodules and minerals for La, Sm, and Yb. All were enriched in light lanthanides relative to chondrites. The garnet and Ca-rich pyroxenes did not account well for the La and Yb in the whole rocks. Mitchell and Carswell attributed the differences to contamination by host kimberlite on the basis that the kimberlites are strongly enriched in light lanthanides.

Reid and Frey (1971) made an extensive study of peridotite nodules from basalts of Salt Lake Crater, Hawaii. All were relatively enriched in light lanthanides compared with chondrites, some showing a broad peak for light to medium lanthanides. Frey and Green (1974) extensively studied peridotite inclusions from alkali lavas of Western Victoria, Australia. Five nodules analyzed were relatively enriched in light lanthanides, with overall concentrations ranging from ~ 0.1 to 10 times those of chondrites. Two were slightly depleted in light lanthanides (concentrations 0.5–2 times chondrites) and one slightly enriched (0.3–1 time chondrites).

Clearly, there is no simple interpretation of ultramafic inclusions in lavas in terms of primitive lanthanide distributions or lanthanide distributions complementary to those found in the crust. Some peridotites do have nearly chondritic lanthanide distributions, some are strongly depleted in light lanthanides, but most nodules in lavas are enriched in light lanthanides relative to chondrites.

6.3. Eclogites

In search for mantle sources of basalt liquids or residues, eclogites, another type of material occurring as nodules, are important. Eclogites have major element compositions similar to those of basalts and, if melted and extruded, would solidify to produce a mineral assemblage that would be regarded as basaltic. At depth, that assemblage is unstable, and eclogites consist mainly of garnet and sodium and aluminum-rich, high-Ca pyroxene. The bulk properties of eclogites, like those of peridotites, are consistent with the bulk properties of the upper mantle. Whether there are extensive amounts of eclogite actually present in the upper mantle, or whether eclogite is important as a source for basalts is not known. Eclogite nodules are substantially more rare than peridotite nodules.

Most eclogites studied have lanthanide distributions that are fairly flat relative to those of chondrites (but not as smoothly so as those of ocean floor basalts) or are enriched somewhat in light lanthanides (fig. 21.17). Lanthanide concentrations are mostly in the range 5–20 times chondritic (e.g., Haskin et al., 1966a; Philpotts et al., 1972; Early, unpublished).

Eclogites are also found in strongly metamorphosed terranes and were presumably produced by the heat and pressure associated with the metamorphosing event. Garmann et al. (1975) analyzed ten such eclogites from western Norway. Lanthanide distributions were flat to significantly depleted in light lanthanides, relative to chondrites. Concentrations of heavy lanthanides varied over a range of ~5–~30 times those of chondrites and those of La varied more widely, 1–~30 times.

Several of the above authors and also White et al. (1972) analyzed garnet and pyroxene separated from eclogites and showed that the heavier lanthanides concentrate in garnet, the light lanthanides in pyroxene.

Eclogites have been regarded as recrystallized basalts, mantle sources of basalt, or precipitates from basalt liquids at depth. The lanthanide distributions

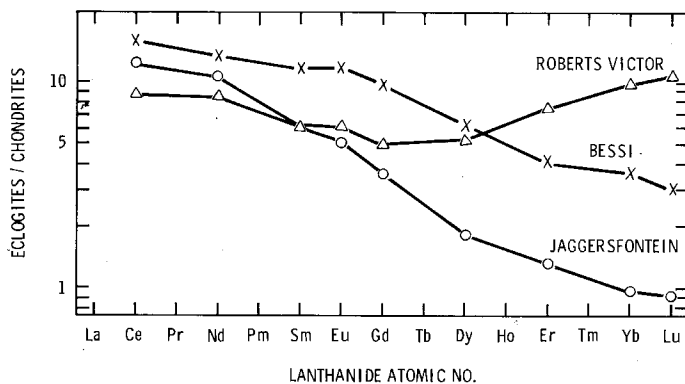


Fig. 21.17. Comparison diagrams for two African (Roberts Victor, Jagersfontein) and one Japanese (Bessi) eclogites (Philpotts et al., 1972).

observed in most eclogites do not match those found in most basalts, so a simple, closed system recrystallization at high pressure and temperature is an inadequate explanation. It is difficult to melt eclogite partially and leave one phase preferentially behind, because under mantle conditions the temperature interval between beginning and completion of melting is very small.

7. Toward a quantitative understanding

Those who have studied lanthanides in ultramafic rocks have interpreted their results in several ways. They have concluded, with varying displays of confidence, that nodules are primitive mantle matter suitable as source material for crustal rocks, or that nodules are precipitates from the host liquids that eventually bore them to the surface, or that nodules are mantle residues related (or not related) to their host lavas, or that certain massive peridotites are (or are not) sources (or residues) from the mantle and are (or are not) kin to associated mafic rocks. These various conclusions do not correlate in any straightforward way with different characteristics of the nodules and must be gracefully accepted as preliminary opinions in a rapidly advancing field of science. Some peridotites are clearly parts of layered intrusive bodies; those bodies, unlike the mantle sources of basalts, can be observed and sampled directly.

Similarly, those studying extrusive and intrusive liquids have struggled over relative importances of partial melting, total melting, and extents of fractional crystallization. Understanding how the lanthanides are distributed among the various segments of Earth's crust and mantle depends on our knowledge of how mantle and crustal materials form. As it is not possible to construct a planet in the laboratory, it is necessary to produce a fully self-consistent concept of the nature of Earth from circumstantial evidence that can be extracted from many kinds of observations. Lanthanide distributions are an important part of that evidence. Thus our knowledge of crustal and mantle materials and how they formed is equally dependent on our understanding of lanthanide behavior during rock-forming events.

So far a general picture has been presented here of the various major segments of Earth and the abundances of the lanthanides in the materials composing those segments, plus some indication of the possible processes relating the segments and their distributions. The ultimate value of lanthanide abundances as a tool for understanding the history of Earth or other planets depends on how quantitatively we can predict lanthanide behavior during different hypothesized processes. It depends on combining knowledge of lanthanide distributions with results from many other fields, e.g., studies of major and other trace elements, phase diagrams, geological field relationships, geophysical constraints, and textures and mineralogy of rocks. In this section, quantitative modelling of lanthanide behavior is discussed, and examples of particularly careful and useful recent work are described.

7.1. *Mathematical models*

During rock-forming or magma-forming processes in nature, with several major and minor minerals involved, what do the lanthanides do? In most systems they do not form their own minerals, but disperse themselves as trace constituents of phases in which they are not essential components.

Numerous attempts have been made by geochemists to account for the ways in which trace elements distribute themselves. It has not been possible to define the energies of different possible locations of trace elements so that their equilibrium distributions can be accurately predicted. There are primitive notions, e.g., that the lanthanides merely follow calcium, that are too crude to be of much use, although there is a grain of truth in them. The most useful rule is that lanthanides (and other trace cations) readily enter those sites in crystals normally occupied by more common cations of approximately equal ionic radius (e.g., Neumann et al., 1966). Effects on lanthanide behavior of balancing charge in the event that the cation substituted for was not 3+ seem to be second order for chemically complex natural systems as long as lanthanide concentrations are low (tens of ppm or less).

Morris (1975) synthesized several silicate and aluminate compounds some of which are end members of important naturally occurring solid solution minerals. The compounds were doped with Gd(III) or Eu(II). From electron paramagnetic resonance studies Morris showed that in Ca and Ca-Mg ortho- and metasilicates, both Gd(III) and Eu(II) entered mineral crystal sites normally occupied by Ca(II). Charge compensation was apparently remote from the lanthanide-occupied sites since it had no effect on the spectra. In triclinic anorthite (CaAl_2O_8), the end-member of the major natural feldspar group, Eu(II) entered the Ca(II) site but Gd(III) showed the disordered spectrum characteristic of a glass, either because the Gd(III) was small relative to the size of the site or because the 3+ ion so strained the site that its symmetry was disrupted. (The affinity of feldspars for Eu relative to other lanthanides has been mentioned previously.) Both Gd(III) and Eu(II) tended to form clusters of several ions in pure Mg ortho- and metasilicates, indicating that those ions did not substitute for Mg(II) in regular structural sites. (Nevertheless, the ferromagnesian ortho- and metasilicates in nature each show strong and characteristic selectivity favoring the heavy lanthanides.)

Common, rock-forming silicate minerals are regarded as excluding lanthanides from their structures. Cullers et al. (1970) indicate, however, that substantial concentrations (hundreds of ppm) of lanthanides can be readily incorporated into such minerals; apparently the minerals do not compete successfully against silicate liquids to obtain them.

The currently most useful approximations of trace element behavior for quantitative prediction are based on a simple Nernst distribution for equilibrium partitioning of a solute between two phases. This concept can be formalized to account for exchange between the trace element and the major ion it is deemed to replace, to account for effects of compensation of charge, etc. (e.g., McIntire,

1963). For purposes of this discussion (and for most practical purposes at the present level of sophistication of the field), a simple mass concentration ratio is adequate; i.e., a distribution coefficient, D , is defined as the ratio of the concentration of a trace element in ppm in a crystal to the concentration of that trace element in ppm in the liquid in equilibrium with that crystal. (A similar ratio between two solid phases is sometimes also useful.)

The limitations on this approach (e.g., Cullers et al., 1970) are that the trace ion in question be so dilute in the system that no possible means of distributing it among the phases will affect the thermodynamic activities of the major ions and required charge-compensating species, including defects. In such a case, the ratio of the activity of the trace ion in the solid phase to that of the liquid phase is a constant. The value of D is equal to that constant times the dilute solution activity coefficient of the trace ion in the liquid phase divided by that in the solid phase. It is presumed that those activity coefficients are insensitive to trace element concentration and that changes in temperature, pressure, or bulk composition of liquid and solid phases do not affect the properties of those phases as solvents, which would change the value of D . Of course, all those conditions are violated in nature, and in ways that could ultimately prove useful in providing information about the history and origin of a rock. These violations appear to have only second order effects on values of distribution coefficients for lanthanides between common silicate liquids and minerals, especially on values of individual lanthanide distribution coefficients relative to values for the other lanthanides in the same system. The values of D reflect the selectivity of individual phases for different members of the lanthanide series.

As mentioned above, the concept of the distribution coefficient implies equilibrium among phases. Rocks seldom crystallize under conditions approaching true equilibrium. For example, minerals are often zoned, i.e., their major and trace element compositions change systematically from their interiors to their rims, reflecting substantial changes in composition of the liquid as fractional crystallization proceeded. Equilibrium in such cases can only obtain between the newly forming surfaces of crystals and their parent liquids. Interior portions of crystals are effectively isolated from the system and do not further react to maintain liquid-solid equilibrium in the general sense. The Nernst distribution can still be considered to hold between the bulk residual liquid and the forming crystal surface. The mathematical description of this process was given by Doerner and Hoskins (1925). Many variants tailored to geochemical uses are given in the literature (e.g., McIntire, 1963; Schilling and Winchester, 1967; Gast, 1968; Haskin et al., 1970; Shaw, 1970; Greenland, 1970; Banno and Matsui, 1973; Hertogen and Gijbels, 1976). In this approach, the concentration $C_{L,m}$ of trace element m in the residual liquid from a parent liquid with initial concentration $C_{A,m}$ when fraction X of the original liquid has solidified is given by eq. (21.1)

$$C_{L,m} = C_{A,m}(1 - X)^{D_{w,m}-1}. \quad (21.1)$$

The parameter $D_{w,m}$ is the solid/liquid distribution coefficient for element m . From a mass balance, the average concentration $C_{S,m}$ in the solid at the same

extent (X) of crystallization is given by eq. (21.2)

$$C_{S,m} = C_{A,m}[1 - (1 - X)^{D_{w,m}}]/X. \quad (21.2)$$

If the value of $D_{w,m}$ exceeds unity, the liquid becomes depleted exponentially in element m as crystallization proceeds (fig. 21.18), and the average concentration of m in the solid decreases accordingly. If the value of $D_{w,m}$ is less than unity, the concentration of m increases exponentially in the liquid and, therefore, in the solid. At $X = 1$, the average concentration of the solid equals $C_{A,m}$, the concentration of the starting material.

To put this simple model into practice for describing a natural system is

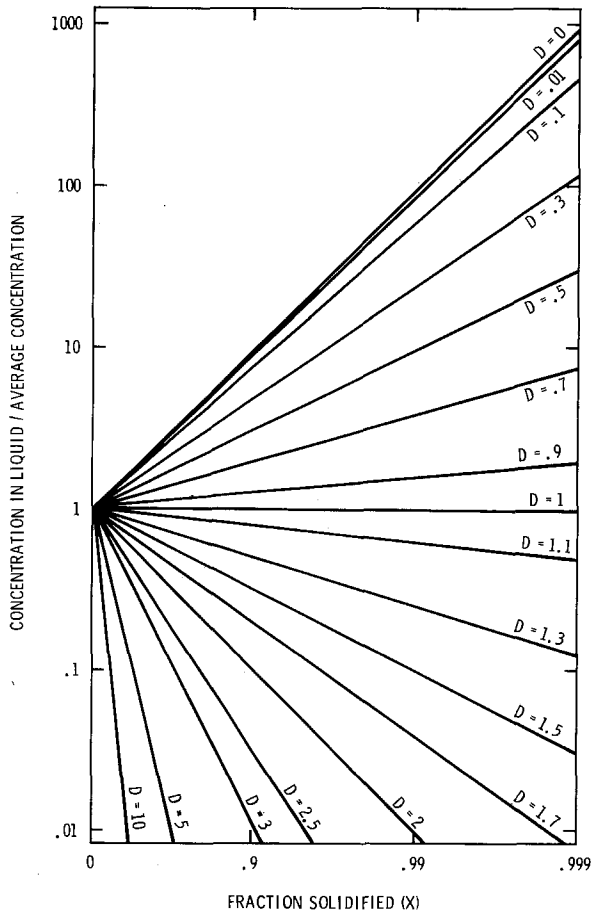


Fig. 21.18. Theoretical behavior of a trace element during fractional crystallization of a liquid, according to eq. (21.1). Concentration of the trace element relative to that of the starting composition for the liquid (or average composition for the entire system) is given as a function of the fraction of the original liquid solidified, for various values of the distribution coefficient (i.e., concentration of the trace element in the crystallizing solid/concentration in equilibrium liquid).

substantially more complicated than equations (21.1) and (21.2) might imply, but fairly straightforward (e.g., Helmke et al., 1972; Paster et al., 1974). Values of $D_{w,m}$ are sums of individual values for each crystallizing mineral, weighted according to the fraction of the precipitating solid that corresponds to each mineral. Compositional fractionation is so severe that some minerals may cease to form and new minerals begin, so the calculation must be done in stages, with appropriate changes in mineral proportions and values of distribution coefficients.

Then there remains the question of whether the process by which a natural rock formed has been adequately described. If the minerals form too rapidly, the liquid will not be well stirred and at the surface of the crystal will be depleted relative to its bulk concentration in those elements with values of D exceeding unity and enriched in those elements with values of D less than unity. The effect is for the minerals to crystallize according to apparent values of D that are closer to unity than are the equilibrium values. This and other complications have been considered by Albarede and Bottinga (1972).

Similar considerations arise as solids partially melt to form liquids. The entire liquid formed can reach equilibrium with the residual solid (e.g., Shaw, 1970), can reach equilibrium with the solid in increments only, which are separated away as melting continues (an extreme case which can be described by equations similar to (1) and (2); e.g., Haskin et al., 1970), can derive from lowest melting fractions too rapidly for any significant equilibrium to be established, or can establish surface equilibrium with the residual solid (e.g., Shaw, 1970). Because of the combination of thermal and pressure gradients with depth, a zone of liquid might rise from the mantle, extracting trace elements along its path (e.g., Schilling and Winchester, 1967).

In order to use any of the above models for fractional crystallization or partial melting, values for distribution coefficients must be obtained. Many are given in the literature. The extent to which they are applicable to quantitative modelling of natural systems has yet to be defined.

7.2. *Distribution coefficients*

Values for lanthanide distribution coefficients have been estimated from observed partitioning of lanthanides in natural systems and from laboratory measurements. The advantage of using natural materials is that the lanthanides in those have distributed themselves under fully natural conditions in real rock systems. The disadvantage is that the materials on which measurements are made may not actually represent the sort of natural, equilibrium systems that we imagine them to be. The advantage of measurements in the laboratory is our ability to control compositions, temperatures, pressures, and other conditions of the experiments. The disadvantage is that we may improperly simulate natural situations and only imagine that we are measuring parameters of useful predictive value.

Even if we do measure valid distribution coefficients for a given natural or

experimental system, those values may not be applicable to the next natural system of interest. Values of D depend, as pointed out earlier, on temperature, pressure, and bulk compositions of liquid and solid phases; these parameters vary widely in nature. Then there remains the question of which form, if any, of the mathematical models using distribution coefficients properly describes the system in question.

Enough studies have been done to demonstrate unequivocally the value of mathematical models to estimate lanthanide behavior during rock and magma-forming processes. Most results are rather semiquantitative, subject to substantial uncertainties. The extent to which lanthanide distributions can yield more quantitatively accurate information such as lanthanide concentrations in source regions, or fractions of liquids solidified or solids melted, or to enable establishment of clear-cut genetic relationships is still being evaluated. One of the crucial steps in this evaluation is accurate determination of values for lanthanide distribution coefficients and the extent to which those values depend on pressure, temperature, and composition. Several studies have been done, but few systematic measurements to show effects of temperature, pressure, and composition have been done.

Schnetzer and Philpotts (1968) obtained values for lanthanide distribution coefficients by the "phenocryst-host matrix" method. Phenocrysts are large mineral crystals found in otherwise fine-grained frozen lavas. The phenocrysts are presumed to have grown in equilibrium with the lava at depth prior to eruption of the lava. On eruption, the phenocrysts are swept along with the host lava, which quickly chills around them. By measuring the lanthanide concentrations in the phenocrysts (solid phase) and the host matrix (liquid phase) and taking the ratio, values for distribution coefficients are obtained. Accuracy depends on whether the phenocrysts truly grew in equilibrium with the liquid, whether the host matrix really represents that liquid, and whether both phases can be sampled without contamination by each other and accurately analyzed.

The principal result of Schnetzer's and Philpotts' work was demonstration that values obtained for a given mineral (e.g., high-Ca pyroxene) from different phenocryst-matrix pairs are very similar *in a relative sense*. This success has prompted many more measurements on phenocryst-matrix pairs (some of which it is a strain to imagine to represent actual equilibrium pairs; some phenocrysts are severely zoned, some may not be phenocrysts, and some matrices are not obviously chilled parent liquids). Values have been presented by Schnetzer and Philpotts (1968, 1970), Onuma et al. (1968), Higuchi and Nagasawa (1969), Nagasawa and Schnetzer (1971), and Dudas et al. (1971). Typical values are shown in fig. 21.19 for phenocryst-matrix distribution coefficients for the minerals feldspar, high-Ca pyroxene, low-Ca pyroxene, olivine, garnet, and apatite.

Estimates of values have been obtained in other ways on natural systems by Frey (1969), Balashov (1972), Paster et al. (1974), and Haskin and Korotev (1977), some to be discussed later.

Values on synthetic systems have been made in several laboratories by

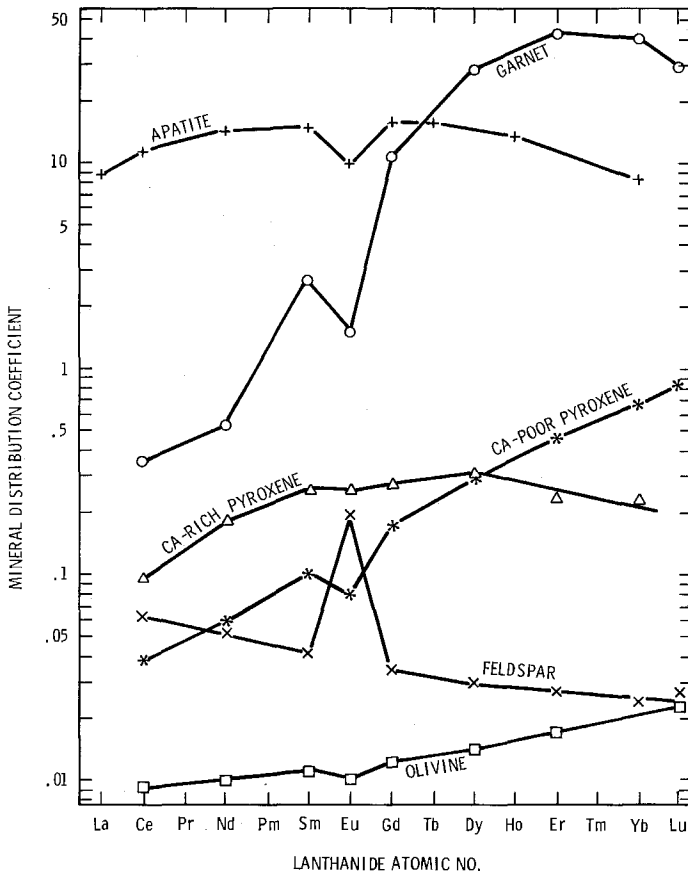


Fig. 21.19. Typical values of lanthanide distribution coefficients for common, rock-forming minerals. Values for apatite inferred from analysis of Skaergaard intrusion (Paster et al., 1974); rest from phenocryst-matrix analyses (Schnetzler and Philpotts, 1970).

different techniques. Cullers et al. (1970, 1973) synthesized pure silicate minerals in the presence of water and trace amounts of lanthanides. They measured their distributions against water and also the distribution between water and a silicate liquid. They derived estimates for lanthanide distribution coefficients that were consistent with those from phenocryst-matrix measurements but in the lowest part of the range. They found that both relative and, to a greater degree, absolute values were sensitive to the temperature of equilibration. Zielinski and Frey (1974) did nearly identical experiments on Ca-rich pyroxene and water but found nonequilibrium effects not observed by Cullers et al. (1973) that they felt might be responsible for some of the apparent effects of temperature. The reasons for the differences in results between the two laboratories are still not known. The technique of equilibrating minerals with water instead of with their parent silicate liquids makes possible a clean separation between the phases after the

furnace charge is quenched. The potential of the method as a means of providing accurate values of distribution coefficients and the effects of temperature, pressure, and composition on them has not been fully evaluated. It seems inherently less promising than methods that rely on the direct synthesis of crystals from silicate melts.

Balashov et al. (1970b) did zone melting experiments on synthetic metasilicates that indicated that the light lanthanides were more easily extracted into the liquid phase than were the heavy ones, especially when Mg(II) was the major cation (as opposed to Ca(II)). Equilibrium between melt and crystals was thought not to have been attained, so no values of distribution coefficient were given.

Masuda and Kushiro (1970) synthesized lanthanide-doped, Ca-rich pyroxene from silicate liquid and measured values of distribution coefficients. Values fell near the middle and upper part of the range of those obtained by the phenocryst matrix method. Such measurements are very difficult because even small inclusions of glass (quenched silicate liquid) with the crystals analyzed can contribute significantly to the measured concentration of a lanthanide if its true value for D is ≤ 0.2 . This problem was recognized but not fully solved by Masuda and Kushiro.

Grutzeck et al. (1974) measured values for lanthanide distribution coefficients in Ca-rich pyroxene grown from a silicate liquid. They obtained values near the middle of the range found in phenocryst-matrix studies. They showed that, at low partial pressures of oxygen, Eu was preferentially excluded relative to other lanthanides from the pyroxene because much of it was in the 2+ oxidation state, which has a lower value of D than Eu in the 3+ state. To avoid the necessity of separating crystals from glass, sufficiently high lanthanide concentrations were used ($\geq 1\%$) so that they could be determined by electron microprobe. Such high concentrations are in risk of violating the dilute solution behavior of the lanthanides, thereby yielding erroneous values for D ; such effects were not found by Grutzeck et al. Weill et al. (1974) used the results of Grutzeck et al. to model the behavior of Sm and Eu during lunar igneous differentiation.

Drake and Weill (1975) used the same experimental technique as Grutzeck et al. to determine lanthanide distribution coefficients for feldspar crystallized from a silicate liquid. Values fell about the middle of the range observed for phenocryst-matrix pairs. They found, as expected, that D for Eu increased as the partial pressure of oxygen was decreased (f_{O_2} ranged from $10^{-0.7}$ to $10^{-12.5}$).

Lanthanide distribution coefficients were determined by Shimizu and Kushiro (1975) on a synthetic garnet. The garnet was separated from the quenched parent liquid for measurement of lanthanide concentrations by isotope dilution mass spectrometry. Values for the heavier lanthanides (fig. 21.20) are not appreciably disturbed by possible contamination by quenched liquid, but those for the lightest lanthanides may be substantially too high.

Mysen (1976) measured distribution coefficients for Sm in olivine and Ca-poor pyroxene by beta track mapping of synthetic silicates. That technique allows use of very low concentrations of a trace element. Mysen reported a strong concen-

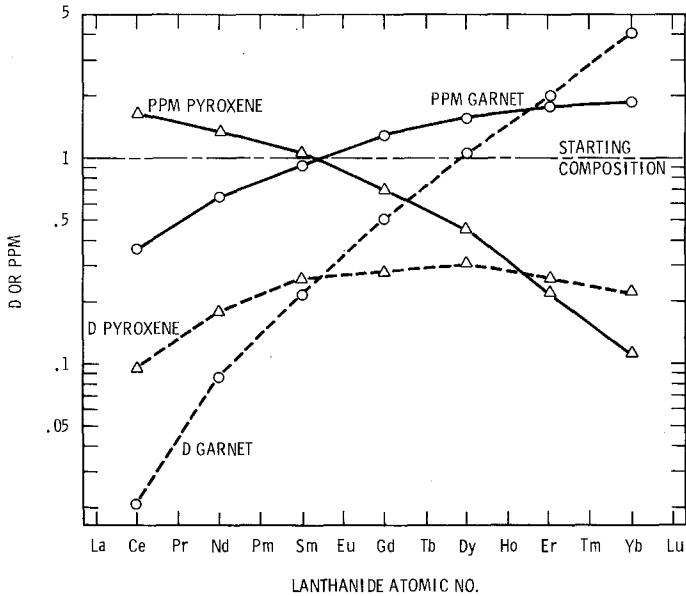


Fig. 21.20. Comparison diagram for a hypothetical eclogite consisting of equal parts of garnet and Ca-rich pyroxene, grown under closed system conditions from a liquid with 1 ppm of each lanthanide and with distribution coefficients as shown (that for garnet from Shimizu and Kushiro, 1975, and that for pyroxene from Schnetzler and Philpotts, 1970). Note that the pyroxene is strongly enriched in light lanthanides despite its preference for heavy ones.

tration dependence of D for Sm in olivine and orthopyroxene, a phenomenon not observed by other investigators. The concentration range studied gave olivine ranging from 0.04 to 1.6 ppm and that for low-Ca pyroxene from 0.08 to 2.6 ppm. The range of concentrations of Gd in the experiments by Cullers et al. (1970) for olivine was ~ 0.003 to >1000 ppm and for low-Ca pyroxene was ~ 0.005 to >1000 ppm, without measurable deviation from constant values. Those experiments were for partitioning between the minerals and an aqueous phase, rather than between minerals and silicate liquid. However, the lowest values of D reported by Mysen were for the liquids most concentrated in Sm, so failure of the liquid to retain increasing quantities of Sm was not important. The reasons for the discrepancies between the two experiments are not known.

From the data in fig. 21.19 it can be seen that most minerals do not remove lanthanides effectively from silicate liquids (i.e., lanthanide D values are mostly less than unity). Exceptions are apatite (a lanthanide-concentrating mineral that is a common late-stage product of crystallization of mafic liquids) and garnet (which concentrates heavy lanthanides but not light lanthanides). In acid magmas, lanthanide minerals may precipitate; these are discussed in later sections. Ca-rich clinopyroxenes and hornblendes (related to pyroxenes, but more compositionally complex) compete for lanthanides successfully against somewhat acidic lavas (Nagasawa and Schnetzler, 1971).

Crystallization of garnet from a liquid will rapidly change the lanthanide distribution of that liquid. Derivation of a liquid from a solid containing several percent or more of garnet will produce a liquid with a lanthanide distribution very different from that of the initial solid. Crystallization of apatite from a liquid can lower the lanthanide concentrations, but is more likely to decrease the rate at which lanthanide concentrations of the liquid increase, since the fraction of the total solid precipitating at any given time that is apatite is likely to be small. Partial melting of most sources containing apatite would be expected to melt all the apatite during the first very few percent of melting, so only in a special case would there be partitioning of lanthanides between residual apatite and a derived liquid. Crystallization of plagioclase can deplete Eu significantly relative to neighboring lanthanides. Partial melting against plagioclase can produce liquids relatively deficient in Eu. Crystallization of Ca-rich pyroxenes slowly changes the lanthanide distribution of the parent liquid. Crystallization of Ca-poor pyroxene or olivine or of plagioclase (except for Eu) scarcely affects the lanthanide distributions of the parent liquids; although those minerals are strongly selective in which lanthanides they remove, they tend to remove such small amounts that the effect on the distribution of the residual liquid is nearly negligible. Precipitation of lanthanide minerals, which appears to occur in granitic magmas, can deplete the residual liquid, sometimes selectively, in lanthanides.

Observed lanthanide distributions in analyzed minerals do not always reflect in an obvious way their distribution coefficients. The coefficients act on some parent distribution, which may differ substantially from the chondritic values commonly used as a standard for producing comparison diagrams. Also, when a liquid crystallizes as a closed system (Helmke et al., 1972), essentially all the lanthanides may enter major minerals, each mineral becoming most enriched in the trace elements against which it discriminates least. For example, fig. 21.20 shows the lanthanide distributions for garnet and high-Ca pyroxene from a hypothetical eclogite. The heavy-lanthanide selective pyroxene is rich in the light lanthanides and depleted in the heavy ones because it has equilibrated with garnet, which has a stronger affinity than the pyroxene for the heavy lanthanides and a weaker affinity for the light ones.

7.3. *Eu anomaly*

The anomalous behavior of Eu that results because Eu can be readily reduced to a 2+ ion with chemical properties unlike those of the 3+ lanthanides has been evident in many of the lanthanide distributions shown above. The existence of this anomaly has been known for a long time (e.g., Goldschmidt, 1938). There has been discussion about whether the anomaly observed in igneous rocks is a result of conversion of Eu(III) to Eu(II) in the liquid phase or of crystallochemical effects (i.e., ready acceptance of Eu(II) but rejection of Eu(III) by some mineral, e.g., feldspar) (e.g., Philpotts and Schnetzler, 1968, 1969; Towell et al., 1969). Both effects are important, of course. No mineral can take up Eu(II)

if conditions are so oxidizing that virtually none of the Eu is in that oxidation state. On the other hand, Eu will not separate from the other lanthanides under reducing conditions unless some mineral or process discriminates against the 3+ lanthanides in its favor, or vice versa. Several measured values for distribution coefficients show negative Eu anomalies for ferromagnesian minerals such as pyroxene, indicating that those minerals selectively favor the 3+ lanthanides. A similar effect can result from closed-system crystallization of pyroxene in the presence of plagioclase, but discrimination by pyroxene against Eu relative to its 3+ neighbors seems well established, especially for lunar materials (e.g., Philpotts, 1970; Haskin and Korotev, 1977).

It has not been possible to measure concentrations of Eu(II) and Eu(III) in most common, rock-forming, natural minerals because of low concentrations and interferences. Philpotts (1970) has suggested a means of estimating such concentrations in minerals and parent liquids that, for some rock systems, gives values that are self-consistent and consistent with concentrations inferred from other evidence. According to Philpotts, given two mineral phases j and k in a rock, the concentration of Eu(III) in phase j , $C_{j,3}$, is given in terms of the total concentration of Eu in each phase, $C_{j,Eu}$ and $C_{k,Eu}$, and the distribution coefficients for Eu(III) and Sr between the two phases, $D_{ij,3}$ and $D_{ij,Sr}$, as follows:

$$C_{j,3} = (C_{i,Eu} - D_{ij,Sr}C_{j,Eu}) / (D_{ij,3} - D_{ij,Sr}) \quad (21.3)$$

This treatment assumes that phases i and j are in full equilibrium with respect to Eu and that the value for the distribution coefficient for Eu(II) equals that for Sr. Values for $D_{ij,3}$ are obtained by interpolation of values for Sm and Gd. Philpotts found values for the concentration ratio of Eu(II) to that of Eu(III) ranging from 0.03 to 2.6 for matrices of basalts and values ranging from 1.8 to 85 for feldspar phenocrysts from those lavas. He also showed an empirical correlation of increasing size of Eu anomaly for feldspar with increasing proportion of Na and decreasing proportion of Ca. He found that negative Eu anomalies were more prominent in Ca-rich pyroxenes with high Fe contents, as opposed to high Mg contents. He found no correlation between relative amounts of Eu(II) and Eu(III) and relative amounts of Fe(II) and Fe(III). He showed that the highest ratios of Eu(II) and Eu(III) in matrices (chilled liquids) were found in more acidic (andesitic and rhyolitic) lavas, in comparison to those found in basalts. Philpotts suggested that the ratio of Eu(II) and Eu(III) might serve as a useful indicator of oxygen fugacity for crystallization of lavas.

Nagasawa (1971) measured Eu anomalies in coexisting Ca-feldspars and K-feldspars (two distinct minerals) from acid igneous rocks. He concluded that Eu(II) was present, that it behaved very much like Sr(II), and that the method of Philpotts (1970) for estimating concentration ratios of Eu(II) to Eu(III) should be reasonable.

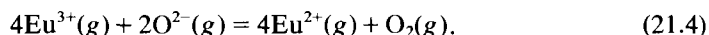
Weill and Drake (1973) measured the distribution of Eu between silicate liquid and crystallizing feldspar as a function of temperature and oxygen fugacity. They developed a model based on their experimental observations to account

quantitatively for the size of the Eu anomaly in feldspar as a function of those two variables. An assumption of the model is a similar temperature dependence for Sr and Eu(II) distribution coefficients. They show that the trend toward higher Eu(II) to Eu(III) concentration ratios in terrestrial acid magmas is a natural consequence of the change in oxygen fugacity and, therefore, redox conditions of terrestrial magmas with temperature. This effect also explains the larger Eu anomalies in Na-rich (lower temperature) feldspars relative to Ca-rich (higher temperature) ones. The results are restricted to systems with bulk compositions similar to that studied. Also, the statement that the ratio of D for Eu in a mineral to that of D for Eu(III) in that mineral by analyses of natural minerals while true, must be regarded with caution in practice. The size of the Eu anomaly in a feldspar is sensitive to effects of closed system crystallization so a measured value could be misleading.

Values of D for Eu and Sr in feldspar and Ca-rich pyroxene in a molten ocean floor basalt doped with oxides of those elements were obtained as functions of temperature and oxygen fugacity by Sun et al. (1974). The range of temperatures studied was narrow (50°C for feldspar, 20°C for pyroxene). Values of D for Eu were found not to be strongly dependent on temperature but to be quite dependent, as anticipated, on oxygen fugacity. Comparison of their results with those of Weill and Drake (1973) indicated a dependence of D for Eu on bulk composition.

Morris and Haskin (1974) and Morris et al. (1974), using electron paramagnetic resonance, measured concentration ratios of Eu(II) to Eu(III) in quenched silicate liquids of a variety of compositions of geochemical interest. They found that, for constant oxygen fugacity, very large differences in concentration ratios occurred for different bulk compositions. For example, the mole fraction of Eu(II) in liquids ranging in composition from Ca-rich pyroxene ($\text{CaMgSi}_2\text{O}_6$) to Ca-feldspar ($\text{CaAl}_2\text{Si}_2\text{O}_8$) at constant temperature and oxygen fugacity ranged from 0.11 to 0.6. This demonstrates clearly the importance of bulk composition to the distribution of variable-valence elements in natural systems.

Morris and Haskin (1974) discussed their observations in terms of the equilibrium given below for Eu(II) and Eu(III) as ions in an ideal gas.



They introduced a solvent coefficient (Henry's law constant) for each Eu species to account for the energy difference between the ideal gas and the particular liquid in question. They found, for a particular choice of major cation (i.e., Ca or Mg) in the solvent, 2EuO to be more soluble than Eu_2O_3 in going from the ortho- or metasilicate end member of the mixture to the aluminosilicate end member. This result was not expected because the aluminosilicate end member has a higher fraction of its oxygen bound into polymer chains. This would be expected to decrease the activity of free oxide ion in the aluminosilicate melts, which according to eq. (21.4) would favor formation of Eu(III) at the expense of Eu(II), just opposite to what was observed.

Fraser (1975) showed that the observations could be readily understood if

Eu_2O_3 were regarded as amphoteric, i.e., in addition to dissociating to produce a solvated $3+$ ion, it would react with oxide ion to produce EuO_2^- . The EuO_2^- would behave as a polymer network forming cation similar to silicate and aluminate. This useful idea would apply to other ions of variable valence as well. Additional testing of the ideas of Fraser is needed. There is no evidence from studies of Gd(III) in minerals (Morris, 1975) for behavior of that ion as a network-forming entity. Morris et al. (1974) concluded from their studies of the composition dependence of concentration ratios of Eu(II) to Eu(III) that the structures of silicate liquids, in terms of the environments available to the Eu species, were probably very similar to those of the solid minerals that would crystallize on cooling of those liquids.

Drake (1975) integrated the method of Philpotts (eq. (21.3) above) with results of experimental work to use empirical concentration ratios of Eu(II) to Eu(III) in feldspar and liquid to determine oxygen partial pressures during crystallization. The method developed does not account for effects of bulk composition on the concentration ratio. Drake pointed out that natural magmas do not cover such a broad range of compositions as that studied by Morris and Haskin (1974). For eight cases reported by Philpotts for which Eu concentration ratios were available for both plagioclase and matrix, Drake obtained internal consistency within a range of -2.3 to 2.8 orders of magnitude for the oxygen fugacity. Most of the values were consistent in a broad sense with those obtained for similar rocks by other means. This consistency is comforting, but Eu concentration ratios as an oxygen barometer have not yet been developed into a method of admirable precision.

7.4. *Developing, testing, and applying the models*

In a sense, the models for describing lanthanide behavior during rock-forming processes do not need testing. They are based on solid chemical grounds. Their applicability to actual natural situations has to be proven, however. To various extents this is recognized and worried about by the various investigators and can be studied in their papers. Some examples of developing and testing of models are given below.

A very important, broad scale application of models for trace element behavior was developed by Gast (1968) in considering the differences between tholeiitic and alkali basalts of the oceanic environment. In this work, Gast considered not only lanthanide abundances between ocean floor tholeiites (light-lanthanide depleted relative to chondrites) and ocean island alkali basalts (light-lanthanide enriched), but abundances of other trace elements (K, Rb, Sr, Ba, Cr, Ni, U, Th, and Pb), major elements and their pertinent mineral assemblages, isotopic data for Sr and Pb, heat budgets, effects of temperature and pressure (depth) on melting, reaction of a magma with surrounding wall rock, new geophysical ideas about magma generation at ocean ridges and sea-floor spreading, available information leading to trace-element distribution coefficients, and relative abundances of ocean floor tholeiites and ocean island alkali basalts

(~100:1). From this study Gast estimated that the source for ocean floor tholeiite was ~50% depleted in the incompatible trace elements. He showed that small extents of partial melting of mantle material of plausible starting composition and mineralogy could produce substantial differences in trace element distributions in liquids, but that implausible extents of fractional crystallization were required to do so. He concluded that the ocean floor tholeiites were derived by extensive (20–30%) partial melting and alkali basalts by a much smaller extent (3–7%). Some of the conclusions have been bent somewhat by further work (e.g., Kay et al., 1970; Schilling, 1975; Blanchard et al., 1976) but the paper stands out as an early test of the adaptability of the model to a specific geologic setting and an integration of lanthanide distributions with other information to obtain a useful, self-consistent description of lava-forming processes.

Subsequent applications of the model have shown the effects of fractional crystallization on specific basalt systems. Usually these are small. Kay et al. (1970) showed that crystallization of olivine, Ca-rich pyroxene, and feldspar could account for some of the variations in lanthanide concentrations observed in ocean floor basalts. Small negative Eu anomalies could be observed after extensive crystallization of feldspar. Helmke and Haskin (1973) showed that the petrographic character, bulk compositions, and lanthanide concentrations of 52 lavas from a single source, Steens Mt., Oregon, were all consistent with crystallization of different amounts of Ca-rich pyroxene, feldspar, and olivine from a common parent in magma chambers prior to eruption of the basalts. Lanthanide concentrations were the key to determining the quantity and composition of material solidified. Solid materials were estimated to have lanthanide distributions peaking around Nd, as often found in gabbros (intrusive rocks similar to basalts in composition). Zielinski and Frey (1970) and Zielinski (1975) showed that extreme extents of fractional crystallization of basaltic magma could account for the relatively rare, acidic volcanic rocks of oceanic islands (Gough island and Reunion island) (fig. 21.6). The comprehensive work of Schilling (1973) on the origin of Iceland magmas was mentioned previously.

A rather specific test of the model was its application to the Skaergaard intrusion. The Skaergaard intrusion is regarded as an example of mafic magma, intruded into a bowl-shaped chamber, that cooled slowly (except where it came in contact with wall rock) and differentiated by fractional crystallization. As it cooled, early-formed crystals settled to the bottom. Later-formed crystals fell on top of those, and so on, leaving a layered rock series that, on being exposed by uplift and erosion, allowed partial sampling of the trends of fractional crystallization. The rocks toward the bottom of the series consist mainly of accumulated crystals of olivine, Ca-rich pyroxene, and Ca-rich feldspar. Farther up, olivine ceased to crystallize in favor of Ca-poor pyroxene. Higher still, crystallization of Ca-poor pyroxene ceased and olivine reappeared. In a systematic manner, from bottom to top, the feldspar became poorer in Ca and richer in Na and the olivine and pyroxenes become richer in Fe and poorer in Mg, in line with known phase relationships for crystallization of such a liquid. Near the top of the series, *P* became so abundant that the lanthanide-concentrating mineral apatite accumulates along with the major minerals.

In terms of the model for fractional crystallization, a cumulate crystal would form in and separate from such a large volume of liquid that there would be no change in the composition of the liquid during formation of the crystal. Thus, any narrow band of accumulated crystals would be equivalent in the surface-equilibrium model to a single increment of new growth on a crystal growing throughout solidification of a melt. Since values for distribution coefficients of all lanthanides in all minerals precipitating (except apatite, very near the top) are less than unity, concentrations of the lanthanides should increase smoothly in successive residual liquids with increasing fraction of the magma solidified. The concentrations in the cumulate crystals should show a corresponding increase with height in the layered series.

Haskin and Haskin (1968) analyzed rocks from the layered series and found the expected increase in lanthanide concentrations for successive residual liquids calculated from a mass balance, but nearly constant lanthanide concentrations for the successive rocks (fig. 21.21) except those highest in the series,

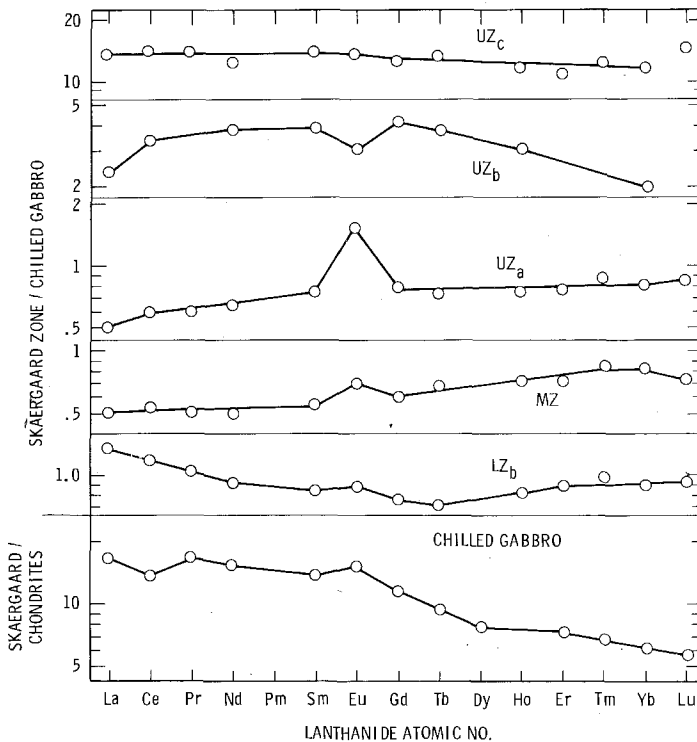


Fig. 21.21. Comparison diagram to chondrites (lowest portion) of Skaergaard chilled marginal gabbro, taken to represent the composition of the starting material for the layered intrusion, and used as the basis of comparison for Skaergaard rocks from different zones of the layered series (rest of diagram). Note the rather abrupt increase in lanthanide concentrations, only for the highest zones of the series, rather than a systematic increase from lower zone (LZ) through middle zone (MZ), to upper zone (UZ).

not at all as expected from the simplest application of the model. Paster et al. (1974) showed that the discrepancy arose from failure to take into account the parent liquid trapped among the accumulated crystals. The trapped liquid solidified as a closed system, increasing the sizes of the cumulate crystals and introducing into them and into the rocks as a whole lanthanide concentrations as large or larger than those already contributed by crystals grown in equilibrium with the bulk melt.

Paster et al. developed a formulation of the model to account for changes in mineralogy on distribution coefficients and for crystallization of trapped liquid. They showed that the approximate constancy of lanthanide concentrations for rocks throughout most of the series was a fortuitous opposition of trends of increasing lanthanide concentrations in the cumulate crystals and decreasing proportions of trapped liquid with increasing height in the intrusion.

Paster et al. showed that the required average values of distribution coefficients to describe solidification of the Skaergaard intrusion fell within the range for phenocryst-matrix systems, but toward the lowest values. Prior to this work, the Skaergaard intrusion was thought to have a large hidden zone (70–80 percent of the total mass) still beneath the surface and inaccessible to sampling. Paster et al. determined that the size of the hidden zone was much less, a result confirmed by geophysical studies.

Some investigators have analyzed separated minerals from the groundmass (not phenocrysts) of basalts or other igneous rocks, then divided their lanthanide concentrations by those for the whole rock to obtain values for distribution coefficients. They reason that the whole rock corresponds to the parent liquid from which the minerals grew. That is so for a closed system, but the minerals do not represent the products of equilibrium crystallization from a parent of the whole rock composition. Rather, the minerals are the integrated products of incremental crystallization from the series of successive parent liquids that formed as the original parent underwent fractional crystallization. Effects on mineral composition of closed-system crystallization must be taken into account. Similarly, some investigators measure lanthanide concentrations in minerals separated from a rock or of unknown origin and, using literature values for distribution coefficients, estimate the lanthanide distribution of the parent liquid. This also fails to account for compositional effects of closed-system crystallization on the minerals. Helmke et al. (1972) developed a model to account for closed-system effects. Haskin and Korotev (1977) tested it on minerals separated from a sample of lunar basalt (figs. 21.22–23). The separates consisted of Ca-rich pyroxene, Ca feldspar, a mixture of olivine and Ca-poor pyroxene, and ilmenite (FeTiO_3). A fifth analyzed "phase" consisted of mesostasis, a partly crystalline, lanthanide-rich glass corresponding to the last dregs (final ~0.6 percent) of the basalt liquid to solidify. Haskin and Korotev showed by use of a mixing model that the mineral separates plus mesostasis accounted accurately for the composition of the whole rock, although single fragments of the minerals did not. They applied the model for closed-system crystallization to the basalt, using values for distribution coefficients taken from studies of other rocks, and found

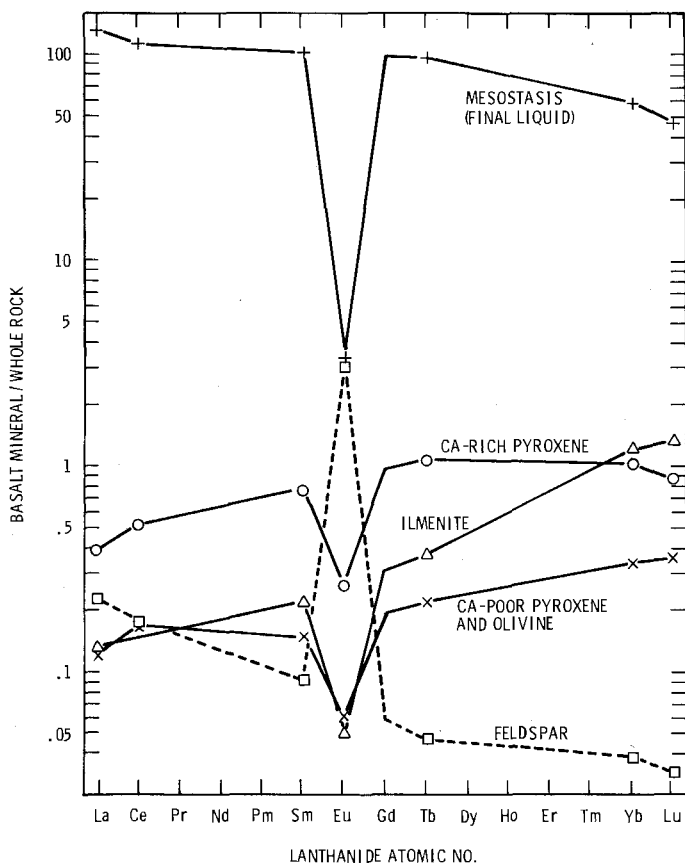


Fig. 21.22. Comparison diagram relative to whole rock, not chondrite, for minerals and mesostasis (final, most differentiated liquid, partly fine crystals, partly glass) from a basalt (lunar basalt 70135) (Haskin and Korotev, 1977). Note the selectivity of the individual minerals and their effect on the relative abundances in the mesostasis, especially for Eu.

that it predicted the trends fairly well. They then assumed the validity of the model and calculated values for distribution coefficients appropriate to the crystallization of that particular basalt, thus providing a set of values from a natural system independent of the relationships assumed between phenocrysts and host matrices in different systems. Haskin and Korotev also showed that variations in the quantity of mesostasis from one chip of the basalt to another corresponded to a concentration range for lanthanides equal to that observed among all chips analyzed from all different basalts taken from the same landing site. Fractional crystallization and partial melting models have been used, unsuccessfully, to explain those variations.

Consideration of effects of trapped liquid enabled Haskin et al. (1974) to determine the lanthanide concentrations of the parent liquid of a lunar cumulate rock consisting mainly of feldspar and olivine. The concentrations ranged from

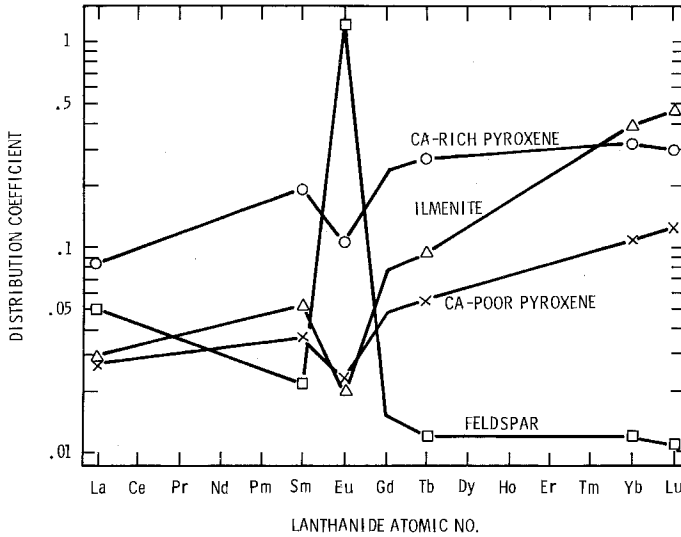


Fig. 21.23. Distribution coefficients required, on basis of closed-system, surface-equilibrium, fractional crystallization model, to account for observed lanthanide concentrations in minerals and mesostasis for basalt 70135 (fig. 21.22). Note that the trends for the distribution coefficients strongly resemble, but differ from, the lanthanide distributions in the minerals, and the values for the distribution coefficients are much lower than the ratios of mineral concentrations to whole-rock concentrations.

~13 times the chondritic value for Lu to ~27 times for La, with little or no Eu anomaly. Laul and Schmitt (1975) showed that trapped liquid was responsible for the variation in concentrations of lanthanides and other incompatible elements in a lunar cumulate rock consisting of nearly pure olivine. The parent liquid estimated for the cumulate was enriched in La relative to Lu to about the same extent as that estimated for the feldspar-olivine cumulate, but with a somewhat different shape, a probable positive Eu anomaly, and lanthanide concentrations approximately one-half as high. The lanthanide distributions are similar to those estimated by Taylor (1975) as the average for the lunar highlands; the concentrations estimated by Taylor are more than twice as high as those for the parent of the feldspar-olivine rock.

Frey and co-workers have done an especially careful job of integrating a variety of constraints into their interpretations of the origins of ultramafic rock nodules in basalts. Frey and Green (1974) found that peridotite nodules (olivine, Ca-rich clinopyroxene, Ca-poor clinopyroxene, and spinel) from alkali basalts of southeastern Australia are of two types with respect to lanthanide distributions. One type has low lanthanide concentrations and distributions depleted in the light lanthanides as might be expected for the source region for ocean floor igneous rocks or the residues of partial melting to produce light-lanthanide rich lavas (fig. 21.24). The other type had slightly lower concentrations of heavy lanthanides but substantial concentrations of light lanthanides as if parental to

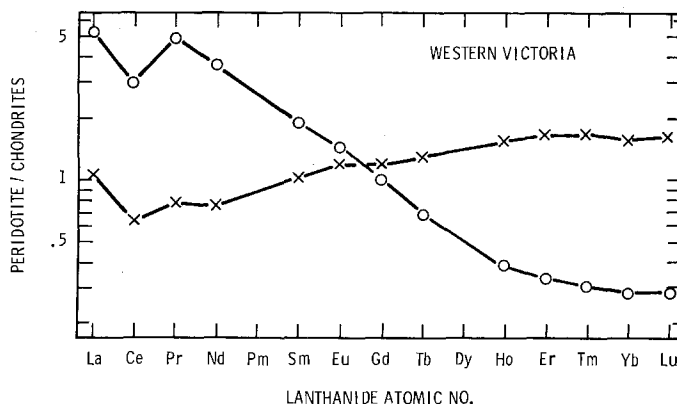


Fig. 21.24. Comparison diagrams for two types of peridotite inclusions found in alkali-rich lavas of southeastern Australia (Frey and Green, 1974).

alkali basalts. Based on lanthanide distributions alone, such an interpretation might have been made. Mineralogy of the nodules was consistent with crystallization or recrystallization within the upper mantle. Pyroxene textures and Sr isotope ratios indicated that the inclusions were chunks of wall rock torn off by the basaltic liquid rather than products of accumulation of crystals from the basalts themselves. However, the nodules with the most refractory, residue-like bulk compositions and mineralogy (poor in Ca-rich pyroxene, rich in Mg relative to Fe) were those with the highest concentrations of incompatible elements (P, K, Ti, U, Th, light lanthanides), making them unsuitable as parents that would leave the other type as residues. Frey and Green concluded that the lanthanide distributions were a mixture of two components, one that of the type with approximately flat distributions and one highly enriched in light lanthanides. The first component was regarded as the residue of early partial melting and is similar to or may correspond to the source for ocean floor volcanics. The second was taken to be the result of a very small degree of partial melting at greater depth, in equilibrium with garnet, and therefore enriched in light lanthanides. The present mineralogy results from mixing and equilibration of the two components at shallow mantle depths, prior to incorporation in lavas rushing to the surface.

In a study of nodules from Hawaiian basalts, Reid and Frey (1971) examined two types. One consisted of olivine, Ca-rich pyroxene, Ca-poor pyroxene, and spinel. The other consisted mainly of garnet and Ca-rich pyroxene, with smaller proportions of the other minerals. Some nodules consisted of both types in intergrading contact. Reid and Frey concluded that the garnet-free variety was produced by partial melting and recrystallization of the garnet-rich type. The liquid removed was estimated from Ca-rich pyroxene distribution coefficients to be similar in lanthanide distribution to common Hawaiian alkali basalts. The garnet-rich variety of nodule was suggested to be a more primitive type of mantle material than the garnet-free variety, yielding incompatible elements to

provide liquids extruded onto the crust. The residual garnet-free variety corresponds mineralogically to the nodules from Australia (and many other localities) and is consistent with a widespread ultramafic mantle material from which incompatible elements have been partially extracted.

A systematic study has been made of lanthanide distributions in rocks from an early Precambrian terrane of Minnesota and Ontario by Hanson and Goldich (1972) and Arth and Hanson (1972, 1975). This terrane consists of metamorphosed tholeiitic basalts, more acidic volcanic rocks, and intruded granite-related rocks. It is typical of much of the Earth's early crust.

The tholeiites (fig. 21.25) have lanthanide distributions like those of their younger counterparts and ranging from essentially flat as is characteristic of ocean floor basalts to slightly enriched in light lanthanides as found in some continental tholeiites. The more acid volcanic rocks and the granite-related rocks

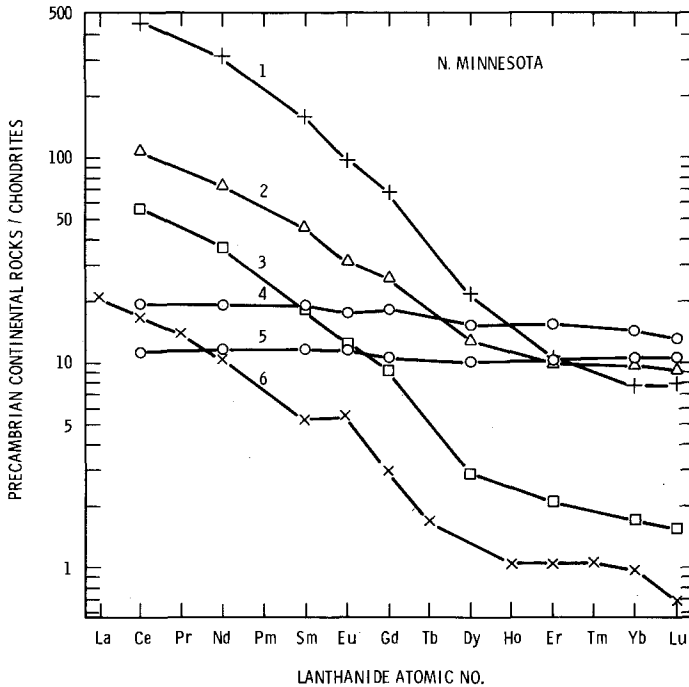


Fig. 21.25. Comparison diagram for Precambrian rocks of northeastern Minnesota interpreted by Arth and Hanson (1975) as possibly representing the formation of continental crust from mantle-derived material. Nos. 4 and 5 are early stage tholeiitic basalts, nos. 2, 3, and 6 are intrusive and extrusive granite-related rocks of main, intermediate stages, and no. 1 is a late-stage, intrusive, granite-related rock. Intermediate and late-stage rocks may have derived from material of the approximate composition of tholeiite, but at depths where garnet was a stable residual mineral, accounting for the severe depletion of the granite-related rocks in heavy lanthanides.

(fig. 21.25) all show strong relative enrichment in the light lanthanides, with lower concentrations of heavy lanthanides than is typical of crustal materials. This was recognized as evidence for equilibration of the liquids that produced these rocks with a residue containing granite.

Using models for estimating lanthanide distributions along with information on major and other trace elements, field relationships among the rocks, phase melting relationships, and isotopic information on Sr and Pb, Arth and Hanson (1975) have outlined the sequence and nature of events that might have led to formation of that portion of the crust. Initially, the tholeiitic volcanics extruded onto the surface; just what kind of surface was not specified, but there is no evidence for any pre-existing continental surface. The tholeiites could have derived from partial melting of mantle peridotite at relatively shallow depth (<30 km). Some of the tholeiitic liquids fractionally crystallized, but not sufficiently to produce acidic lavas. After a substantial quantity of tholeiite was emplaced, granite-related magmas intruded into them. The lanthanide distributions of these rocks are consistent with an origin by partial melting of eclogite or garnet-bearing peridotite; this requires a depth of ≥ 45 km in order for garnet to be stable in the residue. The composition of the eclogite could have been essentially that of the tholeiitic basalts. The volcanic rocks eroded rapidly during and after emplacement of the above rocks, and eventually the buried sediments underwent partial melting to produce a new class of granite-related magmas that intruded into the preceding rock formations. A time scale of ~ 50 million years was deduced for this process. Minor volcanic activity from garnet peridotite or eclogite followed.

Hanson and co-workers argue that this sequence of rocks derived by direct differentiation from the mantle. They point out that if all similar Precambrian terranes can be explained in that manner, the development of those terranes 2.7–3.3 billion years ago represents the derivation of a significant part of our present continental crust from the mantle. It appears that this could be true even if the mantle source of the Precambrian tholeiites had yielded up a portion of its incompatible elements in an earlier episode. The only reason to suggest that it might have done so is the similarity of the tholeiite lanthanide distributions to those of younger ocean floor or early island arc tholeiitic basalts and the interpretation given to them. It is interesting to note that Jahn et al. (1974) also studied volcanic rocks from the same area in northern Minnesota and proposed from considerations of their results and information on other ancient volcanic rocks that trace elements have been repeatedly and fully recycled in a more or less closed system consisting of crust and upper mantle for the past 3 billion years, with relatively minor addition of new trace elements from deep mantle sources during that time.

It is not clear whether the terrane described by Hanson and co-workers would yield the lanthanide distribution characteristic of continental crust (the NASC distribution). A comprehensive model for the derivation of the crust and that lanthanide distribution remains to be developed.

7.5. *Sm-Nd age measurements*

Lugmair et al. (1975) demonstrated that the decay of ^{147}Sm yielded a sufficient change in the isotopic composition of Nd to be useful in determining the age of lunar basalts. ^{147}Sm decays by alpha particle emission with a half-life of 1.06×10^{11} years to give ^{143}Nd . The age obtained for the rock was 3.70 ± 0.07 billion years, in excellent agreement with that obtained by other investigators using different isotopic dating methods.

The technique is made possible because when an igneous rock solidifies different minerals take up different lanthanides selectively, as reflected in their distribution coefficients. This means that different minerals can have different ratios of Sm to Nd at the time of their crystallization. As the ^{147}Sm decays it will change the isotopic composition of the Nd to different extents for each different mineral. If the Sm and Nd concentrations and the Nd isotopic composition are determined for each mineral they can be related by the radioactive decay law to yield the span of time that passed since the minerals crystallized. Similar work has been done with K-Ar, Rb-Sr, U-Pb, and Th-Pb isotopic pairs. Each pair has its advantages and disadvantages. The Sm-Nd pair complements the others nicely in that both elements, being lanthanides, have very similar chemical properties, so no aberrant behavior by one member of the pair can cause a peculiar result.

Any large-scale change in concentration ratio of Sm to Nd in the Moon as a whole would produce, with time, regions with different Nd isotopic compositions. Lugmair et al. (1975) show evidence for a major lunar differentiation 4.35 \pm 0.10 billion years ago. This is also consistent with evidence from other isotopic systems.

De Paolo and Wasserburg (1976) have measured Nd isotopic ratios in terrestrial materials. Their work so far confirms the chondritic relative abundances for Sm and Nd hypothesized for the Earth as a whole. They show that the mantle is now heterogeneous with reservoirs of different Nd isotopic ratios. They find that crustal rocks reflect a long-standing enrichment of the crust in Nd relative to Sm, as compared with chondrites. They show that oceanic island alkali basalt and ocean floor tholeiite come from sources that have had, on the average, Nd-Sm ratios lower than the chondritic, for time spans corresponding to the age of the Earth. Ancient granitic rocks appear to have derived directly from a mantle source with a chondritic concentration ratio of Nd to Sm.

Richard et al. (1976) also found the mantle source of ocean floor tholeiite to have a light-lanthanide depleted distribution. However, they found oceanic island alkali basalts to have higher relative amounts of ^{143}Nd than the ocean floor tholeiites. They suggested that the alkali basalts derived from a source region with a chondritic concentration ratio of Nd to Sm.

Future studies of these isotopic variations will do much to clarify the time scales for major differentiating events and the nature of the processes by which lanthanide distributions of various classes of rocks were attained.

8. Lanthanide mineral resources

Because the lanthanides and yttrium are dispersed elements they are found mainly as trace constituents of common rocks. Within those rocks they occur partly as trace constituents of the major, rock-forming minerals and partly in accessory minerals in which the lanthanides are either essential constituents (e.g., monazite) or are concentrated (e.g., apatite). More than 100 different lanthanide and lanthanide-concentrating minerals are known. Most of these form from liquids that are highly differentiated chemically relative to common magmas. Such liquids are rich in a wide variety of elements that are trace elements in terms of their natural abundances but major constituents of the final dregs of liquid when magmas freeze.

8.1. *Formation of lanthanide ores*

Nature concentrates lanthanide minerals into commercially useful ores mainly by three processes. Minerals such as monazite are dilute accessories in common rocks, but are fairly resistant to weathering and have high densities. As their host rocks weather away, they remain intact and are moved by water and high-graded into placer deposits as less dense minerals are swept away from them.

Another means of concentrating lanthanides is in pegmatites. Pegmatites are final products of crystallization of some magma bodies. Providing that conditions of crystallization of the bulk magma caused concentration of lanthanides in the final liquid, a pegmatite will contain high concentrations of lanthanide-bearing minerals. Pegmatites are relatively small in comparison to lava flows or granite bodies, but they are numerous and some of them can serve as sources of lanthanide ores.

Lanthanides are abundant in magmas yielding highly alkali basalts and related materials. In some cases, when these magmas cool beneath the surface, minerals accumulate as in the Skaergaard intrusion described earlier. If titanium is sufficiently abundant, the magma may crystallize perovskite, thereby concentrating the lanthanides in a form that may later be exposed for use. Also, carbonatites are associated with some alkalic magma suites and contain lanthanide minerals (e.g., apatite) that potentially could be used commercially.

Placer deposits of potential future value as lanthanide ores invariably have the lanthanides present in common lanthanide or lanthanide-concentrating minerals (e.g., apatite, allanite, monazite, xenotime, zircon). Most pegmatites of potential value as ore have the lanthanides as common lanthanide-bearing minerals too (those previously mentioned plus fluorite). Alkalic rock complexes may produce commercially useful concentrations of common lanthanide-bearing minerals (e.g., apatite, perovskite) or rare ones (e.g., bastnaesite).

8.2. *Commercially important lanthanide minerals*

Even a brief introduction to the wide variety of lanthanide minerals exceeds the scope of this chapter. Properties of many are given by Roberts et al. (1974), Palache et al. (1951, vols. 1 and 2), Deer et al. (1962, vols. 1 and 5), Frondel (1958), Fleischer (1966), and Vlasov (1966, vol. 2). Extensive bibliographies have been compiled by Adams and Iberall (1973), Mineev (1969), and Paster (to be published).

Levinson (1966) has discussed the problems of nomenclature. The mineralogists' propensity for sticking names on complex natural chemical phases (minerals) that give no clue whatsoever as to the nature of those phases runs amuck with lanthanide minerals. In those, a simple shift in lanthanide relative abundances changes the phase from that of mainly one chemical element to that of mainly another, with irresistible possibilities for a new and unrelated mineral name.

Most lanthanide-bearing minerals are listed as Ce-group, Y-group, or complex. This is a useful approximate classification for those in which lanthanides are essential constituents. The different ionic radii of the lanthanides can cause different crystal habits to be favored. When sufficient light lanthanides and phosphate are present, and other conditions are right, the light-lanthanide phosphate monazite may form. This mineral is usually dominated by Ce because it is usually the most abundant light lanthanide present. It can be considered a solid solution of all lanthanide phosphates that have similar properties. Monazite has a monoclinic crystal habit. The smaller ionic radii of the heavier lanthanides and yttrium cause them to require a tetragonal structure. Thus, monazite discriminates against those elements. If the concentration of heavy lanthanides is sufficient, the tetragonal phosphate xenotime, dominated usually by yttrium, will form. These minerals are genuinely selective with respect to the lanthanides.

Lanthanide-concentrating minerals can also be selective, depending on which lanthanides more readily substitute into their structures. The true extent of their selectivity is less easily inferred from compositions of natural minerals than for the lanthanide minerals proper. Their lanthanide abundances tend to reflect those of their parent liquids, which are usually not known. Those minerals that do not show a consistent pattern of domination by light lanthanides, heavy lanthanides, or even middle lanthanides are usually listed as complex. Presumably, whatever selectivity they have is insufficient to overcome variations in composition caused by variations in parent liquid composition. Because many of these minerals form late in a crystallization sequence, the lanthanide distributions of their parents may differ considerably from those of the original magmas or those of the rocks in which the minerals occur.

Eight common lanthanide or lanthanide-bearing minerals that account for most concentrated supplies of lanthanides in nature are discussed briefly below. Another mineral (bastnaesite) that is of present commercial importance is discussed also.

Allanite is a complex, lanthanide-concentrating mineral of generalized

composition $(Ca, Fe^{2+})_2(R, Al, Fe^{3+})_3Si_3O_{13}H$. R normally represents the light lanthanides; rarely the heavy lanthanides and yttrium predominate. Allanite is a common accessory mineral in granite-related rocks and pegmatites. It is found as a product of metamorphism of rocks with granite-related compositions. Fig. 21.26 shows lanthanide distributions for some allanites taken from the work of Semenov and Barinskii (1958).

Apatite is a lanthanide-concentrating mineral represented by the composition $Ca_5(PO_4)_3X$ where X is usually F^- , sometimes OH^- , sometimes a mixture, or occasionally Cl^- . More complex varieties, some containing CO_3^{2-} , are known. Apatite is ubiquitous in mafic and granite-related igneous rocks, sediments, and metamorphic rocks. It is common in pegmatites. The distribution coefficients shown in fig. 21.19 imply mild selectivity in favor of the light lanthanides; values derived from studies of Skaergaard apatite implied a preference for middle lanthanides. Most apatites analyzed are enriched in light lanthanides. Fleischer and Altschuler (1969) have noted the tendency for lanthanide-bearing minerals from silica-rich rocks to be richer in heavy lanthanides than their counterparts from silica-poor, alkali-rich rocks. This tendency is clear in apatites from mafic, granite-related, and alkalic rocks studied by them and shown in fig. 21.27. This is principally a result of the average parent lanthanide distributions for those

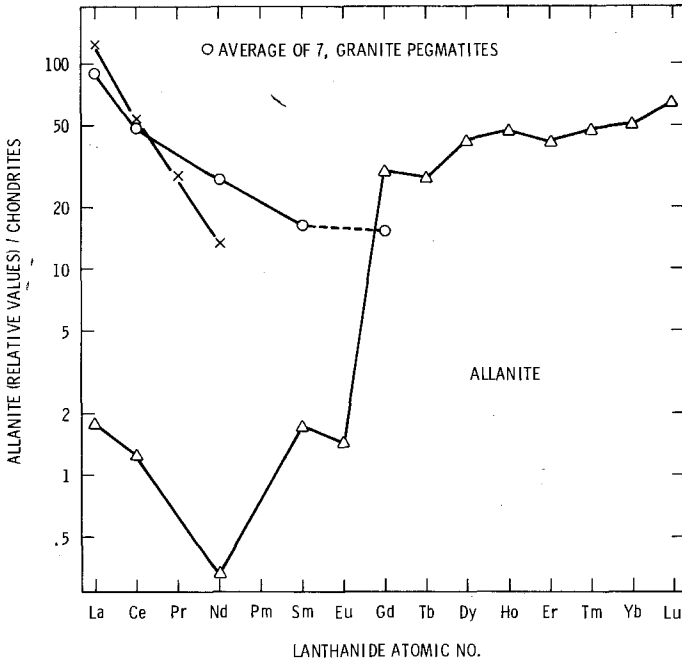


Fig. 21.26. Comparison diagram for allanites (Semenov and Barinskii, 1958). In this and subsequent figures, only relative values for lanthanides are plotted (as reported in the references) rather than concentration ratios. Allanite enriched in light lanthanides is rare.

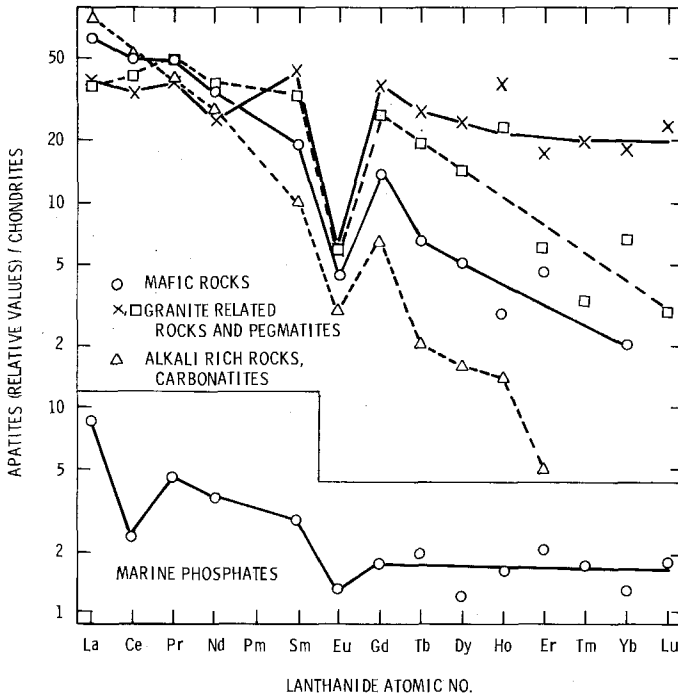


Fig. 21.27. Comparison diagram for apatites, based on averages for different rock types (Fleischer and Altschuler, 1969).

different rock types. An average for sedimentary apatites in marine deposits (fig. 21.27) shows the Ce deficiency characteristic of lanthanide distributions derived from that of sea water.

The bastnaesite-synchisite series of lanthanide minerals can be considered in terms of stoichiometric ratios of RCO_3F to CaCO_3 in proportions 1:0, 1:1, 2:1, and 3:2. The minerals of this series are much more rare than allanite or apatite but are fairly common in alkalic rock suites and in some metamorphic terrains. This mineral occurs in commercially important amounts in carbonatite associated with other alkalic rocks at Mountain Pass, California. The mineral is usually light-lanthanide rich, although rare heavy-lanthanide rich examples are known (fig. 21.28).

Fluorite is a lanthanide-concentrating mineral that is normally rather pure CaF_2 . It is a common, late-crystallizing mineral in granite-related rocks and pegmatites, usually strongly alkaline varieties. It appears to favor heavy lanthanides as it seldom shows really strong light-lanthanide enrichment. This apparent preference may be due less to crystal structure than to the ability of fluoride to hold heavy lanthanides in solution better than light lanthanides to a late stage of crystallization. Some representative lanthanide distributions for fluorite are given in fig. 21.28.

Monazite is a light-lanthanide mineral of composition RPO_4 . It is a common

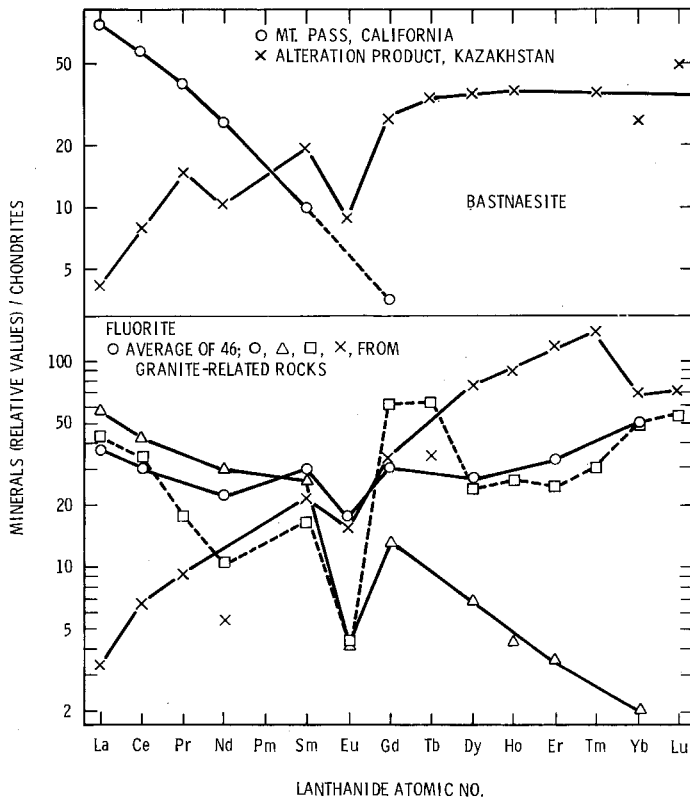


Fig. 21.28. Comparison diagram for bastnaesites, including rare, heavy-lanthanide rich variety (Semenov and Barinskii, 1958; Vlasov, 1966) and fluorites (Fleischer, 1969).

accessory mineral of low abundance in many granite-related rocks and pegmatites and is often associated with xenotime, its heavy-lanthanide counterpart. The strong selectivities of these two minerals are apparent in the distributions shown in figs. 21.29 and 21.30.

Perovskite is a lanthanide-concentrating mineral that in pure form would be CaTiO_3 but tends to be complex with several elements (e.g., Na, Fe, Th, U, Mn, R) substituting for Ca, and several (e.g., Nb, Ta, Fe, Mg, Zr) substituting for Ti. Lanthanide-rich varieties are mainly associated with alkalic igneous rock suites. Those suites tend to be strongly enriched in light lanthanides. Perovskites (fig. 21.30) are enriched in light lanthanides, but so strongly that the mineral is selective in favor of those elements.

Sphene is another Ca, Ti mineral that in some cases concentrates lanthanides. Its composition is characterized as $\text{CaTiSiO}_4\text{X}_2$ where X is $\frac{1}{2}\text{O}^{2-}$, OH^- , F^- . The lanthanide-rich variety sometimes occurs as an accessory mineral in coarse-grained granite-related rocks, pegmatites, and some metamorphic terrains. Most

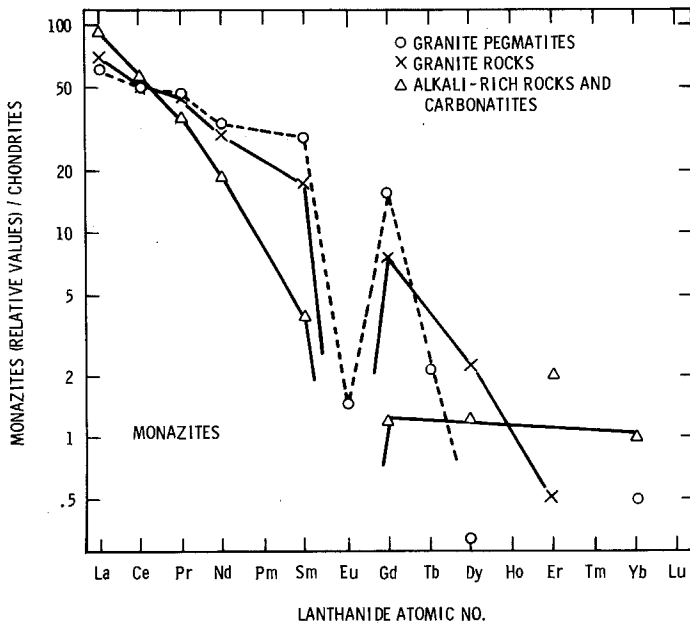


Fig. 21.29. Comparison diagram for monazites from different rock types (Fleischer and Altschuler, 1969).

sphenes for which analyses have been reported are enriched in light lanthanides relative to chondrites (fig. 21.31).

Zircon, $ZrSiO_4$, is a common but sparse accessory mineral in alkaline igneous rocks and some pegmatites. It is fairly resistant to weathering and metamorphic processes and can be concentrated in placer or beach sand deposits. Zircons accept a spectrum of lanthanide distributions as is evident from the two shown in fig. 21.32.

It is not yet possible to explain the variations in lanthanide distributions of these minerals in terms of those of their parent liquids. There are many analyses of lanthanide minerals in the literature, but very few by modern techniques, so that extents of variation or sizes of Eu anomalies are not well known. Most of the mineral analyses are not complemented by whole-rock analyses for their hosts. In many cases, the minerals crystallized from very late-stage differentiates within their hosts and the distributions of lanthanides in those differentiates cannot be determined by direct analysis.

For commercial producers, an otherwise lanthanide-rich ore can prove disappointing if it is deficient in a vital element. In particular, separation of Eu from the other lanthanides by incorporation at low concentrations in feldspars during magmatic differentiation depletes many mineral supplies in that important element. Analyses of potential ores for all lanthanides can be prohibitively expensive. Haskin and Korotev (1973) showed the use of interpolating and extrapolating analytical data for a few elements on a chondrite comparison diagram as a

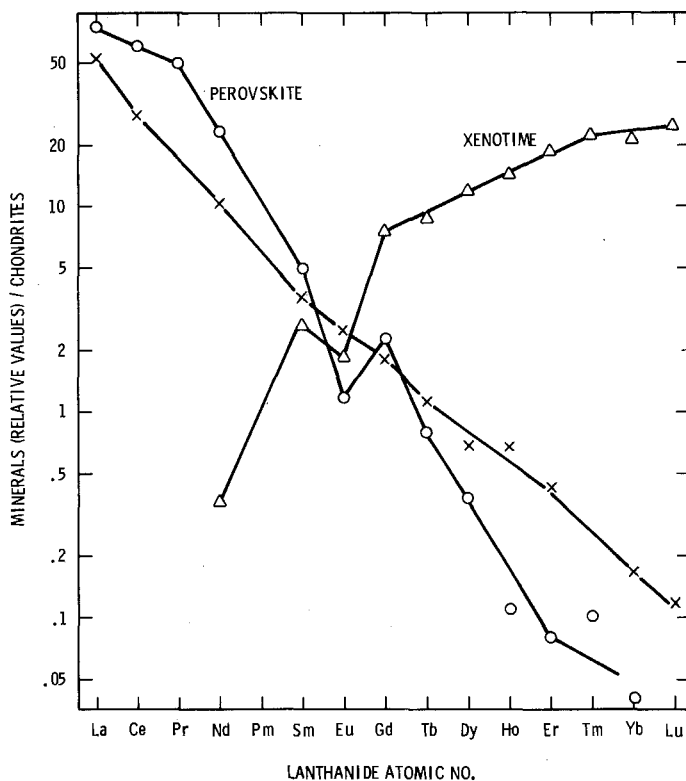


Fig. 21.30. Comparison diagram for perovskites (Bulakh et al., 1973; Haskin and Korotev, 1973) and xenotime (Åmli, 1975).

means of estimating concentrations of elements not analyzed. Such a procedure cannot allow for Eu anomalies.

8.3. Uses of lanthanides

In the early 1960's the total consumption of lanthanides was $\sim 1.6 \times 10^3$ metric tons, used mainly in lighter flints, carbon arc electrodes, and glass polishing powders (Petrick et al., 1973). By 1975 the consumption was more than 20×10^3 metric tons and the main uses were in metallurgy ($\sim 45\%$), catalysts and chemicals ($\sim 36\%$), glasses and ceramics ($\sim 17\%$), and electronics ($\sim 2\%$) (Cannon, 1976). The increase and changes in emphasis were the direct result of much research on the nature and possible applications of those elements.

The principal metallurgical applications are additions to iron, steel, aluminum, and magnesium. The major consumption is in the iron and steel industry; yet, only 0.3% of the annual tonnage from that industry is currently treated with lanthanides (J.G. Cannon, personal communication). Lanthanides provide improved physical properties to iron and steel through deoxidation, desul-

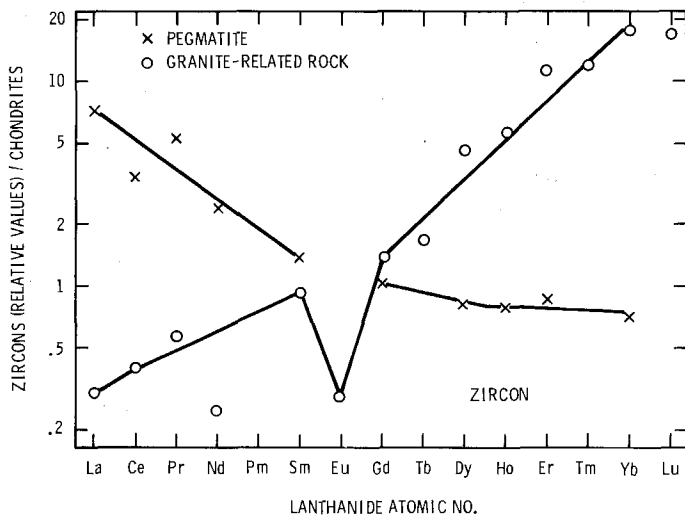


Fig. 21.31. Comparison diagram for sphenes (Semenov and Barinskii, 1958; Panov and Tarnovskaya, 1973).

phurization, sulphide shape control, hot corrosion resistance, grain refinement, and tramp element control. Major steel producers are still evaluating the economics of lanthanide additions. When they have worked out the optimum amounts to use, their consumption is expected to rise.

Unlike competitor alloy metals, the lanthanides have not increased much in

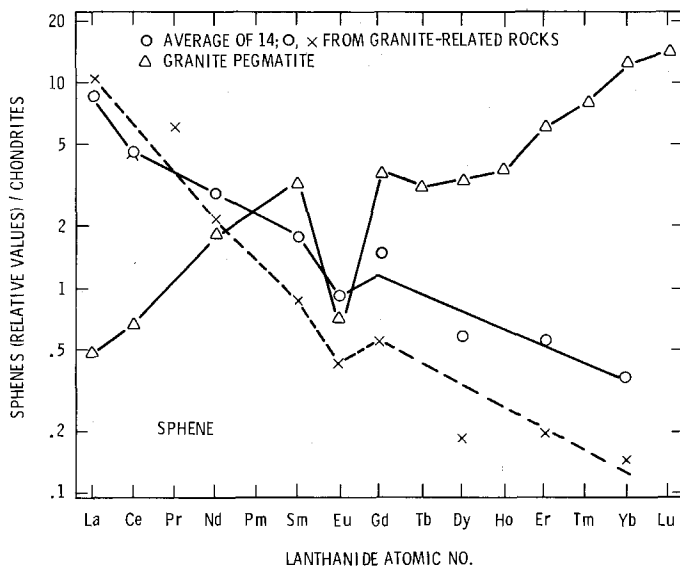


Fig. 21.32. Comparison diagram for zircons (Semenov and Barinskii, 1958; Vlasov, 1966).

price over the past decade, primarily due to the fast expansion of their market. For this reason plus the diversity of products they provide to iron and steel producers, the lanthanides will likely become components of new alloys such as high strength, low alloy steel. An increase from the present 0.3% lanthanide-treated iron and steel to 1.0% would raise world consumption of lanthanides by ~15%. The main lanthanide product used in metallurgy is mischmetal, a mixture of light lanthanide metals. Other additives include ferrosilicides, pure metal, and master alloys containing calcium, aluminum or magnesium. Samarium-cobalt alloy is currently used in the manufacture of permanent magnets for motors. These magnets provide ~50% greater torque horsepower than in conventional motors of the same size.

Lanthanides have been used in catalysts for petroleum cracking since 1966. Zeolite-based lanthanide cracking catalysts increase gasoline production by 3 gallons per barrel of crude oil as compared with silica-alumina catalysts.

Lanthanides have many uses in the chemical industry. They are provided in many product forms, e.g., as mixed chlorides with the same distribution as their parent (bastnaesite) ore and refined, individual oxides of 99.9% or better purity (Cannon, 1976). Separating individual lanthanides by ion exchange or liquid-liquid extraction is costly compared, for example, with the hydrometallurgical purification of vanadium, cobalt, or nickel. Only a few of the purified lanthanides are in demand and their sale must cover the entire cost of the elemental separations. If all the purified elements could be marketed, the cost of each would decrease, to the extent that the unit costs for some would be lower than those of competing alloy metals.

In glasses, cerium oxide is widely used as a decoloring agent; other lanthanide oxides are used to color glass. Lanthanides are used in glass polishing compounds. They are sometimes added to optical glass to increase the refractive index. Lanthanides also serve in ceramics as coloring agents. They are added to stabilize the structures of refractory zirconia and hafnia used in thermal cycling applications.

High purity oxides of yttrium and europium provide the red in color television picture tubes. Although the oxides sold for this purpose represent less than 1% of the annual tonnage of lanthanides used, they account for about 25% of sales. High purity gadolinium oxide is used in diagnostic X-ray screens. A terbium-activated gadolinium oxysulfide phosphor produces a brighter image and 80% lower X-ray dosage to patients in comparison with conventional phosphors.

The lanthanides are also used in the electronics industry in the form of YAG (yttrium-aluminum-garnet) crystals, which are used as microwave filters and control devices. When doped with small quantities of Nd or Er, the garnets can be used as lasers. These garnets have a brilliance similar to diamond and are used as gem stones. Lanthanides are also used to a limited degree in the miniturization of capacitors and the production of thermistors.

The major uses of lanthanides today are not necessarily those of tomorrow. The metallurgical industry uses ~45% of the total and indications are for modest growth of ~5% annually. The uses of lanthanide metallo-organic compounds as

anti-knock fuel additives and lanthanide catalytic converters for auto exhausts are under study. Adoption of either of these uses could make the catalyst/chemical category the leading consumer. The affinity of the lanthanides for phosphate is being investigated as a possible solution to fresh-water lake eutrophication. Treatment of all waste water in the United States would nearly double the present annual U.S. production.

Significant uses of the future might also include additives in nuclear control rods to absorb thermal neutrons, production of solid electrolytes for fuel cells that can convert hydrogen directly into electricity, and as substrates for bubble domain memory devices, possibly the basis for the next generation of computers.

8.4. *Assessment of lanthanide resources*

The lanthanides are more abundant in the Earth's crust than many better known metals. The other metals are better known in part because nature has concentrated them in forms that make their recovery economical. The lanthanides are rarely concentrated and even when they are, their chemical beneficiation is usually more costly than for competing metals. In some cases, lanthanides become available as coproducts from mining operations for other metals, e.g., placer tin and titanium deposits, uranium processing liquors. In these operations the burden of mining cost is borne by the other metals.

The minerals from which most lanthanide production currently comes are bastnaesite, monazite, and xenotime. Bastnaesite is the major source for the light lanthanides (La-Gd) and xenotime-monazite mixtures for the heavy lanthanides, with the light lanthanides as coproducts.

More than 70% of the world's production of lanthanides since 1973 has come from the bastnaesite-rich carbonatite body at Mountain Pass, California. This ore body, operated by Molycorp, Inc., has the capacity to meet world demand at the present rate for ~100 years. No other lanthanide ore body of comparable size and grade is known. The development of the Mountain Pass ore body was a major factor in bringing about the current uses and research into industrial applications of the lanthanides. It made them available in reasonably large quantities at competitive prices.

There are no significant amounts of monazite production or of heavy lanthanide production in the U.S. at present. Most U.S. and foreign needs for heavy lanthanides are met through placer operations in Malaysia, Thailand, Brazil, and India, where byproduct monazite and xenotime are recovered from the mining of titanium and tin. A heavy lanthanide concentrate (primarily Y) is produced in Canada from the processing stream of a uranium extraction mill.

What does the future hold for lanthanide needs and supplies? By the time the Mountain Pass deposit has been depleted, supplies of many metals with which lanthanides compete will also have been depleted. This could make lanthanides indispensable in applications that now use other metals. This would cause the

economics of the industry to change. Ores that now yield lanthanides as byproducts or coproducts might become principal ores.

The use of monazite and xenotime is generally linked to the demand of other economically recoverable elements, e.g., titanium (sphene, rutile, ilmenite), tin (cassiterite), niobium (euxenite), zirconium (zircon) in placer alluvial, fluvial, eluvial, and beach deposits. Rarely has monazite or xenotime occurred in great enough concentration to make it economically recoverable as a primary ore mineral. Nevertheless, there is a considerable worldwide reserve of these minerals which could be processed in the future under more favorable economic conditions.

Should thorium become important for nuclear reactors, a surge in production of monazite, a principal thorium source, would result. Lanthanide sulfates are a byproduct of thorium production from monazite. Placer rutile reserves are already nearly depleted and ilmenite is expected to be the primary titanium source in the years to come. Monazite would be a byproduct of placer ilmenite production.

Zircon is a potential source of yttrium and heavy lanthanides. However, the present demand for zirconium is not great nor is it expected to be in the intermediate future. The principal use for zirconium is in nuclear reactor core material and refractories.

Although they are not usually considered as part of the world reserves of titanium, there are very large tonnages of lanthanide-bearing perovskite. Some perovskite bodies in alkaline complexes contain an average grade of 10–20% perovskite. If even one such ore body were to be developed for titanium, by-product light lanthanides would become available with an estimated tonnage that, at current consumption rates, could supply the world market for 25–100 years. The world demand for titanium, however, is not expected to be large enough to consume the amount of titanium generated from such an operation over that period of time.

Another possible type of low grade lanthanide deposit is carbonatite laterites. The insolubility of lanthanide compounds during weathering and the solubility of carbonates results in slight enrichment in lanthanide concentration for the weathered product relative to the parent carbonatite. Reliable estimates of grade and tonnage are lacking. The affinity of lanthanides for phosphates released during the weathering of apatite causes the lanthanides to precipitate in secondary minerals (e.g., rhabdophane, monazite, and goyazite-gorceixite). The low concentrations, the contained impurities and the exceedingly fine-grained nature of these minerals present make it unlikely that such deposits could become a competitive, primary source now or in the long term.

Apatite could eventually become an important lanthanide source. Marine apatites of biological origin are surprisingly enriched in lanthanides in view of the low lanthanide contents of seawater. Lanthanides liberated during commercial production of phosphoric acid could be recovered. Lanthanide concentrations in these apatites are low compared to those of currently used ores but

tonnages processed are high and reserves are great. The demand for phosphate fertilizers would seem to assure a steady source of byproduct lanthanide. Adams and Staatz (1973) have estimated that 4000 tons of yttrium are being mined annually from the Retort and Meade Peak Members of the Phosphoria Formation in the western United States. Although their figures are based on insufficient sampling for this purpose by Gulbrandsen (1966) (who had different objectives in mind) they indicate the tendency of the marine phosphates to concentrate yttrium.

Igneous apatites could also serve as lanthanide sources; byproduct lanthanides have been recovered from a vein-type occurrence of apatite in Finland. Many igneous apatite ores are mined for fertilizer in Brazil, South Africa, and the U.S.S.R., but in none of these operations are the lanthanides extracted. More than enough tonnage of lanthanides is presently being discarded during phosphate production than is needed to meet current world needs for those elements.

Some other lanthanide-bearing mineral could become a significant ore in the future if a suitable deposit were discovered, but the main tonnage and the certain supply are those more dilute occurrences discussed above. Lanthanide reserves appear adequate to meet anticipated needs into the distant future.

References

- Adams, J.W. and E.R. Iberall, 1973, U.S.G.S. Bull. 1366.
- Adams, J.W. and M.H. Staatz, 1973, U.S.G.S. Prof. Paper 820, 547-556.
- Albarede, F. and Y. Bottinga, 1972, *Geochim. Cosmochim. Acta* **36**, 141.
- Aleksiyev, E.I., 1970, *Geochem. Int.* **7**, 127.
- Aleksiyev, E.I. and M. Zhelyazkova-Panayotova, 1972, *Geochem. Int.* **8**, 779.
- Ämli, R., 1975, *Am. Mineral.* **60**, 607.
- Anderson, J.L. and R.L. Cullers, 1976, *Geochim. Cosmochim. Acta*, to be published.
- Arth, J.G. and G.N. Hanson, 1972, *Contrib. Mineral. Petrol.* **37**, 161.
- Arth, J.G. and G.N. Hanson, 1975, *Geochim. Cosmochim. Acta* **39**, 325.
- Balashov, Yu.A., 1972, *Geochem. Int.* **9**, 320.
- Balashov, Yu.A. and G.V. Nesterenko, 1966, *Geochem. Int.* 672.
- Balashov, Yu.A., A.B. Ronov, A.A. Migdisov and N.V. Turanskaya, 1964, *Geochem. Int.* 951.
- Balashov, Yu.A., M.A. Kekeliya and D.G. Nadareyshvili, 1969, *Geochem. Int.* **6**, 476.
- Balashov, Yu.A., L.V. Dmitriev and A.Ya. Sharas'kin, 1970a, *Geochem. Int.* **7**, 456.
- Balashov, Yu.A., M.Ya. Frenkel' and A.A. Yaroshevskiy, 1970b, *Geochem. Int.* **7**, 611.
- Banno, S. and Y. Matsui, 1973, *Chem. Geol.* **11**, 1.
- Bender, M., W. Broecker, V. Gornitz, U. Middel, R. Kay, S.-S. Sun and P. Biscaye, 1971, *Earth Planet. Sci. Lett.* **12**, 425.
- Blanchard, D.P., L.A. Haskin, J.W. Jacobs, J.C. Brannon and R.L. Korotev, 1975a, *The Moon* **14**, 359.
- Blanchard, D.P., R.L. Korotev, J.C. Brannon, J.W. Jacobs, L.A. Haskin, A.M. Reid, C.H. Donaldson and R.W. Brown, 1975b, *Proc. Sixth Lunar Sci. Conf., Geochim. Cosmochim. Acta, Suppl.* **6** 2, 2321.
- Blanchard, D.P., J.M. Rhodes, M.A. Dungan, K.V. Rodgers, C.H. Donaldson, J.C. Brannon, J.W. Jacobs and E.K. Gibson, 1976, *J. Geophys. Res.* **81**, 4231.
- Borchardt, G.A., M.E. Harward and R.A. Schmitt, 1971, *Quaternary Res.* **1**, 247.
- Bowden, P. and J.E. Whitley, 1974, *Lithos* **7**, 15.
- Boynton, W.V., 1975, *Geochim. Cosmochim. Acta* **39**, 569.
- Bryan, W.B., G. Thompson, F.A. Frey and J.S. Dickey, 1976, *J. Geophys. Res.* **81**, 4285.
- Bulakh, A.G., V.N. Karpatenkov and G.F. Anastasanko, 1973, *Miner. Paragenезisy Miner. Gorn. Porod*, 7-17 (in Russian).
- Tatarinov, P.M., ed., "Nauka," Leningrad. Otd: Leningrad, USSR Chem. Abs., 1974, **80**, No. 147667.
- Buma, G., F.A. Frey and D.R. Wones, 1971, *Contrib. Mineral. Petrol.* **31**, 300.
- Cannon, J.G., 1976, *Engineering Mining J.* **177**, 184.
- Capaldi, G., P. Gasparini, A. Moauro, E. Salvia and O. Travaglione, 1972, *Earth Planet. Sci. Lett.* **17**, 247.
- Clayton, D.D., 1968, *Principles of Stellar Evolution and Nucleosynthesis* (McGraw-Hill, Inc., New York).
- Condie, K.C. and W.R.A. Baragar, 1974, *Contrib. Mineral. Petrol.* **45**, 237.
- Condie, K.C. and D.L. Hayslip, 1975, *Geochim. Cosmochim. Acta* **39**, 1165.

- Condie, K.C. and H.H. Lo, 1971, *Geochim. Cosmochim. Acta* **35**, 1099.
- Condie, K.C. and D.H. Swenson, 1973, *Bull. Volcanol.* **37**, 205.
- Copeland, R.A., F.A. Frey and D.R. Wones, 1971, *Earth Planet. Sci. Lett.* **10**, 186.
- Cullers, R.L., L.G. Medaris, Jr. and L.A. Haskin, 1970, *Science* **169**, 580.
- Cullers, R.L., L.G. Medaris and L.A. Haskin, 1973, *Geochim. Cosmochim. Acta* **37**, 1499.
- Cullers, R.L., S. Chaudhuri, B. Arnold, M. Lee and C.W. Wolf, Jr., 1975, *Geochim. Cosmochim. Acta* **39**, 1691.
- Deer, W.A., R.A. Howie and J. Zussman, 1962, *Rock-Forming Minerals*, vols. 1 and 5 (John Wiley, New York).
- DePaolo, D.J. and G.J. Wasserburg, 1976, *Geophys. Res. Lett.* **3**, 249.
- Doerner, H. and W. Hoskins, 1925, *J. Am. Chem. Soc.* **47**, 662.
- Drake, M.J., 1975, *Geochim. Cosmochim. Acta* **39**, 55.
- Drake, M.J. and D.F. Weill, 1975, *Geochim. Cosmochim. Acta* **39**, 689.
- Duchesne, J.C., I. Roelands, D. Demaiffe, J. Hertogen, R. Gijbels and J. de Winter, 1974, *Earth Planet. Sci. Lett.* **24**, 325.
- Dudas, M.J., R.A. Schmitt and M.E. Harward, 1971, *Earth Planet. Sci. Lett.* **11**, 440.
- Eby, G.N., 1975, *Geochim. Cosmochim. Acta* **39**, 597.
- Ehrlich, A.M., 1968, Rare earth abundances in manganese nodules, Ph.D. Thesis, MIT.
- Ewart, A., W.B. Bryan and J.B. Gill, 1973, *J. Petrol.* **14**, 429.
- Fesq, H.W., E.J.D. Kable and J.J. Gurney, 1975, *Phys. Chem. Earth* **9**, 687.
- Fleet, A.J., P. Henderson and D.R.C. Kempe, 1976, *J. Geophys. Res.* **81**, 4257.
- Fleischer, M., 1966, *Am. Mineral.* **51**, 1247.
- Fleischer, M., 1969, *Indian Mineral.* **10**, 36.
- Fleischer, M. and Z.S. Altschuler, 1969, *Geochim. Cosmochim. Acta* **33**, 725.
- Flower, M.F.J., 1971, *Contrib. Mineral. Petrol.* **31**, 335.
- Fraser, D.G., 1975, *Geochim. Cosmochim. Acta* **39**, 1525.
- Frey, F.A., 1969, *Geochim. Cosmochim. Acta* **33**, 1429.
- Frey, F.A., 1970, *Earth Planet. Sci. Lett.* **7**, 351.
- Frey, F.A. and D.H. Green, 1974, *Geochim. Cosmochim. Acta* **38**, 1023.
- Frey, F.A. and L. Haskin, 1964, *J. Geophys. Res.* **69**, 775.
- Frey, F.A., M.A. Haskin, J.A. Poetz and L.A. Haskin, 1968, *J. Geophys. Res.* **73**, 6085.
- Frey, F.A., L.A. Haskin and M.A. Haskin, 1971, *J. Geophys. Res.* **76**, 2057.
- Frey, F.A., W.B. Bryan and G. Thompson, 1974, *J. Geophys. Res.* **79**, 5507.
- Frondel, C., 1958, *U.S.G.S. Bull.* **1064**, 11.
- Fujimaka, H., 1975, *J. Facul. Science, Univ. of Tokyo* **19**, 81.
- Ganapathy, R. and E. Anders, 1974, *Proc. Fifth Lunar Sci. Conf.*, *Geochim. Cosmochim. Acta, Suppl.* **5** 2, 1181.
- Garmann, L.B., A.O. Brunfelt, K.G. Finstad and K.S. Heier, 1975, *Chem. Geol.* **15**, 103.
- Gast, P.W., 1968, *Geochim. Cosmochim. Acta* **32**, 1057.
- Gerasimovskiy, V.I., Yu.A. Balashov and V.A. Karpushina, 1972, *Geochem. Int.* **9**, 305.
- Glasby, G.P., 1972-73, *Mar. Chem.* **1**, 105.
- Glassley, W., 1974, *Geol. Soc. Am. Bull.* **85**, 785.
- Goldberg, E.D., M. Koide, R.A. Schmitt and R.H. Smith, 1963, *J. Geophys. Res.* **68**, 4209.
- Goldschmidt, V.M., 1938, *Skrifter Norske Videnskaps-Akad. Oslo, I: Matnaturv. Kl.*, No. 4, 1.
- Green, D.H. and A.E. Ringwood, 1963, *J. Geophys. Res.* **68**, 937.
- Green, T.H., A.O. Brunfelt and K.S. Heier, 1969, *Earth Planet. Sci. Lett.* **7**, 93.
- Green, T.H., A.O. Brunfelt and K.S. Heier, 1972, *Geochim. Cosmochim. Acta* **36**, 241.
- Greenland, L.P., 1970, *Am. Mineral.* **55**, 455.
- Griffin, J.B., A.A. Grodus and G.A. Wright, 1969, *Am. Antiquity* **34**, 1.
- Griffin, W.L., B. Sundvoll and H. Kristmannsdottir, 1974, *Earth Planet. Sci. Lett.* **24**, 213.
- Grossman, L., 1972, *Geochim. Cosmochim. Acta* **36**, 597.
- Grossman, L., 1973, *Geochim. Cosmochim. Acta* **37**, 1119.
- Grossman, L. and S.P. Clark, Jr., 1973, *Geochim. Cosmochim. Acta* **37**, 635.
- Grutzeck, M., S. Kridelbaugh and D. Weill, 1974, *Geophys. Res. Lett.* **1**, 273.
- Gulbrandsen, R.A., 1966, *Geochim. Cosmochim. Acta* **30**, 769.
- Hanson, G.N. and S.S. Goldich, 1972, *Geol. Soc. Amer. Mem.* **135**, 179.
- Haskin, L.A. and F.A. Frey, 1966, *Science* **152**, 299.
- Haskin, L.A. and M.A. Gehl, 1962, *J. Geophys. Res.* **67**, 2537.
- Haskin, L.A. and M.A. Haskin, 1968, *Geochim. Cosmochim. Acta* **32**, 433.
- Haskin, L.A. and R.L. Korotev, 1973, Determination of rare earths in geological samples and raw materials, in: *Analysis and Application of Rare Earth Materials. Proceedings of NATO Institute of Rare Earth Analysis.*
- Haskin, L.A. and R.L. Korotev, 1977, *Geochim. Cosmochim. Acta* **41**, 921.
- Haskin, L.A., F.A. Frey, R.A. Schmitt and R.H. Smith, 1966a, Meteoritic, solar and terrestrial rare earth distributions, in: *Physics and Chemistry of the Earth* (Pergamon Press, New York) pp. 167.
- Haskin, L.A., T.R. Wildeman, F.A. Frey, K.A. Collins, C.R. Keedy and M.A. Haskin, 1966b, *J. Geophys. Res.* **71**, 6091.
- Haskin, L.A., M.A. Haskin, F.A. Frey and T.R. Wildeman, 1968, Relative and absolute terrestrial abundances of the rare earths, in: *Origin and Distribution of the Elements* (Pergamon Press, New York), pp. 889-912.
- Haskin, L.A., R.O. Allen, P.A. Helmke, T.P. Paster, M.R. Anderson, R.L. Korotev and

- K.A. Zweifel, 1970, Proc. Apollo 11 Lunar Sci. Conf., *Geochim. Cosmochim. Acta*, Suppl. 1 2, 1213.
- Haskin, L.A., P.A. Helmke, D.P. Blanchard, J.W. Jacobs and K. Telander, 1973, Proc. Fourth Lunar Sci. Conf., *Geochim. Cosmochim. Acta*, Suppl. 4 2, 1275.
- Haskin, L.A., C.-Y. Shih, B.M. Bansal, J.M. Rhodes, H. Wiesmann and L.E. Nyquist, 1974, Proc. Fifth Lunar Sci. Conf., *Geochim. Cosmochim. Acta*, Suppl. 5 2, 1213.
- Haskin, M.A. and L.A. Haskin, 1966, *Science* **154**, 507.
- Hayes, D.W., J.F. Slowey and D.W. Hood, 1965, *Trans. Am. Geophys. Union* **46**, 548.
- Helmke, P.A. and L.A. Haskin, 1973, *Geochim. Cosmochim. Acta* **37**, 1513.
- Helmke, P.A., L.A. Haskin, R.L. Korotev and K.E. Ziege, 1972, Proc. Third Lunar Sci. Conf., *Geochim. Cosmochim. Acta*, Suppl. 3 2, 1275.
- Henderson, P., S.J. Fishlock, J.C. Laul, T.D. Cooper, R.L. Conard, W.V. Boynton and R.A. Schmitt, 1976, *Earth Planet. Sci. Lett.* **30**, 37.
- Herrmann, A.G., 1968, *Contrib. Mineral. Petrol.* **17**, 275.
- Herrmann, A.G. and D. Jung, 1970, *Contrib. Mineral. Petrol.* **29**, 33.
- Herrmann, A.G. and K.H. Wedepohl, 1966, *Contrib. Mineral. Petrol.* **13**, 366.
- Herrmann, A.G. and K.H. Wedepohl, 1970, *Contrib. Mineral. Petrol.* **29**, 255.
- Herrmann, A.G., M.J. Potts and D. Knake, 1974, *Contrib. Mineral. Petrol.* **44**, 1.
- Herrmann, A.G., D.P. Blanchard, L.A. Haskin, J.W. Jacobs, D. Knake, R.L. Korotev and J.C. Brannon, 1976, *Contrib. Mineral. Petrol.* **59**, 1.
- Hertogen, J. and R. Gijbels, 1976, *Geochim. Cosmochim. Acta* **40**, 313.
- Higuchi, H. and H. Nagasawa, 1969, *Earth Planet. Sci. Lett.* **7**, 281.
- Høgdahl, O., NATO Research Grant #203 Semiannual Progress Reports Nos. 1-6, Scientific Affairs Division, Paris, 1965-1968.
- Høgdahl, O.T., S. Melson and V. Bowen, 1968, *Adv. Chem. Ser.* **73**, 308.
- Hubbard, N.J., 1969, *Earth Planet. Sci. Lett.* **5**, 346.
- Hubbard, N.J. and P.W. Gast, 1971, Proc. Second Lunar Sci. Conf., *Geochim. Cosmochim. Acta*, Suppl. 2 2, 999.
- Hubbard, N.J. and J.W. Minear, 1975, Proc. Sixth Lunar Sci. Conf., *Geochim. Cosmochim. Acta*, Suppl. 6 1, 1057.
- Hubbard, N.J., J.M. Rhodes and P.W. Gast, 1973, *Science* **181**, 339.
- Jahn, B.-M., C.-Y. Shih and V.R. Murthy, 1974, *Geochim. Cosmochim. Acta* **38**, 611.
- Jakeš, P. and J. Gill, 1970, *Earth Planet. Sci. Lett.* **9**, 17.
- Jakeš, P. and S.R. Taylor, 1974, *Geochim. Cosmochim. Acta* **38**, 739.
- Jibiki, H. and A. Masuda, 1974, *Mar. Geol.* **16**, 205.
- Kay, R.W. and P.W. Gast, 1973, *J. Geol.* **81**, 653.
- Kay, R. and R. Senechal, 1972, *Trans. Am. Geophys. Union* **53**, 536.
- Kay, R., N.J. Hubbard and P.W. Gast, 1970, *J. Geophys. Res.* **75**, 1585.
- Koljonen, T. and R.J. Rosenberg, 1974, *Lithos* **7**, 249.
- Laul, J.C. and R.A. Schmitt, 1975, Proc. Sixth Lunar Sci. Conf., *Geochim. Cosmochim. Acta*, Suppl. 6 2, 1231.
- Levinson, A.A., 1966, *Am. Mineral.* **51**, 152.
- Loubet M., M. Bernat, M. Javoy and C.J. Allegre, 1972, *Earth Planet. Sci. Lett.* **14**, 226.
- Lugmair, G.W., N.B. Scheinin and K. Marti, 1975, Proc. Sixth Lunar Sci. Conf., *Geochim. Cosmochim. Acta*, Suppl. 6 2, 1419.
- Lyakhovich, V.V., 1968, *Geochem. Int.* **4**, 691.
- Masuda, A., 1966, *Geochem. J.* **1**, 11.
- Masuda, A., 1968, *Earth Planet. Sci. Lett.* **4**, 284.
- Masuda, A. and H. Jibiki, 1973, *Geochem. J.* **7**, 55.
- Masuda, A. and I. Kushiro, 1970, *Contrib. Mineral. Petrol.* **26**, 42.
- Masuda, A., T. Shimokawa, H. Jibiki and T. Nagawa, 1974, *Contrib. Mineral. Petrol.* **48**, 265.
- McIntire, W., 1963, *Geochim. Cosmochim. Acta* **27**, 1209.
- Menzies, M., 1976, *Earth Planet. Sci. Lett.* **28**, 427-438.
- Minami, E., 1935, *Nachr. Ges. Wiss. Göttingen, Math.-Physik, Kl. IV.* **1**, 155.
- Mineev, D.A., 1969, *Lantanoidy v Mineralakh (Izdatel'stvo Nedra, Moscow, U.S.S.R.)* 182 p.
- Mineev, D.A., T.I. Lavrishcheva and A.V. Bykova, 1970, *Zap. Vses. Mineral. Obshchest.* **99**, 328 (in Russian). *Am. Mineral.* **1972**, **57**, 594.
- Mineyev, D.A., 1963, *Geochemistry* **12**, 1129.
- Mitchell, R.H. and A.O. Brunfelt, 1975, *Phys. Chem. Earth* **9**, 671.
- Mitchell, R.H. and D.A. Carswell, 1976, *Earth Planet. Sci. Lett.* **31**, 175.
- Montigny, R., H. Bougault, Y. Bottinga and C.J. Allegre, 1973, *Geochim. Cosmochim. Acta* **37**, 2135-2147.
- Moorbath, S., R.K. O'Nions and R.J. Pankhurst, 1975, *Earth Planet. Sci. Lett.* **27**, 229.
- Morris, R.V., 1975, *Geochim. Cosmochim. Acta* **39**, 621.
- Morris, R.V. and L.A. Haskin, 1974, *Geochim. Cosmochim. Acta* **38**, 1435.
- Morris, R.V., L.A. Haskin, G.M. Biggar and M.J. O'Hara, 1974, *Geochim. Cosmochim. Acta* **38**, 1447.
- Mysen, B., 1976, *Earth Planet. Sci. Lett.* **31**, 1.
- Nagasawa, H., 1971, *Earth Planet. Sci. Lett.* **13**, 139.
- Nagasawa, H., 1973, *Contrib. Mineral. Petrol.* **39**, 301.
- Nagasawa, H. and C.C. Schnetzler, 1971, *Geochim. Cosmochim. Acta* **35**, 953.
- Nagasawa, H., H. Wakita, H. Higuchi and N. Onuma, 1969, *Earth Planet. Sci. Lett.* **5**, 377.
- Nakamura, N., 1974, *Geochim. Cosmochim. Acta* **38**, 757.

- Nakamura, N. and A. Masuda, 1971, *Nature Phys. Sci.* **233**, 130.
- Nakamura, N. and A. Masuda, 1973, *Meteoritics* **8**, 149.
- Neumann, H., B.B. Jensen and A.O. Brunfelt, 1966, *Norsk Geologisk Tidsskrift* **46**, 141.
- Nicholls, G.D. and M.R. Islam, 1971, *Phil. Trans. Roy. Soc. Lond. A* **268**, 469.
- O'Nions, R.K. and K. Grönvold, 1973, *Earth Planet. Sci. Lett.* **19**, 397.
- O'Nions, R.K. and R.J. Pankhurst, 1974, *Earth Planet. Sci. Lett.* **22**, 328.
- Onuma, N., H. Higuchi, H. Wakita and H. Nagasawa, 1968, *Earth Planet. Sci. Lett.* **5**, 47.
- Osawa, M. and G.G. Goles, 1970, Trace element abundances in Columbia River basalts, in: Gilmour, E.H. and D. Stradling, eds., *Proceedings of the Second Columbia River Basalt Symposium*, Cheney, Washington, March 1969 (Eastern Washington State College Press, Cheney) pp. 55.
- Palache, C., H. Berman and C. Frondel, 1951, *System of Mineralogy (of Dana)*, vols. I and II, 7th ed. (John Wiley, New York).
- Panov, E.N. and A.N. Tarnovskaya, 1973, *Geochim. Int.* **10**, 102.
- Paster, T.P., D.S. Schauwecker and L.A. Haskin, 1974, *Geochim. Cosmochim. Acta* **38**, 1549.
- Paul, D.K., P.J. Potts, I.L. Gibson and P.G. Harris, 1975, *Earth Planet. Sci. Lett.* **25**, 151.
- Petric, A. Jr., H.J. Benett, K.E. Starch and R.C. Weisner, *The Economics of Byproduct Metals (in two parts) Part II*, Bureau of Mines Information Circular 8570, 1973, p. 69.
- Philpotts, J.A., 1970, *Earth Planet. Sci. Lett.* **9**, 257.
- Philpotts, J.A. and C.C. Schnetzler, 1968, *Chem. Geol.* **3**, 5.
- Philpotts, J.A. and C.C. Schnetzler, 1969, *Chem. Geol.* **4**, 464.
- Philpotts, J.A. and C.C. Schnetzler, 1970, *Geochim. Cosmochim. Acta* **34**, 307.
- Philpotts, J.A., C.C. Schnetzler and H.H. Thomas, 1966, *Nature* **212**, 805.
- Philpotts, J.A., C.C. Schnetzler and S.R. Hart, 1969, *Earth Planet. Sci. Lett.* **7**, 293.
- Philpotts, J.A., W. Martin and C.C. Schnetzler, 1971, *Earth Planet. Sci. Lett.* **12**, 89.
- Philpotts, J.A., C.C. Schnetzler and H.H. Thomas, 1972, *Geochim. Cosmochim. Acta* **36**, 1131.
- Philpotts, J.A., S. Schuhmann, C.W. Kouns, R.K.L. Lum and S. Winzer, 1974, *Proc. Fifth Lunar Sci. Conf.*, *Geochim. Cosmochim. Acta*, Suppl. **5**, 2, 1255.
- Piper, D.Z., 1974, *Chem. Geol.* **14**, 285.
- Potts, M.J. and K.C. Condie, 1971, *Contrib. Mineral. Petrol.* **33**, 245.
- Press, F. and R. Siever, 1974, *Earth (W.H. Freeman & Co., San Francisco)*.
- Price, R.C. and S.R. Taylor, 1973, *Contrib. Mineral. Petrol.* **40**, 195.
- Ragland, P.C., A.O. Brunfelt and P.W. Weigand, 1971, Rare earth abundances in Mesozoic dolerite dikes from eastern United States, in: Brunfelt, A.O. and E. Steignes, eds., *Activation Analysis in Geochemistry and Cosmochemistry (Universitetsforlaget)* pp. 227.
- Randle, K., G.G. Goles and L.R. Kittleman, 1971, *Quaternary Res.* **1**, 261.
- Reid, J.B. Jr. and F.A. Frey, 1971, *J. Geophys. Res.* **76**, 1184.
- Richard, P., N. Shimizu and C.J. Allègre, 1976, *Earth Planet. Sci. Lett.* **31**, 269.
- Ridley, W.I. and J.B. Dawson, 1975, *Phys. Chem. Earth* **9**, 559.
- Roaldset, E., 1975, *Geochim. Cosmochim. Acta* **39**, 455.
- Roberts, W.L., G.R. Rapp Jr. and J. Weber, 1974, *Encyclopedia of Minerals (Van Nostrand Reinhold, New York)*.
- Robertson, A.H.F. and A.J. Fleet, 1976, *Earth Planet. Sci. Lett.* **28**, 385.
- Ronov, A.B., Yu. A. Balashov, Yu. P. Girin, R. Kh. Bratishko and G.A. Kazakov, 1972, *Geochim. Int.* **9**, 987.
- Ronov, A.B., Yu. A. Balashov, Yu. P. Girin, R. Kh. Bratishko and G.A. Kazakov, 1974, *Sedimentology* **21**, 171.
- Ross, J.E. and L.H. Aller, 1976, *Science* **191**, 1223.
- Schilling, J.-G., 1971, *Phil. Trans. Roy. Soc. Lond. A* **268**, 663.
- Schilling, J.-G., 1973, *Nature* **246**, 141.
- Schilling, J.-G., 1975a, *J. Geophys. Res.* **80**, 1459.
- Schilling, J.-G., 1975b, *Earth Planet. Sci. Lett.* **25**, 103.
- Schilling, J.-G. and A. Noe-Nygaard, 1974, *Earth Planet. Sci. Lett.* **24**, 1.
- Schilling, J.-G. and J.W. Winchester, 1967, Rare-earth fractionation and magmatic processes, in: Runcorn, S.K., ed., *Mantles of the Earth and Terrestrial Planets (Interscience Publishers, New York)* pp. 267.
- Schilling, J.-G. and J.W. Winchester, 1969, *Contrib. Mineral. Petrol.* **23**, 27.
- Schmitt, R.A., A.W. Moser, C.S. Suffredini, J.E. Lasch, R.A. Sharp and D.A. Olehy, 1960, *Nature* **186**, 863.
- Schnetzler, C.C. and J.A. Philpotts, 1968, Partition coefficients of rare-earth elements and barium between igneous matrix material and rock-forming-mineral phenocrysts—I, in: Ahrens, L.H., ed., *Origin and Distribution of the Elements (Pergamon Press, New York)* pp. 929.
- Schnetzler, C.C. and J.A. Philpotts, 1970, *Geochim. Cosmochim. Acta* **34**, 331.
- Schubert, C.E., 1972, *Nature Phys. Sci.* **237**, 26.
- Semenov, E.I. and R.L. Barinskii, 1958, *Geochim. Acta*, **3**, 398.
- Shaw, D.M., 1970, *Geochim. Cosmochim. Acta* **34**, 237.
- Shih, C.-Y., L.A. Haskin, H. Wiesmann, B.M. Bansal and J.C. Brannon, 1975, *Proc. Sixth Lunar Sci. Conf.*, *Geochim. Cosmochim. Acta*, Suppl. **6**, 2, 1255.
- Shimizu, N., 1975, *Earth Planet. Sci. Lett.* **25**, 26.
- Shimizu, N. and R.J. Arculus, 1975, *Contrib. Mineral. Petrol.* **50**, 231.

- Shimizu, N. and I. Kushiro, 1975, *Geophys. Res. Lett.* **2**, 413.
- Shimokawa, T. and A. Masuda, 1972, *Contrib. Mineral. Petrol.* **37**, 39.
- Shimokawa, T., A. Masuda and K. Izawa, 1972, *Geochem. J.* **6**, 75.
- Spirn, R.V., 1965, Rare earth distribution in the marine environment, Ph.D. Thesis, MIT.
- Sun, C.-O., R.J. Williams and S.-S. Sun, 1974, *Geochim. Cosmochim. Acta* **38**, 1415.
- Sun, S.S. and G.N. Hanson, 1975a, *Contrib. Mineral. Petrol.* **52**, 77.
- Sun, S.S. and G.N. Hanson, 1975b, *Geology*, 297.
- Tanaka, T. and A. Masuda, 1973, *Icarus* **19**, 523.
- Tanaka, T. and R. Sugisaki, 1973, *J. Petrol.* **14**, 489.
- Tanaka, T., N. Nakamura, A. Masuda and N. Onuma, 1975, *Nature* **256**, 27.
- Tauson, L.V., V.I. Kovalenko, A.S. Znamenskaya, L.L. Petrov, V.A. Legeido, E.I. Popolitov and S.R. Prokopenko, 1968, Distribution of rare earth elements (RE), yttrium, beryllium and tin in alkaline granitoids and their metasomatites, in: Ahrens, L.H., ed., *Origin and Distribution of the Elements* (Pergamon Press, New York) pp. 663.
- Taylor, S.R., 1975, *Lunar Science: A Post-Apollo View* (Pergamon Press, New York).
- Taylor, S.R., A. Ewart and A.C. Capp, 1968, *Lithos* **1**, 179.
- Taylor, S.R., A.C. Capp, A.L. Graham and D.H. Blake, 1969, *Contrib. Mineral. Petrol.* **23**, 1.
- Towell, D.G., J.W. Winchester and R.V. Spirn, 1965, *J. Geophys. Res.* **70**, 3485.
- Towell, D.G., R.V. Spirn and J.W. Winchester, 1969, *Chem. Geol.* **4**, 461.
- Tugarinov, A.I., Yu. A. Balashov and L.K. Gavrilova, 1973, *Geochem. Int.* **10**, 24.
- Unsöld, A.O.J., 1969, *Science* **163**, 1015.
- Varne, R. and A.L. Graham, 1971, *Earth Planet. Sci. Lett.* **13**, 11.
- Vlasov, K.A., 1966, *Geochemistry and Mineralogy of Rare Elements and Genetic Types of their Deposits*, vol. II, *Mineralogy of Rare Elements*, Academy of Sciences of the USSR, in translation, Israel Program for Scientific Translations, Jerusalem, pp. 220.
- Weill, D. and M. Drake, 1973, *Science* **180**, 1059-1060.
- Weill, D.F., G.A. McKay, S.J. Kridelbaugh and M. Grutzeck, 1974, *Proc. Fifth Lunar Sci. Conf.*, *Geochim. Cosmochim. Acta*, Suppl. 5, **2**, 1337.
- White, A.J.R., B.W. Chappell and P. Jakeš, 1972, *Contrib. Mineral. Petrol.* **34**, 185.
- Wildeman, T.R. and K.C. Condie, 1973, *Geochim. Cosmochim. Acta* **37**, 439.
- Wildeman, T.R. and L. Haskin, 1965, *J. Geophys. Res.* **70**, 2905.
- Wildeman, T.R. and L.A. Haskin, 1973, *Geochim. Cosmochim. Acta* **37**, 419.
- Yajima, T., H. Higuchi and H. Nagasawa, 1972, *Contrib. Mineral. Petrol.* **35**, 235.
- Zielinski, R.A., 1975, *Geochim. Cosmochim. Acta* **39**, 713.
- Zielinski, R.A. and F.A. Frey, 1970, *Contrib. Mineral. Petrol.* **29**, 242.
- Zielinski, R.A. and F.A. Frey, 1974, *Geochim. Cosmochim. Acta* **38**, 545.

Chapter 22

SEPARATION CHEMISTRY

Jack E. POWELL

Ames Laboratory – US DOE, Iowa State University, Ames, Iowa 50011, USA

Contents

1. Introduction	82
2. Preliminary processing	83
2.1. Monazite	83
2.2. Bastnaesite	84
2.3. Others	84
3. Exploiting oxidation states	84
3.1. Cerium	84
3.2. Europium	85
4. Classical methods	86
4.1. Fractional crystallization	86
4.2. Fractional precipitation	86
5. Ion exchange	86
5.1. Cation elution chromatography	87
5.2. Anion elution chromatography	89
5.3. Displacement chromatography	93
5.4. Elutions with EDTA and its homologues	98
5.5. Elutions with HEDTA and some of its analogues	100
5.6. Elutions with DTPA	102
6. Liquid-liquid ion-exchange chromatography	103
7. Solvent extraction	104
7.1. Neutral phosphorus agents	105
7.2. Monoacidic phosphate and phosphonate esters	106
7.3. Primary, secondary, tertiary and quaternary ammonium ions	107
References	108

Symbols

c = concentration of A in the effluent solution (meq/ml)
 c^* = maximum concentration of A in the

effluent (meq/ml)
 v = volume of effluent at which concentration c is noted (ml)
 v^* = volume of effluent at which the maximum concentration c^* is noted (ml)
 $N' = \frac{1}{2}(N - N_0)$ = the number of theoretical plates from the center of the original band to the bottom of the column (actually with light loading, $N' = N$)
 m = amount of A loaded (meq)
 L = length of bed.
 h = theoretical plate height (same units as L)
 w = band width on a volume of effluent bases (ml) measured where $c = c^*/e = 0.368c^*$, i.e., the mean band width
 K_d = distribution coefficient
 α_B^A = separation factor
 R = performance factor
 ν = the minimum number of displacements of the sorbed mixture required for separation
 ϵ = amount by which α exceeds one
 HETP = height equivalent to a theoretical plate
 N_0 = mole fraction of the first component in the mixture
 $(B/C)_0$ = ratio of components B and C at some reference point in the sorbed band
 $(B/C)_m$ = ratio of components B and C at another point in the band m theoretical plates or L centimeters further down the bed

1. Introduction

The history of rare earth separations dates back to the discovery of yttria in the year 1794, and the isolation of ceria in 1803; after which a total of 17 rare earth elements, Sc, Y, La, Ac and the lanthanide elements (except Pm), were isolated laboriously (in varying degrees of purity) by relatively inefficient fractional precipitation methods, prior to 1947. Such methods have (for the most part) been outmoded by the development of more elegant counter-current techniques during the last 30 years. While the purpose of this chapter is to summarize and comment upon recent progress in means of isolating individual lanthanides and yttrium, some mention of well-developed processes for the preliminary treatment of rare earth mixtures must be made, to place the subject of component resolution in proper context.

The lanthanides comprise a series of inner-transition elements in which the number of 4-f electrons increases from 1 to 14. The main effect of increasing the number of electrons in this internal energy sublevel, as the nuclear charge increases, is to gradually decrease the cationic radius of consecutive Ln^{3+} ions, so that they range in size from that of La^{3+} to that of Sc^{3+} (elements of the Sc-Y-La-Ac group).

Due to the remarkable similarities in their cationic charge and their radii, lanthanons form many isomorphous series of compounds, and are always found as complex mixtures (not always of exactly the same composition) in rocks and minerals which comprise the earth's crust.

The problem of separating them by reactions in aqueous media is aggravated further by the fact that increased charge density, which accompanies lanthanide contraction, promotes a greater overall degree of aquation and renders individual hydrated cationic radii even more similar.

The principally exploited mineral sources have been monazite, gadolinite, xenotime, bastnaesite and euxenite; but greater sophistication in chemical processing has made rare earth concentrates an exploitable by-product of other industries, e.g., the phosphate fertilizer industry. Of perhaps 160 minerals known to contain rare earths, only a few contain lanthanons or yttrium in amounts that

TABLE 22.1

Crystal ionic radii of the rare earth elements in the trivalent oxidation state [data of Templeton et al. (1954)]

Element	At. No.	Radius (Å)	Element	At. No.	Radius (Å)	Element	At. No.	Radius (Å)
(Ac)	(89)	1.08	Sm	62	0.964	(Y)	(39)	0.88
La	57	1.061	Eu	63	0.950	Er	68	0.881
Ce	58	1.034	Gd	64	0.938	Tm	69	0.869
Pr	59	1.013	Tb	65	0.923	Yb	70	0.858
Nd	60	0.995	Dy	66	0.908	Lu	71	0.848
Pm	61	0.979	Ho	67	0.894	(Sc)	(21)	0.68

TABLE 22.2
Principal minerals of the rare earth elements.

Mineral	Chemical nature	Percentage	
		Ce group	Y group
monazite	LnPO ₄ with thorium orthophosphate	42.3–66.9	0.5–4.8
bastnaesite	LnFCO ₃	73–76	very little
cerite	hydrated lanthanide silicate	59.4–67.9	very little
loparite	titanoniobate of Ca, Ln, alkali metals	30.7–34.1	very little
orthite	hydrated Al, Ln, Ca, Fe silicate	13.4–27.4	very little
yttrocerite	hydrated Ca, Ln, Y fluoride	8.5–15.5	14.3–24.1
xenotime	Y, Ln orthophosphate	0.3–4.6	51.9–62.6
gadolinite	Y, Ln, Be, Fe silicate	2.9–7.9	30.9–46.6
euxenite	titanoniobate of Y, Ln	0.2–4.3	18.2–28.1
fergusonite	Y, Ln, Fe niobotitanotantalate	0.9–6.2	31.2–42.3
samarskite	Y, Ln pyrotantaloniobate	0.3–1.7	9.1–37.7

warrant current interest. Trifonov (1963) compiled the list given in table 22.2, which is similar to a listing cited in several reviews by Moeller (1963, 1968).

2. Preliminary processing

Processing amounts to: breaking down the mineral; recovering lanthanide, yttrium, thorium and other values; removing thorium, uranium and iron (if present); and separating the yttrium and individual lanthanons. It is generally expedient to remove cerium before fractionating the other rare earths.

2.1. Monazite

Monazite sand occurs extensively in alluvial deposits, from which it is mined (along with other dense minerals) by placer techniques. It is separated from gangue and associated minerals, such as magnetite, ilmenite, rutile, zircon, garnet and xenotime, by ore beneficiation methods, including electrostatic and electromagnetic separations, prior to chemical processing.

Treatment with 93% sulfuric acid for several hours at 210°C yields a gray mud that partially dissolves in cold water, leaving behind extraneous SiO₂, TiO₂, ZrSiO₄, etc. The extract contains Ln³⁺, Th⁴⁺, H₃O⁺, SO₄²⁻, HSO₄⁻, and H₂PO₄⁻, as well as traces of many other elements, including uranium and iron.

Alternate treatment with 73% NaOH at 140°C yields a mud that is first leached with water at 100°C to remove PO₄³⁻, SiO₄⁴⁻, and excess OH⁻; then the metal hydroxide-oxide residue is leached with hot aqueous HCl to leave behind extraneous TiO₂, ZrSiO₄, etc., providing a solution containing Ln³⁺, Th⁴⁺, H₃O⁺ and Cl⁻, along with traces of other elements including uranium and iron.

2.2. Bastnaesite

Bastnaesite is found associated with a variety of other minerals (chiefly BaSO_4 , CaCO_3 , SrCO_3 , and SiO_2) from which it is obtained by hot froth flotation (after crushing and grinding). After filtration, the LnFCO_3 may be attacked by H_2SO_4 or HCl immediately, or subjected to an oxidizing roast (620°), followed by leaching with 0.5 molar HCl . The leachate from the latter treatment contains principally La^{3+} and the light lanthanons (Pr^{3+} through Gd^{3+}); whereas, the residue is chiefly CeO_2 and mixed lanthanide fluorides.

2.3. Others

The treatment of xenotime parallels the H_2SO_4 treatment of monazite, while the minerals gadolinite, cerite and orthite are best attacked by the NaOH route. The more refractory complex minerals, such as fergusonite, loparite, euxenite and samarskite, are somewhat more difficult to deal with, and are generally processed for their niobium and/or tantalum values.

3. Exploiting oxidation states

Although valence states other than +3 are rare among the lanthanons, especially in aqueous media, in several instances it is expedient to exploit alternate oxidation states.

3.1. Cerium

Cerium, the first lanthanide, is the only rare earth element that has a tetra-positive state stable enough to be exploited in aqueous systems. Thus the removal of cerium (the most abundant rare earth element), which frequently becomes a nuisance by forming precipitates in ion-exchange systems, can be undertaken very early. Brill (1964) reviewed methods used to partition monazite sulfate liquor, and cites a method developed by Smutz and others at the Ames Laboratory as being particularly effective in ridding the trivalent lanthanons of other cations. This scheme calls for dilution to a rare earth oxide concentration of about 15 g/l, neutralization to pH 1.5 with ammonia, and treatment with oxalic acid to precipitate thorium and the rare earths away from uranium, iron, and most other cationic and anionic impurities. The recovered precipitate is then treated with caustic (to permit recycling of the oxalate), and the hydroxides obtained are gently calcined in air to convert $\text{Ce}(\text{OH})_3$ to CeO_2 . The oxides are then dissolved in nitric acid; whereupon, both Th^{4+} and Ce^{4+} can be removed by solvent extraction with tributyl phosphate. This scheme could be applied to any acid leachate solution containing rare earths.

Practically all methods for cerium separation are based upon the easy oxidation of cerium to the tetravalent state. Air oxidation of dried hydroxides at

100–150°C, calcination at 650°C, chlorination of aqueous hydroxide suspensions, and electrolysis are the most common methods for large-scale operations. In the laboratory, oxidations with permanganate, bromate, persulfate, bismuthate, hydrogen peroxide, Co(III), and even dichromate or oxygen have been exploited.

From rare earth hydroxide or oxide mixtures in which cerium has been oxidized, the separation of cerium is usually accomplished by selective leaching away of the more soluble tervalent hydroxides with dilute acid, or by complete dissolution in a more concentrated acid followed by hydrolytic precipitation.

Moeller (1973) cites the hydrolysis of Ce^{4+} to a basic nitrate or sulfate; selective precipitation from buffered solution (pH 3–4), after chemical or electrochemical oxidation; and crystallization of $(NH_4)_2[Ce(NO_3)_6]$ from strong nitric acid solution as effective means of removing much of the cerium from crude rare earth solutions. The separations are not quantitative, however.

Solvent extraction of Ce(IV) nitrate has been studied extensively as an alternative method for separating cerium from rare earth mixtures. Alcohols, ethers, organic and inorganic esters, ketones, etc., have all been studied as extractants.

Like Th^{4+} , Ce^{4+} (but not Ln^{3+}) forms a sparingly soluble iodate that can be exploited for cerium removal.

3.2. Europium

Three lanthanides (samarium, europium and ytterbium) have divalent states that are capable of being exploited, but only Eu^{2+} has any appreciable stability in aqueous solutions. Furthermore, due to the relatively low abundance of all three, it is not expedient to utilize the properties of the divalent state until a moderate degree of enrichment has been achieved by other means. Then Eu(III) is easily reduced to Eu(II) by zinc, and europium(II) sulfate can be recovered as a precipitate isomorphous with $BaSO_4$, McCoy (1935).

Samarium, europium and ytterbium can readily be removed from lanthanon mixtures by reductive extraction from a buffered acidic solution into a dilute (0.5% or less) sodium amalgam, Marsh (1957), or by electrolyzing an alkaline citrate solution with a lithium amalgam cathode, Onstott (1955, 1956). Europium can be obtained especially pure from such amalgams by treatment with cold concentrated HCl, which causes precipitation of sparingly soluble $EuCl_2 \cdot 2H_2O$, Hulet et al. (1972), by the common-ion effect. Both Sm(II) and Yb(II) are rapidly oxidized by hydronium ion to the very soluble trihalides, but oxidation of Eu(II) in the absence of oxygen proceeds slowly.

Farah et al. (1972) have recently studied the recovery of Sm and Eu from Egyptian monazite by extraction with sodium amalgam. Their recommendations include utilization of acetate buffering with no less than 65 ml of glacial acetic acid per liter of (35 g/l Ln) feed and 0.26% sodium amalgam. Addition of NaCl to the feed (up to 0.2 N) decreased the pollution of recovered Sm and Eu by La (the major component in the feed stock), and a working temperature near 0°C was cited as optimum.

4. Classical methods

The two methods most widely used, prior to the development of ion-exchange elution, as means of separating rare earth mixtures were fractional crystallization and fractional precipitation. Such practices have been summarized by numerous experts on rare earth separations, e.g., Spencer (1919), Yost et al. (1947), Kremers (1953), Vickery (1953), Healy et al. (1961), Bouissères et al. (1959), Bril (1964), Moeller (1963), and Moeller (1973).

4.1. Fractional crystallization

Fractional crystallization is most effective at the lower (lanthanum) end of the lanthanide series, where differences in cationic radius are greatest. The separation of lanthanum as the double ammonium nitrate, $\text{La}(\text{NO}_3)_3 \cdot 2\text{NH}_4\text{NO}_3 \cdot 4\text{H}_2\text{O}$, from praseodymium and other trivalent lanthanons (after prior removal of cerium in its tetravalent state) is sufficiently rapid and effective to be of commercial significance, but no other procedure of this type is of technical importance today.

4.2. Fractional precipitation

This technique is similar in concept to fractional crystallization and has generally been effected by addition of hydroxide ion, or by the generation of this ion in solution. Hydrolysis occurs less extensively with La^{3+} than with the other lanthanons; and, due to the greater solubility product of $\text{La}(\text{OH})_3$ compared to those of the smaller trivalent rare earth cation hydroxides (ca. 10^{-19} for $\text{La}(\text{OH})_3$ compared to 10^{-24} for $\text{Lu}(\text{OH})_3$), it is feasible to precipitate the bulk of the other rare earths in the presence of ammonium ion and leave La^{3+} , for the most part, behind.

Moeller (1973) reminds us that homogeneous generation of anions, such as carbonate (from urea) and oxalate (from dimethyl oxalate), is more efficient than adding a soluble carbonate or oxalate, and that fractional precipitation by such means in the presence of selective complexing agents could have applications in resolving rare earth mixtures.

5. Ion exchange

Development of ion-exchange processes for isolating individual lanthanons and yttrium has been prompted by: (1) a need to separate small amounts of rare earths from each other to facilitate analyses of mixtures; (2) a need to isolate gross quantities of highly purified individual lanthanides and yttrium, to supply increasing demands of research and technology. One might expect that a single procedure would perform both tasks equally well; but, unfortunately, this is not so. For analytical purposes, separations of microgram and milligram quantities

are performed most rapidly and efficiently by the methodology of "elution chromatography" and by "extractive chromatography". For production of useful quantities, methods related to "displacement chromatography" have been found to be the most economical.

5.1. Cation elution chromatography

Plate theory was adapted to partition chromatography by Martin and Synge (1941) and to ion-exchange chromatography by Mayer and Tompa (1947). In the development of this theory, three assumptions were made: (1) an ion-exchange column can be considered to be a stack of hypothetical compartments of uniform length, each comprising an effective theoretical plate; (2) the solute concentrations in the exchanger and in the interstitial solution are uniform and at equilibrium with each other within the confines of a given plate; (3) the column loading and elution conditions are such that a distributing cation constitutes only a minute fraction of the total number of exchangeable ions in any plate, so that its sorption can be considered a linear function of its concentration in the interstitial solution, i.e., its distribution coefficient can be regarded as a constant.

It was pointed out by Glueckauf (1955) that the shape of the elution curve may be represented by expressions:

$$c = c^* \exp[-N'(v^* - v)^2/2vv^*], \quad \log_{10} c = \log_{10} c^* - 0.217N'(v^* - v)^2/vv^*$$

and that the maximum concentration of a component A is related to the total amount (in meq) of A loaded by the expression:

$$c^* = (m/v^*)(N'/2\pi)^{1/2},$$

where c = concentration of A in the effluent solution (meq/ml), c^* = maximum concentration of A in the effluent (meq/ml), v = volume of effluent at which concentration c is noted (ml), v^* = volume of effluent at which the maximum concentration c^* is noted (ml), $N' = \frac{1}{2}(N - N_0)$ = the number of theoretical plates from the center of the original band to the bottom of the column (actually with light loading, $N' \cong N$), m = amount of A loaded (meq).

The number of theoretical plates in a given column under a given set of conditions is customarily computed from an experimental elution curve. In terms of known and measurable quantities,

$$N = L/h \cong 2\pi(c^*v^*/m)^2 \cong 8(v^*/w)^2,$$

where L = length of bed, h = theoretical plate height (same units as L), w = band width on a volume of effluent basis (ml) measured where $c = c^*/e = 0.368c^*$, i.e., the mean band width.

Note that h (and consequently N and w) depends on the kinetics of exchange rate of the species in question, as well as the set of experimental conditions chosen.

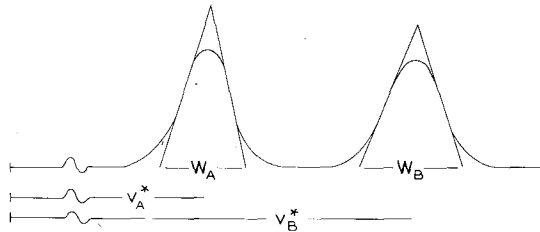
If K_d remains constant for all concentrations of the component under consideration, a constant fraction of the component is always in solution and being

transported by the mobile phase. Consequently, the separation factor or distribution coefficient ratio can be expressed in terms of the respective volumes at which the maxima in individual component concentrations appear in the elution curve.

$$\alpha_B^A = K_{dA}/K_{dB} = (v_B^* - v_0)/(v_A^* - v_0) \cong v_B^*/v_A^*,$$

where v_0 , the free volume in the column, includes both the interstitial volume of the bed and other dead space in the system (i.e., that between the bottom of the bed and column outlet).

Performances of elution chromatographic systems are frequently compared by the resolution of individual components, defined as twice the difference between peak volumes divided by the sum of the approximated peak widths, $W_A + W_B$, on a volume basis, by Ambrose et al. (1960). That is: $R = 2(v_B^* - v_A^*)/(W_A + W_B)$.



Others, e.g., Dybczynski (1970), favor a statistically more exact relationship: $R = (v_B^* - v_A^*)/n(\sigma_A + \sigma_B)$, where: $\sigma = w/2\sqrt{2}$ is the standard deviation of the particular peak width (see definition of w given previously).

Much use has been made of cation-exchange elution chromatography, since the subject was comprehensively reviewed by Powell (1964), as a means of analyzing traces of rare earths encountered in rocks and minerals and in fission-product mixtures. For the most part, however, few improvements have been made in the basic techniques.

Gradient-elution techniques date back to a 9 h, pH-gradient elution of complex lanthanon mixtures with lactate described by Nervik (1955), a 30 min, pH-gradient resolution of a Y-Tb-Er-Tm-Lu mixture with glycolate by Stewart (1955), and a 5 min, concentration-gradient separation of Yb and Lu activities by Preobrazhenskii et al. (1957) using lactate. Further application of the pH-gradient technique, employing ammonium α -hydroxyisobutyrate (which is superior to either glycolate or lactate) has been reported by Wolfsberg (1962), Massart + Hoefle (1963), and Foti et al. (1967). The latter performed a tracer-level separation of 9 rare earth elements in 14 h with 0.25 M α -hydroxyisobutyrate in the pH range 3.83–8.34, on a -200 + 400 mesh, ammonium-form, Dowex 50W-X4, resin bed, 47 inches long and 3 mm in diameter, at room temperature, using a flow rate of 0.125 ml/min.

With fission-product mixtures and in some cases of activation analysis it is expedient, even imperative, to complete an analysis within a short time span. Campbell (1973), working with α HIB in pressurized Dowex 50W-X8 systems,

has exploited very small resin particle sizes, elevated temperature, and the concentration-gradient elution technique to accomplish resolutions of 15-component, rare earth mixtures in less than 2 h. In one experiment, 75 mg of lanthanon mixture (5 mg of each) was loaded on a 33 cm long, 0.9 cm diameter, -400 mesh, Dowex 50W-X8, resin bed and eluted with excellent results at a flow rate of 10 ml/min with pH 4.4, ammonium α HIB, employing a stepwise increase in eluant concentration from 0.1 to 1.0 molar. The elution time required was 100 min.

In confirmation of the work of Nishi and Fujiwara (1964), Karol (1973) found that 2-hydroxy-2-methylbutyrate, the next higher homologue, provides a larger separation for most Ln^{3+} pairs than α -hydroxyisobutyrate.

5.2. Anion elution chromatography

Separation of lanthanons on anion-exchange columns depends upon the ability of trivalent cations to form anionic complexes of differing stability with negatively charged ligands. The art dates back to a report by Huffman and Oswalt (1950) than ^{147}Pm and ^{154}Eu tracers could be resolved on a Dowex 1 anion-exchange column, pretreated with citric acid, by sorption from and elution by 0.0125 M citric acid solution at pH 2.1. The rough separation factor, calculable from their observed Pm and Eu peak volumes was only 1.3; and the order of elution was Pm-Eu . . . the reverse of that observed in cation-exchange elutions.

Lanthanons are not sorbed to any appreciable extent on anion exchangers from aqueous HCl, HNO_3 and H_2SO_4 , and are only weakly sorbed from solutions of salts such as sulfites, sulfates, thiosulfates, nitrates, nitrites and thiocyanates. Marcus and Neel (1959), however, demonstrated that gradient elution, from 6 M to 3 M, with LiCl at 78°C would elute cations in the sequence Cs-Ba-Yb-Eu-Sm-Nd-Pr-Ce-La. From this it is apparent that the lighter lanthanons form the most stable anionic species with Cl^- .

Hamaguchi et al. (1965), using 3 M $\text{Mg}(\text{NO}_3)_2$, demonstrated that the lighter lanthanons could be resolved in the order Gd-Eu-Sm-Nd-Pr-Ce-La (as with Cl^-), but that the heavier rare earths, Er-Lu, separated very little.

Korkisch and Tera (1961) and Faris and Wharfe (1962) demonstrated that adding methanol to aqueous HNO_3 systems markedly improved the distribution coefficients for sorption of lanthanons in anion-exchange systems; and Faris et al. (1962) listed separation factors relative to gadolinium from which the following separation factors for adjacent lanthanons were estimated.

Other water-miscible solvents also enhance Ln distribution coefficients, including: higher alcohols, acetone, cellosolve, dioxane and tetrahydrofuran. Methanol is the solvent of choice, however, simply because it is a better solvent for rare earth nitrates than most of the others.

Molnar et al. (1967) reviewed previous anion-exchange separations and improved the distribution coefficients somewhat by employing nitrate-form Amberlite IRA-400 and 80% MeOH-20% aqueous NH_4NO_3 . Log K_d increased

TABLE 22.3
Separation factors for Dowex 1 with 90% MeOH-10% (1 M
HNO₃).

Pair	α_Z^{Z+1}	Pair	α_Z^{Z+1}	Pair	α_Z^{Z+1}
Lu-Yb	1.0	Dy-Tb	1.1	Pm-Nd	2.6
Yb-Tm	1.0	Tb-Gd	1.3	Nd-Pr	2.2
Tm-Er	1.0	Gd-Eu	1.6	Pr-Ce	1.7
Er-Ho	1.0	Eu-Sm	1.9	Ce-La	1.7
Ho-Dy	1.0	Sm-Pm	2.3		

linearly with NH₄NO₃ concentration in a parallel manner, so that the separation factors remained virtually constant.

Faris (1967) studied the elution of rare earths, on α -hydroxyisobutyrate-charged Dowex 1-X4, with 0.0125 M α HIB in 25% aqueous methanol (propanol, ethanol, isopropanol, tetrahydrofuran, acetone, cellosolve, dioxane, etc.). The elution order was La-Ce-Pr-Nd-Sm-Eu-Gd-Tb-Dy-Ho-Er-Tm-Yb-Lu... the reverse of that observed in cation-exchange elution experiments with α HIB. Yttrium eluted with Dy. From the distribution data, the individual separation factors appear to diminish from about 2.8 for La-Ce to about 1.1 for Yb-Lu.

Dybczynski (1959) initiated an investigation of the anion-exchange elution behavior of lanthanides in ethylenediamine-*N,N,N',N'*-tetraacetate systems and continued this work in collaboration with Minczewski (1962). They proposed that the separations observed stem from the varying ability of the hydrated LnCh⁻ species to undergo the exchange: $2\text{LnCh}^- + \text{H}_2\text{Ch}^{2-} \rightleftharpoons 2\text{LnCh}^- + \text{H}_2\text{Ch}^{2-}$. Their assumption was that associations of LnCh⁻ with $-\text{N}(\text{CH}_3)_3^+$ on the resin lattice are somewhat analogous to the solubilities exhibited by NaLnCh salts in water given by Marsh (1955) and dependent on the hydration of the cations. The distribution coefficients first increase from La to Eu and then decrease from Eu through Lu, while the solubilities of the NaLnCh salts decrease from La to Sm or Eu and then increase. The elution sequence at room temperature is: Lu-Yb-Tm-Er \cong Y-Ho-La-Dy-Ce-Tb-Pr-Nd-Gd-Pm-Sm-Eu, with light Ln species interspersed among the heavy ones. Dybczynski (1964) next demonstrated that raising the temperature effected an increase in the quality of the separation. Not only did the exchange kinetics and theoretical plate heights improve... values of the distribution coefficients underwent changes, so that fewer light Ln species were interspersed in the heavy Ln sequence than at room temperature. The sequence at 92°C became: Lu-Yb-Tm-Er-Y-Ho-Dy-Tb-Gd-La-Eu-Sm-Ce-Pm-Pr-Nd. That is, La shifted its position three places as the distribution maximum changed from Eu to Nd. An additional benefit of elevated temperature was that reduced viscosity diminished the hydraulic resistance and permitted greater flow rates without the necessity of a large increase in pressure.

Dybczynski (1967) expanded upon the various phenomena observed with temperature changes. He cautioned that increasing the temperature does not necessarily lead to improved separations. Both the separation factor and plate

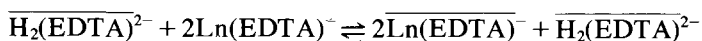
height can either decrease or increase (or remain constant) with an increase in temperature . . . depending on the species to be separated and the ion-exchange system employed.

According to Dybczynski (1970), optimum resolutions in anion-exchange separations of lanthanon pairs on Dowex 1 are achieved with nominally 4% crosslinked resin (Dowex 1-X4). Although separation factors increased rather regularly with increased crosslinkage (from X2 to X16), the plate height was the factor that determined the quality of the resolution and was lowest in 4% crosslinked resin beds. Plate height increased by two orders of magnitude in going from X4 to X16 resin. A sieve effect, heralded by a sudden drop in distribution coefficients, was noted at the higher crosslinkings; because a resin that cannot become highly swollen with water cannot utilize all of its potential capacity in sorbing large species. On the other hand, resins that swell excessively dilute their capacity to sorb species by ion exchange.

Papers by Wodkiewicz ^{Dybczynski} (1967, 1972) and Dybczynski and Wodkiewicz ^C regarding the merits of DCTA (trans-1,2-diaminocyclohexane-*N,N,N',N'*-tetraacetate), compared to EDTA, as an eluant in the anion-exchange separation of lanthanons, reveal that DCTA is inferior to EDTA for this purpose in most respects. The individual distribution coefficients are (for the most part) lower; the separation factors are smaller; and more sluggish exchange kinetics cause larger theoretical plate heights than are observed with EDTA under comparable conditions. Similar to the nonmonotonic sequence observed with EDTA, the elution order with DCTA is: Lu-Yb-Tm-Er-Y-Ho-Dy-Tb-La-Gd-Eu-Ce-Pr-Sm-Nd-Pm, at 25°. As with EDTA, the best component resolutions were obtained with Dowex 1-X4 resin.

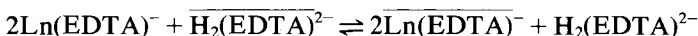
The sieve effect due to high resin crosslinkage was even more pronounced with DCTA than with EDTA chelate species . . . probably because of greater bulk.

Schoebrechts et al. (1973) studied the distribution of trivalent lanthanides between *N'*-hydroxyethylethylenediamine-*N,N,N'*-triacetate- and nitrilotriacetate-charged Dowex 1-X4 resin and solutions of HEDTA or EDTA. The experimental results indicated that the extraction mechanism is a chelating reaction between HEDTA or NTA sorbed on the anion-exchange sites of the resin and the 1:1 complex, Ln(HEDTA) or Ln(EDTA)⁻, in the aqueous phase. The kinetics of reaction were rapid, and the theoretical plate heights obtained from column elution experiments were in good agreement with this chelation model (according to the investigators). They remarked that K_d of the lanthanons, in that system in which NTA was on the resin and EDTA was in the aqueous phase, increased in order Tm-Tb-Gd, in agreement with the trend reported by Geier and Harlen (1971) for formation constants of the mixed Ln(EDTA)(IDA)³⁻ species formed from Ln(EDTA)⁻ and IDA²⁻. They further compared Geier's data trend with $-\Delta G$ values given by Brücher et al. (1972) for the presumed reaction:

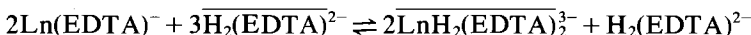


and noted a remarkable correlation which might be an indication that the mode of distribution in the EDTA and DCTA systems studied by Minczewski (1962) and Wodkiewicz ^{Polaczynski} (1967) was analogous to that in their mixed exchange systems.

As a matter of fact, on a tracer scale, the slope of $-\frac{1}{2}$ observed by Minczewski in log-log plots of K_d vs. $[\text{H}_2(\text{EDTA})^{2-}]$ does not differentiate between the reaction favored by Minczewski,



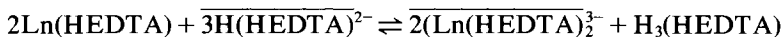
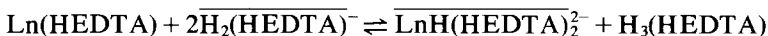
and the reaction



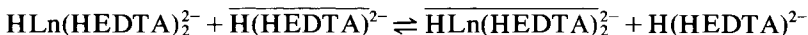
required to account for sorption of a singly charged lanthanon chelate on a diprotonated EDTA anion already on the resin. The first reaction is disfavored by your writer, however, on the grounds that the observed K_d values would imply that the anion exchanger was exhibiting a preference for monovalent anions over divalent anions. In the latter case, trivalent anions being favored over divalent anions agrees with the usual observation. This reaction is, of course, completely analogous to the mechanism proposed by Schoebrechts et al. (1973) for $\text{Ln}(\text{EDTA})^-$ from the aqueous phase associating with resin-bound $\text{H}(\text{NTA})^{2-}$.



In the case of $\text{Ln}(\text{HEDTA})$ associating with resin bound $\text{H}_2(\text{HEDTA})^-$ and $\text{H}(\text{HEDTA})^{2-}$, however, the aqueous 1:1 chelate species bears no charge and the reactions:



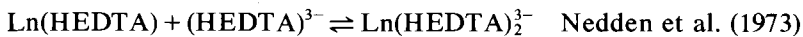
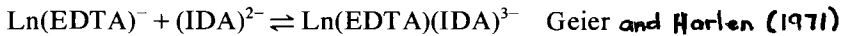
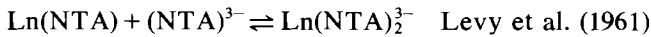
are stoichiometrically feasible. The last one could, in tracer-scale experiments at 2.25, account for the $-\frac{1}{2}$ slope in log-log plots of K_d vs. total HEDTA concentration observed by Schoebrechts et al. (1973); but none of the above accounts for the observation that the slope changed from $-\frac{1}{2}$ to -1 when the pH changed from 2.25 to 6.00. On the other hand, a slope of -1 would be expected if the exchange reaction at pH 6 (where $\text{H}(\text{HEDTA})^{2-}$ comprises nearly 100% of the anions present in both phases) were:



This course of events would stem from prior formation (almost 100%) of the $\text{HLn}(\text{HEDTA})_2^{2-}$ species from $\text{Ln}(\text{HEDTA})$ and $\text{H}(\text{HEDTA})^{2-}$ in the aqueous phase.

Whatever the actual mechanism in anion-exchange distributions of rare earths between an aminopolycarboxylate-charged resin and an aqueous solution of the same (or different) aminopolycarboxylate anion, the Ln distribution curve (log K_d vs. Z) peaks at (or near) the same Z as does the second step chelate formation constant. For example; in the case of $\overline{H}_2(EDTA)^{2-}/H_2(EDTA)^{2-}$, Minczewski et al. (1962) found the K_d a maximum at about $Z = 63$ (Eu), corresponding rather well with the K_2 value maximum observed by Brücher et al. (1975) at $Z = 62$ (Sm).

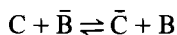
The order, $K_{d_{Gd}} > K_{d_{Tb}} \gg K_{d_{Tm}}$, given by Schoebrechts et al. (1973) in the $\overline{H}(NTA)^{2-}/H_2(EDTA)^{2-}$ and $\overline{H}(HEDTA)^{2-}/H(HEDTA)^{2-}$ systems at about pH 6.00, reflects a similar increase to a maximum followed by a decline in K_2 as Z increases, which has been repeatedly observed in such cases as:



The consensus regarding such systems is that, although separation factors for adjacent elements are in some cases large enough to be of interest in analyses by anion exchange, the nonmonotonic trend (of K_d as Z increases) causes separation factors for intermediate lanthanons to be too low (near the K_d maximum) and causes elution peaks of the lighter lanthanons to be interspersed among the heavier ones.

5.3. Displacement chromatography

Displacement chromatography makes it possible to utilize a large fraction of the exchange capacity of a given resin bed as well as the entire driving potential of the eluant. In the simplest case, B and C, the species to be separated, are sorbed on an exchange bed which has previously been loaded with species A (which either B or C will readily displace by a favorable mass-action reaction . . . due to their greater affinities for the exchange sites), and eluted with a solution containing a fourth species, D, which readily displaces A, B and C. If the equilibrium constant for the exchange reaction:



exceeds unity, C displaces \overline{B} while D is displacing both \overline{B} and \overline{C} . Since A was chosen such that B will displace \overline{A} (the sorbed A species), B will rapidly segregate as \overline{B} at the front of the sorbed $\overline{B} - \overline{C}$ band. This tendency, coupled with favorable front-end and rear-end displacement reactions, promotes development of a steady-state condition, wherein adjacent bands of \overline{B} and \overline{C} , of

constant length, progress down the system head-to-tail under the displacing influence of D as it encounters the rearmost sorbed species \bar{C} . Due to the fixed capacity of a given system, A is forced to vacate the bed as D deposits, at a concentration equivalent to the concentration of D in the eluant. When species A has all been displaced from the system, first B, then C, and finally D appear in the effluent. By collecting appropriate fractions of the effluent solution as it issues from the bed system, it is possible to isolate substantial amounts of all desired products in a high state of purity. While a certain amount of overlapping is inherent, the relative degree of overlap can be controlled very effectively by adjusting the system diameter and the eluant flow rate to the amount of mixture to be separated.

Column performance depends upon two parameters: the separation factor, and the height equivalent to a theoretical plate (HETP). The separation factor is defined as the ratio of the respective distribution coefficients, that is,

$$\alpha_C^B = K_{dC}/K_{dB} = [B][\bar{C}]/[C][\bar{B}]$$

In this definition: [B], [C], $[\bar{B}]$ and $[\bar{C}]$ refer to the total concentrations of B and C in the mobile and static phases, rather than to individual ions or complex species. It will be seen that complexing or chelating agents can alter the distribution constants markedly, thus affecting the separation factor.

HETP is the distance by which attainment of the condition of dynamic equilibrium, representative of a static system, is displaced by the motion of one phase with respect to the other. That is to say, it is the distance, measured along the bed, between points at which the ratio of B to C in the solution and the ratio of \bar{B} to \bar{C} in the resin phase differ by one separation factor. HETP is a function of the time of contact and the rates of exchange of species; hence, it depends upon flow rate, particle size, concentration, pH, temperature, and even the various stabilities of individual chelate species which may be present. Although HETP is difficult to predict with precision, it can be measured accurately for virtually any set of experimental conditions if the separation factor is known. The fundamental equations which apply to the separation of binary mixtures by displacement chromatography are:

$$\nu = (1 + \epsilon N_0)/\epsilon \quad \log \frac{(B/C)_m}{(B/C)_0} = m \log \alpha = \frac{L \log \alpha}{h}$$

where ν = the minimum number of displacements of the sorbed mixture required for separation, ϵ = amount α exceeds one ($\epsilon = \alpha - 1$), N_0 = mole fraction of the first component in the mixture, $(B/C)_0$ = ratio of components B and C at some reference point in the sorbed band, $(B/C)_m$ = ratio of components B and C at another point in the band m theoretical plates or L cm further down the resin bed, m = number of theoretical plates between the points where ratios $(B/C)_0$ and $(B/C)_m$ are observed, h = HETP, the height equivalent to a theoretical plate in cm, L = length measured along column . . . equal to m theoretical plates.

Powell (1964) cautions that the relation, $\nu = (1 + \epsilon N_0)/\epsilon$, applies only when: (1) the HETP is sufficiently small; and (2) the value of ϵ is sufficiently large that the

region of inherent gross overlap between resolved bands is small compared to their lengths. Adjusting the bed diameter to the amount of rare earths to be separated makes it possible to apply this treatment even though HETP is of some magnitude and the value of ϵ is fairly small.

If one defines the region of gross overlap as the region wherein the percentage of one component falls from 99.9 to 0.1, $\log(B/C)_m/(B/C)_0$ becomes equal to six; and $m = 6/\log \alpha$ plates and $L = 6h/\log \alpha$ then comprise the region of gross overlap under steady-state conditions. Care must be exercised in designing equipment to ensure that the length of the sorbed band exceeds $6h/\log \alpha$ sufficiently that substantial yields of pure components result.

If the yield is poor in a given experiment, a larger load and a proportionately longer system will generally improve the separation efficiency. Reduction of HETP is also advantageous. The most practical ways to accomplish this are: (1) decrease the diameter of the resin particles; and (2) elevate the temperature to increase reaction and diffusion rates. Decreasing the flow rate decreases the HETP, to be sure, but unfortunately increases the elution time. Decreasing resin crosslinkage allows more rapid diffusion of species in the static phase, but much of the advantage is offset by the reduced exchange capacity of a more swollen media and less dimensional stability in a packed column (low crosslinked resins expand and contract remarkably between exchange cycles and with changes in concentration of the mobile phase).

The above treatment (applicable to a binary system) has been adapted to ternary mixtures by Powell et al. (1968) and James et al. (1968); and to yet more complex systems by Powell et al. (1971) and Helfferich et al. (1970). While the solutions to more complex systems are quite straightforward, the mathematical expressions rapidly become tedious.

Simple cation-exchange separation of neighboring rare earths by displacement chromatography is not generally feasible, since all the lanthanons exhibit the same affinity for most cation-exchange media (chelating resins excepted). That is, separation factors for adjacent rare earths undergoing simple cation exchange are nearly unity. The reader is referred to the data of Surls et al. (1957). This circumstance has necessitated the use of chelating agents to enhance separation factors.

To be useful in the separation of rare earths by displacement chromatography, a chelant must possess the following characteristics: (1) the reagent and its metal chelates must be reasonably soluble in some inexpensive but compatible solvent (preferably water); (2) the reagent must be selective in its chelating action; (3) the reagent must form rare earth chelates of sufficient stability to promote clean-cut displacement of rare earths from the resin bed by ammonium or alkali-metal ions; (4) the reagent must form labile chelate species which must not be of such great stability that the accompanying cation-exchange process is hampered unnecessarily.

Citrate, nitrilotriacetate (NTA), and many polyaminopolycarboxylate anions form 1:1 chelate species with yttrium and the lanthanons that are either neutral or negatively charged, so that they can be exploited in an aqueous mobile phase

in conjunction with a cation-exchange resin to promote displacement chromatographic separations of these elements. Citrate was tried very early by Spedding et al. (1950) and ultimately abandoned, because of the low solubility of the hydrated 1:1 LnCit·2H₂O species. 1:1 Ln(NTA) species are not very soluble either. With both citrate and NTA, 1:2 Ln chelate species form when the ligand is in excess. To complicate matters further the 1:2 LnCh³⁻ species forms protonated versions at lower pH values; and the 1:1 LnCh species reacts with OH⁻ at higher pH to form LnCh(OH)⁻. The separation factors with citrate and NTA as the eluant, therefore, are markedly pH dependent.

$$\alpha_B^A = \frac{[\bar{B}^{3+}][A^{3+}ACh + ACh_2^{3-} + HACH_2^{2-} + \dots + ACh(OH)^-]}{[\bar{A}^{3+}][B^{3+} + BCh + BCh_2^{3-} + HBCh_2^{2-} + \dots + BCh(OH)^-]}$$

As a group, polyaminopolycarboxylate anions, having 3, 4, or 5-CH₂COO⁻ radicals, form extremely stable (but generally labile) 1:1 chelate species with the lanthanons and yttrium. Although secondary and binuclear chelate species (1:2 and 2:3) do form, the second step formation constants are generally less than 10⁻¹⁰ as large as the first ones (e.g., Brücher et al. (1976) list log $K_{Eu(EDTA)_2^{5-}}$ as 3.60 compared to the Schwarzenbach et al. (1954) value of log $K_{Eu(EDTA)^-}$ = 17.35). Because of this, separation factors with polyaminopolycarboxylate eluants in displacement chromatographic systems can be approximated by:

$$\alpha_B^A = \frac{[ACh^{3-n}][\bar{B}^{3+}]}{[BCh^{3-n}][\bar{A}^{3+}]} = \frac{K_{ACh}[A^{3+}][Ch^{-n}][\bar{B}^{3+}]}{K_{BCh}[B^{3+}][Ch^{-n}][\bar{A}^{3+}]} \cong \frac{K_{ACh}}{K_{BCh}}$$

Note that [Ch⁻ⁿ] cancels and [A³⁺][B³⁺]/[B³⁺][A³⁺] is approximately equal to 1.0 for adjacent lanthanons.

The formation constant sequences of a number of 1:1 species formed between trivalent rare earth cations and polyaminopolycarboxylate species have been determined:

EDTA (ethylenediamine-*N,N,N',N'*-tetraacetate), Wheelwright et al. (1953).

EDTA (ethylenediamine-*N,N,N',N'*-tetraacetate), Schwarzenbach et al. (1954).

DCTA (trans-1,2-diaminocyclohexane-*N,N,N',N'*-tetraacetate), Schwarzenbach et al. (1954).

HEDTA (*N'*-hydroxyethylethylenediamine-*N,N,N'*-triacetate), Spedding et al. (1956).

DTPA (diethylenetriamine-*N,N,N',N',N''*-pentaacetate), Harder et al. (1959).

ME (bis(2-aminoethyl)ether-*N,N,N',N'*-tetraacetate), Mackey et al. (1962).

DE (ethyleneglycolbis(2-aminoethyl)ether-*N,N,N',N'*-tetraacetate), Mackey et al. (1962).

EDDM (ethylenediamine-*N,N'*-dimalonate), Gorelev et al. (1972).

EDDS (ethylenediamine-*N,N'*-disuccinate), Babich et al. (1971).

DPTA (1,2-diaminopentane-*N,N,N',N'*-tetraacetate), Novak et al. (1974).

DHTA (1,2-diaminohexane-*N,N,N',N'*-tetraacetate), Novak et al. (1974).

EDDA (ethylenediamine-*N,N'*-diacetate), Thompson (1962).

TABLE 22.4
Stability constant sequences for selected 1:1 Ln chelates

Ln	log K_{LnCh}							
	EDTA	PDTA	BDTA	DBTA	DCTA	DPTA	DHTA	3MDBTA
La	15.50	16.42	(16.3*)	16.58	16.26	16.61	16.52	16.41
Ce	15.98	16.79	(16.8*)	17.15	16.78	17.13	17.11	16.98
Pr	16.40	17.17	17.49	17.49	17.31	17.48	17.36	17.28
Nd	16.61	17.54	17.70	17.77	17.68	17.76	17.67	17.57
Pm	(16.9*)	(17.8*)	(18.0*)	(18.0*)	(18.0*)	(18.0*)	(17.9*)	(17.8*)
Sm	17.14	17.97	18.32	18.25	18.38	18.25	18.24	18.12
Eu	17.35	18.26	18.61	18.38	18.62	18.38	18.32	18.30
Gd	17.37	18.21	18.84	18.56	18.77	18.53	18.47	18.44
Tb	17.93	18.64	19.45	19.03	19.50	19.02	18.98	18.97
Dy	18.30	19.05	19.93	19.48	19.69	19.48	19.42	19.39
Ho	(18.6*)	19.30	20.27	19.80	(20.2*)	19.77	19.72	19.70
Er	18.85	19.61	20.68	20.11	20.68	20.09	19.87	19.97
Tm	19.32	20.08	20.96	20.52	20.96	20.46	20.40	20.38
Yb	19.51	20.25	21.29	20.87	21.12	20.80	20.61	20.65
Lu	19.83	20.56	21.33	20.97	21.51	20.99	20.81	20.79

Ln	log K_{LnCh}							
	4MDPTA	HEDTA	MEDTA	BEDTA	DTPA	ME	DE	EDDM
La	16.45	13.82	11.50	10.81	19.96	16.21	15.63	9.80
Ce	17.02	14.45	11.87	11.28	(20.9*)	16.90	15.78	10.42
Pr	17.32	14.96	12.33	11.70	21.85	17.57	16.13	10.50
Nd	17.65	15.16	12.51	11.82	22.24	17.88	16.36	10.71
Pm	(17.9*)	(15.4*)	(12.7*)	(12.0*)	(22.5*)	(18.2*)	(16.7*)	(10.9*)
Sm	18.20	15.64	12.86	12.19	22.84	18.40	16.96	11.00
Eu	18.45	15.62	12.96	12.35	22.91	18.52	17.18	11.04
Gd	18.48	15.44	12.98	12.40	23.01	18.34	17.02	10.83
Tb	18.99	15.55	13.35	12.79	23.21	18.52	17.35	11.19
Dy	19.47	15.51	13.61	13.02	23.46	18.42	17.50	11.08
Ho	19.71	15.55	13.81	13.26	(23.3*)	18.34	17.46	11.04
Er	19.99	15.61	14.04	13.47	23.18	18.20	17.48	11.05
Tm	20.40	16.00	14.31	13.65	22.97	18.04	17.56	11.04
Yb	20.74	16.17	14.43	13.85	23.01	18.06	17.86	10.96
Lu	20.92	16.25	14.51	13.93	(23.0*)	17.96	17.89	11.21

*These values in parentheses have been interpolated.

PDTA (1,2-propylenediamine-*N,N,N',N'*-tetraacetate), Irving et al. (1971).
 BDTA (2,3-diaminobutane-*N,N,N',N'*-tetraacetate), Irving et al. (1971).
 MEDTA (*N'*-methylethylenediamine-*N,N,N'*-triacetate), Powell et al. (1973).
 BEDTA (*N'*-benzylethylenediamine-*N,N,N'*-triacetate), Miller et al. (1976).
 DBTA (1,2-diaminobutane-*N,N,N',N'*-tetraacetate), Novak et al. (1968a).

3-MDBTA (3-methyl-1,2-diaminobutane-*N,N,N',N'*-tetraacetate), Novak et al. (1968b).

4-MDPTA (4-methyl-1,2-diaminopentane-*N,N,N',N'*-tetraacetate), Novak et al. (1968b).

The more interesting of these data are tabulated in table 22.4.

5.4. *Elutions with EDTA and its homologues*

When EDTA is used as the eluant at room temperature, a retaining ion other than H^+ is used because of the insolubility of the $H_4(EDTA)$ species. Spedding et al. (1954) originally proposed Fe^{3+} , Cu^{2+} and Ni^{2+} . Of these, Cu^{2+} has been the most widely used. If retention of the heavier yttrium-group elements is not required (as with monazite or bastnaesite concentrates containing insignificant amounts of Ho, Er, Tm, Yb and Lu), Zn^{2+} may be used as the retaining ion. Krumholz et al. (1958) proposed the use of EDTA on Zn^{2+} charged resin beds for the recovery of pure rare earths from Brazilian monazite, and Powell (1961) suggested a practical procedure for using Zn^{2+} as the retaining ion following a short elution with EDTA on a Cu^{2+} bed. After the sorbed bed has moved as little as one fourth of its length, the heavy lanthanons (Ho–Lu) can be set aside on a diversion bed, and elution of the rest of the group can be continued with Zn^{2+} as the retaining ion. This procedure is especially useful with yttrium-rich concentrates (e.g., those from xenotime, gadolinite and euxenite). Its use results in a considerable saving, because most of the complexing agent (as well as the Zn^{2+}) can be recovered very easily and recycled. Recovery of Cu^{2+} is more difficult from $Cu(EDTA)^{2-}$ solutions because its 1:1 chelate is some 200 times as stable as $Zn(EDTA)^{2-}$. At the lower pH required to decompose $Cu(EDTA)^{2-}$, $H_5(EDTA)^+$ and $H_6(EDTA)^{2+}$ species form, and $H_4(EDTA)$, which is sparingly soluble and precipitates in the presence of Zn^{2+} at about pH 2, does not precipitate.

In elutions with EDTA, the prior removal of cerium and lanthanum is highly advantageous, since hydrated $HCe(EDTA)$ and $HLa(EDTA)$ species tend to precipitate and fill the interstices of the resin bed at eluant concentrations even lower than 0.015 molar (the concentration used successfully with the remaining lanthanons (Pr–Lu) and yttrium at pH 8.4). Although Powell et al. (1967) obviated the necessity of using a metal retaining ion by using elevated temperatures, at which $H_4(EDTA)$ is more soluble, the maximum EDTA concentration that can be employed at 92°C is about 0.01 M. At elevated temperatures, the $HLn(EDTA) \cdot H_2O$ species of lanthanum, cerium and praseodymium are even more prone to precipitate than at room temperature.

According to Mackey et al. (1970) the multihydrates, $HLa(EDTA) \cdot 7H_2O$, $HSm(EDTA) \cdot 6H_2O$ and $HEu(EDTA) \cdot 6H_2O$, separate from aqueous media below room temperature, but $HLa(EDTA) \cdot 7H_2O$ is much less soluble than the others. In the case of the heavier lanthanons, Gd–Lu, only anhydrous species can be prepared. Above 25°C, $HSm(EDTA) \cdot 6H_2O$ dehydrates irreversibly to $HSm(EDTA) \cdot H_2O$ (which is 10-fold less soluble than the hexahydrated form).

The decomposition of $\text{HLa(EDTA)} \cdot 7\text{H}_2\text{O}$ to a less soluble (probably polymeric) $\text{HLa(EDTA)} \cdot \text{H}_2\text{O}$ composition, occurs irreversibly at about 45°C .

Although the solubilities of HHo(EDTA) and $\text{HSm(EDTA)} \cdot \text{H}_2\text{O}$ increase with temperature, the solubility of $\text{HLa(EDTA)} \cdot \text{H}_2\text{O}$ (which is very low) does not increase appreciably. While the solubility of $\text{HLa(EDTA)} \cdot 7\text{H}_2\text{O}$ increases from ca. 1.1×10^{-3} at 25° to about 2.5×10^{-3} moles per liter at 45°C , the solubility of the monohydrate is less than 5×10^{-4} moles per liter at all temperatures.

Benefits of operating at 92°C include: (1) feasibility of $\text{H}_4(\text{EDTA})$ recovery; (2) improved HETP values; (3) increase in the Gd–Eu separation factor from 1.1 to 1.5; (4) increase in the Eu–Sm separation factor from 1.4 to 1.8. Hagiwara et al. (1970) reported improved separation factors in the Sm–Gd region even at 60°C . They gave the Gd–Eu separation as 1.37.

Yttrium elutes between dysprosium and terbium at all temperatures. However, the Tb separation improves somewhat and the separation of Dy from Y diminishes a little from 25°C to 92°C .

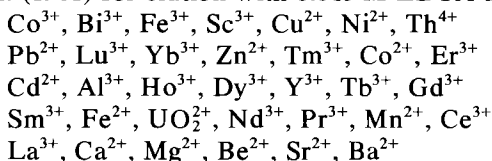
A number of homologues of EDTA have been investigated as chelating agents for the rare earths (see list). Apparently additions of alkyl groups to the ethylenediamine backbone of EDTA has some effect on the overall stabilities of the sequences of chelates formed, but such alterations have very little effect on the magnitudes of $\Delta \log K = \log \alpha_Z^{Z+1}$. That is to say, the relatively small increases in chelate stability occur in a parallel manner and do not alter the basic separation factors provided by the basic EDTA ligand. Recognizing this, one can average the $\Delta \log K$ values for a large number of sets of data to smooth out individual errors in precision and arrive at a list of useful individual (25°C) lanthanide separation factors for EDTA (and a number of its homologues). The values thus obtained agree better with results obtained directly in displacement chromatographic experiments than some of those obtained from Ln(EDTA) chelate stability constant ratios.

Because certain common cations frequently are present in many rare earth concentrates, knowledge of their elution position with respect to the rare earth

TABLE 22.5
Averaged values of individual separation factors for adjacent pairs of lanthanons being eluted with EDTA and its homologues (calculated from 9 sets of stability constant data).

Pair	α_Z^{Z+1}	Pair	α_Z^{Z+1}	Pair	α_Z^{Z+1}
Lu–Yb	1.6	Gd–Eu	1.1	Dy–Y	1.6
Yb–Tm	1.8	Eu–Sm	1.5	Y–Tb	1.5
Tm–Er	2.0	Sm–Pm	(1.8)		
Er–Ho	2.0	Pm–Nd	1.9		
Ho–Dy	2.0	Nd–Pr	2.0		
Dy–Tb	2.7	Pr–Ce	2.4		
Tb–Gd	3.5	Ce–La	3.3		

elements is advantageous. The following sequence has been reported by James et al. (1961) for elution with 0.015 M EDTA at pH 8.4 on Dowex 50 at 25°C.



James et al. (1961) pointed out that the positions of divalent species with regard to the lanthanon sequence should be both pH and concentration dependent; and pH dependence arises from the fact that protonated, divalent-metal chelate species, HMCh^- , are substantially weaker acids than protonated trivalent-lanthanon chelate species, HLnCh .

The separation of Th–Pb–Lu–Yb mixtures with EDTA at 25°C is very difficult because of small separation factors and adverse kinetic effects. Such mixtures, however, are readily resolved at 92°C, due to a reordering of the elution sequence as temperature increases. Powell et al. (1966) report that both Pb and Th readily separate from Lu and Yb when the temperature is raised. Th shifts toward the light end of the series from almost on Lu at 25°C to about the position of Er at 90°C. Lead shifts its position from just ahead of Lu to a spot between Tb and Gd.

5.5 Elutions with HEDTA and some of its analogues

$\text{H}_3(\text{HEDTA})$, hydroxyethylethylenediaminetriacetic acid, and the lighter Ln(HEDTA) chelate species are more soluble in water than $\text{H}_4(\text{EDTA})$ and the $\text{HLa}(\text{EDTA})\cdot 7\text{H}_2\text{O}$, $\text{HLa}(\text{EDTA})\cdot \text{H}_2\text{O}$, $\text{HCe}(\text{EDTA})\cdot \text{H}_2\text{O}$ and $\text{HPr}(\text{EDTA})\cdot \text{H}_2\text{O}$ species. This permits ammonium HEDTA to be used as the eluant with H^+ -ion retaining beds at all temperatures and greatly simplifies reagent recovery. Even the effluent water can be reused. Table 22.6 lists the separation factors available with HEDTA at 92°C, as well as at 25°C.

At room temperature, using HEDTA, good separations are possible with either La–Ce–Pr–Nd–Sm or Ho–Er–Tm–Yb–Lu mixtures, but only poor results are obtained with the Sm–Eu–Gd–Tb–Dy–Ho group. Powell (1964) highly recommends the use of HEDTA for resolving Tm–Yb–Lu concentrates. Th, however, in elutions with HEDTA at 25°C, tends to congregate between Yb and Tm and to be poorly separated from Yb. Eu actually tends to elute ahead of Gd at 25°C, and Y nearly coincides with Nd. At 92°C the Gd–Eu separation becomes about 1.00; whereas, the other α_Z^{Z+1} values, from Pr through Er, improve substantially. According to Powell et al. (1968), this marked improvement in separability, noted in the middle of the Ln sequence, and the considerable shift in the elution position of Y (from almost on Nd to between Gd and Tb) stems from the ability of HEDTA to bond hexadentately to the larger, lighter lanthanons at 25°C but only pentadentately to the smaller, heavier lanthanons, Er–Lu, and to Y. Increasing the temperature to 92°C simply prevents formation of the sixth bond with any lanthanon, so that stability constants increase in a more or less

TABLE 22.6

Comparison of Ln separation factors obtained at 25°C and 92°C with HEDTA to those estimated from LnCh formation constants for MEDTA and BEDTA at 25°C.

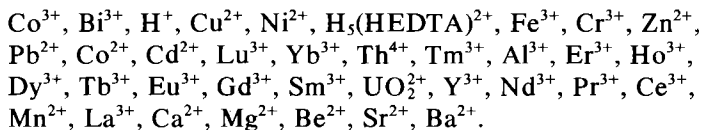
Pair	HEDTA $\alpha_Z^{Z+1}(25^\circ\text{C})^*$	HEDTA $\alpha_Z^{Z+1}(92^\circ\text{C})$	MEDTA $\alpha_Z^{Z+1}(25^\circ\text{C})^*$	BEDTA $\alpha_Z^{Z+1}(25^\circ\text{C})^*$
Lu-Yb	1.3	1.55	1.2	1.2
Yb-Tm	1.6	1.74	1.3	1.3
Tm-Er	2.0	1.55	1.9	1.5
Er-Ho	1.2	1.74	1.7	1.6
Ho-Dy	1.0	1.82	1.6	1.7
Dy-Tb	1.0	1.90	1.8	1.7
Tb-Gd	1.0	2.04	2.3	2.5
Gd-Eu	0.7	1.00	1.1	1.1
Eu-Sm	1.0	1.48	1.3	1.4
Sm-Pm	(1.6)	(1.8)	(1.5)	(1.5)
Pm-Nd	(1.6)	(1.8)	(1.5)	(1.5)
Nd-Pr	1.8	2.09	1.5	1.4
Pr-Ce	2.8	—	2.9	2.7
Ce-La	5.0	—	2.3	2.4
Sm-Nd	2.6	3.16	2.3	2.4

*Subject to errors up to 20% of the value reported. () Estimated from the Sm-Nd separation factor below.

monotonic manner and separations improve throughout about two-thirds of the sequence.

Powell et al. (1973) went on to substantiate their contention that the HEDTA ligand tended to loosen its (hexadentate) hold on the larger lanthanons as entropy increased at higher temperatures. They reasoned that replacement of the *N'*-hydroxyethyl (by substituting a donorless methyl group, for example) would have the same effect on the ethylenediamine-*N,N,N'*-triacetate moiety at 25°C as was observed with increased temperature. Tables 22.4 and 22.6 show that their surmise regarding HEDTA and its analogues, *N'*-methylethylenediamine-*N,N,N'*-triacetate and *N'*-benzylethylenediamine-*N,N,N'*-triacetate (MEDTA and BEDTA) was correct.

Few common elements elute within the rare earth sequence when 0.018 M HEDTA at pH 7.4 is the eluant at 25°C. James et al. (1961) reported the sequence to be:



A very interesting application of elution of rare earths with ammonium HEDTA is the analysis of the heavy elements, Er, Tm, Yb and Lu (in the absence of Th). Brunisholz and Roulet (1973) reported that they were able to

ascertain the composition of Er-Tm-Yb-Lu mixtures to a precision of $\pm 1\%$ by development of a displacement type chromatogram of these elements on a bed of very fine Dowex 50W-X4 cation exchanger (pretreated with Morin) in a capillary tube. Under UV light, the Er, Tm, Yb and Lu zones fluoresce red-brown, grey, beige and white. The individual zone lengths (zone volumes) are directly proportional to the number of millimoles of a species present in the system.

5.6. Elutions with DTPA

Although diethylenetriamine-*N,N,N',N',N''*-pentaacetic acid is appreciably soluble in water, there are several considerations that render it unattractive as a general eluant for lanthanon separations. (1) The extreme stability of all rare earth DTPA species introduces a kinetic factor which unduly increases the theoretical plate height. This can be countered to a degree by operation at elevated temperatures and at lower pH values. (2) A reversal (maximum) occurs in the chelate stability constant sequence at room temperature, so that the heavy rare earths (Ho-Lu) become interspersed among the lighter elements (Sm-Dy). At elevated temperatures fairly good separations are obtained with the lighter lanthanons and yttrium, but the heavier half of the sequence is poorly resolved. The elution sequences under two different conditions have been reported as follows:

5 g/l DTPA at pH 8.74 and 25°C, data of James et al. (1960).

Cu²⁺, Th⁴⁺, Ni²⁺, UO₂²⁺, Zn²⁺, Dy³⁺, Ho³⁺, Er³⁺, Yb³⁺, Sm³⁺, Y³⁺, Co²⁺, Cd²⁺, Pb²⁺, Nd³⁺, Pr³⁺, Ce³⁺, La³⁺, Mn²⁺, Al³⁺, Fe³⁺, Ca²⁺, Mg²⁺, Be²⁺, Sr²⁺, Ba²⁺.

0.05 M DTPA at pH 6.0 at 70°C, data of Hale and Hammer (1972).

Pu⁴⁺, Ga³⁺, Bi³⁺, (Fe³⁺, In³⁺, Cr³⁺), Cu²⁺, Ni²⁺, Fm³⁺, Es³⁺, Cf³⁺, Th⁴⁺, Sc³⁺, Co²⁺, Bk³⁺, Zn²⁺, Cd²⁺, Pb²⁺, Cm³⁺, Al³⁺, (Yb³⁺, Tm³⁺, Ho³⁺, Er³⁺), Dy³⁺, Lu³⁺, Am³⁺, Tb³⁺, (Gd³⁺, Eu³⁺), Sm³⁺, Y³⁺, Pm³⁺, Nd³⁺, Pr³⁺, Ce³⁺, La³⁺, Mn²⁺, Be²⁺, Mg²⁺, Ca²⁺, Sr²⁺, Ba²⁺.

Harder et al. (1959) reported that the acid dissociation constants for the species HLn(DTPA)⁻ is 10^{-2.8} for both HYb(DTPA)⁻ and HLa(DTPA)⁻. From this it is clear that the formation constants for HLn(DTPA)⁻ from H⁺ and Ln(DTPA)⁻ are about 10^{2.8}, and nearly independent of the lanthanon chelated by the ligand. It can be seen then that the separation factors for pairs of lanthanons in DTPA systems,

$$\alpha_B^A = \frac{\{[ACH^{2-}] + [HACH^{-}]\}[B^{3+}]}{\{[BCH^{2-}] + [HBCH^{-}]\}[A^{3+}]} \cong \frac{K_{ACH}\{1 + K_{HACH}[H^{+}]\}}{K_{BCH}\{1 + K_{HBCH}[H^{+}]\}}$$

are little affected by pH changes. Therefore, minor changes in the lanthanon series (such as Yb³⁺ moving from after Dy³⁺ to ahead of it) observed in the above sequences are probably temperature related, rather than due to the change in pH. In the case of divalent metal DTPA chelate species, however, the formation constants of protonated species HM(DTPA)²⁻ from H⁺ and

$M(DTPA)^{3-}$ are several orders of magnitude greater than those for $HLn(DTPA)^-$, thus shifts of elution positions of divalent cations relative to lanthanons are to be expected as the eluant pH is varied (note what happened to Co^{2+} , Cd^{2+} , and Pb^{2+} in the above sequences).

Although DTPA is essentially worthless as an eluant for the heavier lanthanons, it has found some usage in resolving light rare earth mixtures. Wheelwright (1969), summarizing efforts to produce Pm^{3+} from nuclear reactor wastes, advised that while DTPA was superior to both EDTA and HEDTA (for the rapid elutions required to minimize radiation damage to the cation-exchange resin) it was inferior NTA for this purpose. With NTA the HETP values are more favorable at accelerated flow rates than with DTPA, and component resolution is not complicated by the presence of Y^{3+} in the Nd-Sm gap where Pm elutes. The sequence with 0.050 M DTPA, at pH 6.5 and 60°C, is: Zn-(Cm, Ho, Am)-Gd-Eu-Sm-Y-Pm-Nd-Pr-Ce-La; and with 0.105 M NTA, at 60° and pH 6.4, it is: Zn-(Cm, Y)-Gd-(Eu, Am)-Sm-Pm-Nd-Pr-Ce-La.

6. Liquid-liquid ion-exchange chromatography

Certain reagents originally developed as extractants for solvent extraction schemes can be considered to be ion-exchange media (e.g., protonated amine cations and quaternary ammonium ions as anion exchangers; and dialkyl orthophosphate anions and alkyl (alkyl or aryl)-phosphonate anions as cation exchangers). Those materials of this kind which are insoluble enough in water can be immobilized by deposition in thin films on various inert media and utilized like solid anion- and cation-exchange media. They are also exploited in paper chromatography. The very-thin-film aspect of their utilization overcomes the problem of slow diffusion in solid ion-exchange resin particles and reduces HETP values. The need to supply an inert support, however, reduces exchange-column capacity to such a degree that thin-film, liquid, ion-exchange chromatography is mostly exploited as an analytical tool. In general, the exchange capacity of a liquid ion-exchange column is 4- to 10-fold less than a similar column filled with a solid ion-exchange resin.

Hulet et al. (1972), in a summary of ion-exchange extraction chromatography, cite a more extensive review of the subject by Cerrai et al. (1970), and list the most commonly employed inert support materials as: polytrifluoroethylene, polytetrafluoroethylene, polyvinylchloride-vinylacetate copolymer, SiO_2 , and silica gel.

The HETP of such systems depends largely upon the state of subdivision of the support and the degree to which it is loaded with the extractant material. HETP can be as small as 0.2 mm for particles of 15 μm diameter. Best results are obtained at elevated temperatures, with thin extractant films, and with light loadings of the mixtures to be resolved.

Representative cation-exchange extractants include: di-2-ethylhexyl orthophosphoric acid (HDEHP), di-n-octyl orthophosphoric acid (HDOP), 2-ethyl-

TABLE 22.7
Separation factors observed in liquid ion-exchange chromatography with HDEHP and HEHP under various conditions.

Pair	Sochaska (25°C) HDEHP		Bosholm (40°C) HDEHP		Pierce (60°C) HDEHP		Fidelis (20°C) HEHP	
	HCl	HNO ₃	HCl	HCl	HCl	HClO ₄	HCl	HNO ₃
La-Ce	2.8	2.7	3.1	2.4	4.7		3.3	
Ce-Pr	1.5	(1.3)	1.7	1.5	1.3		1.5	
Pr-Nd	1.3	(1.2)	1.4	1.4	1.4		1.3	
Nd-Pm	2.7	2.1	2.3	1.9	2.1		2.8	
Pm-Sm	3.2	2.7	2.2	2.3	2.6		3.6	
Sm-Eu	2.2	2.1	2.2	2.0	1.8		2.3	
Eu-Gd	1.5	1.7	1.6	1.4	1.5		1.6	1.8
Gd-Tb	5.0	5.5	4.4	3.3	5.2		5.4	5.9
Tb-Dy	2.6	3.0	2.2	1.9	1.9		2.1	2.3
Dy-Ho	2.1	2.2	2.0	1.9	1.8		1.9	2.0
Ho-Er	2.8	2.7	2.5	2.7	2.7		2.9	3.0
Er-Tm	3.4	3.5	2.5	1.8	3.3		3.8	4.0
Tm-Yb	2.8	3.1	2.7	3.1	2.2		3.2	3.4
Yb-Lu	1.9	1.9	1.8	2.1	1.8		3.0	2.1

hexyl phenylphosphonic acid (HEHP), and di-2-ethylhexyl pyrophosphoric acid. Representative anion-exchange materials include trioctyl-, triisooctyl-, tridecyl- and tridodecyl-(trilauryl-) ammonium ions; and trioctyl-, tridecyl- and trilauryl-methylammonium ions. Better separation factors for adjacent lanthanons are obtained with the cation-exchange materials than with the anion-exchange liquids. Pierce et al. (1963) reported comparative separation factors for adjacent pairs for the entire lanthanon series on HDEHP exchange columns, using dilute HClO₄ and HCl as eluants at 60°C. Sochaska et al. (1964) made a similar study at room temperature with HCl and HNO₃. Bosholm et al. (1964) gave separation factors at 40°C with HDEHP and HCl. Holzappel et al. (1966) gave results for HDEHP with HCl and HNO₃. Fidelis et al. (1965) studied HEHP at 20°C with HCl and HNO₃ eluants. HEHP is the most efficient extractant for resolving lanthanons, and nitric acid is the best eluant (for the heavier lanthanons at least). Separation tends to decrease with increased temperature.

7. Solvent extraction

At the outset it was the intent of your writer to review all phases of the separation chemistry of the lanthanons in depth, but upon delving into the literature it was found that others, including Hulet et al. (1972) and Weaver (1974), had recently reviewed solvent extraction processes in much greater detail than would be feasible in this chapter. Any attempt to wade through the morass of sometimes fragmentary and generally intertwined works involving separations

of lanthanons and actinide elements was judged redundant, if not futile, at this time. Consequently, it was decided to rely principally upon the diligence, expertise, insight and consensus of previous reviewers in discussing this subject.

Excluding consideration of a multitude of representatives of solvent extraction classes (water-insoluble alcohols, ethers, acids, esters, ketones and diketones) that have been examined and found to be inadequate in some respect or another, it is the intent here to focus upon only a few representatives of just three classes of extractants: (1) neutral phosphorous agents; (2) monoacidic orthophosphate and phosphonate esters; and (3) primary, secondary, tertiary and quaternary ammonium ion species.

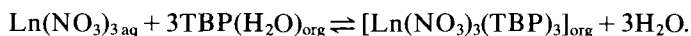
Separation of lanthanons by solvent extraction depends upon a preferential distribution of individual lanthanons (either in cationic form or as complex anions) between two immiscible liquid phases that are in contact with each other. One of the liquids is generally an aqueous solution, usually containing a mineral acid or an inorganic salting-out agent, and in some instances an organic acid or anion that acts as a chelating agent. Ideally one hopes to achieve distributions of all components that are independent of their dilution and which can be represented (under a given set of conditions) as distribution coefficient constants ($K_d = C_{org}/C_{aq}$) which can be used to estimate practical separation factors. The separation factor (ratio of distribution coefficients) dictates how many stages will be required to accomplish the attainment of two products of some specified purity from a binary mixture, or needed to partition a more complex mixture into two less complex mixtures (both of which contain less than specified amounts of components of the other set). Unfortunately, except at very low concentrations, distribution coefficients and, hence, separation factors change markedly with composition and concentration in many systems. Thus, extrapolations (from the tracer-scale) applied to bulk separations are not always valid.

7.1. Neutral phosphorus agents

Many representatives of the trialkyl orthophosphate ester, dialkyl alkyl (or aryl) phosphonate ester, alkyl dialkyl (or diaryl)-phosphinate, and trialkyl (or triaryl) phosphine oxide class have been investigated. Judging from the reviews available, none of the more exotic types appears to offer any particular advantage over tributyl orthophosphate as a selective extractant for resolving lanthanide mixtures. Most are either viscous liquids or solids that require a diluent, and for the most part the individual separation factors to be had are unspectacular.

With TBP, from aqueous solutions greater than 8 M in HNO_3 , extraction into the organic phase increases in the order of increased atomic number, but separation of the Ln's beyond Tb is rather difficult. With TBP, lanthanum, praseodymium and neodymium of rather high purity have been obtained by extracting from 13–14 M HNO_3 in as few as 10–14 stages. Similar results have been obtained from nearly saturated rare earth nitrate solutions of low acidity.

In 15 M HNO₃, $K_{d,Ln}$ ranges from 0.2 for La to 450 for Lu. The extraction mechanism appears to be:

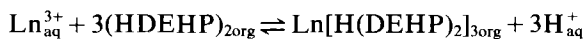


Apparently the extraction into TBP from HClO₄ and NaClO₄ solutions is of different character than extractions from HNO₃ and HCl. The separation factors are lower, although extractability is higher, and the lighter element extracts more readily than the heavier one (Eu/Yb). The extraction mechanism is purported to involve $[\text{Ln}(\text{ClO}_4)_3(\text{TBP})_6]_{\text{org}}$.

Extraction of lanthanides from thiocyanate solutions by TBP has also been studied, but the highest (Yb/La) separation factor observed was only about 10. Thus, there appears to be no practical application of a TBP-SCN⁻ system to separation of lanthanons.

7.2. Monoacidic phosphate and phosphonate esters

The most thoroughly studied and widely applied compound of this class is di-2-ethylhexyl orthophosphoric acid (HDEHP). It is readily available and has low aqueous solubility. It is quite viscous, however, presumably because it exists as a hydrogen-bonded dimeric species, and it must be employed with a diluent. At low acidities the extraction mechanism appears to be a cation-exchange process:



but at high acidities extraction as a simple trisolvate apparently occurs in addition to cation-exchange. Data on individual separation factors observed by Pierce et al. (1963) are listed in table 22.8.

Kolařík et al. (1966) studied extraction of lanthanons by HDEHP, di-n-amyl phosphoric acid (HDAP), diisooamyl phosphoric acid (HDiAP), and di-n-octyl phosphoric acid (HDOP) from HNO₃ and HClO₄. All systems showed a 3rd-order dependence on the extracting agent and a reciprocal 3rd-order dependence on [H⁺]. HDEHP, the most branched, was the least effective extractant, although the separation factors are little affected by chain length and branching.

In the case of isomeric compounds, less sterically hindered di-n-octyl phos-

TABLE 22.8
Separation factors for HDEHP-HCl and HDEHP-HClO₄,
toluene-water systems at 25°C.

Pair	HCl	HClO ₄	Pair	HCl	HClO ₄
La-Ce	2.4	3.0	Gd-Tb	3.2	5.0
Ce-Pr	2.8	2.1	Tb-Dy	2.0	2.1
Pr-Nd	1.7	1.4	Dy-Ho	2.1	1.9
Nd-Pm	2.1	2.2	Ho-Er	2.1	2.3
Pm-Sm	2.4	3.1	Er-Tm	2.5	2.5
Sm-Eu	2.2	1.9	Tm-Yb	1.8	3.1
Eu-Gd	1.6	1.4	Yb-Lu	2.2	1.9

phoric acid extracts M^{3+} ions 100 times as strongly as does di-2-ethylhexyl phosphoric acid and about 1000 times as strongly as di-2,2-dimethylhexyl phosphoric acid.

While 3rd-order dependence of K_d on the extractant (consistent with formation of $Ln(HA_2)_3$ species in the organic phase) is the rule with dialkyl phosphate esters in most solvents, there is considerable evidence that the organic phase species may be $LnA(HA_2)_2$ in some solvents and with aromatic diesters of phosphoric acid. By no means can the solvent used for dilution be considered inert. Extractions are definitely lower in those diluents which can interact with the extraction agent.

Replacing an alkoxy group attached to P by an alkyl or aryl group (which converts a phosphoric acid diester into a phosphonic acid monoester) yields a considerably stronger extractant for lanthanons, in general, but only slightly increases separation factors for neighboring lanthanons. In toluene, K_d 's with alkyl phenylphosphonic acid esters obey the same 3rd-power dependence on extractant concentration as with di-2-ethylhexyl phosphoric acid. An increase in temperature decreases K_d values as a general rule and has a small effect on separation factors. Separation factors for light Ln's increase, while those for heavy Ln's decrease.

A promising application of HDEHP extraction appears to lie in the partitioning of actinides from lanthanides. The TALSPEAK process (Trivalent Actinide Lanthanide Separation by Phosphorus Reagent Extraction from Aqueous Komplexes) involves extraction of Ln's with HDEHP from an aqueous solution of a complex (such as DTPA) which has a high affinity for and represses extraction of the middle and heavier lanthanons "and actinide elements most of all". The separation factor between the An's, Am^{3+} and Cm^{3+} , and the Ln's exceeds 100.

HDEHP is also exploited in the commercial production of Eu from bastnaesite concentrates. By a few stages of extraction with HDEHP, from dilute HCl solution, it is possible to remove nearly all of the lighter lanthanons, leaving a mixture containing several percent of Eu, which may then be recovered easily and in high purity by a reduction method.

HDEHP has also been utilized in one facet of a dual extraction process for purifying yttrium.

7.3. Primary, secondary, tertiary and quaternary ammonium ions

In general, extraction of trivalent lanthanons from mineral acid solutions by long-chain amines is not highly favorable unless high concentrations of acids or salts are present in the aqueous phase. Separation factors for adjacent Ln's are not especially attractive, but the extraction of An's is remarkable. Thus, tertiary amine extraction is the basis for the TRAMEX process for purification of Cm.

In nitrate media light Ln's extract more readily than the heavier ones, but in chloride solutions Eu is the most extractable lanthanon.

Quaternary ammonium compounds with high molecular weights behave chemically as strong-base anion exchangers and require lower concentrations of

salting-out agents. Again selectivity for individual lanthanons is low and apparently non-monotonic in SCN^- . Eu^{3+} is the most extractable Ln from SCN^- , but extracts much less readily than Am^{3+} and Cm^{3+} . In nitrate the lighter lanthanons are more extractable than the heavier ones.

Apparently the favorite tertiary amines and quaternary alkyl ammonium salts are those containing a mixture of eight- and ten-carbon chains. Commercial materials in popular usage are Alamine 336 and Aliquat 336, and their equivalents Adogen 364 and 464.

Acknowledgement

This work was supported by the US Department of Energy, Division of Basic Energy Sciences.

References

- Ambrose, D., A.T. James, A.I.M. Keulemans, E. Kovats, H. Röck, C. Rouit and F.H. Stross, 1960, *Pure Appl. Chem.* **1**, 177.
- Babich, V.A. and I.P. Gorelov, 1971, *Zhur. Anal. Khim.* **26**, 1832.
- Bosholm, J. and H. Grosse-Ruyken, 1964, *J. Prakt. Chem.* **26**, 83.
- Bouissères, G., F. Gaume-Mahn, H. La Blanchetais, J. Loriers and F. Trombe, 1959, Scandium, Yttrium, Elements de Terres Rares, Actinium, in: Pascal, P., ed., *Nouveau Traite de Chimie Minerale*, Vol. VII, Parts I and II (Masson, Paris).
- Bril, K.J., 1964, Mass Extraction and Separation, in: Eyring, L., ed., *Progress in the Science and Technology of the Rare Earths*, Vol. 1 (Pergamon Press, Oxford) pp. 30-61.
- Brücher, E. and I. Toth, 1972, *Radiochem. Radioanal. Lett.* **12**, 53.
- Brücher, E., R. Kiraly and I. Nagypal, 1975, *J. Inorg. Nucl. Chem.* **37**, 1009.
- Brücher, E., R. Kiraly and I. Toth, 1976, *J. Inorg. Nucl. Chem. Lett.* **12**, 167.
- Brunisholz, G. and R. Roulet, 1973, *J. Chromatogr.* **75**, 101.
- Cerrai, E. and G. Ghersini, 1970, Reversed-Phase Extraction Chromatography in Inorganic Chemistry, in: Giddings, J.C. and R.A. Keller, eds., *Advances in Chromatography*, Vol. 9 (Marcel Dekker, New York) pp. 3-189.
- Campbell, D.O., 1973, *J. Inorg. Nucl. Chem.* **35**, 3911.
- Dybczynski, R., 1959, *Chem. Anal. (Warsaw)* **4**, 531.
- Dybczynski, R., 1964, *J. Chromatogr.* **14**, 79.
- Dybczynski, R., 1967, *J. Chromatogr.* **31**, 155.
- Dybczynski, R. and L. Wodkiewicz, 1969, *J. Inorg. Nucl. Chem.* **31**, 1495.
- Dybczynski, R., 1970, *J. Chromatogr.* **50**, 487.
- Farah, M.Y., F.A. Saleh and M. Moustafa, 1972, *Zeit. Allg. Chem.* **392**, 69.
- Hale, W.H., Jr., and C.A. Hammer, 1972, *Ion Exchange Membranes*, **1**, 81.
- Faris, J.P. and J.W. Wharton, 1962, *Anal. Chem.* **34**, 1077.
- Faris, J.P., 1967, *J. Chromatogr.* **26**, 232.
- Fidelis, I. and S. Siekierski, 1965, *J. Chromatogr.* **17**, 542.
- Foti, S.C. and L. Wish, 1967, *J. Chromatogr.* **29**, 203.
- Geier, G. and U. Harlen, 1971, *Helv. Chim. Acta* **54**, 135.
- Glueckauf, E., 1955, *Trans. Faraday Soc.* **51**, 34.
- Gorelov, I.P. and V.A. Babich, 1972, *Zhur. Neorg. Khim.* **17**, 641.
- Hagiwara, Z. and M. Noguchi, 1970, *Bull. Chem. Soc. Japan* **43**, 401.
- Hamaguchi, H., I. Hikawa and R. Kuroda, 1965, *J. Chromatogr.* **18**, 556.
- Harder, R. and S. Chaberek, 1959, *J. Inorg. Nucl. Chem.* **11**, 197.
- Healy, R.M. and H.E. Kremers, 1961, Separation of Rare Earths by Fractional Crystallization, in: Spedding, F.H. and A.H. Daane, eds., *The Rare Earths* (John Wiley and Sons, New York) pp. 29-37.
- Helferich, F. and D.B. James, 1970, *J. Chromatogr.* **46**, 1.
- Holzappel, H., Le Viet-Lan and G. Werner, 1966, *J. Chromatogr.* **24**, 153.
- Huffman, E.H. and R.L. Oswald, 1950, *J. Amer. Chem. Soc.* **72**, 3323.
- Hulet, E.K. and D.D. Bodé, 1972, Separation Chemistry of Lanthanides and Transplutonium Actinides, in: Emelius, H.J. and K.W. Bagnall, eds., *MTP International Review of Science*, Vol. 7, Lanthanides and Actinides (Butterworths, London) pp. 1-45.
- Irving, H.M.N.H. and J.P. Conesa, 1964, *J. Inorg. Nucl. Chem.* **26**, 1945.
- Irving, H.M.N.H. and K. Sharpe, 1971, *J. Inorg. Nucl. Chem.* **33**, 217.
- James, D.B., J.E. Powell and F.H. Spedding, 1961, *J. Inorg. Nucl. Chem.* **19**, 133.

- James, D.B., J.E. Powell and H.R. Burkholder, 1968, *J. Chromatogr.* **35**, 423.
- Karol, P.J., 1973, *J. Chromatogr.* **79**, 287.
- Kolařík, K. and H. Pankova, 1966, *J. Inorg. Nucl. Chem.* **28**, 2325.
- Korkisch, J. and F. Tera, 1961, *Anal. Chem.* **33**, 1264.
- Kremers, H.E., 1953, Rare Earth Metals, in: Kirk-Othmer, eds., *Encyclopedia of Chemical Technology*, Vol. XI (Interscience Publications, New York) pp. 503-521.
- Krumholz, P., K. Bril, S. Bril, J. Behmoiras, F. Gottdenker and F.W. Lima, 1958, *Proc. 2nd U.N. Int. Conf. on Peaceful Uses of Atomic Energy, A/Conf. 15/P/2491* (Brazil).
- Levy, S.C. and J.E. Powell, 1961, USAEC Report IS-421, p. 27.
- Mackey, J.L., M.A. Hiller and J.E. Powell, 1962, *J. Phys. Chem.* **66**, 311.
- Mackey, J.L., D.E. Goodney and J.R. Cast, 1970, Different Forms of the Ethylenediaminetetraacetate Complexes of the Rare Earths, in: Henrie, T.A. and R.E. Linstrom, eds., *Proceedings of the 8th Rare Earth Research Conference*, Vol. 1 (Reno Metallurgy Research Center) pp. 277-292.
- Massart, D.L. and J. Hoste, 1963, *Anal. Chim. Acta* **28**, 278.
- Marcus, Y. and F. Nelson, 1959, *J. Phys. Chem.* **63**, 77.
- Marsh, J.K., 1943, *J. Chem. Soc.* **8**, 531.
- Marsh, J.K., 1955, *J. Chem. Soc.* 451.
- Marsh, J.K., 1957, *Inorganic Synthesis*, **5**, 32.
- Martin, A.J.P. and R.L.M. Synge, 1941, *Biochem. J.* **35**, 1385.
- Mayer, S.W. and E.R. Tompkins, 1947, *J. Amer. Chem. Soc.* **69**, 2866.
- McCoy, H.N., 1935, *J. Amer. Chem. Soc.* **57**, 1756.
- Miller, J.H. and J.E. Powell, 1976, unpublished data.
- Minczewski, J. and R. Dybczynski, 1962, *J. Chromatogr.* **7**, 98.
- Moeller, T., 1963, *The Chemistry of the Lanthanons* (Reinhold, New York).
- Moeller, T., 1973, *The Lanthanides*, in: Bailar, J.C., H.J. Emelius, R. Nyholm and A.F. Trotman-Dickenson, eds., *Comprehensive Inorganic Chemistry*, Vol. 4 (Pergamon Press, Oxford) pp. 1-101.
- Molnar, F., A. Horvath and V.A. Khalkin, 1967, *J. Chromatogr.* **26**, 215, 225.
- Nedden, P.Z., E. Merciny and G. Duyckaerts, 1973, *Anal. Chim. Acta* **64**, 197.
- Nervik, W.E., 1955, *J. Phys. Chem.* **59**, 690.
- Nishi, T. and I. Fujiwara, 1964, *Nippon Genshiryoku Gakkaiishi* **6**, 15.
- Novak, V., J. Lucansky and J. Majer, 1968a, *Chem. Zvesti* **22**, 721.
- Novak, V., J. Lucansky and J. Majer, 1968b, *Chem. Zvesti* **22**, 733.
- Novak, V., J. Lucansky, M. Svickova and J. Majer, 1974, *Chem. Zvesti* **28**, 324.
- Onstott, E.I., 1955, *J. Amer. Chem. Soc.* **77**, 2129.
- Onstott, E.I., 1956, *J. Amer. Chem. Soc.* **78**, 2070.
- Pierce, T.R., P.F. Peck and R.S. Hobbs, 1963.
- Powell, J.E. H.R. Burkholder and K. Gondo, 1971, *J. Chromatogr.* **54**, 259.**
- Spedding, F.H., J. E. Powell and E.J. Wheelwright, 1954, *J. Amer. Chem. Soc.* **76**, 2557.**
- Wodkiewicz, L. and R. Dybczynski, 1967, *Inst. Nucl. Res. (Warsaw), Rep. No. 860/VII/C.***
- J. Chromatogr.* **12**, 81.
- Powell, J.E., 1961, paper 4, Symposium on Rare Earths (1960) Lake Arrowhead, Calif., in: Kleber, E.V., ed., *Rare Earths*, Vol. 1 (Macmillan, New York).
- Powell, J.E., 1964, *The Separation of Rare Earths by Ion Exchange*, in: Eyring, L., ed., *Progress in the Science and Technology of the Rare Earths*, vol. 1 (Pergamon Press, Oxford) pp. 62-84.
- Powell, J.E. and H.R. Burkholder, 1966, USAEC Report IS-1305.
- Powell, J.E. and H.R. Burkholder, 1967, *J. Chromatogr.* **29**, 210.
- Powell, J.E. and H.R. Burkholder, 1968a, *J. Chromatogr.* **36**, 99.
- Powell, J.E., H.R. Burkholder and D.B. James, 1968b, *J. Chromatogr.* **32**, 559.
- Powell, J.E., D.A. Johnson, H.R. Burkholder and S.C. Vick, 1973, *J. Chromatogr.* **87**, 437.
- Preobrashenskii, B.K., A.V. Kalyamin and D.M. Lilova, 1957, *Zhur. Neorg. Khim.* **2**, 1164.
- Schoebrechts, F., E. Merciny and Duyckaerts, 1973, *J. Chromatogr.* **79**, 293.
- Schwarzenbach, G., R. Gut and G. Anderegg, 1954, *Helv. Chim. Acta* **37**, 937.
- Sockaska, R.J. and S. Siekierski, 1964, *J. Chromatogr.* **16**, 376.
- Spedding, F.H., E.I. Fulmer, T.A. Butler and J.E. Powell, 1950, *J. Amer. Chem. Soc.* **72**, 2349, 2354.
- Spedding, F.H., J.E. Powell and E.J. Wheelwright, 1956, *J. Amer. Chem. Soc.* **78**, 34.
- Spencer, J.F., 1919, *The Metals of the Rare Earths* (Longmans, Green, London).
- Stewart, D.C., 1955, *Anal. Chem.* **27**, 1279.
- Surls, J.P. and G.R. Choppin, 1957, *J. Amer. Chem. Soc.* **79**, 855.
- Templeton, D.H. and C.H. Dauben, 1954, *J. Amer. Chem. Soc.* **76**, 5237.
- Thompson, L.C., 1962, *J. Inorg. Nucl. Chem.* **24**, 1083.
- Trifonov, D.N., 1963, *The Rare Earth Elements* (Macmillan, New York).
- Vickery, R.C., 1953, *Chemistry of the Lanthanons* (Academic Press, New York).
- Weaver, B., 1974, *Solvent Extraction in the Separation of Rare Earths and Trivalent Actinides*, in: Marinsky, J.A. and Y. Marcus, eds., *Ion Exchange and Solvent Extraction*, Vol. 6 (Marcel Dekker, New York) pp. 189-277.
- Wheelwright, E.J., F.H. Spedding and G. Schwarzenbach, 1953, *J. Amer. Chem. Soc.* **75**, 4196.
- Wheelwright, E.J., 1969, *J. Inorg. Nucl. Chem.* **31**, 3287.
- Wodkiewicz, L. and R. Dybczynski, 1968, *J. Chromatogr.* **32**, 394.
- Wodkiewicz, L. and R. Dybczynski, 1972, *J. Chromatogr.* **68**, 131.
- Wolfsberg, K., 1962, *Anal. Chem.* **34**, 518.
- Yost, R.M., H. Russell and C.S. Garner, 1947, *The Rare Earth Elements and Their Compounds* (John Wiley and Sons, New York).

Chapter 23

THEORETICAL CHEMISTRY OF RARE EARTHS

Christian K. JØRGENSEN

Department of Inorganic and Analytical Chemistry, University of Geneva,
 CH 1211 Geneva 4, Switzerland

Contents

1. Electronic densities of spherical symmetry	112
1.1. Ionic radii and coordination number N	114
1.2. Ionization energies and hydration energies	122
1.3. Chemical polarizability and Pearson softness	133
2. Electronic configurations and multiplet structure	138
2.1. Huge differences between ionization energy and electron affinity, and the phenomenological baricenter polynomial	139
2.2. Spin-pairing energy and the double zig-zag curve	143
2.3. Electron transfer spectra and redox processes	147
2.4. The conditions for unusual oxidation states	151
2.5. Photo-electron spectra (ESCA)	153
2.6. Metallic and semi-conducting solids	157
2.7. Evidence for weak covalent bonding and the nephelauxetic effect	159
2.8. Collective effects in transparent materials	163
References	166

Symbols

A_* = parameter of interelectronic repulsion
 A_l = angular function

a = L.C.A.O. coefficient
 B = Racah parameter of inter-electronic repulsion in d groups
 D = spin-pairing energy parameter
 d = Rydberg defect
 dI = chemical shift of photo-electron signals
 $d\beta$ = nephelauxetic shift relative to R(III) aqua ions
 E^0 = standard oxidation potential
 E^1 and E^3 = Racah parameters of inter-electronic repulsion in f groups
 $(E - A)$ = parameter of spin-pairing energy theory
 E_{kin} = kinetic energy of photo-electron
 $h\nu$ = photon energy
 I = orbital ionization energy
 I^* = ionization energy of solid relative to Fermi level
 I_{chem} = chemical ionization energy
 I_n = ionization energy of gaseous ion
 \mathcal{J} = Heisenberg parameter
 J = total angular quantum number of many-electron system
 j = one-electron angular quantum number
 K_{av} = exchange integral of two-electron operator
 L = orbital angular quantum number of many-electron system
 l = one-electron orbital angular quantum number
 M_S = component along linear axis of total spin quantum number
 \mathcal{N} = number of nuclei in poly-atomic entity
 N = coordination number

q = number of 4f electrons	ΔH = change of enthalpy
R = internuclear distance	ΔH_{atom} = heat of atomization
r_{ion} = ionic radius	ΔH_{hydr} = hydration energy of gaseous ion
S = total spin quantum number	ϵ_{nl} = binding energy of single electron to closed-shell core
S_{max} = highest S of electron configuration	ζ_{nl} = Landé parameter of spin-orbit coupling
T = absolute temperature	κ = parameter of hydration energy difference
U = Hubbard parameter	ν_{aqua} = wavenumber of sharp bands of R(III) aqua ion
$U(r)$ = central field	$\nu_{\text{e.t.}}$ = wavelength of first strong electron transfer band
x_{opt} = optical electronegativity	σ_{A} = softness parameter according to Ahrland
x_{uncorr} = uncorrected optical electronegativity of 4f group central atom	σ_{K} = softness parameter according to Klopman
Z = atomic number	
z = ionic charge (or oxidation state)	
α = electric dipolar polarizability	
β = nephelauxetic ratio	
ΔG = change of free energy	

1. Electronic densities of spherical symmetry

The title of this chapter "Theoretical Chemistry" should not be extrapolated precociously to a situation where the thermodynamic equilibria determined by free energy differences, and the kinetic reaction rates, can be calculated with sufficient precision. One of several major difficulties is that a (non-linear) molecule or polyatomic ion containing \mathcal{N} nuclei has its energy determined by potential surfaces having $(3\mathcal{N} - 6)$ spatial variables, assuming the validity of the Born-Oppenheimer approximation (where three rotational and three translational degrees of freedom can be neglected). The typical quantum-chemical calculation assumes a fixed set of internuclear distances (by the way, this manifold of distances is sufficient to characterize the nuclear skeleton without any explicit reference to the point-group, if the distinction between optically active enantiomers is neglected). Hence, such a calculation is intrinsically suitable for spectroscopic transitions and for ionization processes studied in photo-electron spectra, in both cases obeying the Franck-Condon principle, where a definite distribution of nuclear positions occurs. On the other hand, the general chemical reaction is adiabatic in the sense that the internuclear distances are allowed to vary.

Obviously, the evaluation of potential surfaces in $(3\mathcal{N} - 5)$ -dimensional spaces becomes far more complicated and time-consuming, when the number \mathcal{N} of nuclei increases. This is one reason why theoretical chemistry in the strong sense is generally restricted to small molecules in the gaseous state. However, it is not possible to conclude from the positive dissociation energy of a given molecule (to isolated, gaseous atoms) that there is stability in the condensed states (liquids, amorphous and crystalline solids). For instance, the diatomic molecules BH and SiO rearrange by condensation, and NO is thermodynamic-

ally highly unstable relative to N_2 and O_2 . The same is true (at moderate temperature) for CO in spite of this molecule having one of the highest known dissociation energies. The gaseous state is particularly favourable toward unipositive complex ions if the criterion of dissociation energies to monatomic species is accepted. It is confirmed by mass-spectra that nearly all combinations MX^+ (including noble gases being M) are stable toward dissociation, whereas the calculations for neutral HLiHe (containing six electrons) show marginal stability, as the only probable case of a neutral helium compound. On the other hand, quantum-chemical studies of H_3^+ , CH_5^+ , HeH^+ , HeO^+ , C_2^+ (having a ground state with a total *spin quantum number* $S = \frac{3}{2}$) and ArF^+ have been thorough and convincing. All of these species are far too oxidizing or too acidic to be compatible with any known solvents or anions to form solid salts.

Nevertheless, there are a quite specific set of properties of lanthanide compounds closely related to the behaviour of gaseous atoms and positive ions. For instance, a system containing q electrons can show the values of

$$S = 0 \text{ (singlet), } 1 \text{ (triplet), } 2 \text{ (quintet), } 3 \text{ (septet), } 4 \text{ (nonet), } \dots$$

when the number q is even, and

$$S = \frac{1}{2} \text{ (doublet), } \frac{3}{2} \text{ (quartet), } \frac{5}{2} \text{ (sextet), } \frac{7}{2} \text{ (octet), } \dots$$

when q is odd. The words in parentheses are the old names, customary in atomic spectroscopy, when Russell–Saunders coupling is a good approximation. In actual practice, it is of little importance that the highest possible value of S is $\frac{1}{2}q$. Whereas the two-electron atoms He, Li^+ , Be^{+2} , ... have sharply defined singlet and triplet energy levels, the lowest quartet levels of the three-electron atoms Li, Be^+ , ... have far higher energies than the first ionization energy corresponding to formation of the closed-shell electron configuration $1s^2$ (containing only one state, a singlet) by belonging to the highly excited configuration $1s2s2p$. The strong bonding of two electrons in the inner shell $1s$ prevents S values higher than 2 from being readily observed in the six-electron atoms C, N^+ , O^{+2} , ... and in the eight-electron atoms O, F^+ , Ne^{+2} , ...

The general consensus among organic chemists is that normal molecules are diamagnetic and have $S = 0$. Species having positive S are called "free radicals" and are expected rapidly to dimerize or to perform other reactions, with S vanishing in all end products. This does not prevent a few molecules (such as NO and ClO_2) containing an odd number of electrons and having ground states with $S = \frac{1}{2}$. It is much more striking that certain molecules have positive S in spite of an even number of electrons. O_2 was shown by Faraday to be paramagnetic, and Lennard–Jones demonstrated that the six states of the lowest M.O. (molecular orbital) configuration constitute three energy levels, the lowest with $S = 1$ and the other two with $S = 0$. This case of a triplet ground state is a consequence of a general result of two orbitals having exactly the same energy for group-theoretical reasons, containing only two of the four possible electrons. Such behaviour is far more frequent in the transition groups. Thus, the large majority of manganese(II) and iron(III) compounds contain five 3d-like electrons

and show $S = \frac{5}{2}$ in their ground states. Actually, in the 3d group, the compounds seem to be particularly stable when S is high.

However much the positive S values may seem unexpected to chemists working mainly with elements outside the transition groups, the high S values of ground states belonging to an electron configuration with one or several partly filled shells are well known in monatomic entities. Charlotte Moore has compiled all the energy levels except for the lanthanides and the elements from thorium onwards. It is to be hoped that the fourth volume of "Atomic Energy Levels" will be published soon. Even before 1927, Hund had established rules for the various quantum numbers of the ground state of a monatomic species containing one partly filled l -shell. For historical reasons, these non-negative integers are called:

$$l = 0 \quad 1 \quad 2 \quad 3 \quad 4 \quad 5 \dots$$

$$s \quad p \quad d \quad f \quad g \quad h \dots$$

and a given shell characterized by the combination of the positive integer n (larger than l) and l is able to accommodate a maximum of $(4l + 2)$ electrons. Until the half-filled shell containing $(2l + 1)$ electrons is reached, the ground state of a system containing q electrons (written as right-hand superscripts $3d^q$ or $4f^q$) has $S = \frac{1}{2}q$. In the second half of the shell, $S = \frac{1}{2}(4l + 2 - q)$ in agreement with Pauli's hole-equivalence principle (actually, the number of states and the distribution of other quantum numbers such as L and J are also the same in the two cases). It is important for chemists not to confuse the spin component M_S along a selected linear axis with S . Though the highest M_S value of a given system corresponds to the highest S , it is not valid to conclude that a lower M_S necessarily belongs to a lower S . The psychological problem is that boxes with arrows pointing in one of two opposite directions have been very popular among chemists as a representation of M_S being the arithmetic sum of $+\frac{1}{2}$ or $-\frac{1}{2}$ of each electron. However, quintet, triplet and singlet states can all have M_S zero.

The concepts derived from atomic spectra have been very important in the recent progress of understanding spectroscopic properties and such chemical questions as the deviations of the oxidation state from M(III) and the conditions for metallic character of the compounds. We return to these individual properties specifically dependent on $4f^q$ in section 2, and we start with the smoothly varying properties which can be described as if the lanthanide M(III) is a sphere of electronic density gradually decreasing its radius from lanthanum to lutetium. The contributions of quantum chemistry to this, apparently simpler problem, have been much more qualitative than the specifically spectroscopic statements.

1.1 Ionic radii and coordination number N

Seen from the point of view of quantum mechanics, a monatomic entity has no distinct surface. The structure of Schrödinger's equation indicates an exponential decrease of the wave function (and its square) as a function of large ~~inter~~ nuclear distance r . Actually, the wave function of a one-electron atom

decreases asymptotically as $\exp(-(2E)^{1/2}r)$ in atomic units

length: 1 bohr = $0.52917 \text{ \AA} = 5.2917 \times 10^{-11} \text{ m}$,

energy: 1 hartree = 2 rydberg = $27.2116 \text{ eV} = 219474.6 \text{ cm}^{-1}$,

velocity of light in vacuo: $137.036 \dots$ bohr/atomic unit of time,

where $-E$ is the negative energy of a stationary state. Though one might choose a limit of negligible size of the exponential function as a measure of the radius there is no doubt that such a choice would produce atomic radii of the type known from solidified noble gases, much larger than the radii known from ordinary compounds. It is general experience from crystallography of solids that the closest interatomic contacts fall into two categories: the former type of Van der Waals radii well-known from internuclear distances between two adjacent neutral molecules in a crystal, and the chemical bonds. The few exceptions of internuclear distances falling in the open interval between the two categories are quite interesting; one type is due to short contacts between metalloids due to strong hydrogen bonds (Speakman, 1972) such as FHF^- and H_2OH_2^+ and another type is due to residual chemical interactions which are quite frequent between adjacent sulfur atoms or between iodine atoms (Murray-Rust et al., 1975).

Slater (1964) emphasized that Bragg's original suggestion was to assign atomic radii to each element independent of the nature of the chemical bonding. This proposal is remarkably accurate but has certain weaknesses. Thus, the cesium-cesium distances in colorless NaCl-type CsF are shorter than in metallic cesium, though the former compound shows no sign of not being almost exclusively electrovalent. Students are often impressed by the highly different ionic and covalent radii given in text-books for a given element. This distinction is to a large extent an illusion. Roughly speaking, the cation M^{+z} in a compound MX_z is said to have an ionic radius 0.8 \AA smaller than the covalent radius of the M atoms, whereas the anion X^- is said to have an ionic radius 0.8 \AA larger than the covalent radius of X. Since the observable quantity is the M-X distance, the discrepancy between the two descriptions usually falls within the same interval of about 0.1 \AA as defined from the dispersion of apparent ionic radii of the same M^{+z} in different compounds. It must be added, in all fairness, that a certain boundary condition exists for this problem of dividing the M-X internuclear distance in two ionic radii so that the choice of crystal type in highly electrovalent compounds can be rationalized by the packing of hard spheres of two distinct radii. Thus, the iodide-iodide contacts in NaCl-type LiI and the oxide-oxide contacts in CaF₂-type CeO₂ give higher limits to the ionic radii of iodide and oxide.

It may be worthwhile considering explicitly the methodology of determining internuclear distances. Diffraction techniques of crystalline solids provide a time-average picture of the average content of the distinct unit cell, which is able exactly to fill the crystal without gaps or overlap by translations in three directions. Some internuclear distances are particularly well known, when they are geometrical constants multiplying the unit cell lengths (in which case the

atoms considered are said to occupy special positions). Thus, the cubic (having three equivalent cartesian axes) crystal types CsCl, NaCl, CuCl (frequently called zincblende, because it is one of the modifications known of ZnS) and CaF₂ have all their atoms at special positions. The distances to atoms at general positions (e.g. the Pt-Cl distances in the regular octahedron found in the cubic type K₂PtCl₆) are much more difficult to evaluate with great precision, and the experimental data needed are relative intensities of spots on a Weissenberg diagram, or less preferably, lines on a Debye powder diagram. Actually, one of the early arguments for almost exclusive electrovalent bonding was the vanishing intensity of reflections dependent only on the difference between the two constituents in NaCl-type NaF, KCl and RbBr having both the cation and the anion isoelectronic with neon, argon and krypton, respectively.

There is no doubt that crystallographers tend to overestimate the symmetry of their crystals, either by neglecting weak reflections, by studying twin samples, or simply by putting atoms on esthetically satisfactory positions and obtaining reasonable agreement with the calculated intensities. In the chemistry of the rare earths, one frequently meets statistically disordered, non-stoichiometric compounds, even of cubic symmetry. It is quite obvious that many inorganic compounds do not contain distinct molecules. Thus, in NaCl, each Na⁺ is surrounded by a regular octahedron of six Cl⁻, and each Cl⁻ is surrounded by a regular octahedron of six Na⁺. Hence, in both cases, the *coordination number* $N = 6$ for both the cation and the anion. In CsCl, they both have $N = 8$. In a way, CaF₂ is a super-structure of CsCl, lacking half the cations in a systematic manner (and retaining cubic symmetry). Ca⁺² has $N = 8$ with eight F⁻ forming a cube, whereas F⁻ has $N = 4$ with four Ca⁺² forming a regular tetrahedron. Goldschmidt pointed out that many CaF₂-type minerals are strongly non-stoichiometric. Thus, yttrifluorite Ca_{1-x}Y_xF_{2+x} contains yttrium(III) to the extent of x up to 0.3, and the excess fluoride is situated on the empty cation positions (compared with CsCl) like the excess oxide in the non-stoichiometric UO_{2+x}. On the whole, it is more usual to have a deficit of anions in the statistically disordered fluorites, as is known from thorianite Th_{1-x}R_xO_{2-0.5x} (in the following, R denotes a mixture of various lanthanides). It is possible to drive synthetic samples of Th_{1-x}La_xO_{2-0.5x} up to $x = 0.54$. The Nernst lamp (Möbius, 1962, 1964) is a mixed oxide such as CaF₂-type Zr_{1-x}Y_xO_{2-0.5x} or Zr_{1-x}Mg_xO_{2-x} (with x around 0.1) conducting electricity above 500°C, not by transport of electrons (like in metals and semiconductors) but by diffusion of oxide anions among the vacant positions (more similar to hot AgI or to molten salts). Such mixed oxides are conveniently prepared by co-precipitating mixed aqueous solutions (containing the quadrivalent and trivalent metals) with aqueous ammonia (not producing non-volatile cations). The hydroxide precipitate is washed, dried and calcined, say at 800°C, to an intimately mixed oxide, though the crystal type (Jørgensen and Rittershaus, 1967) identified with Debye powder diagrams does not always correspond to thermodynamic equilibrium. Thus, equal amounts of erbium(III) and zirconium(IV) produce the disordered fluorite Er_{0.5}Zr_{0.5}O_{1.75} statistically lacking an eighth of the oxide. The same result is obtained with dysprosium(III)

when the mixed hydroxide is calcined at moderate temperatures, whereas $\text{Dy}_2\text{Zr}_2\text{O}_7$ prepared at 1200°C is a cubic superstructure of fluorite, pyrochlore, where M(III) has $N = 8$ in a distorted cube and M(IV) has $N = 6$ in a distorted octahedron. The pyrochlore structure has been carefully investigated in $\text{Er}_2\text{Ti}_2\text{O}_7$ where the smaller Ti(IV) pulls the oxide anions away from Er(III). Caro (1972) has discussed the interesting situation that certain disordered mixed oxides show epitaxial layer structures which also can be studied using electron micrographs.

One of the striking aspects of certain crystal structures containing rare earths is that small but systematic deviations occur from high symmetries. Thus, the cubic perovskite SrTiO_3 has the large strontium(II) surrounded by twelve oxide anions forming a tetrakaidecahedron (usually called a cuboctahedron) and the smaller titanium(IV) surrounded by six oxide anions in a regular octahedron. Related materials such as BaTiO_3 (which should not be called titanates because they do not contain discrete titanate anions like carbonate in BaCO_3 or phosphate and orthovanadate in RPO_4 and RVO_4) have transitions between crystal-line modifications of slightly different symmetry. In particular, some of these modifications are ferroelectric, having quite unusually large dielectric constants. This phenomenon has not been reported for the perovskites RMO_3 formed by a large R(III) and a small M(III), such as aluminum. However, these perovskites have generally non-cubic symmetries. Their magnetic properties can be rather unusual in cases of $M = \text{chromium}$ (having $S = \frac{3}{2}$) and iron ($S = \frac{5}{2}$) having a high spin quantum number. Another interesting fact (Schneider and Roth, 1960) is that La(III) and the heaviest lanthanides have sufficiently different ionic radii that LaErO_3 , LaTmO_3 and LaYbO_3 are perovskites though some of these samples decompose by heating above 650°C , forming among other products a type of mixed oxide NdYO_3 only characterized by its powder diagram (Jørgensen and Rittershaus, 1967). However, there is spectroscopic evidence (Faucher and Caro, 1975) that perovskites containing lanthanides such as $\text{La}_{1-x}\text{Eu}_x\text{AlO}_3$ have rather low local symmetry, and one should not expect $N = 12$ to correspond to roughly equal La-O distances.

The three classical types of rare earths are the hexagonal A-type R_2O_3 where R has $N = 7$ (two triangles in planes perpendicular on the axis containing the seventh neighbor atom), the complicated and low-symmetry B-type, and finally the cubic C-type (also known for Sc_2O_3 , In_2O_3 and Tl_2O_3) where $N = 6$. A quarter of R in the C-type has a surrounding similar to Ti in pyrochlore $\text{Er}_2\text{Ti}_2\text{O}_7$ whereas 75% of the R have six oxide neighbors very far from forming a regular octahedron. Bergerhoff (1964) and Caro (1968) have pointed out that these highly irregular structures are much more regular when seen from the point of view of the oxygen atom. Actually, these and many other oxides have to a good approximation four atoms M in a circumscribing regular tetrahedron, as is known from the so-called basic beryllium acetate $\text{OBe}_4(\text{O}_2\text{CCH}_3)_6$ whereas N is also 4 in BeO and ZnO , but the structure is hexagonal (like in the wurtzite modification of ZnS). The corundum type ($\alpha\text{-Al}_2\text{O}_3$) is also known from V_2O_3 (which is a physical metal above the Mott transition temperature), Cr_2O_3 , Fe_2O_3 and Ga_2O_3 and has $N = 4$ for oxide and $N = 6$ for M(III) being much closer to a

regular octahedron than is the case for C-type rare earths. It may be noted that in a binary compound M_aX_b where all the M atoms are equivalent, and where all the X atoms are equivalent, it is obvious that N (the number of M–X contacts) for M is (b/a) times N of X.

The whole question of N for trivalent lanthanides does not have the same context as in the iron(3d), palladium(4d) and platinum(5d) transition groups. The number q of 4f electrons does not have a specific influence on N going from one lanthanide to the next, whereas the d groups are very sensitive in this respect. It may be instructive to compare with one of the least transition-group-like elements, nickel. It is beyond discussion that certain compounds exist of Ni(IV), Ni(III) and Ni(0). These oxidation states are defined (Jørgensen, 1969a) from the presence of six, seven and ten 3d-like electrons in the preponderant electron configuration. However, the large majority is nickel(II) containing eight 3d-like electrons. Among these compounds, both the aqua ion $Ni(H_2O)_6^{+2}$, the NaCl-type NiO, the highest ammonia complex $Ni(NH_3)_6^{+2}$ and a large number of other examples have $N = 6$ with the neighbor atoms in a regular octahedron, and all the known $Ni(NH_3)_n(H_2O)_{6-n}^{+2}$ are approximately octahedral. Such cases, also known from rutile-type (a tetragonal modification of TiO_2) NiF_2 and cubic perovskites such as $KNiF_3$, all have $N = 6$ and are paramagnetic, corresponding to $S = 1$ of the ground state. The diamagnetic ($S = 0$) nickel(II) complexes usually have $N = 4$ with the four neighbor atoms in a square, such as $Ni(CN)_4^{-2}$ with all nine nuclei situated on a Greek cross, or in a rectangle, such as many sulfur-containing complexes like dithiocarbamates $Ni(S_2CNX_2)_2$ and dithiophosphates $Ni(S_2P(OX)_2)_2$ where X is CH_3, C_2H_5, \dots (Jørgensen, 1968b). However, other diamagnetic nickel(II) complexes have $N = 5$ like the red–orange $Ni(CN)_5^{-3}$ (formed in strong cyanide solutions) which is tetragonal-pyramidal like $Cu(NH_3)_5^{+2}$ formed in concentrated ammonia (Romano and Bjerrum, 1970). A few sporadic examples of unusual stereochemistry among paramagnetic ($S = 1$) complexes are now known, such as $N = 4$ in regular tetrahedral $NiCl_4^{-2}$ and $NiBr_4^{-2}$ occurring in certain non-aqueous solvents, e.g. CH_3CN , and in salts of large cations, e.g. $N(C_2H_5)_4^+$. This summary of nickel(II) chemistry shows that N has the moderate values 4, 5 and 6 also known from elements outside the transition groups such as phosphorus(V), indium(III) and tin(IV) and that spectroscopic properties (color and absorption spectra) and the choice between the alternatives $S = 1$ and 0 are intimately connected with the stereochemistry. The octahedral cases with $S = 1$ have one anti-bonding electron in each of the two d-orbitals (pointing towards the neighbor atoms) having angular functions proportional to $(x^2 - y^2)$ and $(3z^2 - r^2)$, whereas the three other d-orbitals with angular functions proportional to (xz) , (yz) and (xy) are filled with six electrons. The former feature (of two electrons in two orbitals having the same energy) provides a ground state with $S = 1$ as in O_2 . The quadratic (“square-planar” is rather redundant) cases with $S = 0$ have the strongly anti-bonding orbital $(x^2 - y^2)$ directed toward the four ligating atoms situated on the x - and y -axes empty, and the four other d-orbitals filled. The tetragonal-pyramidal cases of $N = 5$ and $S = 0$ have essentially the same distribution of electrons on the four lower

orbitals, but an additional complication is the absence of a centre of inversion allowing the mixture of *l*-values of the nickel atom with opposite parity. Such weak intermixing has observable effects on the intensities of the absorption bands due to internal transitions in the partly filled shell (Jørgensen, 1975b).

For reasons to be discussed below, it is quite certain that the 4f orbitals hardly have any influence on the chemical bonding in trivalent lanthanide compounds. This by no means excludes a considerable amount of covalent bonding. Unfortunately, it is very difficult to obtain reliable evidence for such bonding, because in the L.C.A.O. (linear combination of atomic orbitals) model, it is due to the five empty 5d orbitals and the empty 6s orbital. The same difficulty occurs at the end of the d groups, where the covalent bonding in copper(I), zinc(II) and gallium(III) compounds is highly probably, and due to the empty 4s orbital and, perhaps to a much lower extent, to the three empty 4p orbitals. We return below to the more qualitative reasoning behind the comparison of compounds with metalloids of varying electronegativity, but it may be mentioned that strongly calcined CeO₂ and ThO₂ dissolve remarkably slowly in acids, even in boiling sulfuric acid. Though it cannot be excluded that the exceedingly large Madelung potential in these fluorite-type crystals provides a high Arrhenius activation energy for dissolution, it would seem likely to be an expression of partly covalent bonding. Actually, the X-ray emission spectra (Bonnelle, 1976) of these oxides suggest a certain covalence involving a mixture of oxygen 2p orbitals with Ce4f and Th5f orbitals, e.g. having the angular function proportional to (*xyz*) pointing toward all eight neighbor atoms. Anybody dissolving sesquioxides in aqueous acids will also notice that A-type oxides react rapidly, if not violently, like MgO, whereas calcined C-type containing no carbonate is unreactive. Furthermore, it is striking that one may heat the suspension for some twenty minutes, and then, within a few minutes, a kind of autocatalytic reaction seems to occur, producing a limpid solution.

For many years the general model used for M.O. calculations in molecules was L.C.A.O., which might be justified by the very weak effects of chemical bonding (except hydrogen) compared with the binding energy (roughly $Z^{2.4}$ rydberg) of the atoms consisting of a nucleus with the charge $+Z$ surrounded by Z electrons. However, this is a rather vague argument, because the loosest bound electrons have ionization energies I between 0.4 and 1.2 rydberg, not much more than the bond dissociation energies. Whereas attempts to solve the Schrödinger equation directly with a self-consistent potential for electrons were previously made for infinite crystals (in the model of augmented plane waves) there has recently been a certain interest in the $X\alpha$ model for oligoatomic systems (Johnson, 1973) providing I in good agreement with photo-electron spectra. One of the qualitative descriptions related to such direct techniques disregarding the LCAO hypothesis is the valence-shell electron-pair repulsion (VSEPR) elaborated by Gillespie (1972). This description has certain virtues for molecules formed by elements outside the transition groups, where a given spherical region of the valence shells is divided between bulky lone-pairs, and bonding electron pairs having smaller angular requirements when the other atom

has a higher electronegativity. It is obvious that such a description is related to the virial theorem, that the electronic kinetic energy in any stationary state cancels exactly half the potential energy. Orbitals with high l can tolerate being confined in a smaller volume, since the kinetic energy (assuming identical shapes) is inversely proportional to the square of the scaling factor expressing the relative linear extension. However, the weak point is that it is an empirical fact that the 2p group elements (boron to fluorine) have four electron pairs in their valence shell (as first suggested by Lewis in the so-called octet hypothesis) whereas the subsequent elements tend to have six pairs. Such behavior could be rationalized if the idea of Kimball of non-overlapping spheres each containing two electrons was a good approximation, yielding a picture of tetrahedral or octahedral distributions of spheres. Quantitatively, this picture is unsatisfactory by yielding far too high values for the kinetic energies of the electrons confined in the spheres, and in the writer's opinion, it is a misunderstanding to explain the more or less successful VSEPR description by Pauli's exclusion principle. This principle only demands mutual orthogonality of the orbitals each containing at most two electrons, but does not demand lack of coexistence of several orbitals in our three-dimensional space. Thus, the integral of the product $A_1^2 A_2^2$ of the square of two angular functions A_1 and A_2 on a spherical surface with constant r is $\frac{3}{5}$ for the two p-orbitals (x) and (y) compared with A_3^2 of the d-orbital having A_3 proportional to (xy) . Again, this integral expressing spatial coexistence is $\frac{5}{7}$ for the two d-orbitals (concentrated in the xy -plane) having angular functions proportional to $(x^2 - y^2)$ and (xy) compared with A_3^2 for the corresponding g-orbital. It is a much more profound fact that in spite of electrostatic interactions being the only attraction acting in atoms, molecules and crystals, the kinetic operator is the specific feature of quantum mechanics preventing implosion, since the potential energy of a stable electrostatic system becomes x times more negative, when all the distances are divided by x . Ruedenberg (1962) analyzed thoroughly how the changes of kinetic energy are the driving force behind covalent bonding. It may be noted that the kinetic operator and the virial theorem also determine the average radius of the 1s electron in a hydrogen atom, where Pauli's exclusion principle plays no rôle. A fundamental difficulty for electron-pair descriptions is that it is by no means certain that all chemical bonds can be assigned two electrons in a significant way. Whereas the 18-electron rule (that N of d^q systems, assuming even q , is $\frac{1}{2}(18 - q)$) has a certain success, in particular for organometallic complexes (though many exceptions are known, such as square d^8 $\text{Ni}(\text{CN})_4^{-2}$ and linear d^{10} $\text{Cu}(\text{CN})_2$) there are all kinds of difficulties involved in assigning $2N$ electrons to covalent bonding, culminating in NaCl-type oxides, nitrides and carbides (e.g. NiO, CdO, LaN and HfC) where $N = 6$ in excess of the number 4 of conceivable valence orbitals, and in CaF_2 -type Be_2C with $N = 8$ of carbon (Jørgensen, 1971b).

When considering the high variability of N of lanthanides recently reviewed by Sinha (1976), it is not probable that any intrinsic property of the 4f group atoms predetermines a high propensity for a given N and symmetry, as known from octahedral $3d^3$ chromium(III), $3d^6$ cobalt(III), $3d^8$ nickel(II), $4d^6$

rhodium(III) and $5d^6$ iridium(III) and platinum(IV). In the lanthanides, $N = 3$ is represented not only by gaseous RBr_3 and RI_3 (of which certain optical transitions have great theoretical interest, seen below) but also by the tris-complex of $N(Si(CH_3)_3)_2^-$ containing the chromophore (central atom plus the surrounding nearest neighbour atoms) $R(III)N_3$ (Bradley et al., 1973). The lutetium complex anion containing $Lu(III)C_4$ (like tetraphenylborate) with four 1-deprotonated 2,6-dimethyl benzene ligands represents one of the rare well-established cases of $N = 4$. The chromophore $Er(III)S_4$ can be realized by incorporating small amounts of erbium in crystalline $CdGa_2S_4$. Though $N = 6$ is not rare, the regular octahedron is not at all frequent. RCl_6^{-3} , RBr_6^{-3} and RI_6^{-3} are known in aprotic solvents (Ryan and Jørgensen, 1966; Ryan, 1969) such as acetonitrile, and in certain salts (Schwartz, 1975; Serra and Thompson, 1976) such as $Cs_2NaEuCl_6$. The crystalline structures show a distribution of $N = 7, 8$ and 9 peaking perhaps slightly above 8 . In most cases, one cannot determine a generally valid description of the ligating atoms forming a definite polyhedron. $N = 12$ is known (Zalkin et al., 1963) in the cubic crystals $[Mg(H_2O)_6^{+}]_3[R(O_2NO)_6^{-3}]_2 \cdot 6H_2O$ where twelve oxygen atoms from six bidentate nitrate ligands form an approximately regular icosahedron. Interestingly enough, Judd (1957) had predicted the icosahedral chromophore $Nd(III)O_{12}$ from the fine-structure of the J -levels studied by absorption spectra, before the crystal structure was determined. Whereas boron chemistry represents several cases of icosahedral cage structures, they are not frequent, because a repeated crystal lattice cannot contain five-fold axes. This does not prevent oligoatomic subsystems in a crystal having rotational axes of any order. Thus, the cerium(III) cyclooctatetraenide complex $Ce(C_8H_8)_2^-$ is isosteric with uranocene $U(C_8H_8)_2$ and has $N = 16$, the ligands forming two regular octagons in parallel planes. Quite generally, the recently developing organolanthanide chemistry shows many examples of high N (though the tetra-phenyl derivatives have $N = 4$ only) such as the bridged chloro- and cyclopentadienide complex $(C_5H_5)_2YbCl_2Yb(C_5H_5)_2$ with $N = 12$, containing the chromophore $Yb(III)C_{10}Cl_2$ and the cyclohexylisonitrile adduct of ytterbium(III) cyclopentadienide $(C_5H_5)_3YbCNC_6H_{11}$ having $N = 16$, quite analogous to the uranium(IV) complex $(C_5H_5)_3UCl$. At this point, it may be worthwhile noting that the only reasonable definition of N in ferrocene $Fe(C_5H_5)_2$ is 10 because 10 equivalent $Fe-C$ distances occur. A superstitious respect for the 18-electron rule has induced some authors to the almost metaphysical opinion that $N = 6$ in this molecule, in spite of 3 and 5 containing no common prime factors.

We may return to the meaning of interatomic distances and of the coordination number N . It is a minor detail that diffraction of X-rays indicates the centre of electronic density and diffraction of neutrons (disregarding the effects of partly filled shells observed in magnetically ordered compounds) indicates the position of the nuclei. Even when not demanded by symmetry, these two techniques agree very closely, and actually, the electronic densities seem to be a superposition of standard atomic quantities, with the marginal exception of hydrogen atoms, which are deformed and somewhat contracted (as predicted by

Ruedenberg, 1962) in compounds. A more serious problem is the time-average of the vibrational motion distorting the instantaneous picture obtained by spectroscopic techniques. In modern, refined crystal structures, ellipsoids of thermal motion are determined. By the same token, the rotational spectra (studied in the microwave region) of gaseous molecules give a time-average. Diatomic molecules show the average of R^{-2} from which a so-called internuclear distance R can be given with five or six decimals, in spite of the standard deviation on an instantaneous picture being several percent. On the other hand, electron diffraction of gaseous molecules produce time-average interatomic distances much like X-ray diffraction but lacking the anisotropic information derived from the spatial orientation in the crystal. In all cases, it can become a problem to define N if a distribution of non-equivalent distances is obtained. For instance, La(III) in LaF_3 has eleven fluorine neighbors, but two have such long distances that $N = 9$ may be the better description. It is a matter of taste whether CsCl with identical Cs and Cl (known from metallic iron and tungsten) has $N = 8$ or 14, six of the distances being 15.47% longer than the eight.

1.2. Ionization energies and hydration energies

Alfred Werner was the first to argue that aqua ions $\text{M}(\text{H}_2\text{O})_N^{z+}$ are complexes of coordinated water molecules on an equal footing with ammonia or other complexes. The prototype of an aqua ion is the mixed complex $\text{Co}(\text{NH}_3)_5(\text{H}_2\text{O})^{+3}$ studied by S.M. Jørgensen, where a reversible (pH dependent) equilibrium occurs with H_{aq}^+ (in contrast to NH_4^+ in liquid ammonia, it is not certain that H_3O^+ or H_9O_4^+ occur in aqueous solution, and such species last for a *very* short time before the proton is somewhere else in the solvent) and $\text{Co}(\text{NH}_3)_5\text{OH}^{+2}$. As early as 1909, Niels Bjerrum suggested that $\text{Cr}(\text{H}_2\text{O})_6^{+3}$ would persist, both in alums and in water, partly based on the slow equilibrium with Cl^- and with NCS^- to form $\text{Cr}(\text{H}_2\text{O})_5\text{Cl}^{+2}$ and $\text{Cr}(\text{H}_2\text{O})_5\text{NCS}^{+2}$. Regularities in kinetic evidence suggested that the rate-determining step in all such reactions is the dissociation to a highly reactive $\text{Cr}(\text{H}_2\text{O})_5^{+3}$ but this could not be firmly proven before Taube (1952) used the isotope oxygen 18 for tracer experiments, finding a half-life of the exchange of water molecules with the bulk solvent about 1 day at 25°C. A similar (much cheaper) experiment with deuterium does not yield a significant result because of the rapid equilibrium with $\text{Cr}(\text{H}_2\text{O})_5\text{OH}^{+2}$ (and H_{aq}^+) recombining with D_{aq}^+ to form $\text{Cr}(\text{H}_2\text{O})_5(\text{DOH})^{+3}$ and finally $\text{Cr}(\text{D}_2\text{O})_6^{+3}$ without ever breaking the Cr–O bonds. The latter reactions can be recognized by having rates inversely proportional to the concentration of H_{aq}^+ as found by Niels Bjerrum for the reaction between chromium(III) aqua ions and anions.

From a classical physico-chemical point of view, it is not possible to determine the coordination number N of an aqua ion from equilibria in a strong excess of water, or for that matter of an ammonia complex in liquid ammonia. As first pointed out by Niels Bjerrum the fact that visible absorption spectra of colored complexes are almost exclusively determined by the first coordination sphere (the immediate neighbor atoms forming what we call the inorganic

chromophore) can be used to recognize a definite complex, even when it is an aqua ion with well-defined N and symmetry. This approach has been favored by the comparison with reflection or absorption spectra of solids with known crystalline structure, and by the understanding of the excited levels of the partly filled d shell using what is traditionally called the "ligand field" theory, though it is really MO theory with particular emphasis on effects of interelectronic repulsion (which are generally smaller for the high S values, explaining Hund's rule). Since about 1955, it has been possible in many cases to recognize N and the geometry of the chromophore. The nature of the ligands determines the numerical values (when sufficient information is known about the central atom) of the parameters of the description in the spectrochemical series and the nephelauxetic series. On the other hand, arguments derived from transport properties in electrolysis, or from extraction into other solvents, may give an idea about how many water molecules are transported together with an aqua ion, but they do not give reliable information about how many of these molecules are situated in the first coordination sphere. There is little doubt that the ligating water molecules are particularly apt to form intricate hydrogen bonds to the solvent just outside the first coordination sphere. This is one reason why aqua ions can be so remarkably reluctant to react with anions. Thus, $[\text{Al}(\text{H}_2\text{O})_6]\text{Cl}_3$ can be crystallized from concentrated hydrochloric acid. This is also true for grey-violet $[\text{Cr}(\text{H}_2\text{O})_6]\text{Cl}_3$ though the equilibrium in the supernatant solution contains green species such as $[\text{Cr}(\text{H}_2\text{O})_4\text{Cl}_2]^+$.

At the present time, the central atoms fall in two rather distinct groups as far as identification of a definite aqua ion in an aqueous solution goes. The absorption spectra and "ligand field" arguments have put $N = 6$ with regular octahedral symmetry on a firm basis for Ti(III), V(II), V(III), Cr(III), Mn(II), Fe(II), Fe(III), Co(II), Ni(II), Ru(II), Ru(III) and Rh(III) in agreement with Werner's ideas. There are some problems with Jahn-Teller unstable Cr(II), Mn(III) and Cu(II) which we do not need to discuss here. Palladium(II) seems to form a square $\text{Pd}(\text{H}_2\text{O})_4^{+2}$ though certain aspects of formation constants and band intensities (Jørgensen, 1963a and 1975b) may indicate weak deviations from high symmetry on an instantaneous picture, as is also true for copper(II). The progress in the field of colorless aqua ions has been more difficult, and conclusive evidence for N has mainly been obtained from oxygen 17 nuclear magnetic resonance. It is no great surprise that $\text{Be}(\text{H}_2\text{O})_4^{+2}$ is regular tetrahedral; in alkaline solution, it is deprotonated to the anion $\text{Be}(\text{OH})_4^{-2}$ (corresponding to the amphoteric behaviour of the beryllium hydroxide precipitate being soluble in an excess of OH^-). The hexaqua ions of magnesium(II), aluminum(III), zinc(II) and gallium(III) have been fully established. Following the pioneering work of Jannik Bjerrum (1941, 1950) on the mixed aqua-ammonia complexes $\text{Ni}(\text{NH}_3)_n(\text{H}_2\text{O})_{6-n}^{+2}$ there was a tendency to identify the highest n for the ammonia complex of a given central atom (in a definite oxidation state) with N for the aqua ion. This has been verified for Cr(III), Fe(II), Co(II), Co(III), Ni(II), Ru(II), Ru(III) and Rh(III) but is not necessarily universally valid. Though $\text{Zn}(\text{NH}_3)_4^{+2}$ is tetrahedral, the overwhelming majority of zinc(II) aqua ions are

octahedral. It is true that the linear $\text{Ag}(\text{NH}_3)_2^+$ has not been shown to react with additional ammonia in aqueous solution, but this is no proof of the constitution of the silver(I) aqua ion, and there is actually evidence (Gans et al., 1976) that liquid ammonia contains $\text{Ag}(\text{NH}_3)_4^+$. Generally, the linear d^{10} systems are always somewhat suspected for increasing their N to 3, 4 or 6. The isoelectronic species $\text{Au}(\text{NH}_3)_2^+$, $\text{Au}(\text{CH}_3)_2^-$, $\text{Hg}(\text{NH}_3)_2^{+2}$, $\text{Hg}(\text{CH}_3)_2$ and $\text{Tl}(\text{CH}_3)_2^+$, or the linear pentatomic NCAuCN^- and NCHgCN are strikingly stable, but most of them are known to add the same or differing ligands to form tetrahedral mercury(II) and thallium(III) complexes, e.g. HgX_4^{-2} and TlX_4^- . On the other hand, octahedral TlCl_6^{3-} is only known from crystals such as the highly insoluble $[\text{Co}(\text{NH}_3)_6]\text{TlCl}_6$ but has not been detected in concentrated hydrochloric acid containing TlCl_4^- .

To the author's best knowledge, N has not been established for the aqua ions of Li(I), Na(I), Ca(II), Sc(III), Ag(I), Cd(II), In(III), Hg(II), Tl(I), Tl(III), Pb(II), Bi(III), Th(IV) and U(IV). Sufficiently large (and weakly positive) cations such as K^+ , Rb^+ , Cs^+ and Ba^{+2} have not been included in this list, recognizing the high probability that these ions do not fix a definite number of water molecules. In view of the discussion of the concept N given above, we must distinguish two kinds of difficulties: in an instantaneous picture, the aqueous solution may contain a mixture of different aqua ion species, either differing in symmetry alone, or also in N , but having roughly equal M–O internuclear distances compatible with an unusual vibrational motion, or another situation may occur where not only the number of nearest oxygen neighbor atoms varies, but also a great dispersion of different distances to the same central atom M. Though the two situations are not separated by a clear-cut dividing line, it is obvious that the description of the aqua ion as a distinct stoichiometric species cannot be taken seriously in the second case, whereas it is still legitimate to speak about the thermodynamic quantities characterizing the "standard state of the aqua ion in dilute aqueous solution" though these quantities may have somewhat unexpected differential quotients with respect to the temperature, due to a continuous rearrangement of the probability distribution of the various instantaneous pictures. The chemist should not yield to a conditional reflex of agnostic doubt in all such cases. For instance, the kinetic behaviour of chromium(III) in aqueous solution would be entirely different if concentrations above 10^{-14} M of $\text{Cr}(\text{H}_2\text{O})_5^{+3}$ or $\text{Cr}(\text{H}_2\text{O})_7^{+3}$ (with roughly equal Cr–O distances) occurred. Furthermore, a small concentration of distorted nickel(II) aqua ions (say 1%) would show up in a comparison of the absorption spectrum of $\text{Ni}(\text{H}_2\text{O})_6^{+2}$ in water with a crystalline sample, because most conceivable distortions strongly enhance the band intensities. For instance, a chromophore with odd N cannot possess a centre of inversion, and we know from the hundred times higher band intensities of CoX_4^{-2} and NiX_4^{-2} compared with the aqua ions what influence the lack of a centre of inversion has. This does not prevent systems containing more than three nuclei (considered as points) from nearly always belonging to the point-group C_1 (having only identity as symmetry element) and not to the (frequently highly symmetric) point-group characterizing the time-average picture.

In a sense, the aqua ions of the rare earths (including scandium, yttrium and the elements from lanthanum to lutetium) fall in between the two cases of defined and indefinite N . It is highly probable that N of the scandium(III) aqua ion is above 6 in spite of octahedral Sc(III) anion complexes (such as ScF_6^{-3}) existing. This difference from iron(III) and gallium(III) aqua ions may explain the discrepancies between the trend in observed formation constants of 3d group M(III) complexes and the interpolation (Jørgensen, 1974a) expected from "ligand field" arguments. The first crystal structure of a lanthanide aqua ion without anions in the first coordination sphere was $[\text{Nd}(\text{H}_2\text{O})_9](\text{BrO}_3)_3$ determined by Helmholtz (1939), and yttrium and all the lanthanides form isotypic ennea-aqua bromates. Another complete series of ennea-aqua salts is the ethylsulfates $[\text{R}(\text{H}_2\text{O})_9](\text{C}_2\text{H}_5\text{SO}_4)_3$. In both these series, six of the oxygen nuclei from the water molecules form almost exactly a trigonal prism. The three other oxygen nuclei are situated in an equilateral triangle in the plane midway between the other two triangles parallel to it, but rotated 60° in the middle plane. This geometry for $N = 9$ is not very frequent; one clear-cut analogy is the rhenium(VII) hydride complex ReH_9^{-2} . Going from $\text{R} = \text{La}$ to Lu , the three R-O distances in the equatorial plane tend to diminish much less than the six R-O distances in the trigonal prism, with the result that N shows a tendency to decrease from 9 to 6 (the α -Fe vs. CsCl problem mentioned above) for the smallest (heaviest) lanthanides, though the two series (of bromates and ethylsulfates) do not show modified crystal types. The calorimetric heat of dissolution of ethylsulfates in water changes in a very smooth way from La to Lu (Staveley et al., 1968; Mioduski and Siekierski, 1975).

There have been many discussions (Moeller et al., 1965) on whether N is the same from La(III) to Lu(III) aqua ions in solution. Seen from the point of view of formation constants (i.e. changes ΔG of free energy) and enthalpy differences ΔH , there is no doubt that irregularities are frequently found in the region around samarium, europium and gadolinium. However, this may be more a question of changes in the structure of mixed aqua-ligand complexes than in the aqua ions themselves. For instance, a clear-cut (but minute) shift occurs between two exceptionally sharp absorption lines of europium(III) ethylenediaminetetraacetates (Geier and Jørgensen, 1971) showing a temperature-dependent equilibrium between two forms $\text{Eu}(\text{H}_2\text{O})_{x+1}(\text{enta})^-$ and $\text{Eu}(\text{H}_2\text{O})_x(\text{enta})^-$ differing in constitution by one ligated water molecule. A more classical approach would be to determine the formation constants for binding water to anhydrous lanthanide salts in a non-aqueous solvent. Based on a rich material of absorption spectra photographed by Harry C. Jones before 1911, it was shown that the sharp bands of neodymium(III) of NdCl_3 in anhydrous methanol change in a characteristic way when small amounts of water are added. Actually, this change is half finished in 3 molar (5 vol.%) water, and almost complete in 10 molar water. Jannik Bjerrum and the author (1953) argued that the most probable N was 6, but actually, the formation curve is equally compatible with $N = 8$ or 9. Unfortunately, the situation is far more complicated by the Katzin effect that metal ions in anhydrous alcohols are particularly able to coordinate anions

(including nitrate) whereas small amounts of water (not increasing the dielectric constant significantly) displace the anions quantitatively. Hence, it is highly probable that the spectral changes serve, at the same time, as an indicator of loss of chloride from $\text{Nd}(\text{CH}_3\text{OH})_x\text{Cl}^{+2}$. This is an interesting contrast to the behaviour of Nd(III) in aqueous hydrochloric acid, where outer-sphere ion-pairs without perceptible influence on the visible spectra (but decreasing the thermodynamic activity of both $\text{Nd}_{\text{aq}}^{+3}$ and Cl^- seen from the point of ion-exchange resin and electrode equilibria) are formed with the formation constant K_1 close to 1, whereas a genuine $\text{Nd}(\text{H}_2\text{O})_x\text{Cl}^{+2}$ with a different spectrum (Malkova et al., 1964) is formed in 8 to 11 molar hydrochloric acid. It has long been known that moderate nitrate concentrations (say 1 molar) have a much stronger influence on the absorption spectra. This may be connected with the bidentate behaviour of lanthanide nitrate complexes, as well as the discrimination against more Pearson-soft ligands (discussed below) compared with fluoride and oxygen-containing ligands.

One of the most striking arguments for $N = 9$ of aqua ions in solution was given in 1931 by Freed who found the same band positions of the strong $4f \rightarrow 5d$ transitions in the ultra-violet of cerium(III) incorporated in $[\text{La}(\text{H}_2\text{O})_9](\text{C}_2\text{H}_5\text{SO}_4)_3$ and of the aqueous solution. A very curious situation persists for the first, relatively much weaker, band at 297 nm or 33700 cm^{-1} which is known (Heidt and Berestecki, 1955) to increase its intensity considerably, not only as a function of increasing temperature, but even by replacing D_2O by H_2O (this is an almost unique isotope effect). One conceivable interpretation is that it is due to an ennea-aqua ion with different symmetry from the crystal, or more likely, to an aqua ion with different N . The temperature influence suggests a lower N (such as 8) and the relative band intensities a concentration of this rare species of a few percent. However, it is entirely possible that the weak band belongs to the ennea-aqua ion, but is unusually weak because of a selection rule. Many cerium(III) anion complexes (Jørgensen, 1956a) have strong absorption bands in this region, including (Ryan and Jørgensen, 1966) the octahedral CeCl_6^{-3} and CeBr_6^{-3} . Krumholz (1958) suggested that $N = 9$ for the neodymium(III) aqua ion because of striking similarities between the spectrum of its solution in ice-cold, dilute perchloric acid and of the crystals. There is no comparable spectroscopic evidence available for the heavier lanthanides. It is not possible to conclude from the salt hydrates how big N is, even in the crystal. Thus, $\text{GdCl}_3 \cdot 6\text{H}_2\text{O}$ contains the grouping $[\text{GdCl}_2(\text{H}_2\text{O})_6]^+$ with $N = 8$ in much the same way as $\text{CoCl}_2 \cdot 6\text{H}_2\text{O}$ and $\text{NiCl}_2 \cdot 6\text{H}_2\text{O}$ contain the chromophore *trans*- $\text{M}(\text{II})\text{O}_4\text{Cl}_2$. Crystalline anhydrous LaCl_3 to GdCl_3 (but not TbCl_3 and YCl_3 with a distorted $N = 6$) and LaBr_3 to GdBr_3 have the trigonal chromophore with $N = 9$ known from the ennea-aqua ion, with each halide anion bound to three R. The general consensus today is that it seems plausible that all the aqua ions have $N = 9$, but it must be admitted that the evidence decreases as one goes from Ce(III) to Lu(III).

It is striking that even the six shortest R–O distances in the crystals containing ennea-aqua ions are 0.1 to 0.3 Å longer than in the hexagonal A-type and cubic

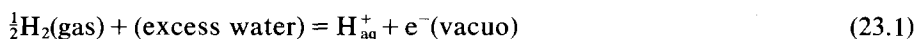
C-type R_2O_3 . This observation suggests a lack of angular directed (and important) covalent bonding in the aqua ions, but does not explain the reluctance to replace a water molecule with a chloride ligand (though $[Al(H_2O)_6]Cl_3$ may serve as an analogy). It is unlikely that the highly irregular disposition of $N = 6$ in the C-type sesquioxide reflects an intrinsic property of the lanthanides, since it is also found in Sc_2O_3 , In_2O_3 and the physical metal Tl_2O_3 (and the chronological prototype, the mineral bixbyite which is essentially Mn_2O_3 with a certain amount of iron(III) impurity) and Caro (1968) is quite correct in suggesting the C-type as an acceptable mode of packing regular tetrahedral OM_4 . It is not always easy to draw conclusions from salts of oxygen-containing anions. It is well understood that cubal $N = 8$ is known only in solids, such as the fluorite type, because any reasonable model of the inter-ligand repulsion makes the Archimedean anti-prism more stable in a monomeric eight-coordinated complex than in a cube (not all of the five regular polyhedra are favored) and it only needs very small fluctuations of energy to obtain competing geometries with $N = 8$. Actually, the zircon type $ZrSiO_4$ is represented by the mineral xenotime and the synthetic compounds YPO_4 and YVO_4 containing such Y(III) and Zr(IV) with $N = 8$. The phosphate mineral monazite and the orthoniobates and orthotantalates found in the mineral fergusonite contain comparable packing of tetrahedral monomeric anions. Sometimes, the choice of N seems rather indifferent. Among the two modifications of $CaCO_3$, aragonite has $N = 9$ and calcite (also represented by $MnCO_3$, $FeCO_3$, $CoCO_3$ and $NiCO_3$) has $N = 6$. There is no serious discrepancy between the lanthanides most frequently having $N = 6, 7$ and 8 in oxides and salts of oxygen-containing anions, but 9 in aqua ions, in view of the longer R-O distances in the latter case.

In 1927, when Hund wrote his book about atomic line spectra and the Periodic Table, it was not fully realized that there is no direct and simple relationship between the electron configuration to which the ground state of the neutral gaseous atom belongs, and the chemical behaviour of the element. Thus, there is less similarity between the chemistry of iron and ruthenium with homologous $[Ar]3d^64s^2$ and $[Kr]4d^65s^2$ than between nickel $[Ar]3d^84s^2$, palladium $[Kr]4d^{10}$ and platinum $[Xe]4f^{14}5d^96s$. A typical case of the discrepancies between the spectroscopic and the chemical versions of the Periodic Table is that not only the conventional alkaline earths, but also helium (in contrast to the other noble gases), zinc, cadmium, ytterbium and mercury are spectroscopic alkaline earths, with ground state closed-shell configurations terminating with two s electrons. Though it is obvious that the most common oxidation states of vanadium $[Ar]3d^34s^2$ and chromium $[Ar]3d^54s$ are not V(II) and Cr(I), Hund (1927) extrapolated from the ground state of the lanthanum atom belonging to $[Xe]5d6s^2$, and the almost invariant trivalence of the fourteen subsequent elements, that the ground states of the neutral atoms all belong to $[Xe]4f^95d6s^2$. This extrapolation (which was not based on spectroscopic observations) is now known to be valid only for cerium $[Xe]4f5d6s^2$, gadolinium $[Xe]4f^75d6s^2$ and lutetium (which it is most practical to consider as the first member of the 5d

group continuing with hafnium, tantalum, ...) whereas the eleven other lanthanides actually have ground states belonging to $[\text{Xe}]4f^{n-1}6s^2$ with only two "valence electrons".

Connick (1949) was the first to emphasize that the predominant trivalence of the lanthanides has nothing to do with the ground states of the neutral atoms, but is a numerical question of the relative size of the consecutive ionization energies, I_n , for the removal of an electron $M^{+n-1} \rightarrow M^{+n} + e^-$ in the gaseous state (with this definition, I_0 is the electron affinity of the M atom to form M^-) compared with the chemical stabilization going from the oxidation state $(n-1)$ to n . This problem arose in connection with the rather violent discussion between 1946 and 1956 on whether the presence of 5f electrons in trans-thorium elements necessarily induces a propensity toward trivalence. This is one more instance of differing spectroscopic and chemical versions of the Periodic Table, the ground state of the uranium atom belonging to $[\text{Rn}]5f^36d7s^2$ does not prevent U(VI) and U(IV) from being far more common than U(III), any more than the ground state of the neodymium atom belonging to $[\text{Xe}]4f^46s^2$ makes Nd(II) frequent.

In classical physical chemistry (Adamson, 1973) there is a strong reluctance to speak about thermodynamic properties of individual ions, and all species transported across the border between two phases have to be neutral, for instance by being a manifold of positive and negative ions accompanying each other. This voluntary restriction is justified by the almost incredibly exact electroneutrality of all macroscopic samples of matter. As a measure of what a chemist considers invariant, the rest mass of all chemical reactions is invariant to better than one part per 10^9 with the exception of the Langmuir torch combining two hydrogen atoms. However, deviations in typical macroscopic bodies from electroneutrality upto 10^{-9} correspond to electrostatic effects greatly in excess of the gravitational attraction at the Earth's surface. One corollary of the rule that one should not consider the energy of an electrically charged species in thermodynamics is that one does not speak about the ionization energy of condensed matter, losing an electron to the vacuo at a large distance. Another ingredient of this convention is that the electric potential zero is said to be possessed by the Earth in spite of the observations (first made by Benjamin Franklin) of large electric potential gradients in the vertical direction in the atmosphere. Nevertheless, for the atomic spectroscopist, there is nothing indecent about the ionization energy I_n of the monatomic entity M^{+n-1} (in fortunate cases of one loosely bound electron it may be determined with a precision approaching that of the wave-numbers of individual spectral lines, typically one part in a million, though it is obtained by extrapolation of observable energy levels and may be uncertain by several percent in complicated atoms) and the threshold of Einstein photo-electron emission from metallic surfaces indicates an I of condensed matter. A closer analysis of this problem boils down to the estimate of the absolute energy for the ionization process



traditionally taken (in the form of the standard hydrogen electrode) as the zero-point for *standard oxidation potentials* E^0 (which are now internationally agreed to be positive for the oxidation of $\text{Fe}(\text{H}_2\text{O})_6^{+2}$ to $\text{Fe}(\text{H}_2\text{O})_6^{+3}$ and negative for species sufficiently reducing to evolve molecular hydrogen, though many American authors previously used the opposite sign for E^0). Seen from a spectroscopic point of view, there is no doubt that the chemical ionization energy I_{chem} (an adiabatic quantity, allowing the internuclear distances to vary, in contrast to a process restricted to invariant nuclear positions by Franck and Condon's principle) is larger than E^0 by a definite constant. The best estimate of the latter constant is given by Rosseinsky (1965), after he had considered a large number of thermodynamic results, as being between 4.4 and 4.6 V, and probably quite close to 4.5 V. It is not certain that the entropy difference determining the distinction between ΔG and ΔH for the reaction (23.1) is completely defined, but the two quantities seem closely similar. Once it is accepted that

$$I_{\text{chem}} = E^0 + 4.5 \text{ eV} \quad (23.2)$$

is a legitimate quantity, the way is open for the discussion of *hydration energy* of gaseous M^{+z} to the standard state of the aqua ion (independent of whether it has a definite N and symmetry). Thus, H^+ has $\Delta H_{\text{hydr}} = -11.30 \text{ eV} = -260.5 \text{ kcal/mol}$ (Rosseinsky, 1965) compensating most of the ionization energy of 1 rydberg = 13.606 eV of the hydrogen atom. We use the convenient unit of energy

$$1 \text{ eV} = 23.06 \text{ kcal/mol} = 8065.48 \text{ cm}^{-1} = 96484 \text{ J/mol} \quad (23.3)$$

for obtaining better agreement between the data from atomic spectra and photo-electron spectra.

The three consecutive $I_1 = 5.577$, $I_2 = 11.06$ and $I_3 = 19.175 \text{ eV}$ of the gaseous lanthanum atom (Moore, 1970) have the sum $\Sigma I = 35.81 \text{ eV}$ which has to be compensated, for the major part, by ΔH_{hydr} (given by Rosseinsky (1965) as -784 kcal/mol) as one of the necessary, though not sufficient, conditions for maintaining lanthanum(III) aqua ions as a chemically viable species, not evolving oxygen and being reduced. It is fairly obvious that the much higher $I_4 = 45.95 \text{ eV}$ (Reader and Epstein, 1975) cannot conceivably be compensated for by the additional hydration energy of a hypothetical La(IV). These types of arguments were mainly used by Rabinowitch and Thilo (1930) combined with the Madelung potential provided by the anions in fairly electrovalent compounds such as LaF_3 or LaCl_3 . As a matter of fact, La(III) is the only oxidation state known of lanthanum in non-metallic compounds. It is roughly true that the aqua ion of M^{+z} does not develop hydrogen if the corresponding I_{z+1} of the gaseous ion is above z times 15 eV. This type of empirical rule is fairly good in the iron(3d) group, but the constant is smaller, somewhere between 12 and 13 eV, in the lanthanides. It is clear that such a difference exists, because gaseous Ti^{+3} has $I_4 = 43.27 \text{ eV}$ and Ce^{+3} $I_4 = 36.76 \text{ eV}$ in spite of titanium(III) aqua ions being much easier to oxidize than cerium(III) aqua ions. Actually, $E^0 = -0.1$ and $+1.7 \text{ V}$ relative to the standard hydrogen electrode in 1 molar non-complexing acid ($\text{pH} = 0$) does not

refer to the formation of the (unknown) Ti(IV) and Ce(IV) aqua ions, but the mixture of hydroxo complexes of ill-defined composition prevailing in such a solution. However E^0 for the genuine aqua ions are expected to be only a few tenths eV higher.

The first quantitative treatment of hydration energy by Latimer (1955) was not so much intended to answer the specific chemical question of which oxidation states are stable for aqua ions of a given element, but rather the more physical question of whether the dielectric properties of water can explain the huge affinity to gaseous ions. In view of the moderate precision of these arguments, we may as well consider the reciprocal dielectric constant 0.013 of water to be negligible, in which case the stabilization of M^{+z} with the ionic radius r_{ion} by a perfect dielectric is $z^2/2r_{\text{ion}}$. Since the atomic unit of e^2/bohr is equivalent to 14.4 eV/Å, this dielectric stabilization is expected to be 7.2 eV divided by r_{ion} in Å. Actually, the four halide anions F^- , Cl^- , Br^- and I^- have experimental ΔH_{hydr} (= 5.4, 3.9, 3.8 and 3.2 eV) in good agreement with this hypothesis giving 5.41, 3.98, 3.67 and 3.27 eV assuming Goldschmidt ionic radii. It has long been known that this agreement cannot be reached for both cations and anions. Fajans pointed out as early as 1919 (cf. Morris, 1969) that most halides MX of the alkaline metals dissolve in water almost without evolution of heat. Only when M^+ and X^- have highly different ionic radii, such as CsF and the lithium salts of the heavier halides, is an exothermic dissolution observed. This fact suggests an approximate equality of the Madelung energy $-1.7476/(r_M + r_X)$ for NaCl-type crystals with the sum of the two solvation energies ($1/2r_M$) and ($1/2r_X$) in perfect dielectrics. It is clear that the sum of the two latter quantities corresponds to the Madelung constant 2 in the special case $r_M = r_X$ and to an even larger Madelung constant in all other cases. If the dielectric theory works for X^- it cannot apply the same small r_M as the crystalline ionic radii, since the dissolution then would be far more exothermic than observed. Latimer (1955) noted that the r_M values could be chosen as the sum of 0.82 Å and the conventional ionic radii. It is difficult to attach a definite physical model to this surprising regularity applying both to the octahedral hexaqua ions of Mg(II), Al(III), Zn(II) and Ga(III) and to alkaline metal M_{aq}^+ . An alternative model would be a local dielectric constant (Schwarzenbach, 1970, 1973) close to 2, but this would not really be in agreement with the evidence obtained from formation constants of complexes of differently charged ligands, where the local dielectric constant varies from 10 to 40 as a function of increasing distance from M^{+z} . Anyhow, it is not generally recognized that a corollary of the Latimer hypothesis is a definite value for eq. (23.1). Actually, the very small proton does not fit the cation model since $7.2 \text{ eV}/0.82 = 8.8 \text{ eV}$ is smaller than the hydration energy 11.3 eV of the proton.

Rather than discussing the complete hydration energy of M^{+z} one may also (Jørgensen, 1969a,b) consider the *difference* between the hydration energy of M^{+z-1} and of M^{+z} and compare it with the difference between I_z of the gaseous ion M^{+z-1} . This is particularly interesting in the transition groups, because E^0 for several oxidation states are known. Surprisingly enough, it turns out to be a good approximation in *each* group to write for aqua ions of the oxidation state $(z - 1)$

$$I_{\text{chem}} = E^0 + 4.5 \text{ eV} = I_z - (2z - 1)\kappa \quad (23.4)$$

where the parameter κ is

$$5.3 \text{ eV for 3d group, } 4.3 \text{ eV for the 4f group, } 3.9 \text{ eV for the 5f group} \quad (23.5)$$

whereas a lower limit to κ for beryllium and aluminium is 5.3 eV. Thus, the E^0 expected for titanium(III) aqua ions is $43.27 - 7 \times 5.3 - 4.5 = +1.7 \text{ V}$ and for cerium(III) aqua ions $36.76 - 7 \times 4.3 - 4.5 = +2.2 \text{ V}$ in moderate agreement with the observed values, but the interesting aspect is that the same value of κ applies to other oxidation states of the same transition group, such as iron(II) $30.65 - 5 \times 5.3 - 4.5 = -0.35 \text{ V}$, copper(I) $20.29 - 3 \times 5.3 - 4.5 = -0.1 \text{ V}$ and europium(II) $24.7 - 5 \times 4.3 - 4.5 = -1.3 \text{ V}$ compared with the observed $E^0 = +0.77, +0.52$ and -0.4 V . It may be argued (Jørgensen, 1956b) that "ligand field" stabilization effects increase E^0 for $\text{Fe}(\text{H}_2\text{O})_6^{+2}$ by some 0.5 V and decrease E^0 for copper(I) aqua ions by some 0.8 V but it is difficult to have great confidence in these arguments, though they explain the rather oscillating variation of E^0 for the 3d group M(II) aqua ions. It must be noted that the theory of hydration energy differences can only be applied in the absence of strong complexation, including the spontaneous formation of hydroxo and oxo complexes by deprotonation of aqua ions. In the case of the rare earths, the M(II) and M(III) aqua ions do not present such problems, only the cerium(IV) is hydrolyzed in aqueous solution, whereas praseodymium(IV) and terbium(IV) are known in binary CaF_2 -type oxides and a variety of mixed oxides (Jørgensen and Rittershaus, 1967; Hoefdraad, 1975; Blasse, 1976) and in fluorides, as is true for the only known instances of neodymium(IV) and dysprosium(IV) in Cs_3RF_7 . It should not be construed that the chemical stability of ruthenium(VIII) oxide has anything to do with I_8 of gaseous Ru^{+7} though it is formally a deprotonation product of the hypothetical (and exceedingly acidic) $\text{Ru}(\text{H}_2\text{O})_4^{+8}$ and though $E^0 = +1.00 \text{ V}$ (and hence $I_{\text{chem}} = 5.5 \text{ eV}$) is known for perruthenate RuO_4^- . The latter type of problem involves central atoms with fractional charges well below the oxidation state (and typically between 2 and 3) as can be treated in the theory of differential ionization energies (Jørgensen et al., 1967; Jørgensen, 1969a) including the Madelung potential.

Table 23.1 gives the ionization energies I_3 and I_4 of gaseous R^{+2} and R^{+3} recently tabulated by Sugar and Reader (1973). With the exception of La^{+2} and Gd^{+2} , the ground states of all these ions belong to the electron configurations $[\text{Xe}]4f^q$ and table 23.1 is arranged according to q showing interesting regularities, and a striking similarity between $(7 + q)$ and q electrons in the 4f shell as discussed below in subsection 2.2. The ground state of La^{+2} belongs to $[\text{Xe}]5d$ and the first (of the two) level of $[\text{Xe}]4f$ occurs at 0.89 eV higher energy. By the same token, the lowest level of $[\text{Xe}]4f^8$ is now known (Johansson and Litzén, 1973) to occur 0.295 eV above the ground state of Gd^{+2} belonging to $[\text{Xe}]4f^75d$. In the two cases, the I_3 given in parentheses in table 23.1 refers to the straightforward removal of a 4f electron from the excited state of R^{+2} . Table 23.1 also gives I_5 of R^{+4} between Pr^{+4} and Hf^{+4} (Sugar, 1975).

TABLE 23.1.
 Ionization energies (in eV) of monatomic $4f^q$ systems M^{+2} , M^{+3} and M^{+4} (The ground states of La^{+2} and Gd^{+2} would show I_3 0.89 and 0.295 eV higher, respectively).

q	R^{+2}	I_3	R^{+3}	I_4	R^{+4}	I_5
1	La	18.28	Ce	36.76	Pr	57.53
2	Ce	20.20	Pr	38.98	Nd	60.0
3	Pr	21.62	Nd	40.41	Pm	61.7
4	Nd	22.14	Pm	41.1	Sm	62.7
5	Pm	22.3	Sm	41.37	Eu	63.2
6	Sm	23.43	Eu	42.65	Gd	64.8
7	Eu	24.70	Gd	44.01	Tb	66.5
8	Gd	20.34	Tb	39.79	Dy	62.1
9	Tb	21.91	Dy	41.47	Ho	63.9
10	Dy	22.79	Ho	42.48	Er	65.1
11	Ho	22.84	Er	42.65	Tm	65.4
12	Er	22.74	Tm	42.69	Yb	65.6
13	Tm	23.68	Yb	43.74	Lu	66.8
14	Yb	25.03	Lu	45.19	Hf	68.36

The most interesting aspect of table 23.1 is the variation with q , the highest I_3 corresponding to the existence of europium(II) and ytterbium(II) aqua ions and the lowest I_4 to the existence of cerium(IV) in aqueous solution (in spite of Eu(II) and Yb(II) being thermodynamically unstable at pH = 0 toward evolution of hydrogen, and Ce(IV) toward evolution of oxygen). It is discussed below in subsection 2.2 how the "refined spin-pairing energy theory" can explain the detailed variation with q . It is possible to use eq. (23.4) to determine individual κ values from the known (Nugent et al., 1973) $E^0 = -0.4$ V for Eu(II) and -1.1 V for Yb(II) aqua ions, viz. $\kappa = (I_3 - E^0 - 4.5)/5 = 4.01$ eV and 4.33 eV respectively. The increase in κ of 0.32 eV in going from Eu(II) to Yb(II) undoubtedly corresponds to one of the effects of decreasing ionic radii. It may be noted that values of I_3 very similar to the values found by Sugar and Reader (1973) were derived by Johnson (1969) and by Faktor and Hanks (1969) from the heat of formation of R_2O_3 and their Madelung energy.

It is possible to make a summation of eq. (23.4) from the neutral atom to M^{+z} and find the corollary that the total hydration energy of the latter ion is $-\kappa z^2$ not showing any evidence of a differential change of the ionic radii as a function of varying z for a given element. Thus, the hydration energies (Rosseinsky, 1965; Jørgensen, 1975b) -34.0 eV for La^{+3} and -65.1 eV for Ce^{+4} can be interpreted in this sense as $\kappa = 3.78$ and 4.07 eV, respectively. These values may be compared with κ (in eV):

$$\begin{array}{cccccc}
 \text{Mg}^{+2} & 4.98 & \text{Ca}^{+2} & 4.12 & \text{Mn}^{+2} & 4.78 & \text{Zn}^{+2} & 5.30 & \text{Sr}^{+2} & 3.75 & \text{Cd}^{+2} & 4.68 \\
 \text{Al}^{+3} & 5.37 & \text{Sc}^{+3} & 4.51 & \text{Fe}^{+3} & 5.04 & \text{Ga}^{+3} & 5.39 & \text{Y}^{+3} & 4.17 & \text{In}^{+3} & 4.73
 \end{array}
 \tag{23.6}$$

showing a mild dependence on the ionic radius in qualitative agreement with Latimer's suggestion of the denominator ($r_{\text{ion}} + 0.82 \text{ \AA}$).

1.3. Chemical polarizability and Pearson softness

Goldschmidt was the first to describe the formation of minerals in the Earth's crust as an extraction process on a geological time-scale and in particular, two major categories of this geochemical classification are *lithophilic elements* (such as all the alkaline and alkaline-earth metals, aluminum, silicon, titanium, yttrium, zirconium, niobium, all the lanthanides, hafnium, tantalum, thorium and uranium) preferentially occurring in silicates and mixed oxides, and *chalkophilic elements* (such as copper, zinc, arsenic, selenium, silver, cadmium, antimony, tellurium, mercury, thallium, lead and bismuth) preferring sulfur-containing minerals. Certain elements, such as nickel, germanium, indium and tin are intermediate cases, occurring in both types of minerals. The practical consequence of this distinction is that many elements with low total abundance can be found in relatively high concentration in comparatively rare sulfide and arsenide minerals.

In a comparative study of complex formation constants, Ahrland, Chatt and Davies (1958) pointed out that A-type central atoms (essentially corresponding to lithophilic elements) consistently have the highest affinity to fluoride and to oxygen-containing ligands, whereas B-type (chalkophilic) central atoms are the only ones to prefer iodide to the lighter halides, sulfur-containing ligands relative to corresponding oxygen-containing ligands, and phosphines to amines and ammonia. It is striking that among the 24 conceivable permutations of the order of $\log K_1$ for the first halide complexes, only the A-type ($F^- \gg Cl^- > Br^- > I^-$) and the B-type ($F^- < Cl^- < Br^- < I^-$) are realized. Seen from this point of view, cadmium(II) and lead(II) are marginally B-type, whereas zinc(II) and indium(III) are among the closest not to belong to the A group. It is somewhat unfortunate that the symbols A and B may remind chemists about the "short-period" version of the Periodic Table with eight columns (which is rather objectionable for many reasons, such as the inherent difficulty in equalling 18 with twice 8) since the division in A and B is *almost* the same, but has the drawback that iron and platinum both belong to the eighth column. Though formation constants are not generally known, there is ample evidence that low oxidation states of d group elements, such as chromium(0) and manganese(I) intrinsically show strong B character. On the other hand, chromium(III) and manganese(II) show almost as much A character as Al(III) and Mg(II).

As early as the beginning of this century, Abegg and Bodländer pointed out that noble metals (having positive E^0 relative to hydrogen) prefer to form complexes with iodide, sulfide and cyanide, and hence have what Ahrland et al. call B characteristics. For some reason, this is fairly valid, with the striking exception of thallium(I) and (III), and lead(II), where the metallic elements have negative E^0 . Seen from the point of view of complex formation constants (Bjerrum, 1950) and in particular of the influence of substitution of a ligating

atom in multidentate ligands (Schwarzenbach, 1956, 1961, 1973) many further remarks have been made. However, this problem was suddenly placed in the lime-light by Pearson (1963, 1968, 1973) who called A-type central atoms and other antibases (the name proposed by J. Bjerrum (1951) for Lewis acids) *hard acids*, fluoride, oxygen-containing ligands *hard bases*, B-type anti-bases *soft acids*, and the ligands preferred by soft anti-bases (iodide, sulfur-containing ligands, phosphine and cyanide) *soft bases* and Pearson proposed the *Dual principle*

Hard anti-bases react preferentially with hard bases, and
Soft anti-bases react preferentially with soft bases.

In view of what we said above, there is no doubt that this principle is not entirely new, but there are convincing reasons for arguing (Jørgensen, 1974b, 1975b) that soft behaviour is not exactly the same thing as covalent bonding, though it may be fair to say that hardness is to a good approximation synonymous with electrovalent bonding. However, Pearson added new perspectives by emphasizing the soft character of the hydride ligand (for which formation constants cannot be found in aqueous solution), CO, carbanions and other ligands which are generally known only from preparative chemistry (recent years have seen the preparation of ReH_9^{2-} , $\text{W}_6(\text{P}(\text{C}_6\text{H}_5)_3)_3$, $\text{W}(\text{CH}_3)_6$, $\text{Ir}(\text{CO})\text{Br}_5^{2-}$, $\text{IrH}_5(\text{P}(\text{C}_6\text{H}_5)_3)_2$, $\text{Pt}(\text{CH}_3)_6^{2-}$ and $\text{Au}(\text{CH}_3)_4^-$ containing the oxidation states Re(VII), W(VI), Ir(III), Ir(V), Pt(IV) and Au(III) which are not particularly low) and further on, Pearson suggested that metallic surfaces *ipso facto* are soft.

If one concentrates attention too much on the four halide ligands alone, it is possible to get a wrong impression from the many properties varying $\text{F}^- \gg \text{Cl}^- > \text{Br}^- > \text{I}^-$ in the same order as the hardness. For instance, the electronegativities 3.9, 3.0, 2.8 and 2.5 which can also be recognized from electron transfer spectra (Jørgensen, 1962d, 1970b) and from ionization energies in photo-electron spectra (Jørgensen, 1973c, 1975e) are not necessarily connected with the hard or soft behavior. Seen from the point of optical electronegativities of central atoms, there is a certain correlation between softness and oxidizing character, but exceptions are again thallium(III) and mercury(II) and, on the other hand, the low oxidation states already mentioned. Seen from the point of view of photo-electron spectra, there is even less correlation with soft character of central atoms, thallium(III) having far higher ionization energy I than manganese(I), though the chemical shift of I of inner shells contains a substantial contribution from the interatomic relaxation effect corresponding to chemical polarization (Jørgensen, 1974b; Wagner, 1976).

When chemists argue that the polarizability increases from F^- to I^- it is necessary to stress two points: that the electric dipolar polarizability α for weak field strengths (generally obtained via the Lorentz formula for molar refractivity from measurements of the refractive index of light) are much smaller for chemical species such as hydride ($-I$) and fluoride ($-I$) than for gaseous H^- and F^- , and furthermore that the α values (in \AA^3 below, 1 cm^3 of molar refractivity corresponding to 0.392 \AA^3) of cations have very little to do with Pearson

softness. The author (Salzmann and Jørgensen, 1968; Jørgensen, 1975b) argues that the α values are much closer to being linearly additive than is usually assumed in literature. Since we only measure the sum of α of a manifold of species being neutral, we meet the same problem as with many other thermodynamic properties of the ion M^{+z} (z reckoned negative for anions) that one may add an arbitrary constant Cz and obtain the same observed result for neutral matter. By the way, this is the reason why E^0 zero can be assigned by classical physico-chemists to eq. (23.1). This indeterminacy can frequently be circumvented by plausible arguments. Thus, the ionic conductivities are only known in aqueous solution for cations and anions together, but it is reasonable to use Stokes' law assuming that sufficiently large polyatomic ions have very small conductivities. By the same token, it can be argued that within 0.2 \AA^3 α vanishes for Li(I), Be(II), Mg(II) and Al(III). Though α for oxygen (-II) definitely changes from 1.25 to slightly above 2 \AA^3 as a function of the positively charged neighbor atom, it is remarkably illustrative to indicate the α values in \AA^3 :

F(-I)	0.8	Cl(-I)	3.0	Br(-I)	4.2	I(-I)	6.3	
Ne	0.39	Ar	1.63	Kr	2.46	Xe	4.0	
Na(I)	0.3	K(I)	1.2	Rb(I)	1.9	Cs(I)	2.9	
Mg(II)	0.1	Ca(II)	0.9	Sr(II)	1.4	Ba(II)	2.4	(23.7)
Al(III)	0.0	Sc(III)	1.1	Y(III)	1.5	La(III)	2.2	
		Mn(II)	1.3	Ag(I)	2.3	Ce(IV)	4	
		Cu(II)	1.0	Cd(II)	1.7	Hf(IV)	1.7	
		Zn(II)	0.9	In(III)	1.6	Th(IV)	2.7	

Though α is larger for the halide anion isoelectronic with a given noble gas, and smaller for the isoelectronic cations, there is not the dramatic decrease as a function of increasing oxidation state (as one would expect from calculations for gaseous ions) and actually, a minimum is observed somewhere between M(II) and M(III). As one would expect from α being proportional to a summation over all excited states of the oscillator strength divided by the square of the wave-number of the transition, the low-lying electron transfer bands of PtX_6^{2-} produce a high and variable estimate of α for platinum(IV). This fact also contributes to α of titanium(IV) being some 4 to 5 \AA^3 and $\alpha = 2.2 \text{ \AA}^3$ of iron(III) being twice as large as for Fe(II), compared with 1.6 \AA^3 of Cr(III). The intense $6s \rightarrow 6p$ transitions in the near ultra-violet produce $\alpha = 5.0 \text{ \AA}^3$ for the gaseous mercury atom and α between 3 and 5 \AA^3 for the isoelectronic thallium(I), lead(II) and bismuth(III). Penneman et al. (1973) have commented on the additivity of α values in double fluorides formed by the 4f and 5f group with other cations. For our purposes, the major result is a marginal increase of α from La(III) to 2.4 \AA^3 for Ce(III) followed by a smooth decrease to 1.6 \AA^3 for Yb(III). In this connection the variation of the refractive indices of $[\text{R}(\text{H}_2\text{O})_9](\text{BrO}_3)_3$ (Schumann, 1952) should also be noted.

Since it became obvious that α has little to do with what a chemist calls polarization (compare Ca(II) with Cu(II), Ag(I) with Cs(I) and Cd(II) with Ba(II) in eq. (23.7)) several authors have attempted to define physical quantities related

to Pearson softness. The most clear-cut case is the parameter σ_A of Ahrlund (1968a,b) as the energy of the process

$$M_{\text{gas}} = M_{\text{aq}}^{+z} + z e_{\text{gas}}^{-}, \quad (23.8)$$

divided by z . This parameter (in eV) has the following values:

H(I) 2.3	K(I) 1.0	Fe(III) 3.1	Sr(II) 0.8	La(III) 0.6
Li(I) 0.0	Ca(II) 0.7	Ni(II) 2.0	Y(III) 0.6	Ce(IV) 2.0
Be(II) 1.2	Sc(III) 1.2	Cu(II) 3.1	Cd(II) 3.6	Hg(II) 5.1
Na(I) 0.9	Cr(II) 2.1	Zn(II) 3.1	In(III) 3.3	Tl(I) 2.7
Mg(II) 1.4	Mn(II) 2.0	Ga(III) 2.9	Cs(I) 1.2	Tl(III) 4.3
Al(III) 1.6	Fe(II) 2.0	Rb(I) 1.0	Ba(II) 0.9	Pb(II) 3.6

(23.9)

obviously much more closely related to Pearson's ideas than eq. (23.7). There are a few discrepancies between the physico-chemical parameter σ_A and Pearson's qualitative ideas, one being that there is a trend to overestimate the softness in eq. (23.9) to an extent proportional to z . It must also be realized that no convincing chemical evidence is available for the alkaline metal ions, their only complexes known (Lehn, 1973; Truter, 1973; Winkler, 1972) are highly stabilized for entropy reasons by multidentate ligands.

If one neglects the distinction between enthalpy and free energy (which is, of course, the central subject of classical physical chemistry) it is possible to reconsider σ_A in such a way as to almost bring it back to the suggestion of Abegg and Bodländer (Jørgensen, 1975b). In such an approximation

$$\sigma_A = (E^0 + 4.5) - (\Delta H_{\text{atom}}/z), \quad (23.10)$$

where E^0 is the standard oxidation potential of the metallic element and ΔH_{atom} its heat of atomization (which may be higher than the heat of evaporation if the vapor contains stable diatomic or oligoatomic molecules). It may be noted that the hydrogen electrode constant 4.5 only shifts σ_A by a constant amount, and that the monatomic I_n are not needed in eq. (23.10). The approximate value derived for magnesium(II) is 1.29, for yttrium(III) 0.64 and for lanthanum(III) 0.71 in good agreement with eq. (23.8). Other examples of such σ_A values are

$$\text{Cr(III) 2.6} \quad \text{Co(III) 3.4} \quad \text{Cu(I) 1.55} \quad \text{Pd(II) 3.5} \quad \text{Ag(I) 2.35} \quad \text{Bi(III) 4.1} \quad (23.11)$$

which again seem rather on the high side for M(III) compared with M(I). It is, of course, possible to draw the analogy that for the noble gases eq. (23.8) would be almost zero, representing the negligible heat of solution in water. With good estimates of E^0 for metallic lanthanides (Johnson, 1974) and ΔH_{atom} (Johansson and Rosengren, 1975) available, eq. (23.10) also provides σ_A values such as

$$\begin{array}{cccc} \text{Ce(III) 0.72} & \text{Pr(III) 0.93} & \text{Nd(III) 1.05} & \text{Sm(III) 1.51} \\ \text{Gd(III) 0.85} & \text{Dy(III) 1.18} & \text{Er(III) 1.07} & \text{Tm(III) 1.45} \end{array} \quad (23.12)$$

which are rather difficult to take seriously in the case of metals such as

samarium and thulium which have particularly low heats of atomization Klopman (1968) suggested an alternative softness parameter σ_K giving roughly the same order of the central atoms as σ_A with the major exception that H(I) is situated between Li(I) and Na(I). The derivation of σ_K is interesting, but highly complicated, and is not discussed in further detail here. Seen from the point of view of Pearson, some ligands do not show a clear-cut hard or soft character. Thus, OH^- reacts with most central atoms in M(II) and higher oxidation states (except for Ca, Sr, Ba, Eu and Ra) regardless of their softness. To the first approximation (Jørgensen, 1963c) the consecutive deprotonation of ligated water molecules to hydroxo, and then to oxo complexes, is a function of increasing pH (the available range in aqueous solution is from -1 to $+15$, more extreme cases are hardly typical of water anymore) and a function of increasing (z/r_{ion}) explaining the "diagonal similarities" in the Periodic Table between Be(II) and Al(III), between B(III) and Si(IV) and between C(IV) and P(V), whereas N(V) and S(VI) almost arrive at the situation known from Cl(VII), Mn(VII), Re(VII) and Ru(VIII) that only oxo complexes occur, the hydroxo complexes being too strong Brønsted acids to exist in aqueous solution except at very low pH. Though the parameter (z/r_{ion}) is satisfactory for electrostatic reasons, it cannot be concealed that noble metal central atoms Pd(II), Pt(IV), Au(III), Hg(II), once more Tl(III), and halogens in positive oxidation states Cl(I), Br(I) and I(I) have much more pronounced Brønsted acidity than expected from electrostatic considerations.

Most authors join Pearson in saying that H(I) is hard, perhaps in analogy to the small Li(I). This is not the observed trend, H_{aq}^+ having an enormous affinity to H^- , CH_3^- , CN^- (though not to CO and C_6H_6) and qualifying as an exceptionally soft anti-base. The obvious counter-argument is the pH of about 3 for HF in aqueous solution being about 10 units higher than the values (extrapolated from behaviour in non-aqueous solvents and from the minute vapour pressure in 1 M aqueous solution) of HCl, HBr and HI. However, this distinction from the other hydrohalic acids seems to be due to rather specific properties of HF, one being a very high stabilization by hydrogen bonding to water* as a solvent. Ahrlund (1968a, 1973) has rightfully pointed out that many hard complexes are formed endothermally in aqueous solution, having positive ΔH and negative ΔG . This is particularly true for most fluoride complexes, whereas the reaction between soft central atoms and soft ligands generally has comparable, negative values of ΔH and ΔG with a much more moderate change of entropy. The entropy of fluoride and certain oxygen-containing ligands, combined with the enigmatic stability of many aqua ions, makes inorganic chemistry rather inadaptably to simplistic models. It may be noted that the total hydration energy divided by z^2 is 3.37 eV for Ba^{+2} , considerably lower than for Sr^{+2} and Ca^{+2} in eq. (23.6) whereas it is 4.75 eV for Hg^{+2} , 4.82 eV for Tl^{+3} and 3.82 eV for Pb^{+2} in spite of larger ionic radii than Cd^{+2} , In^{+3} and Sr^{+2} , respectively. In other words, we lack a detailed

*Vibrational spectra (Giguère, 1976) suggest that the species having $\text{pK} = 3$ is a strongly bound ion-pair OH_3^+F^-

understanding of hydration energy, though the approximate proportionality with z^2 supports electrostatic arguments at their face value. However, it may also be argued that since I_z of M^{z-1} tends to be proportional to z (as long as a closed-shell configuration is not opened up) corresponding to the total energy being $k(z^2 + z)$ relative to the ground state of the neutral atom, the hydration energy must compensate more or less exactly the quadratic dependence on z .

It is worthwhile noting (Jørgensen, 1962b, table 24) that the formation of aqua ions in solution and liberated electrons at great distances in vacuo from a given neutral atom is *endothermic* (with the marginal exception of lithium). The apparent paradox that chemically unreactive aqua ions, say of calcium(II), have positive heats of formation, can be resolved when it is realized that electrons with zero energy (relative to vacuo) are not available in water, though it is much closer the truth for the blue solutions of solvated electrons in liquid ammonia. Actually, the condition for being in thermodynamic equilibrium at 25°C with 1 atm H_2 is $E^0 = -0.059$ pH or $I_{\text{chem}} = 4.5 - 0.059$ pH, whereas the more strongly oxidizing solution in equilibrium with 0.2 atm O_2 (as found in air) has $I_{\text{chem}} = 5.7 - 0.059$ pH. Hence, reactions producing electrons with an energy of -4 eV proceed by evolution of molecular hydrogen. Among the complexes with the highest known formation constants (many are known qualitatively to be stronger, but cannot be readily determined) $Hg(CN)_4^{2-}$ with $\log \beta_4 = 41.5$ and $\Delta H = -63$ kcal/mol is a quite good example, but nevertheless, the covalent bonding pays back only 2.8 eV of the $2\sigma_A = 10.2$ eV lacking when gaseous mercury atoms form electrons with zero energy and Hg(II) aqua ions.

It is considered a serious defect of Pearson's concept of hardness and softness that one cannot predict ΔH or ΔG as an explicit function, say as the sum of two products of two parameters, one characterizing the anti-base and the other the base. In many ways, this is a discussion between Descartes and Riemann about geometry, the former evaluating any distance between two points with definite coordinates, and the latter making a geometry of a sequence of meeting-points. It is an indisputable fact that the exceptions to Pearson's Dual Principle are far less frequent than uncorrelated statistics would produce, and many valuable aspects of chemistry are exclusively sequences of properties, like the chemical version of the Periodic Table before Stoner (1924) suggested each nl -shell to contain $(4l + 2)$ electrons. Though the old concepts of weak and strong acids, and of strongly and weakly reducing species, to a large extent have been quantified by pH and E^0 there is no reason to discriminate against hard and soft anti-bases and bases, even if a comparable numerical scale should never be found.

2. Electronic configurations and multiplet structure

The 5d group can most conveniently be said to start with lutetium, followed by hafnium, tantalum, tungsten, . . . There is no particular reason to place the 4f group as an inclusion in the 5d group from cerium to lutetium though it is true that the ground state of the gaseous lanthanum atom belongs to $[Xe]5d6s^2$. However, this has no more influence on the chemistry of the invariantly trivalent

lanthanum than $[\text{Ar}]3d4s^2$ has on the chemistry of scandium. As emphasized by Connick (1949) it is not plausible that the lanthanides are trivalent simply because their neutral atoms contain $(Z - 57)$ 4f electrons, since the actual fact is that eleven of the gaseous elements are barium-like with $q = (Z - 56)$ and two 6s electrons. There is no striking difference between the chemistry of the four lanthanum-like ground states (La, Ce, Gd and Lu) and the 11 others. As we have seen in the previous sections, the reason for almost invariant trivalence is that I_3 is so small, compared with 5κ , that the M(II) aqua ions have negative E^0 and are able to evolve hydrogen gas, and that I_4 is so large, compared with 7κ , that the M(IV) species in acidic solution have E^0 sufficiently positive to evolve oxygen. Our primordial question is: why is $(I_4 - I_3)$ so overwhelmingly large compared with 2κ ? Obviously, we do not have the simple situation of crossing a closed shell, as when aluminum has $I_4 = 120.0$ eV (depleting the neon shells) much higher than $I_3 = 28.45$ eV (losing only a 3s electron) or when scandium has $I_4 = 73.47$ eV (3p) considerably higher than $I_3 = 24.76$ eV (3d). Table 23.1 shows the lanthanides to have I_4 some 20 eV higher than I_3 (disregarding the effects of $q = 7$) though a 4f electron is removed in both cases (excepting La^{+2} and Gd^{+2} , and even there it hardly makes any difference). In other words, the electron affinity of a partly filled 4f shell is *far smaller* than the corresponding I .

Curiously enough, the linear trend of I as a function of Z (and hence of the number q of 4f electrons) and the almost constant κ serve as an empirical background with only qualitative theoretical justification, whereas many fine details of the small deviations from linearity as a function of q are well understood. Judd (1970) once remarked in a book review that the writer "regards atoms and other comparatively simple systems as analog computers for the very properties they exhibit and hence in need of no special analysis". This is a profound observation (though it may be accompanied by a few explanatory comments given below) but it is perfectly true that the monatomic entities of which the discrete energy levels are classified by Moore (1949, 1952, 1958) are the best (and only) quality available, and that the solution of the Schrödinger equation would yield the observed energy differences, if it is valid. Furthermore, transparent lanthanide compounds are entirely exceptional by having recognizable J -levels corresponding to approximate spherical symmetry (Jørgensen, 1955b; Carnall et al., 1968) analogous to atomic spectra.

2.1. *Huge differences between ionization energy and electron affinity, and the phenomenological baricenter polynomial*

One of the great difficulties for good approximations (such as Hartree-Fock calculations) to the Schrödinger equation for atoms containing many electrons is that the eigen-values E are negative, out of all proportion with chemical experience. A remarkably good approximation to the total binding energy of Z electrons to their nucleus with Z protonic charges has been given by Gombas and Gaspar as $-Z^{2.4}$ rydberg (where 1 rydberg = 13.60 eV). This expression only deviates seriously (for relativistic reasons) for Z above 90. One way of alleviating this difficulty is to consider the atomic core consisting of strongly bound,

closed shells as the zero-point of energy, and to consider a single electron bound to this core. If the ionic charge is $+z$, Rydberg suggested the binding energy

$$-\epsilon_{nl} = -(z + 1)^2 \text{rydberg}/(n - d)^2, \quad (23.13)$$

where the *Rydberg defect* d is a strongly decreasing function of l (being larger for s than for p electrons, and so on) but generally varying very little with the principal quantum number n . By the way, the success of eq. (23.13) in line spectra showing long series (of increasing n) was the reason why (negative) term values were generally given (relative to an ionization limit) the first half of this century, whereas more complicated spectra without clear-cut ionization limits were tabulated relative to the ground state of the monatomic entity as zero-point. For the sake of uniformity, the latter practice has now been generalized (Moore, 1949). Though this is a minor detail in most atomic spectra, we consider the baricenter of the relativistic effect *spin-orbit coupling* in eq. (23.13), the two j -values $(l + \frac{1}{2})$ and, at lower energy, $(l - \frac{1}{2})$ possible for positive l corresponding to $(2l + 2)$ and $(2l)$ states (with identical energy in spherical symmetry) separated by $(l + \frac{1}{2})$ times the *Landé parameter* ζ_{nl} . Hence, the baricenter is situated $\frac{1}{2}l\zeta_{nl}$ below the higher of the two j -levels. It is an empirical fact (Landé, 1924; Jørgensen, 1955a) that ζ_{nl} is roughly proportional to $(z + 1)^2 Z^2$ but, under equal circumstances, much larger for external p than for external d electrons, and usually negligible for external f electrons (this statement starts to break down from barium with $Z = 56$). In typical cases, ζ_{nl} is at most a few percent of ϵ_{nl} .

When two electrons occur in two *different* shells outside the atomic core, several energy levels (characterized by the quantum number J) are observed, each corresponding to $(2J + 1)$ states (independent, mutually orthogonal wave functions) and which in (the usually satisfactory approximation of) *Russell-Saunders Coupling* can be assembled in *terms* each characterized by the quantum numbers S and L , and each containing $(2S + 1)(2L + 1)$ states. If one of two electrons has $l = 0$, the two terms with $S = 0$ (singlet) and $S = 1$ (triplet) and L equal to l of the other electron is formed. Since the triplet (at lower energy) contains 3 times as many states as the singlet, the baricenter of such a configuration is situated a quarter of the singlet-triplet distance above the triplet energy. In the general case of two different shells (nl) and ($n'l'$) there occur many terms, $L = (l + l')$, $(l + l' - 1)$, $(l + l' - 2)$, \dots , $(|l - l'| + 1)$, $|l - l'|$ combined both with $S = 0$ and $S = 1$. In all of these cases, the number of mutually orthogonal states is $(4l + 2)(4l' + 2)$. The situation is entirely different in the case of two electrons in the same nl shell, where only $(2l + 1)(4l + 1)$ states occur, distributed on the series of terms

$$^1S, ^3P, ^1D, ^3F, ^1G, ^3H, ^1I, \dots, ^3(2l - 1), ^1(2l) \quad (23.14)$$

not given in order of decreasing energy, though 1S is always the highest and (according to Hund's rules) the lowest is the triplet with $L = (2l - 1)$. The number of states for one partly filled shell l^q is the permutational expression for q indiscernible objects distributed on $(4l + 2)$ distinct sites, and the general recursion formula for the number of terms has been given by Karayianis (1965). Thus f^3 and f^{11} present the terms

$${}^4S, {}^4D, {}^4F, {}^4G, {}^4I, {}^2P, a^2D, b^2D, a^2F, b^2F, a^2G, b^2G, a^2H, b^2H, {}^2I, {}^2K, {}^2L \quad (23.15)$$

again not in energetic order (the Hund ground term is 4I). It is noted that the same combination of S and L may be present twice, and for the more complicated configurations (such as f^6 , f^7 or f^8) such a combination may be present many times. The numbers of states, J -levels and terms are:

$q =$	0.14	1.13	2.12	3.11	4.10	5.9	6.8	7	
States	1	14	91	364	1001	2002	3003	3432	
J -levels	1	2	13	41	107	198	295	327	(23.16)
S, L -terms	1	1	7	17	47	73	119	119	
Hund	1S	2F	3H	4I	5I	6H	7F	8S	
Highest L	1S	2F	1I	2L	1N	2O	1Q	2Q	

We return below to the interesting consequences for the properties of lanthanide compounds containing a partly filled $4f$ shell, that the number of different energy levels of $4f^q$ is as high as given in eq. (23.16). It is also possible to study the energy differences between various configurations of the same monatomic entity M^{+n} or between configurations of M^{+n+1} and M^{+n} representing ionization energies. A closer analysis (Jørgensen, 1969a, 1973a) shows that it is interesting to evaluate the *baricenter* of each configuration by weighting the energies of each J -level with their number $(2J + 1)$ of states, and when necessary, supplementing the observed J -levels with calculated positions of missing J -levels. It is noted that this baricenter refers to the actual J -levels belonging (in a classificatory way) to a given configuration, and hence includes conceivable differences of correlation energy in the monatomic entities. A parameter $A_*(nl, n'l')$ of interelectronic repulsion is defined for the energy of the baricenter of $(nl)^1(n'l')^1$ (or alternatively $(nl)^2$ giving $A_*(nl, nl)$) of M^{+n-2} outside the closed shells of the ground state of M^{+n} by using the latter ground state as the zero-point of energy

$$-\epsilon_{nl} - \epsilon_{n'l'} + A_*(nl, n'l') \quad (23.17)$$

with the two one-electron energies taken from eq. (23.13). Since the baricenters of the $(4l + 2)(4l' + 2)$ or $(2l + 1)(4l + 1)$ states are usually known with a great precision, table 23.2 gives such values in the unit $1000 \text{ cm}^{-1} = 0.12398 \text{ eV}$ for the systems Cs, Ba^+ , La^{+2} , Ce^{+3} and Pr^{+4} containing one electron and Ba, La^+ , Ce^{+2} and Pr^{+3} containing two electrons ($4f$, $5d$ or $6s$) outside the xenon closed shells. For comparison, ϵ_{nl} for Rb, Sr^+ , Y^{+2} and Zr^{+3} and $A_*(nl, n'l')$ for Sr, Y^+ and Zr^{+2} are also given for $4d$, $5s$ and $5p$ electrons outside the krypton closed shells. More extensive tables of this type are given in a recent chapter in Gmelin (Jørgensen, 1976b).

One of the conclusions from table 23.2 is that $4f$ electrons are distinctly external before barium and distinctly inside the closed shells after cerium, as first discussed theoretically by Maria Goeppert Mayer (1941). The Rydberg defect d increases from 0.31 in Ba^+ to 1.40 in La^{+2} and $A_*(4f, 4f)$ is already 13 eV in La^+ and 19.4 eV in Pr^{+2} to be compared with more usual values such as $A_*(5s, 5s) = 6.3 \text{ eV}$ in Y^+ . Although parameters such as A_* are derived from

TABLE 23.2.
One- and two-electron parameters (in the unit $1\,000\text{ cm}^{-1} = 0.12398\text{ eV}$) from eq.(23.17) for selected monatomic entities

	ϵ_{4d}	ϵ_{5s}	ϵ_{5p}		$A_*(4d,4d)$	$A_*(4d,5s)$	$A_*(4d,5p)$	$A_*(5s,5s)$	$A_*(5s,5p)$
Rb	14	34	21						
Sr ⁺	74	89	65	Sr	58	47	39	45	35
Y ⁺²	165	158	123	Y ⁺	78	60	52	51	46
Zr ⁺³	276	238	194	Zr ⁺²	95	75	65	52?	52
	ϵ_{4f}	ϵ_{5d}	ϵ_{6s}		$A_*(4f,4f)$	$A_*(4f,5d)$	$A_*(4f,6s)$	$A_*(5d,5d)$	$A_*(5d,6s)$
Cs	7	17	31						
Ba ⁺	32	75	81	Ba	—	—	25	51	43
La ⁺²	146	153	141	La ⁺	104	75	56	65	52
Ce ⁺³	295	245	210	Ce ⁺²	139	90	67	77	63
Pr ⁺⁴	461	346	284	Pr ⁺³	156	98	71	64?	—

relative positions of observed configuration baricenters, it is clear that there is a close relation to the reciprocal average radius of the orbital considered, as would also be true for the calculated integrals of interelectronic repulsion for Hartree-Fock radial functions (Freeman and Watson, 1962). Whereas eq. (23.17) is a definition of A_* it is possible to define a *phenomenological baricenter polynomial* using the same set of parameters for various ionic charges of a given element containing a electrons in the nl shell and b electrons in the $n'l'$ shell:

$$-a\epsilon_{nl} - b\epsilon_{n'l'} + \frac{1}{2}a(a-1)A_*(nl, nl) + abA_*(nl, n'l') + \frac{1}{2}b(b-1)A_*(n'l', n'l') \quad (23.18)$$

which can be easily generalized to three or more partly filled shells, the coefficients to A_* being $\frac{1}{2}q(q-1)$ for q electrons in the same shell and q_1q_2 for q_1 electrons in one shell repelling q_2 electrons in another shell. It turns out that eq. (23.18) is not a perfect approximation, but explains a variety of facts somewhat surprising to chemists expecting a linear and not a parabolic (quadratic) dependence of the baricenter energies on the occupation numbers of the two shells. The reason for the non-linearity is that $A_*(nl, n'l')$ tends to be considerably smaller than the arithmetic average value of $A_*(nl, nl)$ and $A_*(n'l', n'l')$ when the average radii of nl and $n'l'$ are highly disparate, as is normally the case when f or d orbitals are compared with s orbitals. Thus, Sc^+ has $[\text{Ar}]3d4s$ at about equal distances below *both* $[\text{Ar}]3d^2$ and $[\text{Ar}]4s^2$ and La^+ has $[\text{Xe}]5d6s$ below both $[\text{Xe}]5d^2$ and $[\text{Xe}]6s^2$. These are special cases of the tendency of nd group neutral atoms to contain two (or less frequently one) $(n+1)s$ electrons in the ground state, as if nd were less stable than $(n+1)s$ though the latter electron is lost at first by ionization. This situation is even more striking in the beginning of the lanthanides, where $[\text{Xe}]4f^2$ and $[\text{Xe}]4f5d$ almost coincide in Ce^{+2} but the baricenter of $[\text{Xe}]5d^2$ occurs 5 eV higher. It is almost certain that the unknown configuration $[\text{Xe}]4f^4$ of the neutral cerium atom would spontaneously ionize to a free electron and the ground state of Ce^+ belonging to $[\text{Xe}]4f5d^2$. Starting with

praseodymium, the neutral atom $[\text{Xe}]4f^36s^2$ contains two $6s$ electrons in the ground state (and already $[\text{Xe}]4f^46s$ would be an excited configuration) whereas the ground state of Pr^+ belongs to $[\text{Xe}]4f^36s$ and of Pr^{+2} to $[\text{Xe}]4f^3$ with $[\text{Xe}]4f^25d$ starting at 12847 cm^{-1} (1.6 eV) higher energy. The baricenter of $[\text{Xe}]4f^3$ is situated 2.4 eV above the ground state of Pr^{+2} , of $[\text{Xe}]4f^25d$ at 3.2 eV and of $[\text{Xe}]4f^36s$ at 4.7 eV which can be compared with eq. (23.18) and the data from table 23.2 giving much closer coinciding baricenters (in units of 1000 cm^{-1}) -915 , -916 and -908 . This somewhat unsatisfactory agreement must be seen against the background that the observed ground state energy of Pr^{+2} (relative to Pr^{+5}) is -952.0 and of the $[\text{Xe}]4f^3$ baricenter -932.5 showing a reasonable percentage agreement. Apparently, $A_*(4f, 4f)$ does not stay perfectly constant.

2.2. Spin-pairing energy and the double zig-zag curve

There is no doubt that the overall separation between $[\text{Xe}]4f^q$ of M^{+n} and $[\text{Xe}]4f^{q-1}$ of $M^{+(n+1)}$ mainly determined by $A_*(4f, 4f)$ because its coefficient in eq. (23.18) changes $(q-1)$ units, actually shows a characteristic variation as a function of q , as evident in table 23.1. It is possible to describe the deviation from the smooth variation by the fact that the baricenter of all states having the maximum value S_{max} is situated below the baricenter of the configuration $4f^q$ for q between 2 and 12. Actually, the fraction of all the states having S_{max} decreases sharply in the vicinity of the half-filled shell and is $(7/13)$ for $q = 2$ and 12 , $(5/13)$ for $q = 3$ and 11 , $(25/143)$ for $q = 4$ and 10 , $(9/143)$ for $q = 5$ and 9 , $(7/429)$ for $q = 6$ and 8 , and only $(1/429)$ for $q = 7$. It is possible to consider the parameters of interelectronic repulsion in the theories of Slater (Condon and Shortley, 1953) and Racah (1949) as entirely phenomenological parameters to be compared with the observed distribution of energy levels. The writer (Jørgensen, 1957b) pointed out that the baricenter of all the states of l^q having a given value of S and the baricenter (at higher energy) of all the states having $(S-1)$ are separated to the extent $2DS$ where D is a definite linear combination of Slater-Condon-Shortley or of Racah parameters. Whereas it is a tautological statement to say that the triplet and singlet baricenters of a two-electron system are separated by $2D$, it is not trivial that the same linear combination of parameters of interelectronic repulsion can be used for all the q (with the same l) and that it can be used for configurations (such as f^4 , f^5 , f^6 and f^7) presenting three or four alternatives of S . The separation $2DS$ is the difference quotient of $-DS(S+1)$ and it is actually possible (Jørgensen, 1962d, 1969a) to write the deviation of the baricenter of all the states having a given S from the baricenter of all the states of l^q as

$$D[\langle S(S+1) \rangle - S(S+1)] \quad (23.19)$$

where the average value of the $S(S+1)$ for the whole configuration can be written in various equivalent ways

$$\langle S(S+1) \rangle = \frac{1}{4}q(q+2) - \frac{2l+2}{4l+1} \frac{1}{2}q(q-1) = \frac{3}{4}q - \frac{3}{8l+2} \frac{1}{2}q(q-1) = \frac{3q(4l+2-q)}{16l+4}, \quad (23.20)$$

where the first way is related to Racah's theory, S_{\max} for $q \leq (2l + 1)$ being $\frac{1}{2}q$, where the coefficient to $\frac{1}{2}q(q - 1)$ indicates what multiple of D might be added to A_* if one so desires, the second way illustrates how the Pauli exclusion principle decreases $\langle S(S + 1) \rangle$ from the value $\frac{3}{4}q$ it would have had for non-equivalent electrons (it is actually multiplied by the factor $1 - (q - 1)/(4l + 1)$) and the last way emphasizes Pauli's hole-equivalence principle by being symmetric in $(4l + 2 - q)$ and q electrons. The coefficients in eq. (23.19) for various l and q have been explicitly tabulated (Jørgensen, 1962a). In the case of a partly filled f shell, S_{\max} corresponds to a *spin-pairing stabilization* going down to a sharp minimum $-168D/13$ at $q = 7$ and generally having the expression $-8D/13$ multiplied by $\frac{1}{2}q(q - 1)$ for q below 7 as easily seen from the first part of eq. (23.20). Chemists should be warned not to confuse the quantum number S with the component M_S along a linear axis. Actually, it is possible (Jørgensen, 1969a, 1971a) to write expressions analogous to eq. (23.19) containing $-(M_S)^2$ rather than $-S(S + 1)$, but it is not feasible to speak in a significant way about spin-pairing energy related to reversal of the "spin direction" of a number of electrons, because M_S lower than S_{\max} does not normally correspond to a definite S in the eigenvalues. Though D is $(2l + 3)/(2l + 2)$ times the average value of the "exchange integral of the two-electron operator" K_{av} (the strict definition being the average value of the $(4l^2 + 2l)$ integrals stabilizing a closed-shell Hartree-Fock function relative to its Hartree product) and $\frac{9}{8}E^1$ for f electrons, it is not appropriate to relate $2DS$ with the corresponding multiple of K_{av} in representative Slater anti-symmetrized determinants. A classical case is p^2 having the baricenter of its 15 states containing no contribution of K_{av} if $J(x, x)$ is written $J(x, y) + 2K_{av}$ but shows the terms 3P at $-K_{av}$, 1D at $+K_{av}$ and 1S at $+4K_{av}$. Among the 15 Slater determinants, 3 contain the contribution $J(x, x)$ forming 1S and two of the five 1D states. The spin-pairing energy parameter D is $\frac{5}{4}K_{av}$. It is an obvious statement that if several terms show S_{\max} and differ in energy, the lowest has a lower energy than the baricenter of all the states having S_{\max} . For $4f^q$ this happens to be a distinct function of L of the ground term. Actually, the further stabilization is $-9E^3$ for 3H ($q = 2$ and 12) and 6H ($q = 5$ and 9) and is $-2\frac{1}{2}E^3$ for 4I ($q = 3$ and 11) and 5I ($q = 4$ and 10) ground terms. As a numerical question, the Racah parameter E^3 turns out quite accurately to be one tenth of E^1 .

The *refined spin-pairing energy theory* was originally introduced in an attempt (Jørgensen, 1962c) to rationalize the variation of the wave numbers of electron transfer bands, where an electron provided by one or more reducing ligands reduces R(III) having $4f^q$ ground state to R(II) with $4f^{q+1}$. The "refinements" are a question of the coefficient to E^3 and of the first-order spin-orbit coupling stabilizing the lowest J -level to the extent $-\frac{1}{2}(L + 1)\zeta_{4f}$ for q below 7 and $-\frac{1}{2}L\zeta_{4f}$ for q above 7. For our purposes, it is most useful to consider the difference of spin-pairing energy removing an electron from $4f^q$ to form $4f^{q-1}$ and we introduce two parameters of a linear variation of the one-electron energy differences, V as a zero-point and $(E - A)$ as a parameter indicating the stabilization of 4f electrons from one element to the next.

$$\begin{aligned}
q = 1 & \quad V + 2\zeta_{4f} \\
q = 2 & \quad V + (E - A) + \frac{8}{13}D + 9E^3 + \zeta_{4f} \\
q = 3 & \quad V + 2(E - A) + \frac{16}{13}D + 12E^3 + \frac{1}{2}\zeta_{4f} \\
q = 4 & \quad V + 3(E - A) + \frac{24}{13}D \\
q = 5 & \quad V + 4(E - A) + \frac{32}{13}D - 12E^3 - \frac{1}{2}\zeta_{4f} \\
q = 6 & \quad V + 5(E - A) + \frac{40}{13}D - 9E^3 - \zeta_{4f} \\
q = 7 & \quad V + 6(E - A) + \frac{48}{13}D - 2\zeta_{4f} \\
q = 8 & \quad V + 7(E - A) - \frac{48}{13}D + \frac{3}{2}\zeta_{4f} \\
q = 9 & \quad V + 8(E - A) - \frac{40}{13}D + 9E^3 + \zeta_{4f} \\
q = 10 & \quad V + 9(E - A) - \frac{32}{13}D + 12E^3 + \frac{1}{2}\zeta_{4f} \\
q = 11 & \quad V + 10(E - A) - \frac{24}{13}D \\
q = 12 & \quad V + 11(E - A) - \frac{16}{13}D - 12E^3 - \frac{1}{2}\zeta_{4f} \\
q = 13 & \quad V + 12(E - A) - \frac{8}{13}D - 9E^3 - \zeta_{4f} \\
q = 14 & \quad V + 13(E - A) - \frac{3}{2}\zeta_{4f}
\end{aligned} \tag{23.21}$$

The same expressions can be used with opposite sign when adding an electron to $4f^{q-1}$ forming $4f^q$. Since V (obviously) is another, new zero-point, such expressions start $V - (q - 1)(E - A)$. The experimentally known fact that the ionization energy for $q = 7$ is marginally larger in condensed matter than for $q = 14$ is an indication that $7(E - A)$ approximately equals $48D/13$. In such a case, eq. (23.21) predicts comparable ionization energies for q and for $(7 + q)$ electrons. It is an interesting (but difficult) question whether one should assume invariant parameters for a definite oxidation state, or allow a smooth variation from one element to the next. It has been the general attitude to evaluate $(E - A)$ as one parameter from experimental data (a typical value is 3000 cm^{-1}), to assume a fixed value of $D = 6500 \text{ cm}^{-1}$ (one reason for this choice is the divisibility with 13) and either a fixed value of E^3 , say 500 cm^{-1} , or allow E^3 to increase smoothly from the known values 460 cm^{-1} for $q = 2$ in Pr(III) to 630 cm^{-1} for $q = 12$ in Tm(III). The minor relativistic effect expressed as a spin-orbit coupling is usually taken into account accepting the smooth (but not linear) increase of ζ_{4f} from 650 cm^{-1} for $q = 1$ in Ce(III) to 2950 cm^{-1} for $q = 13$ in Yb(III). As a numerical example, we may consider the expressions added to V with $(E - A) = 3.2$, $D = 6.5$, $E^3 = 0.5$ and empirically varying ζ_{4f} all in units of 1000 cm^{-1} :

$$\begin{array}{rcccccc}
q = 1: & 1.3 & 2: 12.5 & 3: 20.9 & 4: 21.6 & 5: 22.2 & 6: 30.2 \\
& 7: 40.3 & & & & & \\
q = 8: & 0.8 & 9: 11.9 & 10: 19.8 & 11: 20.0 & 12: 20.0 & 13: 27.2 \\
& 14: 37.2 & & & & &
\end{array} \tag{23.22}$$

Though it is obvious that the decimal lacks physical significance, it is quite characteristic to find the same development (the double zig-zag curve) repeated between $q = 1$ and 7, and between $q = 8$ and 14. The almost horizontal plateaux at $q = 3, 4, 5$ and $10, 11, 12$ are very characteristic features of the refined spin-pairing energy theory. Whereas eq. (23.22) is intended for applications to

condensed matter, as discussed below, the ionization energies for gaseous ions in table 23.1 suggest somewhat larger $(E - A)$. If $D = 6500$ and $E^3 = 500 \text{ cm}^{-1}$ are maintained, I_3 of M^{+2} corresponds to $(E - A)$ close to 4200 cm^{-1} and I_4 to an even larger value, unless D is considerably larger. However, it is probably not worthwhile analyzing this situation in detail, because the mean value of the I of $q = 7$ and 8 according to eq. (23.21) should be close to the mean value of I for $q = 1$ and 14 at equal distance. Actually, the mean value of I_4 for Gd^{+3} and Tb^{+3} is 5.14 eV higher than I_4 of Ce^{+3} but only 3.29 eV below I_4 of Lu^{+3} , and by the same token, I_5 of Pr^{+4} is 6.74 eV below the mean value of I_5 for Tb^{+4} and Dy^{+4} , which again is only 4.09 eV below I_5 of Hf^{+4} . It is not easy to fix a definite value of these two distances, which should both be $13(E - A)/2$. One way out of this situation would be to assume that $(E - A)$ decreases as a function of increasing Z , as rationalized by Vander Sluis and Nugent (1972) by $(E - A)$ being a difference between two huge parameters with A representing effects of interelectronic repulsion, where it is highly probable that $A_*(4f, 4f) = 156000 \text{ cm}^{-1}$ for Pr^{+3} given in table 23.2 increases percentagewise to the same extent as E^3 and hence some 5000 cm^{-1} per unit of Z . This argument is far too strong to explain the effect observed in the gaseous ions, and opens the fascinating discussion as to why the description using the phenomenological baricenter polynomial (Jørgensen, 1969a, 1973a) is so constructive, when one might have expected enormous effects of differential changes of the various parameters (in particular of A_*) going from one configuration to another. The whole concept of one-electron energies is exceedingly difficult to transfer from one ionic charge to another of a monatomic entity, or from one oxidation state to another.

The refined spin-pairing energy theory is also used for a purpose where one would not have expected it to work very well. If one compares the lowest energy level of the configuration $4f^{q-1}5d$ with the $4f^q$ ground state, McClure and Kiss (1963) pointed out that it followed eq. (23.21) for small amounts of R(II) incorporated in CaF_2 in spite of the large parameters of interelectronic repulsion involving $4f$ and $5d$ orbitals simultaneously, and in spite of the cubic rather than spherical symmetry separating the two $5d$ sub-shells by 1 to 2 eV . Similar observations were made by Loh (1966) for small amounts of R(III) in CaF_2 crystals, where the transitions were found below 10 eV in eleven elements, to be compared with aqua ions and some other complexes of Ce(III) , Pr(III) , Tb(III) previously discussed (Jørgensen, 1956a, 1962c; Jørgensen and Brinen, 1963; Ryan and Jørgensen, 1966). Martin (1971) called the corresponding energy difference between the lowest J -level of $[\text{Xe}]4f^{q-1}5d$ and the lowest J level of $[\text{Xe}]4f^q$ in monatomic ions the *system difference* and pointed out, almost at the same time as Brewer (1971) and Nugent and Vander Sluis (1971) that the variation with q is almost exactly described by the refined spin-pairing energy theory. It is also possible to define this system difference between the lowest J -level of $[\text{Xe}]4f^{q-1}5d6s$ and of $[\text{Xe}]4f^q6s$ in gaseous R^+ , and between the lowest J -level of $[\text{Xe}]4f^{q-1}5d6s^2$ and of $[\text{Xe}]4f^q6s^2$ in the neutral atom R^0 . The curves (as a function of q) run parallel with a few thousand cm^{-1} between R^{+2} and R^+ , and between R^+ and R^0 in striking contrast to the large distance 50000 cm^{-1}

between R^{+3} and R^{+2} . It may be noted that the conditional oxidation state M[III] or M[II] determined from the number of 4f electrons (Jørgensen, 1969a) is the ionic charge in the latter ions, but is M[II] for M^+ and M^0 considered here. In eight cases (La^0 , La^+ , La^{+2} , Ce^0 , Ce^+ , Gd^0 , Gd^+ and Gd^{+2}) the system differences are negative, the configuration with one 5d electron being the more stable. The results for R(II) in CaF_2 (McClure and Kiss, 1963) are similar to the system differences found in gaseous R^+ , whereas those for R(III) in CaF_2 (Loh, 1966) are much closer to R^{+3} than to R^{+2} , and actually about 17000 cm^{-1} below R^{+3} for q below 7, and about 10000 cm^{-1} below the gaseous ion for q at least 8.

The minute irregularities in the variation of complex formation constants (relative to R(III) aqua ions) as a function of q discovered by Fidelis and Siekierski (1966), cf. Mioduski and Siekierski (1975), now called the *tetrad effect* can be explained (Jørgensen, 1970a; Nugent, 1970) as covalent bonding decreasing E^3 to a slightly larger extent than E^1 .

2.3. Electron transfer spectra and redox processes.

The clear-cut analogy between spectral lines of monatomic entities and the narrow absorption bands due to transitions between the energy levels belonging to the partly filled 4f shell of lanthanide(III) compounds convinced most physicists about the essentially monatomic character of all transitions to be expected. Hence, it was not surprising that inter-shell transitions to the excited configuration $4f^{q-1}5d$ could be identified, but it was not generally felt that electron transfer bands would be prominent. This statement has a necessary exception: the orange or yellow colours of a large majority of cerium(IV) compounds, corresponding to very strong, broad absorption bands in the violet or the near ultra-violet, cannot be connected with the absent 4f electrons, and the comparison with iron(III) suggests that an electron is transferred from the surrounding reducing anions to the oxidizing central atom. It might be argued that the empty orbital accepting the electron is 5d (rather than 4f) since the absorption band is so strong. This is in contrast to the first (and frequently luminescent) excited level of the linear uranyl ion UO_2^{+2} which is about 1000 times less intense (Jørgensen, 1957 a; Jørgensen and Reisfeld, 1975). There is no doubt today that it is due to electron transfer from two MO consisting essentially of oxygen 2p orbitals, to the empty 5f shell. Because of strong spin-orbit coupling (large ζ_{5f}) and unusual conditions (almost identical one-electron energies of at least four of the seven 5f orbitals) it is not meaningful to ask whether the excited level is a singlet or a triplet. Concomitant with its long half-life (10^{-4} to 10^{-3} s) is its strongly oxidizing character as a photo-chemical reactant, for instance, hydrogen atom abstraction from organic molecules (Rabinowitch and Linn Belford, 1964; Burrows and Kemp, 1974) and it has been established that $Mn(H_2O)_6^{+2}$ yields a quasi-stationary concentration of manganese(III) by flash photolysis (Burrows et al., 1976).

The first authors to mention the possibility of electron transfer bands in trivalent lanthanides were Banks et al. (1961) noting an absorption edge in the

ultra-violet of Eu(III) and Yb(III) in molten chlorides. The first systematic study of such electron transfer bands (Jørgensen, 1962c) was made on solutions of anhydrous RBr_3 in almost anhydrous ethanol, or on perchlorates plus excess bromide in this solvent. The stoichiometry of the prevailing complex is not perfectly certain, though it is probable that it is mainly solvated RBr^{+2} . Anyhow, the wave-numbers of the broad moderately intense electron transfer band increase in a characteristic fashion

$$Eu(III) < Yb(III) < Sm(III) < Tm(III) < \dots \quad (23.23)$$

dependent on the oxidizing properties of the lanthanide, europium(III) being the most readily reduced. As can be seen in table 23.3, similar observations were made from reflection spectra of anhydrous RBr_3 and of various mixed oxides (Barnes and Pincott, 1966) and from solution spectra of oxygen-containing anions, such as sulfate (Barnes and Day, 1964). It is particularly important also that R_2O_3 shows edges or band maxima according to Eq. (23.23) (Ropp, 1965; Jørgensen et al., 1965a) because the luminescent energy transfer to excited $4f^q$ levels (Blasse and Brill, 1966; Blasse, 1976) from such electron transfer bands in mixed oxides can be quite effective.

Though the complexes are quite atypical by low coordination number N , octahedral symmetry, and the need for solvents without mobile protons (such as acetonitrile) the best defined cases included in table 23.3 are the hexa-chloro and -bromo complexes RCl_6^{-3} and RBr_6^{-3} (Ryan and Jørgensen, 1966) and the even more reactive hexa-iodo species RI_6^{-3} (Ryan, 1969) of which the extreme cases are the dark green EuI_6^{-3} and the wine-red YbI_6^{-3} though it may be noted that both anhydrous $EuBr_3$ and $EuBr_6^{-3}$ are orange-yellow. Quite generally, it is rather difficult to find clear-cut cases for electron transfer bands in R(III) because the pronounced A character (Pearson hardness) of lanthanides almost removes the affinity to

TABLE 23.3.

Wave-numbers (cm^{-1}) of the electron transfer bands of $4f$ group complexes in solution and in reflection spectra of crystals.

	Sm	Eu	Tm	Yb
RCl^{+2} in ethanol	45 700	36 200	—	41 000
RCl_6^{-3} in acetonitrile	43 100	33 200, 42 600	—	36 700
RBr^{+2} in ethanol	40 200	31 200	44 500	35 500
RBr_3 , anhydrous	34 500	26 000	—	28 200
RBr_6^{-3} in acetonitrile	35 000	24 500, 32 400, 37 000	38 600	29 200, 41 700
RI_6^{-3} in acetonitrile	24 900, 32 800	14 800, 22 200, 26 700	28 000	17 850, 22 400, 27 000
R(III) aqua ion	—	53 200	—	—
$R_2(CO_3)_3 \cdot 3H_2O$	52 100	42 400	—	47 800
RPO_4 , anhydrous	52 000	43 500	—	48 400
$R_2(SO_4)_3$, anhydrous	50 800	42 200	—	48 500
$R_2(SO_4)_3 \cdot 8H_2O$	50 300	41 700	—	47 200
RSO_4^+ in water	48 100	41 700	—	44 500

reducing ligands, and furthermore, most polyatomic reducing ligands have strong internal transitions in the near ultra-violet frequently masking the conceivable electron transfer bands. Nevertheless, it is possible (Jørgensen, 1962c) to prepare the orange europium(III) dithiocarbamate $\text{Eu}(\text{S}_2\text{CN}(\text{C}_4\text{H}_9)_2)_3$ and the corresponding yellow ytterbium(III) compound. The same two colors due to electron transfer spectra are observed (Bradley et al., 1973) in the $\text{R}(\text{N}(\text{Si}(\text{CH}_3)_3)_2)_3$ with the low $N = 3$. The most extreme example is the green color of $\text{Yb}(\text{C}_5\text{H}_5)_3$ due to an electron transfer band in the red (Pappalardo and Jørgensen, 1967).

In the 4d and 5d groups, a large amount of experimental data is available (Jørgensen, 1963a, 1970b) about electron transfer bands of hexahalide complexes MX_6^{+z-6} and one of the most striking regularities is that the wave-number $\nu_{\text{e.t.}}$ of the first strong electron transfer band within a few thousand cm^{-1} is

$$\nu_{\text{e.t.}} = [x_{\text{opt}}(\text{X}) - x_{\text{uncorr}}(\text{M})]30000 \text{ cm}^{-1}, \quad (23.24)$$

where x_{opt} is the *optical electronegativity* of the ligand. When the constant is chosen as 30000 cm^{-1} , it is possible to give the four halide ligands the values of $x_{\text{opt}} = 3.9(\text{F}^-)$, $3.0(\text{Cl}^-)$, $2.8(\text{Br}^-)$ and $2.5(\text{I}^-)$ also characterizing the Pauling electronegativities. It is not necessary here to repeat the arguments transforming the uncorrected optical electronegativity $x_{\text{uncorr}}(\text{M})$ derived from eq. (23.24) to $x_{\text{opt}}(\text{M})$ though it may be mentioned that it increases with increasing oxidation state of a given element, and also increases smoothly with increasing Z for a set of M(III) or M(IV) crossing a given transition group in a way related to our parameter $(E-A)$. In the hexahalide complexes in table 23.3 there are slightly larger differences between $\text{X} = \text{Cl}$, Br and I than are suggested by eq. (23.24) and actually, x_{uncorr} of Sm(III) seems to increase from 1.56 to 1.67, x_{uncorr} of Eu(III) from 1.89 to 2.01 and x_{uncorr} of Yb(III) from 1.78 to 1.90, but conserving the trend of eq.(23.23) made quantitative in the refined theory of spin-pairing energy. It is perhaps less surprising that R(III) seems to have x_{uncorr} about 0.2 unit lower in RBr^{+2} dissolved in ethanol than in RBr_6^{-3} in acetonitrile, because the former complexes have higher N and longer R-Br distances. Much stronger examples of *anisotropic behavior* is found in uranyl and neptunyl complexes (Ryan and Jørgensen, 1963) such as $\text{UO}_2\text{Br}_4^{-2}$ or $\text{NpO}_2\text{Cl}_4^{-2}$ having much longer internuclear distances in the equatorial plane than along the axis of the two oxo ligands.

In the lanthanides, R(IV) are far more oxidizing than R(III). Correspondingly, strong absorption bands are observed in the visible of Pr(IV) and Tb(IV) incorporated in mixed oxides (Jørgensen and Rittershaus, 1967; Hoefdraad, 1975; Blasse, 1976). Contrary to the hypothesis of a constant x_{opt} of oxide, the wave-numbers are much lower in ThO_2 and ThGeO_4 corresponding to deep purple colors compared with CeO_2 and the characteristic orange color in Y_2O_3 . It is no accident that the best known R(II) are Eu(II) and Yb(II) with the highest I according to the refined spin-pairing energy theory, whereas the best known R(IV) have the lowest electron affinities (i.e. the lowest I of the corresponding R(III) with $q = 2$ and 8) such as Pr(IV) and Tb(IV) of comparable oxidizing character, and Ce(IV) considerably less oxidizing. Among the best characterized cerium(IV) complexes are orange CeCl_6^{-2} having a very strong electron transfer

band at 26600 cm^{-1} and the purple CeBr_6^{-2} at 19200 cm^{-1} (Ryan and Jørgensen, 1966) corresponding to x_{uncorr} of cerium(IV) slightly above 2.1. The highest $x_{\text{uncorr}} = 3.0$ can be derived for Nd(IV) and Dy(IV) from the reflection spectrum (Varga and Asprey, 1968) in the orange solids Cs_3NdF_7 and Cs_3DyF_7 .

Certain electron transfer bands are due to transfer from one metallic element to another, rather than from a ligand to such an atom. Typical cases are the electron transfer from $\text{Ag}4d$ or $\text{Tl}6s$ to the partly filled $5d$ shell producing striking colors and new bands in the reflection spectra (Jørgensen, 1963b) of silver(I) and thallium(I) salts of rhenium(IV), osmium(IV) and iridium(IV) hexahalide anions (as is also known from red Ag_2CrO_4 and blue AgMnO_4) and also of ferrocyanides (Braterman, 1966) of copper(II) and uranyl having excited states containing Fe(III), Cu(I) and U(V). On the other hand, Herbison-Evans et al. (1965) found that $\text{Tl}_3\text{Fe}(\text{CN})_6$ has excited states due to Tl(II) and Fe(II). There is not a large difference between such cases and electron transfer between atoms of the same element in different oxidation states in mixed-valence compounds (Robin and Day, 1967). Thus, Prussian Blue contains the chromophores $\text{Fe}(\text{II})\text{C}_6$ and $\text{Fe}(\text{III})\text{N}_6$ in the ground state (with $S = 0$ and $\frac{5}{2}$, respectively) to be compared with $\text{Fe}(\text{III})\text{C}_6$ and $\text{Fe}(\text{II})\text{N}_6$ with $S = \frac{1}{2}$ and 2 in the excited state. The corresponding purple ruthenium(II) compound goes from $\text{Ru}(\text{II})\text{C}_6$ and $\text{Fe}(\text{III})\text{N}_6$ to $\text{Ru}(\text{III})\text{C}_6$ and $\text{Fe}(\text{II})\text{N}_6$. Another example (Day, 1963) is the dark blue colour of cubic crystals simultaneously containing SbCl_6^{-3} and SbCl_6^- . Somewhat unexpectedly, the ground state contains Sb(III) and Sb(V) whereas the excited state has equilibrated to Sb(IV). These facts must be connected with unexpected features of the potential hypersurfaces in the $(3N - 5)$ dimensional space for N nuclei, as also discussed by Blasse (1976) in connection with the influence of electron transfer bands of R(III) and R(IV) on the luminescent behavior of lanthanide compounds. Hofmann and Höschele (1915) ascribed the dark blue color of $\text{Ce}_{1-x}\text{U}_x\text{O}_2$ to "oscillating valences" also supposed to occur in Prussian Blue, but when it was realized (Magneli and Kihlberg, 1951) that this (completely miscible) series of fluorite crystals follows Vegard's rule, it was assumed that the ground state contains Ce(IV) and U(IV) and the excited state of the electron transfer band Ce(III) and U(V), an electron jumping from uranium to cerium. However, recent photo-electron spectra (Keller and Jørgensen, 1975) might be interpreted as indicating that some U(V) even occurs in the ground state. Allen et al. (1973) made a careful study of the reduction of pale yellow CeO_2 to dark blue CeO_{2-x} and finally olive-yellow Ce_2O_3 . The air oxidation of precipitated $\text{Ce}(\text{OH})_3$ to blue-grey intermediates is somewhat comparable to the classical case of $\text{Fe}(\text{OH})_{2+x}$ being dark green, almost black. There are not many other clear-cut cases of electron transfer between two oxidation states of the same lanthanide, though Allen et al. (1973) argue this to be the case for Eu_3O_4 . It seems also that fox-red stoichiometric PrO_2 and TbO_2 are not as strongly colored as black Pr_6O_{11} and brown Tb_4O_7 .

An important difference between optical transitions (including electron transfer bands) and chemical reactions is that the former obey Franck and Condon's principle that the distribution of internuclear distances in the electronic ground

state (due to the lowest, or population of several other, vibrational functions) is conserved in the excited state in spite of a conceivable large amount of co-excited vibrations. The picture of the potential curve of a diatomic molecule has given the name *vertical transitions* in such a case, projecting the vibrational function originally prevailing up on the excited potential curve. Chemical reactions are intrinsically *adiabatic* allowing the internuclear distances to change. A typical case is the reaction between 2Cu^{+2} in aqueous solution with four I^- forming a precipitate of 2CuI and a diatomic I_2 molecule. Under the same circumstances, the broader an electron transfer band the more likely it is to produce such a redox reaction. It is quite characteristic that one of the lowest wave-numbers known for the electron transfer bands of a monomeric halide complex is the $5d^4$ osmium(IV) OsI_6^{-2} at 9400 cm^{-1} in the near infra-red (Jørgensen, 1963b; Jørgensen et al., 1971; Piepho et al., 1975) where the band-width is exceptionally narrow. On the other hand, broad absorption bands of cerium(IV) complexes are far more liable to conduct to photo-chemical decomposition. In the specific case where the stoichiometry of the excited state does not differ from the ground state (and the excitation energy is due to differing internuclear distances) there is no obvious lower limit to the wave number, but several such compounds containing one Fe(II) and one Fe(III) have been shown in recent years to have a strong, rather broad band between 6000 and 10000 cm^{-1} such as $\text{Fe}_2(\text{CN})_{10}^{5-}$ (Emschwiller and Jørgensen, 1970) probably containing two cyanide bridges, whereas a crystal structure (Ludi and Güdel, 1973; Glauser et al., 1973) has been shown to have one cyanide bridge in the analogous $\text{Fe}_2(\text{CN})_{11}^{6-}$. Besides the question of co-excited vibrations, there is the more fundamental problem with electron transfer between distant atoms that it is very difficult to provide sufficient oscillator strength for the transition. Seen from this point of view, it would be quite interesting to look for weak electron transfer bands between lanthanides and rather distant atoms. One case is black EuTiO_3 (Brous et al., 1953) containing Eu(II) and Ti(IV) in the ground state. The excited states of this perovskite may be intermediate (or superposed) between $4f^65d$ of Eu(II) such as in the NaCl-type monochalkogenides, and electron transfer yielding Eu(III) and Ti(III).

2.4. The conditions for unusual oxidation states

In aqueous 1 molar non-complexing acid ($\text{pH} = 0$) or 0.1 molar H_{aq}^+ ($\text{pH} = 1$) there is not the slightest doubt that only R(III) aqua ions are thermodynamically stable. It is true that the H_2 evolution of europium(II) aqua ions and the O_2 evolution of the not too well-defined cerium(IV) hydroxo-aqua complexes are so slow (in the absence of suitable catalysts and ultra-violet radiation) that solutions can be kept in practice for several months. Alkaline conditions forming the highly insoluble yellow $\text{Ce}(\text{OH})_4$ and many complexing anions (nitrate, phosphate, sulfate, chromate and in roughly neutral solutions peroxide) stabilize Ce(IV). In spite of many attempts to prepare praseodymium(IV) and terbium(IV) from aqueous solution, this does not seem to have succeeded as yet,

though mixed oxides, for instance obtained by calcining the mixed hydroxides made with aqueous ammonia (Jørgensen and Rittershaus, 1967) at 600°C, or by calcining mixed nitrate solutions on cotton Auer mantles (Jørgensen, 1975d and 1976a), readily contain these two oxidation states, and actually it can be quite difficult to reduce them to R(III) by heating in hydrogen. The three R(IV) mentioned form many colorless fluorides and double fluorides, whereas Nd(IV) and Dy(IV) are only known in the orange Cs_3RF_7 (Varga and Asprey, 1968).

Though solid-state chemistry and the use of non-aqueous solvents have extended our previous possibilities of preparing R(II) and R(IV) there are other limitations to the production of unusual oxidation states which have become apparent from recent physical measurements. Since crystalline fluorides are more difficult to reduce than water is, it is not surprising that traces of syncrystallized R(II) can be detected. Contrary to the d groups (Jørgensen, 1969a) where certain types of ligands, such as CO and PF_3 , are particularly able to stabilize central atoms in very low, zero or negative oxidation states, no conjugated ligands (e.g. of the dipyriddy or phenanthroline type) which significantly stabilize R(II) are found. Actually, most complex formation constants for a given ligand are larger for R(III) than for R(II) with the result that the standard oxidation potential E^0 of the R(II) complex is normally more negative than for the aqua ion. Nugent et al. (1973) have used the refined spin-pairing energy theory to predict and rationalize the variation of E^0 for both R(II) and R(III) aqua ions as a function of varying number q of 4f electrons. The general trends in the phenomenological baricenter polynomial clearly show that no R(I) compounds are expected in the sense of containing the appropriate number of 4f electrons. This does not prevent clusters from forming, stabilized by the presence of electrons not in the 4f shell. A typical case is the metallic compound Gd_2Cl_3 (Lokken and Corbett, 1970) having magnetic properties ($S = \frac{7}{2}$) corresponding to the conditional oxidation state Gd(III). In spite of the extremely positive E^0 values evaluated for R(III) aqua ions (Nugent et al., 1973) making eleven of the hypothetical R(IV) aqua ions more oxidizing than F_2 it is much more difficult to present a clear-cut argument against rather unexpected ligands stabilizing a given R(IV) at least kinetically for a short time. We have already seen a rather curious example (Ryan and Jørgensen, 1966) in the admittedly highly reactive CeBr_6^{-2} . It is known in the 3d group that both dithiocarbamates (Hendrickson et al., 1975; Willemse et al., 1976) and a diphosphine (Warren and Bennett, 1974) are able to stabilize unusually high oxidation states such as iron(IV), nickel(IV) and copper(III), and it may be mentioned that the only two known iridium(V) complexes are IrF_6^- and $\text{H}_5\text{Ir}(\text{P}(\text{C}_6\text{H}_5)_3)_2$. Such paradoxes must be explained by a delicate balance between the ligand to be oxidized (and perhaps dimerized) leaving the central atom in a lower oxidation state, and the stronger covalent bonding, in particular of Pearson-soft, ligands when the oxidation state increases. It is quite conceivable that rather soft ligands stabilize R(IV). On the other hand, the $I(\text{R}4\text{f})$ determined by photo-electron spectra exclude (Jørgensen, 1973b,c) R(V) being produced in condensed matter.

It is not easy to have a completely sharp classification of how many oxidation

states are known in non-metallic compounds of the elements scandium ($Z = 21$) to fermium ($Z = 100$) though 238 were definitely known in 1968 (Jørgensen, 1969a). It is curious how few have been determined since: gold(V) in AuF_6^- (Leary and Bartlett, 1972), manganese(-III) and rhenium(-III) in $\text{M}(\text{CO})_4^{-3}$ (Ellis and Faltynek, 1975), nickel(I) complexes of certain macrocyclic ligands (Tait et al., 1976) and finally dark green monomeric nickel(I) in a zeolite (Garbowski, 1976) not to be confused with dimeric $(\text{NC})_3\text{NiNi}(\text{CN})_3^{-4}$. Quite generally, we do not count catenated species with homo-atomic bonds of chromium, manganese, gallium, selenium, molybdenum, ruthenium, rhodium, palladium, tellurium, rhenium and mercury as distinct oxidation states, though their oxidation number (for use in redox equations) is defined. It is difficult to know whether there is an absolute sense in which the discovery of new oxidation states has passed its climax, or whether we are just waiting for a new combination of ligands ready to produce a new manifold of oxidation states. The most oxidizing elements, fluorine and oxygen, already seem to have done their best for the lanthanides. The characteristic electron spin resonance spectrum of $4f^7$ may perhaps assist in detecting traces of terbium(IV) on unusual sites. The electron transfer spectra probably provide intense colors of transient R(IV) intermediates.

2.5. Photo-electron spectra (ESCA)

A neutral or positive system with access to open space always has a set of discrete stationary states followed by a continuum of overall dense states starting with the lowest ionization energy I . This corresponds to the threshold of Einstein photo-emission from a metallic sample, and a large number of gaseous molecules (Watanabe, 1957) were studied with respect to the photon energy threshold for photo-conductivity. It was felt by many quantum chemists that the higher I values corresponding to ionization of penultimate MO in molecules were somewhat an artifact by being situated inside the continuum. However, an experimental technique became available for verifying these penultimate orbitals by photo-electron spectra where

$$I = h\nu - E_{\text{kin}} \quad (23.25)$$

Solid samples are generally bombarded with 1253.6 eV photons originating in a magnesium anti-cathode, or $h\nu = 1486.6$ eV from aluminum. This technique was developed by Kai Siegbahn and his group in Uppsala based on experience with β -spectrographs, and was originally considered an alternative to the classical determination of I for inner shells by X-ray spectra. When Hagström et al. (1964) found a strong chemical shift dI between the two non-equivalent sulfur atoms in thiosulfate $\text{S}_2\text{O}_3^{-2}$ the interest for chemical effects on photo-electron spectra rapidly grew, and the acronym "Electron Spectroscopy for Chemical Applications" was coined. The "A" was "Analysis" until it turned out that the technique is only interesting as a semi-quantitative analysis method for extremely specific problems of surface chemistry, though it can be of unique help

(Jørgensen, 1975a, 1977; Berthou and Jørgensen, 1975; Pitton et al., 1976). By the way, the shift of about 10 eV between the sulfur 1s absorption edges in sulfates and in sulfides was previously found by Stelling (1928) in Lund and was also shown to occur in the X-ray absorption in thiosulfates. Gaseous samples can either be studied with the photon energies given above, or with the 584 Å resonance line (21.2 eV) of the helium atom or 304 Å ($h\nu = 40.8$ eV) of He^+ . Since 1962, David Turner developed this technique, first in Imperial College of Science and Technology in London and later at the University of Oxford (Turner et al., 1970) confirming the penultimate MO of a large number of simple, and in particular di- and triatomic molecules. In such cases, the resolution can be as good as 0.01 eV allowing the vibrational structure to be identified. Solid samples have a variety of experimental problems, one being connected with the mean escape-width of the electron not undergoing inelastic scattering being about 20 Å (some 4 to 6 monomolecular layers), only a percent of the average penetration of the 1253.6 or 1486.6 eV soft X-rays. Correspondingly, the mildly undulating background of inelastically scattered electrons with E_{kin} lower than given by eq.(23.25) has a very large area and is half as high as the strongest peaks. The resolution obtained is not much better than 1 eV. An additional problem for non-conducting samples is that they develop a quasi-stationary positive potential between 1 and 5 V decreasing E_{kin} and increasing the apparent value of I . This charging effect can be evaluated (Jørgensen and Berthou, 1975) by comparison with the C1s signals of the hydrocarbon from one-sided scotch tape. Recent reviews on photo-electron spectra of metallic (Watson and Perlman, 1975) and non-metallic (Jørgensen, 1975e) solids can be consulted for further information. In Geneva, a systematic study of 600 compounds containing 77 elements was made with a Varian IEE-15 photo-electron spectrometer (Jørgensen and Berthou, 1972).

For the chemists, the most interesting aspect of the photo-electron spectra of lanthanides is the valence region containing the signals due to R4f. The resolution is by far the best in the metallic elements but a major experimental problem is that one needs to work at very high vacuo (10^{-10} torr and not 10^{-7} torr as frequent for most compounds) and with freshly evaporated samples (it is here useful that oxygen 1s signals can be used to detect oxides, even if they are amorphous) as first done by Hedén et al. (1971) but later continued to a large extent by Baer and Busch (1974). These results were discussed in a three-laboratory note by Cox, Baer and Jørgensen (1973) as the effect of forming various energy levels of $4f^{q-1}$ by ionization of $4f^q$. In table 23.4 the I^* values relative to the Fermi level are given for the more complicated cases. The corresponding I values relative to vacuo are roughly 3 eV higher. Metallic europium and gadolinium both have the half-filled shell $4f^7$ and hence the conditional oxidation states Eu[II] and Gd[III] with a single signal at two different positions, $I^* = 2.1$ and 8.0 eV, respectively. The excited states formed of $4f^6$ all belong to the lowest term 7F less than $\frac{1}{2}$ eV wide. Metallic ytterbium and lutetium are closed-shell systems, and the sets of I^* values, 1.1 and 2.4 eV for Yb[II] and 7.1 and 8.6 eV for Lu[III] corresponding to the two $J = \frac{7}{2}$ and $\frac{5}{2}$ of the unique term 2F of $4f^{13}$. As seen in table 23.4 the metallic elements between terbium and thulium have rather complicated

TABLE 23.4.

Photo-electron spectra $4f^q \rightarrow 4f^{q-1}$ of metallic lanthanides and NaCl-type antimonides. I^* (in eV relative to the Fermi level) and assignments of ionized states in parentheses.

(q - 1)		4.6	
1	Pr 3.3($^2F_{5/2}$)	PrSb 2.5 ($^2F_{5/2}$)	
2	Nd 4.8(3H_4), 5.4(3F_2)	NdSb 5.8(3H_4), 6.4(3F_2)	
4	Sm 5.3(5I), 6.8(5F), 7.6(5G), 9.4(5D)	SmSb 6.1(5I), 8.5(5G)	
6	Gd 8.0(7F)	GdSb 9.1(7F)	
7	Tb 2.3(8S), 7.4(6I), 9.3(6G), 10.3(6H)	TbSb 3.2(8S), 8.2(6I), 10.1(6G), 11.1(6H)	
8	Dy 3.9(7F_6), 6.7(5D_4), 7.7($^5L_{10}$), 8.6(5H_7), 9.3(5I_8), 10.5(5K_9), 12.5(triplet or $4f^7$ shake-off)	DySb 5.0(7F_6), 8.3(5D_4), 8.7($^5L_{10}$), 9.7(5H_7), 10.3(5I_8), 11.5(5K_9), 13.5(triplet or $4f^7$ shake-off)	
9	Ho 5.3($^6H_{15/2}$), 6($^6F_{11/2}$), 8.7($^4M_{21/2}$), 9.5($^4L_{19/2}$)	HoSb 6.0($^6H_{15/2}$), 7.0($^6F_{11/2}$), 9.4($^4M_{21/2}$), 10($^4L_{19/2}$)	
10	Er 4.8(5I_8), 5.4(5I_7), 6.8(5F_5), 7.7(3G_6), 8.7(3L_9), 9.4($^3M_{10}$)	ErSb 5.6(5I_8), 6.3(5I_7), 8(5F_5), 8.7(3G_6), 9.6(3L_9), 10.2($^3M_{10}$)	
11	Tm 4.6($^4I_{15/2}$), 5.8($^4I_{13/2}$), 7($^2H_{11/2}$), 8.3($^4G_{11/2}$ and $^2K_{15/2}$), 10.1($^2L_{17/2}$)	TmSb 5.5($^4I_{15/2}$), 6.5($^4I_{13/2}$), 8.2($^2H_{11/2}$), 9.3($^4G_{11/2}$ and $^2K_{15/2}$), 11.2($^2L_{17/2}$)	

spectra, but are not as widely distributed as one would predict if all the $4f^{q-1}$ terms enumerated in eq.(23.16) were formed with a probability proportional to their number $(2S + 1)(2L + 1)$ of states. As frequently happens in atomic spectroscopy, the ionization process is both limited by symmetry-determined *selection rules* (in Russell-Saunders coupling, S changes $\pm \frac{1}{2}$ and L can at most change by 3 units) and by numerical conditions related by Cox (1975) to the *squared coefficients of fractional parentage* of the final $4f^{q-1}$ states in the $4f^q$ ground state (assuming spherical symmetry and definite S, L, J). The resulting intensity distribution is in remarkable agreement (Cox et al., 1973) with the observed signals, if the configuration $4f^{q-1}$ is compared with the known distribution of J -levels (Carnall et al., 1968) for the R(III) aqua ion of the preceding element with Z one unit lower. However, we are here in the presence of two isoelectronic species, R[IV] formed by ionization of R[III], and R(III). One would have expected parameters of interelectronic repulsion about 20% larger in the former case, but as a matter of fact, this increase is only 6% in Tm[IV] compared with $4f^{11}$ Er(III) but about 12% when comparing Dy[IV] with $4f^8$ Tb(III) or Tb[IV] with $4f^7$ Gd(III). These regularities can be used for discussing the nephelauxetic effect in the final ionized states (Jørgensen, 1975c).

The first compounds which were compared with the metallic elements were EuS having $I^*(Eu4f) = 1.8$ eV, and $I^*(S3p)$ about 3.8 eV, and the metallic NaCl-type stoichiometric compound GdS having $I^*(Gd4f) = 8.9$ eV (Eastman and Kuznietz, 1971). Campagna et al. (1974b, 1976) compared a large number of semi-conducting NaCl-type antimonides RSb of which $I^*(R4f)$ shows almost the same

structure as the metallic elements, but 1 eV higher values, as seen in table 23.4. What is quite interesting is that $I^*(\text{Sb}5p)$ in all the antimonides is close to 2.0 eV, much lower than $I^*(\text{R}4f)$. The partly filled 4f shell going from R = Ce to Tm does not form such strongly covalent bonds that the structure of $4f^{q-1}$ in approximately spherical symmetry (the strong photo-electron signals usually correspond to the lowest J -level of terms with relatively high L) cannot be recognized and actually, the term distances (e.g. between ${}^2L_{17/2}$ and ${}^4I_{15/2}$ of f^{11}) are marginally larger in the later antimonides (5.7 eV in TmSb to be compared with 5.5 eV in metallic thulium) corresponding to a slightly less pronounced nephelauxetic effect, whereas the opposite may be true for terbium, dysprosium and holmium. The situation is slightly less clear-cut in insulating fluorides, iodates, sulfates and oxides (Jørgensen and Berthou, 1972; Cox et al., 1973) where it is not perfectly clear whether the blurring out of the narrow signals compared with those found in antimonides is due to the inhomogeneous Madelung potential on the surface of the crystals, spatially distributed variations of the quasi-stationary positive potential due to the loss of photo-electrons, or the chemically more interesting effect of splitting of individual J -levels into sub-levels (each containing a few of the $(2J + 1)$ states) due to deviations from effective spherical symmetry corresponding to extensive covalent bonding. However, independently of how the observed broadening is distributed on these three effects, it is normally below 1 eV and, for instance smaller than the typical sub-shell energy difference Δ (called $10Dq$ in ancient literature) in octahedral 3d, 4d and 5d group complexes.

The photo-electron spectra of NaCl-type lanthanide compounds have provided even more surprising observations. An almost unique case is TmTe apparently containing comparable concentrations of $4f^{12}$ thulium(III) and $4f^{13}$ thulium(II) in the ground state (Campagna et al., 1974a) though some criticism has recently been directed (Suryanarayanan et al., 1975) against this description of stoichiometric thulium telluride. Since the crystal remains strictly cubic with no lasting non-equivalence, the fluctuations of oxidation state must be very rapid, though not as rapid as the time-scale (of the order of magnitude 10^{-17} s) of the photo-electron spectra, establishing an almost instantaneous picture (Jørgensen, 1971a). The analogous selenide TmSe has about 80% thulium(III) and 20% thulium(II) on an instantaneous picture (Campagna et al., 1974a). Perhaps the most amazing result is that the nephelauxetic effect is perceptible in $4f^{11}$ formed by ionization of Tm(III) and comparable to TmSb (Campagna et al., 1974b) whereas $4f^{12}$ formed by ionization of Tm(II) at the same time hardly shows any nephelauxetic effect because levels such as 1I_6 and 3H_6 are separated at distances decreased by 2% or less compared with the well-known energy levels obtained by the study of visible and ultra-violet spectra of thulium(III) compounds, as discussed in this series by Carnall in Chapter 25. Whereas NaCl-type samarium(II) sulfide is a straightforward Sm(II) compound showing photo-electron signals due to $4f^6 \rightarrow 4f^5$ ionization, the metallic NaCl-type crystals such as $\text{Sm}_{0.82}\text{Gd}_{0.18}\text{S}$ and $\text{Sm}_{0.85}\text{Th}_{0.15}\text{S}$ obtained by substitution with gadolinium(III) or thorium(IV) seem to contain comparable amounts of Sm[II] and Sm[III] on an

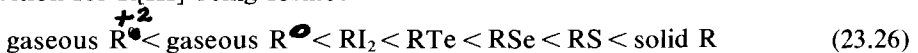
instantaneous picture (Campagna et al., 1974c, 1976). Such collective effects are not due exclusively to a change of lattice constants (comparable to well-known (Jayaraman et al., 1974) transformations of many R(II) compounds to R(III) by external high pressure) since certain substituents increase the unit cell dimension. The relation of such behavior to the energy band model was recently reviewed by Wilson (1977).

2.6. *Metallic and semiconducting solids*

In contrast to the chemical metallic character of an element (evaluated according to the acidic or basic character of the hydroxide, and several other criteria) strongly dependent on the oxidation state (e.g. chromium and manganese) the *physical metal* is best defined as a conducting material not having its electric resistance decreased with increasing temperature. The typical metal actually has its resistivity roughly proportional to the absolute temperature T , whereas the typical semiconductor follows the same exponential decrease as the kinetic reaction-times according to the Arrhenius equation, the logarithm of the electric resistivity being a linear function of $(1/T)$. It is worthwhile noting that elements and non-stoichiometric alloys are not the only feasible physical metals, many strictly stoichiometric compounds can be physical metals. For our purposes, it is interesting to note the cubic NaCl-type compounds TiC, LaS, GdS and ThS and other examples, such as LaI₂ and ThI₂. Certain metallic elements, such as the alkaline metals (Li, Na, K, Rb and Cs) and the coinage metals (Cu, Ag, Au) almost certainly consist of closed-shell ions M^+ surrounded by the Fermi sea of conduction electrons containing one electron from each M atom. However, most metallic elements are much less conducting, and though it cannot be argued that the resistivity is inversely proportional to the number of conduction electrons (because their mobility depends on many additional parameters) it seems likely that most heavier elements are a kind of homo-atomic compounds (with long internuclear distances corresponding to the high coordination number N) containing a relatively low number of mobile electrons. A typical case is mercury (which was used for many years to define an ohm, before the electrical units were incorporated in the m-k-g-s system) or antimony and bismuth, and the chemist cannot help feeling that metallicity must be something slightly superficial. It is beyond doubt that even highly isolating compounds become metallic, even at room temperature or below, at sufficiently high pressure. For the experimentalist, it is sad that one cannot remove metallicity by applying a negative pressure, increasing the internuclear distances, because the strength of most materials toward cavitation is very moderate.

In the lanthanide compounds, the observation that the mono-chalkogenides RX ($X = S, Se, Te$) are physical metals for $R = La, Ce, Pr, Nd, Gd, Tb, Dy, Ho, Er$ (for Tm, cf. the remarks above for photo-electron spectra) but typical semiconductors for $R = Sm, Eu$ and Yb suggested the correlation (Jørgensen, 1964) with the lowest level of the next configuration $4f^{q-1}5d$. The argument then ran that in stoichiometric, undiluted compounds the lowest conduction band is

constituted by 5d orbitals being sufficiently delocalized. This is not true in highly dilute fluorites $R_xCa_{1-x}F_2$ where McClure and Kiss (1963) detected $R = La, Ce$ and possibly Gd with the ground state belonging to 5d, 4f5d and 4f⁷5d respectively, in spite of certain complications (Drotning and Drickamer, 1973) for instance in the case of $R = Tb$. After the establishment of the system differences discussed in subsect. 2.2 and the refined spin-pairing energy theory, it would seem more plausible to say that the metallicity is connected with the removal of one 4f electron of R(II) whereas it is less imperative that it becomes exactly a 5d electron. Any loss of a 4f electron to an indefinite reservoir of conduction electrons would show the same trend and become easier along the elements $Eu < Yb < Sm < Tm < \dots$ in the order given in eq. (23.23). It was also noted (Jørgensen, 1964) that bivalent iodides are more apt to remain non-metallic, since both TmI_2 and NdI_2 are dark colored semi-conductors like ThI_3 . Hulliger (1968) analyzed these conditions further and concluded that there was a parallel shift of 4f^{q-1}5d to higher wave numbers in iodides rather than in chalcogenides. On the other hand, the metallic elements slide a further step down along eq.(23.23) in the sense of M[II] occurring in europium and ytterbium only (though remaining metallic with properties comparable to strontium and barium) and all the other elements being M[III] with one 4f electron less for a given element. It is a characteristic feature of classical physical chemistry that such phase transformations frequently correspond to almost the same free energy G for a highly different set of internuclear distances, as most strikingly seen in the equilibrium of a saturated vapor and its condensed solid. Hence, the transitions between M[II] and M[III] cannot at all be expected to be spectroscopic in the sense of following Franck and Condon's principle. Whereas large chunks of a given solid have almost identical thermodynamic properties, sufficiently small particles are more volatile, soluble, ... corresponding to slightly higher free energy, but at the same time, the strong surface tension imitates many of the effects of high external pressure, and in particular, the internuclear distances are perceptibly shorter than in the large crystal. Vergand and Bonnelle (1972, cf. also Bonnelle and Vergand, 1975) found from the X-ray spectra of small globules of metallic ytterbium that they become Yb[III] when their radii are below 30 Å. This observation was confirmed by electron diffraction, whereas small globules of metallic gadolinium gradually decrease their internuclear distances much less. It is possible to generalize these recent facts to the condition for R[III] being formed



increasing with decreasing R-R distances. The differentiation between tellurides, selenides and sulfides is derived from the observations of Campagna et al. (1974a, 1976). The condition for the transition from R(II) to R[III] is clearly that the ionization energy I forming the ground state of 4f^{q-1} is lower than the electron affinity of the available orbitals with vacant positions, effectively the conduction band. However, this question is adiabatic and not directly spectroscopic.

We have not yet discussed the transition from M[III] to M[IV] though the two isotypic modifications of metallic cerium, cubic α -Ce and γ -Ce at least for a large part contain Ce[IV] without a localized 4f and Ce[III] with one 4f electron, respectively (for a thorough review, see Jayaraman, 1965) compared with the hexagonal β -Ce being Ce[III]. Weaver and Schirber (1976) studied P and As nuclear magnetic resonance of NaCl-type of CeP and CeAs with unusual behavior, and Jayaraman et al. (1976) discussed the high-pressure transformation of cubic NaCl-type CeP from Ce[III] to Ce[IV] with an additional conduction electron. Otherwise, all the RP, RAs and RSb of NaCl-type seem to be low-energy-gap semiconductors and RN seems to have intrinsically a rather large energy gap (say 2 eV) though it seems to be very difficult to prepare them without crystalline defects or chemical impurities making them behave as physical metals. Obviously, alloys of cerium and thorium are also quite interesting (Gschneidner et al., 1962; Edelstein et al., 1976). It may be noted that Johansson (1974, 1975) argues that the transition from γ -Ce to α -Ce is a *Mott transition* (Mott, 1974, describes how a given lattice of e.g. sodium atoms suddenly becomes metallic below a critical limit of internuclear distances, whereas the large difference between I and the electron affinity, called the Hubbard parameter U , prevents electron hopping at higher distances) with itinerant 4f electrons in the latter case as known from compounds in the beginning of the 5d group such as the metallic Na_xWO_3 and ReO_3 . Johansson and Rosengren (1975) have discussed the cohesive energies (heats of atomization) of 4f and 5f elements. Though Johansson (1974) argues that α -Ce cannot be Ce[IV] because its $\Delta H_{\text{atom}} = 103$ kcal/mol is within 2% of that for La, γ -Ce, Lu (and Y) whereas ΔH_{atom} is from 146 to 143 kcal/mol for metallic Zr, Hf and Th, this is only an indicator that the valence state energy of Ce[IV] if it is a predominant constituent of α -Ce is 1.8 eV higher than of Ce[III]. Such differences are both adiabatic and collective (as seen from the absence of intermediate unit cell sizes) and cannot be adequately described by spectroscopic "vertical" transitions. The difference between the two isotypic cerium modifications is of the same type as the well-known Orgel gap (Orgel, 1957) between high-spin and low-spin forms of the same chromophore MX_6 where a given interval of M-X distances still implying S_{max} is thermodynamically unstable relative to a contraction permitting the lower S value. This does not prevent the two energy minima (for different distances) from sometimes being identical.

2.7. Evidence for weak covalent bonding and the nephelauxetic effect

The transitions in the partly filled 4f shell of lanthanide compounds are sufficiently similar to spectral lines of monatomic entities that the overall, small shift toward lower wave numbers is a rather direct indicator of partly covalent bonding. Hofmann and Kirmreuther (1910) suggested that the electronic orbits had slightly larger radii in Er_2O_3 than in hydrated erbium(III) salts, and Ephraim et al. (1926, 1928, 1929) made an extensive systematic study of band shifts in Pr(III), Nd(III) and Sm(III). Such work was continued by Boulanger (1952) and

Jørgensen (1956a, 1962d), but it was only after the identification of twelve J -levels of the lowest configuration $[\text{Xe}]4f^2$ of gaseous Pr^{+3} by Sugar (1965) that it became clear that even fluorides, double nitrates and aqua ions have lower term differences than gaseous R^{+3} as had been suspected for a long time

The situation was very different in the d groups, where the energy levels of gaseous M^{+2} and M^{+3} were generally well-known (Moore, 1952, 1958), but where the deviations from spherical symmetry due to chemical bonding are so strong that the term distances cannot be recovered without a considerable amount of mathematical manipulation (Tanabe and Sugano, 1954; Griffith, 1961), with the fortunate exception of octahedral and tetrahedral manganese(II) complexes (Orgel, 1955; Jørgensen, 1969a) where a direct comparison is possible between the ${}^6\text{S}-{}^4\text{G}$ distance 26846 cm^{-1} in the lowest configuration $[\text{Ar}]3d^5$ of gaseous Mn^{+2} and a sharp absorption band moving from 25300 cm^{-1} in MnF_2 and KMnF_3 both containing the chromophore $\text{Mn}(\text{II})\text{F}_6$ to 21600 cm^{-1} in the sulfides. Though it is beyond doubt that this shift is due to an expansion of the $3d$ radial function corresponding to the modified central field screened by the invading electronic density from the neighbor atoms, Orgel (1955) pointed out that it is not easy to evaluate how much of the electronic density has been transferred to the central atom by the partly covalent bonding. Thus, the lowest configuration $[\text{Ar}]3d^54s^2$ of the gaseous manganese atom has the distance 25279 cm^{-1} between the two terms ${}^6\text{S}$ and ${}^4\text{G}$ showing that the two $4s$ electrons together only decrease the term distance 5.8%. Schäffer and Jørgensen (1958) analyzed the general problem of how to obtain the phenomenological parameters of repulsion between d electrons from the observed absorption band maxima of octahedral and tetrahedral complexes, and the late Kaj Barr proposed the word *nephelauxetic* (cloud-expanding) for this effect. The nephelauxetic ratio β is the ratio between the phenomenological Racah parameter B in the compound and B_0 in the corresponding gaseous ion M^{+2} . Interestingly enough, the difference $(1 - \beta)$ can in most cases be written as the product of one parameter characterizing the central atom (in a definite oxidation state) and another parameter for the ligand. Since the problems in the lanthanides are rather different, we are not going to discuss these two nephelauxetic series at length here.

Actually, the major difficulty in the $4f$ group compounds is that the seven $4f$ -like electrons have *slightly* different one-electron energies, typically spread over 800 cm^{-1} or 0.1 eV . The corresponding six independent energy differences cannot be significantly evaluated from the original model of the electrostatic crystal field, which is a first-order perturbation from the (very small) difference between the Madelung potential and its spherical average for a given r . On the other hand, the *angular overlap model* was developed as M.O. theory for anti-bonding effects proportional to the square of the overlap between the orbitals of the central atom and of the ligands having the same symmetry type in the point-group considered (Jørgensen et al., 1963). It was later shown (Schäffer and Jørgensen, 1965; Schäffer, 1968, 1973; Jørgensen, 1971a) that the angular overlap model is equi-consequential with a contact term at the ligand nuclei acting on the square of the (real) $4f$ orbital. Anyhow, this model has been shown

to be compatible with much experimental evidence (Burns, 1967; Kuse and Jørgensen, 1967; Vishwamittar and Puri, 1973; Linares et al., 1977) but the relation between the one-electron energy differences in the 4f shell and the separation of sub-levels (each containing one or a few of the $(2J + 1)$ states) of a given J -level is, unfortunately, rather complicated. Because the M.O. configurations are highly mixed, the total splitting of a given J -level is usually 20 to 120% of the spread of one-electron energy differences, but varies strongly from one J -level to another. In crystals of comparatively high local symmetry, thorough studies of the line absorption spectra at low T allow all the sub-levels to be identified, so that they can be weighted by their number of states, and the baricentre of each J -level can be experimentally established. Typical cases of $d\beta$ (defined as the best straight line going through the J -level baricenters of $[\text{R}(\text{H}_2\text{O})_9](\text{C}_2\text{H}_3\text{SO}_4)_3$ compared with the compound, and assuming invariant ζ_{4f} as discussed below) are 0.0075 for $\text{Nd}_x\text{La}_{1-x}\text{Cl}_3$ (Carlson and Dieke, 1961), 0.012 for $\text{Nd}_x\text{La}_{1-x}\text{Br}_3$ (Richman and Wong, 1962) 0.031 for $\text{Nd}_x\text{Y}_{2-x}\text{O}_3$ (Chang, 1966) relative to the ennea-aqua ion, and for erbium(III) compounds 0.004 for $\text{Er}_x\text{La}_{1-x}\text{Cl}_3$, but the higher value 0.013 for $\text{Er}_x\text{Y}_{1-x}\text{Cl}_3$ (Rakestraw and Dieke, 1965), 0.007 for $\text{Er}_x\text{La}_{1-x}\text{Br}_3$ (Kiess and Dieke, 1966) and 0.015 for $\text{Er}_x\text{Y}_{2-x}\text{O}_3$ (Kisliuk et al., 1964) which is almost as high as 0.016 for undiluted Er_2O_3 (Gruber et al., 1966). Comparable values are obtained by the more accessible, but less accurate technique (Jørgensen et al., 1965a; Jørgensen and Rittershaus, 1967) of finding the best straight line

$$\nu - \nu_{\text{aqua}} = d\nu - (d\beta)\nu_{\text{aqua}} \quad (23.27)$$

with the slope $d\beta$ by comparing the baricenter of band intensity of each J level of the compound considered (ν) and in the aqua ion (ν_{aqua}). The parameter $d\nu$ contains several contributions. Most mixed oxides have rather large $d\beta$, slightly below the undiluted sesquioxides. The only two categories of compounds having even larger $d\beta$ are sulfides (Jørgensen, Pappalardo and Flahaut, 1965b) and cyclopentadienides. Such cases are $d\beta = 0.042$ in BaNd_2S_4 , 0.038 in $\text{Nd}(\text{C}_5\text{H}_5)_3$, 0.036 in $\text{CdGa}_{2-x}\text{Er}_x\text{S}_4$ and 0.028 in $\text{Er}(\text{C}_5\text{H}_5)_3$ though it must be noted that the corresponding $d\nu$ are rather large, 300 to 400 cm^{-1} . The interpolation of the term distance ${}^6\text{S}-{}^4\text{G}$ of manganese(II) compounds (according to their nephelauxetic effect) between the isoelectronic gaseous ions Cr^+ and Mn^{+2} can be repeated by comparison of neodymium(III) compounds with the gaseous Pr^{+2} (Sugar, 1963; Trees, 1964) rather systematically having all J -level energy differences 23% smaller than $\text{Nd}(\text{III})$ aqua ions.

A characteristic feature of lanthanide(III) compounds is that only the term distances dependent on phenomenological parameters of interelectronic repulsion are significantly diminished by the nephelauxetic effect, whereas the spin-orbit Landé parameter ζ_{4f} hardly changes at all. In a delocalized L.C.A.O. description where the electronic density of the partly filled shell on the central atom is depleted by being multiplied by the factor $(1 - a^2)$, ζ_{4f} is expected to be multiplied by the same factor, whereas the nephelauxetic ratio β should be approximately $(1 - a^2)^2 \sim 1 - 2a^2$ with the result that $d\beta$ is roughly $2a^2$. An

expansion of the partly filled 4f shell by a modified central field $U(r)$ (or for that matter an increased Watson effect in the compounds) may change β by more than twice the change of ζ_{4f} . It is important to note for the chemist that all these effects pull in the same direction, and since their sum is moderate, the results put an upper limit to each of the conceivable contributions. Caro and Derouet (1972) compared a large number of neodymium(III) compounds, and recently Caro et al. (1976) have performed a careful analysis of all the phenomenological parameters one may introduce in the description of $[\text{Xe}]4f^3$.

Recently, Kaufman and Sugar (1976) found that ${}^2F_{5/2}$ of Yb^{+3} is situated $10\,214\text{ cm}^{-1}$ above the ground state ${}^2F_{7/2}$. This new result agrees with an extrapolation from gaseous Yb^{+2} where Bryant (1965) derived values of ζ_{4f} between $2\,910$ and $2\,950\text{ cm}^{-1}$ from different configurations such as $4f^{13}6s$, $4f^{13}5d$, $4f^{13}6p$ and $4f^{13}7s$, and Meggers (1947) found a distance $10\,149\text{ cm}^{-1}$ between the two J -levels of the excited configuration $4f^{13}6s^2$ of Yb^+ . This invariance of $\frac{7}{2}\zeta_{4f}$ very close to $10\,200\text{ cm}^{-1}$ of $4f^{13}$ systems with highly differing ionic charge is comparable to the situation described by Dunn (1961) of $3d^q(\text{M}^{+2})$, $3d^q4s(\text{M}^+)$ and $3d^q4s^2$ (neutral atoms) having almost the same ζ_{3d} when the additional 4s electrons do not modify the conditional oxidation state $\text{M}[\text{II}]$. In the cases where the distance between the baricenter of the four lower Kramers doublets (${}^2F_{7/2}$) and the three higher Kramers doublets can be found with a high experimental accuracy in ytterbium(III) compounds, it is also between $10\,100$ and $10\,200\text{ cm}^{-1}$. A comparable invariance is exemplified by the levels 7F_0 , 7F_1 , 7F_2 , 7F_3 , ... of a series of crystals containing samarium(II) compared with $[\text{Xe}]4f^6$ of Sm^{+2} and $[\text{Xe}]4f^6s^2$ of the neutral atom (Dupont, 1967). Solids containing thulium(II) are also comparable to Tm^{+2} with the distance $8\,774\text{ cm}^{-1}$ (Sugar, 1970) 14% smaller than in the isoelectronic Yb^{+3} .

In the 3d, 4d and 5d group compounds, the dispersion of nephelauxetic effect from fluorides to sulfur-containing complexes is about three times as large for a given central ion as $(1 - \beta)$ for the fluoride. It might be argued that the dispersion of nephelauxetic effect as indicated by $d\beta$ from eq.(23.27) in lanthanides is smaller than $(1 - \beta)$ of the aqua ion or the fluoride. Until now, a reliable estimate for term distances in R^{+3} is only available for Pr^{+3} where we may evaluate the energy difference 3P_0 above 3F_3 in cm^{-1} :

$$\begin{array}{ll}
 14\,975\ \text{Pr}^{+3} & 14\,145\ \text{Pr}_x\text{La}_{1-x}\text{Cl}_3 \\
 14\,375\ \text{Pr}_x\text{La}_{1-x}\text{F}_3 & 14\,084\ \text{Pr}_x\text{La}_{1-x}\text{Br}_3 \\
 14\,330\ \text{Pr}(\text{H}_2\text{O})_9^{+3} & \approx 13\,800\ \text{BaPr}_2\text{S}_4
 \end{array} \tag{23.28}$$

showing β values 0.96 for the fluoride and 0.94 for the bromide which have indeed a smaller dispersion than $\beta = 0.94$ for MnF_2 , $\beta = 0.93$ for $\text{Mn}(\text{H}_2\text{O})_6^{+2}$ and 0.87 for MnBr_2 (Jørgensen, 1969a). However, it would be surprising if β is below 0.97 for $\text{Nd}(\text{III})$ and 0.985 for $\text{Er}(\text{III})$ aqua ions, though direct information about gaseous Nd^{+3} and Er^{+3} or Tm^{+3} would be very helpful. We discussed above the related arguments about the moderate nephelauxetic effect in $\text{R}[\text{IV}]$ obtained from photo-electron spectra of $\text{R}(\text{III})$ compounds or $\text{R}[\text{III}]$ in metallic samples. It

may be interesting to compare with $3d^3$ chromium(III) where $\beta = 0.89$ for CrF_6^{-3} , 0.79 for $\text{Cr}(\text{H}_2\text{O})_6^{+3}$, 0.71 for $\text{Cr}(\text{NH}_3)_6^{+3}$, 0.62 for $\text{Cr}(\text{NCS})_6^{-3}$, 0.52 for undiluted Cr_2O_3 (to be compared with 0.71 in ruby) and 0.47 for the dithiocarbamate $\text{Cr}(\text{S}_2\text{CN}(\text{C}_2\text{H}_5)_2)_3$. Seen from this point of view, there is no doubt that the 4f shell is protected to a great extent against the influence of reducing ligands. Another characteristic difference in the d groups is the compensation of increasing oxidation state by more pronounced covalent bonding; iron(III) has similar or smaller term distances than the isoelectronic manganese(II) with the same ligands (Jørgensen, 1969a).

2.8. Collective effects in transparent materials

The small average radius of the partly filled 4f shell compared with the internuclear distances strongly attenuates the collective effects well-known from d group compounds, and for instance, one has to cool to very low temperatures before antiferromagnetic behavior can be observed in lanthanide compounds, with a few remarkable exceptions such as EuTe and metallic ferromagnetic gadolinium. It is very difficult to observe *simultaneous excitation* of two atoms (each containing a partly filled shell) by the same photon, as is known from the classical case (Linz and Newnham, 1961) where narrow absorption bands in the near ultra-violet of ruby $\text{Cr}_x\text{Al}_{2-x}\text{O}_3$ are due to the spin-forbidden transition ($S = \frac{3}{2} \rightarrow \frac{1}{2}$) in the red occurring simultaneously in both chromium(III) in a CrOCr grouping. In materials such as the perovskite KMgF_3 it is possible to observe simultaneous transitions in pairs of manganese(II) (Güdel, 1975) or in Mn(II) and Ni(II) at the same time (Ferguson et al., 1975). Such transitions in pairs of praseodymium(III) were found by Varsanyi and Dieke (1961) in $\text{Pr}_x\text{La}_{1-x}\text{Cl}_3$ and Dieke and Dorman (1963) reported 90 weak lines of this origin between 22 220 and 28 100 cm^{-1} of undiluted PrCl_3 . The most striking example are the absorption lines between 20 490 and 21 858 cm^{-1} of undiluted Yb_2O_3 (Schugar et al., 1975) having an intensity of about 10^{-3} of the near infra-red bands. They were not detected (and are at least ten times weaker) in YbF_3 , $\text{Yb}(\text{OH})_3$ and in LaYbO_3 .

The *antiferromagnetic coupling* that lower values of combined S of paramagnetic systems have slightly lower energy than higher S (in the simplest Heisenberg case, a contribution proportional to $S(S+1)$ occurs in the energy) has the same origin as the slightly lower energy of the singlet (compared with the triplet) of two hydrogen atoms at a large distance (Jørgensen, 1971a; Glerup, 1972; Ammeter, 1975) and the Heisenberg parameter \mathfrak{J} is intimately connected with the square of the exchange integral (representing the non-diagonal element of interelectronic repulsion) divided by electron transfer energies (representing the formation of $\text{H}(-\text{I})$ and $\text{H}(\text{I})$ in H_2 or of $\text{Cr}(\text{II})$ and $\text{Cr}(\text{IV})$ in $(\text{NH}_3)_5\text{CrO}(\text{Cr}(\text{NH}_3)_5)^{+4}$). Examples of antiferromagnetic effects between R(III) and Cr(III) on 4f group absorption bands are the (not perfectly cubic) perovskites NdCrO_3 (Hornreich et al., 1975) and ErCrO_3 (Hasson et al., 1975).

The practically most important cases of *energy transfer* yielding narrow-line luminescence of trivalent lanthanides are from organic ligands having strong

absorption bands (Halverson et al., 1964; Sinha, 1967) and several biologically important systems (Nieboer, 1975) have been studied along the lines of the rather surprising observation (Charles and Riedel, 1966) that terbium(III) shows strong emission lines from 5D_4 in aqueous solution if *both* a sulfosalicylate and an ethylenediaminetetra-acetate ligand are bound. Several polycarboxylate ligands (Luk and Richardson, 1975) were recently shown to promote energy transfer from Tb(III) to 5D_0 of Eu(III) because the same ligand binds two lanthanides. This may be a rather frequent case as Berzelius has already noted that strong R(III) solutions can be obtained in ammonium tartrate containing a small excess of aqueous ammonia. If desiccated, such solutions provide reversibly a candy-like transparent glass, giving the impression of a disordered cross-linked polymer, and the nephelauxetic effect of the Nd(III) solution is considerable (Jørgensen, 1956a). Energy transfer between two lanthanides in inorganic glasses has been reviewed by Reisfeld (1973, 1975). The mechanism is "physical" in the sense of not involving the negligible overlap between the 4f shells of distant atoms, but though the dipole-dipole or dipole-quadrupole theory of Dexter gives the correct dependence on the mutual distance (assuming a statistical distribution, which can only be valid beyond a certain lower limit of distance) the numerical parameters predicted are several orders of magnitude too low. This phenomenological proliferation is quite frequent in many theoretical descriptions of lanthanides. For instance, the first treatment of *intensities* of internal transitions in the partly filled 4f shell by Broer et al. (1945) developed into the Judd-Ofelt parametrization discussed by several authors in this Handbook. Jørgensen and Judd (1964) pointed out that many "conjugated" types of ligands (β -diketonates, carboxylates, nitrate and, curiously enough, gaseous RI_3) develop strong pseudoquadrupolar *hypersensitive transitions* having selection rules like electric quadrupole transitions (in Russell-Saunders coupling, S of the ground state is conserved, whereas the typical cases decrease both L and J by two units) but with unaccessibly large numerical values of the oscillator strength. This intricate subject has recently been reviewed (Peacock, 1975) and the author persists in believing that the inhomogeneous local dielectric constant is the main origin. An opposite case is $R_xLa_{1-x}F_3$ showing particularly strong pseudo-64-polar transitions, a quite fascinating situation in view of the vanishing (within experimental uncertainty) pseudoquadrupolar intensities also known (Carnall et al., 1968) for the aqua ions.

Though the most conspicuous impact on daily life of lanthanide luminescence at this time is the red color television using the *cathodoluminescence* (a phenomenon discovered by Crookes) of europium(III) studied by Urbain (1909) and used, first in the orthovanadate $Eu_xY_{1-x}VO_4$ (Brecher et al., 1967) and later in the oxysulfide $Eu_xY_{2-x}O_2S$ (Sovers and Yoshioka, 1969) giving a more saturated red color because of slightly more pronounced nephelauxetic effect, and much stronger pseudoquadrupolar $^5D_0 \rightarrow ^7F_2$ emission at lower wavenumbers, it seems likely that the line emission of *lasers* may have more important consequences for the future of humanity (Reisfeld and Jørgensen, 1977). Since the major competitive process (diminishing or preventing lumines-

cence) is multi-phonon de-excitation (Reisfeld, 1973, 1975; Reisfeld et al., 1976a) it is obvious that materials with heavy atoms and low force constants (the two conditions for a lower value of the highest phonon normal frequencies) have great propensity for fluorescing, as known from crystalline $R_xLa_{1-x}Br_3$. However, glasses containing germanate, tellurite or tungstate anions are also quite effective, and a thorough study has been performed of the many decay rates of several excited states of thulium(III) and erbium(III) (Reisfeld and Eckstein, 1975) and of holmium(III) (Reisfeld et al., 1976b) in tellurite glasses. The general subject of luminescence of crystalline and vitreous solids was recently reviewed by Thomson (1976).

In actual practice, the most important energy transfer is from other (strongly absorbing or long-lived) species to the lanthanides, allowing steady-state pumping of energy to maintain a high yield of line luminescence (Reisfeld, 1975, 1976; Reisfeld and Jørgensen, 1977). Among such excited states of other species are the [Xe]5d configuration of cerium(III), [Xe]4f⁷5d of terbium(III), [Xe]4f¹⁴5d¹⁰6s6p (though the description with quantum numbers of spherical symmetry may be less appropriate) of thallium(I), lead(II) and bismuth(III) isoelectronic with the mercury atom, and the electron transfer state (promoting one π_n electron from the oxygen 2p orbitals to the empty uranium 5f shell) of the uranyl ion (Jørgensen and Reisfeld, 1975). Blasse (1976) has recently discussed the importance of electron transfer states for "non-vertical" energy transfer.

As first pointed out by Maria Goeppert Mayer (1941) the distinctive feature of the 4f group is the low average radius $\langle r \rangle$ combined with a large amount of angular kinetic energy $\frac{1}{2}l(l+1)\langle r^{-2} \rangle$ atomic units corresponding to 540 eV for Gd^{+3} using Dr. Watson's Hartree-Fock radial function. Though the reluctance of the 4f group to change oxidation state is related to the difference between the ionization energy and the electron affinity (presumably proportional to $\langle r^{-1} \rangle$ as are other parameters of interelectronic repulsion) the isolated character with $\langle r \rangle$ about 40% of the Goldschmidt ionic radius is even more striking, corresponding to the weak nephelauxetic effect and much weaker variation of the spin-orbit coupling going from gaseous monatomic entities to compounds or to metallic elements. At sufficiently small internuclear distances, there may remain an itinerant tendency of the 4f electron in cerium(III) but the photo-electron spectra and the surprisingly weak collective effects in non-metallic solids indicate clearly the invariant characteristic of a given configuration 4fⁿ imitating atomic spectra to a remarkable degree. Another important difference between the 4f and the 5f group is that the parameter $(E - A)$ of eq.(23.21) is much larger in the latter case (Jørgensen, 1968a, 1969b, 1973a) like in the 4d group compared with the 3d group, corresponding to higher and more varying oxidation states in the beginning of the 4d and the 5f groups, whereas they are exceptionally low at the end, such as silver(I), mendelevium(II) and nobelium(II). The 4f group is the only one known where the half-filled shell europium(II) is more difficult to oxidize (because of the large spin-pairing energy parameter D) than the filled shell ytterbium(II), a final exception to conceived ideas in general chemistry. A fascinating group, indeed.

References

- Adamson, A.W., 1973, *A Textbook of Physical Chemistry* (Academic Press, New York).
- Ahrland, S., J. Chatt and N.R. Davies, 1958, *Quart. Rev. (London)* **12**, 265.
- Ahrland, S., 1968a, *Structure and Bonding* **5**, 118.
- Ahrland, S., 1968b, *Chem. Phys. Lett.* **2**, 303.
- Ahrland, S., 1973, *Structure and Bonding* **15**, 167.
- Allen, G.C., M.B. Wood and J.M. Dyke, 1973, *J. Inorg. Nucl. Chem.* **35**, 2311.
- Ammeter, J.H., 1975, *Chimia* **29**, 504.
- Baer, Y. and G. Busch, 1974, *J. Electron Spectr.* **5**, 611.
- Banks, C.V., M.R. Heusinkveld and J.W. O'Laughlin, 1961, *Anal. Chem.* **33**, 1235.
- Barnes, J.C. and P. Day, 1964, *J. Chem. Soc.*, 3886.
- Barnes, J.C. and H. Pincott, 1966, *J. Chem. Soc. A*, 842.
- Bergerhoff, G., 1964, *Angew. Chem.* **76**, 697.
- Berthou, H. and C.K. Jørgensen, 1975, *Anal. Chem.* **47**, 482.
- Bjerrum, J., 1941 (reprint 1957), *Metal Ammine Formation in Aqueous Solution* (Haase and Son, Copenhagen).
- Bjerrum, J., 1950, *Chem. Rev.* **46**, 381.
- Bjerrum, J., 1951, *Naturwiss.* **38**, 461.
- Bjerrum, J. and C.K. Jørgensen, 1953, *Acta Chem. Scand.* **7**, 951.
- Bjerrum, N., 1909, *Z. Anorg. Chem.* **63**, 140.
- Blasse, G. and A. Brill, 1966, *J. Chem. Phys.* **45**, 2350 and 3327.
- Blasse, G., 1976, *Structure and Bonding* **26**, 43.
- Bonnelle, C., and F. Vergand, 1975, *J. Phys. Chem. Solids* **36**, 575.
- Bonnelle, C., 1976, *Structure and Bonding* **31**, 23.
- Boulanger, F., 1952, *Ann. Chim. (Paris)* **7**, 732.
- Bradley, D.C., J.S. Ghotra and F.A. Hart, 1973, *J.C.S. Dalton*, 1021.
- Braterman, P.S., 1966, *J. Chem. Soc. A*, 1471.
- Brecher, C., H. Samelson, A. Lempicki, R. Riley and T. Peters, 1967, *Phys. Rev.* **155**, 178.
- Brewer, L., 1971, *J. Opt. Soc. Amer.* **61**, 1101 and 1666.
- Broer, L.J.F., C.J. Gorter and J. Hoogschagen, 1945, *Physica* **11**, 231.
- Brous, J., I. Fankuchen and E. Banks, 1953, *Acta Crystallogr.* **6**, 67.
- Bryant, B.W. 1965, *J. Opt. Soc. Amer.* **55**, 771.
- Burns, G., 1967, *Phys. Letters* **25A**, 15.
- Burrows, H.D. and T.J. Kemp, 1974, *Chem. Soc. Rev. (London)* **3**, 139.
- Burrows, H.D., S.J. Formosinho, M. da Graça Miguel and F. Pinto Coelho, 1976, *J.C.S. Faraday Trans. I* **72**, 163.
- Campagna, M., E. Bucher, G.K. Wertheim, D.N.E. Buchanan and L.D. Longinotti, 1974a, *Phys. Rev. Letters* **32**, 885.
- Campagna, M., E. Bucher, G.K. Wertheim, D.N.E. Buchanan and L.D. Longinotti, 1974b, *Proceed. 11th Rare Earth Conference*, Traverse City, Michigan.
- Campagna, M., E. Bucher, G.K. Wertheim and L.D. Longinotti, 1974c, *Phys. Rev. Lett.* **33**, 165.
- Campagna, M., G.K. Wertheim and E. Bucher, 1976, *Structure and Bonding* **30**, 99.
- Carlson, E. and G.H. Dieke, 1961, *J. Chem. Phys.* **34**, 1602.
- Carnall, W.T., P.R. Fields and K. Rajnak, 1968, *J. Chem. Phys.* **49**, 4412, 4424, 4443, 4447 and 4450.
- Caro, P., 1968, *J. Less-Common Metals* **16**, 367.
- Caro, P., 1972, *Proceed. 5. Materials Research Symposium*, Nat. Bur. Standards Special Publication no. 364, p. 367.
- Caro, P. and J. Derouet, 1972, *Bull. Soc. Chim. Fr.* **46**.
- Caro, P., O. Beaury and E. Antic, 1976, *J. de Phys.* **37**, 671.
- Chang, N.C., 1966, *J. Chem. Phys.* **44**, 4044.
- Charles, R.G. and E.P. Riedel, 1966, *J. Inorg. Nucl. Chem.* **28**, 527.
- Condon, E.U. and G.H. Shortley, 1953, *Theory of Atomic Spectra* (Cambridge University Press, Cambridge).
- Connick, R.E., 1949, *J. Chem. Soc. Suppl.* 235.
- Cox, P.A., Y. Baer and C.K. Jørgensen, 1973, *Chem. Phys. Lett.* **22**, 433.
- Cox, P.A., 1975, *Structure and Bonding* **24**, 59.
- Day, P., 1963, *Inorg. Chem.* **2**, 452.
- Dieke, G.H. and E. Dorman, 1963, *Phys. Rev. Lett.* **11**, 17.
- Drotning, W.D. and H.G. Drickamer, 1973, *J. Chem. Phys.* **59**, 3482.
- Dunn, T.M., 1961, *Trans. Faraday Soc.* **57**, 1441.
- Dupont, A., 1967, *J. Opt. Soc. Amer.* **57**, 867.
- Eastman, D.E. and M. Kuznietz, 1971, *J. Appl. Phys.* **42**, 1396.
- Edelstein, A.S., H.R. Child and C. Tranchita, 1976, *Phys. Rev. Lett.* **36**, 1332.
- Ellis, J.E. and R.A. Faltynek, 1975, *J.C.S. Chem. Comm.*, 966.
- Emschwiller, G. and C.K. Jørgensen, 1970, *Chem. Phys. Lett.* **5**, 561.
- Ephraim, F. and R. Bloch, 1926, *Ber. Deutsch. Chem. Ges.* **59**, 2692.
- Ephraim, F. and R. Bloch, 1928, *Ber. Deutsch. Chem. Ges.* **61**, 65 and 72.
- Ephraim, F. and P. Rây, 1929, *Ber. Deutsch. Chem. Ges.* **62**, 1509, 1520 and 1639.
- Faktor, M.M. and R. Hanks, 1969, *J. Inorg. Nucl. Chem.* **31**, 1649.
- Faucher, M. and P. Caro, 1975, *J. Chem. Phys.* **63**, 446.
- Ferguson, J., H.U. Güdel and E.R. Krausz, 1975, *Mol. Phys.* **30**, 1139.
- Fidelis, I. and S. Siekierski, 1966, *J. Inorg. Nucl. Chem.* **28**, 185.
- Freed, S., 1931, *Phys. Rev.* **38**, 2122.
- Freeman, A.J. and R.E. Watson, 1962, *Phys. Rev.* **127**, 2058.
- Gans, P., J.B. Gill and M. Griffin, 1976, *J.C.S. Chem. Comm.*, 169.
- Garbowski, E., 1976, *Thesis at University of Lyon, France*.

- Geier, G. and C.K. Jørgensen, 1971, *Chem. Phys. Lett.* **9**, 263.
- Giguère, P.A., 1976, *Chem. Phys. Lett.* **41**, 598.
- Gillespie, R.J., 1972, *Molecular Geometry* (Van Nostrand, London).
- Glauser, R., U. Hauser, F. Herren, A. Ludi, P. Roder, E. Schmidt, H. Siegenthaler and F. Wenk, 1973, *J. Amer. Chem. Soc.* **95**, 8457.
- Glerup, J., 1972, *Acta Chem. Scand.* **26**, 3775.
- Griffith, J.S., 1961, *The Theory of Transition-metal Ions*. (Cambridge University Press, Cambridge).
- Gruber, J.B., J.R. Henderson, M. Muramoto, K. Rajnak and J.G. Conway, 1966, *J. Chem. Phys.* **45**, 477.
- Gschneidner, K.A., R.O. Elliott and R.R. McDonald, 1962, *J. Phys. Chem. Solids* **23**, 555, 1191 and 1201.
- Güdel, H.U., 1975, *Chem. Phys. Letters* **36**, 328.
- Hagström, S., C. Nordling and K. Siegbahn, 1964, *Z. Physik* **178**, 439.
- Halverson, F., J.S. Brinen and J.R. Leto, 1964, *J. Chem. Phys.* **41**, 157 and 2752.
- Hasson, A., R.M. Hornreich, Y. Komet, B.M. Wanklyn and I. Yaeger, 1975, *Phys. Rev.* **B12**, 5051.
- Hedén, P.O., H. Löfgren and S.B.M. Hagström, 1971, *Phys. Rev. Letters* **26**, 432.
- Heidt, L.J. and J. Berestecki, 1955, *J. Amer. Chem. Soc.* **77**, 2049.
- Helmholz, L., 1939, *J. Amer. Chem. Soc.* **61**, 1544.
- Hendrickson, A.R., R.L. Martin and N.M. Rohde, 1975, *Inorg. Chem.* **14**, 2980.
- Herbison-Evans, D., P.B.P. Phipps and R.J.P. Williams, 1965, *J. Chem. Soc.*, 6170.
- Hoefdraad, H.E., 1975, *J. Inorg. Nucl. Chem.* **37**, 1917.
- Hofmann, K.A. and H. Kirmreuther, 1910, *Z. Phys. Chem.* **71**, 312.
- Hofmann, K.A. and K. Höschele, 1915, *Ber. Deutsch. Chem. Ges.* **48**, 20.
- Hornreich, R.M., Y. Komet, R. Nolan, B.M. Wanklyn and I. Yaeger, 1975, *Phys. Rev.* **B12**, 5094.
- Hulliger, F., 1968, *Helv. Phys. Acta* **41**, 945.
- Hund, F., 1927, *Linienpektren und Periodisches System der Elemente* (Springer, Berlin).
- Jayaraman, A., 1965, *Phys. Rev.* **A137**, 179.
- Jayaraman, A., A.K. Singh, A. Chatterjee and S.U. Devi, 1974, *Phys. Rev.* **B9**, 2513.
- Jayaraman, A., W. Lowe, L.D. Longinotti and E. Bucher, 1976, *Phys. Rev. Letters* **36**, 366.
- Johansson, B., 1974, *Phil. Mag.* **30**, 469.
- Johansson, B., 1975, *Phys. Rev.* **B11**, 2740.
- Johansson, B. and A. Rosengren, 1975, *Phys. Rev.* **B11**, 1367 and 2836.
- Johansson, S. and U. Litzén, 1973, *Physica Scripta* (Stockholm) **8**, 43.
- Johnson, D.A. 1969, *J. Chem. Soc. A.*, 1525.
- Johnson, D.A., 1974, *J.C.S. Dalton*, 1671.
- Johnson, K.H., 1973, *Advan. Quantum Chem.* **7**, 143.
- Jones, H.C., J.A. Anderson and W.W. Strong, 1909 to 1911, *Carnegie Institute Publications* (Washington D.C.) no. 110, 130 and 160.
- Judd, B.R., 1957, *Proc. Roy. Soc.* **A241**, 122.
- Judd, B.R., 1970, *J. Franklin Institute* **289**.
- Jørgensen, C.K., 1955a, *J. Inorg. Nucl. Chem.* **1**, 301.
- Jørgensen, C.K., 1955b, *Mat. fys. Medd. Dan. Vid. Selskab* **29**, no 11.
- Jørgensen, C.K., 1956a, *Mat. fys. Medd. Dan. Vid. Selskab* **30**, no. 22.
- Jørgensen, C.K., 1956b, *Acta Chem. Scand.* **10**, 1505.
- Jørgensen, C.K., 1957a, *Acta Chem. Scand.* **11**, 166.
- Jørgensen, C.K., 1957b, *Energy Levels of Complexes and Gaseous Ions* (Gjellerup, Copenhagen).
- Jørgensen, C.K., 1962a, *Solid State Phys.* **13**, 375.
- Jørgensen, C.K., 1962b, *Absorption Spectra and Chemical Bonding in Complexes* (Pergamon Press, Oxford).
- Jørgensen, C.K., 1962c, *Mol. Phys.* **5**, 271.
- Jørgensen, C.K., 1962d, *Orbitals in Atoms and Molecules* (Academic Press, London).
- Jørgensen, C.K., 1963a, *Advan. Chem. Phys.* **5**, 33.
- Jørgensen, C.K., 1963b, *Acta Chem. Scand.* **17**, 1034 and 1043.
- Jørgensen, C.K., 1963c, *Inorganic Complexes* (Academic Press, London).
- Jørgensen, C.K., and J.S. Brinen, 1963, *Mol. Phys.* **6**, 629.
- Jørgensen, C.K., R. Pappalardo and H.H. Schmidtke, 1963, *J. Chem. Phys.* **39**, 1422.
- Jørgensen, C.K., 1964, *Mol. Phys.* **7**, 417.
- Jørgensen, C.K., and B.R. Judd, 1964, *Mol. Phys.* **8**, 281.
- Jørgensen, C.K., R. Pappalardo and E. Ritterhaus, 1965a, *Z. Naturforsch.* **A20**, 54.
- Jørgensen, C.K., R. Pappalardo and J. Flahaut, 1965b, *J. Chim. Phys.* (Paris) **62**, 444.
- Jørgensen, C.K., and E. Ritterhaus, 1967, *Mat. fys. Medd. Dan. Vid. Selskab* **35**, no. 15.
- Jørgensen, C.K., S. M. Horner, W.E. Hatfield and S.Y. Tyree, 1967, *Int. J. Quantum Chem.* **1**, 191.
- Jørgensen, C.K., 1968a, *Chem. Phys. Letters* **2**, 549.
- Jørgensen, C.K., 1968b, *Inorg. Chim. Acta Rev.* **2**, 65.
- Jørgensen, C.K., 1969a, *Oxidation Numbers and Oxidation States* (Springer, Berlin).
- Jørgensen, C.K., 1969b, *Chimia* **23**, 292.
- Jørgensen, C.K., 1970a, *J. Inorg. Nucl. Chem.* **32**, 3127.
- Jørgensen, C.K., 1970b, *Progress Inorg. Chem.* **12**, 101.
- Jørgensen, C.K., 1971a, *Modern Aspects of Ligand Field Theory* (North-Holland Publishing Co., Amsterdam).
- Jørgensen, C.K., 1971b, *Chimia* **25**, 109.
- Jørgensen, C.K., W. Preetz and H. Homborg, 1971, *Inorg. Chim. Acta* **5**, 223.
- Jørgensen, C.K., and H. Berthou, 1972, *Mat. fys. Medd. Dan. Vid. Selskab* **38**, no. 15.
- Jørgensen, C.K., 1973a, *Angew. Chem.* **85**, 1 (Int. Ed. **12**, 12).

- Jørgensen, C.K., 1973b, *Structure and Bonding* **13**, 199.
- Jørgensen, C.K., 1973c, *Chimia* **27**, 203.
- Jørgensen, C.K., 1974a, *Chimia* **28**, 6.
- Jørgensen, C.K., 1974b, *Advan. Quantum Chem.* **8**, 137.
- Jørgensen, C.K., 1975a, *Chimia* **29**, 53.
- Jørgensen, C.K., 1975b, *Topics in Current Chemistry* **56**, 1.
- Jørgensen, C.K., 1975c, *Structure and Bonding* **22**, 49.
- Jørgensen, C.K., 1975d, *Chem. Phys. Letters* **34**, 14.
- Jørgensen, C.K., 1975e, *Structure and Bonding* **24**, 1.
- Jørgensen, C.K., and H. Berthou, 1975, *Chem. Phys. Letters* **31**, 416.
- Jørgensen, C.K., and R. Reisfeld, 1975, *Chem. Phys. Letters* **35**, 441.
- Jørgensen, C.K., 1976a, *Structure and Bonding* **25**, 1.
- Jørgensen, C.K., 1976b, *Gmelin's Handbuch der anorganischen Chemie, Seltene Erden* (39B1) **17**.
- Jørgensen, C.K., 1977, *Fresenius' Z. Anal. Chem.* **288**, 161.
- Karayianis, N., 1965, *J. Math. Phys.* **6**, 1204.
- Kaufman, V. and J. Sugar, 1976, *J. Opt. Soc. Amer.* **66**, 439.
- Keller, C. and C.K. Jørgensen, 1975, *Chem. Phys. Letters* **32**, 397.
- Kiess, N.H. and G.H. Dieke, 1966, *J. Chem. Phys.* **45**, 2729.
- Kisluk, P., W.F. Krupke and J.B. Gruber 1964, *J. Chem. Phys.* **40**, 3606.
- Klopman, G., 1968, *J. Amer. Chem. Soc.* **90**, 223.
- Krumholz, P., 1958, *Spectrochim. Acta* **10**, 274.
- Kuse, D. and C.K. Jørgensen, 1967, *Chem. Phys. Letters* **1**, 314.
- Landé, A., 1924, *Z. Physik* **25**, 46.
- Latimer, W.M., 1955, *J. Chem. Phys.* **23**, 90.
- Leary, K. and N. Bartlett, 1972, *J.C.S. Chem. Comm.*, 903.
- Linares, C., A. Louat and M. Blanchard, 1977, *Structure and Bonding* **33**, 179.
- Linz, A. and R.E. Newnham, 1961, *Phys. Rev.* **123**, 500.
- Loh, E., 1966, *Phys. Rev.* **147**, 332.
- Lokken, D.A. and J.D. Corbett, 1970, *J. Amer. Chem. Soc.* **92**, 1799.
- Ludi, A. and H.U. Güdel, 1973, *Structure and Bonding* **14**, 1.
- Luk, C.K. and S.F. Richardson, 1975, *J. Amer. Chem. Soc.* **97**, 6666.
- Magnéli, A. and L. Kihlberg, 1951, *Acta Chem. Scand.* **5**, 578.
- Malkova, T.V., G.A. Shutova and K.B. Yatsimirskii, 1964, *Russ. J. Inorg. Chem.* **9**, 993.
- Martin, W.C., 1971, *J. opt. Soc. Amer.* **61**, 1682.
- Mayer, M.G., 1941, *Phys. Rev.* **60**, 184.
- McClure, D.S. and Z. Kiss, 1963, *J. Chem. Phys.* **39**, 3251.
- Meggers, W.F., 1947, *J. Opt. Soc. Amer.* **37**, 988.
- Mioduski, T. and S. Siekierski, 1975, *J. Inorg. Nucl. Chem.* **37**, 1647.
- Moeller, T., D.F. Martin, L.C. Thompson, R. Ferrus, G.R. Feistel, W.J. Randall, 1965, *Chem. Rev.* **65**, 1.
- Moore, C.E. (1949, 1952 and 1958) *Atomic Energy Levels. Nat. Bur. Stand. Circular no. 467, vol. I, II and III* (Washington, D.C.).
- Moore, C.E. (1970). *Ionization Potentials and Ionization Limits Derived from the Analyses of Optical Spectra. NSRDS-NBS 34* (National Bureau of Standards, Washington, D.C.).
- Morris, D.F.C., 1969, *Structure and Bonding* **6**, 157.
- Mott, N.F., 1974, *Metal-Insulator Transitions* (Taylor and Francis, London).
- Möbius, H.H., 1962, *Z. Chem.* **2**, 100.
- Möbius, H.H., 1964, *Z. Chem.* **4**, 81.
- Murray-Rust, P., H.B. Bürgi and J.D. Dunitz, 1975, *J. Amer. Chem. Soc.* **97**, 921.
- Nieboer, E., 1975, *Structure and Bonding* **22**, 1.
- Nugent, L.J., 1970, *J. Inorg. Nucl. Chem.* **32**, 3485.
- Nugent, L.J. and K.L. Vander Sluis, 1971, *J. Opt. Soc. Amer.* **61**, 1112.
- Nugent, L.J., R.D. Baybarz, J.L. Burnett and J.L. Ryan, 1973, *J. Phys. Chem.* **77**, 1528.
- Orgel, L.E., 1955, *J. Chem. Phys.* **23**, 1004, 1819, 1824 and 1958.
- Orgel, L.E., 1957, *Nature* **179**, 1348.
- Pappalardo, R. and C.K. Jørgensen, 1967, *J. Chem. Phys.* **46**, 632.
- Peacock, R.D., 1975, *Structure and Bonding* **22**, 83.
- Pearson, R.G., 1963, *J. Amer. Chem. Soc.* **85**, 3533.
- Pearson, R.G., 1968, *J. Chem. Educ.* **45**, 581 and 643.
- Pearson, R.G. (ed.), 1973, *Hard and Soft Acids and Bases* (Dowden, Hutchinson and Ross in Stroudsburg, Penn.).
- Penneman, R.A., R.R. Ryan and A. Rosenzweig, 1973, *Structure and Bonding* **13**, 1.
- Piepho, S.B., W.H. Inskeep, P.N. Schatz, W. Preetz and H. Homborg, 1975, *Mol. Phys.* **30**, 1569.
- Pitton, O., C.K. Jørgensen and H. Berthou, 1976, *Chem. Phys. Letters* **40**, 357.
- Rabinowitch, E. and E. Thilo, 1930, *Periodisches System, Geschichte und Theorie* (Ferdinand Enke, Stuttgart).
- Rabinowitch, E. and R. Linn Belford, 1964, *Spectroscopy and Photochemistry of Uranyl Compounds* (Pergamon Press, Oxford).
- Racah, G., 1949, *Phys. Rev.* **76**, 1352.
- Rakestraw, J.W. and G.H. Dieke, 1965, *J. Chem. Phys.* **42**, 873.
- Reader, J. and G.L. Epstein, 1975, *J. Opt. Soc. Amer.* **65**, 638.
- Reisfeld, R., 1973, *Structure and Bonding* **13**, 53.
- Reisfeld, R., 1975, *Structure and Bonding* **22**, 123.
- Reisfeld, R. and Y. Eckstein, 1975, *J. Chem. Phys.* **63**, 4001.
- Reisfeld, R., 1976, *Structure and Bonding* **30**, 65.

Lehn, J.M., 1973, Structure and Bonding 16, 1.

- Reisfeld, R., C.K. Jørgensen and H. Berthou, 1976a, *Chimia* **30**, 202.
- Reisfeld, R., J. Hormadaly and A. Muranevich, 1976b, *Chem. Phys. Letters* **38**, 188.
- Reisfeld, R. and C.K. Jørgensen, 1977, *Lasers and Excited States of Rare Earths* (Springer, Berlin).
- Richman, I. and E.Y. Wong, 1962, *J. Chem. Phys.* **37**, 2270.
- Robin, M.B. and P. Day, 1967, *Advan. Inorg. Chem. Radiochem.* **10**, 248.
- Romano, V. and J. Bjerrum, 1970, *Acta Chem. Scand.* **24**, 1551.
- Ropp, R.C., 1965, *J. Electrochem. Soc.* **112**, 181.
- Rosseinsky, D.R., 1965, *Chem. Rev.* **65**, 467.
- Ruedenberg, K., 1962, *Rev. Mod. Phys.* **34**, 326.
- Ryan, J.L. and C.K. Jørgensen, 1963, *Mol. Phys.* **7**, 17.
- Ryan, J.L. and C.K. Jørgensen, 1966, *J. Phys. Chem.* **70**, 2845.
- Ryan, J.L., 1969, *Inorg. Chem.* **8**, 2053.
- Salzmann, J.J. and C.K. Jørgensen, 1968, *Helv. Chim. Acta* **51**, 1276.
- Schneider, S.J. and R.S. Roth, 1960, *J. Res. Nat. Bur. Stand.* **A64**, 317.
- Schugar, H.J., E.I. Solomon, W.L. Cleveland and L. Goodman, 1975, *J. Amer. Chem. Soc.* **97**, 6442.
- Schumann, H., 1952, *Z. Anorg. Chem.* **271**, 29.
- Schwartz, R.W., 1975, *Mol. Phys.* **30**, 81.
- Schwarzenbach, G., 1956, *Experientia Suppl.* **5**, 162.
- Schwarzenbach, G., 1961, *Advan. Inorg. Radiochem.* **3**, 257.
- Schwarzenbach, G., 1970, *Pure Appl. Chem.* **24**, 307.
- Schwarzenbach, G., 1973, *Chimia* **27**, 1.
- Schäffer, C.E. and C.K. Jørgensen 1958, *J. Inorg. Nucl. Chem.* **8**, 143.
- Schäffer, C.E. and C.K. Jørgensen, 1965, *Mol. Phys.* **9**, 401.
- Schäffer, C.E., 1968, *Structure and Bonding* **5**, 68.
- Schäffer, C.E., 1973, *Structure and Bonding* **14**, 69.
- Serra, O.A. and L.C. Thompson, 1976, *Inorg. Chem.* **15**, 504.
- Sinha, S.P., 1966, *Complexes of the Rare Earths* (Pergamon Press, Oxford).
- Sinha, S.P., 1967, *Europium* (Springer, Berlin).
- Sinha, S.P., 1976, *Structure and Bonding* **25**, 69.
- Slater, J.C., 1964, *J. Chem. Phys.* **41**, 3199.
- Sovers, O.J. and T. Yoshioka, 1969, *J. Chem. Phys.* **51**, 5330.
- Speakman, J.C., 1972, *Structure and Bonding* **12**, 141.
- Staveley, L.A.K., D.R. Markham and M.R. Jones, 1968, *J. Inorg. Nucl. Chem.* **30**, 231.
- Stelling, O., 1928, *Z. Physik* **50**, 506.
- Stoner, E.C., 1924, *Phil. Mag.* **48**, 719.
- Sugar, J., 1963, *J. Opt. Soc. Amer.* **53**, 831.
- Sugar, J., 1965, *J. Opt. Soc. Amer.* **55**, 1058.
- Sugar, J., 1970, *J. Opt. Soc. Amer.* **60**, 454.
- Sugar, J. and J. Reader, 1973, *J. Chem. Phys.* **59**, 2083.
- Sugar, J., 1975, *J. Opt. Soc. Amer.* **65**, 1366.
- Suryanarayanan, R., G. Güntherodt, J.L. Freeouf and F. Holtzberg, 1975, *Phys. Rev.* **B12**, 4215.
- Tait, A.M., M.Z. Hoffman and E. Hayon, 1976, *Inorg. Chem.* **15**, 934.
- Tanabe, Y. and S. Sugano, 1954, *J. Phys. Soc. Japan* **9**, 753 and 766.
- Taube, H., 1952, *Chem. Rev.* **50**, 69.
- Thomson, A.J., 1976, in P. Day (ed.): *Electronic Structure and Magnetism of Inorganic Compounds* **4**, p. 149 (Chemical Society, London).
- Trees, R.E., 1964, *J. Opt. Soc. Amer.* **54**, 651.
- Truter, M.R., 1973, *Structure and Bonding* **16**, 71.
- Turner, D.W., C. Baker, A.D. Baker and C.R. Brundle, 1970, *Molecular Photo-electron Spectroscopy* (Interscience, London).
- Urbain, G., 1909, *Ann. Chim. Phys. (Paris)* **18**, 222 and 289.
- Vander Sluis, K.L. and L.J. Nugent, 1972, *Phys. Rev.* **A6**, 86.
- Varga, L.P. and L.B. Asprey, 1968, *J. Chem. Phys.* **48**, 139 and **49**, 4674.
- Varsanyi, F. and G.H. Dieke, 1961, *Phys. Rev. Letters* **7**, 442.
- Vergand, F. and C. Bonnelle, 1972, *Solid State Comm.* **10**, 397.
- Vishwamittar and S.P. Puri, 1973, *Chem. Phys. Letters* **23**, 510.
- Wagner, C.D., 1976, *Discuss. Faraday Soc.* **60**, 291.
- Warren, L.F. and M.A. Bennett, 1974, *J. Amer. Chem. Soc.* **94**, 3340.
- Watanabe, K., 1957, *J. Chem. Phys.* **26**, 542.
- Watson, R.E. and M.L. Perlman, 1975, *Structure and Bonding* **24**, 83.
- Weaver, H.T. and J.E. Schirber, 1976, *Phys. Rev.* **B13**, 1363.
- Willemse, J., J.A. Cras, J.J. Steggerda and C.P. Keijzers, 1976, *Structure and Bonding*, **28**, 83.
- Wilson, J.A., 1977, *Structure and Bonding* **32**, 57.
- Winkler, R., 1972, *Structure and Bonding* **10**, 1.
- Zalkin, A., J.D. Forrester and D.H. Templeton, 1963, *J. Chem. Phys.* **39**, 2881.

Chapter 24

THE ABSORPTION AND FLUORESCENCE SPECTRA OF RARE EARTH IONS IN SOLUTION

William T. CARNALL

*Chemistry Division, Argonne National Laboratory, Argonne,
 IL 60439, USA*

Contents

1. Introduction	172
1.1. Scope	172
1.2. Historical development	173
2. Absorption spectra in solution	175
2.1. Nature of the transitions	175
2.2. Absorption spectra of the R ³⁺ ions. Experimental results	176
2.3. Absorption spectra of the R ²⁺ ions. Experimental results	184
3. Theoretical treatment of 3+ lanthanide solution absorption spectra	184
3.1. Energy level calculations	185
3.2. Experimental determination of intensities of absorption bands	188
3.3. Model calculation of absorption intensity. General considerations	188
3.4. Induced electric dipole transitions	189
3.5. Magnetic dipole transitions	191
3.6. Comparison of experimental and calculated oscillator strengths	191
3.7. Use of intensity parameters to estimate oscillator strengths of infrared transitions	194
3.8. Hypersensitive transitions	194
4. Fluorescence spectra in solution	195
4.1. Historical development	195
4.2. Relaxation of excited states in solution. General considerations	196
4.3. Radiative relaxation	196
4.4. Non-radiative relaxation. General considerations	197

4.5. Multiphonon-like processes in solution	198
4.6. Other non-radiative relaxation mechanisms in solution	200
4.7. Theoretical models for radiationless relaxation of excited states in solution	200
4.8. Hydration and coordination numbers of R ³⁺ (aquo). Application of fluorescence lifetime measurements	201
5. Oxidation states of the lanthanides observed in dilute aqueous solution	203
5.1. Standard oxidation potentials	203
5.2. Production of unusual oxidation states in solution by pulse radiolysis	204
References	205

Symbols

ϵ	= Molar absorptivity of an absorption band
F^k	= Slater integral
ζ	= Spin-orbit coupling integral
P	= Oscillator strength
I, I_0	= Light intensity
σ	= Energy of a transition (cm ⁻¹)
A	= Transition probability (sec ⁻¹)
\bar{F}^2	= Electric dipole operator
\bar{M}^2	= Magnetic dipole operator
χ, χ'	$\chi = (n^2 + 2)^2/9n, \quad \chi' = n(n^2 + 2)^2/9,$ where n is the bulk refractive index of the medium
T_λ	= Intensity parameter defined in Judd-Ofelt theory

ν = Frequency of a transition (sec^{-1})	δ = Kronecker delta
ψJ = Designation of a particular intermediately coupled <i>SLJ</i> electronic state in the f^N configuration	\hbar = Planck's constant divided by 2π
$U^{(\lambda)}$ = Unit tensor operator of rank λ	β_R = Branching ratio for radiative relaxation to a particular final state
$\mathcal{T}_\lambda, \Omega_\lambda$ = Alternative forms of the intensity parameter T_λ defined by the Judd-Ofelt theory	τ_R = Radiative lifetime of an excited state
α = All quantum numbers and suffixes in addition to <i>SLJ</i> needed to specify a particular state	τ_T = Total lifetime (radiative and non-radiative) of an excited state
	W_T = Non-radiative relaxation rate of an excited state
	ρ_E = Density of states

1. Introduction

1.1. Scope

This chapter deals almost exclusively with absorption and fluorescence spectra in aqueous solution. In outlining the present status of the experimental results and their theoretical interpretation, the attempt is made to identify those areas that are currently undergoing active development. Practically all of the experimental and interpretive techniques cited are directly applicable to investigations in non-aqueous solvents, but no effort has been made to cover that extensive literature.

Some of the main currents of thought that have contributed significantly to our present understanding of rare earth spectra in solution are outlined in the next section. At an early stage it was recognized that the spectra of certain members of the group serve as a sensitive probe to monitor changes in the ionic environment. Such spectra can provide one basis for the development of models of the structure of solutions.

The theoretical interpretation of solution spectra has undergone significant advances in recent years. It is now possible to compute both the energies and intensities of bands in good agreement with experiment. While the intensity calculations normally involve parameters evaluated from experimental data, these parameters can be calculated from first principles based on a model for at least the immediate environment of the ion. Some attempts have been made to explore the type of model required by the intensity theory, but the problem is complex and progress along these lines has been slow. At present it appears that intensity correlations play a much more immediate role in the interpretation of the mechanisms of relaxation of excited states of the ions in solution. The concepts involved have been widely applied in investigations of lanthanide lasers.

1.2. Historical development

Although many published accounts of research involving the spectra of lanthanide ions in solution predate the 1930's, this was the era of extensive development that provided the basis for many concepts that are still under active investigation. In one of the classic papers in rare earth spectroscopy, the outgrowth of many years' effort to purify materials, Prandtl and Scheiner (1934) presented an essentially complete collection of trivalent lanthanide solution absorption spectra. This collection, covering the region 7000–2000 Å, stimulated and influenced the thinking of many subsequent investigators at a time when the theoretical interpretation of such spectra was just developing. The authors emphasized an apparent symmetry in region of absorption with band structure shifting toward the ultraviolet in approaching the center of the series from both ends.

Ce (colorless)
Pr (yellow green)
Nd (red violet)
61 (unknown)
Sm (yellow)
Eu (essentially colorless)
Gd (colorless)
Tb (essentially colorless)
Dy (light yellow green)
Ho (brownish yellow)
Er (pink)
Tm (light green)
Yb (colorless)

This apparent symmetry, which had been pointed out earlier by Main-Smith (1927) based on color alone, led to the expectation that bands for members at the beginning and end of the series might be found in the infrared region. Indeed several such observations were noted.

Three years later, interpretation of lanthanide spectra was placed on a much firmer basis when Van Vleck (1937) summarized the evidence for attributing the sharp absorption bands observed in both solutions and solids to transitions within the $4f^N$ configuration. While a number of investigators had espoused this interpretation (Freed, 1931; Tomaschek, 1932; Lang, 1936; Mukherji, 1936), it was by no means universally accepted. Van Vleck pointed out that the intensities reported for Pr^{3+} and Nd^{3+} absorption bands were a factor of 10^6 weaker than would have been expected for normal electric dipole transitions, and concluded that there were probably several contributing mechanisms that could account for the magnitude of the observed transitions.

Progress was also being made during this period in the theoretical interpretation of the spectra of rare earth compounds and solutions in terms of energy level structure as Bethe and Spedding (1937), Lange (1938), and Spedding

(1940) published analyses of the free-ion energy level schemes in $\text{Pr}^{3+}(4f^2)$ and $\text{Tm}^{3+}(4f^{12})$. Differences in interpretation were not fully resolved in favor of the intra f-configuration concept until later, when Broer et al. (1945) reexamined Van Vleck's arguments and revised some of the intensity estimates. It was not until 1953 that the energy level analysis was extended to more complex spectra when Satten (1953) undertook the analysis of $\text{Nd}^{3+}(4f^3)$. Jørgensen (1955) was one of the first to attempt to identify systematically lanthanide aquo ion energy levels.

While to a first approximation, the spectra of the lanthanides in solution were known to be rather insensitive to the environment, the significance of the relatively small but distinctive changes that could be induced in certain absorption bands was pointed out at an early stage. The smaller number of lines observed in bands in $\text{Eu}(\text{NO}_3)_3$ solution compared to those in EuCl_3 solution led Freed and Weissman (1938) to ascribe a higher symmetry to the immediate environment in the nitrate case. Freed (1942) summarized much of the early work on environmental effects in both crystals and solutions.

In a series of papers published from the Zeeman Laboratory in Amsterdam in the early 1940's, quantitative measurements of the solution absorption spectra of the lanthanides, corrected for known impurities in the samples, were made. This constituted the first systematic investigation of band intensities (oscillator strengths) for these ions (Woudenberg, 1942a,b; Franzen et al., 1943; Hoogschagen et al., 1943, 1946a,b; Hoogschagen, 1946; Hoogschagen and Gorter, 1948). Based on the relative magnitudes of the electrostatic and spin-orbit interactions, Bethe and Spedding (1937), and Spedding (1940), Broer et al. (1945) concluded that the energy levels must be treated in the intermediate coupling approximation, i.e., J is a good quantum number, but L and S are not. It was also noted that the J and g -values associated with the ground states deduced from magnetic data agreed with those calculated from Hund's rule.

While much of the data published prior to 1945 is accurate and consistent with more recent results, there have been significant improvements in both purity of materials and in the resolution of recording spectrophotometers. Comprehensive investigations of lanthanide spectra have been published by Moeller and Brantley (1950), Holleck and Hartinger (1955), Banks and Klingman (1956) and Stewart (1959), and extended to the near infrared region by Carnall et al. (1962, 1964) and Carnall (1963).

Along with the increased availability of quantitative measurements of band intensities and energies in solution, there has been a rapid development in the theoretical interpretation of the energy level structures of the lanthanide ions. Much of the latter is based primarily on experimental results obtained with single crystals (Dieke (1968)).

Exciting new possibilities for interpretation of the fundamental processes of absorption and emission of radiation by lanthanide ions in solution were opened up by the publication by B.R. Judd (1962) and independently by G.S. Ofelt (1962) of a theory which made possible quantitative interpretation of intensities associated with observed absorption bands. This development has played a decisive role in much of the subsequent research involving the spectra of these ions.

2. Absorption spectra in solution

2.1. Nature of the transitions

Systematic variation in the energy differences between the lowest levels of the $4f^N$ and higher-lying configurations in various ionization states of the lanthanides was pointed out almost simultaneously by Brewer (1971a,b), Nugent and Vander Sluis (1971), and Martin (1971). For the trivalent lanthanides, the emission spectroscopic results establish $4f^N$ as the ground configuration. The lowest energy level belonging to the next higher ($4f^{N-1}5d$) configuration follows the trend shown in fig. 24.1. In solution, the energy of these $4f \rightarrow 5d$ transitions is lowered by $\sim 15000 \text{ cm}^{-1}$ compared to that of the gaseous ion, and the corresponding relatively intense (parity allowed) bands can be observed in the ultraviolet region for $\text{Ce}^{3+}(\text{aquo})$, $\text{Pr}^{3+}(\text{aquo})$, and $\text{Tb}^{3+}(\text{aquo})$. As indicated in fig. 24.1, the electronic absorption spectra for most of the 3+ lanthanides within the spectral range normally observed (to 200 nm), only involves transitions within the $4f^N$ -configuration.

In several rare earth ions, Sc^{3+} , Y^{3+} , La^{3+} , Ce^{4+} (iso-electronic with La^{3+}), and Lu^{3+} , the core electronic structure comprises completely filled shells. In such cases, no electronic absorption spectra at $>200 \text{ nm}$ is expected because the corresponding process of promoting an electron out of a filled shell requires much higher energies. Broad absorption that appears to increase exponentially is observed in the ultraviolet region of a number of rare earth ions and is particularly apparent in $\text{Eu}^{3+}(\text{aquo})$, $\text{Yb}^{3+}(\text{aquo})$ and $\text{Ce}^{4+}(\text{aquo})$. For complexes

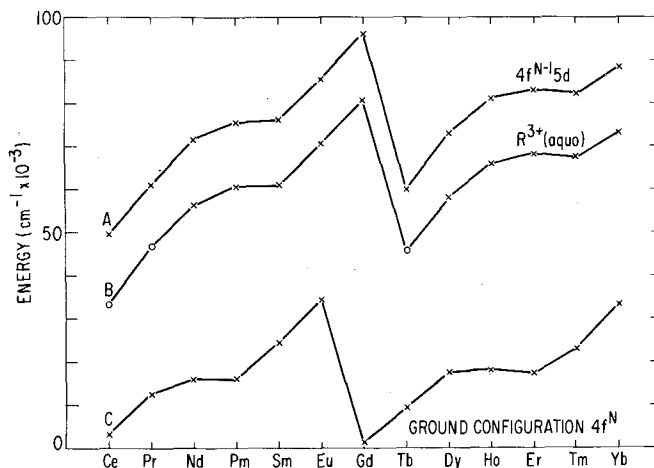


Fig. 24.1. Energy of the lowest level in the $4f^{N-1}5d$ configuration relative to that of $4f^N$ for the lanthanides. (A) Lanthanide 3+ gaseous ion spectra (Brewer, 1971). (B) Data of (A) corrected to spectra observed in dilute acid solution. The results for $\text{Ce}^{3+}(\text{aquo})$, $\text{Pr}^{3+}(\text{aquo})$ and $\text{Tb}^{3+}(\text{aquo})$ are experimental (Jørgensen and Brinen, 1963). (C) Lanthanide 2+ gaseous ion spectra. For Gd^{2+} , the $4f^75d$ -configuration lies lowest and the $4f^8$ is at 1500 cm^{-1} (Brewer, 1971).

such as CeCl_6^{-2} and CeBr_6^{-2} , pronounced absorption bands are apparent, and they extend well into the visible range (Ryan and Jørgensen, 1966). The absorption mechanism involved in these cases is the electron transfer process (Jørgensen and Brinen, 1963; Jørgensen, 1973), where in general the absorption of energy results in the transfer of an electron from molecular orbitals on the ligands to the nl -shell of the central atom.

Those divalent lanthanides whose absorption spectra have been observed under normal conditions in solution, $\text{Sm}^{2+}(4f^6)$, $\text{Eu}^{2+}(4f^7)$, and $\text{Yb}^{2+}(4f^{14})$ (Butement, 1948), have much lower-lying $4f^{N-1}5d$ configurations than is the case with the trivalent ions which possess the corresponding f^N configuration (Brewer, 1971b), fig. 24.1. In all three cases, only the $f \rightarrow d$ transitions are actually observed in solution. The weak $f \rightarrow f$ transitions in Sm^{2+} and Eu^{2+} that are expected to occur in the visible-ultraviolet region are lost in the strong $f \rightarrow d$ bands.

2.2. Absorption spectra of R^{3+} ions. Experimental results

The region of the spectrum in which lanthanide absorption bands can be observed in aqueous solution is restricted as indicated in fig. 24.2. In the ultraviolet range, aqueous solvents are suitable to ~ 200 nm, which is also the usual spectrophotometer limit. Absorption bands characteristic of Pr^{3+} , Nd^{3+} , Sm^{3+} , Dy^{3+} , Ho^{3+} , and Er^{3+} in the 900–1100 nm range in aqueous solution were

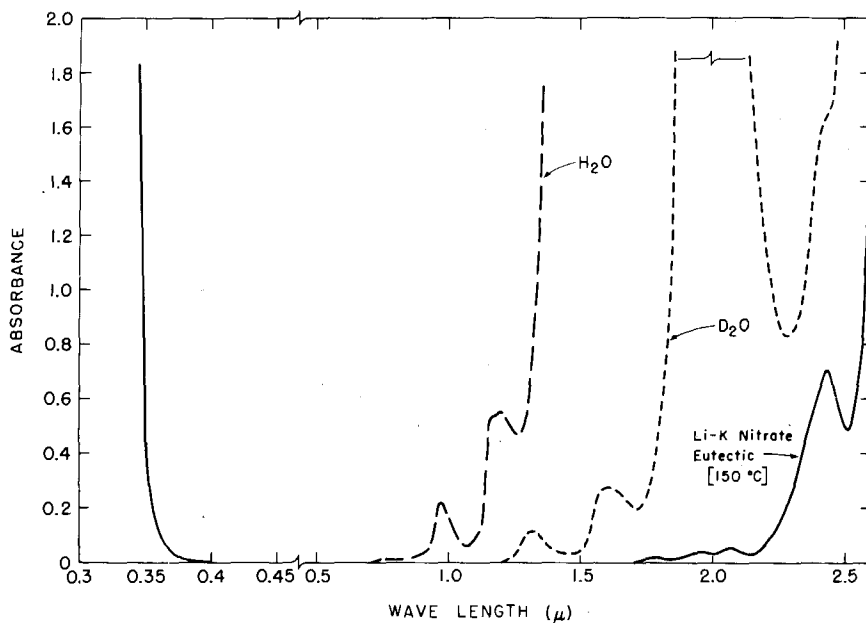


Fig. 24.2. Comparative absorption spectra of different solvent systems in 1 cm path length cells.

reported at a very early date (Freyman and Takvorian, 1932). Stewart (1959) extended observations to the ~ 1400 nm cut-off in H_2O in his systematic investigation. More extensive spectra using D_2O as the solvent, published by Carnall et al. (1962, 1964), Carnall (1963), revealed a number of bands in the ~ 1400 – 1800 nm region. The same authors further extended observations to ~ 2600 nm by using the molten $LiNO_3$ - KNO_3 eutectic ($\sim 150^\circ C$) as a solvent, and the advantages of using characteristic bands in this region in the analysis of mixtures of lanthanides were pointed out (Carnall, 1962).

Fused salts have been a popular solvent medium for lanthanide ion spectroscopy. Typical systematic investigations were carried out in molten fluorides (Young and White, 1960a,b) and in molten chlorides (Banks et al., 1961). Measurements in the $LiCl$ - $NaCl$ - KCl eutectic ($333^\circ C$) included the near infrared range (Mamiya, 1965), and a more comprehensive investigation was carried out in $LiCl$ - KCl eutectic at $450^\circ C$ (Johnson and Sandoe, 1968). The oxidizing character of the nitrate melt makes it an ideal medium for stabilizing the trivalent state of the lanthanides at 150 – $200^\circ C$, whereas in the chloride melt, some evidence of reduction or charge transfer absorption is noted in the spectra of the most easily reduced species, Sm^{3+} , Eu^{3+} , and Yb^{3+} . Lanthanide absorption spectra covering a range similar to that observed in the $LiNO_3$ - KNO_3 eutectic at $150^\circ C$ have also been recorded in non-aqueous solvents at $25^\circ C$ (Heller, 1968).

The absorption spectra shown in figs. 24.3–24.15 represent a consistent set of results in dilute $HClO_4$ or $DClO_4$ solution. In cases where the $f \rightarrow f$ transitions are superimposed on broad bands that are attributed to other processes such as charge transfer or $f \rightarrow d$ transitions, the background absorption has been subtracted where possible.

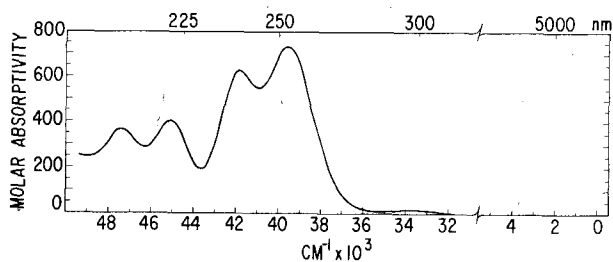


Fig. 24.3. Solution absorption spectrum of Ce^{3+} (aqo). Jørgensen and Brinen (1963) report an additional band at 200 nm (50000 cm^{-1}) not shown.

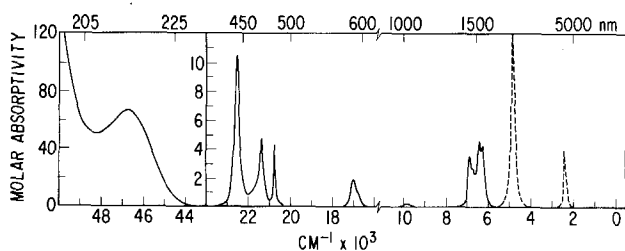


Fig. 24.4. Solution absorption spectrum of Pr^{3+} (aqo). Dashed lines indicate calculated curves (section 3.7).

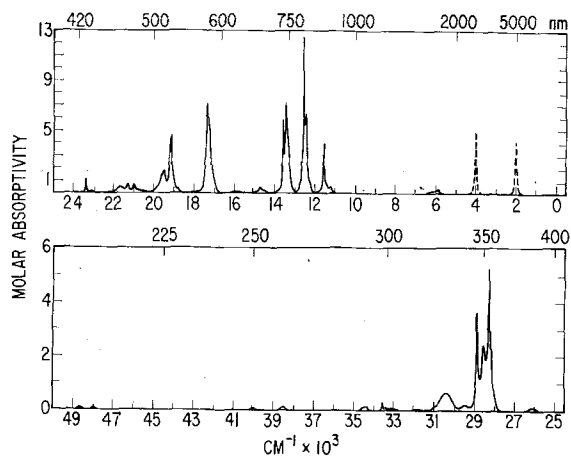


Fig. 24.5. Solution absorption spectrum of $\text{Nd}^{3+}(\text{aquo})$. Dashed lines indicate calculated curves (section 3.7).

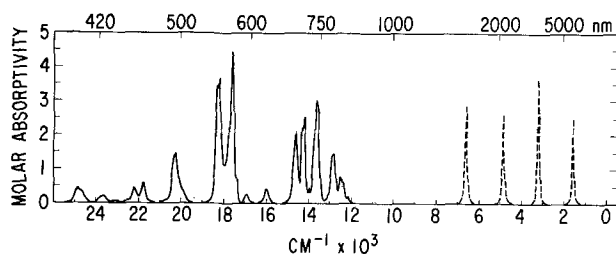


Fig. 24.6. Solution absorption spectrum of $\text{Pm}^{3+}(\text{aquo})$. Dashed lines indicate calculated curves (section 3.7).

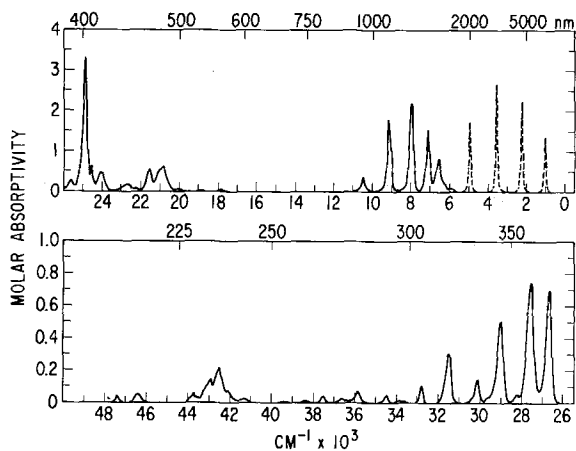


Fig. 24.7. Solution absorption spectrum of $\text{Sm}^{3+}(\text{aquo})$. Dashed lines indicate calculated curves (section 3.7).

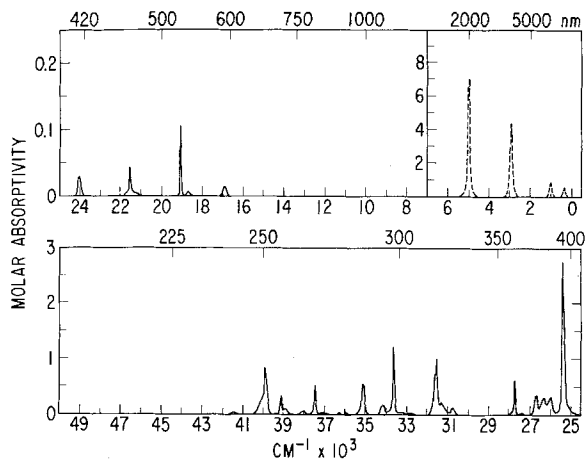


Fig. 24.8. Solution absorption spectrum of $\text{Eu}^{3+}(\text{aq})$. Dashed lines indicate calculated curves (section 3.7).

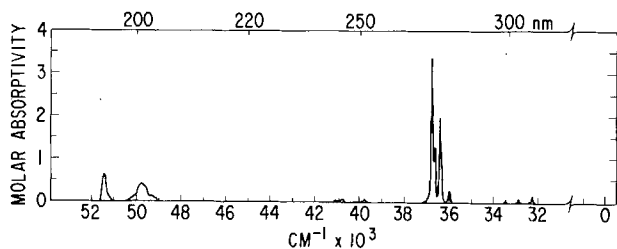


Fig. 24.9. Solution absorption spectrum of $\text{Gd}^{3+}(\text{aq})$.

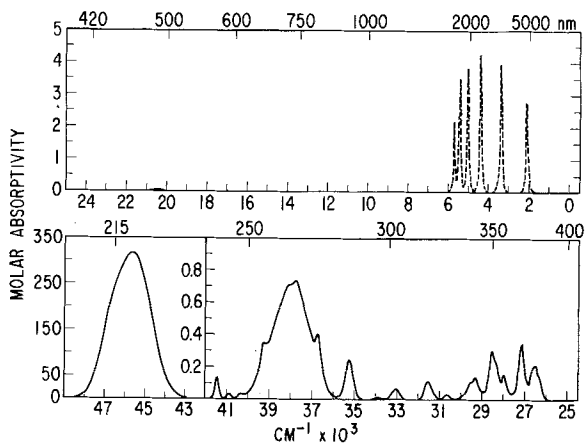


Fig. 24.10. Solution absorption spectrum of $\text{Tb}^{3+}(\text{aq})$. Dashed lines indicate calculated curves (section 3.7).

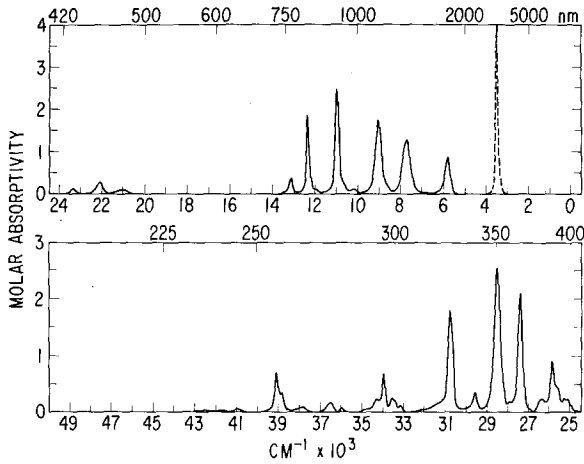


Fig. 24.11. Solution absorption spectrum of $\text{Dy}^{3+}(\text{aquo})$. Dashed lines indicate calculated curves (section 3.7).

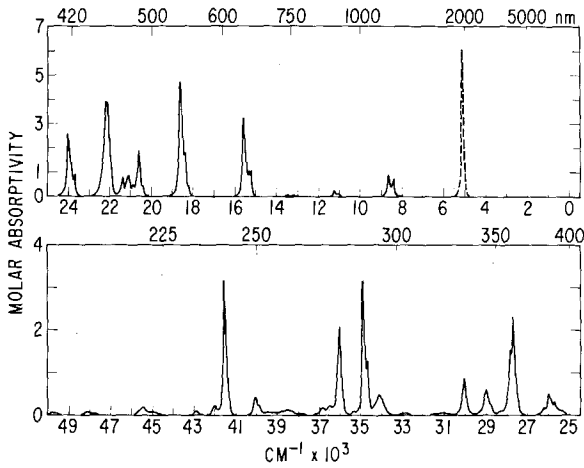


Fig. 24.12. Solution absorption spectrum of $\text{Ho}^{3+}(\text{aquo})$. Dashed lines indicate calculated curves (section 3.7).

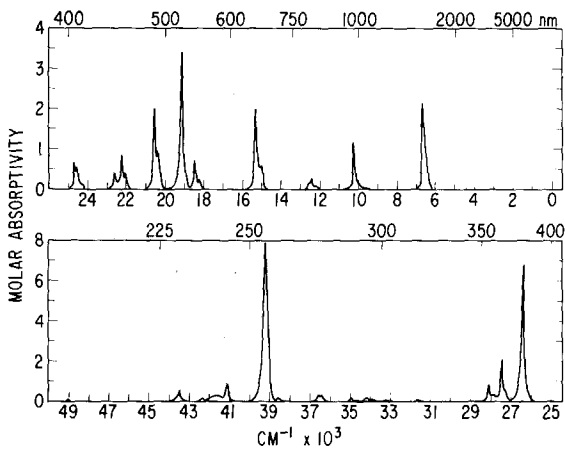


Fig. 24.13. Solution absorption spectrum of $\text{Er}^{3+}(\text{aquo})$.

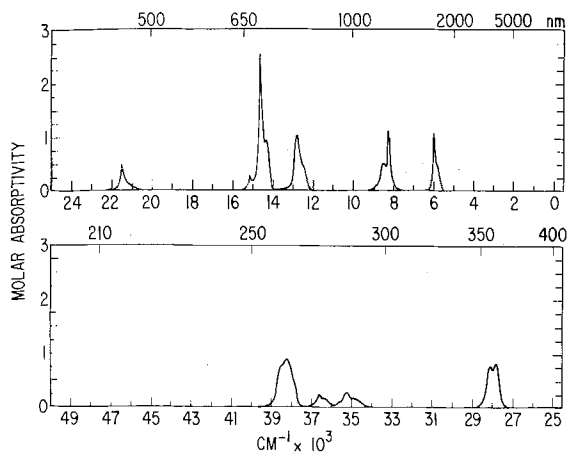


Fig. 24.14. Solution absorption spectrum of $\text{Tm}^{3+}(\text{aq})$.

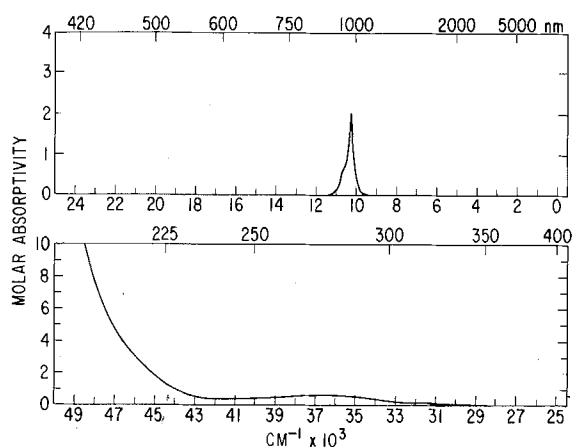


Fig. 24.15. Solution absorption spectrum of $\text{Yb}^{3+}(\text{aq})$.

As noted earlier, bands characteristic of the lanthanides are observed in non-aqueous solvents at lower energies than is possible in DClO_4 . In a subsequent section, the quantitative treatment of band intensities is discussed. As a result of this work, the energies and intensities of all the transitions characteristic of the lanthanides in aqueous solution in the energy range 0 – 5500 cm^{-1} can be computed. The corresponding bands are included in the spectra shown in figs. 24.4–24.12 and discussed in section 3.7.

A band register which includes the molar absorptivities (ϵ) for all trivalent lanthanide absorption band maxima with $\epsilon > 0.2$ is given in table 24.1. The region of the spectrum covered is that which can be observed in H_2O and D_2O .

TABLE 24.1
Band register for $R^{3+}(\text{aquo})$ ions in $\text{H}_2\text{O}-\text{D}_2\text{O}$ with molar absorptivity (ϵ) > 0.2.

Band peak		Ion	ϵ	Band peak		Ion	ϵ
(cm^{-1})	(nm) ^a			(cm^{-1})	(nm) ^a		
5837	1713	Dy	0.84	15608	641	Ho	3.19
5988	1670	Nd	0.25	16000	625	Pm	0.44
6006	1665	Tm	1.04	16920	591	Pm	0.26
6309	1585	Pr	4.18	16980	589	Pr	1.88
6451	1550	Pr	4.51	17373	576	Nd	7.20
6622	1510	Sm	0.79	17605	568	Pm	4.43
6667	1500	Er	2.11	18215	549	Er	0.21
6896	1450	Pr	3.60	18235	548	Pm	3.68
7143	1400	Sm	1.54	18315	546	Pm	3.45
7707	1297	Dy	1.22	18399	544	Ho	1.81
8051	1242	Sm	2.02	18477	541	Er	0.72
8278	1208	Tm	1.11	18632	537	Ho	4.74
8417	1188	Ho	0.74	19128	523	Er	3.40
8529	1172	Tm	0.50	19198	521	Nd	4.33
8673	1153	Ho	0.87	19522	512	Nd	1.76
9066	1103	Dy	1.72	20242	494	Pm	1.47
9199	1087	Sm	1.77	20375	491	Er	0.93
9876	1012	Pr	0.20	20542	487	Er	2.02
10262	974	Yb	2.03	20614	485	Ho	1.84
10262	974	Er	1.14	20772	481	Pr	4.29
10520	951	Sm	0.36	20833	480	Ho	0.48
10995	910	Dy	2.44	20894	479	Sm	0.60
11235	890	Ho	0.22	21017	476	Nd	0.72
11556	865	Nd	4.01	21106	474	Ho	0.82
12398	806	Dy	1.82	21308	469	Nd	0.78
12462	802	Er	0.27	21349	468	Pr	4.59
12472	802	Nd	6.42	21377	468	Ho	0.82
12484	801	Pm	0.74	21533	464	Tm	0.48
12586	794	Nd	12.5	21580	463	Sm	0.54
12804	781	Pm	1.46	21668	462	Nd	0.52
12820	780	Tm	1.02	21786	459	Pm	0.63
13210	757	Dy	0.35	22056	453	Er	0.38
13508	740	Nd	7.27	22065	453	Dy	0.26
13624	734	Pm	3.04	22185	451	Ho	3.90
13665	732	Nd	5.93	22222	450	Pm	0.46
13980	715	Pm	0.48	22242	450	Er	0.88
14239	702	Pm	2.54	22522	444	Pr	10.4
14347	697	Tm	0.92	22624	442	Er	0.43
14600	685	Nd	0.22	23386	428	Nd	1.14
14625	684	Pm	2.11	23640	423	Pm	0.20
14663	682	Tm	2.43	23708	422	Ho	0.89
14721	679	Nd	0.50	24033	416	Ho	2.55
15015	666	Er	0.54	24096	415	Sm	0.47
15179	659	Tm	0.27	24570	407	Er	0.53
15238	656	Ho	1.03	24582	407	Sm	0.61
15314	653	Ho	1.01	24704	405	Er	0.67
15328	652	Er	1.97	24876	402	Pm	0.46

TABLE 24.1. (Contd.)

Band peak			Band peak				
(cm ⁻¹)	(nm) ^a	Ion	ε	(cm ⁻¹)	(nm) ^a	Ion	ε
24925	401	Sm	3.31	31505	317	Eu	1.01
25227	396	Dy	0.23	31546	317	Sm	0.31
25419	393	Eu	2.77	33580	298	Dy	0.21
25602	390	Sm	0.26	33580	298	Nd	0.33
25680	389	Ho	0.29	33602	298	Eu	1.21
25840	387	Dy	0.89	33944	295	Dy	0.67
25974	385	Ho	0.49	34153	293	Ho	0.47
25988	385	Eu	0.33	34320	291	Dy	0.22
26330	380	Eu	0.31	34420	290	Nd	0.27
26334	379	Dy	0.24	34674	288	Ho	1.26
26385	379	Er	6.68	34891	287	Ho	3.16
26510	377	Tb	0.21	35100	285	Eu	0.57
26624	376	Eu	0.36	35211	284	Tm	0.27
26702	374	Eu	0.36	35223	284	Tb	0.25
26752	374	Sm	0.70	35920	278	Gd	0.29
27137	368	Tb	0.34	35997	278	Ho	2.07
27427	365	Dy	2.11	36258	276	Gd	0.92
27457	364	Er	2.08	36337	275	Gd	2.00
27624	362	Sm	0.75	36443	274	Er	0.31
27678	361	Eu	0.64	36536	274	Gd	1.38
27716	361	Ho	2.27	36550	274	Ho	0.20
27809	360	Tm	0.80	36576	273	Gd	1.22
27932	358	Er	0.31	36576	273	Tm	0.23
28090	356	Tm	0.76	36603	272	Er	0.30
28120	356	Er	0.85	36710	272	Gd	3.41
28296	353	Nd	5.30	37439	267	Eu	0.54
28545	350	Tb	0.31	38226	262	Tm	0.90
28555	350	Nd	2.46	38490	260	Nd	0.22
28556	350	Dy	2.54	38850	257	Dy	0.32
28892	346	Nd	3.71	39093	256	Dy	0.68
28985	345	Ho	0.59	39108	256	Eu	0.35
29070	344	Sm	0.50	39200	255	Er	7.89
29410	340	Nd	0.21	39872	251	Eu	0.80
29595	338	Dy	0.34	40064	250	Ho	0.39
30039 ^b	333	Pm	4.73	41152	243	Er	0.89
30048	333	Ho	0.82	41560	241	Ho	3.16
30469	328	Nd	0.68	41666	240	Er	0.31
30478 ^b	328	Pm	4.96	42016	238	Ho	0.21
30798	325	Dy	1.78	42553	235	Sm	0.22
31250 ^b	320	Pm	2.53	43525	230	Er	0.58
31270	320	Eu	0.24				

^aMeasured center of observed band. The value in cm⁻¹ is the converted value; ^bGruber and Conway (1960).

2.3. Absorption spectra of R^{2+} ions. Experimental results

Since the lanthanides that exhibit the divalent state in aqueous solution, Sm^{2+} , Eu^{2+} , and Yb^{2+} , are all readily oxidized to the trivalent state, attempts to record their absorption spectra have usually proceeded from the rapid dissolution of a soluble anhydrous compound. The absorption spectra shown in fig. 24.16 for Sm^{2+} , Eu^{2+} , and Yb^{2+} were adapted from results published by Butement and Terrey (1937), Butement (1948), and Christensen et al. (1973). Production of other divalent lanthanide ions by pulse radiolysis, and the observation of their spectra is discussed in section 5.2.

3. Theoretical treatment of 3+ lanthanide solution absorption spectra

We are concerned here exclusively with the trivalent lanthanides since there has been little progress made beyond a general interpretation of the band structure observed in solutions containing the divalent ions. Two aspects of the interpretation of the spectra will be considered. First, the energy level structure is calculated in agreement with experiment using a model that includes sufficiently high order interactions to insure accurate intermediate coupling eigenvectors for states over the whole energy range of observation. Second, the intensities of the observed bands are related to a semi-empirical theory, which in turn can be used to predict properties of the absorption and fluorescence spectra. The parameters of the intensity theory can be calculated on a first

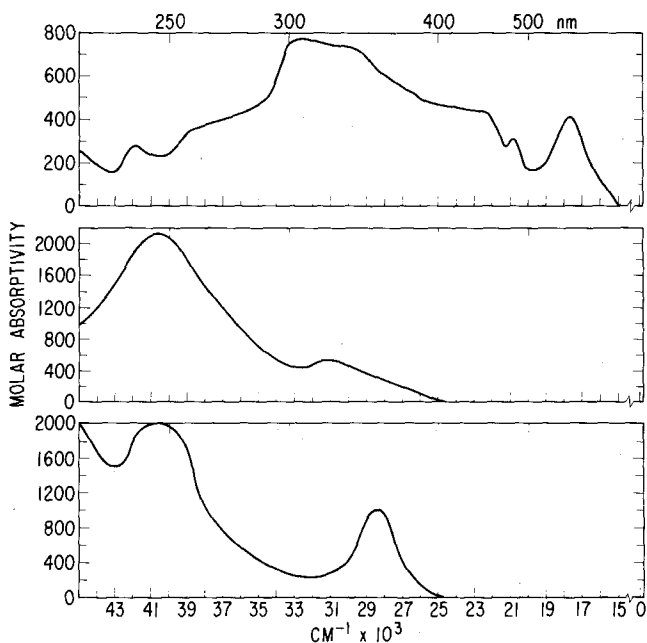


Fig. 24.16. Solution absorption spectra of Sm^{2+} (aquo), Eu^{2+} (aquo), and Yb^{2+} (aquo) adapted from Butement (1948).

principles basis, but in practice this approach suffers from the same lack of an accurate model of the environment that limits the first principles computation of lanthanide crystal-field parameters.

3.1. Energy level calculations

A number of sources present extensive development of the energy level structure theory in lanthanide spectra, but works by Wybourne (1965), Judd (1963), and Dieke (1968) are particularly useful. Only a brief summary that includes recent developments in the theoretical model will be included here.

Since for present purposes interest is entirely centered on transitions within the $4f^N$ configuration, it can be taken as a good simplifying approximation that electrons in closed shells in a lanthanide ion exert a constant influence on all of the f^N -states. The problem then is to identify those effective interactions operating within the f^N configuration that reproduce the observed structure. The principal terms of the current model can be written:

$$E = \sum_{k=0}^6 F^k(nf, nf)f_k + \zeta_{4f}A_{SO} + E_{CI} + E_{CF} \quad (k \text{ even}) \quad (24.1)$$

where f_k and A_{SO} represent the angular parts of the electrostatic and spin-orbit interactions, respectively. The F^k are Slater integrals, $F^2 = 225F_2$, $F^4 = 1089F_4$, and $F^6 = 184\,041/25F_6$, representing the purely electrostatic interaction between the f electrons, and ζ_{4f} is the spin-orbit coupling constant. The term E_{CI} is used here to represent the two-body and three-body effective operators that have been added to the model in recent years to account for the effects of configuration mixing, and E_{CF} is the crystal or ligand field interaction term.

The relative magnitudes of the principal terms in eq. (24.1) are indicated in fig. 24.17 which shows the experimentally well established energy level scheme for $\text{Pr}^{3+}:\text{LaCl}_3$ (Dieke, 1968). The fact that several of the excited states in $\text{Pr}^{3+}:\text{LaCl}_3$ are isolated in energy, makes it possible to identify the transitions responsible for the corresponding absorption bands in fig. 24.4.

While the principal interactions that give rise to the structure of the f^N configuration are the electrostatic and spin-orbit terms of eq. (24.1), and the corresponding degenerate states are the free-ion states, computation of the energies of spectroscopic states based solely on these interactions are only approximate. Even in the relatively simple case of $\text{Pr}^{3+}(4f^2)$, differences between observed and calculated free-ion levels of $>500 \text{ cm}^{-1}$ are encountered (Spedding, 1940; Carnall, 1974).

In recent analyses of lanthanide spectra, the term E_{CI} in eq. (24.1) has included the effects of configuration interaction as expressed in the Trees correction $\alpha L(L+1)$, and the parametrized Casimir operators $\beta G(G_2)$ and $\gamma G(G_7)$ (Trees, 1964; Rajnak and Wybourne, 1963). The additional terms represent those effects of configuration interaction that can be accounted for by two-body effective operators that do not transform as the f_k in eq. (24.1). For configurations of three or more equivalent f -electrons, the three-particle operators of Judd (1966a), $T^i t_i$

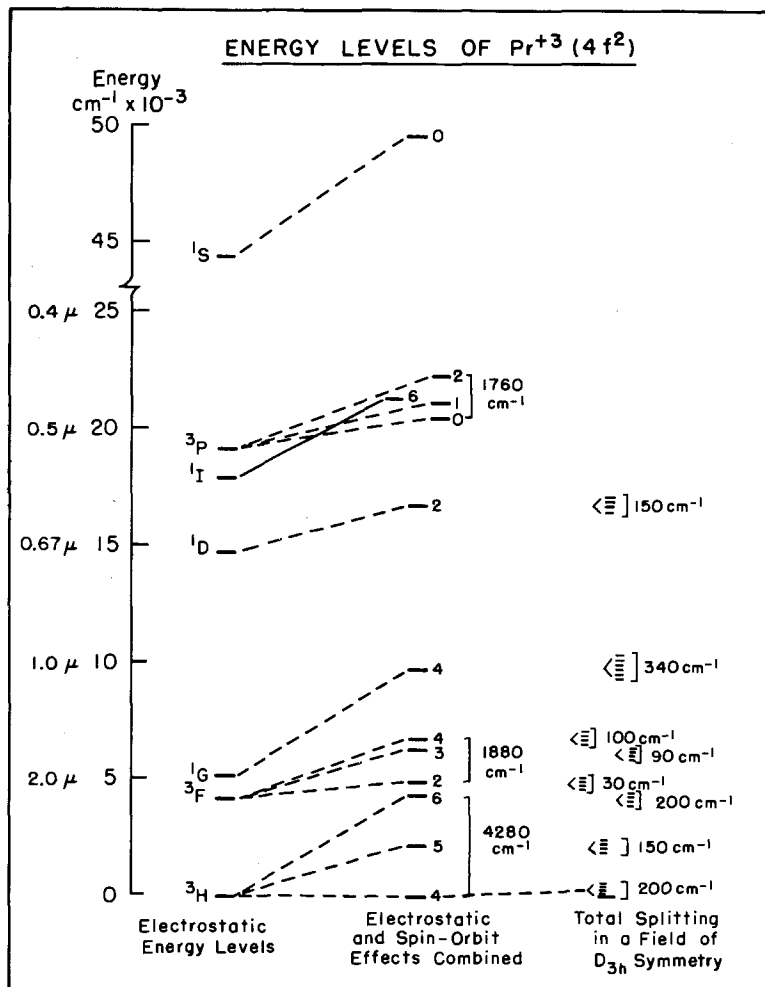


Fig. 24.17. Schematic energy level structure for $\text{Pr}^{3+}(4f^2)$.

($i = 2,3,4,6,7,8$) where T^i are the parameters and t_i are the operators, have been included to account for the perturbing influence of those configurations that differ from f^N in the quantum numbers of a single electron. In addition to the electrostatically correlated interactions, Judd et al. (1968) have provided the basis for including a number of magnetically correlated interactions in the parametric analysis. The effects represented by E_{CI} are not small. They may shift the energies of individual terms by several hundred wavenumbers.

Approximate values for the radial integrals associated with the electrostatic and spin-orbit interactions can be obtained from both relativistic and non-

relativistic Hartree-Fock methods (Lewis et al., 1970; Crosswhite and Cowan, 1976). Such computed values are in general too large because they do not include the effects of configuration interaction. They may be scaled down by systematic comparison with results obtained semi-empirically. The magnitudes of some of the important parameters of configuration interaction and the screening of the electrostatic integrals have also been computed (Morrison and Rajnak, 1971; Newman and Taylor, 1971, 1972). However, all of these integrals are in practice treated as parameters to be evaluated from experimental data. The angular parts of the interactions can be calculated exactly using Racah's tensor operator methods (Judd, 1963). The *ab initio* methods do, however, yield values for the parameters of configuration interaction that are in good agreement with those obtained by parameterization, and thus tend to confirm the validity of the latter procedure.

Recent investigations of the spectra of $\text{Nd}^{3+}:\text{LaCl}_3$ (Crosswhite et al., 1976), and $\text{Pm}^{3+}:\text{LaCl}_3$ (Carnall et al., 1976), provide examples of the results obtained using the expanded parameterization model. The fits to observed "free-ion" states have an RMS deviation of $<20\text{ cm}^{-1}$, and the parameter values exhibit regular trends over the whole lanthanide series (Crosswhite et al., 1975).

The fact that 4f-electrons are well shielded from the environment by filled $5s^2$ and $5p^6$ shells (Wybourne, 1965), results in there being a close similarity in the level structure derived from the analysis of lanthanide spectra in crystalline solids such as $\text{R}^{3+}:\text{LaCl}_3$ and that observed for the $\text{R}^{3+}(\text{aquo})$ ion. Indeed evidence was presented at an early stage to show that the spectroscopic properties of Eu^{3+} ions in solution at reduced temperature were very similar to those of the ions in crystals (Freed and Weissman, 1938). Subsequent experiments with mixed component solutions containing Eu^{3+} (Sayre et al., 1957), and Nd^{3+} and Sm^{3+} (Freed and Hochanadel, 1950), demonstrated the continuity between the numerous sharp lines which could be identified as crystal-field components in a microfield of clearly defined site symmetry in solution at low temperature, and the band envelope of these lines that developed as the temperature was raised.

For solution spectra at room temperature, the term in eq. (24.1) which expresses the effects of the crystal field is not included. Instead what is calculated is the center of gravity of the absorption bands. While the term "free-ion" calculation is used, the level scheme is clearly not that that would be characteristic of the gaseous free-ion. Each different medium shifts the center of gravity of the envelopes of crystal-field components to slightly different energies. This screening effect on the f-electrons has been referred to by Jørgensen (1969) as the nephelauxetic effect.

Values of the energy level parameters obtained from a fit to lanthanide solution absorption spectra are given in table 24.2 (Carnall et al., 1968a). While more accurate values can now be derived from a consistent treatment of data in crystals, the indicated results constitute a useful set for computing eigenvectors of states in intermediate coupling as required in the intensity calculations to be discussed next.

TABLE 24.2.
Energy level parameter values calculated for the R^{3+} (aquo) ions^a (in cm^{-1})

	F^2	F^4	F^6	ζ_{4f}	α	β	γ
Pr^{3+}	68674	50395	32648	740.75	21.255	-799.93	1342.9
Nd^{3+}	72412	50394	34698	884.58	0.5611	-117.15	1321.3
$\text{Pm}^{3+ \text{ b}}$	76585	54538	35135	1022.8	20.692	-616.29	1967.5
Sm^{3+}	82008	61766	39922	1157.3	22.250	-742.55	796.64
Eu^{3+}	83162	61245	41526	1326.0	25.336	-580.25	1155.7
Gd^{3+}	86625	62890	42513	1450.0	22.552	-103.7	996.98
Tb^{3+}	90358	66213	44262	1709.5	20.131	-370.21	1255.9
Dy^{3+}	91730	65886	46194	1932.0	37.062	-1139.1	2395.3
Ho^{3+}	94448	70849	49835	2141.3	23.635	-807.20	1278.4
Er^{3+}	99182	72778	53812	2380.7	18.347	-509.28	649.71
Tm^{3+}	103887	77024	57449	2628.7	14.677	-631.79	—

^aCarnall et al. (1968a). ^bFree-ion parameters from data for $\text{Pm}^{3+}:\text{LaCl}_3$ (Carnall et al., 1976).

3.2. Experimental determination of intensities of absorption bands

The quantitative treatment of the intensities of 3+ lanthanide absorption bands relates an experimentally determined quantity, a normalized band envelope, to a theoretical model based on the mechanisms by which radiation can be absorbed. The integrated absorption bands observed in a solution of known concentration can be used to calculate the number of classical oscillators in one ion, which is more commonly referred to as the probability for absorption of radiant energy P (oscillator strength) by the expression (Hoogschagen, 1946):

$$P = \frac{2303 mc^2}{N\pi e^2} \int \epsilon_i(\sigma) d\sigma = 4.32 \times 10^{-9} \int \epsilon_i(\sigma) d\sigma \quad (24.2)$$

where ϵ_i is the molar absorptivity of a band at the energy $\sigma(\text{cm}^{-1})$, and the other symbols have their usual meaning. P is here a dimensionless quantity. The molar absorptivity at a given energy is computed from the Beer-Lambert law:

$$\epsilon = \frac{1}{cl} \log I_0/I \quad (24.3)$$

where c is the concentration of the lanthanide ion in moles/liter, l is the light path in the solution (cm), and $\log I_0/I$ is the absorptivity or optical density. Maximum molar absorptivities of lanthanide absorption bands in dilute non-complexing acid solution are usually <10 and average nearer unity as shown in table 24.1. Oscillator strengths are in general of the order of 1×10^{-6} .

3.3. Model calculation of absorption intensity. General considerations

As Van Vleck (1937) and Broer et al. (1945) pointed out, there is some magnetic dipole character in a few transitions (P_{MD}), but an induced electric-

dipole mechanism (P_{ED}) must be invoked to account for the intensities of most lanthanide absorption bands. The term induced or forced electric dipole is used to emphasize that true electric dipole transitions require the initial and final states to be of different parity, whereas no parity change is involved in transitions *within* a configuration. In contrast, magnetic dipole transitions within a configuration are (parity) allowed. The weak intra f^N transitions are thus accounted for by assuming that a small amount of the character of higher-lying opposite parity configurations is mixed into the f^N states via the odd terms in the potential due to the ligand field (Wybourne, 1965). We can therefore write $P_{\text{expt}} = P_{ED} + P_{MD}$.

In view of the interest in both absorption and fluorescence processes in solution, there is an advantage in pointing out the basic role of the Einstein coefficient in expressing the transition probability due to dipole radiation:

$$A(i, f) = \frac{64\pi^4\sigma^3}{3h} |\langle i|\mathbf{D}|f\rangle|^2 \quad (24.4)$$

where i and f signify the initial and final states, A is the (spontaneous) transition probability per unit time, σ (cm^{-1}) is the energy difference between the states, and \mathbf{D} is the dipole operator (Condon and Shortley, 1957).

In addressing the problem of the absorption of energy, Broer et al. (1945) expressed eq. (24.4) in terms of oscillator strength using the relationship $P = Amc/8\pi^2\sigma^2e^2$. The factor $2J + 1$ was added since the matrix elements of \mathbf{D} are summed over all components of the initial state i . A refractive index correction χ was also included giving:

$$P = \frac{8\pi^2mc\sigma}{3he^2(2J + 1)} [\chi\bar{F}^2 + n\bar{M}^2] \quad (24.5)$$

where \bar{F}^2 and \bar{M}^2 represent the matrix elements of the electric dipole and magnetic dipole operators, respectively, joining an initial state J to the final state J' , $\chi = (n^2 + 2)^2/9n$, and n is the refractive index of the medium.

3.4. Induced electric dipole transitions

Judd (1962) and Ofelt (1962) independently derived expressions for the oscillator strength of induced electric dipole transitions within the f^N configuration. This was a signal accomplishment. Much of the highly significant theoretical interpretation of the fluorescence process and the prediction of the properties of solid state lanthanide lasers, ch. 35, was made possible by this work. Since their results are similar, and were published simultaneously, the basic theory has become known as the Judd-Ofelt theory. However, Judd's expression, eq. (24.6), was cast in a form that could be directly related to oscillator strengths derived from lanthanide solution spectra, and he was the first to show that the model satisfactorily reproduced the experimental results for $\text{Nd}^{3+}(\text{aquo})$ and

$\text{Er}^{3+}(\text{aquo})$.

$$P_{\text{ED}} = \sum_{\lambda=2,4,6} T_{\lambda} \nu (\psi J \| U^{(\lambda)} \| \psi' J')^2 \quad (24.6)$$

where $\nu(\text{sec}^{-1})$ is the frequency of the transition $\psi J \rightarrow \psi' J'$, $U^{(\lambda)}$ is a unit tensor operator of rank λ , the sum running over the three values $\lambda = 2, 4, 6$, and the T_{λ} are three parameters which can be evaluated from experimental data. These parameters involve the radial parts of the $4f^N$ wave functions, the wave functions of perturbing configurations such as $4f^{N-1}5d$, and the interaction between the central ion and the immediate environment.

In order to facilitate the intercomparison of parameters for different lanthanide ions, eq. (24.6) was modified by the substitution $T_{\lambda} = \mathcal{T}_{\lambda}/2J + 1$, and results for all of the lanthanides in dilute acid solution have been reported in terms of \mathcal{T}_{λ} (Carnall et al., 1965, 1968b). However, those investigators who have studied lanthanide intensities in crystals have followed an alternate parameterization proposed by Axe (1963). The latter has clear advantages in describing both the absorption and fluorescence processes in terms of a single set of adjustable parameters.

The expression for T_{λ} given by Judd was:

$$T_{\lambda} = \frac{8\pi^2 m}{3h(2J+1)} \left\{ \frac{(n^2+2)^2}{9n} \right\} (2\lambda+1) \sum_t (2t+1) B_t \Xi^2(t, \lambda) \quad (24.7)$$

Substituting $\nu = c\sigma$ and eq. (24.7) into eq. (24.6) gives

$$P_{\text{ED}} = \frac{8\pi^2 m c \sigma}{3h(2J+1)} \left\{ \frac{(n^2+2)^2}{9n} \right\} \sum_{\lambda=2,4,6} \Omega_{\lambda} (\psi J \| U^{(\lambda)} \| \psi' J')^2 \quad (24.8)$$

where $\Omega_{\lambda} = (2\lambda+1) \sum_t (2t+1) B_t \Xi^2(t, \lambda)$ (Axe, 1963), and in terms of \bar{F}^2 , eq. (24.5),

$$\bar{F}^2 = e^2 \sum_{\lambda=2,4,6} \Omega_{\lambda} (\psi J \| U^{(\lambda)} \| \psi' J')^2 \quad (24.9)$$

The matrix elements of eq. (24.8) are calculated in the LS basis using the relation (Judd, 1962),

$$\begin{aligned} & (f^N \alpha SLJ \| U^{(\lambda)} \| f^N \alpha' S' L' J') \\ &= \delta(S, S') (-1)^{S+L+J+\lambda} [(2J+1)(2J'+1)]^{1/2} \begin{Bmatrix} J & J' & \lambda \\ L' & L & S \end{Bmatrix} (f^N \alpha SL \| U^{(\lambda)} \| f^N \alpha' S' L') \end{aligned} \quad (24.10)$$

Selection rules imposed by the nature of the mechanism assumed are discussed by Ofelt (1962). The reduced matrix elements on the right side of eq. (24.10) have been tabulated by Nielson and Koster (1963). The matrix elements as computed must be transformed from the LS basis to intermediate coupling before being squared and substituted into eq. (24.8).

The intermediate-coupling eigenvectors, $|f^N \psi J\rangle$, are expressed in terms of LS basis states, $|f^N \alpha SLJ\rangle$, by:

$$|f^N \psi J\rangle = \sum_{\alpha, S, L} c(\alpha, S, L) |f^N \alpha SLJ\rangle$$

where $c(\alpha, S, L)$ are the numerical coefficients resulting from the simultaneous diagonalization of the terms indicated in eq. (24.1).

3.5. Magnetic dipole transitions

Following the results of Condon and Shortley (1957), the magnetic dipole operator is given as $M = (-e/2mc)\sum_i(L_i + 2S_i)$. The matrix elements of the operator \bar{M}^2 in eq. (24.5) can then be written,

$$\bar{M}^2 = (\hbar^2/4m^2c^2)(\psi J \| L + 2S \| \psi' J')^2. \quad (24.11)$$

The non-zero matrix elements will be those diagonal in the quantum numbers α , S , and L . The selection rule on J , $\Delta J = 0, \pm 1$, restricts consideration to three cases,

$$(1) \quad J' = J \quad (\alpha SLJ \| L + 2S \| \alpha SLJ') = g\hbar[J(J+1)(2J+1)]^{1/2} \quad (24.12)$$

$$\text{where } g = 1 + \frac{J(J+1) + S(S+1) - L(L+1)}{2J(J+1)}$$

$$(2) \quad J' = J - 1 \quad (\alpha SLJ \| L + 2S \| \alpha SLJ - 1) \\ = \hbar \left[\frac{(S+L+J+1)(S+L+1-J)(J+S-L)(J+L-S)}{4J} \right]^{1/2} \quad (24.13)$$

$$(3) \quad J' = J + 1 \quad (\alpha SLJ \| L + 2S \| \alpha SLJ + 1) \\ = \hbar \left[\frac{(S+L+J+2)(S+J+1-L)(L+J+1-S)(S+L-J)}{4(J+1)} \right]^{1/2}. \quad (24.14)$$

The matrix elements calculated in eqs. (24.12–24.14) must be transformed into the intermediate coupling scheme before computation of the magnetic dipole contribution represented by eq. (24.11).

Values of the quantity $P' > 0.015 \times 10^{-8}$ where $P_{MD} = P'n$ have been calculated for all of the trivalent lanthanide ions based on eigenvectors derived from energy level schemes for $R^{3+}(\text{aquo})$ (Carnall et al., 1968a). The principal magnetic dipole transitions in the absorption spectra of the 3+ lanthanides are identified in table 24.3.

3.6. Comparison of experimental and calculated oscillator strengths

The most complete oscillator strength data for lanthanide solution absorption spectra have been given by Stewart (1959) and by Carnall et al. (1968a). The results obtained when the parameters of eq. (24.8) are determined by a least squares fitting procedure to the data for a given R^{3+} ion, corrected for P_{MD} where appropriate, are summarized in table 24.4. As was pointed out in section 3.4, the parameterization in terms of Ω_λ lends itself readily to discussion of both absorption and fluorescence spectra, and has been used almost exclusively in describing data obtained in crystals, ch. 35. It serves no purpose to continue to preserve several different parameterizations. We adopt here the use of Ω_λ .

TABLE 24.3.

Oscillator strengths (P') of the principal magnetic dipole transitions in the absorption spectra of the 3+ lanthanides in solution.

	Excited ^a state	E_{calc}^b (cm^{-1})	$P' \times 10^8$ ^{b,c}		Excited ^a state	E_{calc}^b (cm^{-1})	$P' \times 10^8$ ^{b,c}
Pr ³⁺	³ H ₅	2322	9.76	Tb ³⁺	⁷ F ₅	2112	12.11
					⁷ F ₄	26425	5.03
Nd ³⁺	⁴ I _{11/2}	2007	14.11		³ F ₅	34927	1.87
Pm ³⁺	⁵ I ₅	1577	16.36	Dy ³⁺	⁶ H _{13/2}	3506	22.68
					⁴ I _{15/2}	22293	5.95
Sm ³⁺	⁶ H _{7/2}	1080	17.51				
	⁴ G _{5/2}	17924	1.76	Ho ³⁺	⁵ I ₇	5116	29.47
					³ K ₈	21308	6.39
Eu ³⁺	⁷ F ₁	350	17.73				
	⁵ D ₁	19026	1.62	Er ³⁺	⁴ I _{13/2}	6610	30.82
	³ F ₁	33429	2.16		² K _{15/2}	27801	3.69
Gd ³⁺	⁶ P _{7/2}	32224	4.13	Tm ³⁺	³ H ₅	8390	27.25
	⁶ P _{5/2}	32766	2.33				
				Yb ³⁺	² F _{3/2}	10400	17.76

^aPrincipal $L-S$ state. ^bCalculated using parameters given in table 24.4. ^cResults are given for $P' > 1.5 \times 10^{-8}$ where $P_{\text{MD}} = P'n$ and $n = 1.33$ for dilute acid solutions.

TABLE 24.4.

Values of the Judd-Ofelt intensity parameters, Ω_λ , for the lanthanides in dilute acid solution^a.

R ³⁺	$\Omega_2(\text{cm}^2)$	$\Omega_4(\text{cm}^2)$	$\Omega_6(\text{cm}^2)$
Pr ^b	32.6×10^{-20}	5.7×10^{-20}	32.0×10^{-20}
Nd	0.93	5.00	7.91
Pm	2.80	2.52	4.20
Sm	0.91	4.13	2.70
Eu ^c	1.46	6.66	5.40
Gd	2.56	4.70	4.73
Tb	.004	7.19	3.45
Dy	1.50	3.44	3.46
Ho	0.36	3.14	3.07
Er	1.59	1.95	1.90
Tm	0.80	2.08	1.86
Yb	—	1.65	1.65

^aOriginal results from Carnall et al. (1968b).
^bFrom Carnall et al. (1965). ^cFor purposes of comparison with other members of the series, the parameters for Eu³⁺ were increased by a factor of 1.546. See Carnall et al. (1968b).

Conversion factors for the various parameterizations of the electric dipole oscillator strength are:

$$(a) \mathcal{T}_\lambda(\text{cm}) \text{ (Carnall et al., 1965)} = (2J + 1)cT_\lambda \text{ (Judd, 1962)}$$

$$(b) \Omega_\lambda(\text{cm}^2) \text{ (Axe, 1963)} = \left[\frac{8\pi^2 mc}{3h} \right]^{-1} \mathcal{T}_\lambda = (1.086 \times 10^{11})^{-1} \mathcal{T}_\lambda$$

Use of the parameters in table 24.4 is illustrated by the comparison of calculated and observed data for $\text{Tb}^{3+}(\text{aq})$ shown in table 24.5. It is evident that large variations in intensities between different groups are reproduced by the theory. Typically, several excited states are encompassed by a single complex absorption envelope, and the matrix elements of $U^{(\lambda)}$ are summed over these states. The energy in this case becomes that of the center of gravity of the envelope. While many transitions are weak, as judged from the magnitude of the corresponding matrix elements, the few transitions principally responsible for the intensity of a given band can be readily identified. At an earlier stage, this fact was the basis for the extensive use of intensity correlations as a means of making energy level assignments to solution spectra. It resulted in the first successful effort to derive a consistent set of free-ion energy level parameters including effective operators of configuration interaction for the whole series of trivalent lanthanide ions, as shown in table 24.2 (Carnall et al., 1968a).

TABLE 24.5.
Observed and calculated oscillator strengths for $\text{Tb}^{3+}(\text{aq})$.

SLJ ^a	Spectral range ^b (cm^{-1}) $\times 10^{-3}$	$P \times 10^6$	
		Expt.	Calc. ^c
7F_5	2.112	—	0.16 ^d 1.04 ^e
7F_4	3.370	—	1.54
7F_3	4.344	—	1.35
7F_2	5.028	—	0.98
7F_1	5.481	—	0.70
7F_0	5.703	—	0.28
5D_4	20–21.2	0.52	0.21
${}^5D_3, {}^5G_6, {}^5L_{10}$	25.9–27.6	8.46	{ 0.07 ^d 7.61 ^e
${}^5G_5, {}^5D_2, {}^5G_4, {}^5L_9$	27.6–28.95	7.46	7.61
${}^5G_3, {}^5L_8, {}^5L_7, {}^5L_6, {}^5G_2$	28.95–30.2	3.04	4.03
5D_1	30.4–30.9	0.37	0.32
${}^5D_0, {}^5H_7$	30.95–32.0	2.02	1.85
5H_6	32.5–33.5	1.20	1.41
5H_5	33.6–34.1	0.18	0.47
${}^5H_4, {}^5F_5, {}^5H_3, {}^5I_8, {}^5F_4$	34.4–35.8	5.05	5.32

^aThe principal L–S component(s) is shown. ^bThe calculated free-ion energy of the state is shown for the levels of the 7F -multiplet. For the observed bands, the range encompassed by the band group is noted. ^cCalculated using the parameters of table 24.4. ^dCalculated magnetic-dipole strength. ^eCalculated electric-dipole strength.

3.7. Use of intensity parameters to estimate oscillator strengths of infrared transitions

In addition to the use of intensity correlations as an aid in making energy level assignments, the parameters given in table 24.4 can be used to predict the oscillator strength associated with transitions that cannot be observed in aqueous solution. The results given for $\text{Tb}^{3+}(\text{aquo})$, table 24.5, illustrate this by the inclusion of calculated intensities associated with bands in the infrared region. In many cases such bands will be intense compared to those observed in the visible region and can be observed if an appropriate solvent is used. See section 2.2. While the energy of the center of gravity (free-ion level energy) is known for these infrared transitions, the band width, the complex structure, and the associated intensities are not known.

In order to emphasize the relative intensities of the infrared bands in R^{3+} spectra, a computer program was developed to calculate the molar absorptivity of a Gaussian curve of specified base energy interval, width at half-height, and area. The half-width was arbitrarily set at 50 cm^{-1} . The energy interval was taken as that observed for the corresponding R^{3+} bands observed in $\text{LiNO}_3\text{-KNO}_3$ eutectic at 150°C (Carnall et al., 1965), where possible. Otherwise an arbitrary scale based on the energy of the transition was used. The results are included as dashed line curves in figs. 24.4–24.12. The parameters used to compute the band areas for Pr^{3+} were those for Pr^{3+} in $\text{LiNO}_3\text{-KNO}_3$ eutectic (Carnall et al., 1965). For Pr^{3+} the band at $\sim 5000 \text{ cm}^{-1}$, fig. 24.4, encompasses two levels.

3.8. Hypersensitive transitions

The fact that the intensities of certain bands in the solution spectra of the trivalent lanthanides are remarkably sensitive to changes in the environment has been known for many years. For example, in an investigation of the effects of nitrate ion concentration on the spectra of a number of lanthanides, Selwood (1930) showed that relative to the other bands, one or two bands in the spectra of Nd^{3+} , Eu^{3+} , Ho^{3+} and Er^{3+} exhibited greatly increased intensities at high nitrate concentration compared to dilute solution. Such bands have subsequently been labeled "hypersensitive". These transitions follow electric quadrupole selection rules, $\Delta J \leq \pm 2$. Increases in oscillator strength by more than a factor of 3 are observed in some environments.

With the development of the Judd–Ofelt Theory, Judd (1962) pointed out that of the three parameters, T_1 , eq. (24.6), T_2 most closely monitors changes in the environment, and that hypersensitivity was strongly correlated with those transitions having large matrix elements of $U^{(2)}$. Jørgensen and Judd (1964) examined some of the potential mechanisms for hypersensitive transitions, discarding the possibility that they could exhibit electric quadrupole character. It was suggested that the origin might lie in an inhomogeneous dielectric. Subsequently Judd (1966b) pointed out that symmetry arguments could be introduced to classify site symmetries in which hypersensitivity might be in-

duced. Peacock (1975) has reviewed some of the arguments but no definitive interpretation has been offered. Hendrie et al. (1976) have discussed hypersensitivity in terms of a correlation which they found between oscillator strength and ligand basicity. The term "hypersensitive transitions" as used by the above authors and by Jørgensen and Judd (1964) refers to a limited clearly defined set of experimental observations. Unfortunately the term is occasionally used by other authors in a very broad, ill-defined manner.

4. Fluorescence spectra in solution

The existence of characteristic fluorescence spectra in aqueous solutions of the lanthanides was extensively reported in the early 1930's. Much of the data was qualitative, but a number of transitions were identified, and recent characterization of the energy level schemes involved makes possible considerable additional interpretation. The analytical potential of the fluorescence spectra was recognized and exploited at an early stage. More recent interest in fluorescence in solution derives in part from the ability to determine lifetimes of the fluorescing states and to use this as a basis for exploring excited state relaxation and energy transfer mechanisms. With laser excitation, micro to nanosecond lifetimes can be readily measured. Thus in contrast to absorption spectra where only shifts in band energy or changes in band shape can be correlated with changes in the ionic environment, fluorescence spectra investigations can also yield characteristic lifetimes of the relaxing states. It will be shown that such measurements provide a highly sensitive monitor of changing environment.

The forced-electric and magnetic dipole mechanisms discussed relative to the absorption of radiation are also primarily responsible for the radiative relaxation of excited states. Non-radiative relaxation, which usually competes strongly with the radiative mode, is under active investigation, and several different mechanisms have been discussed.

4.1. *Historical development*

It was pointed out at an early stage that those lanthanides that fluoresced in solid compounds at room temperature, also exhibited fluorescence in solution at approximately the same energy and with the same relative intensities (Tomaschek and Deutschbein, 1933; Deutschbein and Tomaschek, 1937). Maximum fluorescence yield was observed at the center of the series, Eu^{3+} , Gd^{3+} , Tb^{3+} , with intensity dropping rapidly at Sm^{3+} and Dy^{3+} (Tomaschek and Mehnert, 1937; Gobrecht, 1938), and transitions between a number of well characterized excited states and components of the ground term multiplet were identified (Zaidel, 1937). The particular sensitivity of both the intensity and energy of fluorescing transitions in Eu^{3+} to changes in the ionic environment was discussed by Tomaschek (1939, 1942). Deutschbein and Tomaschek (1937) attributed the

existence of structure in the weak ${}^5D_0 \rightarrow {}^5F_0$ transition in Eu^{3+} to the presence of multiple species of Eu^{3+} .

The analytical aspects of fluorescence spectra in lanthanide solutions were exploited by a number of groups to detect Ce^{3+} , Sm^{3+} , Gd^{3+} , Tb^{3+} , and Dy^{3+} as impurities in solutions of other lanthanides (Gobrecht and Tomaschek, 1937; Zaidel et al., 1938; Zaidel and Lavionov, 1939, 1943). Fassel and Heidel (1954) used the intense fluorescence of $\text{Tb}^{3+}(\text{aquo})$ as the basis for developing quantitative analytical procedures.

4.2. Relaxation of excited states in solution. General considerations

A great deal of progress has been made in analyzing the mechanisms of excited state relaxation of lanthanides in crystal hosts, ch. 35, and these concepts have also diffused into the literature on solutions. Two modes of relaxation can be recognized: radiative and non-radiative processes. Axe (1963) addressed the problem of expressing the radiative process in quantitative terms using the Judd-Ofelt theory. Non-radiative relaxation was already being formulated in terms of multiphonon processes in the early 1960's (Barasch and Dieke, 1965; Riseberg and Moos, 1968). Such processes become less probable as the energy gap between an excited state and the next lower energy state increases.

4.3. Radiative relaxation

In treating the fluorescence process, the Einstein coefficient, eq. (24.4) is used directly to express the rate of relaxation of an excited state (ψJ) to a particular final state ($\psi' J'$). Following Axe (1963), the counterpart of eq. (24.5) becomes

$$A(\psi J, \psi' J') = \frac{64\pi^4 \sigma^3}{3h(2J+1)} [\chi' \bar{F}^2 + n^3 \bar{M}^2] \quad (24.15)$$

where $\sigma(\text{cm}^{-1})$ represents the energy gap between states (ψJ) and ($\psi' J'$), $\chi' = n(n^2 + 2)^2/9$, and n is the refractive index of the medium. As in the absorption process, there is an implicit assumption that all (crystal-field) components of the initial state are equally populated. In principle, if fluorescence can be detected, the lifetime of the state is long compared to the rate at which it is populated in the excitation process, so thermal equilibrium at the temperature of the system can be achieved prior to emission.

The matrix elements of the electric and magnetic dipole operators, \bar{F}^2 and \bar{M}^2 , are identical to those in eq. (24.9) and eq. (24.11), respectively. However, the form of the refractive index correction in eq. (24.15) is not the same as for the absorption process, eq. (24.5). Equation (24.15) can be evaluated using parameters Ω_λ established from measurement of the absorption spectrum of the lanthanide ion in a solution identical to that studied in fluorescence.

Since excited state relaxation generally involves transitions to several lower-lying states, we define a total radiative relaxation rate, $A_T(\psi J)$

$$A_T(\psi J) = \sum_{\psi' J'} A(\psi J, \psi' J') \quad (24.16)$$

where the sum runs over all states lower in energy than the fluorescing state.

It is useful to define in addition the radiative branching ratio, β_R , from the relaxing state (ψJ) to a particular final state ($\psi' J'$):

$$\beta_R(\psi J, \psi' J') = \frac{A(\psi J, \psi' J')}{A_T(\psi J)} \quad (24.17)$$

and the radiative lifetime of a state

$$\tau_R(\psi J) = [A_T(\psi J)]^{-1} \quad (24.18)$$

The principal fluorescing states in aqueous solutions containing the lanthanide ions were identified in experimental investigations undertaken in the 1930's. Toward the beginning and end of the series, lifetimes were too short for fluorescence to be detected, but lines characteristic of Sm^{3+} , Eu^{3+} , Gd^{3+} , Tb^{3+} , and Dy^{3+} were discerned. Since the parameters, Ω_λ , have been determined for all the lanthanides in dilute acid solution, table 24.4, the total radiative lifetime of any excited state can be readily computed. The results shown in table 24.6 are in most cases for the resonance level which is the excited state which has the largest energy gap to the next lower state. As will be discussed in section 4.5, non-radiative relaxation is at a minimum in $\text{Gd}^{3+}(\text{aq})$ so that the measured lifetime of Gd^{3+} in H_2SO_4 ($\tau \approx \sim 2$ msec) (Kondrat'eva and Lazeeva, 1960), compares well with the calculated radiative lifetime of the state.

4.4. Non-radiative relaxation. General considerations

Although much is known about the non-radiative mechanisms of relaxation of fluorescing states in aqueous solution, there is presently no quantitative theory. Consequently, the symbolism used here follows that introduced in the study of the solid state where the theory has undergone more extensive development.

Since in the usual case both radiative and non-radiative processes operate to relax an excited state, we can express the total fluorescence lifetime of the state as

$$(\tau_T)^{-1} = A_T(\psi J) + W_T(\psi J) \quad (24.19)$$

TABLE 24.6.
Calculated radiative lifetimes of excited states of $\text{R}^{3+}(\text{aq})^a$.

Excited state ^b	Nd $^4\text{F}_{3/2}$	Pm $^5\text{F}_1$	Sm $^4\text{G}_{5/2}$	Eu $^5\text{D}_0$	Gd $^6\text{P}_{7/2}$	Tb $^5\text{D}_4$	Dy $^4\text{F}_{9/2}$	Ho $^5\text{S}_2$	Er $^4\text{S}_{3/2}$
Energy of excited state (cm^{-1})	11460	12400	17900	17277	32200	20500	21100	18500	18350
$\tau_R(\psi J)$ (msec)	0.42	0.65	6.26	9.67	10.9	9.02	1.85	0.37	0.66

^aThe total radiative (electric and magnetic dipole) lifetime, eq. (24.18), is given. The electric-dipole contribution was calculated from eq. (24.9) using values of Ω_λ given in table 24.4. ^bMajor component of the eigenvector is indicated.

where A_T is the radiative rate and $W_T(\psi J)$ is the sum of the rates of the various non-radiative processes. In crystalline hosts it has been shown that the dependence of the non-radiative rate on the energy gap (ΔE) between the excited level and the next lower-lying level is of the form:

$$W_T = Ce^{\alpha\Delta E} \quad (24.20)$$

where C and α are constants characteristic of a particular crystal (Riseberg and Moos, 1968). The relaxation mechanism is interpreted as a multiphonon process which becomes less probable as the number of phonons that must be simultaneously excited to conserve energy increases.

4.5. Multiphonon-like processes in solution

Investigations of the enhancement of the fluorescence yield of lanthanide ions in D_2O compared to H_2O provided the basis for extending the concepts of multiphonon relaxation to aqueous solutions. The H_2O - D_2O system was selected for fluorescence enhancement experiments since the substitution of D_2O for H_2O has been shown to exert no change in the absorption spectrum of a lanthanide ion (Kropp and Windsor, 1965; Gallagher, 1965; Borkowski et al., 1965). Such spectra are known to be sensitive to the effects of complexing by many different anionic species even in very dilute solutions (Kondrat'eva, 1960; Kondrat'eva and Lazeeva, 1960; Gallagher, 1964). Complexing measurably influences the radiative lifetime of the fluorescence. In contrast to the behavior reported for lanthanide ions, the spectra of a number of transition metal ions were displaced toward higher energies when H_2O was substituted for D_2O . The necessity for the isotopic substitution to take place in the inner coordination sphere to achieve an effect was noted (Halpern and Harkness, 1959; Bigeleisen, 1960).

In their pioneering work, Kropp and Windsor (1963, 1965, 1966) pointed out that the ratio of the intensity of fluorescence of a given R^{3+} state in D_2O to that of the same state in H_2O bore an inverse relation to the energy gap. This is illustrated in table 24.7 where the original data has been supplemented with similar results obtained later by others.

Kropp and Windsor (1965) concluded that quenching of fluorescence in aqueous solution occurred via $-OH$ coupled modes and that the rate was proportional to the number of such modes associated with the lanthanide ions. Gallagher (1965) found that the experimentally observed decay curves of the $Eu^{3+}(\text{aquo}) \ ^5D_0 \rightarrow \ ^7F_1$ emission as a function of increasing H_2O concentration in D_2O could be resolved into the sum of two exponentials. The results were interpreted as indicating that the introduction of a single OH group into the inner coordination sphere of Eu^{3+} was sufficient to reduce the fluorescence lifetime of the $\ ^5D_0$ state from 3.9 to 0.12 msec. Heller (1966) used the relative intensity of fluorescence in D_2O to H_2O , (I_D/I_H) as a function of $[H_2O]$ at low concentrations in D_2O to show that the rate determining step in the quenching of lanthanide fluorescence in H_2O was associated with transfer of energy to a single vibrational mode (OH) which is subsequently excited to high vibrational states. This

TABLE 24.7.
Fluorescence intensities and lifetimes of lanthanide excited states in H₂O
and D₂O.

	I_D/I_H^a	$\Delta E^b(\text{cm}^{-1})$	Lifetime ^c (msec)	
			$\tau_{\text{H}_2\text{O}}$	$\tau_{\text{D}_2\text{O}}$
Gd ³⁺	1.0 ± 0.2	32100	2 ^d (2.3) ^e	
Tb ³⁺	7.8 ± 0.8	14700	.39(.48) ^f	3.3(4.0) ^f
Eu ³⁺	18.0 ± 1.8	12300	.10(.12) ^f	1.9(4.0) ^f
Dy ³⁺	12 ± 3	7800	≤.003 ^f (.0023) ^e	.06 ^f (.038) ^e
Sm ³⁺	12 ± 6	7500	≤.003 ^f (.0022) ^e	.075 ^f (.053) ^e

^aSolutions were 0.1 M R(NO₃)₃ in H₂O or D₂O, and the intensity of fluorescence in D₂O was normalized to unity in H₂O in each case. ^b ΔE is the difference in energy between the excited (resonance) level and the next lower energy level. ^cThe results are from Kropp and Windsor (1965) except as indicated. ^dKondrat'eva and Lazeeva (1960). ^eStein and Würzburg (1975). ^fKazanskaya and Sveshnikova (1970).

was contrasted to possible alternative processes which would have involved either several different modes of a simple molecule or energy transfer to vibrational modes of several molecules. Haas and Stein (1971a) interpreted structure observed in Gd³⁺(aquo) as vibronic satellites due to coupling -OH or -OD to the 312 nm fluorescing state.

As pointed out by Heller (1966), the changes in the vibrational quantum numbers necessary to bridge the energy gaps already cited, using ν_1 (OH) = 3405 cm⁻¹ (O-H fundamental) and ν_1 (OD) = 2520 cm⁻¹ (Hornig et al., 1958), are as follows:

$\Delta E/\nu_1$	OH	OD
Gd ³⁺	10	13
Tb ³⁺	5	6
Eu ³⁺	4	5
Dy ³⁺	3	4
Sm ³⁺	3	4

Since the lifetimes associated with Sm³⁺(aquo) and Dy³⁺(aquo) were short, Stein and Würzburg (1975) give ~2 μ sec in each case, and other ions with $\Delta E < 6500$ cm⁻¹ (Pr³⁺, Nd³⁺, Ho³⁺, Er³⁺) barely fluoresce in H₂O or D₂O (Ermolaev and Sveshnikova, 1970), the results in solution appear to be comparable to those pointed out by Barasch and Dieke (1965) as characteristic of the LaCl₃ host. Fluorescence at room temperature was not observed from an excited state if the energy gap to the next lower level were <1000 cm⁻¹. Since the phonon density of states cuts off at ~260 cm⁻¹ in LaCl₃, this gap corresponds to an ~3 phonon emission process.

Similarly, at the other extreme, Kropp and Windsor (1965), pointed out that the gap in Gd³⁺ is so large that multiphonon-like relaxation is already a very high order (and thus low probability) process when the coordinating group is OH.

Substitution of D₂O therefore has no further detectable effect. Their computed value of τ_R based on integrated absorption measurements was 5.4 msec compared to a measured value of ~ 2 msec (Kondrat'eva and Lazeeva, 1960), and they concluded that non-radiative processes other than those associated with OH-modes must contribute to this relaxation process. The results in table 24.6 based on theory in section 3.4 suggest that the emission is consistent with a purely radiative relaxation mechanism.

4.6. *Other non-radiative relaxation mechanisms in solution*

Fluorescence yield studies have shown that mechanisms other than multiphonon-like processes can play an important part in the non-radiative relaxation of some states. For example, Kropp and Windsor (1965) pointed out that for Eu(NO₃)₃ in CH₃OH, only about one-half of the energy associated with the excited ⁵D₁ state is transferred to the lower ⁵D₀ state. The remainder is transferred to ground by other processes. This fast non-radiative decay of the ⁵D₁ state also accounts for the temperature dependent decrease in the lifetime of the ⁵D₀ state, since at higher temperature some thermal excitation to the ⁵D₁ from the ⁵D₀ state occurs, and the very rapid non-radiative decay associated with the ⁵D₁ state aids in the deactivation of the ⁵D₀ state (Kropp and Dawson, 1966).

It may be noted in passing that no quenching effect on fluorescence was attributable to dissolved O₂ in aqueous solution nor to the presence of I⁻ (Kropp and Windsor, 1965), but ion-ion interaction may be a mode of relaxation depending upon the energy level scheme. It can operate to deactivate the ⁵D₃ state in Tb³⁺ directly to the ⁷F-multiplet (Goldschmidt et al., 1975). Stein and Würzberg (1975) have also pointed out cases where radiationless relaxation occurs by modes other than those associated with multiphonon-like processes and have made approximate calculations.

4.7. *Theoretical models for radiationless relaxation of excited states in solution*

In their discussion of the rates of non-radiative energy transfer in molecules (Robinson and Frosch, 1963) pointed out that large isotope effects may arise in solution where significant amounts of electronic energy are converted into vibrational modes in the system. This motivated some of the earlier investigations of lanthanides in H₂O-D₂O systems. More recently Siebrand (1967) carried out an extensive investigation of the Franck-Condon factors that are part of the Robinson and Frosch theory and obtained the expression:

$$W_{AB} = (2\pi\rho_E/\hbar)J^2F \quad (24.21)$$

where W is the radiationless transition probability per unit time, ρ_E is the density of final states within which vibrational deactivation is rapid relative to any electronic relaxation, J is Siebrand's electronic transition matrix element between the initial (A) and final (B) states, and F is the Franck-Condon factor. If it is assumed that changes in the radiationless rate constant are due primarily to F ,

that is, that ρ_E and J are effectively constant, then it can be shown that $F(E)$, for small values of the energy gap E , varies essentially exponentially with the order of the vibrational process (Henry and Kasha, 1968). Bodunov and Sveshnikova (1974) reached the same conclusion with respect to the exponential dependence of W_{AB} on the order of the process based on modeling the intramolecular vibrations of H_2O by Morse oscillators. Thus for R^{3+} (aquo) ions, a multiphonon-like process similar in form to that given by Riseberg and Moos (1968) for crystals, eq. (24.20), is an important relaxation mode.

Haas and Stein (1972) using the Siebrand model and spectroscopic results for Gd^{3+} (aquo), calculated non-radiative relaxation rates for different order processes, and compared them with rates determined experimentally for several lanthanide ions. There was good correlation in the magnitude of change with the order of the process, but quantitative agreement was not achieved. Sveshnikova and Ermolaev (1971) used a dipole-dipole interaction approximation to compute rate constants for non-radiative relaxation, but the correlation with experimental results was poor.

Further development of theoretical models that can be used to interpret non-radiative relaxation processes in solution in greater detail is certain to be fruitful. At present a basic result obtained is that multiphonon-like processes of order greater than 5 or 6 cannot compete effectively with radiative modes of relaxation.

4.8. *Hydration and coordination numbers of R^{3+} (aquo). Application of fluorescence lifetime measurements*

When a cation such as R^{3+} is thrust into aqueous solution, the bulk structure is modified and two different regions about the ion can be arbitrarily defined. Region A: The H_2O molecules in the direct vicinity of the ion constitute the primary (inner) coordination sphere, and there is a kinetic distinction between these molecules and those in the bulk solvent (Hindman and Sullivan, 1971). The number of molecules in this sphere is the coordination number. Region B: Extending beyond the first region is a second (outer) shell which contains H_2O molecules that are not in contact with the central ion. They interact with the inner sphere, and consequently this region has a structure that is different from that of the bulk solvent. The extent of the outer shell is defined by the measurable effect it has on processes occurring in solution (Rosseinsky, 1965; Entelis and Tiger, 1976).

As Spedding et al. (1974) pointed out, the increase in charge density on the surface of a lanthanide ion as the ionic radius decreases, results in an increase in the total extent of hydration (Regions A and B) with atomic number. This is consistent with trends in conductivity and viscosity measurements. Choppin and Grafeo (1965) estimated hydration numbers from conductance data obtaining 12.8 ± 0.1 for La^{3+} – Nd^{3+} , 13.1 – 13.4 for Sm^{3+} – Gd^{3+} , and 13.9 ± 0.1 for Dy^{3+} – Yb^{3+} .

Since the coordination number of a lanthanide ion can only be accurately defined with respect to a crystal lattice, the concept must remain approximate

when applied to solutions. Nevertheless, a number of estimates have been made, and conflicting viewpoints exist as to whether or not there is a change in coordination number across the series. Undoubtedly part of the problem lies in the interpretation given to different experiments. Karraker (1970) found the spectra of Nd^{3+} in dilute solutions and in crystalline $\text{Nd}(\text{BrO}_3)_3 \cdot 9\text{H}_2\text{O}$ to be very similar and took this as evidence supported by other measurements for the coordination number of 9 in $\text{Nd}^{3+}(\text{aq})$. Geier et al. (1969) and Reuben and Fiat (1969a,b) interpreted their spectroscopic and NMR results, respectively, as indicating that the coordination number (probably 9), is constant in dilute solution. Hinchley and Cobble (1970) found no evidence for a change in coordination number over the series from their correlation between ionic entropy and radius. This was in contrast to the conclusions of a similar study by Bertha and Choppin (1969).

More recently Spedding et al. (1974), Habenschuss and Spedding (1974), and Rard and Spedding (1974) have summarized evidence based on X-ray as well as a number of different thermodynamic studies supporting the position that there is a change in coordination number of $\text{R}^{3+}(\text{aq})$ across the series. The hydrated lanthanide ions in dilute solution exhibit a coordination number of 9 from La^{3+} to Nd^{3+} , and 8 from Tb^{3+} to Yb^{3+} . The intermediate ions presumably exhibit a mixture of these coordination numbers.

Insight into the nature of the coordination sphere in $\text{R}^{3+}(\text{aq})$ was obtained by Kropp and Windsor (1967) from fluorescence lifetime studies. The addition of acetate ion (Ac^-) to solutions of EuCl_3 or TbCl_3 in H_2O increases both the total fluorescence intensity and the lifetime of the fluorescing states. In contrast, the lifetimes decrease in D_2O with increasing $[\text{Ac}^-]$. Comparison of the rates of relaxation in H_2O and D_2O made it possible to determine the radiative rate constant for fluorescence emission which could be related to the fraction of the hydration shell not replaced by Ac^- , m/m_s , as a function of $[\text{Ac}^-]$. The variation of m/m_s with $[\text{Ac}^-]$ was compared to data on Ac^- complexing of R^{3+} obtained by Sonesson (1958), and this resulted in the relationship $m_s/n = 6$ where m_s is the hydration number for pure H_2O and n is the number of H_2O molecules replaced by each Ac^- . If n is assumed to be 2, the resulting hydration number of 12 is near the value estimated by Choppin and Graffeo (1965) from conductance measurements. A similar experiment in which the fluorescence lifetime of the $^5\text{D}_0$ state of Eu^{3+} was monitored in $\text{H}_2\text{O}-\text{CH}_3\text{CN}$ mixtures was interpreted by Haas and Stein (1971b) in terms of a step-wise quenching mechanism. By comparing the bimolecular rate constant for quenching due to one molecule of H_2O , (1100 sec^{-1}) as determined from quantum yield and total fluorescence lifetime data, with the total quenching rate constant in aqueous solution (9800 sec^{-1}), it appears that formally, only 9 molecules of H_2O participate in the quenching process in aqueous solution. This is close to the expected coordination number for $\text{Eu}^{3+}(\text{aq})$, but should be taken as the effective number for the $^5\text{D}_0$ excited state.

5. Oxidation states of the lanthanides observed in dilute aqueous solution

5.1. Standard oxidation potentials

Standard oxidation potentials referred to the normal hydrogen electrode (E°) for the divalent and trivalent lanthanide aquo ions are given in table 24.8 based primarily on the selected experimental results compiled by Charlot et al. (1971) and the systematic correlations summarized by Nugent (1975). Only Eu^{2+} and Yb^{2+} can persist for times of the order of minutes to hours in dilute acid solution, and can be readily produced by reduction of the trivalent ionic species (Laitinen and Taebel, 1941; Laitinen, 1942; Christensen et al., 1973). The value of $E^\circ = -0.43$ V for the $\text{Eu}(\text{II-III})$ couple quoted in many previous compilations was obtained using both potentiometric and polarographic techniques. However, in a reevaluation of the solution thermodynamic properties of europium, Morss and Haug (1973) recommended the value $E^\circ = -0.35$ V.

The III-IV potentials of both Pr and Tb were placed in the $+(3.3-3.4)$ V range by Nugent et al. (1973) based on correlations between E° and observed spectroscopic properties, as well as by use of Jørgensen's refined electron spin-pairing theory. However, the reported oxidation of Pr III to Pr IV by the OH radical during pulse radiolysis experiments, section 5.2, suggests that the esti-

TABLE 24.8.
Standard oxidation potentials (relative to the standard
hydrogen electrode).^a

	II-III Potential ^b $E_{298\text{K}}^\circ$ (volts)	III-IV Potential ^b $E_{298\text{K}}^\circ$ (volts)
Ce	-3.2	1.70 ^c , 1.74
Pr	-2.7	ca. 2.9 ^d , 3.4
Nd	-2.6	4.6
Pm	-2.6	4.9
Sm	-1.56 ^e	5.2
Eu	-0.35 ^e	6.4
Gd	-3.9	7.9
Tb	-3.7	3.3
Dy	-2.6	5.0
Ho	-2.9	6.2
Er	-3.1	6.1
Tm	-2.3	6.1
Yb	-1.15 ^f	7.1

^aThe 1969 IUPAC sign convention is used. The greater the positive potential, the more stable the reduced form. ^bExcept where specifically cited, the values shown were calculated or derived from spectrophotometric data by Nugent et al. (1973). ^cCharlot et al. (1971). ^dEyring et al. (1952). ^eMorss and Haug (1973). ^fLaitinen (1942).

mated (III–IV) potentials previously cited may be too high. At pH ~ 6 , the oxidizing potential of the OH radical would be estimated to be only ~ 2.4 V (Henglein, 1974). Jørgensen (1976) has pointed out that the calculated III–IV potentials refer to the formation of a hypothetical highly acid R(IV) aquo ion. It can be argued that at pH ≥ 5 , a much more stable species $R(OH)^{3+}$ or $R(OH)_2^{2+}$ may be formed. In this case the E° value would be less positive than that predicted. Results of pulse radiolysis experiments with Gd^{3+} and Ho^{3+} quoted in section 5.2 indicate that the II–III oxidation potentials of these ions lie in the range ca. $-(2.3-2.8$ V).

5.2. Production of unusual oxidation states in solution by pulse radiolysis

One of the most powerful techniques of radiation chemistry is pulse radiolysis. Accelerators capable of producing electron pulses on the micro to nanosecond time scale are now in wide-spread use and provide a unique means for studying oxidation-reduction reactions in aqueous solution. The interaction of high energy electrons with H_2O results in the net ionization reaction $2H_2O \rightarrow H_3O^+ + OH + e_{aq}^-$ which is complete in $\approx 10^{-11}$ sec. Since the hydrated electron, e_{aq}^- and the OH-radical represent, respectively, an extremely strong reducing/oxidizing agent, unusual reactions can be induced. By the addition of a suitable scavenger to the system, it is possible to selectively study the reaction of either e_{aq}^- or OH with solute species. For example, H_2 rapidly converts the OH-radical to e_{aq}^- by the reactions $OH + H_2 \rightarrow H_2O + H$, $H + OH^- \rightleftharpoons e_{aq}^-$.

The potentials associated with the redox reactions of $R^{3+}(\text{aquo})$ span a wide range, table 24.8, and characteristic absorption spectra are obtained for the various oxidation states. As a consequence, this represents an interesting area for pulse radiolysis studies. Hart and Anbar (1960) give $E^\circ = 2.77$ V for the reaction $e_{aq}^- + H^+ \rightarrow 1/2 H_2$. Based on the reaction $Cu II + OH \rightarrow Cu III$ (Baxendale et al., 1965) and the calculations of Henglein (1974), a standard oxidizing potential, E° , of the order of 2 V may be associated with the OH radical. Reaction products with e_{aq}^- or OH frequently have only a transient existence, but recent developments permit recording time-resolved spectra on the nanosecond time scale (Schmidt et al., 1976).

The spectra of Sm^{2+} , Eu^{2+} , and Yb^{2+} in good agreement with fig. 24.16 have been obtained by several groups on the reduction of $R^{3+}(\text{aquo})$ with e_{aq}^- (Gordon, 1965; Faraggi and Tendler, 1972; and Pikaev, 1974). Pikaev et al. (1973) have also reported the reduction of Tm to the divalent state (pH 3–6) with a characteristic band at 280 nm ($\epsilon_{max} \sim 750 M^{-1} sec^{-1}$). Both Faraggi and Feder (1972) and Pikaev et al. (1973) report the successful oxidation of Pr III to Pr IV on reaction with OH radicals. A characteristic intense absorption band was observed at 290 nm. Based on the trends in the potentials estimated by Nugent (1975), if the $OH + Pr^{3+} \rightarrow Pr^{4+}$ reaction can occur, then it should be possible to obtain Tb^{4+} under similar conditions.

Tendler and Faraggi (1972) used the pulse radiolysis technique to produce $R^{2+}(\text{aquo})$, and studied the rate of oxidation of $R^{2+}(\text{aquo})$ by NO_2^- . The results

were interpreted in terms of an outer sphere electron transfer mechanism and used to compute E° for the R^{2+}/R^{3+} couple, but the values obtained are much too low. They also suggest an essentially constant (II-III) potential across the series except for those couples that have been measured. This was not confirmed by the results cited below, nor is it consistent with spectroscopic correlations (Nugent et al., 1973).

Recently Gordon et al. (1976) reexamined the reaction of e_{aq}^- with $R^{3+}(\text{aquo})$ in a study which included all of the lanthanides. Their rate constant data could be used to divide the series into three groups in terms of reactivity: (1) readily reduced ions Sm, Eu, Yb with rate constants in the range of $10^{10} \text{ M}^{-1} \text{ sec}^{-1}$, (2) an intermediate group, Gd, Ho, Er, and Tm, with rate constants (10^7 – 10^8), and (3) a relatively unreactive group, Pr, Nd, Dy, Tb, and Lu with rate constants $\leq 10^6$. Using streak camera techniques they obtained the first spectroscopic evidence for Gd^{2+} and Ho^{2+} , fig. 24.18.

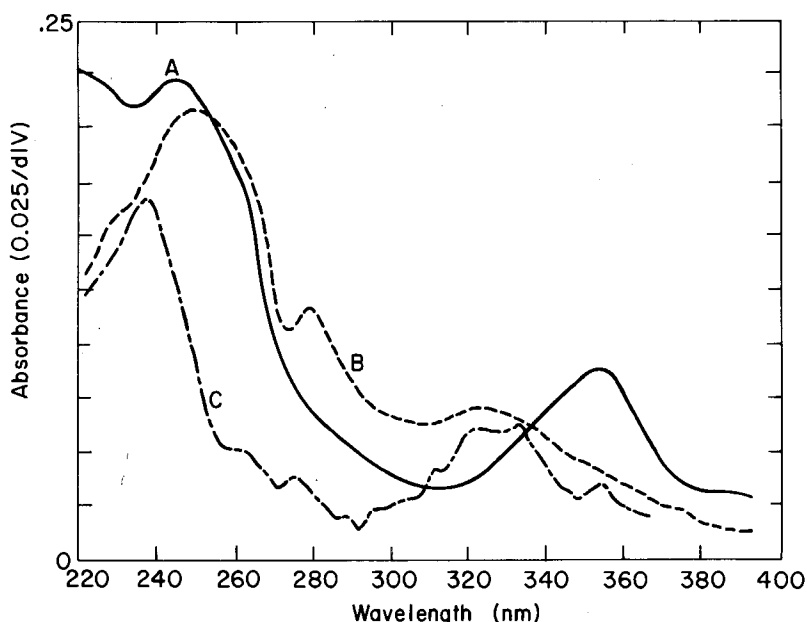


Fig. 24.18. Absorption spectra obtained by pulse radiolysis of lanthanide solutions. (A) Tm^{2+} , (B) Gd^{2+} , (C) Ho^{2+} , from Gordon et al. (1976).

References

- Axe, J.D., 1963, *J. Chem. Phys.* **39**, 1154.
 Banks, C.V. and D.W. Klingman, 1956, *Anal. Chim. Acta* **15**, 356.
 Banks, C.V., M.R. Heusinkveld, J.W. O'Laughlin, 1961, *Anal. Chem.* **33**, 1235.
 Barasch, G.E. and G.H. Dieke, 1965, *J. Chem. Phys.* **43**, 988.
 Baxendale, J.H., E.M. Fielden, and J.P. Keene, 1965, Formation of CuIII in the Radiolysis of Cu^{2+} Solutions, in: A.J. Swallow and J.H. Baxendale, eds., *Pulse Radiolysis*, (Academic Press, London), p. 217.
 Bertha, S.L. and G.R. Choppin, 1969, *Inorg. Chem.* **8**, 613.

- Bethe, H.A. and F.H. Spedding, 1937, *Phys. Rev.* **52**, 454.
- Bigeleisen, J., 1960, *J. Chem. Phys.* **32**, 1583.
- Bodunov, E.N. and E.B. Sveshnikova, 1974, *Opt. Spectrosc.* **36**, 196.
- Borkowski, R., H. Forest, and D. Grafstein, 1965, *J. Chem. Phys.* **42**, 2974.
- Brewer, L., 1971a, *J. Opt. Soc. Am.* **61**, 1101.
- Brewer, L., 1971b, *J. Opt. Soc. Am.* **61**, 1666.
- Broer, L.J.F., C.J. Gorter, and J. Hoogschagen, 1945, *Physica* **11**, 231.
- Butement, F.D.S., and H. Terrey, 1937, *J. Chem. Soc.*, 1112.
- Butement, F.D.S., 1948, *Trans. Faraday Soc.* **44**, 617.
- Carnall, W.T., 1962, *Anal. Chem.* **34**, 786.
- Carnall, W.T., D.M. Gruen, and R.L. McBeth, 1962, *J. Phys. Chem.* **66**, 2159.
- Carnall, W.T., 1963, *J. Phys. Chem.* **67**, 1206.
- Carnall, W.T., P.R. Fields and G.E. Toogood, 1964, *J. Phys. Chem.* **68**, 2351.
- Carnall, W.T., P.R. Fields, and B.G. Wybourne, 1965, *J. Chem. Phys.* **42**, 3797.
- Carnall, W.T., P.R. Fields, and K. Rajnak, 1968a, *J. Chem. Phys.* **49**, 4424, 4443, 4447, 4450.
- Carnall, W.T., P.R. Fields and K. Rajnak, 1968b, *J. Chem. Phys.* **49**, 4412.
- Carnall, W.T., 1974, Recent Developments in the Interpretation of Trivalent Lanthanide and Actinide Absorption Spectra, in: Trzebiatowska, B.J. and M. Rudolf, eds., Section Lectures of the Thirteenth International Conference on Coordination Chemistry, Polish Academy of Sciences, Warsaw, p. 89.
- Carnall, W.T., H. Crosswhite, H.M. Crosswhite, and J.G. Conway, 1976, *J. Chem. Phys.* **64**, 3582.
- Charlot, G., A. Collumeau, and M.J.C. Marchon, 1971, Selected Constants. Oxidation-Reduction Potentials of Inorganic Substances in Aqueous Solution, I.U.P.A.C., (Butterworths, London).
- Choppin, G.R. and A.J. Graffeo, 1965, *Inorg. Chem.* **4**, 1254.
- Christensen, R.J., J.H. Espenson, and A.B. Butcher, 1973, *Inorg. Chem.* **12**, 564.
- Condon, E.U. and G.H. Shortley, 1957, *The Theory of Atomic Spectra*, (Cambridge Univ. Press, London) pp. 91-109.
- Crosswhite, H.M., H. Crosswhite, and W.T. Carnall, 1975, Atomic Electronic Parameters Derived from Lanthanide and Actinide Crystal Spectra, in: Abstracts of the Atomic Spectroscopy Symposium, National Bureau of Standards, Gaithersburg, Md.
- Crosswhite, H.M., H. Crosswhite, F.W. Kaseta, and R. Sarup, 1976, *J. Chem. Phys.* **64**, 1981.
- Crosswhite, H.M. and R.D. Cowan, 1976, private communication.
- Deutschbein, O. and R. Tomaschek, 1937, *Ann. Physik.* **29**, 311.
- Dieke, G.H., 1968, Spectra and Energy Levels of Rare Earth Ions in Crystals, H.M. Crosswhite and H. Crosswhite, eds., (Wiley, New York).
- Entelis, S.D. and R.P. Tiger, 1976, *Reaction Kinetics in the Liquid Phase*. (Wiley, New York), p. 71.
- Ermolaev, V.L. and E.B. Sveshnikova, 1970, *Opt. Spectry.* **28**, 98.
- Eyring, L., H.L. Lohr, and B.B. Cunningham, 1952, *J. Am. Chem. Soc.* **74**, 1186.
- Faraggi, M. and Y. Tendler, 1972, *J. Chem. Phys.* **56**, 3287.
- Faraggi, M. and A. Feder, 1972, *J. Chem. Phys.* **56**, 3294.
- Fassel, V.A. and R.H. Heidel, 1954, *Anal. Chem.* **26**, 1134.
- Franzen, P., J.P.M. Woudenberg, and C.J. Gorter, 1943, *Physica* **10**, 365.
- Freed, S., 1931, *Phys. Rev.* **38**, 2122.
- Freed, S. and S.I. Weissman, 1938, *J. Chem. Phys.* **6**, 297.
- Freed, S., 1942, *Rev. Mod. Phys.* **14**, 105.
- Freed, S. and C.J. Hochanadel, 1950, *J. Chem. Phys.* **18**, 780.
- Freymann, R. and S. Takvorian, 1932, *Compt. Rend.* **194**, 963.
- Gallagher, P.K., 1964, *J. Chem. Phys.* **41**, 3061.
- Gallagher, P.K., 1965, *J. Chem. Phys.* **43**, 1742.
- Geier, G., U. Karlen, and A. v. Zelewsky, 1969, *Helv. Chem. Acta* **52**, 1967.
- Gobrecht, H. and R. Tomaschek, 1937, *Ann. Physik.* **29**, 324.
- Gobrecht, H., 1938, *Ann. d. Phys.* **31**, 181.
- Goldschmidt, R., G. Stein, and E. Würzberg, 1975, *Chem. Phys. Ltrs.* **34**, 408.
- Gordon, S., 1965, in: A.J. Swallow and J.H. Baxendale, eds., *Pulse Radiolysis*, (Academic Press, London) p. 285.
- Gordon, S., J.C. Sullivan, W.A. Mulac, D. Cohen, and K.H. Schmidt, 1976, Pulse Radiolysis of the Lanthanide and Actinide Elements, in: Proc. Fourth Symposium on Radiation Chemistry, Keszthely, Hungary.
- Gruber, J.B. and J.G. Conway, 1960, *J. Inorg. Nucl. Chem.* **14**, 303.
- Haas, Y. and G. Stein, 1971a, *Chem. Phys. Ltrs.* **11**, 143.
- Haas, Y. and G. Stein, 1971b, *J. Phys. Chem.* **75**, 3677.
- Haas, Y. and G. Stein, 1972, *Chem. Phys. Ltrs.* **15**, 12.
- Haas, Y., G. Stein, and E. Würzberg, 1973, *J. Chem. Phys.* **58**, 2777.
- Habenschuss, A. and F.H. Spedding, 1974, A Survey of Some Properties of Aqueous Rare Earth Salt Solutions. I. Volume, Thermal Expansion, Raman Spectra, and X-ray Diffraction, in: J.H. Haschke and H.A. Eick, eds., *Proceedings of the 11th Rare Earth Research Conference*, (Tech. Inform. Center, Oak Ridge, Tenn.) p. 909.
- Halpern, J. and A.C. Harkness, 1959, *J. Chem. Phys.* **31**, 1147.
- Hart, E.J. and M. Anbar, 1970, *The Hydrated Electron*, (Wiley-Interscience, N.Y.) p. 102 and 255.
- Heller, A., 1966, *J. Am. Chem. Soc.* **88**, 2058.
- Heller, A., 1968, *J. Mol. Spectro.* **28**, 208.
- Hendrie, D.E., R.L. Fellows, and G.R. Choppin, 1976, *Coord. Chem. Rev.* **18**, 199.

- Henglein, A., 1974, *Ber. Bunsen-ges. für Physikal. Chemie*, **78**, 1078.
- Henry, B.R. and M. Kasha, 1968, *Ann. Rev. Phys. Chem.* **19**, 161.
- Hinchley, R.J. and J.W. Cobble, 1970, *Inorg. Chem.* **9**, 917.
- Hindman, J.C. and J.C. Sullivan, 1971, *Principles and Methods for the Study of Metal Complex Ion Equilibrium*, in: Martell, A.E. ed., *Coordination Chemistry*, Vol. 1, ACS Monograph 168, (Van Nostrand Reinhold, N.Y.), Chapter 7.
- Holleck, L. and C. Hartinger, 1955, *Angew. Chemie*, **67**, 648.
- Hoogschagen, J., A.P. Snoek, and C.J. Gorter, 1943, *Physica* **10**, 693.
- Hoogschagen, J., 1946, *Physica* **11**, 513.
- Hoogschagen, J., A.P. Snoek, and C.J. Gorter, 1946, *Physica* **11**, 518.
- Hoogschagen, J., Th. G. Scholte, and S. Kruyer, 1946, *Physica* **11**, 504.
- Hoogschagen, J. and C.J. Gorter, 1948, *Physica* **14**, 197.
- Hornig, D.F., H.F. White, and F.P. Redding, 1958, *Spectrochim. Acta* **12**, 338.
- Johnson, K.E. and J.N. Sandoe, 1968, *Can. J. Chem.* **46**, 3457.
- Jørgensen, C.K., 1955, *Dan. Mat. Fys. Medd.* **29**, No. 11.
- Jørgensen, C.K. and J.S. Brinen, 1963, *Mol. Phys.* **6**, 629.
- Jørgensen, C.K., 1969, *Oxidation Numbers and Oxidation States*, (Springer-Verlag, Berlin).
- Jørgensen, C.K., 1973, *Struct. Bonding* **13**, 199.
- Jørgensen, C.K. and B.R. Judd, 1964, *Mol. Phys.* **8**, 281.
- Jørgensen, C.K., 1976, Private communication.
- Judd, B.R., 1962, *Phys. Rev.* **127**, 750.
- Judd, B.R., 1963, *Operator Techniques in Atomic Spectroscopy*, (McGraw-Hill, N.Y.).
- Judd, B.R., 1966a, *Phys. Rev.* **141**, 4.
- Judd, B.R., 1966b, *J. Chem. Phys.* **44**, 839.
- Judd, B.R., H.M. Crosswhite, and H. Crosswhite, 1968, *Phys. Rev.* **169**, 130.
- Karraker, D.G., 1970, *J. Chem. Ed.* **47**, 424.
- Kazanskaya, N.A. and E.B. Sveshnikova, 1970, *Opt. Spectry.* **28**, 376.
- Kondrat'eva, E.V., 1960, *Opt. Spectry.* **8**, 66.
- Kondrat'eva, E.V. and G.S. Lazeeva, 1960, *Opt. Spectry.* **8**, 67.
- Kropp, J.L. and M.W. Windsor, 1963, *J. Chem. Phys.* **39**, 2769.
- Kropp, J.L. and M.W. Windsor, 1965, *J. Chem. Phys.* **42**, 1599.
- Kropp, J.L. and W.R. Dawson, 1966, *J. Chem. Phys.* **45**, 2419.
- Kropp, J.L. and M.W. Windsor, 1966, *J. Chem. Phys.* **45**, 761.
- Kropp, J.L. and M.W. Windsor, 1967, *J. Phys. Chem.* **71**, 477.
- Laitinen, H.A. and W.A. Taebel, 1941, *Ind. Eng. Chem., Anal. Ed.* **13**, 825.
- Laitinen, H.A., 1942, *J. Am. Chem. Soc.* **64**, 1133.
- Lang, R.J., 1936, *Can. J. Research* **14A**, 127.
- Lange, H., 1938, *Ann. d. Phys.* **31**, 609.
- Lewis, W.B., J.B. Mann, D.A. Liberman, D.T. Cromer, 1970, *J. Chem. Phys.* **53**, 809.
- Main-Smith, J.D., 1927, *Nature* **120**, 583.
- Mamiya, M., 1965, *Bull. Chem. Soc. Japan* **38**, 178.
- Martin, W.C., 1971, *J. Opt. Soc. Am.* **61**, 1682.
- Moeller, T. and J.C. Brantley, 1950, *Anal. Chem.* **22**, 433.
- Morrison, J.C. and K. Rajnak, 1971, *Phys. Rev.* **A4**, 536.
- Morss, L.R. and H.O. Haug, 1973, *J. Chem. Thermodyn.* **5**, 513.
- Mukherji, P.C., 1936, *Indian J. Phys.* **10**, 319.
- Newman, D.J. and C.D. Taylor, 1971, *J. Phys.* **B 4**, 241.
- Newman, D.J. and C.D. Taylor, 1972, *J. Phys.* **B 5**, 2332.
- Nielson, C.W. and G.F. Koster, 1963, *Spectroscopic Coefficients for pⁿ, dⁿ, and fⁿ Configurations*, (M.I.T. Press, Cambridge).
- Nugent, L.J. and K.L. VanderSluis, 1971, *J. Opt. Soc. Am.* **61**, 1112.
- Nugent, L.J., R.D. Baybarz, J.L. Burnett, J.L. Ryan, 1973, *J. Phys. Chem.* **77**, 1528.
- Nugent, L.J., 1975, *Chemical Oxidation States of the Lanthanides and Actinides*, in: Bagnall, K.W., ed., *International Review of Science, Inorganic Chemistry Series Two*, Vol. 7, (University Park Press, Baltimore), Chapter 6.
- Ofelt, G.S., 1962, *J. Chem. Phys.* **37**, 511.
- Peacock, R.D., 1975, *Struct. Bonding* **22**, 83.
- Pikaev, A.K., G.K. Sibirskaia, V.I. Spitsyn, 1973, *Dokl. Akad. Nauk SSSR*, **209**, 1154.
- Pikaev, A.K., 1974, *Rad. Res. Reviews* **5**, 177.
- Prandtl, W. and K. Scheiner, 1934, *Zeit. Anorg. Allgem. Chem.* **220**, 107.
- Rajnak, K. and B.G. Wybourne, 1963, *Phys. Rev.* **132**, 280.
- Rard, J.A. and F.H. Spedding, 1974, *A Survey of Some Properties of Aqueous Rare Earth Salt Solutions. II. Heats of Dilution, Heat Capacities, Activity Coefficients, Electrical Conductances, and Relative Viscosities*, in: J.H. Haschke and H.A. Eick, eds., *Proceedings of the 11th Rare Earth Research Conference*, (Tech. Inform. Center, Oak Ridge, Tenn.) p. 919.
- Reuben, J. and D. Fiat, 1969a, *J. Chem. Phys.* **51**, 4909.
- Reuben, J. and D. Fiat, 1969b, *J. Chem. Phys.* **51**, 4918.
- Riseberg, L.A. and H.W. Moos, 1968, *Phys. Rev.* **174**, 429.
- Robinson, G.W. and R.P. Frosch, 1963, *J. Chem. Phys.* **38**, 1187.
- Rosseinsky, D.R., 1965, *Chem. Rev.* **65**, 467.
- Ryan, J.L. and C.K. Jørgensen, 1966, *J. Phys. Chem.* **70**, 2845.
- Satten, R.A., 1953, *J. Chem. Phys.* **21**, 637.
- Sayre, E.V., D.G. Miller, and S. Freed, 1957, *J. Chem. Phys.* **26**, 109.
- Schmidt, K.H., S. Gordon, and W.A. Mulac, 1976, *Rev. Sci. Instrum.* **47**, 356.
- Selwood, P.W., 1930, *J. Am. Chem. Soc.* **52**, 4308.
- Siebrand, W., 1967, *J. Chem. Phys.* **46**, 440.

- Sonesson, A., 1958, *Acta Chem. Scand.* **12**, 165, 1937.
- Spedding, F.H., 1940, *Phys. Rev.* **58**, 255.
- Spedding, F.H., P.F. Cullen, and A. Habenschuss, 1974, *J. Phys. Chem.* **78**, 1106.
- Stein, G. and E. Würzberg, 1975, *J. Chem. Phys.* **62**, 208.
- Stewart, D.C., 1959, *Absorption Spectra of Lanthanide Rare Earths*, in: Pascal, P. ed., *Nouveau Traité de Chimie Minerale*, Vol. 7, Part II, (Masson et C^{ie}, Paris), p. 1201.
- Sveshnikova, E.B. and V.L. Ermolaev, 1971, *Opt. Spectry.* **30**, 208.
- Tendler, Y. and M. Faraggi, 1972, *J. Chem. Phys.* **57**, 1358.
- Tomaschek, R., 1932, *Physik. Zeitschr.* **33**, 878.
- Tomaschek, R. and O. Deutschbein, 1933, *Physik. Zeitschr.* **34**, 374.
- Tomaschek, R. and E. Mehnert, 1937, *Ann. Phys.* **29**, 306.
- Tomaschek, R., 1939, *Faraday Soc. Trans.* **35**, 148.
- Tomaschek, R., 1942, *Ergeb. exakt. Naturwiss.* **20**, 268.
- Trees, R.E., 1964, *J. Opt. Soc. Am.* **54**, 651.
- Van Vleck, J.H., 1937, *J. Phys. Chem.* **41**, 67.
- Woudenberg, J.P.M., 1942a, *Physica* **9**, 217.
- Woudenberg, J.P.M., 1942b, *Physica* **9**, 936.
- Wybourne, B.G., 1965, *Spectroscopic Properties of Rare Earths*, (Wiley, N.Y.).
- Young, J.P. and J.C. White, 1960a, *Anal. Chem.* **32**, 799.
- Young, J.P. and J.C. White, 1960b, *Anal. Chem.* **32**, 1658.
- Zaidel, A.N., 1937, *Nature*, **139**, 248.
- Zaidel, A.N., Ya. I. Larionov, and A.N. Filipov, 1938, *J. Gen. Chem. (USSR)* **8**, 943.
- Zaidel, A.N. and Ya. I. Larionov, 1939, *Uspekki Fiz. Nauk* **21**, 211.
- Zaidel, A.N. and Ya.I. Larionov, 1943, *Trudy Vsesoyuz. Konferentsii Anal. Khim.* **2**, 615.

Chapter 25

COMPLEXES

Larry C. THOMPSON

Department of Chemistry, University of Minnesota, Duluth, MN 55812,
USA

Contents

1. Introduction	210
2. Complex formation	213
2.1. Properties of the rare earth ions	213
2.2. Types of donor atoms	215
2.3. Nature of rare earth-ligand bonding	216
2.4. Relationship of scandium to the other rare earths	218
3. Coordination numbers	219
3.1. Factors affecting coordination numbers and coordination polyhedra	219
3.2. Coordination number 3	221
3.3. Coordination number 4	222
3.4. Coordination number 5	223
3.5. Coordination number 6	224
3.6. Coordination number 7	226
3.7. Coordination number 8	229
3.8. Coordination number 9	234
3.9. Coordination number 10	237
3.10. Coordination number 12	239
4. Complexes in solution	239
4.1. Types of complexes	239
4.2. Stability constants and thermodynamic data	240
5. Spectra and magnetic properties – solutions and solids	244
5.1. Absorption	244
5.2. Emission	250
5.3. Mössbauer spectroscopy	253
5.4. Magnetic susceptibility	254
5.5. NMR and ESR	255
6. Specific types of complexes	257
6.1. Inorganic	257

6.2. Organic oxygen donors	261
6.3. Organic nitrogen donors	271
6.4. Organic nitrogen-oxygen donors	275
6.5. Other donor atoms	279
7. Organometallic complexes	280
7.1. Tris-cyclopentadienides	281
7.2. Di-cyclopentadienides	282
7.3. Adducts	283
7.4. $R(C_5H_5)_2X$ and $R(C_5H_5)Cl_2$	283
7.5. Idenyl complexes	286
7.6. Cyclooctatetraenyl compounds	286
7.7. Miscellaneous compounds	288
References	290

Symbols

acac = anion of acetylacetone
BuL = γ -butyrolactam
COT = dianion of cyclooctatetraene
dien = diethylenetriamine
Dip = 1,2-di(4-pyridyl)ethane
dipy = 2,2'-dipyridyl
dipyO ₂ = 2,2'-dipyridyl-1,1'-dioxide
DMA = N,N-dimethylacetamide
DMF = dimethylformamide
DMP = 2,6-dimethyl-4-pyrone
DMSO = dimethylsulfoxide
DPM = anion of dipivaloylmethane (2,2,6,6-tetramethyl-3,5-heptanedione)
dpae = 1,2-bis(pyridine-2-aldimino)ethane
DPSO = diphenylsulfoxide
EDTA = anion of ethylenediaminetetraacetic acid
en = ethylenediamine
facam = anion of 3-trifluoroacetyl-d-camphor

fod = anion of 1,1,1,2,2,3,3-heptafluoro-7,7-dimethyl-4,6-octanedione	Pip = piperidine
HEDTA = anion of hydroxyethylethylenediaminetriacetic acid	py = pyridine
HFA = anion of hexafluoroacetylacetone	pyNO = pyridine-N-oxide
HMPA = hexamethylphosphoramide	salen = bis(salicylaldehyde)ethylenediimine
IMDA = anion of iminodiacetic acid	TBP = tributylphosphate
mal = anion of malonic acid	terpy = 2,2',6',2''-terpyridine (terpyridyl)
NTA = anion of nitrilotriacetic acid	THF = tetrahydrofuran
OPPh ₃ = triphenylphosphine oxide	TMMA = N,N,N',N'-tetramethylmalonamide
o-phen = ortho-phenanthroline	TMU = N,N,N',N'-tetramethylurea
PDC = anion of pyridine-2,6-dicarboxylic acid	tren = β,β',β'' -triaminotriethylamine
4-pic = 4-picoline	trien = triethylenetetramine
	TTA = anion of 4,4,4-trifluoro-1-(2-thienyl)-1,3-butanedione (thenoyltrifluoroacetone)

1. Introduction

The early history of the rare earth elements is primarily dominated by the attempts to separate and purify the individual elements using the classical techniques of fractional crystallization and precipitation (Vickery, 1953). These procedures generally involved aqueous solutions which contained the hydrated ion and in this sense could be considered as the earliest examples of studies of the complexing properties of the rare earths. From a practical standpoint, however, the existence of the complexed ions was only incidental and was probably not even considered by the early workers. Early reference works of the 1920's which summarize the extant information discuss only some double salts and adducts of the rare earths and do not consider them in terms of coordination compounds (Moeller, 1967). The first chelates prepared were probably the acetylacetonates used by Urbain (1896) in a separation procedure.

The extensive studies of the complexes of these elements began both as a cause and result of the improved separation procedures worked out during the early 1940's (Peppard, 1961; Powell, 1961). The ion exchange and solvent extraction techniques developed to separate small amounts of the elements and which have since been extended for the separation of larger quantities, resulted in the availability of substantial quantities of pure materials with which various properties, including complexing behavior, could be investigated. Since these separations made use of the differing degrees of complex formation of the various elements, the search for new and better complexing agents was given an added impetus. Perhaps it can be said that the lack of substantial quantities of the pure individual rare earths was the major cause for the lack of effort devoted to the study of their complexing tendencies until the 1940's. However, it is also fair to comment that of equal importance may well have been the feeling of the chemists of that period that because of the similarities of the rare earth elements

to the alkali and alkaline earth elements they would form very few coordination compounds and that these would most likely be of little interest either from a chemical or practical viewpoint. The influence of the availability of the elements in a pure form, the preparation of new and stronger complexing agents, and the recognition that they form a wide variety of complexes with interesting and useful properties is exemplified by the fact that in 1953 the significant research was summarized in some 60 references (Moeller, 1953) whereas a review published in 1965 covering only the literature to 1962 contained 651 references and made no attempt to be complete (Moeller et al., 1965). Although two comprehensive books have appeared (Sinha, 1966; Melson, 1975), publication has been at such an accelerated rate that most recent reviews have no longer attempted to deal with all aspects of the complexes of the rare earths but instead have been narrowly focused on a very limited range of topics (for example, Brown, 1975; Moeller, 1972; Moeller et al., 1968).

The study of the complexes of the rare earth elements has been marked by several periods of renewed interest. As already mentioned, the first intensive work was carried out to find those ligands which would be effective in conjunction with ion exchange or in solvent extraction procedures for the separation of the elements one from another. In the initial phase these studies focused primarily on the determination of equilibrium constants and distribution coefficients (Moeller et al., 1965). The compounds that were studied as ligands in both cases were almost exclusively limited to molecules that used oxygen as the donor atom, either alone, or as in the case of the aminopolycarboxylic acids, in combination with nitrogen donors within the same molecule. This phase started in the early 1940's and lasted into the 1960's. Toward the end of this period the equilibrium measurements were supplemented with calorimetric studies of the enthalpy of formation of the complexes in solution in order to define more clearly the nature of the complexation process (Moeller, 1973). However, during much of this time there was very little effort devoted to the study of the solid complexes which could be isolated from solutions.

The search for efficient luminescent compounds and lasers generated an intense activity in the late 1950's and through the early 1960's (Crosby, 1966). As a part of these studies a great number of compounds were prepared and their physical and chemical properties were intensively studied. The main emphasis was on the complexes with the β -diketones but it was soon realized that molecules that did not utilize oxygen atoms as the donors would also complex with the rare earth ions. During this period several solid compounds were characterized by definitive structural studies using X-ray diffraction and the results showed that the common coordination number for yttrium and the lanthanides was greater than the six that had been generally assumed (Moseley, 1975). This led to a radical change in thinking and, as a result, the variety of compounds that can be prepared has been markedly increased.

As interest in the luminescence properties of the β -diketones began to wane, the late 1960's and early 1970's saw the use of complexes of the rare earths as

the so-called shift reagents which are used to simplify nuclear magnetic resonance spectra, particularly of organic compounds. From the first demonstration of this effect by Hinckley (1969) until the publication of the proceedings of a symposium four years later (Sievers, 1973), more than 400 publications appeared. Although most of these covered work in which the rare earth complex served as a probe and the adduct was generally not isolated, this is unquestionably the facet of the chemistry of the rare earth complexes that has most readily captured the attention of chemists in general.

During the latter 1960's and continuing on into the present, an increasing amount of research has been devoted to preparing and studying complexes of the rare earths that are unstable in aqueous solution (Forsberg, 1973). By utilizing non-aqueous solvents it has been possible to prepare complexes with ligands such as the aliphatic polyamines. In aqueous solution these systems yield the rare earth hydroxide and for many years it was felt that the metal ion-aliphatic nitrogen bond was too weak to exist. In addition to these kinds of complexes there has been a renewed and increasing interest in the preparation and study of organometallic compounds.

Finally, because of the similarity in size and bonding properties between the alkaline earth ions and the rare earth ions, principally the lanthanide ions, the latter are increasingly being used in studies involving biological systems as probes for the binding sites for the alkaline earth ions (Nieboer, 1975). Several of the properties of the lanthanides (absorption spectra, luminescence spectra, paramagnetism, etc.) can be used to elucidate the role of the lanthanide ion and thus, by inference, that of the alkaline earth ion. Such studies are currently increasing and there is optimism that they will become even more important in the future.

The major drawbacks to the preparation, characterization, and study of complexes of the rare earth ions seem now to have been overcome. The elements are available in quantity as well as in high purity, there is a general recognition that they can form complexes under appropriate conditions with most types of ligands, and modern physical methods are readily available to aid in the characterization and study of the properties of the complexes. The unique electronic properties of some of these ions and their tendency to form complexes with high coordination numbers have been, and will continue to be, exploited both from the standpoint of developing a clearer understanding of the chemistry of the elements themselves as well as being developed into practical applications.

It is the purpose of this chapter to discuss and evaluate the factors leading to the formation of rare earth complexes and to consider illustrative examples of the various types of complexes that have been prepared. The examples are taken whenever possible from the most recent literature available. In an article of this length it is impossible to cover the topic exhaustively. In so far as possible, the major topics are considered in reasonable detail and extensive reference is made to the more comprehensive review articles that exist for some of the topics.

Since the ligands which are to be considered are so varied and are often

complicated organic molecules, it has become customary to employ appropriate abbreviations in order to avoid problems with the nomenclature. The abbreviations used in this chapter have been kept to as few as convenient and are listed at the beginning of the chapter.

2. Complex formation

2.1. Properties of the rare earth ions

The ability and tendency of a metal ion to form complexes depends very strongly on a number of factors. For the rare earth ions these are such that the nature and type of complexes which are formed are different from those formed by the d-transition elements. The trivalent rare earth ions have a completely filled set of electronic subshells with the exception that for the lanthanides, the 4f orbitals may be partially filled (Moeller, 1973). In either case the important point is that the R^{3+} ions are essentially spherical and should present an environment very much like that of the alkali and alkaline earth ions toward complex formation. The 4f orbitals are, in general, not available for chemical bonding and are sufficiently shielded that the stabilization due to crystal field effects is only of the order of 100 cm^{-1} , whereas with the d-transition elements this stabilization may be as large as $30\,000 \text{ cm}^{-1}$. Consequently it is expected that the predominant description of the bonding will be in ionic terms and the geometrical arrangements of the ligands will not be due so much to specific bonding requirements as to steric requirements.

The ionic radii of the trivalent rare earth ions are given in table 25.1. It can be seen that with the exception of the value for scandium these ionic radii are quite large and, in fact, are among the largest values for any trivalent ions. These large

TABLE 25.1.
Ionic radii of the trivalent rare earths in six-coordination*.

Symbol	Radius (Å)	Symbol	Radius (Å)
Sc	0.68	Gd	0.938
Y	0.88	Tb	0.923
La	1.061	Dy	0.908
Ce	1.034	Ho	0.894
Pr	1.013	Er	0.881
Nd	0.995	Tm	0.869
Pm	(0.979)	Yb	0.858
Sm	0.964	Lu	0.848
Eu	0.950		

*Lanthanide values from Templeton and Dauben (1954), scandium and yttrium values from Zachariasen (1954).

radii mean that the charge to radius ratio (ionic potential) is relatively low which results in a very low polarizing ability. (Scandium is somewhat different in this respect and is considered more fully in section 2.4.) This, of course, is reflected in the predominantly ionic character in the metal-ligand bonds. The other major effect of the large ionic radii is to influence in a marked fashion the coordination number of the rare earth complexes. These two factors serve to produce complexes which in general have coordination numbers in excess of six, which is the most common coordination number for the d-transition elements.

A third characteristic of the rare earths that influences the type of complex that they form is their strong tendency to bind water molecules. Hydrolysis of the rare earth ions is not so extensive as for other trivalent ions but the affinity of the rare earth ions for the hydroxide ion is still rather substantial. [Representative values of the equilibrium constant for the reaction $R^{3+} + H_2O \rightleftharpoons ROH^{2+} + H^+$ are: Sc^{3+} , $\log K_1 = -5.1$ (1M $NaClO_4$) (Aveston, 1966); La^{3+} , $\log K_1 = -9.1$ (0.3M $NaClO_4$); Lu^{3+} , $\log K_1 = -7.9$ (0.3M $NaClO_4$); Y^{3+} , $\log K_1 = -8.3$ (0.3M $NaClO_4$) (Frolova et al., 1966).] (The scandium(III) ion has a very strong affinity for the hydroxide ion and indeed aqueous solutions of scandium(III) are both extensively hydrolyzed and polymerized.) Aliphatic amines are sufficiently basic, for example, that in aqueous solutions with the rare earth ions they precipitate the hydroxides rather than resulting in R^{3+} -N complex bond formation. As a result, for many years it was thought that this bond was so weak that complexes of this type could not be formed. More recently such compounds have been prepared by working under scrupulously anhydrous conditions.

The rare earth ions belong to class (a) in the Ahrlund, Chatt and Davies (1958) classification or to the hard acid class in the Pearson (1963) designation. Ions in this class bond to hard bases, primarily those which contain oxygen and nitrogen as the donor atoms, and bond only weakly to the soft bases which contain, for example, sulfur or phosphorous as the donor atoms. This means that by far the majority of rare earth complexes contain ligands which utilize at least one oxygen atom. As a result, the variety of types of complexes which can be formed easily with the rare earth ions is more restricted than that which is formed with the d-transition elements.

The final factor to be considered is a kinetic one. The experimental information that is available from those kinetic studies that have been conducted clearly indicates that reactions between the rare earth ions and various ligands in solutions is generally fast (Reidler and Silber, 1973). The possibility of observing isomerism is thus drastically reduced and probably only in the case of *cis*- and *trans*-[Sc(o-phen)₂(NCS)₂](NCS) and [Sc(dipy)₂(NCS)₂](NCS) is there substantial evidence that isomers can be isolated (Melson, 1975). This lability of the rare earth complexes naturally places restrictions on the numbers and types of complexes that can be isolated from solutions. Moreover, it is much more difficult to be assured that the species which is isolated is in fact identical to the one that exists in solution. Physical methods, particularly those which are spectroscopic in nature, have been utilized in attempting to resolve questions of this type.

The factors considered above demonstrate that in many respects the rare earth ions resemble the alkaline earth ions in their complex-forming tendencies more closely than they do the d-transition elements. Indeed one of the more recent uses of the rare earth ions is as a substitute for calcium in biological systems.

Element 39, yttrium, although it has no f orbitals at a reasonable energy, has a coordination chemistry essentially identical to that of the lanthanides. This is due to the fact that the trivalent yttrium ion has an inert gas configuration and, as can be seen in table 25.1, the ionic radius of the Y^{3+} ion, 0.88 Å, is intermediate between that of Ho^{3+} , 0.891 Å, and that of Er^{3+} , 0.881 Å. Primarily because the lanthanide ions have similar ionic radii, varying from 1.06 Å for La^{3+} to 0.848 Å for Lu^{3+} , the overall general properties with respect to complexation are similar. However, in many cases the effect of this gradual change in the ionic radius plays a significant role in the differences that develop in complex formation from element to element. Consequently it is not surprising that this similarity between yttrium and the lanthanides exists. The only significant differences are in those properties which are related to the presence of the partially-filled 4f orbitals which do not exist in yttrium.

2.2. Types of donor atoms

Although nearly all the early work, as mentioned previously, involved ligands having at least one oxygen atom as donor, recent studies have been directed toward preparing complexes which have other donor atoms in order to broaden the types of complexes and their resulting properties (Moeller et al., 1973). In the preparation of these non-oxygen donor complexes it is generally necessary to employ a solvent having low inherent donating ability (Forsberg, 1973). Thus, although it is possible to isolate complexes of glycine from aqueous solution, complexes of o-phenanthroline must be prepared in alcoholic media, and complexes of ethylenediamine can only be isolated from solvents such as acetonitrile which is completely free from hydroxylic impurities.

Since the rare earth ions form bonds of the ionic or electrostatic type with most ligands, the most abundant and stable complexes (in the sense of resistance to hydrolysis) are those formed with ligands having a negatively charged oxygen atom. Complexes of ligands containing the carboxylate group are particularly abundant and important in the coordination chemistry of the rare earths as are complexes of the β -diketonates. Complexes formed from ligands containing uncharged oxygen atoms such as alcohols, ethers, and ketones do exist but are very much less stable than those containing anionic oxygen donors (Moeller et al., 1965). Moreover, these ligands cannot compete successfully for the rare earth ion in the presence of water molecules and the reactions must also be carried out in weakly-coordinating solvents. Often the ligand itself is a liquid and serves as the solvent. These very weak donor molecules can form adducts with coordinately unsaturated complexes like $R(fod)_3$ in non-coordinating solvents such as carbon tetrachloride or hexane (Cockerill et al., 1973). Although complexes containing aliphatic nitrogen donors must be synthesized in inert

media and must be kept in total absence of moisture, the carboxylate ion is such a good donor that the nitrogen atoms in the aminopolycarboxylates can be bonded to the rare earth ion and such bonds can persist even in the presence of water.

A variety of ligands which have heterocyclic nitrogen as the donor atom are known to form complexes with the rare earth ions (Forsberg, 1973). These ligands are only weakly basic and so the complexes can often be prepared in alcoholic solutions in which there is little competition for the coordination sites. The electronic factors which usually stabilize complexes of these ligands are absent with the rare earth ions and the detailed nature of the interactions is not well understood at the present time. A particularly common type of complex is that in which only part of the coordination positions are occupied by the heterocyclic nitrogen ligand and the remainder are occupied by one or more of the anions in the compound.

Complexes formed from organic ligands which have these donor atoms occurring either singly or in combination, are by far the most common. Simple complexes of the halide ions, oxygen-containing anions, and nitrogen-containing anions also exist (Moeller et al., 1965). As expected from their hard-acid character, the rare earths are more readily and more strongly complexed by the fluoride ion than the other halide ions. In addition there are a few compounds known that contain ligands in which the sulfur atom serves as the donor. In keeping with the predominant ionic character of the rare earth-ligand bond, the most stable of these involve compounds in which the sulfur atom carries a negative charge and is contained in a chelating species such as the dithiocarbamate ion.

The final class of ligands to be mentioned are the organic anions of compounds such as cyclopentadiene and cyclooctatetraene (Kanellakopoulos and Bagnell, 1972). Compounds containing these ligands must be prepared in systems that are both anhydrous and oxygen-free since the compounds are hydrolyzed instantaneously and many of them inflame on contact with air. These complexes might perhaps be the best examples in which covalency in the metal-ligand bonds would be expected. However, as will be discussed in later sections, the available evidence once again supports a predominantly ionic interaction.

2.3. *Nature of rare earth-ligand bonding*

The tremendous advances made in the coordination chemistry of the d-transition elements in the past thirty years have come about largely as a direct consequence of the theoretical approaches which have been adopted to treat the nature of the metal-ligand bond (Cotton and Wilkinson, 1972). The earlier valence bond approach due to Pauling was gradually replaced by the simple crystal field approach which itself has been more recently supplanted by the ligand field and molecular orbital theories. In all of these it has been recognized that there is a varying amount of covalent character in the metal-ligand bond

depending primarily on the type of donor atom presented by the ligand and the detailed nature of the bonds within the ligand molecule. The essential demise of the crystal field theory for the d-transition elements was due in part to a series of experimental measurements which showed that even in complexes with the fluoride ion there is some delocalization of electrons between the ligands and the metal ion. Recognition of this has led to the preparation of a large number and variety of types of complexes with a myriad of kinds of ligands. Of particular interest as examples would be the carbonyl complexes and the metallocene-types of complexes.

The rare earths on the other hand form large ions in which the ns , np , and $(n-1)d$ orbitals are empty and in the case of the lanthanides the $4f$ orbitals are partially filled. It is particularly attractive to attempt to involve these $4f$ orbitals in chemical bonding to the ligands and several such attempts have been made (Henrie et al., 1976). In all cases, however, the amount of involvement of the $4f$ orbitals has been found to be quite small although covalency may contribute significantly to the crystal field splitting (Burns and Axe, 1967; Newman, 1971; Sengupta and Artman, 1971). In view of the relatively efficient shielding of the $4f$ orbitals by the electrons in the $5s$ and $5p$ orbitals, this is not really surprising. The impetus for these considerations has been to provide a more satisfactory interpretation for the results obtained from various physical measurements such as optical, NMR, ENDOR, and ESR spectra. These results do show that addition of overlap and covalency effects results in improvements between the experimental and calculated parameters (Jørgensen, 1975). Although magnetic neutron scattering clearly demonstrates that compounds of the 3d-transition elements have considerable covalent bonding, similar studies with rare earth compounds yield, at most, only very slight effects that can be attributed to covalency involving the $4f$ orbitals (Tofield, 1975).

The question of the involvement of the outer $6s$, $6p$, and $5d$ orbitals in the case of the lanthanides has also been considered. Although there has been evidence presented that the gaseous halides, RX_3 , can be treated by a covalent model better than an ionic model (Myers, 1975), it is not clear yet to what extent this might prevail. In their properties rare earth complexes behave as would be expected of predominantly ionic complexes. The overwhelming bulk of evidence suggests that the main contribution to the bonding in the rare earth complexes can be classified as ionic although in certain selected types of complexes there may well be some degree of covalency (Moeller, 1972).

The most favorable complexes in which substantial covalency would be expected to be found would be in σ - or π -bonded organometallic complexes. However, even in these cases the overwhelming weight of the evidence points to a predominantly ionic type of interaction (see section 7). Since this is a relatively new area in the complex chemistry of the rare earths, a definitive answer to the question of the role of covalent effects in rare earth complexes will only be forthcoming after considerable additional work.

The question of covalency in the bonds formed by the rare earth elements is considered in detail in ch. 23 and so will not be discussed any further here.

2.4. Relationship of scandium to the other rare earths

Although scandium is formally a member of the rare earth family of elements, it differs from yttrium and the lanthanide elements in rather significant ways. Of primary importance is the fact that the ionic radius of scandium(III) which is 0.68 Å is much smaller than that of yttrium(III) (0.88 Å) or the lanthanide(III) ions (1.06 Å to 0.85 Å). On this basis the chemistry of yttrium should be very similar to that of the lanthanides, as it is. On the other hand, since the chemistry of these elements results from chemical bonding which is essentially ionic in nature, this smaller size for scandium has a marked influence on the nature and coordination number of the complexes which it forms.

Scandium(III) also differs from yttrium and the lanthanide ions in that it is very extensively hydrolyzed in aqueous solution. This means for example that in the measurement of the stability constants for complexes formed with scandium(III) in aqueous media the existence of these hydrolyzed and polymerized scandium(III) species must be taken into consideration. For yttrium and the lanthanides, hydrolysis is so slight that it is not necessary, except when dealing with very weak complexes in nearly neutral or basic solutions, to consider hydrolysis of the metal ion. This hydrolysis of scandium can be circumvented in the presence of sufficiently strong ligands. However, although it is often possible to prepare complexes of relatively weak ligands with yttrium and the lanthanides by using the hydrated salts and ethanolic solutions, the corresponding scandium complexes can only be prepared from the anhydrous salts and in solutions in which precautions have been taken to ensure the absence of water.

The other major effect of this marked difference in size appears in the coordination numbers of complexes. As mentioned previously, yttrium and the lanthanides are very large ions and as a result form discrete complexes in which the coordination number is generally greater than six. The ionic size of scandium is much smaller and most of its discrete complexes have coordination number six. Although eight-coordinated scandium(III) has been described in polymeric networks in compounds such as ScPO_4 , ScAsO_4 , ScVO_4 (Schwarz, 1963) and $\text{Sc}_2(\text{C}_2\text{O}_4)_3 \cdot 6\text{H}_2\text{O}$ (Hansson, 1972), only one discrete complex having this coordination number has been reported, hydrogen tetrakis(oxalato)scandium(III) (Davis and Einstein, 1974; Anderson et al., 1974b).

Complexes of scandium(III) often appear to be more covalent than those of yttrium(III) and the lanthanides (Melson, 1975). This trend is the one that would be expected because of the smaller size of the scandium(III) ion. The covalency in the scandium-ligand bonds is illustrated with the β -diketone ligands which give complexes that have relatively low melting points, fairly high volatility, and are soluble in a number of types of non-polar solvents. For a given β -diketone ligand the scandium complex generally has the lowest melting point of the rare earth complexes. For example, the melting points of the tris-dipivaloylmethanato complexes of scandium(III), lanthanum(III), and lutetium(III) are $\sim 153^\circ\text{C}$, 243°C , and 173°C respectively (Eisentraut and Sievers, 1965).

The coordination chemistry of scandium has been extensively reviewed

recently by Melson and Stotz (1971) and by Melson (1975). These references should be consulted for additional details on the similarities and differences between the complexes of scandium and the other rare earths.

3. Coordination numbers

3.1. *Factors affecting coordination numbers and coordination polyhedra*

One of the most interesting and useful developments in the chemistry of the complexes of the rare earths during the past fifteen years has been the recognition that this chemistry for yttrium and the lanthanides is dominated by large coordination numbers. Although the structure of $\text{Nd}(\text{BrO}_3)_3 \cdot 9\text{H}_2\text{O}$ had been determined in 1939 by Helmholtz (1939) and showed that the neodymium ion was surrounded by nine water molecules in a face-centered trigonal prismatic arrangement, the commonly held opinion even into the early 1960's was that the rare earth ions formed six-coordinate, octahedral complexes (Moeller et al., 1965). In part this was based on the almost universal octahedral, six-coordination known at that time for most trivalent metal ions of both the d-transition and representative metals. Moreover, many of the rare earth complex species had formulations which could be rationalized in these terms.

Schwarzenbach and his co-workers in their studies of the stability constants of the 2:1 complexes of nitrilotriacetic acid with yttrium and the lanthanides (Andergg, 1960) and of the 1:1 complex of the potentially octadentate ligand, diethylenetriaminepentaacetic acid with the cerium(III) ion (Anderegg et al., 1959), alluded to this tendency for the adoption of large coordination numbers. This possibility was, however, still largely ignored. A number of investigations were carried out in the period between 1959 and 1965 in which the only reasonable explanation for the results involved postulating that the metal ions were adopting coordination numbers greater than six (Moeller et al., 1965). Among these were the relative values determined for the stability constants of complexes with ligands presenting a large number of potential donor atoms, solvent extraction results, the stability constants for mixed complexes, and the synthesis of complexes such as the tetrakis- β -diketonates in which there were eight possible donor atoms. The final death blow to the six-coordinate thinking was provided in 1965 by Hoard and his co-workers in their classic papers on the crystal and molecular structures of the lanthanum ethylenediaminetetraacetic acid complexes (Lind et al., 1965; Hoard et al., 1965). These complexes which had the formulas $\text{NH}_4\text{La}(\text{EDTA}) \cdot 8\text{H}_2\text{O}$ and $\text{HLa}(\text{EDTA}) \cdot 7\text{H}_2\text{O}$ were found to contain nine and ten-coordinate lanthanum(III) respectively. Many structures have since been determined and the compounds invariably have large coordination numbers (Moseley, 1975). In fact, as will be discussed later, compounds having coordination numbers less than seven are exceedingly rare for yttrium and the lanthanides.

The chemical composition of a rare earth complex is of only limited value in

determining the coordination number of the central ion. There are now numerous examples in which the water molecules contained in the formula are not all waters of hydration but may also be coordinated and thereby increase the coordination number. In addition it is quite often found that at least some of the anions, either simple halide or pseudohalide ions or oxyanions, are coordinated. Both of these factors severely complicate the determination of rare earth coordination numbers.

The NTA complexes of praseodymium and dysprosium serve as examples of the former problem. These two compounds which have the formulae $\text{PrNTA}\cdot 3\text{H}_2\text{O}$ and $\text{DyNTA}\cdot 4\text{H}_2\text{O}$ contain nine-coordinate praseodymium with one water of hydration (Martin and Jacobson, 1972a) and eight-coordinate dysprosium with two water molecules of hydration (Martin and Jacobson, 1972b). It is clear that neither of these is predicted by the stoichiometry of the complexes. The second problem is illustrated by the complexes $\text{R}(\text{NO}_3)_3\cdot n\text{DMSO}$ ($n = 3$ or 4). The complex $\text{Nd}(\text{NO}_3)_3\cdot 4\text{DMSO}$ (Aslanov et al., 1972b) has all the nitrate ions coordinated in a bidentate fashion which results in overall ten-coordination. The complex $\text{Lu}(\text{NO}_3)_3\cdot 3\text{DMSO}$ (Aslanov et al., 1973) also has all three nitrate ions coordinated and the lutetium is nine-coordinate.

The coordination number can sometimes be reasonably established by a combination of physical measurements such as conductance, molecular weight determination, infrared, ultraviolet-visible-near-infrared, and emission spectroscopy (Moeller, 1972). The method of choice for the determination of the coordination numbers for solid complexes is, however, X-ray diffraction and the tremendous progress in rare earth coordination chemistry is in large part due to the improvements in X-ray diffraction techniques and the availability of large computers to aid in the data reduction and solution of the structures. As a case in point, the dimethylsulfoxide complexes mentioned above were assigned coordination numbers eight and seven respectively on the basis of the infrared spectra of the nitrate groups and their conductance behavior (Ramalingam and Soundararajan, 1967).

Coordination numbers of complexes in solution are even more difficult to determine and are usually rationalized from spectroscopic and conductance measurements by inference.

The existence of complexes of the rare earths with larger coordination numbers is a natural consequence of their large size and the predominantly ionic bonding which they exhibit. Since there is no strong, directional bonding, the arrangement of the ligands is influenced both by the size of the rare earth ion and the properties of the ligands and steric factors seem to play a dominant role in determining the coordination numbers. In the absence of adverse steric factors the rare earth ion seems to achieve a coordination number of eight or larger. (The differences between scandium and the other rare earths in this regard were considered in section 2.4.) For example, only the tris-chelates exist for the dipivaloylmethane complexes (Eisentraut and Sievers, 1965). The *t*-butyl groups clearly are so bulky that a fourth β -diketone ligand cannot coordinate. On the other hand, the tetrakis-chelate of dibenzoylmethane is easily prepared

(Melby et al., 1964). Even though the tetrakis-dipivaloylmethane complex does not exist, the tris-chelate is still capable of adding one or two additional ligands, such as pyridine, picoline, or o-phenanthroline, to form seven- and eight-coordinate species (Selbin et al., 1971).

Although seven- and eight-coordination are known for each of the rare earth ions, higher coordination numbers depend critically on the size of the metal ion as well as the nature of the ligands. For example, although the dysprosium ions in DyNTA·4H₂O are eight-coordinate (Martin and Jacobson, 1972b), the praseodymium ions in the corresponding compound, PrNTA·3H₂O (Martin and Jacobson, 1972a), are nine-coordinate. This change in coordination number is consistent with the dependence of steric interactions upon the size of the central metal ion. Complexes having coordination numbers greater than nine appear to be limited to terbium and the lighter lanthanides (lanthanum to gadolinium) (Moseley, 1975).

It is useful at this point to comment briefly on coordination number six in the rare earths. Although this is the most common coordination number for scandium (Melson, 1975), authentic six-coordinate complexes with yttrium and the lanthanides are severely limited (see section 3.5). From the few compounds that are known it is apparent that steric factors are of overriding importance. Several examples of six-coordination involve uninegative anions as the ligands which results in a complex ion with three negative charges. Since there does not seem to be any steric reason to limit to six the number of these simple ions that could coordinate to the metal ion, it can be concluded that the high total negative charge and the packing considerations for the compensating cation are also of significance.

In the following sections some examples of complexes having coordination numbers from three to twelve will be presented. The listing is illustrative only with the majority of the examples from the most recent literature available. The review by Moseley (1975) covers the structures known up until 1973 and should be consulted for a more extensive listing. Also it should be pointed out that the coordination polyhedron for a complex with a large coordination number is rarely uniquely determined and that it is usually possible to describe the polyhedron as related to more than one of the idealized structures. The description of the coordination polyhedron is often influenced by the compounds with which comparisons are to be made (see e.g. Hansson, 1973e).

3.2. Coordination number 3

The compounds R{N(SiMe₃)₂}₃ have been prepared for Sc, Y, La, Ce, Pr, Nd, Sm, Eu, Gd, Ho, Yb, and Lu (Bradley et al., 1973). The scandium, europium, and ytterbium compounds are isomorphous and thus it would appear that all the complexes have the same structure. This structure has been determined for the scandium and europium complexes by Ghotra et al. (1973) and is somewhat different from that for the analogous compounds with aluminum, iron, and other first-row transition elements. The iron compound has a three-coordinate planar

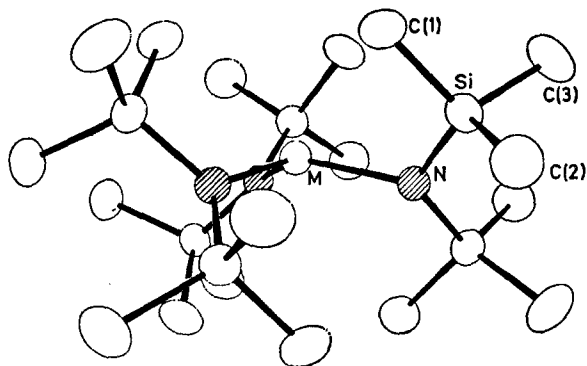


Fig. 25.1. The molecular structure of $R\{N(SiMe_3)_2\}_3$ ($R = Sc, Eu$). (Reprinted with permission from Ghotra, J.S., Hursthouse, M.B. and Welch, A.J., 1973, *J. Chem. Soc., Chem. Comm.*, 669-670.)

arrangement which allows for delocalization of the π -electrons. The scandium and europium compounds adopt true three-coordination but the ligands are arranged in a pyramidal fashion with N-M-N bond angles of approximately 116° . This pyramidal coordination appears to be explicable in terms of bonding which is predominantly ionic. The existence of this structure with ions as large as the lanthanides implies that there is a substantial ligand steric effect. Because the compounds have zero dipole moment in solution, which implies that they are planar, it is possible that packing considerations are important in the crystalline phase.

3.3. Coordination number 4

The only example of this coordination number which is known at the present time occurs in the compound $[Li(C_4H_8O)_4][Lu(C_8H_9)_4]$ (Cotton et al., 1972). (The anion is the tetrakis(2,6-dimethylphenyl)lutetate(III) anion.) The structure of this compound is given in fig. 25.2 and shows that the lutetium-carbon bonds

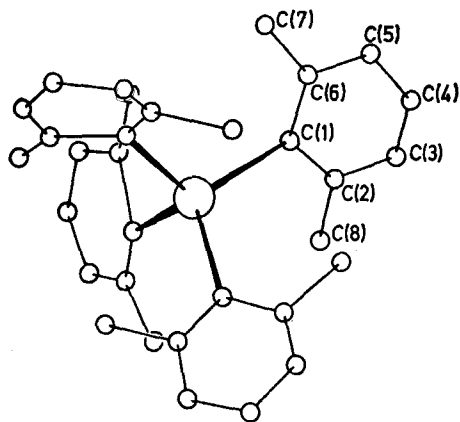


Fig. 25.2. The structure of the anion $Lu(C_8H_9)_4^-$. (Reprinted with permission from Cotton, S.A., F.A. Hart, M.B. Hursthouse and A.J. Welch, 1972, *J. Chem. Soc., Chem. Comm.*, 1225-1226.)

(2.42–2.50 Å) approximate a tetrahedral arrangement. The bulkiness of the ligands in this case must also impose a severe steric requirement on the complex. Although the analogous ytterbium complex could be prepared and is isomorphous with the lutetium compound, complexes with the lighter lanthanides could not be synthesized.

3.4. Coordination number 5

Treatment of $\text{La}\{\text{N}(\text{SiMe}_3)_2\}_3$ with an excess of triphenylphosphine oxide results in the formation of $\text{La}_2\text{O}_2\{\text{N}(\text{SiMe}_3)_2\}_4(\text{OPPh}_3)_2$. The crystal structure of this compound has been determined and contains a doubly bidentate bridging peroxy group (Bradley et al., 1974). If the peroxy group is considered to occupy two coordination positions, then as shown in fig. 25.3, the lanthanum is five-coordinate. Similar compounds have been prepared for praseodymium, samarium, and europium.

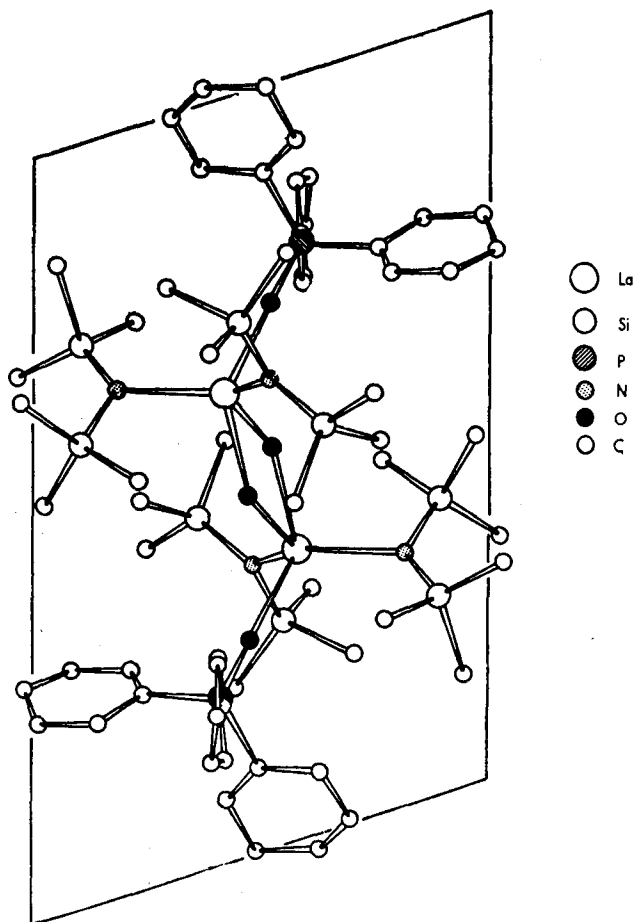


Fig. 25.3. The molecular structure of $\text{La}_2\text{O}_2\{\text{N}(\text{SiMe}_3)_2\}_4(\text{OPPh}_3)_2$. (Reprinted with permission from Bradley, D.C., J.S. Ghotra, F.A. Hart, M.B. Hursthouse and P.R. Ruithby, 1974, *J. Chem. Soc., Chem. Comm.*, 40–41.)

3.5. Coordination number 6

The first structural study of an authentic six-coordinate lanthanide complex was carried out in 1968 by Martin et al. (1968) although the spectroscopic work of Ryan and Jørgensen (1966) on the LnX_6^{3-} species which are probably octahedral had been published two years earlier. The number of six-coordinate complexes studied by X-ray diffraction is quite small and this coordination number is still often inferred from the chemical formula.

The geometrical arrangement predicted for six unidentate ligands is octahedral with distortions of a tetragonal or rhombic nature if the ligands are not identical. The other commonly expected six-coordinate species, $\text{R}(\text{bidentate})_3^{n+}$, is expected to be octahedral with distortions toward trigonal prismatic stereochemistry as the "bite" of the bidentate ligand is progressively decreased (Moseley, 1975).

These stereochemical predictions have been found to be upheld in the few examples that have been completely characterized. The complex anion, $\text{Er}(\text{NCS})_6^{3-}$, in $\{(\text{C}_4\text{H}_9)_4\text{N}\}_3\text{Er}(\text{NCS})_6$ is six-coordinate and almost perfectly octahedral (Martin et al., 1968). All the lanthanides from praseodymium to lutetium and yttrium form this hexaisothiocyanato complex and all are isostructural. The lanthanum complex was formulated as $\{(\text{C}_4\text{H}_9)_4\text{N}\}_4\text{La}(\text{NCS})_7$ but the molecular structure has not as yet been solved. Since lanthanum is the largest of the rare earths, it may adopt the six-coordinate structure even less readily.

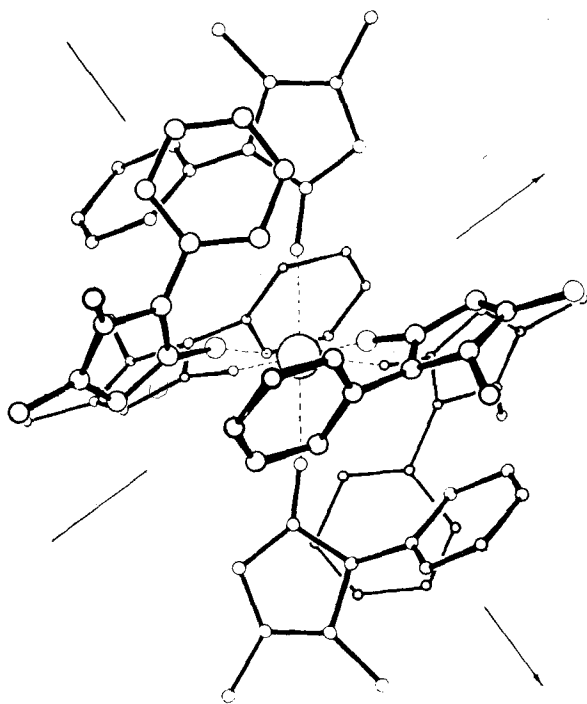


Fig. 25.4. The molecular structure of the hexakisantipyrineyttrium(III) cation. (Reprinted with permission from Baker, R.W. and J.W. Jeffery, 1974, *J. Chem. Soc., Dalton Trans.*, 229-232.)

The structure of the gadolinium complex $\text{Gd}(\text{DMP})_3\text{Cl}_3$ has been found to be six-coordinate and basically octahedral (Tazzoli et al., 1972). The coordination polyhedron must be irregular since the Gd–O distances are 2.30, 2.31, and 2.35 Å whereas the Gd–Cl distances are 2.64, 2.65, and 2.66 Å.

One further example of six-coordination involving unidentate ligands is found in hexakisantipyreneytterbium(III) iodide (Baker and Jeffery, 1974). The antipyrene ligand is quite large and the six oxygen atoms coordinated to the yttrium form an essentially regular octahedron. This regularity is reflected in the molecular symmetry which is S_6 .

The only six-coordinate tris-bidentate complexes that have been structurally identified are those of dipivaloylmethane with the lanthanides from holmium to lutetium. The coordination polyhedron of the erbium complex, $\text{Er}(\text{DPM})_3$, (deVilliers and Boeyens, 1971b), is built up from three, planar bidentate ligands and deviates only very slightly from the ideal trigonal prism. The larger lanthanide ions do not adopt this coordination number with DPM but rather the structure is a seven-coordinate one achieved by dimerization (Erasmus and Boeyens, 1970). Again this is probably a consequence of the larger ionic radius in the lighter lanthanides.

This coordination number is the one that is most common for scandium(III) complexes but there have not been a large number of complexes for which the detailed molecular structure has been determined. The structure of $\text{Sc}(\text{acac})_3$ consists of discrete molecular units with slight deviations from D_3 symmetry

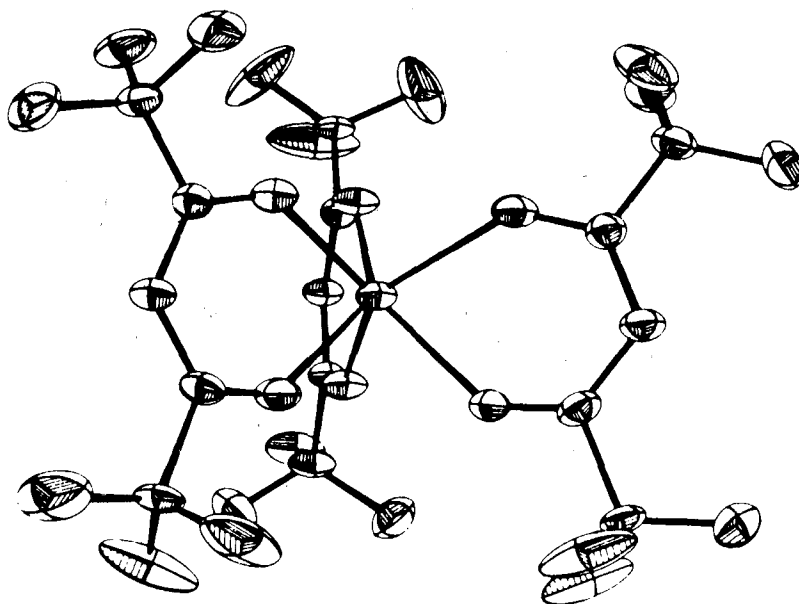


Fig. 25.5. Trigonal prismatic coordination in $\text{Er}(\text{DPM})_3$. (Reprinted with permission from deVilliers, J.P.R. and J.C.A. Boeyens, 1971, *Acta Crystallogr.* **B27**, 2335–2340.)

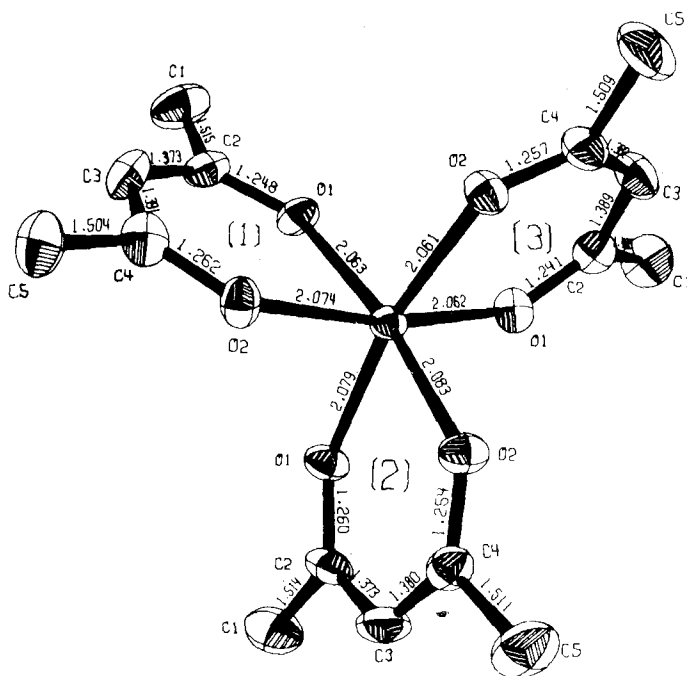


Fig. 25.6. The molecular structure of $\text{Sc}(\text{acac})_3$. (Reprinted with permission from Anderson, T.J., M.A. Neuman and G.A. Melson, 1973, *Inorg. Chem.* **12**, 927-930.)

(Anderson et al., 1973). The coordination polyhedron can best be described as a distorted octahedron. The tris(tropolonato)scandium(III) complex also consists of discrete molecular units which have crystallographically imposed D_3 symmetry (Anderson et al., 1974a). In this case the coordination polyhedron is intermediate between the octahedron and the trigonal prism. The twist angle of 33° compares to that of 47° found for $\text{Sc}(\text{acac})_3$ and 60° expected for the octahedron. The scandium-oxygen bond lengths are approximately the same for the two compounds. The adoption of this structure for the tropolonato complex is due to the fact that the ligand is rigid and has a fixed bite. In the absence of any electronic preference, such as exists for the corresponding octahedral cobalt(III) complex, these steric factors are the most important and the structure is distorted toward the trigonal prism.

3.6. Coordination number 7

There is now a substantial number of complexes known to have this coordination number (Moseley, 1975). Nearly all of them have the basic formulation $\text{R}(\text{bidentate})_3(\text{unidentate})^{n+}$ in which the bidentate ligand is a β -diketonate. The preferred coordination polyhedra for complexes of this type have been deter-

TABLE 25.2.
 Seven-coordinate rare earth complexes.

Complex	Basic polyhedron	Reference
Ho(C ₆ H ₅ COCHCOC ₆ H ₅) ₃ ·H ₂ O	mono-capped octahedron	Zalkin et al. (1969)
Y(C ₆ H ₅ COCHCOC ₆ H ₅) ₃ ·H ₂ O	mono-capped octahedron	Cotton and Legzdins (1968)
Dy(DPM) ₃ ·H ₂ O	mono-capped trigonal prism	Erasmus and Boeyens (1971)
Lu(DPM) ₃ ·C ₆ H ₇ N	mono-capped trigonal prism	Wasson et al. (1973)
Yb(acac) ₃ ·H ₂ O	mono-capped trigonal prism	Cunningham et al. (1969)
Eu(DPM) ₃ ·DMSO	pentagonal bipyramid	Dyer et al. (1973)

mined by Kepert (1974) from consideration of the ligand–ligand repulsion energies using a “normalized bite” of 1.22. (The term “normalized bite” refers to the distance between the two donor atoms divided by the metal atom–donor atom distance.) This results in three favored coordination polyhedra: (a) the mono-capped octahedron; (b) a figure with no elements of symmetry that can be loosely described as the capped trigonal prism; and (c) a figure intermediate between the pentagonal bipyramid and the capped trigonal prism. No examples of coordination polyhedron (c) had been identified at that time for complexes of this type with the rare earth ions. Kepert predicted that this polyhedron would be adopted only by those complexes in which the unidentate ligand formed an unusually strong bond with the rare earth ion.

Some examples of seven coordination in the rare earths are given in table 25.2. As predicted, it is apparent that the differences necessary to stabilize one

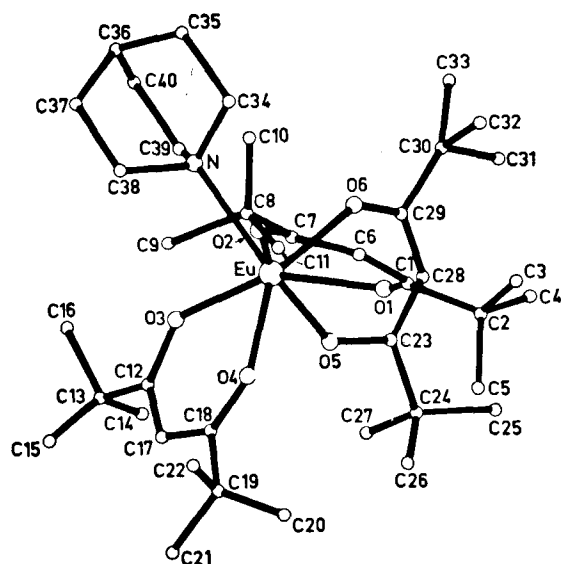


Fig. 25.7. The molecular structure of the quinuclidine adduct of Eu(DPM)₃. (Reprinted with permission from Bye, E., *Acta Chem. Scand.* **A28**, 731–739.)

structure over another are very subtle. In addition to these all four structures that have been determined recently involve the basic $R(DPM)_3$ unit and, depending on the metal ion and the nature of the seventh ligand, all three geometries predicted by Kepert have been found.

The molecular structure of the quinuclidine adduct of $Eu(DPM)_3$ has been determined by Bye (1974). The coordination polyhedron is best described as a distorted octahedron formed by the six oxygen atoms with the nitrogen atom from the quinuclidine located above the center of one of the faces, yielding overall threefold symmetry (type a).

The coordination polyhedron for the 3,3-dimethylthietane-1-oxide adduct of $Eu(DPM)_3$ (Wing et al., 1973) and for the 3-methylpyridine adduct of $Lu(DPM)_3$ (Wasson et al., 1973) can both be described as capped trigonal prisms. Of particular interest is the adoption of essentially the same polyhedron by complexes in which the metal ion radii are substantially different. Moreover, Erasmus and Boeyens (1970) had previously concluded from their study of $Pr_2(DPM)_6$ that seven-coordination would be impossible if the metal-oxygen distances were less than 2.27 Å. In the europium complex the europium-DPM oxygen distances

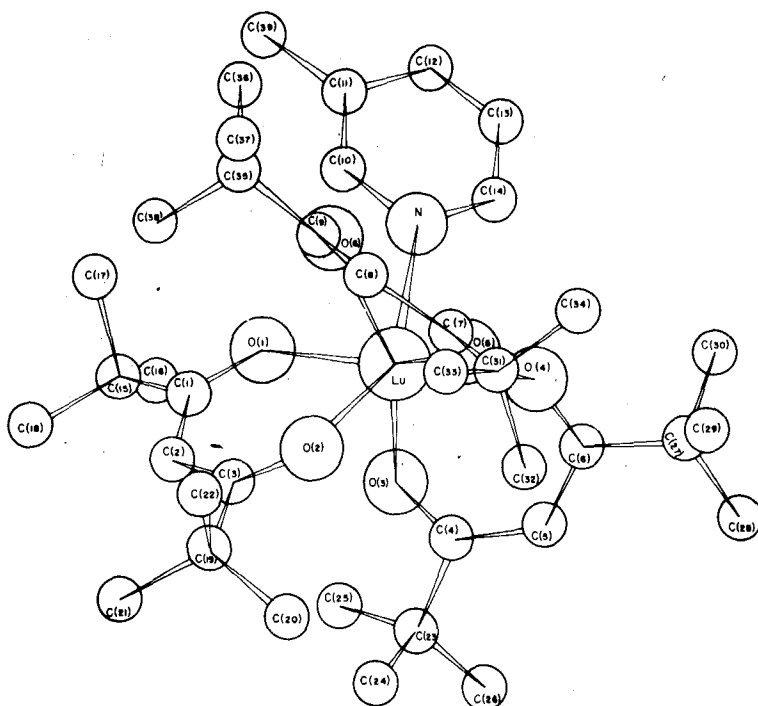


Fig. 25.8. The molecular structure of 3-methylpyridine- $Lu(DPM)_3$. (Reprinted with permission from Wasson, S.J.S., D.E. Sands and W.F. Wagner, 1973, *Inorg. Chem.* **12**, 187-190.)

average to 2.33 Å but in the lutetium complex the lutetium–DPM oxygen distances only average to 2.24 Å. For the other exceptions to this suggestion of Erasmus and Boeyens it is possible to consider the existence of seven-coordination as a consequence of hydrogen bonding. Since this is not possible for the lutetium complex, this suggestion seems to have lost some of its predictive power.

The complex $\text{Eu}(\text{DPM})_3 \cdot \text{DMSO}$ exists in a seven coordinate structure with two slightly different coordination polyhedra (Dyer et al., 1973). The two polyhedra can be considered to be distorted pentagonal bipyramids (type c). As such, they would be the first example of this geometrical arrangement found in rare earth complexes. Since it is known that dimethyl sulfoxide forms reasonably strong bonds to the rare earth ions, the existence of this geometrical arrangement would be consistent with the hypothesis put forth by Kepert. The fact that the two isomers are slightly different supplies clear evidence of the ease with which complexes having coordination number seven can be deformed.

3.7. Coordination number 8

Perhaps the most common of the coordination numbers exhibited by yttrium and the lanthanides is eight. Numerous attempts have been made to determine the coordination polyhedra to be expected by considering the interligand repulsions (Hoard and Silvertov, 1963; King, 1970a; and Porai-Koshits and Aslanov, 1972). The results obtained point to the dodecahedron with triangular faces and the square antiprism as the two most likely polyhedra. Although the cubic arrangement is found in many simple ionic lattices, its existence in discrete complexes probably would require participation of the f-orbitals in the bonding in order to overcome the strong inter-ligand repulsions (Kettle and Smith, 1967). The earlier work on complexes that have eight coordination has been reviewed by Lippard (1967) and by Muetterties and Wright (1967).

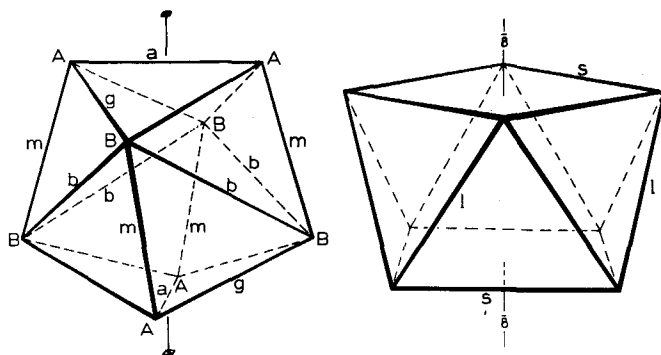


Fig. 25.9. Idealized eight-coordination polyhedra: left, triangular-faced dodecahedron; right, square antiprism. (Reprinted with permission from Hoard, J.L. and J.V. Silvertov, 1963, *Inorg. Chem.* 2, 235–243.)

The variety of chemical formulations for which eight-coordination is found is large, but the two most common are $R(\text{bidentate})_4^{n+}$ and $R(\text{bidentate})_3(\text{unidentate})_2^{n+}$. Blight and Kepert (1972) have carried out a detailed analysis of the inter-ligand repulsions in $R(\text{bidentate})_4^{n+}$ in which they found that the potential energy surface is critically dependent on the "bite" of the bidentate ligand. For ligands having small bites, there is a single minimum corresponding to the D_{2d} dodecahedron. As the bite of the bidentate ligand is increased, a continuous change is predicted toward that polyhedron approximating the D_2 square antiprism. Further increase in the bite leads progressively to stereochemistries which appear to be nearly equally probable, the D_2 square antiprism, the D_4 square antiprism, and the D_2 dodecahedron. (In all these computations it was assumed that the four bidentate ligands span equivalent polyhedral edges.) The known crystal structures are in agreement both with these general predictions and with the predicted detailed geometry.

It should be mentioned that the two basic polyhedra are very closely related and only a very small spatial rearrangement is necessary to interconvert them. This means that it is often a difficult matter to decide which idealized geometry affords the more appropriate description. There have been attempts to define parameters in such a way that it will be possible to decide which is the appropriate polyhedron (Lippard and Russ, 1968). However, these are in reality only rejection tests and it is necessary to carry out a comprehensive analysis to arrive at a satisfactory assignment in cases of distorted polyhedra (Penneman et al., 1973). Only rarely has this analysis actually been carried out.

3.7.1. Dodecahedron

A number of lanthanide and yttrium complexes having the basic dodecahedral coordination polyhedron have been described and some representative examples are given in table 25.3. Of particular interest are the tetrakis hexafluoroacetylacetonates of europium and yttrium. These are isomorphous (Burns and Danford, 1969) and adopt the D_2 dodecahedral arrangement with the chelate rings spanning the g edges of the polyhedron (Bennett et al., 1968). In this structure and in that of $(\text{NH}_4)[\text{Pr}(\text{TTA})_4] \cdot \text{H}_2\text{O}$ (Lalancette, 1967) the rings interconnect the two trapezoids of the dodecahedron. The yttrium complex is quite volatile and the structure is in accord with a strong ion pair with the cesium ion surrounded by eight fluorine atoms from two neighboring $\text{Y}(\text{HFA})_4^-$ moieties.

The m edges are spanned in the compound $\text{NH}_4[\text{Ho}(\text{tropolanato})_4]$ (Day, 1970) as would be expected for a complex having a very small bite. The compound isoquinolinium tetrakis[4,4,4-trifluoro-1-(2-thienyl)-1,3-butanediono]cerium(III) also has the chelating ligands spanning the m edges and the dodecahedron is distorted by the formation of a hydrogen bond from the isoquinolinium ion to one of the chelated oxygen atoms (McPhail and Tschang, 1974).

There are a number of complexes of the type $R(\text{bidentate})_3(\text{unidentate})_2^{n+}$ and although the majority of these have the basic square antiprismatic stereochemistry there are some examples that have the basic dodecahedron. The complex tris[4,4,4-trifluoro-1-(2-thienyl)-1,3-butanediono]bis(triphenylphosphineoxide)-

TABLE 25.3.
Eight-coordinate rare earth complexes.

Complex	Basic polyhedron	Reference
$R(C_2O_4)_3 \cdot 6H_2O$ (R = Ho–Lu, Y, Sc)	Dodecahedron	Hansson (1972, 1973a)
$R(HOCH_2COO)_3 \cdot 2H_2O$ (R = Tb–Lu)	Dodecahedron	Grenthe (1971b)
$[R(HOCH_2COO)(OCH_2COO)(H_2O)] \cdot H_2O$	Dodecahedron	Grenthe (1969)
$Ho(acac)_3 \cdot 4H_2O$	Dodecahedron	Aslanov et al. (1971a)
$DyNTA \cdot 4H_2O$	Dodecahedron	Martin and Jacobson (1972b)
$CsR(HFA)_4$ (R = Y, Eu)	Dodecahedron	Bennett et al. (1968)
$La(C_5H_5NO)_8(ClO_4)_3$	Square antiprism	Burns and Danford (1969)
$Eu(DPM)_3(py)_2$	Square antiprism	Al-Karaghoulis and Wood (1972a)
$Ho(DPM)_3(4-pic)_2$	Square antiprism	Cramer and Seff (1972)
$Eu(acac)_3 \cdot o\text{-phen}$	Square antiprism	Horrocks, Jr. et al. (1971)
$Nd(TTA)_3 \cdot Dip \cdot H_2O$	Square antiprism	Watson et al. (1972)
$Y(acac)_3 \cdot 3H_2O$	Square antiprism	Leipoldt et al. (1976)
$HPip[Eu(C_6H_5COCHCOCH_3)_4]$	Square antiprism	Cunningham et al. (1967)
$R(nicotinate)_3 \cdot 2H_2O$ (R = La–Lu)	Square antiprism	Il'inskii et al. (1972)
		Moore et al. (1972)
		Aslanov et al. (1972a)
$Pr_2(fod)_6 \cdot 2H_2O$	(1) dodecahedron and (2) bicapped trigonal prism	deVilliers and Boeyens (1971a)
$Eu(acac)_3 \cdot 3H_2O$	bicapped trigonal prism	Il'inskii et al. (1969)
$Nd(acac)_3 \cdot 2H_2O$	indeterminate	Aslanov et al. (1971b)

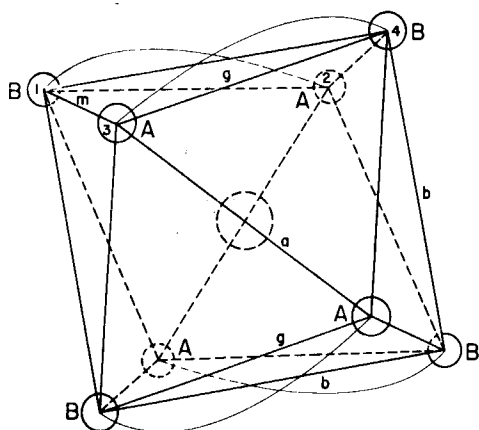


Fig. 25.10. Coordination dodecahedron in the tetrakis(hexafluoroacetylacetonato)yttrate(III) ion viewed down the two-fold axis through the yttrium ion. (Reprinted with permission from Bennett, M.J., F.A. Cotton, P. Legzdins and S.J. Lippard, 1968, *Inorg. Chem.* 7, 1770–1776.)

neodymium(III) forms a basic dodecahedron with two chelating ligands spanning the *g* edges and one spanning an *m* edge (Leipoldt et al., 1975). The two unidentate ligands occupy different sites in the polyhedron, one in the A position and one in the B position.

The compound $Pr_2(fod)_6 \cdot 2H_2O$ is very interesting in that it contains dimeric, eight-coordinate groups (deVilliers and Boeyens, 1971). The two praseodymium

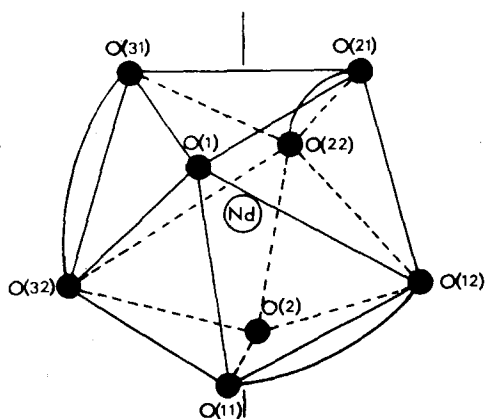


Fig. 25.11. The coordination polyhedron in $\text{Nd}(\text{TTA})_3(\text{Opph}_3)_2$. (Reprinted with permission from Leipoldt, J.G., L.D.C. Bok, A.E. Laubscher and S.S. Bosson, 1975, *J. Inorg. Nucl. Chem.* **37**, 2477-2480.)

atoms in the dimer are not identical, one being easily recognizable as dodecahedral and the other being most conveniently described as a bicapped trigonal prism. The chelate rings are very similar to those in the seven-coordinate $\text{Pr}_2(\text{DPM})_6$.

3.7.2. Square antiprism

Examples of complexes adopting the square antiprismatic geometry are also given in table 25.3. Both the compounds $\text{Ce}(\text{CH}_3\text{COCHCOCH}_3)_4$ (Titze, 1969) and $\text{HPip}[\text{Eu}(\text{C}_6\text{H}_5\text{COCHCOCH}_3)_4]$ (Il'inskii et al., 1972) adopt this geometry with the chelate rings spanning the *s* edges as expected. This arrangement is very common for the bis-adducts of the tris- β -diketone complexes and a number of examples have been described. The subtle interplay of interligand steric effects, crystal packing effects and bonding considerations is once again seen in the fact that the coordination polyhedron in $[\text{Y}(\text{CH}_3\text{COCHCOCH}_3)(\text{H}_2\text{O})_2] \cdot \text{H}_2\text{O}$ is best described as a slightly distorted square antiprism (Cunningham et al., 1967) whereas the corresponding complex $[\text{Ho}(\text{CH}_3\text{COCHCOCH}_3)_3(\text{H}_2\text{O})_2]$ is best described in terms of a dodecahedron (Aslanov et al., 1971a).

In the compound tris-[4,4,4-trifluoro-1-(2-thienyl)-1,3-butanediono]europium(III) dihydrate the two water molecules are diagonally opposite one another on one square face which means that one ring spans *s*-edges while the other two rings span *l*-edges (White, 1976). Because of the tremendous interest in the lanthanide shift reagents, structures of their adducts have become very important. Although most of these adducts seem to be of the 1:1 variety, and thus are presumably seven-coordinate, at least two 2:1 adducts have been reported, $\text{Eu}(\text{DPM})_3(\text{py})_2$ (Cramer and Seff, 1972) and $\text{Ho}(\text{DPM})_3(4\text{-picoline})_2$ (Horrocks, Jr. et al., 1971). Both of these are basically square antiprismatic. In both complexes the two nitrogen atoms are on opposite square faces located as far from one another as possible. The positions occupied by the pyridine molecules in $\text{Eu}(\text{DPM})_3(\text{py})_2$ are very crowded and larger ligands would not be

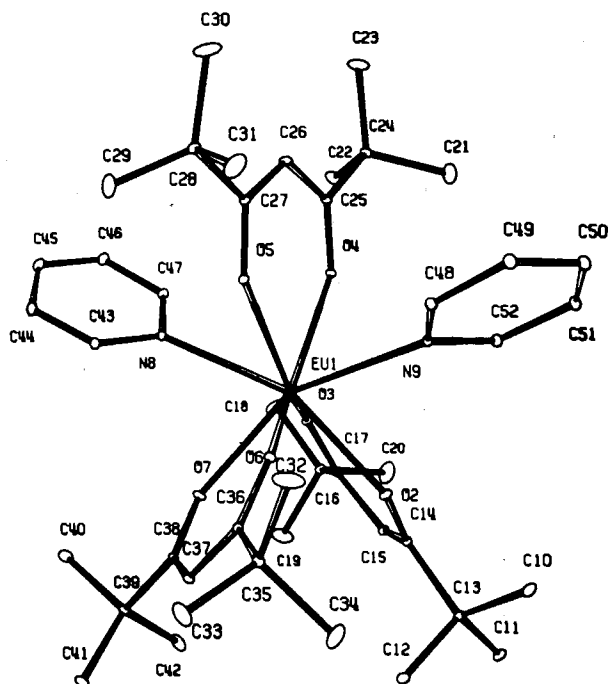


Fig. 25.12. The molecular structure of $\text{Eu}(\text{DPM})_3(\text{py})_2$. (Reprinted with permission from Cramer, R.E. and K. Seff, 1972, *Acta Crystallogr.* **B28**, 3281-3293.)

expected to adopt this configuration. One mole of pyridine is readily lost to give the monopyridine adduct but at present its molecular structure is unknown (Selbin et al., 1971).

In contrast to these two compounds $\text{Eu}(\text{DPM})_3(\text{DMF})_2$ is square antiprismatic with the two DMF molecules occupying *cis* positions on the same square face

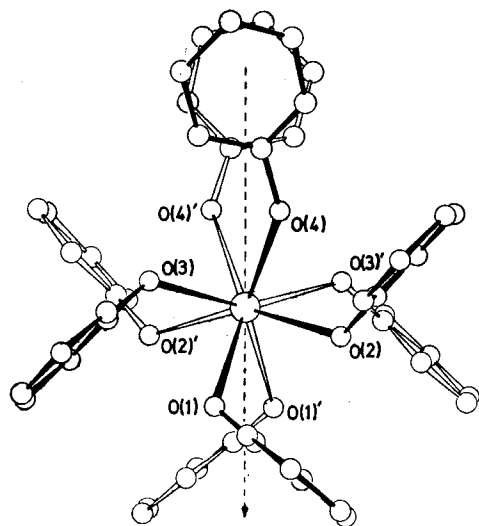


Fig. 25.13. The molecular structure of the octakis(pyridine-N-oxide) lanthanum(III) ion. (Reprinted with permission from A.R. Al-Karaghoul and J.S. Wood, 1972, *J. Chem. Soc., Chem. Comm.*, 516-517.)

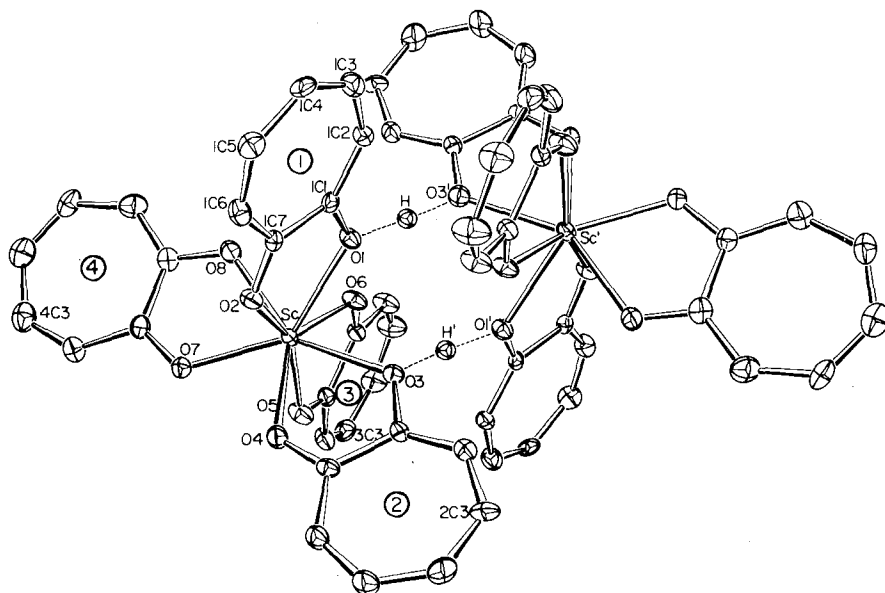


Fig. 24.14. The molecular structure of the eight-coordinate acid dimer of tetrakis(tropolonato)scandium(III). (Reprinted with permission from Davis, A.R. and F.W.B. Einstein, 1974, *Inorg. Chem.* 13, 1880–1884.)

(Dyer et al., 1973). All three chelate rings span *s*-edges. It would seem clear from these results that any extrapolation of structural results from the solid state to solution must be done with great care.

The complex ion in octakis(pyridine-*N*-oxide)lanthanum(III) perchlorate (Al-Karaghoulis and Wood, 1972a) is one of the very few examples of an eight-coordinate complex formed with monodentate ligands for which structural information is available. The complex ion is square antiprismatic and has almost perfect D_4 symmetry. Consideration of the detailed coordination polyhedron suggests strongly that the ion is distorted toward the cube.

The acid dimer of tetrakis(tropolonato)scandium(III) exists in a centrosymmetric structure in which each scandium is eight-coordinate and the two units are held together by two nearly linear hydrogen bonds (Davis and Einstein, 1974; Anderson et al., 1974b). The coordination polyhedron is best described as an irregular bicapped trigonal prism distorted toward a dodecahedron. The achievement of this larger coordination number of scandium(III) is a consequence of the compact shape, skeletal rigidity, and small bite of the tropolonate anionic ligand.

3.8. Coordination number 9

There is a substantial number of complexes having nine-coordination and a representative list is presented in table 25.4. Additional examples can be found in

TABLE 25.4.
 Nine-coordinate rare earth complexes.

Complex	Basic polyhedron	Reference
R(HOCH ₂ COO) ₃ (orthorhombic) (R = La-Tb)	Tricapped trigonal prism	Grenthe (1972)
R(HOCH ₂ COO) ₃ (monoclinic) (R = Pr-Tb)	Tricapped trigonal prism	Grenthe (1971a)
R ₂ (C ₂ O ₄) ₃ ·10H ₂ O (R = La-Nd)	Tricapped trigonal prism	Ollendorf and Weigel (1969)
Na ₃ R(PDC) ₃ ·15H ₂ O (triclinic) (R = Ce-Dy)	Tricapped trigonal prism	Albertsson (1972c)
Na ₃ R(PDC) ₃ ·14H ₂ O (orthorhombic) (R = Dy-Lu)	Tricapped trigonal prism	Albertsson (1970)
Na ₃ R(PDC) ₃ ·13H ₂ O (monoclinic) (R = Ho-Tm)	Tricapped trigonal prism	Albertsson (1972a)
Na ₃ R(PDC) ₃ ·NaClO ₄ ·10H ₂ O (hexagonal) (R = Ho-Lu)	Tricapped trigonal prism	Albertsson (1972b)
Er(NO ₃) ₃ ·3DMSO	Tricapped trigonal prism	Aslanov et al. (1972c)
Yb(NO ₃) ₃ ·3DMSO	Tricapped trigonal prism	Bhandory et al. (1975)
Lu(NO ₃) ₃ ·3DMSO	Tricapped trigonal prism	Aslanov et al. (1973)
Nd(NO ₃) ₃ ·3 antipyrène	Tricapped trigonal prism	Bhandory et al. (1976)
Nd(OCOCH ₂ SCH ₂ COO)Cl·4H ₂ O	Tricapped trigonal prism	Malmberg and Oskarsson (1973)
Pr(terpy)Cl ₃ ·8H ₂ O	Monocapped square anti- prism	Radonovich and Glick (1971)
Nd ₂ (malonato) ₃ ·8H ₂ O	Monocapped square anti- prism	Hansson (1973b)
RNTA·3H ₂ O (R = Pr-Tb)	Indeterminate	Martin and Jacobson (1972a)

the reviews by Meutterties and Wright (1967) and Moseley (1975). The expected polyhedra based on the equal-distance-equal-charge model (King, 1970a) are the symmetrically-tricapped trigonal prism and the capped square antiprism. The tricapped trigonal prism occurs for a wide variety of kinds of ligands and is found in many simple hydrated compounds such as Nd(H₂O)₉(BrO₃)₃ (Helmholz, 1939) and [R(H₂O)₉](C₂H₅SO₄)₃ (R = Pr, Er, Ho, Y) (Fitzwater and Rundle, 1959; Hubbard et al., 1974).

This is the expected geometrical arrangement for tridentate ligands and indeed the trisdipicolinate and trisoxodiacetate lanthanide complexes utilize this structure (Albertsson, 1972d). The trisglycolate and trisoxalate complexes are polymeric but also form the tricapped trigonal prism as the coordination polyhedron (Hansson, 1973e). The situation with these complexes is complicated by polymorphism. For example, two forms of the trishydroxyacetates (Grenthe, 1971a, 1972) and three forms of the trisdipicolinates (Albertsson, 1970, 1972a, c) have been identified. The differences are mainly due to the different numbers of molecules of water of crystallization since the coordination polyhedra are nearly identical (Albertsson, 1972c).

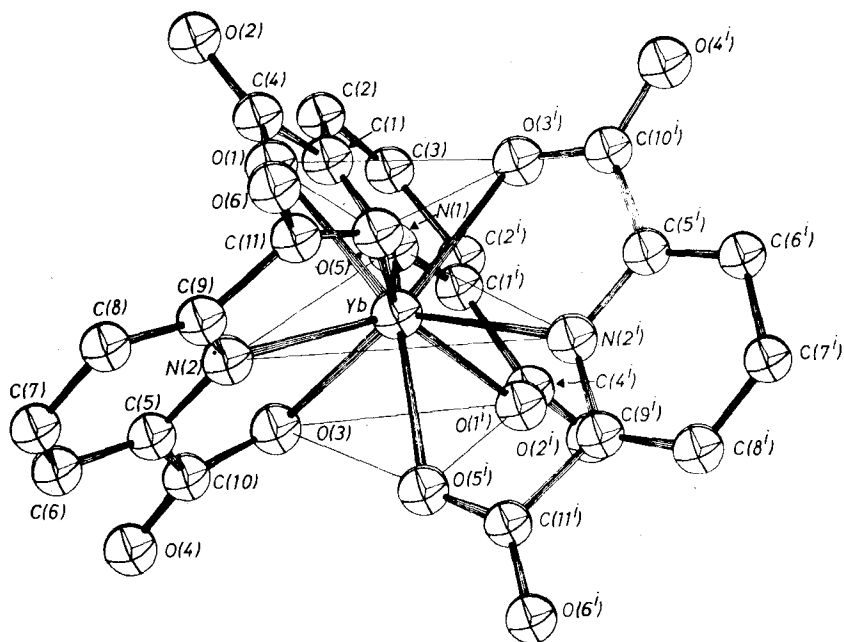


Fig. 25.15. The nine-coordinate structure of $\text{Yb}(\text{DPC})_3$. (Reprinted with permission from Albertsson, J., 1970, *Acta Chem. Scand.* **24**, 1213–1229.)

The europium malonate, $\text{Eu}_2(\text{mal})_3 \cdot 8\text{H}_2\text{O}$, is interesting since there are two different coordination geometries around the europium atoms and only five of the water molecules are coordinated (Hansson, 1973d). One of the europium atoms is eight-coordinate in the form of a distorted square antiprism whereas the other is a nine-coordinate, distorted tricapped trigonal prism. The influence of the ionic radius is apparent in the analogous neodymium compound in which six of the water molecules are coordinated (Hansson, 1973b). The larger neodymium atoms in this complex are all nine-coordinate and the coordination geometry is the monocapped square antiprism.

A second form of neodymium malonate, $\text{Nd}_2(\text{mal})_3 \cdot 6\text{H}_2\text{O}$, also exists (Hansson, 1973c). In this compound each neodymium is also nine-coordinate, surrounded by six carboxylate and three water oxygen atoms, and the coordination polyhedron is intermediate between the distorted capped square antiprism and the distorted tricapped trigonal prism.

The structure of the dimethylformamide adduct of a chiral shift reagent based on 3-trifluoroacetyl-*d*-camphor has been determined (Cunningham and Sievers, 1975). This compound is a dimeric species, $(\text{facam})_3\text{Pr}(\text{DMF})_3\text{Pr}(\text{facam})_3$ in which the three DMF molecules serve as bridging groups. The two praseodymium atoms are nine-coordinate with the oxygen atoms occupying the vertices of a distorted monocapped square antiprism. This structure is particularly

interesting since it had previously been suggested that a coordination number in excess of eight could not exist with these types of complexes (Horrocks, Jr., 1973). The stability of this dimer and its ability to accommodate the three DMF ligands demonstrates that although intramolecular steric factors are important, the influence of other factors such as the nucleophilic strength of the substrate ligand, intermolecular packing considerations, and hydrogen bonding may be the deciding factors in determining the coordination number.

3.9. Coordination number 10

As expected, the situation with respect to the coordination polyhedra for 10-coordination is complex. Three polyhedra are generally considered (Al-Karaghoulis and Wood, 1972b): the bicapped square antiprism, the bicapped dodecahedron, and a polyhedron of C_{2v} symmetry derived from the triangular-faced dodecahedron in which two of the trans equatorial B positions are each "divided" between two pairs of ligands. Calculation of the ligand-ligand repulsion energies shows that the bicapped square antiprism is the favored arrangement (King, 1970b). As shown in table 25.5, however, examples of all three polyhedra are known.

The classical ten-coordinate lanthanide structure is that of $H[La(EDTA)(H_2O)_4] \cdot 3H_2O$ (Lind et al., 1965). Although there are severe restraints placed on the coordination polyhedron by the EDTA ligand, this coordination polyhedron can be considered to approximate the bicapped square antiprism.

The existence of a coordination number as large as ten generally requires that small chelating ligands be used in order to minimize the interligand repulsions and most other examples of ten-coordination contain the chelated nitrate ion. The coordination polyhedron in $La(NO_3)_3 \cdot 2bipyridyl$ approximates the bicapped dodecahedron (Al-Karaghoulis and Wood, 1972b), whereas the polyhedron of C_{2v} symmetry is approximated by the coordination around lanthanum in

TABLE 25.5.
Ten-coordinate rare earth complexes.

Complex	Basic polyhedron	Reference
$HLa(EDTA) \cdot 7H_2O$	Bicapped square antiprism	Lind et al. (1965)
$La(NO_3)_3 \cdot 4DMSO$	C_{2v} based on dodecahedron	Bhandary and Manohar (1973)
$La(NO_3)_3 \cdot dipy$	Bicapped dodecahedron	Al-Karaghoulis and Wood (1972b)
$Gd(NO_3)_3 \cdot dpae$	Distorted pentagonal bipyramid	Smith et al. (1973)
$Ce(NO_3)_4 \cdot 2\{(C_6H_5)_3PO\}$	Octahedral*	Mazhar-Haque et al. (1971)
$[(C_6H_5)_3C_2H_5P]_2Ce(NO_3)_5$	Trigonal bipyramid*	Al-Karaghoulis and Wood (1973)

*Nitrate groups are assumed to occupy only one coordination position.

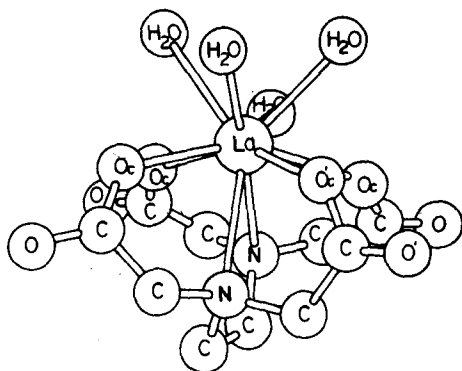


Fig. 25.16. The structure of the ten-coordinate cation in $\text{H}[\text{La}(\text{EDTA})(\text{H}_2\text{O})_4] \cdot 3\text{H}_2\text{O}$. (Reprinted with permission from Lind, M.D., B. Lee and J.L. Hoard, 1965, *J. Amer. Chem. Soc.* **87**, 1611–1612.)

$\text{La}(\text{NO}_3)_3 \cdot 4\text{DMSO}$ (Bhandary and Manohar, 1973). (The importance of ionic radius is again demonstrated since the ytterbium complex is formulated $\text{Yb}(\text{NO}_3)_3 \cdot 3\text{DMSO}$ and its coordination polyhedron is the nine-coordinate, tri-capped trigonal prism (Bhandary et al., 1975).

The nitrate complex ions $\text{Ce}(\text{NO}_3)_5^{2-}$ (Al-Karaghoulis and Wood, 1973) and $\text{Ho}(\text{NO}_3)_5^{2-}$ (Toogood and Chieh, 1975) cannot be rationalized easily in terms of the idealized polyhedra. However, if each nitrate group is considered to occupy only one coordination position, the nitrogen atoms then closely approximate a trigonal bipyramid. If a ten-coordinate description is desired, the D_2 bicapped dodecahedron is the most appropriate polyhedron.

The final example of ten-coordination to be mentioned is that found in trinitrato-1,2-bis(pyridine-2-aldimino)ethanegadolinium(III) (Smith et al., 1973). The coordination polyhedron approximates a pentagonal bipyramid (considering the nitrate ions to occupy a single coordination position) with four of the five equatorial positions occupied by the nitrogen atoms of the tetradentate amine ligand and the remaining three positions occupied by the three nitrate ions.

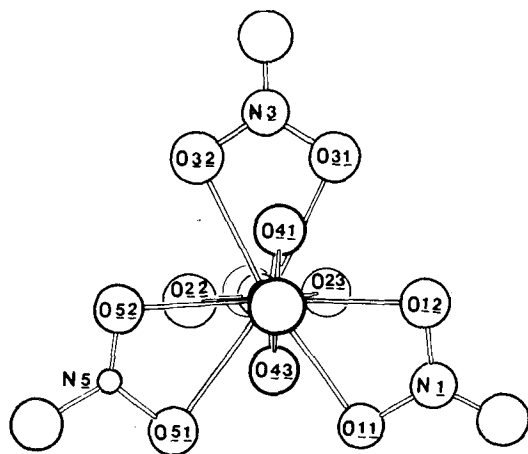


Fig. 25.17. The structure of the $\text{Ho}(\text{NO}_3)_5^{2-}$ anion in $(\text{NO})_2[\text{Ho}(\text{NO}_3)_5]$. (Toogood and Chieh, 1975). (Reproduced by permission of the National Research Council of Canada, 1975, *Can. J. Chem.* **53**, 831–835.)

3.10. Coordination number 12

Very few examples of twelve coordination are known and they are limited to the nitrate ion functioning as a bidentate ligand. In all cases the coordination polyhedron is the icosahedron. In both $\text{Ce}_2\text{Mg}_3(\text{NO}_3)_{12}\cdot 24\text{H}_2\text{O}$ (Zalkin et al., 1963) and $(\text{NH}_4)_2[\text{Ce}(\text{NO}_3)_6]$ (Beineke and Delgaudio, 1968) the cerium(III) and (IV) ions are surrounded by nitrate ions such that the six nitrogen atoms define an octahedron and the oxygen atoms define the icosahedron.

4. Complexes in solution

4.1. Types of complexes

The rare earth ions form a variety of types of complexes in both aqueous and non-aqueous solution and these have been studied extensively. The initial impetus for studies of the solution chemistry was centered on the development of more efficient ligands for use in the ion exchange separation of yttrium and the lanthanides. Likewise, a large portion of the work devoted to the study of complexes in non-aqueous solutions was ultimately directed toward improvements in the solvent extraction separation.

The most common complex in solution is the aquated ion $\text{R}(\text{H}_2\text{O})_x^{3+}$. (The possibility of anion coordination may change the nature of this simple ion. See below.) The value of x is not known with certainty although it is apparently not constant even in the lanthanide series. Because of the importance of the aquated ions there has been considerable effort expended in studies designed to determine the value of x and the various results obtained by different techniques have been subjected to different interpretations. The latest work (Habenschuss and Spedding, 1974), however, seems now to have established that from lanthanum to neodymium the inner sphere water coordination is nine and for the elements terbium to lutetium it is eight. For the ions from neodymium to terbium the steric hindrance for nine-coordination becomes critical and the hydrated ions exist in an equilibrium between the two coordinated forms with the equilibrium shifting gradually toward eight-coordination. The inner hydration sphere for yttrium is similar to that for erbium whereas the scandium(III) ion has six-coordination (Melson, 1975).

The actual situation that exists in solutions of rare earth salts in either aqueous or non-aqueous solution is complicated by concentration effects that can lead to both inner and outer sphere anion coordination as well as to the possibility of hydroxo-containing species particularly in the case of scandium. Inner sphere complexes containing halide ions, nitrate ions, sulfate ions (Choppin, 1971) and even the perchlorate ion (Fратиello et al., 1973; Silber, 1974) have been identified. Consequently, the interpretation of results obtained from measurements of conductance, density, partial molal volume, reaction kinetics, formation constants, and solution spectra can be extraordinarily complicated.

In aqueous solution the complexes that exist must compete with a large excess

TABLE 25.6.
Representative types of rare earth complexes in solution.*

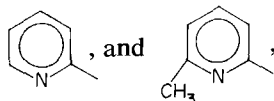
<i>Inorganic ligands</i>	<i>Organic ligands</i>
RX^{2+} (X = F, Cl, Br, I)	$R(C_2H_3O_2)_n^{(3-n)+}$ ($n = 1-3$)
RX_2^+ (X = Cl, Br)	$R(HOCH_2COO)_n^{(3-n)+}$ ($n = 1-4$)
$RCIO_3^+$	$R(EDTA)^-$
RNO_3^+	$R(NTA)_n^{(3-3n)+}$ ($n = 1, 2$)
$R(P_2O_7)_n^{(3-4n)+}$ ($n = 1, 2$)	$R(HEDTA)(IMDA)^{2-}$
	$R(HEDTA)(OH)^-$
	$R(\beta\text{-diketone})_n^{(3-n)+}$ ($n = 1-3$)
	$R(PDC)_n^{(3-2n)+}$ ($n = 1-3$)
	$R(NO_3)_3 \cdot 3TBP$ (kerosine as solvent)

*Moeller et al. (1965).

of water and must involve ligands that are not so basic that hydroxides or hydroxo species are precipitated. The requirements for solubility in non-aqueous solvents place stringent restrictions on the ligands that can form complexes in these solvents. A representative sample of the types of complexes that exist in solutions is given in table 25.6. Additional details can be found in chs. 22, 24 (Separation Chemistry and Solution Chemistry).

Stability constants have been measured in solution for a large number of ligands (Moeller et al., 1965, and Sillén and Martell, 1971). However, because the rare earth ions are hard acids or class (a) metals, most of these involve at least one oxygen as a donor atom. The carboxylic acids, hydroxycarboxylic acids, and various substituted aminopolycarboxylic acids have been most widely studied. Inorganic ligands, in general, form only very weak complexes or, as in the case of a number of oxyanions, form precipitates. By a judicious choice of experimental conditions the stability constants for a number of these have been measured, however.

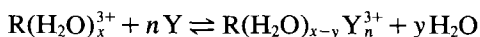
The relative tendencies of various donor groups such as HO-, CH₃O-, CH₃S-,



to coordinate to the lanthanides has been estimated from the stability constants for the appropriate N-substituted iminodiacetic acid (Thompson et al., 1967). The extra stability imparted by these donor groups is approximately the same for each element and in units of $\Delta \log K$ the values are 2.9, 1.6, 0.0, 3.3, and 1.0 respectively. These values are consistent with the class (a) character of the lanthanides except that the affinity for the pyridyl group seems remarkably large.

4.2. Stability constants and thermodynamic data

The period between 1945 and 1970 saw a particularly intense effort devoted to measuring the stability constants for complexes of the rare earth ions. Most of these were carried out in aqueous solution and only a relatively few were ever measured in non-aqueous solutions. The reaction that was studied was



and the corresponding stepwise stability constants, K , or overall stability constants, β , were obtained. Most of the values which have been measured were obtained in media of constant ionic strength, usually 0.1 M or 2 M. Very few data have been determined at infinite dilution. The formation constants have been determined by a variety of physical measurements that depend on the nature of the complexes: potentiometric, conductmetric, or spectrophotometric, to mention those that are most common. Several extensive compilations of stability constants have been published (Moeller et al., 1965, ; Sillén and Martell, 1971) and only representative values will be discussed here.

The data in table 25.7 show that although the stability constants for the rare earth complexes are large, they are not in general as large as those for the d -transition elements. Moreover, upon detailed examination it is clear that the stability constants across the lanthanide series do not follow the same trend for every ligand listed. If the only important factor in determining the stabilities of the complexes were the simple ionic interaction between the metal ion and the ligand, then they would increase monotonically as the ionic radius decreased. Clearly this is not the case and many other factors such as the nature of the aquated ion (since the complexation reaction actually involves the displacement of one ligand, water, by another), degree of aquation of the complex, changes in

TABLE 25.7.
Formation constants for some selected 1:1 complexes.

R ³⁺	log K ₁				
	Acetate ^a	Glycolate ^b	Diglycolate ^c	EDTA ^d	IMDA ^e
Sc ³⁺			8.31	25.05	
Y ³⁺	1.57	2.47	5.24	18.09	3.24
La ³⁺	1.58	2.19	4.93	15.50	2.80
Ce ³⁺	1.71	2.35	5.16	15.98	3.11
Pr ³⁺	1.84		5.33	16.40	3.48
Nd ³⁺	1.93	2.50	5.45	16.61	3.68
Sm ³⁺	2.04	2.55	5.55	17.14	4.11
Eu ³⁺			5.53	17.35	4.23
Gd ³⁺	1.87	2.48	5.40	17.37	4.30
Tb ³⁺			5.32	17.93	3.98
Dy ³⁺	1.71	2.54	5.31	18.30	3.84
Ho ³⁺	1.66		5.28	18.74	3.54
Er ³⁺	1.65	2.61	5.34	18.85	3.25
Tm ³⁺			5.49	19.32	2.86
Yb ³⁺	1.69	2.72	5.55	19.51	2.55
Lu ³⁺			5.64	19.83	2.51

^aSonesson (1958a, b); ^bSonesson (1959); ^dGrenthe and Tobiasson (1963); scandium, Grenthe and Hansson (1969); ^dSchwarzenbach et al. (1954); scandium, Bottari and Anderegg (1967); ^eR(EDTA)⁻ + IMDA²⁻ ⇌ R(EDTA)(IMDA)³⁻; Geier and Karlen (1971).

coordination number, and steric effects within the ligands must have varying degrees of importance (Moeller et al., 1965).

The stability constants for the lighter lanthanides, La^{3+} – Eu^{3+} or Gd^{3+} , always increase in the expected monotonic fashion regardless of the ligand which indicates that for complexes of these ions other factors are relatively unimportant. In the heavier lanthanides, however, at least three distinct types of behavior have been noted: (1) a more or less regular increase with increasing atomic number and corresponding decrease in ionic radius, (2) essential constancy for the ions Gd^{3+} – Lu^{3+} , and (3) an increase to a maximum in the vicinity of Dy^{3+} followed by a decrease. There is no obvious correlation among the ligands which give one or the other of these trends. Since the first trend is the simple one that is expected in the absence of any complicating effects, it has been rationalized in the Coulombic terms mentioned previously. This is consistent with the observation that the formation constant for the yttrium complex nearly always falls in the holmium–erbium region just as consideration of the ionic radius predicts. Rationalization of the other two trends almost certainly requires consideration of changes in coordination number, steric effects, and differences in the coordinating abilities of the various donor atoms of the ligand.

The values of $\log K$ (or ΔG) are composed of both enthalpy (ΔH) and entropy ($T\Delta S$) terms and these have been determined in an attempt to provide more insight into the trends which are observed both for polydentate ligands and for the individual steps with simpler ligands (Grenthe, 1964b; Choppin, 1971). Although the values obtained aid in interpreting the trends, the various results can still be interpreted in more than one way and the problems are still not resolved. It is useful to recall that the complexation reaction in solution is a complex process involving hydration of all species and changes in the solvent structure, all of which contribute to the magnitude of the problem.

The enthalpy changes observed for complexation reactions reflect the processes mentioned above and are related to the difference in energy between the cation–ligand bond and the cation–coordinated–solvent molecule bond. Both of these will also include any effects due to a change in solvation and any that occur in the bulk solvent (Moeller, 1972). As shown in table 25.8 for some typical ligands, the experimental values obtained for the enthalpy change accompanying complex formation generally do not change monotonically from lanthanum to lutetium. The values of ΔH usually become more positive with perhaps a slight decrease again at the end of the series.

For most complexes the entropy term is dominant. The entropy change upon complexation is related to the change in the number of particles and to changes in the various modes of vibration of these particles. For reactions in aqueous solution the release of bound water molecules contributes substantially to the entropy change and is particularly favorable in the case of chelation. These trends in ΔH and ΔS have been rationalized both in terms of changes in the hydration number of the lanthanide ions (Choppin, 1971) or of the complex species (Geier and Karlen, 1971; Grenthe and Ots, 1972; Ots, 1973). The latter arguments now seem particularly convincing for the EDTA and diglycolate complexes.

TABLE 25.8.
Enthalpy and entropy changes for 1:1 complexes.

R ³⁺	Acetate ^a		Glycolate ^a		Diglycolate ^b		EDTA ^c		IMDA ^d	
	ΔH	ΔS	ΔH	ΔS	ΔH	ΔS	ΔH	ΔS	ΔH	ΔS
Sc					-0.47	36.3				
Y	3.26	18.1	-0.07	11.1	1.73	30.0	-0.59	80.7	-6.53	-7.4
La	2.18	14.6	-0.63	7.9	-0.07	22.3	-2.93	60.9	-1.56	7.6
Ce	2.09	14.8	-0.81	8.0	-0.40	22.2	-2.94	63.0	-1.60	8.8
Pr	1.72	14.2			-0.68	22.1	-3.20	64.1	-3.05	5.5
Nd	1.71	14.6	-1.19	7.4	-0.85	22.1	-3.62	63.7	-2.66	7.8
Sm	1.45	14.2	-1.03	8.1	-1.05	21.8	-3.35	67.0	-4.26	4.3
Eu					-0.78	22.6	-2.56	70.6	-5.57	0.3
Gd	1.87	14.8	-0.61	9.3	-0.36	23.5	-1.73	73.6	-6.61	-2.9
Tb					0.77	27.0	-1.11	78.3	-8.10	-9.4
Dy	2.93	17.6	-0.16	11.0	1.32	28.8	-1.21	79.6	-7.46	-7.9
Ho	3.17	18.3			1.59	29.6	-1.36	81.1	-7.14	-8.2
Er	3.28	18.5	-0.19	11.3	1.66	30.1	-1.71	80.4	-6.99	-9.0
Tm					1.57	30.5	-1.87	82.0	-6.50	-9.1
Yb	3.51	19.5	-0.29	11.4	1.42	30.2	-2.31	81.4	-5.54	-7.2
Lu					1.23	30.0	-2.51	82.2	-4.00	-2.2

^aGrenthe (1964a); ^bGrenthe (1963); Scandium; ^cGrenthe and Hansson (1969); ^dMackey et al. (1962); ^eREDTA⁻ + IMDA²⁻ → R(EDTA)(IMDA)³⁻, Geier and Karlen (1971).

For many reactions it has been found that there is a relationship between ΔH and ΔS : the more negative the value of ΔH , the less positive the value of ΔS (Choppin and Strazik, 1965). For 1:1 complexes of unidentate ligands it has been further suggested that for outer sphere complex formation ΔH should favor complexation and ΔS should oppose it. This circumstance would result from the essential retention of the primary hydration sphere of the rare earth ion. This is the behavior found for dilute solutions containing the nitrate or thiocyanate ion and should correspond to the formation of outer sphere complexes for these ligands. If the converse relationship exists for ΔH and ΔS , such as with the fluoride ion or carboxylate ions, then it is assumed that the primary hydration sphere has been ruptured and the resulting complex is of the inner-sphere type (Choppin, 1971).

In the discussion above the relatively strongly complexed water molecules in the hydration sphere of the lanthanide ion or the corresponding complex contribute to the uncertainty in the interpretation of the results. Moeller and his co-workers have removed some of this difficulty by measuring the thermodynamics of the formation of complexes with ethylenediamine and diethylenetriamine under anhydrous conditions in acetonitrile as the solvent (Forsberg, 1973). This solvent is only weakly coordinating toward the lanthanides and complexes with these aliphatic-nitrogen donors can thus be formed. With the anhydrous lanthanide(III) perchlorates ethylenediamine forms $R(en)_x^{3+}$ ($x = 1, 2, 3$, and 4) and diethylenetriamine forms $R(dien)_x^{3+}$ ($x = 1, 2, 3$). These complexes are strongly enthalpy stabilized and the entropy changes oppose complex formation. The enthalpy results suggest a strong R-N interaction. Moreover, the importance of steric effects is apparent in the 3:1 diethylenetriamine complex which becomes increasingly less stable as the ionic radius decreases with a substantial change occurring between gadolinium and dysprosium.

5. Spectra and magnetic properties – solutions and solids

5.1. Absorption

Those rare earth ions in which the 4f electronic orbitals are incompletely filled absorb electromagnetic radiation in the spectral region which is experimentally easily accessible, *i.e.*, the near-ultraviolet, the visible, and the near-infrared (Dieke, 1968). The transitions that occur in these regions are caused by or result from the incomplete 4f subshell and are either due to intra-4fⁿ transitions, the 4fⁿ → 4fⁿ⁻¹5d¹ transition, or charge transfer transitions.

The 4fⁿ → 4fⁿ⁻¹5d¹ transition occurs in the near-ultraviolet for cerium(III) praseodymium(III) and terbium(III). These transitions tend to be broad and the upper 5d level is split by the ligand field surrounding the ion. Ryan and Jørgensen (1966) have prepared the RCl_6^{3-} , and RBr_6^{3-} ions with the triphenylphosphonium cation and measured their spectra in an acetonitrile-succinonitrile mixed solvent. For the cerium(III) compounds the 4fⁿ → 4fⁿ⁻¹5d¹ transition

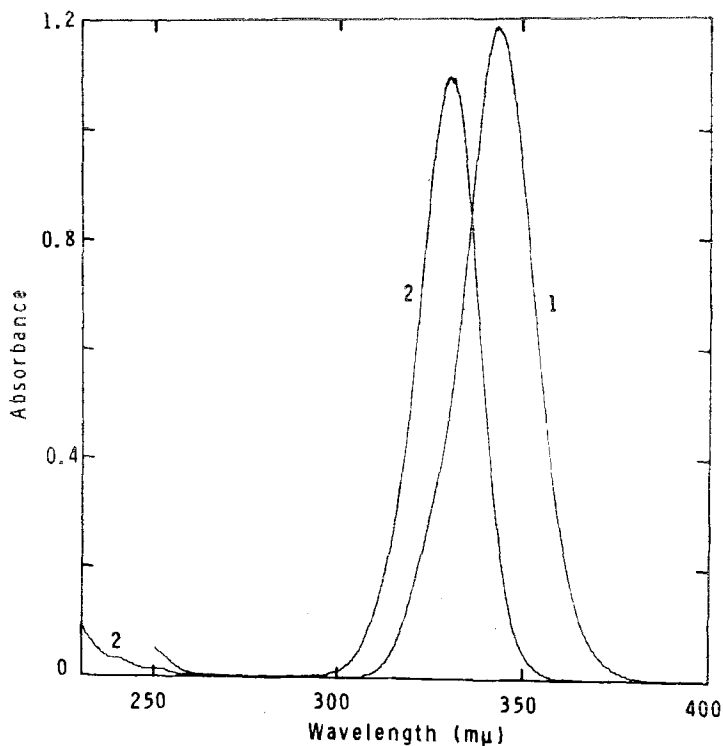


Fig. 25.18. The $4f-5d$ transitions for (1) CeBr_6^{3-} , (2) CeCl_6^{3-} in acetonitrile. (Reprinted with permission from Ryan, J.L. and C.K. Jørgensen, 1966, *J. Phys. Chem.* **70**, 2845-2857.)

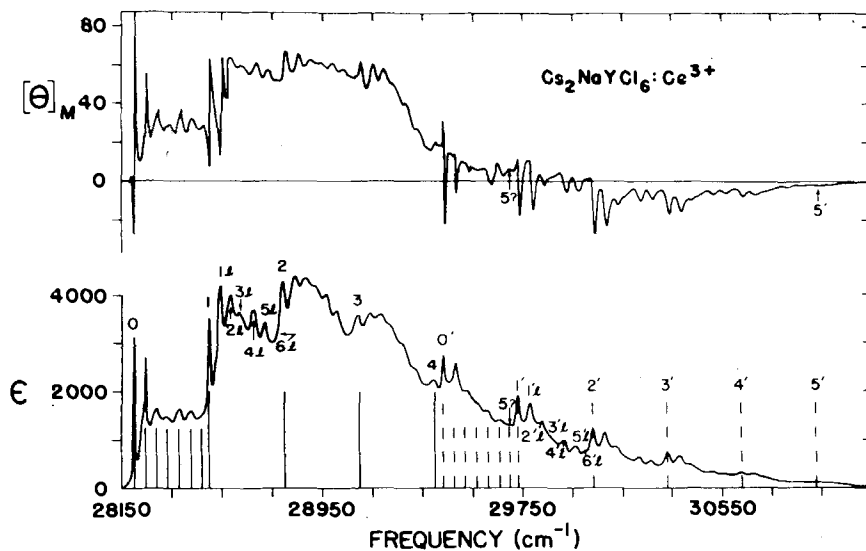


Fig. 25.19. Absorption (bottom) and Magnetic Circular Dichroism (top) spectra of $\text{Cs}_2\text{NaYCl}_6:\text{Ce}^{3+}$ at about 6 K. (Reprinted with permission from Schwartz, R.W. and P.N. Schatz, 1973, *Phys. Rev.* **B8**, 3229-3236.)

occurs at 330 nm and 342 nm for the chloride and bromide respectively. For the terbium(III) complexes there are two bands at 272 nm and 234 nm for the chloro complex and one band at 278 nm for the bromo complex. It has also been possible to correlate the position of these $4f \rightarrow 5d$ transitions with the standard (III–II) and (IV–III) reduction potentials for the lanthanides (Nugent et al., 1971, 1973).

A detailed study of the absorption and magnetic circular dichroism spectra of cerium(III) doped in $\text{Cs}_2\text{NaYCl}_6$ has been reported by Schwartz and Schatz (1973). In this interesting compound, which can be prepared for all the trivalent rare earth ions, the yttrium and cerium ions occupy an essentially perfect octahedral site surrounded by six chloride ions. The $4f \rightarrow 5d$ transition for cerium(III) has two components at $28\,196\text{ cm}^{-1}$ and $29\,435\text{ cm}^{-1}$ as a result of the splitting of the upper T_{2g} state by the strong spin-orbit coupling. Because no other transitions are observed out to $50\,000\text{ cm}^{-1}$, $10Dq$ must be $\geq 20\,000\text{ cm}^{-1}$ in the excited state. Besides these electronic transitions there is considerable vibronic structure due to the $\nu_1(a_{1g})$ vibration of the CeCl_6^{3-} moiety and the low-energy lattice vibrations. The magnetic circular dichroism spectrum is in complete accord with the absorption spectra results.

Charge transfer bands result whenever an easily oxidized ligand is bound to a trivalent lanthanide ion which can be reduced to the divalent state or when the ligand is bound to one of the tetravalent ions (Jørgensen, 1970). Such transitions are commonly observed in the spectra of complexes of samarium(III), europium(III), thulium(III), ytterbium(III), and cerium(IV). The position of these bands in the spectrum is markedly dependent on the ligand and the metal ion. For example, in the ions RCl_6^{3-} the charge transfer bands for europium(III),

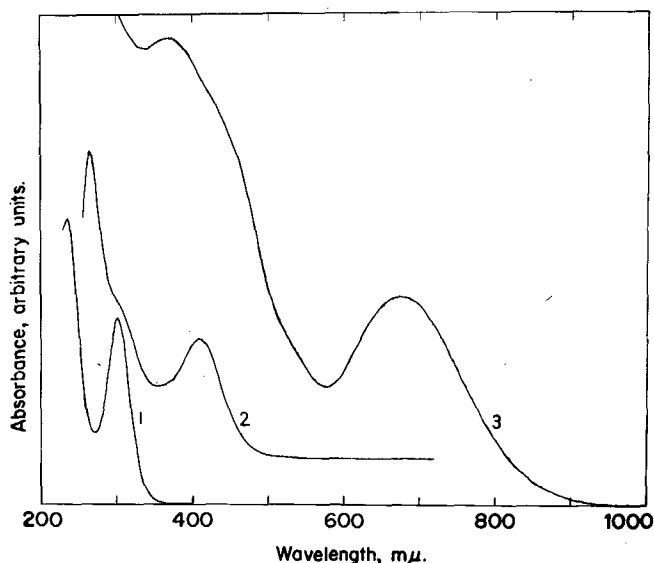


Fig. 25.20. Electron-transfer spectra of (1) EuCl_6^{3-} in acetonitrile, (2) EuBr_6^{3-} in acetonitrile, and (3) solid $[(\text{C}_6\text{H}_5)_3\text{PH}]_3\text{EuI}_6$. (Reprinted with permission from Ryan, J.L., 1969, *Inorg. Chem.* **8**, 2053–2058.)

ytterbium(III), and samarium(III) occur at 301 nm, 273 nm, and 232 nm respectively (Ryan and Jørgensen, 1966). The corresponding bands in the RI_6^- complex ions occur at 675 nm, 560 nm, and 402 nm (Ryan, 1969). The energy of the charge transfer band decreases as the ease of oxidation of the halide ion increases and as the ease of reduction of the lanthanide ion increases. The standard lanthanide (III–II) and (IV–III) reduction potentials have also been correlated with the energy of the first charge-transfer band (Nugent et al., 1971, 1973).

By far the most useful and interesting transitions in the spectra of the lanthanide complexes are the intra-4f transitions (Moeller, 1973). These are formally Laporte-forbidden and as a result tend to be very weak. In addition to being Laporte-forbidden those transitions that do not occur within the ground multiplet may also be spin-forbidden. Because of the shielding of the 4f electrons, the transitions that are observed are very sharp and line-like even in solution. These spectra are quite different from those of the d-transition elements and this can be explained by examining the magnitude of the perturbations acting on the two types of electrons (Figgis, 1966):

d-transition metal complexes

interelectronic repulsions \approx crystal field \gg spin-orbit coupling $>$ thermal energy

f-transition metal complexes

interelectronic repulsions \gg spin-orbit coupling $>$ crystal field \approx thermal energy

This order means that the crystal field in the lanthanides is acting to remove some of the degeneracy contained in the individual values of the J quantum number. This additional splitting is generally only on the order of two hundred wave numbers or so whereas in the d-transition elements it is on the order of 10 000–30 000 wave numbers.

When the spectrum of a complexed lanthanide(III) ion is compared to that of the aquated ion (the spectra of the “free” ions are in general not known), three effects are observed: (1) there are small changes usually toward longer wave lengths, (2) the bands undergo additional (or at least different) splitting, and (3) there is a significant change in the molar absorptivity of the individual bands. Each of these can be readily related to the changes in the strength and symmetry of the crystal field produced by the ligands.

For certain transitions which have $|\Delta J| \leq 2$, $|\Delta L| \leq 2$, and $\Delta S = 0$, the intensities are far more sensitive to complexation than for the other transitions. These have been termed “hypersensitive transitions” by Jørgensen and Judd (1964). The intensities of these transitions may be up to 200 times greater than the corresponding transition in the aquo ion whereas the intensities of the other transitions are generally approximately the same as in the aquo ion. The sensitivity of these transitions to the environment has led to their use in determining the coordination number for lanthanide complexes in solution. Since the subject of hypersensitivity has been reviewed recently by Henrie et al. (1976) and is covered in ch. 24 (Solution Chemistry), the phenomenon is only mentioned briefly here.

The shifts in the baricenters of the peaks in the spectra of rare earth complexes relative to the aquo ion are caused by what has been termed the nephelauxetic effect by Jørgensen (1971) and are related to the decrease in the interelectronic repulsion parameters in the complex. Numerous attempts have been made to relate this effect to weak covalency effects and these are considered in ch. 23 (Theoretical Chemistry of Rare Earths).

Transitions in the absorption spectra of the lanthanides are generally of the forced electric dipole type and, although formally Laporte-forbidden, gather intensity by mixing in states having opposite parity. In a few cases, particularly in europium(III), transitions that are magnetic dipole allowed ($\Delta J = 0, \pm 1$, but not $0 \leftrightarrow 0$) have been observed and from the polarization properties the magnetic dipole character has been confirmed. The spin selection rule is relaxed by spin-orbit coupling and so the transitions are observed even though they are weak. Transitions that are magnetic dipole in origin are generally at least an order of magnitude weaker than those that are electric dipole in origin. A comprehensive review of the intensities of lanthanide f-f transitions has recently been published (Peacock, 1975) and details of the various mechanisms responsible for electronic transitions in lanthanide compounds can be found there.

The symmetry of the environment determines the removal of the degeneracy of the values of J and which of the possible electric and/or magnetic dipole transitions will be allowed. In principle then the analysis of the number of observed bands for each transition permits the symmetry of the coordinated groups around the lanthanide ion to be determined. In practice this is often not possible, particularly in solutions where the solvent effects may broaden the bands so that the details of the splitting are obscured or in cases where more than one symmetry gives rise to the same splitting pattern. If the spectrum of a single crystal can be examined, then additional information can sometimes be obtained from the polarized absorption spectrum. It is self-evident that the success of these spectral techniques depends on having well-defined, pure compounds.

Because the spectral properties of the lanthanides are treated in detail in other chapters in this volume, only two examples of the use of the $4f^n$ absorption spectrum will be considered here. The absorption spectra of solutions containing the RCl_6^{3-} ions in acetonitrile-succinonitrile solutions obtained by Ryan and Jørgensen (1966) consisted of very weak transitions in most of the $4f^n \rightarrow 4f^n$ region and led them to the conclusion that the compounds were essentially octahedral. For the reasons mentioned above, however, it is generally more useful to have the solid-state spectrum in order to determine the symmetry more conclusively. The spectrum of a single crystal of $[\text{C}_6\text{H}_5)_3\text{PH}]_3\text{NdCl}_6$ has, therefore, been carefully measured at 77 K (Gruber et al., 1969). The spectrum is consistent with an octahedral symmetry surrounding the neodymium(III) ions with a slight distortion along one axis. In addition it appears that there are two slightly inequivalent neodymium(III) sites. The effects of the deviation from octahedral symmetry and the two inequivalent sites are sufficiently small that they do not affect a first-order crystal field analysis.

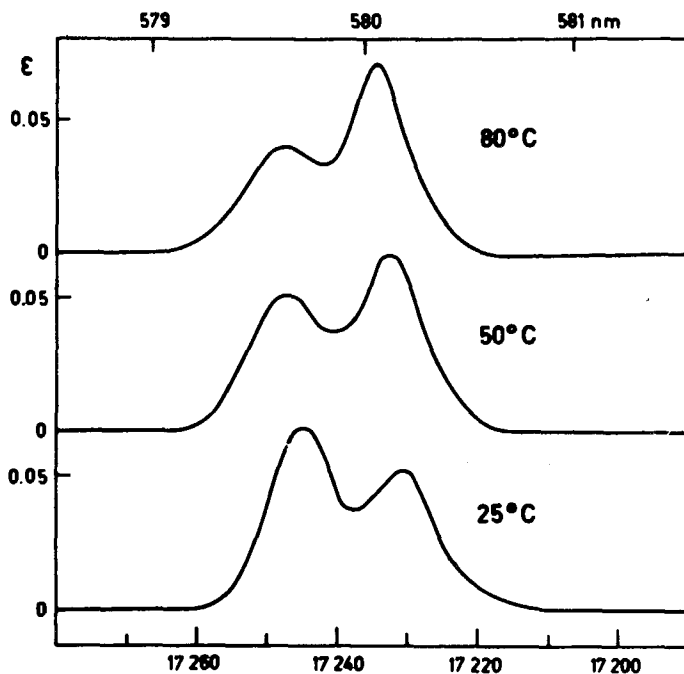


Fig. 25.21. Absorption spectra of $\text{Eu}(\text{EDTA})(\text{H}_2\text{O})_{x,y}$ as a function of temperature. (Reprinted with permission from Geier, G. and C.K. Jørgensen, 1971, *Chem. Phys. Lett.* **9**, 263–265.)

As discussed in section 4.2 the thermodynamic data for the formation of lanthanide complexes with EDTA have been interpreted in terms of a change in the degree of hydration of the complex between the light and heavier members of the series (Geier and Karlen (1971)). It has been further postulated that the complexes of samarium, europium, and gadolinium exist in an equilibrium mixture of the two forms which most plausibly differ by one molecule of water. The position of the equilibrium should be shifted to the less highly hydrated form by increasing the temperature. The ${}^7\text{F}_0 \rightarrow {}^5\text{D}_0$ transition of europium(III) in aqueous solutions of EuEDTA^- has two components separated by 14 cm^{-1} at about 580 nm (Geier and Jørgensen (1971)). These are shifted only very slightly (4 cm^{-1}) as the temperature changes from 25°C to 80°C. The relative intensities, however, change markedly and this is taken to be spectral evidence for the above equilibrium since $J = 0$ cannot be split by the crystal field.

Several studies of the circular dichroism (CD) spectra of aqueous solutions of the lanthanides in the presence of optically active ligands have been made (Katzin, 1970; Misumi et al., 1974; Prados et al., 1974). The CD spectra are highly structured in the region of the intra-4f transitions and are very sensitive to change in the pH of the solution particularly at values for which polynuclear hydroxo complexes could be formed.

5.2. Emission

The lanthanide ions, particularly those near the middle of the series, samarium, europium, terbium, and dysprosium, form complexes that often emit visible radiation when excited in the near-ultraviolet. This emission spectrum can be analyzed by essentially the same procedure as for the absorption spectrum except that the nature of the emission process will generally yield additional information concerning the ground multiplet of the ion. The technique can be applied to solutions and solids but in solution various processes operate to reduce the intensity of the emitted light and to broaden the bands which can result in a reduction of the amount of information that can be obtained.

There are still some unsettled points but the mechanism proposed by Crosby (1966) seems to be operative in the majority of complexes. In this mechanism there is excitation of the ligand portion of the molecule to the first excited singlet state, non-radiative decay to the ligand triplet state, further non-radiative decay to the excited terms of the lanthanide(III) ion and fluorescent emission upon decay to the ground state. If the complex does not contain organic ligands that absorb in the ultraviolet, then the initial excitation may be in a charge-transfer band or perhaps in the $4f^n \rightarrow 4f^{n-1}5d^1$ band with subsequent non-radiative decay to the excited terms of the $4f^n$ configuration (Blasse and Brill, 1970).

The complexes of the rare earths can be divided into three groups depending on their emission characteristics:

(1) Sc^{3+} , Y^{3+} , La^{3+} , and Gd^{3+} – For the first four ions no $4f \rightarrow 4f$ transitions are possible. For $\text{Gd}^{3+}(4f^7)$ the lowest lying excited term (${}^6\text{P}$) lies at a level too high for efficient energy-transfer to occur.

(2) Sm^{3+} , Eu^{3+} , Tb^{3+} , and Dy^{3+} – Complexes of these four ions yield very strong fluorescence characteristic of the lanthanide ion. This is a consequence of the fact that the resonance energy level of the metal ion is closely matched with the appropriate energy level (usually the lowest-lying triplet state) of the ligand and the efficiency of energy transfer is relatively high.

(3) Ce^{3+} , Pr^{3+} , Nd^{3+} , Ho^{3+} , Er^{3+} , Tm^{3+} , and Yb^{3+} – For each of these ions only small energy differences exist between terms, and the probability of non-radiative energy transfer is increased leading only to weak fluorescence.

The energy levels in europium are particularly favorable for analysis of the emission spectrum since the transitions occur between levels which have small (generally <3) values of J and by far the majority of the complexes that have been studied have contained europium(III) as the central ion. The energy levels of europium(III) and terbium(III) are given in table 25.9 from which it can be seen that the lowest transitions for europium, ${}^5\text{D}_0 \rightarrow {}^7\text{F}_J$ ($J = 0, 1, 2$) would be much easier to analyze than the lowest transitions for terbium, ${}^5\text{D}_4 \rightarrow {}^7\text{F}_J$ ($J = 6, 5, 4, 3, 2$).

The greatest volume of emission work has been done with the various β -diketone complexes particularly in the search for compounds that could be utilized as lasers (see ch. 35). Much of this work, unfortunately, involved complexes of uncertain composition and purity. The early work on the lumines-

TABLE 25.9.
Low-lying energy levels for europium(III) (Carnall et al., 1968b) and terbium(III) (Carnall et al., 1968a) in aqueous solution.

Eu(III) 4f ⁷		Tb(III) 4f ⁹	
Level	Energy (cm ⁻¹)	Level	Energy (cm ⁻¹)
⁷ F ₀	0	⁷ F ₆	85
⁷ F ₁	360	⁷ F ₅	2100
⁷ F ₂	1020	⁷ F ₄	3356
⁷ F ₃	1887	⁷ F ₃	4400
⁷ F ₄	2865	⁷ F ₂	5038
⁷ F ₅	3909	⁷ F ₁	5440
⁷ F ₆	4980	⁷ F ₀	5700
⁵ D ₀	17 277	⁵ D ₄	20 500
⁵ D ₁	19 028	⁵ D ₃	26 356 (calc.)
⁵ D ₂	21 519	⁵ D ₂	28 150 (calc.)
⁵ D ₃	24 408	⁵ D ₁	30 650
⁵ D ₄	27 670	⁵ D ₀	31 228 (calc.)

Emission in complexes generally occurs from the resonance levels ⁵D₀ and ⁵D₁ for europium(III) and ⁵D₄ for terbium(III).

cence of organic complexes of the rare earths has been reviewed by Crosby (1966).

More recently the emission spectra of the β -diketone complexes are being re-examined both to obtain additional structural information (Baczynski et al., 1973; Razvina et al., 1973) and to gain further insight into the nature of the energy transfer process between the ligand and lanthanide ion and within the excited manifold of the lanthanide ion (Dean and Shepherd, 1975; Fukuzawa et al., 1975; Neilson and Shepherd, 1976; Watson et al., 1975). Although the details of these studies are outside the scope of this chapter, the results from two interesting studies will be mentioned.

In n-butanol as solvent at 293 K Tb(acac)₃·3H₂O undergoes intermolecular energy transfer to the complexes R(acac)₃·3H₂O (R = Pr, Nd, Sm, Eu, Dy, Ho, or Er) (Napier et al., 1975). Measurement of the decay time of the ⁵D₄ level of the terbium(III) ion indicates that transfer takes place from that level to the excited levels of the other rare earths with bimolecular rate constants of 0.5–4.9 × 10⁵ dm³ mol⁻¹ s⁻¹. The fluorescence lifetime for the ⁵D₄ state of terbium in gaseous Tb(DPM)₃ has also been determined. These measurements have been made by Jacobs et al. (1975) as a function of temperature and pressure and the results demonstrate that intermolecular collisional deactivation is not important. Rather, the non-radiative deactivation is an intramolecular process and occurs by means of a transfer to low-lying excited states of the chelate. The fluorescence decay time is ≤ 1 μs at 200°C which is very much shorter than those observed in 95% ethanol (~600 μs) and in the solid state (~500 μs) at room temperature.

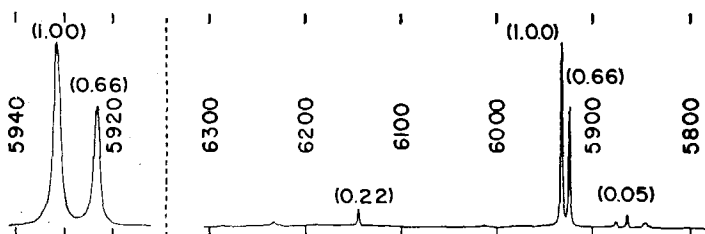


Fig. 25.22. Emission spectrum of octakis(4-picoline-N-oxide)europium(III) hexafluorophosphate at ~ 77 K. The numbers in parentheses are relative intensities. (Reprinted with permission from Rose, N.J. and E. Abramson, 1965, *J. Chem. Phys.* **42**, 1849–1850.)

The use of the fluorescence spectrum as an aid in structure indication for favorable cases can be illustrated by the work of Rose and Abramson (1965). The complex octakis(4-picoline-N-oxide)europium(III) hexafluorophosphate, since it involves unidentate ligands, would be expected to be either dodecahedral or square antiprismatic. The emission spectrum of this compound at 77 K is quite simple and consists of two peaks in the ${}^5D_0 \rightarrow {}^7F_1$ region and a very much weaker peak in the ${}^5D_0 \rightarrow {}^7F_2$ region. The former is a magnetic dipole transition and the latter is an electric dipole transition. If the complex is derived from the square antiprism, the symmetry around the europium(III) ion is D_{4d} (considering the oxygen atoms only) and if it is dodecahedral, the symmetry would be D_{2d} . Application of the appropriate selection rules for these two transitions (table 25.10) predicts two magnetic dipole transitions and no electric dipole transitions for the D_{4d} geometry but two magnetic and two electric dipole transitions for the D_{2d} geometry. (The irreducible representations and selection rules in the original paper are incorrect but the errors are compensating and the conclusions are correct.) This is strong indication that the complex has the square antiprismatic

TABLE 25.10.
Irreducible representations and allowed transitions in D_{2d}
(dodecahedron) and D_{4d} (square antiprism) symmetries.

J	D_{2d}	D_{4d}
0	A_1	A_1
1	$A_2 + E$	$A_2 + E_3$
2	$A_1 + B_1 + B_2 + E$	$A_1 + E_2 + E_3$
${}^5D_0 \rightarrow {}^7F_1$	$A_1 \rightarrow A_2$ $A_1 \rightarrow E$	$A_1 \rightarrow A_2$ $A_1 \rightarrow E_3$
${}^5D_0 \rightarrow {}^7F_2$	$A_1 \rightarrow B_2$ $A_1 \rightarrow E$	None

Magnetic dipole operator (D_{2d} : A_2, E ; D_{4d} : A_2, E_3) for ${}^5D_0 \rightarrow {}^7F_1$ and Electric dipole operator (D_{2d} : B_2, E ; D_{4d} : B_2, E_1) for ${}^5D_0 \rightarrow {}^7F_2$.

geometry. Although the X-ray structure of the complex has never been determined, the analogous octakis(pyridine-N-oxide)lanthanum(III) ion is essentially square antiprismatic (Al-Karaghoulis and Wood, 1972a).

The emission spectra of the europium(III) ion in $\text{Cs}_2\text{NaEuCl}_6$ and in $\text{Cs}_2\text{Na}(\text{Eu}_x\text{Y}_{1-x})\text{Cl}_6$ ($x = 0.01$ and 0.1) have recently been reported by Serra and Thompson (1976). In this compound the rare earth ion is in a site of perfect octahedral symmetry and as a result of the inversion symmetry only magnetic dipole transitions are allowed. The usually more intense electric dipole transitions are replaced by weak vibronic transitions. In the doped compound all possible magnetic dipole transitions between the ${}^5\text{D}_J$ levels ($J = 0, 1, 2, 3$) and the ${}^7\text{F}_J$ levels ($J = 0, 1, 2, 3, 4$) have been observed. Weak additional lines on the magnetic dipole transitions and the weak vibronic lines have been correlated with the various vibrational modes of the compound. The emission spectra complement the absorption spectra determined earlier by Schwartz (1975) and illustrate how the two types of spectra can be used to obtain a more complete picture of the energy levels.

The possibility of obtaining additional information about the excited states of fluorescent complexes of the rare earth ions europium and terbium using circularly polarized luminescence (CPL) has recently been advanced (Luk and Richardson, 1974, 1975). In principle CPL measurements will provide the same structural information about emitting states as CD measurements provide about the molecular ground state. CPL involves measuring the differential intensities of left- and right-circularly polarized radiation in the spontaneous emission spectrum of a chiral luminescent system. Luk and Richardson (1975) have begun studies of the CPL spectra of aqueous solutions of the complexes of europium and terbium with a number of optically active ligands such as malic and aspartic acids and alanine and serine. The CPL spectra are remarkably sensitive and may yield several peaks in regions where the total luminescence gives only a single unresolved or asymmetric peak. Changes in ligand type and donor atom availability by altering the pH of these solutions lead to marked changes in the sign and intensity patterns in the CPL spectra. This promises to be a valuable additional tool in the study of rare earth complexes and will probably make its most significant contribution in the study of the complexes formed by the rare earth ions with ligands of biological interest and importance.

5.3. Mössbauer spectroscopy

The Mössbauer effect should in principle provide useful information with respect to the bonding in rare earth complexes (Ofer et al., 1968) since the isomer shift is dependent on the electron density at the nucleus. A large number of rare earth nuclei are suitable for Mössbauer spectroscopy, but only for ${}^{151}\text{Eu}$ have complexes been extensively studied. Although a number of early papers appeared, the results were based on the report that the isomer shift in Eu_2O_3 relative to EuF_3 was less than 0.05 mm s^{-1} whereas recent investigations have shown that for commercial Eu_2O_3 the ${}^{151}\text{Eu}$ isomer shift relative to $\text{EuF}_3 \cdot 2\text{H}_2\text{O}$ is

1.06 mm s⁻¹ (Large et al., 1969). Several europium(III) complexes including aminocarboxylates, β -diketones, and 1,10-phenanthroline complexes have now been re-investigated by Glentworth et al. (1973). The range of isomer shifts found for thirty-three complexes is quite small (0.8 mm s⁻¹) signifying that the measured isomer shift is insensitive to the nature of the coordinating ligand. The data again indicate that the bonding in these complexes is predominantly ionic. Additional europium complexes have been studied by Lyle and Witts (1975), Taragin and Eisenstein (1973), and Zaheer et al. (1974). The results obtained from these measurements confirm the suggestions made above. The existence of a slight degree of covalency is suspected and it is postulated that this involves a shift of a small amount of electron density from the ligands into the 6s orbital of europium. Any involvement of the 4f orbitals in covalent bonding must be quite small for these compounds.

The area under the curve of resonant absorption has been termed the resonant effect. Complexes that give large resonant effects, such as some of the aminopolycarboxylate chelates and oxalate complexes, are thought to be polymeric with carboxyl groups serving as the bridging ligands. For example, NH₄[Eu(EDTA)]·8H₂O gives a small resonant effect whereas H[Eu(EDTA)] gives a large effect (Mackey and Greenwood, 1972). The Mössbauer effect is treated in detail in ch. 18 of vol. 2.

5.4. Magnetic susceptibility

Because the 4f electrons in the lanthanides are at most only slightly involved in the bonding in complexes, the magnetic moments found for complexes are very close to those observed for simple compounds (Moeller, 1973). This means that measurements of the magnetic susceptibility are of limited use in the study of rare earth complexes. Very careful measurements over a range of temperatures can be used, however, to determine the nature of the lowest components of the ground multiplet and to arrive at a set of crystal field parameters. Early measurements were made on some powdered lanthanide trisacetylacetonates and EDTA complexes by Fritz et al. (1961).

The magnetic susceptibilities of single crystals of the hexakisantipyrenelanthanide(III) iodides (R = Ce, Pr, Nd, Eu, Tb, Dy, Er, Tm, and Yb) have been studied in the temperature range 80–300 K (Gerloch and Mackey, 1970a, b, 1971a, b, c, 1972a, b, c, d). These are six-coordinate complexes which have rigorous D_{3d} symmetry and the results have been analyzed to obtain a set of crystal field parameters.

The compound Cs₂NaRCl₆ mentioned previously contains an octahedral RCl₆³⁻ anionic grouping and the magnetic susceptibility of nine lanthanide ions (Ce, Pr, Nd, Tb, Dy, Ho, Er, Tm, and Yb) have been determined in this compound in the temperature range 2.5 to ~80 K (Karraker, 1971; Hoehn and Karraker, 1974). The values determined for the parameters A₄ and A₆ are essentially constant over the compounds considered. Attempts to explain these crystal-field parameters in this series of simple isomorphous compounds in terms

of a point-charge model were completely unsuccessful (Dunlap and Shenoy, 1975).

5.5. NMR and ESR

Studies of the proton magnetic resonance of complexes of the rare earths, with the exception of the adducts of the shift reagents (see ch. 38) and the studies with biological ligands (see ch. 39), have been much fewer than for the d-transition complexes. One group of measurements has been directed toward the determination of the cation hydration number for the rare earth ions in both aqueous solutions and in mixed solvent systems (Fратиello et al., 1971, 1973). By appropriate experimental techniques paramagnetic ions as well as diamagnetic ions have been studied. Although a coordination number of six is implied from the pmr results, it is not possible to rule out the possibility that there are other water molecules that are exchanging more rapidly. However, even at -130°C the lutetium(III) hydration number remains six in perchlorate solutions. There is strong evidence for coordination by the nitrate ion and displacement of some of the water molecules in the rare earths and a clear indication of hydrolysis for scandium(III) even in acidified solutions (Fратиello et al., 1970). An NMR investigation of the hydration of lanthanum(III) in various solutions using ^{139}La has also demonstrated the existence of inner-sphere complexes with nitrate and sulfate ions and suggests that there is an equilibrium between $\text{La}(\text{H}_2\text{O})_9^{3+}$ and $\text{La}(\text{H}_2\text{O})_8^{3+}$ (Nakamura and Kawamura, 1971). Studies of the pmr and oxygen-17 spectra by Reuben and Fiat (1969a, b) suggested, however, that only a single hydrated species is present which persists over a wide range of concentrations. Their results indicate that perchlorate ions do not form inner-sphere complexes whereas acetate, nitrate, and probably chloride ions do. Lower limits for the rate contents of water exchange with solvent water have also been estimated for Tb^{3+} , Dy^{3+} , Ho^{3+} , Er^{3+} , and Tm^{3+} . Some of the difficulties inherent in measurements of hydration numbers with this technique have been discussed by Haas and Navon (1972).

The use of pmr in elucidating the process of ligand exchange is illustrated by studies on tetrakis- β -diketone yttrium(III) complexes. The ligand exchange equilibria in this system for hexafluoroacetylacetonate and trifluoroacetylacetonate (Cotton et al., 1966; Serpone and Isheyek, 1971) have been studied in some detail using the methylene proton resonances. In the temperature range -58 to -16°C in deuteriochloroform, the equilibrium quotients for the formation of mixed complexes are three-five times larger than those expected statistically with the assumption of random distribution of ligands. These deviations have been ascribed to enthalpy changes since the entropy changes are essentially zero. Moreover, analysis of the coalescence behavior indicates that the hexafluoroacetylacetonate ligands exchange faster than the trifluoroacetylacetonate ligands.

Kinetic information has been obtained from the pmr spectra for other systems such as EDTA (Sc, Y, La, Lu) (Merbach and Gnaegi, 1969), NTA (Sc, Y, La, Lu)

(Merbach and Gnaegi, 1971), and 4,4'-di-n-butyl-2,2'-bipyridine and 5,5'-di-n-butyl-2,2'-bipyridine (Y, La, Ce, Pr, Nd, Sm, Eu, Lu) (Hart et al., 1970b).

The isotropic shifts in the proton resonances observed in the presence of a paramagnetic lanthanide ion could arise both from a Fermi contact term and the geometric dipolar term (as an example see Quereshi and Walker (1974)). In rare earth complexes, particularly in aqueous solution where there are uncertainties regarding the geometry and composition of the coordination sphere and where there may be substantial interactions between the cation and solvent molecules, the division of the observed shift into its components is not an easy problem. Treatment of data in terms of the pseudo-contact shift only must be made with some caution even in what would appear to be the most favorable cases (Moeller, 1972). (A complete discussion of problems of these sorts will be found in chs. 18, 38, 39 and in Fischer (1973)).

The fact that the scandium(III) ion has the $3d^0$ electronic configuration severely limits the kinds of physical methods that can be brought to bear on determining the nature of the chemical environment in its complexes. The ^{45}Sc nuclide has 100% natural abundance and a high sensitivity compared to protons and NMR studies using ^{45}Sc may well prove to be a powerful tool (Melson et al., 1974). NMR spectra of aqueous solutions of scandium(III) chloride, perchlorate, nitrate, and sulfate have been obtained and it has been demonstrated that the chemical shifts for ^{45}Sc at very low concentrations for the chloride, bromide, and perchlorate are independent of the anion and may be characteristic of the $[\text{Sc}(\text{OH})]^{2+}$ ion. At higher concentrations the chemical shifts are both anion- and concentration-dependent and reflect the formation of bromo and chloro complexes and in the case of the perchlorate, polymeric hydroxo species. The chemical shifts for the nitrate and sulfate are different from the others and indicate that even at low concentrations there must be significant quantities of the respective complexes.

When the change in chemical environment is more pronounced, there is a considerable chemical shift. For example the chemical shift for $\text{Sc}(\text{acac})_3$ in benzene is +85 ppm relative to 0.1 M aqueous $\text{Sc}(\text{ClO}_4)_3$. Thus it seems that this experimental technique holds considerable promise for the study of scandium complexes.

Electron spin resonance measurements yield detailed information with respect to the splitting of the ground state and can be used to determine the crystal field parameters (see ch. 18 for a complete discussion). The complexes that have been studied include $\text{Ln}(\text{C}_2\text{H}_5\text{SO}_4)_3 \cdot 9\text{H}_2\text{O}$ (which contains the nine-coordinate hydrated ion), the double nitrate $\text{Ln}_2\text{Mg}_3(\text{NO}_3)_{12} \cdot 24\text{H}_2\text{O}$ (which contains the icosahedral $\text{R}(\text{NO}_3)_6^{3-}$ ion), and the hexakis(antipyrene) iodides as well as a number of simple compounds that contain extended lattices (Abragam and Bleaney, 1970). The ion to be studied is generally doped into the appropriate lanthanum, lutetium, or yttrium compound.

Recently the esr spectra of Ce^{3+} , Dy^{3+} , and Yb^{3+} have been determined in $\text{Cs}_2\text{NaYCl}_6$ (Schwartz and Hill, 1974). The spectra are isotropic and reconfirm the octahedral nature of the RCl_6^{3-} moiety in this compound. The g -values imply

that there is a small amount of covalency in the bonds. ENDOR measurements on the ytterbium salt give a g -value that differs slightly from the esr results and the crystal field splitting of 225 cm^{-1} is greater than that determined from the magnetic susceptibility (Devaney and Stapleton, 1975). Schwartz et al. (1976) have also reported from esr measurements on gadolinium-doped compounds that there is a phase change between room temperature and 77 K for the complexes with the lighter lanthanides. This could be due to an order-disorder transformation involving the cesium ions.

6. Specific types of complexes

In this section a representative number of types of ligands which have been found to form solid rare earth complexes will be discussed and contrasted. Because the number of publications describing solid complexes is now very large and increasing at a substantial rate, the coverage will of necessity not encompass all of the known complexes. However, insofar as possible, examples of all the major types of complexes will be given and the emphasis will be on the more recent work, although for completeness, reference will be made to earlier work for particularly important ligands. There have been several previous reviews of solid rare earth complexes (Forsberg, 1973; Melson, 1975; Moeller, 1972; Moeller et al., 1965, 1968, 1973; Moseley, 1975; Sinha, 1966; Stevenson and Nervik, 1961).

6.1. Inorganic

6.1.1. Halides and pseudohalides

Large numbers of compounds have been prepared that contain the rare earth ion coordinated to the halide and pseudohalide ions and representative examples are given in table 25.11.

The complexes with the halide ions, although they often appear to have six ligands bound to the rare earth ion, are generally extended lattice compounds and are not octahedral. This is particularly true with the fluoro complexes. For example, although the formula of $(\text{NH}_4)_2\text{CeF}_6$ implies the existence of six-coordination about the Ce(IV) ion, the crystal structure determined by Ryan et al. (1969) clearly shows that the coordination is approximately square antiprismatic and the cerium has eightfold coordination. The compounds A_2BRF_6 (A, B = alkali metals) (Bucher et al., 1974) and $\text{Cs}_2\text{NaRCl}_6$ (Morss et al., 1970), however, have octahedral coordination and are particularly suited for studies designed to provide spectral and magnetic information as has been discussed in previous sections. The vibrational Raman spectra have been determined for the lanthanum (Papatheodorou, 1975), praseodymium (Amberger et al., 1975), neodymium and erbium (Barbanel et al., 1975) complexes. The far infrared spectra have also been determined for the latter two lanthanides. The results

TABLE 25.11.
Representative complexes with inorganic ligands.*

<i>Halide ions</i>		
MRF_4	(R = La-Lu, Y, Sc)	Brown (1968)
M_3RF_6	(R = La-Lu, Y, Sc)	Brown (1968)
M_2CeF_6		Brown (1968)
Cs_3RF_7	(R = Ce, Pr, Nd, Tb, Dy)	Brown (1968)
Cs_2KRF_6		Siddigi and Hoppe (1970)
M_3RCl_6		Ryan and Jørgensen (1966)
$M_3R_2Cl_6$		Brown (1968)
M_2CeCl_6		Brown (1968)
Cs_2NaRCl_6	(R = La-Lu, Y, Sc)	Morss et al. (1970)
M_3RBr_6		Ryan and Jørgensen (1966)
M_3RI_6		Ryan (1969)
<i>Pseudohalide ions</i>		
$M_3R(NCS)_6$	(R = Pr-Lu, Y, Sc)	Martin et al. (1968) Burmeister et al. (1969) Eremin et al. (1970)
$M_3R(NCSe)_6$	(R = Pr-Er, Y)	Burmeister and Deardorff (1970)
$M_3R(NCO)_6$	(R = Eu-Yb, Y, Sc)	Dieck and Moeller (1973a)
$M_3R(NCO)_3(NO_3)_3$	(R = La-Yb)	Dieck and Moeller (1974)
$M_3R(NCO)_3X_3$	(X = Cl, NCS; R = Dy, Er, Yb, Y)	Dieck and Moeller (1973b)
<i>Oxyanions</i>		
$M_3R(NO_3)_6$	(R = La-Sm)	Walker and Weeden (1973)
$M_2R(NO_3)_5$	(R = Nd-Lu)	Walker and Weeden (1973) Quereshi and Walker (1974)
$(NH_4)_2Ce(NO_3)_6$		Beineke and Delgaudio (1968)
$M_3Sc(PO_4)_3$	(M = Sr, Ba, Pb)	Engel (1972)

*In this and subsequent tables M signifies an alkali metal or organic ammonium, phosphonium, etc., cation. If the scandium complex has been prepared, this will be specifically noted.

confirm the octahedral coordination around the lanthanide ion and the totally symmetric A_{1g} band appears at 274 cm^{-1} for lanthanum, 281 cm^{-1} for praseodymium, 278 cm^{-1} for neodymium, and 289 cm^{-1} for erbium. In addition the Raman spectrum of the praseodymium complex at 10 K contains electronic lines due to electronic transitions within the lowest lying levels. The number and spacing of these bands suggest that the praseodymium complex is weakly distorted, in agreement with the esr results (Schwartz et al., 1976).

The first solid chloro complexes of the trivalent ions to be isolated were $[(C_6H_5)_3PH]_3RX_6$ and $[C_5H_5NH]_3RX_6$ for which octahedral coordination was established from the visible spectra (Ryan and Jørgensen, 1966). The far infrared and Raman spectra have also shown that the ions have essentially perfect octahedral coordination (Choca et al., 1974, 1975). The totally symmetric stretching frequency is similar to that found for Cs_2NaRCl_6 , varying from

252 cm^{-1} for neodymium to 263 cm^{-1} for ytterbium. It appears that these anionic, low-coordination complexes can only be stabilized by a large counter ion and similar compounds have been prepared using the tetrabutylammonium ion (Walker et al., 1971).

Prior to 1968 a number of complexes of the thiocyanate ion had been prepared but each of them contained additional adduct molecules (such as dioxane or alcohol) that were most likely coordinated as well (Golub and Borsch, 1967). In 1968 the preparation of the complexes $[(\text{C}_4\text{H}_9)_4\text{N}]_3\text{R}(\text{NCS})_6$ was reported along with the crystal structure of the erbium complex (Martin et al., 1968). This was the first six-coordinate, discrete, anionic complex for which an X-ray diffraction study had been made. These compounds are quite stable, non-hygroscopic, soluble in many organic solvents, and melt without decomposition (Burmeister et al., 1969). The corresponding selenocyanates have also been prepared and, as expected, they are considerably less stable decomposing quite rapidly in moist air or in solution (Burmeister and Dearnorff, 1970).

Although initial attempts to prepare similar complexes with the cyanate ion were unsuccessful, Dieck and Moeller (1973a) were able to isolate $[(\text{C}_2\text{H}_5)_4\text{N}]_3\text{R}(\text{NCO})_6$ ($\text{R} = \text{Sc}, \text{Y}, \text{Eu}, \text{Gd}, \text{Dy}, \text{Ho}, \text{Er}, \text{and Yb}$) complexes from the reaction of the anhydrous chlorides with excess tetraethylammonium cyanate in absolute ethanol. All indications are that these are six-coordinate, octahedral complexes (Amberger et al., 1976), and the infrared spectrum shows that the cyanate is N-bonded as is also the case for the thiocyanate and selenocyanate complexes. In addition the complexes $[(\text{C}_2\text{H}_5)_4\text{N}]_3[\text{R}(\text{NCO})_3\text{X}_3]$ ($\text{R} = \text{Dy}, \text{Er}, \text{and Yb}, \text{X} = \text{Cl and NCS}$) could be isolated when the ratio of reactants was 3 : 1 and all experimental results point to six coordination (Dieck and Moeller, 1973b). Reaction of the anhydrous nitrates with tetraethylammonium cyanate in a 1 : 3 molar ratio resulted in the mixed complexes $[(\text{C}_2\text{H}_5)_4\text{N}]_3[\text{R}(\text{NCO})_3(\text{NO}_3)_3]$ ($\text{R} = \text{La}, \text{Pr}, \text{Nd}, \text{Sm}, \text{Eu}, \text{Gd}, \text{Er}, \text{and Yb}$) (Dieck and Moeller, 1974). Infrared studies again indicate that the cyanate is ligated through the nitrogen atom and that all three nitrate groups are coordinated. It is likely that the nitrate groups are bidentate which would give a coordination number of nine.

The difficulties inherent in trying to assign coordination numbers, and even in deciding which groups are coordinated, is illustrated by the compounds $\text{K}_4\text{Nd}(\text{NCS})_7 \cdot 4\text{H}_2\text{O}$ and $\text{K}_4\text{Eu}(\text{NCS})_7 \cdot 6\text{H}_2\text{O}$ reported by Lazarev et al. (1973). These compounds contain eight-coordinate neodymium and europium in the $[\text{Ln}(\text{NCS})_4(\text{H}_2\text{O})_4]^-$ unit. The coordination polyhedron is a dodecahedron in which each trapezoid contains two water molecules on the A vertices and two nitrogen atoms from the thiocyanates on the B vertices. The other three thiocyanate ions are not coordinated to the lanthanide ion.

In addition to these simple halide and pseudohalide complexes there are many complexes with organic ligands in which all or part of the halide or pseudohalide ions are coordinated as well. Because of the relatively weak interactions between these donor atoms and the rare earth ions, the metal-ligand stretching occurs in the far-infrared and it is generally difficult to differentiate these from

the low-energy vibrations of the organic ligands. Many examples of these kinds of complexes are considered in later sections.

6.1.2. Oxyanions

A number of oxyanions form complexes (inner- and outer-sphere) in aqueous solution with the rare earth ions. However, the number of authenticated solid complexes is much smaller. By far the greatest number of complexes is formed with the nitrate ion and the structure of some of these were discussed previously (sections 3.9, 3.10). In addition to these it is possible to prepare $[(C_4H_9)_4N]_3[R(NO_3)_6]$ for $R = La, Ce, Pr, Nd,$ and Sm and $[(C_4H_9)_4N]_2[R(NO_3)_5]$ for $R = Ho, Er, Tm, Yb,$ and Lu and $[(C_3H_7)_4N]_2[R(NO_3)_5]$ for $R = Nd, Ho, Tm,$ and Yb (Walker and Weeden, 1973). The role of the size of both the cation and lanthanide ion in determining the coordination number is again demonstrated. At least in the case of neodymium the visible spectra of both salts in nitrobenzene and dichloromethane are identical which indicates that $Nd(NO_3)_6^{3-}$ is unstable in these solvents.

Lanthanide nitrates are soluble in $LiNO_3$ - KNO_3 eutectic and the complex nitrates $K_3R_2(NO_3)_9$ ($R = Pr, Nd,$ and Sm) can be isolated (Carnall et al., 1973). The praseodymium compound is surrounded by twelve oxygen atoms belonging to six nitrate ions and is in the form of a distorted icosahedron.

There is a large variety of complexes that contain organic ligands as well as nitrate ions. For many of these complexes it can be suspected from the formulation that at least some of the nitrate ions are coordinated and these can be differentiated by an examination of the infrared and Raman spectra (Brown, 1975). The ionic nitrate group has D_{3h} symmetry and four fundamental vibrations, three of which are infrared active and one which is Raman active only. Upon coordination either as a bidentate or monodentate ligand, the symmetry is reduced to C_{2v} , which gives six infrared active vibrations and six Raman active vibrations. The doubly degenerate ν_4 band of the ionic nitrate (700 cm^{-1}) is split into the ν_3 and ν_5 bands of the coordinated nitrate. In addition Raman polarization studies can distinguish monodentate coordinated nitrate from bidentate and bridging nitrate. As an example the presence of only coordinated nitrate is indicated for the compound $La(HMPA)_3(NO_3)_3$ whereas in $Yb(HMPA)_4(NO_3)_3$ both coordinated and ionic nitrate are present (Sylvanovich, Jr. and Madan, 1972).

The nitrite ion forms a series of complexes having the formula $Cs_2NaLn(NO_2)_6$ ($Ln = La$ - Er) and $Rb_2NaLn(NO_2)_6$ ($Ln = La$ - Nd). The infrared and Raman spectra have been interpreted in terms of T_h symmetry and a weak lanthanide-nitrogen bond (Barnes and Peacock, 1971).

Although the perchlorate ion is generally a non-coordinating anion, there are examples in which it is coordinated to the lanthanide ions. With hexamethylphosphoramide the lanthanides form the complexes $R(HMPA)_4(ClO_4)_3$ (Durney and Marianelli, 1970). The infrared and Raman spectra of these complexes have bands that correspond both to ionic perchlorate and coordinated perchlorate

(Scholer and Merbach, 1975). The Raman band at 436 cm^{-1} is indicative of a perchlorate having C_{2v} symmetry; that is, the perchlorate is a bidentate ligand. The spectra from lanthanum to ytterbium undergo a slow change that is interpreted as indicating a decrease in the amount of ionic perchlorate and a gradual replacement of bidentate perchlorate coordination with monodentate coordination.

6.2. Organic oxygen donors

Because of their class (a) behavior the rare earth ions form the largest number of complexes with ligands that utilize oxygen as the donor atom. The types of ligands are varied but can be broken down into six groups: (a) carboxylic and hydroxycarboxylic acids, (b) carbonyl compounds, (c) β -diketones, (d) alcohols and alkoxides, (e) macrocyclic polyethers, and (e) $Q_nX \rightarrow O$ compounds ($X = N, P, S, \text{ etc.}$, and $Q = \text{an organic group}$). Included among these are both unidentate ligands as well as polydentate ligands. Most of the rare earth complexes that are formed with unidentate ligands involve ligands from this group, particularly the carbonyl ligands and $Q_nX \rightarrow O$ ligands. Among these are a variety of formulations and it is now quite clear as shown earlier that conclusions with regard to coordination number based on the chemical formulation, particularly with the unidentate ligands in this class, can only be made with considerable caution. The possibility of anion coordination when the anion is nitrate, thiocyanate, or one of the halides, is relatively high. The maximum number of coordinated unidentate organic ligands is generally only found in those compounds in which the counter anion is of low coordinating tendency toward the rare earth ion such as the perchlorate, iodide, or more recently, the hexafluorophosphate ion or the tetraphenylborate(III) ion. It is important to note that in a series of complexes of the same ligand the chemical formulation may well change as the size of the lanthanide ion decreases reflecting a change in the coordination number. This may also be reflected not by a change in the number of bound organic ligands but rather in the change from coordinated anion to uncoordinated anion due to the increased steric crowding and, consequently, by a decrease in the coordination number.

6.2.1. Carboxylic and hydroxycarboxylic acids

Complexes of the rare earth ions with carboxylic and hydroxycarboxylic acids were of importance in the development of ion exchange methods for the separation of the rare earths. A large number of complexes have been prepared and characterized and these have been reviewed recently by Bagnall (1975). In the solid state most of these compounds are hydrated and have structural forms of some complexity in which the carboxylate anions also may serve as bridging groups between metal ions. As might be expected, polydentate ligands have a greater tendency to bond only to a single metal ion. Some representative compounds are presented in table 25.12.

TABLE 25.12.
Representative complexes with carboxylic and hydroxycarboxylic acids.*

$R(C_2H_3O_2)_3 \cdot 4H_2O$	(R = Sm-Lu)
$R_2(C_2O_4)_3 \cdot 10H_2O$	
$R_2(C_2O_4)_3 \cdot 6H_2O$	(R = Ho-Lu, Sc)
$R_2(\text{malonate})_3 \cdot 8H_2O$	(R = Ce-Gd)
$R_2(\text{malonate})_3 \cdot 6H_2O$	(R = Ce-Eu)
$Sc(OH)(\text{malonate}) \cdot 2H_2O$	
$R(C_2H_3O_2)_3 \cdot o\text{-phen}$	
$M[R(C_2H_3O_2)_4] \cdot xH_2O$	
$M_2[R(C_2H_3O_2)_5] \cdot xH_2O$	
$M_3[R(C_2H_3O_2)_6] \cdot xH_2O$	
$M[R(C_2O_4)_2] \cdot xH_2O$	
$R(\text{tartrate})Cl \cdot xH_2O$	
$R(\text{citrate}) \cdot xH_2O$	
$K_3R(\text{citrate})_2 \cdot 3H_2O$	

*Bagnall (1975), Hansson (1973e), Melson (1975).

The complexes formed by oxalic and malonic acids have been carefully studied and the detailed structural features have been obtained from X-ray diffraction measurements (Hansson, 1973e). The oxalate ions in these complexes serve as bridging ligands and the larger metal ions have coordination number nine whereas the smaller ions have coordination number eight. The malonate ions in the rare earth malonates are of two different types, those that are involved in six-membered chelate ring formation and those which are not.

The most extensively studied of the hydroxycarboxylic acids is glycolic acid. This ligand forms neutral tris complexes with the lanthanide ions, $R(\text{HOCH}_2\text{COO})_3$ (Grenthe, 1971a,b, 1972), in which the coordination numbers are greater than six by the sharing of carboxylate groups between polyhedra as well as having chelated glycolate anions. Hydrothermal treatment of the tris-glycolate complexes of the heavier lanthanides converts them into $[R(\text{HOCH}_2\text{COO})(\text{OCH}_2\text{COO})(\text{H}_2\text{O})] \cdot \text{H}_2\text{O}$ the structure of which was mentioned previously (Grenthe, 1969).

The nicotinic and isonicotinic acid complexes with the lanthanide ions also show the presence of both chelated and bridging carboxylate groups (Kay et al., 1972). The details of the structures vary according to the lanthanide ion and counter ions present.

The ligand diglycolic acid (oxydiacetic acid) is a terdentate ligand which forms the complexes $\text{Na}_3[R(\text{OCOCH}_2\text{OCH}_2\text{OCO})_3] \cdot 2\text{NaClO}_4 \cdot 6\text{H}_2\text{O}$ (Albertsson, 1972d). As suggested previously, this ligand forms nine-coordinate complexes in which the coordination positions are occupied by the two carboxylate groups which function in a unidentate fashion and by the ether oxygens. As expected the metal ion-ether oxygen distance is longer than the metal ion-carboxylate oxygen distance.

6.2.2. Carbonyl compounds

The number of complexes formed by ligands containing the carbonyl group is very large. Some typical examples of these complexes are given in table 25.13. The largest numbers of compounds are derived from urea and its derivatives and the various amides.

The ligand N,N,N',N'-tetramethylurea forms different types of complexes with the rare earths depending on the counter anion. With the perchlorate ion the compounds have the formula $R(TMU)_6(ClO_4)_3$ for all the lanthanides (Giesbrecht and Kawashita, 1970). With the chlorides the compounds $La(TMU)_{3.5}Cl_3$ (probably dimeric) and $R(TMU)_3Cl_3$ are formed (Perrier et al., 1970; Seminara et al., 1969). For the nitrates the complexes $R(TMU)_3(NO_3)_3$ were found to contain coordinated nitrate ions (Vicentini and Najjar, 1970) and with the thiocyanate ion the compounds $R(TMU)_5(NCS)_3$ ($R = La-Nd$), $R(TMU)_4(NCS)_3$ ($R = Sm-Er, Y$), and $R(TMU)_3(NCS)_3$ ($R = Tm-Lu$) were prepared (Perrier and Vicentini, 1973). In all of these except the perchlorate compounds there must be a substantial amount of anion coordination. The effects of differing coordination tendencies of the anions and of the lanthanide contraction are clearly evident. The molecular structure of $Eu(TMU)_3(NO_3)_3$ has now been determined (Chieh et al., 1976) and the three nitrate ions are coordinated in a bidentate manner to give a coordination number of nine to the complex. The polyhedron of the europium coordination sphere does not conform to either the tricapped trigonal prism or the monocapped square antiprism. Presumably this is due to the small bite of the nitrate ions and the structure is best described in terms of a pseudo octahedral arrangement with each nitrate ion occupying one of the octahedral coordination positions.

The complexes of dimethylacetamide have been extensively studied with a large number of lanthanide salts (Moeller and Vicentini, 1965; Vicentini and de Carvalho Filho, 1966; Vicentini et al., 1969). The results are basically the same as observed with tetramethylurea except that the steric requirements here must be somewhat less since it was possible to prepare $R(DMA)_8(ClO_4)_3$ ($R = La-Nd$), $R(DMA)_7(ClO_4)_3$ ($R = Sm-Er, Y$), and $R(DMA)_6(ClO_4)_3$ ($R = Tm-Lu$). Similar differences between the complexes of the two ligands were noted for the other series of anions.

The Brazilian workers have also studied complexes formed with the diamides, diacetamide (Airoldi and Gushikem, 1972), di-n-butyramide (Gushikem et al., 1973), N,N-dimethylacetoacetamide (Perrier and Vicentini, 1974), N,N,N',N'-tetramethylmalonamide (Vicentini, 1972; Vicentini et al., 1974a), and N,N,N',N'-tetramethyladipamide (Vicentini and Isuyama, 1975). The perchlorates of each of these have the formula $R(diamide)_4(ClO_4)_3$ with the exception of N,N,N',N'-tetramethyladipamide for which the complexes of samarium to lutetium have only three molecules of the diamide. In all these complexes the T_d symmetry of the perchlorate ion is preserved which implies that it is not coordinated. The complexes with other anions show a reduction in the number of coordinated organic ligands.

RCl ₃ ·3(biuret)·3H ₂ O	(R = La-Ho)	Seminara et al. (1969)
RL ₃ ·8DMF	(R = La-Gd)	Moeller and Galasya (1960)
R(ClO ₄) ₃ ·xDMA	(x = 8, R = La-Nd)	Moeller and Vicentini (1965)
	(x = 7, R = Sm-Er, Y)	
	(x = 6, R = Tm-Lu)	
R(NO ₃) ₃ ·xDMA	(x = 4, R = La-Pr)	Vicentini and de Carvalho Filho (1966)
	(x = 3, R = Sm-Lu, Y)	
	(x = 5, R = La-Nd)	
	(x = 4, R = Sm-Lu, Y)	Vicentini et al. (1969)
R(NCS) ₃ ·xDMA		
R(ClO ₄) ₃ ·8(γ-butyrolactam)	(x = 8, R = La-Gd)	Miller and Madan (1968b)
R(NO ₃) ₃ ·x(γ-butyrolactam)	(x = 3, R = Dy, Er, Yb)	Miller and Madan (1968a)
	(x = 8, R = La-Gd)	
R(ClO ₄) ₃ ·x(N-methyl-γ-butyrolactam)	(x = 7, R = Dy, Er, Yb, Y)	Miller and Madan (1968b)
R(ClO ₄) ₃ ·4(N,N-dimethylacetamide)		Perrier and Vicentini (1974)
R(ClO ₄) ₃ ·4TMMA		Vicentini (1972)
R(NO ₃) ₃ ·2TMN:A		Vicentini (1972)
RCl ₃ ·2TMMA	(R = La-Yb, Y)	Vicentini et al. (1974a)
R(NCS) ₃ ·4TMMA		Vicentini et al. (1974a)
Lu(NCS) ₃ ·3TMMA		Vicentini et al. (1974a)
Sc(ClO ₄) ₃ ·3TMMA		Vicentini and Isuyama (1972)
RX ₃ ·6(antipyrène)	(x = ClO ₄ , I, NCS, B(C ₆ H ₅) ₄)	Bashoum et al. (1973)
R(NO ₃) ₃ ·3(antipyrène)		Krishnamurthy and Soundararajan (1967b)

The cyclic ligand, cyclopropyleneurea (tetrahydro-2-pyrimidone), forms the complexes $R(\text{CPU})_3X_3$ ($X = \text{ClO}_4^-$ or NO_3^-) (Burgess and Toogood, 1971). The perchlorates for all the lanthanides were prepared but for the nitrates only the compounds from lanthanum to gadolinium could be formed. In both cases the infrared evidence indicates that the anions are not coordinated. The emission spectra of the europium compounds with perchlorate, nitrate, iodide, and hexafluorophosphate as the anions indicate that the symmetry around the rare earth ion is the same in all of them (Vanderveer, 1972). The reason for the different behavior for this cyclic ligand from that of the straight chain amides is not well understood at present but probably is related to the cyclic nature of the ligands and a reduction in the steric effect.

6.2.3. β -diketones

The β -diketones are excellent chelating ligands for the rare earth ions and typical examples of the types of complexes that are formed are presented in table 25.14. (The functioning of these complexes as lasers is discussed in ch. 35.) The complexes that might have been expected, $R(\beta\text{-diketone})_3$, rarely form, except for scandium, because of the tendencies of these compounds to add one or more additional ligands, particularly water molecules. Attempts to dehydrate most of these hydrated species leads either to destruction of the complex or the formation of polymeric hydroxo species (Pope et al., 1961). If, however, the substituents on the β -diketone are large, *t*-butyl groups as an example, then the anhydrous tris chelate can be prepared (eisentraut and Sievers, 1965). The anhydrous trisacetylacetonato complexes have been prepared, however, in the absence of any possible adduct formation by the reaction of acetylacetonone directly with a rare earth hydride (Przystal et al., 1971). The anhydrous acetyl-

TABLE 25.14.
Representative complexes with β -diketone ligands.

Compound		Reference
$R(\text{acac})_3 \cdot x\text{H}_2\text{O}$	($x = 1$ or 3)	Pope et al. (1961)
$\text{Sc}(\text{acac})_3$		Melson (1975)
$(R(\text{DPM}))_3$	($R = \text{La-Lu, Y, Sc}$)	Eisentraut and Sievers (1965)
$R(\text{fod})_3 \cdot x\text{H}_2\text{O}$	($x = 0$ or 1)	Springer, Jr. et al. (1967)
	($x = 0$ for Sc)	
$R(\text{acac})_2\text{OH}$		Pope et al. (1961)
$M[R(\text{hexafluoroacetylacetonato})_4]$	($R = \text{La-Lu, Y, Sc}$)	Melby et al. (1964)
		Melson (1975)
$R(\beta\text{-diketone})_3 \cdot x\text{L}$	(x may be 1 or 2 depending on L and β -diketone;	Melby et al. (1964)
	$L =$ triphenylphosphine oxide,	Bauer et al. (1964)
	<i>o</i> -phen, dipy, terpy, DMSO, etc.)	Selbin et al. (1971)
	($R = \text{La-Lu, Y; Sc rarely}$)	Melson (1975)

acetates of erbium and dysprosium have now also been synthesized by the co-condensation of metal atoms prepared by the laser/thermal metal evaporation procedure with acetylacetone at -196°C (Blackborow et al., 1976). Recrystallization from toluene/ether mixtures gave the pure materials. This technique which obviates complex purification procedures may well prove to be extremely useful for the preparation of other complexes as well.

In general it is possible to add a fourth β -diketone ligand to the tris complex providing the substituents are small enough. Consequently, complexes of the general formula $\text{M}[\text{R}(\beta\text{-diketone})_4]$ can be prepared in which M^+ can be either a univalent metal cation or an organic cation (Bauer et al., 1964; Melby et al., 1964). Nearly any kind of additional ligand can be added to the tris complex and adducts with triphenylphosphine oxide, dipyriddy, terpyridyl, ortho-phenanthroline, and picoline-N-oxide, among others, have been prepared. This ability to coordinate an additional ligand is one of the factors that has made the β -diketone complexes $\text{R}(\text{DPM})_3$ and $\text{R}(\text{fod})_3$ valuable as the so-called shift reagents (see ch. 38). These β -diketone complexes are useful in various studies because the metal ion is relatively shielded from the environment around the complex and because of the nature of the organic ligands the complexes are often soluble in a variety of nonaqueous solvents.

The mass spectra of the lanthanide complexes of thenoyltrifluoroacetone, $[\text{R}(\text{CF}_3\text{COCHCOC}_4\text{H}_3\text{S})_3]$, have been obtained for samarium, europium, gadolinium, and terbium (Das and Livingstone, 1975). The spectra are similar and fluorine migration to the metal ion with concomitant loss of $:\text{CF}_2$ occurs. The species RF_2^+ was observed for samarium, gadolinium, and terbium and RF^+ was observed for the easily reduced ions samarium and europium. No oxidation of terbium to terbium(IV) occurred. A mechanism for the fragmentation has been presented.

6.2.4. Alcohols and alkoxides

Because of the affinity of the rare earth ions for water molecules, it is not surprising that corresponding alcoholates have also been isolated (Melson, 1975; Moeller et al., 1965). These complexes are generally not particularly stable and they do not seem to have been extensively investigated. The alkoxides can be prepared in the usual ways and triisopropoxides in particular have been studied (Bradley, 1972). Other alkoxides can be prepared by alcoholysis of the isopropoxides. The methoxides and ethoxides are insoluble solids but the higher alkoxides are soluble in typical organic solvents. The triisopropoxides sublime at $200\text{--}300^{\circ}\text{C}$ at 0.1 mm Hg and it is now clear that they are polymeric. The extent of this polymerization is not certain but mass spectral results have given evidence for dimers and tetramers.

The compounds $\text{R}[\text{Al}(\text{OC}_3\text{H}_7)_4]_3$ have been synthesized in a variety of ways (Mehrotra et al., 1973a). These complexes are volatile and can be distilled under reduced pressure. As expected, the scandium compound is the most volatile boiling at 145°C at 0.5 mm Hg, whereas the lanthanum compound is least volatile

and boils at 208°C at 0.5 mm Hg. Interestingly the cerium(III) complex could be made, whereas the synthesis of the simple isopropoxide results in oxidation to cerium(IV). The compounds are monomeric in benzene and the suggested structure involves a six-coordinate rare earth ion in which one half of the isopropoxide ions are in bridging positions between the rare earth ion and the three aluminum ions. The corresponding complexes $R[Ga(OC_3H_7)_4]_3$ have been synthesized and are even more volatile (Mehrotra, 1973b).

The ligand, 2-acetamidohexafluoro-2-propanol ($CH_3CONHC(F_3)_2OH$) acts as a bidentate, uninegative ligand to give CeL_4 and $NH_4(RL_4)$ (MacDonald and Willis, 1973). The ammonium salts are volatile and can be sublimed without decomposition. In organic solvents, however, the complexes decompose in the absence of excess ligand.

6.2.5. Macrocyclic polyethers

The macrocyclic polyethers form complexes with the rare earths and although these have not been extensively studied up to now, because of their relationship to biologically important substances, they may ultimately assume an important position. The ligand benzo-15-crown-5 reacts with the hydrated Lanthanide(III) nitrate in acetone to yield the 1:1 complexes $R(NO_3)_3 \cdot C_{14}H_{20}O_5$ ($R = La-Sm$) and $R(NO_3)_3 \cdot C_{14}H_{20}O_5 \cdot 3H_2O \cdot (CH_3)_2CO$ ($R = Sm-Lu$) (King and Heckley, 1974). The ligand dibenzo-18-crown-6 forms the complexes $R(NO_3)_3 \cdot C_{20}H_{24}O_6$ ($R = La-Nd$) from acetonitrile solution (King and Heckley, 1974). The formation of these complexes is predicated on the size relationships between the radius of the rare earth ion and the cavity of the ligand. The crystal structure of the lanthanum complex of the saturated analog cyclohexyl-18-crown-6, $La(NO_3)_3 \cdot C_{20}H_{36}O_6$, has been determined (Hart, 1976). The six ether oxygens are coordinated to the lanthanum(III) ion as are all three nitrate ions, yielding an effective coordination number of twelve.

6.2.6. $Q_nX \rightarrow O$ compounds

Complexes of ligands in this class are widespread. Some examples in which they form adducts with chelated rare earth ions have been mentioned previously (6.2.3). The most common compounds are those in which X is phosphorus, arsenic, sulfur, or heterocyclic nitrogen and some typical examples are given in table 25.15. The complexes are similar in many respects to those formed with the carbonyl ligands particularly insofar as potential coordination of the anions is concerned and different coordination numbers for complexes with a given organic ligand will be found depending on the anion present. In all of these complexes coordination through the oxygen atom has been well-established from the infrared spectra and in a few examples by a complete structure determination by X-ray diffraction. Although the synthesis of these compounds is generally relatively straightforward, there are many inconsistencies reported in the literature. Some of these have now been resolved but many of them remain.

As an example, two groups reported the preparation of the complexes $R(\text{HMPA})_6(\text{ClO}_4)_3$ in which the perchlorate ions were found to be ionic on the basis of the infrared spectra (Donoghue et al., 1969), Giesbrecht and Zinner, 1969). However, neither of these syntheses could be repeated and the compounds $R(\text{HMPA})_4(\text{ClO}_4)_3$ were found instead and on the basis of the infrared spectra both ionic and coordinated perchlorate groups were assigned (Durney and Marianelli, 1970). By changing the reaction conditions and solvents it has now been conclusively demonstrated that both groups of complexes can be synthesized (Scholer and Merbach, 1975). Moreover, very careful handling of the reaction conditions can result in the isolation of the two kinds of complexes from the same solution (Serra et al., 1971).

Complexes derived from the pyridine-N-oxide ligands seem to be well-behaved. The largest number of coordinated pyridine-N-oxide ligands occurs as expected with perchlorate (Krishnamurthy and Soundararajan, 1967a), iodide (Ramakrishnan and Soundararajan, 1975), or hexafluorophosphate (Melby et al., 1964) as the anion. The steric requirements are such that eight ligands are coordinated throughout the lanthanide series. Complexes of one bidentate ligand, 2,2'-dipyridyl-1,1'-dioxide, have been prepared (Mehs and Madan, 1968). As in the case of the unidentate ligands of this type, all the lanthanides form complexes having the same number of ligands coordinated, $R(\text{dip}y\text{O}_2)_4(\text{ClO}_4)_3$. The europium and terbium complexes are very strongly fluorescent.

Introduction of methyl groups into the 2- and 6-positions of pyridine-N-oxide does not seem to introduce any adverse steric effect since the maximum number of ligands coordinated remains eight for the perchlorate salts (Vicentini and de Oliveira, 1975). However, only three ligands are coordinated with chloride as the anion and only four with nitrate.

The sulfoxide group has proven to be a good donor toward the rare earth ions. The simplest sulfoxide, dimethyl sulfoxide, forms complexes with varying numbers of organic ligands coordinated depending both on the anion present and on the size of the rare earth ion (Ramalingam and Soundararajan, 1967). With the perchlorate ion the three series of complexes $R(\text{DMSO})_8(\text{ClO}_4)_3$ ($R = \text{La-Nd}$), $R(\text{DMSO})_7(\text{ClO}_4)_3$ ($R = \text{Sm-Ho, Y}$), and $R(\text{DMSO})_6(\text{ClO}_4)_3$ ($R = \text{Er-Lu}$) result (Kutek, 1968). More recent workers have obtained slightly different results for the complexes of the heavier lanthanides in that the complexes all analyze for "approximately" seven ligands (Iwase and Toda, 1973). With iodide as the anion, the complexes have the formula $R(\text{DMSO})_8\text{I}_3$ ($R = \text{La-Er, Y}$) (Koppiker and Soundararajan, 1975). The corresponding hexafluorophosphates contain only seven organic ligands with the heavier lanthanides and the lighter lanthanides resulted in formulations that could not be rationalized as mixtures (Kuya et al., 1975). It is clear in all these cases that the choice of solvent and conditions of precipitation are very important.

A further illustration of the difficulties inherent in the synthesis of these types of complexes is illustrated by diphenyl sulfoxide. The perchlorates were reported to combine with only six ligands to give $R(\text{DPSO})_6(\text{ClO}_4)_3$ which existed for all the lanthanides with only ionic perchlorate ions (Ramalingam and Soun-

dararajan, 1968). The iodides, however, yield complexes formulated as $R(\text{DPSO})_8\text{I}_3$ ($R = \text{La}-\text{Y}$) (Koppiker and Soundararajan, 1975). This result is at variance with most other experience. In an attempt to repeat the perchlorate work, Serra and Thompson (1973) could only obtain $R(\text{DPSO})_7(\text{ClO}_4)_3$ ($R = \text{Sm}, \text{Eu}, \text{Yb}$) using varying ratios of DPSO to metal from 4:1 to 9:1. Moreover, the complex $\text{Eu}(\text{DPSO})_7(\text{PF}_6)_3$ was easily obtained.

The current status of knowledge concerning these dimethyl sulfoxide and diphenyl sulfoxide complexes is thus rather uncertain and is typical of many complexes of this class. Most of the complexes have not been subjected to extensive study by physical chemical means. In general, the compounds have been characterized only through measurements of the molar conductivity and infrared spectra. Additional work, particularly measurements of the absorption and emission spectra and ultimately structure determinations by x-ray diffraction, will be necessary to resolve these uncertainties.

Other sulfoxides that have been studied recently include thioxane oxide (Vicentini and Vieira, 1973; Vicentini and Perrier, 1974; Serra et al., 1976), tetramethylenesulfoxide (Bertan and Madan, 1972; Vicentini and Zinner, 1975), and trans-1,4-dithiane-1,4-dioxide (Vicentini et al., 1975). The results that have been obtained follow the same general patterns previously discussed.

The most common ligand of the oxides of the Group V elements is triphenylphosphine oxide which yields a variety of types of complexes having the composition $R(\text{NO}_3)_3\text{L}_2 \cdot \text{EtOH}$, $R(\text{NO}_3)_3\text{L}_3$, $R(\text{NO}_3)_3\text{L}_3(\text{Me}_2\text{CO})_2$, $R(\text{NO}_3)_3\text{L}_4 \cdot \text{Me}_2\text{CO}$, $R(\text{NO}_3)_3\text{L}_4 \cdot \text{EtOH}$, $[\text{R}(\text{NO}_3)_2\text{L}_4](\text{NO}_3)$, RCl_3L_3 , RCl_3L_4 , $\text{R}(\text{NCS})_3\text{L}_3$ and $\text{R}(\text{NCS})_3\text{L}_4$. With triphenylarsine oxide the complexes $\text{R}(\text{NCS})_3\text{L}_3$, $\text{R}(\text{NO}_3)_3\text{L}_2 \cdot \text{EtOH}$, $\text{R}(\text{NO}_3)_3\text{L}_3$, and $\text{R}(\text{NO}_3)_3\text{L}_4$ have been prepared (Cousins and Hart, 1967a, b, 1968). In line with the greater dipole moment of triphenylarsine it appears to complex more strongly than does triphenylphosphine oxide. Complexes of neodymium with a number of phosphine oxides having varying organic groups have also been prepared (Serra et al., 1972). The perchlorate ion in these complexes is both coordinated and ionic and from the infrared spectra and the molar conductivity they have been formulated as $[\text{NdL}_4(\text{ClO}_4)_2]\text{ClO}_4$.

In addition complexes of various phosphinamides (Zinner and Vicentini, 1975) and substituted phosphinamides (Vicentini et al., 1974b) have been reported. The formulation of the compounds is again in agreement with the principle considered before. N-substitution apparently results in a steric effect and the number of coordinated ligands is reduced.

6.3. Organic nitrogen donors

Until the middle 1960's there were no really well-characterized rare earth complexes with ligands that contained only nitrogen donor atoms. Although there had been prior reports of complexes with ammonia and various simple amines, the information concerning their composition and properties was, at best, only very sketchy (Moeller et al., 1965). The rapid development in the

preparation and characterization of complexes utilizing nitrogen donors parallels the intense study of the β -diketone complexes and the search for more efficient luminescent materials. The first complexes to be prepared (Hart and Laming, 1963; Lobanov and Smirnova, 1963a, b) involved ligands containing heterocyclic nitrogen atoms which had low enough basicities that the complexes could be prepared in alcoholic or even aqueous media. Only later were the complexes with ligands containing aliphatic nitrogen donors synthesized (Forsberg and Moeller, 1968). These require far more involved procedures and scrupulously anhydrous conditions to avoid the formation of hydroxo species and precipitation of these undesired complexes. Typical complexes of both types of ligands are presented in table 25.16. There are three recent review articles

TABLE 25.16.
Representative complexes with ligands having nitrogen donor atoms.*

Heterocyclic	
$R(o\text{-phen})_2X_3 \cdot (H_2O \text{ or } C_2H_5OH)_n$	(X = Cl, NO ₃ , SCN, SeCN; n = 0-5)
$Sc(o\text{-phen})_2X_3$	(X = Cl, SCN, NO ₃)
$R(o\text{-phen})_3X_3$	(X = SCN, SeCN)
$Sc(o\text{-phen})_3X_3$	(X = SCN, SeCN, Cl)
$R(o\text{-phen})_4(CIO_4)_3$	
$R(dipy)_2X_3 \cdot (H_2O \text{ or } C_2H_5OH)_n$	(X = Cl, NO ₃ , SCN, SeCN; n = 0-5)
$Sc(dipy)_2X_3$	(X = Cl, SCN, NO ₃)
$R(dipy)_3X_3$	(X = SCN, SeCN)
$Sc(dipy)_3X_3$	(X = SCN, SeCN)
$R(terpy)X_3 \cdot nH_2O$	(X = Cl, Br, NO ₃ ; n = 0-3)
$R(terpy)_2X_3$	(X = Cl, Br, ClO ₄)
$R(terpy)_3(CIO_4)_3$	
Aliphatic	
$[R(en)_4(NO_3)](NO_3)_3$	(R = La-Sm)
$[R(en)_4](NO_3)_3$	(R = Eu-Yb)
$[R(en)_3(NO_3)_2][NO_3]$	(R = Gd-Ho)
$[R(en)_4Cl]Cl_2$	(R = La, Nd)
$[R(en)_4]Cl_3$	(R = Sm-Lu)
$[R(en)_3Cl_2]Cl$	(R = Gd, Er)
$[Sc(en)_3]Cl_3$	
$[Sc(en)_2Cl_2]Cl$	
$[R(en)_4Br]Br_2$	(R = La)
$[R(en)_4]Br_3$	(R = Nd, Gd)
$[R(en)_3Br_2]Br$	(R = Gd)
$[Sc(en)_3]Br_3$	
$[Sc(en)_2Br_2]Br$	
$[R(en)_4](ClO_4)_3$	(R = La-Nd)
$[R(dien)_3](NO_3)_3$	(R = La-Gd)
$[R(dien)_2(NO_3)_2](NO_3)$	(R = La-Yb)
$[R(trien)_2](NO_3)_3$	(R = Pr-Eu)
$[R(trien)_2](ClO_4)_3$	(R = La-Ho)
$Sc(amine)_2Cl_3$	(amine = C ₂ H ₅ NH ₂ , C ₆ H ₅ NH ₂ , (CH ₃) ₂ NH, etc.)

*Lanthanides: Forsberg (1973); Moeller et al. (1973). Scandium: Melson (1975).

covering rare earth complexes from nitrogen donor ligands so the examples considered below will only be illustrative (Forsberg, 1973; Moeller et al., 1973; Melson, 1975).

The two ligands that have been most extensively studied are ortho-phenanthroline and 2,2'-bipyridyl. Both of these ligands are bidentate and are only weakly basic. With ortho-phenanthroline the maximum number of bound ligands is four when the anion is the perchlorate ion (Krishnamurthy and Soundararajan, 1966). The tris-complex with one coordinated perchlorate ion (as indicated by the infrared spectrum) has also been obtained (Grandey and Moeller, 1970). There do not appear to have been any dipyriddy complexes with the lanthanide perchlorates prepared at the present time, although there does not seem to be any reason they would not form.

For both of these ligands the complexes formed when the acetates, chlorides, nitrates, and thiocyanates are used as the starting materials have a smaller number of organic ligands, coordination of some or all of the anions (the structure of the ten-coordinate complex $[\text{La}(\text{o-phen})_2(\text{NO}_3)_3]$ has been discussed earlier, section 3.9), and perhaps may be solvated as well (Forsberg, 1973). Most of the preparations can be carried out in aqueous or anhydrous ethanol. The existence of the lanthanide-nitrogen bond is clearly implied in these compounds and the infrared spectra (Sinha, 1964) and ultimately, complete structure determination, have verified that this interaction does take place. It should also be noted that both of these molecules form adducts with the tris- β -diketone complexes and the structures of two of these with ortho-phenanthroline have been determined (Watson et al., 1972; Cunningham, 1973).

The terdentate ligand, terpyridyl, follows the same pattern as bipyridyl and ortho-phenanthroline (Durham et al., 1969). The maximum number of coordinated ligands (three) occurs with the perchlorate. Since only ionic perchlorate was observed in the infrared spectrum, the molecule was presumed to be nine-coordinate. The emission spectrum of the europium complex was consistent with the expected D_3 symmetry with a very slight distortion and this has been confirmed by a complete structure determination (Frost et al., 1969).

The ligand bis(2'-quinolyl)-2,6-pyridine is similar to terpyridyl except that there is an additional ring fused to each of the peripheral pyridyl groups converting them into quinolyl groups. Complexes of this ligand are different from those of terpyridyl in that only one of the ligands can be coordinated even with perchlorate as the anion and these are solvated with three molecules of water (Gurrieri et al., 1976). The molar conductivities suggest that the thiocyanate and nitrate complexes are non-electrolytes and that the perchlorate complexes are 1:3 electrolytes, in agreement with the infrared spectra.

The ligand, 1,8-naphthyridine, forms complexes with what appear to be very high coordination numbers. With perchlorate as the anion the complexes $\text{R}(\text{napy})_6(\text{ClO}_4)_3$ ($\text{R} = \text{La}-\text{Pr}$) and $\text{R}(\text{napy})_5(\text{ClO}_4)_3$ ($\text{R} = \text{Nd}-\text{Eu}$) are isolated from ethyl acetate solutions (Foster et al., 1972). The infrared evidence indicates that in all cases the naphthyridine is functioning as a bidentate ligand and that the perchlorate is present in the ionic form. This would require that the larger lanthanide ions be twelve-coordinate and that the heavier lanthanides be

ten-coordinate. With the nitrate ion both 1,8-naphthyridine (Foster and Hendricker, 1972) and 2,7-dimethyl-1,8-naphthyridine (Hendricker and Foster, 1972) form the complexes $RL_2(NO_3)_3$ with all the lanthanides. In these the nitrate groups all appear to be coordinated to the metal ion. Since the smaller d-transition metal ions are known to form eight-coordinate complexes with 1,8-naphthyridine (Clearfield et al., 1970), the suggestion of ten- and twelve-coordination with the lanthanides seems reasonable. Because the only authenticated twelve-coordinate complexes involve the nitrate ion as the sole ligand, a complete structural determination of these complexes would be of interest.

The first definitive work on the lanthanide complexes with polydentate aliphatic amines was reported by Forsberg and Moeller, (1968). By working in completely anhydrous systems using acetonitrile as the solvent, they were able to prepare complexes of the lanthanide ions with ethylenediamine. Later, complexes with diethylenetriamine, 1,2-propanediamine, β,β',β'' -triamino-triethylamine, and triethylenetetramine, were also reported (Forsberg, 1973). In contrast to the complexes of the weakly-basic amine ligands, high coordinate complexes containing only nitrogen atoms in the coordination sphere can be prepared with these strongly basic ligands even in the presence of strongly coordinating anions, which is indicative of the fact that strong lanthanide-aliphatic nitrogen bonds must be formed. Although they are readily hydrolyzed upon exposure to the atmosphere, these complexes possess considerable thermal stability.

When the ligand is ethylenediamine (Forsberg and Moeller, 1969) or 1,2-propanediamine (Carpentier and Moeller, 1970), addition of the reagents in stoichiometric quantities results in $R(\text{diamine})_3X_3$ and addition of excess amine yields $R(\text{diamine})_4X_3$ ($X = Cl^-, Br^-, NO_3^-,$ or ClO_4^-). Infrared data established that for the tetrakisethylenediamine complexes of the lighter lanthanides (La-Sm) there is both coordinated and ionic nitrate whereas for the heavier lanthanides (Eu-Yb) there are only ionic nitrate ions, an observation consistent with the decreasing ionic radius. Coordination of the diamine nitrogen atoms was established from the decrease in the N-H stretching mode in the infrared spectrum which was independent of the anion. In the trisethylenediamine complexes a coordination number of eight was assigned to all the complexes whereas in the tetrakis complexes of the lighter lanthanides, a coordination number of nine was assigned. These need to be established firmly by a definitive structural study, however.

With diethylenetriamine two types of complexes are formed with nitrate as the anion (Forsberg and Walthen, 1971): $R(\text{dien})_3(NO_3)_3$ ($R = La-Gd$) and $R(\text{dien})_2(NO_3)_3$ ($R = La-Yb, Y$). The tris complexes contain only ionic nitrate whereas the bis complexes contain both ionic and coordinated nitrate groups. Coordination number nine was thus assigned to the tris complexes but the coordination number in the bis complexes remains undetermined due to the impossibility of determining the relative numbers of ionic and coordinated nitrate groups solely by means of the infrared spectra.

Both mono and bis complexes can be isolated from acetonitrile solutions of lanthanide nitrates and tren (Forsberg et al., 1971). The two series of complexes $[R(\text{tren})(\text{NO}_3)_3]$ and $R(\text{tren})_2(\text{NO}_3)_3$ exist for all the lanthanides. In the bis complexes there are both ionic and coordinated nitrate groups for the larger ions (La–Nd) but only ionic groups for the smaller lanthanides (Sm–Yb). The perchlorate salts, $R(\text{tren})(\text{ClO}_4)_3$ ($R = \text{Pr, Gd, Er}$) and $R(\text{tren})_2(\text{ClO}_4)_3$ ($R = \text{La, Pr, Nd, Gd, Er, Y}$), have also been obtained (Johnson and Forsberg, 1976). The mono complexes contain complexed perchlorate ions but the bis complexes contain only ionic groups. The exchange kinetics of the reaction between tren and $\text{Nd}(\text{tren})_2^{3+}$ in acetonitrile has been measured using the NMR line-broadening technique (Johnson and Forsberg, 1972). The reaction is first order in both ligand and complex and the proposed mechanism involves simultaneous partial attachment of the free ligand and partial unwrapping of coordinated ligand.

The ligand 1,2-bis(pyridine- α -aldimino)ethane, which is a Schiff base (see section 6.4) and has four nitrogen donor atoms, forms solid 1:1 complexes with the lanthanide chlorides, nitrates, thiocyanates, or salicylates (Durham and Hart, 1969). Infrared spectra for the nitrates show that the anions are all coordinated and the ring-breathing vibration for the pyridyl group is shifted to higher energy suggesting coordination. It has not been possible to isolate complexes that contain two ligands from ethanolic solution, even with perchlorate as the anion, although spectral evidence indicates that they exist in solution.

Several reports in the chemical literature deal with the formation of rare earth complexes formed with phthalocyanines. Although both the mono- and bis-phthalocyanine complexes have been reported, the nature of the complexes is still not well-characterized (Forsberg, 1973; Moeller et al., 1973). The synthesis of porphyrin complexes has recently been realized for scandium (Buchler et al., 1971), and yttrium (Wong and Horrocks, Jr., 1975) and the lanthanides (Wong et al., 1974). Reaction of hydrated tris(2,4-pentanedionato)rare earth(III) with meso-tetraphenylporphine or a substituted meso-tetraphenylporphine in 1,2,4-trichlorobenzene at 214°C results in the formation of $R(\text{porphyrin})(\text{C}_5\text{H}_7\text{O}_2)$. Other β -diketonates can be used with similar results. These complexes are soluble in organic solvents, stable in air, and to water when the latter is added to an organic solvent with which it is miscible. Addition of hydrogen chloride gas to a solution of the complex results in immediate destruction with the formation of the green porphyrin dication. The NMR spectra suggest that the lanthanide ion is considerably displaced from the porphyrin plane. These complexes have an obvious potential in the study of biological materials.

6.4. Organic nitrogen–oxygen donors

This group, since it incorporates at least two donor atoms in each molecule, contains only chelating ligands. By far the most common types of ligands in this category are the aminopolycarboxylic acids (Bagnall, 1975). However, a substantially greater effort has been devoted to the solution chemistry of these ligands than to the preparation and characterization of the solid compounds and

many of the results have been conflicting. Most complexes of the aminopolycarboxylates are hydrated and it is difficult to differentiate coordinated water from lattice water short of carrying out a complete structural determination.

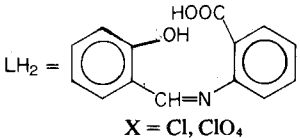
Another class of ligands in this category contains a heterocyclic nitrogen atom. For these compounds the infrared spectra can be used to determine the nitrogen coordination since the ring breathing vibration at about 990 cm^{-1} is shifted to higher energy upon coordination (Thompson and Mannila, 1968). Typical ligands are dipicolinic acid and 8-hydroxyquinoline.

The third class of ligands includes the Schiff bases derived, in general, from salicylaldehyde or its derivatives. In many of these complexes the phenolic group is not ionized which leads to complexes that are less stable and more difficult to characterize than for the d-transition elements.

A few typical examples of the complexes formed by each of these types of ligands are given in table 25.17.

Some of the lanthanide complexes of EDTA and NTA have been considered previously in the section dealing with the structural characteristics of the ions (section 3). In addition to the heptahydrates for which Hoard and his co-workers determined the detailed structure, the protonated 1:1 chelates also exist in the

TABLE 25.17.
Representative complexes with ligands having nitrogen and oxygen donor atoms.

Aminopolycarboxylic acids (Bagnall, 1975)		
$R(\text{IMDA})\text{Cl} \cdot x\text{H}_2\text{O}$		(R = La-Lu, Y, Sc)
$R_2(\text{IMDA})_3 \cdot \text{H}_2\text{O}$		(R = La-Lu, Y, Sc)
$K[\text{R}(\text{IMDA})_2] \cdot x\text{H}_2\text{O}$		(R = La-Lu, Y, Sc)
$M_3[\text{R}(\text{IMDA})_3] \cdot x\text{H}_2\text{O}$		(R = La-Lu, Y, Sc)
$\text{R}(\text{NTA}) \cdot x\text{H}_2\text{O}$		(R = La-Lu, Y, Sc)
$K_3\text{R}(\text{NTA})_2 \cdot x\text{H}_2\text{O}$		(R = La-Lu, Y, Sc)
$\text{HR}(\text{EDTA}) \cdot x\text{H}_2\text{O}$		(R = La-Lu, Y, Sc)
$\text{MR}(\text{EDTA}) \cdot x\text{H}_2\text{O}$		(R = La-Lu, Y, Sc)
Heterocyclic nitrogen - oxygen		
$\text{Na}_3[\text{R}(\text{PDC})_3] \cdot x\text{H}_2\text{O}$		Albertsson (1972)
$\text{ScL}_3 \cdot \text{HL}$	(HL = 8-hydroxyquinoline)	Melson (1975)
$\text{R}(\text{8-hydroxyquinolate})_3$		Jackson (1950)
Schiff Bases		
$R_2(\text{salen})_3 \cdot (\text{C}_2\text{H}_5\text{OH or H}_2\text{O})_n$ $[\text{R}(\text{LH})_2(\text{H}_2\text{O})]\text{X}$		Dutt and Nag (1968) de Sá et al. (1975)
$\text{R}(\text{N-alkylsalicylidineiminato})_3 \cdot x\text{H}_2\text{O}$		Yamada et al. (1971)

monohydrate form if they are crystallized above 45°C (Mackey et al., 1971). Detailed thermograms have been recorded for some of the complexes of the light lanthanides and from these it has been possible to show that the multihydrates and monohydrates undergo different types of decomposition probably related to structural differences in the way EDTA is bound to the metal ions. The multihydrates do not show a weight loss that corresponds to the formation of either the monohydrate or anhydrous forms. Although there are no structural determinations, it has been suggested from this study and from the Mössbauer results (Mackey and Greenwood, 1972) that these are most likely polymeric with carboxylate bridging.

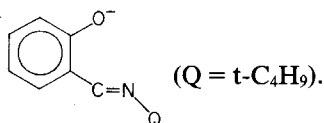
The complexities that are inherent in the preparation of these types of compounds are illustrated by the iminodiacetic acid complexes. In an attempt to prepare $\text{Nd(IMDA)Cl}\cdot n\text{H}_2\text{O}$, equimolar aqueous solutions of $\text{Nd}_2(\text{IMDA})_3$ and NdCl_3 were mixed (Albertsson and Oskarsson, 1968). Addition of ethanol after concentration to a syrup resulted in a microcrystalline precipitate which after hydrothermal treatment at 80°C for three weeks was found to be $\text{Nd}_2(\text{IMDA})_3\cdot 2\text{HCl}\cdot 7\text{H}_2\text{O}$. The structural determination showed that two protons were bound to two of the nitrogen atoms of the IMDA ligands to give the >NH_2^+ group. If the pH of the initial solution is above 4.5, the compound $\text{Nd(IMDA)Cl}\cdot 3\text{H}_2\text{O}$ is isolated (Oskarsson, 1971, 1972). The coordination around the neodymium ion can be described as a distorted tricapped trigonal prism with each iminodiacetate chelated to three neodymium atoms.

The ligand pyridine-2,6-dicarboxylic acid was mentioned previously in connection with the coordination numbers of lanthanide complexes (section 3). The cerium complex of this ligand, $\text{Na}_3[\text{Ce}(\text{C}_7\text{H}_3\text{NO}_4)_3]\cdot 15\text{H}_2\text{O}$, can be obtained as large triclinic, single crystals by crystallization at 14 to 18°C (Albertsson et al., 1972). Crystals as large as $20 \times 20 \times 4 \text{ mm}^3$ could be obtained in less than 14 days. The interest in this complex is related to its potential use as an alternative to cerium magnesium nitrate for very low temperature thermometry using its magnetic susceptibility (Doran et al., 1972).

This same ligand forms two additional types of complexes (Hoof et al., 1973). Reaction of the hydrated acetates with pyridine-2,6-dicarboxylic acid in aqueous solution results in $\text{R(DPC)(DPCH)}\cdot 6\text{H}_2\text{O}$ ($\text{R} = \text{La} \rightarrow \text{Tb}$) and $\text{R(DPCH)}_3\cdot \text{H}_2\text{O}$ ($\text{R} = \text{Sm} - \text{Yb}$). Within each series the compounds appear to be isostructural as judged by the similarity of their infrared spectra and their X-ray powder diffraction patterns. The complexes $\text{R(DPCH)}_3\cdot \text{H}_2\text{O}$ are easily dehydrated without any accompanying change in the C=O stretching region of the infrared spectrum. This supports the above formulation rather than $\text{H}_3\text{O}^+[\text{R(DPC)(DPCH)}_2]$. The structure has been considered to contain nine-coordinated metal ions with three monoanionic terdentate (DPCH) groups. No detailed conclusions could be drawn concerning the structure of $\text{R(DPC)(DPCH)}\cdot 6\text{H}_2\text{O}$ although bridging carboxylate groups are suspected.

The situation with the Schiff base complexes is not entirely clear and some points are still confusing. It has been reported, for example, that the

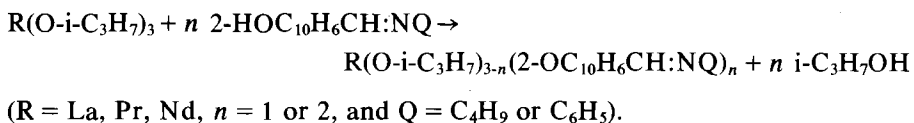
lanthanide(III) ions form complexes with *t*-butyl-salicylideneimine of the type $R(L)_2 \cdot 3H_2O$ (Yamada et al., 1971) in which the phenolic proton is lost and the ligand coordinates as the anion



The reaction reportedly takes place without the addition of base. The corresponding yttrium complexes in which $Q = CH_3, C_2H_5, n-C_3H_7,$ and $i-C_3H_7$ were prepared by the same workers at a later date but it was found that the ligand binds in the neutral form (Kuma and Yamada, 1975). From the analyses and conductivity measurements it was concluded that the compounds should be formulated as $[Y(LH)_3Cl_2]Cl$. The only apparent synthetic differences were that the reaction with the lanthanides was carried out at temperatures less than $50^\circ C$ in the absence of a solvent whereas the reaction with yttrium took place in refluxing ethanol.

The complexes of the Schiff base derivatives of acetylacetone, 2,4-pentanedioneanil, and 2,4-pentanedionebenzylamine, with the lanthanide nitrates have also been prepared by reaction in acetone (Agarwal and Tandon, 1975). The resulting compounds contain the neutral ligand molecule and were formulated as $[R(L-LH)_3(NO_3)](NO_3)_2$ for the lighter ions and $[R(L-LH)_2(NO_3)](NO_3)_2$ for ytterbium. On the other hand, reaction of ethanolic solutions of the hydrated lanthanide chlorides with bis-salicylaldehydeethylenediimine followed by the addition of ammonia results in complexes in which the phenolic proton is removed (Dutt and Nag, 1968). The corresponding derivative of 1,3-diaminopropane precipitates complexes containing the neutral ligand from ethanolic solutions of the lanthanide nitrates (Condorelli et al., 1975).

The Schiff base complexes formed in the reaction between the lanthanide isopropoxides and 2-hydroxy-1-naphthylidene-*n*-butylamine and 2-hydroxy-1-naphthylideneaniline in anhydrous benzene have been described (Agarwal and Tandon, 1974). The products that are isolated depend on the molar ratio of the reactants according to



The complexes are light yellow or brown crystalline solids and are non-volatile. The di-isopropoxy-mono-Schiff base derivatives are dimeric in boiling benzene. Both types of complex undergo exchange reactions with an excess of *t*-butyl alcohol in the presence of benzene to yield the corresponding *t*-butoxy complexes which are monomeric in boiling benzene probably because of the increased steric effect of the *t*-butoxy groups. In all these complexes the Schiff base is coordinated in the anionic form.

The difficulties that have been encountered in the studies of the Schiff base complexes illustrate once again the necessity of working under anhydrous

conditions in order to prepare complexes with relatively weak donors. The interactions are generally not strong enough to cause ionization of the phenolic group except in the presence of a base. This base has the additional effect of causing the formation of hydroxo species and the resulting materials are intractable. The recent work in which the isopropoxides are used as the starting materials obviates these difficulties (Agarwal and Tandon, 1975) by supplying a strongly basic anion and permitting the use of anhydrous conditions since the isopropoxides are soluble in benzene.

6.5. Other donor atoms

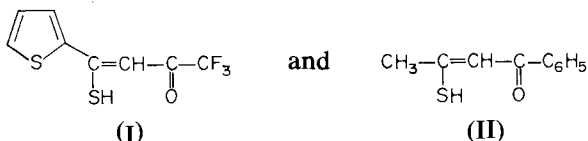
The number of complexes formed by the rare earths with ligands having donor atoms other than oxygen or nitrogen (excluding organometallic complexes which are considered separately in section 7) is very small and it appears that all of these involve coordination with a sulfur atom which, as has been shown previously in this discussion, is only weakly coordinating toward the rare earth ions in aqueous solutions. Thiourea and some substituted thioureas have been reported to form complexes in which infrared evidence indicates coordination through the sulfur atom. Complexes with various 1-substituted tetrazoline-5-thiones are purported to involve coordination through the sulfur atom and one nitrogen atom to yield polymeric substances. A recent review by Moeller et al. (1973) has considered these kinds of complexes with neutral sulfur donor molecules.

More definitive results have been obtained with the N-substituted dithiocarbamates. Brown and Holah (1968) synthesized the first solid, well-characterized tris species by carrying out the reaction between stoichiometric quantities of diethyldithiocarbamate and the anhydrous lanthanide bromides in anhydrous ethanol. Reaction with an excess of the ligand yielded the tetrakis complex which was precipitated as the tetraethylammonium salt. All the available evidence supports coordination of the sulfur atoms in the usual way to the lanthanide. Similar compounds with the N,N-di-iso-butylthiocarbamate ligand have also been prepared (Siddall, III and Stewart, 1970). The electronic spectra and proton magnetic resonance spectra have been interpreted to indicate that the symmetry of the tetrakis complex is C_{2v} or lower. Additionally, the room temperature magnetic moments for the neodymium, praseodymium, samarium, and europium complexes are all in the normal range and rule out any unusual bonding effects. As expected these complexes are soluble in a number of organic solvents including chloroform. The tetrakis complexes are iso-structural with the neptunium(III) complex which is a grossly distorted dodecahedron (Brown et al., 1970).

Complexes of the bisethoxydithiophosphate ion $[(C_2H_5O)_2PS_2^-]$ for all the lanthanides are readily obtained by adding the tetraphenylarsonium ion to an ethanolic solution of the ligand and the hydrated lanthanide chlorides (Pinkerton, 1974). Recrystallization from ethanol/iso-propanol mixtures yields the tetrakis complexes $[(C_6H_5)_4As]RL_4$. The sodium salts can also be prepared although they

tend to be more hygroscopic. The properties of the complexes are very similar to those reported for the dithiocarbamate complexes. A band at approximately 255 cm^{-1} which appears in both the infrared and Raman spectra has tentatively been assigned to the metal-sulfur vibration.

The first reports of the formation of solid complexes between the lanthanide ions and the monothio derivatives of the β -diketones appeared in 1976 (Nag and Chaudhury, 1976). Complexes of the types $\text{RL}_3 \cdot \text{H}_2\text{O}$, $\text{RL}_3 \cdot \text{dipy}$, $\text{RL}_3 \cdot \text{o-phen}$, and $\text{RL}_3 \cdot 2\text{pyNO}$ have been prepared with 1,1,1-trifluoro-4-(2-thienyl)-4-mercaptobut-3-en-2-one(I) and 3-mercapto-1-phenylbut-2-en-1-one(II).



The synthesis of these complexes is essentially the same as for the corresponding β -diketone complexes and the complexes are also soluble in organic solvents such as methanol, ethanol, acetone, chloroform, and benzene. The neodymium-sulfur band in the infrared is tentatively located at about 370 cm^{-1} . Since the neodymium-oxygen band in $\text{Nd}(\text{DPM})_3$ is located at 402 cm^{-1} (Lee et al., 1972), this value seems somewhat high. There is a significant tail from the ligand absorption band into the visible and this will complicate any detailed examination of the $4f-4f$ transitions in these complexes.

The recent preparation of these complexes containing sulfur donor ligands and of the complexes of aliphatic amines, suggests very strongly that if the appropriate experimental conditions are obtained, particularly the utilization of completely anhydrous, weakly coordinating solvents, and weakly coordinating anions such as perchlorate, hexafluorophosphate, or tetraphenylborate, the scope of rare earth coordination chemistry could be significantly expanded.

7. Organometallic complexes

Although the first lanthanide organometallic compounds were reported only three years after the discovery of ferrocene (Birmingham and Wilkinson, 1956), the years until 1968 saw only limited interest in this area. However, after the suggestion in that year that there is f orbital involvement in uranocene (Streitwieser, Jr. and Müller-Westerhoff, 1968), there has been a notable resurgence of interest in these complexes. The field has been surveyed in two comprehensive reviews (Hayes and Thomas, 1971; Kanellakopoulos and Bagnall, 1972) and each year there is a summary of the reported research in the *Journal of Organometallic Chemistry*.

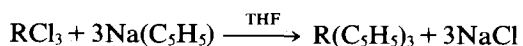
The types of compounds that have been prepared are nearly all derived from cyclopentadiene, indene, or cyclooctatetraene and only very recently have compounds containing direct metal-carbon σ -bonds been formed. Examples of the kinds of complexes that are known are listed in table 25.18.

TABLE 25.18.
General types of organometallic complexes of the rare earths.

Type		Reference
<i>Cyclopentadienyl compounds of the divalent rare earths</i>		
(C ₅ H ₅) ₂ R	(R = Eu, Yb)	Kanellakopulos and Bagnall (1972)
(C ₅ H ₅) ₂ Sm·OC ₄ H ₈ O		
<i>Cyclopentadienyl compounds of the trivalent rare earths</i>		
<i>Tricyclopentadienyl compounds</i>		
(C ₅ H ₅) ₃ R	(R = La–Lu, Y, Sc)	Kanellakopulos and Bagnall (1972) Melson (1975)
(C ₅ H ₅) ₃ R·X	(X = cyclohexyliso-nitrile, THF, ammonia, triphenylphosphine)	
<i>Dicyclopentadienyl compounds</i>		
(C ₅ H ₅) ₂ RX	(R = Sm–Lu)	Kanellakopulos and Bagnall (1972)
(CH ₃ C ₅ H ₄) ₂ RX	(R = Gd–Yb)	
	(X = chloride, formate, acetate, benzoate, methoxy, phenoxy, iodide)	
(C ₅ H ₅) ₂ RQ	(Q = methyl, phenyl, phenylacetylide, allyl)	Ely and Tsutsui (1975) Tsutsui and Ely (1975a, b) Melson (1975)
<i>Indenyl compounds</i>		
(C ₉ H ₇) ₃ R·OC ₄ H ₈ O	(R = La–Yb)	Kanellakopulos and Bagnall (1972)
<i>Cyclooctatetraenyl compounds</i>		
R(C ₈ H ₈)	(R = Eu, Yb)	Hayes and Thomas (1969)
K[R(C ₈ H ₈) ₂]	(R = La–Tb, Y)	Hodgson et al. (1973)
[R(C ₈ H ₈)Cl·2C ₄ H ₈ O] ₂	(R = Ce–Sm)	Hodgson et al. (1973)
(C ₅ H ₅)R(C ₈ H ₈)·THF	(R = Nd, Sm, Ho, Er, Y)	Jamerson et al. (1974)
[Nd(C ₈ H ₈)(OC ₄ H ₈)] [Nd(C ₈ H ₈) ₂]		Ely et al. (1976)
<i>Alkyl and aryl compounds</i>		
R(C ₆ H ₅) ₃	(R = Sc, Y)	Hart et al. (1970a)
[(CH ₃) ₃ CCH ₂] ₃ Sc·2THF		Lappert and Pearce (1973)
[(CH ₃) ₃ SiCH ₂] ₃ Sc·2THF		Lappert and Pearce (1973)
[o-CH ₃ OC ₆ H ₄ Si(CH ₃) ₂ CH ₂] ₃ Sc		Lappert and Pearce (1973)
{[(CH ₃) ₃ Si] ₂ CH] ₃ Y		Barker and Lappert (1974)
{[(CH ₃) ₃ Si] ₂ CH] ₃ R·2THF	(R = Y, Sc)	Barker and Lappert (1974)

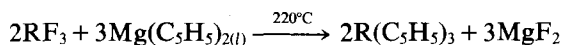
7.1. Tris-cyclopentadienides

The cyclopentadienides were the first complexes verified and consequently the ones about which the most is known. The tris complexes were initially prepared by the reaction



(R = Sc, Y, La, Ce, Pr, Nd, Sm, Gd, Dy, Er, and Yb)

and after sublimation they were found to be free of solvent although they form as the THF adducts. The synthesis can be modified by utilizing $K(C_5H_5)$ and benzene or diethyl ether as solvent but the resulting compounds are the same. All the triscyclopentadienides, including that of promethium, have now been prepared by these two methods (Kanellakopoulos and Bagnall, 1972). The europium complex does not sublime and removal of the THF must be carried out at a lower temperature. A third general method of synthesis (Reid and Wailes, 1966) involves the reaction:



This procedure has the advantage that the products are obtained free of solvents and the great difference in sublimation temperatures of the magnesium and lanthanide cyclopentadienides makes purification a relatively simple process.

The results of the measurements of the physical properties of these air- and moisture-sensitive complexes are consistent with their formulation as ionic compounds. The electronic spectra indicate that any involvement of the 4f electrons must be minimal. Moreover, the magnetic movements are essentially those expected for the free ions. The detailed molecular structure of $Sm(C_5H_5)_3$ has been determined and it is found to have a complex polymeric arrangement with considerable disorder involving as many as four different types of samarium-carbon bonds (Wong et al., 1969). The situation has been somewhat clarified with the report of the structure of neodymium tris(methylcyclopentadienide) (Burns et al., 1974). In this compound each neodymium atom is bonded in a pentahepto manner to three cyclopentadienide rings and in a monohapto manner to another ring of an adjacent $(C_6H_7)_3Nd$ unit. This sharing of a carbon atom between two neodymium atoms is repeated in a manner which produces the tetrameric units $[(C_6H_7)_3Nd]_4$. The types of bonds found for this structure are in accord with the bonding between the neodymium and the ring being primarily ionic.

The crystal structure of triscyclopentadienylscandium has been determined (Atwood and Smith, 1973a) and in agreement with expectation supports the idea that the bonding between scandium and the carbon atoms should be more covalent than for the lanthanides. The structure consists of $Sc(C_5H_5)_2$ units bridged by the third cyclopentadienyl group. The scandium atom is thus bonded to two rings in a pentahapto manner and to the two bridging rings in a monohapto manner. The preferred orientations of the two monohapto C_5H_5 groups are taken to imply that there is an appreciable amount of covalency in the compound.

7.2. Di-cyclopentadienides

In addition to the cyclopentadienides of the trivalent lanthanides, complexes of the divalent ions of samarium, europium, and ytterbium have been prepared (Fischer and Fischer, 1965). The europium and ytterbium dicyclopentadienides

are formed by the reaction



and the anhydrous compounds are obtained by removal of the ammonia by prolonged heating under vacuum. The samarium compound (Watt and Gillow, 1969) has been prepared by the reaction



Apparently removal of the solvated THF results in decomposition.

7.3. Adducts

The lanthanide tris-cyclopentadienides are strong Lewis acids and form 1:1 adducts with a number of donor molecules (Fischer and Fischer, 1966). Among these are ammonia, tetrahydrofuran, cyclohexylisocyanide, and triphenylphosphine. Although not all the lanthanides have been studied with each of these, there is no reason to expect that they all could not be formed. The isonitrile adducts are particularly stable and sublime without decomposition. The $C \equiv N$ stretching frequency is shifted approximately 70 cm^{-1} to higher frequencies which is in accord with the isonitrile acting as a σ -donor with little or no π -involvement. Lewis acidity toward the oxygen atoms in NO and CO in various transition metal organometallic compounds has been observed for $R(C_5H_5)_3$ or $R(CH_3C_5H_4)_3$ ($R = Nd, Sm, Gd, Dy, Ho, Er, \text{ and } Yb$) from a lowering of the NO or CO stretching frequencies (Crease and Legzdins, 1973) and by the isolation of solid compounds. The tris-cyclopentadienides are sufficiently soft Lewis acids that they can interact with soft bases such as transition metals in appropriate complexes, some carbon-carbon triple bonds (Crease and Legzdins, 1973) and phosphines and sulfides as indicated by substantial isotropic shifts in the proton magnetic resonance spectra (Marks et al., 1973) and by the isolation of compounds such as $cp_2RW(\pi-C_5H_5)(CO)_3$ ($cp = C_5H_5$ or C_6H_7 , $R = Dy, Ho, Er, \text{ or } Yb$).

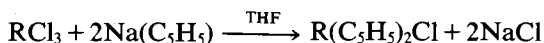
7.4. $R(C_5H_5)_2X$ and $R(C_5H_5)Cl_2$

For the lanthanides samarium through lutetium the compounds $R(C_5H_5)Cl_2$ can be prepared (Manastyrskyj et al., 1963) by the reaction of a stoichiometric quantity of RCl_3 and $Na(C_5H_5)$ according to

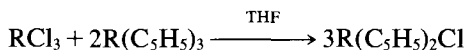


The compounds do not sublime and when heated under reduced pressure they decompose.

Similarly, the compounds $R(C_5H_5)_2Cl$ and $R(C_6H_7)_2Cl$ ($C_6H_7 =$ methylcyclopentadienide) can be prepared (Maginn et al., 1963) according to:



or



These complexes sublime between 150 and 250°C (10⁻⁵ mm) and are soluble in some organic solvents. The methylcyclopentadienides are dimeric in benzene presumably with chloride in the bridging positions and monomeric in THF. They are stable indefinitely in vacuum or under nitrogen but they decompose in a matter of minutes in air. They are also readily decomposed by protolytic solvents. The chloride ion can be easily replaced by alkoxide, aryloxy, amide, or carboxylate ions by reaction with the corresponding sodium salts.

The structure of the ytterbium complex, $[\text{Yb}(\text{C}_5\text{H}_4\text{CH}_3)_2\text{Cl}]_2$, has now been reported (Baker et al., 1975) and is shown in fig. 25.23. The dimeric structure is connected by chloride bridges and the average bond positions around ytterbium can be approximately described as tetrahedral. The rings are symmetrically bound to the metal atoms and the bridge is essentially symmetric. The structure of the closely related scandium compound, $[(\text{C}_5\text{H}_5)_2\text{ScCl}]_2$ has also been determined (Atwood and Smith, 1973b). The essential features of this structure are very similar to the ytterbium compound with the rings bound in a pentahapto fashion and with a symmetrical chloride bridge.

More recently the reaction of $(\text{C}_5\text{H}_5)_2\text{RCl}$ with QLi has been shown to yield $(\text{C}_5\text{H}_5)_2\text{RQ}$ (R = Gd, Er, and Yb) (Tsutsui and Ely, 1974, 1975; Ely and Tsutsui, 1975). These compounds in which Q is methyl, phenyl, or phenylacetylde are among the very few lanthanide compounds in which there are well-characterized metal-carbon σ -bonds. A di-phenylacetylde of holmium was also prepared from $\text{Ho}(\text{C}_5\text{H}_5)\text{Cl}_2 \cdot \text{THF}$. The compounds are sensitive to oxygen and moisture and decompose in air in a matter of seconds, but they have high thermal stabilities.

All the complexes have bands in the infrared spectra at ~ 3100 , 1400, 1010, and 780 cm^{-1} which are indicative of η^5 -cyclopentadienyl ligands. In addition each compound has characteristic bands which support the σ -nature of the Q groups. For example, the methyl derivatives all have one band at $\sim 1190 \text{cm}^{-1}$

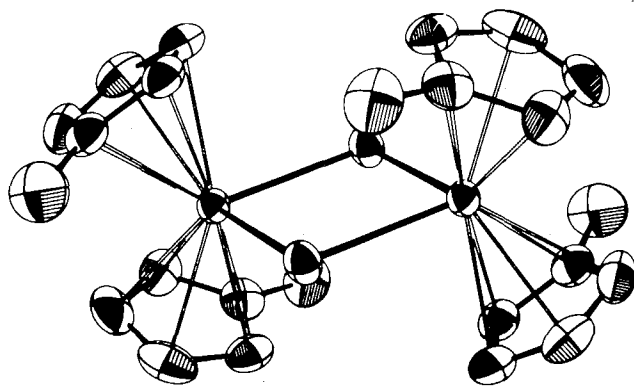


Fig. 25.23. The dimeric structure of $[\text{Yb}(\text{C}_5\text{H}_4\text{CH}_3)_2\text{Cl}]_2$. (Reprinted with permission from Baker, E.C., L.D. Brown and K.N. Raymond, 1975, *Inorg. Chem.* **14**, 1376-1379.)

TABLE 25.19.
 Some σ -bonded organometallic rare earth complexes.

Compound	Color	μ_{eff}	Reference
$(\text{C}_5\text{H}_5)_2\text{YbC}\equiv\text{CC}_6\text{H}_5$	Orange	4.31	Ely and Tsutsui (1975)
$(\text{C}_5\text{H}_5)_2\text{ErC}\equiv\text{CC}_6\text{H}_5$	Pink	9.64	Ely and Tsutsui (1975)
$(\text{C}_5\text{H}_5)_2\text{HoC}\equiv\text{CC}_6\text{H}_5$	Sand	10.08	Ely and Tsutsui (1975)
$(\text{C}_5\text{H}_5)_2\text{Ho}(\text{C}\equiv\text{CC}_6\text{H}_5)_2$	Sand	10.48	Ely and Tsutsui (1975)
$(\text{C}_5\text{H}_5)_2\text{GdC}\equiv\text{CC}_6\text{H}_5$	Yellow	7.98	Ely and Tsutsui (1975)
$(\text{C}_5\text{H}_5)_2\text{YbC}_6\text{H}_5$	Orange	3.86	Ely and Tsutsui (1975)
$(\text{C}_5\text{H}_5)_2\text{GdC}_6\text{H}_5$	Lavender	7.69	Ely and Tsutsui (1975)
$(\text{C}_5\text{H}_5)_2\text{ErCH}_3$	Pink	9.41	Ely and Tsutsui (1975)
$(\text{C}_5\text{H}_5)_2\text{YbCH}_3$	Orange	4.14	Ely and Tsutsui (1975)
$(\text{C}_5\text{H}_5)_2\text{ScC}\equiv\text{CC}_6\text{H}_5$	Yellow	—	Coutts and Wailes (1970)
$(\text{C}_6\text{H}_5)_3\text{Sc}$	Yellow-brown	—	Hart et al. (1970a)
$(\text{C}_6\text{H}_5\text{C}\equiv\text{C})_3\text{Sc}$	Brown	—	Hart et al. (1970a)
$(\text{C}_6\text{H}_5)_3\text{Y}$	Brown	—	Hart et al. (1970a)
$\text{Li}[\text{Pr}(\text{C}_6\text{H}_5)_4]$	Dark brown	—	Hart et al. (1970a)
$[(\text{CH}_3)_3\text{CCH}_2]_3\text{R}\cdot 2\text{THF}$ (R = Sc, Y)	Colorless	—	Lappert and Pearce (1973)
$[(\text{CH}_3)_3\text{SiCH}_2]_3\text{R}\cdot 2\text{THF}$ (R = Sc, Y)	Colorless	—	Lappert and Pearce (1973)
$[\text{o}-\text{CH}_3\text{OC}_6\text{H}_4\text{Si}(\text{CH}_3)_2\text{CH}_2]_3\text{Sc}$	Colorless	—	Lappert and Pearce (1973)
$\{[(\text{CH}_3)_3\text{Si}]_2\text{CH}\}_3\text{R}\cdot 2\text{THF}$ (R = Sc, Y)	White	—	Barker and Lappert (1974)
$\{[(\text{CH}_3)_3\text{Si}]_2\text{CH}\}_3\text{Y}$	White	—	Barker and Lappert (1974)

which arises from the symmetric deformation of the methyl group and which is characteristic of a methyl ligand bound to a metal. The absorption spectra contain in addition to the $4f-4f$ transitions a charge-transfer band that tails into the visible and is most likely of the ligand to metal type. Hypersensitive transitions are observed in both the erbium and holmium compounds. Conclusions concerning possible covalency based on this hypersensitivity would seem to be premature. The magnetic susceptibility for the compounds are in close agreement with the theoretically predicted values. However, the μ_{eff} values decrease with decreasing temperature which is in contrast to the values for other types of lanthanide cyclopentadienyl complexes. Whether or not this indicates "covalent" involvement of the f orbitals remains to be seen.

A similar reaction of $(\text{C}_5\text{H}_5)_2\text{RCl}$ (R = Sm, Er, or Ho) with allyl-magnesium bromide in a THF-ether solution at -78°C has resulted in the preparation of $(\text{C}_5\text{H}_5)_2\text{RC}_3\text{H}_5$ (Tsutsui and Ely, 1975b). These allyl compounds are also sensitive to air and moisture but are thermally quite stable. The infrared spectra indicate the η^5 -cyclopentadienyl ligand and the strong band at 1533 cm^{-1} is characteristic of π - or η^3 -allyl moieties. This is the first example of such an interaction in the rare earths. It is not clear why the allyl group bounds in the π -fashion in view of the σ -bonded complexes discussed above. Formally the σ -bonded complexes have a coordination number of seven and the allyl complexes have a coordination number of eight. The solids are all brightly colored and undergo a color change when dissolved in THF. For example the samarium complex is yellow

but gives a burgandy solution. Since this color change does not occur in benzene solutions, this is indicative of adduct formation in solution.

7.5. Indenyl complexes

Complexes of the indenyl group have been prepared by Tsutsui and Gysling (1968, 1969) from the reaction of the anhydrous trichlorides with sodium indenide in THF solution. The compounds are of the general formula $R(C_9H_7)_3 \cdot OC_4H_8$ ($R = La, Sm, Gd, Tb, Dy, \text{ and } Yb$). The magnetic moments of the complexes are normal and the THF can be removed by heating under vacuum or replaced by other donor molecules such as p-dioxane or triphenylphosphine. The NMR spectrum of the lanthanum compound is similar to that of the ionic sodium compound but the spectrum of the samarium compound was interpreted as indicating a decrease in the amount of ionic character. The detailed molecular structure of triindenylsamarium has now been determined (Atwood et al., 1973) and it is found that the samarium atom is symmetrically coordinated to the five-membered rings of the indenyl systems with an average Sm-C distance of 2.75 Å. The placement of the indenyl moieties is such that the angles between the samarium atom and the normals to the planes of the rings are approximately 120°. The rings are bonded in a pentahapto manner to the samarium and there is no preference for bonding to the electron-rich C-1 position which indicates that the bonds are primarily ionic in character.

7.6. Cyclooctatetraenyl compounds

Shortly after the preparation of uranocene, Streitwieser and his co-workers also prepared $K[R(COT)_2]$ ($R = Y, La, Ce, Pr, Nd, Sm, Gd, \text{ and } Tb$) by adding a

TABLE 25.20.
Cyclooctatetraenyl complexes.*

Compound	Color	Magnetic moment (B.M.)
$K[Y(C_8H_8)_2]$	Yellow	—
$K[La(C_8H_8)_2]$	Green	—
$K[Ce(C_8H_8)_2]$	Pale green	1.88
$K[Pr(C_8H_8)_2]$	Yellow-gold	2.84
$K[Nd(C_8H_8)_2]$	Pale green	2.98
$K[Sm(C_8H_8)_2]$	Brown	1.42
$K[Gd(C_8H_8)_2]$	Yellow	—
$K[Tb(C_8H_8)_2]$	Yellow-brown	9.86
$[Ce(C_8H_8)Cl \cdot 2C_4H_8O]_2$	Yellow-green	1.79
$[Pr(C_8H_8)Cl \cdot 2C_4H_8O]_2$	Pale green	3.39
$[Nd(C_8H_8)Cl \cdot 2C_4H_8O]_2$	Bright green	3.37
$[Sm(C_8H_8)Cl \cdot 2C_4H_8O]_2$	Purple	1.36

*Hodgson et al. (1973).

suspension of the anhydrous trichloride in THF to a mixture of 1.5 equivalents of K_2COT and 0.5 equivalent of COT dissolved in THF (Mares et al., 1970, 1971; Hodgson et al., 1973). In addition to the $K[R(COT)_2]$ complexes the compounds $[R(C_8H_8)Cl \cdot 2C_4H_8O]$ ($R = Ce, Pr, Nd, \text{ and } Sm$) have also been prepared. Although the europium and ytterbium compounds could not be prepared in this way, the preparation of the corresponding complexes of these elements in the divalent state by reaction of the metals with cyclooctatetraene in liquid ammonia had already been reported (Hayes and Thomas, 1969). The compounds have the formulae $EuCOT$ and $YbCOT$ and are orange and pink respectively. They are stable to $500^\circ C$, do not sublime even at 10^{-3} mm, but are explosively oxidized by air. Their solubility in basic solvents suggests that complexes are being formed.

The biscyclooctatetraene complexes have similar properties, are colored, decompose when heated above $160^\circ C$ under vacuum, and do not sublime even at 1×10^{-4} mm. However, they are thermally stable when heated to $360^\circ C$ in sealed tubes under one atmosphere of argon. They are insoluble in $CHCl_3$, CCl_4 , and hexane, and are moderately soluble in THF and dioxane. The molecular structure of the cerium complex has been determined (Hodgson and Raymond, 1972b) and is shown in fig. 25.24. The important feature is the symmetric coordination of the two $C_8H_8^{2-}$ rings in a π -fashion. The molecular symmetry is very close to D_{8d} .

The monocyclooctatetraene complexes are chloride-bridged dimers and have physical properties that are very similar to the bis-complexes. The THF is slowly

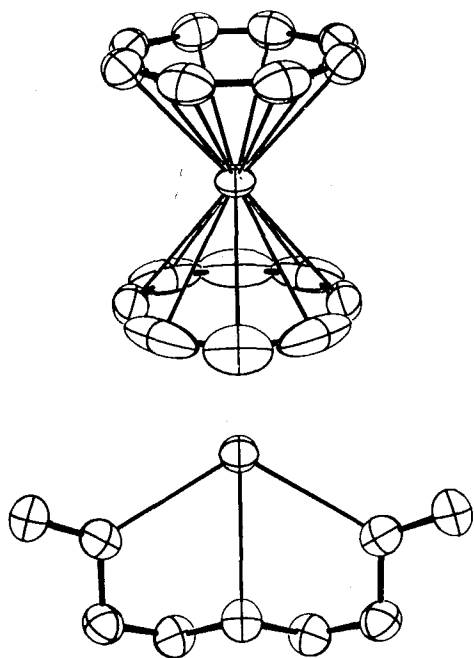
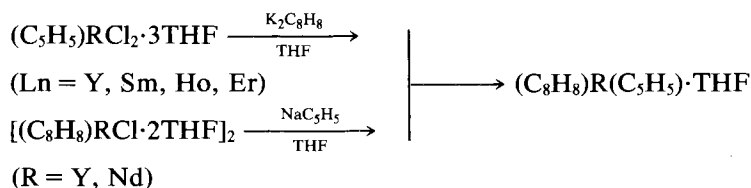


Fig. 25.24. The structure of the contact ion pair, $[K(diglyme)][Ce(C_8H_8)_2]$. (Reprinted with permission from Hodgson, K.O. and K.N. Raymond, 1972, *Inorg. Chem.* **11**, 3030-3035.)

lost when they are heated under vacuum and this is accompanied by some decomposition. The complexes cannot be sublimed at 10^{-3} mm and begin to decompose as the temperature is raised to 100°C . The structure of $[\text{Ce}(\text{C}_8\text{H}_8)\text{Cl}\cdot 2\text{C}_4\text{H}_8\text{O}]_2$ consists of two cerium atoms bridged asymmetrically by the chlorines (Hodgson and Raymond, 1972a). The C_8H_8 ring is a planar octagon with aromatic C–C bond distances and the coordination is completed by the oxygen atoms from the THF molecules.

The chemical and spectral (infrared, NMR, visible-near-infrared, and Raman) data confirm that these are highly ionic compounds relative to the analogous actinide compounds. Some slight degree of involvement of the 4f electrons is indicated by the presence bands in the visible assigned as ligand to metal charge transfer transitions.

An interesting extension of the chemistry in this field is the preparation of mixed cyclopentadiene–cyclooctatetraene complexes (Jamerson et al., 1974) according to the reactions



The complexes are exceedingly air sensitive, inflaming on contact with air. The THF can be removed by vacuum drying at 10^{-3} mm at 50°C . The infrared spectra again indicate that the bonding is primarily ionic. The complexes form adducts with molecules other than THF such as ammonia, pyridine, and cyclohexylisocyanide.

More recently the codeposition of lanthanide metal atoms, prepared by high-temperature vacuum evaporation, with cyclooctatetraene at 77 K has resulted in the formation of $\text{R}_2(\text{C}_8\text{H}_8)_3$ (Ely et al., 1976). The neodymium compound was purified by Soxhlet extraction into THF from which bright green crystals of $[\text{Nd}(\text{C}_8\text{H}_8)(\text{THF})_2][\text{Nd}(\text{C}_8\text{H}_8)_2]$ grew. The structure of this compound has been determined and is given in figure 25.25. The $\text{C}_8\text{H}_8^{2-}$ rings clearly demonstrate ten- π -electron aromatic character. The coordination about the neodymium in $[\text{Nd}(\text{C}_8\text{H}_8)(\text{THF})_2]^+$ is completed by coordination to at least one of the carbon atoms in the neodymium anion and perhaps to as many as three. The two rings in $[\text{Nd}(\text{C}_8\text{H}_8)_2]^-$ are inclined to each other by 8.25° and the Nd–C distances in the two rings are different, thus giving rise to the first lanthanide or actinide complex in which the $\text{M}(\text{C}_8\text{H}_8)_2$ unit is asymmetric.

7.7. Miscellaneous compounds

The codeposition of lanthanide atoms and carbon monoxide in an oxygen matrix at liquid helium temperatures leads to a series of carbonyl complexes which from an analysis of the infrared spectra have been assigned the formulae $\text{R}(\text{CO})_{1-6}$ (Sheline and Slater, 1975). The ytterbium compounds have distinctly

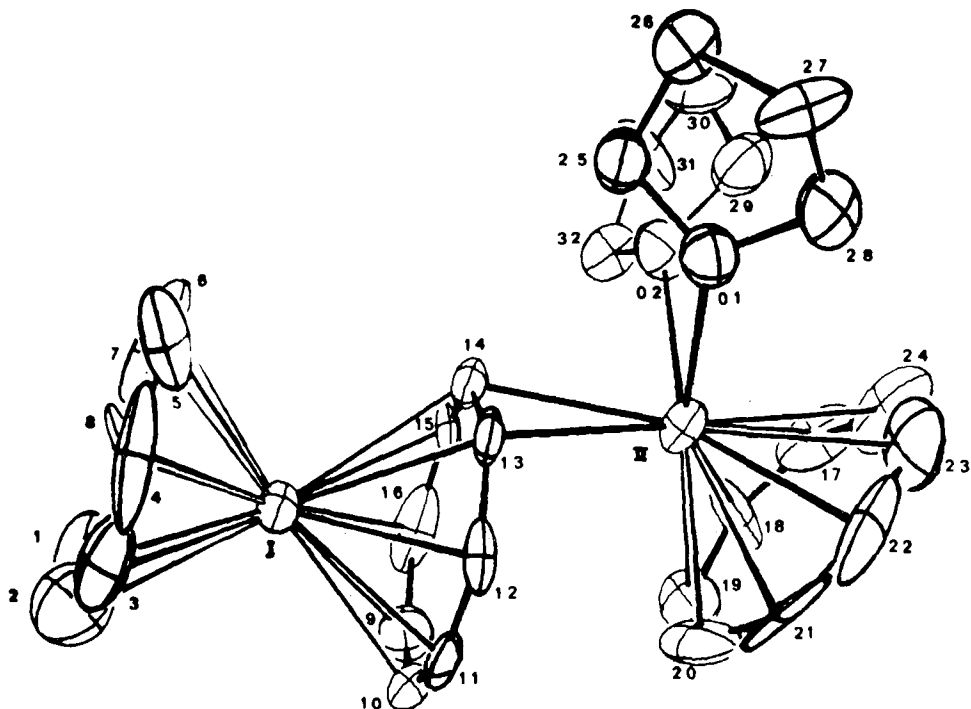
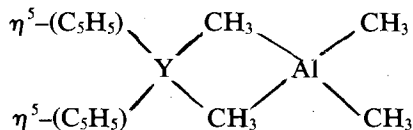


Fig. 25.25. The structure of $[\text{Nd}(\text{COT})(\text{THF})_2][\text{Nd}(\text{COT})_2]$. (Reprinted with permission from Ely, S.R., T.E. Hopkins and C.W. DeKock, 1976, *J. Amer. Chem. Soc.* **98**, 1624–1625.)

different infrared spectra which was attributed to the lack of one electron for a filled set of 4f orbitals. All considerations of bonding and structures at this point would be very speculative.

There have been a few reports of simple lanthanide alkyl and aryl compounds (see table 25.19). The structure of the $\text{Lu}(\text{C}_8\text{H}_9)_4^-$ anion ($\text{C}_8\text{H}_9^- = 2,6\text{-dimethylphenyl ion}$) was discussed earlier (section 3.3). Hart and his co-workers (Hart et al., 1970a) have described some trimethyl and triphenyl complexes as well as some more complicated compounds of formula $\text{LiR}(\text{C}_6\text{H}_5)_4$. There is reasonable chemical evidence for the formation of these compounds but more physical and spectroscopic data are needed.

The compound $[(\eta^5\text{-C}_5\text{H}_5)_2\text{YMe}_2\text{AlMe}_2]$ has been prepared by the reaction of lithium tetramethylaluminate(III) with $[(\text{Y}(\eta^5\text{-C}_5\text{H}_5)_2\text{Cl})_2]$ in toluene at 0°C (Ballard and Pearce, 1975). This compound sublimes at 120°C and 0.05 mmHg without decomposition. The proposed structure



is supported by the proton NMR spectrum at -45°C .

References

- Abragam, A. and B. Bleaney, 1970, *Electron Paramagnetic Resonance of Transition Ions* (Clarendon Press, Oxford) pp. 277-345.
- Agarwal, S.K. and J.P. Tandon, 1974, *Syn. React. Inorg. Metal-Org. Chem.* **4**, 387-401.
- Agarwal, S.K. and J.P. Tandon, 1975, *Z. Naturforsch.* **B30**, 50-53.
- Ahrland, S., J. Chatt and N.R. Davies, 1958, *Quart. Rev. Chem. Soc.* **12**, 265-276.
- Albertsson, J., 1970, *Acta Chem. Scand.* **24**, 1213-1229.
- Albertsson, J., 1972a, *Acta Chem. Scand.* **26**, 985-1004.
- Albertsson, J., 1972b, *Acta Chem. Scand.* **26**, 1005-1017.
- Albertsson, J., 1972c, *Acta Chem. Scand.* **26**, 1023-1044.
- Albertsson, J., 1972d, *On the Stereochemistry of Nine-Coordinate Lanthanoid Compounds*, Thesis, Lund.
- Albertsson, J. and A. Oskarsson, 1968, *Acta Chem. Scand.* **22**, 1700-1702.
- Albertsson, J., S. Mroczkowski and J.C. Doran, *J. Cryst. Growth* **16**, 159-162.
- Airolidi, C. and Y. Gushikem, 1972, *J. Inorg. Nucl. Chem.* **34**, 3921-3925.
- Al-Karaghoul, A.R. and J.S. Wood, 1972a, *Chem. Commun.* 516-517.
- Al-Karaghoul, A.R. and J.S. Wood, 1972b, *Inorg. Chem.* **11**, 2293-2299.
- Al-Karaghoul, A.R. and J.S. Wood, 1973, *J. Chem. Soc., Dalton Trans.* 2318-2321.
- Amberger, H.-D., R.D. Fischer and G.G. Rosenbauer, 1975, *Ber. Bunsenges. Phys. Chem.* **79**, 1226-1230.
- Amberger, H.-D., R.D. Fischer and G.G. Rosenbauer, 1976, *Z. Naturforsch.* **B31**, 1-11.
- Anderegg, G., 1960, *Helv. Chim. Acta* **43**, 825-830.
- Anderegg, G., P. Nägeli, F. Müller and G. Schwarzenbach, 1959, *Helv. Chim. Acta* **42**, 827-836.
- Anderson, T.J., M.A. Neuman and G.A. Melson, 1973, *Inorg. Chem.* **12**, 927-930.
- Anderson, T.J., M.A. Neuman and G.A. Melson, 1974a, *Inorg. Chem.* **13**, 158-163.
- Anderson, T.J., M.A. Neuman and G.A. Melson, 1974b, *Inorg. Chem.* **13**, 1884-1890.
- Aslanov, L.A., E.F. Korytyni and M.A. Porai-Koshits, 1971a, *Zh. Strukt. Khim.* **12**, 661-666; *J. Struct. Chem. (USSR)* 1972, **12**, 600-604.
- Aslanov, L.A., M.A. Porai-Koshits and M.O. Dekaprilevich, 1971b, *Zh. Strukt. Khim.* **12**, 470-473; *J. Struct. Chem. (USSR)* 1971, **12**, 431-434.
- Aslanov, L.A., I.K. Abdul-Minev and M.A. Porai-Koshits, 1972a, *Zh. Strukt. Khim.* **13**, 468-472; *J. Struct. Chem. (USSR)*, 1972, **13**, 437-440.
- Aslanov, L.A., L.I. Soleva, M.A. Porai-Koshits and S.S. Goukhberg, 1972b, *Zh. Strukt. Khim.* **13**, 655-659; *J. Struct. Chem.*, 1972, **13**, 610-613.
- Aslanov, L.A., L.I. Soleva and M.A. Porai-Koshits, 1972c, *Zh. Strukt. Khim.* **13**, 1101-1104; *J. Struct. Chem. (USSR)*, 1972, **13**, 1021-1023.
- Aslanov, L.A., L.I. Soleva and M.A. Porai-Koshits, 1973, *Zh. Strukt. Khim.* **14**, 1064-1066; *J. Struct. Chem. (USSR)*, 1973, **14**, 998-1000.
- Atwood, J.L. and K.D. Smith, 1973a, *J. Amer. Chem. Soc.* **95**, 1488-1491.
- Atwood, J.L. and K.D. Smith, 1973b, *J. Chem. Soc. Dalton Trans.* 2487-2490.
- Atwood, J.L., J.H. Burns and P.G. Laubereau, 1973, *J. Amer. Chem. Soc.* **95**, 1830-1833.
- Aveston, J., 1966, *J. Chem. Soc. A*, 1599-1601.
- Baczynski, A., Z. Rozploch and W. Orzeszko, 1973, *Acta Phys. Pol.* **A43**, 211-218.
- Bagnall, K.W., 1975, *MTP (Med. Tech. Publ. Co.) Int. Rev. Sci.: Inorg. Chem., Ser. Two* **7**, 41-63.
- Baker, E.C., L.D. Brown and K.N. Raymond, 1975, *Inorg. Chem.* **14**, 1376-1379.
- Baker, R.W. and J.W. Jeffery, 1974, *J. Chem. Soc., Dalton Trans.* 229-232.
- Ballard, D.G.H. and R. Pearce, 1975, *J. Chem. Soc., Chem. Comm.* 621.
- Barbanel, Y.A., R.B. Dooshin, V.V. Kolin, N.K. Michaelov and G.P. Choodnovskaa, 1975, *Koord. Khim.* **1**, 411-415.
- Barker, G.K. and M.F. Lappert, 1974, *J. Organometal. Chem.* **76**, C45-C47.
- Barnes, J.C. and R.D. Peacock, 1971, *J. Chem. Soc. A* 558-562.
- Bashium, R.W., R.L. Dieck and T. Moeller, 1973, *Inorg. Nucl. Chem. Lett.* **9**, 773-776.
- Bauer, H., J. Blanc and D.L. Ross, 1964, *J. Amer. Chem. Soc.* **86**, 5125-5131.
- Beineke, T.A. and J. Delgaudio, 1968, *Inorg. Chem.* **7**, 715-721.
- Bennett, M.J., F.A. Cotton, P. Legzdins and S.J. Lippard, 1968, *Inorg. Chem.* **7**, 1770-1776.
- Bertan, P.B. and S.K. Madan, 1972, *J. Inorg. Nucl. Chem.* **34**, 3081-3087.
- Bhandary, K.K. and H. Manohar, 1973, *Acta Crystallogr.* **B29**, 1093-1098.
- Bhandary, K.K., H. Manohar and K. Venkatesan, 1975, *J. Chem. Soc., Dalton Trans.* 288-291.
- Bhandary, K.K., H. Manohar and K. Venkatesan, 1976, *Acta Crystallogr.* **B32**, 861-867.
- Birmingham, J.M. and G. Wilkinson, 1954, *J. Amer. Chem. Soc.* **76**, 6210.
- Blackborow, J.R., C.R. Eady, E.A.K. von Gustorf, A. Scrivanti and O. Wolfbeis, 1976, *J. Organometal. Chem.* **108**, C32-C34.
- Blasse, G. and A. Brill, 1970, *Philips Tech. Rev.* **31**, 304-314.
- Blight, D.G. and D.L. Kepert, 1972, *Inorg. Chem.* **11**, 1556-1561.
- Bottari, E. and G. Anderegg, 1967, *Helv. Chim. Acta* **50**, 2349-2356.
- Bradley, D.C., 1972, *Adv. Inorg. Chem. Radiochem.* **15**, 290-293.

- Bradley, D.C., J.S. Ghotra and F.A. Hart, 1973, *J. Chem. Soc., Dalton Trans.* 1021-1023.
- Bradley, D.C., J.S. Ghotra, F.A. Hart, M.B. Hursthouse and P.R. Raithby, 1974, *J. Chem. Soc., Chem. Commun.* 40-41.
- Brown, D., 1968, *Halides of the Lanthanides and Actinides* (Wiley-Interscience, London).
- Brown D., 1975, MTP (Med. Tech. Publ. Co.) *Int. Rev. Sci.: Inorg. Chem.*, Ser. Two 7, 111-150.
- Brown, D. and D.G. Holah, 1968, *Chem. Commun.* 1545-1546.
- Brown, D., D.G. Holah and C.E.F. Rickard, 1970, *J. Chem. Soc. A* 786-790.
- Bucher, E., H.J. Guggenheim, K. Andres, G.W. Hull, Jr. and A.S. Cooper, 1974, *Phys. Rev.* **B10**, 2945-2951.
- Buchler, J.W., G. Eikermann, L. Puppe, K. Rohbock, H.H. Schneehage and O. Weck, 1971, *Justus Liebigs Ann. Chem.* **745**, 135-151.
- Burgess, C.M. and G.E. Toogood, 1971, *Inorg. Nucl. Chem. Lett.* **7**, 761-766.
- Burmeister, J.L., S.D. Patterson and E.A. Deardorff, 1969, *Inorg. Chim. Acta* **3**, 105-109.
- Burmeister, J.L. and E.A. Deardorff, 1970, *Inorg. Chim. Acta* **4**, 97-100.
- Burns, G. and J.D. Axe, 1967, *Covalent Bonding Effects in Rare Earth Crystal Fields*, in: H.M. Crosswhite and H.W. Moos, eds.: *Optical Properties of Ions in Crystals* (Interscience Publishers, New York) pp. 53-71.
- Burns, J.H. and M.D. Danford, 1969, *Inorg. Chem.* **8**, 1780-1784.
- Burns, J.H., W.H. Baldwin and F.H. Fink, 1974, *Inorg. Chem.* **13**, 1916-1920.
- Bye, E., 1974, *Acta Chem. Scand.* **A28**, 731-739.
- Carnall, W.T., P.R. Fields and K. Rajnak, 1968a, *J. Chem. Phys.* **49**, 4447-4449.
- Carnall, W.T., P.R. Fields and K. Rajnak, 1968b, **49**, 4450-4455.
- Carnall, W.T., S. Siegel, J.R. Ferraro, B. Tani and E. Gebert, 1973, *Inorg. Chem.* **12**, 560-564.
- Carpentier, L.J. and T. Moeller, 1970, *J. Inorg. Nucl. Chem.* **32**, 3575-3584.
- Chieh, C., G.E. Toogood, T.D. Boyle and C.M. Burgess, 1976, *Acta Crystallogr.* **B32**, 1008-1011.
- Choca, M., J.R. Ferraro and K. Nakamoto, 1974, *Coord. Chem. Rev.* **12**, 295-307.
- Choca, M., J.R. Ferraro and K. Nakamoto, 1975, *J. Inorg. Nucl. Chem.* **37**, 1425-1428.
- Choppin, G.R., 1971, *Pure Appl. Chem.* **27**, 23-41.
- Choppin, G.R. and W.F. Strazik, 1965, *Inorg. Chem.* **4**, 1250-1254.
- Clearfield, A., P. Singh and I. Bernal, 1970, *Chem. Commun.* 389-390.
- Cockerill, A.F., G.L.O. Davies, R.C. Harden and D.M. Rackham, 1973, *Chem. Rev.* **73**, 553-588.
- Condorelli, G. and A. Seminara, 1967, *Boll. Sedute Accad. Gioenia Sci. Natur. Catania* **9**, 87-92.
- Condorelli, G., I. Fragala, S. Giuffrida and A. Cassol, 1975, *Z. Anorg. Allgem. Chem.* **412**, 251-257.
- Cotton, F.A. and P. Legzdins, 1968, *Inorg. Chem.* **7**, 1777-1783.
- Cotton, F.A. and G. Wilkinson, 1972, *Advanced Inorganic Chemistry: A Comprehensive Text*, 3rd ed. (Interscience Publishers, New York) pp. 555-556 and 599-604.
- Cotton, F.A., P. Legzdins and S.J. Lippard, 1966, *J. Chem. Phys.* **45**, 3461-3462.
- Cotton, S.A., F.A. Hart, M.B. Hursthouse and A.J. Welch, 1972, *J. Chem. Soc., Chem. Commun.* 1225-1226.
- Cousins, D.R. and F.A. Hart, 1967a, *J. Inorg. Nucl. Chem.* **29**, 1745-1757.
- Cousins, D.R. and F.A. Hart, 1967b, *J. Inorg. Nucl. Chem.* **29**, 2965-2974.
- Cousins, D.R. and F.A. Hart, 1968, *J. Inorg. Nucl. Chem.* **30**, 3009-3015.
- Coutts, R.S.P. and P.C. Wailes, 1970, *J. Organometal. Chem.* **25**, 117-122.
- Cramer, R.E. and D. Seff, 1972, *Acta Crystallogr.* **B28**, 3281-3293.
- Crawford, N.P. and G.A. Melson, 1969, *J. Chem. Soc. A* 1049-1052.
- Crawford, N.P. and G.A. Melson, 1970, *J. Chem. Soc. A* 141-145.
- Crease, A.E. and P. Legzdins, 1973, *J. Chem. Soc., Dalton Trans.* 1501-1507.
- Crosby, G.A., 1966, *Mol. Cryst.* **1**, 37-81.
- Cunningham, J.A., 1973, personal communication.
- Cunningham, J.A. and R.E. Sievers, 1975, *J. Amer. Chem. Soc.* **97**, 1586-1587.
- Cunningham, J.A., D.E. Sands and W.F. Wagner, 1967, *Inorg. Chem.* **6**, 499-503.
- Cunningham, J.A., D.E. Sands, W.F. Wagner and M.F. Richardson, 1969, *Inorg. Chem.* **8**, 22-28.
- Das, M. and S.E. Livingstone, 1975, *Aust. J. Chem.* **28**, 1513-1516.
- Davis, A.R. and F.W.B. Einstein, 1974, *Inorg. Chem.* **13**, 1880-1884.
- Day, V.W., 1970, *Diss. Abstr. Int.* **B30**, 4079-4080.
- Dean, C.R.S. and T.M. Shepherd, 1975, *Chem. Phys. Lett.* **32**, 480-482.
- de Sa, G.F., E. Giesbrecht and L.C. Thompson, 1975, *J. Inorg. Nucl. Chem.* **37**, 109-112.
- Devaney, P. and H.J. Stapleton, 1975, *J. Chem. Phys.* **63**, 5459-5461.
- de Villiers, J.P.R. and J.C.A. Boeyens, 1971a, *Acta Crystallogr.* **B27**, 692-702.
- de Villiers, J.P.R. and J.C.A. Boeyens, 1971b, *Acta Crystallogr.* **B27**, 2335-2340.
- Dieck, R.L. and T. Moeller, 1973a, *J. Inorg. Nucl. Chem.* **35**, 3781-3785.
- Dieck, R.L. and T. Moeller, 1973b, *J. Less-Common Metals* **33**, 355-360.
- Dieck, R.L. and T. Moeller, 1974, *J. Inorg. Nucl. Chem.* **36**, 2283-2286.
- Dieke, G.H., 1968, *Spectra and Energy Levels of Rare Earth Ions in Crystals* (Interscience Publishers, New York).

- Donoghue, J.T., 1970, *Bull. Chem. Soc. Jap.* **43**, 932-934.
- Donoghue, J.T. and E. Fernandez, 1970, *Bull. Chem. Soc. Jap.* **43**, 271-273.
- Donoghue, J.T. and D.A. Peters, 1969, *J. Inorg. Nucl. Chem.* **31**, 467-470.
- Donoghue, J.T., E. Fernandez, J.A. McMillan and D.A. Peters, 1969, *J. Inorg. Nucl. Chem.* **31**, 1431-1433.
- Doran, J.C., U. Erich and W.P. Wolf, 1972, *Phys. Rev. Lett.* **28**, 103-106.
- Dunlap, B.D. and G.K. Shenoy, 1975, *Phys. Rev.* **B12**, 2716-2724.
- Durham, D.A. and F.A. Hart, 1969, *J. Inorg. Nucl. Chem.* **31**, 145-157.
- Durham, D.A., G.H. Frost and F.A. Hart, 1969, *J. Inorg. Nucl. Chem.* **31**, 833-838.
- Durney, M.T. and R.S. Marianelli, 1970, *Inorg. Nucl. Chem. Lett.* **6**, 895-902.
- Dutt, N.K. and K. Nag, 1968, *J. Inorg. Nucl. Chem.* **30**, 2493-2499.
- Dyer, D.S., J.A. Cunningham, J.J. Brooks, R.E. Sievers and R.E. Rondeau, 1973, *Interactions of Nucleophiles with Lanthanide Shift Reagents*, in R.E. Sievers, ed., *Nuclear Magnetic Shift Reagents*, (Academic Press, New York) pp. 21-51.
- Edwards, J.O., R.J. Goetsch and J.A. Stritar, 1967, *Inorg. Chim. Acta* **1**, 360-362.
- Eisentraut, K.J. and R.E. Sievers, 1965, *J. Amer. Chem. Soc.* **87**, 5254-5266.
- Ely, N.M. and M. Tsutsui, 1975, *Inorg. Chem.* **14**, 2680-2687.
- Ely, S.R., T.E. Hopkins and C.W. DeKock, 1976, *J. Amer. Chem. Soc.* **98**, 1624-1625.
- Engel, G., 1972, *Z. Anorg. Allgem. Chem.* **387**, 22-30.
- Erasmus, C.S. and J.C.A. Boeyens, 1970, *Acta Crystallogr.* **B26**, 1843-1854.
- Erasmus, C.S. and J.C.A. Boeyens, 1971, *J. Cryst. Mol. Struct.* **1**, 83-91.
- Eremin, Yu.G., V.S. Katochkina and L.N. Komissarova, 1970, *Zh. Neorg. Khim.* **15**, 1248-1254; *Russ. J. Inorg. Chem.* 1970, **15**, 640-644.
- Figgis, B.N., 1966, *Introduction to Ligand Fields* (Interscience Publishers, New York) pp. 324-327.
- Fischer, E.O. and H. Fischer, 1965, *J. Organometal. Chem.* **3**, 181-187.
- Fischer, E.O. and H. Fischer, 1966, *J. Organometal. Chem.* **6**, 141-148.
- Fischer, R.D., 1973, *Lanthanide and Actinide Complexes*, in: G.N. LaMar, W.deW. Horrocks, Jr. and R.H. Holm, eds., *NMR of Paramagnetic Molecules: Principles and Applications* (Academic Press, New York), pp. 521-553.
- Fitzwater, D.R. and R.E. Rundle, 1959, *Z. Krist.* **112**, 362-374.
- Forsberg, J.H., 1973, *Coord. Chem. Revs.* **10**, 195-226.
- Forsberg, J.H. and T. Moeller, 1968, *J. Amer. Chem. Soc.* **90**, 1932.
- Forsberg, J.H. and T. Moeller, 1969, *Inorg. Chem.* **8**, 883-888.
- Forsberg, J.H. and C.A. Wathen, 1971, *Inorg. Chem.* **10**, 1379-1383.
- Forsberg, J.H., T.M. Kubik, T. Moeller and K. Gucwa, 1971, *Inorg. Chem.* **10**, 2656-2660.
- Foster, R.J. and D.G. Hendricker, 1972, *Inorg. Chim. Acta* **6**, 371-375.
- Foster, R.J., R.L. Bodner and D.G. Hendricker, 1972, *J. Inorg. Nucl. Chem.* **34**, 3795-3799.
- Fratiello, A., V. Kubo, S. Peak, B. Sanchez and R.E. Shuster, 1971, *Inorg. Chem.* **10**, 2552-2557.
- Fratiello, A., V. Kubo and G.A. Vidulich, 1973, *Inorg. Chem.* **12**, 2066-2071.
- Fratiello, A., R.E. Lee and R.E. Shuster, 1970, *Inorg. Chem.* **9**, 391-392.
- Fritz, J.J., P.E. Field and I. Grenthe, 1961, *J. Phys. Chem.* **65**, 2070-2074.
- Frolova, U.K., V.N. Kumok and A. Serebrennikov, 1966, *Izv. Vyssh. Ucheb. Zaved. Khim. Khim. Technol.* **9**, 176-179.
- Frost, G.H., F.A. Hart, C. Heath and M.B. Hursthouse, 1969, *Chem. Commun.* 1421-1422.
- Fukuzawa, T., N. Ebara, M. Katayama and H. Koizumi, 1975, *Bull. Chem. Soc. Jap.* **48**, 3460-3463.
- Geier, G. and C.K. Jørgensen, 1971, *Chem. Phys. Lett.* **9**, 262-265.
- Geier, G. and U. Karlen, 1971, *Helv. Chim. Acta* **54**, 135-153.
- Gerloch, M. and D.J. Mackey, 1970a, *J. Chem. Soc. A* 3030-3040.
- Gerloch, M. and D.J. Mackey, 1970b, *J. Chem. Soc. A* 3040-3050.
- Gerloch, M. and D.J. Mackey, 1971a, *J. Chem. Soc. A* 2605-2612.
- Gerloch, M. and D.J. Mackey, 1971b, *J. Chem. Soc. A* 2612-2616.
- Gerloch, M. and D.J. Mackey, 1971c, *J. Chem. Soc. A* 3372-3377.
- Gerloch, M. and D.J. Mackey, 1972a, *J. Chem. Soc. A* 37-42.
- Gerloch, M. and D.J. Mackey, 1972b, *J. Chem. Soc. A* 42-45.
- Gerloch, M. and D.J. Mackey, 1972c, *J. Chem. Soc. A* 410-414.
- Gerloch, M. and D.J. Mackey, 1972d, *J. Chem. Soc. A* 415-418.
- Ghotra, J.S., M.B. Hursthouse and A.J. Welch, 1973, *J. Chem. Soc., Chem. Commun.* 669-670.
- Giesbrecht, E. and M. Kawashita, 1970, *J. Inorg. Nucl. Chem.* **32**, 2461-2464.
- Giesbrecht, E. and L.B. Zimmer, 1969, *Inorg. Nucl. Chem. Lett.* **5**, 575-579.
- Glentworth, P., A.L. Nichols, D.A. Newton, N.R. Large and R.J. Bullock, 1973, *J. Chem. Soc., Dalton Trans.* 546-550.
- Golub, A.M. and A.N. Borsch, 1967, *Ukr. Khim. Zh.* **32**, 923-925.
- Grandey, R.C. and T. Moeller, 1970, *J. Inorg. Nucl. Chem.* **32**, 333-336.
- Grenthe, I., 1963, *Acta Chem. Scand.* **17**, 2487-2498.
- Grenthe, I., 1964a, *Acta Chem. Scand.* **18**, 283-292.
- Grenthe, I., 1964b, *Acta Chem. Scand.* **18**, 293-299.

- Grenthe, I., 1969, *Acta Chem. Scand.* **23**, 1253-1269.
- Grenthe, I., 1971a, *Acta Chem. Scand.* **25**, 3347-3359.
- Grenthe, I., 1971b, *Acta Chem. Scand.* **25**, 3721-3736.
- Grenthe, I., 1972, *Acta Chem. Scand.* **26**, 1479-1489.
- Grenthe, I. and E. Hansson, 1969, *Acta Chem. Scand.* **23**, 611-627.
- Grenthe, I. and H. Ots, 1972, *Acta Chem. Scand.* **26**, 1229-1242.
- Grenthe, I. and E. Tobiasson, 1963, *Acta Chem. Scand.* **17**, 2101-2112.
- Gruber, J.B., E.R. Menzel and J.L. Ryan, 1969, *J. Chem. Phys.* **51**, 3816-3819.
- Gurrieri, S., S. Musumeci, E. Rizzarelli and A. Seminara, 1976, *J. Inorg. Nucl. Chem.* **38**, 259-263.
- Gushikem, Y., C. Airoldi and O.L. Alves, 1973, *J. Inorg. Nucl. Chem.* **35**, 1159-1169.
- Haas, Y. and G. Navon, 1972, *J. Phys. Chem.* **76**, 1449-1455.
- Habenschuss, A. and F.H. Spedding, 1974, A Survey of Some Properties of Aqueous Rare Earth Salt Solutions. I. Volume, Thermal Expansion, Raman Spectra and X-Ray Diffraction, in: J.M. Haschke and H.A. Eick, eds., Proceedings of the 11th Rare Earth Conference, Traverse City, vol. 2 (United States Atomic Energy Commission, Oak Ridge), pp. 909-918.
- Hansson, E., 1972, *Acta Chem. Scand.* **26**, 1337-1350.
- Hansson, E., 1973a, *Acta Chem. Scand.* **27**, 823-834.
- Hansson, E., 1973b, *Acta Chem. Scand.* **27**, 2441-2454.
- Hansson, E., 1973c, *Acta Chem. Scand.* **27**, 2813-2826.
- Hansson, E., 1973d, *Acta Chem. Scand.* **27**, 2827-2840.
- Hansson, E., 1973e, On the Structures of Solid Rare Earth Oxalates and Malonates, Thesis, Lund.
- Hart, F.A., 1976, personal communication.
- Hart, F.A. and F.P. Laming, 1963, *Proc. Chem. Soc. London* 107.
- Hart, F.A., A.G. Massey and M.S. Saran, 1970a, *J. Organometal Chem.* **21**, 147-154.
- Hart, F.A., J.E. Newbery and D. Shaw, 1970b, *J. Inorg. Nucl. Chem.* **32**, 3585-3597.
- Hayes, R.G. and J.L. Thomas, 1969, *J. Amer. Chem. Soc.* **91**, 6876.
- Hayes, R.G. and J.L. Thomas, 1971, *Organometal. Chem. Rev. Sect. A7*, 1-50.
- Helmholz, L., 1939, *J. Amer. Chem. Soc.* **61**, 1544-1550.
- Hendrick, D.G. and R.J. Foster, 1972, *J. Inorg. Nucl. Chem.* **34**, 1949-1954.
- Henrie, D.E., R.L. Fellows and G.R. Choppin, 1976, *Coord. Chem. Rev.* **18**, 199-224.
- Hinckley, C.C., 1969, *J. Amer. Chem. Soc.* **91**, 5160-5162.
- Hoard, J.L. and J.V. Silverton, 1963, *Inorg. Chem.* **2**, 235-243.
- Hoard, J.L., B. Lee and M.D. Lind, 1965, *J. Amer. Chem. Soc.* **87**, 1612-1613.
- Hodgson, K.O. and K.N. Raymond, 1972a, *Inorg. Chem.* **11**, 171-175.
- Hodgson, K.O. and K.N. Raymond, 1972b, *Inorg. Chem.* **11**, 3030-3035.
- Hodgson, K.O., F. Mares, D.F. Starks and A. Streitwieser, Jr., 1973, *J. Amer. Chem. Soc.* **95**, 8650-8658.
- Hoehn, M.V. and D.G. Karraker, 1974, *J. Chem. Phys.* **60**, 393-397.
- Hoof, D.L., D.G. Tisley and R.A. Walton, 1973, *J. Chem. Soc., Dalton Trans.* 200-204.
- Horrocks, Jr., W.DeW., 1973, Lanthanide Shift Reagents and other Analytical Applications, in: G.N. LaMar, W.DeW. Horrocks, Jr. and R.W. Holm, eds., *NMR of Paramagnetic Molecules* (Academic Press, New York) pp. 492-495.
- Horrocks, Jr., W.DeW., J.P. Sipe III and J.R. Lubert, 1971, *J. Amer. Chem. Soc.* **93**, 5258-5260.
- Hubbard, C.R., C.O. Quicksall and R.A. Jacobson, 1974, *Acta Crystallogr.* **B30**, 2613-2619.
- Il'inskii, A.L., L.A. Aslanov, V.I. Ivanov, A.D. Khalidov and O.M. Petrukhin, 1969, *Zh. Struct. Khim.* **10**, 285-289; *J. Struct. Chem. (USSR)*, 1969, **10**, 263-266.
- Il'inskii, A.L., M.A. Porai-Koshits, L.A. Aslanov and P.I. Lazarev, 1972, *Zh. Struct. Khim.* **13**, 277-286; *J. Struct. Chem. (USSR)*, 1972, **13**, 254-262.
- Iwase, A. and S. Tada, 1973, *Nippon Kagaku Kaishi*, 60-63.
- Jackson, D.E., 1950, Doctoral Dissertation, University of Illinois.
- Jacobs, R.R., M.J. Weber and K. Pearson, 1975, *Chem. Phys. Lett.* **34**, 80-83.
- Jamerson, J.D., A.P. Mosino and J. Takats, 1974, *J. Organometal. Chem.* **65**, C33-C36.
- Johnson, M.F. and J.H. Forsberg, 1972, *Inorg. Chem.* **11**, 2683-2686.
- Johnson, M.F. and J.H. Forsberg, 1976, *Inorg. Chem.* **15**, 734-737.
- Jørgensen, C.K., 1970, *Progr. Inorg. Chem.* **12**, 132-138.
- Jørgensen, C.K., 1971, *Modern Aspects of Ligand Field Theory* (North-Holland Publishing Company, Amsterdam) pp. 293-313.
- Jørgensen, C.K., 1975, *Struct. Bonding (Berlin)* **22**, 49-81.
- Jørgensen, C.K. and B.R. Judd, 1964, *Mol. Phys.* **8**, 281-290.
- Kanellakopoulos, B. and K.W. Bagnall, 1972, *MTP (Med. Tech. Publ. Co.) Int. Rev. Sci.: Ser. One* **7**, 299-322.
- Karraker, D.G., 1971, *J. Chem. Phys.* **55**, 1084-1086.
- Katzin, L.I., 1970, *Coord. Chem. Rev.* **5**, 279-292.
- Kay, J., J.W. Moore and M.D. Glick, 1972, *Inorg. Chem.* **11**, 2818-2826.
- Keper, D.L., 1974, *J. Chem. Soc., Dalton Trans.* 617-621.
- Kettle, S.F.A. and A.J. Smith, 1967, *J. Chem. Soc. A* 688-692.
- King, R.B., 1970a, *J. Amer. Chem. Soc.* **92**, 6455-6460.

- King, R.B., 1970b, *J. Amer. Chem. Soc.* **92**, 6460-6466.
- King, R.B. and P.R. Heckley, 1974, *J. Amer. Chem. Soc.* **96**, 3118-3123.
- Koppikar, D.K. and S. Soundararajan, 1975, *J. Inorg. Nucl. Chem.* **38**, 174-176.
- Krishnamurthy, S.S. and S. Soundararajan, 1966, *Z. Anorg. Allgem. Chem.* **348**, 309-312.
- Krishnamurthy, V.N. and S. Soundararajan, 1967a, *Can. J. Chem.* **45**, 189-191.
- Krishnamurthy, S.S. and S. Soundararajan, 1967b, *J. Less-Common Metals* **13**, 619-625.
- Kuma, H. and S. Yamada, 1975, *Inorg. Chim. Acta* **15**, 213-215.
- Kutek, F., 1968, *Coll. Czech. Chem. Commun.* **33**, 1341-1345.
- Kuya, M.K., O.A. Serra and V.K.L. Osorio, 1975, *J. Inorg. Nucl. Chem.* **37**, 1998-1999.
- Lalancette, R.A., M. Cefola, W.C. Hamilton and S.J. LaPlaca, 1967, *Inorg. Chem.* **6**, 2127-2134.
- Lappert, M.F. and R. Pearce, 1973, *J. Chem. Soc., Chem. Comm.* 126.
- Large, N.R., R.J. Bullock, P. Glentworth and D.A. Newton, 1969, *Phys. Lett.* **A29**, 352-353.
- Lazarev, P.I., V.M. Ionov, L.A. Aslanov and M.A. Porai-Koshits, 1973, *Zh. Strukt. Khim.* **14**, 168; *J. Russ. Struct. Chem.* 1973, **14**, 151-152.
- Lee, H.-Y., F.F. Cleveland, J.S. Ziomek and F. Jarke, 1972, *Appl. Spectrosc.* **26**, 251-256.
- Leipoldt, J.G., L.D.C. Bok, A.E. Laubscher and S.S. Basson, 1975, *J. Inorg. Nucl. Chem.* **37**, 2477-2480.
- Leipoldt, J.G., L.D.C. Bok, S.S. Basson, J.S. van Vollenhoven and A.E. Laubscher, 1976, private communication.
- Lind, M.D., B. Lee and J.L. Hoard, 1965, *J. Amer. Chem. Soc.* **87**, 1611-1612.
- Lippard, S.J., 1967, *Progr. Inorg. Chem.* **8**, 109-193.
- Lippard, S.J. and B.J. Russ, 1968, *Inorg. Chem.* **7**, 1686-1688.
- Lobanov, N.I. and V.A. Smirnova, 1963a, *Zh. Neorg. Khim.* **8**, 2206-2207.
- Lobanov, N.I. and V.A. Smirnova, 1963b, *Zh. Neorg. Chem.* **8**, 2208-2209.
- Luk, C.K. and F.S. Richardson, 1974, *Chem. Phys. Lett.* **25**, 215-220.
- Luk, C.K. and F.S. Richardson, 1975, *J. Amer. Chem. Soc.* **97**, 6666-6675.
- Lyle, S.J. and A.D. Witts, 1975, *J. Chem. Soc., Dalton Trans.* 185-188.
- MacDonald, C. and C.J. Willis, 1973, *Can. J. Chem.* **51**, 732-740.
- Mackey, J.L. and N.N. Greenwood, 1972, *J. Inorg. Nucl. Chem.* **34**, 1529-1534.
- Mackey, J.L., J.E. Powell and F.H. Spedding, 1962, *J. Amer. Chem. Soc.* **84**, 2047-2050.
- Mackey, J.L., D.E. Goodney and J.R. Cast, 1971, *J. Inorg. Nucl. Chem.* **33**, 3699-3706.
- Maginn, R.E., S. Manastyrskiy and M. Dubeck, 1963, *J. Amer. Chem. Soc.* **85**, 672-676.
- Malmberg, T. and A. Oskarsson, 1973, *Acta Chem. Scand.* **27**, 2923-2929.
- Manastyrskiy, S., R.E. Maginn and M. Dubeck, 1963, *Inorg. Chem.* **2**, 904-905.
- Mares, F., D. Hodgson and A. Streitwieser, Jr., 1970, *J. Organometal. Chem.* **24**, C68-C70.
- Mares, F., K. Hodgson and A. Streitwieser, Jr., 1971, *J. Organometal. Chem.* **28**, C24-C26.
- Marks, T.J., R. Porter, J.S. Kristoff and D.F. Shriver, 1973, in: R.E. Sievers, ed., *Nuclear Magnetic Resonance Shift Reagents* (Academic Press, New York) pp. 247-264.
- Martin, J.L., L.C. Thompson, L.J. Radinovich and M.D. Glick, 1968, *J. Amer. Chem. Soc.* **90**, 4493-4494.
- Martin, L.L. and R.A. Jacobson, 1972a, *Inorg. Chem.* **11**, 2785-2789.
- Martin, L.L. and R.A. Jacobson, 1972b, *Inorg. Chem.* **11**, 2789-2795.
- Mazhar-UI-Haque, C.N. Coughlin, F.A. Hart and R. van Nice, 1971, *Inorg. Chem.* **10**, 115-122.
- Mehrotra, R.C., M.M. Agarwal and A. Mehrotra, 1973a, *Syn. Inorg. Metal-Org. Chem.* **3**, 181-191.
- Mehrotra, R.C., M.M. Agarwal and A. Mehrotra, 1973b, *Syn. Inorg. Metal-Org. Chem.* **3**, 407-414.
- Mehs, D.M. and S.K. Madan, 1968, *J. Inorg. Nucl. Chem.* **30**, 3017-3021.
- Melby, L.R., N.J. Rose, E. Abramson and J.C. Caris, 1964, *J. Amer. Chem. Soc.* **86**, 5117-5125.
- Melson, G.A., 1975, *Organic Compounds in: C.T. Horovitz, ed., Scandium: Its Occurrence, Chemistry, Physics, Metallurgy, Biology, and Technology*, (Academic Press, London) pp. 111-138 and 323-384.
- Melson, G.A. and R.W. Stoiz, 1971, *Coord. Chem. Rev.* **7**, 133-160.
- Melson, G.A., D.J. Olszanski and E.T. Roach, 1974, *J. Chem. Soc. Chem. Comm.* 229-230.
- Merbach, A. and F. Gnaegi, 1969, *Chimia* **23**, 271-273.
- Merbach, A. and F. Gnaegi, 1971, *Helv. Chim. Acta* **54**, 691-710.
- Miller, W.V. and S.K. Madan, 1968a, *J. Inorg. Nucl. Chem.* **30**, 2785-2793.
- Miller, W.V. and S.K. Madan, 1968b, *J. Inorg. Nucl. Chem.* **30**, 3287-3294.
- Misumi, S., T. Isobe and H. Furuta, 1974, *Bull. Chem. Soc. Jap.* **47**, 421-423.
- Moeller, T., 1953, *Record Chem. Progr.* **14**, 69-81.
- Moeller, T., 1967, *Coordination Chemistry of the Lanthanide Elements - One Hundred Years of Development and Understanding*, in: G. Kauffman, ed., *Werner Centennial* (American Chemical Society, Washington, D.C.) pp. 306-317.
- Moeller, T., 1972, *MTP (Med. Tech. Publ. Co.) Int. Rev. Sci. Inorg. Chem. Ser. One* **7**, pp. 275-298.
- Moeller, T., 1973, *The Lanthanides*, in: J.C. Bailar, Jr., H.J. Emeléus, R. Nyholm and A.F. Trotman-Dickenson, eds., *Comprehensive Inorganic Chemistry*, vol. 4 (Pergamon Press, Oxford) pp. 1-101.

- Moeller, T. and V. Galasyn, 1960, *J. Inorg. Nucl. Chem.* **12**, 259-265.
- Moeller, T. and G. Vicentini, 1965, *J. Inorg. Nucl. Chem.* **27**, 1477-1482.
- Moeller, T., E.R. Birnbaum and J.H. Forsberg, 1968, *Progr. Sci. Tech. Rare Earths* **3**, 61-128.
- Moeller, T., R.L. Dieck and J.E. McDonald, 1973, *Rev. Chim. Miner.* **10**, 177-198.
- Moeller, T., D.R. Martin, L.C. Thompson, R. Ferrús, G.R. Feistel and W.J. Randall, 1965, *Chem. Revs.* **65**, 1-50.
- Moore, J.W., M.D. Glick and W.A. Baker, Jr., 1972, *J. Amer. Chem. Soc.* **94**, 1858-1865.
- Morss, L.R., M. Siegal, L. Stenger and N. Edelstein, 1970, *Inorg. Chem.* **9**, 1771-1775.
- Moseley, P.T., 1975, MTP (Med. Tech. Publ. Co.) *Int. Rev. Sci.: Ser. Two* **7**, 65-110.
- Muettterties, E.L. and C.M. Wright, 1967, *Quart. Rev. (London)* **21**, 109-194.
- Myers, C.E., 1975, *Inorg. Chem.* **14**, 199-201.
- McPhail, A.T. and P.-S.W. Tschang, 1974, *J. Chem. Soc., Dalton Trans.* 1165-1171.
- Nag, K. and M. Chaudhury, 1976, *Inorg. Nucl. Chem. Lett.* **12**, 307-311.
- Nakamura, K. and K. Kawamura, 1971, *Bull. Chem. Soc. Jap.* **44**, 330-334.
- Napier, G.D.R., J.D. Neilson and T.M. Shepherd, 1975, *J. Chem. Soc. Faraday Trans. 2*, **71**, 1487-1496.
- Neilson, J.D. and T.H. Shepherd, 1976, *J. Chem. Soc. Faraday Trans. 2*, **72**, 557-564.
- Newman, D.J., 1971, *Advan. Phys.* **20**, 197-256.
- Nieboer, E., 1975, *Struct. Bonding (Berlin)* **22**, 1-47.
- Nugent, L.J., R.D. Baybarz, J.L. Burnett and J.L. Ryan, 1971, *J. Inorg. Nucl. Chem.* **33**, 2503-2530.
- Nugent, L.J., R.D. Baybarz, J.L. Burnett and J.L. Ryan, 1973, *J. Phys. Chem.* **77**, 1528-1539.
- Ofer, S., J. Nowik and S.G. Cohen, 1968, *The Mössbauer Effect in Rare Earths and Their Compounds*, in: V.I. Goldanskii and R.H. Herber, eds., *Chemical Application of Mössbauer Spectroscopy* (Academic Press, New York) pp. 427-503.
- Ollendorf, F.W. and F. Weigel, 1969, *Inorg. Nucl. Chem. Lett.* **5**, 263-269.
- Oskarsson, A., 1971, *Acta Chem. Scand.* **25**, 1206-1216.
- Oskarsson, A., 1972, *Acta Chem. Scand.* **26**, 2126-2127.
- Ots, H., 1973, *Acta Chem. Scand.* **27**, 2351-2360.
- Papatheodorou, G.N., 1975, *Inorg. Nucl. Chem. Lett.* **11**, 483-490.
- Peacock, R.D., 1975, *Struct. Bonding (Berlin)* **22**, 83-122.
- Pearson, R.G., 1963, *J. Amer. Chem. Soc.* **85**, 3533-3539.
- Penneman, R.A., R.R. Ryan and A. Rosenzweig, 1973, *Struct. Bonding (Berlin)* **13**, 1-52.
- Peppard, D.F., 1961, *Separation of Rare Earths by Liquid-Liquid Extraction*, in: F.H. Spedding and A.H. Daane, eds., *The Rare Earths* (John Wiley and Sons, New York) pp. 38-54.
- Perrier, M. and G. Vicentini, 1973, *J. Inorg. Nucl. Chem.* **35**, 555-559.
- Perrier, M. and G. Vicentini, 1974, *J. Inorg. Nucl. Chem.* **36**, 1187-1190.
- Perrier, M., R. Najjar and G. Vicentini, 1970, *An. Acad. Brasil. Cienc.* **42**, 439-443.
- Pinkerton, A.A., 1974, *Inorg. Nucl. Chem. Lett.* **10**, 495-497.
- Pope, G.W., J.F. Steinbach and W.F. Wagner, 1961, *J. Inorg. Nucl. Chem.* **20**, 304-313.
- Porai-Koshits, M.A. and L.A. Aslanov, 1972, *Zh. Strukt. Khim.* **13**, 266-276; *J. Struct. Chem. (USSR)*, 1972, **13**, 244-253.
- Powell, J.E., 1961, *Separation of Rare Earths by Ion Exchange*, in: F.H. Spedding and A.H. Daane, eds., *The Rare Earths* (John Wiley and Sons, New York) pp. 55-73.
- Prados, R., L.G. Stadtherr, H. Donato, Jr. and R.B. Martin, 1974, *J. Inorg. Nucl. Chem.* **36**, 689-693.
- Przystal, J., W.G. Bos and I.B. Liss, 1971, *J. Inorg. Nucl. Chem.* **33**, 679-689.
- Querishi, N.S. and I.M. Walker, 1974, *Inorg. Chem.* **13**, 2896-2900.
- Radonovich, L.J. and M.D. Glick, 1971, *Inorg. Chem.* **10**, 1463-1468.
- Ramakrishnan, L. and S. Soundararajan, 1975, *Monatsh. Chem.* **106**, 625-632.
- Ramalingam, S.K. and S. Soundararajan, 1967, *J. Inorg. Nucl. Chem.* **29**, 1763-1768.
- Ramalingam, S.K. and S. Soundararajan, 1968, *Bull. Chem. Soc. Jap.* **41**, 106-110.
- Razvina, T.I., V.S. Khomenko, V.V. Kuznetsova and R.A. Puko, 1973, *Zh. Prikl. Spektrosk.* **19**, 866-871; *J. Appl. Spectrosc. (USSR)*, 1973, **19**, 1461-1465.
- Reid, A.F. and P.D. Wailes, 1966, *Inorg. Chem.* **5**, 1213-1216.
- Reidler, J. and H. Silber, 1973, *J. Phys. Chem.* **77**, 1275-1280.
- Reuben, J. and D. Fiat, 1969a, *J. Chem. Phys.* **51**, 4909-4917.
- Reuben, J. and D. Fiat, 1969b, *J. Chem. Phys.* **51**, 4918-4927.
- Rose, N.J. and E. Abramson, 1965, *J. Chem. Phys.* **42**, 1849-1850.
- Ryan, J.L., 1969, *Inorg. Chem.* **8**, 2053-2058.
- Ryan, J.L. and C.K. Jørgensen, 1966, *J. Phys. Chem.* **70**, 2845-2857.
- Ryan, R.R., A.C. Larson and F.H. Kruse, 1969, *Inorg. Chem.* **8**, 33-36.
- Scholer, R.P. and A.E. Merbach, 1975, *Inorg. Chim. Acta* **15**, 15-20.
- Schwartz, R.W., 1975, *Mol. Phys.* **30**, 81-95.
- Schwartz, R.W. and N.J. Hill, 1974, *J. Chem. Soc. Faraday Trans. 2* **70**, 124-131.
- Schwartz, R.W. and P.N. Schatz, 1973, *Phys. Rev.* **B8**, 3229-3236.
- Schwartz, R.W., S.F. Watkins, C.J. O'Connor and R.L. Carlin, 1976, *J. Chem. Soc. Faraday Trans. 2* **72**, 565-570.
- Schwarz, W., 1963, *Z. Anorg. Allg. Chem.* **323**, 44-56.
- Schwarzenbach, G., R. Gut and G. Anderegg, 1954, *Helv. Chim. Acta* **37**, 937-957.

- Selbin, J., N. Ahmad and N. Bhacca, 1971, *Inorg. Chem.* **10**, 1383-1387.
- Seminara, A. and G. Condorelli, 1969, *Ann. Chim. (Rome)* **59**, 990-996.
- Seminara, A., A. Musumeci and G. Condorelli, 1969, *Ann. Chim. (Rome)* **59**, 978-989.
- Sengupta, D. and J.Q. Artman, 1971, *J. Chem. Phys.* **54**, 1010-1014.
- Serpone, N. and R. Ishayek, 1971, *Inorg. Chem.* **10**, 2650-2656.
- Serra, O.A. and L.C. Thompson, 1973, Rare Earth Complexes of Diphenyl Sulfoxide, in: C.J. Kavane and T. Moeller, eds., *Proceedings of the Tenth Rare Earth Research Conference (National Technical Information Service, Washington, D.C.)* pp. 325-333.
- Serra, O.A. and L.C. Thompson, 1976, *Inorg. Chem.* **15**, 504-507.
- Serra, O.A., M.L.R. Gibran and A.M.B. Galindo, 1972, *Inorg. Nucl. Chem. Lett.* **8**, 673-678.
- Serra, O.A., M. Kawashita, E. Giesbrecht and L.C. Thompson, 1971, unpublished results.
- Serra, O.A., M. Perrier, V.K.L. Osorio and Y. Kawano, 1976, *Inorg. Chim. Acta* **17**, 135-138.
- Sheline, R.K. and J.L. Slater, 1975, *Angew. Chem. Int. Ed. Eng.* **14**, 309-313.
- Siddall, III, T.H. and W.E. Stewart, 1970, *J. Inorg. Nucl. Chem.* **32**, 1147-1158.
- Siddigi, I. and R. Hoppe, 1970, *Z. Anorg. Allg. Chem.* **374**, 225-228.
- Sievers, R.E., 1973, *Nuclear Magnetic Shift Reagents* (Academic Press, New York).
- Silber, H.B., 1974, *J. Phys. Chem.* **78**, 1940-1944.
- Sillén, L.G. and A.E. Martell, 1971, *Stability Constants of Metal-Ion Complexes*, Supplement No. 1, Special Publication No. 25 (The Chemical Society, London).
- Sinha, S.P., 1964, *Spectrochim. Acta* **20**, 879-886.
- Sinha, S.P., 1966, *Complexes of the Rare Earths* (Pergamon Press, Ltd., Oxford).
- Smith, G.D., C.N. Caughlin, Mazhar-ul-Haque and F.A. Hart, 1973, *Inorg. Chem.* **12**, 2654-2658.
- Sonesson, A., 1958a, *Acta Chem. Scand.* **12**, 165-181.
- Sonesson, A., 1958b, *Acta Chem. Scand.* **12**, 1937-1954.
- Sonesson, A., 1959, *Acta Chem. Scand.* **13**, 998-1010.
- Springer, Jr., C.S., D.W. Meek and R.E. Sievers, 1967, *Inorg. Chem.* **6**, 1105-1110.
- Stevenson, P.C. and W.E. Nervik, 1961, *The Radiochemistry of the Rare Earths, Scandium, Yttrium, and Actinium* (National Academy of Sciences - National Research Council, Washington, D.C.).
- Streitwieser, Jr., A. and U. Müller-Westerhoff, 1968, *J. Amer. Chem. Soc.* **90**, 7364.
- Sylvanovich, Jr., J.A. and S.K. Madan, 1972, *J. Inorg. Nucl. Chem.* **34**, 1675-1683.
- Taragin, M.F. and J.C. Eisenstein, 1973, *J. Inorg. Nucl. Chem.* **35**, 3815-3819.
- Tazzoli, V., A. Della Giusta, M. Cola, A. Coda and C. Castellani Bisi, 1972, *Acta Crystallogr.* **28A**, S88.
- Templeton, D.H. and C.H. Dauben, 1954, *J. Amer. Chem. Soc.* **76**, 5237-5239.
- Thompson, L.C. and K.D. Mannila, 1968, *J. Inorg. Nucl. Chem.* **30**, 1109-1112.
- Thompson, L.C., B.L. Shafer, J.A. Edgar and K.D. Mannila, 1967, *Advan. Chem. Ser.* **71**, 169-179.
- Titze, H., 1969, *Acta Chem. Scand.* **23**, 399-408.
- Tofield, B.C., 1975, *Struct. Bonding (Berlin)* **21**, 78-82.
- Toogood, G.E. and C. Chieh, 1975, *Can. J. Chem.* **53**, 831-835.
- Tsutsui, M. and N. Ely, 1974, *J. Amer. Chem. Soc.* **96**, 4042-4043.
- Tsutsui, M. and N. Ely, 1975a, *J. Amer. Chem. Soc.* **97**, 1280-1281.
- Tsutsui, M. and N. Ely, 1975b, *J. Amer. Chem. Soc.* **97**, 3551-3553.
- Tsutsui, M. and H.J. Gysling, 1968, *J. Amer. Chem. Soc.* **90**, 6880-6881.
- Tsutsui, M. and H.J. Gysling, 1969, *J. Amer. Chem. Soc.* **91**, 3175-3178.
- Urbain, G., 1896, *Bull. Soc. Chim.* **15**, 347.
- Vanderveer, M.C., 1972, *Master's Thesis*, University of Minnesota.
- Vicentini, G., 1972, *J. Inorg. Nucl. Chem.* **34**, 669-672.
- Vicentini, G. and E. de Carvalho Filho, 1966, *J. Inorg. Nucl. Chem.* **28**, 2987-2992.
- Vicentini, G. and W. de Oliveira, 1975, *J. Inorg. Nucl. Chem.* **37**, 2018-2021.
- Vicentini, G. and R. Isuyama, 1972, *An. Acad. Brasil Cienc.* **44**, 423-425.
- Vicentini, G. and R. Isuyama, 1975, *J. Inorg. Nucl. Chem.* **37**, 1810-1812.
- Vicentini, G. and R. Najjar, 1970, *Inorg. Nucl. Chem. Lett.* **6**, 571-577.
- Vicentini, G. and M. Perrier, 1974, *J. Inorg. Nucl. Chem.* **36**, 77-79.
- Vicentini, G. and A.M.S. Vieira, 1973, *An. Acad. Brasil Cienc.* **45**, 371-376.
- Vicentini, G. and L.B. Zinner, 1975, *J. Inorg. Nucl. Chem.* **37**, 607-609 and references cited therein.
- Vicentini, G., R. Najjar and C. Airoidi, 1969, *An. Acad. Brasil Cienc.* **41**, 375-380.
- Vicentini, G., M. Perrier, L.B. Zinner and M.I. Amin, 1974a, *J. Inorg. Nucl. Chem.* **36**, 771-776.
- Vicentini, G., L.B. Zinner and L. Rothschild, 1974b, *Inorg. Chim. Acta* **9**, 213-216 and references cited therein.
- Vicentini, G., L.B. Zinner and L.R.F. de Carvalho, 1975, *J. Inorg. Nucl. Chem.* **37**, 2021-2023 and references cited therein.
- Vickery, R.C., 1953, *Chemistry of the Lanthanons*, (Butterworths Scientific Publications, London), pp. 1-13.
- Walker, I.M., L. Rosenthal and M.S. Quereshi, 1971, *Inorg. Chem.* **10**, 2463-2471.
- Walker, I.M. and D.H. Weeden, 1973, *Inorg. Chem.* **12**, 772-777.
- Wasson, S.J.S., D.E. Sands and R.F. Wagner, 1973, *Inorg. Chem.* **12**, 187-190.
- Watson, W.H., R.J. Williams and N.R. Stemple, 1972, *J. Inorg. Nucl. Chem.* **34**, 501-508.

- Watson, W.M., R.P. Zerger, J.T. Yardley and G.D. Stucky, 1975, *Inorg. Chem.* **14**, 2675-2680.
- Watt, G.W. and E.W. Gillow, 1969, *J. Amer. Chem. Soc.* **91**, 775-776.
- White, J.G., 1976, *Inorg. Chim. Acta* **16**, 159-162.
- Wing, R.M., J.J. Uebel and K.K. Andersen, 1973, *J. Amer. Chem. Soc.* **95**, 6046-6056.
- Wong, C.-H., T.-Y. Lee and Y.-T. Lee, 1969, *Acta Cryst.* **B25**, 2580-2587.
- Wong, C.-P., R.F. Venteicher and W.DeW., Horrocks, Jr., 1974, *J. Amer. Chem. Soc.* **96**, 7149-7150.
- Wong, C.-P. and W. DeW., Horrocks, Jr., 1975, *Tetrahedron Lett.* **31**, 2637-2640.
- Yamada, S., K. Yamanonchi and H. Kuma, 1971, *Synth. Inorg. Metal-Org. Chem.* **1**, 9-12.
- Zachariasen, W.H., 1954, *Crystal Chemistry of the 5f Elements*, in: G.T. Seaborg and J.J. Katz, eds., *The Actinide Elements*, (McGraw-Hill Book Co., New York) pp. 769-796.
- Zaheer, A.H., I.B. Liss, N.B. Keck, W.G. Bos and P.J. Ouseph, 1974, *J. Inorg. Nucl. Chem.* **36**, 2515-2520.
- Zalkin, A., J.D. Forrester and D.H. Templeton, 1963, *J. Chem. Phys.* **39**, 2881-2891.
- Zalkin, A., D.H. Templeton and D.G. Karraker, 1969, *Inorg. Chem.* **8**, 2680-2684.
- Zinner, L.B. and G. Vicentini, 1975, *Inorg. Chim. Acta* **15**, 235-238 and references therein.

Chapter 26

HYDRIDES

G.G. LIBOWITZ and A.J. MAELAND

Materials Research Center, Allied Chemical Corporation, Morristown,
 New Jersey 07960, USA

Contents			
1. Introduction	299	8. Rare earth alloy hydrides	329
2. Phase relations and crystal structures	301	8.1. Reaction of RM_5 and related compounds with hydrogen	329
2.1. Phase relations	301	8.2. Other rare earth intermetallic hydrides	332
2.2. Crystal structures	303	8.3. Development of new alloy hydrides	332
3. Thermodynamic properties	307	References	333
3.1. Dihydrides	308		
3.2. Trihydrides	312		
3.3. Specific heat data	314		
4. Magnetic properties	315		
5. Electronic properties	319		
5.1. Dihydrides	319		
5.2. Trihydrides	321		
5.3. Electronic structure of cerium hydride	322		
6. Kinetics of hydride formation and hydrogen diffusion	323		
6.1. Reaction mechanisms	323		
6.2. Diffusion of hydrogen in hydrides	324		
7. Other measurements related to bonding and structure	325		
7.1. Inelastic neutron scattering	325		
7.2. Positron annihilation	327		
7.3. Specific heat measurements	327		
7.4. Mössbauer spectroscopy	328		

Symbols

δ, ϵ, x = deviations from stoichiometry
 E_a = activation energy
 ΔG° = standard free energy
 ΔG_f = free energy of formation
 Γ = spectroscopic electronic energy state
 ΔH° = standard enthalpy
 ΔH_f = enthalpy of formation
 \bar{H}_H = partial molal enthalpy
 H/M = hydrogen-to-metal atom ratio
 K = equilibrium constant
 μ = Bohr magneton
 P_{H_2} = hydrogen pressure
 ΔS° = standard entropy
 \bar{S}_H = partial molal entropy

1. Introduction

All of the rare earth metals react directly with hydrogen to form dihydrides according to the following reaction



In addition, most of the rare earths will also form trihydrides. Both the dihydrides and trihydrides are normally nonstoichiometric, usually exhibiting very wide existence ranges. The rate at which reaction (26.1) proceeds depends upon temperature, hydrogen pressure, and the condition of the metal surface. In some cases, the reaction will occur at room temperature and low pressures (<1 torr) if the surface is clean (Beavis et al., 1974; Curzon and Singh, 1975). In all cases, however, the reaction will proceed readily at moderate temperatures (100–500°C) and pressures (≤ 1 atm of H_2). A more detailed discussion of the reaction mechanisms is given in section 6.

Libowitz (1972a) has classified the rare earth hydrides into three groups on the basis of their crystal structures. The first group contains the hydrides of the rare earths, La, Ce, Pr, Nd, which have a cubic (fluorite-type) dihydride structure. They form continuous solid solutions with the trihydrides. (Sc may also be included in the first group, although it does not form a trihydride.) Members of the second group also have a fluorite-type dihydride structure, but their trihydrides are hexagonal. This group includes Y, Sm, Gd, Tb, Dy, Ho, Er, Tm, and Lu. The third group consists of only europium and ytterbium dihydrides, which have an orthorhombic structure and resemble the alkaline earth hydrides. The structures and phase relations of the rare earth hydrides are discussed in detail in section 2.

The nature of the chemical bonding in the transition metal hydrides, in general, has been the subject of a great deal of controversy in the past (Libowitz, 1965). Hydrogen may be considered a metal, in which case, it would form an alloy with the transition metal with electrons from the hydrogen atoms occupying the d-band of the transition metal. Therefore, the hydrogen would exist as screened protons in the metal sublattice of the hydride. Conversely, hydrogen may be viewed as the first member of the halogen series needing one electron to complete its outer shell. In this case, the hydride would be predominantly ionic, consisting of hydrogen anions and metal cations. There are experimental data supporting each concept, although in the case of the rare earth hydrides most of the evidence appears to favor the anionic hydrogen model (Libowitz, 1972b). The disparity between the two models has been resolved in band energy calculations of metal hydrides by Switendick (1971, 1974). The behavior of metal hydrides may be correlated with the position of the hydrogen energy levels with respect to the Fermi level of the metal. For the case of the rare earth hydrides, the hydrogen energy levels always fall below the Fermi energy and, therefore, the electrons from the hydrogen atoms will occupy such energy levels in preference to existing unfilled metallic energy states. Consequently, the rare earth hydrides behave like ionic compounds. In this chapter (particularly section 5) it is more convenient to discuss the properties of the rare earth hydrides in terms of ionic bonding rather than band structure. It should be mentioned that the bonding in Eu and Yb hydrides is decidedly more ionic; they resemble the alkaline earth hydrides in most of their properties. This is attributed to the stability of the underlying 4f states, since they are fully

occupied in the case of Yb and exactly one half occupied (one electron in each orbital according to Hund's rule) in the case of Eu.

The properties and characteristics of the rare earth hydrides have been extensively reviewed in the past by Bos and Gayer (1966) and Mueller (1968), and the information updated by Libowitz (1972b). Consequently, emphasis will be placed on work published subsequent to those dates.

2. Phase relations and crystal structures

2.1. Phase relations

The reaction between hydrogen and the rare earth metals is most conveniently illustrated by pressure-composition isotherms such as those shown in fig. 26.1. The first ascending branch, AB, of an isotherm in fig. 26.1 (a and b) reflects the pressure dependence of the solubility of hydrogen in the metal (α -phase). The constant-pressure plateau region, BC corresponds to a two-phase system consisting of a saturated solution of hydrogen in the metal and a nonstoichiometric dihydride phase, $MH_{2-\delta}$. The overall composition in the plateau region is determined by the relative amounts of the two phases present, but the pressure is invariant. When the hydrogen saturated α -phase has been completely converted to the dihydride, point C, members of the first group, except scandium, continue to absorb hydrogen with increasing pressure until a composition

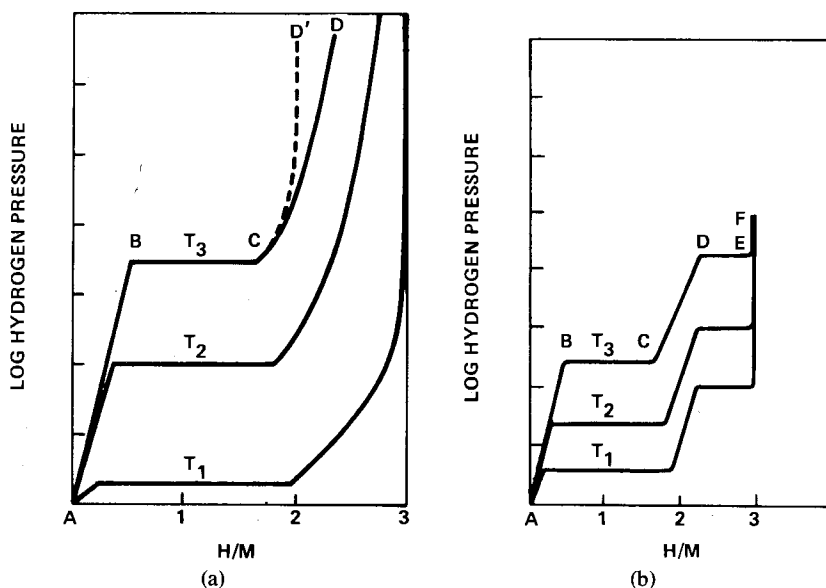


Fig. 26.1. Pressure-composition isotherms for metal-hydrogen systems.

near MH_3 is reached. This continuous solid solution behavior is indicated by the second ascending branch, CD, in fig. 26.1a. The behavior of scandium and europium, which do not form trihydrides, is illustrated by the very rapidly rising portion of the isotherm in fig. 26.1a, CD', which indicates a limiting composition of ScH_2 and EuH_2 . The second group of rare earth hydrides displays a much narrower range of solid solutions as shown by the ascending portion, CD, in fig. 26.1b; the solid solution region is followed by a second plateau region, DE, where the nonstoichiometric di- and tri-hydrides coexist. The final ascending part of the isotherm in fig. 26.1b, EF, shows the dependence of hydrogen pressure on composition of the nonstoichiometric trihydride. The regions of rapidly rising pressures in the middle and right-hand side of fig. 26.1 represent single-phase hydride regions.

A schematic generalized phase diagram for rare earth-hydrogen systems is shown in fig. 26.2. The two-phase cubic + hexagonal region does not occur in systems where the rare earth dihydrides form continuous solid solutions with their trihydrides; in those cases the cubic hydride phase field extends to $H/M = 3$. The actual positions of the phase boundaries depend on the particular metal-hydrogen system involved, as well as the temperature. Room temperature existence ranges of the rare earth hydrides are summarized in table 26.1.

The rare earth metals undergo phase changes at elevated temperatures and the simple phase diagram of fig. 26.2 consequently becomes much more complex at higher temperatures. The complexity is illustrated in figs. 26.3, 26.4 and 26.5. In the lanthanum-hydrogen system, the face centered cubic to body centered cubic transition in the metal at $860^\circ C$ leads to an additional two-phase region as shown in fig. 26.3. (Peterson and Straatmann, 1966). In the neodymium-hydrogen system,

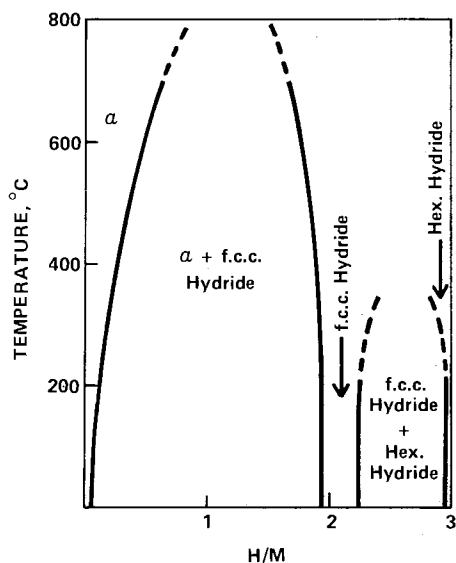


Fig. 26.2. Generalized phase diagram for rare earth-hydrogen systems.

the phase transition in the metal at 862°C is from hexagonal to body centered cubic, which again results in an additional two-phase region as seen in fig. 26.4 (Peterson et al., 1971). The metal-rich intermediate phase, γ , observed between 680–880°C could not be positively identified by X-ray diffraction, but appears to be well established by other measurements. The cerium–hydrogen phase diagram, fig. 26.5 (Libowitz and Pack, 1967), shows a peritectic point at about 1010°C resulting from the fact that cerium melts at 795°C.

Recently, Mintz et al. (1974) reported that neodymium trihydride, $\text{NdH}_{3-\delta}$, samples prepared at or below 350°C have a hexagonal structure ($a_0 = 3.84 \text{ \AA}$, $c_0 = 6.80 \text{ \AA}$) similar to the hexagonal trihydrides of the heavier rare earths. If this phase is heated above $\sim 300^\circ\text{C}$ it transforms to the f.c.c. neodymium hydride, and it retains the cubic structure when cooled down again.

2.2. Crystal structures

The fluorite type structure, common to the first and second group of rare earth hydrides, consists of a face-centered cubic metal sub-lattice with hydrogen atoms situated in the tetrahedral sites. Thus the ideal structure corresponds to MH_2 , but due to hydrogen vacancies (on tetrahedral sites) or interstitial hydrogen atoms in octahedral sites both negative and positive deviations from stoichiometry are observed, i.e. $\text{MH}_{2\pm\delta}$. An early neutron diffraction study by Holley et al. (1955) on CeH_2 and $\text{CeD}_{2.48}$ established that in CeH_2 the hydrogen atoms were in tetrahedral sites, and in $\text{CeD}_{2.48}$, the deuterium atoms in excess of those required to fill the tetrahedral sites were statistically distributed in the octahedral sites of the fluorite structure. The fluorite structure was also confirmed for TbD_2 and HoD_2 by neutron diffraction measurements by Cox et al.

TABLE 26.1
Estimated existence ranges of rare earth hydrides

Group I	Group II		Group III
	Fluorite	Hexagonal	
$\text{LaH}_{1.95-3}^a$	$\text{YH}_{1.90-2.23}^{b*}$	$\text{YH}_{2.77-3}^{b*}$	$\text{EuH}_{1.86-2}^c$
$\text{CeH}_{1.8-3}^d$	$\text{SmH}_{1.92-2.55}^b$	$\text{SmH}_{2.59-3}^b$	$\text{YbH}_{1.80-2}^c$
$\text{PrH}_{1.9-3}^b$	$\text{GdH}_{1.8-2.3}^f$	$\text{GdH}_{2.85-3}^f$	
$\text{NdH}_{1.9-3}^b$	$\text{TbH}_{1.90-2.15}^b$	$\text{TbH}_{2.81-3}^b$	
	$\text{DyH}_{1.95-2.08}^b$	$\text{DyH}_{2.86-3}^b$	
	$\text{HoH}_{1.95-2.24}^b$	$\text{HoH}_{2.95-3}^g$	
	$\text{ErH}_{1.86-2.13}^b$	$\text{ErH}_{2.97-3}^i$	
	$\text{TmH}_{1.99-2.41}^b$	$\text{TmH}_{2.76-3}^b$	
	$\text{LuH}_{1.85-2.23}^b$	$\text{LuH}_{2.78-3}^b$	

*X-ray studies by Lundin and Blackledge (1962) indicate somewhat narrower existence range. ^aMulford and Holley (1955); ^bPebler and Wallace (1962); ^cZanowick and Wallace (1962); ^dStreck and Dialer (1960); ^eMesser et al. (1967); ^fSturdy and Mulford (1956); ^gPerkins and Lundin (1968); ^hSingh et al. (1976); ⁱLundin (1968a).

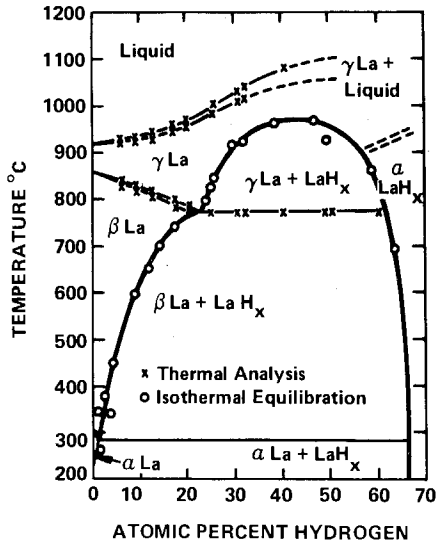


Fig. 26.3. The lanthanum-hydrogen system (Peterson and Straatmann, 1966).

(1963). Karimov et al. (1967) in a neutron diffraction study of CeD_3 reported that the deuterium atoms were located in the tetrahedral and octahedral sites of the face centered cubic metal lattice. All available sites are filled at this composition.

More recent neutron diffraction work by Cheetham and Fender (1972) on $CeD_{2.0}$, $CeD_{2.15}$ and $CeD_{2.75}$ and by Titcomb et al. (1974) on $CeD_{2.29}$, $CeD_{2.51}$, $LaD_{2.30}$, and $PrD_{2.37}$ have revealed some additional structural features. For $CeD_{2.0}$

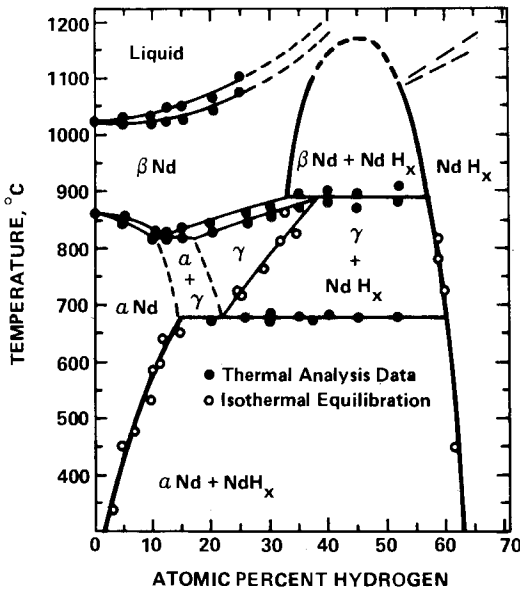


Fig. 26.4. The neodymium-hydrogen system (Peterson et al., 1971).

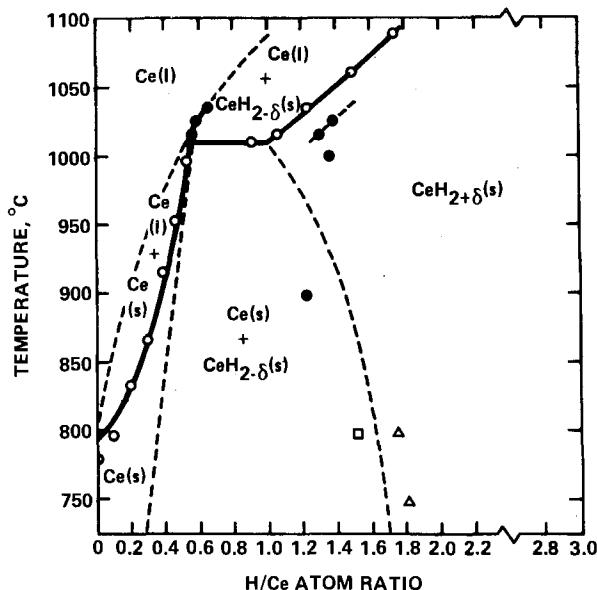


Fig. 26.5. The cerium-hydrogen system (Libowitz and Pack, 1967).

the data indicated no significant deviations from the perfect fluorite structure as had been suggested from NMR measurements by Schreiber and Cotts (1963) on $\text{LaH}_{2.00}$. In $\text{LaH}_{2.00}$, Schreiber and Cotts found that $2\frac{1}{2}\%$ of the tetrahedral sites are vacant and that those hydrogen atoms are to be found in the octahedral positions. Cheetham and Fender (1972) suggested that there might be a real difference between these two hydride systems or that small levels of oxygen impurities were present in the $\text{LaH}_{2.00}$ sample causing blocking of a relatively large number of hydrogen sites (Kofstad et al., 1959). However, it would be thermodynamically impossible for $\text{CeD}_{2.0}$ to have a perfect fluorite structure; at any temperature above absolute zero, there must be a finite concentration of lattice defects (in this case, predominantly hydrogen vacancies and interstitials). Libowitz and Lightstone (1967) calculated intrinsic defect concentrations in some rare earth dihydrides from thermodynamic data. For cerium dihydride, they found about 2 to 5% defects in the temperature range 300–800°C. Extrapolation to room temperature yields an intrinsic defect concentration of about 0.2%, which is far too low to be detected in any neutron diffraction experiment. Oxygen and other impurities certainly could enhance the apparent defect concentration as suggested by Kofstad et al. (1959). Additional evidence that octahedral sites are being occupied by hydrogen atoms before all the tetrahedral sites are filled, is the sharp increase in entropy from $\text{CeH}_{1.9}$ to $\text{CeH}_{2.0}$ (section 3.2), the rapid rise in resistivity in the same composition range (section 5.1), and peaks observed in inelastic neutron scattering (section 7.1) which are due to hydrogen vibrations in octahedral sites.

In $\text{CeD}_{2.29}$, $\text{LaD}_{2.30}$ and $\text{PrD}_{2.37}$, Titcomb et al. (1974) found evidence for small displacements of deuterium atoms from both the tetrahedral and octahedral

positions and an increase in the number of octahedral interstitial deuterium atoms formed at the expense of vacant tetrahedral sites. The tetrahedral occupancy number varies between 1.96 and 1.87 leading to an intrinsic disorder; in a perfect fluorite structure the occupancy number would, of course, be 2.00. The rare earth atoms are displaced very slightly from those of the fluorite structure, but the displacement is not large enough to produce observable superlattice reflections in X-ray patterns. It is interesting to note, however, that Libowitz et al. (1972) observed a tetragonal distortion in $\text{CeD}_{2.75}$ by X-ray measurements below ~ 252 K (section 5.3). Titcomb et al. (1974) proposed a partially ordered tetragonal superstructure for $\text{CeD}_{2.29}$. Because of the higher degree of intrinsic disorder at increasing hydrogen contents, the octahedral hydrogen atoms became completely disordered at $\text{CeD}_{2.5}$, in agreement with the work of Holley et al. (1955). The data of Titcomb et al. (1974) suggested that intrinsic disorder was greatest in $\text{LaD}_{2+\delta}$ and least in $\text{PrD}_{2+\delta}$.

Somenkov et al. (1975) have used neutron diffraction methods to study another kind of ordering in cerium trihydride, i.e., the distribution of hydrogen isotopes in octahedral and tetrahedral positions in CeD_2H in the temperature range 4.2–300 K. It was shown that atoms of the light isotope occupy octahedral sites in the face centered cubic lattice with a higher probability than that predicted by random distribution, and that the probability increased with decreasing temperature. This kind of ordering is due to a decrease in local vibrational energy as the light atom jumps into an octahedral site.

The structure of the hexagonal trihydride phase has been determined in a neutron diffraction study of HoD_3 by Mansmann and Wallace (1964). Earlier X-ray diffraction studies by Pebler and Wallace (1962) had been indexed on the basis of a simple hexagonal close-packed metal lattice. In the actual structure the a_0 parameter is 3 times that of the hexagonal close-packed cell as determined by X-rays. The deuterium atoms are situated in tetrahedral and octahedral sites, but slightly displaced from the ideal positions in order to provide the required space. The other hexagonal rare earth trihydrides are presumably isostructural with HoH_3 although small deviations of atomic parameters are possible (Mansmann and Wallace, 1964).

X-ray studies (Korst and Warf, 1956) of europium and ytterbium dihydrides have shown that these hydrides have an orthorhombic structure similar to that found in the alkaline earth dihydrides. Recent values of the lattice parameters are listed in table 26.2. There have been no neutron studies of europium or ytterbium dihydrides, but the hydrogen positions may be deduced from orthorhombic calcium deuteride, which presumably is isostructural with these hydrides and has recently been studied by neutron diffraction (Andresen et al., 1977). Ytterbium under high hydrogen pressure also forms a face centered cubic hydride of limiting composition $\text{YbH}_{2.55}$ with $a_0 = 5.192$ Å (Warf and Hardcastle, 1966). A second "metastable" face centered cubic phase with $a_0 = 5.253$ Å was observed when $\text{YbH}_{2.55}$ was partially decomposed followed by rapid quenching. Messer and Gianoukas (1968) reported formation of both of these cubic phases on heating the orthorhombic dihydride above 125°C ; all three phases were found

TABLE 26.2
Lattice parameters of rare earth hydrides.

Hydride	Structure	Parameters (Å)	Ref.	Hydride	Structure	Parameters (Å)	Ref.
ScH ₂	f.c.c.	$a = 4.783$	^a				
LaH ₂	f.c.c.	$a = 5.663$	^b	LaH ₃	f.c.c.	$a = 5.604$	^b
CeH ₂	f.c.c.	$a = 5.580$	^c	CeH ₃	f.c.c.	$a = 5.539$	^a
PrH ₂	f.c.c.	$a = 5.515$	^c	PrH ₃	f.c.c.	$a = 5.486^1$	^c
NdH ₂	f.c.c.	$a = 5.469$	^c	NdH ₃	f.c.c.	$a = 5.42^1$	^c
YH ₂	f.c.c.	$a = 5.205$	^d	YH ₃	hex	$a = 3.672^2$	^d
						$c = 6.659$	
SmH ₂	f.c.c.	$a = 5.363$	^e	SmH ₃	hex	$a = 3.782^2$	^d
						$c = 6.779$	
GdH ₂	f.c.c.	$a = 5.303$	^f	GdH ₃	hex	$a = 3.73$	^f
						$c = 6.71$	
TbH ₂	f.c.c.	$a = 5.246$	^d	TbH ₃	hex	$a = 3.700^2$	^d
						$c = 6.658$	
DyH ₂	f.c.c.	$a = 5.201$	^d	DyH ₃	hex	$a = 3.671^2$	^d
						$c = 6.615$	
HoH ₂	f.c.c.	$a = 5.165$	^d	HoH ₃	hex	$a = 3.642$	^d
						$c = 6.560$	
ErH ₂	f.c.c.	$a = 5.123$	^d	ErH ₃	hex	$a = 3.621$	^d
						$c = 6.526$	
TmH ₂	f.c.c.	$a = 5.090$	^d	TmH ₃	hex	$a = 3.599^2$	^d
						$c = 6.489$	
LuH ₂	f.c.c.	$a = 5.033$	^d	LuH ₃	hex	$a = 3.558^2$	^d
						$c = 6.443$	
EuH ₂	ortho.	$a = 6.254$ $b = 3.806$ $c = 7.212$	^e				
YbH ₂	ortho.	$a = 5.904$ $b = 3.580$ $c = 6.794$	^g	YbH _{2.55}	f.c.c.	$a = 5.192$	^g

¹The lattice parameter is a linear function of H/M. Values listed are extrapolated to H/M = 3. ²H/M > 2.90. ^aHardcastle and Warf (1966); ^bGoon (1959); ^cKorst and Warf (1966); ^dPebler and Wallace (1962); ^eHaschke and Clark (1975); ^fSturdy and Mulford (1956); ^gWarf and Hardcastle (1966).

in the range 250°C to 600°C. A corresponding higher hydride of europium could not be prepared when europium was exposed to 33–61 atm of hydrogen and temperatures ranging from 300–500°C (Hardcastle and Warf, 1966).

Lattice parameters for all the rare earth di- and trihydrides are presented in table 26.2. Lattice parameters of the corresponding deuterides are usually a few tenths of a percent smaller.

3. Thermodynamic properties

Thermodynamic properties of the rare earth hydrides are usually obtained from measurements of hydrogen pressures in equilibrium with hydrides of

varying composition as a function of temperature (p - c - T measurements). The relationship between standard free energy, ΔG° , and equilibrium constant, K , for a chemical reaction may be written

$$\Delta G^\circ = \Delta H^\circ - T\Delta S^\circ = -RT \ln K. \quad (26.2)$$

For reaction (26.1), $K = 1/P_{\text{H}_2}$, and eq. (26.2) becomes

$$\Delta G_f = \Delta H_f - T\Delta S_f = RT \ln P_{\text{H}_2} \quad (26.3)$$

where P_{H_2} is the hydrogen pressure in equilibrium with the hydride phase and ΔG_f , ΔH_f , and ΔS_f are the free energy, enthalpy, and entropy of formation of the dihydride. Since the rare earth hydrides are normally nonstoichiometric, it is more convenient to define these thermodynamic quantities per mole of hydrogen, rather than per mole of hydride. Equation (26.3) may be re-written:

$$\ln P_{\text{H}_2} = (\Delta H_f/RT) - (\Delta S_f/R). \quad (26.4)$$

If $\ln P_{\text{H}_2}$ is plotted against reciprocal temperature for pressures in the first plateau regions of fig. 26.1, a straight line is obtained whose slope will yield the enthalpy of formation, ΔH_f , of the nonstoichiometric (hydrogen-deficient) dihydride from hydrogen saturated rare earth metal. The corresponding entropy of formation, ΔS_f , is obtained from the intercept. These plateau pressures are referred to as the dissociation pressures of the dihydrides at each temperature. Similar plots at any given composition in the solid solution regions to the left and right of the pressure plateaus of fig. 26.1a yield values for the partial molal enthalpies and entropies of hydrogen in the metal phase and in the hydride phase, respectively. For the case of the hydrides which form a hexagonal trihydride phase, the use of eq. (26.4) in the second plateau region yields enthalpies and entropies of formation of the hydrogen-deficient trihydride from the non-stoichiometric (hydrogen excess) dihydride.

3.1. Dihydrides

The enthalpies and entropies of formation of the (hydrogen-deficient) dihydrides as obtained from the application of eq. (26.4) to the experimental data are tabulated in table 26.3. The values shown are in many cases averages of two or more investigations. In some cases, previously cited values (Mueller, 1968) were rejected because they were out of line with two or more subsequent studies, or because the authors felt that some recent investigations were more reliable. For almost all metal hydrides, eq. (26.4) yields a straight line over wide temperature ranges (Libowitz, 1965). A typical $\log P_{\text{H}_2}$ vs $1/T$ curve is illustrated for the case of lutetium dihydride in fig. 26.6 where it can be seen that a straight line is obtained over a 400° temperature range. The lower-limit composition of the dihydride phase also changes with temperature in all these hydride systems as illustrated in fig. 26.1a. Therefore, ΔH_f and ΔS_f are generally independent of temperature and composition over the ranges studied. In the case of yttrium dihydride, the large differences in the values of ΔH_f and ΔS_f between the two

TABLE 26.3
Thermodynamic properties of rare earth dihydrides as calculated from dissociation pressure data.

Dihydride	$-\Delta H_f$ (kcal/mole H ₂)	$-\Delta S_f$ (cal/mole H ₂ /deg)	$-\Delta G_f(298\text{ K})$ (kcal/mole H ₂)	Ref.
Sc	48.0	34.8	37.6	a
Y(<900°C)	54.3	34.9	43.9	b
Y(>900°C)	44.4	27.1	—	c
La	49.6	35.7	39.0	d,e
Ce	49.3	35.6	38.7	e,f,g
Pr	49.8	35.0	39.4	e,h
Nd	50.5	34.8	40.1	e
Sm	48.2	32.6	38.5	i,j
Gd	46.9	31.7	37.5	j,k,l,m
Tb	50.9	33.8	40.8	h,m
Dy	52.7	35.8	42.0	h,m
Ho	54.0	36.7	43.0	h,n
Er	53.5	36.3	42.7	h,i,o,p
Tm	53.8	36.3	43.0	h
Yb	43.3	33.4	33.3	q
Lu	49.5	36.3	38.7	h,m

^aLiebermann and Wahlbeck (1965); ^bYannopoulos et al. (1965); ^cLundin and Blackledge (1962); ^dMulford and Holley (1955); ^eKorst and Warf (1966); ^fFadayeve and Izhvanov (1973); ^gLundin (1966); ^hJones et al. (1964); ⁱMulford (1958); ^jJones et al. (1966); ^kSturdy and Mulford (1956); ^lLibowitz and Pack (1969a); ^mMcQuillan (1976); ⁿPerkins and Lundin (1968); ^oLundin (1968a); ^pMaurin (1965); ^qMesser et al. (1967).

different investigations as shown in table 26.3, have been attributed (Blackledge, 1968) to experimental error rather than to the different temperature ranges over which the studies were performed. However, Fadayeve (1972) has shown that there were indeed inflections in the $\log P_{\text{H}_2}$ vs $1/T$ lines in the range 770–920°C. Further, his data agreed with those of Yannopoulos et al. (1965) below 900°C and with those of Lundin and Blackledge (1962) above 900°C.

The free energy of formation, ΔG_f (298 K), is an indication of the stability of a hydride. The rare earth hydrides are among the most stable of the transition metal hydrides (Libowitz, 1972b). From the data shown in table 26.3, there does not appear to be any pronounced trend in hydride stability within the lanthanide series, although the hydrides of the metals in the range Dy through Tm appear more stable than the other lanthanide hydrides. YbH₂ has a considerably lower (absolute) free energy of formation because its bonding (ionic) is basically different from the other rare earth dihydrides. There is no thermodynamic data available for EuH₂, but for the same reason it should have a lower (absolute) value of ΔG_f .

The stabilities of hydrides are usually greater than the corresponding deuterides or tritides. This is illustrated by the more negative values of the free

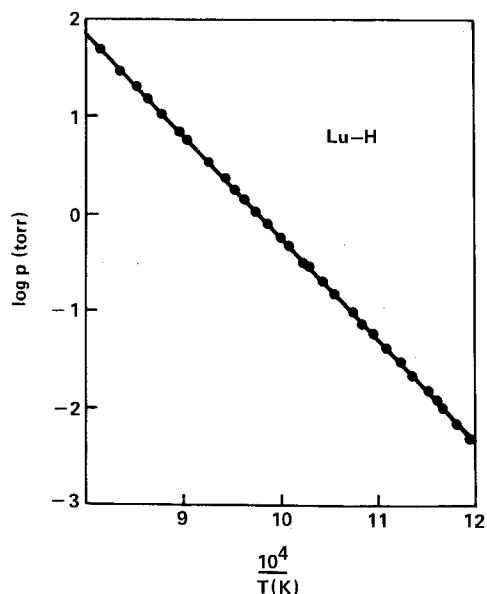


Fig. 26.6. Logarithm of dissociation pressure vs reciprocal temperature for lutetium dihydride (taken from McQuillan, 1976).

energies of formation of the hydrides (table 26.3) as compared with those of the deuterides given in table 26.4. The greater stability of the hydride (more negative value for ΔG_f) is usually attributed to two factors (Libowitz, 1965). The greater strength of the hydrogen-metal bond (as compared to the deuterium-metal bond) leads to a more negative value for ΔH_f . Also, the higher absolute entropy of deuterium over hydrogen gas will yield a more negative value for ΔS_f of the deuteride. However, for the rare earth hydrides, ΔS_f (hydride) is more negative than ΔS_f (deuteride) as seen by comparison of tables 26.3 and 26.4. This may be explained by the higher vibrational frequency of hydrogen in the hydride (as

TABLE 26.4
Thermodynamic properties of rare earth deuterides.

Dihydride	$-\Delta H_f$ (kcal/mole H ₂)	$-\Delta S_f$ (cal/mole H ₂ /deg)	$-\Delta G_f(298\text{ K})$ (kcal/mole H ₂)	Ref. (see table 26.3)
YD ₂ (<900°C)	51.7	33.2	41.8	h
LaD ₂	46.5	33.1	36.6	e
CeD ₂	46.3	33.5	36.3	e
PrD ₂	48.0	33.7	38.0	h
TbD ₂	49.6	33.6	39.6	h
DyD ₂	52.2	35.0	41.8	h
HoD ₂	52.8	36.3	42.0	h,n
ErD ₂	52.6	35.9	41.9	h, Lundin (1968b)
TmD ₂	51.5	36.2	40.7	h
LuD ₂	47.3	31.5	37.9	h

compared to deuterium in the deuteride), and hence a lower value of the absolute entropy of the hydride (see Libowitz, 1965, p. 58). Consequently, the greater stabilities of the rare earth hydrides are mainly due to the larger negative values of ΔH_f (hydride).

In order to obtain thermodynamic properties of hydride compositions other than the hydrogen-deficient dihydride phase (which is normally in equilibrium with the metal phase), it is necessary to use partial molal quantities of hydrogen in the hydride, as illustrated for the calculation of enthalpy in the following expression:

$$\Delta H_f(\text{MH}_{2+x}) = \frac{1}{2}(2 - \delta)\Delta H_f(\text{MH}_{2-\delta}) + \frac{1}{2} \int_{2-\delta}^{2+x} \bar{H}_H dr, \quad (26.5)$$

where $\Delta H_f(\text{MH}_{2+x})$ is the enthalpy of formation of the hydride (per mole of hydride) at any hydrogen to metal ratio, $2 + x$, $\Delta H_f(\text{MH}_{2-\delta})$ is the enthalpy of formation of the hydrogen-deficient dihydride (the values shown in table 26.3), \bar{H}_H is the partial molal enthalpy of solution per mole of H_2 , and dr is the change in hydrogen-to-metal ratio.

The use of eq. (26.5) may be illustrated for the case of cerium hydride. From calorimetric measurements, Sieverts and Gotta (1928) obtained a value of -56.8 kcal/mole hydride for the enthalpy of formation $\text{CeH}_{2.69}$. To calculate a value from dissociation pressure measurements, the partial molal enthalpies of hydrogen in cerium hydride as a function of the H/Ce ratio shown in fig. 26.7 can be used in eq. (26.5). The area under the curve from H/Ce = 1.89 to H/Ce = 2.69 represents the term under the integral sign. One half this value (-8.4 kcal/mole H_2) is added to $(1.89/2)\Delta H_f(\text{CeH}_{1.89}) [= (1.89/2)(-49.3)]$, and a

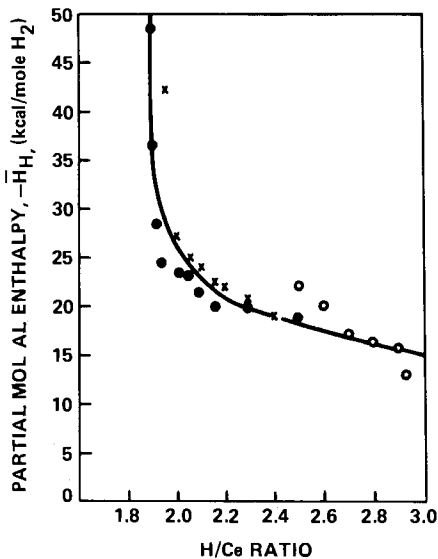


Fig. 26.7. Partial molal enthalpies of hydrogen in cerium dehydride. ●, Streck and Dialer (1960); ○, Hardcastle and Warf (1966); ×, Lundin (1966).

value of -55.0 kcal/mole hydride is obtained for $\Delta H_f(\text{CeH}_{2.69})$, which is in fairly good agreement with the calorimetric value.

Sieverts and Gotta (1928) also obtained a calorimetric value of -56.1 kcal/mole for the enthalpy of formation of $\text{PrH}_{2.84}$. Using the partial molal enthalpies determined by Messer and Park (1972) in eq. (26.5), a value of -57.2 kcal/mole is calculated from dissociation pressure data, which is in very good agreement with the calorimetric value. (The values for partial molal quantities given by Messer and Park are actually per gram-atom of hydrogen although they are labeled per mole.)

3.2. Trihydrides

The enthalpies of formation of the stoichiometric trihydrides of the first group of rare earths (La through Nd) also may be calculated from eq. (26.5) by integrating the last term up to $H/M = 3$. Using fig. 26.7 for cerium hydride, the partial molal quantity data of Hardcastle and Warf (1966) and Messer and Hung (1968) for lanthanum hydride, and Messer and Park (1972) for praseodymium and neodymium hydrides along with the data in table 26.3, the values for ΔH_f shown in table 26.5 were calculated. Within the uncertainty of the data and the calculations therefrom, the value for ΔH_f is approximately the same, -58 kcal/mole, for all four trihydrides.

Partial molal entropies of cerium hydride as a function of r as calculated from the data of Lundin (1966), Streck and Dialer (1960), and Hardcastle and Warf (1966) are shown in fig. 26.8. The minimum in the curve at about $H/\text{Ce} = 2$ is probably due to a maximum in the configurational entropy at this composition since hydrogen atoms enter the octahedral interstices in the rare earth dihydrides before all the tetrahedral sites are occupied (see section 2.2). Therefore, there is disorder in both the tetrahedral and octahedral sublattices near the stoichiometric dihydride composition.

An equation equivalent to eq. (26.5) can be written for the entropy of a cubic trihydride

$$\Delta S_f(\text{MH}_3) = \frac{1}{2}(2 - \delta)\Delta S_f(\text{MH}_{2-\delta}) + \frac{1}{2} \int_{2-\delta}^3 \bar{S}_H dr. \quad (26.6)$$

For cerium hydride, the last term in eq. (26.6) is obtained from the area under

TABLE 26.5
Thermodynamic properties of cubic rare earth trihydrides.

	$\Delta H_f(\text{kcal/mole})$	$\Delta S_f(\text{cal/deg}\cdot\text{mole})$
LaH ₃	-58.9	-49.1
CeH ₃	-57.5	-48.5
PrH ₃	-58.3	-48.1
NdH ₃	-58.3	-46.5

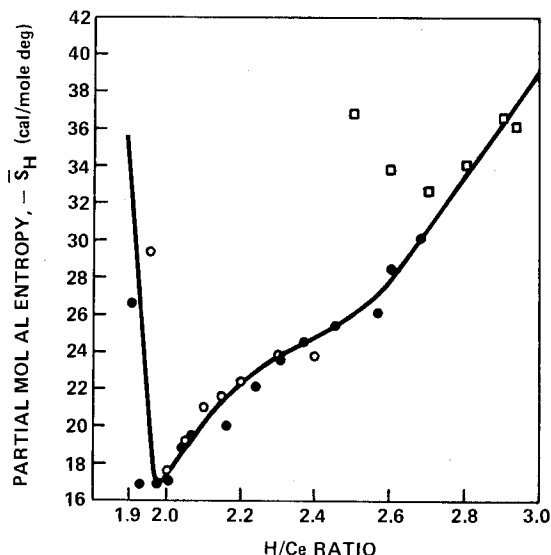


Fig. 26.8. Partial molal entropies of hydrogen in cerium dihydride. ●, Streck and Dialer (1960); ○, Lundin (1966); □, Hardcastle and Warf (1966).

the curve in fig. 26.8. The resulting value for the entropy of formation of CeH_3 is -48.5 cal/deg mole. In a similar manner, the entropies of formation of LaH_3 , PrH_3 , and NdH_3 can be calculated from the partial molal entropy data of Hardcastle and Warf (1966), Messer and Hung (1968), and Messer and Park (1972) and the values of $\Delta S_f(\text{MH}_{2-\delta})$ listed in table 26.3. Although the data for the other three hydrides are not as extensive as for cerium hydride, the values of ΔS_f for the trihydrides calculated from estimated values of \bar{S}_H are shown in table 26.5.

It should be mentioned that since the hydrogen solubility of hydrogen in the metal phase is relatively low, the contribution from the enthalpies (and entropies) of solution of hydrogen in the metal phase is neglected. For completeness, however, eqs. (26.5) and (26.6) should include a term containing the partial molal enthalpy (and entropy) of hydrogen in the metal phase.

The thermodynamic properties of the hexagonal trihydrides (Sm, Gd, Tb, Dy, Ho, Er, Tm, Lu) could be calculated from a modification of eqs. (26.5) and (26.6) as follows:

$$\Delta H_f(\text{MH}_3) = \frac{1}{2}(2 - \delta)\Delta H_f(\text{MH}_{2-\delta}) + \frac{1}{2} \int_{2-\delta}^{2+x} \bar{H}_1 dr + \frac{1}{2}(1 - x - \epsilon)\Delta H_f(\text{MH}_{3-\epsilon}) + \frac{1}{2} \int_{3-\epsilon}^3 \bar{H}_2 dr, \quad (26.7)$$

where \bar{H}_1 is the partial molal enthalpy in the composition region ranging from the hydrogen-rich side of the first plateau ($2 - \delta$) to the hydrogen-poor side of the second plateau ($2 + x$) in fig. 26.1b. \bar{H}_2 is the partial molal enthalpy in the region from the hydrogen-rich side of the second plateau (i.e. the hydrogen-deficient trihydride) to $\text{H/M} = 3$. $\Delta H_f(\text{MH}_{3-\epsilon})$ is the enthalpy of formation of the

hydrogen-deficient trihydride from the hydrogen-rich dihydride (MH_{2+x}). An equation similar to eq. (26.7) can be written for the entropy of formation of the trihydride. The values of $\Delta H_f(\text{MH}_{3-\epsilon})$ and $\Delta S_f(\text{MH}_{3-\epsilon})$ as determined by van't Hoff plots of the logarithm of the second plateau pressure vs reciprocal temperature are listed in table 26.6 for a few hexagonal hydrides where data are available. The values for samarium and gadolinium trihydrides were estimated from rather sparse data. Also listed in the table are enthalpy values for the transition $\text{MH}_{2-\delta} \rightleftharpoons \text{MH}_{3-\epsilon}$ [including the reported (section 2.1) low temperature hexagonal neodymium hydride phase] as obtained by Mintz et al. (1976) from DTA curves. The agreements between the two sets of ΔH values are excellent for Ho and Er, and also are satisfactory for Sm and Gd in view of the uncertainty in the values obtained from van't Hoff plots of dissociation pressure data.

Values for \bar{H}_1 for these hydrides can be obtained from data in the references shown and from Lundin and Blackledge (1962) for YH_2 and Libowitz and Pack (1969a) for GdH_2 . However, because of the high pressures involved, there are no data available to calculate \bar{H}_2 in eq. (26.7).

3.3. Specific heat data

Thermodynamic quantities may be computed from specific heat data using the following relations:

$$S_T^\circ = \int_0^T (C_p/T) dT \quad (26.8)$$

and

$$H_T^\circ - H_0^\circ = \int_0^T C_p dT \quad (26.9)$$

where S_T° and H_T° are the absolute entropy and enthalpy, respectively at temperature, T , and C_p is the specific heat. The values of these quantities at 298 K have been computed from measurements of specific heat as a function of temperature for the hydrides and deuterides of yttrium, and the dihydrides of La, Ce, Pr, Nd, and Dy using eqs. (26.8) and (26.9); they are listed in table 26.7. Also listed in the table are the entropies of formation, ΔS_f , at 298 K as computed from the absolute entropy of the hydride, S° .

$$\Delta S_f(298) = S^\circ - S_M - S_{\text{H}_2}$$

The values for the absolute entropy of the metal, S_M , at 298 K were obtained from Kelly and King (1961) and a value of 31.2 cal/deg mole was used for the entropy of hydrogen gas, S_{H_2} . Where data were available, the entropies of formation also were computed for the stoichiometric dihydride using eq. (26.6) and the values obtained from dissociation pressure data (table 26.5). Except for YH_2 , the agreement between the two methods of calculating ΔS_f is fairly good.

TABLE 26.6
Enthalpies and entropies of formation of hydrogen-deficient hexagonal rare earth trihydrides from hydrogen-rich dihydrides.

Trihydride	$-\Delta H$ (kcal/mole H ₂)	$-\Delta S$ (cal/deg/mole H ₂)	Ref. (see table 26.3)
Y	21.5	33.3	b
Sm	25 (est.)	42 (est.)	r
Sm	18		s
Gd	12 (est.)	18 (est.)	k
Gd	22		s
Tb	23		s
Dy	22		s
Ho	18.7	28.6	n
Ho	18		s
Er	19.8	30.1	o
Er	20		s
Tm	26		s
Lu	25		s

^aMesser and Park (1972); ^sMintz et al. (1976).

TABLE 26.7
Thermodynamic properties of rare earth hydrides from specific heat measurements at 298 K.

Hydride	$H^\circ - H_0^\circ$ (cal/mole)	S° (cal/deg mole)	$-\Delta S_f$ (cal/deg mole)		Ref.
			(from S° value)	(from eq. (26.6))	
YH ₂	1403	9.18	33.0	38.4	a
YD ₂	1659	10.29	35.3	—	b
YH ₃	1613	10.02	47.8	—	a
YD ₃	2025	12.03	50.9	—	b
LaH ₂	1810	12.35	32.5	35.4	c
CeH ₂	1776	13.33	34.5	34.7	c
PrH ₂	1832	13.57	35.2	35.3	c
NdH ₂	1882	14.08	34.6	34.4	c
DyH ₂	1853	15.45	33.7	—	d

^aFlotow et al. (1962); ^bFlotow et al. (1963); ^cBieganski (1972); ^dBieganski and Opyrchal (1972).

4. Magnetic properties

Magnetic properties of the rare earth hydrides are summarized and compared with the properties of the rare earth metals in table 26.8. The decrease in magnetic susceptibility of the metal on hydride formation, which is characteristic of most transition metal hydrides (Libowitz, 1965, 1972b), occurs only in the

TABLE 26.8
Magnetic properties of the rare earth hydrides

Metal or hydride	Magnetic susceptibility		Magnetic moment (Bohr magnetons)	Weiss constant (K)	Ordering temperature (K) $T_C = \text{Curie}$ $T_N = \text{Néel}$	References
	$\times 10^4$	room temp. (emu/mole)				
La	0.95					Stalinski (1957a)
LaH ₂	0.59					
LaH ₃	-0.20					
Ce	25		2.54	-37	$T_N = 12.5$	Stalinski (1959) Kopp and Schreiber (1967a)
CeH ₂	25		2.50	-16		
CeH _{2.9}	23		2.44	-16		
CeH _{2.1-2.5}					$T_N = 5.0-5.4$	
Pr	49		3.41	7	$T_N = 25$	Wallace and Mader (1968); Kubota and Wallace (1963a)
PrH _{2.0}	51		3.69	-33	N.O.*	
PrH _{2.7}	48		3.36	-34	N.O.*	Wallace (1963a)
Nd	44		3.33	4	$T_N = 19$	Kubota and Wallace (1963a); Kopp and Schreiber (1967b)
NdH _{2.0}	50		3.38	-30, 4	$T_N = 6.2$	Schreiber (1967b)
NdH _{2.7}	45		3.41	-39, 1	$T_N = 3$	Bieganski et al. (1975a); Bieganski and Druilis (1976)
Sm	11				$T_N = 106$	Kubota and Wallace (1963a)
SmH _{2.0}	11				N.O.*	
SmH _{2.9}	9				N.O.*	
Eu	330		7.94		$T_N = 95$	Zanowick and Wallace (1962); Mustachi (1974)
EuH _{1.9}	240		7.0	25	$T_C = 16$	

Gd	2500	7.94	302	$T_C = 293$	Wallace et al. (1963)
GdH ₂	250	7.7	3	$T_N = 21, 30, 5$	Kopp and Schreiber (1967b); Flood (1976)
GdH ₃	215	7.3	-3	$T_N = 3.3$	Wallace et al. (1963)
Tb	1380	9.85	230	$T_N = 235$	Bieganski et al. (1975b)
TbH _{2,0}	350	9.8	-6	$T_N = 16$	Kubota and Wallace (1963b); Bieganski et al. (1975c); Hubbard et al. (1964); Flood (1975)
TbH _{3,0}		9.7	-7	N.O.*	Kubota and Wallace (1963b); Bieganski et al. (1975c); Hubbard et al. (1964); Flood (1975)
Dy	910	9.9	160	$T_N = 184$	Kubota and Wallace (1963b); Bieganski et al. (1975c); Hubbard et al. (1964); Flood (1975)
DyH _{2,0}	465	10.8	-16	$T_N = 5.0$	Kubota and Wallace (1963b); Bieganski et al. (1975c); Hubbard et al. (1964); Flood (1975)
DyH _{3,0}	390	9.5	-2	$T_N = 3.5$	Kubota and Wallace (1963b); Bieganski et al. (1975c); Hubbard et al. (1964); Flood (1975)
Ho	650	10.4	86	$T_N = 135$	Kubota and Wallace (1962); Bieganski and Stalinski (1976)
HoH _{2,0}	395	9.9	-5	$T_N = 8$	Flood (1976)
HoH _{3,0}	425	10.1	-8	N.O.*	Kubota and Wallace (1963b); Opyrchal and Bieganski (1976)
Er	510	9.9	56	$T_N = 88$	Shenoy et al. (1976)
ErH _{2,0}	360	9.8	-18	$T_N = 2.1-2.4$	Kubota and Wallace (1963b); Opyrchal and Bieganski (1976)
ErH ₃	350	9.5	-19	N.O.*	Shenoy et al. (1976)
Tm	365	7.5	32	$T_N = 56$	Kubota and Wallace (1963b)
TmH _{2,0}	220	7.6	-40	N.O.*	Warf and Hardcastle (1966)
TmH _{3,0}	210	7.5	-34	N.O.*	Parks and Bos (1970)
YbH ₂	~3				
YbH _{2,55}	40				
Y	165				
YH _{2,1}	95				
YH _{2,8}	55				

*No magnetic ordering observed down to 4 K.

heavier rare earth metals (Gd to Tm) including yttrium. The lighter rare earths, Ce, Pr, Nd, and Sm show essentially no change in magnetic susceptibility on hydride formation. The lanthanum-hydrogen system, which has no f electrons, exhibits the susceptibility behavior to be expected if the trihydride is ionic. The paramagnetic susceptibility decreases on formation of the dihydride, and the trihydride is diamagnetic.

The fact that the effective magnetic moments do not change on hydride formation establishes that the f electrons in the rare earth metals do not take part in chemical bonding with hydrogen. However, the decrease in magnetic ordering with hydride formation in every case indicates that it is the conduction band electrons which are removed during reaction of the metal with hydrogen. Since magnetic interactions between the paramagnetic ions in the rare earth metals are transmitted via conduction electrons, the substantial decrease in magnetic ordering temperatures on hydride formation may be explained by a suppression of these interactions due to removal of the conduction band electrons to more localized energy states (Wallace, 1972). The decrease in Weiss constant is also indicative of decreased magnetic ordering.

Most of the rare earth hydrides are antiferromagnetic (except EuH_2 , see below). However, neodymium dihydride appears to exhibit ferrimagnetic ordering. Kubota and Wallace (1963a) reported a Curie temperature of 9.5 K on the basis of magnetic susceptibility measurements. More recent specific heat measurement (Bieganski et al., 1975a) and NMR studies (Kopp and Schreiber, 1967b) both indicate a magnetic ordering transition at 6.2 K. The Weiss constants obtained from the magnetic susceptibility measurements (-30 K) and the NMR studies (4 K) differ by a greater amount.

In the case of terbium dihydride, Bieganski et al. (1975b) observed no specific heat anomaly corresponding to the ordering at 40 K obtained by Wallace et al. (1963) in susceptibility measurements. However, a sharp specific heat anomaly was observed at 10 K, which Bieganski et al. (1975b) interpreted as the Néel temperature since it agreed with their susceptibility data indicating antiferromagnetic ordering at about 18 K. Bieganski et al. (1975c) also observed somewhat lower magnetic ordering temperatures in DyH_2 than the value of 8 K obtained by Kubota and Wallace (1963b). Actually, Bieganski et al. (1975c) observed two specific heat anomalies at 3.3 and 4.5 K. They attributed the lower one to antiferromagnetic ordering, but the higher temperature anomaly appears to be in better agreement with the value of 5 K obtained by Hubbard et al. (1964). In DyH_3 , Hubbard et al. (1964) observed slightly positive Weiss constants and large variations of Néel temperature with magnetic field. They suggested that the magnetic ordering in DyH_3 involved a complicated spin structure rather than simple antiferromagnetism. This appears to be corroborated by neutron diffraction studies (Pickart, 1968) indicating a spiral magnetic structure in DyH_3 .

As discussed earlier, europium and ytterbium differ from the other rare earth hydrides because of their more stable +2 oxidation state. Therefore, the magnetic moment of europium dihydride (7μ) is closer to the theoretical value for the Eu^{2+} state (7.94μ) than the Eu^{3+} state (zero). Because of the seven

unpaired f electron spins in Eu^{2+} , it is strongly magnetic. As seen in table 26.8, EuH_2 becomes ferromagnetic at 25 K.

On the other hand, because of its closed electronic configuration, YbH_2 should be diamagnetic. Measurements by Wallace et al. (1963) and Warf and Hardcastle (1966) indicated that YbH_2 was weakly paramagnetic. $\text{YbH}_{2.55}$, however, appears to be more strongly paramagnetic, presumably because of unpairing of the f electrons.

The magnetic susceptibility measurements of Wallace and Mader (1968) on PrH_2 also have led to further insight into the bonding in the rare earth hydrides. They observed that below 100 K, the susceptibility data deviated from Curie-Weiss behavior in that susceptibility values became too high. These results could be explained in terms of crystal field splitting. The eight hydrogen ions surrounding the Pr^{3+} ion in the fluorite structure generate an electrostatic field which causes splitting of the degenerate $^3\text{H}_4$ ground state of the Pr^{3+} ion into four states. If the hydrogen were negatively charged (anionic) the lowest lying state of the Pr^{3+} ion would be the Γ_5 triplet state. Conversely, if the hydrogen existed as protons (positive charge) in the lattice, the energy spectrum of the Pr^{3+} would be reversed and the Γ_1 singlet state would be the lowest lying state. If the magnetic susceptibilities are calculated on the basis of each of these configurations, it is found that for anionic hydrogen, the magnetic susceptibility would increase as observed, while for protonic hydrogen the magnetic susceptibility would tend towards constancy. Consequently, these results may be taken as evidence that in the rare earth hydrides, the bonding more closely resembles the anionic case. Similar results were obtained in specific heat measurements and these are discussed in section 7.3.

Nuclear magnetic and electron paramagnetic resonance studies have been of great value in obtaining fundamental properties of metal hydrides. Structural details in hydrides can be deduced from the mean square width of the resonance lines (second moments), the shifts of the resonance peaks (Knight shift) in metallic hydrides leads to an understanding of the electronic structure, and the change in linewidth with temperature, as well as measurements of nuclear spin system longitudinal spin-lattice relaxation times or transverse spin-spin relaxation times yield the diffusion parameters for hydrogen through metal hydrides. The principles behind NMR and EPR studies and their application to metal hydrides are discussed by R.G. Barnes in ch. 18 of Volume I and hence will not be covered here. However, some of the results on hydrogen diffusion will be included in section 6.2.

5. Electronic properties

5.1. Dihydrides

As is true for the transition metal hydrides in general, the rare earth dihydrides (except for YbH_2 and EuH_2) are metallic conductors. The hydrogen deficient dihydrides ($\text{MH}_{1.8}$ to $\text{MH}_{1.9}$) are actually better electronic conductors than the

Table 26.9
Resistivity ratios of hydrogen-deficient rare earth dihydrides to the corresponding rare earth metal.

	$MH_{2-\beta}/\rho_M$	Refs.
La	0.28, 0.31	a,b
Ce	0.44	a,b
Pr	0.37	a
Nd	0.37, 0.39	a,b
Gd	0.35, 0.34	a,b
Dy	0.28	a
Ho	0.23	b
Er	0.23, 0.19	a,b
Lu	0.16, 0.17	a,c
Y	0.27	d

^aViallard and Daou (1973);
^bHeckman (1969); ^cDaou and Bonnet (1965); ^dBlackledge (1968).

corresponding rare earth metals as shown in table 26.9 which summarizes recent resistivity data for these hydrides. In every case, the resistivity of the hydride is less than one-half that of the metal. Viallard and Daou (1973) explain the increased conductivity of the hydride phase in terms of the density of states at the Fermi level of the metal. Because the density of states in the d-band of a transition metal is high, there is also a large probability of electronic transitions from the s- to d-bands. Consequently, the increased d-band scattering of the conduction electrons results in higher resistivities for the transition metals (including rare earths) as compared to other metals (Mott and Jones, 1958). On formation of the hydride phase, de-population of the d-band by the production of hydride anions leads to a decrease in the density of states (the protonic model in which the d-band is filled by electrons from the hydrogen atom will lead to the same effect), and the corresponding decrease in d-band scattering results in a higher conductivity for the hydride. It is assumed that because the hydrogen ions are in ordered positions on the tetrahedral sites of the metal sublattice, they do not perturb the crystalline field of the metal and therefore the effect of hydrogen scattering on the resistivity is negligible.

As more hydrogen is added to the hydrogen-deficient dihydride, the hydrogen atoms commence to randomly occupy the octahedral positions in the metal sublattice (see section 2.2) and the resistivity increases as illustrated for several hydrides in fig. 26.9. It is of interest to note that the resistivities of several different hydrides all fall on approximately the same curve and that the variation in temperature appears to have negligible effect. The latter observation indicates that although the resistivity rises with hydrogen content, the samples remain

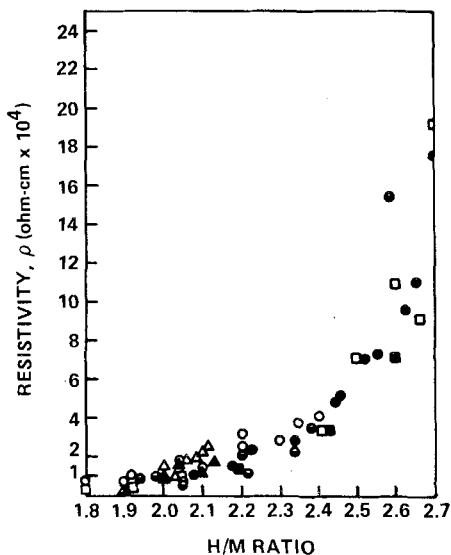


Fig. 26.9. Resistivity as a function of hydrogen contents for several rare earth hydrides. \circ , $\text{CeH}_{2.8}$ at 23°C (Heckman, 1964); \bullet , $\text{CeH}_{2.8}$ at 23°C (Libowitz and Pack, 1969b); \bullet , $\text{CeH}_{2.8}$ at 200°C (Heckman, 1967); \square , $\text{LaH}_{2.8}$ at 25°C (Heckman, 1969); \blacksquare , $\text{NdH}_{2.8}$ at 200°C (Heckman, 1968); \triangle , $\text{GdH}_{2.8}$ at 23°C (Heckman, 1964); \blacktriangle , $\text{ErH}_{2.8}$ at 340°C (Heckman, 1969).

metallic conductors. This conclusion was confirmed by Libowitz and Pack (1969b) and Libowitz (1972a) who measured resistivities as a function of temperature (in the range 140 K to 310 K) of several cerium hydride samples ranging in hydrogen content from $\text{CeH}_{1.98}$ to $\text{CeH}_{2.55}$. In all cases there was a positive coefficient of resistivity with temperature.

Because europium and ytterbium dihydrides resemble the ionic alkaline earth dihydrides, it is expected that these hydrides would be poor electronic conductors (insulators or semiconductors). There have been no reported electronic measurements on EuH_2 , but Heckman (1969) obtained a resistivity value of about 10^7 ohm-cm for $\text{YbH}_{1.90}$ at room temperature. Heating the hydride resulted in a monotonic decrease in resistivity to a value of 2.5×10^4 ohm-cm at 150°C . The logarithm of the resistivity varied linearly with reciprocal temperature which is indicative of semiconductor behavior.

5.2. Trihydrides

Early studies on polycrystalline samples of lanthanum and cerium hydrides by Stalinski (1957b, 1959) indicated that these materials become semiconductors as the trihydride composition is approached. More recent studies on single crystals of cerium hydride by Libowitz and Pack (1969b) showed a sharp increase in resistivity as the hydride composition approached $\text{CeH}_{2.8}$; illustrated in fig. 26.10. As mentioned in section 5.1, samples in which $\text{H/Ce} < 2.7$ showed metallic behavior. However, samples with $\text{H/Ce} > 2.8$ exhibited typical semiconductor behavior with a linear increase in resistivity with reciprocal temperature. Clearly, there is a metal-to-semiconductor transition in cerium hydride at an

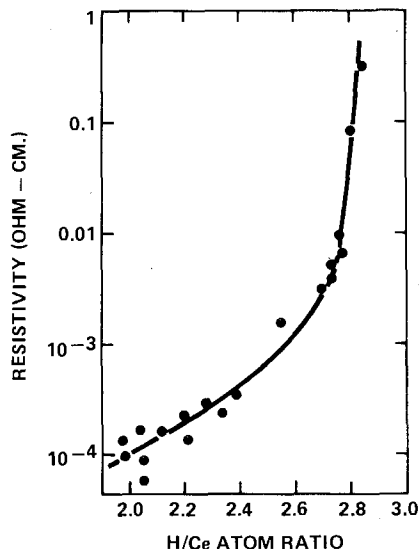


Fig. 26.10. Resistivity of cerium hydride as a function of hydrogen content (Libowitz and Pack, 1969b).

H/Ce value of about 2.8. X-ray and neutron diffraction data (Libowitz et al., 1972) revealed no structural change at this composition.

There have been no reported resistivity data for the hexagonal trihydrides although Wallace et al. (1963) reported that the resistivities of dysprosium and holmium hydrides increase by five orders of magnitude when these hydrides are fully hydrogenated. Singh et al. (1976) found semiconductor-type behavior for erbium trihydride. It is generally believed that the hexagonal rare earth hydrides are semiconductors.

5.3 Electronic structure of cerium hydride

The observed compositional dependent metal-to-semiconductor transition in cerium hydride (section 5.2) can be explained in terms of the band structures shown in fig. 26.11. If cerium hydride is viewed as an ionic compound, the composition CeH_3 would be an insulator (or semiconductor). As hydrogen atoms are removed from CeH_3 to form vacancies in the octahedral hydrogen sublattice, donor levels are introduced into the band gap as shown in fig. 26.11 for $\text{H/Ce} > 2.8$ and the resistivity of the hydride decreases. A value of 0.30 eV was calculated by Libowitz and Pack (1969b) for the energy difference between the donor levels and the bottom of the conduction band for $\text{CeH}_{2.85}$. As more hydrogen is removed from the hydride, the concentration of donors increases, and at $\text{H/Ce} \approx 2.8$ there is overlap between the wave functions of the donor electrons and the E_g orbitals of the 5d cerium states to form a half-filled defect band with corresponding metallic behavior (fig. 26.11). This model requires that the semiconducting compositions be *n*-type, which appears to be confirmed by

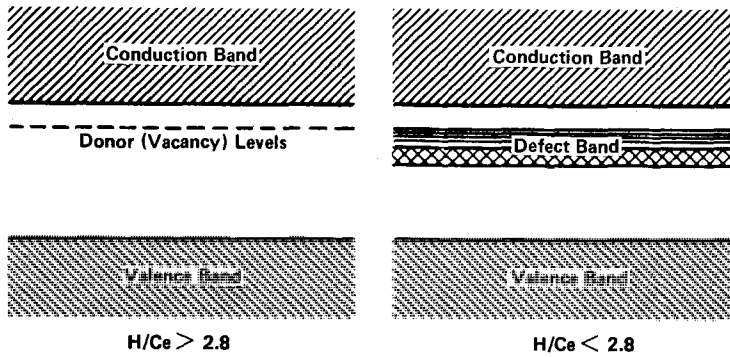


Fig. 26.11. Proposed electronic band structure for cerium hydride (Libowitz et al., 1972).

observations of negative Seebeck coefficients in thermoelectric power measurements (Libowitz et al., 1972). The thermoelectric power measurements, however, indicate *p*-type conductivity for the metallic compositions ($H/Ce < 2.8$) in agreement with Hall effect studies by Heckman (1967).

When metallic cerium hydride at compositions close to the transition ($H/Ce = 2.7$ to 2.8) are cooled from room temperature, there is a sharp increase in resistivity at about 250 K, indicative of a temperature-dependent metal-to-semiconductor transition (Libowitz et al., 1972). A specific heat anomaly also was observed at about the same temperature by Bieganski et al. (1965). Neutron diffraction investigations of $CeH_{2.75}$ revealed no hydrogen ordering at 250 K, but X-ray diffraction studies showed that the hydride lattice becomes tetragonal at this temperature with an increasing *c/a* ratio as temperature is further decreased. At 100 K, the *c/a* ratio is 1.007. Libowitz et al. (1972) have suggested that the temperature-dependent transition may be due to a splitting of the narrow defect band in fig. 26.11.

6. Kinetics of hydride formation and hydrogen diffusion

6.1. Reaction mechanisms

There has been only a limited number of kinetic studies of hydrogenation rates of rare earth metals. In general, isothermal curves of hydrogen absorption vs time exhibit a sigmoidal shape which may be explained in terms of a four stage reaction (Gayer and Bos, 1964; Gayer and Milotik, 1968; Gayer and Grunwald, 1969). There is an initial induction period which Gayer and coworkers explain by a nucleation process that requires hydrogen to reach the surface of the metal by penetrating an oxide or other contaminating layer. Viillard (1960) proposed that this induction period may be due to a chemisorption process (of hydrogen) in which the hydrogen molecules are dissociated into atoms. The second stage is autoacceleration which is a result of the growth of the nuclei, thereby exposing

more of the metal surface to hydrogen gas. The induction and autoacceleration stages generally do not occur at higher temperatures. The third stage is a linear decrease in pressure with time representing a constant rate of reaction. During this stage of the reaction, the brittle hydride phase tends to disintegrate the sample thereby continually exposing more metal surface for reaction. The final stage is deceleration as the hydride phase approaches saturation. This latter stage is probably diffusion controlled since hydrogen must diffuse through the dihydride phase as the trihydride composition is approached. Viallard (1960) found that under certain conditions an initially hydrogen-rich hydride is formed, which then becomes less rich in hydrogen as further hydride is formed from metal. In studying the formation of cerium hydride, Gayer and Melotik (1968) observed that at lower temperatures, the reaction curve no longer had a sigmoidal shape but was parabolic, indicative of a diffusion controlled reaction.

Because rare earth-hydrogen reaction rates are dependent upon sample and surface condition and the presence of impurities, it has been difficult to get sufficient data on activation energies for cases where the reactions appear to be diffusion controlled. Consequently there are no data available to compare with the results of NMR diffusion studies.

6.2. Diffusion of hydrogen in hydrides

All available data on diffusion of hydrogen in rare earth hydrides are obtained from nuclear magnetic resonance studies. Values for activation energies are summarized in table 26.10.

Schreiber and Cotts (1963) observed a decrease in activation energy with increasing hydrogen content in lanthanum hydride. NMR data for the dihydride composition indicated that hydrogen diffuses via a vacancy mechanism from tetrahedral site to tetrahedral site through an octahedral site (t-o-t). As the hydrogen content increases, more octahedral sites become occupied and the corresponding repulsion between hydrogen atoms on the two types of sites decreases the energy necessary to move a hydrogen from a tetrahedral to an octahedral site, thus explaining the lower activation energy of diffusion.

In scandium hydride, Weaver (1972a) observed two activation energies at compositions close to stoichiometry (see table 26.10). At the lower compositions and temperatures, he proposed a simple vacancy mechanism, t-t. However, at the higher temperatures and hydrogen contents, more octahedral sites are occupied and the mechanism becomes t-o-t. It is of interest to note that on the basis of energetic considerations, Khodosov (1971) proposed that in fluorite-type hydrides at sufficiently high temperatures, there may be more hydrogen atoms in octahedral sites than in tetrahedral sites so that the diffusion mechanism would be o-t-o.

NMR diffusion studies on hexagonal yttrium trihydride by Weaver (1972b) were difficult to interpret. However, in the $\text{YH}_{2.83}$ sample, the NMR results are in agreement with a vacancy diffusion model involving octahedral sites. In the hexagonal trihydride there are two types of octahedral hydrogen sites; four of

TABLE 26.10
 Activation energies, E_a , for hydrogen diffusion in rare earth
 hydrides

Hydride	E_a (kcal/mole)	Reference
LaH _{1.92}	23	Schreiber and Cotts (1963)
LaH _{1.96}	10	Schreiber and Cotts (1963)
LaH _{2.00}	8	Schreiber and Cotts (1963)
LaH _{2.47}	8	Schreiber and Cotts (1963)
LaH _{2.61}	5	Schreiber and Cotts (1963)
LaH _{2.85}	3	Schreiber and Cotts (1963)
ScH _{1.7}	13	Weaver (1972a)
ScH _{1.8}	17	Weaver (1972a)
ScH _{1.9}	10 (<620°C)	Weaver (1972a)
	26 (>620°C)	Weaver (1972a)
ScH _{1.98}	9 (<520°C)	Weaver (1972a)
	18 (>520°C)	Weaver (1972a)
YH _{1.91}	8.0	Stalinski et al. (1969)
YH _{1.96}	9.8	Khodosov and Andrievskii (1967)
YH _{2.00}	10.0	Stalinski et al. (1969)
YH _{2.83}	20	Weaver (1972b)
YH _{2.93}	6	Weaver (1972b)

one type, O(4), and two of the second type O(2) in each unit cell. It is the O(2) site which is involved in the diffusion mechanism.

7. Other measurements related to bonding and structure

7.1. Inelastic neutron scattering

In the incoherent inelastic neutron scattering from a solid, lattice vibrational quanta (phonons) are exchanged with the incident neutrons. Energy analysis of the scattered neutrons, obtained by the time-of-flight technique, results in a spectrum which directly reflects the vibration spectrum of the solid. Such information can generally not be obtained on metallic hydrides by conventional infrared techniques because of the interaction of light with conduction electrons. Hydrogen also has a very large incoherent scattering cross section compared to other elements and any motion involving hydrogen, therefore, will be manifested as an enhanced peak in the neutron spectrum.

Rush et al. (1966) studied the Y-H₂ system. In YH₂ they observed a single peak which they assigned to the vibration of hydrogen in tetrahedral sites in the face centered cubic lattice. The spectrum for YH₃ was considerably more complex, exhibiting several maxima, due to hydrogen atoms in different sites in the hexagonal lattice, but the spectrum could be correlated reasonably well with the known crystal structure. Karimov et al. (1967) found one optical peak in

CeH₂, due to vibrations of hydrogen atoms in tetrahedral sites; in CeH₃ this peak had shifted to higher energies and an additional peak at lower energies was observed. The additional peak was assigned to hydrogen vibrating in the octahedral sites. Maeland and Holmes (1971) obtained similar results for LaH_{1.94} and LaH_{2.82}, but in addition they found evidence for a small number of octahedral hydrogen atoms in LaH_{1.94}. Vorderwisch and Hautecler (1974b) also concluded from their inelastic scattering work on CeH_{1.98} that hydrogen occupied a small number of octahedral sites in the structure. The inelastic neutron spectrum of YbH₂ was found to be similar to those of the orthorhombic alkaline earth hydrides confirming the structural similarities of these hydrides (Maeland, 1970). Optical peak energies observed in rare earth hydrides are listed in table 26.11.

Inelastic neutron scattering data have been analyzed on the basis of a central force lattice dynamical model for CeH₂ and CeH₃ (Vorderwisch et al., 1974). Glinka et al. (1977) have recently completed a study of the phonon dispersion relation in a single crystal of CeD_{2.12}. The results bear little resemblance to the predictions of the simplified model derived by Vorderwisch et al. (1974) to fit incoherent neutron scattering results. Even when the model is extended considerably, it cannot reproduce the optic mode data. Attempts are underway to derive a more satisfactory description of the dynamics of this system (Rush, 1976).

TABLE 26.11
Optical peak energies in rare earth hydrides

Hydride	Structure	Peak energies (meV)*	Ref.
CeH ₂	f.c.c.	105 (t)	a
CeH ₃	f.c.c.	115 (t); 65 (o)	a
CeH _{1.98}	f.c.c.	106 (t); 74 (o)	b,c
CeH _{2.72}	f.c.c.	110 (t); 65 (o)	b
LaH _{1.94}	f.c.c.	102 (t) (corr)	d
LaH _{2.82}	f.c.c.	116 (t); 64 (o) (corr)	d
PrH _{1.94}	f.c.c.	108 (t)	e
PrD _{2.3}	f.c.c.	75 (o); 52 (o)	e
HoH _{1.98}	f.c.c.	126 (t)	e
YH ₂	f.c.c.	127 (t) (corr)	f
YD ₂	f.c.c.	90 (t) (corr)	f
YH ₃	hexagonal	136; 94; 62 (corr)	f
YD ₃	hexagonal	96; 68; 41 (corr)	f
YbH ₂	orthorhombic	130; 91; 81; 71 (corr)	g

*Vibrations due to hydrogen in octahedral and tetrahedral sites are designated (o) and (t), respectively. Peaks in the approximate frequency distributions, calculated from the time-of-flight spectra, are marked (corr); ^aKarimov et al. (1967); ^bVorderwisch and Hautecler (1974a); ^cVorderwisch and Hautecler (1974b); ^dMaeland and Holmes (1971); ^eHunt and Ross (1976); ^fRush et al. (1966); ^gMaeland (1970).

7.2. Positron annihilation

Annihilation of a positron by combination with an electron in a solid results in the emission of a pair of photons (for singlet states) in opposite directions (i.e. 180 degrees apart) in the zero momentum case. The electrons in a solid have a momentum distribution, however, and the photons will, therefore, be separated by an angle $180 \text{ degrees} \pm \Theta$, where Θ depends on the momentum of the electrons. By measuring the angular distribution of the emitted photons the momentum distribution of electrons in the solid may be obtained and this, in turn, may lead to information on the electronic structure.

The life-times of positrons in a solid depend upon the particular mechanism of annihilation (e.g. through formation of positronium or positron-ion combinations). Consequently, measurements of positron annihilation rates give results which again may be interpreted in terms of electronic structure.

Chouinard et al. (1969) measured angular correlations of positron annihilation in cerium hydride. In the composition range $\text{CeH}_{1.8-2.2}$ they found that the correlations were nearly parabolic, increased in width with increasing hydrogen concentration, and were broader (larger Θ values) than for cerium metal. For $\text{H/Ce} \gg 2.2$ the angular correlations not only increased in width, but also began to deviate significantly from parabolic. The authors claimed that these observations were consistent with the protonic model for hydrogen which, according to their calculations, predicted expanded angular correlation functions (with respect to cerium metal). The anionic model was rejected because computed values, based on this model, predicted narrower correlations. Green et al. (1971) disagreed with these conclusions stating that the calculation of Chouinard et al. (1969) for the case of the hydridic model was overly simplified. They pointed out that the measured angular correlation for LiH , a compound in which hydrogen is definitely anionic, was also broader than that predicted by the same type of calculation. Green et al. (1971) measured annihilation rates in lanthanum hydride as a function of hydrogen concentration and found that they were constant from LaH_2 to $\text{LaH}_{2.7}$. This, they claimed, was consistent with a reaction mechanism in which the annihilation occurred primarily within a positron-hydride-ion pair. The increase in annihilation rates at $\text{H/La} > 2.7$ was attributed to a different type of positron interaction with the localized electrons of the semiconductor phase.

In a later paper Chouinard and Gustafson (1971) reported angular correlations of positron annihilation in erbium, gadolinium, holmium and ytterbium hydrides. The correlations were again claimed to be consistent with the predictions of the protonic model. Recent studies on yttrium dihydride (Sabin et al., 1972; Rozenfeld and Debowska, 1975) were interpreted on the basis of the proton model, but it was pointed out that the model fails for higher hydrogen concentrations, i.e. $\text{YH}_2\text{-YH}_3$ (Rozenfeld and Debowska, 1975).

7.3. Specific heat measurements

A number of properties of the rare earth hydrides have been studied by determining the temperature variation of their specific heat. Bieganski et al.

(1965) observed a λ -type, specific heat anomaly at 255 K in $\text{CeH}_{2.86}$, which Libowitz et al. (1972) associated with the metal-to-semiconductor transition discussed in section 3.3. In another study Bieganski (1971a) observed broad and diffuse anomalies in $\text{LaH}_{2.00}$ and $\text{LaH}_{2.02}$ over the temperature range 170–270 K. They assumed that this anomalous behavior was due to hydrogen diffusion. Low temperature λ -type specific heat anomalies due to ferro- or antiferromagnetic transitions have been observed in many rare earth dihydrides (section 4). Specific heat measurements have also been used to obtain information about the state of hydrogen in the rare earth dihydrides, i.e. whether protonic or ionic (Bieganski and Stalinski, 1970; Bieganski, 1971a; Bieganski, 1971b; Bieganski and Opyrchal, 1972; Bieganski, 1972; Bieganski et al., 1973; Bieganski, 1973; Bieganski et al., 1975c; Opyrchal and Bieganski, 1976). The electronic contributions to the specific heat in these measurements are associated with the splitting of the degenerate ground states of the tripositive isolated Ln^{+3} ion by the crystal field in the fluorite lattice. This splitting, however, will be different for H^+ and H^- (section 4). If the specific heat contributions from the electronic transition between the two lowest levels (Schottky functions) at low temperature are computed and compared with the experimentally observed values, the nature of hydrogen in the rare earth hydrides may be deduced. The results of measurements on CeH_2 (Bieganski, 1970, 1971a, 1972), PrH_2 (Bieganski, 1970; Bieganski, 1972; Bieganski, 1973), NdH_2 (Bieganski, 1970; Bieganski, 1971b; Bieganski, 1972), DyH_2 (Bieganski and Opyrchal, 1972; Bieganski et al., 1975c), HoH_2 (Bieganski et al., 1973) and ErH_2 (Opyrchal and Bieganski, 1976) are in much better agreement with the anionic than with the protonic model.

7.4. Mössbauer spectroscopy

Mössbauer spectroscopy is a relatively new technique for studying the electronic structure of solids. The method is based on the fact that the spacing of nuclear energy levels is affected by the chemical environment around the nucleus. Therefore, the energy associated with a transition between a nuclear ground state and an excited state of a particular nucleus in a series of compounds will, in general, vary from compound to compound. The changes in the spacing of nuclear energy levels are measured in Mössbauer spectroscopy and these changes are referred to as isomer shifts. Abeles et al. (1969) used this technique to study the isomer shifts of ^{161}Dy in $\text{DyH}_{2.1}$ and $\text{DyH}_{2.9}$ at room temperature. The isomer shifts, when compared with isomer shifts in other dysprosium compounds and with the predictions of the protonic and hydridic models for these two hydrides, appeared to favor the hydridic model. Mustachi (1974) measured isomer shifts in $\text{YbH}_{1.94}$ and $\text{EuH}_{1.92}$ and their data was shown to be consistent with the hydridic model. In $\text{EuH}_{1.92}$ Mustachi (1974) observed splitting of the single line spectrum at low temperatures which he attributed to the ferromagnetic transition in EuH_2 (see section 4); the Curie point was estimated to be 16.2 K. Zaheer et al. (1976) studied the ferromagnetic ordering in $\text{EuH}_{1.90}$ by Mössbauer spectroscopy and concluded that the predominant

exchange interaction was via the hydride anions (superexchange). The gadolinium-hydrogen system was studied by Lyle et al. (1975) and their isomer shift data were in agreement with the anionic model. Splitting of the single line spectrum of GdH_2 was observed at low temperature in agreement with the known antiferromagnetic ordering transition in this compound (see table 26.8). There was also evidence for magnetic ordering in the trihydride at 1.3 K which has since been confirmed by magnetic susceptibility studies (see table 26.8). Erbium dihydride was studied by Shenoy et al. (1976). These authors observed typical hyperfine splitting of the spectrum at low temperatures (due to magnetic ordering) and obtained an ordering temperature of 2.4 K. From a detailed analysis of their data, Shenoy et al. (1976) found that the crystal field ground state was Γ_6 (see section 4) which implies an anionic environment surrounding the Er^{+3} ion.

8. Rare earth alloy hydrides

A hydride formed by the reaction of a binary solid solution alloy with hydrogen can be considered as a solid solution of two binary hydrides. The properties of this type of hydride are related to the properties of the constituent binary hydrides and may, with some degree of confidence, be predicted from a knowledge of the properties of the constituent binary hydrides. However, a hydride formed by the reaction of an intermetallic compound with hydrogen, in general, has properties which bear little or no resemblance to those of the constituent metal hydrides (vanMal, 1976; Libowitz, 1976). Intermetallic compound hydrides may conveniently be viewed as pseudo-binary metal hydrides. This section will deal only with intermetallic compound hydrides.

While investigating the magnetic properties of SmCo_5 , Zijlstra and Westendorp (1969) observed that the coercivity of this material depended on certain etching techniques. Believing this to be due to hydrogen dissolved in the crystal during etching, these authors made coercivity measurements with the sample under various pressures of hydrogen and discovered that SmCo_5 absorbed a surprisingly large amount of hydrogen ($\text{H}/\text{SmCo}_5 > 2$ at 20 atm. H_2 pressure). This discovery set off a flurry of investigations of hydrogen absorption by RM_5 and related compounds (M is a transition metal, usually cobalt, nickel or iron). The extensive literature that followed has recently been reviewed (Newkirk, 1976) and will not be repeated here. The following discussion deals with some of the more important aspects of these systems.

8.1. Reaction of RM_5 and related compounds with hydrogen

The RM_5 compounds have the hexagonal CaCu_5 type structure and they form orthorhombic hydride phases (Bowman et al., 1973; Kuijpers and Loopstra, 1974). Pressure-composition isotherms for the representative $\text{LaNi}_5\text{-H}_2$ system are shown in fig. 26.12 (van Vucht et al., 1970). The hydride formed has a

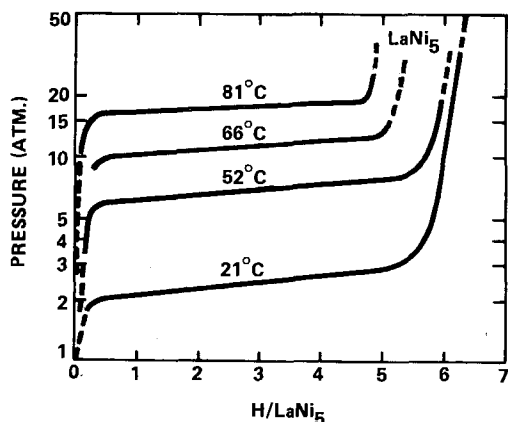


Fig. 26.12. Pressure-composition isotherms for the $\text{LaNi}_5\text{-H}_2$ system (van Vucht et al., 1970).

composition near LaNi_5H_6 at 21°C and the dissociation pressure is ~ 2.5 atm. At higher pressures, further absorption takes place; the highest reported composition is $\text{LaNi}_5\text{H}_{7.8}$ at 23°C and 130 atm. pressure (Anderson et al., 1973). The enthalpy of formation, calculated from the plateau pressures, is -7.2 kcal/mole. VanVucht et al. (1970) reported similar behavior for SmCo_5 , but the limiting composition of the hydride was only SmCo_5H_3 . Kuijpers (1972) studied the $\text{LaCo}_5\text{-H}_2$ and the $\text{CeCo}_5\text{-H}_2$ systems and found the $\text{CeCo}_5\text{-H}_2$ system to be similar to the $\text{SmCo}_5\text{-H}_2$ system. The $\text{LaCo}_5\text{-H}_2$ system, however, was more complicated as seen from fig. 26.13. Two plateau regions were found, indicating two different hydride phases; one $\text{LaCo}_5\text{H}_{3.35\pm 0.1}$ and the other $\text{LaCo}_5\text{H}_{4.3\pm 0.1}$. Steward et al. (1976) have extended these measurements to higher pressures and found a third plateau region near 10^3 atm. pressure. The composition of the sample was $\text{LaCo}_5\text{H}_{>8}$ at 1300 atm. of H_2 pressure. Steward et al. (1977) claimed

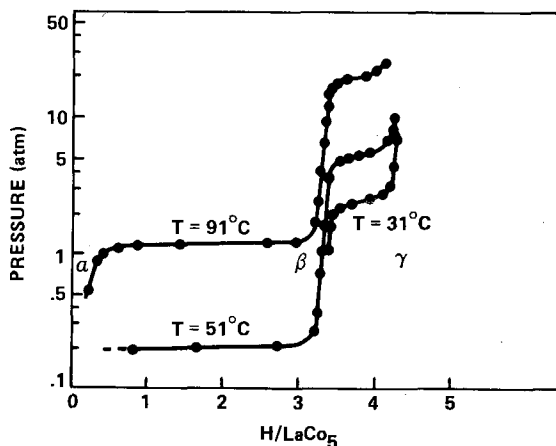


Fig. 26.13. Pressure-composition isotherms for the $\text{LaCo}_5\text{-H}_2$ system (Kuijpers, 1972).

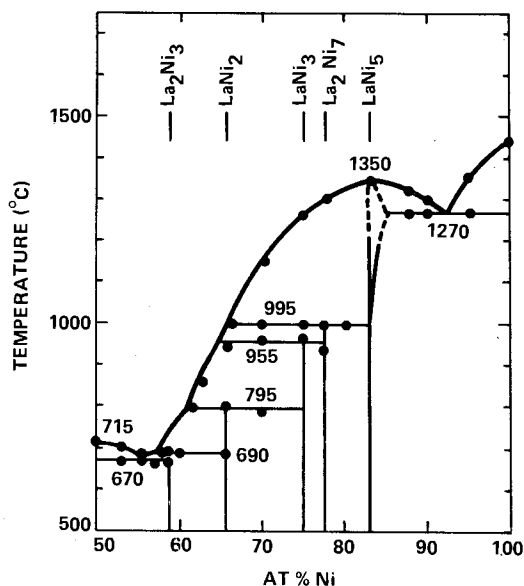


Fig. 26.14. The La-Ni system in the range 50-100 atomic percent Ni (Buschow and van Mal, 1972).

this result was consistent with the number of available sites in the CaCu_5 structure.

The RM_5 structure is but one of many intermetallic compounds formed between the rare earths and transition metals. Figure 26.14, which shows the La-Ni system, will serve as an illustration. It is seen that no less than six

TABLE 26.12
Intermetallic compounds in the La-Ni system and some corresponding hydrides.

Compound	Structure	Structure type	Ref.	Observed hydrides	Ref.
LaNi	orthorhombic	CrB	^a	LaNiH _{2.6} LaNiH _{3.0} LaNiH _{3.6}	^c ^d ^e
La ₂ Ni ₃	orthorhombic	New (La ₂ Ni ₃)	^b	La ₂ Ni ₃ H(?)	^d
LaNi ₂	cubic	MgCu ₂	^a	LaNi ₂ D _{4.10} LaNi ₂ H _{4.5}	^c ^e
LaNi ₃	rhombohedral	PuNi ₃	^a	LaNi ₃ H _{5.3} LaNi ₃ H ₅	^c ^e
La ₂ Ni ₇	hexagonal	Ce ₂ Ni ₇	^a	La ₂ Ni ₇ H _{11.3} La ₂ Ni ₇ H ₁₀	^d ^e
LaNi ₅	hexagonal	CaCu ₅	^a	LaNi ₅ H _{6.5} LaNi ₅ H _{7.8}	^d ^f

^aBuschow and van Mal (1972); ^bvan Vucht and Buschow (1976); ^cMaeland et al. (1976); ^dvan Mal (1976); ^eOesterreicher et al. (1976); ^fAnderson et al. (1973).

intermetallic phases, which contain at least 50 atomic percent of La, are formed. (Two phases with less than 50 atomic percent La are also known.) All of these compounds have been found to react with hydrogen to form hydrides. In table 26.12 we have listed crystallographic data for the intermetallic phases and reported compositions of the various hydrides formed in the La-Ni system.

8.2. Other rare earth intermetallic hydrides

LiEuH₃ has been prepared by heating LiH and EuH₂ together under an atmosphere of hydrogen; YbH₂ and LiH did not form a ternary hydride under similar conditions (Messer and Hardcastle, 1964). LiEuH₃ is isostructural with LiBaH₃ which has the inverse cubic perovskite structure (Maeland and Andresen, 1968). Mikheeva and Kost (1969) reported that LiEuH₃ melts incongruently at 760°C and found evidence for an additional hydride, LiEu₂H₅. Greedan (1970) has grown single crystals of LiEuH₃ and measured the electrical resistivity and optical absorption properties (Greedan, 1971b) as well as the magnetic properties (Greedan, 1971a). Greedan's results strongly suggested that EuH₃ is a semiconducting ferromagnet with $T_c = 38$ K and $\Theta_c = 40$ K.

Thompson et al. (1975) prepared Eu₂RuH₆ by reacting EuH₂ and Ru metal at 800°C in 1 atm. H₂. The structure of the metal lattice was reported to be of the fluorite type with ruthenium occupying the 8-fold sites and europium the 4-fold sites. Neutron diffraction results indicated that the hydrogen atoms occupied the octahedral positions. Electrical resistivity measurements pointed toward semiconductor behavior and magnetic susceptibility measurements showed that Eu₂RuH₆ obeys a Curie-Weiss law with $\Theta = 43$ K. The corresponding Yb₂RuH₆ compound has recently been reported and shown to have the same structure as Eu₂RuH₆ and quite similar properties (Lindsay et al., 1976).

Toma (1975) has found that La₂Mg₁₇ forms a hydride of composition La₂Mg₁₇H₁₂. The related compounds Ce₂Mg₁₇, Pr₂Mg₁₇ and Nd₂Mg₁₇ also absorb large amounts of hydrogen. At 50°C and 10 atm hydrogen pressure the compositions are Pr₂Mg₁₇H₉, Ce₂Mg₁₇H₇ and Nd₂Mg₁₇H₉ (Yajima, 1974).

8.3. Development of new alloy hydrides

The current interest in metal hydrides for energy storage systems (Libowitz, 1976) has led to an intensive search for new alloy hydrides. Since there are a very large number of known and possible intermetallic compounds, and since intermetallic compound hydrides bear little or no resemblance to the properties of the constituent metal hydrides, it would be useful to have a procedure for predicting which intermetallic compounds will form hydrides and the approximate properties of such hydrides. Investigators at the Philips Research Laboratories, Eindhoven, The Netherlands, have developed such a procedure (vanMal et al., 1974; Buschow et al., 1974; Buschow et al., 1975; Miedema et al., 1976; vanMal, 1976). Their approach consists in evaluating the enthalpy of formation

of a hypothetical intermetallic hydride, MM'_aH_{b+c} in terms of the enthalpies of formation of the constituent metal hydrides, $\Delta H(MH_b)$ and $\Delta H(M'H_c)$, and the enthalpy of formation of the intermetallic compound, $\Delta H(MM'_a)$. When $a \geq 1$ and M is a strong hydride forming metal, the following equation is applicable:

$$\Delta H(MM'_aH_{b+c}) = \Delta H(MH_b) + \Delta H(M'_aH_c) - \Delta H(MM'_a) \quad (26.10)$$

This approach has resulted in the Rule of Reversed Stability (vanMal et al., 1974) which states that, within a given series of intermetallic compounds, the greater the stability of the intermetallic compound, the less stable its hydride. It is immediately obvious that eq. (26.10) has limited applicability since the heats of formation of many or most intermetallic compounds are unknown and must be estimated by semiempirical methods. Furthermore, the equation is limited to a particular structural or compositional series, there is no reliable procedure for estimating $\Delta H(M'_aH_c)$, and there frequently is some arbitrariness in choosing the composition of the constituent hydrides (Libowitz, 1976). It should be pointed out, however, that the rule is particularly successful in predicting the effects of alloying elements on the properties of known intermetallic compound hydrides. However, it is clearly necessary to develop new correlations which can assist in developing alloy hydrides with the required properties for hydrogen storage.

References

- Abeles, T.P., W.G. Bos and P.J. Ouseph, 1969, *J. Phys. Chem. Solids* **30**, 2159.
- Anderson, J.L., T.C. Wallace, A.L. Bowman, C.L. Radosevich and M.L. Courtney, 1973, Hydrogen Absorption by AB_3 Compounds, Rept. LA-5320-MS, Los Alamos Scientific Laboratory, Univ. of California, Los Alamos, N.M.
- Andresen, A.F., A.J. Maeland and D. Slotfeldt-Ellingsen, 1977, *J. Sol. State Chem.* **20**, 93.
- Beavis, L.C., R.S. Blewer, J.W. Guthrie, E.J. Nowak and W.G. Perkins, 1974, The Formation and Properties of Rare Earth and Transition Metal Hydrides, Veziroglu, T.N., ed., *Proceedings of the Hydrogen Economy Miami Energy Conference*, (Univ. of Miami, Coral Gables, Fla.) pp. S4-38 to S4-49.
- Bieganski, Z., W. Fesenko and B. Stalinski, 1965, *Bull. Acad. Pol. Sci., Ser. Sci. Chim.* **13**, 227.
- Bieganski, Z. and B. Stalinski, 1970, *Phys. Status Solidi(a)* **2**, K 161.
- Bieganski, Z., 1971a, *Bull. Acad. Pol. Sci., Ser. Sci. Chim.* **19**, 581.
- Bieganski, Z., 1971b, *Phys. Status Solidi(b)* **47**, 93.
- Bieganski, Z., 1972, *Ber. Bunsenges. Phys. Chem.* **72**, 1183.
- Bieganski, Z. and J. Opyrchal, 1972, *Bull. Acad. Pol. Sci., Ser. Sci. Chim.* **20**, 775.
- Bieganski, Z., 1973, *J. Chem. Thermodynamics* **5**, 1.
- Bieganski, Z., J. Opyrchal and M. Drulis, 1973, *Bull. Acad. Pol. Sci., Ser. Sci. Chim.* **21**, 703.
- Bieganski, Z., J. Opyrchal, M. Drulis and B. Stalinski, 1975a, *Phys. Status Solidi(a)* **31**, 289.
- Bieganski, Z., J. Opyrchal and M. Drulis, 1975b, *Solid State Comm.* **17**, 353.
- Bieganski, Z., J. Opyrchal and M. Drulis, 1975c, *Phys. Status Solidi(a)* **28**, 217.
- Bieganski, Z. and M. Drulis, 1976, *Phys. Status Solidi(a)* **35**, K127.
- Bieganski, Z. and B. Stalinski, 1976, *J. Less-Common Metals* **49**, 421.
- Blackledge, J.P., 1968, Yttrium and Scandium Hydrides, in: Mueller, W.M., J.P. Blackledge and G.G. Libowitz, eds., *Metal Hydrides* (Academic Press, New York), Chap. 10, pp. 441-489.
- Bos, W.G. and K.H. Gayer, 1966, *J. Nucl. Mater.* **18**, 1.
- Bowman, A.L., J.L. Anderson and N.G. Nereson, 1973, A Neutron Diffraction Study of $LaNi_5H_7$, in: Kevane, C.J. and T. Moeller, eds., *Proceedings of the 10th Rare Earth Research Conference*, Carefree, Arizona, pp. 485-489.
- Buschow, K.H.J. and H.H. vanMal, 1972, *J. Less-Common Metals* **29**, 203.
- Buschow, K.H.J., F.A. Kuijpers, A.R. Miedema and H.H. vanMal, 1974, Hydrogen in Rare Earth Intermetallics, in: Haschke, J.M. and H.A. Eick, eds., *Proceedings of the 11th*

- Rare Earth Research Conference, Traverse City, Michigan, pp. 417-429.
- Buschow, K.H.J., H.H. vanMal and A.R. Miedema, 1975, *J. Less-Common Metals* **42**, 163.
- Cheatham, A.K. and B.E.F. Fender, 1972, *J. Phys. C: Solid State Phys.* **5**, L35.
- Chouinard, M.P., D.R. Gustafson and R.C. Heckman, 1969, *J. Chem. Phys.* **51**, 3554.
- Chouinard, M.P. and D.R. Gustafson, 1971, *J. Chem. Phys.* **54**, 5082.
- Cox, D.E., G. Shirane, W.J. Takei and W.E. Wallace, 1963, *J. Appl. Phys., Suppl.* **34**, 1352.
- Curzon, A.E. and O. Singh, 1975, *J. Phys. D: Appl. Phys.* **8**, 1703.
- Daou, J.N. and J. Bonnet, 1965, *Compt. Rend., Gr. 7*, 261, 1675.
- Fadayev, V.N., 1972, *Izv. Akad. Nauk SSSR Metal* **5**, 210.
- Fadayev, V.N. and L.A. Izhyvanov, 1973, *Izv. Akad. Nauk SSSR Metal* **6**, 97.
- Flood, D.J., 1975, *Bull. Am. Phys. Soc.* **20**, 499.
- Flood, D.J., 1976, *Bull. Am. Phys. Soc.* **21**, 442.
- Flotow, H.E., D.W. Osborne and K. Otto, 1962, *J. Chem. Phys.* **36**, 866.
- Flotow, H.E., D.W. Osborne, K. Otto and B.M. Abraham, 1963, *J. Chem. Phys.* **38**, 2620.
- Gayer, K.H. and W.G. Bos, 1964, *J. Phys. Chem.* **68**, 2569.
- Gayer, K.H. and D.J. Melotik, 1968, *Z. Anorg. Allg. Chem.* **367**, 105.
- Gayer, K.H. and J.J. Grunwald, 1969, *Z. Anorg. Allg. Chem.* **368**, 327.
- Glinka, C.J., M.R. Rowe, J.J. Rush, G.G. Libowitz and A.J. Maeland, 1977, *Solid State Commun.* **22**, 541.
- Goon, E.J., 1959, *J. Phys. Chem.* **63**, 2018.
- Greedan, J.E., 1970, *J. Cryst. Growth* **6**, 119.
- Greedan, J.E., 1971a, *J. Phys. Chem. Solids* **32**, 819.
- Greedan, J.E., 1971b, *J. Phys. Chem. Solids* **32**, 1039.
- Green, R., W.G. Bos and W.F. Huang, 1971, *Phys. Rev.* **B3**, 64.
- Hardcastle, K.I. and J.C. Warf, 1966, *Inorg. Chem.* **5**, 1728.
- Haschke, J.M. and M.R. Clark, 1975, *High Temp. Sci.* **7**, 152.
- Heckman, R.C., 1964, *J. Chem. Phys.* **40**, 2958.
- Heckman, R.C., 1967, *J. Chem. Phys.* **46**, 2158.
- Heckman, R.C., 1968, *J. Chem. Phys.* **48**, 5281.
- Heckman, R.C., 1969, *Electronic Properties of Rare Earth Hydrides*, Report No. SC-RR-69-571, Sandia Laboratories, Albuquerque, N.M., November 1969.
- Holley, C.E., Jr., R.N.R. Mulford, F.H. Ellinger, W.C. Koehler and W.H. Zachariasen, 1955, *J. Phys. Chem.* **59**, 1226.
- Hubbard, W.M., R.E. Brava and J.F. Haben, 1964, *Ferromagnetism in the System Dysprosium-Hydrogen*, in *Proceedings of the International Conference on Magnetism*, Nottingham, p. 525.
- Hunt, D.G. and D.K. Ross, 1976, *J. Less-Common Metals* **49**, 169.
- Jones, P.M.S., J. Southall and K. Goodhead, 1964, *The Thermal Stability of Metal Hydrides. Part 1: Rare Earth and Yttrium Hydrides and Deuterides*, United Kingdom Atomic Energy Authority, AWRE Report No. 0-22/64.
- Jones, P.M.S., P. Ellis and T. Aslett, 1966, *The Thermal Stability of Metal Hydrides. Part 2: Samarium and Gadolinium Hydrides*, United Kingdom Atomic Energy Authority, AWRE Report No. 0-31/66.
- Karimov, I., M.G. Zemlyanov, M.E. Kost, V.A. Somenkov and N.A. Chernoplekov, 1967, *Fiz. Tverd. Tela* **9**, 1740.
- Kelly, K.K. and E.G. King, 1961, *Contributions to the Data on Theoretical Metallurgy. XIV Entropies of the Elements and Inorganic Compounds*, U.S. Bureau of Mines Bulletin No. 592.
- Khodosov, E.F. and R.A. Andrievskii, 1967, *Soviet Powder Met.* **7**, 65.
- Khodosov, E.F., 1971, *Soviet Phys.-Cryst.* **16**, 369.
- Kofstad, P., W.E. Wallace and L.J. Hyvönen, 1959, *J. Amer. Chem. Soc.* **81**, 5015.
- Kopp, J.P. and D.S. Schreiber, 1967a, *J. Appl. Phys.* **38**, 1373.
- Kopp, J.P. and D.S. Schreiber, 1967b, *Phys. Lett.* **A24**, 323.
- Korst, W.L. and J.C. Warf, 1956, *Acta Cryst.* **9**, 452.
- Korst, W.L. and J.C. Warf, 1966, *Inorg. Chem.* **5**, 1719.
- Kubota, Y. and W.E. Wallace, 1962, *J. Appl. Phys. Suppl.* **33**, 1348.
- Kubota, Y. and W.E. Wallace, 1963a, *J. Appl. Phys.* **34**, 1348.
- Kubota, Y. and W.E. Wallace, 1963b, *J. Chem. Phys.* **39**, 1285.
- Kuijpers, F.A., 1972, *J. Less-Common Metals* **27**, 27.
- Kuijpers, F.A. and B.O. Loopstra, 1974, *J. Phys. Chem. Solids* **35**, 301.
- Libowitz, G.G., 1965, *The Solid State Chemistry of Binary Metal Hydrides*, (W.A. Benjamin, Inc., New York).
- Libowitz, G.G. and J.G. Pack, 1967, *The Growth and Some Properties of Cerium Hydride Single Crystals*, in: *Proceedings of the International Conference on Crystal Growth*, Boston, Mass. June 1966 (Pergamon Press, N.Y.) pp. 129-132.
- Libowitz, G.G., 1967, *Point Defects in Some Rare Earth Dihydrides*, in: Kohler, W.C. ed., *Proceedings of the Sixth Rare Earth Research Conference*, Gatlinburg, Tenn. pp. 132-141.
- Libowitz, G.G. and J.G. Pack, 1969a, *J. Phys. Chem.* **73**, 2352.
- Libowitz, G.G. and J.G. Pack, 1969b, *J. Chem. Phys.* **50**, 3557.
- Libowitz, G.G., J.G. Pack and W.P. Binnie, 1972, *Phys. Rev.* **B6**, 4540.
- Libowitz, G.G., 1972a, *Ber. Bunsenges. Phys. Chem.* **76**, 837.

- Libowitz, G.G., 1972b, Solid State Properties of Metallic and Saline Hydrides, in: L.E.J. Roberts, ed., MTP International Review Science, Vol. 10: Solid State Chemistry, (Butterworth, London) pp. 79-116.
- Libowitz, G.G., 1976, Metal Hydrides for Energy Storage, in: C. Stein, ed., Critical Materials Problems in Energy Production, (Academic Press, N.Y.) pp. 825-852.
- Lieberman, M.L. and P.G. Wahlbeck, 1965, J. Phys. Chem. **69**, 3514.
- Lindsay, R., R.O. Moyer, Jr., J.S. Thompson and D. Kuhn, 1976, Inorg. Chem. **15**, 3050.
- Lundin, C.E. and J.P. Blackledge, 1962, J. Electrochem. Soc. **109**, 838.
- Lundin, C.E., 1966, Trans. Met. Soc. AIME **236**, 978.
- Lundin, C.E., 1968a, Trans. Met. Soc. AIME **242**, 903.
- Lundin, C.E., 1968b, Trans. Met. Soc. AIME **242**, 1161.
- Lyle, S.J., P.T. Walsh and A.D. Witts, 1975, J. Chem. Soc. Dalton Transactions, 1406.
- Maeland, A.J. and A.F. Andresen, 1968, J. Chem. Phys. **48**, 4660.
- Maeland, A.J., 1970, J. Chem. Phys. **52**, 3952.
- Maeland, A.J. and D.E. Holmes, 1971, J. Chem. Phys. **54**, 3979.
- Maeland, A.J., A.F. Andresen and K. Videm, 1976, J. Less-Common Metals **45**, 347.
- Mansmann, M. and W.E. Wallace, 1964, J. Phys. (Paris) **25**, 454.
- Maurin, J.F., 1965, Study of the Hydrides of Erbium and Yttrium, Centre d'Etudes Nucleaires, Report No. NT/ACC-65/06.
- McQuillan, A.D., 1976, J. Less-Common Metals **49**, 431.
- Messer, C.E. and K.I. Hardcastle, 1964, Inorg. Chem. **3**, 1327.
- Messer, C.E., T.Y. Cho and T.R.P. Gibb, Jr., 1967, J. Less-Common Metals **12**, 411.
- Messer, C.E. and G.W. Hung, 1968, J. Phys. Chem. **72**, 3958.
- Messer, C.E. and P.C. Gianoukos, 1968, J. Less-Common Metals, **15**, 377.
- Messer, C.E. and M.K. Park, 1972, J. Less-Common Metals **26**, 235.
- Miedema, A.R., K.H.J. Buschow and H.H. vanMal, 1976, J. Less-Common Metals **49**, 463.
- Mikheeva, V.I. and M.E. Kost, 1969, Dokl. Akad. Nauk SSSR **189**, 553.
- Mintz, M.H., Z. Hadari and M. Bixon, 1974, J. Less-Common Metals **37**, 331.
- Mintz, M.H., D. Hiershler and Z. Hadari, 1976, J. Less-Common Metals **48**, 241.
- Mott, N.F. and H. Jones, 1958, The Theory and Properties of Metals and Alloys, (Dover Publications, Inc., New York) p. 267.
- Mueller, W.M., 1968, The Rare Earth Hydrides, in: Mueller, W.M., J.P. Blackledge and G.G. Libowitz, eds., Metal Hydrides, (Academic Press, N.Y.) Chap. 9, pp. 384-440.
- Mulford, R.N.R. and C.E. Holley, Jr., 1955, J. Phys. Chem. **59**, 1222.
- Mulford, R.N.R., 1958, Los Alamos Scientific Laboratory, U.S. Atomic Energy Commission Report No. AECU-3813.
- Mustachi, A., 1974, J. Phys. Chem. Solids **35**, 1447.
- Newkirk, H.W., 1976, Hydrogen Storage by Binary and Ternary Intermetallics for Energy Applications - A Review, Lawrence Livermore Laboratory, Livermore, CA, Report No. UCRL-V 52110.
- Oesterreicher, H., J. Clinton and H. Bittner, 1976, Mat. Res. Bull. **11**, 1241.
- Opyrchal, J. and Z. Bieganski, 1976, Solid State Comm. **20**, 261.
- Parks, C.D. and W.G. Bos, 1970, J. Solid State Chem. **2**, 61.
- Pebler, A. and W.E. Wallace, 1962, J. Phys. Chem. **66**, 148.
- Perkins, F.C. and C.E. Lundin, 1968, J. Electrochem. Soc. **115**, 21.
- Peterson, D.T. and J.A. Straatmann, 1966, J. Phys. Chem. **70**, 2980.
- Peterson, D.T., T.J. Poskie and J.A. Straatmann, 1971, J. Less-Common Metals **23**, 177.
- Pickart, S.J., 1968, Bull. Am. Phys. Soc. **13**, 573.
- Rozenfeld, B. and E. Debowska, 1975, Acta Phys. Pol. A, **A47**, 37.
- Rush, J.J., H.E. Flotow, D.W. Connor and C.L. Thaper, 1966, J. Chem. Phys. **45**, 3817.
- Rush, J.J., 1976, Private Communication.
- Sabin, V.I., R.A. Andrievskii, V.V. Gorbachev and A.D. Tsyganov, 1972, Fiz. Tverd. Tela **14**, 3320.
- Schreiber, D.S. and R.M. Cotts, 1963, Phys. Rev. **131**, 1118.
- Shenoy, G.K., B.D. Dunlap, D.G. Westlake and A.E. Dwight, 1976, Phys. Rev. **B14**, 41.
- Sieverts, A. and A. Gotta, 1928, Z. Anorg. Allg. Chem. **172**, 1.
- Singh, B., N.A. Surplice and J. Müller, 1976, J. Phys. D.: Appl. Phys. **9**, 2087.
- Somenkov, V.A., I.R. Entin, M.E. Kost and S. Sh. Shilshtein, 1975, Fiz. Tverd. Tela **17**, 2368.
- Stalinski, B., 1957a, Bull. Acad. Pol. Sci., Cl. III **5**, 997.
- Stalinski, B., 1957b, Bull. Acad. Pol. Sci. Cl. III **5**, 1001.
- Stalinski, B., 1959, Bull. Acad. Pol. Sci. Ser. Sci. Chim. **7**, 269.
- Stalinski, B., O.J. Zogal and H. Drulis, 1969, Bull. Acad. Pol. Sci., Ser. Sci. Chim. **17**, 121.
- Steward, S.A., J.F. Lakner and F. Uribe, Storage of Hydrogen Isotopes in Intermetallic Compounds, 1977, in J.B. Goodenough and M.S. Whittingham, eds., Solid State Chemistry of Energy Conversion and Storage (Advances in Chemistry series No. 163, American Chemical Society, Washington, D.C.) chap. 16, pp. 284-297.
- Streck, R. and K. Dialer, 1960, Z. Anorg. Allg. Chem. **306**, 141.
- Sturdy, G.E. and R.N.R. Mulford, 1956, J. Amer. Chem. Soc. **78**, 1083.

- Switendick, A.C., 1971, *Int. J. Quant. Chem.* **5**, 459.
- Switendick, A.C., 1974, Hydrogen in Metals - A New Theoretical Model, in: Veziroglu, T.N. ed., *Proceedings of the Hydrogen Economy Miami Energy Conference*, (Univ. of Miami, Coral Gables, Fla.) pp. S6-1 to S6-12.
- Thompson, J.S., R.O. Moyer, Jr. and R. Lindsay, 1975, *Inorg. Chem.* **14**, 1866.
- Titcomb, C.G., A.K. Cheetham and B.E.F. Fender, 1974, *J. Phys. C: Solid State Phys.* **7**, 2409.
- Toma, H., Rare Earth Information Center News, 1975, Iowa State Univ., Ames, Iowa, Vol. X, No. 1, March 1.
- van Mal, H.H., K.H.J. Buschow and A.R. Miedema, 1974, *J. Less-Common Metals* **35**, 65.
- van Mal, H.H., 1976, *Philips Res. Repts. Suppl.*, No. 1.
- van Vucht, J.H.N., F.A. Kuijpers and H.C.A.M. Bruning, 1970, *Philips Res. Repts.* **25**, 133.
- van Vucht, J.H.N. and K.H.J. Buschow, 1976, *J. Less-Common Metals* **46**, 133.
- Viallard, R., 1960, Kinetic Studies of Hydride Formation of the Lanthanides, in: *Proceedings 4th International Symposium on Reactivity of Solids*, Amsterdam, p. 168.
- Viallard, R. and J.N. Daou, 1973, *Hydrogène Met., Comp. Int.*, 1972, **1**, 123.
- Vorderwisch, P. and S. Hautecler, 1974a, *Phys. Status Solidi(b)*, **64**, 495.
- Vorderwisch, P. and S. Hautecler, 1974b, *Phys. Status Solidi(b)* **66**, 595.
- Vorderwisch, P., S. Hautecler and H. Deckers, 1974, *Phys. Status Solidi(b)* **65**, 171.
- Wallace, W.E., Y. Kubota and R.L. Zanowick, 1963, Magnetic Characteristics of Gd, Tb, and Yb Hydrides in Relation to the Electronic Nature of the Lanthanide Hydrides, in: *Nonstoichiometric Compounds, Advances in Chemistry Series No. 39*, (American Chemical Society, Washington, D.C.) pp. 122-130.
- Wallace, W.E. and K.H. Mader, 1968, *J. Chem. Phys.* **48**, 84.
- Wallace, W.E., 1972, *Ber. Bunsenges. Phys. Chem.* **76**, 832.
- Warf, J.C. and K.I. Hardcastle, 1966, *Inorg. Chem.* **5**, 1736.
- Weaver, H.T., 1972a, *Phys. Rev.* **B5**, 1663.
- Weaver, H.T., 1972b, *J. Chem. Phys.* **56**, 3193.
- Yajima, S., 1974, Japanese Patent Application No. 7481342, July 16.
- Yannopoulos, L.N., R.K. Edwards and P.G. Wahlbeck, 1965, *J. Phys. Chem.* **69**, 2510.
- Zaheer, A.H., W.G. Bos and P.J. Ouseph, 1976, *J. Inorg. Nucl. Chem.* **38**, 103.
- Zanowick, R.L. and W.E. Wallace, 1962, *Phys. Rev.* **126**, 537.
- Zijlstra, H. and F.F. Westendorp, 1969, *Sol. State. Comm.* **7**, 857.

Chapter 27

THE BINARY RARE EARTH OXIDES

LeRoy EYRING

Department of Chemistry and the Center for Solid State Science, Arizona
 State University, Tempe, Arizona 85281, USA

Contents

1. Introduction	338
2. Stable phases in the rare earth oxides and their structures	340
2.1. The lower oxides	340
2.2. The sesquioxides	340
2.3. The higher oxides	352
3. Hysteresis and pseudophase formation	364
4. Thermodynamics	366
5. Phase reactions in rare earth oxides	374
5.1. Material transport in rare earth oxides	376
6. The tarnishing of rare earth metals by oxygen	381
7. Growth of single crystals and the preparation of special specimen forms	382
7.1. The Verneuil method	382
7.2. Flux growth	383
7.3. Hydrothermal growth	383
7.4. Miscellaneous observations	383
7.5. Preparation of sintered transparent polycrystalline materials	384
8. The physical properties of the rare earth oxides	385
8.1. The electrical properties of the rare earth oxides	385
8.2. Magnetism in rare earth oxides	388
8.3. Optical properties of the rare earth oxides	391
8.4. Mechanical and thermal properties	393
References	394

Symbols

A = hexagonal A-type sesquioxide
B = monoclinic B-type sesquioxide
C = cubic C-type sesquioxide
D = selfdiffusion coefficient
H = high temperature hexagonal sesquioxide
X = high temperature cubic sesquioxide
Z = atomic number
k = rate constant
n = inter denoting a member of a homologous series
u = structural parameter
x = a variable ratio of oxygen atoms to metal atoms
$\alpha = \text{RO}_x, 1.72 \leq x \leq 2.0$
$\beta = \text{R}_{12}\text{O}_{22}$
$\delta = \text{R}_{11}\text{O}_{20}$; deviation from stoichiometry
$\epsilon = \text{R}_{10}\text{O}_{18}$
$\zeta = \text{R}_9\text{O}_{16}$
$\iota = \text{R}_7\text{O}_{12}$
$\mu = 10^{-6} \text{ m}$; electron mobility
$\sigma = \text{RO}_x, 1.5 \leq x \leq 1.71$; electrical conductivity
$\varphi = \text{R}_2\text{O}_3$
χ = magnetic susceptibility
CN = coordination number
C_p = molar heat capacity
D_0 = diffusion constant
E_a = energy of activation
t_i = transference number
ΔG_{f298}^0 = standard free energy of formation at 298 K
ΔH = high temperature enthalpy of reaction
ΔH_{f298}^0 = standard enthalpy of formation at 298 K

$\bar{\Delta H}_{O_2}$ = partial molar enthalpy of solution of oxygen

$\Delta H_{T_0}^0$ = standard enthalpy of reaction at T K

ΔS_{T_0} = standard entropy of reaction at T K

OR_4 = oxygen coordination tetrahedra

S_{298}^0 = molar entropy at 298 K

$\square R$ = vacant cation position

$\square O$ = vacant oxygen position

$\square O_6$ = octahedrally coordinated anion vacancy

$\square R_6$ = octahedral voids in the fluorite structure

1. Introduction

The dominating theme of this chapter is a delineation of the full range of binary rare earth oxide phases known to exist together with their concomitant structural, thermodynamic and dynamic characteristics. In addition, some physical properties not covered in other chapters of this Handbook will be stressed to give, if not a balanced picture, at least a broad view of the solid state chemistry of these interesting model materials.

Frequently a prototype of nature is imagined and studies of real systems are undertaken whose results are then used to fill in the idealized image. In such cases the structures derived are those of perfectly ordered materials, the stable compositions are neatly stoichiometric line phases and the mechanisms of reaction consist of simple steps involving obvious species. The result is a carefully edited image of things as they might have been. Such activities have been very useful in laying the foundations but now they are apt to obscure the facts and impede progress in arriving at a more complete and realistic picture of solid state reactions. It is vital that coherent systems which will serve as models be relentlessly pursued until they reveal the full dimension of their deviations from such pat stereotypes and reveal their true natures. It is ugly business but it must be done. The rare earth oxides have the variety to serve such a purpose and in describing them it will be possible to illustrate the state of knowledge available on a series of related real materials.

The rare earths as used here include the fifteen lanthanide elements and scandium and yttrium. This large group of elements with measured differences provides one of the best sources available for studying developing chemical and physical characteristics. They do not possess the full range of solid state properties but they will be appreciated as one of the best of model systems since they provide subtle variations in properties which may be utilized to test hypotheses or theories.

In addition to their intrinsic theoretical interest and as models for other systems, the oxides of the rare earths have many practical uses. They are receiving attention in industry because of their potential use as control rods for nuclear reactors where samarium, gadolinium and europium oxides are incorporated into cermetts or are used in fuel elements as burnable poisons. Radioactive europium and thulium oxides are used as heat sources and promethium oxide as a β source. Lanthanide oxide catalysts may be

combined as phosphors for improved cathodoluminophors in color TV and electrooptic components. In addition they find use in glass making and grinding, alloys and composites, lasers and phosphors.

Certain aspects of the rare earth oxides have been reviewed in the past several years by Eyring and Holmberg (1963); Brauer (1964, 1966, 1968); Eyring (1967); Westrum (1967); Eyring (1970a, b, 1974) and Samsonov and Gil'man (1974). Nevertheless none of these are adequate to the purposes set forth above.

At moderate temperatures any compound of oxygen with a rare earth atom is a solid. The solid state chemistry of an atom in combination with oxygen depends primarily upon its electronic configuration and size. In the lanthanide series of elements the outer valence electrons (the $5d^1$ and $6s^2$ electrons) are effectively shielded from the increasing nuclear charge as electrons are added to the $4f$ orbitals. This results in a trivalent state for all the lanthanides whose energy changes slowly across the series. The size of the atom in combination with oxygen contracts smoothly across the series to produce oxides related to each other in more or less predictable ways. Figure 27.1 illustrates this principle for the main sequence oxides. The data are obtained from Eyring and Holmberg (1963); Templeton and Dauben (1954); Barbezat and Loriers (1952) and Stecura and Campbell (1961). The combination of electronic configuration and size of the lanthanide atoms results in their oxides being among the most thermally stable of all known substances. The nature of the chemical bond varies over each series. It has been proposed that there is a substantial degree of covalence (Jørgensen et al., 1964, 1965; Caro, 1968; Sanderson, 1971) mixed with the predominant ionic character.

Although electrons in the f orbitals are not strongly involved in the formation of compounds they do have a definite second order effect upon the chemical properties. They facilitate, for instance, the valence states other than three

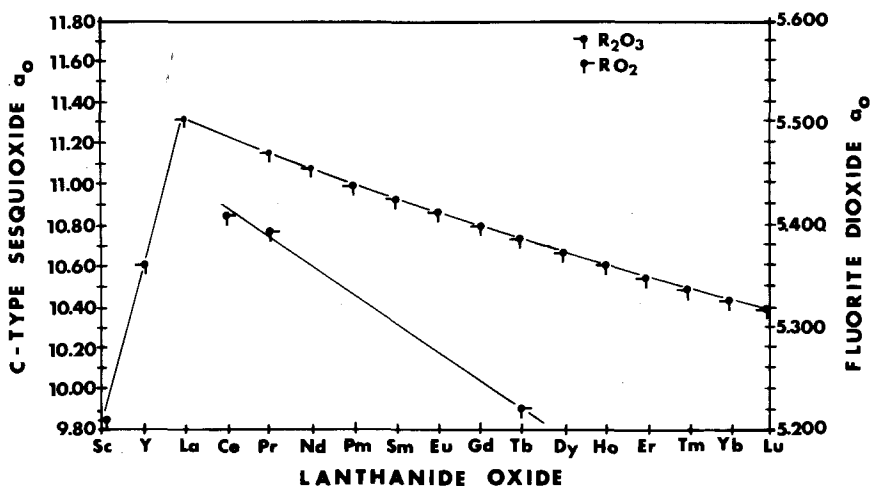


Fig. 27.1. Lattice parameters for the cubic rare earth oxides.

which occur (i.e., divalent samarium, europium and ytterbium; tetravalent cerium, praseodymium and terbium) since, as Hund observed, the energy of the f electronic states changes significantly near the zero, half and completely filled condition.

The filling of the f orbitals according to Hund's rule results in the presence of widely varying numbers of unpaired electron spins. Consequently the oxides have progressive and varied magnetic properties. Indeed, the lanthanide elements and their compounds were the proving ground for the elaboration of the theory of magnetism (Van Vleck, 1965, 1966).

2. Stable phases in the rare earth oxides and their structures

The composition of any rare earth oxide depends upon the temperature, oxygen activity and whether or not it is in equilibrium or metastable equilibrium. The metal will take up oxygen at low temperatures but little is known about ordered-distinct phases very rich in metal (see section 6). At higher oxygen pressures separate oxide phases appear depending upon the particular rare earth under consideration. It will be our purpose in these paragraphs to discuss these phases and their interrelationships. Table 27.1 lists the established phases of the rare earth oxides together with some structural parameters. This list does not include a number of phases which have been reported but not confirmed. Others, especially polymorphs of the intermediate phases will become established.

2.1. *The lower oxides*

A NaCl-type monoxide has been reported for virtually all the rare earth elements. Gradually, however, these have been shown to be ternary phases stabilized by nitrogen or carbon or both (Felmlee and Eyring, 1968; Work and Eick, 1972). At present only EuO and YbO (Eick et al., 1956; Fishel et al., 1970) remain undisputed. EuO is well established, its preparation and range of phase stability is described by Shafer et al. (1972) and more will be said about its properties below and especially in Vol. 2, Chapter 19. YbO has been prepared by a low temperature technique.

Eu₃O₄ is orthorhombic (Bärnighausen and Brauer, 1962; Rau, 1966) of space group *Pnam*. A discussion of methods and results of lower oxide preparation has been offered by Brauer (1966) and more recently by McCarthy and White (1970). Bedford and Catalano (1971) have shown that EuO and Eu₃O₄ have very narrow ranges of composition.

2.2. *The sesquioxides*

2.2.1. *Polymorphism*

All the rare earth elements, under suitable conditions, form a sesquioxide. Polymorphism is common and no fewer than five distinct crystalline types have

been described. Below about 2000°C three types designated as Types A, B and C are commonly observed (Goldschmidt et al., 1925) while above that temperature types designated as H or X are formed (Foëx and Traverse, 1966a; Traverse, 1971; Chikalla et al., 1972). Figure 27.2 illustrates the observed temperature regions of stability of the various polymorphic forms. Observe that in the central region all five polymorphic forms may be exhibited by one oxide. For example, C-type Eu_2O_3 would transform to B-type at $\sim 1100^\circ\text{C}$, to A-type at $\sim 2040^\circ\text{C}$ to H-form at $\sim 2140^\circ\text{C}$ to X-form at $\sim 2280^\circ\text{C}$ before melting at $\sim 2340^\circ\text{C}$. (C \rightarrow B conversion has been observed by X-ray in Eu_2O_3 by abrasion of a pellet on coarse abrasive paper (Ross and Gibby, 1974).)

On the other hand all the rare earths have been reported formed in the C-form oxide although from Nd_2O_3 to La_2O_3 they are probably metastable (Felsche, 1969) or stabilized in that form by impurities. Brauer and Mohr-Rosenbaum (1972) discuss the existence of C-type for the light rare earth oxides. Brauer (1966) had reviewed the status of this work earlier. Structural and kinetic transformation studies have been carried out on the C-type to either the B or A-type. Activation energies were also obtained (Stecura, 1965).

Studies of polymorphism have yielded markedly varying results over the years due to a variety of starting materials sometimes with water present, varying purities of the rare earths and occasionally mistaken identity of the product.

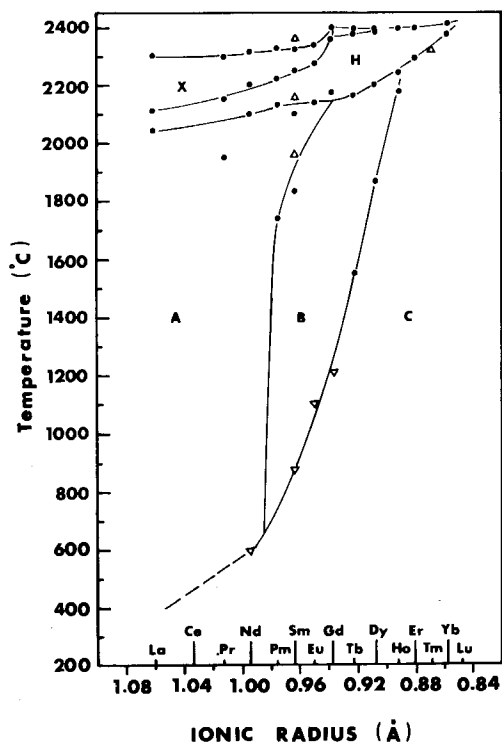


Fig. 27.2. Polymorphic forms and transition temperatures of the rare earth sesquioxides (after Coutures et al., 1975).

TABLE
Lattice parameters of established

Oxide	n in R_nO_{2n-2} (phase name)	Color	Lattice type	Lattice parameter (\AA)	Symmetry
$\text{LaO}_{1.500}$	(sesquioxide)	white	Hex(A)	$a^2 = 3.938(3)$ $c = 6.128(5)$	$P6_3/mmm$
$\text{CeO}_{1.500}$	(sesquioxide)	white	Hex(A)	$a_0^3 = 3.8905(3)$ $c_0 = 6.0589(3)$	$P\bar{3}m1$
$\text{CeO}_{1.714}$	7 (iota)	blue black	Rhomb	$a_r^3 = 6.784$ $\alpha_r = 99.302^\circ$ Hexagonal representation $a_h = 10.3410(7)$ $c_h = 9.6662(6)$	$R\bar{3}$
$\text{CeO}_{1.778}$	9 (zeta)	dark blue			
$\text{CeO}_{1.800}$	10 (epsilon)	dark blue			
$\text{CeO}_{1.818}$	11 (delta)	dark blue			
CeO_2	∞ (dioxide)	pale yellow	fcc(F)	$a_0 = 5.4109(3)$	$Fm\bar{3}m$
$\text{PrO}_{1.5}$	4 (phi)	yellow light green	bcc(C) Hex(A)	$a_0^4 = 11.152(2)$ $a^2 = 3.857(3)$ $c = 6.016(5)$ $a^5 = 11.070$	$Ia\bar{3}$ $P\bar{3}m1$
$\text{PrO}_{1.65}$	(sigma)	black	bcc		
$\text{PrO}_{1.714}$	7 (iota)	black	rhomb	$a^4 = 6.741(3)$ $\alpha = 99.28^\circ$	$R\bar{3}$
$\text{PrO}_{1.778}$	9 (zeta)	black	triclinic	$\alpha^6 = 6.5$ $b = 8.4$ $c = 6.5$ $\alpha = 97.3^\circ$ $\beta = 99.6$ $\gamma = 75.0$	
$\text{PrO}_{1.800}$	10 (epsilon)	black	monoclinic	$a = 6.728(4)$ $b = 19.319(12)$ $c = 15.480(10)$ $\beta = 125.46(4)^\circ$	$(P2_1/C)$
$\text{PrO}_{1.818}$	11 (delta)	black	monoclinic	$a^7 = 6.7$ $b = 42.4$ $c = 15.5$ $\beta = 125.2^\circ$	
$\text{PrO}_{1.826}$	(alpha)	black	fcc	$a_0^4 = 5.469(1)$	

27.1.
phases of the rare earth oxides

Pseudo cell	Crystal radius ¹ CN = 6	Relation to basic structure	Relative volume	No. of vacancies/unit cell (fraction of oxygens missing)
	1.172			
	1.15			
Rhombohedral $a_F = 5.5443(4)$ $\alpha_F = 89.642(0)^\circ$		$a = a_F + \frac{1}{2}b_F - \frac{1}{2}c_F$	7/4	2 (1/7)
Triclinic $a_F^{\frac{1}{2}} = 5.5106(12)$ $b_F = 5.5155(12)$ $c_F = 5.5213(12)$ $\alpha_F = 90.339(0)^\circ$ $\beta_F = 90.595(0)^\circ$ $\gamma_F = 90.204(0)^\circ$				(1/9)
Triclinic $a_F = 5.5076(9)$ $b_F = 5.5100(9)$ $c_F = 5.5112(8)$ $\alpha_F = 90.360(0)^\circ$ $\beta_F = 90.176(0)^\circ$ $\gamma_F = 90.160(0)^\circ$				(1/10)
Rhombohedral $a_F = 5.5023(7)$ $\alpha_F = 89.762(0)^\circ$				(1/11)
	1.11(VIII)	$a = a_F$	1	0 (0)
	1.13	$a = 2a_F$	8	16 (1/4)
$a = 5.5096(5)$ $\alpha = 89.63^\circ$ $a^4 = 5.478(1)$ $b = 5.482(1)$ $c = 5.496(1)$ $\alpha = 90.15^\circ$ $\beta = 90.50^\circ$ $\gamma = 90.91^\circ$		$a = a_F + \frac{1}{2}b_F - \frac{1}{2}c_F$	7/4	2 (1/7)
triclinic $a = b = c = 5.4820(5)$ $\alpha = \beta = 90.28^\circ$ $\gamma = 90.09^\circ$		$a = a_F + \frac{1}{2}b_F - \frac{1}{2}c_F$ $b = \frac{3}{2}b_F + \frac{1}{2}c_F$ $c = \frac{1}{2}a_F - \frac{1}{2}b_F + c_F$	9/4	2 (1/9)
triclinic $a^4 = 5.473$ $b = 5.474$ $c = 5.475$ $\alpha = \beta = \gamma = 90.09^\circ$		$a = a_F + \frac{1}{2}b_F - \frac{1}{2}c_F$ $b = \frac{3}{2}(-b_F - c_F)$ $c = 2(-b_F + c_F)$	10	8 (1/10)
			(22)	(16) (1/11)

TABLE

Oxide	n in R_nO_{2n-2} (phase name)	Color	Lattice type	Lattice parameter (Å)	Symmetry
PrO _{1.833}	12 (beta)	black	monoclinic	$a^8 = 6.6874$ $b = 11.602$ $c = 15.470$ $\beta = 125.257^\circ$	(P2 ₁ /n)
PrO ₂	∞ (dioxide)	black	fcc(F)	$a_0^4 = 5.3932(5)$	Fm3m
NdO _{1.500}		light blue	Hex(A)	$a^2 = 3.829(3)$ $c = 6.002(5)$	P6 ₃ /mmm
PmO _{1.500}	4		bcc(C)	$a^{10} = 11.080$	Ia3
	4		bcc(C) monoclinic(B)	$a^9 = 10.99$ $a = 14.22$ $b = 3.65$ $\beta = 100.10^\circ$	Ia3 C2/m
SmO _{1.500}	4(phi)		Hex(A)	$a = 3.802$ $c = 5.954$	P3ml
			bcc(C) monoclinic(B)	$a^{10} = 10.934$ $a^{11} = 14.177$ $b = 3.633$ $c = 8.847$ $\beta = 99.96^\circ$	Ia3 C2/m
EuO		dark red	rock salt	$a^{12} = 5.1439(5)$	Fm3m
EuO _{1.33}		black	orthorhombic	$a^{13} = 10.094(3)$ $b = 12.068(3)$ $c = 3.500(1)$	Pnam
EuO _{1.500}	4	white	bcc(C)	$a^{14} = 10.869$	Ia3
		white	monoclinic	$a^{14} = 14.082$ $b = 3.604$ $c = 8.778$ $\beta = 100^\circ 00'$	C2/m
GdO _{1.500}	4	white	bcc(C)	$a^{10} = 10.8122$	Ia3
		white	monoclinic(B)	$a^{15} = 14.061(13)$ $b = 3.566(6)$ $c = 8.760(7)$ $\beta = 100.10(8)^\circ$	C2/m
TbO _{1.500}	4	white	bcc(C)	$a^{16} = 10.7281(5)$	Ia3
		white	monoclinic(B)	$a^2 = 14.04(1)$ $b = 3.541(3)$ $c = 8.725(8)$ $\beta = 100.06(5)^\circ$	C2/m
TbO _{1.714}	7 (iota)	brown	rhomb	$a^{16} = 6.509(2)$	R3
TbO _{1.809}	10 $\frac{1}{3}$		triclinic	$\alpha = 99^\circ 21'(5)$ $a^6 = 13.8$ $b = 16.2$ $c = 12.1$ $\alpha = 107.4^\circ$ $\beta = 100.1^\circ$ $\gamma_6 = 92.2$	
TbO _{1.818}	11	dark brown	triclinic	$a^6 = 6.5$ $b = 9.9$ $c = 6.5$ $\alpha = 90.0^\circ$ $\beta = 99.6^\circ$ $\gamma = 96.3^\circ$	

27.1 (Contd.)

Pseudo cell	Crystal radius ¹ CN = 6	Relation to basic structure	Relative volume	No. of vacancies/unit cell (fraction of oxygens missing)
triclinic $a^4 = b = 5.466$ $c = 5.465$ $\alpha = \beta = \gamma = 90.08^\circ$		$a = a_F + \frac{1}{2}b_F - \frac{1}{2}c_F$ $b = \frac{3}{2}(-b_F - c_F)$ $c = 2(-b_F + c_F)$	6	4 (1/12)
	1.10(VIII)	$a = a_F$	1	0 (0)
	1.123	$a = 2a_F$	8	16
	1.11	$a = 2a_F$	8	16
	1.098	$a = 2a_F$	8	16 (1/4)
	1.31			
	1.087	$a = 2a_F$	8	16 (1/4)
	1.078	$a = 2a_F$	8	16 (1/4)
	1.063	$a = 2a_F$	8	16 (1/4)
$a_F = 5.319(1)$ $\alpha = 89^\circ 41'$		$a = a_F + \frac{1}{2}b_F - \frac{1}{2}c_F$	7/4	2 (1/7)
		$a = -\frac{1}{2}a_F + \frac{5}{2}c_F$ $b = -2a_F - 2b_F - c_F$ $c = 2a_F - b_F$	31/2	12 (1/10 $\frac{1}{2}$)
		$a = a_F + \frac{1}{2}b_F - \frac{1}{2}c_F$ $b = -\frac{1}{2}a_F + \frac{3}{2}b_F + c_F$ $c = \frac{1}{2}a_F - \frac{1}{2}b_F + c_F$	11/4	2 (1/11)

TABLE

Oxide	n in R_nO_{2n-2} (phase name)	Color	Lattice type	Lattice parameter (Å)	Symmetry
TbO _{1.833}	12		monoclinic	$a^6 = 6.7$ $b = 23.2$ $c = 15.5$ $\beta = 125.2^\circ$	(Pn)
TbO _{1.95}	∞	dark brown	fcc(F)	$a^{16} = 5.220$	Fm3m
DyO _{1.500}	4(phi)	white	bcc(C)	$a^{10} = 10.6647$	Ia3
		white	monoclinic(B)	$a^2 = 13.97(1)$ $b = 3.519(3)$ $c = 8.661(8)$ $\beta = 100.00(5)^\circ$	C2/m
HoO _{1.500}	4(phi)	white	bcc(C)	$a^{10} = 10.6065$	Ia3
			monoclinic(B)	$a^2 = 13.90(1)$ $b = 3.492(3)$ $c = 8.592(8)$ $\beta = 99.98(5)^\circ$	C2/m
YO _{1.500}	4(phi)	white	bcc(C)	$a^{10} = 10.6021$	Ia3
			monoclinic(B)	$a^2 = 13.91(1)$ $b = 3.483(3)$ $c = 8.593(8)$ $\beta = 100.15(5)^\circ$	C2/m
ErO _{1.500}	4(phi)	pink	bcc(C)	$a^{10} = 10.5473$	Ia3
			monoclinic(B)	$a^2 = 13.87(1)$ $b = 3.470(3)$ $c = 8.555(8)$ $\beta = 100.17(5)^\circ$	C2/m
TmO _{1.500}	4(phi)	white	bcc(C)	$a^{10} = 10.4866$	Ia3
			monoclinic(B)	$a^2 = 13.81(1)$ $b = 3.447(3)$ $c = 8.505(8)$ $\beta = 100.20(5)^\circ$	C2/m
YbO _{1.500}	4(phi)	white	bcc(C)	$a^{10} = 10.4334$	Ia3
			monoclinic(B)	$a^2 = 13.73(1)$ $b = 3.425(3)$ $c = 8.452(8)$ $\beta = 100.17(5)^\circ$	C2/m
LuO _{1.500}	4(phi)	white	bcc(C)	$a^{10} = 10.3907$	Ia3
			monoclinic(B)	$a^2 = 13.70$ $b = 3.410$ $c = 8.425$ $\beta = 100.22^\circ$	C2/m
ScO _{1.500}	4(phi)	white	bcc(C)	$a^{17} = 9.849(1)$	Ia3

¹Shannon, R.D., *Acta Cryst.* (1976).²Hoekstra, H.R., *Inorg. Chem.* **5**, 754 (1966).³Height, T.M. and D.J.M. Bevan, private communication (1976).⁴Sawyer, J.O., B.G. Hyde and L. Eyring, *Bull. Soc. Chim. France* 1190 (1965).⁵Eyring, L. and N.C. Baenziger, *J. Appl. Phys.* **33**, 428 (1962).⁶Kunzmann, P. and L. Eyring, *J. Solid State Chem.* **14**, 229 (1975).⁷Tuenge, R.T. and L. Eyring, *J. Solid State Chem.* **29**, 165 (1979).⁸Lowenstein, M.Z., L. Kihlborg, K.H. Lau, J.M. Haschke and L. Eyring, *NBS Spec. Pub.* 364, 1972, 343.⁹Chikalla, T.D., C.E. McNeilly and F.P. Roberts, *J. Am. Ceram. Soc.* **55**, 428 (1972).

27.1. (Contd.)

Pseudo cell	Crystal radius ¹ CN = 6	Relation to basic structure	Relative volume	No. of vacancies/unit cell (fraction of oxygens missing)
		$a = a_F + \frac{1}{2}b_F - \frac{1}{2}c_F$ $b = 3(-b_F - c_F)$ $c = 2(-b_F + c_F)$	12	8 (1/12)
	1.02(VIII)	$a = a_F$	1	0
	1.052	$a = 2a_F$	8	16 (1/4)
	1.041	$a = 2a_F$	8	16 (1/4)
	1.040	$a = 2a_F$	8	16 (1/4)
	1.030	$a = 2a_F$	8	16 (1/4)
	1.020	$a = 2a_F$	8	16 (1/4)
	1.008	$a = 2a_F$	8	16 (1/4)
	1.001	$a = 2a_F$	8	16 (1/4)
	0.885	$a = 2a_F$	8	16 (1/4)

¹⁰Roth, R.S. and S.J. Schneider, J. Res. Natl. Bur. Std. **64A**, 309 (1960).¹¹Douglass, R.M. and E. Staritzky, Anal. Chem. **28**, 552 (1956).¹²Eick, H.A., N.C. Baenziger and L. Eyring, J. Am. Chem. Soc. **78**, 5147 (1967).¹³Bärnighausen, H. and G. Brauer, Acta Cryst. **15**, 1059 (1962).¹⁴Rau, R.C., in "Rare Earth Research II" (K. Vorres, ed.) (Gordon and Breach, New York, 1964) pp. 117.¹⁵Guentert, O.J. and R.L. Mozzi, Acta Cryst., **11**, 746 (1958).¹⁶Baenziger, N.C., H.A. Eick, H.S. Schuldt and L. Eyring, J. Am. Chem. Soc. **83**, 2219 (1961).¹⁷Norrestam, R., Arkiv. f. Kemi **29**, 343 (1968).

Some observations on the juxtaposition of regions of phase stability in fig. 27.2 are in order. Notice that the order of transition $C \rightarrow B \rightarrow A$ -type occurs for some Z as the temperature is increased or at constant temperature as Z is decreased. The $C \rightarrow B \rightarrow A$ -type transition occurs with an increase in coordination number ($6 \rightarrow (6 + 7) \rightarrow 7$), with a decrease in symmetry and with an increase in density all at odds with expectation for phase changes occurring with temperature increase.

It is clear that the radius ratios for the various structures are at critical values, hence the phase transformations as the rare earth atom is substituted in series in the sesquioxide. Furthermore there is some indication that these transformations may not be reversible at temperatures below 1200–1400°C where metal atom mobility is small. Reports to the contrary usually involve water or special starting material, hence provide an alternative transformation path (Shafer and Roy, 1959; Roth and Schneider, 1960; Warshaw and Roy, 1961; Brauer and Müller, 1963; Sastry et al., 1966a; Mehrotra et al., 1966; Glushkova and Bogdanov, 1965; Bogdanov and Rudenko, 1965; Chapin et al., 1965; Queyroux et al., 1966).

Whatever the cause of the anomalous behavior in the $C \rightarrow B \rightarrow A$ transformation as temperature is increased, the A (B or C) $\rightarrow H \rightarrow X$ appears to obey all the rules. In this case there is an overall symmetry increase and the density decreases. The structural details of the H and X phases are not fully elucidated. It has been observed (Traverse, 1971) that the c/a ratio decreases sharply as does the density as the A -form transforms to H . There is a sharp increase in both a and c but a increases more rapidly, reducing the ratio. Since the space group of H is unknown, one cannot say what changes in symmetry occur when it is formed from A but there is clearly an increase when the hexagonal H decomposes to cubic X . As with other high temperature reactions entropy changes are likely to be of utmost importance. One final observation on fig. 27.2 – the region of stability of each polymorph narrows at some point as the radius of the rare earth atom decreases until finally lutecium (and scandium) transforms directly from C -type to the melt.

The variation of the molar volumes of the polymorphs suggests a profound pressure dependence on the stability regions. The A and B -forms for example would be stabilized with respect to the C -form. Such has clearly been observed (Hoekstra and Gingerich, 1964; Sawyer et al., 1965a; Hoekstra, 1966). For example, at 35 kilobars or higher and 1000°C all the C -type lanthanides from Sm to Lu are in the B -form. Similar shifts occur in the $B \rightarrow A$ transition but the effect is very much less. The high pressure reactions appear to be universally reversible when the pressure is released and the specimens are annealed at 900°C for a few hours.

Few studies of the kinetics of phase transitions without composition change have been made. Stecura (1965) and Ainscough et al. (1975) studied the rate of the $C \rightarrow B$ transformation in Nd_2O_3 , Sm_2O_3 , Eu_2O_3 and Gd_2O_3 . The rate of the $C \rightarrow B$ transition of Eu_2O_3 was calculated by Ainscough et al. (1975) to be 0 at $1074 \pm 5^\circ C$. Above this temperature the rate was observed to be first order. The activation energy is much greater in hydrogen than in air.

The melting points of the sesquioxides are indicated in fig. 27.2. The temperature of solidification has been found by Coutures et al. (1975) to be anomalous for La_2O_3 , Gd_2O_3 and Lu_2O_3 defining clearly the ceric and yttric groups.

2.2.2. *Nonstoichiometry in the sesquioxides*

The composition of the sesquioxide phase depends upon the polymorphic form and its chemical environment. The C-type is the most subject to composition variability of the lower temperature forms. Miller and Daane (1965) produced partially reduced C-type rare earth oxides by codistilling and comelting the sesquioxides with their respective metals and determining the composition of the separated oxide phase by reoxidation to the sesquioxide. The compositions observed were $\text{GdO}_{1.495}$, $\text{YO}_{1.4991}$, $\text{ErO}_{1.489}$ and $\text{LuO}_{1.485}$. Density and X-ray diffraction studies led them to the conclusion that these were nonstoichiometric by loss of oxygen from normal oxygen sites. The oxides are deeply colored presumably from trapping-sites at the oxygen vacancies. Bedford and Catalano (1971) confirm oxygen loss from Yb_2O_3 at high temperatures in the presence of metal to yield $\text{YbO}_{1.495}$ which disproportionates below 1800°C to $\text{Yb} + \text{YbO}_{1.500}$. They also observed a variable composition $\text{EuO}_{1.5-\delta}$ phase down to $\text{EuO}_{1.45\pm 0.01}$ at 1500°C . Mueller-Buschbaum (1968) observed a dark $\text{LaO}_{1.5-\delta}$ with δ undetermined and Ackermann and Rauh (1971) found the congruent vaporizing species of lanthanum oxide from a tungsten effusion cell to be $\text{La}_2\text{O}_{2.980}$ at 2400 K and in rhenium $\text{La}_2\text{O}_{2.998}$ at 2427 K. They also (1973) found the composition of yttria to be $\text{Y}_2\text{O}_{2.89}$ at 2000 K. The noncongruent vaporization of La_2O_3 and Y_2O_3 resulting in a variation in the metal to oxygen ratio is discussed by Trevisan and Depaus (1973).

The composition of the sesquioxide on the hyperstoichiometric side depends very much on the particular oxide. The oxygen excess is small for any but those of cerium, praseodymium and terbium, where for the C-type it can be considerable. There are C-type phases of these latter oxides with composition near $\text{RO}_{1.70}$ (called σ phase). For most of the rare earths only the sesquioxide is known.

Of the sesquioxides perhaps least is known about Ce_2O_3 . Unless it is completely stoichiometric (and A-form) it can be pyrophoric hence preparation and protection from oxygen during study requires serious attention. Sata and Yoshimura (1968a, b) have prepared this material and have studied its chemical and physical properties including its melting point, thermal expansion, and electrical and magnetic properties.

2.2.3. *Structure and syntax of the sesquioxides*

The hexagonal A-type sesquioxide is of space group $\text{P}\bar{3}\text{mL}$ with one formula per unit cell (Pauling, 1928 and Koeller and Wollan, 1953a). The metal atoms are seven coordinated with four oxygens closer than the other three. The four oxygens are bonded to five metals and the three are bonded to four metal atoms.

The A-type structure of La_2O_3 and Nd_2O_3 has been found by Mueller-Buschbaum and Schnering (1965) and Mueller-Buschbaum (1966) to be more

complicated than previously considered. There were a variety of discrepancies in observations such as symmetries of X-ray patterns and systematic absences of certain reflections in the X-ray diffraction patterns. These have all been accounted for by assuming a statistical distribution of two lanthanum atoms over four sites and three oxygens over six sites in microtwinned domains. Neighboring domains, which occur in equal numbers, share faces leading to a higher symmetry of coordination of the lanthanum atoms than in the Pauling model. The high temperature crystal they studied was in the space group $P6_3/mmm$.

Monoclinic B-type sesquioxide with six formulae per unit cell has space group $C2/m$ (Douglass and Staritzky, 1956; Cromer, 1957). The metal atoms are seven- and six-coordinate.

Body-centered cubic C-type sesquioxide is of space group $Ia3$. The unit cell contains 32 metal atoms and 48 oxygen atoms. The metal atoms are six-coordinate. Table 27.1 contains the lattice parameters of the established crystal-line rare earth oxides.

There has been a recurrent debate concerning the actual structure of the C-type rare earth oxides which have been reexamined by X-rays and by neutron diffraction by several persons since the original determination by Pauling and Shappel (1930). This work has been reviewed by Brauer (1966). One of the main themes of the discussion was whether the structure included oxygen vacancies of about full atomic size with six-coordinated metal atoms of two types—one with oxygens missing across the body-diagonal of the coordination cube to give a distorted octahedron and three times as many with oxygens missing across the face diagonal (a strange unsymmetrical coordination). It appears that in spite of results to the contrary showing much more nearly regular octahedral coordination, the preponderance of evidence is for the Pauling structure.

It is useful to consider the relationships between the RO_2 dioxide on the one hand and the A, B and C-form sesquioxides on the other (Eyring and Holmberg, 1963). In the dioxide the metal atoms are eight-coordinate with cubic coordination polyhedra sharing all edges to form a three-dimensional chess-board network. If one-fourth of the oxygen atoms of this network are removed along nonintersecting strings in the four $\langle 111 \rangle$ directions such that every atom is six-coordinate, one has the C-type. In this case one-fourth of the atoms have oxygens missing across the body-diagonal of the coordination cube and three-fourths have oxygens missing across the face-diagonal where the strings come closest to intersection (see fig. 27.3a, b).

On the other hand if the oxygen substructure of the fluorite RO_2 is preserved intact but the metal atoms are moved into interstitial positions such that slabs of RO_2 two atom-layers wide are preserved but shear occurs at these regular intervals, the seven-coordinate A-type is formed. The B-type is very similar to the A-type with six- and seven-coordinate (see fig. 27.3c, d).

These basic structures may also be considered as arrays of OR_4 coordination tetrahedra in three dimensions. In the case of fluorite RO_2 there are sheets of edge sharing OR_4 tetrahedra pointing up and down along $\langle 111 \rangle$ which have

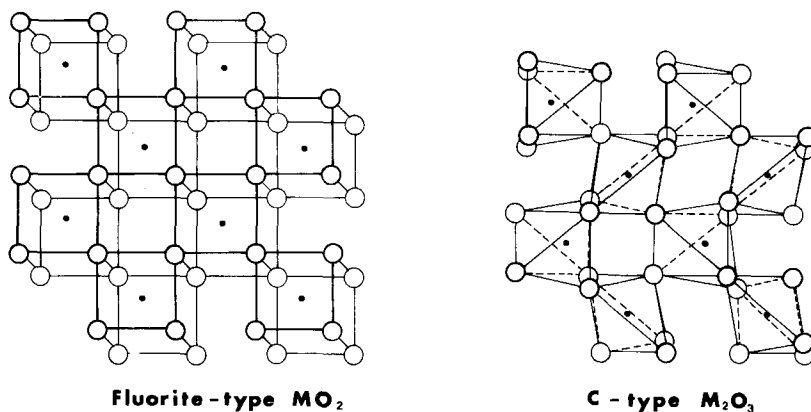


Fig. 27.3a, b. Representations of (a) fluorite-type RO_2 and (b) C-type R_2O_3 . The solid dot represents the metal atom (after Eyring and Holmberg, 1963).

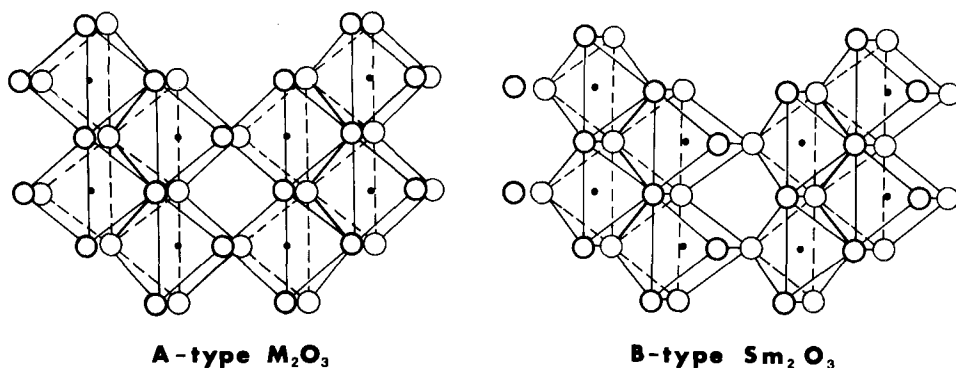


Fig. 27.3c, d. Representations of (c) A-type R_2O_3 and (d) B-type R_2O_3 . The solid dot represents the metal atom (after Eyring and Holmberg, 1963).

embedded in them empty edge-sharing octahedra, $\square\text{R}_6$. These, of course, are the tetrahedral and octahedral holes in a cubic close-packed array of metal atoms. The C-type structure is formed from this by the ordered removal of one-fourth of the oxygen atoms (tetrahedra) which results in the tetrahedra sharing four of their six edges in three dimensions (Caro, 1968). The A-type sesquioxide can be described as layers of $(\text{RO})_n^{n+}$ formed from edge-sharing OR_4 tetrahedra disposed in a two-dimensional hexagonal array perpendicular to the c -axis. These slabs stacked one above the other are separated by a layer of oxygen which does not destroy the hexagonal symmetry. In the monoclinic B-form sesquioxide the $(\text{RO})_n^{n+}$ layers of OR_4 tetrahedra are slipped slightly with respect to each other perpendicular to the c -axis destroying the hexagonal symmetry. These layer-structure characteristics particularly of the A- and B-form oxides are seen as

resulting from considerable covalent bonding of the atoms in the $(\text{RO})_n^{n+}$ sheets (Caro, 1968; Jørgensen et al., 1965).

Caro (1968) has observed the importance of these layers of $(\text{LnO})_n^{n+}$ as building blocks in a wide variety of compounds other than the A- and B-type sesquioxides where the slabs are separated by anions such as Cl^- , Br^- , CO_3^{2-} , S^{2-} , etc. This has been a fruitful idea but although application to the higher oxides has been attempted it does not appear to have usefulness in predicting the members of the homologous series or to suggest structures which are consistent with observation.

Phase transformation growth relationships and twinning in thin oxide films formed by the oxidation of metal films have been studied by electron microscopy (Caro et al., 1970; Boulesteix et al., 1971a). These studies have confirmed the structural relationships between the A-, B- and C-forms of sesquioxides. These investigations have been expanded to include topotactic observations in the $\text{C} \rightarrow (\text{B})$ A-type transition (Boulesteix et al., 1971b, c) in Nd_2O_3 . The B-type structure of Nd_2O_3 and Pr_2O_3 promoted in the transition disappears within minutes after formation by a Martensitic process. Boulesteix et al. (1972) and Boulesteix and Loier (1973) investigated the twinning laws in B-type sesquioxides especially numerous in Sm_2O_3 . Recently, Schiffmacher et al. (1976) have modeled the dislocation boundary between A- and B-type sesquioxides from high resolution structure images.

Hoskins and Martin (1975) have shown the polymorphic relationships of the sesquioxides in terms of their coordinated defect model. Their discussion adds new insight into possible ways of viewing these structures.

The structures of the hexagonal H- and cubic X-forms have not been determined, consequently their relationships to the low temperature phases are not known. Diffraction patterns have been observed for powder (Foëx and Traverse, 1966b) and for crystals which have been beam heated in the electron microscope (Boulesteix et al., 1971a).

2.3. *The higher oxides*

For those rare earth elements which have an energetically accessible oxidation state higher than three in the presence of oxygen, higher oxides in the composition range RO_x ($1.5 \leq x \leq 2.0$) are formed. The composition of these oxides depends entirely upon the temperature, oxygen fugacity, physical state and history of the preparation. Such oxide systems are firmly established only for Ce, Pr and Tb.

The dioxides exhibit the fluorite structure space group $\text{Fm}\bar{3}\text{m}$ containing four RO_2 per unit cell. The fluorite structure may be visualized as a cubic close-packed array of metal atoms with nonmetal atoms filling all the tetrahedral positions (fig. 27.4). Alternatively one may view it as RO_8 coordination cubes sharing all edges in a three-dimensional chess-board array or as OR_4 coordination tetrahedra sharing all edges in three dimensions. When oxygen is removed from this structure the crystalline products are fluorite-related either as

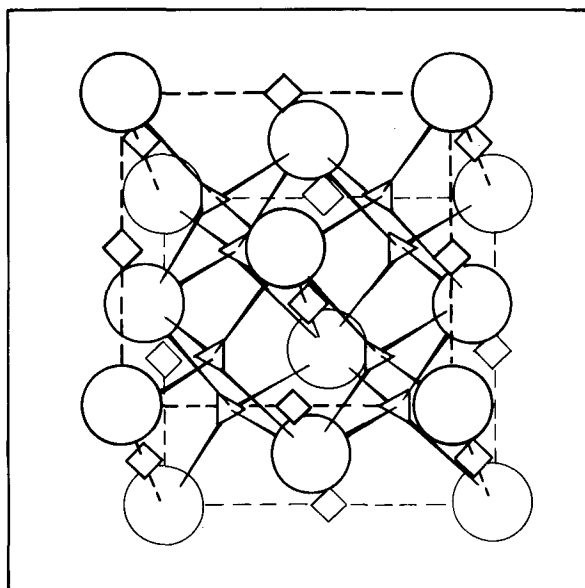


Fig. 27.4. The fluorite structure. The circles represent a close-packed array of metal atoms. The triangles represent the tetrahedral positions occupied by oxygen atoms and the squares mark the empty octahedral positions.

members of an homologous series of intermediate oxides having the generic formula R_nO_{2n-2} or as phases of functionally wide stoichiometric range $RO_{2-\delta}$ (α phase) or $R_2O_{3+\delta}$ (σ phase). The C-type sesquioxide of bixbyite structure described previously, is fluorite-related and the compositional end-member of the higher oxides. It is obvious that there is a great similarity between the oxide systems of Ce, Pr and Tb yet at the present state of knowledge the considerable differences in behavioral details preclude discussing them further as a group. Table 27.1 lists the members of the homologous series which have been observed up until the present in the three systems.

Maps of the new world evolved as exploration continued over the decades of the early Sixteenth Century from those correlating almost not at all with reality to some bearing a very great resemblance to modern maps. A feature such as the northwest passage in North America, evoked largely out of legend and hope, appeared on these evolving maps for scores of years and indeed was not cleared up for more than a century. Clarification of phase diagrams have a great similarity to geographical exploration and even with present techniques can take quite as long to accomplish as ancient quests.

2.3.1. *The cerium–oxygen system*

a. *Phase diagram* – When Brauer and coworkers (Brauer and Holtschmidt, 1951) began publication of their long series on the cerium oxide system a quarter century ago they cited work done more than a half-century earlier providing

pertinent information on this system. Now (in 1976) extensive work is still being done on the phase diagram of this system.

A phase diagram which correlates most of the direct phase analysis work which has been accomplished until the present has been suggested by Height and Bevan (1976) and is shown, in addition to work to be described later, in fig. 27.5. A striking feature of this system is that CeO_2 loses oxygen at lower temperatures depending upon the oxygen pressure to form certain members of the homologous series $\text{R}_n\text{O}_{2n-2}$ ($n = 4, 6(?), 7, 9, 10, 11$ and ∞). Each of the intermediate phases appears to decompose peritectoidally to yield a non-stoichiometric phase and an adjacent ordered phase except the ν -phase ($n = 7$) which decomposes to two distinct nonstoichiometric phases.

The peritectoid decomposition temperatures were observed to be ν , $1025 \pm$

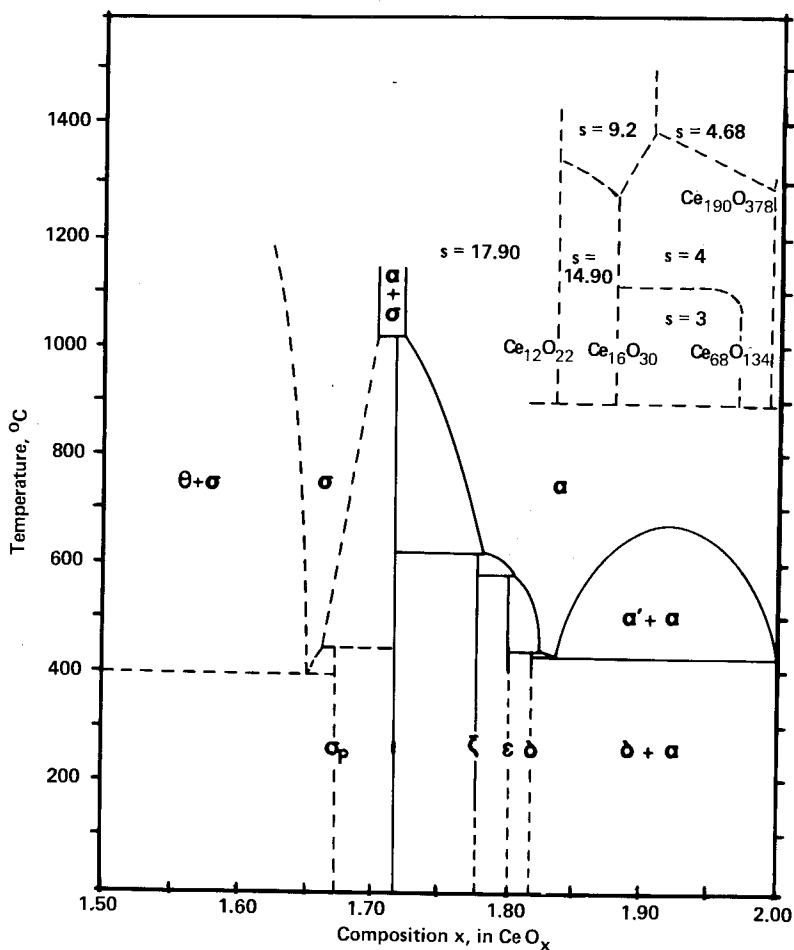


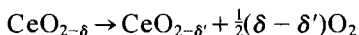
Fig. 27.5. The CeO_x phase diagram. Ordered phases are indicated by Greek letters and s denotes a region where the isotherms have the slope specified.

5°C; ζ , $625 \pm 10^\circ\text{C}$; ϵ , $585 \pm 10^\circ\text{C}$; δ , $445 \pm 10^\circ\text{C}$ and the $\delta + \alpha$ eutectoid occurs at $435 \pm 10^\circ\text{C}$.

At higher temperatures two nonstoichiometric phases, $\sigma(\text{Ce}_2\text{O}_{3+\delta})$ and $\alpha(\text{CeO}_{2-\delta})$, dominate the phase diagram. These appear in high temperature X-ray analysis to be bixbyite-related or fluorite-related respectively with widely varying lattice parameters.

The critical temperature in the $\alpha' + \alpha$ region was established by high temperature X-ray diffraction studies by Brauer and Gingerich (1960).

There have been many studies of the equilibrium dissociation of $\text{CeO}_{2-\delta}$ according to the equation



(Brauer and Holtschmidt, 1955; Brauer et al., 1960; Bevan and Kordis, 1964; Sata and Yoshimura, 1968a, b; Iwasaki and Katsura, 1971; Panlener et al., 1975) where the oxygen fugacity is usually fixed either by $\text{CO}|\text{CO}_2$ or $\text{H}_2|\text{H}_2\text{O}$ mixtures. These studies have evolved to show a greater and greater complexity to the system, first suggesting the ordered intermediate phases and more recently to suggest extensive ordering even at high temperatures (Sørensen, 1976). The inset in fig. 27.5 summarizes the recent careful equilibration studies of $\text{CeO}_x\text{-O}_2$ (CO/CO_2) carried out thermogravimetrically by Sørensen and his review of the work referred to above. The α -phase region, until now considered continuously nonstoichiometric, shows grossly nonideal behavior and is interpreted by Sørensen as divided into several distinct nonstoichiometric subregions which themselves may consist of closely spaced phases belonging to the $\text{R}_n\text{O}_{2n-2}$ homologous series. Results of this sort depend on a trusting interpretation of the most subtle nuances of the data. The experiences of the past quarter century in complex oxides have taught the folly of unyielding disbelief.

b. *Structural properties* – As indicated in the introduction all the well established higher oxides of cerium possess fluorite-related structures. A considerable number of powder diffraction studies of the intermediate phases have been carried out both by quenching the specimens and by high temperature techniques. The earliest serious effort to delineate the complexities of the system was made by Bevan (1955). Table 27.1 presents what appear to be the best lattice parameters available. The sources of the values are indicated in the table.

Ray and Cox (1975) have recently determined the structure of Ce_7O_{12} by neutron diffraction measurements from powders and single crystals. They confirm the compound to be isostructural with Pr_7O_{12} (see section 2.3.2b). The space group is $\text{R}\bar{3}$ with hexagonal unit cell dimensions $a = 10.37 \text{ \AA}$ and $c = 9.67 \text{ \AA}$ (rhombohedral cell $a = 6.79 \text{ \AA}$ and $\alpha = 99.4^\circ$). The hexagonal cell contains three formula units of Ce_7O_{12} . An important feature of this study was that the crystals were extensively twinned and these domains had to be sorted out. There was a differing amount of disorder in powder and single crystals, being greater in the powder. Considerable disorder has been seen in electron micrographs of Pr_7O_{12} (Tuenge and Eyring, 1978) hence it may be characteristic of these materials.

Neutron and X-ray powder diffraction patterns of specimens of composition $\text{CeO}_{1.710}$, $\text{CeO}_{1.781}$, $\text{CeO}_{1.802}$, $\text{CeO}_{1.822}$ and CeO_2 have been studied by Ray et al. (1975). They confirm different structures for these phases establishing $\text{Ce}_{10}\text{O}_{18}$ ($n = 10$) for the first time. The structures of phase $n = 9$ and 10 appear to be different from the unit cells suggested by Kunzmann and Eyring (1975) for the PrO_x system. Height and Bevan (1976) cannot confirm that the homologous series members with $n = 9$ and 10 in the ceria system are isomorphous with the $\text{Pr}_n\text{O}_{2n-2}$ compounds. However, this is not to say that agreement has been established between those studying the ceria phases. Ray et al. (1975) cannot rule out the possibility of isomorphism between the CeO_x and TbO_x for $n = 11$, however current studies (Tuenge and Eyring, 1978) indicate that $\text{Pr}_{11}\text{O}_{20}$ is not isomorphous with $\text{Tb}_{11}\text{O}_{20}$.

The R_7O_{12} phase is isomorphous in Ce, Pr and Tb oxides and appears to be the lower structural end-member of the $\text{R}_n\text{O}_{2n-2}$ series but while other members exist which belong compositionally they display polymorphism at the least. It is clear that there are a great number of possible ways of accommodating a deficiency of 1/9, 1/10 or 1/11 of the oxygen atoms.

A careful study of neutron diffraction from a CeO_2 crystal has provided the nuclear coherent scattering cross-section of cerium and the Debye-Waller factor of cerium and oxygen atoms. The anharmonic contribution to the Debye-Waller factor has been calculated (Valentine and Willis, 1965).

Sørensen (1976) has reported finding a phase (Ce_6O_{11}) isostructural with Pr_6O_{11} with a monoclinic unit cell with $a = 6.781 \pm 0.006 \text{ \AA}$, $b = 11.893 \pm 0.009 \text{ \AA}$, $c = 15.823 \pm 0.015 \text{ \AA}$ and $\beta = 125.04 \pm 0.04^\circ$. This result has not been added to table 27.1 since there has been no verification of the composition and the relative intensity of the subcell and supercell reflections do not appear to be reasonable.

2.3.2. *The praseodymium-oxygen system*

a. *The phase diagram* – The black oxides of praseodymium have been known as long as the pure oxides have been available. If some praseodymium salt which decomposes to the oxide is cooled slowly in air the final composition will be Pr_6O_{11} . Depending upon how high the temperature has been the oxide shall have been many other things before it finally becomes this black material with somewhat odd stoichiometry. Actually the composition of the unit cell is $\text{Pr}_{24}\text{O}_{44}$. This barely hints at the complexity of this oxide system.

The story of praseodymium oxide could not have been written as fully as it is today without the pioneering work of many who will not be named here, such as Prandtl, Marsh, and Pagel and Brinton. Honig (1958) reviewed the early work to some degree in his report to the USAFOSR nearly twenty years ago.

The unfolding of the praseodymia saga in its latest stages began when the Pr-O system was investigated as a stand-in for the newly synthesized and then more exciting americia (Eyring, 1949; Asprey, 1949). These studies revealed a microcosm of solid state chemistry within this system which would require another quarter century to sort out. For example, it has since emerged that not

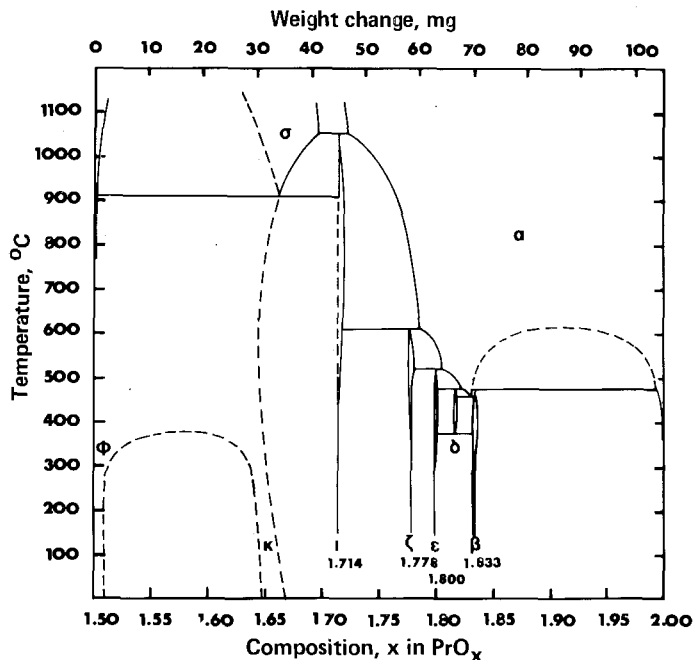


Fig. 27.6. A projection of the PrO_x phase diagram. Metastable or assumed boundaries are dashed.

only are there wide range nonstoichiometric phases but there is also an homologous series of oxides with the generic formula $\text{Pr}_n\text{O}_{2n-2}$ as listed in table 27.1 (Ferguson et al., 1954; Guth et al., 1954; Simon and Eyring, 1954; Sieglaff and Eyring, 1957; Eyring and Baenziger, 1962; Honig et al., 1963a; Hyde et al., 1966; Kordis and Eyring, 1968; Burnham and Eyring, 1968; Jenkins et al., 1970; Turcotte et al., 1971; Parks and Bevan, 1973).

The phase diagram is shown as fig. 27.6 (Hyde et al., 1966; Turcotte et al., 1971). Any member of the series may be prepared by adjustment of the oxygen pressure and temperature taking care to make adjustments depending upon whether one approaches composition in oxidation or reduction. This last proviso is important in-as-much-as hysteresis accompanies all phase reactions (see section 3). The phase diagram was largely arrived at from tensimetric measurements such as are shown in fig. 27.7 (Hyde et al., 1966), however, structural observations by X-ray, neutron and electron interaction and DTA have supplied their own evidence on which the picture is composed as discussed below.

Lott et al. (1969) report a study of the PrO_x system in the region Pr_2O_3 – Pr_7O_{12} utilizing electrochemical cells with solid electrolytes at high temperatures. It is disquieting that their results did not conform to what has been a rather general experience in this composition region. For example they could not confirm the C–A phase transition for the sesquioxide nor the existence of the σ , σ_a and σ_b phases indicated in the phase diagram. A serious effort to account for this

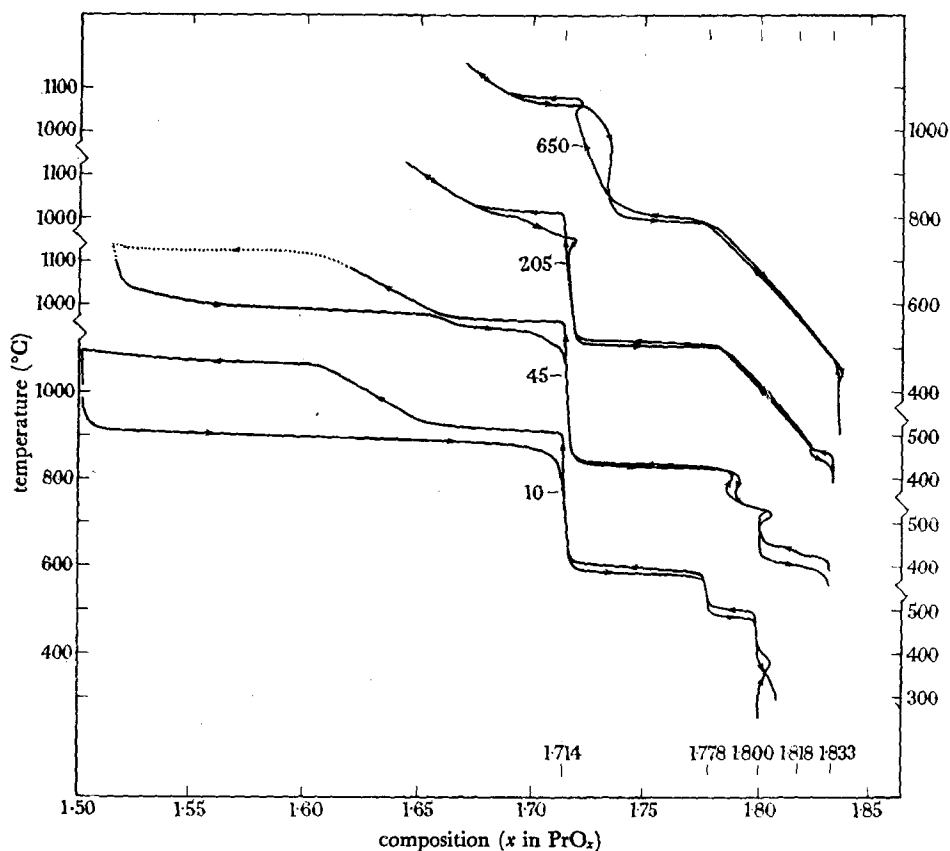


Fig. 27.7. Representative isobaric runs. The nominal oxygen pressure is indicated in torr at each curve. (From Hyde et al., 1966).

discrepancy and to correlate the thermodynamic data with other experience is to be found in Turcotte et al. (1971).

Evidence for members of the homologous series with $4 \leq n \leq 7$ have specifically been searched for (Parks and Bevan, 1973; Kordis and Eyring, 1968) by a low pressure tensimetric technique. In these studies no phases of intermediate stability ($n = 5$ or 6) appeared. Parks and Bevan (1973) also investigated the A-type sesquioxide \rightarrow iota-phase break originally studied by Honig et al. (1963b). In this latter study evidence was found to suggest a high and low temperature form of iota phase with a transformation around 700°C .

The composition of any member of the series varies within narrow but observable limits depending upon the temperature and oxygen pressure and upon the direction of preparation (hysteresis). The most common feature of the phase diagram in the CeO_x and PrO_x systems shows a peritectoidal decomposition of members of the homologous series to at least one disordered phase

of very wide composition. The high pressure and high temperature fields of the phase diagrams are divided between cubic nonstoichiometric phases, fcc for PrO_x $1.72 \leq x \leq 2.0$ and bcc for $1.50 \leq x \leq 1.70$ with a narrow miscibility gap separating these two phases of widely variable composition at high temperatures. This is a common feature of all the systems of either the lanthanide or actinide series and indeed the endless ternary systems of related crystal structure. Jenkins et al. (1970) obtained evidence that the α phase of widely variable composition was complex and consisted of at least four distinct regions. This is analogous to the behavior of $\text{CeO}_{2-\delta}$ studied by Sørensen (1976) (see Chapter 28).

The phase boundary between $\text{PrO}_{2.0}$ and $\text{PrO}_{1.833}$ has been studied by Simon and Eyring (1954), Sieglaff and Eyring (1957) and MacChesney et al. (1964) up to pressures of oxygen reaching 2000 atm. For some time it had been observed that higher oxides (i.e., Pr_6O_{11}) of praseodymium with long exposure to laboratory air disproportionated to PrO_2 and $\text{Pr}(\text{OH})_3$. Subsequently disproportionation has been demonstrated to be a general phenomenon in both the praseodymium and terbium higher oxides (Brauer and Pfeiffer, 1963; Clifford, 1964; Sastry et al., 1966b). In particular the intermediate oxides have been leached (for example with acetic acid) to yield dioxide crystals with the dissolution of the trivalent metal ions into solution. Analogous reactions have been observed in the formation of PbO_2 from Pb_3O_4 or MnO_2 from Mn_2O_3 (Partington, 1953). In the present case, however, certain of the III and IV valent cation sites are crystallographically equivalent. The oxygen is mobile and metal atom mobility is not required in the formation of new phases if one has electron mobility which these oxides do. It will be interesting to pursue the mechanism of this disproportionation.

The breakthrough enabling the structural advance as well as other observations of intrinsic properties came with the hydrothermal growth of single crystals of the higher oxides of praseodymium and terbium by Haschke and Eyring (1971) and the improvement of the technique together with the analysis of data collected on one of the ordered intermediate phases $\text{Pr}_{24}\text{O}_{44}$ (Lowenstein et al., 1972).

b. *On the structure of praseodymium-oxides* – All phases of composition greater than the sesquioxide are fluorite-related. That is to say that their structures may be viewed as formed by the omission of oxygen from normal sites in the fluorite structure accompanied by a relaxation of the remaining atoms appropriate to the existence of the oxygen vacancy. This is to some extent a statement of faith since only one intermediate phase in the binary higher oxides has been determined and that is Pr_7O_{12} . However there is a great body of evidence to support this assertion.

The structure of Pr_7O_{12} has recently been determined by Von Dreele et al. (1975) using a total profile analysis of neutron powder diffraction data. It was found, as expected, to be isomorphous with UY_6O_{12} determined by Bartram (1966) which has strings of oxygen vacancies in the $\langle 111 \rangle$ direction in an hexagonal array of third nearest metal neighbors. This gives a unit cell of composition Pr_7O_{12} with the two oxygens missing across the body diagonal $\langle 111 \rangle$.

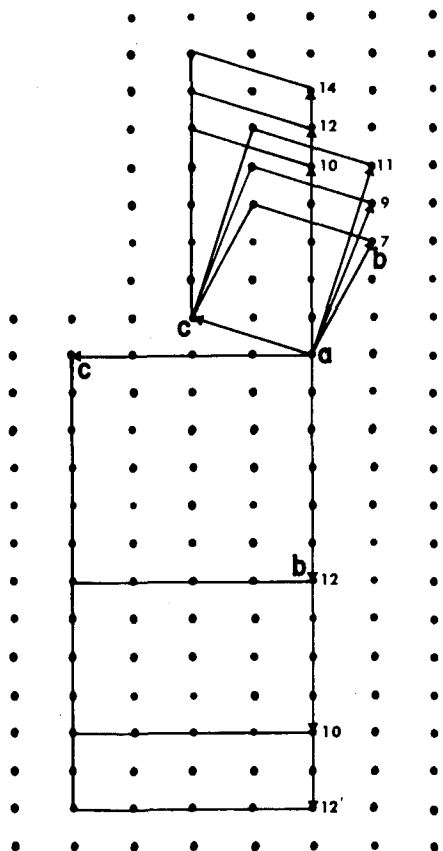


Fig. 27.8. Projections of the unit cells of members of the homologous series along the common a axis $[2\bar{1}\bar{1}]$ fluorite.

It features a six-coordinated metal atom with tridents of seven-coordinate metal atoms above and below rotated 60° with respect to each other. This cluster including the twelve associated oxygen atoms has frequently been advanced as the defect cluster characteristic of the oxygen deficient fluorite structures (Hyde and Eyring, 1965; Thornber et al., 1968; Anderson, 1970).

Powder diffraction studies of many of the phases were carried out by Sawyer et al. (1965b). Unit cells of many members of the homologous series have been determined by electron diffraction by Kunzmann and Eyring (1975). They are listed in table 27.1 and shown projected on the $(2\bar{1}\bar{1})$ in fig. 27.8.

It is apparent that members of the series fall into two categories: the odd members with the same a and c axes but differing in a regular way by a change in the b vector and the even members with identical a and c axes (equal to twice the projection of the c axis for odd members on the $\langle 110 \rangle$ direction) and with a b vector which distinguishes the members of the series.

In other words the a - c plane in each subseries is the same but the distance between the planes differs for each member. The planes are different for the odd

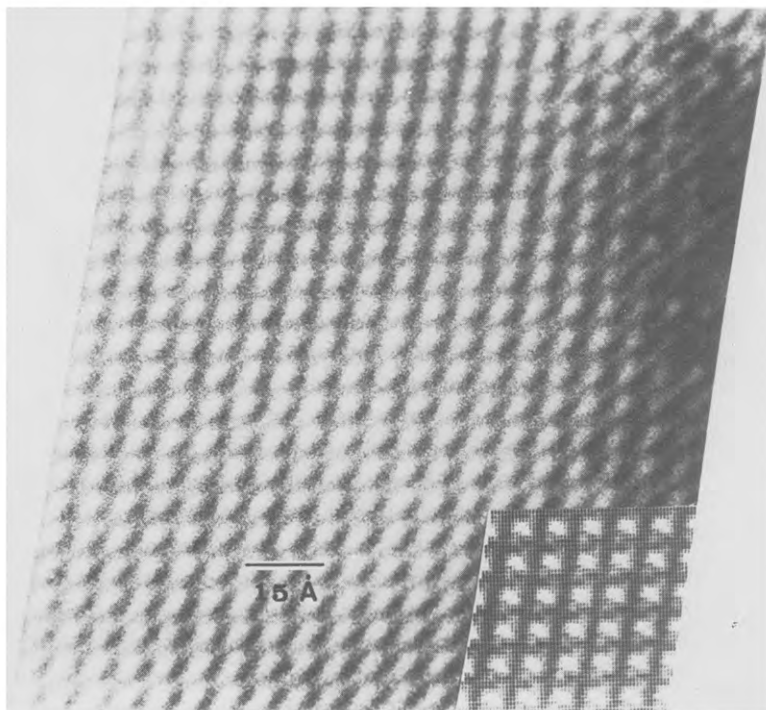


Fig. 27.9. Observed and calculated $(100)_7$ lattice images of Pr_7O_{12} . The calculated image in the lower right corner is based on the known structure for a crystal of about 200 Å thick and about 800 Å underfocus.

and even series but current guesses of the structures from high resolution electron imaging suggest that the even members are twinned at the unit cell level (c even = projection of $2c$ odd on the $\langle 110 \rangle$) hence their vacancy patterns are related by folding in the even series (Summerville et al. 1978). Efforts are being made to determine the structures of additional members of the series but these so far have not been successful.

The deviation of real solid state systems from the classical behavior has, of course, its root in the structure and texture of the samples themselves. The techniques of X-ray and neutron diffraction give little direct information concerning defects in crystals. Many real crystals are full of defects, hence techniques must be utilized which can study their defect structures. Such a technique is high resolution electron microscopy which has been applied to a study of real structures in the rare earth oxides.

As mentioned before, electron diffraction was used by Kunzmann and Eyring (1975) to determine many unit cells of the PrO_x and TbO_x homologous series and imaging was used to suggest the structures of the odd members of the series. Since then the technique has been extended by Skarnulis et al. (1978) to correlate calculated and observed images (see fig. 27.9) and by Summerville et

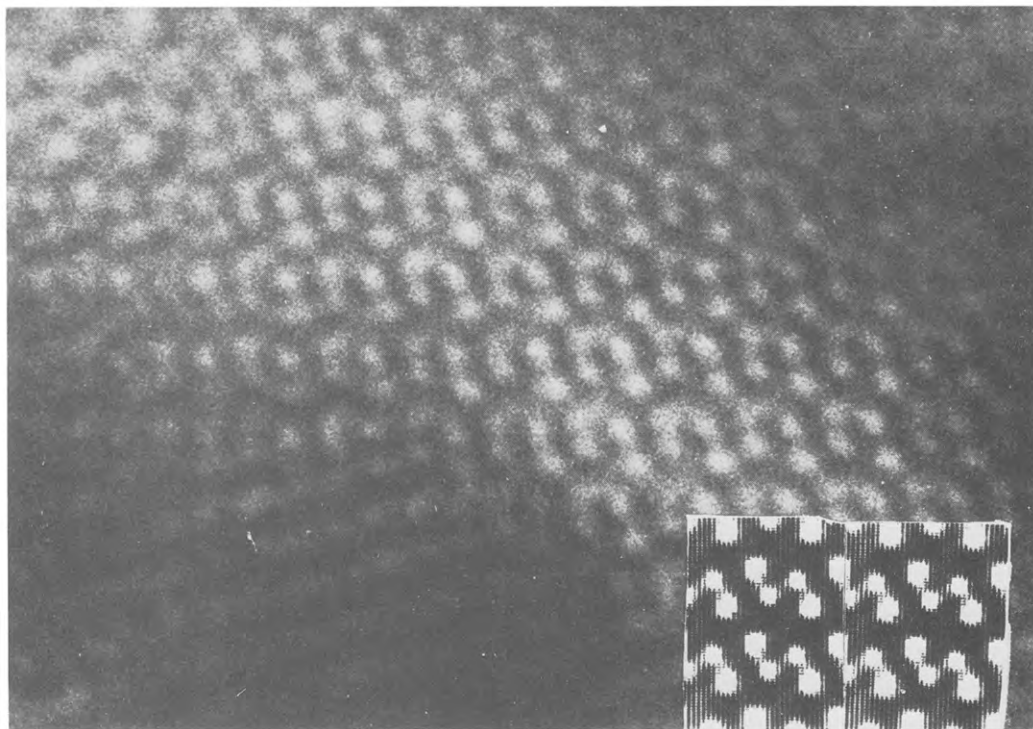


Fig. 27.10. Image of a thin edge of a crystal of $\text{Pr}_{12}\text{O}_{22}$. The calculated image based upon the proposed structure is shown as an insert at the bottom right. The white dots correlate with the projected vacancy rows which exist in the proposed structure.

al. (1978) to image the individual phases and to suggest a structure for the even series member, $\text{Pr}_{12}\text{O}_{22}$ (fig. 27.10). Of at least equal importance, it is possible to observe the nature of defects in these materials and to observe directly the reaction process (Tuenge and Eyring, 1982) (see fig. 27.11). This can hardly be overvalued. It is of fundamental importance to catalog the types of defects which take part in reactions and when these can be seen directly it removes the need for difficult and uncertain indirect methods which have been an almost unlimited source of confusion in the past. At the very least it limits the number of alternatives which must be considered.

There has been marked recent interest in a variety of armchair attempts at predicting the fluorite-related anion deficient homologous series. Martin (1974) and Hoskins and Martin (1975) have constructed an intriguing model based on the octahedrally coordinated anion vacancy $\square\text{O}_6$, known to exist in pairs in Pr_7O_{12} , using available information prior to the recent derivation of the unit cells of the PrO_x and TbO_x systems by Kunzmann and Eyring (1975). This topologically inspired structural theory (for constructing the $\text{R}_n\text{O}_{2n-2}$ series) will be interesting to compare with observations as they unfold but until the present it

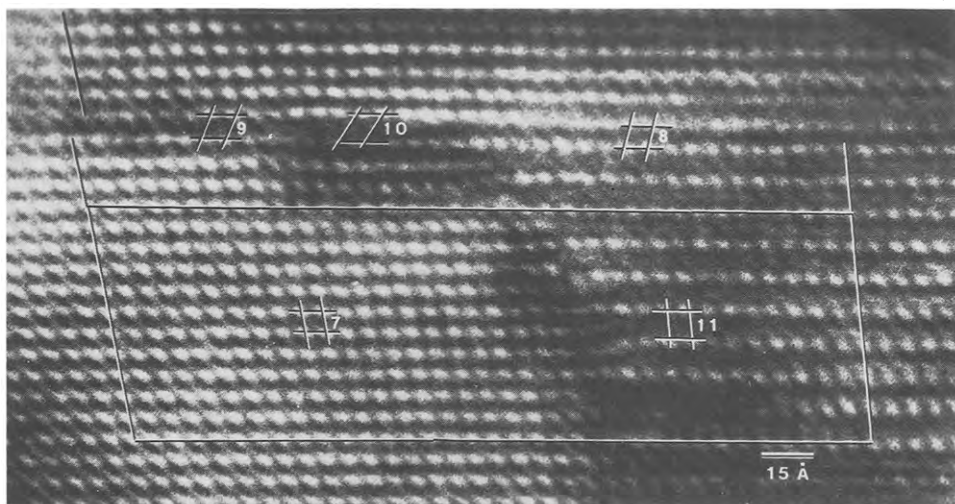


Fig. 27.11. An image of multiple-phased TbO_x down $[2\bar{1}1]_F$. Specimen prepared by reduction of $Tb_{11}O_{20}$ in the microscope to one containing a large amount of Tb_7O_{12} . Integers indicate n in Tb_nO_{2n-2} for cell projections. Mode of reaction at the boundaries is indicated in the darker regions.

does not appear to be a reliable guide to the structures actually found. This points up again the wondrous multiplicity of ways nature can find to order her existence. For example, the $Pr_{12}O_{22}$ unit cell had not been accounted for in the 1974 paper but after the unit cell was published it was possible (Hoskins and Martin, 1975) to evolve a branching structure of coordinated defects consistent with the unit cell.

Mann (1974) has performed a service in making more explicit the relationships between the fluorite-type and C-type oxides to the $MX_3(YF_3)$ type structures. Similar relationships had earlier been pointed out by Hyde (1971).

2.3.3. The terbium–oxygen system

The same techniques as used to study the praseodymium–oxygen system have been used to produce the phase diagram shown as fig. 27.12 (Guth et al., 1954; Simon and Eyring, 1954; Baenziger et al., 1961; Hyde and Eyring, 1965; Sawyer et al., 1965b; Kordis and Eyring, 1968; Burnham et al., 1968; Kunzmann and Eyring, 1975).

Wilbert and Marion (1970) have studied the TbO_x $1.5 < x < 1.714$ region by observation of the electrical resistance as a function of temperature and pressure and by high temperature X-ray diffraction. The same general features as were exhibited by the CeO_x and PrO_x at low temperatures and pressures are seen here. There are members of a homologous series, $n = 4, 7, 11, \infty$ (see table 27.1) but no evidence even at the highest temperature for a nonstoichiometric α or σ phase has

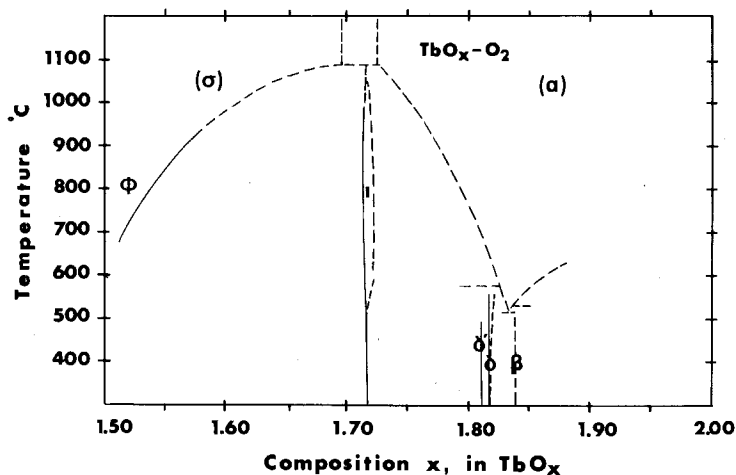


Fig. 27.12. Phase diagram of the TbO_x system. The dashed curves mark the boundaries of the disordered α and σ regions suggested by electron microscopic studies.

been found. It has been supposed that if the pressures were high enough such phases might be observed.

The thermodynamic properties of the terbium oxide system in the composition range $\text{TbO}_{1.50} \rightarrow \text{TbO}_{1.714}$ has been studied by high temperature emf measurements. Thermodynamic properties are derived and a phase diagram for this region was constructed (Vasil'eva et al., 1975).

3. Hysteresis and pseudophase formation

Very extensive temperature-pressure-composition observations have been made on the rare earth higher oxides as is clear from the discussion of the previous sections. Certain observations should be made explicit. There are no instances of classical behavior, i.e., none of the single phases are "line" phases but have at least some range of composition and none of the two-phase isobaric transformations occur at a fixed temperature but rather over a range of temperatures. There is also clearly intrinsic hysteresis in all two-phase regions. Furthermore the hysteresis loops are not symmetric, but rather are skewed such as to give a retarded and almost linear approach when a phase of lower symmetry is being formed. This may occur either in oxidation or reduction; is reproducible and intrinsic - it has been termed pseudophase formation (Hyde et al., 1966).

Hysteresis and pseudophase formation are properly not displayed in equilibrium phase diagrams because they are metastable states but they are nevertheless features of real systems and anyone who wishes to describe real systems must take them into account. Earlier studies by Faeth and Clifford (1963) were

carried out in the PrO_x system without isolating a simple two-phase reaction to be studied. Turcotte et al. (1973) have examined pseudophase behavior in the PrO_x system in several regions. Recently hysteresis in the two major loops of the $\text{TbO}_x\text{-O}_2$ system ($\text{Tb}_2\text{O}_3 \rightleftharpoons \text{Tb}_7\text{O}_{12}$ and $\text{Tb}_7\text{O}_{12} \rightleftharpoons \text{Tb}_{11}\text{O}_{20}$) has been studied by Lowe and Eyring (1975) (see fig. 27.13). In this case the high temperature transition ($\iota \rightleftharpoons \varphi$) was seen to be intrinsic with a wide temperature differential and marked pseudophase formation. Scanning loops showed the durable nature

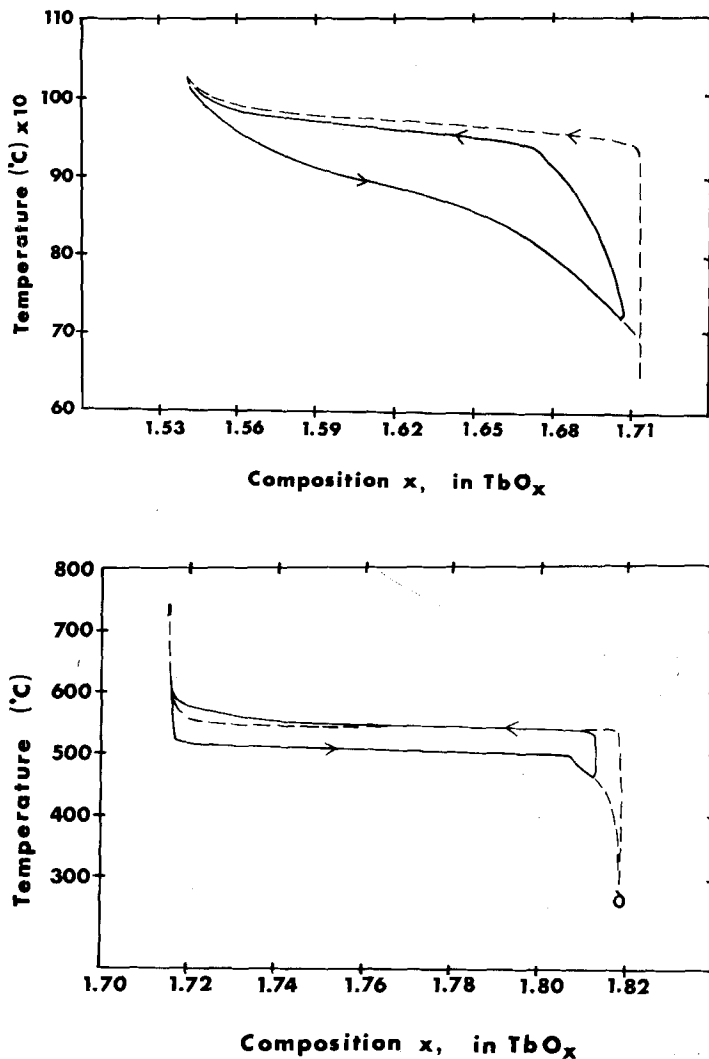


Fig. 27.13. Isobaric hysteresis loop for (a) the reaction $\frac{2}{7}\text{Tb}_7\text{O}_{12} \rightleftharpoons \text{Tb}_2\text{O}_3 + \frac{3}{14}\text{O}_2(\text{g})$. Dashed loop is the intrinsic hysteresis envelope, and (b) the reaction $\frac{7}{11}\text{Tb}_{11}\text{O}_{20} \rightleftharpoons \text{Tb}_7\text{O}_{12} + \frac{4}{11}\text{O}_2$ (after Lowe and Eyring, 1975).

of the pseudophases and distinguished various parts of the loop by their form. The low temperature loop $\iota \rightleftharpoons \delta$ was found to require extremely slow rates of traversal ($\sim 0.05^\circ/\text{min}$) before they were intrinsic. In this case the loop is not simple but involves the path $\delta \rightarrow \iota \rightarrow \delta' \rightarrow \iota$ where δ' is a distinct fluorite-related phase but not one of the homologous series since its n value would be $10\frac{1}{3}$ with a composition $\text{TbO}_{1.809}$. The effect of increasing the crystallite size on hysteresis was studied by Lowe et al. (1975) and found to decrease hysteresis contrary to what might be expected.

Theories based on regular solutions or on heterogeneous domains predict hysteresis behavior. Knittel et al. (1977) are developing these theories and comparing the results with carefully determined intrinsic loops. Hysteresis in solid state reactions is clearly an important property related to the structure and texture and containing a great deal of information and memory.

4. Thermodynamics

A casual perusal of the phase relationships just described together with a glance at such properties as the melting and boiling points of the oxides (table 27.2) will make one acutely aware of the great thermal stability of the reduced oxides of the rare earths. Only ThO_2 stands out among oxides as being more thermally stable while the rare earths are in the same range of thermal stability as CaO and MgO .

It shall be our purpose here to illustrate these facts in tables and graphs. For this purpose we shall rely heavily on a review paper by Westrum (1967) and Holley et al. (1968) particularly for references and data up to the middle sixties including the estimation of entropy values and a review of the high temperature data. Gschneidner et al. (1973) reviewed the literature for information making possible the tabulation of enthalpy and free energy values as a function of temperature. There will be no effort to document values taken from these three sources and only more recent values or those not reviewed by these authors shall be noted separately.

The special ways in which the electronic properties of the oxides impinge on thermodynamics will be discussed later under magnetic and electric properties. In the present treatment these properties are buried in the unreported heat capacity data. These shall be evoked as desired to indicate that interesting atomic or solid-state properties are reflected in the thermodynamic data as would be expected.

Tabulations of values for the entropies, enthalpies and Gibbs free energies for the stable phases where they are known appear in tables 27.2, 27.3 and 27.4 and the Gibbs free energy is plotted against temperature in fig. 27.14.

The thermodynamic values tabulated are derived from the full arsenal of methods available such as enthalpy or internal energy measurements by direct calorimetry, cryogenic heat capacity measurements from sufficiently low temperature to permit entropy evaluation at room temperature, as well as some

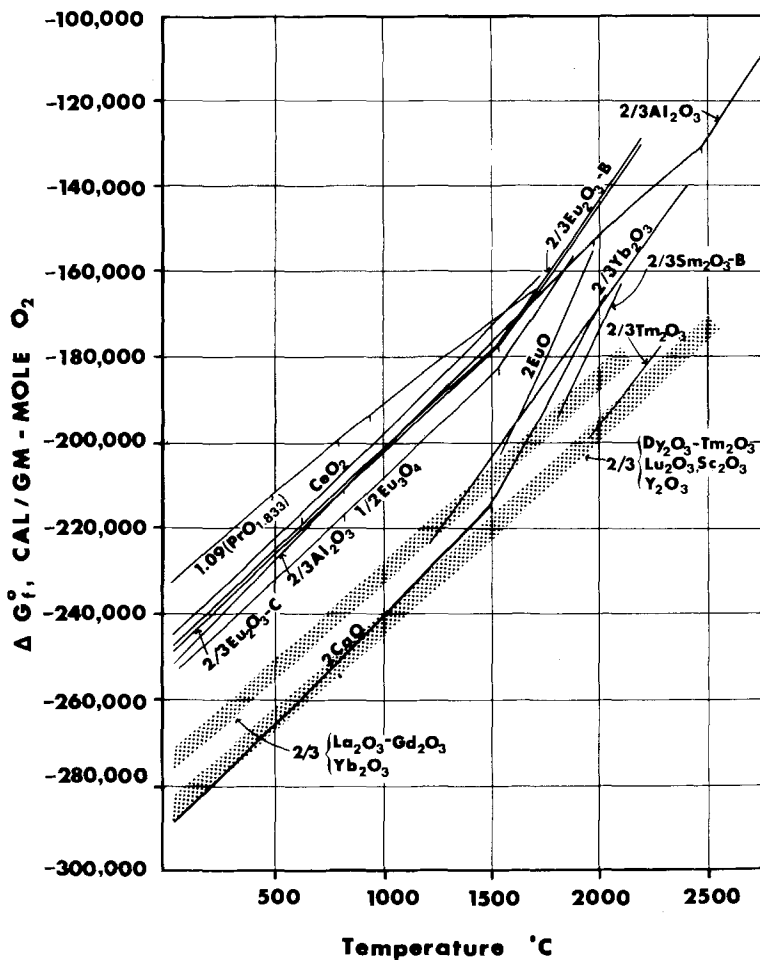
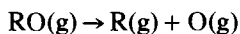


Fig. 27.14. The free-energy of formation of the rare earth oxides. Some common oxides are added for comparison. Dotted regions replace individual curves as indicated (after Gschneidner et al., 1973).

derived from equilibrium methods often at high temperatures and estimation schemes. At high temperatures, for example, studies of the vaporization process



followed by



give information concerning the most common types of gaseous species, the heat of vaporization of the sesquioxides and the dissociation energy of the gaseous monoxide.

TABLE 27.2.
Physical and thermodynamic properties of rare earth sesquioxides.

Rare earth	Electronic Configuration of (III) ions ¹	Ground term ¹	Experimental ¹ magnetic moment (Bohr magnetons)	Freezing point ² (°C)	Boiling point ² (°C)	S ³⁹⁸ for R ₂ O ₃ (cal K ⁻¹ mole ⁻¹)		S ³⁹⁸ for metal ¹ (cal K ⁻¹ mole ⁻¹)	-ΔH ₂₉₈ ⁰ (kcal mole ⁻¹)	-ΔG ₂₉₈ ⁰ (kcal mole ⁻¹)
						(est)	obs			
Sc		¹ S ₀	[0.0]	2403 ⁴ ± 20		19.4	[8.20]		456.2	434.8
Y		¹ S ₀	[0.0]	2376 ^{4,5} 2432 ⁶		22.4	10.63		455.5	434.3
La		¹ S ₀	0.00	2256 ⁴ 2304 ⁵ ± 5	3620	30.4	30.58	13.64	428.8	407.9
Ce	4f ¹	² F _{5/2}	[2.56]	2210 ⁷ ± 10	3730	36.4		16.68	429.3	408.1
Pr	4f ²	³ H ₄	3.55	2183 ⁴	3760	37.9	37.9	17.49	A, C432.52 ⁹	414.4
Nd	4f ³	⁴ I _{9/2}	3.66	2233 ⁴	3760	38.0	36.92	17.54	432.1	411.1
Pm	4f ⁴	⁵ I ₄	[2.83]	2320 ⁸				[17.2]		
Sm	4f ⁵	⁶ H _{5/2}	1.54	2269 ⁴	3780	35.4	36.1	16.64	B435.9	414.8
Eu	4f ⁶	⁷ F ₀	3.51	2291 ⁴	3790	35		[17.0]	C436.8	415.3
Gd	4f ⁷	⁸ S _{7/2}	7.90	2339 ⁴	3900	36.3	36.0	15.77	B394.7	371.9
Tb	4f ⁸	⁷ F ₆	9.63	2303 ⁴		37.5		17.48	C397.4	374.1
Dy	4f ⁹	⁶ H _{15/2}	10.5	2228 ⁴	3900	38.1	35.8	17.87	B433.9	413.5
Ho	4f ¹⁰	⁵ I ₈	10.5	2330 ⁴	3900	38.2	37.8	18.00	C436.6	415.8
Er	4f ¹¹	⁴ I _{15/2}	9.5	2344 ⁴	3920	37.6	36.6	17.52	445.8	424.7
Tm	4f ¹²	³ H ₆	7.39	2341 ⁴	3945	36.5	36.5	17.37	448.9	427.6
Yb	4f ¹³	² F _{7/2}	4.34	2355 ⁴	4070	34.5	31.8	[15.0]	453.7	429.6
Lu	4f ¹⁴	¹ S ₀	[0.0]	2427 ⁴	3980	26.0		12.19	433.7	413.3

- ¹Westrum, E.F.Jr., Developments in Chemical Thermodynamics of the Lanthanides, in: Advances in Chemistry Series, Number 71, American Chemical Society 1967, pp. 25-50.
- ²Benezech, G., J.P. Coutures, M. Foéx, J. Less-Common Metals **38**, 131 (1974).
- ³Gschneidner, K.A., N. Kippenhan and O.D. McMasters, Thermochemistry of the Rare Earths, Report No. IS-RIC-6 Rare Earth Information Center-Institute for Atomic Research, Iowa State University, Ames, Iowa (1973).
- ⁴Noguchi, T., High Temperature Phase Studies with a Solar Furnace, in: Advances in High Temperature Chemistry, Vol. 2 (L. Eyring, ed.) (Academic Press, New York, 1969) pp. 235-262.
- ⁵Sata, T., Rev. Hautes Tempér, et Réfract., **3**, 337 (1966).
- ⁶Sheindlén, A.E., M.M. Kenesarin and V.Ya. Chekhovskoi, Dokl. Akad. Nauk SSSR **216**, 582 (1974).
- ⁷Sata, T. and M. Yoshimura, J. Ceram. Assoc. Japan **76**, 30 (1968).
- ⁸Gibby, R.L., C.E. McNeilly and T.D. Chikalla, J. Nucl. Mat. **34**, 299 (1970).
- ⁹Fitzgibbon, G.C., E.J. Huber, Jr., C.E. Holley, Jr., Rev. Chim. Min. **t10**, 29 (1973).

TABLE 27.3.
Thermodynamic properties of other rare earth oxides.

Oxide	S_{298}^0 ¹ (cal K ⁻¹ mole ⁻¹)	$-\Delta H_{298}^0$ ² (kcal mole ⁻¹)	$-\Delta G_{298}^0$ (kcal mole ⁻¹)
CeO _{1.67}	17.2		
CeO _{1.72}	16.5		
CeO _{1.78}	16.2		
CeO _{1.81}	16.2		
CeO _{2.0}	14.7	260.2	245.1
PrO _{1.703}	[19.1]	223.5	
PrO _{1.717}		224.0	
PrO _{1.74}	[19.2]		
PrO _{1.804}		226.5	
PrO _{1.833}	19.1	225.5 ³	213.5
PrO ₂	19.1		
SmO	[15.7]		
EuO	[16.3]	142.9	136.0
Eu ₃ O ₄		538.9	509.0
TbO _{1.70}		223.3	
TbO _{1.72}	19.3		
TbO _{1.806}		226.4	
TbO _{1.81}	19.4		
TbO _{1.817}		230.0	
TbO _{1.975}		232.0	
TbO _{2.0}	19.8	232.2	
CeO ₂ (g)	$\Delta G_f^0 = -13150 + 6.98T/K$		

¹Westrum, E.F.Jr., Developments in Chemical Thermodynamics of the Lanthanides, in: Advances in Chemistry Series, Number 71, Amer. Chem. Soc., 1967, pp. 25-50.

²Gschneidner, K.A.Jr., N. Kippenhan and O.D. McMasters, IS-RIC-6Aug. 1973, Iowa State Univ., Ames, Iowa. "Thermochemistry of the Rare Earths."

³Fitzgibbon, G.C., E.J. Huber, Jr. and C.E. Holley, Jr., Rev. Chim. Min. t10, 29 (1973).

The enthalpy, entropy and free energy of formation of Ce₂O₃ and CeO₂ are given in table 27.3. The values of these and related thermodynamic quantities as a function of T are given by Kuznetsov et al. (1961) and King and Christensen (1961). The thermodynamic properties of the intermediate phases have been obtained by P , T , X studies as discussed in section 2.3.1 and by utilizing a solid state cell (Kuznetsov et al., 1961) and finally Campserveux and Gerdanian (1974) have made direct high temperature microcalorimetric measurements of the partial molar enthalpy of O₂ in the intermediate oxides mostly in the disordered region. Figure 27.15 shows a plot of $-\Delta\bar{H}_{O_2}$ vs x (in CeO _{x}) from the latter work which agrees rather well with the results of Bevan and Kordis (1964) and of Sørensen (1976).

TABLE 27.4.
 Vaporization characteristics of rare earth oxides¹

Oxide	ΔH_v^0 (kcal/mole)	ΔG_f^0 (kcal/mole)	ΔH_f^0 (kcal/mole)	D_0^0 (eV)	ΔH_S^0 (kcal/mole)	$S_{2900\text{ K}}^0$ (eu)
Y ₂ O ₃	502.6		-5.0 ± 5.0	7.13 ³	99.0	53.4
	318.4 ²	-21800 - 10.96T ⁶		7.03 ²	100.3 ⁴	
La ₂ O ₃	430.2		-27.9 ± 5.0	8.26 ± 0.2	103.0	56.5
		-36940 - 11.73T/K ³	-28.6 ± 1.0 ⁵	7.95 ± 0.04 ³		
Nd ₂ O ₃	428.0		-31.2 ± 7.0	7.24 ± 0.3	76.6	57.4
	361.1 ± 1.1 ⁷		-33.7 ± 0.6 ⁷	7.42 ± 0.1 ⁷		
Sm ₂ O ₃	443.2		-24.0 ± 7.0	5.77 ± 0.3	50.0	57.4
Eu ₂ O ₃				4.80 ± 0.11 ⁸		
Gd ₂ O ₃	453.3		-18.6 ± 7.0	7.02 ± 0.3	84.1	58.2
	468.7 ± 0.8 ⁹					

ΔH_v^0 = Standard enthalpy change at 0 K for the reaction $R_2O_3(c) \rightarrow 2RO(g) + O(g)$.

ΔG_f^0 = Standard Gibbs energy of RO(g) at T K

ΔH_f^0 = Standard enthalpy of formation of RO(g) at 0 K.

D_0^0 = Standard dissociation energy of RO(g) at 0 K.

ΔH_S^0 = Standard enthalpy of sublimation of metal at 0 K.

$S_{2900\text{ K}}^0$ = Entropy of gaseous metal.

¹All values are from Westrum (1967) unless otherwise indicated (see table 27.3).

²Ackermann, R.J. and E.G. Rauh, J. Chem. Thermodyn. **5**, 331 (1973).

³Liu, M.B. and P.G. Wahlbeck, High Temperature Sci. **6**, 179 (1974).

⁴Ackermann, R.J., E.G. Rauh and R.R. Walters, J. Chem. Thermodyn. **2**, 139 (1970).

⁵Ackermann, R.J. and E.G. Rauh, J. Chem. Thermodyn. **3**, 445 (1971).

⁶Ackermann, R.J., E.G. Rauh and R.J. Thorn, J. Chem. Phys. **40**, 883 (1964).

⁷Tetenbaum, M., High Temp. Sci. **7**, 37 (1975).

⁸Hildenbrand, D.L., E.Z. Mural, Z. Naturforsch. **30A**, 1087 (1975).

⁹Messier, D.R., J. Am. Ceram. Soc. **50**, 665 (1967).

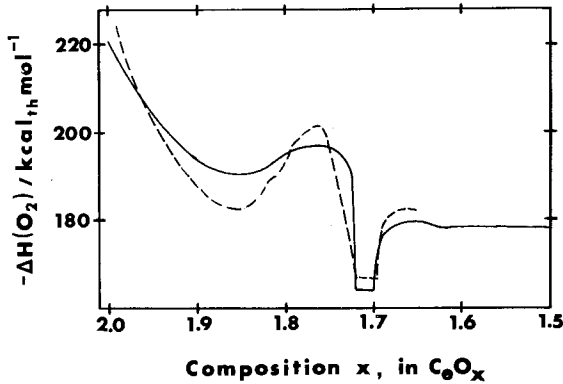


Fig. 27.15. A comparison of the partial molar enthalpy of O_2 in CeO_x . The solid curve follows the results of Compserveux and Gerdanian (1974). The dashed curve represents the results of Bevan and Kordes (1964).

High temperature vaporization studies have yielded the thermodynamic data shown in table 27.5 on the cerium oxide system.

The high temperature enthalpy and specific heat of Y_2O_3 in the range 1300–2100 K has been measured by Landa et al. (1974).

$$\Delta H = H_T - H_{298} = 0.1207T + 0.9 \times 10^{-5}T^2 - \frac{1603}{T} + 42.142 \text{ kcal/kg}$$

$$C_p = 0.1207 + 1.8 \times 10^{-5}T + \frac{1603}{T^2} \text{ kcal/kg degree.}$$

TABLE 27.5.
Some high temperature thermodynamic properties of the CeO_x system.

Phase	$\Delta G_f^\circ(T)$ (cal mol ⁻¹)	$\Delta G_f^\circ(2000 \text{ K})$ (cal mol ⁻¹)	Ref.
Ce(g) 4f ¹ 5d ¹ 6s ²	96500 - 25.2 T/K	46100	1
CeO(g)	-37360 - 10.8 T/K	-58960	2
CeO ₂ (g)	-131350 + 7.0 T/K	-117390	2
Ce ₂ O ₃ (s)	-424100 + 65.8 T/K	-292500	2, 3
CeO ₂ (s)	-259650 + 50.7 T/K	-158250	2, 3
Phase reaction	Enthalpy		Ref.
CeO ₂ (s) → CeO ₂ (g)	$\Delta H_{298}^0 = 135 \pm 6 \text{ kcal mol}^{-1}$		4
Ce(g) + CeO ₂ (g) ⇌ 2CeO(g)	$\Delta H_{298}^0 = -19 \pm 4 \text{ kcal mol}^{-1}$		
Ce ₂ O ₃ (g) ⇌ 2CeO(g)	$\Delta H_{298}^0 = 90 \pm 6 \text{ kcal mol}^{-1}$		
CeO ₂ ⇌ Ce + 2O	$D_{298}^0 = 350 \pm 15 \text{ kcal mol}^{-1}$		
Ce ₂ O ₃ ⇌ 2Ce + 2O	$D_{298}^0 = 474 \pm 15 \text{ kcal mol}^{-1}$		

¹Ackermann, R.J., M. Korima, E.G. Rauh, R.R. Walters, J. Chem. Thermo. **1**, 527 (1969).

²Ackermann, R.J. and E.G. Rauh, J. Chem. Thermo. **3**, 609 (1971).

³Baker, F.B. and C.E. Holley, J. Chem. Eng. Data **13**, 405 (1968).

⁴Piacente, V., G. Bardi, L. Malaspina and A. Desideri, J. Chem. Phys. **59**, 31 (1973).

These relations serve as interpolation formulae in the temperature range 298–1300 K with an average error not exceeding 3.8%.

High-temperature heat-contents, heat capacities and entropies for many of the phases, La_2O_3 (King et al., 1961); Eu_2O_3 , Gd_2O_3 , Nd_2O_3 , Sm_2O_3 , Y_2O_3 (Pankratz et al., 1962); Er_2O_3 , Ho_2O_3 , Tm_2O_3 and Yb_2O_3 (Pankratz and King, 1963) and Lu_2O_3 , Dy_2O_3 and Ce_2O_3 (Pankratz and Kelley, 1963) have been determined.

McMasters et al. (1974) have determined the high temperature enthalpies for EuO and have calculated a variety of thermodynamic functions. McCarthy (1974) has summarized the thermodynamic data on the $\text{Eu}-\text{O}_2$ system to sketch the regions of stability of the various oxides.

The oxygen dissociation pressure at temperatures below those where metal containing species are significant have yielded thermodynamic data on the intermediate oxides of praseodymium and terbium as discussed in section 2.3.

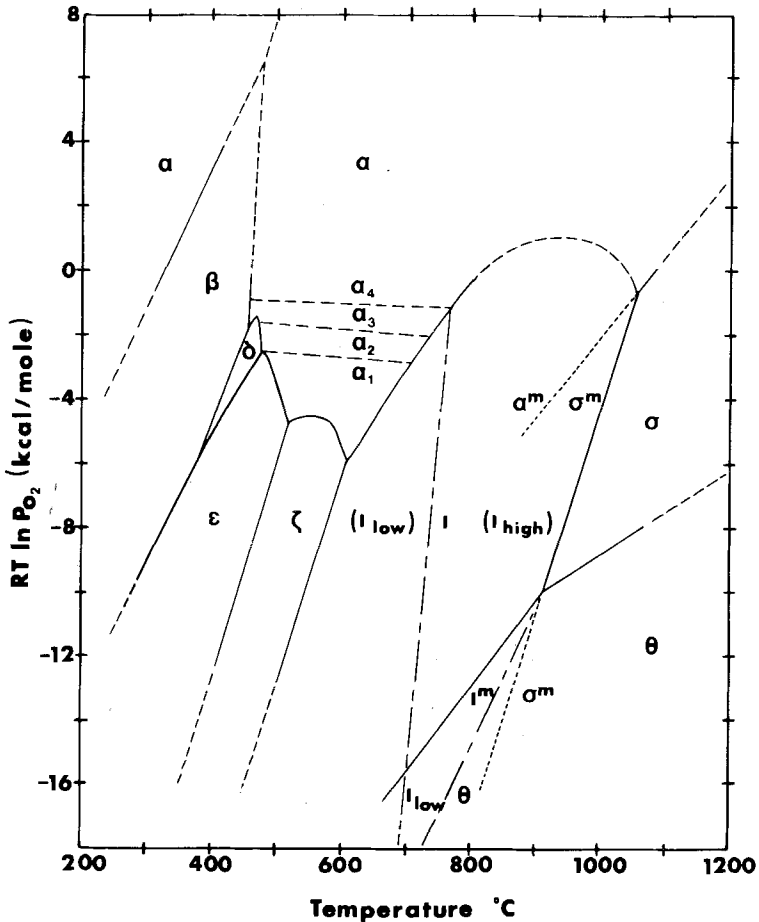


Fig. 27.16. Fields of stability in the PrO_x system. The α phase is shown to be complex.

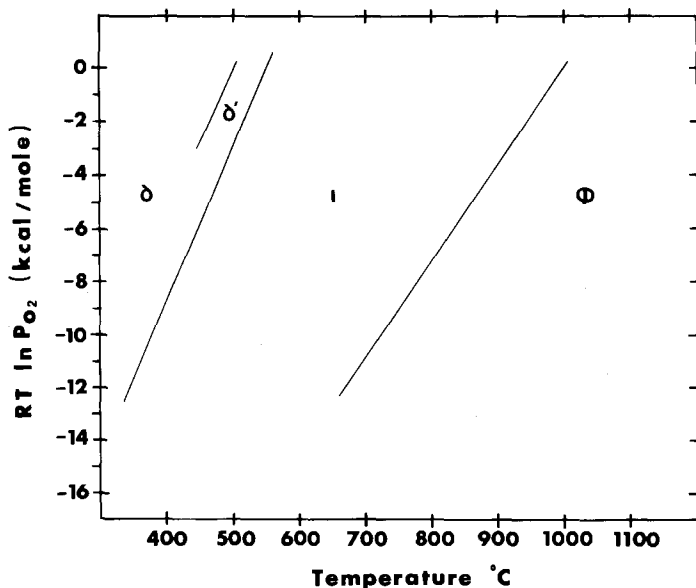


Fig. 27.17. Fields of stability in the TbO_x system.

Figures 27.16 and 27.17 illustrate the stable phase fields for the intermediate compounds in the PrO_x-O_2 and TbO_x-O_2 systems. Derived entropy values in the α -region of the PrO_x-O_2 system which show erratic changes in the regions where ordering is occurring has been commented on by Jenkins et al. (1970).

Haschke and Eick (1969) have studied the vaporization thermodynamics of EuO using a Knudsen effusion technique. The reaction



occurred over the temperature range 1344–1758 K. At 1546 K $\Delta H_T^0 = 75.9 \pm 0.9$ kcal/gfw and $\Delta S_T^0 = 28.6 \pm 0.6$ eu. For EuO $\Delta H_{f298}^0 = 145.2 \pm 4$ kcal/gfw, $\Delta G_{f298}^0 = -139 \pm 4$ kcal/gfw and $S_{298}^0 = 15 \pm 3$ eu.

5. Phase reactions in rare earth oxides

Careful observation of the composition dependence on oxygen pressure at constant temperature or related observations of composition as temperature is changed at constant pressure have been used (tensimetric methods) as described above to determine the regions and range of stability of the multiple phases of the rare earth oxides. Obviously any phase of narrow stability range will show little compositional change as the conditions of temperature or pressure are altered. On the contrary, a rapid compositional change with pressure or temperature change accompanies phase reactions. In this way the phase diagrams have been constructed.

If one observes the details of the pressure composition relationship carefully he will see the implications at the molecular level of the changes occurring as phases pass through the range of their compositional stability and as phase reactions occur when new types replace the old. It is the details of these changes to which we now turn our attention.

The functional relationship of composition and pressure has in it all the information about a solid-gas reaction—deciphering it, however, may be a problem. The solid consists of a three-dimensional array of atoms. At equilibrium at any composition there will be a certain deployment of species characteristic of the solid and the locus of these equilibrium states determines the composition-pressure curve. A phase of variable composition will have defects present at varying concentration and the nature of the defects themselves will be a function of their concentration. All this will be revealed in the functional relationship of temperature, pressure and composition.

Indirect methods having no outside information must consider all thermodynamically plausible species. This includes all plausible omissions of atoms from proper sites, all plausible interpolations of either type of atom as interstitials and all plausible additions or abstractions of electrons from these entities. The problem does not end there since one must consider all plausible interactions of these entities into complex groups or extended defects and, of course, the final analysis must take into account the effect of the occupation of a certain crystal space by a specific entity on the possibility of a second entity being nearby, not to mention, of course, impurities. It is obvious that this is a formidable, even an impossible, task and although there is considerable data delimiting the possibilities in each case one can understand why students of the problem have come up with every plausible answer.

Our discussion of mass transport in the rare earth oxides shall be virtually limited to the C-type and fluorite phases and their fluorite-related intermediates. As we have seen, as oxygen is removed from the fluorite dioxide a series of intermediate fluorite-related phases are formed which have metal atoms on all proper sites and ordered oxygen vacancies. The compositional end-member of the series, C-type oxide, contains vacancies in one-fourth of the normal fluorite oxygen sites. The intermediate R_7O_{12} structure common to all higher oxides has one-seventh of its fluorite oxygen sites vacant and ordered. The similarities of these two to the other phases cannot be ignored. Therefore although a priori there would be no reason not to consider metal atom interstitials of every complexity and charge, all such species must be present in relatively small concentrations considering the extant crystallographic information.

Such density data as exist also confirm the presence in the higher oxides of oxygen vacancies rather than metal interstitials. This is frequently a weak indication, however, since the description of an actual structure can sometimes be made in either terms within the limit of error of this measurement.

With the advent of high resolution electron microscopes capable of resolution of about 3 Å or less which can directly image structures in two dimensions, the types and relative abundance of defect species and the degree of their complex-

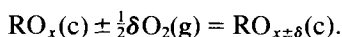
ity in any crystalline material should not be left in much doubt. This makes the indirect methods much more powerful and less arbitrary and subject to error. They can be used to illuminate the blind spots of the direct methods such as serious sampling statistics. Used together they should in time be capable of yielding the truth. The direct observation of defects in these systems is described in section 2.3 and illustrated in figs. 27.9, 27.10 and 27.11.

5.1. *Material transport in rare earth oxides*

Fluorite materials are notorious for the mobility of their nonmetal constituent. Among materials of this class are the best fluorine (PbF₂) and oxygen (calcia-stabilized zirconia) conductors. O'Keeffe (1973) has discussed the high mobility of nonmetal atoms in these structures and has shown that the substructure melts hundreds of degrees below the phenomological melting point. In the fast-ion conducting state the nonmetal atoms spend a substantial fraction of their time moving *between* lattice sites.

In spite of this high mobility of the oxygen substructure these materials are among the most thermally stable known—melting in the range of 2500°C—the metal substructure is rigid up to the melting point and temperatures of the order of 1200–1400°C are required before appreciable metal atom movement occurs. In contrast the oxygen is mobile at 300°C in the rare earth oxides.

Most reactions to be discussed in this section involve a compositional change in the reacting oxide. In these cases some phase RO_x reacts with gaseous oxygen to produce another phase RO_{x±δ} according to the equation



It must be admitted that next to nothing is known about the detailed mechanisms of such reactions at the atomic level since they involve extended defects which have not even been cataloged.

Nevertheless the beginnings of a foundation are being laid for such an understanding in several systems. The rare earth oxides are a suitable choice for such comprehensive studies. The higher oxides of cerium, praseodymium and terbium, especially praseodymium, exhibit complicated phase relationships which have been described in detail above. Furthermore the praseodymium oxide system and certain regions of the terbium oxide system can be studied at temperatures and oxygen pressures where unusual furnace and crucible materials and gas buffer systems with their contamination possibilities are not required. Add to this the feasibility of subtle modifications of the system by the admixture of the chemically and structurally related other rare earths and actinide elements and one sees the practically unlimited possibilities of obtaining experimental information necessary for a comprehensive understanding of solid oxides.

Eyring (1970c) reviewed the studies of oxygen transport in rare earth oxides which had been done up to that time. Some of the parameters describing the transport behavior are presented in tables 27.6 and 27.7.

The results of kinetic measurements of heterogeneous reactions have been

TABLE 27.6.
Heterogeneous reactions in rare earth oxides.

Reactant	Rate controlling mechanism	Activation energy (kcal/mole)	Temperature range (°C)	Oxygen pressure	D_0 (cm ² /s × 10 ⁶)	D (100 K) (× 10 ¹⁰)
PrO _{2.00}	Phase boundary	50	289-347	vac		
PrO _{1.83}	Phase boundary	26.9	265-305	1 atm		
PrO _{1.78}	Phase boundary	49.6	407-493	vac		
PrO _{1.50}	Phase boundary	{ 25 C-type 50 A-type	240-320	138 Torr		
PrO _{1.71}	Diffusion	42	700-970	vac		
*TbO _{1.82}	Diffusion	41.5	383-471	vac		
*TbO _{1.71}	Diffusion	~40	570-643	vac		
CeO _{1.818}	Interstitially	~10	20-40	1 atm, air		
Sc ₂ O ₃	Diffusion with a moving boundary	38.30	1106-1298	air	7.72	2.27
Y ₂ O ₃	Diffusion with a moving boundary	19.58	1064-1241	air	0.0606	27.6
Dy ₂ O ₃	Diffusion with a moving boundary	26.24	1087-1235	air	0.163	5.27
Ho ₂ O ₃	Diffusion with a moving boundary	40.53	1050-1274	air	71.8	8.26
Er ₂ O ₃	Diffusion with a moving boundary	30.12	1060-1292	air	1.31	0.958
Tm ₂ O ₃	Diffusion with a moving boundary	45.56	1015-1235	air	114.0	1.97
Lu ₂ O ₃	Diffusion with a moving boundary	29.76	1020-1297	air	1.88	1.58

*Behavior deviates from diffusion-like mechanism in the early stages of reaction (modified diffusion behavior).

TABLE 27.7.
Oxygen self diffusion in rare earth oxides.

Oxygen self-diffusion	Activation energy (kcal/mole)	Temperature range (°C)	D_0 (cm ² /sec)	D (1000 K)
Zr _{0.858} Ca _{0.142} O _{1.858}	31.20	781-1097	1.8×10^{-2}	8.1×10^{-8}
Nd ₂ O ₃ (99.999%)	31	700-1000	1.3×10^{-4}	7.7×10^{-10}
Sm ₂ O ₃ (99.9%)	23.5	700-950	9.2×10^{-6}	8.96×10^{-10}
Sm ₂ O ₃ (99.998%)	21.3	700-1000	6.0×10^{-6}	1.39×10^{-9}
Er ₂ O ₃ (99.999%)				$\sim 10^{-14}$
Pr ₇ O ₁₂ (low temp)	8.21	725-930	9×10^{-8}	3.58×10^{-9}
Pr ₇ O ₁₂ (high temp)	19.05	725-930	2.9×10^{-8}	1.65×10^{-9}

analyzed by comparing them with the mathematical consequences of a proposed model.

5.1.1. Phase boundary controlled reactions

If the sample consists of spheres whose reaction rate is controlled by a phase boundary retreating into the sphere at a uniform rate, a plot of the cube root of the unreacted remainder against time will be a straight line. In such a reaction, nucleation of the new phase must be rapid over the entire surface yielding a spherical phase boundary. Excellent agreement between this model and the reduction of PrO_{2.00} and oxidation of PrO_{1.833} (Hyde et al., 1965), the reduction of PrO_{1.78} (Kuntz and Eyring, 1959) and the oxidation of PrO_{1.50} (Ramdas et al., 1970) has been observed.

5.1.2. Diffusion controlled reactions

A diffusion mechanism including phase boundary movement has been proposed by Berard et al. (1968) for the oxidation of substoichiometric rare earth sesquioxides although rather than the phase boundary formation itself being rate controlling it is chemical diffusion through the reaction product. If on the other hand the rate controlling step is simply diffusion into the sphere along a radial concentration gradient a plot of the logarithm of the amount of unreacted sample against time gives a curve which falls off rapidly at first while a uniform gradient is being established, then becomes linear. Such a mechanism apparently obtains in the reduction of PrO_{1.71} (Kuntz and Eyring, 1959). In the case of the reduction of TbO_{1.82} and TbO_{1.71} only the linear behavior at longer times is observed (Kuntz and Eyring, 1959). The chemical diffusion coefficient may be calculated from these experiments if one knows the radius of the particles being studied.

5.1.3. Selfdiffusion studies

Studies of selfdiffusion of oxygen in Nd₂O₃, Sm₂O₃ and Er₂O₃ have been undertaken employing heterogeneous isotope exchange (Stone et al., 1968). They

observed a very small oxygen pressure dependence. The results are treated to yield surface and diffusion parameters.

A sectioning technique was used to obtain diffusion and surface parameters for calcia stabilized zirconia by Simpson and Carter (1966). These results are included in table 27.7 for comparison with the data from the rare earth oxides.

5.1.4. Recent experiments

Some more recent dynamic studies of material transport may be noted. Selfdiffusion studies of CeO_{2-x} at high temperatures (850–1150°C) utilizing the isotope exchange technique (Steele and Floyd, 1971) have confirmed oxygen diffusion by a vacancy mechanism. At a composition of $\text{CeO}_{1.92}$ the diffusion coefficient may be written

$$D = 1.5 \times 10^{-5} \exp\left(\frac{-11\,900 \pm 3.9 \text{ cal}}{RT}\right).$$

The activation energy decreases from 24.8 ± 3.5 kcal/mole at CeO_2 to 3.6 ± 4.2 at $\text{CeO}_{1.8}$. The preexponential factor changes from 2×10^{-4} to 6×10^{-6} cm^2/sec in the same composition interval.

Similar selfdiffusion studies on the sesquioxides (Stone et al., 1968) utilizing isotope exchange methods gave such a low activation energy for oxygen diffusion and lack of pressure dependence that transport was considered extrinsic. Under analogous conditions, the oxygen diffusion rate decreased with atomic number of the rare earth atom being slower by a factor of 100 as between lanthanum and erbium.

The isotope exchange method of studying selfdiffusion was extended to the structural prototype of the homologous series Pr_7O_{12} which is isomorphous with the oxides of similar composition in the ceria and terbia systems. These measurements were made on powdered samples by Weber and Eyring (1971) and on polycrystalline specimens and on single crystals by Lau et al. (1976). The dependence of the diffusion coefficient on pressure is shown in fig. 27.18. The results of studies on these three physical forms were remarkably consistent. The temperature dependence of the selfdiffusion coefficient at 106 Torr oxygen, for example, may be expressed as

$$D = 6.275 \times 10^{-7} \exp(-14\,974 \text{ cal}/RT) \text{ cm}^2/\text{sec}$$

in the temperature range $740^\circ\text{C} < T < 900^\circ\text{C}$. The temperature dependence of the diffusion coefficient of oxygen in Pr_7O_{12} was almost independent of the state of subdivision of the specimen and the activation energies for diffusion were the same within experimental error in these independent studies. The $\log D$ vs $1/T$ curves at high pressure and low temperature (high composition) shows a break in all three types of material suggesting a different regime when the defect concentration reaches high levels.

The pressure dependence of the diffusion coefficient showed a distinct transition, even a minimum, in all studies implying a change in the transport mechanism as the composition of the exchanging $\text{Pr}_7\text{O}_{12 \pm \delta}$ changes. These

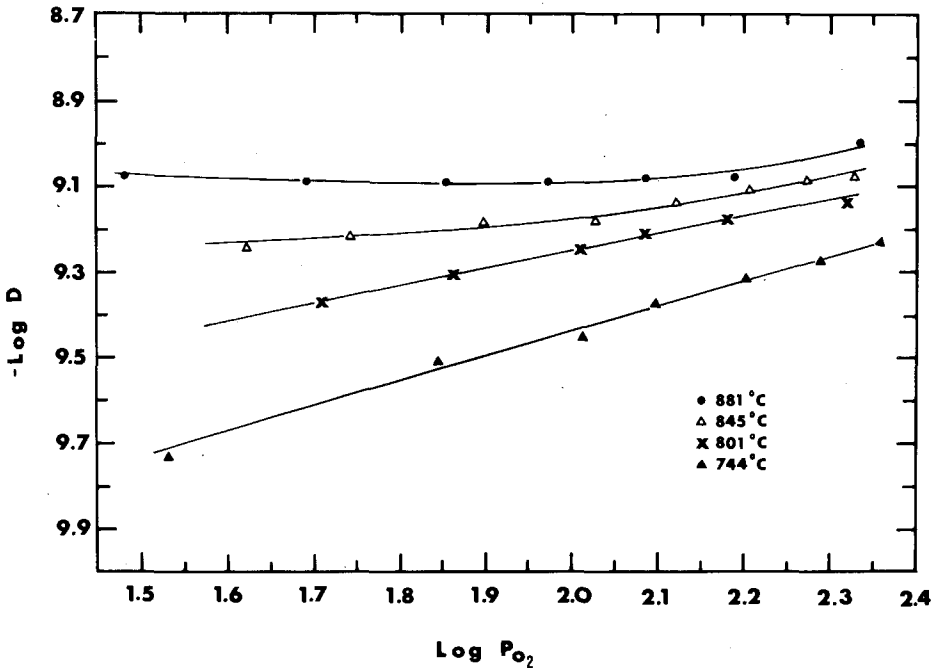


Fig. 27.18. The dependence of the diffusion coefficient on pressure as a function of temperature.

results are interpretable in terms of an interstitialcy mechanism or a vacancy mechanism depending upon whether the material is hyper or hypostoichiometric.

In the stoichiometric range a vacancy mechanism appears to predominate. The selfdiffusion equation is

$$D = 1.28 \times 10^{-3} \exp(-19050 \text{ cal}/RT) f_i$$

where D is the diffusion coefficient and f_i the mole fraction of oxygen in excess of the stoichiometric amount. A quite different behavior is observed at the lowest temperatures and highest pressures suggesting sharp changes in mechanism as the edge of the stability range of the phase is reached.

Ban and Nowick (1972) studied oxygen transport and reaction in large single crystals of CeO_x . These maintained their integrity if $1.67 < x < 2.0$. Reaction occurs in these crystals at just above room temperature and attention was given to maintain constant temperature during reaction. The rapid low temperature oxidation results in a metastable structure called α' of composition close to $x = 1.995$. This material is black and must be heated to at least 350°C before it becomes yellow characteristic of CeO_2 . The diffracted X-ray spots are smeared out and the phase is interpreted to be a domain structure of about 100–1000 atom distances. The electrical conductivity drops by a factor of about 10^5 when α' is oxidized to $\alpha(\text{CeO}_2)$.

It is pointed out that oxygen diffusing in the material possessing extended defects has a diffusion coefficient many orders of magnitude greater than that for stoichiometric CeO_2 . Ban and Nowick (1972) conclude that the low temperature reaction is not diffusion controlled nor is it controlled by surface reaction and suggest that an interstitialcy mechanism (no interstitials in the δ phase) with a low activation energy accounts for the reaction rate. Furthermore the rate limiting process is the transfer of an interstitial oxygen ion in the δ phase over to the α phase at the $\delta - \alpha$ phase boundary.

This occurrence of oxidation at below 50°C is unexpected from extrapolation from high temperature measurements. This suggests a different mechanism based on the ideas of microheterogeneity in the growth of CeO_2 domains in the $\text{CeO}_{1.818}$ matrix. Indeed α' may be an example of a pseudophase known in other regions of the fluorite-related oxide systems.

6. The tarnishing of rare earth metals by oxygen

A few scattered experiments have been performed on the reaction of rare earth metals with oxygen. Some of these have sought to determine the rate law which in the early stages of reaction is parabolic and in nearly all cases is stated to be due to the diffusion of oxygen through the oxide film of increasing thickness.

For example, Vorres and Eyring (1961) reported parabolic oxidation of La, Pr, Nd, Sm, Gd and Yb and a parabolic rate followed by a linear one for Ce. Edmondson et al. (1964) observed a parabolic law for Y, Lu, Er, Ho, Dy and Nd with activation energies in the range of 18 to 25 kcal/mole. In a separate study Jones and Edmondson (1966) followed the oxidation of Pr and found it at first to follow a parabolic law with an activation energy of 27 kcal/mole and then appear to maintain a constant barrier and follow a logarithmic law. This switchover in mechanism was accounted for by outer oxidation of the PrO_x film to give a porous higher oxide (Pr_6O_{11}). The logarithmic rate constant, k , at 500°C is $8.62 \times 10^{-4} \text{ min}^{-1} \text{ cm}^{-2}$ whereas the rate constant, kd , where d is the barrier thickness, at the same temperature is $4.40 \times 10^{-3} \text{ min}^{-1} \text{ mg cm}^{-4}$ where the limiting barrier thickness is 5.1 mg cm^{-2} .

Borchardt (1964) studied the oxidation of Y metal between $900\text{--}1400^\circ\text{C}$ with the following results. The immediate rapid reaction is an appreciable solubility of oxygen in the metal to the extent of 5.1 and 28% for 900 and 1400°C . Diffusion coefficients of oxygen in yttrium metal are approximately 1.3×10^{-6} (900°C) and 2×10^{-5} (1400°C) $\text{cm}^2 \text{ sec}^{-1}$. This phase is followed by a parabolic oxidation with rate constants $k = 1.43 \times 10^{-3} \exp(-44\,500/RT) \text{ g}^2 \text{ cm}^{-4} \text{ sec}^{-1}$. The Y metal was observed to have unusual stability due to a protective oxide scale up to a thickness of $100 \mu\text{m}$. This high temperature oxidation resistance exceeds that of any other elemental base metal. Brett and Seigle (1966) studied the oxidation of liquid rare earth metals. They observed diffusivities of about $10^{-8} \text{ cm}^2/\text{sec}$ at 1600°C . It must be appreciated that experiments on rare earth metal oxidation

are subject to great differences due to metal impurities and experiment design. nevertheless qualitative agreement abounds.

Basler (1972) studied the rate of oxidation of Gd and Dy metal at 727 to 1327°C under oxygen pressures in the range of $10^{-0.3}$ and $10^{-14.5}$ atm. Weight gain as a function of time was followed on a thermobalance. An analysis of the data suggests Gd_2O_3 is p-type at $P_{\text{O}_2} > 10^{-9.4}$ atm from 727 to 1177°C and Dy_2O_3 is p-type at $P_{\text{O}_2} > 10^{-11.3}$ atm between 727 and 1327°C. Utilizing the Wagner parabolic oxidation theory in the semiconducting range self-diffusion coefficients of oxygen were found to be $D = 1.149 \times 10^{-7} \exp(-40\,269/RT)$ cm²/sec for Gd_2O_3 (727–1177°C) and $D = 2.831 \times 10^{-8} \exp(-21\,393/RT)$ cm²/sec for Dy_2O_3 (727–1327°C).

When thin rare earth metal films were begun to be studied in electron microscopes with poor vacuums it quickly became evident that one was studying the characteristics of thin oxide or hydride films. Such studies began with Murr (1967) and were continued by Kumar et al. (1970) and have become a torrent from Caro and coworkers (see section 2.2.3). Kumar et al. (1970) found the films to oxidize by a linear rate law in contrast to Murr (1967) who observed a logarithmic rate.

Bist and Srivastava (1971) and Bist et al. (1972a, b) describe the production of SmO and GdO and Murr (1967) found ErO from the oxidation of thin films in the microscope. They ascribe these compositions to zincblende structures. In view of the established instability of these phases one wonders whether the "zincblende" phases could in fact have been hydrides (Gasgnier et al. (1974).

7. Growth of single crystals and the preparation of special specimen forms

Growth of single crystals of oxides of the lanthanide series of elements presents special problems. They are insoluble in liquid solvents at normal temperatures and pressures. They are high melting ($\sim 2500^\circ\text{C}$) and their congruently melting composition depends upon the temperature and oxygen activity. They are so thermodynamically stable that suitable vapor transport reactions are difficult to find. Frequently they suffer polymorphic transformation and shatter on cooling. Nevertheless, for many studies of problems in solid state chemistry single crystals are necessary. The growth of crystals of higher oxides present additional problems.

It shall be our purpose here to indicate some of those techniques which have proved useful in the growth of single crystals of the oxides being discussed.

7.1. *The Verneuil method*

For those substances which melt congruently and do not suffer reconstructive phase transformations between the melting point and the temperature of interest the flame fusion technique has been successfully applied. The $\text{H}_2 + \text{O}_2$ flame originally used is sometimes replaced by an argon plasma made oxidizing or

reducing by the addition of small concentrations of hydrogen or oxygen. The method consists of adding feed material to a molten region within the flame at the top of a boule which is slowly being withdrawn. The feed material is usually oxide but may be compounds such as an acetate which decompose to yield the oxide. The gaseous environment of the growing boule may be altered within limits to improve results.

7.2. Flux growth

Fused salt solutions may be found in which the solubility of these oxides is appreciable at high temperatures and from which crystals grow as the solution is cooled. Some of the fluxes which have been used for growth of the oxides of concern here are (a) potassium nitrate-sodium nitrate, (b) lead fluoride-bismuth oxide, (c) lead oxide-bismuth oxide, and (d) lithium hydroxide-boric acid-molybdenum oxide. Temperatures frequently are in the range of 1300°C.

7.3. Hydrothermal growth

At high pressure and temperature the solubility of many oxides becomes quite appreciable in water or water containing small concentrations of a mineralizer. The generation of temperature gradients or slow-cooling programs with or without pressure cycling promotes the growth of oxide crystals. This method is of greatest value in the growth of crystals of the thermally unstable intermediate and higher oxides where high oxygen pressures are necessary. Thick walled autoclaves of special alloys are used to contain the high pressure. The reaction mixture may be contained in a gold or platinum capsule and the pressurizing fluid may be water, argon or some other fluid.

Table 27.8 lists some lanthanide oxides whose single crystals have been successfully grown. The method of growth and a suitable reference are indicated.

7.4. Miscellaneous observations

For many of the intermediate phases of interest which belong to the fluorite family the composition may be adjusted by annealing at suitable oxygen pressures and temperatures. It has been established (Lowenstein et al., 1972) that crystal integrity is preserved when PrO_2 crystals are reduced to $\text{PrO}_{1.833}$ and when $\text{CeO}_{2.00}$ crystals are reduced to $\text{CeO}_{1.67}$ (Ban and Nowick, 1972).

Degen and Bondar (1974) report rapid crystal growth of Y_2O_3 at 800–1000°C and again at temperatures in excess of 1200°C where a change in morphology occurs. Round granules show edges at 1000°C and assume hexagonal shape at 1200 to 1600°C.

The physical and chemical properties of a crystal depend on its phase purity and if single phase its stoichiometry. Dramatic property variations are observed on crystals prepared under different chemical and physical conditions. Shafer et

TABLE 27.8.
Growth of lanthanide oxide single crystals.

Crystal	Method	Reference
EuO	Melt	Shafer, M.W., J.B. Torrance and T. Penney, <i>J. Phys. Chem. Solids</i> 33 , 2251 (1972).
Y ₂ O ₃	Gas laser	Gasson, D.B., B. Cockayne, <i>J. Mat. Sci.</i> 5 , 100 (1970).
CeO ₂	Flux	Linares, R.C., <i>J. Phys. Chem. Solids</i> 28 , 1285 (1967).
CeO ₂	Flux	Finch, C.B. and G.W. Clark, <i>J. Appl. Phys.</i> 37 , 3910 (1966).
CeO ₂	Flux	Vinokurov, I.V., Z.N. Zonn and V.A. Ioffe, <i>Soviet Physics Solid State</i> 7 , 814 (1965).
PrO ₂ (TbO _{1.818})	Hydrothermal	Lowenstein, M.Z., L. Kihlborg, K.H. Lau, J.M. Haschke and L. Eyring, <i>Proc. 5th Mat. Res. Sym. on Solid State Chem.</i> , NBS Spec. Pub. 364, 343 (1972).
Sm ₂ O ₃ (B-type)	Verneuil	Lejus, A.M., J.C. Bernier and R. Collongues, <i>Rev. Int. Hautes Temp. Refract.</i> 11 , 183 (1974).
Eu ₂ O ₃	Flux	Drofenik, M., L. Golic and D. Kolar, <i>J. Cryst. Growth</i> 21 , 170 (1974).
R ₂ O ₃	Verneuil	Lefever, R.A., <i>Rev. Sci. Instr.</i> 33 , 1470 (1962). Lejus, A.M. and J.P. Connan, <i>Rev. Int. Hautes Temp. Refract.</i> 11 , 215 (1974). Popova, A.A. and V.B. Zotkina, <i>Soviet Physics Doklady</i> , 11 , 553 (1967). Pastor, R.C. and A.C. Pastor, <i>Mat. Res. Bull.</i> 1 , 275 (1966).

al. (1972) make this point in their demonstration involving ir absorption and conductivity measurements of EuO crystals grown from melts containing excess Eu metal. A similar experience is reported by Massenet et al. (1974) for EuO thin films under conditions expected to provide a range of composition.

7.5. Preparation of sintered transparent polycrystalline materials

Efforts to fabricate transparent polycrystalline rare earth oxides by hot pressing and press forging at high temperatures have been successful. Press forging has produced transparent Y₂O₃ (Lefever and Matsko, 1967 and Dutta and Gazza, 1975) and hot pressing (Gazza et al., 1971) has produced Sc₂O₃.

The sintering characteristics of Sm₂O₃, Eu₂O₃, Gd₂O₃ and Dy₂O₃ were investigated under oxidizing and reducing conditions and by hot pressing (Ploetz et al., 1958). The pure rare earth oxides sintered into dense ceramic bodies at 1500–1800°C promoted mostly by a reducing atmosphere with possibly some reduction. Of the sintered compacts Dy₂O₃ was the most resistant to boiling water. Schieltz and Wilder (1967) found the sintering behavior of Y₂O₃ anomalous in that low values were obtained for the rate of shrinkage.

8. The physical properties of the rare earth oxides

This last section will be rather more in the nature of an annotated bibliography, frequently in the words of the authors cited. The selected references are intended to be enough to launch the interested reader into a more comprehensive search than is provided. This procedure is justified in part by coverage, at least tangentially in other chapters of this Handbook. References to the pertinent sections will be found in the text.

8.1. *The electrical properties of the rare earth oxides*

8.1.1. *The lower oxides*

Because of its potential commercial value as well as its intrinsic scientific interest EuO has been among the most extensively studied of the rare earth compounds. The electrical and magnetic properties of EuO are discussed in detail in Chapter 19 of Volume II and will not be repeated here.

8.1.2. *The sesquioxides*

The electrical properties of the rare earth sesquioxides were studied and the earlier literature commented on by Subba Rao et al. (1970). The results of these and other studies (as noted) are given in table 27.9. The conductivities of these sesquioxides decrease with increasing Z except that Y_2O_3 falls between Ho_2O_3 and Yb_2O_3 .

There is a break near 550–600°C in the $\log \sigma$ vs $1/T$ plots for most of the rare earth oxides. This phenomenon seems independent of P_{O_2} and is free of significant hysteresis. The observed increase in the activation energy with Z is accompanied by a decrease in conductivity.

Appreciable ionic conductivity is established in the rare earth oxides at higher temperatures. It may contribute to the break in the conductivity curve alluded to above. Of course, the low temperature conductivity could have an extrinsic component. Wilbert et al. (1975a, b) following Tare and Schmalzried (1964) have utilized solid electrolyte cells to determine the transference number for ionic conduction as a function of temperature and oxygen pressure. They find, for example, that for Gd_2O_3 $t_i = 0.5$ at $P_{O_2} = 10^{-3}$ atm and 1100°C. For Dy_2O_3 t_i is 0.5 at 1100°C at $P_{O_2} = 6.3 \times 10^{-5}$ and the value goes to ~ 0.9 at 1200°C and 10^{-7} atm oxygen.

Electronic and ionic components of electrical conductivity are resolved for Nd_2O_3 at 500–1000°C by Volchenkova and Chebotin (1974). The effect of oxygen pressure is studied and the conclusion reached that the ionic conduction is due to oxygen vacancies.

The dependence of the conductivity on oxygen pressure has been studied (Subba Rao et al., 1970) and found to vary as $P_{O_2}^{1/5.3}$ in the pressure range

TABLE 27.9.
Transport characteristics of rare earth oxides.

Oxide	$E_a(T > T_B)$ (eV)			$\sigma_{650^\circ\text{C}}^2$ $\times 10^9 (\Omega \text{ cm})^{-1}$
	Noddack ¹	Subba Rao ²	Wilbert ³ (ionic conduction)	
Sc ₂ O ₃	1.70			
Y ₂ O ₃	1.46	1.10		55
La ₂ O ₃	1.05	1.05		1700
Ce ₂ O ₃				
CeO ₂	1.10			
Pr ₂ O ₃		0.95		3450
Pr ₆ O ₁₁	0.55			
PrO ₂				
Nd ₂ O ₃	0.97	1.15	0.87	1450
Sm ₂ O ₃	1.17	1.28	1.28	880
Eu ₂ O ₃	1.24	1.35	1.09-1.41	150
EuO				
Gd ₂ O ₃	1.36	1.57	1.42	130
Tb ₂ O ₃		0.95		200
"Tb ₄ O ₇ "	0.40			
TbO ₂				
Dy ₂ O ₃	1.39		2.28	
Ho ₂ O ₃		1.61	1.89	160
Er ₂ O ₃	1.40		1.29	
Tm ₂ O ₃			1.65	
Yb ₂ O ₃	1.53	1.61	1.49	50
Lu ₂ O ₃			1.96	

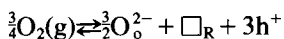
$E_a(T > T_B)$ (eV) \equiv Activation energy in the temperature above the break in the curve
 $\sigma_{650^\circ\text{C}}^2 \equiv$ DC electrical conductivity at 650°C measured at $P_{\text{O}_2} \cong 150$ torr

¹Noddack, W. and H. Walch, Z. Phys. Chem. **211**, 194 (1959).

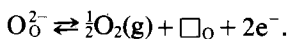
²Subba Rao, G.V., S. Ramdas, P.N. Mehrotra and C.N.R. Rao, J. Solid State Chem. **2**, 377 (1970).

³Wilbert, Y., N. Dherbome~~2~~ and H. Breuil, C.R. Acad. Sci., Paris, Series C **280**, 465 (1975).

2-100 torr for some cases as would be expected if it were *p*-type arising from



where O_O^{2-} is an oxygen ion on an oxygen site, \square_R is a vacant metal atom site and h^+ is an electron hole. At sufficiently low pressures the sesquioxides are *n*-type semiconductors with σ proportional to $P_{\text{O}_2}^{-1/6}$ as expected from



On the other hand Wilbert et al. (1975a, b) have found a pressure dependence of the resistivity to be proportional to the pressure of oxygen to the $-1/m$ power

where m varies between 4 and 6 except for Eu_2O_3 which is higher. Seebeck coefficients confirm p -type semiconduction at 140 torr oxygen which increases sharply at 600°C .

The dielectric behavior of vacuum deposited PrO_x and Dy_2O_3 films has been studied by Goswami and Goswami (1974) and by Goswami and Varma (1975) as a function of frequency and temperature.

The ac conductivity of Sc_2O_3 has been measured by Pike (1972) in the audio-frequency range at temperatures between 4 and 295 K. The results are explained in terms of a new hopping model.

8.1.3. *The higher oxides of the rare earths*

The phase relationships in the higher oxides of Ce, Pr and Tb have been elaborated earlier (see section 2.3). It is clear that these systems are complex and sensitive to environmental conditions and unless extreme care is taken property measurements will be on inadequately characterized materials. The electrical properties made on higher oxides come in this category and only the broadest statements can be made. Subba Rao et al. (1970) have made some observations on the PrO_x and TbO_x systems and have reviewed the previous work on PrO_x – principally by Honig et al. (1963b). There seems to be agreement on the following points. The mixed valence higher oxides are hopping-type electron conductors. In the range $\text{RO}_{1.5}$ – $\text{RO}_{2.0}$ the oxides are p -type between $\text{RO}_{1.5}$ – $\text{RO}_{1.75}$ and n -type above this composition. It should be remembered however that $\text{RO}_{1.75}$ is in a two-phased region in both oxides, R_8O_{14} being unstable. As a matter of fact the minimum in resistivity is shallow and may occur at $\text{RO}_{1.714}$ which is a well-known phase of narrow composition limit where some have argued the minimum should occur (Hyde and Eyring, 1965). It is obvious that a clarification of this work will be possible only when large single crystals of the intermediate phases are available and when sufficient care is taken to characterize their composition, structural and textural details.

Experiments were performed (Subba Rao et al., 1970) on the pressure dependence of the conductivity on the PrO_x system. Pr_6O_{11} was established as n -type but the conductivity was very dependent on oxygen pressure (hence composition). The Pr_7O_{12} conductivity on the other hand was less pressure-dependent as might be expected since it has a much wider temperature range of compositional stability.

Grosvald (1964) has reviewed his and others work on the dielectric properties of nonstoichiometric praseodymium oxides in the composition range Pr_2O_3 – PrO_2 . The coexistence of two relaxation phenomena in the diphasic regions were observed and ordered vacancies in the Pr_6O_{11} phase were obtained.

In addition to phase stability analysis already discussed (see section 2.3.1) the data of Bevan and Kordis (1964) on the $\text{CeO}_{2-\delta}$ – O_2 system and new isothermal data obtained by Panlener et al. (1975) has been analyzed for the composition range $\text{CeO}_{2.0}$ to $\text{CeO}_{1.70}$ over a pressure range of 10^{-2} to 10^{-26} atm of oxygen for a series of isotherms from 750 – 1500°C . Blumenthal (1975) found that in the composition range $0.001 < \delta < 0.01$ the partial molar entropy change was consis-

tent with the presence of randomly distributed doubly ionized oxygen vacancies. Furthermore they observed a $P_{O_2}^{-1/5}$ dependence of composition and conductivity which was also accounted for satisfactorily by doubly ionized oxygen vacancies. In this range $\Delta\bar{H}_{O_2}$ is a mild function of δ but outside the range it is strongly composition-dependent going through a minimum at about $CeO_{1.82}$, the composition of the δ -phase. Apparently the simple application of the mass action law in terms of point defects is inappropriate even at quite low defect concentration and markedly so as the defect concentration increases.

Conductivity studies on sintered specimens of $CeO_{2-\delta}$ as a function of composition at constant temperature have been derived by combining thermogravimetric data with conductivity both taken as a function of pressure and temperature in the range 750–1500°C at oxygen pressures ranging from 1 to 10^{-22} atm (Blumenthal and Sharma, 1975). The results are fit with

$$\sigma = 410[\delta] \exp\left(-\frac{0.158 + \delta}{kT}\right) (\text{ohm cm})^{-1}$$

over the composition range $CeO_{1.999}$ and $CeO_{1.900}$ at 750–1500°C. From this relation the electron carrier concentration, presumed concentrated on cerium atoms between hops, is

$$n'_{CeCe} = 8\delta/a_0^3 \text{ cm}^{-3}$$

where a_0 is the lattice parameter of the fluorite unit cell. The electron mobility is

$$\mu = 5.2 \times 10^{-2} \exp\left(-\frac{0.158 + \delta}{kT}\right) \text{ cm}^2/\text{V sec.}$$

The activation energy derived for electron conduction is a constant 0.22 eV between $\delta = 10^{-3}$ and 1.6×10^{-2} but increases to 0.37 at $\delta = 2 \times 10^{-1}$. At low temperatures E_a is 0.61 ± 0.03 eV and independent of δ .

Earlier work had frequently suggested the presence of such defects as oxygen vacancies, divacancies, cerium interstitials and polarons in CeO_{2-x} based on an analysis of extant information. Land (1973) has discussed these possibilities with the conclusion that the data can be explained by polarons in equilibrium with isolated oxygen vacancies but not with divacancies or interstitial cerium ions.

8.2. Magnetism in rare earth oxides

Rare earth atoms have played a leading role, center stage, in the development of our understanding of magnetism (Van Vleck, 1965). The deeply embedded 4f electrons of the rare earth atoms in the oxides interact weakly with each other such that any cooperative effects occur at quite low temperatures. The Néel points of antiferromagnetic Dy_2O_3 , Er_2O_3 and Yb_2O_3 , for example, are respectively 1.2 K, 3.4 K and 2.3 K.

8.2.1. The lower oxides

Chapter 19 of Volume 2 should be consulted for the magnetic properties of EuO.

8.2.2. *The sesquioxides*

a. *Magnetic characteristics* – Magnetic susceptibilities have been measured for some sesquioxides over a wide temperature range. In general they obey the Curie–Weiss relationship. Smol'kov and Dobroval'skaya (1965) measured the magnetic susceptibility of the sesquioxides of La, Nd and Gd between 20 and 800°C. They obtained results in agreement with Van Vleck's theoretical values with a screening constant, $\sigma = 33$.

The structure and magnetic properties of samarium as the sesquioxide and the metal have been studied by Perakis and Kern (1972). Between 80–154 K the magnetic susceptibility of a purified Sm specimen essentially coincided with that for Sm^{3+} in monoclinic Sm_2O_3 . The minimum of χ (the magnetic susceptibility) was at about 350 K.

Kern and Perakis (1969) observed a slight discontinuity in the χ_λ^{-1} vs T curve at about 1280 K for Eu_2O_3 corresponding to the cubic to monoclinic phase transformation. Earlier Borovik-Romanov and Kreines (1955) had observed the magnetic susceptibility at lower temperatures (12–300 K) where Eu_2O_3 agreed with Van Vleck's theory if a splitting of the first excited level is taken into account. The difference in two crystalline modifications of Sm_2O_3 was commented on and deviations from Van Vleck's theory for the free ions are shown to be adequately accounted for by the splitting of the ground state of Sm^{3+} in the field of the lattice.

The susceptibility of Eu_2O_3 of varying concentration in Y_2O_3 has been measured (Kern and Kosteletzky, 1971) to liquid helium temperatures. The susceptibility and crystal-field splitting remained relatively constant and the "excess" in susceptibility over that calculated from the spectroscopic data is not completely explained even when the presence of the monoclinic phase was considered.

Arajs and Colvin (1962, 1964) made measurements on Eu_2O_3 , Gd_2O_3 and Dy_2O_3 in the approximate temperature range 300–1300 K which were in satisfactory agreement with Van Vleck's theory and Judds' energy levels for free Eu^{3+} . Bonrath et al. (1966) observed the magnetic susceptibility of single crystals of Dy_2O_3 , Er_2O_3 and Yb_2O_3 in the temperature region of 1.1 to 4.2 K in $H_{\text{ext}} \leq 3.5$ kOe. These oxides become antiferromagnetic with Néel temperatures of 1.2, 3.4 and 2.3 K respectively.

The low temperature magnetic susceptibility of monoclinic, cubic, stoichiometric and substoichiometric gadolinium oxides have been measured in the range 1–6 K by Miller et al. (1971). Transformation temperatures and correlations with specific heat peaks in Gd metal containing appreciable amounts of oxygen are made.

In a series of papers the paramagnetic susceptibility of single crystals of the sesquioxides of various rare earths has been reported as a function of crystal orientation with respect to the magnetic field. Measurements have been made at constant temperatures of 5, 77 and 300 K as well as at increasing temperatures from 5–1000 K. The anisotropy observed is interpreted in terms of the layer

structures in the case of the A- and B-type crystals as well as the electronic energy levels in some cases. The sesquioxides studied include La, Pr, Nd, Sm, Gd and Er (Tueta et al., 1972; Tueta and Lejus, 1974; Lejus and Connan, 1974; Lejus et al., 1974, 1976 and Bernier et al., 1973, 1975).

b. *Magnetic structures* – The magnetic scattering of neutrons has been utilized to investigate the magnetic structure of certain of the rare earth oxides. Koehler and Wollan (1953b) studied the angular dependence of paramagnetic scatter for Pr_2O_3 , Nd_2O_3 and Er_2O_3 which have large angular momentum contributions to their magnetic moments. The results were compared to theory. Further work on holmium oxide indicated magnetic ordering at low temperatures.

The C-type rare earth sesquioxide (space group $Ia\bar{3}$) has two sets of metal atom positions. One set of 24 metal atoms has a single parameter u ($u = 0.030$ for the isomorphous mineral bixbyite). Each is coordinated by six oxygens instead of the eight at the corners of a regular cube as in fluorite. Two are removed across the face-diagonal resulting in a C_2 site. In the other set of eight without parameters, the two oxygen vacancies lie at opposite ends of the body-diagonal of the coordination cube yielding a C_{3i} site. Moon et al. (1968) have determined the magnetic structure of Er_2O_3 and Yb_2O_3 . Noncollinear antiferromagnetic structures were found with the moment direction related to the local symmetry axis. For Er_2O_3 the moment on the C_2 site is $5.36 \pm 0.08 \mu_B$ and at the C_{3i} site the moment is $6.06 \pm 0.23 \mu_B$. The Néel points are 3.4 K and 2.3 K respectively. For Yb_2O_3 the corresponding moments are $1.86 \pm 0.06 \mu_B$ and $1.05 \pm 0.06 \mu_B$. The magnetic structure of Er_2O_3 had earlier been obtained by Bertaut and Chevalier (1966).

Recently Moon and Koehler (1975) have used polarized neutron experiments to measure the temperature dependence of the susceptibility of the Gd^+ ion at the two crystallographic sites in cubic Gd_2O_3 in the paramagnetic state. The advantage of this technique is that it can distinguish more than one type of magnetic atom rather than obtaining simply an average response. Below 10 K these susceptibilities are quite different because of the different net exchange interactions with the remainder of the crystal.

The results of this study show the persistence of spin correlations up to 100 times the ordering temperature in Gd_2O_3 , a material previously regarded as an ideal paramagnet. Spin correlations then must be taken into account in obtaining proper form factor data. The paramagnetic form factor for Gd_2O_3 leads to the conclusion that the 4f spin density in this material is the same as in the metal.

Quezel et al. (1970) presented new data on Tb_2O_3 and discussed the magnetic modes allowed for the C_2 and C_{3i} sites for this and for Er_2O_3 and Yb_2O_3 . In the Tb_2O_3 structure at 1.5 K the total moment of Tb is $4.2 \mu_B$, much less than for the free ion.

8.2.3. Higher oxides of the rare earths

As discussed in detail above (see section 2.3) Ce, Pr and Tb oxides are capable of forming many ordered and disordered phases in the composition interval RO_x

$1.5 < x < 2.0$. For this reason one must be conscious of the exact mode of preparation of specimens for magnetic study. MacChesney et al. (1964) studied the magnetic susceptibility of polycrystalline specimens of the praseodymium oxides. PrO_2 prepared at 200 atm of O_2 appears to be antiferromagnetic with a Néel temperature of 14 K in contrast to low pressure preparations reported by Kern (1964) to lack cooperative effects.

MacChesney et al. (1964) compare their results on $\text{PrO}_{1.5}$, $\text{PrO}_{1.83}$ and $\text{PrO}_{2.00}$ with those of Kern (1964) on $\text{PrO}_{1.5}$, $\text{Pr}_{1.72}$, $\text{PrO}_{1.83}$ and $\text{PrO}_{2.01}$ in the range of about 4–300 K. There was agreement that the Curie-Weiss law was found to hold over the upper portion of the temperature range and the magnetic moments were found to be close to the theoretical value predicted for the free ion. Kern and Perakis (1970) have measured the magnetic susceptibility as a function of temperature up to about 1400 K. They consider their results against a view that the mixed oxides are simply a mixture of Pr^{3+} and Pr^{4+} ions. The materials do not appear to have been maintained at composition as the temperature was increased.

MacChesney et al. (1966) have measured the magnetization as a function of temperature for Tb_2O_3 (cubic and monoclinic polymorphs), $\text{TbO}_{1.715}$, $\text{TbO}_{1.809}$, $\text{TbO}_{1.825}$ and TbO_2 between 1.4 and 300 K. With the exception of $\text{TbO}_{1.809}$ each phase ordered antiferromagnetically with Néel temperatures of 2, 7, 7, 6 and 3 K respectively. $\text{TbO}_{1.809}$ was not found ordered above 1.4 K. In the case of some of the lower compositions they may be metamagnetic. $\text{TbO}_{1.823}$ exhibits a tendency toward ferrimagnetic alignment as indicated by remanent magnetization at 1.4 K. At higher temperatures, in the paramagnetic region, all the oxide phases give effective Bohr magneton numbers close to the expected values for the free ions.

The magnetic structure of TbO_2 has been investigated by Quezel-Ambunaz and Bertaut (1972). TbO_2 is antiferromagnetic with a Néel temperature of 3 K. The moments are distributed in the (111) plane along undetermined directions. Terbium possesses a magnetic moment of $6.25 \pm 0.10 \mu_B$ at 1.5 K.

Analysis of the EPR lineshape and width of Tb^{4+} in polycrystalline TbO_2 has been made by Azzoni et al. (1970) who found limited agreement with approximated theoretical calculations.

Schreiner and Czopnik (1973) measured the magnetic susceptibility of Nd_2O_3 , Tb_4O_7 , Pr_6O_{11} between 1.5 and 300 K for Nd and Pr oxides and 4.2 and 300 K for Tb oxide. No magnetic ordering was observed in these materials contrary to the observations of MacChesney et al. (1966). One cannot help wondering how well the materials are characterized since Tb_4O_7 , for example, does not correspond to a known stable oxide of terbium.

8.3. *Optical properties of the rare earth oxides*

The stoichiometric oxides of the rare earths are a light pastel color except for what is PrO_2 and TbO_2 from gravimetric measurements which are black and red respectively. The mixed valence intermediate oxides including the higher oxides of Ce, Pr and Tb and the substoichiometric sesquioxides are all deep colors.

The influence of temperature and magnetic field on the optical transmission of an EuO single crystal has been studied by Skornyakov et al. (1971). In the temperature range 30–293 K and magnetic fields up to 2.7 kOe transmission in the wavelength range 0.9–2.7 μm was observed to change markedly as each condition was varied showing shifts in the position and sharpness of the transmission edge.

Batlogg et al. (1975) have deduced something of the electronic structure of the mixed valence Eu_3O_4 . They investigated the optical reflectivity of single crystal Eu_3O_4 in the photon energy range 0.03 and 12 eV. Interpretations were made in terms of lattice vibrations and interband transitions from initial Eu^{2+} , Eu^{3+} and $2p^0$ states into crystal-field-split 5d bands. In addition, intra $4f^6$ transitions were observed. The coulomb correlation energy between Eu^{2+} and Eu^{3+} was determined. Optical transmission measurements revealed a blue shift of the absorption edge above the Néel point and in $H_{\text{ext}} = 0$ and a red shift for magnetic fields larger than $H_{\text{ext}}^c = 2.4$ kOe confirming the metamagnetic phase above 5.2 ± 0.2 K.

M spectra of Eu, EuO and Eu_2O_3 have been compared by Mariot and Karnatak (1974) and energy level diagrams are proposed. The spectra show an evolution of metallic character in the sequence.

Similar studies of the $M_{4,5}$ emission spectra of Gd_2O_3 and Yb_2O_3 have been made by LaVilla (1974). Differences in profiles due to resonance radiation as compared to spectra excited by electron impact are reported and the photoelectron spectra are discussed.

Infrared absorption spectra have been recorded for most of the sesquioxides by McDevitt and Baun (1964), McDevitt and Davidson (1966), Petru and Muck (1966, 1967a, b) and Faithful et al. (1973) who record not only the bands observed for C, B and A-type sesquioxides but also show their results to be consistent with the statistical structures mentioned earlier for the A-type (Müller-Buschbaum and Schnering, 1965). Optical constants have been observed by Nigara (1968) for Y_2O_3 .

The far-infrared and visible spectra of erbium oxide have been observed by Bloor et al. (1970) about the antiferromagnetic state at 3.4 K. The complex spectra can be interpreted in terms of ions on two nonequivalent sites. The changes in the visible absorption spectrum, together with changes in phonon frequencies, are attributed to the presence of the exchange fields and a magnetostrictive expansion of the crystal lattice in the ordered state.

Reflectance spectra have been observed by Vratny et al. (1961), White (1967), Sinha (1967), McMahan (1967) and Nigara et al. (1971). High-temperature spectral emittance of some oxides have been recorded by McMahan and Wilder (1968) and Guazzoni (1972). A variety of other optical properties have been reported, such as the absorption edge of Sc_2O_3 (Tippins, 1966), the refractivities of rare earth oxides (Levin, 1964), and optical properties by Batsanov et al. (1965) and Ruchkin et al. (1967). Caro and Derouet (1970) have placed Nd_2O_3 in the range of neodymium compounds exhibiting a nephelauxetic effect.

Dulepov et al. (1972) have investigated the dielectric properties and charges on

the atoms of many rare earths in C-type oxides. They tabulate the refractometric constants of many of the rare earth C-type oxides.

Warmkessel et al. (1969) have recorded the absorption spectra of some sesquioxides in the uv and visible and of the higher oxides of PrO_x , $1.5 < x < 2.0$. They found the spectra of the intermediate phases to be suitable fingerprints for each phase and although the ir and visible bands for the sesquioxides could be assigned it was not possible for the intermediate phases.

The refractive index, the absorption index and the absorption coefficient of vacuum deposited films of PrO_x prepared under varying conditions have been evaluated by Goswami and Goswami (1975) from the transmittance data as a function of wavelength in the visible region. The optical energy gap is estimated at 3.40 eV.

Haensel et al. (1970) have observed optical absorption of cerium, cerium oxide, praseodymium, praseodymium oxide and samarium in the extreme ultraviolet using synchrotron radiation from the 7.5 GeV electron synchrotron DESY as the light source. Optical absorption was measured in the energy region 100 eV to 180 eV where numerous sharp maxima are observed. The absorption spectra of Ce and CeO_x show a marked difference whereas those of the metal-metal oxide pairs in Pr and Nd are very similar.

8.4. Mechanical and thermal properties

Gibson and Harvey (1966) and Vier (1975) have collected a wide variety of information on the rare earth oxides and other substances including many mechanical and thermal properties. These publications also list reference sources for the data they include. A few other types of studies should be mentioned. The elastic properties of Gd_2O_3 , Y_2O_3 , Dy_2O_3 , Er_2O_3 and Ho_2O_3 have been measured as a function of temperature by Haglund and Hunter (1973); Manning et al. (1966); Manning and Hunter (1969) and Manning et al. (1969).

The thermal conductivity of EuO between 1 and 200 K has been measured by Martin and Dixon (1972) with attention given to effects of magnetic order. Near the Curie point weak critical scattering was observed. At 1 K the dominant heat carriers were magnons.

Thermal transport in Y_2O_3 has been studied by Klein and Croft (1967), of Eu_2O_3 by Gibby (1973), of Er_2O_3 by Hunter and Calderwood (1973/74) and by Chekhovskoi et al. (1973). Thermal expansion of rare earth oxides utilizing X-ray methods have been studied by Stecura and Campbell (1961) and Hatibarua and Mahanta (1972 and 1975) and for Sc_2O_3 by Hajek et al. (1973).

Thermal conductivity coefficients of CeO_2 in the temperature range 400–1500 K are reported by Chekhovskoi et al. (1971).

Ploetz et al. (1958) determined the coefficient of expansion of Sm_2O_3 ($10.8 \times 10^{-6} \text{ cm cm}^{-1} \text{ }^\circ\text{C}^{-1}$) from 30–740°C. The lowest value measured was for Dy_2O_3 ($8.3 \times 10^{-6} \text{ cm cm}^{-1} \text{ }^\circ\text{C}^{-1}$) from 30–840°C; Eu_2O_3 ($10.5 \times 10^{-6} \text{ cm cm}^{-1} \text{ }^\circ\text{C}^{-1}$) from 30–840°C and for Gd_2O_3 they observed $10.0 \times 10^{-6} \text{ cm cm}^{-1} \text{ }^\circ\text{C}^{-1}$ from 30–850°C.

Sims and Blumenthal (1976a, b, c) have studied the thermal expansion of CeO_2

and $\text{CeO}_{2-\delta}$ in the temperature range 800–1000°C utilizing high temperature X-ray techniques on powders and by macroscopic length measurements under similar conditions. The X-ray studies yielded the following relationship for CeO_2

$$\text{thermal expansion (\%)} = \frac{a_T - a_{25}}{a_{25}} \times 100 = A + BT + CT^2 + DT^3$$

$$A = -2.14 \times 10^{-2}, \quad B = 8.72 \times 10^{-4}, \quad C = 5.83 \times 10^{-7},$$

$$D = 2.56 \times 10^{-10}, \quad T = \text{temperature (}^\circ\text{C)}.$$

In separate experiments the percent expansion as a function of the degree of substoichiometry was observed to increase with δ at an increasing rate. The curve shows two regions, $\text{CeO}_2\text{--CeO}_{1.88}$ and $\text{CeO}_{1.88}\text{--CeO}_{1.77}$. The results of macroscopic length measurements were in substantial agreement.

These studies were examined critically and it was concluded that they were inconsistent with interstitial cerium atoms but consistent with oxygen vacancies if in addition there were other anion and cation vacancies. They also indicated that their results could be interpreted in terms of defect-defect interaction forming extended defects which must be considered a real possibility. The X-ray line profiles did not show evidence of deviation from the cubic structure.

Acknowledgement

The United States Energy, Research and Development Administration and before them the United States Atomic Energy Commission have supported the bulk of the work on rare earth oxides carried out by the author and his many coworkers. Indeed, a large fraction of the American work on the oxides has been sponsored by them. We acknowledge this active interest with gratitude.

References

- Ackermann, R.J. and E.G. Rauh, 1971, *J. Chem. Thermodyn.* **3**, 609.
 Ackermann, R.J. and E.G. Rauh, 1973, *J. Chem. Thermodyn.* **5**, 331.
 Ainscough, J.B., D.A. Moore and S.C. Osborn, 1975, *J. Nucl. Mater.* **55**, 229.
 Anderson, J.S., 1970, Defect chemistry and non-stoichiometric compounds, in: Rao, C.N.R., ed., *Modern Aspects of Solid State Chemistry*, (Plenum Press, New York) p. 29.
 Arajs, S. and R.V. Colvin, 1962, *J. Appl. Phys.* **33**, 2517.
 Arajs, S. and R.V. Colvin, 1964, *J. Appl. Phys.* **35**, 1181.
 Asprey, L.B., 1949, *Equilibria in the Oxide Systems of Praseodymium and Americium*, Ph.D. Thesis, University of California, Berkeley.
 Azzoni, C.B., G.L. DelNero and G. Lanzi, 1970, *Lettere al Nuovo Cimento*, **IV**, 959.
 Ackermann, R.J., E.G. Rauh and R.J. Thorn, 1964, *J. Chem. Phys.* **40**, 883.
 Ackermann, R.J., E.G. Rauh and R.R. Walters, 1970, *J. Chem. Thermodyn.* **2**, 139.
 Baker, F.B. and C.E. Holley, 1968, *J. Chem. Eng. Data* **13**, 405.
 Baenziger, N.C., H.A. Eick, H.S. Schuldt and L. Eyring, 1961, *J. Amer. Chem. Soc.* **83**, 2219.
 Ban, Y. and A.S. Nowick, 1972, Defects and mass transport in reduced CeO_2 single crystals, in: Roth, R.S. and S.J. Schneider, Jr., eds., *NBS Spec. Publ.* **364**, p. 353.
 Barbezat, S. and J. Loriers, 1952, *C.R. Acad. Sci.* **245**, 1978.
 Bärnighausen, H. and G. Brauer, 1962, *Acta Cryst.* **15**, 1059.
 Bartram, S.F., 1966, *Inorg. Chem.* **5**, 749.
 Basler, D.B., 1972, *High Temperature Oxidation of Gadolinium and Dysprosium Under Controlled Oxygen Partial Pressure*, Ph.D. Thesis, Iowa State University, Ames, Iowa.
 Batlogg, B., E. Kaldis, A. Schlegel and P. Wachter, 1975, *Phys. Rev.* **12B**, 3940.
 Batsanov, S.S., A.N. Kastova, E.D. Ruchkin and V.S. Grigor'eva, 1965, *Zhurnal Strukturnoi Khimii*, **6**, 58.

- Bedford, R.G. and E. Catalano, 1971, *J. Solid State Chem.* **3**, 112.
- Berard, M.F., C.D. Wirkus and D.R. Wilder, 1968, *J. Amer. Ceram. Soc.* **51**, 643.
- Bernier, J.C., A.M. Lejus, R. Tueta and R. Collongues, 1973, *Mat. Res. Bull.* **118**, 261.
- Bernier, J.C., A.M. Lejus, R. Tueta and R. Collongues, 1975, *Solid State Comm.* **16**, 349.
- Bertaut, E.F. and R. Chevalier, 1966, *C.R. Acad. Sci., Paris*. **B262**, 1707.
- Bevan, D.J.M., 1955, *Inorg. and Nucl. Chem.* **1**, 49.
- Bevan, D.J.M. and J. Kordis, 1964, *J. Inorg. Nucl. Chem.* **26**, 1509.
- Bist, B.M.S. and O.N. Srivastava, 1971, *Phys. Status Sol.* (a) **7**, 9.
- Bist, B.M.S., J. Kumar and O.N. Srivastava, 1972a, *Phys. Status Sol* (a) **14**, 197.
- Bist, B.M.S., J. Kumar and O.N. Srivastava, 1972b, *Z. Kristallogr.* **136**, 144.
- Bloor, D., J.R. Dean and G.E. Stedman, 1970, *J. Appl. Phys.* **41**, 1242.
- Blumenthal, R.N., 1975, *J. Solid State Chem.* **12**, 307.
- Blumenthal, R.N. and R.K. Sharma, 1975, *J. Solid State Chem.* **13**, 360.
- Bogdanov, A.G. and V.S. Rudenko, 1965, *Doklady Akad. Nauk SSSR*, **161**, 590.
- Bonrath, H., K.H. Hellwege, K. Nicolay and G. Weber, 1966, *Phys. Kondens. Materie.* **4**, 382.
- Borchardt, H.J., 1964, *J. Inorg. Nucl. Chem.* **26**, 711.
- Borovik-Romanov, A.S. and N.M. Kreines, 1955, *J. Exper. Theoret. Phys. USSR*, **29**, 740.
- Boulesteix, C. and Ch. Loier, 1973, *Phys. Stat. Sol.* (a) **18**, 553.
- Boulesteix, C., P. Caro, M. Gasgnier, Ch. Henry LaBlanchetais and G. Schiffmacher, 1971a, Etude par microscopie et diffraction electroniques des transformation, a haute temperatures des sesquioxides de terres rares, in: *Proc. Colloquia Internationaux C.N.R.S.*, No. 205, p. 361.
- Boulesteix, C., P. Caro, M. Gasgnier, Ch.H. LaBlanchetais and G. Schiffmacher, 1971b, *Acta Cryst.* **A27**, 552.
- Boulesteix, C., P. Caro, M. Gasgnier, Ch.H. LaBlanchetais and G. Schiffmacher, 1971c, *Phys. Letters*, **34A**, 437.
- Boulesteix, C., P.E. Caro, Ch. Loier and R. Portier, 1972, *Phys. Status Solidi* (a) **11**, 771.
- Brauer, G., 1964, Kristallchemie der Oxide der Seltenen Erden, in: Eyring, L., ed., *Progress in the Science and Technology of the Rare Earths*, vol. 1 (Pergamon Press, Oxford) p. 152.
- Brauer, G., 1966, Structural and Solid State Chemistry of Pure Rare Earth Oxides, in: Eyring, L., ed., *Progress in the Science and Technology of the Rare Earths*, vol. 2 (Pergamon Press, Oxford) p. 312.
- Brauer, G., 1968, Structural and Solid State Chemistry of Pure Rare Earth Hydroxides, in: Eyring, L., ed., *Progress in the Science and Technology of the Rare Earths*, vol. 3 (Pergamon Press, Oxford) p. 434.
- Brauer, G. and U. Holtschmidt, 1951, *Z. Anorg. Allgem. Chem.* **265**, 105.
- Brauer, G. and U. Holtschmidt, 1955, *Z. Anorg. Allgem. Chem.* **279**, 129.
- Brauer, G. and K.A. Gingerich, 1960, *J. Inorg. Nucl. Chem.* **16**, 87.
- Brauer, G. and R. Müller, 1963, *Z. Anorg. Chem.* **321**, 234.
- Brauer, G. and B. Pfeiffer, 1963, *J. Less-Common Metals*, **5**, 171.
- Brauer, G. and E. Mohr-Rosenbaum, 1972, *Z. Anorg. Allgem. Chem.* **394**, 301.
- Brauer, G., K.A. Gingerich and U. Holtschmidt, 1960, *J. Inorg. Nucl. Chem.* **16**, 77.
- Brett, J. and L. Seigle, 1966, *J. Less-Common Metals* **10**, 22.
- Burnham, D.A. and L. Eyring, 1968, *J. Phys. Chem.* **72**, 4415.
- Burnham, D.A., L. Eyring and J. Kordis, 1968, *J. Phys. Chem.* **72**, 4424.
- Campserveux, J. and P. Gerdanian, 1974, *J. Chem. Thermo.* **6**, 795.
- Caro, P.E., 1968, *J. Less-Common Metals*, **16**, 367.
- Caro, P. and J. Derouet, 1970, *C.R. Acad. Sci., Paris*, **271C**, 1370.
- Caro, P.E., M. Gasgnier and C.H. LaBlanchetais, 1970, *Physics Letters*, **32A**, 361.
- Chapin, D.S., M.C. Finn and J.M. Honig, 1965, The Phase Transition Region of $\text{PrO}_{1.5}$, in: Eyring, L., ed., *Rare Earth Research III* (Gordon and Breach, New York) p. 607.
- Chekhovskoi, V. Ya., G.I. Stavrovskii and A.B. Ivanov, 1971, Consultant's Bureau translation of *Teplofizika Vysokikh Temperature* **9**, 1182.
- Chekhovskoi, V.Ya., G.I. Stavrovskii, A.I. Pustel'nik, T.S. Sedykh and A.B. Ivanov, 1973, *Heat Transfer-Sov. Res.* **5**, 68.
- Chikalla, T.D., C.E. McNeilly and F.P. Roberts, 1972, *J. Amer. Ceram. Soc.* **55**, 428.
- Clifford, A.F., 1964, A Joint Report on the Simultaneous Independent Work in Three Laboratories on the Solvolytic Disproportionation of Intermediate Higher Oxides (R.E.) O_x ($1.50 < x < 2.00$) into (R.E.) (III) and (R.E.) O_2 , in: Vorres, Karl, ed., *Rare Earth Research II* (Gordon and Breach, New York) p. 45.
- Coutures, J.P., R. Verges and M. Foëx, 1975, *Rev. Int. Hautes Temp. Refract.* **12**, 181.
- Cromer, D.T., 1957, *J. Phys. Chem.* **61**, 753.
- Degen, M.G. and I.A. Bondar, 1974, *Dokl. Akad. Nauk SSSR*, **215**(4), 924.
- Douglass, R.M. and E. Staritzky, 1956, *Anal. Chem.* **28**, 552.
- Dulepov, E.V., S.S. Batsanov and G.N. Kustova, 1972, Translated by the Consultant's Bureau from *Zh. Strukturnoi Khimii*, **13**, 935.
- Dutta, S.K. and G.A. Gazza, 1975, U.S. Patent 3878.280.
- Edmondson, W., K. Goodhead and P.M.S. Jones, 1964, The Oxidation of Rare Earth Metals, Part I, Bulk Materials, in: AWRE Rept. No. 0-45/64.
- Eick, H.A., N.C. Baenziger and L. Eyring, 1956, *J. Am. Chem. Soc.* **78**, 5147.
- Benezech, G., J.P. Coutures, M. Foëx, 1974, *J. Less-Common Metals* **38**, 131.
- Drofenik, M., L. Golic and D. Kolar, 1974, *J. Cryst. Growth* **21**, 170.

- Eyring, L., 1949, Thermochemical Studies of Oxides of Praseodymium and Americium and the Estimation of the Praseodymium (III)-Praseodymium (IV), Americium (III)-Americium (IV) Oxidation Potentials, Ph.D. Thesis, University of California, Berkeley.
- Eyring, L., 1967, Fluorite-Related Oxide Phases of the Rare Earth and Actinide Elements, in: Gould, R.F., ed., *Advances in Chemistry Series 71* (Amer. Chem. Soc., Washington, D.C.) p. 67.
- Eyring, L., 1970a, Refractory Oxides of the Lanthanide and Actinide Elements, in: Alper, A.M., ed., *High Temperature Oxides* (Academic Press, New York) p. 41.
- Eyring, L., 1970b, *J. Solid State Chem.* **1**, 376.
- Eyring, L., 1970c, Oxygen Transport Properties of Rare Earth Oxides, in: Belton, G.R. and W. Worrell, eds., *Heterogeneous Kinetics at Elevated Temperatures* (Plenum Press, New York) p. 343.
- Eyring, L., 1974, Lanthanide and Actinide Oxides, A Case Study in Solid State Chemistry, in: Rao, C.N.R., ed., *Solid State Chemistry* (Marcel Dekker, New York) p. 565.
- Eyring, L. and N.C. Baenziger, 1962, *J. Appl. Phys. Suppl.* **33**, 428.
- Eyring, L. and Bo Holmberg, 1963, Ordered Phases and Nonstoichiometry in the Rare Earth Oxide Systems, in: Gould, R.F. ed., *Advances in Chemistry Series 39* (Amer. Chem. Soc., Washington, D.C.) p. 46.
- Faeth, P.A. and A.F. Clifford, 1963, *J. Phys. Chem.*, **67**, 1453.
- Faithful, D.B., S.M. Johnson and I.J. McColm, 1973, *Rev. Chim. Mineral.* **10**, 291.
- Felmlee, T.L. and L. Eyring, 1968, *Inorg. Chem.* **7**, 660.
- Felsche, J., 1969, *Die Naturwissenschaften*, **4**, 212.
- Ferguson, R.E., E.D. Guth and L. Eyring, 1954, *J. Amer. Chem. Soc.* **76**, 3890.
- Fishel, N.A., J.M. Haschke and H.A. Eick, 1970, *Inorg. Chem.* **9**, 413.
- Foëx, M. and J.P. Traverse, 1966a, *Rev. Int. Hautes Temp. Réfract.* **3**, 429.
- Foëx, M. and J.P. Traverse, 1966b, *Bull. Soc. Franc. Mineral. Crist.* LXXXIX, 184.
- Gasnier, M., J. Ghys, G. Schiffmacher, Ch. Henry LaBlanchetais, P. Caro, C. Boulesteix, Ch. Loier and B. Pardo, 1974, *J. Less-Common Metals*, **34**, 131.
- Gazza, G.E., D. Roderick and B. Levine, 1971, *J. Mat. Sci. Lett.* **6**, 1137.
- Gibby, R.L., 1973, Thermal Properties of Boron Carbide and Europium (III) Oxide, in: Rept. HEDL-SA-587.
- Gibson, J.A. and G.S. Harvey, 1966, Properties of Rare Earth Metals and Compounds, Tech. Rept. AFML-TR-65-430, Battelle Mem. Inst.
- Glushkova, V.B. and A.G. Boganov, 1965, *Izv. Akad. Nauk SSSR*, **7**, 1131.
- Goldschmidt, V.M., F. Ulrich and T. Barth, 1925, *Mat. Naturv. Kl.* **5**.
- Goswami, A. and A.P. Goswami, 1974, *Thin Solid Films* **20**, S3.
- Goswami, A. and R.R. Varma, 1975, *Thin Solid Films* **28**, 157.
- Finch, C.B. and G.W. Clark, 1966, *J. Appl. Phys.* **37**, 3910.
- Fitzgibbon, G.C., E.J. Huber, Jr., C.E. Holley, Jr., 1973, *Rev. Chim. Min.* **10**, 29.
- Gasson, D.B. and B. Cockayne, 1970, *J. Mat. Sci.* **5**, 100.
- Gibby, R.L., C.E. McNeilly and T.D. Chikalla, 1970, *J. Nucl. Mat.* **34**, 1970.
- Guentert, O.J. and R.L. Mozzi, 1958, *Acta Cryst.* **11**, 746.
- Hildenbrand, D.L. and E.Z. Mural, 1975, *Z. Naturforsch* **30A**, 1087.
- Goswami, A. and A.P. Goswami, 1975, *Thin Solid Films* **27**, 123.
- Grosvald, G., 1964, Etude du système praséodyme-oxygène par la méthode diélectrique, in: Servant, R. and A. Charru, eds. Proc. of a Conf. "Electronic Magnetic Resonance and Solid Dielectrics," (North-Holland Pub. Co., Amsterdam) p. 398.
- Gschneidner, K.A., Jr. N. Kippenhan and O.D. McMasters, 1973, Thermochemistry of the Rare Earths, Rpt. IS-RIC-6, Iowa State Univ., Ames, Iowa.
- Guazzoni, E., 1972, *Appl. Spectroscopy*, **26**, 60.
- Guth, E.D. and L. Eyring, 1954, *J. Amer. Chem. Soc.*, **76**, 5242.
- Guth, E.D., J.R. Holden, N.C. Baenziger and L. Eyring, 1954, *J. Amer. Chem. Soc.* **76**, 5239.
- Haensel, R., P. Rabe and B. Sountog, 1970, *Solid State Comm.* **8**, 1845.
- Haglund, J.A. and O. Hunter, Jr., 1973, *J. Amer. Ceram. Soc.* **56**, 327.
- Hajek, B., V. Brozek and P.H. Duvigneaud, 1973, *J. Less-Common Metals*, **33**, 385.
- Haschke, J.M. and H.A. Eick, 1969, *J. Phys. Chem.* **73**, 374.
- Haschke, J.M. and L. Eyring, 1971, *Inorg. Chem.* **10**, 2267.
- Hatibara, J. and P.C. Mahanta, 1972, *Indian J. Pure and Appl. Phys.* **10**, 599.
- Hatibara, J. and P.C. Mahanta, 1975, *Indian J. Pure and Appl. Phys.* **13**, 474.
- Height, T.M. and D.J.M. Bevan, 1976, unpublished work.
- Hoekstra, H.R., 1966, *Inorg. Chem.* **5**, 754.
- Hoekstra, H.R. and K.A. Gingerich, 1964, *Sci.* **146**, 1163.
- Holley, C.E., Jr., E.J. Huber, Jr. and F.B. Baker, 1968, The Enthalpies, Entropies and Gibbs Energies of Formation of the Rare Earth Oxides, in: Eyring, L., ed., *Progress in the Science and Technology of the Rare Earths*, Vol. 3 (Pergamon Press, Oxford) p. 343.
- Honig, J.M., 1958, Literature Review on Properties of Praseodymium and Cerium Oxides, Report No. AFOSR-TN-5857, ASTIA Report No. AD148098.
- Honig, J.M., A.F. Clifford and P.A. Faeth, 1963a, *Inorg. Chem.* **2**, 791.
- Honig, J.M., A.A. Cella and J.C. Cornwell, 1963b, Electrical Properties of Praseodymium Oxides, in: Vorres, K., ed., *Rare Earth Research II*, (Gordon and Breach, New York) p. 555.
- Hoskins, B.F. and R.L. Martin, 1975, *J. Chem. Soc. London, Dalton*, 576.
- Hunter, O. and F.W. Calderwood, 1973/74, *J. Nucl. Materials*, **49**, 103.
- Hyde, B.G., 1971, *Acta Cryst.* **A27**, 617.
- Hyde, B.G. and L. Eyring, 1965, On Phase Equilibria and Phase Reaction in TbO₂-O₂ and Related Systems, in: Eyring, L. ed., *Rare Earth Research III* (Gordon and Breach, New York) p. 623.
- Hyde, B.G., E.E. Garver, U.E. Kuntz and L. Eyring, 1965, *J. Phys. Chem.* **69**, 1667.

- Hyde, B.G., D.J.M. Bevan and L. Eyring, 1966, *Phil. Trans. Roy. Soc., London, Ser. A, No. 1106*, **259**, 583.
- Iwasaki, B. and T. Katsura, 1971, *Bull. Chem. Soc. Japan*, **44**, 1297.
- Jenkins, M.S., R.P. Turcotte and L. Eyring, 1970, On the Thermodynamic and X-Ray Diffraction Behavior of a Widely Non-Stoichiometric Region of the Praseodymium Oxide System, in: Eyring, L. and M. O'Keefe, eds., *The Chemistry of Extended Defects in Non-Metallic Solids*, (North-Holland Pub. Co., Amsterdam) p. 36.
- Jones, P.M.S. and W. Edmondson, 1966, The Oxidation of Rare Earth Oxides, Part 2. Praseodymium, in *AWRE Rept. No. 0-72/66*.
- Jørgensen, C.K., R. Pappalardo and E. Rittershaus, 1964, *Z. Naturforsch.* **19A**, 424.
- Jørgensen, C.K., R. Pappalardo and E. Rittershaus, 1965, *Z. Naturforsch.* **20A**, 54.
- Kern, F. and N. Perakis, 1969, *C.R. Acad. Sci. Paris*, **B269**, 241.
- Kern F. and N. Perakis, 1970, *C.R. Acad. Sci. Paris*, **B270**, 1593.
- Kern, S., 1964, *J. Chem. Phys.* **40**, 208.
- Kern, S. and R. Kosteletzky, 1971, *J. Appl. Phys.* **42**, 1773.
- King, E.G. and A.U. Christensen, 1961, High-Temperature Heat Contents and Entropies of Cerium Dioxide and Columbium Dioxide, in: *Bur. Mines Rept. of Inv. 5789*.
- King, E.G., W.W. Weller and L.B. Pankratz, 1961, Thermodynamic Data for Lanthanum Sesquioxide, in: *Bur. Mines Rept. of Inv. 5857*.
- Klein, P.H. and W.J. Croft, 1967, *J. Appl. Phys.* **38**, 1603.
- Knittel, D., S. Pack, S.H. Lin and L. Eyring, 1977, *J. Chem. Phys.* **67**, 134.
- Koehler, W.C. and E.O. Wollan, 1953a, *Acta Cryst.* **6**, 741.
- Koehler, W.C. and E.O. Wollan, 1953b, *Phys. Rev.* **92**, 1380.
- Kordis, J. and L. Eyring, 1968, *J. Phys. Chem.* **72**, 2044.
- Kumar, J., B.M.S. Bist and O.N. Strivastava, 1970, *Mater. Sci. Eng.* **6**, 371.
- Kuntz, U.E. and L. Eyring, 1959, Diffusion of Oxygen in Rare Earth Oxides, in: Kingery, W.D., ed., *Kinetics of High Temperature Processes* (John Wiley and Sons, New York) p. 50.
- Kunzmann, P. and L. Eyring, 1975, *J. Solid State Chem.* **14**, 229.
- Kuznetsov, F.A., V.I. Belyi and T.N. Rezukhina, 1961, *Doklady AN SSSR, Fiz-Khim.* **139**, No. 6, 1405.
- Land, P.L., 1973, *J. Phys. Chem. Solids*, **34**, 1839.
- Landa, Ya.A., Yu.A. Polonskii, B.S. Glazachev and T.V. Milovidova, 1974, *Ogneupory* **2**, 16.
- Lau, K.H., D.L. Fox, S.H. Lin and L. Eyring, 1976, *High Temp. Sci.* **8**, 129.
- LaVilla, R.E., 1974, *Phys. Rev.* **A9**, 1801.
- Lefever, R.A. and J. Matsko, 1967, *Mat. Res. Bull.* **2**, 865.
- Lefever, R.A., 1962, *Rev. Sci. Instr.* **33**, 1470.
- Linares, R.C., 1967, *J. Phys. Chem. Solids* **28**, 1285.
- Liu, M.B. and P.G. Wahlbeck, *High Temperature Sci.* **6**, 179.
- Messier, D.R., 1967, *J. Am. Ceram. Soc.* **50**, 665.
- Lejus, A.M. and J.P. Connan, 1974, *Rev. Int. Hautes Temp. Refract.* **11**, 215.
- Lejus, A.M., J.C. Bernier and R. Collongues, 1974, *Rev. Int. Hautes Temp. Refract.* **11**, 183.
- Lejus, A.M., J.C. Bernier and R. Collongues, 1976, *J. Solid State Chem.* **16**, 349.
- Levin, E.M., 1964, Refractivities of the Rare Earth Oxides, in: Vorres, K.S., ed., *Rare Earth Research II* (Gordon and Breach, New York) p. 339.
- Lott, U., H. Rickert and C. Keller, 1969, *J. Inorg. Nucl. Chem.* **31**, 3427.
- Lowe, A.T. and L. Eyring, 1975, *J. Solid State Chem.* **14**, 383.
- Lowe, A.T., K.H. Lau and L. Eyring, 1975, *J. Solid State Chem.* **15**, 9.
- Lowenstein, M.Z., L. Kihlberg, K.H. Lau, J.M. Haschke and L. Eyring, 1972, Growth and X-Ray Studies of Single Crystals of Higher Oxides of Praseodymium and Terbium, in: *NBS Spec. Pub.* **364**, 343.
- MacChesney, J.B., H.J. Williams, R.C. Sherwood and J.F. Potter, 1964, *J. Chem. Phys.*, **41**, 3177.
- MacChesney, J.B., H.J. Williams, R.C. Sherwood and J.F. Potter, 1966, *J. Chem. Phys.* **44**, 596.
- Mann, A.W., 1974, *J. Solid State Chem.* **11**, 94.
- Manning, W.R. and O. Hunter, 1969, *J. Amer. Ceram. Soc.* **52**, 492.
- Manning, W.R., M.O. Marlowe and D.R. Wilder, 1966, *J. Amer. Ceram. Soc.* **49**, 227.
- Manning, W.R., O. Hunter and B.R. Powell, Jr., 1969, *J. Amer. Ceram. Soc.* **52**, 436.
- Mariot, J.M. and R.C. Karnatak, 1974, *Phys. Fenn.* **9** (Suppl. S1) 96.
- Martin, J.J. and G.S. Dixon, 1972, *Phys. Status Solidi* **B54**, 707.
- Martin, R.L., 1974, *J. Chem. Soc., London, Dalton*, 1335.
- Massenet, O., Y. Capiomont and N.V. Deng, 1974, *J. Appl. Phys.* **45**, 3595.
- McCarthy, G.J., 1974, *J. Amer. Ceram. Soc.* **57**, 502.
- McCarthy, G.J. and W.B. White, 1970, *J. Less-Common Metals* **22**, 409.
- McDevitt, N.T. and W.L. Baun, 1964, *Spectrochimica Acta* **20**, 799.
- McDevitt, N.T. and A.D. Davidson, 1966, *J. Opt. Soc. Amer.* **56**, 636.
- McMahon, W.R., 1967, Hemispherical Spectral Emittance of Selected Rare Earth Oxides, Ph.D. Thesis, Iowa State University, Ames.
- McMahon, W.R. and D.R. Wilder, 1968, *J. Amer. Ceram. Soc.* **51**, 187.
- McMasters, O.D., K.A. Gschneidner, Jr., E. Kaldis and G. Sampietori, 1974, *J. Chem. Thermo.* **6**, 845.
- Mehrotra, P.N., G.V. Chandrashekar, C.N.R. Rao and E.C. Subbarao, 1966, *Trans. Faraday Soc.* **62**, 3586.
- Miller, A.E. and A.H. Daane, 1965, *J. Inorg. Nucl. Chem.* **27**, 1955.
- Miller, A.E., F.J. Jelinck, K.A. Gschneidner, Jr., and B.C. Gerstein, 1971, *J. Chem. Phys.* **55**, 2647.
- Moon, R.M. and W.C. Koehler, 1975, *Phys. Rev.* **B11**, 1609.

- Moon, R.M., W.C. Koehler, H.R. Child and L.J. Raubenheimer, 1968, *Phys. Rev.* **176**, 722.
- Müller-Buschbaum, H., 1966, *Z. Anorg. Allgem. Chem.* **343**, 6.
- Müller-Buschbaum, H., 1968, *J. Inorg. Nucl. Chem.* **30**, 895.
- Müller-Buschbaum, H. and H.G. Schnering, 1965, *Z. Anorg. Allgem. Chem.* **340**, 232.
- Murr, L.E., 1967, *Phys. Status Solidi*, **24**, 135.
- Nigara, Y., 1968, *Japan. J. Appl. Phys.* **7**, 404.
- Nigara, Y., M. Ishigame and T. Sakurai, 1971, *J. Phys. Soc. Japan* **30**, 453.
- O'Keeffe, M., 1973, *Cooperative Aspects of Ionic Motion*, in vanGool, W., ed., *Fast Ion Transport in Solids* (North-Holland Publ. Co. Amsterdam) p. 233.
- Pankratz, L.B. and E.G. King, 1963, *High-Temperature Heat Contents and Entropies of the Sesquioxides of Erbium, Holmium, Thulium and Ytterbium*, in: *Bur. Mines Rept. of Inv.* 6175.
- Pankratz, L.B. and K.K. Kelley, 1963, *High-Temperature Heat Contents and Entropies of the Sesquioxides of Lutetium, Dysprosium and Cerium*, in: *Bur. Mines Rept. of Inv.* 6248.
- Pankratz, L.B., E.G. King and K.K. Kelley, 1962, *High-Temperature Heat Contents and Entropies of the Sesquioxides of Europium, Gadolinium, Neodymium, Samarium and Yttrium*, in: *Bur. Mines Report. of Inv.* 6033.
- Panlender, R.J., R.N. Blumenthal and J.E. Garnier, 1975, *J. Phys. Chem. Solids*, **36**, 1213.
- Parks, T.C. and D.J.M. Bevan, 1973, *Rev. de Chim. Mineral.* **10**, 115.
- Partington, J.R., 1953, *Textbook of Inorganic Chemistry* (Macmillan, London).
- Pauling, L., 1928, *Z. Kristallogr.* **69**, 415.
- Pauling, L. and M.D. Shappel, 1930, *Z. Krist.* **75**, 128.
- Perakis, N. and F. Kern, 1972, *C.R. Acad. Sci. Ser. B*, **275**, 677.
- Petru, F. and A. Muck, 1966, *Z. Chem.* **6**, 386.
- Petru, F. and A. Muck, 1967a, *Z. Chem.* **7**, 27.
- Petru, F. and A. Muck, 1967b, *Z. Chem.* **7**, 159.
- Pike, G.E., 1972, *Phys. Rev.* **B6**, 1572.
- Ploetz, G.L., C.W. Krystyniak and H.E. Dumas, 1958, *J. Amer. Ceram. Soc.* **41**, 551.
- Queyroux, F., A. Harari and R. Collongues, 1966, *Bull. Soc. Franc. Ceram.* **72**, 37.
- Quezel, Mrs. S., E.F. Bertaut and G. Quezel, 1970, *Magnetic Structures and Theory of Representations of Rare Earth Cubic Oxides*, in: *Colloq. Int. Cent. Nat. Rech. Sci.* **180**, 293.
- Quezel-Ambrunaz, S. and E.F. Bertaut, 1972, *Solid State Comm.* **11**, 605.
- Ramdass, S., K.C. Patil and C.N.R. Rao, 1970, *J. Chem. Soc. A*, 64.
- Rau, R.C., 1966, *Acta Cryst.* **20**, 716.
- Ray, S.P. and D.E. Cox, 1975, *J. Solid State Chem.* **15**, 333.
- Ray, S.P., A.S. Nowick and D.E. Cox, 1975, *J. Solid State Chem.* **15**, 344.
- Ross, W.A. and R.L. Gibby, 1974, *J. Amer. Ceram. Soc.* **57**, 46.
- Roth, R.S. and S.J. Schneider, 1960, *J. Res. of NBS* **64A**, 309.
- Ruchkin, E.D., M.N. Sokalova and S.S. Batsanov, 1967, *Trans. from Zhurnal Strukturnoi Khimii*, **8**, 465.
- Samsonov, G.V. and I.Ya. Gil'man, 1974, *Porosh. Met. Akad. Nauk Ukr. SSR*, **11**, 73.
- Sanderson, R.T., 1971, *Chemical Bonds and Bond Energy* (Academic Press, New York) (see Chapter 9).
- Sastry, R.L.N., P.N. Mehrotra and C.N.R. Rao, 1966a, *Trans. Faraday Soc.* **62**, 1632.
- Sastry, R.L.N., P.N. Mehrotra and C.N.R. Rao, 1966b, *J. Inorg. Nucl. Chem.* **28**, 2167.
- Sata, T. and M. Yoshimura, 1968a, *J. Ceram. Soc. Japan*, **76**, 30.
- Sata, T. and M. Yoshimura, 1968b, *Bull. Tokyo Inst. of Techn. No.* **84**, 13.
- Sawyer, J.O., B.G. Hyde and L. Eyring, 1965a, *Inorg. Chem.* **4**, 426.
- Sawyer, J.O., B.G. Hyde and L. Eyring, 1965b, *Bull. Soc. Chim. France*, 1190.
- Schieltz, J.D. and D.R. Wilder, 1967, *J. Amer. Ceram. Soc.* **50**, 439.
- Schiffmacher, G., P.E. Caro and C. Boulesteix, 1976, *Phys. Status Solidi (a)* **33**, K9.
- Schreiner, P. and A. Czopnik, 1973, *Magnetic Investigations of Several Rare Earth Oxides*, in: *Inst. Techn. Jap., AGH Rept. No.* 39/PS.
- Shafer, M.W. and R. Roy, 1959, *J. Amer. Ceram. Soc.* **42**, 563.
- Shafer, M.W., J.B. Torrance and T. Penney, 1972, *J. Phys. Chem. Solids* **33**, 2251.
- Sieglauff, C.L. and L. Eyring, 1957, *J. Amer. Chem. Soc.* **79**, 3024.
- Simon, W. and L. Eyring, 1954, *J. Amer. Chem. Soc.* **76**, 5872.
- Simpson, L.A. and R.E. Carter, 1966, *J. Am. Ceram. Soc.* **49**, 139.
- Sims, J.P., Jr. and R.N. Blumenthal, 1976a, *High Temp. Sci.* **8**, 99.
- Sims, J.P., Jr. and R.N. Blumenthal, 1976b, *High Temp. Sci.* **8**, 111.
- Sims, J.P. Jr. and R.N. Blumenthal, 1976c, *High Temp. Sci.* **8**, 121.
- Sinha, S.P., 1967, *Indian J. of Chem.* **5**, 451.
- Skarnulis, A.J., E. Summerville and L. Eyring, 1978, *J. Solid State Chem.* **23**, 59.
- Skornyakov, G.P., A.A. Samokhvalov and T.P. Chukini, 1971, *Soviet Physics-Solid State* **12**, 1952.
- Smol'kov, N.A. and N.V. Dobroval'skaya, 1965, *Izv. Akad. Nauk SSSR, Neorg. Mater.* **1**, 1564 (see *Chem. Abst.* **64**, 1471f (1966)).
- Sørensen, O.T., 1976, *J. Solid State Chem.* **18**, 217.
- Stecura, S., 1965, *Crystallographic Modifications and Phase Transformation Rates of Five Rare Earth Sesquioxides: Lanthanum Oxide, Neodymium Oxide, Samarium Oxide, Europium Oxide and Gadolinium Oxide*, in: *Bur. of Mines Rept. of Inv.* 6616.
- Stecura, S. and W.J. Campbell, 1961, *Thermal Expansion and Phase Inversion of Rare*

- Earth Oxides, in: Bur. of Mines Rept. No. 5847.
- Steele, B.C.H. and J.M. Floyd, 1971, Proc. Brit. Ceram. Soc. No. 19, p. 55.
- Stone, G.D., G.R. Weber and L. Eyring, 1968, Self-Diffusion of Oxygen in Neodymium and Samarium Sesquioxide, in: Wachtman, J.B., Jr. and A.D. Franklin, eds., Mass Transport in Oxides, NBS Special Publ. 296, p. 179.
- Subba Rao, G.V., S. Ramdas, P.N. Mehrotra and C.N.R. Rao, 1970, J. Solid State Chem. 2, 377.
- Summerville, E., R.T. Tuenge and L. Eyring, 1978, J. Solid State Chem. 24, 21.
- Tare, V.B. and H. Schmalzried, 1964, Z. Phys. Chem. (NF) 43, 30.
- Templeton, D.H. and C.H. Dauben, 1954, J. Amer. Chem. Soc. 76, 5237.
- Thornber, M.R., D.J.M. Bevan and J. Graham, 1968, Acta Cryst. B24, 1183.
- Tippins, H.H., 1966, J. Phys. Chem. Solids, 27, 1069.
- Traverse, J.P. 1971, Contribution au developpement de methodes d'experimentation a temperature elevee. Application a l'etude du polymorphisme des sesquioxides de terres rares et des changements de phases dans les systems zircone-chaux et zircone-oxyde de strontium, Ph.D. Thesis, The Scientific and Medical University of Grenoble.
- Trvisan, G. and R. Depaus, 1973, Z. Naturforsch. A28, 37.
- Tuenge, R. and L. Eyring, 1978, unpublished work.
- Tueta, R. and A.M. Lejus, 1974, Rev. Chim. Mineral. 11, 27.
- Tueta, R., A.M. Lejus, J.C. Bernier and R. Collongues, 1972, C.R. Acad. Sci. Paris 274C, 1925.
- Turcotte, R., J. Warmkessel, R.J.D. Tilley and L. Eyring, 1971, J. Solid State Chem. 3, 265.
- Turcotte, R.P., M.S. Jenkins and L. Eyring, 1973, J. Solid State Chem. 7, 454.
- Valentine, T.M. and B.T.M. Willis, 1965, A Neutron Diffraction Study of Cerium Dioxide at Room Temperature, in AERE-R4939 Report.
- Van Vleck, J.H., 1965, The Magnetic History
- Tetenbaum, M., 1975, High Temp. Sci. 7, 37.
- Tuenge, R.T. and L. Eyring, 1979, J. Solid State Chem. 29, 165.
- Tuenge, R.T. and L. Eyring, 1982, J. Solid State Chem. 41, 75.
- Vinokurov, I.V., Z.N. Zonn and V.A. Ioffe, 1965, Soviet Physics Solid State 7, 814.
- of Rare Earths, in: Eyring, L. ed., Rare Earth Research III (Gordon and Breach, New York) p. 3.
- Van Vleck, J.H., 1966, The Molecular Field Model of Exchange Coupling in Rare Earth Materials, in: Eyring, L. ed., Progress in the Science and Technology of the Rare Earths, Vol. 2 (Pergamon Press) p. 1.
- Vasil'eva, I.A., Ya.I. Gerasimov, A.F. Maiorova and I.V. Pervova, 1975, Dokl. Akad. Nauk SSSR 221, 865.
- Vier, D.T., 1975, Thermal and Other Properties of Refractories, in: Rept. LA-5937-MS, Los Alamos Sci. Lab.
- Volchenkova, Z.S. and V.M. Chebotin, 1974, Dzv. Akad. Nauk SSSR Neorg. Mater. 10, 1275.
- Von Dreele, R.B., L. Eyring, A.L. Bowman and J.L. Yarnell, 1975, Acta Cryst. Sec. B31, 971.
- Vorres, K.S. and L. Eyring, 1961, High-Temperature Oxidation of Rare Earth Metals, in: Kleber, E.V., ed., Rare Earth Research (Macmillan, New York) p. 119.
- Vratny, F., M. Tsai and J.M. Honig, 1961, J. Inorg. Nucl. Chem. 16, 263.
- Warmkessel, J.M., S.H. Lin and L. Eyring, 1969, Inorg. Chem. 8, 875.
- Warshaw, I. and R. Roy, 1961, J. Phys. Chem. 65, 204.
- Weber, G.R. and L. Eyring, 1971, Self-Diffusion of Oxygen in Iota Phase Praseodymium Oxide, in: Hirschfelder, J. and D. Henderson, ed., Chemical Dynamics (Wiley-Interscience, New York) p. 253.
- Westrum, E.F., Jr., 1967, Developments in Chemical Thermodynamics of the Lanthanides, in: Gould, R.F., ed., Advances in Chemistry Series 71 (ACS, Washington, D.C.) p. 25.
- White, W.B., 1967, Appl. Spectroscopy 21, 167.
- Wilbert, Y. and F. Marion, 1970, C.R. Acad. Sci. Ser. C271, 736.
- Wilbert, Y., H. Breuil and N. Dherbomez, 1975a, C.R. Acad. Sci. Paris, Ser. C280, 373.
- Wilbert, Y., N. Dherbomez and H. Breuil, 1975b, C.R. Acad. Sci. Paris, Ser. C280, 465.
- Work, D.E. and H.A. Eick, 1972, J. Less-Common Metals 26, 413.
- Noguchi, T., 1969, "High Temperature Phase Studies with a Solar Furnace, in: Advances in High Temperature Chemistry, Vol. 2, L. Eyring, ed. (Academic Press, New York, 1969), pp. 235-262.
- Norrestam, R., 1968, Arkiv. f. Kemi 29, 343.
- Pastor, R.C. and A.C. Pastor, 1966, Mat. Res. Bull. 1, 275.
- Piacente, V., G. Bardi, L. Malaspina and A. Desideri, 1973, J. Chem. Phys. 59, 31.
- Popova, A.A. and V.B. Zotkina, 1967, Soviet Physics Doklady, 11, 553.
- Rau, R.C., 1964, in Rare Earth Research II, K. Vorres, ed. (Gordon and Breach, New York, 1964), pp. 117.
- Sata, T., 1966, Rev. Hautes Tempér, et Réfract. 3, 337.
- Shannon, R.D., 1976, Acta Cryst. A 32, 751.
- Sheindlén, A.E., M.M. Kenesarin and V.Ya. Chekhovskoi, 1974, Dokl. Akad. Nauk SSSR 216, 582.

Chapter 28

MIXED RARE EARTH OXIDES

D.J.M. BEVAN and E. SUMMERVILLE

School of Physical Sciences, Flinders University of South Australia,
 Bedford Park, South Australia, 5042

Contents	References	519
1. Introduction and scope	402	
2. Phase relationships in mixed sesquioxides of the rare earths	403	
2.1. The systems R_2O_3 - R'_2O_3 (R, R' = Ln, Y, Sc)	403	
2.2. The perovskite-type phase $RR'O_3$	413	
2.3. The systems R_2O_3 - R'_2O_3 - R''_2O_3 (R, R', R'' = Ln, Y, Sc)	414	
3. Phase relationships in the systems MO_2 -(rare earth oxides)	415	
3.1. Mixed oxides of tetravalent elements	415	
3.2. Mixed oxides of the type MO_2 (fluorite)- R_2O_3	417	
4. Mixed oxides of uranium and the rare earths	444	
4.1. The systems UO_{2+x} - R_2O_3 (R = Ln, Y, Sc)	444	
4.2. The system UO_{2+x} - CeO_{2-x}	451	
5. Structures and structural relationships	452	
5.1. NaCl-related structures	452	
5.2. Structures with hexagonal close packed anions	457	
5.3. Perovskite related structures	458	
5.4. Structures deriving from the $CaFe_2O_4$ -type	468	
5.5. Structures related to A-type R_2O_3 : the ψ -phases	486	
5.6. Fluorite-related structures	489	
5.7. Scheelite-related structures	511	
6. Recent developments	518	
	References	519
	Symbols	
	r = ionic radius	
	= parallel to	
	% = percent	
	n = integer	
	°C = degrees Celsius	
	Å = Angström unit	
	t = tolerance factor	
	$a, b, c,$ = lattice parameters	
	α, β, γ	
	R, R', R'' = rare earth elements	
	M, A, B = non-rare earth metals	
	x, m = non-integral numbers, used to designate various chemical compositions	
	N = mole fraction	
	σ = standard deviations: conductivity (depending on context)	
	~ = approximately equal to	
	$p(O_2)$ = oxygen partial pressure	
	$< \leq$ = less than: less than or equal to	
	$> \geq$ = greater than: greater than or equal to	
	T = temperature	
	$\Delta\bar{H}(O_2)$ = partial molar enthalpy of solution of oxygen	
	$\Delta\bar{S}(O_2)$ = partial molar entropy of solution of oxygen	
	x, y, z = fractional atomic coordinates	
	V = vacancy	
	h, k, l = Miller indices	

1. Introduction and scope

There is nothing rare about mixed oxides involving the rare earth elements. On the contrary, even a cursory survey of the published literature reveals a plethora of reports and a wide diversity of types, enough to blanch the countenance of the most hardened reviewer. Inevitably, then, some selection needs to be made, and, just as inevitably, that selection will reflect a personal bias. In this case there will be a strong but unashamed emphasis on structural considerations, although, hopefully, not to the exclusion of other aspects where these seem to be significant. However, there are some types of mixed-oxides involving rare earth oxides, such as the garnets, ch. 29, the perovskites, ch. 29, and the molybdates, ch. 30, which, because of their uniquely important properties, have been studied intensively in recent years: these warrant separate treatment, and are accorded such in this volume. The binary rare earth oxide systems are also discussed separately, ch. 27. On the other hand, there is nothing particularly unique about the chemistry of the rare earth silicates and the related germanates when viewed in the context of silicates in general and their germanate analogues, so these are not treated. A review of rare earth silicates and aluminates has been given by Warsaw and Roy (1964).

In trying to set a pattern for an exercise of this kind there is a strong temptation to adopt one systematic approach favoured by many authors in which pseudo-binary systems are treated in the sequence $M_2O-R_2O_3$, $M_2O_3-R_2O_3$ etc. However, a rigid classification of this kind can be cumbersome, and there is always the problem of where to include certain pseudo-ternary compounds which deserve attention. Accordingly, two quite different types of classification have been used, the first, as above, when the phase relationships appear as perhaps the most important aspect in the total situation, and the second, based on structure-type, when the phase-field of even polynary systems contains simply one or more intermediate stoichiometric compounds. Thus the inter-lanthanide oxide systems, in which the phase relationships are often quite complex and where several different structure types are encountered, are best included in the first category. On the other hand there are many mixed-oxide compounds, often of complex and quite different chemical constitution, which nonetheless have in common a close structural relationship to each other and to some basic structure type: these are discussed in the context of the structural relationships, that is, they are classified on the basis of the second criterion. There will, of course, often be overlap between the two approaches.

Ignoring for the moment the voluminous literature on specific compounds and systems, it is worth noting at the outset the existence of some major review articles which relate to one or more aspects of the whole topic. Keller (1972) has written on "Lanthanide and Actinide Mixed-oxide Systems with Alkali and Alkaline-earth Metals", and an even more recent summary of the data extant in a part of this area has appeared in Gmelin (1974a) under the title "Alkalioxometallates". Gmelin (1974b) also contains much comparatively recent information on the interlanthanide oxide systems, while in late 1975 a further

article by Keller (1975a) on "Lanthanide and Actinide Mixed-oxide Systems of Face-centred-cubic Symmetry" was published. Yet another review by Keller (1975b) on the mixed oxides of uranium and the rare earth elements exists. Of older vintage but nonetheless valuable is an article by Roth (1964) on mixed oxides involving the rare earth elements. These are all valuable sources.

2. Phase relationships in mixed sesquioxides of the rare earths

2.1. *The systems* R_2O_3 - R'_2O_3 ($R, R' = Ln, Y, Sc$)

The individual lanthanide sesquioxides crystallize in one or more of three main polymorphic forms designated A, B, and C. Two further high-temperature forms, H and X, have also been reported by Foex and Traverse (1966). The C- and X-forms are both cubic, the A- and H-forms are hexagonal, while the B-form is monoclinic. Details of these structures, their interrelationships, and their stability ranges are discussed in ch. 27, but the dominant factor in determining which structure is assumed by a given sesquioxide under specified conditions is the cation radius. The trend is $A \rightarrow B \rightarrow C$ with decreasing radius (i.e. $La^{3+} \rightarrow Sc^{3+}$).

In the pseudo-binary mixed-oxides the structure assumed will obviously depend on the structures of the pure oxide components, the mole ratio of these, and (most importantly) on the difference between the radii of the two cations. The first thorough study of these systems was carried out by Schneider and Roth (1960). Their specimens were prepared by solid state reaction to equilibrium of individual oxides at 1650°C or sometimes 1900°C. The phase-fields were then determined from room-temperature X-ray diffraction data, and the results correlated with the "average cation radius". Full details of the observed and predicted phase relationships are best obtained from the original publication, but a general summary can be given here.

If the two component oxides both crystallize in the same structure type (A, B, or C) the mixed-oxide systems form a solid solution of the same structure over the whole range of composition, and Végard's law (a linear relationship between lattice parameter and composition) should apply. This has been confirmed, for example, by Caro et al. (1973) for the system La_2O_3 - Nd_2O_3 , where the structure is A-type, and by Wolf and Schwab (1964) for the system Er_2O_3 - Tb_2O_3 , with the C-type structure. In these cases the differences between the cation radii are very small. Larger differences signify a difference in structure type of the pure sesquioxides, and the corresponding mixed-oxide systems show a diphasic region between two terminal solid solutions of these different structure types. As this difference between the cation radii becomes still larger the binary mixed-oxide system may have solid solution regions of all three structural types, as for example in the cases of La_2O_3 - Dy_2O_3 and Nd_2O_3 - Dy_2O_3 . For still larger differences a nominal 1:1 compound $RR'O_3$ appears, which usually has an orthorhombically-distorted perovskite-type structure.

In most studies of solid phase equilibria the determination of phases present after high-temperature reaction is necessarily carried out at room temperature; specimens are often quenched as rapidly as possible from the annealing temperature in the hope that the high-temperature situation will be "frozen", but uncertainty on this point presents a well-known and serious problem in this kind of work. It has been overcome in recent studies by Foex (1966a, 1966b) and his colleagues, who, using a solar furnace to heat samples in air, have developed techniques for the in situ study of high-temperature phase equilibria. Very recently Coutures et al. (1976a) have published the results of such studies for most of the $\text{La}_2\text{O}_3\text{-R}_2\text{O}_3$ systems. Figures 28.1-28.4 show four representative

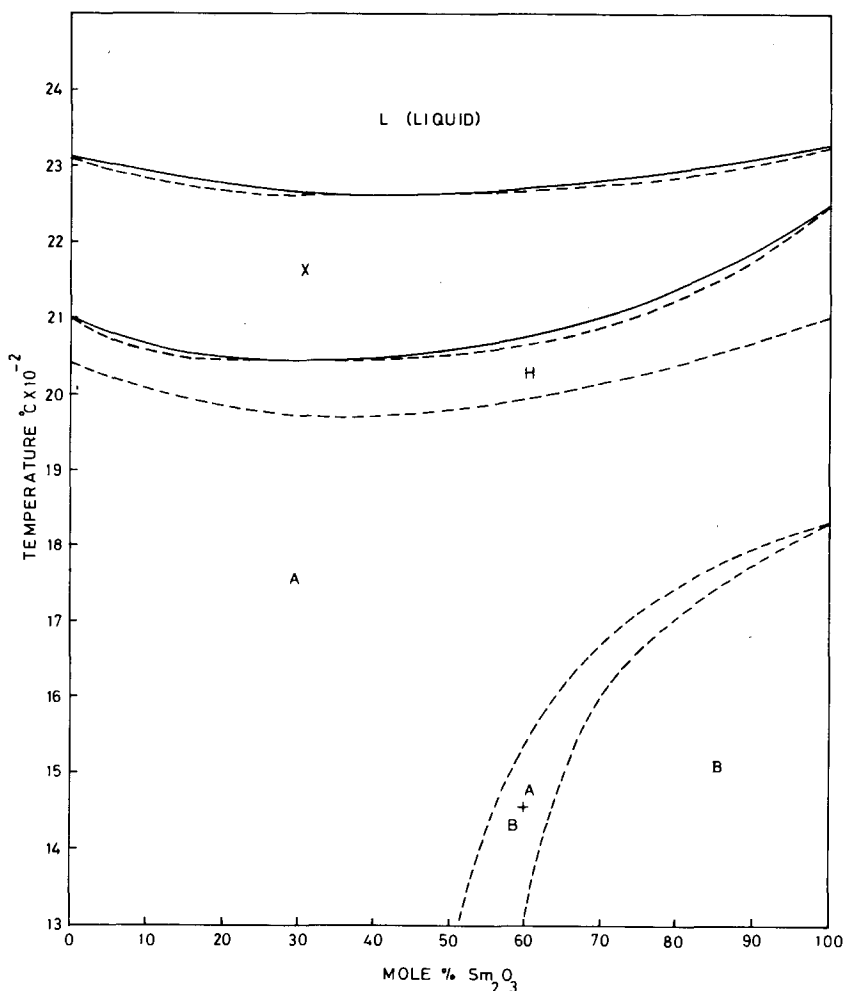


Fig. 28.1. Phase diagram for the system $\text{La}_2\text{O}_3\text{-Sm}_2\text{O}_3$; after Coutures et al. (1976).

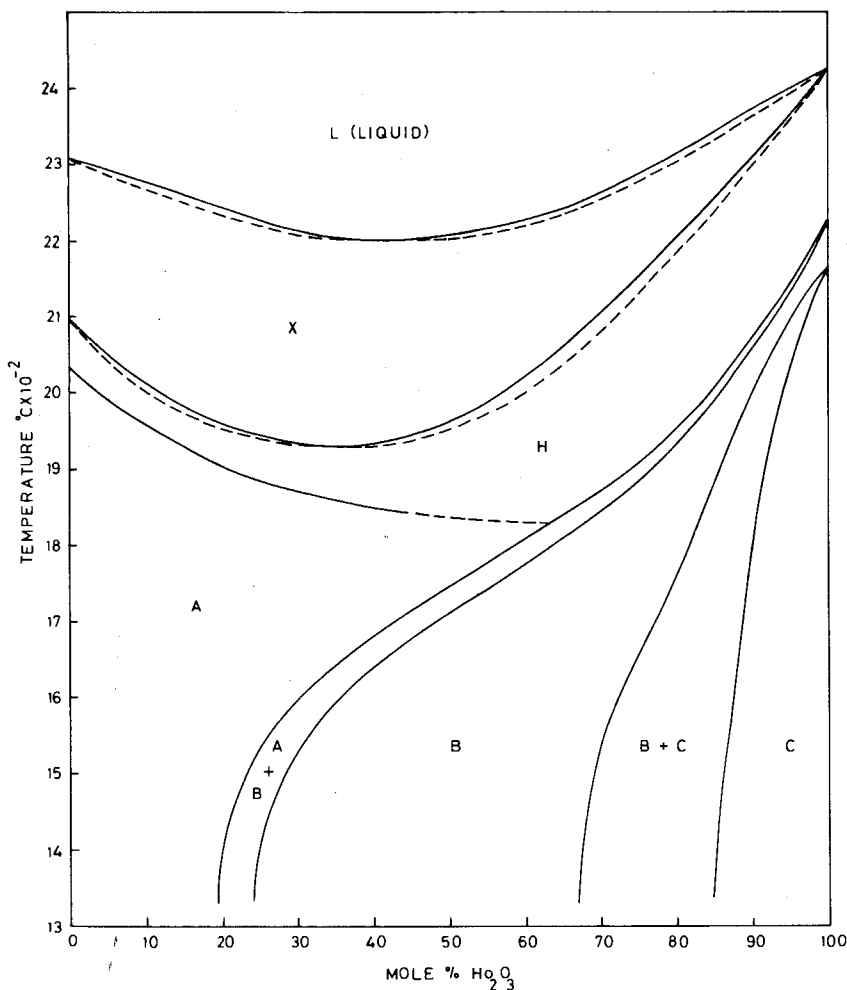


Fig. 28.2. Phase diagram for the system La₂O₃-Ho₂O₃ after Coutures et al. (1976).

phase diagrams taken from their work, and illustrate very clearly the general trends in behaviour already determined by Schneider and Roth (1960). Much more detailed trends, however, have been established. Thus addition of La₂O₃ to those R₂O₃ oxides which have the C-type structure at room temperature (Tb₂O₃ through Lu₂O₃, and both Y₂O₃ and Sc₂O₃) has the effect of sharply increasing the mean cation radius and thereby limiting the extent of the C-type solid solution: the greater the difference $r(\text{La}^{3+}) - r(\text{R}^{3+})$ the more limited the extent, and for the systems La₂O₃-Sc₂O₃ and La₂O₃-Lu₂O₃ respectively Badie (1970) and Berndt et al. (1976) have shown that no C-type solid solutions exist. Within the homogeneity range of the C-type phase the lattice parameter increases linearly with increasing La₂O₃ content. The B-type phase occurs only for R = Sm through

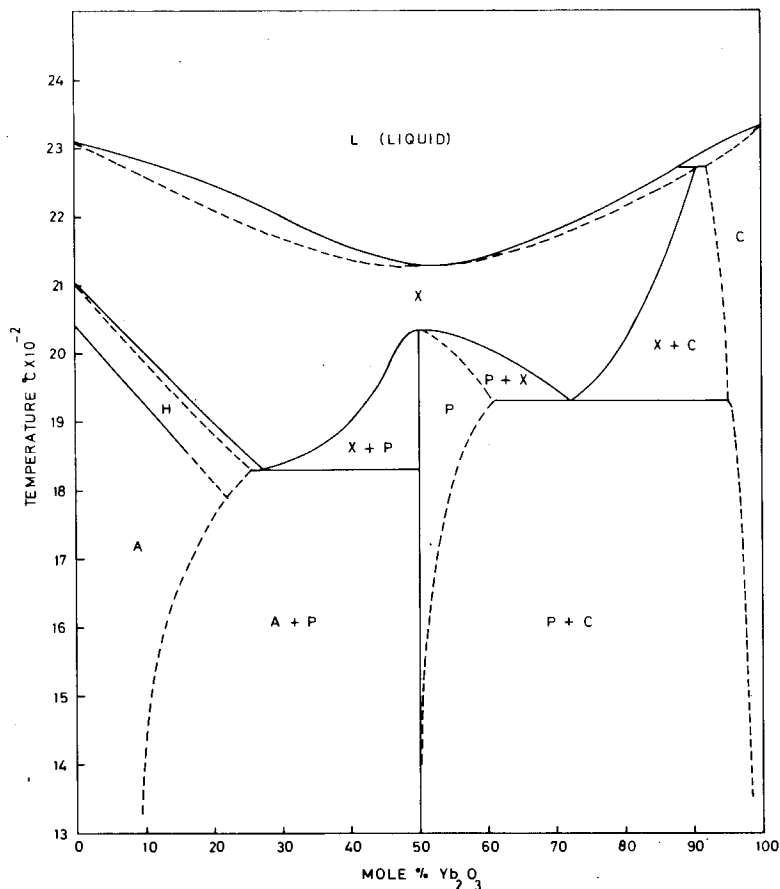


Fig. 28.3. Phase diagram for the system $\text{La}_2\text{O}_3\text{-Yb}_2\text{O}_3$: after Coutures et al. (1976).

Ho, and Y, giving place either to an A-type or perovskite type phase for $R = \text{Nd}$ or $R = \text{Er}$ through Lu respectively. In this respect the system $\text{La}_2\text{O}_3\text{-Y}_2\text{O}_3$ is anomalous: here the perovskite-type phase undergoes a monotectoid decomposition to the B-type phase (see fig. 28.4), and the system $\text{La}_2\text{O}_3\text{-Ho}_2\text{O}_3$ probably shows similar behaviour, but at temperatures below the minimum shown in fig. 28.2, since Berndt et al. (1976) class these two systems together and point out that the perovskite phase LaHoO_3 decomposes at $1300 \pm 30^{\circ}\text{C}$. In all cases, however, the stable existence of the B-type solid solution requires that the mean cation radius lie between 1.01 and 1.09 Å. For the A-type phase the range of existence decreases in general with decreasing $r(R^{3+})$: from $R = \text{Nd}$ through Gd this can extend over the whole range of composition at sufficiently high temperatures.

The high-temperature phases X and H cannot be retained to room temperature on quenching, and their existence could only be shown by the use of high-

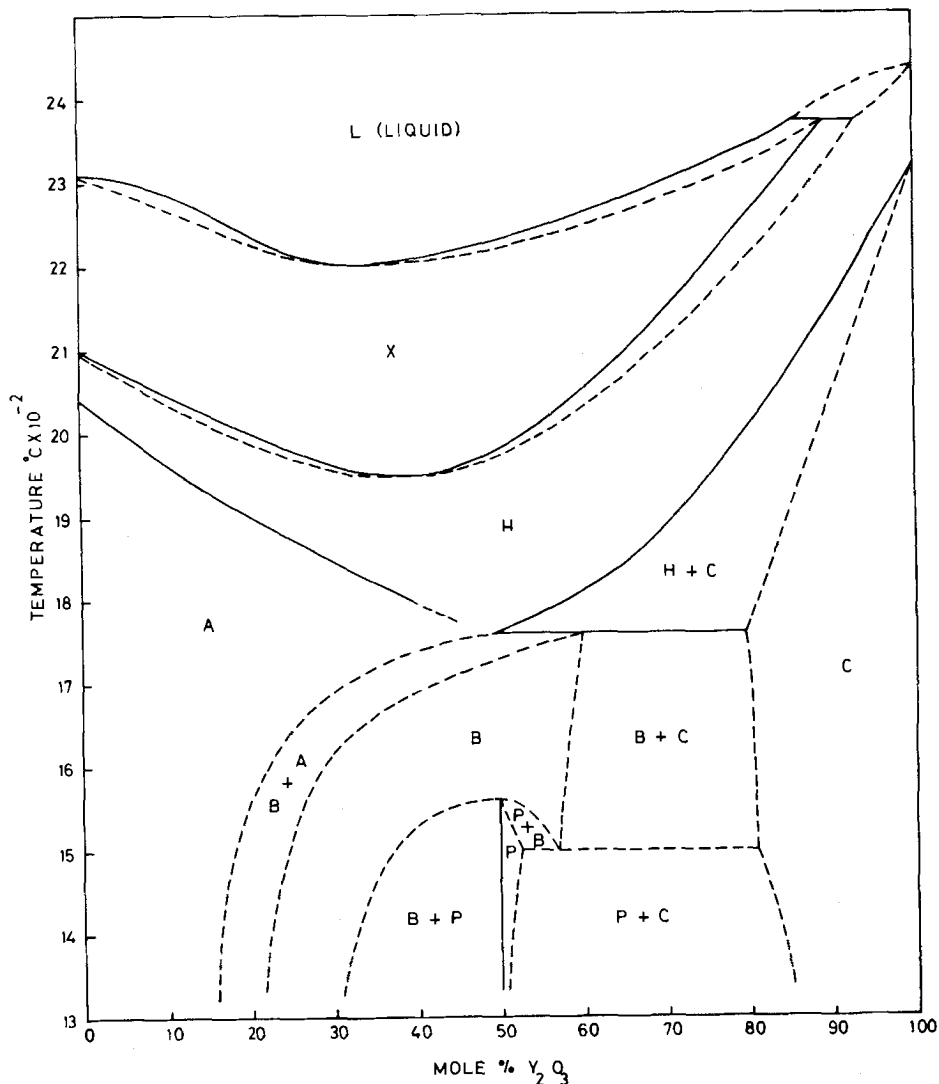


Fig. 28.4. Phase diagram for the system $\text{La}_2\text{O}_3\text{-Y}_2\text{O}_3$: after Coutures et al. (1976).

temperature X-ray diffraction: the phase boundaries down to 1400°C have also been determined in the same way. The liquidus curves and other sub-solidus transformation temperatures have been obtained by thermal analysis; high-temperature X-ray diffraction was again used to identify the phase reactions.

It is of great interest to compare directly, where possible, the results of this kind of work with those obtained by classical quenching techniques. Rouanet et al. (1972), using Foex's techniques, have studied the system $\text{La}_2\text{O}_3\text{-Yb}_2\text{O}_3$, and studies by quenching techniques have been reported for the same system by

Müller-Buschbaum and Teske (1969) for 1650°C, and by Berndt et al. (1975) for 1400°C (see table 28.1).

Significant discrepancies between the comparable data sets are apparent, particularly with respect to the width of the A-type solid solution and both the widths and positioning of the perovskite field. Superficially these may be explained by differences of technique etc., but this state of affairs warrants further probing. Coutures et al. (1974) have also published phase diagrams for the systems $\text{Nd}_2\text{O}_3\text{-Y}_2\text{O}_3$ and $\text{Nd}_2\text{O}_3\text{-Yb}_2\text{O}_3$ (see fig. 28.5), and have shown quite clearly in this work, and even more dramatically by splat-cooling experiments in the systems $\text{La}_2\text{O}_3\text{-R}_2\text{O}_3$ (Coutures et al., 1976b), that the phase relationships determined in situ at high temperatures are often different from those indicated by room-temperature examination of quenched samples. They have also explored what might be termed the effect of a specimen's past history on phase relationships observed at room temperature, or the approach to "equilibrium" from both directions. For this purpose samples were prepared by two methods: (a) the mixed oxides were melted in the solar furnace and then annealed at 1400°C for 72 hours

(b) coprecipitated hydroxides were reacted at 1400°C for 72 hours.

At room temperature the final states achieved in these samples were not identical: cell-parameter data from melted samples indicated an extension of the monophasic B-type solid solution into the diphasic B + C region which data of the same kind from coprecipitated samples had shown was present. The authors conclude from this that it is much more difficult to achieve equilibrium in melted samples than in coprecipitated ones, but it is not clear whether the same final

TABLE 28.1
Comparison of phase-equilibrium data for $\text{La}_2\text{O}_3\text{-Yb}_2\text{O}_3$.

Temp. °C	Phase(s) found and composition range (mole % Yb_2O_3)		
	MBT ^a	BMK ^b	RCF ^c
1650	A: 0-4		A: 0-23
	A + P: 4-39		A + P: 23-47
	P: 39-55		P: 47-63
	P + C: 55-96		P + C: 63-98
	C: 96-100		C: 98-100
1400		A: 0-4	A: 0-20
		A + P: 4-48	A + P: 20-48
		P: 48-52	P: 48-62
		P + C: 52-96	P + C: 62-98
		C: 96-100	C: 98-100

^aMüller-Buschbaum and Teske (1969); ^bBerndt et al. (1975); ^cRouanet et al. (1972); Note: A, P, and C refer respectively to the A-, perovskite-, and C-type phases of this system.

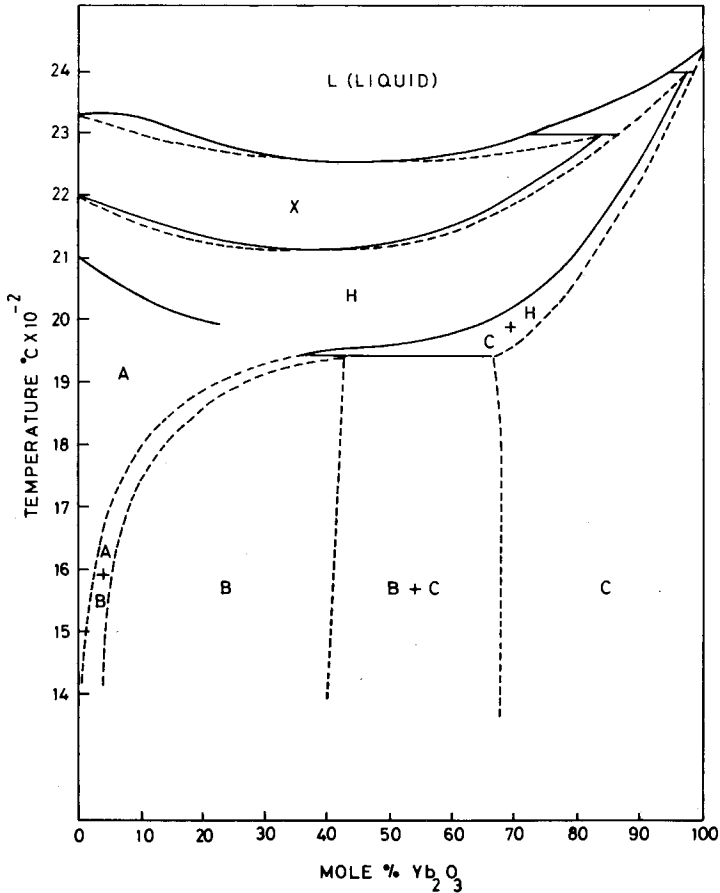


Fig. 28.5. Phase diagram for the system $\text{Nd}_2\text{O}_3\text{-Yb}_2\text{O}_3$; after Coutures et al. (1974).

state (equilibrium?) that is achieved for coprecipitated samples is also eventually reached by the melted samples on longer annealing.

On the other hand, Müller-Buschbaum and Teske (1969) state that essentially identical cell-parameter data at room temperature were obtained both from samples reacted at 1650°C and from those which had been melted and then "slowly cooled". On this evidence it might be concluded that equilibrium had been reached at 1650°C , but the problem of what, if anything, happens on cooling from 1650°C to room temperature still remains.

The results of Caro et al. (1973) on the mixed oxides formed at 1000°C from coprecipitated oxalates of neodymium and yttrium also appear to be inconsistent with the high-temperature data given by Coutures et al. (1974), and the theme of Caro's argument is very relevant to this discussion. In Caro's work it is recognised that the phases involved are all solid solutions, and that the nature of these per se and of their structural transformations assumes considerable

importance in any attempt to understand their interrelationships. These essentially structural considerations have been explained in some detail.

The particular structural description used is one of edge-sharing OLn_4 tetrahedra (Caro, 1972; see also ch. 27), in terms of which the A- and B-type structures are seen to be built up from the trigonal or pseudo-trigonal $(LnO)_n^{n+}$ layers (in which OLn_4 tetrahedra share all edges) linked by intercalated layers of oxygen atoms: the formula is best written then as $(LnO)_2O$. The C-type structure is a three-dimensional network of OLn_4 tetrahedra, each sharing four out of six edges, and as such is quite distinct from the closely-related A- and B-forms. However, electron microscope studies of thin oxide layers (Boulesteix et al., 1971) have shown the possibility of epitaxial relationships between these different structural types. Indeed, quite remarkable phenomena have been observed in this work, in which the electron beam is used for local heating and can induce, for example, the formation of epitaxed microdomains of B-type structure within an A-type host crystal. The observed crystallographic relationships in this case are $(002)_A \parallel (20\bar{1})_B$ (the planes of $(LnO)_n^{n+}$ layers), and $(110)_A \parallel (313)_B$. The contact planes can be any one of the $\{100\}_A$, $\{110\}_A$, and $\{210\}_A$ families.

A similar phenomenon has been reported by Müller-Buschbaum (1967) in an interesting paper concerned with the mechanism of the $A \rightarrow B$ transformation in single crystals of Sm_2O_3 containing varying amounts of La_2O_3 . These crystals were formed from a rapidly-cooled melt, and were studied by standard X-ray diffraction techniques. Crystals containing 20–23 mole % La_2O_3 gave only diffraction patterns of the B-type phase, but a structure determination showed that the atom positions were shifted somewhat from those of the pure B-form towards those of the A-form. In direct contrast, for crystals containing in excess of 28 mole % La_2O_3 the diffraction patterns were A-type, and the atom positions were shifted towards those of the B-type structure. At compositions between 23 and 28 mole % La_2O_3 the X-ray data showed the existence of oriented intergrowth on a sub-microscopic scale of both A- and B-type crystals. Müller-Buschbaum (1967) concludes that the transition between these two structure types in interlanthanide sesquioxide systems is not sudden but continuous, and in the diphasic region (see fig. 28.1) both exist together in a state which he describes as submicroscopic twinning.

Such behaviour is perhaps not so unexpected since the A- and B-type structures are closely related; the $A \rightarrow B$ transition corresponds simply to a slip of the $(LnO)_n^{n+}$ layers with respect to each other in one of the directions $\langle 1\bar{1}0 \rangle_A$. However, similar intergrowths of the B-type phase in a C-type matrix have also been observed: here the crystallographic relationships found by Boulesteix et al. (1971) are $(20\bar{1})_B \parallel (111)_C$ and $(111)_B \parallel (110)_C$, and in the light of all these observations the clearly complex situation of the solid solutions was further studied by Caro and his colleagues, using both spectroscopic techniques (Caro et al., 1973) and electronmicroscopy (Loier et al., 1974). Two very different pictures have emerged.

In the system $\text{La}_2\text{O}_3\text{-Nd}_2\text{O}_3$ the stable structure of both end-members is A-type, and these form a continuous solid solution of identical structure type over the whole range of composition. Moreover, it is ideal in the sense that Végard's law holds. The optical absorption spectra measured at liquid helium temperature show only a single sharp peak, as in pure Nd_2O_3 , corresponding to single site-occupancy for Nd^{3+} , and the inescapable conclusion is that the Nd^{3+} ions simply replace La^{3+} ions at random on normal A-type cation sites. As the Nd^{3+} concentration in the solid solution increases, so the absorption peak shifts regularly towards longer wave length (the nephelauxetic effect) and at the same time broadens to a maximum half-peak-height width for a neodymia mole fraction of 0.5. This latter observation is interpreted as being due to strain in the rigid $(\text{LnO})_n^{n+}$ framework resulting from the substitution of La^{3+} by the slightly smaller Nd^{3+} in the OLn_4 tetrahedra. This system, then, shows the normal type of solid solution behaviour expected for strictly isomorphous components. Similarly, in the system $\text{Nd}_2\text{O}_3\text{-Y}_2\text{O}_3$, whose end-members have the A- and C-type structures respectively, it seems that Y_2O_3 can incorporate a considerable amount of Nd_2O_3 in "ideal" solid solution*. The lattice parameter of the cubic C-type phase increases linearly with increasing neodymia content up to the phase boundary, and the optical absorption data suggest that in this region Nd^{3+} ions replace Y^{3+} ions in the C_{2v} site of the structure. The 6-fold coordination of this site by nearest-neighbour anions is very irregular and therefore able to adjust to the presence of the larger Nd^{3+} ion. Thus this solid solution region can also be said to show normal behaviour, in spite of the fact that the components are not isomorphous.

In marked contrast, however, at the other end of the system incorporation of as little as 0.5 mole % Y_2O_3 in Nd_2O_3 leads to the appearance of a B-type phase, which suggests that Y^{3+} ions cannot occupy the C_{3v} site of Nd^{3+} in the A-type structure. There are sound structural reasons for this, as even in A-type La_2O_3 the oxygen atoms of the OLa_4 tetrahedra are virtually close-packed, and cannot come much closer together around a smaller cation. Indeed, the distortion of the OLn_4 tetrahedra in the B-type structure exhibited by the intermediate rare earth oxides is the result of the lanthanide contraction, and the further transition to the C-type structure, with more loosely-linked OLn_4 tetrahedra, is a direct result of the need to preserve reasonable O-O distances as the Ln^{3+} radius decreases. This same argument should also exclude the possibility of a normal B-type solid solution in which Y^{3+} replaces Nd^{3+} at random in the $(\text{LnO})_n^{n+}$ framework, yet solid solution of a kind does occur over a wide range of composition: but what kind?

In an electron microscope study of this B-type solid solution Loier et al. (1974) prepared thin, single-crystal films of the mixed neodymium and yttrium oxides by careful beam heating of an evaporated metal film containing the appropriate

*The phase diagram for this system, as given by Coutures et al. (1974), is similar in general appearance to that shown in fig. 28.5.

ratio of Nd to Y: residual oxygen within the evacuated instrument was sufficient to effect the oxidation. Most of their reported work is for the composition 10 mole % Y_2O_3 , and the diffraction patterns showed at the outset that the prepared films were B-type and monophasic (in accord with the phase diagram) but strongly twinned. Much of the contrast observed for such specimens was, however, quite different from what had been seen previously in pure Nd_2O_3 samples. The details of these striking observations are best obtained from the original paper, but their implication is quite clear: within the thickness of the single-crystal film ($\sim 1500 \text{ \AA}$) the composition varied by as much as 20%. Whether this fine-scale inhomogeneity is introduced at the stage of metal evaporation or oxidation in the electron beam cannot be determined. The strain arising from this is taken up in the observed system of dislocations. Further beam heating led to the almost complete disappearance of the B-phase and the appearance of epitaxed regions of both A- and C-phases, which had quite specific orientations with respect to each other. Intergrowth of A-type and B-type regions was also observed, as in pure Nd_2O_3 , but the coexistence of B- and C-type phases, which might have been expected according to the phase diagram, was never seen.

What has happened, in effect, is that local beam heating, following the first oxidation of the metal film and subsequent rapid quenching, has produced a more or less random heterogeneity of composition, and the phases observed reflect this. Of course, there is no question of this specimen being at equilibrium, but the important feature of the observations is that different structures with different compositions can intergrow coherently in these systems – a property known as syntaxy. This behaviour is well-documented in the literature on *d*-block transition metal oxides, and the term “microdomain texture” has been coined to describe it.

The argument can now be carried a stage further. There is no a priori reason why such texture in a solid solution should not exist at equilibrium. For large numbers of small microdomains in some matrix the interfacial energy at the microdomain boundaries will be important in determining what structural and compositional differences between microdomains can be sustained. Thus Caro et al. (1973) have explained how it could be that very small amounts of Y_2O_3 introduced into A-type Nd_2O_3 promote the formation of a B-type phase. Microdomains of C-type $(Y, Nd)_2O_3$ relatively richer in yttrium form coherently within the A-type matrix, but the local strains set up induce the displacive transformation $A \rightarrow B$ in the matrix in the same kind of way that local constraints due to beam heating in the electron microscope induce formation of microdomains of B in pure A-type Nd_2O_3 films.

Alternatively, it can be argued that possibly the most important factor in determining what macroscopic phase relationships will be observed for extended-defect systems is the way in which the components are distributed initially, since local fluctuations of composition will profoundly affect microdomain texture. Further discussion of this point is taken up in the section on fluorite-related phases.

2.2. The perovskite-type phase $RR'O_3$

Schneider and Roth (1960), using ionic radii given by Ahrens (1952), have suggested from their observations that a minimum radius difference of 0.25 Å is necessary for a stable perovskite phase to form. Furthermore, using the tolerance factor* derived by Goldschmidt et al. (1926) for this structure type, they proposed again a minimum value of 0.77–0.79 for perovskite formation in these interlanthanide systems. As the tolerance factor tends to unity, so the tendency for stable perovskite formation increases.

However, perovskite phases when formed often exhibit quite wide phase-fields, a complication not discussed by Schneider and Roth (1960). Tolerance factor calculations for such cases have been developed by Müller-Buschbaum and Teske (1969), who took into account the known crystal structures of these perovskite phases. The large and small cations in the 1:1 compound occupy quite distinct lattice sites, and the structure is essentially a rigid, three-dimensional network of corner-sharing $R'O_6$ octahedra, having the formula $(R'O_3)_n^{3n-}$; and R^{3+} ions are incorporated in the large interstices present in this framework. (For a full discussion of the perovskite-type structure, see ch. 29.) These authors assume, then, that any stoichiometric excess of one or other component is accommodated by a statistical distribution of, say, additional R^{3+} ions and the correspondingly fewer R'^{3+} ions on R' sites of the intact structure to form the phase $R^{3+}(R'_{1-x}R_x^{3+})O_3$; the R sites in this case remain fully occupied by R^{3+} ions. For a known composition it is now possible to calculate the mean ionic radius for the ions occupying the R' (or the R) sites, and hence the tolerance factor. The experimental data from samples of mixed lanthanum and ytterbium oxides heated to 1650°C and in excess of 2200°C (no significant differences *at room temperature* were observed for samples given these different heat treatments) indicated a perovskite phase extending from 38.62 mole % to 55.45 mole % Yb_2O_3 . Tolerance factors calculated for these boundary compositions (again based on Ahren's ionic radii) were 0.77(2) and 0.77(9) respectively: for the stoichiometric composition the value is 0.79(5). From all these considerations Müller-Buschbaum and Teske (1969) predicted that it should be possible to prepare the then unknown perovskite phases $LaDyO_3$, $LaHoO_3$, $CeLuO_3$ and $NdLuO_3$. Of these, the last three have recently been prepared in Keller's laboratory, and table 28.2 gives what is probably a complete listing of the $RR'O_3$ perovskites which can be prepared by standard solid-state reaction techniques.

It should be noted that the new compounds prepared by Berndt et al. (1975) only appear to be stable at lower temperatures: at higher temperatures they decompose into one or more solid-solution phases, and it is therefore interesting to speculate on the possibility of the stable existence of other such compounds at even lower temperatures. The lower limit of 0.77–0.79 for the Goldschmidt tolerance factor is, of course, derived empirically from experimental observation

* $t = (r_R + r_0) / \sqrt{2}(r_{R'} + r_0)$, where t is the tolerance factor, r_R is the ionic radius of the smaller cation, and r_0 is the ionic radius of oxygen.

TABLE 28.2
Perovskite-type compounds $RR'O_3$ (Ahren's ionic radii (Å) are given in parentheses: for lattice constants see Berndt et al. (1975)).

R	R'	Y (0.92)	Ho (0.91)	Er (0.89)	Tm (0.87)	Yb (0.86)	Lu (0.85)
La (1.14)	La	LaYO ₃	LaHoO ₃	LaErO ₃	LaTmO ₃	LaYbO ₃	LaLuO ₃
Ce (1.07)					CeTmO ₃	CeYbO ₃	CeLuO ₃
Pr (1.06)						PrYbO ₃	PrLuO ₃
Nd (1.04)							NdLuO ₃

Note: Sc₂O₃ ($r(\text{Sc}^{3+}) = 0.81 \text{ \AA}$) forms perovskite phases RScO₃ for R = La through Ho, and Y.

of perovskite formation, and all of these preparations have involved solid state reaction. In this situation the problem arises that in order to achieve reaction a high temperature is required, and this temperature may exceed the decomposition temperature of the compound sought. Special low-temperature preparation techniques might be worth exploring in this context, although Berndt et al. (1975) have tried hydrothermal reaction of coprecipitated mixed hydroxides at 210°C without success (no perovskite-type compounds at all were obtained by this method). Vapour-phase transport reactions, and homogeneous decomposition of mixed rare earth oxysalts dissolved in a KCl/NaCl melt, are two other possibilities.

2.3. The systems R_2O_3 - R'_2O_3 - $R''O_3$ (R, R', R'' = Ln, Y, Sc)

The very large number of such possible combinations makes any detailed discussion of these quaternary or pseudo-ternary systems impracticable, but it is possible to make intelligent predictions as to how any such system will behave from a consideration of the phase relationships in the pseudo-binary systems. Indeed, Schneider and Roth (1960) have predicted the phase diagram for the system La₂O₃-Sm₂O₃-Lu₂O₃ in just this way. More recently, Keller and his colleagues have studied some of these systems experimentally, and fig. 28.6 shows their results for the system La₂O₃-Er₂O₃-Y₂O₃ (Berndt et al., 1976a). The main feature of this is the existence of a perovskite-type phase extending over the whole composition range from LaErO₃ to LaYO₃. This has its maximum phase width (corresponding to the limits La_{0.47}(Y_{0.265}Er_{0.265})O₃ and La_{0.54}(Y_{0.230}Er_{0.230})O₃ for the ratio Er:Y = 1:1. The B-type phase achieves its maximum ErO_{1.5} content of 11 mole % at the expense of the YO_{1.5} content since the phase boundary on the lanthana-rich side is virtually independent of the ErO_{1.5} content, and the phase width narrows as this maximum ErO_{1.5} content is approached. The A- and C-type phase-fields correspond quite well to what would be expected from the behaviour of the respective pseudo-binary systems.

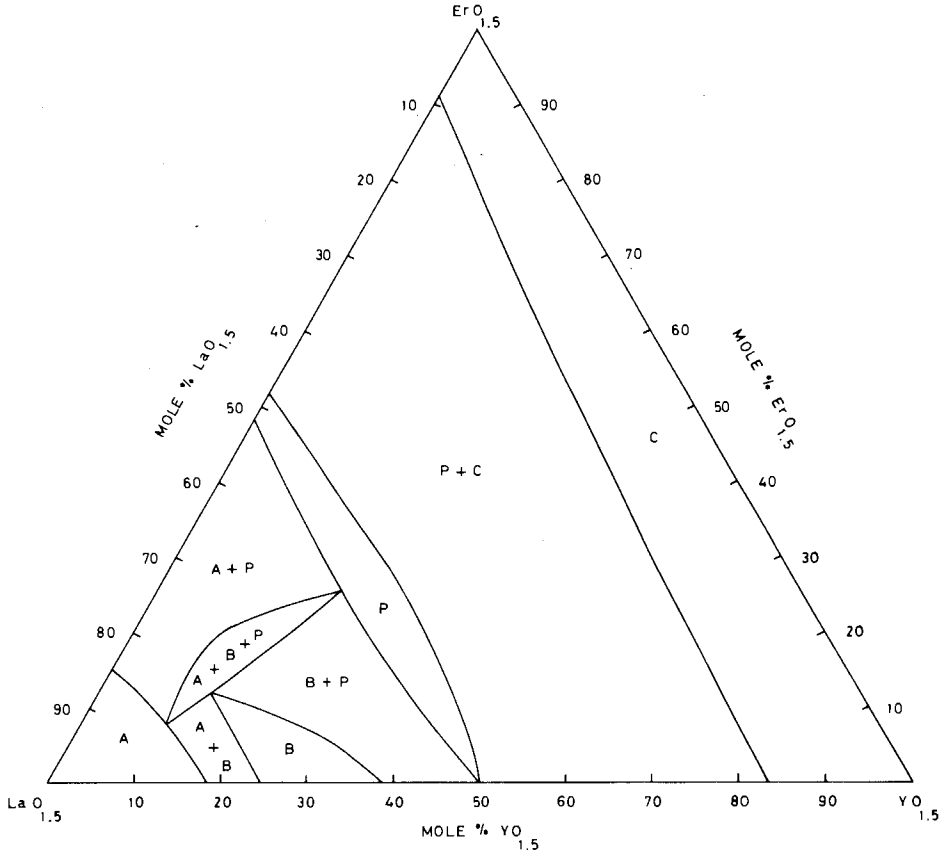


Fig. 28.6. Phase diagram for the system $\text{La}_2\text{O}_3\text{-Er}_2\text{O}_3\text{-Y}_2\text{O}_3$ at 1400°C ; after Berndt et al. (1976a).

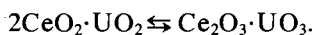
3. Phase relationships in the systems $\text{MO}_2\text{-}$ (rare earth oxides)

3.1. Mixed oxides of tetravalent elements

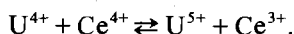
Of the lanthanide elements themselves only Ce , Pr, and Tb can form dioxides, RO_2 , although PrO_2 and TbO_2 do not form easily, particularly the latter. These have the face-centred-cubic fluorite-type structure. Other dioxides with this structure, but not of the rare earth series, are ThO_2 , UO_2 , NpO_2 , PuO_2 , AmO_2 , CmO_2 , and CfO_2 . It might be expected, therefore, that mixed oxides of this type should exhibit normal, "ideal" solid solution behaviour over the whole range of composition, and this has been found in numerous cases. The studies of McCullough (1950) on the system $\text{CeO}_2\text{-PrO}_2$, and of Whitfield et al. (1966) on the system $\text{ThO}_2\text{-CeO}_2$ may be cited as examples.

Several reports of work on the rather intriguing system $\text{CeO}_2\text{-UO}_2$ are also extant (Magnéli and Kihlberg, 1951; Hund et al., 1952; Brauer and Tiessler, 1953;

Rüdorff and Valet, 1953), the most comprehensive being that of Rüdorff and Valet (1953). As early as 1915 Hofmann and Hoeschele (1915) gave the name "Ceruranblau" (cerium-uranium blue) to a dark blue phase obtained at an approximate composition $2\text{CeO}_2 \cdot \text{UO}_2$. They postulated compound formation on account of the colour, and only subsequently was it realized that this was due to the coexistence of different valence states for both cerium and uranium. The situation was represented formally by the equilibrium:



Rüdorff and Valet (1953) showed that in fact there exists a continuous fluorite-type solid solution over the whole range of compositions between CeO_2 and UO_2 , with the cell edge varying linearly in accordance with Végard's law. They also measured the electrical conductivity of their specimens, and found a maximum at 30–40 mole % CeO_2 , where the conductivity was about one order of magnitude higher than that of UO_2 itself. With increasing CeO_2 content above 30–40 mole % CeO_2 the conductivity decreased, and beyond about 50 mole % CeO_2 became less than that of UO_2 . They suggest that this observation is more in accord with the overall electron exchange equilibrium:



The dioxides of both Zr and Hf have monoclinic structures related to the fluorite-type and should behave in this context not too differently from other fluorite-type dioxides, in spite of their smaller cation radii. The system CeO_2 - ZrO_2 has been studied by Longo and Roitti (1971), (1972), using optical microscopy, X-ray diffraction, and electrical conductivity measurements, but their conclusions as to the phase relationships existing at various temperatures are quite at variance with what might be expected, and also with the results of other workers for analogous systems which behave "normally". Thus Longo and Roitti report a quite limited solubility (20 mole %) of ZrO_2 in CeO_2 , in marked contrast to the much higher (~82 mole %) "ideal" solubility of ZrO_2 in AmO_2 (Radzewitz, 1966). For this latter, closely analogous system there is on the zirconia-rich side a diphasic region separating the broad fluorite-type solid solution from a narrow tetragonal solid solution close to the ZrO_2 composition, but in the CeO_2 - ZrO_2 system this diphasic region is unexpectedly wide. Moreover, at temperatures below ~870°C Longo and Minichelli (1973) report the appearance of a tetragonal phase of composition $\text{Ce}_2\text{Zr}_3\text{O}_{10}$ with the following lattice parameters:

$$a = b = 5.267 \pm 0.003 \text{ \AA}, \quad c = 6.034 \pm 0.003 \text{ \AA}.$$

If confirmed, these results for the CeO_2 - ZrO_2 system would imply the operation of factors as yet unknown and unexplained.

Little is known of the binary systems involving RO_2 and the dioxides of still smaller elements, e.g. TiO_2 and SnO_2 , which no longer have a fluorite-related structure but are rutile-type. Lang et al. (1956) have reported no reaction between UO_2 and SnO_2 , and a similar result might be anticipated for CeO_2 and

SnO_2 , but Perez y Jorba et al. (1961) have reported formation of the compound ThTi_2O_6 , and Stöcker (private communication to Radzewitz, 1966) has prepared CeTi_2O_6 with the same monoclinic structure.

3.2. *Mixed oxides of the type MO_2 (fluorite) – R_2O_3*

This area has been widely investigated since the discovery by Zintl and Croatto (1939) of the existence of so-called "anomalous" or "heterotype" mixed crystals in the system CeO_2 – La_2O_3 . These grossly non-stoichiometric phases, which often have wide compositional ranges, are virtually unique in oxide systems, and some have the important property of good anionic conduction (Möbius, 1964). However, in spite of much research effort there is still considerable disagreement on the precise nature of the phase equilibria in such systems.

3.2.1. *The systems ThO_2 – R_2O_3*

Figures 28.7, 28.8, and 28.9 show the results of three recent but quite independent studies of the system ThO_2 – La_2O_3 . These have been redrawn from the published data in such a way as to facilitate comparison, and the designations used throughout for the lanthana-rich intermediate phases of closely similar composition are those of Sibieude and Foex (1975). However, this is not to say that phases with the same designation are necessarily identical. Thus in the paper by Keller et al. (1972) it is stated that X-ray diffraction data for the phases found at 91.7 mole % $\text{LaO}_{1.5}$ are in approximate agreement with those reported by Sibieude and Chaudron (1970) for the Ψ_1 -phase, but that a similar correspondence between data for the phase found in this work at 75.0 mole % $\text{LaO}_{1.5}$ and the metastable Ψ_3 -phase found by the French workers was anomalous in that the Ψ_3 composition was given as 85–87 mole % $\text{LaO}_{1.5}$. No such correspondence with the data of Diness and Roy (1969) could be found.

Inspection of these phase diagrams reveals many significant differences in detail, some of which can be explained readily enough. Keller et al. (1972) and Diness and Roy (1969) based their conclusions essentially on data from quenched samples, whereas Foex (1966a,b) and his colleagues, as mentioned earlier, have developed experimental techniques for studies in situ at high temperature. From this work has come the discovery of the high-temperature H- and X-phases, which cannot be quenched and so could not have been found in the first two studies. However, important differences at lower temperatures remain unexplained, such as the width of the A-type solid solution (negligible at 1600°C in figs. 28.7 and 28.8 but quite significant in fig. 28.9), the boundary of the fluorite-type solid solution, and the whole realm of Ψ -phases. It should also be noted that discrepancies exist between the results obtained by Hund and Metzger (1952) and by Gingerich and Brauer (1963) for the boundary of the fluorite-type solid solution in particular ThO_2 – R_2O_3 systems. It is clearly very difficult to achieve and identify the true equilibrium situation in such systems.

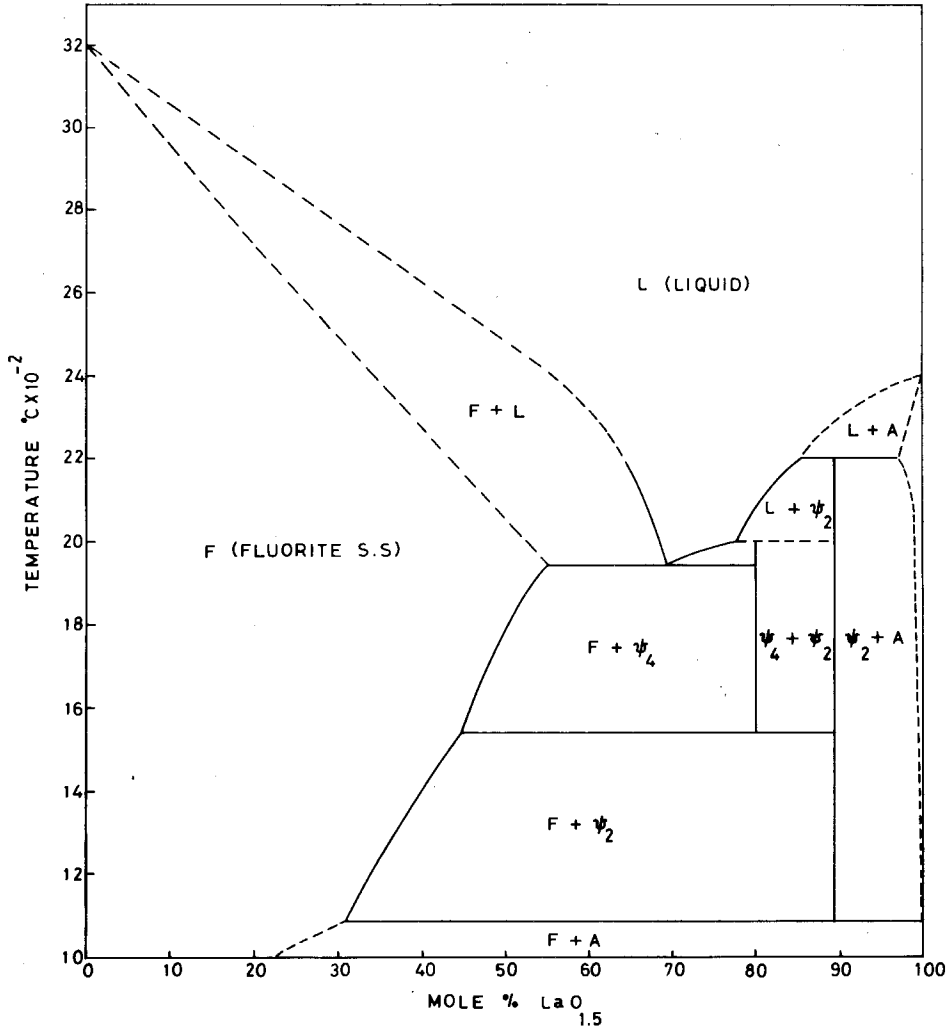


Fig. 28.7. Phase diagram for the system ThO₂-La₂O₃; after Diness and Roy (1969).

Nevertheless, in spite of such problems (to be discussed in more detail later), phase studies have revealed well-defined trends which, for the ThO₂-R₂O₃ systems, have been reviewed by Sibieude and Foex (1975) and by Keller et al. (1972). These papers contain virtually a complete set of phase diagrams which illustrate the evolution of the phase relationships as $r(\text{Th}^{4+})-r(\text{R}^{3+})$ increases. Thus the systems ThO₂-La₂O₃ and ThO₂-Nd₂O₃ are similar in character, as are those of ThO₂-Sm₂O₃, ThO₂-Eu₂O₃, and ThO₂-Gd₂O₃, but in the latter group, phases of both C- and B-type make their appearance, while Ψ -phases (vestigially present in ThO₂-Sm₂O₃ according to Sibieude and Foex (1975), but not in the other two systems) are fading out. As the discrepancy in ionic radii increases the

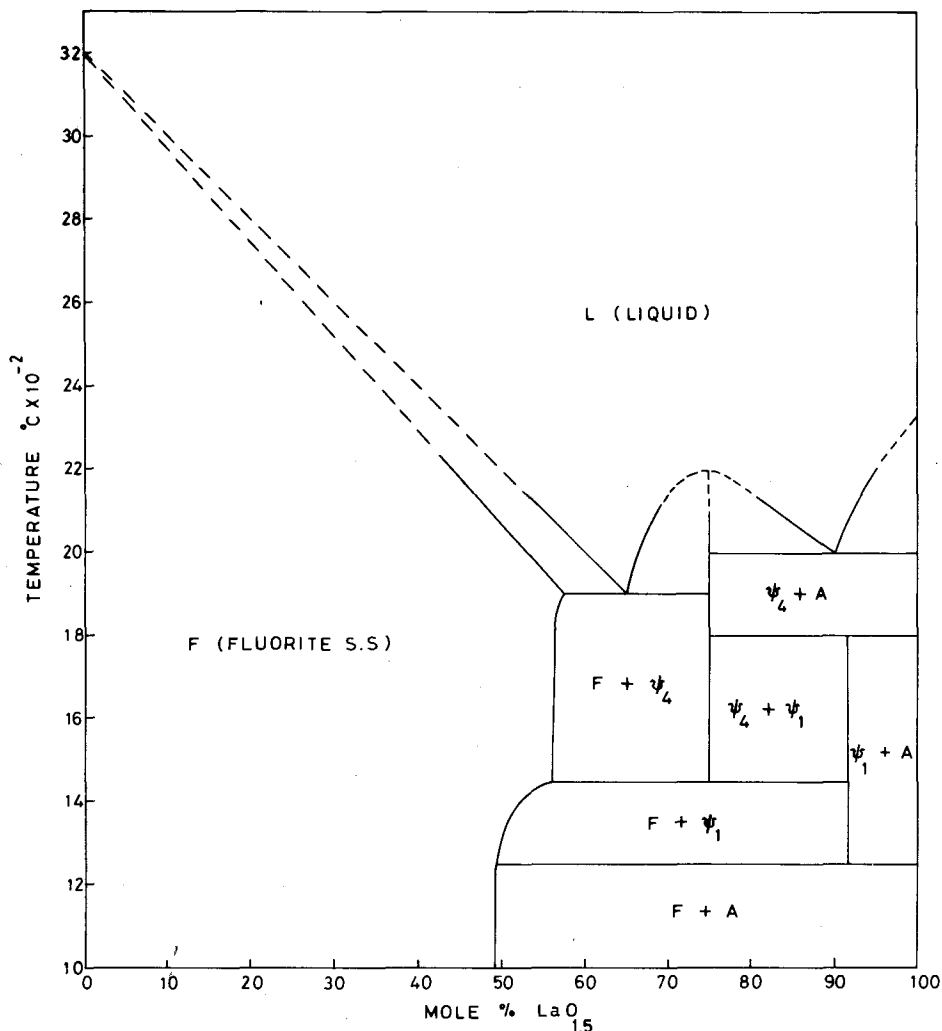


Fig. 28.8. Phase diagram for the system ThO₂-La₂O₃; after Keller et al. (1972).

range of existence of the B-type phase decreases, and it has disappeared completely in the system ThO₂-Er₂O₃. Keller et al. (1972) found no solubility of ThO₂ in B-type R₂O₃, in contrast to the French work. At the same time the C-type solid solution becomes firmly established, and it seems to be stabilized by the presence of Th⁴⁺ in the lattice. Once again however, there are significant differences between phase diagrams for the same system reported by different authors.

Keller's studies go to somewhat lower temperatures than those of the French workers and reveal a marked decrease towards the end of the lanthanide series in the saturation solubility of R₂O₃ in ThO₂ (the fluorite-type solid solution) at

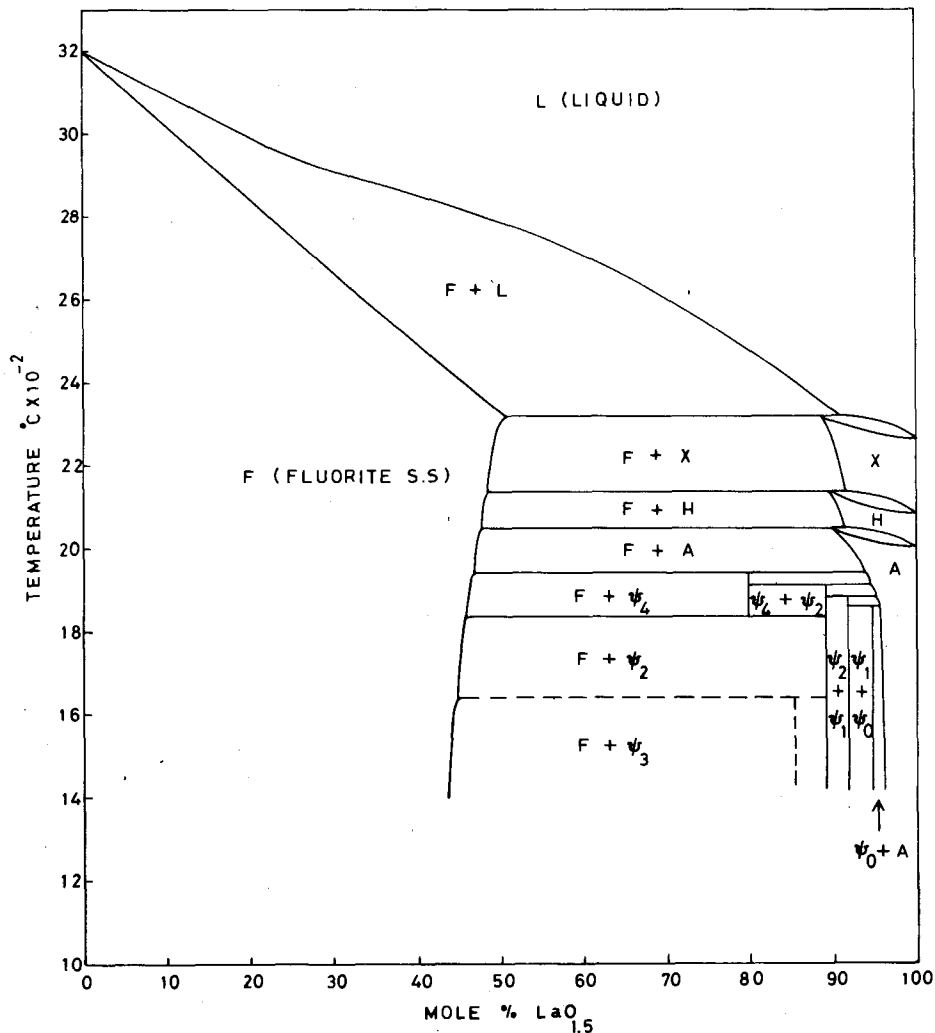


Fig. 28.9. Phase diagram for the system ThO₂-La₂O₃; after Sibicude and Foex (1975).

any given temperature. This is also true for the solubility limit of ThO₂ in C-type R₂O₃, as might be expected. The temperature dependence of this latter solubility limit, however, is somewhat anomalous compared with that of R₂O₃ in ThO₂, which increases significantly with increasing temperature: for the C-type phase there appears to be a minimum solubility of ThO₂ at about 1700°C (except in the case of ThO₂-Lu₂O₃). For further details the original papers should be consulted. There will also be published shortly a very full and comprehensive survey by Keller (1976) of the ternary and polynary oxides of thorium.

When due account is taken of radius differences, the ThO₂-R₂O₃ systems discussed above serve as models for other actinide dioxide - R₂O₃ systems, since

all dioxides of the actinide elements from thorium to californium inclusive have the fluorite-type structure. The sub-solidus regions of some of these systems ($\text{UO}_2\text{-R}_2\text{O}_3$, $\text{NpO}_2\text{-R}_2\text{O}_3$, $\text{PuO}_2\text{-R}_2\text{O}_3$) have been studied recently by Leitner (1967) in Keller's laboratory, and the $\text{UO}_2\text{-Y}_2\text{O}_3$ system was thoroughly investigated many years ago by Ferguson and Fogg (1957). In all cases only fluorite- and C-type solid solutions, separated by a diphasic region, were observed. However, because of the multivalent character of these actinide elements (in contrast to thorium) it is often difficult to retain the +4 oxidation state under experimental conditions, and it has been shown very clearly, particularly for the urania and neptunia systems, that the presence of higher oxidation states profoundly affects the phase equilibria, even to the extent of introducing entirely new phases, the nature of which will be discussed later.

3.2.2. *The systems* $\text{R}'\text{O}_2\text{-R}_2\text{O}_3$ ($\text{R}' = \text{Ce, Pr, Tb}$)

Of these, the $\text{CeO}_2\text{-R}_2\text{O}_3$ systems constitute the majority of those investigated, since for Pr and Tb it is difficult to retain completely the tetravalent state. However, for these last elements some studies have been made. Thus McCullough has reported lattice parameter data for the fluorite-type solid solutions found in the system $\text{PrO}_2\text{-Nd}_2\text{O}_3$ (1950) and for both fluorite- and C-type solid solutions in the system $\text{PrO}_2\text{-Y}_2\text{O}_3$ (1952). In this work specimens were reacted at high temperature (1200–1400°C) in conditions where Pr is predominantly trivalent, but a subsequent low-temperature heating (300–650°C) under high oxygen pressure was used to convert Pr^{3+} to Pr^{4+} . For the $\text{PrO}_2\text{-Y}_2\text{O}_3$ system the authors report a continuous transition from the fluorite- to C-type structure. Wolf and Schwab (1964) have also determined lattice parameters of solid solutions in the systems $\text{TbO}_x\text{-Y}_2\text{O}_3$ and $\text{TbO}_x\text{-Er}_2\text{O}_3$ ($1.5 < x < 2.0$), but for neither of these systems was the oxygen to metal ratio (or $\text{R}^{4+}/\text{R}^{3+}$) determined, so that interpretation of lattice parameter variations is only qualitative. In later work of a similar kind on the systems $\text{PrO}_x\text{-R}_2\text{O}_3$ Brauer and Pfeiffer (1965) did analyse their specimens for Pr (IV) content. The results obtained are interesting and unexpected but will not be discussed here: because of the preparation method, which was similar to McCullough's, the phases formed are almost certainly metastable. Finally, in this area, Kordis and Eyring (1968a, 1968b) have described results of tensimetric studies on the systems $\text{CeO}_x\text{-TbO}_x$ and $\text{PrO}_x\text{-TbO}_x$. In both of these systems (but particularly in the former) there is some evidence that no stabilization of Tb^{4+} occurs, and that therefore the component cationic species independently adjust their respective ratios of tetravalent to trivalent ions in response to changes in oxygen pressure or temperature. Certainly, the isobars for mixed cation ratios (Tb: Ce(Pr)) between approximately 2 and 1.5 are virtually featureless compared with those of the separate binary systems $\text{PrO}_x\text{-O}_2$ and $\text{TbO}_x\text{-O}_2$, in which single phases and diphasic regions are clearly delineated (see ch. 27). On the other hand, for samples much richer in TbO_x (e.g. $\text{Tb}_{0.8}\text{Ce}_{0.2}\text{O}_x$) the isobars obtained, while bearing little resemblance to those for pure terbia, do indicate the existence of a

phase $RO_{1.714}$ (R_7O_{12}), but X-ray diffraction studies show quite clearly that samples of this composition are not rhombohedral (the structure of R_7O_{12}): in fact, according to the X-ray findings, the $Tb_{0.8}Ce_{0.2}O_x$ system was monophasic (fluorite-type with, possibly, some C-type superstructure lines) for all compositions between $Tb_{0.8}Ce_{0.2}O_{1.5}$ and $Tb_{0.8}Ce_{0.2}O_{1.854}$. Thus the same situation obtains here as in the Brauer and Pfeiffer study, and in McCullough's work: a partial equilibrium between the gas and solid phases may well be established, but the solid phase itself is, at this stage, metastable. In the true binary systems the kinetic barrier to achievement of equilibrium in the solid phase is relatively small, even at quite low temperatures ($\sim 400^\circ\text{C}$), since, as is well-known, the anion mobility in fluorite-type structures is high, and adjustment of the cation sub-lattice can occur simply by electron switching: no cation transport need take place. By contrast, in ternary phases (and it is clear that CeO_x - TbO_x and PrO_x - TbO_x are true ternaries, not pseudo-binaries) any rearrangement of the cation sub-lattice must involve cation diffusion, which, for the fluorite-type structure, is extremely slow.

With this in mind, a detailed investigation of the sub-solidus regions of the CeO_2 - R_2O_3 systems was undertaken by Bevan et al. (1965) (1973), with particular attention being paid to the attainment of high-temperature equilibrium. In this work both physically-mixed oxides and coprecipitated hydroxides were repeatedly heated at some high reaction temperature for long periods (days), quenched, and studied at room temperature by powder X-ray diffraction methods. Full details are given in the original papers, but a summary of the phase relationships observed at 1600°C is contained in fig. 28.10. There is a dependence of the phase-boundary compositions on temperature: the fluorite-type solid solution increases in width with increasing temperature, while the C-type phase width decreases.

Certain features apparent in this work are worth emphasizing:

(i) The diphasic region separating the fluorite-type solid solution from the C-type phase. Only in the case of CeO_2 - La_2O_3 does no C-type phase appear, and the tendency of Ce^{4+} , like Th^{4+} , to stabilize this structure is well illustrated. Where the stable structure of R_2O_3 is itself C-type the width of the C-type solid solution decreases, as might be expected, with increasing difference between the ionic radii of Ce^{4+} and R^{3+} . Earlier studies of some of these systems by McCullough (1950, 1952) and by Brauer and Gradinger (1954) had suggested that for $R = \text{Sm, Gd, Dy, Y}$ the transition from the fluorite-type structure to the C-type was continuous as a consequence of the close relationship between the two structure types. The C-type structure is a superstructure of fluorite with double the cell edge of the latter: its diffraction pattern shows very clearly the strong reflections of the fluorite-type sub-cell, and the main evidence for the proposed continuous transition, apart from an apparently monotonic variation of cell edge with composition, was the appearance of diffuse C-type superstructure reflections in diffraction patterns of solid solutions containing as little as 20 mole % $RO_{1.5}$. The intensities of these reflections increased with increasing $RO_{1.5}$ content until the complete C-type diffraction pattern was developed, and it

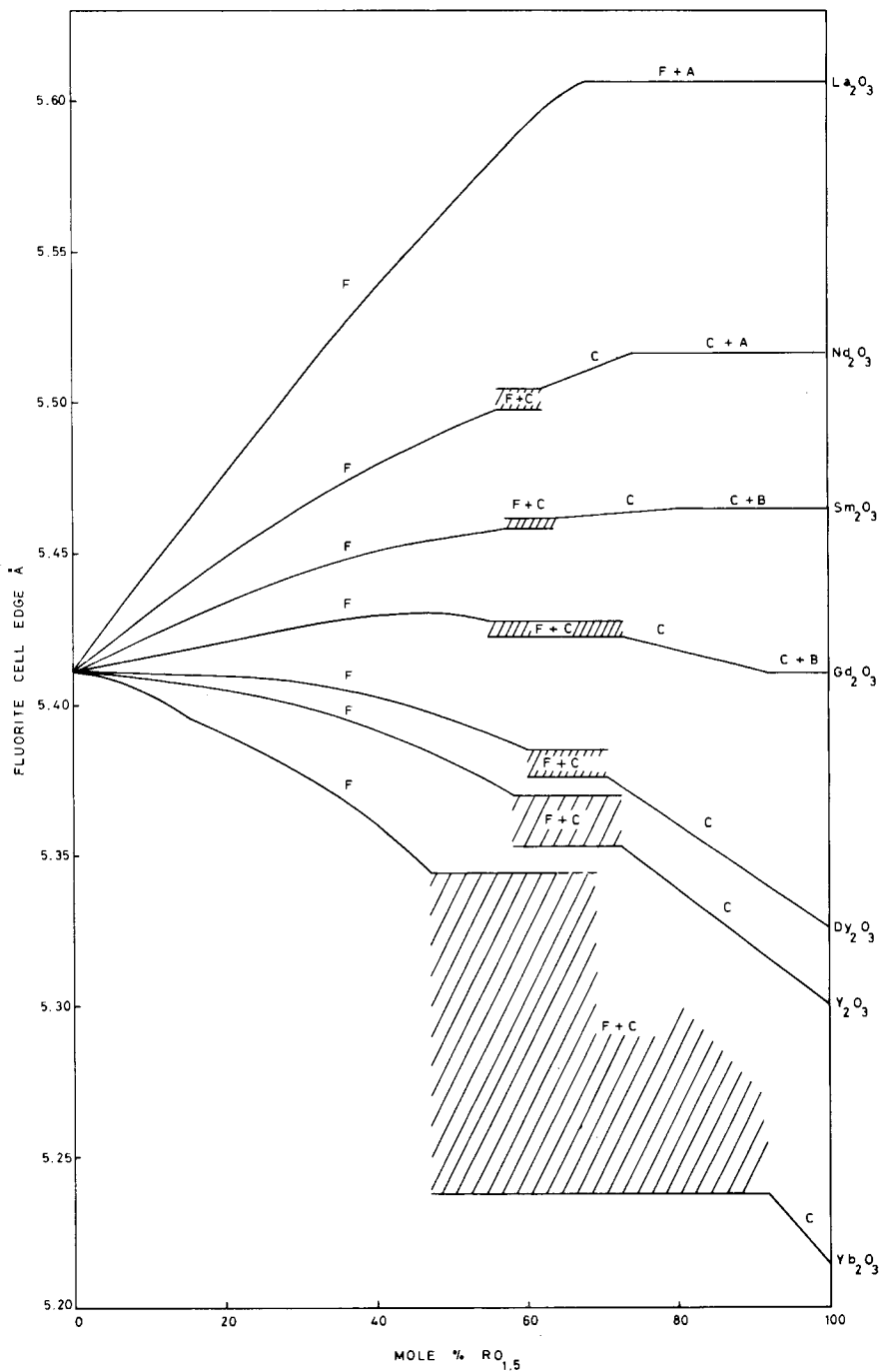


Fig. 28.10. Plot of fluorite type cell edge as a function of mole % $RO_{1.5}$ showing the phase relationships in the systems $CeO_2-R_2O_3$ as determined by room-temperature X-ray powder diffraction from specimens quenched from $1600^\circ C$.

required very close study to establish the existence in all cases of the diphasic region separating the two solid solutions. This appearance and development of C-type superstructure is a widespread phenomenon in such systems: it was observed in the work of Bevan et al. (1965), and Sibieude and Foex (1975) have found it also in their studies of $\text{ThO}_2\text{-R}_2\text{O}_3$ systems. It is almost certainly related to a second feature in Bevan's $\text{CeO}_2\text{-R}_2\text{O}_3$ data, now to be described.

(ii) The pronounced curvature in the plots of fluorite cell edge against composition for the fluorite-type solid solution. This is also widespread, and it is in direct contrast to the linear plots for the C-type solid solution. Indeed, for the system $\text{CeO}_2\text{-Yb}_2\text{O}_3$ (see fig. 28.10) two curves are identified in this region. This same latter behaviour is exhibited in the system $\text{CeO}_2\text{-Y}_2\text{O}_3$, where it has been more thoroughly investigated. Figure 28.11 shows an expanded plot of the fluorite cell parameter against mole % $\text{YO}_{1.5}$ up to 25 mole %, and clearly reveals the existence of two curves. Figure 28.12 shows a plot of the same cell parameters against the square of the yttria mole fraction, and this is linear, although the extrapolated value of a at zero mole % $\text{YO}_{1.5}$ does not coincide with

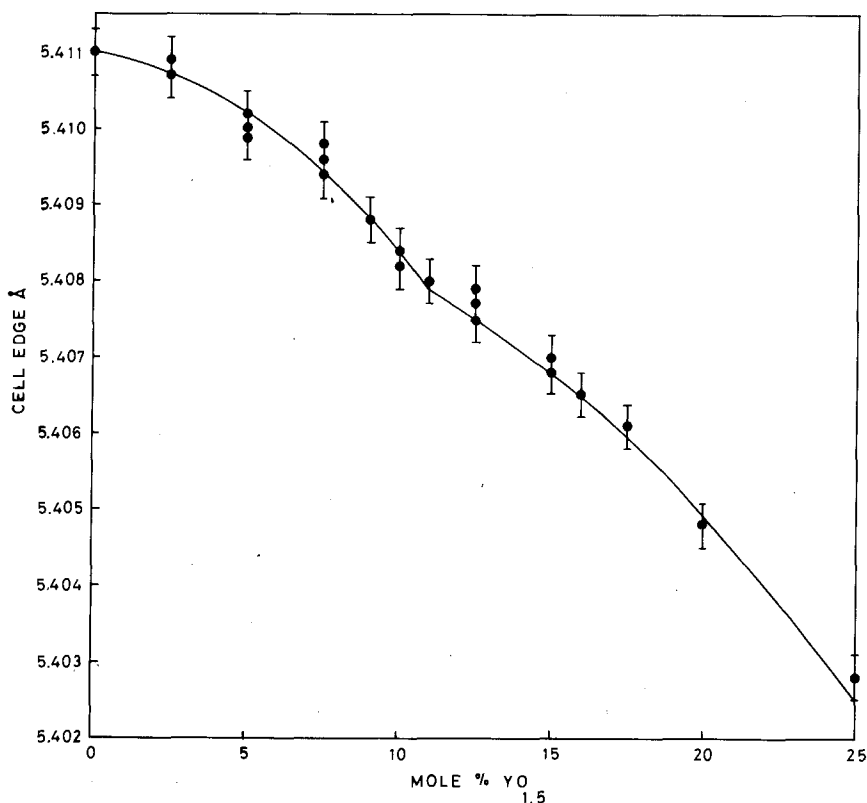


Fig. 28.11. Expanded plot of the fluorite-type cell edge as a function of mole % $\text{YO}_{1.5}$ for the system $\text{CeO}_2\text{-Y}_2\text{O}_3$; after Bevan et al. (1965).

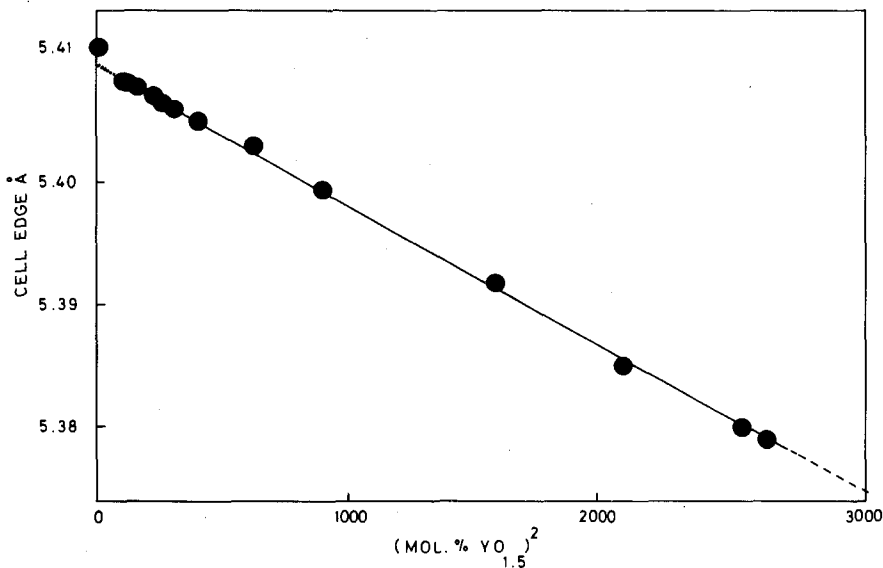


Fig. 28.12. The fluorite-type cell edge plotted as a function of the square of mole % $\text{YO}_{1.5}$ for the system $\text{CeO}_2\text{-Y}_2\text{O}_3$ in the region 0–10 mole % $\text{YO}_{1.5}$: reproduced from Bevan et al. (1965) by courtesy of Gordon and Breach, New York.

the CeO_2 cell edge. If, however, a similar plot is made of the data in the region 0–10 mole % $\text{YO}_{1.5}$ (fig. 28.13) another straight line is obtained. The two curves shown in fig. 28.11 are thus described individually by two quadratic equations, the parameters of which have been calculated: these are given below:

$$0\text{--}10 \text{ mole } \%. \quad a = 5.4110 - (3.248 \times 10^{-5})N_Y - (2.240 \times 10^{-5})N_Y^2$$

$$\sigma = 9.91 \times 10^{-5}$$

$$10\text{--}55 \text{ mole } \%. \quad a = 5.4088 + (4.896 \times 10^{-5})N_Y - (1.196 \times 10^{-5})N_Y^2$$

$$\sigma = 2.91 \times 10^{-4}$$

N_Y in each equation refers to mole % of $\text{YO}_{1.5}$. Bevan et al. (1965) have suggested that there are therefore two factors which determine the cell parameter of a fluorite-type solid solution; first, a purely geometrical one related to the difference in ionic radii between Ce^{4+} and R^{3+} (the first-order term), and secondly, an attractive defect interaction (the second-order term) which strongly contracts the unit cell. Competition between these two factors is well illustrated in the system $\text{CeO}_2\text{-Gd}_2\text{O}_3$ where the cell edge shows a maximum. It has further been suggested that the appearance of the diffuse C-type superstructure reflections might indicate the existence of small microdomains of C-type structure coherently intergrown in a fluorite-type matrix. It must be remembered, however, that the X-ray data were obtained at room temperature on quenched specimens, so the high-temperature situation is unresolved. It may be that on

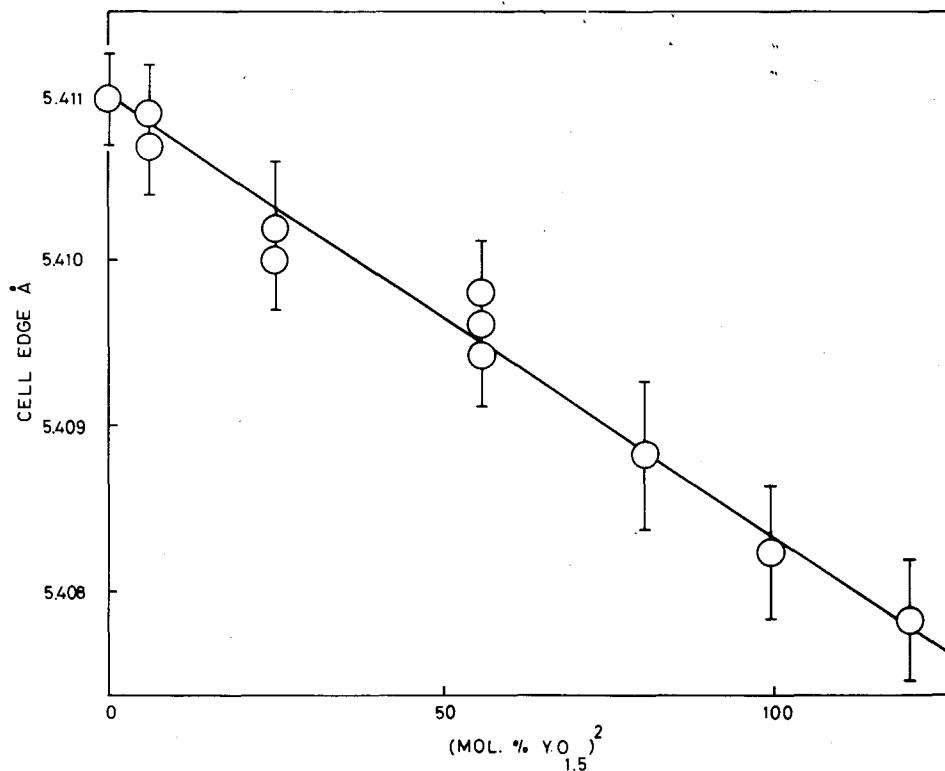


Fig. 28.13. Expanded plot of the fluorite-type cell edge as a function of the square of mole % $\text{YO}_{1.5}$ for the system $\text{CeO}_2\text{-Y}_2\text{O}_3$ in the region 0–10 mole % $\text{YO}_{1.5}$; reproduced from Bevan et al. (1965) by courtesy of Gordon and Breach, New York.

cooling there is coherent precipitation of a C-type phase, although this seems unlikely, but in either case it should be possible to observe C-type regions in dark-field electron microscopy.

3.2.3. The systems $\text{MO}_2\text{-R}_2\text{O}_3$ (M = Zr, Hf)

Although the dioxides of zirconium and hafnium crystallize at room temperature in the monoclinic baddeleyite-type structure, this is closely related to fluorite, and they do form fluorite-type solid solutions with rare earth oxides which have important ceramic properties. Compared with Th^{4+} , U^{4+} , Ce^{4+} etc., Zr^{4+} and Hf^{4+} have considerably smaller ionic radii which are close to that of the smallest R^{3+} ion (Sc^{3+}), and this fact has an important influence on the phase relationships in these systems, leading to the appearance of intermediate phases not encountered in other $\text{MO}_2\text{-R}_2\text{O}_3$ systems. They have been studied extensively, particularly in the first instance by Collongues et al. (1965 and references therein). Work published prior to 1964 has been reviewed by Möbius (1964).

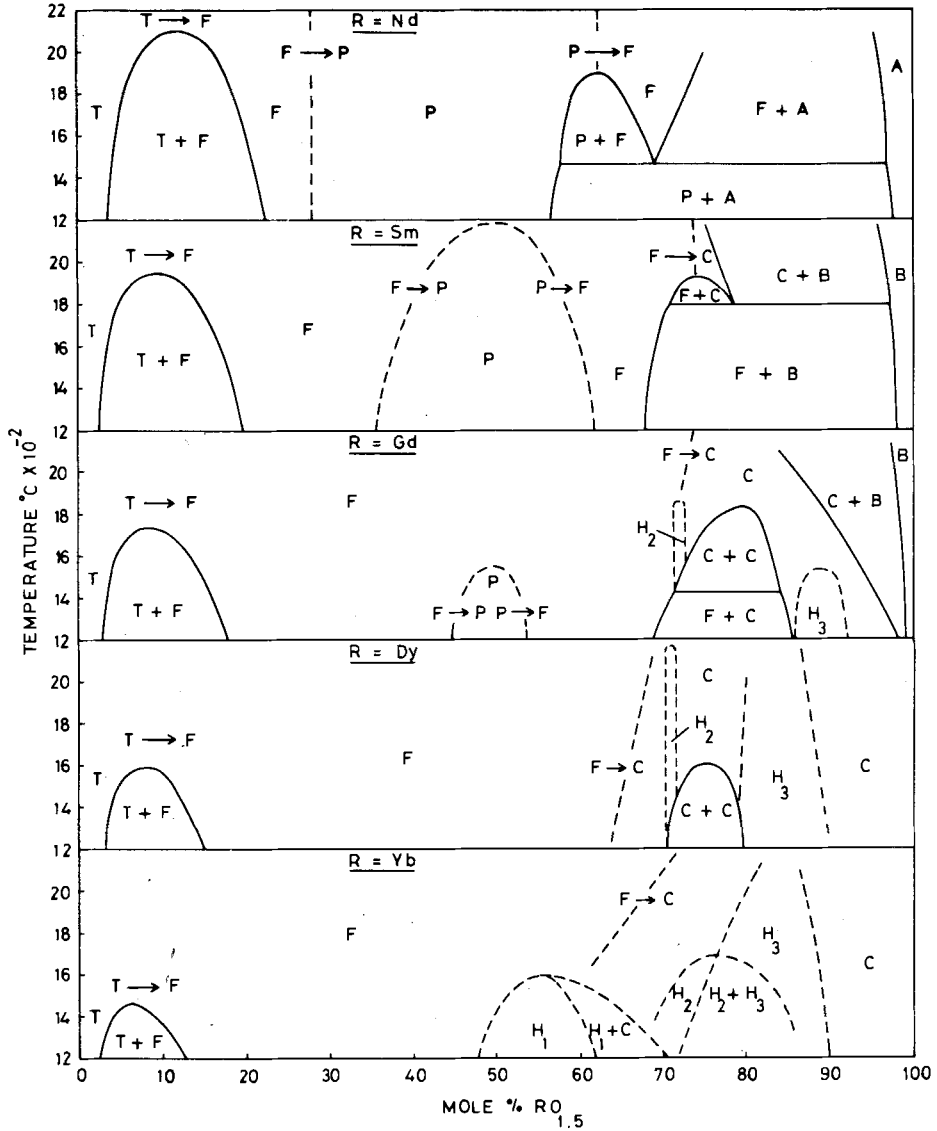


Fig. 28.14. Phase relationships for several $ZrO_2-R_2O_3$ systems as determined by Collongues and his colleagues.

Apart from the ceramic applications which inspired much of this work, new understanding of fundamental solid state chemistry has also emerged in recent years, in spite of and even because of still greater discrepancies and contradictions between the results of different workers than those already emphasized in discussions of other systems.

Figure 28.14 shows in consolidated form the phase relationships determined in

Collongues' laboratory for a number of $ZrO_2-R_2O_3$ systems: these are both complex and peculiar. Certain features stand out:

(i) The appearance of a pyrochlore-type phase in all systems from La through Gd. The ideal formula for this is $R_2M_2O_7$, but the phase occurs over quite a wide range of composition extending on either side of the ideal. The empirical evidence shows that a pyrochlore-type phase can only be formed if the ratio r (M^{4+}): r (R^{3+}) is greater than 1.22. A brief discussion of the pyrochlore structure in this context will be given later.

(ii) Continuous transformations between different structure types. Thus above some critical temperature the tetragonal solid solution rich in zirconia is shown as transforming continuously to the fluorite-type solid solution. This in turn transforms continuously to the pyrochlore-type solid solution in those systems where the latter can form, and with increasing R_2O_3 content this transforms back again to the fluorite-type. (Similar behaviour has been reported for some of the $ZrO_2-R_2O_3$ and $HfO_2-R_2O_3$ systems investigated by Radzewitz (1966) in Keller's laboratory.) With further increase in R_2O_3 content the fluorite-type solid solution in all systems shown, with the exception of $ZrO_2-Nd_2O_3$, then transforms continuously into a C-type phase.

(iii) The appearance of hexagonal phases, designated H_1 , H_2 , and H_3 . The H_1 -phase, appearing only in the system $ZrO_2-Yb_2O_3$, is the δ -phase of the $ZrO_2-Sc_2O_3$ system (see below), whose ideal composition is $Zr_3Sc_4O_{12}$. The genuine existence of the H_2 and H_3 phases is open to doubt; in later work Rouanet (1971) did not report them, and Thornber et al. (1970) state that they were not observed when the starting rare earth oxides were purified prior to sample preparation.* Moreover, Thornber (1969) noted the close similarity of the diffraction patterns of these hexagonal phases to that of the C-type phase, and suggested that H_2 and H_3 might, in fact, be mixtures of the C-type phase and impurities. However, Spiridonov et al. (1968) have reported the occurrence of H_2 and H_3 in the system $HfO_2-Gd_2O_3$, while Spiridonov and Komissarova (1970) have found H_3 in the system $HfO_2-Er_2O_3$; further clarification is clearly needed.

More recently, Rouanet (1971) has published high-temperature phase diagrams for many of the $ZrO_2-R_2O_3$ systems: his results for the systems $ZrO_2-La_2O_3$ and $ZrO_2-Nd_2O_3$ are shown in figs. 28.15 and 28.16. A comparison of the latter with the appropriate sections of fig. 28.14 shows the existence of significant differences. Thus in Rouanet's diagram the relationships involving the tetragonal and fluorite-type solid solutions are quite conventional: there is no continuous transformation between the two phases, which are separated by a diphasic region. Similarly, at temperatures below about 2100°C there are diphasic regions separating the fluorite-type solid solution and the pyrochlore-type phase on the one hand, and the pyrochlore- and C-type phases on the other. At higher temperatures, however, continuous transitions of the type $F \rightarrow P$ and $P \rightarrow C$ (or

*In this context it is worth noting that the stated purity of most commercially-available rare earth oxides (99.9%, 99.99% etc.) is only with respect to other rare earths; other impurities may be present in larger amounts.

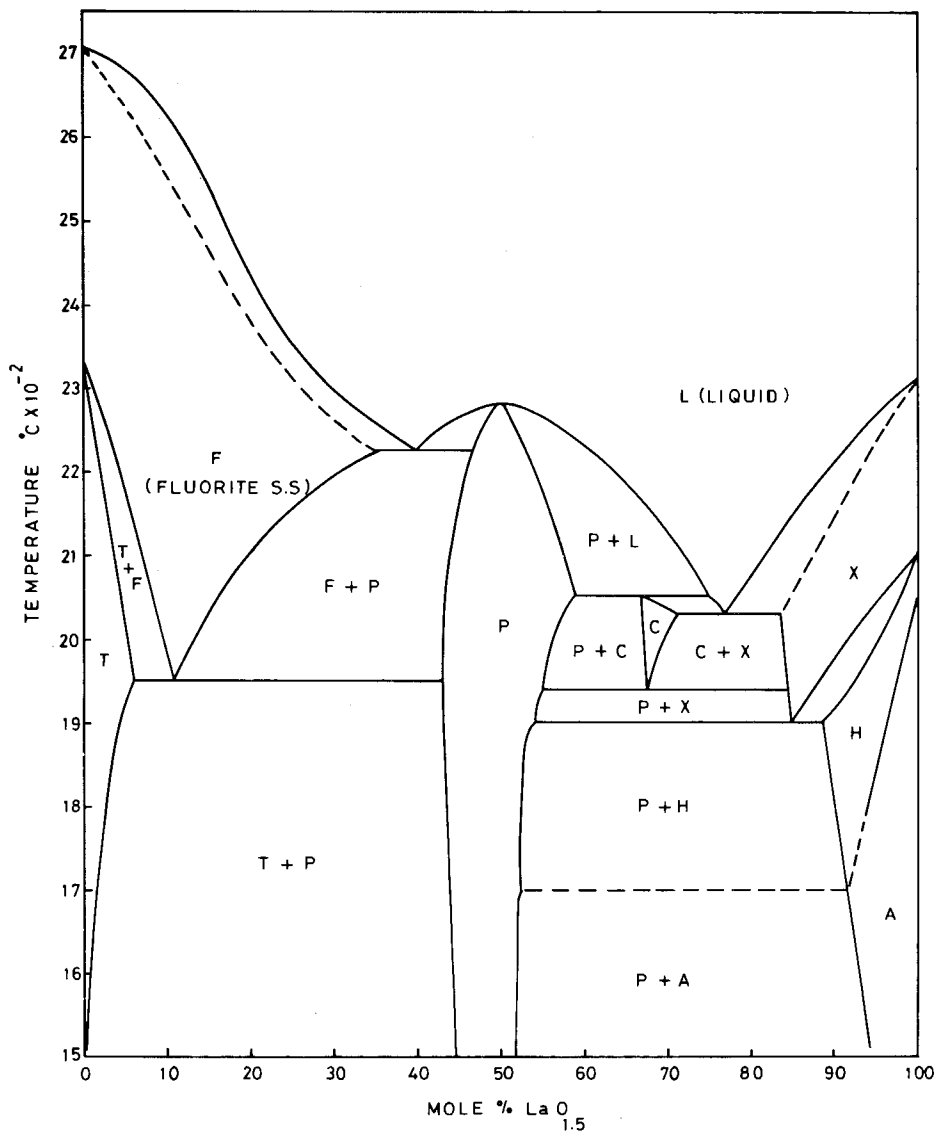


Fig. 28.15. Phase diagram for the system $\text{ZrO}_2\text{-La}_2\text{O}_3$: After Rouanet (1971).

$\text{P} \rightarrow \text{F}$) are implied, and at still higher temperatures, where the pyrochlore-type phase is no longer stable, the $\text{F} \rightarrow \text{C}$ transition is also shown as continuous.

This same general pattern is evident in all the other diagrams given by Rouanet except that for $\text{ZrO}_2\text{-La}_2\text{O}_3$ (fig. 28.15): however, the R_2O_3 -rich ends are well behaved and similar to those of the $\text{ThO}_2\text{-R}_2\text{O}_3$ systems. This theme of continuous transitions, particularly between the fluorite- and C-type phases, is dominant in much of this work, and is very reminiscent of the early results on

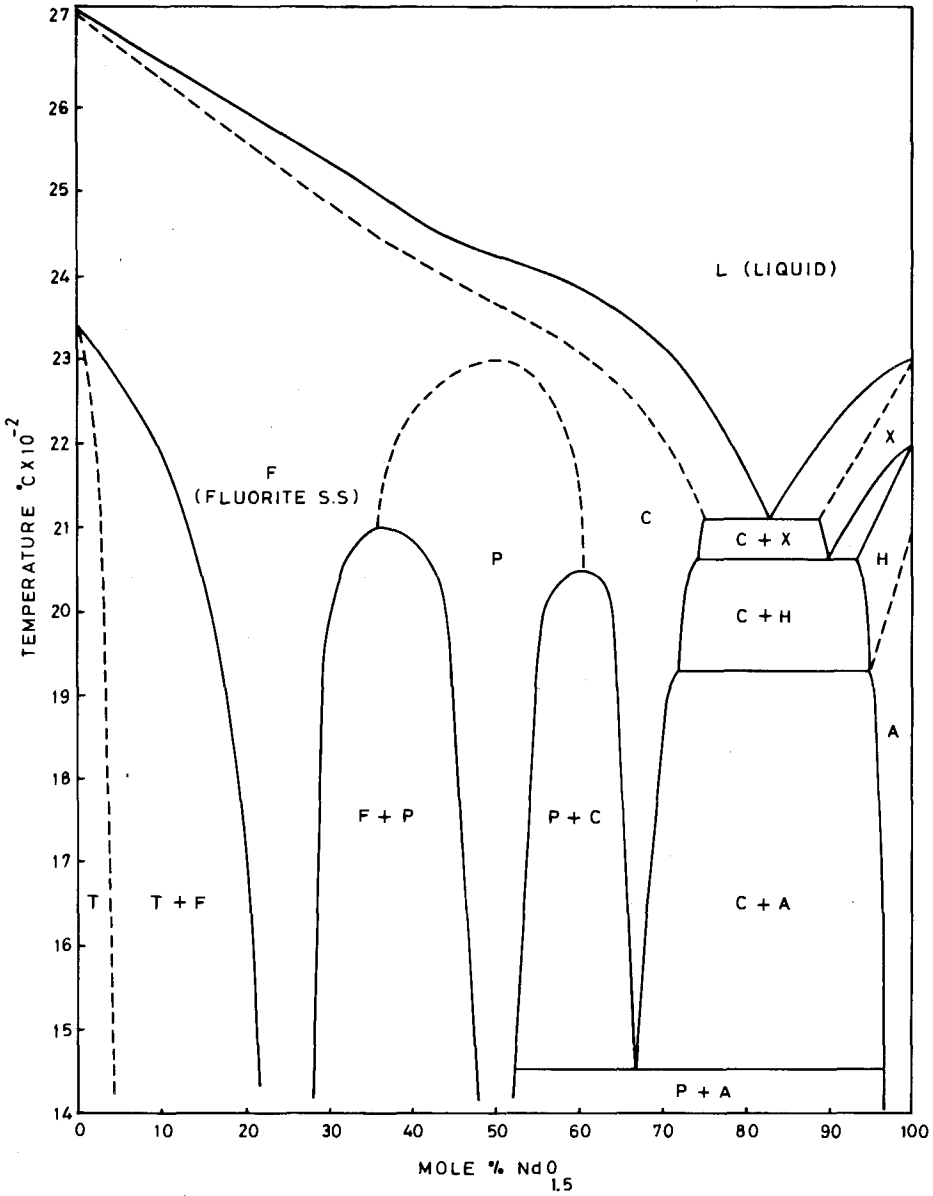


Fig. 28.16. Phase diagram for the system $ZrO_2-Nd_2O_3$; after Rouanet (1971).

some of the $CeO_2-R_2O_3$ systems already discussed, results which were later shown to be incorrect. In these systems, at least to temperatures of $\sim 1600^\circ C$, the fluorite- and C-type phases are separated by a diphasic region, albeit a very narrow one in some cases, and the question arises as to whether or not the same situation obtains in the $ZrO_2-R_2O_3$ systems.

Thorner et al. (1970) have studied the systems ZrO_2 - Dy_2O_3 , ZrO_2 - Er_2O_3 , and ZrO_2 - Yb_2O_3 at $1600^\circ C$ in some detail, and their results are summarized in fig. 28.17. These show quite clearly that at this temperature a diphasic region between the fluorite- and C-type phases of the first two systems does exist. For the third, where the δ -phase ($Zr_3Yb_4O_{12}$) is present as an intermediate phase, diphasic regions between the fluorite phase and $Zr_3Yb_4O_{12}$ on the one hand, and between $Zr_3Yb_4O_{12}$ and the C-type phase on the other, also occur. Spiridonov and Komissarova (1970) have also reported a diphasic region between the fluorite- and C-type phases of the system HfO_2 - Er_2O_3 , extending at least to $2000^\circ C$, and a similar result was found by Spiridonov et al. (1969) for the system HfO_2 - Y_2O_3 . There is, then, much evidence suggesting that diphasic regions should intervene between the solid solutions of different structure types which occur in these systems. Intermediate phases (compounds) might also be expected to melt congruently, as found for the pyrochlore-type phases of the systems ZrO_2 - La_2O_3 (Rouanet, 1971), HfO_2 - La_2O_3 (Komissarova et al., 1964), and HfO_2 - Gd_2O_3 (Spiridonov et al., 1968), or incongruently, as in the case of ZrO_2 - Pr_2O_3

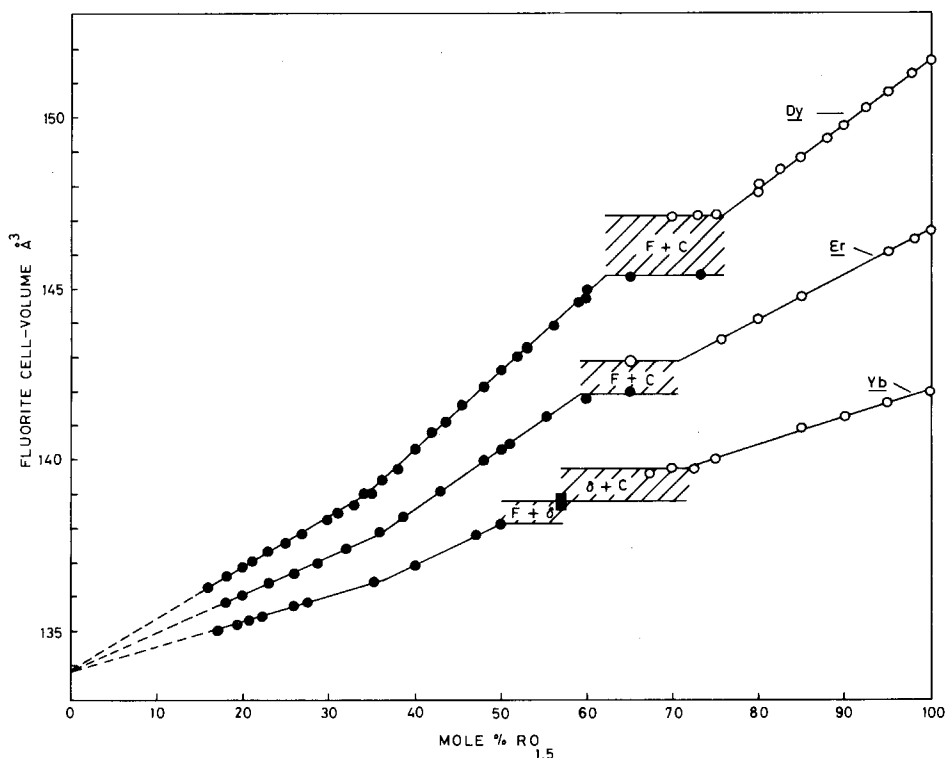


Fig. 28.17. Plot of fluorite-type cell edge as a function of mole % $RO_{1.5}$ showing the phase relationships in the systems ZrO_2 - R_2O_3 ($R = Dy, Er, Yb$) as determined by room-temperature X-ray powder diffraction from specimens quenched from $1600^\circ C$. The blocked rectangle represents the δ -phase ($Zr_3Yb_4O_{12}$): after Thorner et al. (1970).

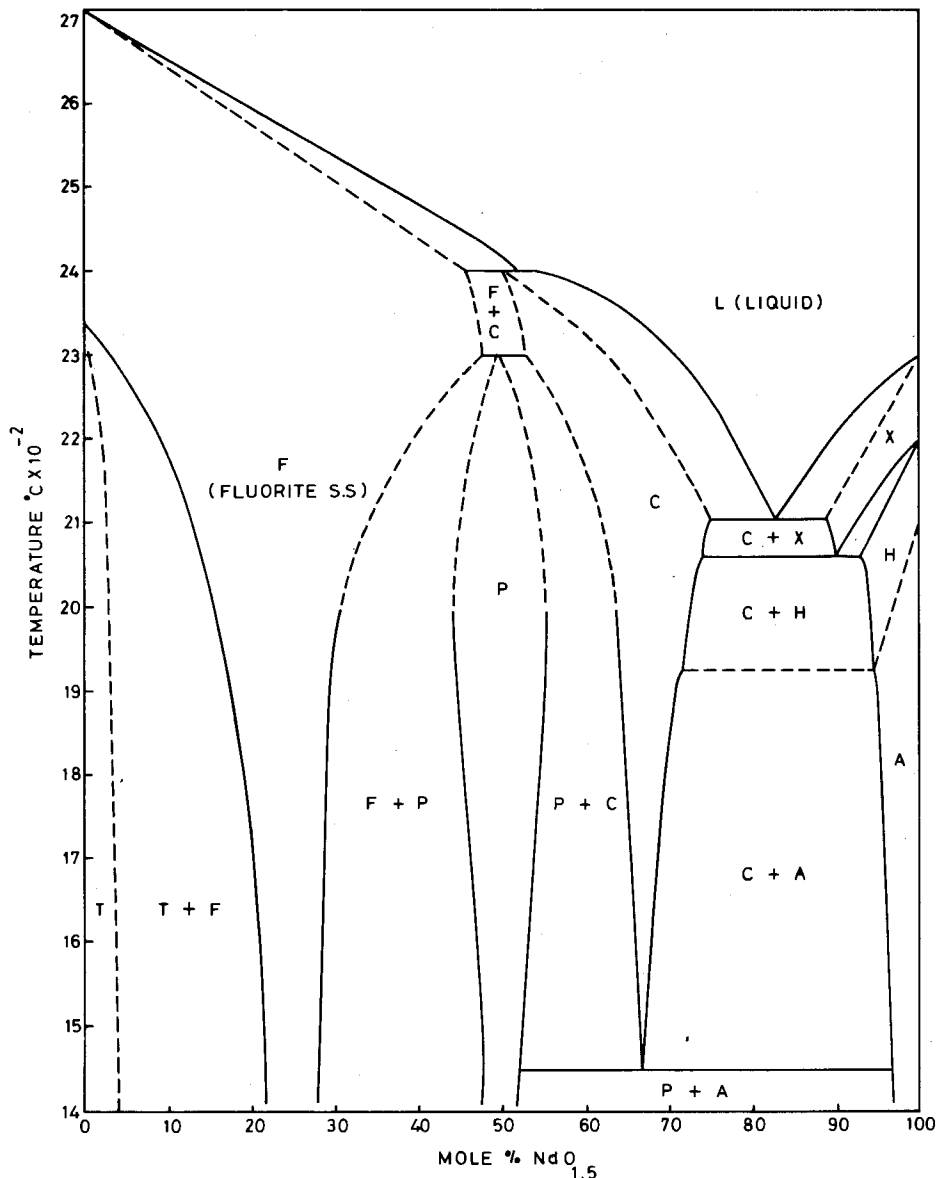


Fig. 28.18. Proposed phase diagrams for the system $\text{ZrO}_2\text{-Nd}_2\text{O}_3$. (see text).

(Rouanet, 1971), or to undergo a peritectoid decomposition rather than an order-disorder transformation. Thus fig. 28.18 is a redrawn version of fig. 28.16 incorporating these proposed features.

Much less research has been devoted to the analogous $\text{HfO}_2\text{-R}_2\text{O}_3$ systems, and some of it has already been cited. In general, as would be expected, the

behaviour is very similar to that of the $ZrO_2-R_2O_3$ systems, but intermediate phases seem to be stable to higher temperatures. A pyrochlore-type phase occurs in the system $HfO_2-Tb_2O_3$ (Klee and Weitz, 1969) although not in the system $ZrO_2-Tb_2O_3$.

The ionic radii of Sc^{3+} , Zr^{4+} , and Hf^{4+} are almost identical, as a result of which the systems $ZrO_2-Sc_2O_3$ and $HfO_2-Sc_2O_3$ possess certain unique and very significant characteristics. The former was first studied in Collongues' laboratory, with samples quenched from high temperature, and fig. 28.19 shows the phase diagram reported by Lefèvre (1963). The most significant feature of this is the appearance of the three intermediate phases, β , γ , and δ . On the zirconia-rich side of the diagram two tetragonal phases are shown to coexist, but with increasing Sc_2O_3 content a fluorite-type solid solution becomes established. Diphasic regions are shown between γ and δ , and between δ and the scandia-rich C-type phase. The ideal compositions of δ and γ are $Zr_3Sc_4O_{12}$ and $Zr_3Sc_2O_{13}$ respectively, but there is some uncertainty about that of β : following Strickler and Carlson (1964), Spiridonov et al. (1970) and other authors have assumed the ideal formula $Zr_2Sc_2O_{17}$. Thornber et al. (1970), however, have proposed the formula $Zr_{48}Sc_{14}O_{117}$, which is in accord with the unit-cell data obtained from both powder and single-crystal X-ray diffraction patterns. All three have structures which are superstructures of the fluorite-type, and these will be discussed subsequently. The same intermediate phases were observed by Kalinovskaya et al. (1969) in the system $HfO_2-Sc_2O_3$, while Duclot et al. (1970) have reported the presence of a β -phase (but not γ and δ) in the system $HfO_2-Y_2O_3$. In the $ZrO_2-R_2O_3$ systems other than $ZrO_2-Sc_2O_3$ the δ -phase has been found for $R = Er, Yb, Tm, \text{ and } Lu$, but not β and γ (Rossell, 1976).

Fig. 28.19 is a somewhat crude phase diagram, but its appearance sparked several other independent studies of the $ZrO_2-Sc_2O_3$ system. Figs. 28.20(a), (b), and (c) illustrate the wide divergence of results from three such studies, and serve to emphasize the problem, already touched on, in determining equilibrium phase relationships in systems of this kind. The diagram proposed by Thornber et al. (1970) is a composite, constructed from data obtained by Lefèvre (1963), Strickler and Carlson (1964), Domagala (1966), Ruh (1967), and from their own experiments. It is an attempt to rationalize the evidence available, to extrapolate observed trends in data from incompletely equilibrated specimens, and to take cognisance of the fact that many of the data are from quenched samples. It is a tentative *equilibrium* diagram, but begs the question of whether or not such equilibria can ever be achieved. By contrast, the other two diagrams represent what might be termed "observational equilibria", i.e. simply the phase relationships observed under the conditions of the performed experiment. Two questions immediately arise. Is there evidence that very different "observational equilibria" can be attributed to experimental factors, and if so, what are the factors responsible? On these points two independent studies of the $ZrO_2-Sc_2O_3$ system are highly relevant. Spiridonov et al. (1970) noted that for the fluorite-type solid solutions formed in excess of $\sim 600^\circ C$ in the composition range of the β -phase, the rate and extent of the reverse transformation $F \rightarrow \beta$ on cooling is

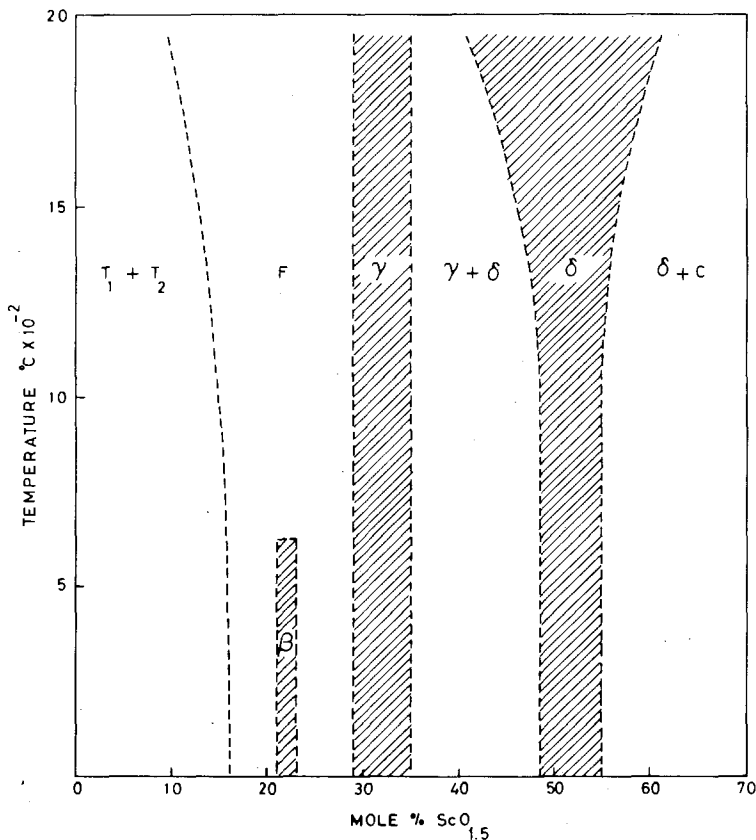


Fig. 28.19. Phase diagram for the system $\text{ZrO}_2\text{-Sc}_2\text{O}_3$; after Lefèvre (1963).

very dependent on the preceding heat treatment. Thus, provided this did not exceed 1200°C , the transformation was fully realized, but for treatments at higher temperatures it is slowed down considerably, or even does not occur. Similar behaviour is said to have been observed in the region of the β -phase composition in the system $\text{HfO}_2\text{-Sc}_2\text{O}_3$ quenched from $\sim 2550^\circ\text{C}$. The following two paragraphs are quoted from Spiridonov's paper:

The reason for this is probably tied to the fact that the higher temperatures of tempering gradually eliminate the microdisorders of the lattice that aid formation of crystalline seeds of the low-temperature compounds.

The persistence of 'super-cooled' metastable solid solutions in the specimens may be the source of the discrepancies in equilibrium studies in the system $\text{ZrO}_2\text{-Sc}_2\text{O}_3$.

No comment is made on what these microdisorders might be.

Further work by Summerville and Bevan (to be published) on this system has confirmed such behaviour. The techniques applied were both ambient- and

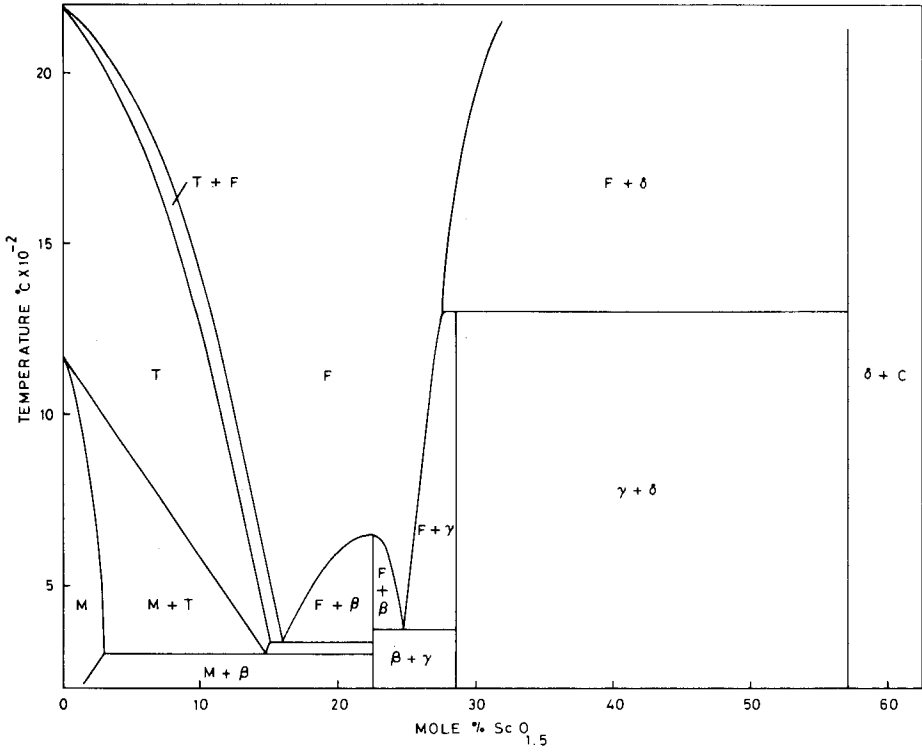


Fig. 28.20(a). Phase diagram for the system ZrO_2 - Sc_2O_3 : after Thornber et al. (1970).

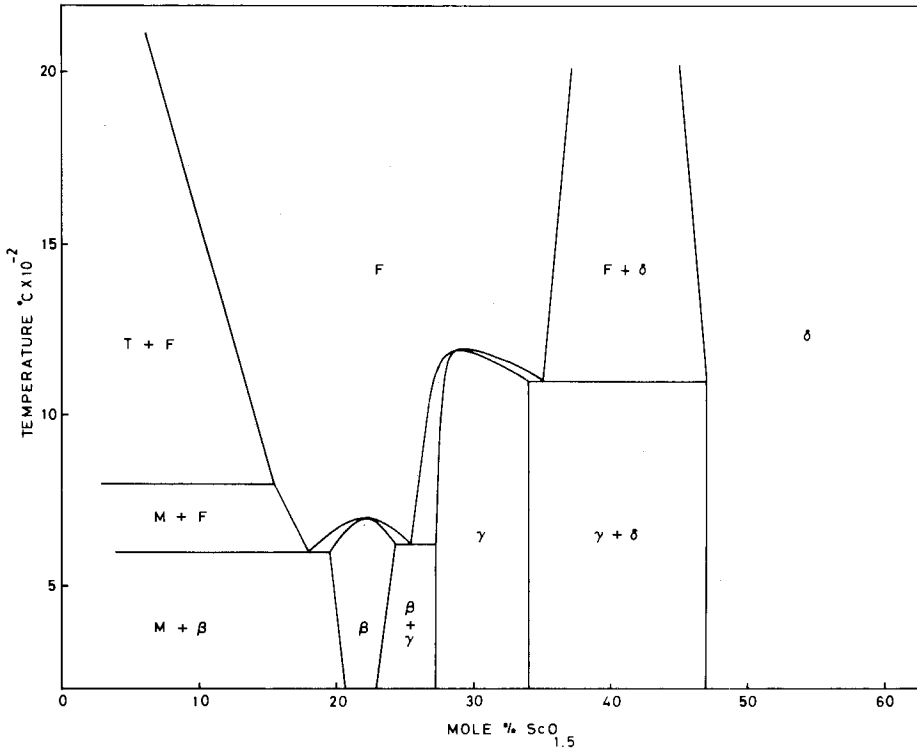


Fig. 28.20(b). Phase diagram for the system ZrO_2 - Sc_2O_3 : after Spiridonov et al. (1970).

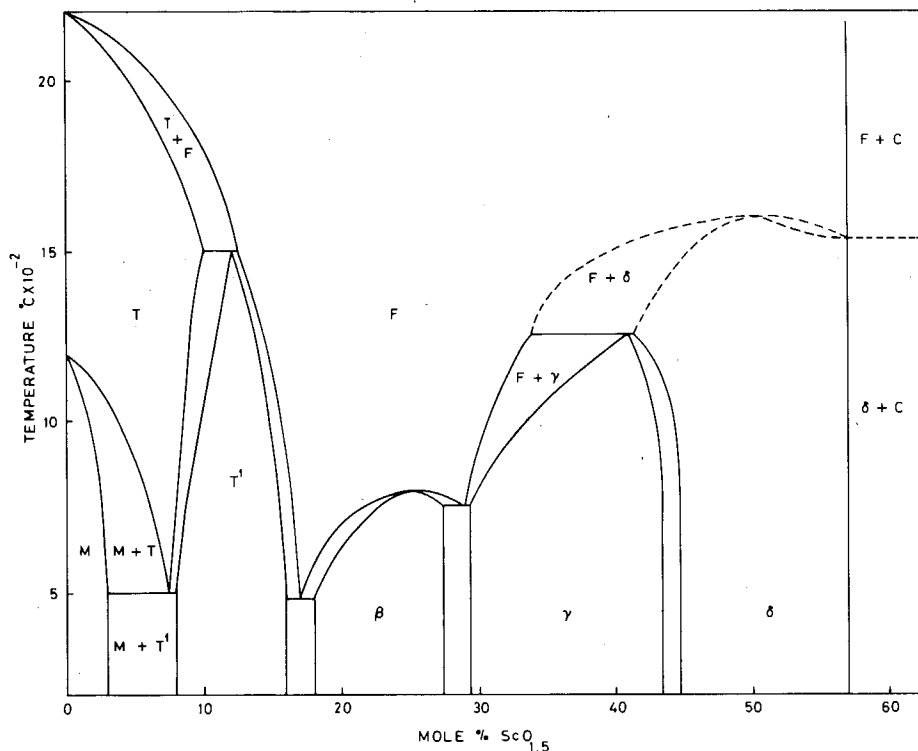


Fig. 28.20(c). Phase diagram for the system $\text{ZrO}_2\text{-Sc}_2\text{O}_3$: after Ruh (1967).

high-temperature X-ray diffraction and metallography, and electron diffraction. Samples were prepared both by standard coprecipitation methods, and by arc-melting of physical mixtures of the component oxides under argon. Coprecipitated samples were also arc-melted in some cases. Many different heat treatments were given, often for very long times (months to years). This is not the place to record details which will be published elsewhere: it is sufficient to state that many of the data obtained were clearly non-equilibrium, often mutually contradictory, and unreproducible. In this work the microdisorders invoked by Spiridonov are identified with compositional heterogeneities, and although these occur on such a fine scale that their presence can often only be evidenced by electron microscopy*, their effects, allied to the unique transport properties of fluorite-type phases and the close structural relationships (see below) between the phases F, β , γ , and δ , may be very profound. Thus it now appears that a broad

* It is worth noting in parenthesis that there are many published pictures of electron microscope lattice images of d -transition metal oxides in which compositional heterogeneities are apparent: see, for example, Allpress and Sanders (1973), Iijima (1973).

spectrum of results can be obtained from a phase analysis experiment at any composition in this system, depending on the *degree of heterogeneity* of the sample. Because cation mobility in the system is so low, this degree of heterogeneity will not be changed significantly except by annealing at very high temperatures: complete equilibrium is only attainable under these conditions.

In such fluorite-related systems, where the "characteristic temperatures" (to use a spectroscopic term) of the two sub-lattices are about 1000°C apart, low-temperature equilibrium is unattainable by conventional techniques. If a sample were heated at a temperature where equilibrium in the cation sub-lattice could be achieved without undue kinetic hindrance, the resulting cation distribution would be that appropriate to a disordered, virtually liquid anion array. Subsequent annealing of the sample at a lower temperature would then do no more than permit the anions to achieve the lowest energy configuration consistent with the "frozen" high-temperature cation distribution. Moreover, since the anions are so mobile, even quenching of samples from high temperature will not prevent some adjustment of the anion sub-lattice, although again the high-temperature cation configuration will be frozen. The low-temperature situation is thus seen to be the direct consequence of the high-temperature cation distribution.

In view of this, some reference state for the cation distribution needs to be defined to serve as a bench mark to which observed low-temperature states can be referred. Summerville (1973) has coined the phrase "operational equilibrium" to describe the state achieved after a low-temperature anneal when the anion sub-lattice adjusts to a *random* cation distribution: this should be reproducible. Operational equilibrium will be achieved in principle with samples that have been melted initially, or in practice perhaps with those which have been heated above, say, 2000°C. Any tendency for changes in the random cation distribution thus achieved, which might stem from the stable existence below, say, 1600°C of some intermediate compound of defined composition, would only be revealed if the sample were annealed at close to this temperature for sufficient time for the diffusion-controlled reaction to take place. So it is that for the ZrO_2 - Sc_2O_3 system, arc-melted samples of compositions between those of the γ - and δ -phases appear optically, to X-rays, but *not* to electrons as monophasic. However, after a week's annealing at 1600°C and subsequent quenching, phase separation does occur on a sub-microscopic scale, and is clearly shown in X-ray diffraction.

Summerville's evidence suggests that both γ and δ are "line phases" *at equilibrium*, having no compositional width and occurring at the ideal compositions. However, in the context of operational equilibrium, a sample with a statistical distribution of cations may contain regions whose composition corresponds to that of an intermediate phase, and transformation of these "nuclei" on cooling to the ordered-phase structure, coherently intergrown in the matrix, must set up stresses which could then propagate the same transformation through the nonstoichiometric material (c.f. the electron microscope studies of Loier et al. (1974) on induced transformations, discussed in 2.1). In an *observational* sense,

then, each intermediate phase will exhibit a range of composition, but the extent of this might be small. On the other hand, if the overall sample composition is well removed from any ordered-phase composition, no transformation would be likely to occur. However, if such a sample did not have its cations randomly distributed, but contained inhomogeneities significantly above the statistical level, the chances of transformation to an intermediate-phase structure would be enhanced. In such a case the phase width would appear greater. It now seems likely that true operational equilibrium occurs rather rarely in these systems, and that while the various workers believed that they had achieved initially a random cation distribution by one preparative means or another, none did so consistently: each experimenter had imparted a unique inhomogeneity profile to the samples used, and this may well have been a major factor in determining the phase relationships observed in each experiment.

Lefèvre's phase diagram for the ZrO_2 - Sc_2O_3 system is the one which probably reflects most accurately the operational equilibrium situation, and hence from a technological point of view may be the most valuable. Ruh's diagram exemplifies observational equilibrium far removed from the operational equilibrium condition, where major inhomogeneities have resulted in the appearance of broad monophasic regions separated by narrow diphasic regions. The diagrams of Thornber et al. (1970) and Spiridonov et al. (1970) are hybrids of both observational and thermodynamic equilibrium, the former in particular resulting from attempts to extrapolate observed trends to the true equilibrium state. As such they represent approximations to the equilibrium phase diagram, but it is unlikely that significant improvements can ever be made for low temperature. The phase diagram for the closely analogous system HfO_2 - Sc_2O_3 , reported by Kalinovskaya et al. (1969), is probably another example of a rather extreme case of observational equilibrium.

These two systems, ZrO_2 - Sc_2O_3 and HfO_2 - Sc_2O_3 , are only a fraction of the many in which fluorite-related phases occur, but their importance lies in the fact that the intermediate phases β , γ , and δ possess disordered cation sub-lattices. (This is certainly true for γ and δ in the ZrO_2 - Sc_2O_3 system (Thornber et al., 1968), and is likely to be a general property of these systems.) Had this not been so, the probability of the existence of transformable nuclei would have been much less because of the additional requirement that the cation configuration be right, and the internal inconsistencies in both Summerville's and Spiridonov's results, from which these ideas developed, might not have been so obvious.

These same concepts may well apply to the much-studied CeO_2 - Y_2O_3 system and its analogues, even though no intermediate phases seem to exist. An account of this work has already been given. Indeed, assuming that coherently intergrown microdomains of C-type structure within the fluorite-type phase do occur (a proposal which has already been advanced to account for the appearance of diffuse C-type superstructure reflections in the diffraction patterns), their very existence implies compositional heterogeneities. However, it is clear that further work needs to be carried out in order to resolve the issues raised.

Finally, it is worth commenting on the absence of intermediate phases in most ternary systems of this type. A clear consequence of the large gap between the characteristic temperatures of the cation and anion sub-lattices in fluorite-type phases is the unattainability of low-temperature equilibrium. Thus all extant phase diagrams in this area are merely statements concerning observational equilibrium: only at the highest temperatures, achieved mainly in the French work, can these diagrams be considered to show the true equilibrium phase relationships. What, then, is the status of intermediate phases in those systems where they have not as yet been found? Are they incapable of existence, or have they just not been prepared because kinetic barriers to their formation exist in the methods tried so far? Answers to these questions are not unimportant since it is common practice (*vide* the interlanthanide perovskite phases discussed in 2.2) to develop crystallochemical generalizations relating, say, differences in cationic radii to the occurrence of particular structure types. Perhaps the best indicator comes from the phase studies on the binary systems CeO_x , PrO_x , and TbO_x , where there is little kinetic hindrance to the attainment of true thermodynamic equilibrium. This work is discussed in detail in ch. 27. Allied to the results of Kordis and Eyring (1968a, 1968b), on $\text{CeO}_x\text{-TbO}_x$ and $\text{PrO}_x\text{-TbO}_x$, which have already been outlined in this chapter, the picture is fairly clear. The most stable phase of the binary systems is $\text{R}_3^{4+}\text{R}_4^{3+}\text{O}_{12}$, yet this still decomposes in the vicinity of 1000°C to give fluorite- and C-type solid solutions. This temperature is well below that for significant mobility of the fluorite-type cation sub-lattice. $\text{Ce}_3^{4+}\text{Ce}_4^{3+}\text{O}_{12}$ exists as an ordered phase, and by analogy the formation of such isostructural compounds as $\text{Ce}_3^{4+}\text{La}_4^{3+}\text{O}_{12}$ and $\text{Ce}_3^{4+}\text{Nd}_4^{3+}\text{O}_{12}$ would certainly be expected since $r(\text{La}^{3+})$, $r(\text{Ce}^{3+})$, and $r(\text{Nd}^{3+})$ are all very similar. However, these have never been formed by solid state reaction for the simple reason that at temperatures where they would be stable there is too high a kinetic barrier to the ordering of the cation sub-lattice required for this structure (Von Dreele, ^{et al.} 1975; Rossell, 1976). The same explanation for the non-appearance of ternary phases in the systems $\text{CeO}_2\text{-La}_2\text{O}_3$ and $\text{CeO}_2\text{-Nd}_2\text{O}_3$ analogous to the members $n = 9, 10, 11$, and 12 of the binary series $\text{R}_n\text{O}_{2n-2}$ applies *a fortiori* since these phases in the binary systems are even less stable than R_7O_{12} . Conversely, if such ternary phases analogous to the $\text{R}_n\text{O}_{2n-2}$ binary compounds could be made by some low-temperature method, once prepared they could be retained, albeit metastably, to quite high temperatures.

The ternary system $\text{CeO}_2\text{-Y}_2\text{O}_3$, on the other hand, is analogous to the systems $\text{ZrO}_2\text{-Sc}_2\text{O}_3$ and $\text{HfO}_2\text{-Sc}_2\text{O}_3$ in the sense that the cation radii of Ce^{4+} and Y^{3+} are almost identical, yet no intermediate phases have been observed. Those which do occur in the last-named systems have their cation sub-lattices disordered (Thorner et al., 1968; Rossell, 1976), and form so readily just because of this. It follows, then, that the non-appearance of these phases in the $\text{CeO}_2\text{-Y}_2\text{O}_3$ system probably derives from the fact that they can not exist rather than that they cannot form. This must be due to the considerably larger ionic radii of Ce^{4+} and Y^{3+} compared with those of $\text{Zr}^{4+}(\text{Hf}^{4+})$ and Sc^{3+} .

3.2.4. *The systems $\text{MO}_2\text{-R}_2\text{O}_3$ ($M = \text{Ti, Sn}$).*

As the formal cation radii of the tetravalent elements become smaller the structure of the dioxides is no longer fluorite-type or fluorite-related. Thus TiO_2 and SnO_2 have the rutile structure in which octahedral coordination of oxygen about the metal has become firmly established. As might be expected then, the phase relationships involving R_2O_3 oxides and dioxides with the rutile structure are somewhat different from those already discussed: in the main intermediate line phases are found, and these are considered in more detail later in terms of structure. The first detailed phase study was carried out by MacChesney and Sauer (1962) on the system $\text{TiO}_2\text{-La}_2\text{O}_3$. Three intermediate compounds were found, namely La_2TiO_5 , the pyrochlore-type $\text{La}_2\text{Ti}_2\text{O}_7$, and $\text{La}_4\text{Ti}_9\text{O}_{24}$. Subsequently, Queyroux (1963) reported a tentative phase diagram for the system $\text{TiO}_2\text{-Gd}_2\text{O}_3$ in which not only the Gd_2TiO_5 phase and the pyrochlore-type phase were prominent but also a high-temperature fluorite-type solid solution. The same system was studied in more detail by Waring and Schneider (1965), whose phase diagram is shown in fig. 28.21. There is general agreement between

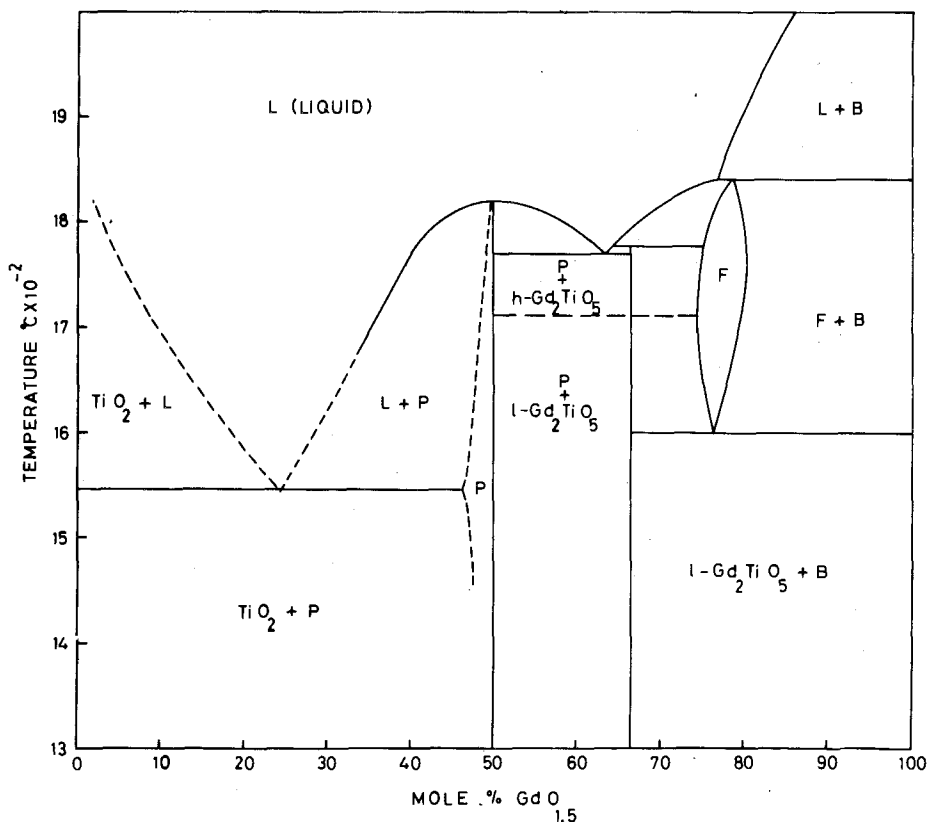


Fig. 28.21. Phase diagram for the system $\text{TiO}_2\text{-Gd}_2\text{O}_3$: after Waring and Schneider (1965).

the results of Queyroux (1963) and those of Waring and Schneider (1965), but the latter authors have shown that the pyrochlore-type phase melts congruently at 1820°C and possesses some homogeneity range, while the other intermediate phase, Gd_2TiO_5 , melts incongruently at 1775°C and exists in both high- and low-temperature forms. The fluorite-type solid solution is limited to the quite narrow composition range between approximately 74 and 81 mole % $GdO_{1.5}$, and to the temperature range 1600–1840°C (see fig. 28.21).

Ault and Welch (1966) reported somewhat different results for the system TiO_2 - Y_2O_3 based on room-temperature X-ray diffraction data from samples quenched from 1500°C. In this work the phase Y_2TiO_5 is not reported, but both the pyrochlore- and fluorite-type phases were found, the former extending from 45 to 59 mole % $YO_{1.5}$ and the latter from 63 to 76 mole % $YO_{1.5}$. These authors comment on the rather unexpected appearance of the fluorite-type phase: within the range of its existence the ratio of the average cation radius to the anion radius is always less than the value 0.73, taken empirically as the lower limit for the stability of this structure. Subsequently, Mumme and Wadsley (1968) prepared the compound Y_2TiO_5 and solved its structure, proving thereby that it is not fluorite-related, as originally supposed, but more akin to the B-type rare earth oxides. The structure is discussed in more detail later.

Other R_2TiO_5 ($R = Sm, Eu$) phases have been prepared by Waring and Schneider (1965), and Queyroux (1964) has found Dy_2TiO_5 . However, this compound does not seem to occur for the smaller rare earth ions.

3.2.5. *Electrical properties of the system MO_2 - R_2O_3*

Although the emphasis in this review is on phase relationships and structure, it would not be complete without some account of the important electrical properties of certain MO_2 - R_2O_3 mixed oxides. About the turn of the century Nernst (1899) discovered that a fluorite-type solid solution of 9 mole % Y_2O_3 in ZrO_2 possessed good ionic conductivity, and in more recent years this and similar types of anionically-conducting solids have been widely used as electrolytes in high-temperature electrochemical cells for such purposes as the determination of the chemical potential of oxygen in non-stoichiometric oxides, the measurement of the oxygen content of molten metals and hot gases, and the generation of electrical power in high-temperature fuel-cells. There is now much published work in this general area, and the electrical properties of the MO_2 - R_2O_3 solid electrolytes have been thoroughly reviewed in a number of places (Etsell and Flengas, 1970; Steele, 1972; Keller, 1976). Thus, apart from considerations of space, the existence of these excellent reviews makes anything more than a brief survey here quite redundant. Moreover, there are other review articles cited below which further discuss the properties of these solid electrolytes in the context of more specific electrochemical applications, such as high-temperature fuel cells (Goto and Pluschkell, 1972; Worrell and Hladik, 1972; Hladik, 1972; Takahashi, 1972; Steele, 1976).

The four most commonly used solid electrolyte systems coming within the

scope of this chapter are $\text{ZrO}_2\text{-Y}_2\text{O}_3$, $\text{HfO}_2\text{-Y}_2\text{O}_3$, $\text{CeO}_2\text{-Y}_2\text{O}_3$, and $\text{ThO}_2\text{-Y}_2\text{O}_3$; $\text{ZrO}_2\text{-CaO}$ (calcia-stabilized-zirconia) electrolytes are also widely used. Fig. 28.22 shows the general features, now firmly established, of the ionic conductivity of these fluorite-type solids: it also includes data for the system $\text{ZrO}_2\text{-Sc}_2\text{O}_3$, which has the highest conductivity of all, but general use of this electrolyte is precluded because of the high cost of Sc_2O_3 and the readiness with which the ordered intermediate phases occur at lower temperatures. Indeed, "ageing" phenomena related to ordering processes occur to a greater or lesser degree in all systems, and lead to a lowering of the conductivity, but these processes are slow enough in the commonly used electrolytes not to affect their

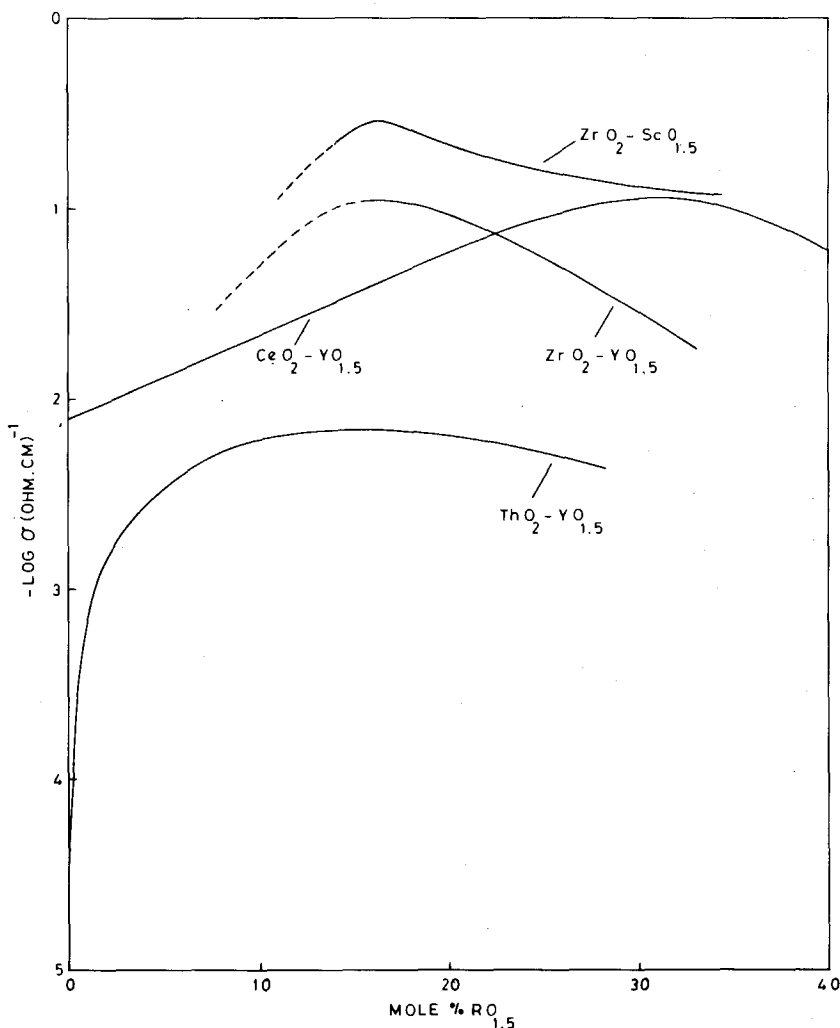


Fig. 28.22. Ionic conductivities of several solid electrolytes at 1000°C as a function of composition.

performance significantly over long terms. All these systems exhibit a maximum in the conductivity *vs* composition isotherms, which, for the zirconia and hafnia systems, occurs near to the zirconia- or hafnia-rich boundary of the fluorite-type phase. In the ceria and thoria systems the conductivity of the pure dioxide is significantly enhanced by the addition of Y_2O_3 , and this increase in conductivity

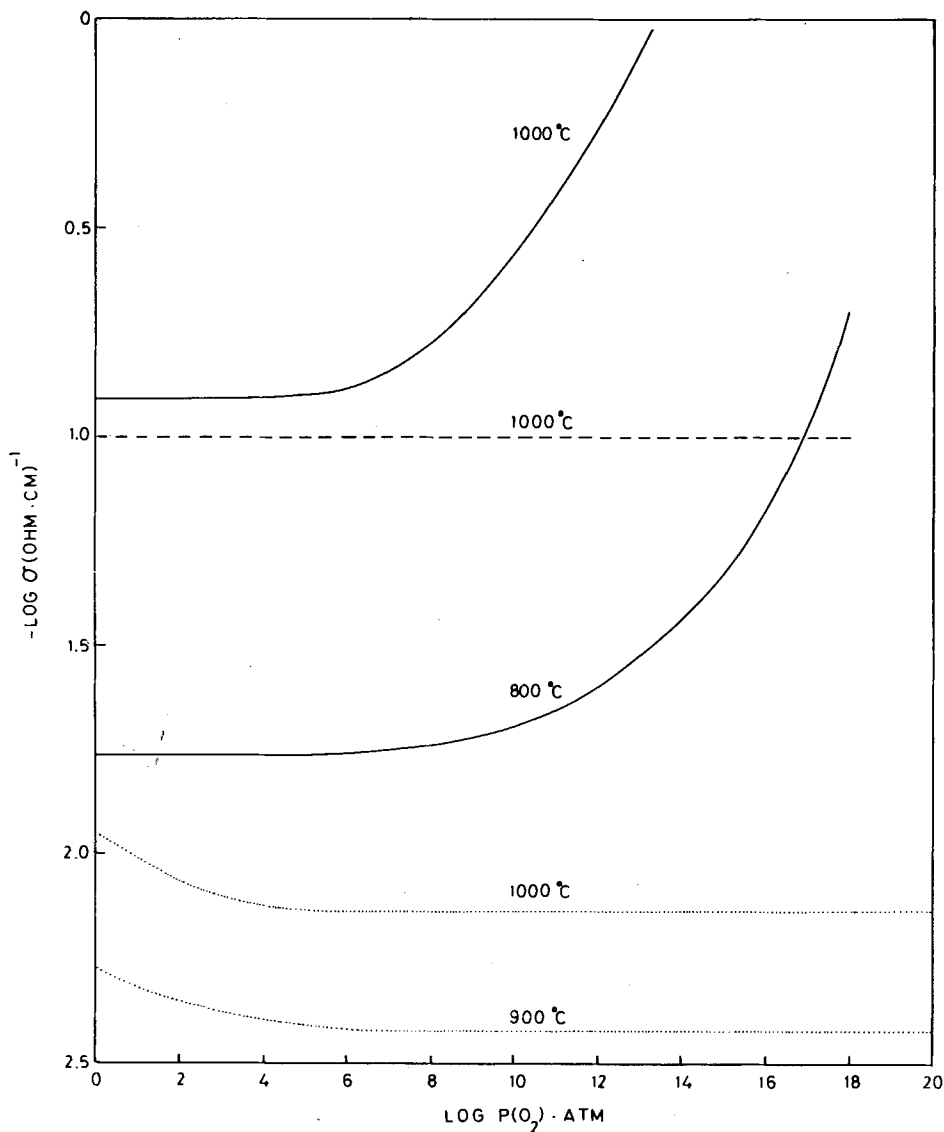


Fig. 28.23. Total conductivity as a function of oxygen pressure for three common solid electrolytes. Full lines: CeO_2 (9.5 mole % $YO_{1.5}$); Tuller and Nowich (1975). Dashed line: ZrO_2 (18.2 mole % $YO_{1.5}$); Etsell and Flenglas (1970). Dotted lines: ThO_2 (15 mole % $YO_{1.5}$); Lasker and Rapp (1966).

is closely related to the increase in the number of defects thus created in the anion sub-lattice, but with further increase in the number of anion defects resulting from further addition of Y_2O_3 , defect interactions assume a significant role, leading to a decrease in the conductivity.

It is tacitly assumed that "conductivity" in the foregoing discussion refers to anionic conductivity, and insofar as the total conductivity measured is ionic conductivity, this assumption is justified on the basis of the well-known and much-invoked transport properties of fluorite-type solids: anion diffusion coefficients in these oxides are at least five to six orders of magnitude greater than cation diffusion coefficients at $1000^\circ C$. However, any significant electronic contribution to the total conductivity would seriously limit the usefulness of these materials as electrolytes, and it is therefore important to know under what conditions this may arise. The theory of *p*- and *n*-type semiconduction in oxide materials is well documented and need not be reiterated here: as it applies to this problem it is discussed briefly in several of the reviews already cited. What emerges is that any significant electronic component of the total conductivity should reveal itself in an observable dependence of the measured conductivity on oxygen pressure, whereas pure ionic conductivity is independent of this. Fig. 28.23 shows data for various electrolyte materials, and it is clear that $ThO_2-Y_2O_3$ electrolytes become *p*-type semiconductors at higher oxygen pressures while $CeO_2-Y_2O_3$ electrolytes rapidly become *n*-type semiconductors with decreasing oxygen pressure. $ZrO_2-Y_2O_3$ electrolytes would seem to be pure ionic conductors over a wide oxygen-pressure range, but there is evidence (Friedman et al., 1973) that significant *n*-type conductivity is developed in certain commercial stabilized-zirconia products at $1000^\circ C$ if the oxygen pressure is below 10^{-17} atm. Steele and Dudley (1975) have commented on the important role which complex microstructural features, such as those discussed in 3.2.3. above, might play in determining the transport properties of such electrolytes, and it is not surprising that general agreement has not been reached on what constitutes the so-called "electrolyte domain" of these materials. Nevertheless, there is no doubt that $CeO_2-Y_2O_3$ electrolytes are only useful at relatively high oxygen pressures, whereas at very low oxygen pressures $ThO_2-Y_2O_3$ solid solutions are preferable.

4. Mixed oxides of uranium and the rare earths

4.1. *The systems* $UO_{2+x}-R_2O_3$ ($R = Ln, Y, Sc$)

In expanding the discussion to true ternary systems of the general type $U + R + O_2$ a much more complex situation is encountered, but one which is nonetheless of great significance not only from the point of view of basic solid state chemistry but also in the applied area of nuclear technology, where the interactions of fission-product rare earth oxides with the urania fuel itself can have important consequences.

Early studies by Hund et al. (1952a, 1952b, 1952c, 1952d, 1955) on the mixed

oxides U_3O_8 - R_2O_3 had shown that at temperatures up to 1200°C a grossly non-stoichiometric fluorite-type phase occurred, separated on either side from the end-members by diphasic regions. In this work no determination of the mean uranium valency, and hence of the overall O:(R + U) ratio, was made, so the data are incomplete. The first thorough study of such a system was carried out by Bartram et al. (1964) for the case UO_3 - UO_2 - Y_2O_3 . From the results of this work a complete ternary phase diagram (except for the UO_3 corner) was constructed for two temperature regions, 1000 - 1700°C and $<1000^\circ\text{C}$. Specimens of varying U:Y ratio were separately heated in air, in a ten to one $CO_2 + CO$ mixture, and in hydrogen to appropriate temperatures, then quenched and subsequently analysed to determine the $U^{4+}:U^{6+}$ ratio. In summary, the results show the existence of four phases between 1000°C and 1700°C : β - U_3O_8 , a grossly non-stoichiometric fluorite-type phase, a fluorite-related rhombohedral phase (designated RI), and a C-type phase.

There seems to be no solubility of Y_2O_3 in β - U_3O_8 , but the fluorite-type phase has a wide range of existence; this is probably temperature dependent and extends on either side of the ideal value (2.00) for the oxygen:metal ratio in the fluorite-type structure. Samples of this phase prepared under strongly reducing conditions are readily oxidized in air at room temperature. The C-type phase-field at high temperatures appears to be quite narrow: in the pseudo-binary system UO_2 - Y_2O_3 the maximum solubility of UO_2 in $YO_{1.5}$ is 7-8 mole %, but there appears to be no solubility of UO_3 in Y_2O_3 . The rhombohedral RI phase was found under all conditions to have a constant O:(Y + U) ratio of 12:7, and is identified with the δ -phase of the MO_2 - R_2O_3 systems (the ι -phase of the binary rare earth oxides, Ch. 27). In this case, however, it does extend over a range of composition with respect to the Y:U ratio, and its composition can be formulated as $U_m Y_{7-m} O_{12}$ ($1 < m < 3.4$): these compositions lie on the line joining the fully-oxidized phase UY_6O_{12} (obtained in air) to the hypothetical phase $U_3Y_4O_{12}$ of the UO_2 - Y_2O_3 system. During low-temperature oxidation of reduced RI compositions a closely related rhombohedral phase (designated RII) was found to occur as an intermediate. Although assumed to be metastable, it too was shown to have variable composition with respect to the Y:U ratio but a constant O:(Y + U) ratio of 15:8. The observed composition range was given as $17UO_{2.67} \cdot 18Y_2O_3$ to $2UO_3 \cdot 3Y_2O_3$.

Subsequent studies on the system UO_{2+x} - R_2O_3 (R = Ho, Er, Tm, Yb, Lu) at an oxygen pressure of one atmosphere have been reported by Keller et al. (1969). These confirm in some measure and extend the findings of Bartram et al. (1964), particularly in respect of the RI and RII phases. In this work, at $RO_{1.5}$ contents in excess of about 70 mole %, the uranium was shown to exist in the fully-oxidized +6 state, but only the RI phase was found. This phase, however, was reported as occurring over a range of composition (72-85.7 mole % $RO_{1.5}$, or $U_2R_5O_{13.5}$ to UR_6O_{12}) which includes the two fixed compositions ($U_2Y_6O_{15}$ and UY_6O_{12} respectively) found by Bartram et al. (1964). The status of RII on this evidence is clearly suspect, but there does seem to be a real discrepancy between the two sets of findings which only further work would resolve.

The most comprehensive study in this area is that of Diehl and Keller (1971) on the system $\text{UO}_3\text{--UO}_2\text{--LaO}_{1.5}$, and the results probably typify, apart from relatively minor details, the general behaviour of all the rare earth oxide/urania systems. In order to achieve both desired O: (La + U) and U:La ratios many specimens were prepared by weighing the required amounts of $\text{LaO}_{1.5}$, UO_2 , and U_3O_8 . After careful mixing these were then sealed under a low argon pressure inside fused-quartz ampoules, reacted at 1250°C for 15 to 20 days, and finally quenched. They were handled subsequently under argon in a glove-box to prevent oxidation. Other coprecipitated specimens were reacted in oxygen ($p(\text{O}_2) = 1 \text{ atm}$) at temperatures between 1000°C and 1550°C . All specimens were analysed to determine the mean valence state of the uranium.

The phase relationships thus determined at 1250°C are shown in fig. 28.24, which reveals again the existence of the $\beta\text{-U}_3\text{O}_8$ containing no dissolved $\text{LaO}_{1.5}$, the fluorite-type phase occupying the greater part of the diagram and extending between the limits $(\text{U, La})\text{O}_{1.60}$ and $(\text{U, La})\text{O}_{0.25}$ on either side of the ideal fluorite

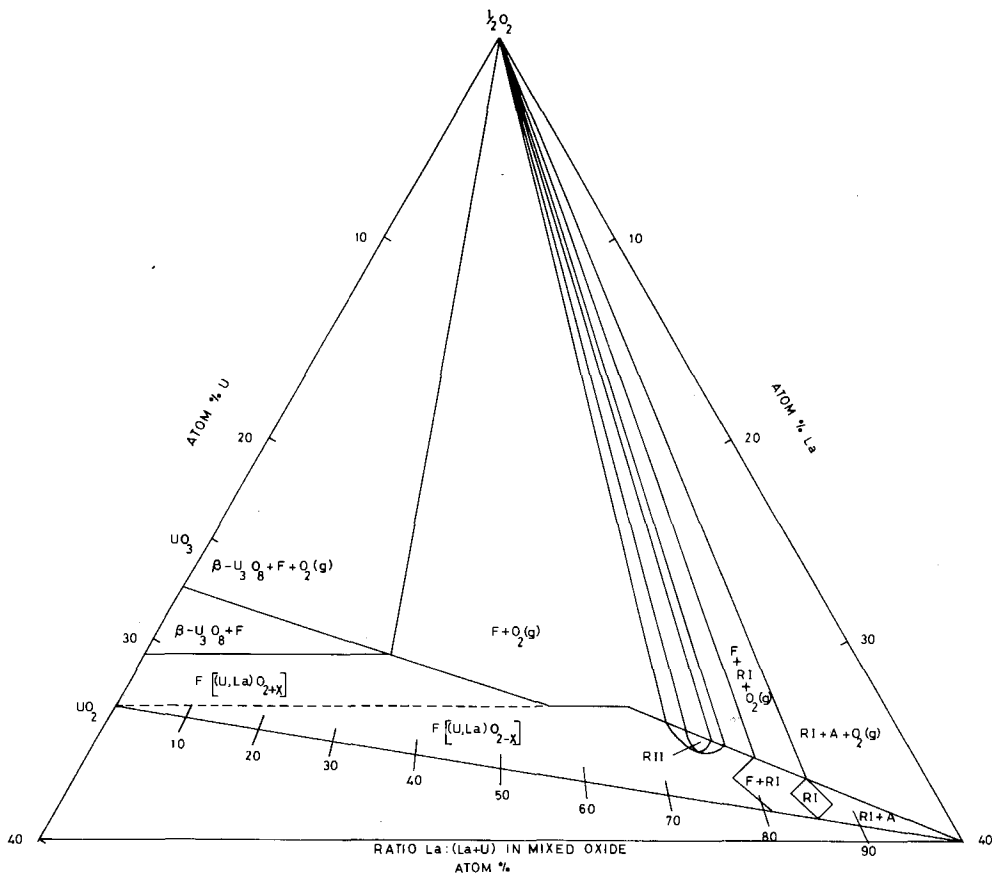


Fig. 28.24. Phase diagram for the system U-La-O at 1250°C : after Diehl and Keller (1971).

stoichiometry, the fluorite-related RI and RII phases, A-type $\text{LaO}_{1.5}$ containing no dissolved UO_{2+x} , and the associated diphasic regions. The RII phase is thus established as a stable entity in the phase diagram. Figure 28.25 shows the phase relationships for $p(\text{O}_2) = 1 \text{ atm}$.

The rhombohedral RI phase is shown in fig. 28.24 as having an extraordinarily wide composition range overall, although in terms of the ratio $\text{La}:(\text{La} + \text{U})$ it occurs only between the limits 83.3 mole $\text{LaO}_{1.5}$ and 87.5 mole % $\text{LaO}_{1.5}$. Diehl and Keller (1971) have represented the phase field as follows:

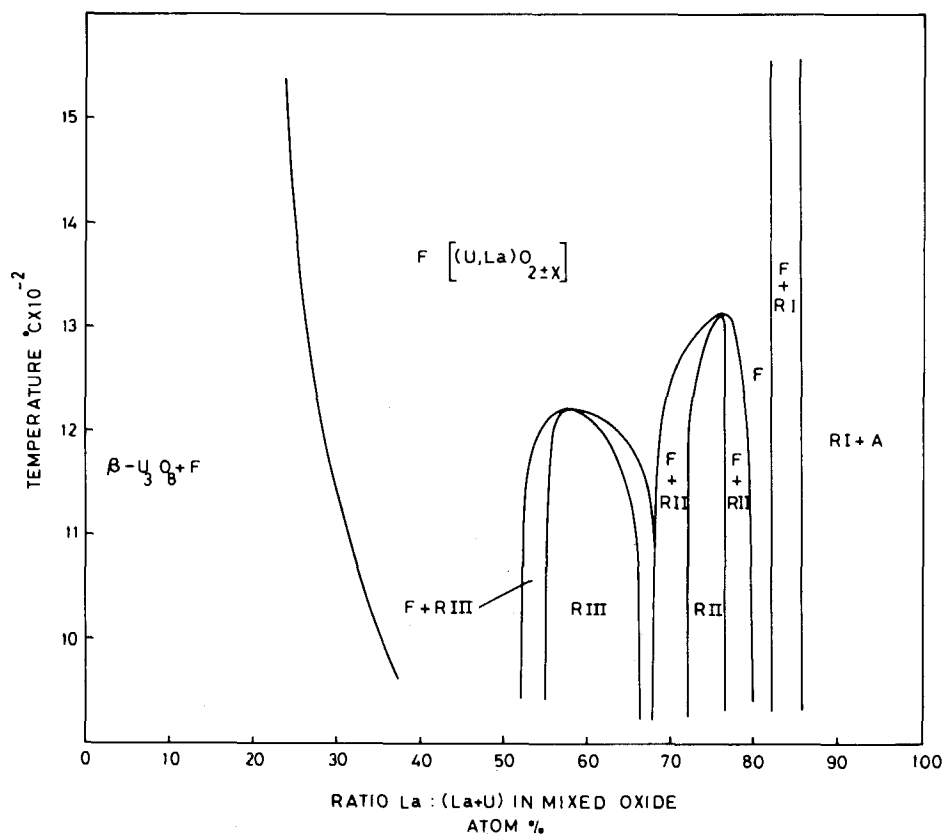
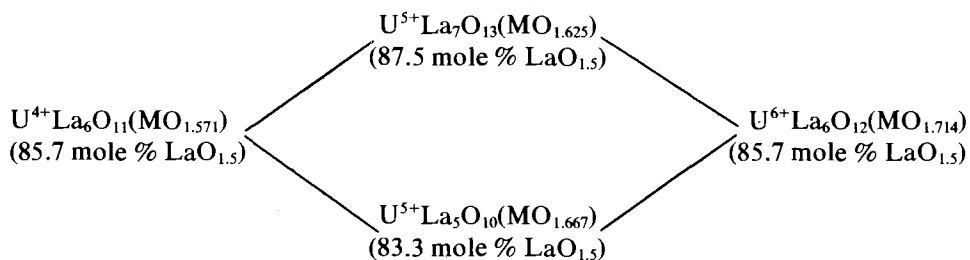


Fig. 28.25. Phase diagram for the system U-La-O at $p(\text{O}_2) = 1 \text{ atm}$: after Diehl and Keller (1971).

It is doubtful whether the indicated stoichiometries have any real significance since it must be remembered that only a single phase exists within these extremities, but the variation in O:(La + U) ratio between 1.714 and 1.571 is very large. Neither should too much emphasis be given to the authors' formal description of solid solution processes: they point out that the mean composition of the two limits with U:La = 1:6, namely $U^{5+}La_6O_{11.5}$, might be thought of as dissolving $UO_{2.5}$ to give $U^{5+}La_5O_{10}$ ($\frac{5}{6}U^{5+}La_6O_{11.5} + \frac{1}{6}UO_{2.5} \rightarrow U^{5+}La_5O_{10}$), or as dissolving $LaO_{1.5}$ to give $U^{5+}La_7O_{13}$. These issues will be raised later in the context of the structure of the RI phase. At $p(O_2) = 1$ atm. RI is fully oxidized (see fig. 28.26) so appears on fig. 28.25 as a line phase in agreement with the representation in fig. 28.24. It is clearly stable to very high temperatures.

The closely related rhombohedral phase RII, however, does have a range of composition at 1250°C, even when fully oxidized, as is shown in fig. 28.24 on the UO_3 - $LaO_{1.5}$ join: it is 73–76.5 mole % $LaO_{1.5}$, corresponding to $1.86 < O:(La + U) < 1.90$. With decreasing uranium valency the width of this phase decreases rapidly, and it ceases to exist at 1250°C at the composition 75 mole % $LaO_{1.5} + 25$ mole % $UO_{2.76}$ ($O:(La + U) = 1.82$), being converted to the fluorite-type phase. At $p(O_2) = 1$ atm. the RII phase, like RI, is fully oxidized (see fig. 28.26), but it is less stable and transforms at $1310 \pm 10^\circ C$ and at the ratio $O:(La + U) = 1.86$ into the fluorite-type phase. The reverse transformation does take place, but is very slow at 1100°C.

A new development in this work is the appearance of yet a third fluorite-related rhombohedral phase designated RIII. This had been reported previously by Russian workers (Koshcheev and Kovba, 1966) who had assigned it the formula $U_3O_8 \cdot 2La_2O_3 (M_7O_{14})$, but Diehl and Keller (1971) discount this: however, the only basis for their rejection of this formula is their indexing of the powder diffraction pattern in terms of an M_8O_{16} rhombohedron.

The phase is shown in fig. 28.25 between the limits 55 mole % $LaO_{1.5}$ and 66.7 mole % $LaO_{1.5}$, but its O:(La + U) ratio is constant at 2.00, which implies a fully-occupied fluorite-type lattice. What makes this possible is the quite rapid decrease in the mean uranium valency at $p(O_2) = 1$ atm., $T = 1000^\circ C$, with decreasing lanthana content below 66.7 mole %, i.e. in the phase-field of RIII, and this is shown in fig. 28.26. The RIII phase transforms into the fluorite-type phase at $1220 \pm 10^\circ C$ at the monotectoid composition of 57.2 mole % $LaO_{1.5}$: the reverse transformation is significantly faster at 1100°C than in the case of the RII phase.

In subsequent work Stadlbauer et al. (1974) have used a high-temperature, solid-state electrochemical cell to study the thermodynamic properties of this system. These will not be discussed here, but it should be recorded that thermodynamic measurements on systems of this kind, in which the equilibrium oxygen pressure is determined as a function of both temperature and O:M ratio ($M = U + R$), have shown that O:M ratios very close to the ideal fluorite stoichiometry (2.00) are retained over a wide range of oxygen pressure (many orders of magnitude), whereas for compositions MO_{2+x} with x greater than about 0.01 quite small changes in oxygen pressure produce significant changes in x . It

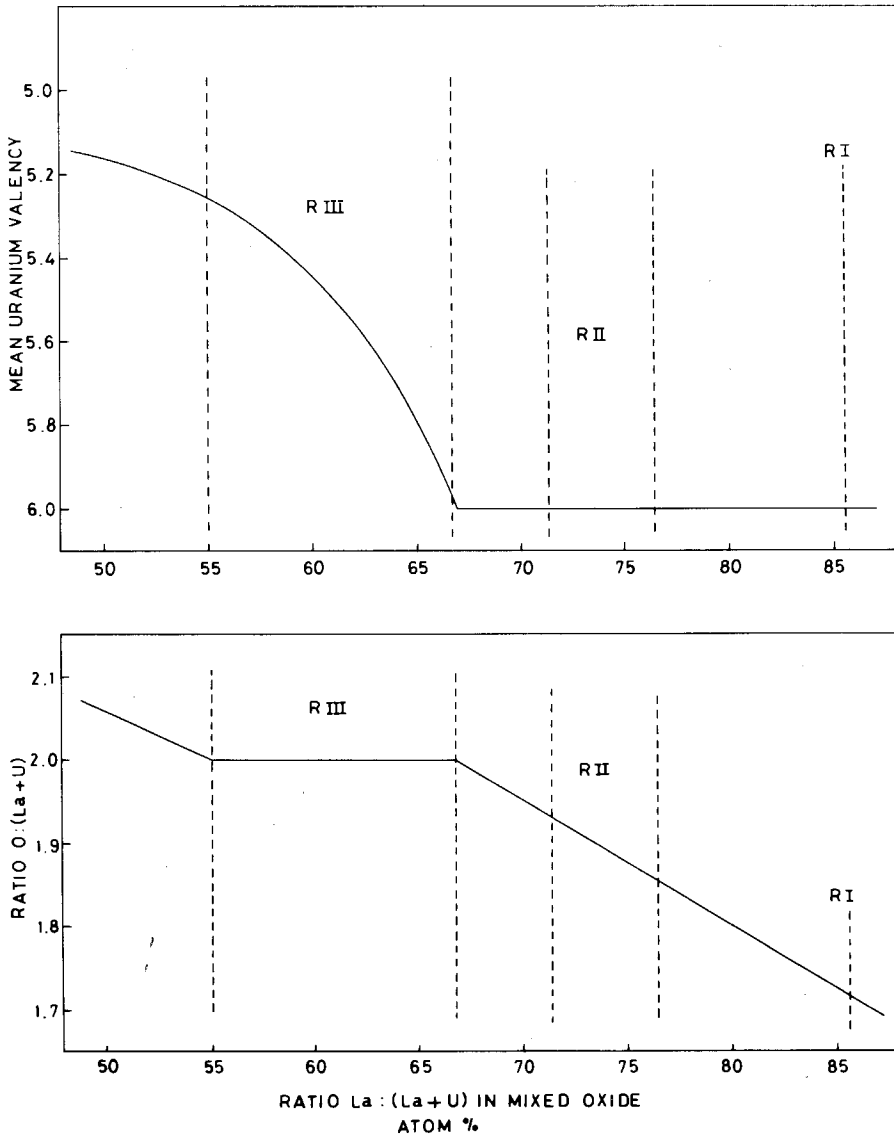


Fig. 28.26. Mean uranium valency (top) and oxygen: total metal ratio (bottom) plotted as a function of lanthanum: total metal ratio for the system U-La-O at 1000°C: $p(\text{O}_2) = 1 \text{ atm}$: after Diehl and Keller (1971).

is this behaviour which underlies the data shown in fig. 28.26 and thus allows the RIII phase at $p(\text{O}_2) = 1 \text{ atm}$. to exist over such a wide range of La:U ratios while retaining a constant O:(La + U) ratio of 2.0.

The three fluorite-related rhombohedral phases, RI, RII and RIII, occurring in the system $\text{UO}_3\text{-UO}_2\text{-LaO}_{1.5}$, present something of an enigma. RIII has been

reported only for this system, and RII for this and the system $\text{UO}_3\text{-UO}_2\text{-SmO}_{1.5}$ (Koshcheev et al., 1967). Although Bartram et al. (1964) described the occurrence of RII, with a fixed $\text{O}:(\text{Y} + \text{U})$ ratio of 15:8 but variable $\text{Y}:(\text{Y} + \text{U})$ ratios, as a metastable intermediate in the oxidation of RI in the system $\text{UO}_3\text{-UO}_2\text{-YO}_{1.5}$, Keller et al. (1969) did not find it in analogous heavy rare earth oxide systems: instead they reported a range of composition for RI, both with respect to the $\text{R}:(\text{R} + \text{U})$ ratio and the $\text{O}:(\text{R} + \text{U})$ ratio, which included that of RII. Bartram et al. (1964), however, found no composition range with respect to the $\text{O}:(\text{Y} + \text{U})$ ratio for their RI phase. For the system involving $\text{LaO}_{1.5}$ Diehl and Keller (1971) described the RI phase as having compositional width with respect to both possible variables (see 28.24), yet Keller and Boroujerdi (1972), in their study of the system $\text{UO}_3\text{-UO}_2\text{-NdO}_{1.5}$, found an RI phase with a fixed $\text{Nd}:(\text{Nd} + \text{U})$ ratio of 6:1 but a variable $\text{O}:(\text{Nd} + \text{U})$ ratio ($\frac{11}{7} \leq \text{O}:(\text{Nd} + \text{U}) \leq \frac{12}{7}$). The RII phase reported for the $\text{SmO}_{1.5}$ system below 1100°C by Koshcheev et al. (1967) ranged in composition from a $\text{UO}_3:\text{SmO}_{1.5}$ ratio of 1:1.15 to 1:3.5, which corresponds to the range 60–77.8 mole % $\text{SmO}_{1.5}$ ($\text{Sm}:(\text{Sm} + \text{U})$) and $1.833 \leq \text{O}:(\text{Sm} + \text{U}) \leq 2.10$. This overlaps the RIII range, so there is evidence here for the existence of both RII and RIII, although only a single phase was reported on the basis of X-ray evidence. For the system involving $\text{EuO}_{1.5}$ Berndt et al. (1974) have described an RI phase which extends over the whole region of the reported RI, RII, and RIII phases in so far as the $\text{Eu}:(\text{Eu} + \text{U})$ ratios are concerned (60–85.7 mole % $\text{EuO}_{1.5}$), although the range of the $\text{O}:(\text{Eu} + \text{U})$ ratio is only 1.64–1.71. Later work involving $\text{HoO}_{1.5}$ (Wichmann, 1977) gives the full extent of the RI phase for this system as triangular in the ternary phase diagram for 1250°C , with one edge on the $\text{UO}_3\text{-HoO}_{1.5}$ join (fully-oxidized uranium) and between the compositions 78 mole % $\text{HoO}_{1.5}$ and 87.5 mole % $\text{HoO}_{1.5}$ (earlier data for $p(\text{O}_2) = 1$ atm. gave this range as 72–85.7 mole % $\text{HoO}_{1.5}$), while the third apex of the triangle occurs on the $\text{UO}_2\text{-HoO}_{1.5}$ join (fully-reduced uranium) at 75 mole % $\text{HoO}_{1.5}$.

Here is yet another and quite dramatic example of inconsistencies between various data sets, each of which must therefore be thought of as representing only observational equilibrium. Again the explanation of these differences is probably to be sought in the cation distribution achieved during reaction. What follows is a highly speculative attempt to rationalize in structural terms the reported observations.

The structure of the rhombohedral phase RI (UR_6O_{12}) is well known and is described later. The important feature here is the complete ordering of the highly-charged U^{6+} ions into a special site (0, 0, 0) of the $R\bar{3}$ space group, and indeed this same ordering of the smaller, more highly-charged cation occurs for all isotypic phases with the exception of $\text{Zr}_3\text{Sc}_4\text{O}_{12}$ (see 5.6.1 below). Moreover, the great stability of the UR_6O_{12} phases, already noted, implies a strong tendency for this ordering to be achieved, which will enhance the rate of cation diffusion processes during reaction since these must be thought of as chemical—rather than self-diffusion. Once cation ordering is achieved, the anion sub-lattice, particularly at lower temperatures, is strongly constrained, and the RI phase

results. However, even at compositions well away from UY_6O_{12} , as in RII, RIII, and some RI phases, there will be the same tendency, though less strong perhaps, for this preferred cation ordering to be established, especially if UR_6O_{12} forms initially as an intermediate in the reaction. The final product may then be constrained to adopt what might be termed a "stuffed" or "depleted" RI structure. To some extent this hypothesis has been borne out by structure determinations (Bartram, 1966) on $U_2Y_5O_{12}$ and $U_2Y_5O_{13.3}$, where the observed intensity data are in good accord with this model. The argument should not be pursued further here since so much speculation is involved, but it is worth noting that the observed monotectoid decompositions of both RII and RIII in the $UO_3-UO_2-LaO_{1.5}$ system at temperatures of 1310°C and 1220°C respectively would be interpreted in this context as the breakdown of a particular kind of partial cation order, which is less stable the further the sample composition is from ULa_6O_{12} . The reestablishment of this order on cooling below the transition temperature depends now essentially on cation self-diffusion, and the slow rates observed are understandable.

Finally, this speculation raises the possibility that the H_2 - and H_3 - phases reported for some of the $ZrO_2-R_2O_3$ and $HfO_2-R_2O_3$ systems (see 3.2.3) are examples of a "depleted" M_7O_{12} structure, but further clarification of this issue is required.

4.2. *The system $UO_{2+x}-CeO_{2-x}$*

In this system the situation is still further complicated by the fact that both cations have variable valency. This is not the place to give a detailed description of the data obtained by Markin et al. (1970) on the phase relationships, and by Markin and Crouch (1970) on the thermodynamic properties, but the results of this work further emphasize a major point of the earlier discussion on equilibria involving fluorite-type phases, namely that in ternary systems equilibrium is virtually unattainable at low temperature by conventional means. For this reason a brief discussion is included.

In the phase studies of Markin et al. (1970) samples of various U:Ce ratios were prepared at high temperature (1600°C) in vacuum, quenched, and then brought to the stoichiometric composition $O:(U+Ce) = 2.00$ at 850°C in a 1:1 mixture of CO_2 and CO, which, according to the data of Hoch and Furman (1965), is an appropriate ratio for this temperature. (The large variation in the equilibrium oxygen pressures between the compositions $MO_{1.99}$ and $MO_{2.01}$, mentioned in 4.1 above, is here used to good effect.) Subsequent treatment of these samples, either reduction or oxidation, was then carried out mainly at low temperature (850°C), and was such as to produce only the mixed valence states U^{6+} , U^{5+} , U^{4+} , Ce^{4+} , Ce^{3+} : in no case were the reducing conditions severe enough to produce U^{3+} . As in the case of the systems CeO_x-TbO_x and PrO_x-TbO_x , there was no evidence for any stabilization in the mixed oxides of abnormal valence states, and thus formation of the ordered intermediate phases known to occur in the simple binary systems (e.g. U_4O_9 , Ce_nO_{2n-2} : $n = 7, 9, 10, 11$.) was not, in fact,

observed. Although these authors claim that their results "show conclusively that intermediate phases occur at room temperature when (U, Ce) oxides are reduced . . .", these reported phases are cubic and do not conform in composition to any of the known Ce_nO_{2n-2} compounds. Moreover, although they report the existence of an " M_4O_9 -type" phase in oxidized samples, no superstructure lines were observed. Once again the reported phase relationships refer to observational states in which the mobile anion sub-lattice has adjusted itself to whatever high-temperature cation distribution was achieved in the initial sample preparation. Indeed, Markin and Crouch (1970), in their thermodynamic study of this system, tacitly recognize this in explaining the big differences between the thermodynamic behaviour of the systems $(U, Pu)O_{2+x}$ and $(U, Ce)O_{2+x}$ on the one hand and the simple binary systems on the other. In the latter class there is a large change in the function $\Delta\bar{H}(O_2)$ and $\Delta\bar{S}(O_2)$ as, for example, the Pu valency changes from 3.1 to 3.99, which is explained as due to kinetically unhindered local ordering involving both cations and anions. The much smaller change in these properties for the mixed-oxide systems in the same composition range is attributed to the absence of such local ordering, which could only come about in these systems if the mixed cations were sufficiently mobile, and they are not.

5. Structures and structural relationships

5.1. NaCl-related structures

The so-called α -form of the compounds Na_2RO_3 ($R = Ce^{4+}, Pr^{4+}, Tb^{4+}$) and K_2RO_3 all crystallize in the NaCl-type structure with the two cationic species statistically distributed over the sites of the cation sub-lattice (Hoppe and Lidecke, 1962; Zintl and Morawietz, 1940).

Other compounds of the rare earth and alkali-metal oxides have the stoichiometry ARO_2 and usually form superstructures of the NaCl-type with an ordered arrangement of cations. The basic structure-types reported are:

(i) α - $NaFeO_2$. The unit cell of this structure is rhombohedral. The space group is $R\bar{3}m$ with a (hex) = 3.66 Å, and c (hex) = 18.66 Å for $KCeO_2$ (Clos et al., 1970). Atom positions within the triply-primitive hexagonal unit cell are: M^+ in $3a$ (0, 0, 0); R^{3+} in $3b$ (0, 0, $\frac{1}{2}$); O^{2-} in $6c$ (0, 0, 0.23). The coordinates for the O^{2-} ions in the equivalent hexagonal setting of the ideal NaCl-type structure would be 0, 0, $\frac{1}{4}$. As in NaCl the structure consists of a cubic-close-packed anion array with cations occupying all the octahedral holes, but in this case the one set of cubic {111} planes which has become the unique (001)_{hex} set is composed of alternate planes of K^+ and R^{3+} ions. Structure refinements have been carried out for $KLaO_2$, $KErO_2$ (Clos et al., 1967), $RbHoO_2$ (Seeger and Hoppe, 1969), and $KPrO_2$ (Clos et al., 1970). Compounds crystallizing with this structure are summarized below:

KRO_2 : $R = La$ through Yb (Clos et al., 1967)

$NaRO_2$: $R = Tm$ through Lu , Sc , Y (Murav'eva et al., 1965; Blasse, 1966)

$RbRO_2$: $R = Dy$ through Lu (Seeger and Hoppe, 1969).

The so-called β -forms of K_2CeO_3 and K_2TbO_3 also have the α - NaFeO_2 structure (Hoppe, 1965; Paletta and Hoppe, 1966; Hoppe and Seeger, 1968) so that their general formula is best written as $\text{K}(\text{K}_{1/3}\text{R}_{2/3}^{4+})\text{O}_2$. Here two R^{4+} ions and one K^+ ion have replaced three R^{3+} ions, but since these are randomly distributed, the α - NaFeO_2 structure can be retained. A complete range of solid solution exists between KPrO_2 and K_2PrO_3 (Clos et al., 1970; Devalette et al., 1971) as this substitution occurs. Similar behaviour would be expected of the cerium and terbium analogues, and Devalette et al. (1971) have further shown that solid solutions are formed between KPrO_2 and $\text{K}(\text{Ca}, \text{Pr})\text{O}_2$ as one Ca^{2+} and one Pr^{4+} ion replace two Pr^{3+} ions. It would be interesting to examine such solid solutions by electron microscopy to see just how random the distribution of Ca^{2+} and Pr^{4+} ions really is since the size discrepancy between them (Shannon and Prewitt, 1969) give the ionic radii for six-fold coordination at 1.00 Å and 0.78 Å respectively) might result in some interesting ordering effects.

A number of mixed oxides involving alkali metals and rare earth elements were earlier reported as having the Na_2SnO_3 structure. However, Wyckoff (1964) expresses serious doubt about this structure, and Hoppe and Lidecke (1962) have referred to it as being isomorphous with α - NaFeO_2 . The use of this structure-type has therefore been avoided.

(ii) α - LiFeO_2 . This unit cell is tetragonal, space group $I4_1/amd$. The parameters for the compound LiYO_2 are $a = 4.44$ Å and $c = 10.35$ Å (Bertaut and Gondrand, 1962). Compounds exhibiting this structure are

NaRO_2 : R = La through Gd (Blasse, 1966)

LiRO_2 : R = Er through Lu, Y (Bertaut and Gondrand, 1962) and Sc (Rooymans, 1961).

Atom positions given for LiScO_2 are: Sc^{3+} in $4a$ (0, 0, 0); Li^+ in $4b$ (0, 0, $\frac{1}{2}$); O^{2-} in $8c$ (0, 0, 0.23). A projection of the structure showing the cation ordering within a close-packed anion layer is shown in fig. 28.27.

Two different unit cells have been reported for other LiRO_2 compounds; both have $P2_1/c$ symmetry. One of these was reported by Bärnighausen (1965) for lanthanides from La through Eu: unit cell parameters given for what Bärnighausen has designated α - LiEuO_2 are $a = 5.68$ Å, $b = 5.99$ Å, $c = 5.62$ Å, $\beta = 103^\circ 10'$. Bertaut and Gondrand (1962) reported a different monoclinic cell for

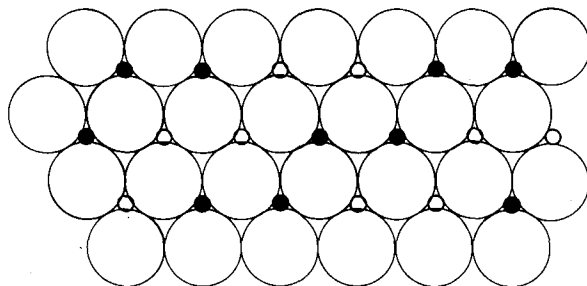


Fig. 28.27. A close packed anion layer of the α - LiFeO_2 -type structure showing the ordered arrangement of the two different cations on the octahedral sites (after Clark, 1972).

the rare earths Y, Dy and Ho. Lattice parameters given for LiDyO_2 are $a = 6.21 \text{ \AA}$, $b = 6.17 \text{ \AA}$, $c = 6.30 \text{ \AA}$, $\beta = 119^\circ 13'$. These two sets of data seem to indicate a genuine difference in structure; they can not be rationalised in terms of a different choice of equivalent unit cells since the unit cell volume of LiDyO_2 is significantly greater than that of LiEuO_2 while $r(\text{Eu}^{3+})$ is greater than $r(\text{Dy}^{3+})$. It might have been expected that all of these LiRO_2 compounds would have been isostructural and that the structure would be a distorted form of $\alpha\text{-LiFeO}_2$ which forms when the radius of the rare earth ion becomes too large. Since both of these unit cells were obtained by indexing X-ray powder patterns it seems possible that one of the unit cells is incorrect and that only one distorted form of $\alpha\text{-LiFeO}_2$ exists.

(iii) $\beta\text{-LiFeO}_2$. Another monoclinic form, this structure is found for compounds of the formula NaRO_2 : R = Dy, Ho, Y and Er (Gondrand et al., 1972). Lattice parameters given for NaDyO_2 are $a = 10.03 \text{ \AA}$, $b = 13.24 \text{ \AA}$, $c = 6.07 \text{ \AA}$, $\beta = 146.83^\circ$: the space group is $C2/c$. Gondrand et al. (1972) and Brunel et al. (1972) have shown that this is a transition structure, intermediate between the $\alpha\text{-LiFeO}_2$ and $\alpha\text{-NaFeO}_2$ structure types. Their description of the three structures is given in terms of the OM_6 cation polyhedra which are of two types depending on the arrangement of R^{3+} and M^+ cations about the anion. The type-1 octahedron has three cations of each type in an equatorial plane of the octahedron while in the type-2 octahedron the three cations of each type occupy opposite

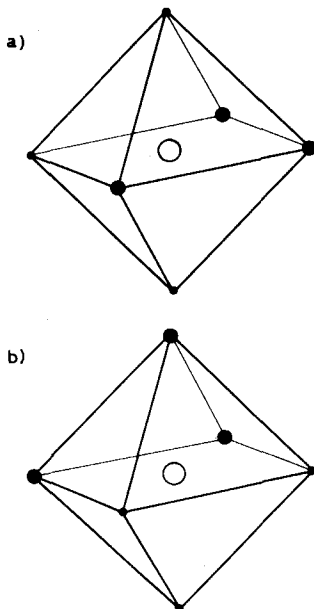


Fig. 28.28. The structural units used to describe the ordered NaCl-type compounds. The OM_6 octahedron in a) is designated as type 1, that in b) as type 2. Small circles represent R^{3+} ions, large circles M^+ ions.

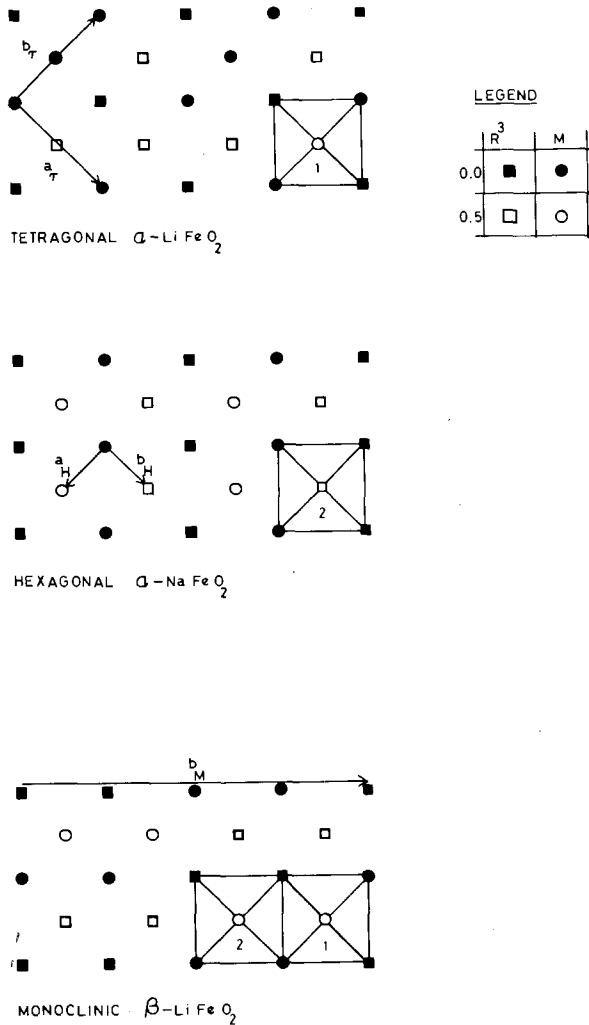


Fig. 28.29. The arrangement of type-1 and type-2 octahedra in α -LiFeO₂, α -NaFeO₂ and β -LiFeO₂. Only cation positions are shown in projection; anions would occupy the same projected positions alternating with the cations.

octahedral faces, as shown in fig. 28.28. α -LiFeO₂ contains only type-1 octahedra, α -NaFeO₂ contains only type-2 octahedra, while β -LiFeO₂ contains both types in the ratio 1:1. Figure 28.29 shows these three situations for a single layer of edge-shared octahedra (two cation layers) projected along [001] of the NaCl-type cell, and illustrates the different types of cation ordering within such layers. In each structure the translation c_{NaCl} leads to a switch of cation types in the positions thus generated for adjacent layers i.e. along [001]_{NaCl} the cation strings contain alternating R³⁺ and M⁺ ions.

(iv) NaHF_2 . The significance of this structure-type in rare earth oxide systems is difficult to assess as some of the published data are insufficiently detailed. The structure has been described by Haas and Kordes (1969), who point out that this structure and that of $\alpha\text{-NaFeO}_2$ both belong to the same space group and that the same point positions are occupied in both structures. The only difference is in the x parameter of the anion array, which results in different modes of anion packing: in the $\alpha\text{-NaFeO}_2$ structure this x parameter lies between $\frac{1}{6}$ and $\frac{1}{3}$ and the anion packing sequence is $-\text{A}-\text{B}-\text{C}-\text{A}-$ (c.c.p.) while in NaHF_2 it lies between 0 and $\frac{1}{6}$ and the corresponding sequence is $-\text{A}-\text{A}-\text{B}-\text{B}-\text{C}-\text{C}-\text{A}-\text{A}-$. It is therefore impossible to decide between these structure types unless a full structure determination is made. Atom positions found for the hexagonal cell of CuLaO_2 are: Cu^+ in $3a$ (0, 0, 0); La^{3+} in $3b$ (0, 0, $\frac{1}{2}$); O^{2-} in $6c$ (0, 0, 0.108). The only substantiated case of a mixed rare earth oxide with the NaHF_2 structure is that of CuLaO_2 (Haas and Kordes, 1969). In this structure La^{3+} is coordinated in a distorted octahedron while Cu^+ occurs in a linear $\text{O}-\text{Cu}-\text{O}$ group parallel to the c -axis. Other mixed rare earth oxides for which the NaHF_2 structure has been reported are CuRO_2 : $\text{R} = \text{La}, \text{Pr}, \text{Nd}, \text{Sm}, \text{Eu}$ (Haas and Kordes, 1969). In addition the NaHF_2 structure appears to be identical with the delafossite structure (Dannhauser and Vaughan, 1955) of certain $\text{A}^+\text{B}^{3+}\text{O}_2$ compounds ($\text{A} = \text{Pt}, \text{Pd}, \text{Cu}, \text{Ag}$) so that PtScO_2 (Shannon et al., 1971) also has the NaHF_2 structure. Presumably other oxides of noble metals and rare-earth elements will be found to have this structure.

The existence regions of a number of the M^+RO_2 phases are shown in table 28.3. A similar table, also including MRO_2 phases with hexagonal-close-packed anions, is given by Spitsyn et al. (1969).

5.2. Structures with hexagonal-close-packed anions

A number of LiRO_2 phases ($\text{R} = \text{Sm}, \text{Eu}, \text{Gd}$) were reported by Gondrand and Bertaut (1963) to have diasporite-related structures. The unit cells are orthorhombic, and for $\beta\text{-LiEuO}_2$ (Bärnighausen, 1963) the space group is $Pnam$ with lattice parameters $a = 11.405 \text{ \AA}$, $b = 5.335 \text{ \AA}$, $c = 3.471 \text{ \AA}$. The diasporite ($\alpha\text{-AlOOH}$) structure consists of h.c.p. O^{2-} and OH^- ions with Al^{3+} ions in half the octahedral sites. From both a structural (Clark, 1972) and diffraction point of view diasporite is similar to $\gamma\text{-MnO}_2$ which consists of h.c.p. O^{2-} ions with Mn^{2+} ions in half the octahedral sites, as shown in fig. 28.30. According to the structural model proposed by Gondrand and Bertaut (1963) for LiRO_2 the RO_2^- arrangement is identical to that of $\gamma\text{-MnO}_2$, the vacant octahedral sites being occupied by Li. Alternatively, the $\gamma\text{-MnO}_2$ structure is one of a number of framework structures composed of ribbons of edge-shared double octahedra, which will be discussed in more detail in the next section. In this context the structure of these mixed rare earth oxides can then be described as consisting of an RO_2^- framework (shown in fig. 28.31) of edge-shared double octahedra with Li^+ ions occupying the remaining octahedral sites. A further, formal description of this structure is that of the NiAs structure with ordered cations.

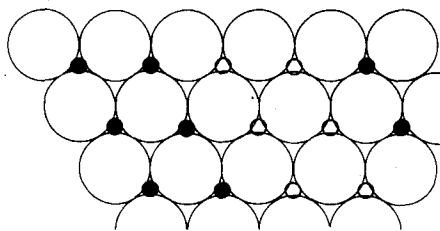


Fig. 28.30. A close-packed anion layer and the associated cations of γ - MnO_2 (after Clark, 1972). Large circles represent anions, filled circles Mn^{3+} ions above the anion plane and small open circles Mn^{4+} ions below the anion plane.

According to Keller (1972) the tetravalent lanthanides form compounds of the type Li_8RO_6 which are isomorphous with Li_8SnO_6 (Trömel and Hauck, 1969). While no parameters are available for the Ce^{4+} , Pr^{4+} or Tb^{4+} compounds, the Sn^{4+} compound is rhombohedral (space group $R\bar{3}$), with a (hex) = 5.464 Å, c (hex) = 15.267 Å; the atom positions are as follows:

Sn^{4+}	in	$3a$	$0, 0, 0$
$\text{Li}^+(1)$		$18f$	$\frac{1}{3}, \frac{1}{3}, 0.11$
$\text{Li}^+(2)$		$6c$	$0, 0, \frac{1}{3}$
O^{2-}		$18f$	$0.31, 0.0, 0.083$

The formula can be written structurally as $(\text{Li})_6(\text{Li}_2\text{Sn})\text{O}_6$. The anions are hexagonal-close-packed with two Li^+ and the Sn^{4+} ions occupying half the octahedral sites in an ordered manner and the remaining six Li^+ ions occupying half the tetrahedral sites.

5.3. Perovskite-related structures

Although perovskite phases as such involving rare earth oxides are dealt with separately in this volume (ch. 29) there are two important series of compounds based on the perovskite structure which occur in mixed rare earth oxide systems and are treated here.

5.3.1. Ruddlesden–Popper phases

The first series consists of phases with the general formula $(\text{M}^{3+}, \text{R}^{3+})_{2n}\text{M}^{2+}\text{O}_{3n+1}$. The structures have been described as consisting of n

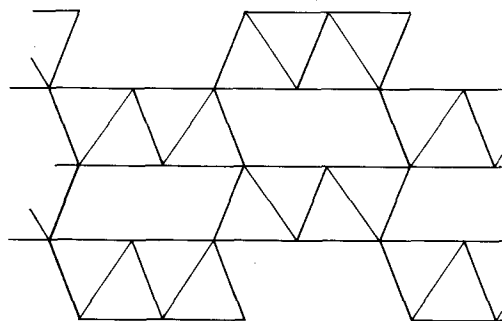


Fig. 28.31. The arrangement of double octahedral ribbons in γ - MnO_2 projected down the two-fold axis of the octahedron. The same arrangement occurs in the diasporite-related LiRO_2 structure with the additional cations occupying the octahedral sites between the ribbons.

layers of perovskite-type structure separated by a layer of stoichiometry MO with NaCl-type structure. In this context a perovskite-type layer is defined as a single layer of corner-shared BO_6 octahedra with one additional A cation per octahedron intercalated as in the ABO_3 perovskite structure. These perovskite-type layers are perpendicular to [001] of the perovskite sub-cell. The structure of the member $n = 1$ is that of K_2NiF_4 , first described by Balz and Plieth (1955) as being tetragonal, space group $I4/mmm$. In rare earth oxide systems it occurs either in the above form (Rabenau and Eckerlin, 1958) or, more often, as an orthorhombically-distorted variant. The orthorhombic cell (space group probably $Fmmm$) is related to the tetragonal cell by

$$\begin{aligned} a &= a_t + b_t \text{ so that } a \approx \sqrt{2} a_t \\ b &= a_t + b_t \quad b \approx \sqrt{2} a_t \\ c &= c_t \quad c \approx c_t \end{aligned}$$

Typical parameters for both types of unit cell are:

La_2NiO_4 $a = 3.855 \text{ \AA}$, $c = 12.652 \text{ \AA}$ (Rabenau and Eckerlin, 1958)

La_2CuO_4 $a = 5.363 \text{ \AA}$, $b = 5.409 \text{ \AA}$, $c = 13.17 \text{ \AA}$ (Longo and Raccah, 1973).

Atom positions are:

La	in	8c	0, 0, 0.3621
Cu		4a	0, 0, 0
O(1)		8i	0, 0, 0.182
O(2)		8i	$\frac{1}{4}, \frac{1}{4}, 0$

The ideal structure (fig. 28.32) consists of single layers of perovskite perpendicular to the c -axis but with successive layers shifted by $\frac{1}{2}a + \frac{1}{2}b + \frac{1}{2}c$ (referred to the sub-cell) which effectively interposes a layer of stoichiometry MO between them. This description of the structure as an intergrowth of perovskite and sodium chloride is most appropriate for K_2NiF_4 itself and would be equally apt for compounds of the type $\text{M}^{2+}\text{O}/\text{M}^{2+}\text{M}^{4+}\text{O}_3$ or $\text{M}^{2+}\text{O}/\text{M}^{3+}\text{O}_3$ (where the first part is the NaCl part and the second the perovskite portion). However, in most such compounds involving the lanthanides the ion in the NaCl layer has a charge of +3, and the octahedral site in the perovskite layer is occupied either by a small divalent cation or by statistically distributed R^{3+} and M^{2+} cations. Thus the rare earth analogues of K_2NiF_4 consist of MO^+/MRO_3 and the charge compensation between the NaCl and perovskite layers is poor. The intergrowth nature of K_2NiF_4 itself is evidenced by its good cleavage parallel to the perovskite layers and by the fact that it melts incongruently forming KF and the perovskite KNiF_3 , whereas some of the oxide compounds are reported to melt congruently. In addition, no member of the series exists with two or more adjacent NaCl-type MO layers. These facts suggest that the relationship between these structures and those of NaCl and perovskite is purely formal, rather than the expression of a structural principle like intergrowth. The structures of the Ruddlesden-Popper phases actually consist simply of layers of perovskite-type structure; the NaCl-type regions result simply from the juxtaposition of adjacent perovskite-type layers.

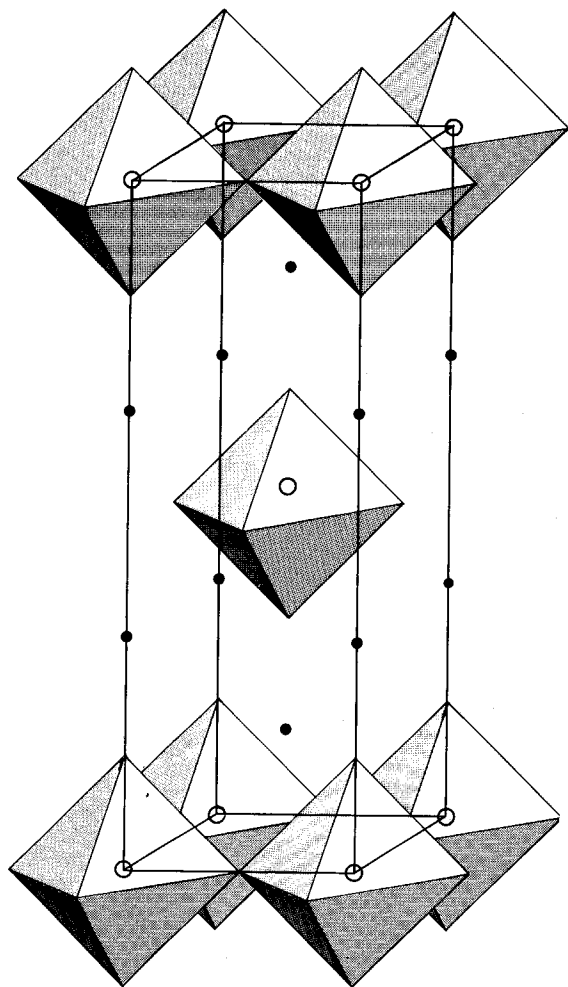


Fig. 28.32. The ideal K_2NiF_4 -type structure of La_2CuO_4 . Filled circles represent La^{3+} ions; open circles Cu^{2+} ions. Anions occur at the apices of the octahedra.

In both the tetragonal and orthorhombic modifications the octahedra around the small B cations are distorted; MO bonds parallel to the c -axis of the tetragonal unit cell may be longer or shorter than those in the ab plane. In the orthorhombically-distorted unit cells the only effect of the distortion is to alter the O-B-O angle in the ab plane from ninety degrees, as shown in fig. 28.33. To emphasise this point a monoclinic cell has sometimes been used to describe the orthorhombic form; this cell uses the axes of the tetragonal unit cell but has $\gamma \neq 90^\circ$. The large A cations of the perovskite layer (which are also the cations of the NaCl layer) have an unusual ninefold coordination. This polyhedron is like a capped, distorted, square antiprism with the cation lying close to the capped face, as shown in fig. 28.34. In perovskite this cation would be twelve-coordinated by the anions in the same sub-lattice.

As shown in table 28.4, the only binary oxides reported to have the K_2NiF_4

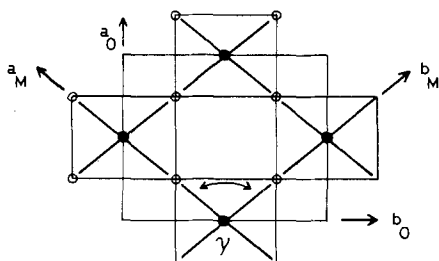


Fig. 28.33. Projection down the c -axis of the orthorhombic form of the K_2NiF_4 -type structure showing the relationship between the orthorhombic and the alternative monoclinic cells of the structure.

structure are those of Co, Ni and Cu with the larger rare earths. In these, the small divalent ions occupy the octahedral sites. Until recently only two of these compounds, La_2NiO_4 and La_2CuO_4 (Rabenau and Eckerlin, 1958; Longo and Racciah, 1973) had been the subject of X-ray structure analysis, and both of these analyses were performed on powder data. Although Longo and Racciah (1973) were able to refine the structure of La_2CuO_4 to the very acceptable R-value of 2.4% they point out that the isotropic temperature factor of one of the anions has the high value of 4 \AA^2 and suggest that the symmetry may be lower than that of $Fmmm$. The situation, however, becomes less clear with the publication by Müller-Buschbaum and Wollschläger (1975) of a single crystal structure determination of Nd_2CuO_4 . This phase has similar unit cell parameters to La_2CuO_4 and belongs to the same space group; however, the structure (fig. 28.35) is different from that of K_2NiF_4 . The anions form a near-cubic array, with Nd^{3+} ions in the eightfold "cubic" sites and the Cu^{2+} ions occupying fourfold sites in the faces of cubes. The structure can be formally derived from K_2NiF_4 by shifting the anion at $0, 0, \frac{1}{6}$ to $0, \frac{1}{2}, \frac{1}{4}$. At the least, it would seem that the publication of this structure analysis throws doubt on the identification of structures of other compounds as being of the K_2NiF_4 -type (since such identification is often based only on lattice parameter measurement and general observation of relative intensities of powder diffraction lines). It seems quite possible that the R_2CuO_4 compounds with $R = Sm$ through Gd are of the Nd_2CuO_4 structure-type. In addition, since it is the above anion (at $0, 0, 0.182$) of

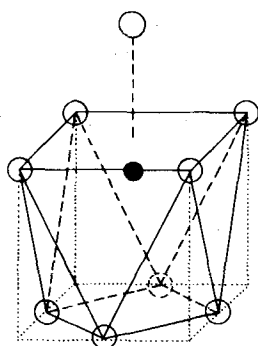


Fig. 28.34. Coordination polyhedron about on La^{3+} ion in the La_2CuO_4 structure. The La^{3+} ion is shown as a filled circle, anions as open circles.

TABLE 28.4
Compounds with the K_2NiF_4 -type structure and associated references

	La	Ce	Pr	Nd	Sm	Eu	Gd	Tb	Dy	Ho	Y	Er
MR_2O_4	Co 2, 8		17	8								
	Ni 2		1, 9	17								
	Cu 1, 9, 18		3	9	9	9	9					
$M^{2+}M^{3+}RO_4$	SrFe 3		3	3	3	3	3	3				
	SrCr 3		3	3	3	3	3	3	3			
	SrAl 15	10, 15	15	10, 15	15	15	15					
	CaAl 4		4	4	4	4	4		4	4	4	4
	CaCr 5		5	5	5	5	5					
	CaGa 6		6	6	6	6	6	6				
	CaMn 7		7	7	7	7	7					
$M^+M^{4+}RO_4$	NaTi 16			16	16		16		16		16	16
	LaSr 11	Co 11	Ni 11	Gd 11	Rh 11	(LiCo) 11	(LiNi) 11	(LiCu) 12				
Others	SrCuLaO ₄ (13), Eu ₂ TiO ₄ (14), SrVLaoO ₄ (1)											

References: 1. Longo and Raccach (1973). 2. Rabenau and Eckerlin (1958). 3. Joubert et al. (1970). 4. Oudalov et al. (1970). 5. Daoudi and Le Flem (1973). 6. Daoudi et al. (1974). 7. Daoudi and Le Flem (1972). 8. Ganguly and Rao (1973). 9. George et al. (1974). 10. Pausch and Müller-Buschbaum (1972). 11. Blasse (1965). 12. Demazeau et al. (1972). 13. Goodenough et al. (1973). 14. Greedan and McCarthy (1972). 15. Fava et al. (1972). 16. Blasse (1968). 17. Willer and Daire (1968). 18. Lehuède and Daire (1973).

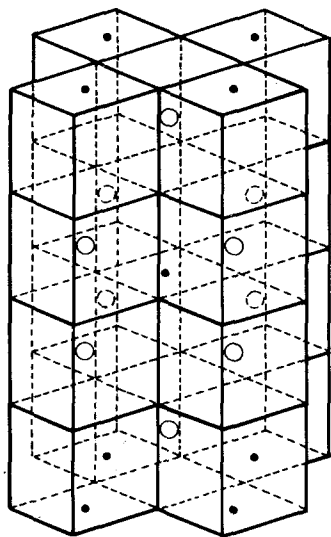


Fig. 28.35. The ideal structure of Nd_2CuO_4 . Cu^{2+} ions are shown as filled circles, Nd^{3+} ions as open circles. Anions occur at all cube corners.

La_2CuO_4 which had a high temperature factor in the analysis by Longo and Raccach (1973), it may be that this site is not occupied and that the structure of La_2CuO_4 is not that of K_2NiF_4 . Such problems can probably be expected in heavy-metal oxides. The significance of Müller-Buschbaum's discovery for the interpretation of the electric and magnetic properties of these compounds is difficult to evaluate without further structural information. If La_2CuO_4 is of the K_2NiF_4 -type, and the remaining R_2MO_4 ($\text{M} = \text{Pr}$ through Gd) compounds are of the Nd_2CuO_4 -type, then the differences in their properties, discussed by Ganguly and Rao (1973), George et al. (1974) and Goodenough (1973) probably arise from structural differences.

The ternary K_2NiF_4 structures are derived from the binary compounds by replacing a small divalent transition-metal cation by a large alkaline-earth ion and by replacing a large rare earth ion with a small (often transition-metal) trivalent cation. With the small trivalent cation on the octahedral site charge compensation between the sodium chloride and perovskite layers is better than in the binary compounds. Attempts have been made with X-ray and neutron powder data to determine the extent of cationic order on the ninefold sites (Daoudi and Le Flem, 1972; Oudalov et al., 1970; Joubert et al., 1970; Daoudi and Le Flem, 1973), and in all cases except that of the NaRTiO_4 compounds (Blasse, 1968) the cations were found to be disordered. In the ordered arrangement found by Blasse (1968) the nine-coordinated sites in one half of the unit cell (along $[001]$) are occupied by Na^+ ions while the R^{3+} ions occupy the corresponding sites in the other half of the unit cell. This leads to very poor

charge compensation between the layers which presumably is balanced by lattice relaxation in the anion sub-lattice. Marchand (1976) recently reported that compounds R_2AlO_3N also have this structure.

With the problems of La_2CuO_4 in mind the reliability of the identification of the ternary compounds might be queried; the only single crystal study of such compounds which has been made is that of Pausch and Müller-Buschbaum (1972) on $SrCeAlO_4$ and $SrNdAlO_4$. Many structure analyses have been performed on X-ray powder data; apart from those which investigated cationic order (above) there are those of $LaSrVO_4$ by Longo and Raccach (1973), of $SrLaAlO_4$ by Ruddlesden and Popper (1957) and of $LaSrCuO_4$ by Goodenough et al. (1973). A number of authors (Blasse, 1965; Demazeau et al., 1972; Daoudi et al., 1974) have assigned this structure type to compounds on the basis of the similarity of their diffraction patterns with those of compounds known to have the K_2NiF_4 structure, a process that may well be appropriate but that is not devoid of risk. A number of structure analyses based on powder data are difficult to evaluate because they either do not report temperature factors or apply an overall temperature factor. Therefore although some of these compounds have been shown unequivocally to have this structure, the possibility remains that some of the other compounds may have other structures. Since it is a truism that a refined structure is no better than the assumptions on which it is based, if isomorphism with the K_2NiF_4 structure is assumed then all that can be obtained from the refinement is the set of atomic parameters for this structure which corresponds to the minimum R value. If the assumption of isomorphism is incorrect so also will be the atomic coordinates. The imposition of an arbitrary overall temperature factor may obscure indications that the atomic coordinates are in error. Thus while the structures of some of the compounds have been proved and most others are probably correct, the possibility remains that some of these phases do not have the K_2NiF_4 structure.

A number of systems show solid solution regions where the transition metal adopts different valence states (Daoudi and Le Flem, 1972, 1973; Chaumont et al., 1975). In $Ca_{2-x}Pr_xMnO_4$ ($0 < x < 0.5$) and $Ca_{2-x}Y_xMnO_4$ ($0 < x < 0.25$) the symmetry is tetragonal for all values for x , whereas in $Ca_{2-x}Gd_xMnO_4$ and $Ca_{1+x}R_{1-x}CrO_4$ ($R = Nd, Gd, 0 < x < 0.5$) the symmetry changes from orthorhombic to tetragonal. Only in the case of $Ca_{2-x}Y_xMnO_4$ do the lattice parameters vary in the simple manner expected from Vegard's law. In all cases except that of $Ca_{2-x}Pr_xMnO_4$ the orthorhombic phase has a much lower c/a ratio than the tetragonal phase (a in c/a for an orthorhombic phase being taken either as $(ab)^{1/2}$ or $\frac{1}{2}(a+b)$).

Daoudi et al. (1974) found that rare earth calcium gallates ($R = La$ through Yb) form with the olivine-type structure, and that some of these are then transformed irreversibly to the K_2NiF_4 -type by the action of pressure ($R = Eu$ through Dy) or temperature ($R = La$ through Sm). The pressure effect is accompanied by a volume decrease of some 16%.

The second member of the Ruddlesden-Popper series of phases is typified by $Sr_3Ti_2O_7$ (Ruddlesden and Popper, 1958). This structure consists of double layers

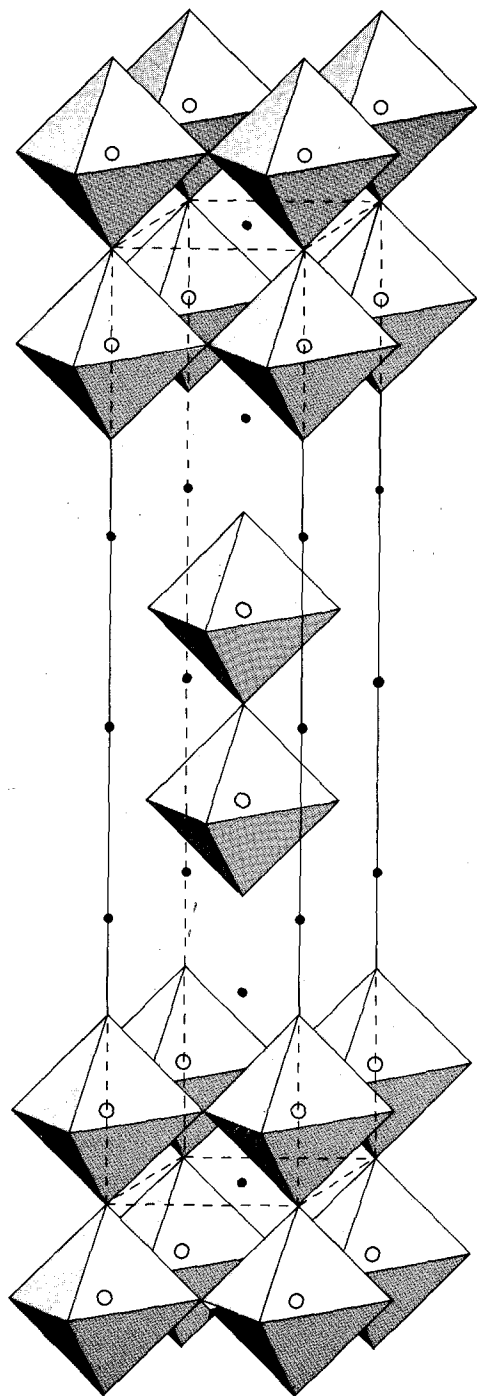


Fig. 28.36. The $\text{Sr}_3\text{Ti}_2\text{O}_7$ -type structure as found in $\text{SrLa}_2\text{Al}_2\text{O}_7$. Filled circles represent sites occupied by randomly distributed Sr^{2+} and La^{3+} ions; open circles represent Al^{3+} ions. Anions occur at the apices of the octahedra. The unit-cell is indicated.

of perovskite separated by layers of stoichiometry MO, with the adjacent double perovskite layers translated as before by $\frac{1}{2}a + \frac{1}{2}b + \frac{1}{2}c$ (fig. 28.36), which again effectively interposes a layer of stoichiometry MO between them. While the parent structure belongs to the space group $I4/mmm$, the only occasions on which such (pseudo) symmetry is observed in ternary rare earth oxide systems is in the case of $BaR_2Fe_2O_7$ ($R = La$ and Nd) where the scattering factor of Ba^{2+} is very close to that of the R^{3+} ion. The most likely space group for the ternary oxides is $P4_2/mnm$ (Drofenik et al., 1973; Joubert et al., 1971) although Fava and Le Flem (1975) used the space group $I4/mmm$ for the refinement of the structures of $SrLa_2Al_2O_7$ and $SrGd_2Al_2O_7$. In this refinement they found the Sr^{2+} and La^{3+} ions to be statistically distributed over the nine- and twelve-coordinated sites and the Al^{3+} ions octahedrally coordinated. Typical parameters for this phase are those of $SrLa_2Al_2O_7$ for which $a = 3.775 \text{ \AA}$, $c = 20.21 \text{ \AA}$.

Atom coordinates for this compound are given below:

Sr, La(1)	in	$2b$	0	0	$\frac{1}{2}$
Sr, La(2)		$4e$	0	0	0.318
Al		$4e$	0	0	0.090
O(1)		$2a$	0	0	0
O(2)		$8g$	0	$\frac{1}{2}$	0.097
O(3)		$4e$	0	0	0.203

Other compounds of this structure-type are $BaR_2Fe_2O_7$ ($R = Sm, Eu, Gd$), $SrR_2Fe_2O_7$ ($R = Nd$ through Tb) reported by Joubert et al. (1971), and $Eu_3Al_2O_7$ (Fava et al., 1972).

$Eu_4Ti_3O_{10}$ appears to be the only documented rare earth oxide phase likely to have $n = 3$ in the Ruddlesden–Popper series (McCarthy et al., 1969). In accord with the above structures it consists simply of triple perovskite layers translated with respect to each other as before.

5.3.2. Structures of the $BaZnF_4$ -type

The second series of perovskite-related phases is an analogue of a series of (sodium, calcium) niobium oxides (Carpy et al., 1973) based on the $BaZnF_4$ -structure (Schnering and Bleckmann, 1968) which has the generic formula $A_nB_nO_{3n+2}$. These structures consist of slabs of perovskite-type structure n octahedra thick ($n \geq 2$), but these layers now contain the c -axis of the sub-cell and are parallel to its (110) plane. This distinguishes them from the perovskite-type layers occurring in the Ruddlesden–Popper phases. Separating these slabs are additional anion-only planes. Lanthanum ditanate ($La_2Ti_2O_7$), the member $n = 4$, was described by Queyroux et al. (1970) as monoclinic, space group $P2_1/m$. Gasperin (1975) found the space group to be $P2_1$ and gave the lattice parameters as $a = 7.800 \text{ \AA}$, $b = 13.011 \text{ \AA}$, $c = 5.546 \text{ \AA}$, $\gamma = 98.6^\circ$, while Scheunemann and Müller–Buschbaum (1975) described the unit cell as orthorhombic, space group $Pna2_1$, with $a = 25.745 \text{ \AA}$, $b = 7.810 \text{ \AA}$, $c = 5.547 \text{ \AA}$. However, as Gasperin (1975) observes, these last two unit cells are simply

related. Atom positions for the monoclinic cell are as given below.

La(1)	0.2789	0.1138	0.2500	O(1)	0.776	0.109	0.799
La(2)	0.7741	0.0993	0.2543	O(2)	0.275	0.090	0.698
La(3)	0.3502	0.3909	0.8026	O(3)	0.030	0.016	0.024
La(4)	0.8525	0.4161	0.8413	O(4)	0.479	0.020	0.026
Ti(1)	0.0320	0.1191	0.7630	O(5)	0.098	0.226	0.969
Ti(2)	0.5271	0.1200	0.7598	O(6)	0.517	0.229	0.963
Ti(3)	0.0780	0.3228	0.2946	O(7)	0.033	0.187	0.460
Ti(4)	0.5833	0.3263	0.2975	O(8)	0.559	0.189	0.455
				O(9)	0.089	0.409	0.554
				O(10)	0.613	0.398	0.569
				O(11)	0.121	0.432	0.078
				O(12)	0.599	0.440	0.089
				O(13)	0.327	0.312	0.323
				O(14)	0.825	0.300	0.221

The structure consists of infinite layers of perovskite, four octahedra wide, separated by regions in which an anion-only plane has been inserted; each slab is translated by $\frac{1}{2}[001]$ of the sub-cell relative to its neighbours. In table 28.5 the unit-cell parameters and space groups of the other members of the series $(\text{Ca}, \text{La})_n\text{Ti}_n\text{O}_{3n+2}$ with $n = 4.5, 5$ and 6 are given. These structures are shown in fig. 28.37.

Neodymium forms apparently analogous compounds with $n = 4$ and 4.5 but those with $n = 5$ and 6 show a doubling of the orthorhombic b -axis (Nanot et al., 1975); however, this effect is due to twinning of structures whose real symmetry is monoclinic. Intergrowth of various homologues has been observed by electron microscopy. In particular, the member with $n = 4.5$ is an ordered intergrowth at the unit cell level of members with $n = 4$ and 5 , and in a sample with a composition appropriate for $n = 6$, isolated planar defects corresponding to layers with $n = 8$ and $n = 9$ have been observed. In addition to these compounds, a rare earth ion may be introduced in $\text{Ca}_2\text{Nb}_2\text{O}_7$ by replacement of two Ca^{2+} ions by an Na^+ and an R^{3+} ion, forming solid solutions $\text{R}_x\text{Na}_x\text{Ca}_{2-2x}\text{Nb}_2\text{O}_7$ where, for Sm, $x \leq 0.25$ and for Eu and Gd, $x \leq 0.20$ (Nanot et al., 1974). Bocquillon et al. (1971) have shown that samarium dititanate has the pyrochlore structure unless formed under high pressure, in which case a second polymorph isostructural with $\text{La}_2\text{Ti}_2\text{O}_7$ may be formed. This transformation is accompanied by a 1% decrease in volume, a quite small motivation for a complete structural reor-

TABLE 28.5

n	Composition	a	b	c	Space group
4.5	$\text{Ca}_{0.5}\text{La}_4\text{Ti}_{4.5}\text{O}_{15.5}$	3.904	57.10	5.536	$P2c, Pmcb$
5	$\text{CaLa}_4\text{Ti}_5\text{O}_{17}$	3.892	31.32	5.520	$Pmnn, P2nn$
6	$\text{Ca}_2\text{La}_4\text{Ti}_6\text{O}_{20}$	3.892	36.80	5.516	$Cmcn, Cmc2, C2cm$

Unit cell parameter data for higher members of the series $(\text{Ca}, \text{La})_n\text{Ti}_n\text{O}_{3n+2}$ (After Nanot et al., 1974).

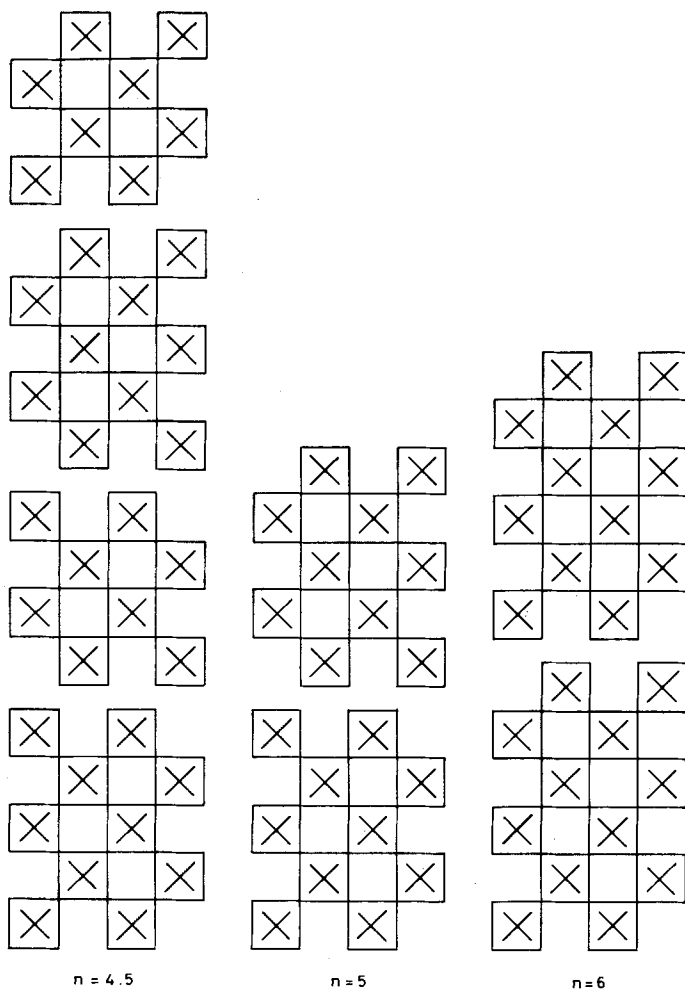


Fig. 28.37. Projection down [100] of the idealised structures of members of the series of $(\text{Ca, La})_n \text{Ti}_n \text{O}_{3n+2}$ with $n = 4.5, 5$ and 6 .

ganisation. However the La and Nd dititanates have molar volumes per cation only 2% and 1% respectively smaller than would be expected for their non-existent pyrochlores.

5.4. Structures deriving from the CaFe_2O_4 -type

The structures of many compounds containing a rare earth sesquioxide (especially those involving alkaline-earth oxides) are composed of two main structural units, the double octahedron and the capped trigonal prism. The double octahedron simply consists of two edge-sharing MO_6 octahedra, and

edge-sharing of these results in an infinitely long double octahedral ribbon. A discussion of the significance of the double ribbons is given by Reid et al. (1968). Across the range of oxide structures described in this section a gradual transition is observed from structures which are most appropriately described in terms of double octahedral ribbons to those most aptly described in terms of capped trigonal prisms (hereafter referred to as m.t.p's, b.t.p's, or t.t.p's depending on whether they are mono-, bi- or tri-capped). At one end of the spectrum the structures consist solely of a double octahedral framework containing sites within capped trigonal prisms whose pseudo-trigonal axes are parallel to the long axis of the ribbons (or to the short c -axis of the unit cell). Towards the other end of the spectrum the proportion of octahedra decreases, the proportion of b.t.p's with their pseudotrigonal axes parallel to the c -axis decreases, and the proportion of m.t.p's with these axes perpendicular to the c -axis increases. At the end of the spectrum there are only m.t.p's of the latter type. In order to illustrate these structures more clearly the structural units are depicted in fig. 28.38. These representations show (in projection) the space-filling properties of the various polyhedra.

The double ribbon of MO_6 octahedra occurs in a number of oxide systems (Clark, 1972). They are often linked by unshared vertices, forming an open framework structure as in α - and γ - MnO_2 . Figure 28.39 is a projection of the

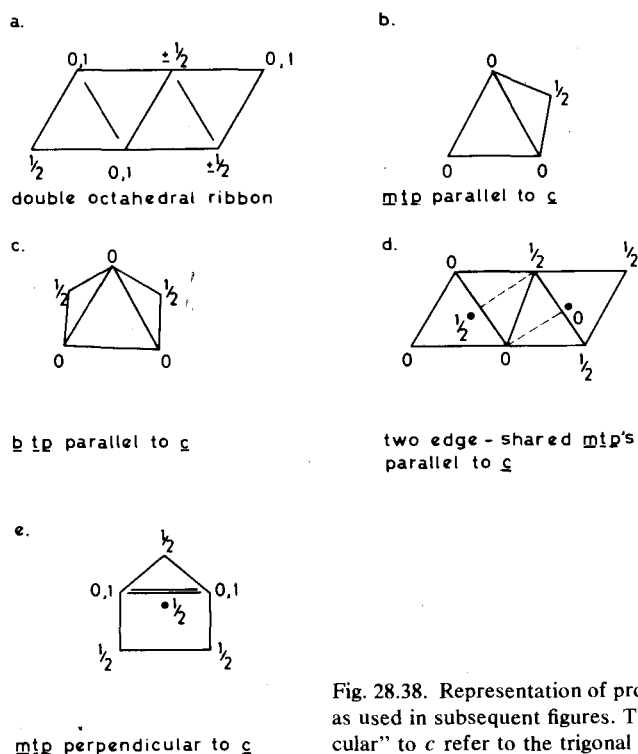


Fig. 28.38. Representation of projections of various structural units as used in subsequent figures. The terms "parallel" and "perpendicular" to c refer to the trigonal axes of the prisms.

atom positions of $\text{SrCa}_2\text{Sc}_6\text{O}_{12}$ down the c -axis. Müller-Buschbaum and Muschick (1975) found this phase to be hexagonal, space group $P6_3/m$ with $a = 9.695 \text{ \AA}$, $c = 3.136 \text{ \AA}$. The atom positions within the unit cell are:

Sc^{3+}	$6h$	0.3460	0.9970	0.250
Ca^{2+}	$2c$	0.3333	0.6667	0.250
$\frac{1}{2}\text{Sr}^{2+}$	$2b$	0.0000	0.000	0.000
O^{2-}	$6h$	0.195	0.309	0.250
O^{2-}	$6h$	0.530	0.398	0.250

As can be seen in fig. 28.39, the structure consists of double octahedral ribbons sharing vertices with four other ribbons, such that each ribbon constitutes a side of two trigonal channels, the overall structure assuming hexagonal symmetry. The Ca^{2+} ions occupy t.t.p. sites parallel to the c -axis, the Sr^{2+} ions are in special octahedral sites at the origin, the Sc^{3+} ions occupy all of the octahedral sites within the double ribbons. Despite the distortion of the octahedra in the ribbons there is no tendency for these to be capped or to form capped trigonal prisms.

Like many of the alkaline-earth/rare earth oxides of formula $\text{M}^{2+}\text{R}_2^{3+}\text{O}_4$, Eu_3O_4 (Rau, 1966) is isotypic with CaFe_2O_4 (Decker and Kasper, 1957). This structure

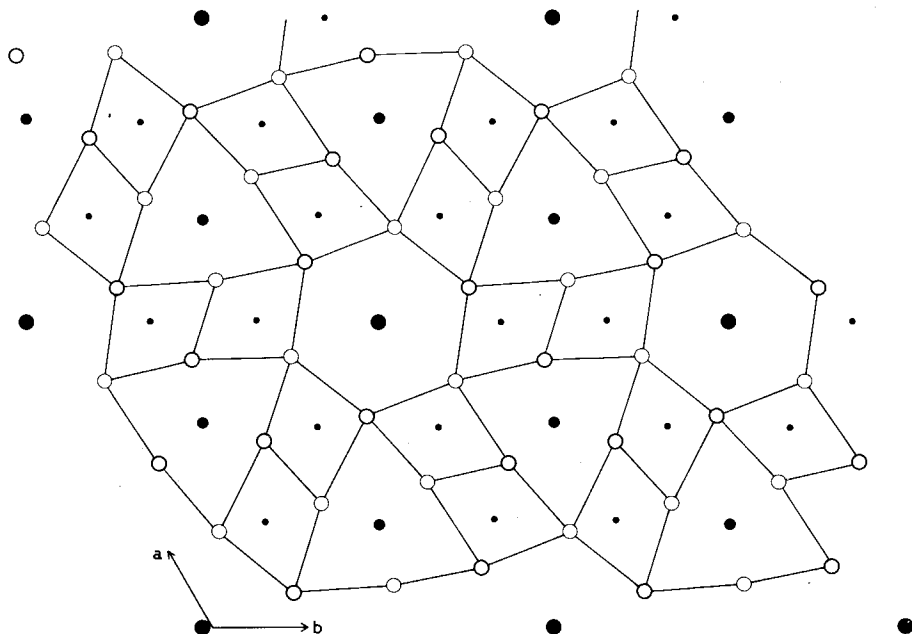


Fig. 28.39. Projection of the structure of $\text{SrCa}_2\text{Sc}_6\text{O}_{12}$ along the hexagonal c -axis. Heavy and light open circles represent anions at different levels along c . Filled circles represent cations as follows: - Large circles - Sr^{2+} , medium circles - Ca^{2+} , small circles - Sc^{3+} . Relative cation levels can be deduced from those of the anions.

belongs to space group $Pnam$ with $a = 10.085 \text{ \AA}$, $b = 12.054 \text{ \AA}$, $c = 3.502 \text{ \AA}$.
Atoms occupy the 4c positions

Eu ³⁺	0.4280	0.6140	0.25	O(1)	0.2150	0.6824	0.25
Eu ³⁺	0.4136	0.1106	0.25	O(2)	0.1334	0.9841	0.25
Eu ²⁺	0.2481	0.3525	0.25	O(3)	0.0055	0.2151	0.25
				O(4)	0.4297	0.9207	0.25

The calcium ferrite structure contains two types of R^{3+} ions on octahedral sites; in one case the RO_6 octahedra are almost undistorted, in the other the distortion is substantial. The most accurate description of the structure involves an $R_2O_4^{2-}$ framework of ribbons of double octahedra with Ca^{2+} ions occupying the b.t.p. sites within this framework, as depicted in fig. 28.40. However an alternative description is that of isolated double octahedral ribbons built into a framework by edge-sharing with b.t.p.'s, the trigonal axes of which are parallel to

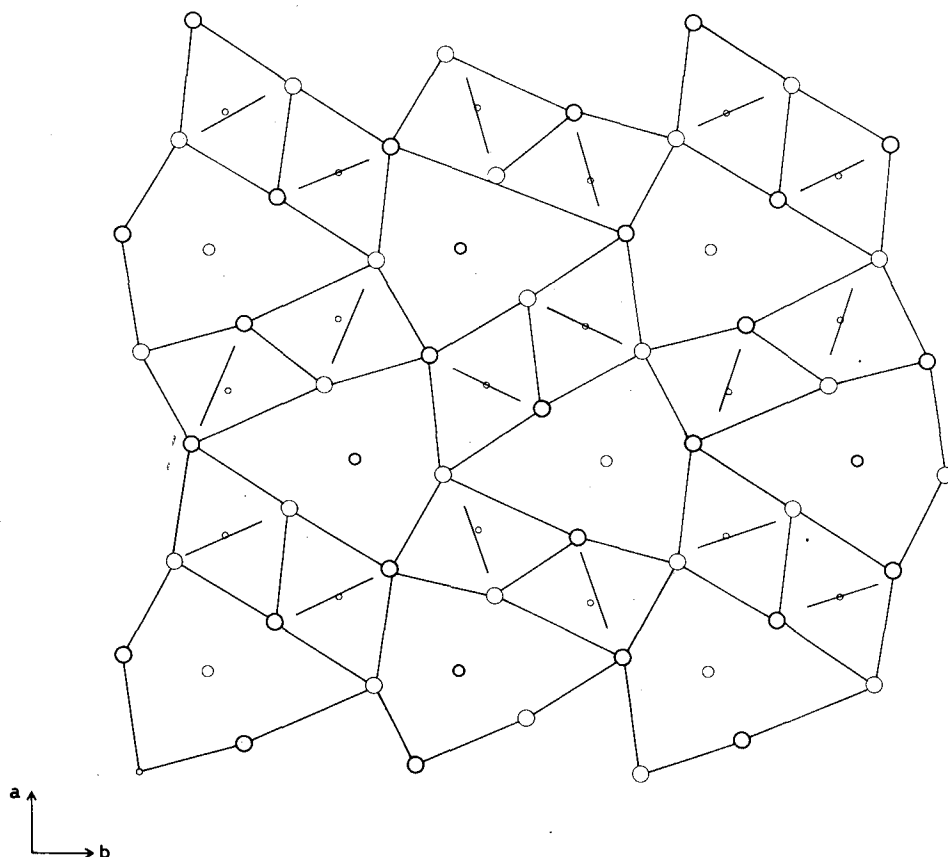


Fig. 28.40. [001] projection of the $CaFe_2O_4$ -Type structure of Eu_3O_4 . Large circles represent anions, medium circles Eu^{2+} ions and small circles Eu^{3+} ions.

the c -axis, and with distorted m.t.p's whose trigonal axes are perpendicular to the c -axis, as shown in fig. 28.41. In this latter case the two types of trigonal prism also shares edges with each other.

The CaFe_2O_4 structure, as exemplified by mixed-oxide phases of the alkaline- and rare earth elements, has been extensively studied by Müller-Buschbaum and his colleagues. Complete structure analyses have been performed on MgSc_2O_4 (Müller-Buschbaum, 1966); CaSc_2O_4 (Müller-Buschbaum and Schnering, 1965); CaYb_2O_4 , CaLu_2O_4 , SrY_2O_4 , and SrTb_2O_4 (Müller-Buschbaum and von Schenck, 1970; Müller-Buschbaum, 1968; Paletta and Müller-Buschbaum, 1968). In all of these except MgSc_2O_4 the cations are fully ordered, with the M^{2+} ion on the b.t.p. site and the R^{3+} ions on the other sites. However, in MgSc_2O_4 the cations are disordered, with a random distribution of Mg^{2+} and Sc^{3+} ions on all cation sites. This disorder is presumably a result of the similarity in the ionic radii of Mg^{2+} and Sc^{3+} ions: Shannon and Prewitt (1969) give the following figures:

for six-fold coordination $r(\text{Sc}^{3+}) = 0.73 \text{ \AA}$, $r(\text{Mg}^{2+}) = 0.72 \text{ \AA}$;

for eight-fold coordination $r(\text{Sc}^{3+}) = 0.87 \text{ \AA}$, $r(\text{Mg}^{2+}) = 0.89 \text{ \AA}$.

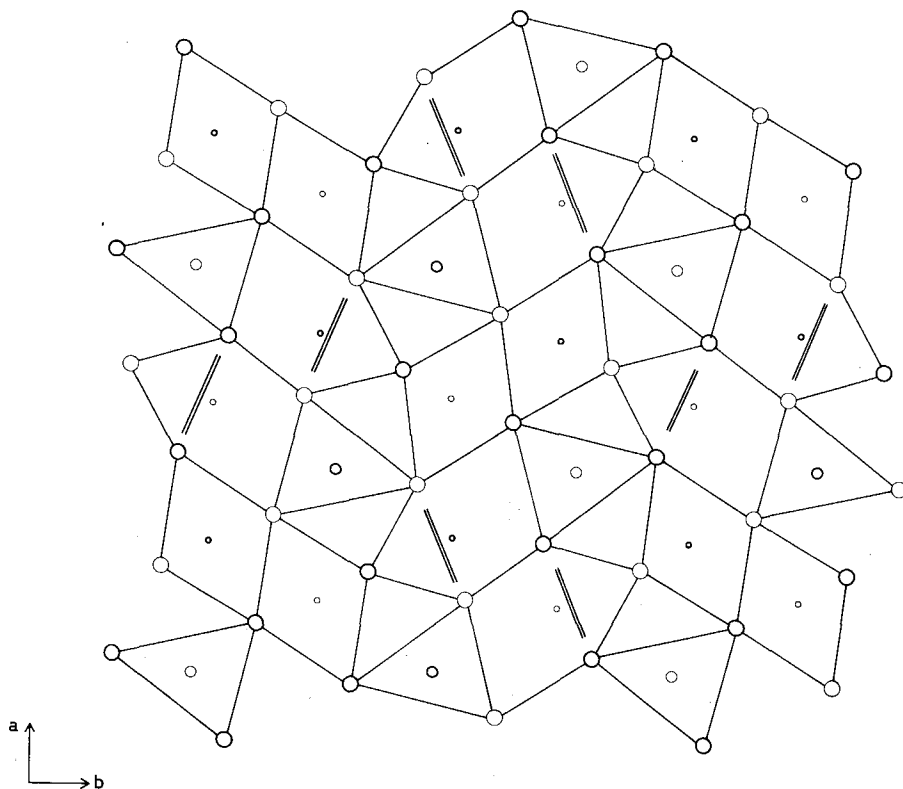


Fig. 28.41. The same projection of the structure of Eu_3O_4 as in fig. 5.14, but with a different description of the cation polyhedra. The distorted octahedra of fig. 5.14 have been replaced by monocapped trigonal prisms.

That MgSc_2O_4 forms at all is surprising; as Müller-Buschbaum (1966) points out, the molar volume of MgSc_2O_4 is some 16% larger than the appropriate sum of the molar volumes of its constituent oxides. Despite the fact that this volume problem would be less with other rare earths, there appears to be no report of a CaFe_2O_4 -type phase in other $\text{MgO-R}_2\text{O}_3$ systems. The other MSc_2O_4 -phases ($M = \text{Ca, Sr}$) appear to have remarkably low unit-cell volumes, as do the isostructural NaScMO_4 compounds with $M = \text{Ti, Sn, Hf}$ and Zr (Reid et al., 1968). In these latter compounds it has been found that the M^{4+} and Sc^{3+} ions are randomly distributed on the octahedral sites, and that the anions do not have anomalous temperature factors despite the fact that they are coordinating dissimilar cations i.e. where it might have been expected that the $\text{Sc}^{3+}\text{-O}$ distances would be greater than the $\text{Ti}^{4+}\text{-O}$ distances in these octahedra, resulting in spreading out of the anions in the $a\text{-}c$ plane, this was not the case. Reid et al. (1968) therefore suggested that the structure imposed a size on the cations. An alternative explanation would be that the structural parameters are determined by the size of the trigonal prisms, which in turn is a function of the radius of the cations on the trigonal prismatic sites. Other phases with the CaFe_2O_4 type structure are listed in table 28.6.

The next stage in the sequence of structures is represented by LiEu_3O_4 . As determined by Bärnighausen (1970), the unit cell is again orthorhombic, space group $Pbnm$, with lattice parameters $a = 11.565 \text{ \AA}$, $b = 11.535 \text{ \AA}$, $c = 3.48 \text{ \AA}$. All atoms are in the $4c$ positions: -

Eu(1)	0.20426	0.35862	0.25	O(1)	0.0450	0.2441	0.25
Eu(2)	0.61529	0.40230	0.25	O(2)	0.3894	0.4369	0.25
Eu(3)	0.52443	0.13562	0.25	O(3)	0.6297	0.0263	0.25
Li	0.9108	0.1555	0.25	O(4)	0.7808	0.2575	0.25

This structure can be described as consisting of a framework of edge-sharing m.t.p's with trigonal axes both parallel and perpendicular to the c -axis, within which there are isolated columns of octahedra. This representation is shown in fig. 28.42, where it can be seen that the m.t.p's with trigonal axes parallel to the c -axis occur in edge-sharing pairs. Li^+ occupy the tetrahedral sites, Eu^{2+} ions occupy the m.t.p's with trigonal axes both perpendicular to and parallel to the c -axis, while the Eu^{3+} ions occupy the octahedra. The alternative representation of this structure (fig. 28.43) shows a framework built up of doubled double ribbons of octahedra (the caps on some have been ignored) between which the Eu^{2+} ions occupy the trigonal prismatic sites and the Li^+ ions the tetrahedral sites. $\text{LiSr}_2\text{EuO}_4$ (Bärnighausen, 1967) and probably $\text{LiBa}_2\text{EuO}_4$ (Bärnighausen and Schmid, 1967) are isostructural with LiEu_3O_4 .

A structure which shows a remarkable similarity to LiEu_3O_4 is that of Y_2BeO_4 as reported by Harris and Yakel (1967). This phase, like the warwickite $(\text{Mg, Fe})_3\text{TiO}_2(\text{BO}_3)_2$ structure, is also orthorhombic, space group $Pm\bar{c}n$, with $a = 3.5315 \text{ \AA}$, $b = 9.899 \text{ \AA}$, $c = 10.400 \text{ \AA}$. A projection of the atom positions down the a -axis is shown in fig. 28.44. The chief difference between the two structures lies in the fact that in Y_2BeO_4 the trigonal prismatic sites are vacant and the Be^{2+}

TABLE 28.6
Unit cell volumes (in Å³) of compounds with the CaFe₂O₄ structure. Superscripts refer to references given in the footnote.

	La	Ce	Pr	Nd	Pm	Sm	Eu	Gd	Tb	Dy	Ho	Y	Er	Tm	Yb	Lu	Sc
Mg ²⁺																	320 ⁽⁸⁾
Ca ²⁺																	375 ⁽³⁾
Eu ²⁺																	335 ⁽⁵⁾
Sr ²⁺				443 ⁽¹⁾		433 ⁽¹⁾	428 ⁽⁷⁾	425 ⁽¹⁾	418 ⁽¹⁾	414 ⁽¹⁾	409 ⁽¹⁾	404 ⁽¹⁾					396 ⁽⁴⁾
Ba ²⁺	500 ⁽¹⁾		481 ⁽¹⁾	475 ⁽¹⁾		462 ⁽¹⁾	457 ⁽¹⁾	452 ⁽¹⁾	444 ⁽¹⁾	440 ⁽²⁾	435 ⁽²⁾	436 ⁽²⁾					392 ⁽¹⁾
Others	Ti	Sn	Hf	Zr													
NaSc	309 ⁽⁶⁾	332 ⁽⁶⁾	338 ⁽⁶⁾	342 ⁽⁶⁾													

References: 1. Schwartz and Bommert (1964). 2. Lopato et al. (1972). 3. Müller-Buschbaum and von Schenck (1970). 4. de Pous et al. (1973). 5. Carter and Feigelson (1964). 6. Reid et al. (1968). 7. Bärnighausen and Brauer (1962). 8. Müller-Buschbaum (1966).

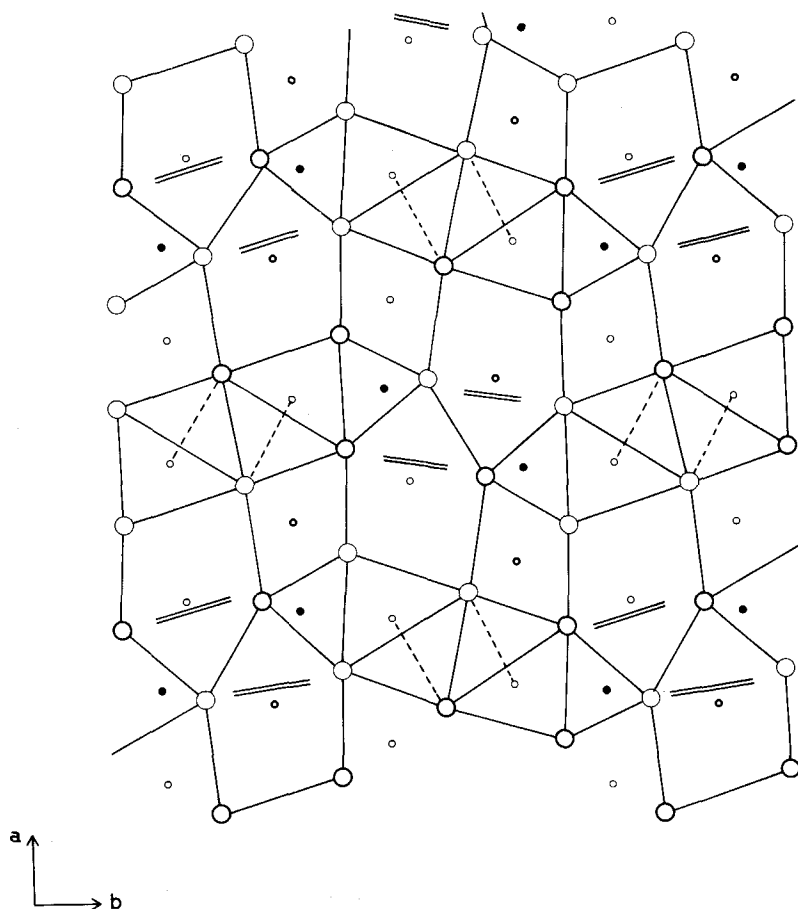


Fig. 28.42. [001] projection of the structure of LiEu_3O_4 . As shown here the structure consists of a framework of edge-shared pairs of monocapped trigonal prisms in two orientations within which are isolated octahedral and tetrahedral sites. Different z coordinates are indicated by light and heavy circles; large circles represent anions, medium circles Eu^{2+} , small open circles Eu^{3+} ions and small filled circles Li^+ ions.

ions lie in the triangular faces of the prism. Hyde et al. (1974) have described this structure as being derived from CaTi_2O_4 by slip of lamellae $\frac{1}{2}a$ thick by $\sim\frac{1}{4}[012]$ on (100). The framework of Y_2BeO_4 produces a significantly smaller triangular edge for the trigonal prism than is the case in the CaFe_2O_4 framework.

Another very close parallel with the LiEu_3O_4 structure is shown by Y_2TiO_5 (Mumme and Wadsley, 1968) and La_2TiO_5 (Guillen and Bertaut, 1966). The orthorhombic unit cell of Y_2TiO_5 has $a = 10.35 \text{ \AA}$, $b = 3.70 \text{ \AA}$, $c = 11.25 \text{ \AA}$ and belongs to space group $Pnma$. All atoms occur in the $4c$ position with the

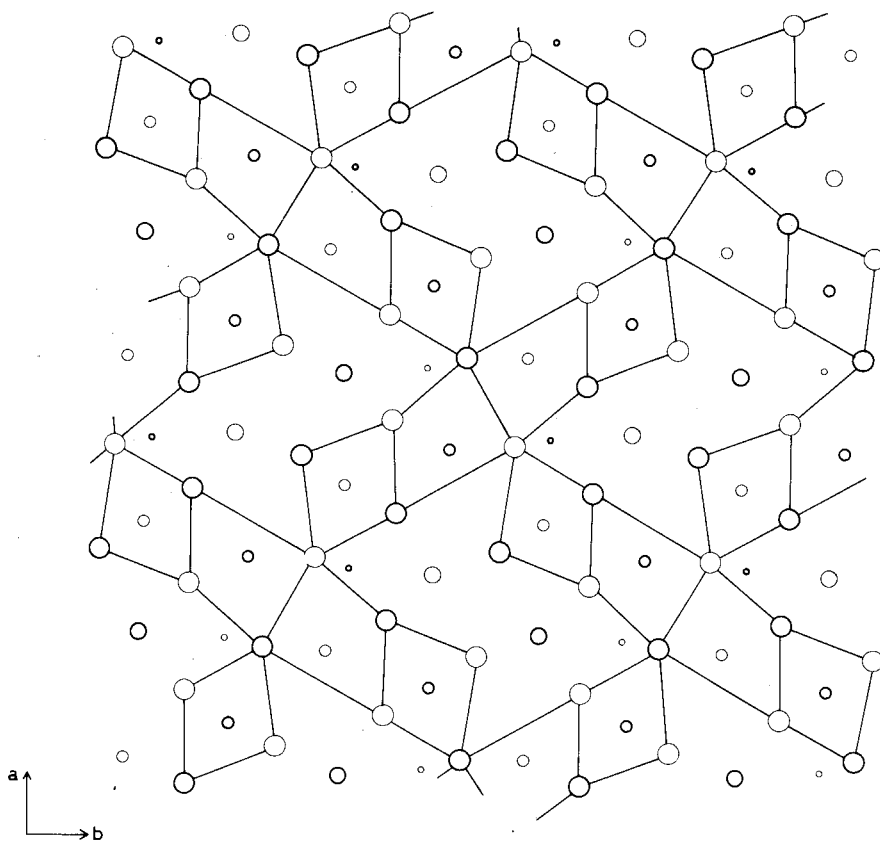


Fig. 28.43. The same projection of LiEu_3O_4 as shown in fig. 28.42 but with different coordination polyhedra indicated.

coordinates given below:

Y(1)	0.1156	$\frac{1}{4}$	0.2231	O(1)	0.495	$\frac{1}{4}$	0.102
Y(2)	0.1366	$\frac{1}{4}$	0.5578	O(2)	0.223	$\frac{1}{4}$	0.045
Ti	0.1745	$\frac{1}{4}$	0.8806	O(3)	0.259	$\frac{1}{4}$	0.734
				O(4)	0.508	$\frac{1}{4}$	0.660
				O(5)	0.269	$\frac{1}{4}$	0.383

As represented in fig. 28.45 the structure consists of edge-sharing m.t.p.'s with trigonal axes perpendicular to the b -axis, forming an $\text{R}_2\text{O}_5^{4-}$ framework within which the Ti^{4+} ions occupy the square-pyramidal sites. The alternative representation in fig. 28.46 shows an $\text{R}_2\text{O}_4^{2-}$ framework composed of doubled octahedral ribbons. The Ti^{4+} and additional O^{2-} ion completes the TiO_5 square pyramid within this framework.

LiSrLaO_3 has been reported by Bärnighausen (personal communication) to be isostructural with K_2CuCl_3 (Brink and MacGillavry, 1949). A discussion of this

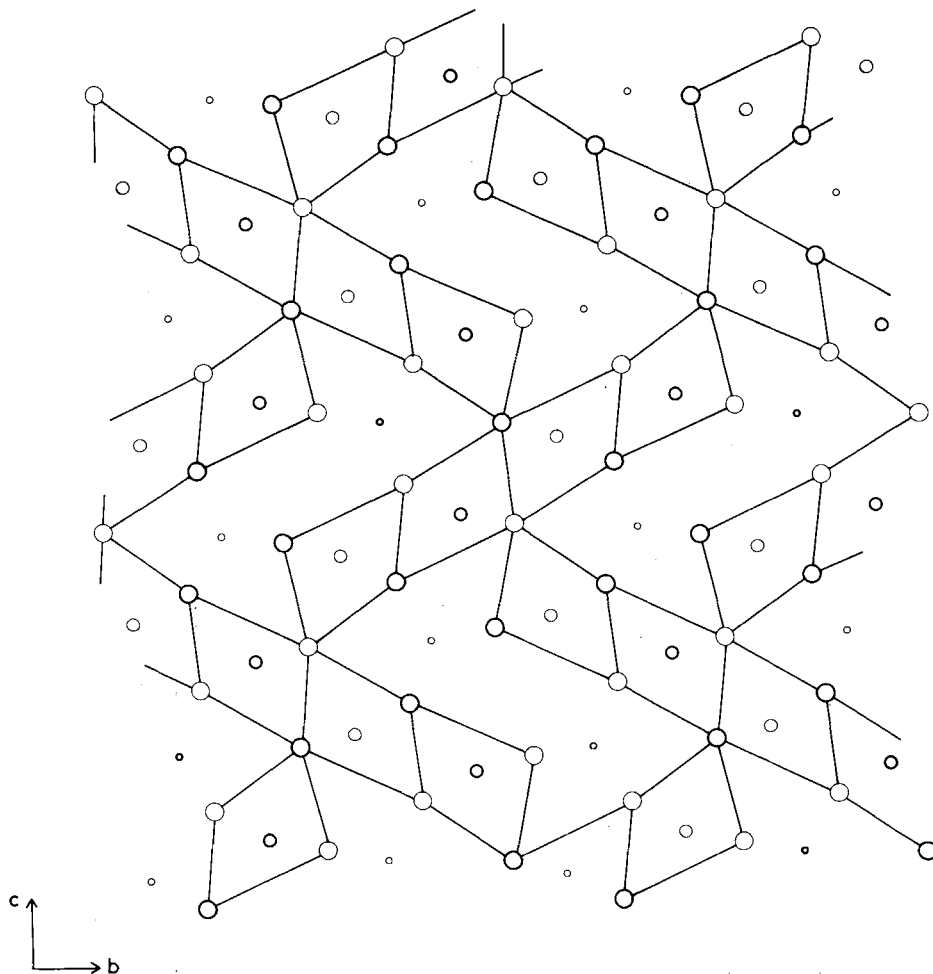


Fig. 28.44. Projection down the a -axis of Y_2BeO_4 showing the close similarity between this structure and that of $LiEu_2O_4$ (fig. 28.43). Relative heights of atoms are shown by light and heavy circles; large circles represent anions, medium circles R^{3+} ions and small circles Be^{2+} ions. These latter occupy the triangular sites at the ends of trigonal prisms.

latter and related structures, including the A-type sesquisulphides and η -sesquichalcogenides of the lanthanides and actinides, is given by Shoemaker (1973). $LiSrLaO_3$ is orthorhombic, space group $Pbnm$ with unit cell axes $a = 9.775 \text{ \AA}$, $b = 9.535 \text{ \AA}$, $c = 3.586 \text{ \AA}$. Atomic positions were not given so those of K_2CuCl_3 have been used in the projection in fig. 28.47.

It can be seen that the structure is composed entirely of edge-sharing $m.t.p$'s of both orientations. Li^+ ions occupy tetrahedral sites, Sr^{2+} ions occupy the $m.t.p$'s with trigonal axes parallel to the c -axis, and La^{3+} ions occupy the $m.t.p$'s with these perpendicular to the c -axis. Again in this structure the $m.t.p$'s with

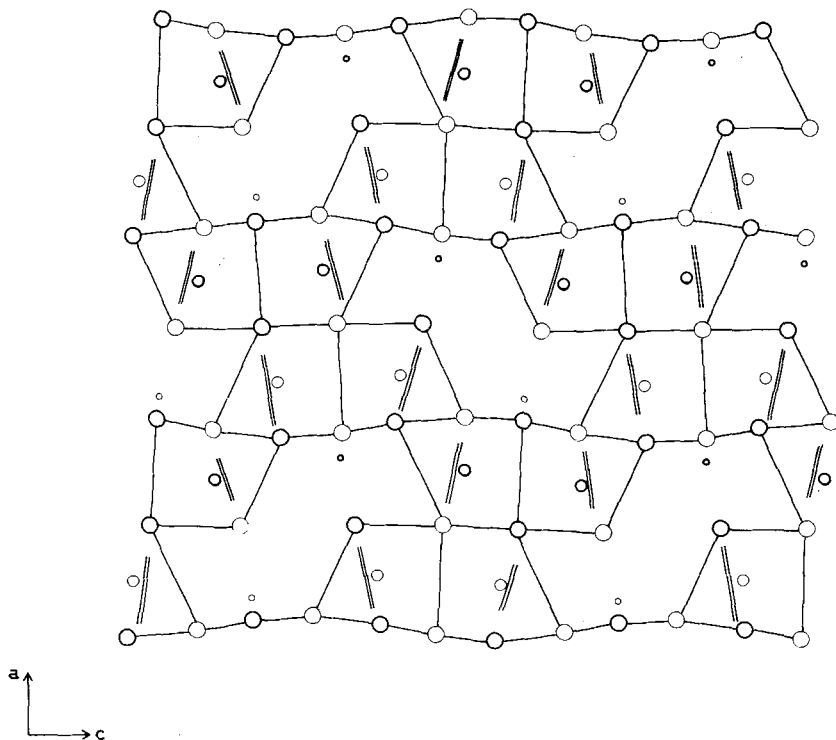


Fig. 28.45. [010] projection of the structure of Y_2TiO_5 showing the framework of mon capped trigonal prisms. Within this framework Ti^{4+} ions occupy square pyramidal sites. Relative atomic levels are indicated by light and heavy circles; anions are represented by large circles, R^{3+} ions by medium circles and Ti^{4+} ions by small circles.

trigonal axes parallel to the c -axis occur in edge-sharing pairs. Other structures reported by Bärnighausen (personal communication) to be isostructural with $LiSrLaO_3$ are $LiMRO_3$, where if $R = La$, $M = Sr$, Eu^{2+} , Ba ; and if $R = Pr$ or Nd , $M = Sr$.

Projections down the c -axes of both α - and β - $Li_2Eu_5O_8$ are shown in figs. 28.48 and 28.49 (Bärnighausen et al., 1973). The former is monoclinic, space group $B2/m$ with $a = 13.378 \text{ \AA}$, $b = 9.666 \text{ \AA}$, $c = 3.539 \text{ \AA}$, $\gamma = 119.52^\circ$. The latter is orthorhombic, space group $A2_1am$, with $a = 13.156 \text{ \AA}$, $b = 17.137 \text{ \AA}$, $c = 3.545 \text{ \AA}$. In α - $Li_2Eu_5O_8$ all atoms occupy $4i$ positions except the Eu^{2+} ions which are on $2b$ sites, while all atoms occupy $4a$ sites in β - $Li_2Eu_5O_8$. Atom parameters for both polymorphs are given on facing page.

Although deviating slightly from Bärnighausen's description, both structures can be regarded as built of units consisting of four edge-sharing $m.t.p$'s with trigonal axes perpendicular to the c -axis, each containing an Eu^{3+} ion. These units can be packed together in two ways leaving channels into which two Li^+ ions and one Eu^{2+} ion must be inserted. In α - $Li_2Eu_5O_8$ both Li^+ ions have tetrahedral coor-

$$\alpha\text{-Li}_2\text{Eu}_5\text{O}_8$$

Eu ²⁺	0.5	0	0
Eu ³⁺ (1)	0.6103	0.437	0
Eu ³⁺ (2)	0.6636	0.813	0.5
Li	0.691	0.262	0.5
O(1)	0.542	0.242	0.5
O(2)	0.736	0.620	0.5
O(3)	0.815	0.936	0
O(4)	0.582	0.656	0

$$\beta\text{-Li}_2\text{Eu}_5\text{O}_8$$

Eu ²⁺	0.5	0.9892	0
Eu ³⁺ (1)	0.4272	0.1884	0
Eu ³⁺ (2)	0.2870	0.3499	0.5
Eu ³⁺ (3)	0.1382	0.1985	0
Eu ³⁺ (4)	0.2521	0.0342	0.5
Li(1)	0.606	0.122	0.5
Li(2)	0.467	0.350	0
O(1)	0.464	0.100	0.5
O(2)	0.457	0.290	0.5
O(3)	0.366	0.430	0
O(4)	0.286	0.271	0
O(5)	0.112	0.291	0.5
O(6)	0.097	0.105	0.5
O(7)	0.177	0.956	0
O(8)	0.281	0.112	0

dination, leaving a distorted cubic site for the Eu²⁺ ion. In $\beta\text{-Li}_2\text{Eu}_5\text{O}_8$ one Li⁺ ion is tetrahedrally coordinated, the Eu²⁺ ion occupies an *m.t.p.* with its trigonal axis parallel to the *c*-axis, and the remaining site for the other Li⁺ ion is square pyramidal. Other phases reported by Bärnighausen et al. (1973) to be isostructural with these two phases are given below.

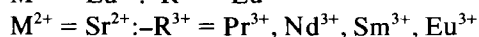
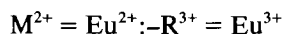
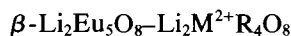
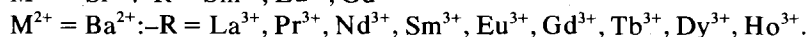
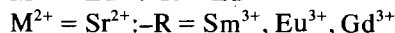
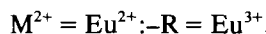
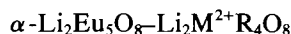


Fig. 28.50 is a projection of B-type Sm₂O₃ down the *b*-axis. Whether this is regarded as consisting entirely of edge-sharing *m.t.p.*'s with trigonal axes

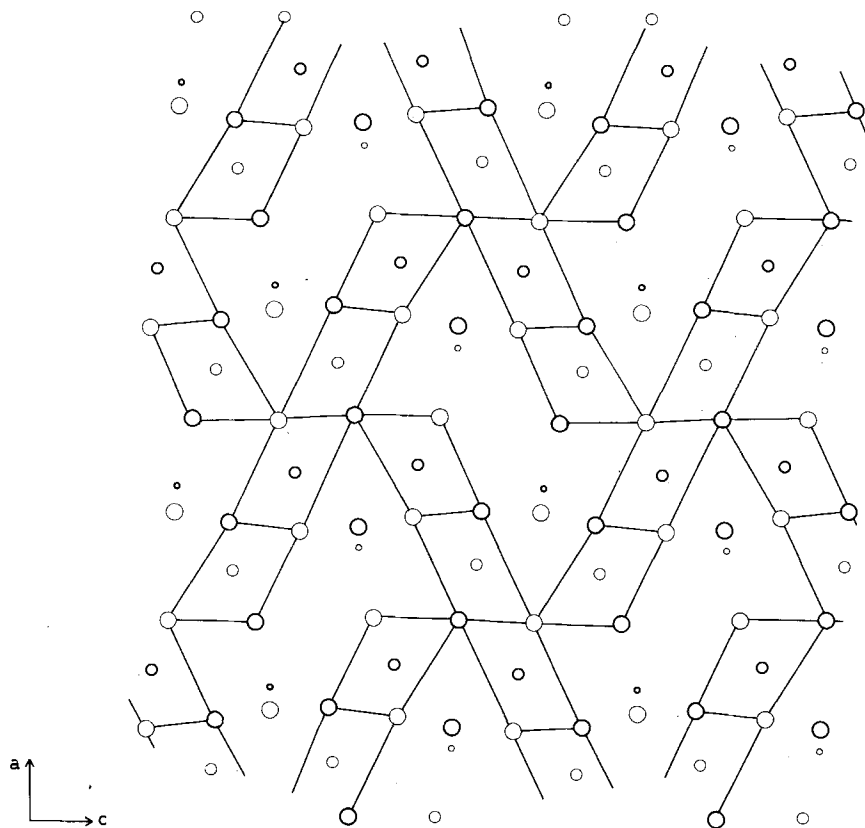


Fig. 28.46. An alternative description of the structure of Y_2TiO_5 in the same projection as fig. 28.45. The similarity between this structure and those of $LiEu_3O_4$ and Y_2BeO_4 can now be seen. The Ti^{4+} ions in this structure occupy the same sites as the Be^{2+} ions in Y_2BeO_4 but the coordination is altered by the additional anion.

perpendicular to the b -axis or as having octahedral coordination of one-third of the cations, the relationship to the above structures is obvious. A summary of the coordination trends in these structures is given in table 28.7.

A number of structures exist which are not directly related to calcium ferrite but which consists of similar coordination polyhedra. The first of these is the RMn_2O_5 structure type shown in fig. 28.51. This structure has been found for $R = La$ through Lu by Quezel-Ambrunaz et al. (1964). The orthorhombic unit cell of this phase belongs to space group $Pbam$ and for $HoMn_2O_5$ has parameters $a = 7.36\text{\AA}$, $b = 8.49\text{\AA}$, $c = 5.69\text{\AA}$. Atom positions for this compound are:

Ho	in	4g	0.143	0.172	0
Mn(1)		4h	0.090	0.848	$\frac{1}{2}$
Mn(2)		4f	0	$\frac{1}{2}$	$\frac{1}{4}$
O(1)		8i	0.10	0.72	$\frac{1}{4}$

O(2)	in	4g	0.14	0.44	0
O(3)		4h	0.14	0.44	$\frac{1}{2}$
O(4)		4e	0	0	$\frac{1}{4}$

As shown in fig. 28.51, the structure contains R^{3+} ions in distorted *t.t.p.*'s with trigonal axes parallel to the *c*-axis, half the Mn ions (presumably Mn^{3+}) on octahedral sites, and the remaining cations (Mn^{4+}) on square-pyramidal sites. The structure is somewhat unusual in that it contains large, unoccupied *t.t.p.* sites, the structure then contains columns of trigonal prisms (sharing triangular faces) which are alternately occupied by R^{3+} ions and vacant. Alternatively occupied trigonal prisms at one level edge share to form an infinite plane. Such planes are separated by [001]. Between these there are planes consisting of discreet pairs of square pyramids having one edge in common. These two kinds of plane are welded together by edge-sharing between the trigonal prisms and the square pyramids to form a rigid three-dimensional network containing octahedral sites which are occupied by the Mn^{3+} ions.

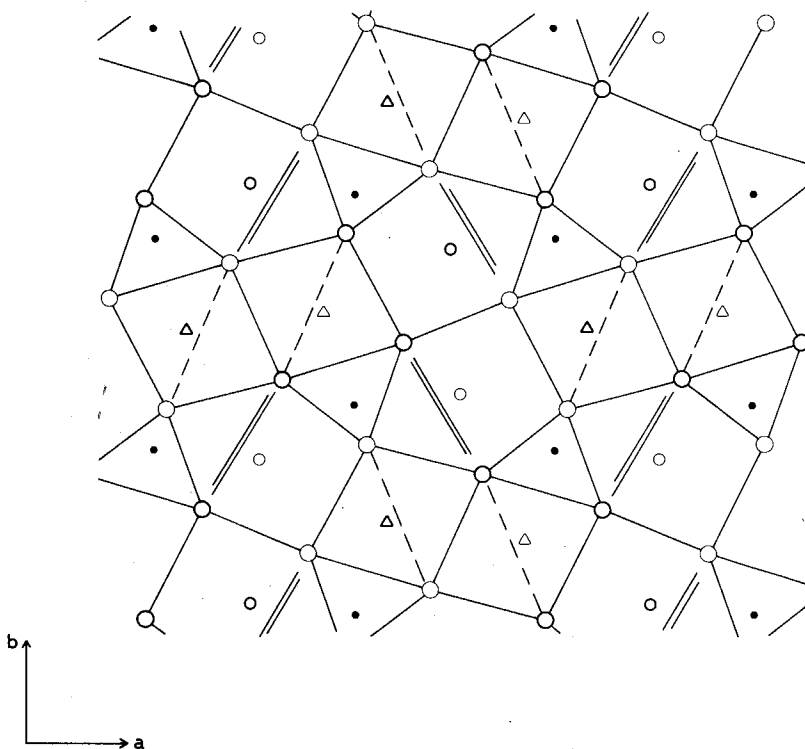


Fig. 28.47. [001] projection of the K_2CuCl_3 structure. $LiSrLaO_3$ and a number of similar compounds are isostructural with K_2CuCl_3 . In $LiSrLaO_3$, Li^+ ions would occupy sites indicated by small filled circles, La^{3+} ions by medium open circles, Sr^{2+} ions by triangles and O^{2-} ions by large circles. Relative heights are indicated by light and heavy triangles or circles for all atoms other than Li^+ .

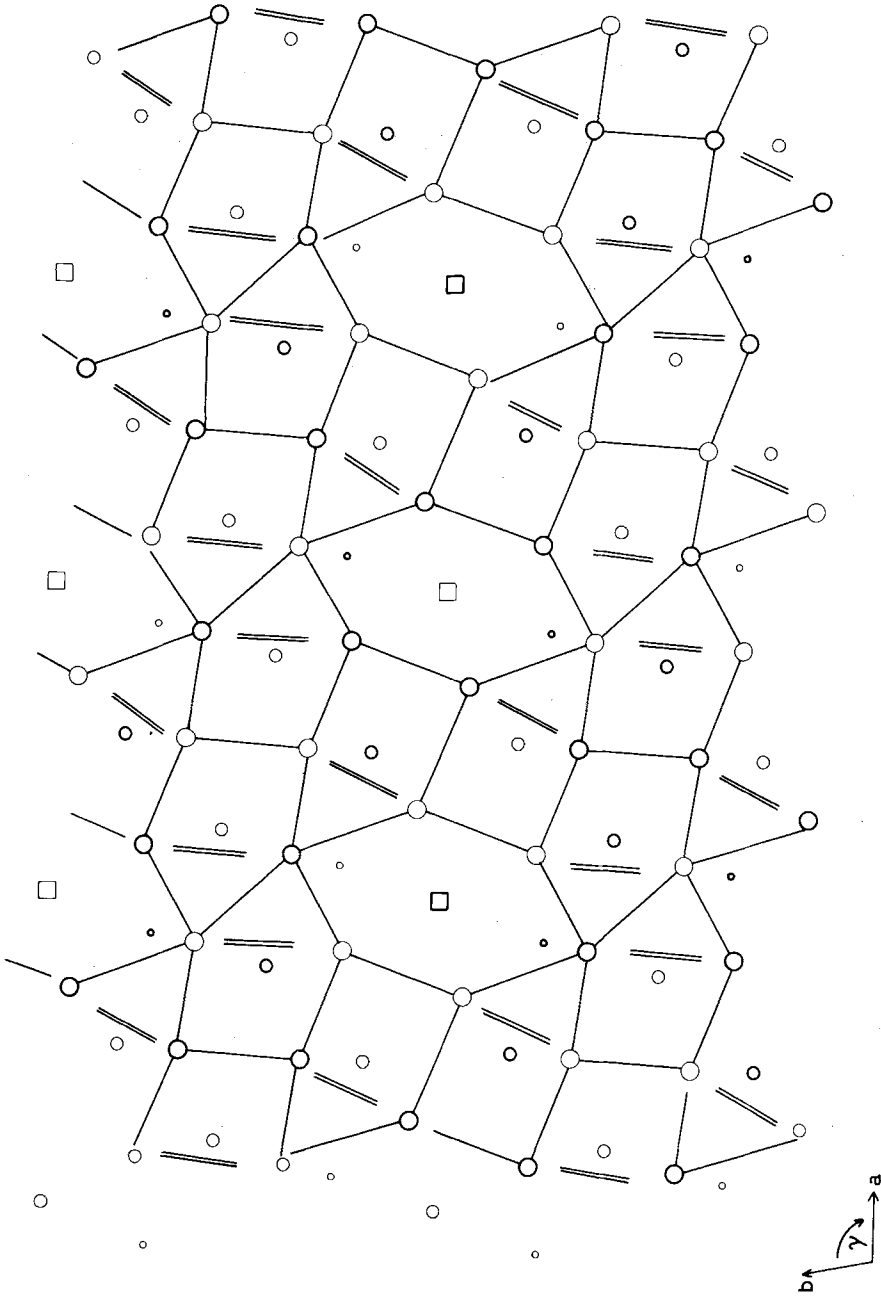


Fig. 28.48. Projection down the c -axis of the structure of $\alpha\text{-Li}_2\text{Eu}_5\text{O}_8$ showing the framework of monoclapped trigonal prisms within which the Li^+ ions occupy tetrahedra and Eu^{2+} ions distorted cubes. Relative atomic levels are shown by light and dark circles; large circles represent anions; medium circles, Eu^{3+} ions; small circles, Li^+ and squares, Eu^{2+} ions.

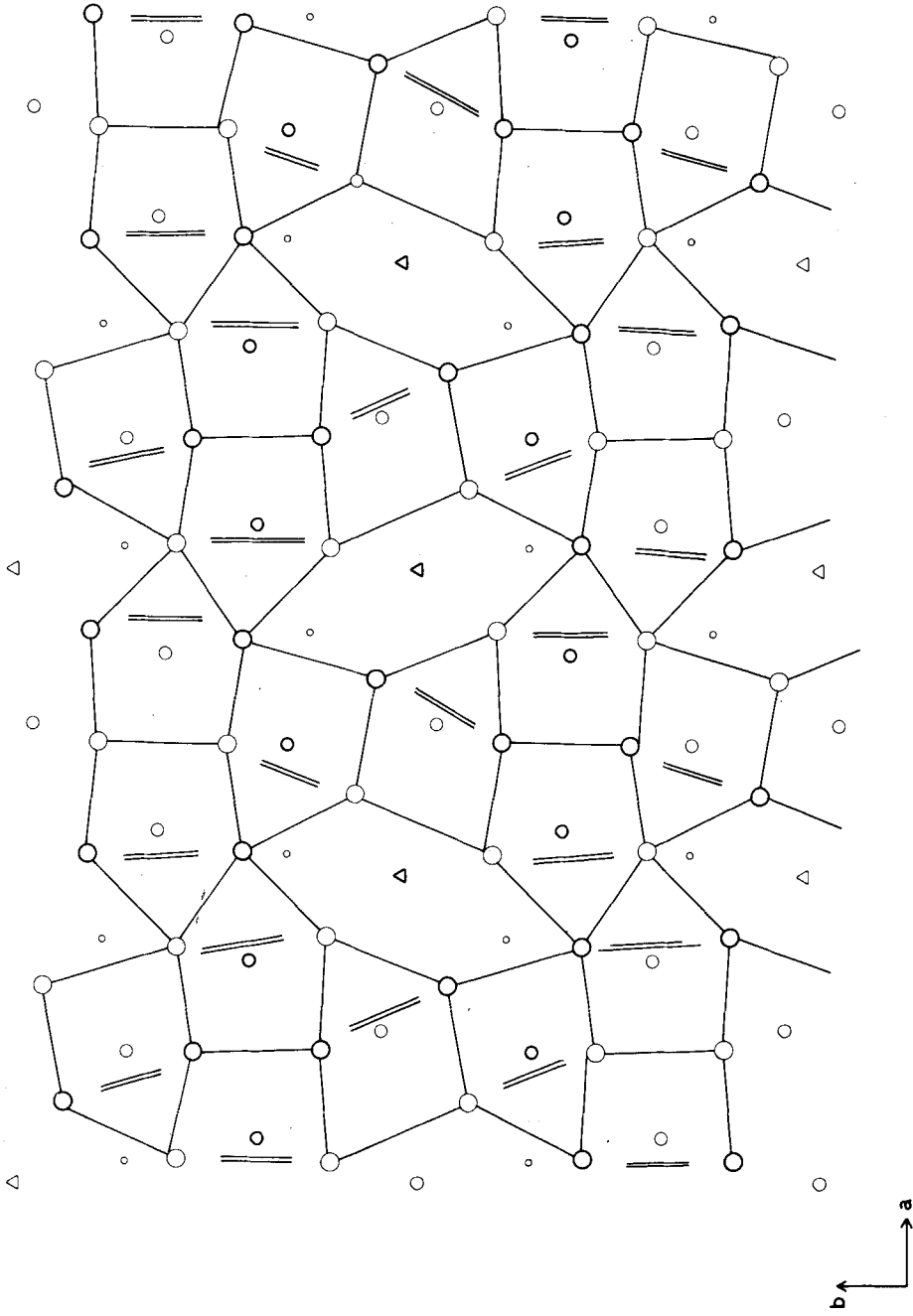


Fig. 28.49. [001] projection of the structure of β - $\text{Li}_2\text{Eu}_3\text{O}_8$. The structure is quite comparable with that of α - $\text{Li}_2\text{Eu}_3\text{O}_8$ (fig. 28.48) except that one Li^{+} ion now occupies a square pyramidal site and the Eu^{2+} ion is now on a monocoordinated trigonal prismatic site with its trigonal axis parallel to [001]. Large circles represent antons, medium circles; Eu^{3+} ions, small circles; Li^{+} ions; triangles; Eu^{2+} ions.

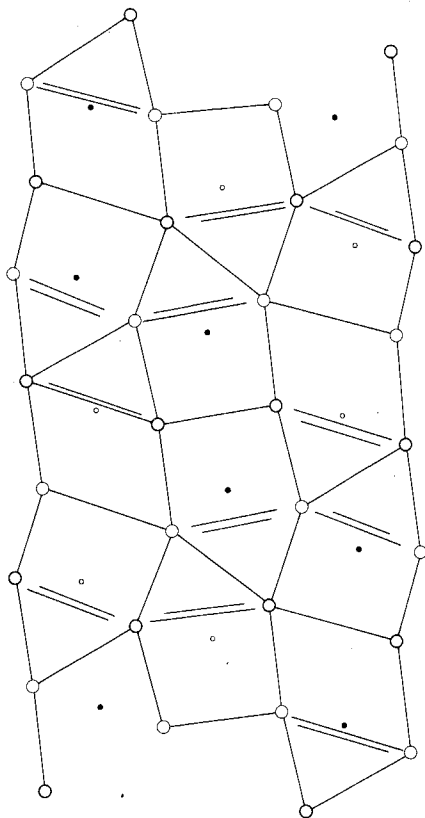


Fig. 28.50. Projection of the structure of B-type Sm_2O_3 along $[010]$ after Eyring and Holmberg (1963). Large heavy circles represent O^{2-} ions at $y = 0$, large light circles O^{2-} ions at $y = \frac{1}{2}$, small filled circles are Sm^{3+} ions at $y = 0$, small open circles are Sm^{3+} ions at $y = \frac{1}{2}$.

TABLE 28.7

Compound	M^+	M^{2+}	M^{3+}
$\text{SrCa}_2\text{Sc}_6\text{O}_{12}$		4 octahedra 2.t.t.p.'s†	4 octahedra
Eu_3O_4		b.t.p.†	m.t.p. octahedron octahedron
LiEu_3O_4	tetrahedron	m.t.p.†	octahedron
LiSrLaO_3	tetrahedron	m.t.p.* m.t.p.†	m.t.p.*
$\alpha\text{-Li}_2\text{Eu}_5\text{O}_8$	2 tetrahedra	distorted cube	4 m.t.p.'s*
$\beta\text{-Li}_2\text{Eu}_5\text{O}_8$	tetrahedron square pyramid	m.t.p.†	4 m.t.p.'s*

†trigonal axis parallel to c -axis. *trigonal axis perpendicular to c -axis.

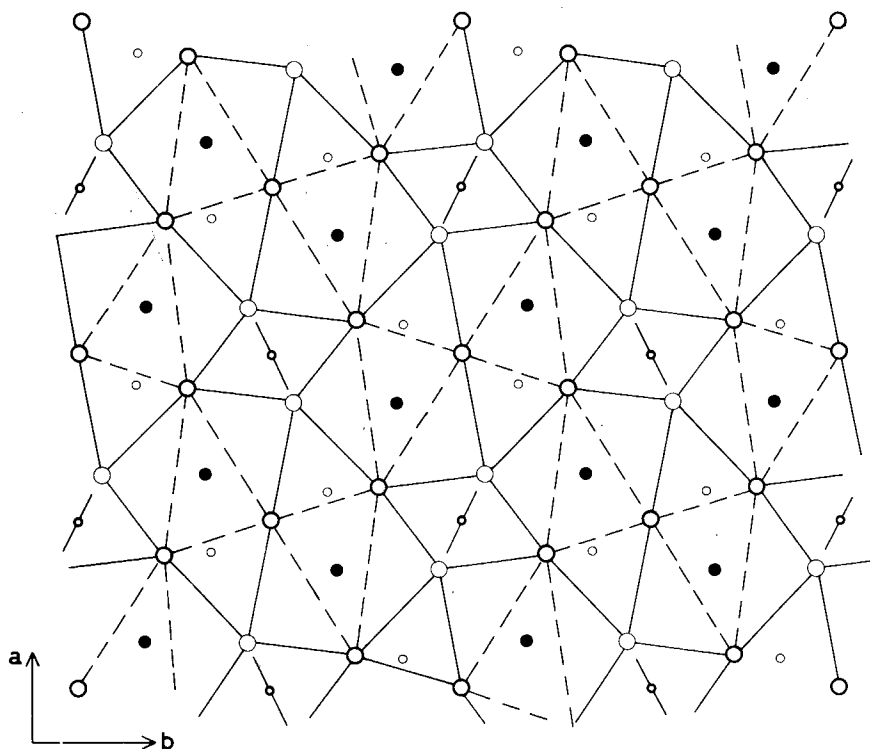


Fig. 28.51. The structure of HoMn_2O_5 projected along the c -axis. Filled circles represent Ho^{3+} ions, large circles are anions, small circles manganese ions. Relative levels of anions and Mn ions are indicated by light and heavy circles.

The second of these structure types is that of aeschynite, CaTa_2O_6 , which has this structure, has an orthorhombic unit cell, space group $Pnma$, with $a = 11.068\text{\AA}$, $b = 7.505\text{\AA}$, $c = 5.378\text{\AA}$ (Jahnberg, 1963). Atoms occupy the following positions:

Ta in	$8d$	0.1412	0.9944	0.0376
Ca	$4c$	0.042	0.25	0.540
O(1)	$8d$	0.976	0.035	0.225
O(2)	$8d$	0.213	0.049	0.383
O(3)	$4c$	0.146	0.25	0.967
O(4)	$4c$	0.122	$\frac{3}{4}$	0.162

It consists of a $\text{Ta}_2\text{O}_6^{2-}$ framework formed by corner-sharing of edge-shared double octahedra, as shown in fig. 28.52. Ca^{2+} ions occupy $b.t.p.$ sites within this framework. Rare earths occur in this structure in compounds of the types

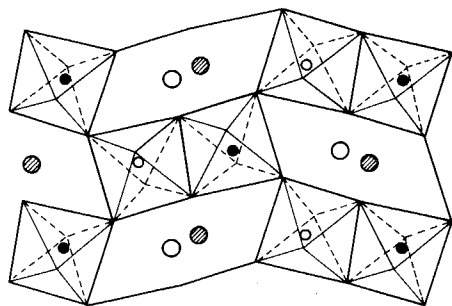
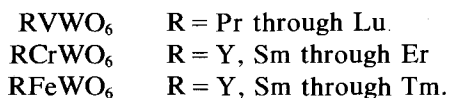
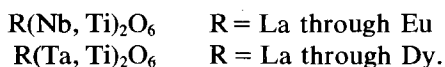


Fig. 28.52. The atom positions of the aeschynite-type structure of CaTa_2O_6 projected along $[001]$ after Jahnberg (1963). The cation ordering shown is that found in YbVWO_6 . Large circles then indicate R^{3+} ions at two levels, small filled circles represent vanadium ions and small open circles tungsten ions. (After Jahnberg, 1963).

ARWO_6 (Salmon et al., 1974; Salmon and Le Flem, 1972)



and $\text{R}(\text{B, Ti})_2\text{O}_6$ (Aleksandrov, 1963; Sych and Klenus, 1973)



In all of these compounds the rare earth ions occupy the $4c$ sites, while the remaining cations are either randomly distributed on the $8d$ sites, as in LaTiNbO_6 (Fauquier and Gasperin, 1970), or ordered on these sites as in YbVWO_6 (Salmon et al., 1974). In this latter case, this cation ordering results in a reduction of symmetry to $Pn2_1a$. A related structure, that of euxenite, is found if yttrium earths replace the cerium rare earths in the above compounds. The euxenite structure is also orthorhombic with $a = 5.604\text{\AA}$, $b = 14.68\text{\AA}$, $c = 5.237\text{\AA}$ for GdNbTiO_6 (Aleksandrov, 1963).

5.5. Structures related to A-type R_2O_3 : the Ψ -phases.

The occurrence of the so-called Ψ -phases in some of the systems $\text{ThO}_2\text{-R}_2\text{O}_3$ has already been described briefly in 3.2.1., and many similar phases have been reported by Sibieude et al. (1974) in the system $\text{CeO}_2\text{-La}_2\text{O}_3$. Sibieude (1973) has proposed a structural model to account for the observed X-ray diffraction patterns, all of which were indexed assuming a hexagonal (or rhombohedral) one-dimensional superstructure of the A-type sesquioxide: these hexagonal unit cells have dimensions $a = a_A$; $c = n \cdot \frac{1}{2}c_A$, where a_A and c_A refer to the A-type sub-cell parameters and n is an integer. The proposed structures of the Ψ_2 -, Ψ_3 -, and Ψ_4 -phases of the $\text{ThO}_2\text{-La}_2\text{O}_3$ system are shown in fig. 28.53, along with equivalent representations of the fluorite- and A-type unit cells of ThO_2 and La_2O_3 , and represent in effect the ordered intergrowth of elements of fluorite-type structure in an A-type matrix. Such intergrowth of two different structure types is only feasible if the atomic arrangements in each are such as to be compatible across some interface. Thus in the hexagonal A-type structure both

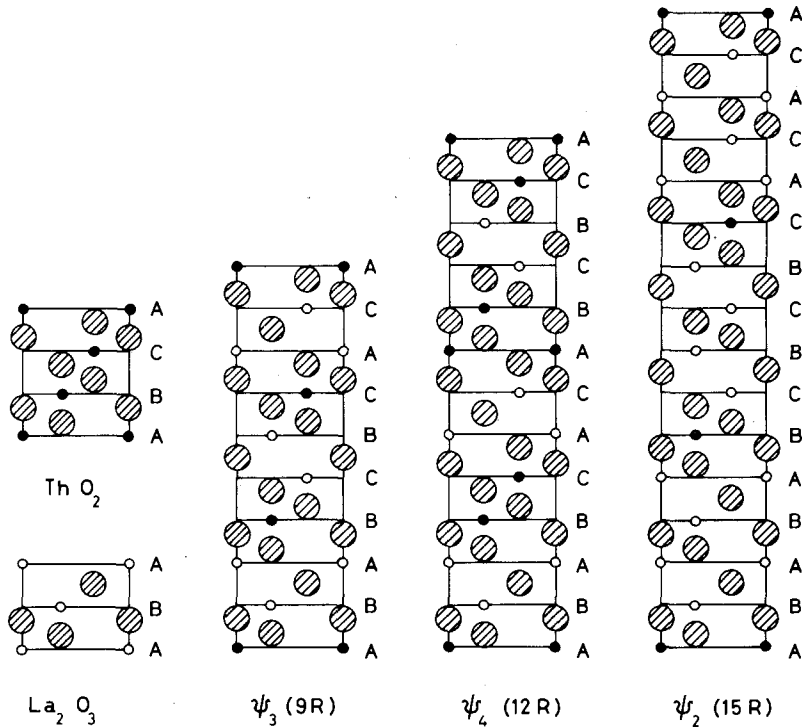


Fig. 28.53. The structures proposed for some ψ -phases in the system $\text{ThO}_2\text{-La}_2\text{O}_3$; reproduced from Sibieude (1973) by courtesy of J. Solid State Chem.

the cations and anions are disposed as in close-packing in layers perpendicular to $[001]_A$, while in the fluorite-type structure a similar disposition of cations and anions occurs in planes perpendicular to $\langle 111 \rangle$. The sequence of layers along these directions respectively, shown schematically, is as follows:

$$\begin{array}{cccccccc}
 \langle 111 \rangle_F & c & A & b & a & B & c & b & C & a \\
 [001]_A & c & A & b & a & B & c & A & b &
 \end{array}$$

Upper-case lettering refers to cations, lower-case lettering to anions, and the notation used is that for close-packed sequences. The compatibility of the two structures in these directions is obvious.

The unit cell of Ψ_3 , as derived from the indexing of the powder pattern, is a 9-fold repeat of the basic half-unit-cell of the A-type structure, and has been described in terms of the cation layer sequence ----ABABCBCAC----: the complete layer sequence can be read from fig. 28.53. An alternative description is that of an ordered sequence of cation stacking faults along $[001]_A$ (the anion layer sequence remains unaltered), and it is tempting to propose a sequence of fully-ordered cation layers (as Sibieude (1973) did) in which the ratio $\text{Th}^{4+}:\text{La}^{3+}$ is 1:2. However this leads to an incorrect composition (66.7 mole % $\text{LaO}_{1.5}$, instead of the observed 75 mole % $\text{LaO}_{1.5}$), so the implication is that the

intergrown fluorite-type phase is a solid solution of composition of 75 mole % ThO_2 if it is assumed that all the Th^{4+} cations are in the fluorite-type layers.

A very recent electron microscope study of the related phases occurring in the system $\text{CeO}_2\text{-La}_2\text{O}_3$ has been carried out by Sibieude et al. (1976)

and the results strongly support the essentials of the postulated model. Fig. 28.54 shows a high-resolution lattice image, obtained with a small number of 001 reflections, in which fringes corresponding to the 6.1\AA spacing of the $(001)_A$ planes of the sub-cell are present along with more widely-spaced but parallel fringes which are interpreted as arising from the presence of stacking faults. However, the spacing of these latter is not quite regular, which shows that the stacking faults are not fully ordered. Thus no clearly-defined unit cell of the superstructure can be derived, although the average spacing of the stacking fault fringes (40.3\AA) is close to one sixth of the c -parameter (247.6\AA) derived from the X-ray diffraction data. Similar results were obtained for other compositions. It is perhaps significant that the composition of the sample from which the comparatively well-ordered stacking fault fringe pattern was obtained (fig. 28.54) was 91.9 mole % $\text{LaO}_{1.5}$, corresponding closely to that of the Ψ_1 -phase reported for the $\text{ThO}_2\text{-La}_2\text{O}_3$ system.

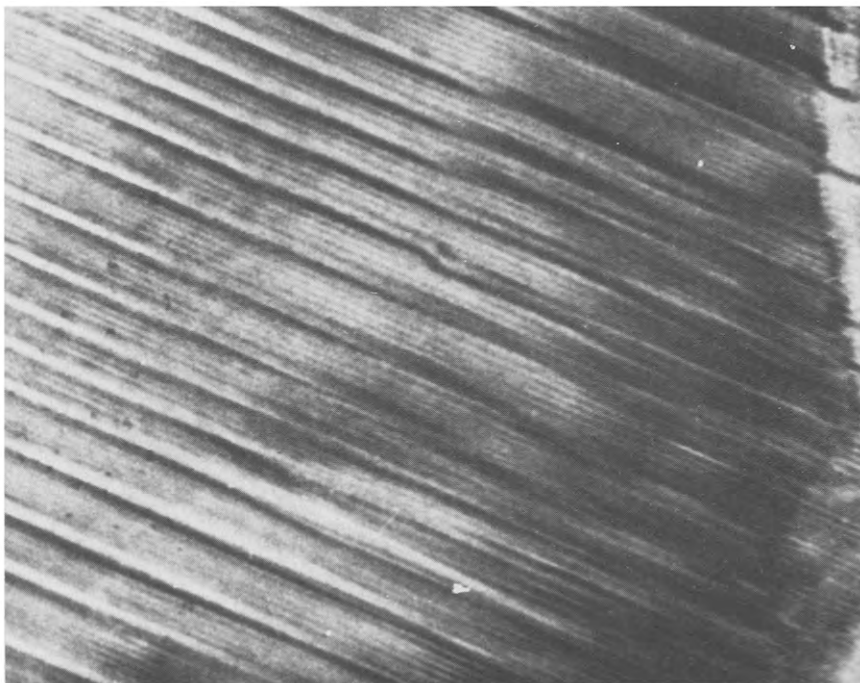


Fig. 28.54. High-resolution lattice image of a ψ -phase in the $\text{CeO}_2\text{-La}_2\text{O}_3$ system showing closely-spaced fringes corresponding to the $(001)_A$ interplanar spacing and more or less ordered stacking faults: reproduced by courtesy of Dr. F. Sibieude.

5.6. Fluorite-related structures

The fluorite structure itself is well-known. The unit cell is face-centred cubic, space group $Fm\bar{3}m$, and the cell edge is commonly about 5.5\AA . There is a face-centred cubic array of cations on the $4a$ sites at $0, 0, 0$; and a primitive cubic array of anions on the $8c$ sites at $\frac{1}{4}, \frac{1}{4}, \frac{1}{4}$. The structure can be described either as edge-shared MO_8 cubes or edge-shared OM_4 tetrahedra.

This basic structure type figures very prominently in much of the solid-state chemistry of the rare earth oxides. Already, in discussing phase relationships, much has been made of the great difference in temperature at which the anion and cation sub-lattices achieve significant mobility. This property and the apparent stability of this structure type, even in grossly non-stoichiometric phases, for anion to cation ratios both greater than and less than two, marks it as rather unique. However, this section of the discussion is not concerned so much with the grossly non-stoichiometric phases *per se* as with the ordered intermediate phases which occur in a variety of systems at particular ideal compositions, all of which have in common a close structural relationship to the fluorite-type parent. These fluorite-related superstructures occur with anion to metal ratios both less than and greater than 2.0.

5.6.1. Structures related to UY_6O_{12}

(i) Phases of stoichiometry M_7O_{12} . The most common of the $\text{R}_{7-x}\text{M}_x\text{O}_{12}$ structures is that of UY_6O_{12} . While a description of this structure has been given in ch. 27, the following points should be included here. This structure can be described in terms of a triply primitive hexagonal unit-cell with parameters typified by those of UY_6O_{12} , which, according to Aitken et al. (1964), are $a = 9.934\text{\AA}$, $c = 9.364\text{\AA}$. The c -axis of this unit cell coincides with both the $[111]$ axis of the primitive rhombohedral unit cell and one of the $\langle 111 \rangle$ axes of the MO_8 fluorite cube. In terms of the hexagonal unit cell, atoms occupy the positions in space group $R\bar{3}$ given below:

U^{6+}	in	$3a$	0	0	0
Y^{3+}		$18f$	0.1224	0.4170	0.0235
O		$18f$	0.191	0.032	0.117
O		$18f$	0.140	0.447	0.268
V		$6c$	0	0	$\frac{1}{4}$

(V refers to a vacant anion site relative to fluorite).

Numerous structure refinements have been performed on isomorphous phases by X-ray powder diffraction (Bartram, 1965; Thornber et al., 1968; Thornber and Bevan, 1970; Rossell, 1976), by neutron powder diffraction (von Dreele et al., 1975), and by single crystal X-ray diffraction (Latavalya, 1976). The UY_6O_{12} structure is a fluorite superstructure resulting from the ordering of cations and formal anion vacancies. These vacancies occur in pairs across the body diagonal of MO_8 cubes so that the special metals in the hexagonal unit cell become

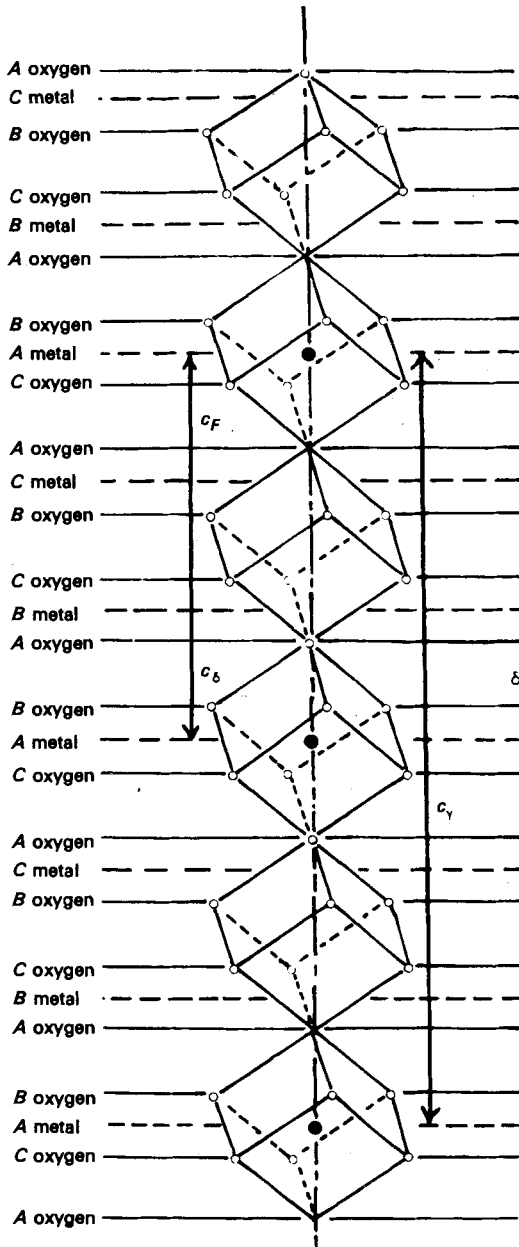


Fig. 28.55. The relationship between the δ -($\text{Zr}_3\text{Sc}_4\text{O}_{12}$) and γ -($\text{Zr}_{10}\text{Sc}_4\text{O}_{26}$) phase structures. The former has strings of anion vacancies along the c -axis, the latter has pairs of vacancies along this axis. (Reproduced from Thornber et al., 1968, with permission of J. Solid State Chem.).

six-coordinated. The remaining six anions have relaxed towards the vacancy so that the special cations have distorted octahedral coordination. The structure is shown in fig. 28.55. Relative to fluorite, the surrounding six cations have relaxed away from the anion vacancy, and their resulting coordination will be between two extremes. One extreme type of coordination is that found in $\text{Zr}_3\text{Sc}_4\text{O}_{12}$

(Thornber et al., 1968) where there are seven anions surrounding the $M(2)$ cation with no substantial disparities in the $M(2)$ -O bond lengths, e.g. in $Zr_3Sc_4O_{12}$ five anions lie between 2.06–2.16Å; the remaining anions lie at distances of 2.34Å and 2.40Å. In the second extreme type of coordination six anions lie much closer to the $M(2)$ cation than the seventh, e.g. in $Ti_3Sc_4O_{12}$ six $M(2)$ -O bond lengths lie between 2.03–2.13Å and the seventh anion lies at 2.65Å (Rossell, 1976). The resulting structure consists of strings of formal anion vacancies parallel to the hexagonal c -axis so that the cations on these strings are six-coordinated and all other cations are seven-coordinated. Thornber et al. (1968) identified an I-unit, composed of one six-coordinated and six seven-coordinated cations with their surrounding anions; these are stacked parallel to the c -axis to produce this structure as shown in fig. 28.56(a). Von Dreele et al. (1975) used a unit half this size, containing the six- and three of the seven-coordinated cations to arrive at a similar structural description.

In all of the phases for which structure refinements have been performed, with but two exceptions, the cations are at least partially ordered. Where the cation molar ratios are 1:6, as in UY_6O_{12} or $NbSc_6O_{11}F$ (Rossell, 1976) complete cationic order exists, with the smaller cation on the special octahedral site. Where the cation ratio is not 1:6, as in $M_3^4R_4^3O_{12}$, one of the small M^{4+} ions occupies the special site and the remaining M^{4+} and R^{3+} ions are randomly distributed on the general site. The only phases for which complete cationic disorder has been observed are $Zr_3Sc_4O_{12}$ (Thornber et al., 1968) and a high-temperature form of $Zr_3Yb_4O_{12}$ (Thornber and Bevan, 1970). A partially-ordered form of $Zr_3Yb_4O_{12}$ was also reported by Thornber and Bevan (1970) and the

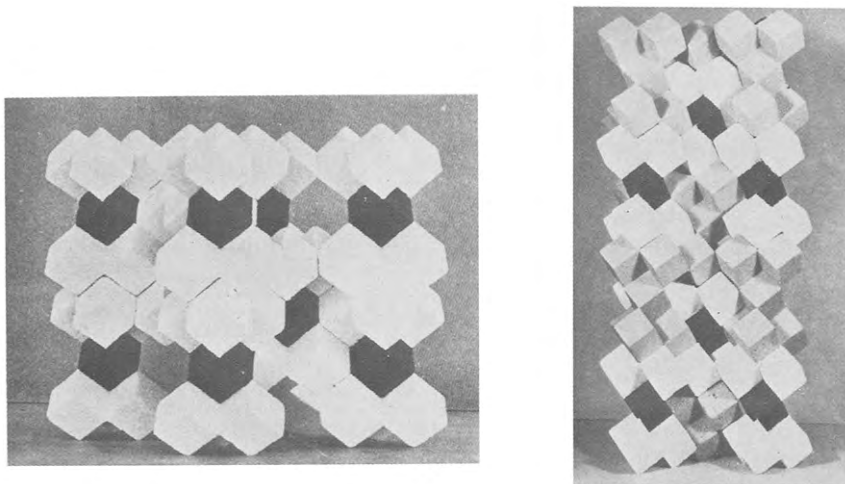


Fig. 28.56(a, b). The structures of δ - $Zr_3Sc_4O_{12}$ and γ - $Zr_{10}Sc_4O_{26}$ as packings of I- and 7F- units, reproduced from Thornber et al. (1968), with permission of J. Solid State Chem. Grey cubes represent MO_8 cubes, white cubes MO_7 polyhedra, and black cubes MO_6 "octahedra" with two anions of an MO_8 cube missing across a cube body-diagonal. The γ -phase consists of an ordered arrangement of I- and 7F- units.

fully-ordered form by both Latavalya (1976) and Rossell (1976). Rossell (1976) found $\text{Hf}_3\text{Sc}_4\text{O}_{12}$ to have slight cationic order, with Hf showing a preference for the special site. Those compounds isostructural with UY_6O_{12} are listed in table 28.8.

The nature of M_7O_{12} phases involving tungsten and the lighter rare earths appears to depend substantially on the preparative temperature. At 1400°C such phases appear to be defective pyrochlores of formula $\text{R}_2(\text{RW}_{1/2})\text{O}_{7-1}$ (Chang and Phillips, 1964), whereas at lower temperatures (1250°C) lower symmetry phases, described as pseudo-cubic, have been obtained (McCarthy^{et al.} 1972; Trunov et al., 1968).

(ii) Phases of stoichiometry $\text{M}_{14}\text{O}_{26}$. The first fluorite-related phase of this composition was reported by Lefèvre (1963) for $\text{Zr}_{10}\text{Sc}_4\text{O}_{26}$ —the so-called γ -phase of the ZrO_2 - $\text{ScO}_{1.5}$ system. This phase is rhombohedral, space-group $R\bar{3}$, with hexagonal parameters $a = 9.53\text{\AA}$, $c = 17.44\text{\AA}$ (Thorner et al., 1968). The unit cell is therefore similar to that of the δ -phase ($\text{Zr}_3\text{Sc}_4\text{O}_{12}$) except for a doubled c -axis. Atoms occupy the positions as follows:

M(1) in	$3a$	0	0	0	O(1)	$18f$	0.1972	0.1976	0.0569
M(2)	$18f$	0.2222	0.1905	0.1721	O(2)	$18f$	0.2066	0.0421	0.2044
M(3)	$18f$	0.2310	0.0427	0.3266	O(3)	$18f$	0.2161	0.2572	0.2929
M(4)	$3b$	0	0	$\frac{1}{2}$	O(4)	$18f$	0.2444	0.0790	0.4540
					O(5)	$6c$	0	0	0.3523

The structure is related to that of the M_7O_{12} phases (δ -phase) by the insertion of pairs of anions into the vacancy strings of the latter such that the atom sequence along these rows is VMVOMVMVOMO etc. (V = vacancy, M = cation, O = oxygen). Both structures are depicted in fig. 28.55. Each anion pair

TABLE 28.8
Occurrence and references for ternary phases of composition M_7O_{12} involving the rare earths.

	Gd	Tb	Dy	Ho	Y	Er	Tm	Yb	Lu	Sc
Ti										1, 11
U	2	2	2	2	2	2	2	2	2	
W	4	3, 4	3, 4	3, 4	3, 4, 5	3, 4	3, 4	3, 4	3, 4	
Mo						6	6	6	6	
Te	6	6	6	6	6	6	6	6	6	6
Zr						7-10	7-9	7-10	11	8-10
Hf								11		10, 12
Nb										10
Sn										11
Np	13	13	13	13	13	13	13	13		

Others include UR_6O_{12} -R = La-Eu(2) $\text{ReY}_6\text{O}_{12}$ (13)
 $\text{NbSc}_6\text{O}_{11}\text{F}$ (10) $\text{NpR}_6\text{O}_{12}$ -R = La-Eu(13).

References: 1. Komissarova et al. (1966). 2. Aitken et al. (1964). 3. Chang and Phillips (1964). 4. McCarthy et al. (1972). 5. Borchardt (1963). 6. Blasse (1969). 7. Collongues et al. (1965). 8. Thorner et al. (1968). 9. Thorner et al. (1970). 10. Rossell (1976). 11. Brisse and Knop (1968). 12. Kalinovskaya et al. (1969). 13. Keller et al. (1969).

completes an MO_8 cube, converting an I-unit (M_7O_{12}) into an M_7O_{14} (the so-called 7F) unit. Thus the γ -phase structure is composed of alternating I- and 7F-units stacked parallel to the hexagonal c -axis ($[111]_F$) as shown in fig. 28.56(b). Thornber et al. (1968) described this structure as an intergrowth of fluorite and δ in a ratio of 1:1.

At first sight the γ -phase appears to be unique, with no analogues in either the binary or ternary systems containing rare earth oxides. However a number of ternary phases have been reported to have stoichiometries close to that of γ , where the O/M ratio is 1.857. These include the phases $7\text{R}_2\text{O}_3 \cdot 4\text{WO}_3$, for $\text{R} = \text{Sm}, \text{Dy}, \text{Eu}, \text{Ho}$ (Chang and Philp, 1964; Ivanova et al., 1972; McCarthy et al., 1972; McCarthy and Fisher, 1971) where the O/M ratio is 1.833, the phase tentatively identified as $11\text{Er}_2\text{O}_3 \cdot 6\text{WO}_3$ (Trunov et al., 1968) with an O/M ratio of 1.821, the X-phase in the $\text{Y}_2\text{O}_3\text{-WO}_3$ system, reported by Borchardt (1963), and its analogue $3\text{La}_2\text{O}_3 \cdot 2\text{WO}_3$, found by Ivanova et al. (1970). These last two have an O/M ratio of 1.875. McCarthy and Fischer (1971) were able to index the diffraction patterns of both $\text{Ho}_{14}\text{W}_4\text{O}_{33}$ by analogy with the R_6WO_{12} phases, but the c -axis had to be doubled and the rhombohedral condition ($-h + k + l = 3n$) had to be relaxed. Thus for $\text{Ho}_{14}\text{W}_4\text{O}_{33}$ the lattice parameters are $a = 9.752\text{\AA}$, $c = 18.796\text{\AA}$. The unit cells of these phases are therefore analogous to that of $\text{Zr}_{10}\text{Sc}_4\text{O}_{26}$ except that the symmetry is apparently hexagonal or primitive trigonal. The volume of this unit cell is then $3(\text{M}_{14}\text{O}_{28-x})$ so that the ideal composition cannot be any of those given above. The only likely composition would appear to be $\text{R}_{32}\text{W}_{10}\text{O}_{78}$ with an O/M ratio of 1.857, that of the γ -phase. Further structural details can be predicted if the assumption is made that this phase, like γ , is composed of I- and 7F-units. An I-unit (M_7O_{12}) in the $\text{R}_2\text{O}_3\text{-WO}_3$ system would have fully ordered cations as in UY_6O_{12} i.e. the I-unit must have the composition $\text{W}^{6+}\text{R}_6^{3+}\text{O}_{12}$ for electrical neutrality. The 7F-units then have a composition of $\text{W}_{7/3}^{6+}\text{R}_{14/3}^{3+}\text{O}_{14}$ with the W^{6+} and R^{3+} ions probably randomly distributed. The "hexagonal" unit cell would then contain three I- and three 7F-units distributed as in the γ -phase. This unit cell would be rhombohedral; presumably the deviation from this condition is due to additional cation ordering, but a complete structural analysis is obviously required.

If a γ -phase does exist in the tungstate systems its absence in other fluorite-related systems could be queried. Does the observed absence of a γ -phase in these systems correspond to equilibrium, or is the situation simply confused by the fact that the temperatures at which cation order could occur and the temperatures at which a cation-ordered γ -phase could exist show no overlap for conventional preparative methods? In other systems where the cation radii are dissimilar the requirement of cation order has been demonstrated if an M_7O_{12} phase is to exist, and is implied for the $\text{M}_{42}\text{O}_{78}$ phases. Thus Rossell (1976) has shown that cation ordering required 4-7 days at 1400°C for $\text{Zr}_3(\text{Yb/Er})_4\text{O}_{12}$ if coprecipitated samples are used, but months for arc-melted samples. This difference in ordering times is probably due to differing levels of partial order in the disordered state. In addition, the reordering that was observed to occur in four days at 1400°C after disordering at 1600°C is probably also commencing

from a partially-disordered state i.e. the sample did not completely disorder on heating at 1600°C. The anion pairs may disorder completely (especially since other Zr^{4+} ions occur in the unit cell), but while some of the Zr^{4+} cations shift off the special site, they probably do not shift far from their ordered positions during the disordering process. Thornber et al. (1970) found that below 1100°C in the ZrO_2 - $ErO_{1.5}$ system the rate of cation ordering was so low that $Zr_3Er_4O_{12}$ was only observed as a very minor constituent of the samples. These facts raise the possibility that a γ -phase may exist in this and related systems, but has not yet been observed because cation mobility has not been achieved in the temperature range where this phase is stable (cf. the discussion in 3.2.3). If this phase does exist in MO_3 -based systems it could certainly be expected in other ZrO_2 -based systems. Moreover, it can be suggested that the compounds which form in the ZrO_2 - $ScO_{1.5}$ system without cation order may well be the equilibrium phases in related systems when cation order is achieved at the appropriate temperature. Certainly however, no equilibrium data are available for zirconia-based systems below $\sim 1200^\circ\text{C}$.

The composition region between $Zr_3Sc_4O_{12}$ and $Zr_{10}Sc_4O_{26}$ has been the subject of a number of investigations. As mentioned elsewhere, Lefèvre (1963) indicated that the δ -phase becomes non-stoichiometric at high temperatures, and there is the possibility of a continuous structural transition between it and the γ -phase above 2000°C. Conversely Ruh (1968) indicated that both phases were grossly nonstoichiometric at all temperatures investigated and were separated by a narrow diphasic region. During an investigation of this composition region quenched arc-melted samples were examined by both powder X-ray diffraction and electron diffraction. With X-ray diffraction the samples were found to be monophasic, but a gradual evolution of the structure from that of the δ -phase to that of the γ -phase occurred (Thornber et al., 1970). Selected area electron diffraction, however, showed the samples to be heterogeneous, (Summerville, 1973), some specimen areas being γ , others δ , and others showing either split superstructure reflections or the presence of satellite reflections. An analysis of the unusual superstructure effects was carried out by examining the geometrical part of the structure factors of $00l$ (hex) reflections from large supercells based on intergrowth of I- and 7F-units, and the conclusion reached was that these effects probably resulted from incipient phase separation. Thus the cation sublattice contains compositional modulations; in regions where the local composition is close to $Zr_{10}Sc_4O_{26}$ the γ -phase structure occurs, and in other regions where the local composition is close to $Zr_3Sc_4O_{12}$ the δ -phase structure exists. The anion array adjusts to maintain local charge balance. However, it should be emphasised that this phase separation occurs in an ordered fashion, so much so that long-period superstructures are observed.

Similar problems appear to exist in R_2O_3 - WO_3 systems. Thus Chang and Phillips (1964) indicate increasing stoichiometric ranges of the M_7O_{12} and $M_{42}O_{78}$ phases at higher temperatures. Conversely Ivanova et al. (1970) report both of these phases to be grossly non-stoichiometric at all temperatures as shown in fig.

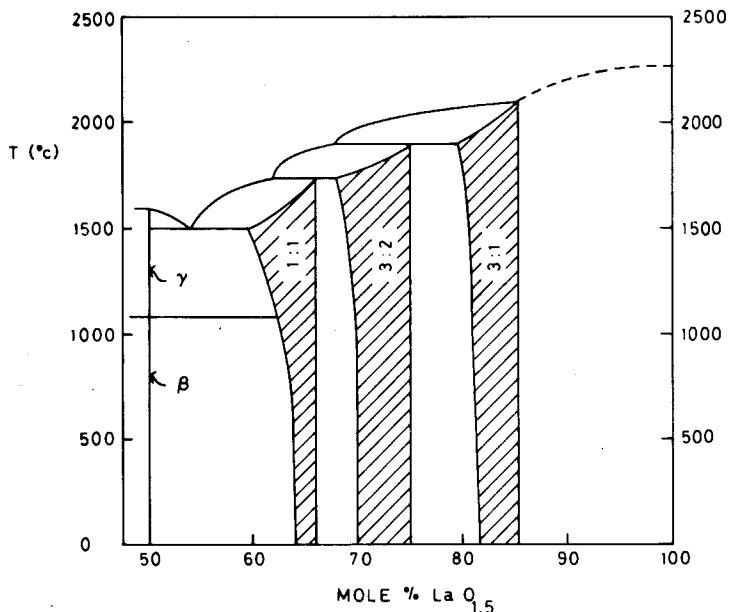


Fig. 28.57. Phase diagram of part of the La_2O_3 - WO_3 system after Ivanova et al. (1970). Phase designations are those used in the original phase diagram and refer to mole ratios of La_2O_3 : WO_3 .

28.57. Several researchers have reported the presence of other ordered phases in this composition region. These include $\text{R}_{10}\text{W}_2\text{O}_{21}$ [where $\text{R} = \text{Dy}$ (Ivanova and Reznik, 1972), Ho (McCarthy and Fisher, 1971), Y (Borchardt, 1963), Gd through Ho and Y (McCarthy et al., 1972)], Nd_4WO_9 (Rode and Harpov, 1966) and $\text{Y}_{18}\text{W}_4\text{O}_{41}$ (Borchardt, 1963).

(iii) The beta phase in $\text{ZrO}_2(\text{HfO}_2)$ - $\text{ScO}_{1.5}$ systems. A number of reports of a phase with a composition of ~ 22 mole % $\text{ScO}_{1.5}$ occur in the literature (Lefèvre, 1963; Strickler and Carlson, 1963; Kalinovskaya et al., 1969; Spiridonov et al., 1970). Because of its composition, its stoichiometry has often been assumed to be $\text{Zr}_7\text{Sc}_2\text{O}_{17}$ (22.22 mole % $\text{ScO}_{1.5}$). However, indexing of electron diffraction patterns and X-ray powder diffraction patterns by Thornber et al. (1970) has shown that the true unit cell of this phase is rhombohedral, space group probably $R\bar{3}$, with hexagonal parameters of $a = 19.801\text{Å}$, $c = 17.996\text{Å}$. The rhombohedral unit cell then contains 62 cations, so that the most likely composition is $\text{Zr}_{48}\text{Sc}_{14}\text{O}_{117}$ (22.58 mole % $\text{ScO}_{1.5}$). If this composition is correct, this phase is unusual in having an odd number of anion vacancies (seven) per unit cell. Refinement of X-ray data from this structure is currently being attempted. As pointed out above, while the ZrO_2 - $\text{ScO}_{1.5}$ system appears to be an odd-ball it may in fact be the only system which isn't odd, and while this phase has not been reported in related systems this may only be because of the difficulty of attaining equilibrium below 600°C .

5.6.2. Compounds with the pyrochlore structure

Compounds with stoichiometry $A_2B_2O_7$ often form with the pyrochlore structure. The unit cell of this structure is face-centred cubic, space group $Fd\bar{3}m$, with double the cell-edge of the fluorite-type structure. Because different workers have chosen different origins the literature is somewhat confusing as to the atom parameters, but this has been clarified by Sleight (1968). With the origin chosen at a centre of symmetry, atoms occupy the positions

R^{3+}	in	$16c$	$0, 0, 0$
M^{4+}		$16d$	$\frac{1}{2}, \frac{1}{2}, \frac{1}{2}$
O		$8a$	$\frac{1}{8}, \frac{1}{8}, \frac{1}{8}$
O		$48f$	$x, \frac{1}{8}, \frac{1}{8}$

For $Er_2Ti_2O_7$ (Knop, et al., 1965) $x = 0.42$. With $x = \frac{3}{8}$ these $48f$ anions would occupy normal fluorite-type anion sites, but the remaining fluorite-type anion sites ($8b$ of the $Fd\bar{3}m$ space group with coordinates $\frac{3}{8}, \frac{3}{8}, \frac{3}{8}$) are unoccupied. The "vacancies" occur in pairs across the body-diagonals of MO_8 cubes in such a way as to form chains of six-coordinated cations parallel to each of the $\langle 110 \rangle$ (fluorite) directions (fig. 28.58). The structure also has the "vacancies" arranged to produce the maximum number of six-coordinated cations, and this is done without affecting the coordination number of any other cation. The six-coordinated cations are the B-cations (usually M^{4+}) while the remaining A-cations (often R^{3+}) have eightfold scalenohedral coordination.

In an alternative, very elegant description the pyrochlore structure is seen as a tunnel structure with a continuous three-dimensional B_2O_6 framework of corner-sharing octahedra, the remaining A_2O atoms being in the tunnels as shown in fig.

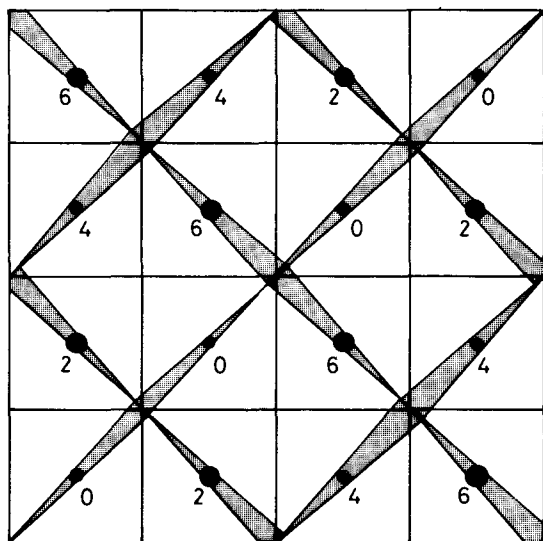


Fig. 28.58. Diagrammatic representation of a projection of the ideal pyrochlore structure along $[100]$. Anions occur at the corners of the cube-projections. Cations occur at different levels as indicated by the different sized circles. The heights of six-coordinated cations are indicated by their height in eighths of a unit-cell edge and the "anion vacancies" responsible for this reduction in coordination number are indicated by the sloping bars. Thus a zig-zag chain of ideal anion vacancies at levels of $1/8$ and $7/8$ results in the $[110]$ string of six coordinated cations at level 0.

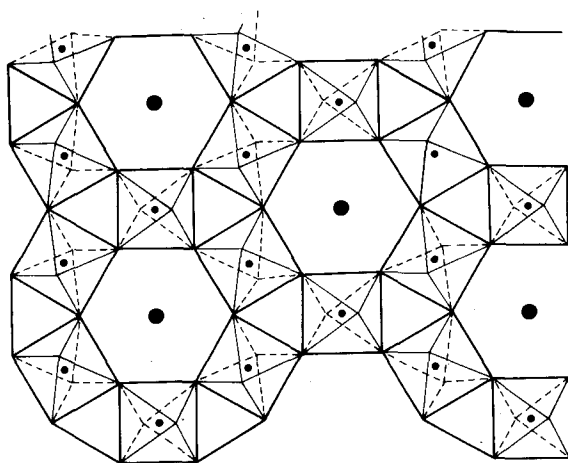


Fig. 28.59. The tunnel representation of the pyrochlore structure projected along [111] (after Knop et al., 1965). The relationship between this projection and that along [001] of a hexagonal tungsten bronze is obvious but in the pyrochlore these "tunnels" run along all $\langle 111 \rangle$ directions (Hyde, B.G., personal communication). The BO_6 octahedra are shown along with the projection of the A atoms in the "tunnels".

28.59. This description correlates well with the physical properties of pyrochlore e.g. the $\text{M}^{4+}\text{-O}(2)$ distances are normal for octahedral coordination of the 4+ ion but the six $\text{M}^{3+}\text{-O}(2)$ bonds are much longer than usual (Knop et al., 1965). The two $\text{M}^{3+}\text{-O}(1)$ bonds between atoms in the tunnels are of normal length. Furthermore, both cation and anion deficiency has been found within the tunnels of $\text{Ce}_{1.56}\text{Sb}_2\text{O}_{6.37}\text{F}_{0.44}$ (Aia et al., 1963), but while this may be possible where a clearly-defined covalent framework is present, the issue is less clear in more ionic compounds.

As mentioned earlier, the pyrochlore phases in fluorite-related systems are grossly non-stoichiometric on both sides of the ideal composition. If the fluorite description of the pyrochlore structure is correct this range of stoichiometry can be accommodated simply by introducing anion vacancies or interstitials at random and adjusting the $\text{M}^{4+}/\text{R}^{3+}$ ratio appropriately. While this may be counter to much current thought on defect structures, such a process would leave the cation sub-lattice intact and introduce defects only into the anion sub-lattice. However, if the structure is fundamentally a framework structure containing an assortment of inserted anions and cations then any defects in the structure could be expected to occur in the tunnels, leaving the framework intact. The observed stoichiometry could then be accommodated on the MO_2 -rich side by the creation of cation vacancies in the tunnels and substitution of M^{4+} for R^{3+} , leading to an extreme composition of $\text{M}_2^4\text{O}_6 \cdot \text{M}_{3/2}^4\text{O}$ (or MO_2). On the R_2O_3 -rich side, non-stoichiometry could be accommodated by formation of anion vacancies in the tunnel and substitution of R^{3+} for M^{4+} in the framework. Again, no obvious composition limit would occur up to $\text{R}_2^3\text{O}_6 \cdot \text{R}_{3/2}^3$ (or pure sesquioxide). An alternative suggestion has been made by Ault and Welch (1966) for accommodation of non-stoichiometry if the framework description of the pyrochlore structure is correct. Their suggestion is that both anionic and cationic occupancy in the tunnels is variable, requiring only charge balance. On this basis MO_2 -rich pyrochlores exist via vacancies of R^{3+} and O^{2-} in the tunnels with a limiting

composition of $M_2^{4+}O_6 \cdot R_{4/3}^{3+}$ or 40 moles % $RO_{1.5}$. This lower limit does not conform with observations in other systems and it is difficult to see how R_2O_3 -excess could be accommodated. In the context of previous assertions about the essentially-complete cation sub-lattice in fluorite-related systems, it seems that the framework description is less likely to be applicable than the defect fluorite description unless the pyrochlore structure is not as closely related to the fluorite-type as has been assumed. This matter could be simply resolved by density measurements of MO_2 -rich pyrochlores.

Regardless of which of the above descriptions is appropriate, accommodation of non-stoichiometry is accompanied by substitution of M^{3+} ions on M^{4+} sites or vice versa. This has enabled Perez y Jorba (1962) to describe the ranges of stoichiometry of ZrO_2 - R_2O_3 pyrochlores in terms of two factors:

(i) The ease with which R^{3+} and Zr^{4+} ions can be interchanged. The closer the radii of the two ions the wider the phase field can be.

(ii) The range over which cationic substitution can occur whilst allowing the ratio $r(A)/r(B)$ to remain above the limit of 1.2 set by the pyrochlore structure, $r(A)$ and $r(B)$ being the average radii of the cations on the A and B sites respectively. Thus when R^{3+} replaces the Zr^{4+} within the framework, $r(B)$ is increased and $r(A)/r(B)$ decreased. As the proportion of R^{3+} increases this ratio decreases until the limiting value of 1.2 is attained. Conversely, as the proportion of ZrO_2 is increased beyond the stoichiometric value, Zr^{4+} enters the A site, so decreasing $r(A)$ and the ratio $r(A)/r(B)$. Again a limiting composition is reached beyond which this ratio is less than 1.2.

Table 28.9 shows the observed and calculated ranges obtained by Perez y Jorba (1962). It can be seen that the agreement between the observed ranges and those calculated on the basis of the average ionic radii of the species on the A and B sites is excellent for $R^{3+} = Nd, Sm, Gd$. For these systems $r(R^{3+})$ is apparently sufficiently close to $r(Zr^{4+})$ that interchange presents no problem. However the observed range for ZrO_2 - La_2O_3 is much narrower than that calculated using the average ionic radii of the species on the A and B sites, indicating that in this case the limiting factor is the difference in ionic radius between Zr^{4+} and La^{3+} .

Solid solutions between $A_2Zr_2O_7$ and $A'_2Zr_2O_7$ can be obtained if the ratio

TABLE 28.9
Stability regions of pyrochlore phases as observed and calculated by Perez y Jorba (1962). Composition in moles % $RO_{1.5}$.

System	Observed range	Calculated range
La_2O_3 - ZrO_2	40.0-57.1	21.6-72.4
Nd_2O_3 - ZrO_2	32.2-64.9	32.1-65.0
Sm_2O_3 - ZrO_2	38.1-60.1	38.2-59.6
Gd_2O_3 - ZrO_2	45.3-54.5	44.6-55.0

$r(A')/r(A)$ is between 1.0 and 1.22. Thus complete solid solution exists between $\text{Gd}_2\text{Zr}_2\text{O}_7$ and $\text{Sm}_2\text{Zr}_2\text{O}_7$ ($r(\text{Sm}^{3+})/r(\text{Gd}^{3+}) = 1.03$) and the pyrochlore ($\text{Dy}_{0.1}\text{Gd}_{0.9}$) $_2\text{Zr}_2\text{O}_7$ ($r(\text{Gd}^{3+})/r(\text{Dy}^{3+}) = 1.05$) can be formed. Surprisingly, however, no pyrochlore exists in the $\text{ZrO}_2\text{-La}_2\text{O}_3\text{-Dy}_2\text{O}_3$ system where the corresponding ratio equals 1.24. Despite the fact that $r(\text{La}^{3+})$ is tending to be too large for the pyrochlore structure, it might have been expected that addition of Dy^{3+} would have aided pyrochlore formation by reducing the average $r(\text{R}^{3+})$, but this is evidently not the case.

Identification of systems containing a pyrochlore-type phase is often extremely difficult because of the similarity of this structure to that of fluorite. Thus the cation sub-lattices of these two structures are identical except for the order present in the pyrochlores, and unless there is a substantial difference in the scattering factors of the two cation types in the pyrochlore there will be little indication of this order in the diffraction pattern. Similarly, the only ways in which the pyrochlore anion array differs from that of fluorite are that one eighth of the anion sites of the latter are vacant and six sevenths of the remaining anions are shifted from their ideal fluorite sites. In most relevant systems any contribution from the anion sub-lattice would be small and not greatly different from that of a fluorite anion array. Pyrochlore-type compounds of oxides of second transition-series metals and those of light rare earth elements, or of the oxides of third transition-series metals and those of heavier rare earth elements, are relatively difficult to distinguish from fluorite.

Identification is further complicated by the fact that some of the pyrochlores are incompletely ordered. In a study of $\text{Eu}_2\text{M}_2\text{O}_7$ compounds ($\text{M} = \text{Sn}, \text{Ti}, \text{Zr}$) Faucher and Caro (1975), using X-ray and spectroscopic techniques, found varying degrees of order depending on the nature of the sample. Klee and Weitz (1969) have found a transition from ordered pyrochlore to disordered fluorite structures in the HfO_2 and ZrO_2 rare earth pyrochlores. The zirconium compounds, for rare earths above gadolinium, and the hafnium compounds for rare earths above terbium, appeared to have fluorite-type X-ray powder patterns. However, infra-red spectra of $\text{Tb}_2\text{Zr}_2\text{O}_7$ and $\text{R}_2\text{Hf}_2\text{O}_7$ ($\text{R} = \text{Ho}$ through Tm) showed some evidence of pyrochlore-type ordering. In fact both the zirconium and hafnium series of rare earth pyrochlores showed a decrease in the intensity of infra-red adsorption bands characteristic of pyrochlore, and a decrease in intensity of pyrochlore-type superstructure lines in X-ray powder patterns with increase in atomic number of the rare earth. The overall effect is of a continuous transition from the fully-ordered state to the disordered state. However, as mentioned earlier, the decomposition temperatures of zirconium and hafnium pyrochlores decrease with increasing atomic number of the rare earth, and since all of the components used by Klee and Weitz (1969) were prepared at 1500°C it seems quite likely that the disordered phases were prepared above the decomposition temperature of the pyrochlore. This would give the appearance of a transition from order to disorder as sequential compounds were annealed closer and closer to, then above, the disordering temperature. If this is so the actual region of stability of the zirconium and hafnium pyrochlores is greater than

TABLE 28.10
Rare earth compounds with the pyrochlore structure and associated references.

	La	Ce	Pr	Nd	Sm	Eu	Gd	Tb	Dy	Ho	Y	Er	Tm	Yb	Lu	Sc
ZrO ₂	14, 1, 2, 13	2	14	2, 13, 14	14, 2, 7	4, 14	2, 14									
TiO ₂					20	20, 22	20, 14	20	20, 14	20	20	20	20	20, 4	20	
					14, 2, 3, 13	3, 4, 14	3, 2, 13	3, 14	3, 2, 13	3, 14	3, 2, 13	3, 14	3, 14	3, 2, 13	3, 2, 14	
SnO ₂	10			10	10	10	10	10	10	10	15, 10	15, 10	10	15, 10	10	
	13, 15		15	13, 15	15, 7	4, 15	5, 6	5	5, 6	5, 6	5, 6	5, 6	6	5, 6	6, 11	
IrO ₂			5	5, 6	5, 6	5, 6	16	16	16	16	16	16	16	16	11, 16	
RuO ₂					16	16	16	16	16	16	16	16	16	16	16	
PtO ₂			9	8, 9, 12	9, 12	9, 12	9, 12, 8	9	9, 12	9, 8, 12	8, 9, 12	9, 12	9, 12	9, 12	9, 12	9, 12
(Fe, Sb)O ₂					17	17	17	17	17	17	17	17	17	17	17	
OsO ₂			11	11	11	11	11	11	11	11	11	11	11	11	11	
HfO ₂	14		14	14	14	14	14	14	14	14	14	14	14	14	14	
TcO ₂					18											
PdO ₂									18			18				12
GeO ₂									12		12	12	12	12	12	12
MoO ₂					21	21	21	19	19	19	19	19	19	19	19	19

References: 1. Deiseroth and Müller-Buschbaum (1970). 2. Perez y Jorba (1962). 3. Brixner (1964). 4. Faucher and Caro (1975). 5. Montmory and Bertaut (1961). 6. Schneider et al. (1965). 7. Bocquillon et al. (1971). 8. Ostorero et al. (1974). 9. Hoekstra and Gallagher (1968). 10. Brisse and Knop (1968). 11. Shaplygin and Lazarev (1973). 12. Sleight (1968). 13. Roth (1956). 14. Klee and Weitz (1969). 15. Whinfrey et al. (1960). 16. Bertaut et al. (1959). 17. Knop et al. (1968). 18. Muller et al. (1964). 19. Shannon and Sleight (1968). 20. Knop et al. (1969). 21. McCarthy (1971). 22. McCarthy et al. (1969).

indicated in table 28.10, but lower ordering temperatures will have to be used to observe this wider region.

The rare earth antimonates R_3SbO_7 ($R = Nd$ through Yb , including Y) were previously thought to be pyrochlores (Nath, 1970). However, recent studies by Boulon et al. (1974), using optical methods on compounds of the type Y_2BSbO_7 ($B = Ga, Lu, Y$), have shown that the site symmetries of the Y and B sites are different, and that neither has the D_{3d} symmetry of the cations in pyrochlore.

Vinson and Faurie (1973) reported that compounds of the type $M_5Y_3Sb_{18}O_{52}$ are pyrochlores of the form $M_{5/8}R_{3/8}^{3+}Sb_{9/4}O_{13/2}$, with defects in both sub-lattices. These compounds were reported for $Na, Rb,$ and Cs when R was Y ; the K compounds were found for $R = Ce$ through Lu , including Y . However X-ray refinements in space group $Fd3m$ were unsatisfactory with the cations on classical sites, and it was only by allowing the cations to shift from these sites that a satisfactory refinement could be obtained. In itself this is not surprising, since there are three types of cations present; however, it is surprising that an ion as large as Cs can be incorporated into pyrochlore. No details of the coordination polyhedra have been given to allow an assessment of the structure to be made.

A structure often mentioned in the context of deformed pyrochlores is that of weberite which is orthorhombic, space group $Imm2$. $Ca_2Sb_2O_7$ has the weberite structure and has lattice parameters $a = 7.28 \text{ \AA}, b = 7.44 \text{ \AA}, c = 10.18 \text{ \AA}$ (Bystrom, 1944). The weberite structure has seven-coordinated B cations and was suggested by Rooksby and White (1964) as the structure of R_3VO_7 compounds where $R = La, Nd; B = Nb, Ta$. The analogous compounds of the remaining rare earths were identified as having the defect fluorite-type structure, although Rooksby and White (1964) and Dyer and White (1964) felt that cationic ordering should result in a pyrochlore structure. Tilloca et al. (1970) found the

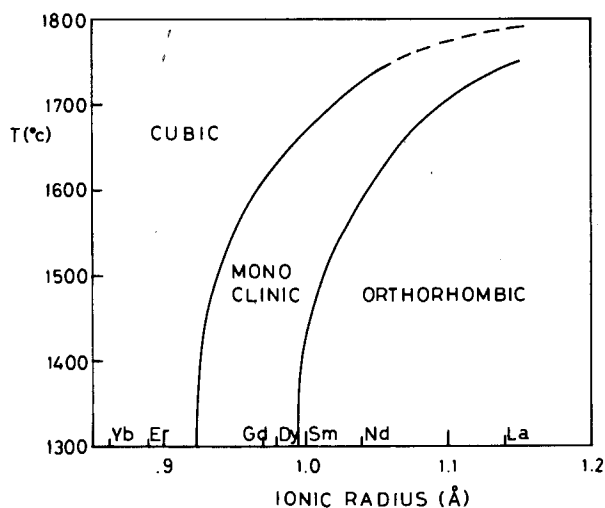


Fig. 28.60. Existence regions of R_3NbO_7 phases (after Collongues et al. 1972).

same unit cell for the La and Nd niobates and showed Sm niobate to be isomorphous. However, they found the space group of single crystals of La_3NbO_7 to be $Pnam$, a result which does not conform to the weberite description. Tilloca et al. (1970) also pointed out that two of the unit cell axes corresponded to $\langle 110 \rangle$ fluorite directions while c corresponded to $2a$ (fluorite). They also observed that the formal fluorite anion vacancies must be disordered because of space group requirements but that the cations could be ordered. Subsequently Collongues et al. (1972) reported that the Eu niobate was monoclinic, space group $P2/m$ with $a = 10.67 \text{ \AA}$, $b = 10.68 \text{ \AA}$, $c = 10.66 \text{ \AA}$, $\beta = 90.42^\circ$. Above 1300°C this phase becomes cubic fluorite, and at 1400°C and 1500°C respectively Sm_3NbO_7 and Gd_3NbO_7 become isomorphous with the low-temperature form of Eu_3NbO_7 . They therefore suggested that the regions of stability of these phases are as shown in fig. 28.60. Recent results by Rossell and Scott (private communication) indicate that the orthorhombic phase extends to holmium, but they found the possible space groups to be $Cmcm$, $Cmc2$, or $C2mc$. They also found that the ordering temperature decreases with increasing atomic number of the rare earth element and observed some interesting ordering effects. Further studies of the structures of these compounds are in progress (Rossell and Scott, private communication).

5.6.3. Fluorite-related structures in rare earth oxide-fluorides

The first report on rare earth oxide fluorides was given by Klemm and Klein (1941) for the system $\text{LaO}_{1.5}\text{-LaF}_3$. These authors described the occurrence of a cubic, fluorite-type solid solution extending from the stoichiometric composition LaOF (LaX_2 : $X = \text{O} + \text{F}$) to the LaF_3 -rich boundary at about $\text{LaX}_{2.45}$. Croatto (1943) later showed from density measurements that the cation sub-lattice of this solid solution was fully occupied, and that the additional anions were therefore incorporated interstitially. Hund (1951) claimed that YOF was dimorphic; fluorite-type at higher temperatures, and having a tetragonally-distorted fluorite-type structure at room temperature, but his specimens contained a slight excess of YF_3 . The situation was clarified somewhat when Zachariasen (1951) showed that both LaOF and YOF existed as stoichiometric phases with identical fluorite-related rhombohedral structures, but that fluoride-rich compositions existed between $\text{RX}_{2.0}$ and $\text{RX}_{2.3}$ in each case with the tetragonal structure. Much subsequent work has shown that ROF is indeed stoichiometric at room temperature and stands on its own as a line-phase in any diagram showing phase relationships. For $R = \text{La}$ through Er , and including Y , the ROF phases are rhombohedral: YbOF and ScOF (and therefore presumably LuOF) have the monoclinic baddeleyite-type structure associated with ZrO_2 . However, at higher temperatures (see table 28.11) these phases transform to the cubic fluorite-type structure, and can then incorporate excess fluoride. While the emphasis in this discussion is on structures rather than phase relationships, it is worth noting for these systems that where fluorite-related phases are concerned phase reactions and order-disorder processes involve predominantly the anion sub-lattice. Since

TABLE 28.11

Crystallographic data for YOF.

Hexagonal cell parameters: $a = 3.797 \pm 0.001 \text{ \AA}$; $c = 18.89 \pm 0.01 \text{ \AA}$. $c/a = 4.97 \pm 0.1$. Cell contents: 6YOFRhombohedral parameters $a = 6.666 \pm 0.002 \text{ \AA}$; $\alpha = 33.09 \pm 0.01^\circ$.Space group $R\bar{3}m$. Cell contents 2YOF.

Atom parameters					Metal-anion distances (\AA) σ		
Atom	x	y	z	$\sigma(z)$	Y-O	2.24	0.02
Y	0	0	0.2412	0.0001	Y-O ¹	2.34	0.02
O	0	0	0.117	0.001	Y-F	2.41	0.02
F	0	0	0.372	0.001	Y-F ¹	2.47	0.02

this is very mobile, quenching techniques are most unlikely to permit retention of high-temperature states which are not stable at lower temperatures (300–400°C). Any adjustment of the uniform cation sub-lattice in response to anion ordering, for example, will be displacive rather than reconstructive, and thus not kinetically hindered. This situation is the direct opposite of that encountered in mixed-cation oxide systems and makes the study of these oxide-fluorides of considerable interest from the point of view of achievement of low-temperature equilibrium.

The structure of the rhombohedral LaOF and YOF phases was first described by Zachariassen (1951) as containing ordered layers of O and F atoms perpendicular to the body diagonal of the rhombohedral cell or to the c -axis of the related hexagonal cell, and a redetermination of the structure of YOF was carried out by Mann and Bevan (1970): it is shown in fig. 28.61. The close relationships to the fluorite-type structure will be apparent from earlier discussion of the hexagonal representation of this. If the O and F atoms shown in fig. 28.61 become randomly distributed in the anion layers a fluorite-type structure results, and this is presumably what happens at higher temperatures in the transformation from rhombohedral to cubic symmetry. However, in fig. 28.61 the ordering sequence of the O and F layers is the inverse of that proposed by Zachariassen (1951), and also by Tanguy et al. (1973) for the structure of EuOF. This warrants some comment. The scattering powers of oxygen and fluorine are very similar so that it is not easy to distinguish between them in an X-ray diffraction study. Mann and Bevan (1970), using diffraction intensities measured from powder patterns obtained with a Hagg-Guinier focussing camera and strictly monochromatic $\text{CuK}\alpha_1$ radiation, refined their data in space group $R\bar{3}m$ for the two possible ordered models, and concluded that the one shown in fig. 28.61 did give a significantly better agreement factor for the data. The consequences of the model so chosen can be seen from the crystallographic data summarised in table 28.12: the Y-O distances are significantly shorter than the Y-F distances, which is in contradiction to the general observation on which Zachariassen (1951) and Tanguy et al. (1973) based their choice. However, in

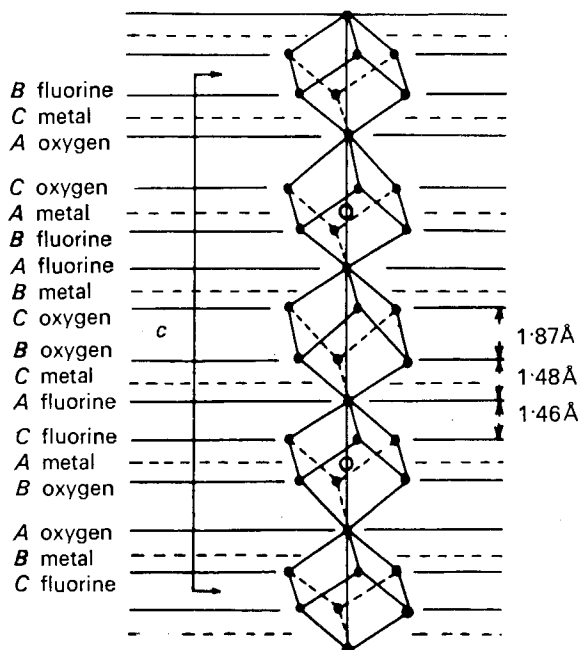


Fig. 28.61. The structure of YOF: reproduced from *Magnani Bevan* (1970) by courtesy of Acta Crystallogr.

Holmberg's (1966) single-crystal study of the structure of ScOF (see below) the Sc–O distances were also found to be less than the Sc–F distances. Some uncertainty on this issue must remain, although electrostatic energy calculations by Templeton (1957) for the two models tend to support that presented here.

There is no argument on the broader details of this superstructure derived from the parent fluorite-type. The distortion which occurs as a result of the anion ordering is an extension along one of the $\langle 111 \rangle$ fluorite vectors which then becomes the unique $[001]$ vector of the hexagonal cell: for the undistorted fluorite-type lattice the equivalent c/a ratio is 4.899 compared with the observed value of 4.97. Furthermore, the three different spacings observed between anion layers perpendicular to the c (hex) axis show that the ordering sequence of these

TABLE 28.12

Crystallographic data for ScOF.

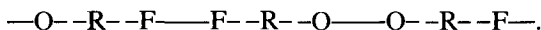
Cell parameters: $a = 5.1673 \pm 0.005 \text{ \AA}$; $b = 5.1466 \pm 0.0005 \text{ \AA}$

$c = 5.2475 \pm 0.0008 \text{ \AA}$; $\beta = 99.70 \pm 0.08^\circ$.

Space group $P2_1/c$ (No. 14): Cell contents 4ScOF.

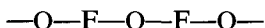
Atom parameters				Metal–anion distances (\AA)			
Atom	x	y	z	Sc–F(3)	2.13 ± 0.02	Sc–O(1)	2.08 ± 0.02
Sc	0.307	0.027	0.213	Sc–F(1)	2.19 ± 0.02	Sc–O(4)	2.08 ± 0.02
F	0.057	0.325	0.343	Sc–F(4)	2.28 ± 0.02	Sc–O(3)	2.10 ± 0.02
O	0.457	0.750	0.490			Sc–O(2)	2.14 ± 0.02

along this direction must be



The structure of ScOF has been determined by Holmberg (1966) and is shown in figs. 28.62a and 28.62b: it is isotypic with the structures of ZrO_2 and HfO_2 , which, because of the small cation radii, do not crystallize with the fluorite-type structure but in the monoclinic system.

Nevertheless, there is a clear relationship between the two structures, the lattice parameters being similar, the cell contents identical, and the cation sub-lattices arranged in much the same way. Crystallographic data for ScOF are given in table 28.12, from which it is seen that Sc is coordinated by seven anions. The structure is probably best described (Hyde and Anderson: private communication) in terms of edge-shared, monocapped trigonal prisms, and this is how it is represented in fig. 28.62. These trigonal prisms are somewhat distorted, and it is this distortion which makes the capping of one of the rectangular faces a reality. Figure 28.62 shows the idealized structure with undistorted trigonal prisms, which are no longer capped, and is a clearer indication of their linkages. The ordering of O and F atoms is seen to be different from that in the rhombohedral ROF compounds: these atoms segregate into more or less puckered layers parallel to the bc plane, and are separated by $\frac{1}{2}a$. The sequence along the [100] direction is



On the fluorite-rich side of the ideal ROF composition, where earlier workers had reported the existence of a grossly non-stoichiometric phase with tetragonal structure, the situation is not as yet completely clear. A thorough study of the yttrium oxide-fluorides has been made by Mann and Bevan (1972) in which attention became focussed on one particular composition region between about $\text{YX}_{2.13}$ and $\text{YX}_{2.22}$ ($X = \text{O} + \text{F}$). At low temperatures this region coexisted on one side with rhombohedral YOF and on the other with orthorhombic YF_3 , and itself appeared at first sight to be a single, grossly nonstoichiometric phase with an orthorhombic (almost tetragonal) fluorite-related sub-cell, but the powder diffraction patterns showed many superstructure reflections. Single-crystal diffraction experiments revealed that the basic structure of any sample within this region was a one-dimensional superstructure of the fluorite-type sub-cell whose true unit cell could be described in terms of the sub-cell vectors as $1 \times n \times 1$ (n integral). However, crystals of different compositions yielded significantly different diffraction patterns, so that in the final analysis it was concluded that there exists a unique n (which may be quite large) for any composition within the range. The details of this analysis are given in the original paper and need not be repeated here. What is important, however, for this review is the structural principle which permits such a state of affairs to exist, and this has been established.

The simplest superstructures which can exist within this composition range are $1 \times 7 \times 1$ ($\text{YX}_{2.143}$), $1 \times 6 \times 1$ ($\text{YX}_{2.167}$), and $1 \times 5 \times 1$ ($\text{YX}_{2.200}$). These constitute

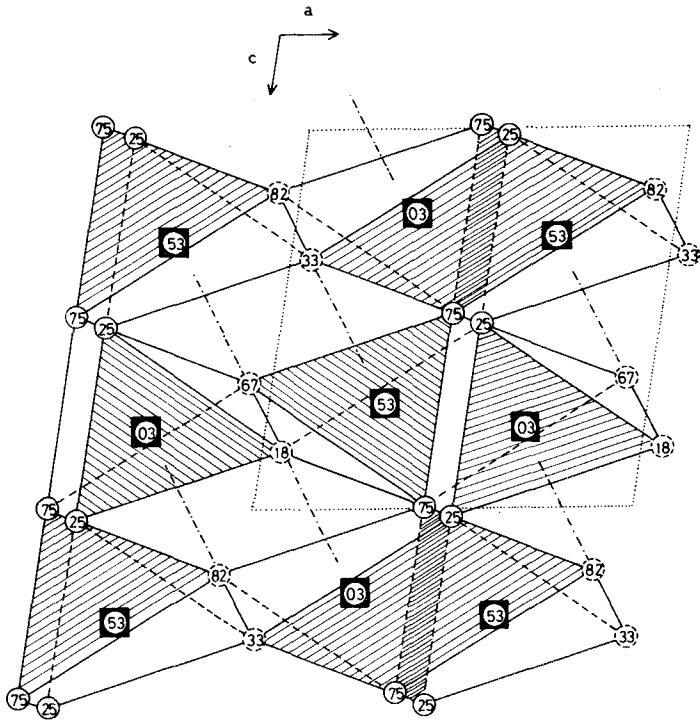


Fig. 28.62(a). The structure of ScOF: after Holmberg (1966). Squares indicate Sc atoms, full circles O atoms, and dashed circles F atom. The numbers refer to y-coordinates.

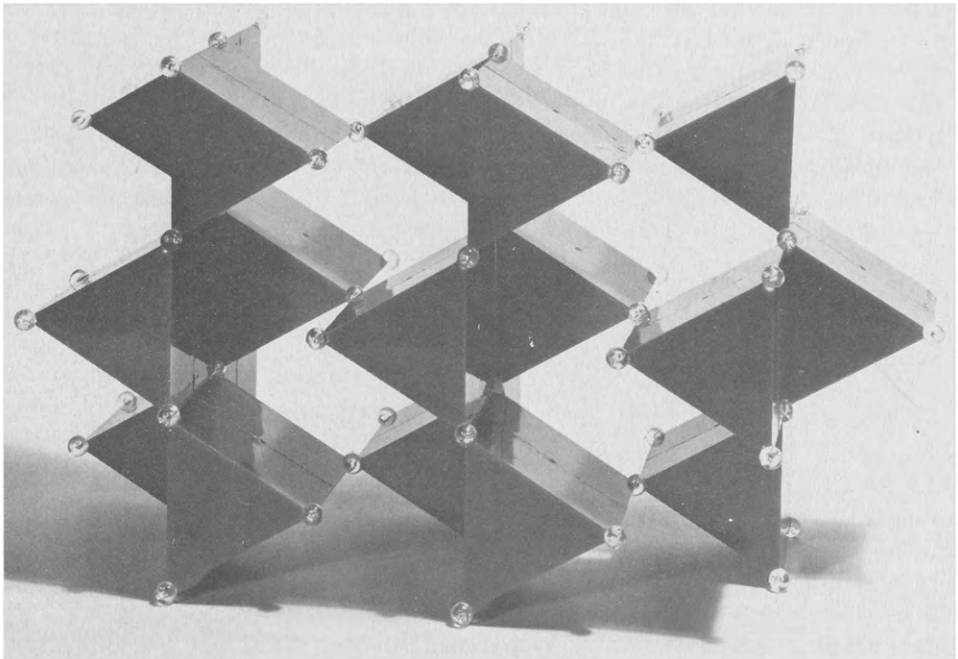


Fig. 28.62(b). The idealized structure of ScOF, comprised of edge-shared trigonal prisms.

the members $n = 7, 6, 5$ of a homologous series of general formula $Y_nO_{n-1}F_{n+2}$, and single crystals of each have been obtained. A full structure analysis has been carried out so far only on $Y_7O_6F_9$ (Bevan and Mann, 1975), and work is proceeding on the other two. Nevertheless, the structural principal seems clear. Crystallographic details for $Y_7O_6F_9$ are as follows:

Cell parameters: $a = 5.420 \pm 0.001 \text{ \AA}$; $b = 38.58 \pm 0.01 \text{ \AA}$ ($7 \times 5.511 \text{ \AA}$)
 $c = 5.527 \pm 0.001 \text{ \AA}$

Space group: $Abm2$: (Cell contents: $(Y_7O_6F_9)_4$)

The structure is shown in fig. 28.63. This representation is that used by Hyde et al. (1974) to illustrate best the "vernier" character of the structure, a term coined by them for a principle which is becoming more widely recognized as applying in many inorganic systems. In fig. 28.63 the Y atoms occupy the sites of an only slightly-distorted fluorite-type cation sub-lattice. In a similar manner the anions at $x = \frac{1}{2}$ are displaced by trivial amounts from the corresponding sites of an ideal fluorite-type anion sub-lattice, and constitute a slightly puckered 4^4 net perpendicular to $[100]$: most of these are O atoms. By contrast, the anions at $x = 0$ (mostly F atoms) are displaced much further from the ideal fluorite-type sites, the more so as y increases from 0 to $\frac{1}{4}$. Because of the mirror plane perpendicular to b at $y = \frac{1}{4}$ this process reverses itself between $y = \frac{1}{4}$ and $y = \frac{1}{2}$, and then repeats the cycle. These atoms constitute a 3^6 net perpendicular to $[100]$. Thus two sets of anion planes perpendicular to $[010]$ can be distinguished, those composed only of anions belonging to the 4^4 nets, and those composed only of anions belonging to the 3^6 nets. Given the approximate equality of the anion-anion spacing within the two types of net it is easy to see how the "vernier" effect arises. Figure 28.63 shows that at $y = 0$ and $y = \frac{1}{2}$ the two anion planes perpendicular to $[010]$, which contain respectively anions belonging to the 3^6 and 4^4 nets, are coincident. Between these limits there are seven planes of anions from the 4^4 nets but eight of those from the 3^6 nets. Thus additional anions have been added to the structure in conformity with the unit cell contents. Moreover, it is easy to see how a change of composition is accommodated without any fundamental change in structure: all that is required is slight adjustment of the respective spacings between the anion planes of each type. There will then be a consequential change in the interval along b between coincidences of the two types of plane, and this may become quite large, giving rise to the very long-period superstructures found in practice.

An alternative way of describing this structure emerges when a comparison is made between the coordination of Y(1) in fig. 28.63 and that of the Y atoms in YF_3 . This is shown in fig. 28.64a and 28.64b, reproduced from the paper by Hyde et al. (1974). These two projections reveal just how similar the two coordinations are, and that that part of the $Y_7O_6F_9$ structure centred on the mirror plane containing Y(4) atoms surrounded entirely by F atoms can accurately be described as an element of the YF_3 structure. The coordination of Y(3), with 6F atoms and 2O atoms around it, also resembles the spatial distribution of the F atoms around Y(4). By contrast, in the vicinity of Y(1) the structure is obviously distorted fluorite-type, with Y(1) coordinating 6O atoms and 2F atoms, whereas

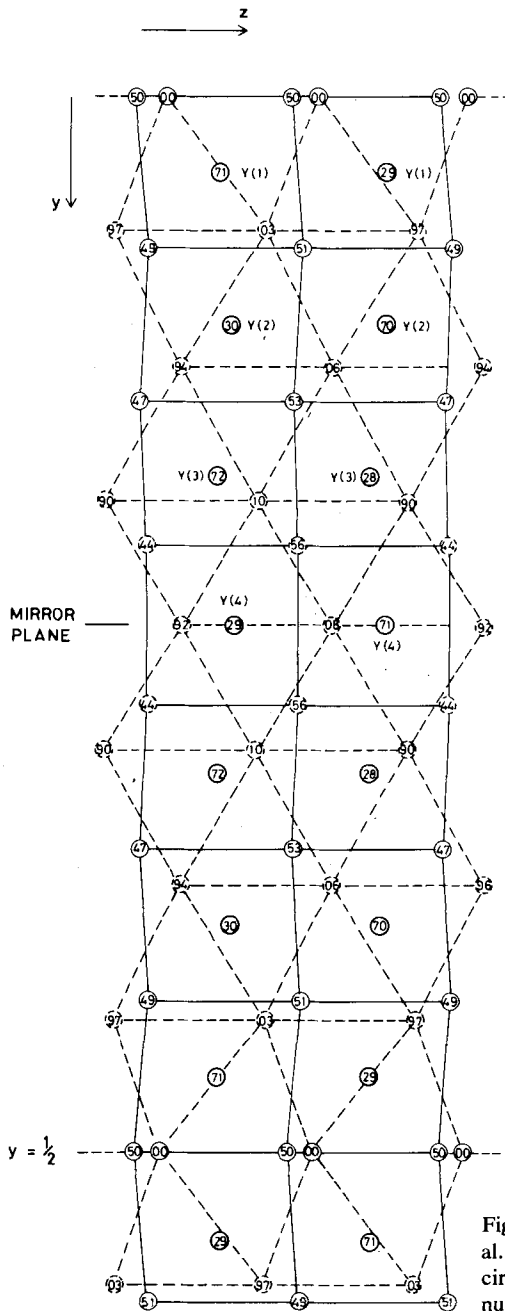


Fig. 28.63. The structure of $Y_7O_6F_9$: after Hyde et al. (1974). Heavy circles represent Y atoms, light circles O atoms, and dashed circles F atoms. The numbers refer to X-coordinates.

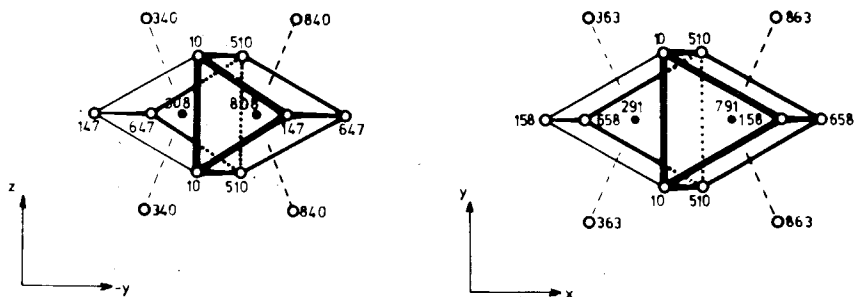


Fig. 28.64(a). The environment of Y atoms in YF_3 (to facilitate comparison with fig. 28.64(b) 0.325 a has been added to the x -coordinates for YF_3).

Fig. 28.64(b). The environment of the Y(4) atom in $Y_7O_6F_9$; reproduced from Hyde et al. (1974) by courtesy of Ann. Review of Mater. Sci. Solid circles represent Y atoms, open circles anions.

the coordination of Y(2), with 4O atoms and 4F atoms around it, is quite similar to that of Sc in ScOF. Thus there exists in $Y_7O_6F_9$ what might be described as a modulation along $[010]$, this modulation involving both composition and structure. Again, variations in overall composition can readily be accommodated by changes in the modulation. Mann and Bevan (1972) described this in terms of ordered intergrowth between adjacent simple superstructure phases (i.e. $Y_nO_{n-1}F_{n+2}$; $n = 5, 6, 7$), and were able to explain their observations adequately in these terms; e.g. a crystal from a sample of analysed composition $YX_{2.17(1)}$ was shown to have a unit cell $1 \times 17 \times 1$, with an intergrowth pattern consisting of $2(1 \times 6 \times 1) + 1(1 \times 5 \times 1)$ – ideal composition $YX_{2.176}$.

There is sufficient evidence available to indicate that the situation as described above for the yttrium oxide-fluorides does *not* apply *in toto* to other rare earth oxide-fluoride systems. Roether (1967), and Brauer and Roether (1968) have investigated a number of these; Tanguy et al. (1973) have studied the europium oxide-fluorides in some detail; and Molyneux (1973) has thoroughly explored the neodymium and samarium systems. Work on the ytterbium oxide-fluorides is also in progress (Bevan et al., to be published). In summary, the results of all these investigations suggest that there is a close parallel between the yttrium and erbium oxide-fluorides, and it might be expected that the holmium and even the dysprosium systems would behave in a similar way. However, with increasing radius of the rare earth cation the stability of the orthorhombic superstructure phases seems to decrease, and these are no longer in evidence in the neodymium and lanthanum systems. Where they do occur the ranges of composition over which they have been observed are much the same as for the yttrium system, and there is no evidence for any members of the $R_nO_{n-1}F_{n+2}$ series other than those with $n = 5, 6$, and 7 . Beginning with the gadolinium system, however, another phase is formed at higher fluoride contents which coexists with the limiting fluoride-rich orthorhombic phase. For this system this new phase only exists at high temperature and is non-stoichiometric: it decomposes below $\sim 700^\circ\text{C}$ at a composition of $GdX_{2.40}$, and at 1000°C extends between the limits $GdX_{2.40}$ and $GdX_{2.34}$ (Roether, 1967). Its apparent unit cell is a monoclinic

distortion of the fluorite-type cell, and is closely related to the tetragonal cell reported by Zachariasen (1951) for $\text{LaX}_{2+\delta}$. With further increase in cation radius this phase becomes more firmly established and is stable to lower temperatures. Thus Tanguy et al. (1973) report its existence at room temperature in the europium system between $\text{EuX}_{2.30}$ and $\text{EuX}_{2.35}$, and between $\text{EuX}_{2.25}$ and $\text{EuX}_{2.37}$ at 500°C , while Molyneux (1973) has shown that it occurs at room temperature over the range $\text{SmX}_{2.30}$ to $\text{SmX}_{2.40}$ in the samarium system and becomes tetragonal at higher temperatures. This range of existence broadens still further in the neodymium and lanthanum systems, being $\text{NdX}_{2.14}$ to $\text{NdX}_{2.40}$ in the former and $\text{LaX}_{2.20}$ to $\text{LaX}_{2.40}$ in the latter. Moreover, in the lanthanum system the apparent unit cell is tetragonal even at room temperature. Roether (1967) also reported the existence of the stoichiometric phase $\text{LaX}_{2.5}$ (La_2OF_4) at temperatures above $\sim 700^\circ\text{C}$ but could not determine its unit cell.

Little is known about the detailed structure of the monoclinic (tetragonal) phase, and in spite of many attempts to obtain a stoichiometric, ordered monoclinic or tetragonal phase within this composition range, no success has been achieved. There is evidence of superstructure ordering from electron diffraction studies (Molyneux, 1973) but the instability of these oxide-fluorides in the electron beam has effectively prevented a detailed investigation. What evidence there is suggests that one-dimensional superstructures probably do form, and that the long axis of the supercell is parallel to a $\langle 110 \rangle$ vector of the fluorite-type sub-cell. Figure 28.65 shows the relationships between a monoclinically distorted fluorite-type cell and an orthorhombic cell for which superstructure ordering perpendicular to a principal axis (as in the case of the yttrium oxide-fluorides) which is a $\langle 110 \rangle$ fluorite-type vector could occur. This derivative cell is only orthorhombic if the a and c vectors of the distorted fluorite-type cell are of equal length, as is observed. If the angle β , which in reality is very close to 90° , becomes 90° the orthorhombic cell degenerates to the tetragonal cell first described by Zachariasen (1951) for the $\text{LaX}_{2+\delta}$ phase. It is perhaps significant that the hexagonal tysonite structure of the lighter rare earth trifluorides (i.e. those rare earth elements with larger cation radii) can best intergrow with the

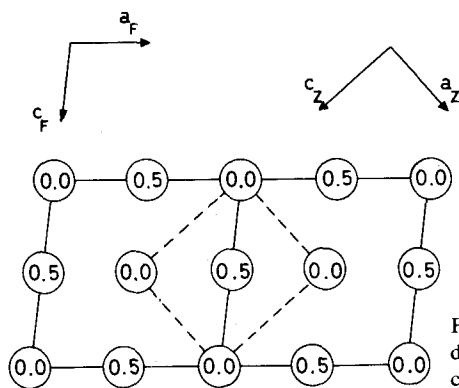


Fig. 28.65. The relationship between a monoclinically-distorted fluorite-type cell and the Zachariasen-type cell.

fluorite-type structure along a $\langle 110 \rangle$ fluorite direction, and the tentative hypothesis advanced by Molyneux (1973) follows the pattern already established for the yttrium oxide fluorides, namely that of a modulated structure in which in this case elements of the hexagonal (tysonite) RF_3 (as opposed to the orthorhombic YF_3) are intergrown in a fluorite-type matrix.

At the other end of the rare earth series the results for the ytterbium system show the stable existence of anion-excess superstructure phases completely analogous to those found in the yttrium system, but there is also evidence for a hypostoichiometric fluorite-related phase $\text{YbX}_{2-\delta}$. Much more work in this general area needs to be done in order to clarify the situation.

5.7. Scheelite-related structures

5.7.1. Scheelite- and fergusonite-type structures

The scheelite structure is tetragonal, space group $I4_1/a$, with $a = 5.411 \text{ \AA}$, $c = 11.936 \text{ \AA}$ for EuWO_4 (McCarthy, 1971). In the parent CaWO_4 structure the atomic coordinates, as given by Wyckoff (1965a), are: –

Ca	in $4b$	$0, 0, \frac{1}{2}$
W	$4a$	$0, 0, 0$
O	$16f$	$\frac{1}{4}, 0.15, 0.075$

Phases with this structure are found as high-temperature polymorphs of many of the rare earth ortho-niobates and ortho-tantalates, and in many of the pseudo-ternary systems involving alkali-metal oxides and rare earth tungstates or molybdates. The niobates and tantalates are discussed below but it is not intended to discuss the pseudo-ternary systems here, despite the fact that with the smaller alkali metals (Li and Na) many $\text{M}^+\text{R}^{3+}(\text{WO}_4)_2$ phases have been reported to have the scheelite structure. (See for example Mokhosov et al., 1967; Klevtsov and Kozeeva, 1970).

Two descriptions of this structure are relevant, depending on whether anion-excess or anion-deficient systems are being considered. In the former case scheelite can be regarded as a superstructure of an anti-cuprite structure, the superstructure deriving from ordering of the cations (Clark, 1972). From this viewpoint scheelite is derived from a corner-sharing array of MO_4 tetrahedra which has been distorted so that the larger cations have eight-fold coordination. The resultant structure is an array of isolated WO_4 tetrahedra between which the Ca^{2+} ions occupy eight-coordinated sites. The alternative view of scheelite is that it is a superstructure of fluorite, the superstructure again deriving from cation order. As shown in fig. 28.66, in scheelite the two cation-types alternate in each row parallel to the c -axis. The anions are then shifted from fluorite sites so that the small, highly-charged cations have tetrahedral coordination, while the larger cations are still eight-coordinated.

These two descriptions are quite pertinent. In anion-deficient systems the cation sub-lattice remains essentially invariant, all defects entering the anion

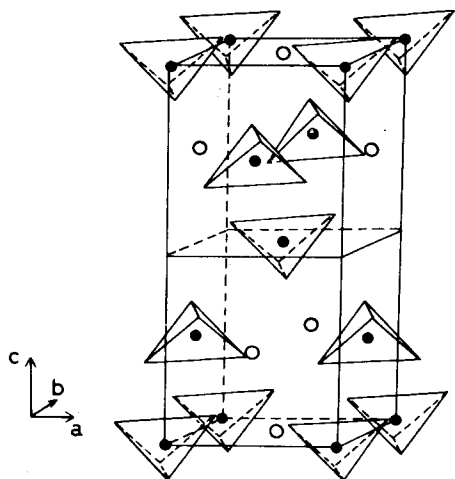


Fig. 28.66. The scheelite structure as an array of MO_4 tetrahedra. Both cation types are indicated.

sub-lattice as in typical fluorite-related systems. In anion-excess, scheelite-related systems deviation from MO_2 stoichiometry is accommodated by the production of cation vacancies (resulting in typical molybdate structures) in contrast with anion-excess fluorite systems where the cation sub-lattice again remains invariant and interstitial anions occur.

A monoclinic form of scheelite has been described by Komkov (1959). This structure is known as fergusonite and belongs to space group $I2$. As a distorted form of scheelite its lattice parameters are similar to those of scheelite; for YTao_4 these are $a = 5.34 \text{ \AA}$, $b = 10.94 \text{ \AA}$, $c = 5.07 \text{ \AA}$, $\beta = 95.3^\circ$ (Ferguson, 1957). Wolten and Chase (1967) have described this phase in terms of cation nets perpendicular to the scheelite c -axis. In scheelite these nets are square and flat, in fergusonite they are puckered and distorted.

A third (M') polymorph of YTao_4 has been described by Wolten (1967) as monoclinic, space group $P2/a$, with $a = 5.292 \text{ \AA}$, $b = 5.451 \text{ \AA}$, $c = 5.110 \text{ \AA}$, $\beta = 96.44^\circ$. The halving of the b -axis relative to the scheelite c -axis is due to a different ordering of the cations, such that the planes of cations perpendicular to the c -axis are alternately all Y^{3+} or all Ta^{5+} , whereas in scheelite and fergusonite these planes all contain cations of both types. According to Wolten, the Y^{3+} ions have distorted cubic coordination and the Ta^{5+} ions distorted tetrahedral coordination, as in the other polymorphs. However, as shown in fig. 28.67, the coordination polyhedron of the Ta^{5+} ion is distorted and the structure is closely related to that of wolframite. The structure could be described as consisting of planes of distorted, edge-sharing WO_6 octahedra sharing vertices with planes of distorted, edge-shared MO_8 cubes. Orthotantalates of Sm through Yb, including Y, can form an M' polymorph isostructural with M' - YTao_4 . The occurrence of the scheelite and fergusonite structures is shown in table 28.13.

The fergusonite structure is the normal low-temperature form found for the rare earth orthoniobates (except Sc^{3+}) and for the orthotantalates of the

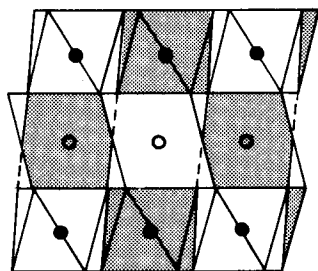


Fig. 28.67. Projection of the structure of M' -fergusonite along [010] showing its relationship to wolframite. Different cation types are indicated by filled and open circles and different heights of these by shading of the polyhedra. Two rows of MO_6 octahedra and one row of MO_4 tetrahedra are shown.

lanthanides Nd through Er and Y. Praseodymium orthotantalate can be stabilised in the fergusonite structure by addition of neodymium i.e. $Pr_{1-x}Nd_xTaO_4$ has the fergusonite structure if $x \geq 0.1$ (Keller, 1962). The tetragonal scheelite structure probably exists as a high-temperature structure for all of these compounds. It has been shown (Rooksby and White, 1963; Stubican, 1964; Wolten and Chase, 1967) that with increasing temperature the monoclinic distortion of fergusonite gradually decreases (the a and c parameters approach each other and β tends to 90°), but no discontinuities are observed. The highest temperature at which the monoclinic distortion is evident has been termed the transformation temperature: for the orthoniobates this ranges from 500°C for $LaNbO_4$ to 825°C for $YbNbO_4$, and from 1325°C for $NdTaO_4$ to 1410°C for $HoTaO_4$.

However, Wolten and Chase (1967) have shown that these M' -fergusonites can only be formed by transformation of the tetragonal scheelite phases. Crystals grown hydrothermally below the monoclinic-tetragonal transformation temperature have the wolframite-related M' structure. On heating the M' -phases above the fergusonite-scheelite transformation temperature a first-order transition to the scheelite form slowly occurs. Subsequent cooling results in formation of the fergusonite form, never the M' form. It seems most likely that the equilibrium low-temperature phase is the wolframite-related M' -phase; at high temperature this transforms to the scheelite structure. On subsequent cooling the tetragonal phase becomes unstable and transformation back to M' should occur, but this process requires cationic reordering, and a much more rapid transition to fergusonite occurs instead. This, then, is another case where the phases *observed* by conventional solid state techniques are indicative of *observational* equilibrium rather than true thermodynamic equilibrium. Once a particular cationic distribution has been obtained at high temperature it becomes invariant, and it is not possible by conventional techniques to attain true thermodynamic equilibrium. The easy reversibility of the second order fergusonite-scheelite transition is no criterion of thermodynamic stability. The phases found for $RTaO_4$ ($R = Tm$ through Lu) are probably isomorphous with the M' -phase, these being formed by conventional solid state reaction below the hypothetical transformation temperatures of the corresponding scheelite phases. If these contentions are correct then the M' -phase is most important from a thermodynamic viewpoint,

and it is suggested that this structure be named woltenite after G.M. Wolten who first determined the structure*.

5.7.2. Zircon- and monazite-type structures

Another structure closely related to that of scheelite, the zircon structure, is again tetragonal but with very different cell-parameters. For HoVO_4 the lattice parameters are $a = 7.121 \text{ \AA}$, $c = 6.293 \text{ \AA}$ (Fuess and Kallel, 1972). The space group is $I4_1/amd$ with atoms in positions

R^{3+}	in	$4a$	$0, 0, 0$
V^{5+}		$4b$	$0, 0, \frac{1}{2}$
O^{2-}		$16h$	$0, 0.186, 0.328$

The resulting eight-fold coordination of the R^{3+} ion is less regular than in scheelite, there now being four longer and four shorter bonds, whereas in scheelite all eight bonds are of very similar length. This structure is found for many rare earth vanadates, arsenates and phosphates of $\text{R}^{3+}\text{B}^{5+}\text{O}_4$ stoichiometry (Carron et al., 1958, and references therein). Numerous structure refinements have been carried out on these compounds by single crystal and powder X-ray diffraction, and by powder neutron diffraction (Wyckoff, 1965b; Fuess and Kallel, 1972, and references therein). The name xenotime, which occasionally occurs in the literature (e.g. Stubican and Roy, 1963) is a pseudonym for zircon.

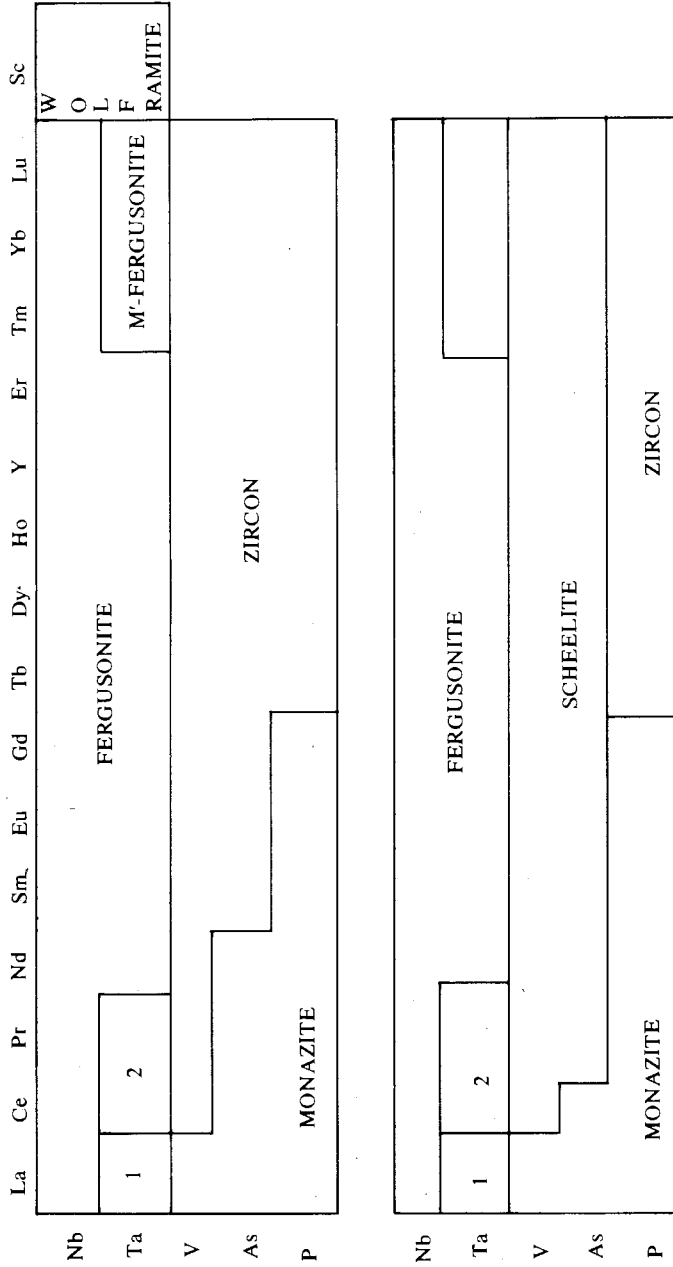
The monazite structure of CePO_4 is very similar to that of zircon. Its space group is $P2_1/n$, and the lattice parameters are $a = 6.76 \text{ \AA}$, $b = 7.00 \text{ \AA}$, $c = 6.44 \text{ \AA}$; $\beta = 103.6^\circ$. Transformations from both the zircon and monazite structures to that of the scheelite have been observed by Stubican and Roy (1963) for a number of arsenates and vanadates of the rare earths. Stability regions of these phases at standard and high pressures are shown in table 28.13. These reactions occurred under the influence of pressures up to 80 000 atm at 600°C and are accompanied by an 11.5% volume decrease; however, transformations between zircon and monazite were not effected because of their similar densities. Praseodymium chromate, prepared by Schwarz (1963a), was a mixture of the monazite and zircon types, and LaCrO_4 had the monazite structure (Schwarz, 1963b). Presumably other rare earth chromates have either the monazite or zircon structures.

5.7.3. Wolframite-type structures

The wolframite structure is another which can be described as having a fluorite-related cation sub-lattice about which the anions adopt some convenient arrangement. The unit cell is monoclinic, space group $P2/c$, and has $a = 4.68 \text{ \AA}$,

*Indeed, as reviewers we have found great confusion in the literature over the naming of phases. $\text{Zr}_3\text{Sc}_4\text{O}_{12}$ has been termed the δ -phase of the $\text{ZrO}_2\text{-Sc}_2\text{O}_3$ system whereas the isotopic phase Pr_7O_{12} is known as ι . $\beta\text{-Na}_2\text{RO}_3$ has the $\alpha\text{-LiFeO}_2$ structure, and so on. There is a clear case for some rationalization and we might do worse than follow the tradition of the mineralogists.

TABLE 28.13
Stability regions of scheelite-related phases at low (top) and high (bottom) pressures. Numerals refer to unknown phases.



$b = 5.66 \text{ \AA}$, $c = 4.92 \text{ \AA}$, $\beta = 89.67^\circ$ (Keeling, 1957). Atom positions are:

Ni	in	$2e$	$\frac{1}{2}, 0.180, \frac{1}{4}$
W		$2f$	$0, 0.653, \frac{1}{4}$
O		$4g$	$0.22, 0.11, 0.96$
O		$4g$	$0.26, 0.38, 0.39$

The structure and its relationship to fluorite are shown in figs. 28.68a and 28.68b. As can be seen in the figures, the structure consists of alternating layers of edge-sharing WO_6 octahedra parallel to $[001]_F$ which share vertices with layers of NiO_6 octahedra. As Clark (1972) points out, this phase is a superstructure of $\alpha\text{-PbO}_2$. The relationship between this structure and that of M' -fergusonite (fig. 28.67) can be seen. ScNbO_4 and ScTaO_4 have this structure (Komissarova et al., 1968; Vladimirova et al., 1970; Dyer and White, 1964).

5.7.4. Compounds with compositions R_2MO_6 and R_3MO_8

The tungstates of this composition fall into three groups:

(i) La_2WO_6 , which is unique and about which little is known.

(ii) The rare earths from Nd through Ho. These form compounds which are monoclinic and scheelite-related. There are two equivalent descriptions of the unit cell which have been used by different authors. The first, used by McCarthy et al. (1972), Polyanskaya et al. (1971) and Wyart et al. (1970), has $a = 15.93 \text{ \AA}$, $b = 11.39 \text{ \AA}$, $c = 5.51 \text{ \AA}$, $\beta = 92^\circ$ for Nd_2WO_6 (Wyart et al., 1970). According to the last two the symmetry is close to body-centred but is actually $P2_1/c$. The alternative cell for Nd_2WO_6 has $a = 16.62 \text{ \AA}$, $b = 11.384 \text{ \AA}$, $c = 5.522 \text{ \AA}$, $\beta = 107.58^\circ$ (Brixner et al., 1973), and the symmetry found for this cell by Pokrovskii et al. (1969) was $C2/c$.

Refinement of the structure of Nd_2WO_6 was performed in space group $I2/c$

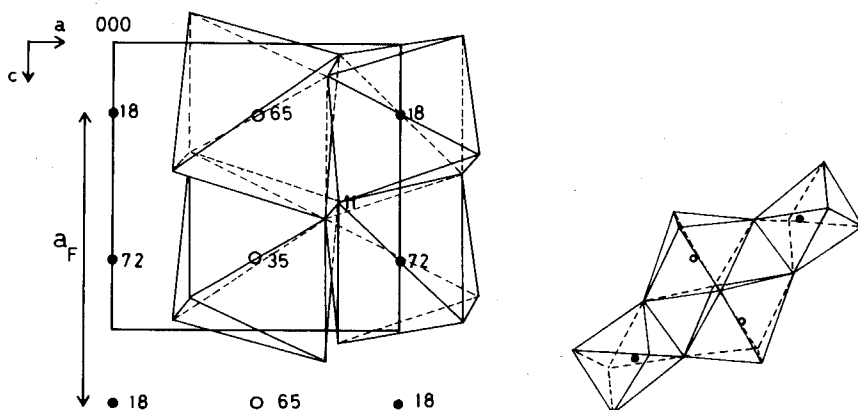


Fig. 28.68(a) and 28.68(b). Two projections of the wolframite structure showing the corner sharing of planes of edge-shared octahedra. The relationship to fluorite is evident in (a) where cation heights in units of $y/100$ are shown. (Figure 28.68(b) after Keeling, 1957).

with atoms in the positions

Nd(1)	0	0.6314	$\frac{1}{4}$
Nd(2)	0.1731	0.8845	0.2859
Nd(3)	0	0.1110	$\frac{1}{4}$
W	0.1531	0.3526	0.2145
O(1)	0.407	0.519	0.485
O(2)	0.420	0.261	0.493
O(3)	0.222	0.035	0.396
O(4)	0.272	0.053	0.117
O(5)	0.270	0.205	0.487
O(6)	0.390	0.222	0.036

Relative to a fluorite sub-cell the unit cell of this structure has one doubled and one trebled axis. The structure analysis performed by Polyanskaya et al. (1971) has shown that the doubling of one axis is due to normal scheelite cation ordering, with cations of both types alternating along the *b*-direction. The trebling of the *a*-axis was found to be due to alternation of two of these planes containing a scheelite distribution of cations with one containing only Nd³⁺ ions. Thus the planes perpendicular to *a* are successively (Nd_{1/2}W_{1/2})(Nd_{1/2}W_{1/2})(Nd) etc. A similar sort of ordering is found in La₂MoO₆, Bi₂NbO₅F and Bi₂(Mo/W)O₆ where every third cation plane contains the smaller cations. The anion distribution found for Nd₂WO₆ corresponds to five-coordinated W⁶⁺ ions and distorted cubic coordination for the Nd³⁺ ions. This structure is referred to below as the "body-centred" form of R₂WO₆ compounds.

(iii) The smaller rare earths. These form tungstates which again are monoclinic but with $a = 11.35 \text{ \AA}$, $b = 5.330 \text{ \AA}$, $c = 7.678 \text{ \AA}$, $\beta = 104.45^\circ$ for the Ho₂WO₆, according to Pokrovskii et al. (1969). The unit cells have the symmetry of one of the space groups *P2/m*, *P2*, *P2₁/m* or *P2₁*, and since Brixner et al. (1973) find them to be centrosymmetric the choice is limited to *P2/m* or *P2₁/m*. This structure exists for R = Dy through Lu so that the Dy and Ho tungstates are dimorphic. Brixner et al. (1973) found they were able to transform the "body-centred" structures of both Dy₂WO₆ and Ho₂WO₆ to the *P*-forms. Where the *I*-form is scheelite-related, the *P*-form appears to behave more like a fluorite-related structure. Thus the addition of 0.01 mole of Bi to Er₂WO₆ resulted in a rhombohedral structure with hexagonal parameters $a = 9.767 \text{ \AA}$, $c = 9.373 \text{ \AA}$. This cell may be related to UY₆O₁₂ or to the rhombohedral R(III) phase found by Koshcheev and Kovba (1966) or to the R₂TeO₆ compounds discussed below.

The rare earth tellurates R₂TeO₆, described by Natansohn (1968), crystallise in two forms. The powder patterns of both forms have been indexed in terms of hexagonal unit cells with $a = 10.96 \text{ \AA}$, $c = 10.35 \text{ \AA}$ for La₂TeO₆ and $a = 8.94 \text{ \AA}$, $c = 5.08 \text{ \AA}$ for Lu₂TeO₆. The former unit cell is found for the rare earths from La through Tm, including Y, the latter for Lu and Sc. Yb₂TeO₆ is dimorphic as both forms were present in its samples.

Three types of rare earth rhenates have been found by Baud and Besse (1974). La₃ReO₈ is orthorhombic with $a = 17.53 \text{ \AA}$, $b = 11.90 \text{ \AA}$, $c = 12.78 \text{ \AA}$; the possible

space groups are *Ccmm*, *Ccm2*, *Cc2m*. Analogous compounds for the rare earths between Nd and Gd are also orthorhombic, space group *B22₁2₁*, with $a = 8.540 \text{ \AA}$, $b = 6.124 \text{ \AA}$, $c = 12.26 \text{ \AA}$ for Pr_3ReO_8 . The remaining lanthanides have fluorite-type unit cells with a varying linearly from about 5.39 \AA for Tb to about 5.25 \AA for lutecium. For the first two structure types, where the number of formula units (z) is respectively 16 and 4, there is no valency problem – the average valence of the Re is simply $4\frac{1}{2}$. However, in the fluorite-type unit cell, where $z = 1$, the actual valence of Re would have to be $4\frac{1}{2}$ unless either the true cell is larger than that proposed or the anion sublattice is defective to a significant extent.

The unique character of fluorite-related structures is seen to emerge again in drawing together the various structural theories which have been discussed above. There is a host of solid phases of widely differing chemical composition for which a common feature is the stable arrangement of cations, either ordered or disordered, on a sub-lattice which is essentially that of the cations of the fluorite-type structure. The stability of this cation arrangement is then such that the anions of the associated anion sub-lattice can adopt a variety of configurations around individual cations, each of which is the most appropriate for the particular cation/anion combination. Such behaviour has also been recognised by Polyanskaya et al. (1971). A good example of the application of this principle is the structure of $\text{Y}_7\text{O}_6\text{F}_9$, already discussed. Another even more striking example is that of the structure of $\text{Na}_7\text{Zr}_6\text{F}_{13}$ (Burns et al., 1968) in which the ordered cations constitute an almost undistorted fluorite-type cation sub-lattice. The coordination of F atoms around these cations however, varies continuously and regularly from octahedral around the Na atom at the origin to trigonal pyramidal around the Zr atoms. Moreover the anion sub-lattices thus produced are clearly very flexible and can adjust within wide limits to changes in cation composition and distribution so long as the cation sub-lattice per se retains its relationship to that of the fluorite-type structure, and gross non-stoichiometry in fluorite-type phases is a direct consequence of this.

6. Recent developments

Two local developments relevant to this chapter are recorded here to update the section on rare earth tantalates and niobates and rare-earth tungstates. The latter negates much of the speculation on tungstate structures included earlier.

Recent work by Allpress and Rossell (1978) and Rossell (1978) has shown that all rare earths other than scandium form niobates and tantalates with an O/M ratio of 1.75. These compounds are superstructures of fluorite: they are orthorhombic with probable space groups *Cmcm* for the La compound and *C22₁2₁* for those containing Nd, Gd, Ho and Y. Both structures are very similar to each other and to both pyrochlore and weberite: they are related to fluorite by $a = [200]_{\text{F}}$, $b = [011]_{\text{F}}$, $c = [0\bar{1}1]_{\text{F}}$. While the fluorite cation array is again intact, the anion arrangement results in the formation of slabs within which the cations all have cubic or

octahedral coordination, and between which the cations are seven-coordinated. The octahedrally coordinated cations are in strings parallel to one of the $\langle 110 \rangle_F$ axes and alternate with similar strings of cations which have cubic coordination. In Y_3TaO_7 the six-coordination results from loss of anions across the body diagonals of MO_8 cubes to form zig-zag strings of "vacancies" using two of the $\langle 111 \rangle_F$ directions. This is analogous to the situation in pyrochlore depicted in fig. 28.58. For Er, and under some conditions Ho and Y, samples consisted of a high-temperature defect fluorite phase containing microdomains of an orthorhombic phase of unknown structure. The order-disorder transformation temperature probably decreases with cationic radius.

Recent results on the rare earth oxide-tungsten trioxide system by Summerville et al. (1978), and since then extended in this laboratory, have revised the description of these systems. The only R_6WO_{12} phase found was that isostructural with UY_6O_{12} (Bartram, 1966), which was found for $R = Nd-Er$ and Y . This phase is orthorhombic, space group either $Pnma$ or $Pbcn$, with $a = 2a_F$, $b = 3b_F$, $c = 2c_F$. This high-temperature phase appears to undergo eutectoid decomposition, the decomposition temperature increasing with increasing atomic number. A trigonal phase has been found for rare earths from $Nd-Lu$ and Y at the ideal composition $R_{14}W_4O_{33}$. The unit cell is related to fluorite by $a = [1\bar{1}0]_F$, $b = [01\bar{1}]_F$, $c = [111]_F$; the space group is either $P\bar{3}m1$, $P3m1$, or $P321$, and the contents of the unit cell are $M_{12}O_{22}$. The phase appears to have a range of composition which is associated with an increase in the unit cell volume and a reduction in symmetry to triclinic. The unit cell of the R_2WO_6 phase for $R = Ho-Lu$ and Y has been identified as monoclinic, space group either Pc or $P2/c$, related to fluorite by $a = [10\bar{1}]_F$, $b = [010]_F$, $c = [102]_F$.

Acknowledgements

The author gratefully acknowledge the considerable help and cooperation generously given by their colleagues mentioned below: Professor H. Bärnighausen, Dr. P. Caro, Dr. J. Coutures, Professor B.G. Hyde, Professor C. Keiler, Dr. H.J. Rossell, and Dr. F. Sibieude.

References

- Ahrens, L.H., 1952, *Geochim. Cosmochim. Acta* **2**, 155.
 Aia, M.A., R.W. Mooney and C.W.W. Hoffman, 1963, *J. Electrochem. Soc.* **110**, 1048.
 Aitken, E.A., S.F. Bartram and E.F. Juenke, 1964, *Inorg. Chem.* **3**, 949.
 Aleksandrov, V.B., 1963, *Dokl. Akad. Nauk SSSR—Mineralogy* **153**, 129.
 Allpress, J.G. and J.V. Sanders, 1973, *J. Appl. Crystallogr.* **6**, 165.
 Ault, J.D. and A.J.E. Welch, 1966, *Acta Crystallogr.* **20**, 410.
 Badie, J.-M. 1970, *High Temp. High Pressures* **2**, 309.
 Balz, D. and K. Plieth, 1955, *Z. Electrochem.* **59**, 545.
 Bärnighausen, H., 1963, *Acta Crystallogr.* **16**, 1073.
 Bärnighausen, H., 1965, *Acta Crystallogr.* **19**, 1048.

- Bärnighausen, H., 1967, *Z. Anorg. Allg. Chem.* **349**, 280.
- Bärnighausen, H., 1970, *Z. Anorg. Allg. Chem.* **374**, 201.
- Bärnighausen, H., and G. Brauer, 1962, *Acta Crystallogr.* **15**, 1059.
- Bärnighausen, H. and R.D. Schmid, 1967, *Z. Anorg. Allg. Chem.* **354**, 27.
- Bärnighausen, H., R. Schuster and K. Vogt, 1973, The crystal structures of two modifications of the new Eu(II)-Eu(III) Compound $\text{Li}_2\text{Eu}_3\text{O}_8$ and the crystal data of the isostructural compounds $\text{Li}_2\text{Ba Eu}_4\text{O}_8$ in: *Proc. 10th Rare Earth Research Conference*, Vol. 1, 490-499.
- Bartram, S.F., 1966, *Inorg. Chem.* **5**, 749.
- Bartram, S.F., E.F. Juenke and E.A. Aitken, 1964, *J. Amer. Ceram. Soc.* **47**, 171.
- Baud, G. and J.P. Besse, 1974, *Mater. Res. Bull.* **9**, 1499.
- Berndt, U., D. Maier and C. Keller, 1975, *J. Solid State Chem.* **13**, 131.
- Berndt, U., D. Maier and C. Keller, 1976, *J. Solid State Chem.* **16**, 189.
- Bertaut, F., F. Forrat and M-C. Montmory, 1959, *Bull. Soc. Chim. Fr.* 829.
- Bertaut, F. and M. Gondrand, 1962, *C.R. Acad. Sci., Paris, Ser. C* **255**, 1135.
- Bevan, D.J.M. and A.W. Mann, 1975, *Acta Crystallogr.* **B31**, 1406.
- Bevan, D.J.M., W.W. Barker, R.L. Martin and T.C. Parks, 1965, Mixed Oxides of the Type $\text{MO}_2(\text{Fluorite})-\text{M}_2\text{O}_3$, Part 2, Non-stoichiometry in ternary rare-earth oxide systems, in: *Eyring, L., ed., Proc. of the Fourth Conference on Rare Earth Research*, (Gordon and Breach, New York), pp. 441-468.
- Blasse, G., 1965, *J. Inorg. Nucl. Chem.* **27**, 2683.
- Blasse, G., 1966, *J. Inorg. Nucl. Chem.* **28**, 2444.
- Blasse, G., 1968, *J. Inorg. Nucl. Chem.* **30**, 656.
- Blasse, G., 1969, *J. Inorg. Nucl. Chem.* **31**, 3335.
- Bocquillon, G., F. Queyroux, C. Susse and R. Collongues, 1971, *C.R. Acad. Sci., Paris, Ser. C* **272**, 572.
- Borchardt, H.J., 1963, *Inorg. Chem.* **2**, 170.
- Boulesteix, C., P.E. Caro, M. Gagnier, Ch. Henry La Blanchetais and G. Schiffmacher, 1971, *Acta Crystallogr.* **A27**, 552.
- Boulon, G., J.P. Faurie and C. Madej, 1974, *J. Solid State Chem.* **10**, 167.
- Brauer, G. and H. Gradinger, 1954, *Z. Anorg. Allg. Chem.* **276**, 209.
- Brauer, G. and B. Pfeiffer, 1965, *J. Prakt. Chem.* **34**, 23.
- Brauer, G. and U. Roether, 1968, Contributions to Solid State Chemistry of Rare Earth Fluorides, in: *Proc. of 7th Rare Earth Research Conf.*, P. 253.
- Brauer, G. and R. Tiessler, 1953, *Z. Anorg. Allg. Chem.* **271**, 273.
- Brink, C. and C.H. MacGillavry, 1949, *Acta Crystallogr.* **2**, 158.
- Brise, F. and O. Knop, 1968, *Can. J. Chem.* **46**, 859.
- Brixner, L.H., 1964, *Inorg. Chem.* **3**, 1065.
- Brixner, L.H., A.W. Sleight and C.M. Foris, 1973, *J. Solid State Chem.* **7**, 418.
- Brunel, M., F. de Bergevin and M. Gondrand, 1972, *J. Phys. Chem. Solids* **33**, 1927.
- Burns, J.H., R.D. Ellison and H.A. Levy, 1968, *Acta Crystallogr.* **B24**, 230.
- Bystrom, A., 1944, *Ark. Kemi, Mineral. Geol.* **18**, 1.
- Caro, P.E., 1972, *Nat. Bur. Stand. Spec. Publication* 364, *Proc. 5th Mater. Res. Symp.*, p. 367.
- Caro, P.E., M. Faucher, J. Derouet and M.G. Alves, 1973, *Rev. Chim. Mineral.* **10**, 317.
- Carpy, A., P. Amestoy and J. Galy, 1973, *C.R. Acad. Sci., Paris, Ser. C* **277**, 501.
- Carron, M.K., M.E. Mrose and K.J. Murata, 1958, *Amer. Mineral.* **43**, 985.
- Carter, J.R. and R.S. Feigelson, 1964, *J. Amer. Ceram. Soc.* **47**, 141.
- Chang, L.L.Y., and B. Phillips, 1964, *Inorg. Chem.* **3**, 1792.
- Chaumont, C., A. Daoudi, G. Le Flem and P. Hagenmuller, 1975, *J. Solid State Chem.* **14**, 335.
- Clark, M.C., 1972, The structure of non-molecular solids (*Applied Science*, London).
- Clos, R., M. Devalette, P. Hagenmuller, R. Hoppe and E. Paletta, 1967, *C.R. Acad. Sci., Paris, Ser. C* **265**, 801.
- Clos, R., M. Devalette, C. Fousassier and P. Hagenmuller, 1970, *Mater. Res. Bull.* **5**, 179.
- Collongues, R., M. Perez y Jorba and G. Tilloca, 1972, *Monatsh. Chem.* **103**, 571.
- Collongues, R., F. Queyroux, M. Perez y Jorba and M.J.-C. Gilles, 1965, *Bull. Soc. Chim. Fr.*, 1141.
- Coutures, J., A. Rouanet, R. Verges and M. Foex, 1976a, *J. Solid State Chem.* **17**, 171.
- Coutures, J., F. Sibieude and M. Foex, 1976b, *J. Solid State Chem.*, in press.
- Coutures, J., R. Verges and M. Foex, 1974, *Mater. Res. Bull.* **9**, 1603.
- Croatto, U., 1943, *Gazz. Chim. Ital.* **73**, 257.
- Dannhauser, W. and P.A. Vaughan, 1955, *J. Amer. Chem. Soc.* **77**, 896.
- Daoudi, A., G. Demazeau and G. Le Flem., *Rev. Chim. Mineral.* **11**, 327.
- Daoudi, A. and G. Le Flem, 1972, *J. Solid State Chem.* **5**, 57.
- Daoudi, A. and G. Le Flem, 1973, *Mater. Res. Bull.* **8**, 1103.
- Decker, B. F. and J.S. Kasper, 1957, *Acta Crystallogr.* **10**, 332.
- Deiseroth, H.-J. and Hk Müller-Buschbaum, 1970, *Z. Anorg. Allg. Chem.* **375**, 152.
- Demazeau, G., C. Parent, M. Pouchard and P. Hagenmuller, 1972, *Mater. Res. Bull.* **7**, 913.
- de Pous, O., L. Albert and J.-C. Achard, 1973, *C.R. Acad. Sci., Paris, Ser. C* **276**, 763.
- Devallette, M., C. Fouassier and P. Hagenmuller, 1971, *C.R. Acad. Sci., Paris, Ser. C* **272**, 73.
- Berndt, U., R. Tanamas and C. Keller, 1976b, *J. Solid State Chem.* **17**, 113.

- Diehl, H.G. and C. Keller, 1971, *J. Solid State Chem.* **3**, 621.
- Diness, A.M. and R. Roy, 1969, *J. Mater. Sci.* **4**, 613.
- Domagala, R.F., 1966, Aerospace Research Laboratories Report 66-0230.
- Drofenik, M., D. Kolar and L. Golič, 1973, *J. Cryst. Growth* **20**, 75.
- Duclot, M., J. Vicat and C. Deportes, 1970, *J. Solid State Chem.* **2**, 236.
- Dyer, A.J. and E.A.D. White, 1964, *Trans. Brit. Ceram. Soc.* **63**, 301.
- Etsell, T.H. and S.N. Flenglas, 1970, *Chem. Rev.* **70**, 339.
- Eyring, L. and B. Holmberg, 1963, Ordered phases and nonstoichiometry in rare earth oxide systems, in: *Non-stoichiometric Compounds, Advances in Chemistry 39* (American Chemical Society, Washington, D.C.) pp. 46-57.
- Faucher, M. and P. Caro, 1975, *J. Solid State Chem.* **12**, 1.
- Fauquier, D. and M. Gasperin, 1970, *Bull. Soc. Fr. Mineral. Cristallogr.* **93**, 258.
- Fava, J. and G. Le Flem, 1975, *Mater. Res. Bull.* **10**, 75.
- Fava, J., Y. Oudalov, J.-M. Reau, G. Le Flem and P. Hagenmuller, 1972, *C.R. Acad. Sci., Paris. Ser. C* **274**, 1837.
- Ferguson, I.F. and P.G.T. Fogg, 1957, *J. Chem. Soc.* 3679.
- Ferguson, R.B., 1957, *Can. Mineral.* **6**, 72.
- Foex, M., 1966, *Rev. Int. Htes Temp. Refr.* **3**, 309.
- Foex, M. and J.P. Traverse, 1966a, *Bull. Soc. Fr. Mineral. Cristallogr.* **89**, 184.
- Foex, M. and J.P. Traverse, 1966b, *Rev. Int. Htes. Temp. Refr.* **3**, 429.
- Friedman, L.M., K.E. Oberg, W.M. Boorstein and R.A. Rapp, 1973, *Met. Trans.* **4**, 69.
- Fuess, H. and A. Kallel, 1972, *J. Solid State Chem.* **5**, 11.
- Ganguly, P. and C.N.R. Rao, 1973, *Mater. Res. Bull.* **8**, 405.
- Gasperin, M., 1975, *Acta Crystallogr.* **B31**, 2129.
- George, A.M., I.K. Gopalakrishnan and M.D. Karkhanavala, 1974, *Mater. Res. Bull.* **9**, 721.
- Gingerich, K.A. and G. Brauer, 1963, *Z. Anorg. Allg. Chem.* **324**, 48.
- Gmelin, 1974a, Alkali oxometallates and alkali hydroxometallates of Sc, Y, La, and the lanthanides, in: *Handbuch de Anorganischen Chemie, 8 Auflage, System—Nummer 39, Seltenerdelemente Teil C2* (Springer-Verlag, Berlin) pp. 114-142.
- Gmelin, 1974b, Sc_2O_3 , Y_2O_3 , La_2O_3 and In_2O_3 . Comparative data, in: *Handbuch der Anorganischen Chemie, 8 Auflage, System—Nummer 39, Seltenerdelemente Teil C1* (Springer-Verlag, Berlin) pp. 104-436.
- Goldschmidt, V.M., T. Barth, G. Lunde, W.H. Zachariasen, 1926, *Skr. Norske Vidensk.-Akad. Oslo I. Mat.-Naturvidensk. Kl.*, **2**.
- Gondrand, M. and E.F. Bertaut, 1963, *Bull. Soc. Fr. Mineral. Cristallogr.* **86**, 301.
- Gondrand, M., M. Brunel and F. de Bergevin, 1972, *Acta Crystallogr.* **B28**, 722.
- Goodenough, J.B., 1973, *Mater. Res. Bull.* **8**, 423.
- Goodenough, J.B., G. Demazeau, M. Puchard and P. Hagenmuller, 1973, *J. Solid State Chem.* **8**, 325.
- Goto, K.S. and W. Plushkell, 1972, Oxygen concentration cells, in: *Physics of Electrolytes, Vol. 2*, (Academic Press, London) pp. 540-622.
- Greedan, J.E. and G.J. McCarthy, 1972, *Mater. Res. Bull.* **7**, 531.
- Guillen, M. and E.F. Bertaut, 1966, *C.R. Acad. Sci., Paris, Ser. C* **262**, 962.
- Haas, H. and Kordes, E., 1969, *Z. Kristallogr.* **129**, 259.
- Harris, L.A. and H.L. Yakel, 1967, *Acta Crystallogr.* **22**, 354.
- Hladik, J., 1972, Reference Electrodes, in: *Hladik, J., ed., Physics of Electrolytes, Vol. 2*, (Academic Press, London) pp. 839-865.
- Hoch, M. and F.J. Furman, 1965, Thermodynamics, Proceedings IAEA Symposium, Vienna, 1965, Vol. 2, pp. 849-853.
- Hoekstra, H.R. and F. Gallagher, 1968, *Inorg. Chem.* **7**, 2553.
- Hofmann, K.A., K. Hoeschele, 1915, *Ber. dtch. hem. Ges.* **48**, 20.
- Holmberg, B., 1966, *Acta Chem. Scand.* **20**, 1082.
- Hoppe, R., 1965, *Bull. Soc. Chim. Fr.* **4**, 1115.
- Hoppe, R. and W. Lidecke, 1962, *Naturwissenschaften* **49**, 255.
- Hoppe, R. and K. Seeger, 1968, *Naturwissenschaften* **55**, 297.
- Hund, F., 1951, *Z. Anorg. Allg. Chem.* **265**, 62.
- Hund, F. and U. Peetz, 1952a, *Z. Anorg. Allg. Chem.* **271**, 6.
- Hund, F. and U. Peetz, 1952b, *Z. Anorg. Allg. Chem.* **267**, 189.
- Hund, F. and U. Peetz, 1952c, *Z. Elektrochem.* **56**, 223.
- Hund, F., R. Wagner and U. Peetz, 1952d, *Z. Elektrochem.* **56**, 61.
- Hund, F. and R. Metzger, 1952e, *Z. Phys. Chem. (Leipzig)* **201**, 268.
- Hund, F., U. Peetz and G. Kottenhahn, 1955, *Z. Anorg. Allg. Chem.* **278**, 184.
- Hyde, B.G., A.M. Bagshaw, S. Andersson and M. O'Keefe, 1974, *Ann. Rev. Mater. Sci.* **4**, 43.
- Iijima, S., 1973, *Acta Crystallogr.* **A29**, 18.
- Ivanova, M.M., G.M. Balagina and E.Y. Rode, 1970, *Inorg. Mater.* **6**, 801.
- Ivanova, M.M. and E.M. Reznik, 1972, *Inorg. Mater.* **8**, 863.
- Jahnberg, L., 1963, *Acta Chem. Scand.* **71**, 2548.
- Joubert, J.C., A. Collomb, D. Elmaleh, G. Le Flem, A. Daoudi and G. Ollivier, 1970, *J. Solid State Chem.* **2**, 343.
- Joubert, J.C., D. Samaras and A. Collomb, 1971, *Mater. Res. Bull.* **6**, 341.
- Kalinovskaya, G.A., R.M. Spiridonov and L.N. Komissarova, 1969, *J. Less-Common Metals* **17**, 151.

- Keeling, R.O., 1957, *Acta Crystallogr.* **10**, 209.
- Keller, C., 1962, *Z. Anorg. Allg. Chem.* **318**, 89.
- Keller, C., 1972, Lanthanide and actinide mixed oxide systems with alkali and alkaline-earth metals, in: Bagnall, K.W., ed., *MTP International Review of Science, Inorganic Chemistry Series One, Vol. 7, Lanthanides and Actinides* (Butterworths, London), pp. 47-85.
- Keller, C., 1975a, Lanthanide and actinide mixed oxide systems of face-centred cubic symmetry, in: Bagnall, K.W., ed., *MTP International Review of Science, Inorganic Chemistry Series Two, Vol. 7, Lanthanides and Actinides* (Butterworths, London) pp. 1-39.
- Keller, C., 1975b, Ternary and polynary oxides of uranium, in: Gmelin, *Handbuch der Anorganischen Chemie, 8 Auflage, System-Nummer 55, Uran Teil C3* (Springer-Verlag, Berlin) pp. 197-249.
- Keller, C. 1976, Ternary and polynary oxides of thorium, in: Gmelin, *Handbuch der Anorganischen Chemie, 8 Auflage, System-Nummer 44, Thorium Teil C2* (Springer-Verlag, Berlin) to be published.
- Keller, C., U. Berndt, H. Engerer and L. Leitner, 1972, *J. Solid State Chem.* **4**, 453.
- Keller, C. and A. Boroujerdi, 1972, *J. Inorg. Nucl. Chem.* **34**, 1187.
- Keller, C., H. Engerer, L. Leitner and U. Sriyoth, 1969, *J. Inorg. Nucl. Chem.* **31**, 965.
- Keller, C., H. Engerer and H. Seiffert, 1969, *J. Inorg. Nucl. Chem.* **31**, 2727.
- Klee, W.E. and G. Weitz, 1969, *J. Inorg. Nucl. Chem.* **31**, 2367.
- Klemm, W. and H.A. Klein, 1941, *Z. Anorg. Allg. Chem.* **248**, 167.
- Klevtsov, P.V. and L.P. Kozeeva, 1970, *Soviet Phys.—Crystallogr.* **15**, 44.
- Knop, O., F. Brisse and L. Castelliz, 1969, *Can. J. Chem.* **47**, 971.
- Knop, O., F. Brisse, L. Castelliz and Sutarno, 1965, *Can. J. Chem.* **43**, 2812.
- Knop, O., F. Brisse, R.E. Meads and J. Bainbridge, 1968, *Can. J. Chem.* **46**, 3829.
- Komissarova, L.N., B.I. Pokrovskii and V.V. Nechaeva, 1966, *Dokl. Akad. Nauk, SSSR* **168**, 1076.
- Komissarova, L.N., S.S. Plotkin and V.E. Plyuschchev, 1968, *Russ. J. Inorg. Chem.* **13**, 934.
- Komissarova, L.N., K-S. Wang, V.I. Spitsyn and Y.P. Simanov, 1964, *Russ. J. Inorg. Chem.* **9**, 383.
- Komkov, A.I., 1959, *Soviet Phys.—Crystallogr.* **4**, 796.
- Kordis, J. and L. Eyring, 1968a, *J. Phys. Chem.* **72**, 2030.
- Kordis, J. and L. Eyring, 1968b, *J. Phys. Chem.* **72**, 2044.
- Koshcheev, G.G. and L.M. Kovba, 1966, *Inorg. Mater.* **2**, 1070.
- Koshcheev, G.G., L.M. Kovba and V.I. Spitsyn, 1967, *Dokl. Akad. Nauk SSSR* **175**, 92.
- Lang, S.M., F.P. Knudsen, C.L. Fillmore and R.S. Roth, 1956, *Natl. Bur. Stds. Circ. No.* 568.
- Lasker, M.F. and R.A. Rapp, 1966, *Z. Physik. Chem.* **49**, 198.
- Latavalya, N., 1976, Ph.D. Thesis, Flinders University of South Australia.
- Lefèvre, J., 1963, *Ann. Chim.* **8**, 117.
- Lehuéde, P. and M. Daire, 1973, *C.R. Acad. Sci., Paris, Ser. C* **276**, 1011.
- Leitner, L., 1967, KFK-521.
- Loier, C., P. Caro, R. Portier and M. Fayard, 1974, *Mater. Res. Bull.* **9**, 1553.
- Lopato, L.M., I.M. Maister and A.V. Shevchenko, 1972, *Inorg. Mater.* **8**, 861.
- Longo, V. and D. Minichelli, 1973, *J. Amer. Ceram. Soc.* **56**, 600.
- Longo, J.M. and P.M. Raccach, 1973, *J. Solid State Chem.* **6**, 526.
- Longo, V. and S. Roitti, 1971, *Ceramurgia* **1**, 4.
- McCarthy, G.J., 1971, *Mater. Res. Bull.* **6**, 31.
- McCarthy, G.J. and R.D. Fischer, 1971, *Mater. Res. Bull.* **6**, 591.
- McCarthy, G.J., R.D. Fisher, G.G. Johnson and C.E. Gooden, 1972, *N.B.S. Special Publication* 364, 397.
- McCarthy, G.J., W.B. White and R. Roy, 1969, *J. Inorg. Nucl. Chem.* **31**, 329.
- MacChesney, J.B. and H.A. Saver, 1962, *J. Am. Ceram. Soc.* **45**, 416.
- McCullough, J.D., 1950, *J. Amer. Chem. Soc.* **72**, 1386.
- McCullough, J.D. and J.D. Britton, 1952, *J. Amer. Chem. Soc.* **74**, 5225.
- Magnéli, A. and E. Kihlberg, 1951, *Acta Chem. Scand.* **5**, 578.
- Mann, A.W. and D.J.M. Bevan, 1970, *Acta Crystallogr.* **B26**, 2129.
- Mann, A.W. and D.J.M. Bevan, 1972, *J. Solid State Chem.* **5**, 410.
- Marchand, R., 1976, *C.R. Acad. Sci., Paris, Ser. C* **282**, 329.
- Markin, T.L. and E.C. Crouch, 1970, *J. Inorg. Nucl. Chem.* **32**, 77.
- Markin, T.L., R.S. Street, and E.C. Crouch, 1970, *J. Inorg. Nucl. Chem.* **32**, 59.
- Möbius, H-H., 1964, *Z. Chem.* **4**, 81.
- Mokhosoev, M.V., V.I. Krivobok, S.M. Aleikina, N.S. Zhigulina and N.G. Kisel, 1967, *Inorg. Mater.* **3**, 1444.
- Molyneux, A.R.M., 1973, Ph.D. Thesis, Flinders University of South Australia.
- Montmory, M-C. and F. Bertaut, 1961, *Bull. Soc. Chim. Fr.* 4171.
- Muller, O., W.B. White and R. Roy, 1964, *J. Inorg. Nucl. Chem.* **26**, 2075.
- Müller-Buschbaum, Hk., 1966, *Z. Anorg. Allg. Chem.* **343**, 113.
- Müller-Buschbaum, Hk., 1967, *Z. Anorg. Allg. Chem.* **335**, 41.
- Müller-Buschbaum, Hk., 1968, *Z. Anorg. Allg. Chem.* **358**, 138.
- Müller-Buschbaum, Hk. and W. Muschick, 1975, *Z. Anorg. Allg. Chem.* **412**, 209.
- Müller-Buschbaum, Hk. and R. von Schenck, 1970, *Z. Anorg. Allg. Chem.* **377**, 70.
- Müller-Buschbaum, Hk. and H.G. Schnering, 1965, *Z. Anorg. Allg. Chem.* **336**, 295.
- Müller-Buschbaum, Hk. and C. Teske, 1969, *Z. Anorg. Allg. Chem.* **369**, 249.

- Müller-Buschbaum, Hk. and W. Wollschläger, 1975, *Z. Anorg. Allg. Chem.* **414**, 76.
- Mumme, W.G. and A.D. Wadsley, 1968, *Acta Crystallogr.* **B24**, 1327.
- Murav'eva, I.A., L.M. Kovba, L.I. Martynenko and V.I. Spitsyn, 1965, *Russ. J. Inorg. Chem.* **10**, 959.
- Nanot, M., F. Queyroux, J.-C. Gilles, R. Portier and M. Fayard, 1975, *Mater. Res. Bull.* **10**, 313.
- Nanot, M., F. Queyroux, J.-C. Gilles, A. Carpy and J. Galy, 1974, *J. Solid State Chem.* **11**, 272.
- Natansohn, S., 1968, *J. Inorg. Nucl. Chem.* **30**, 741.
- Nath, D.K., 1970, *Inorg. Chem.* **9**, 2714.
- Nernst, W., 1899, *Z. Elektrochem.* **6**, 41.
- Ostorero, J., H. Makram and J. Loriers, 1974, *C.R. Acad. Sci., Paris, Ser. C* **278**, 737.
- Oudalov, J.P., A. Daoudi, J.-C. Joubert, G. Le Flem and P. Hagenmuller, 1970, *Bull. Soc. Chim. Fr.* 3408.
- Paletta, E. and R. Hoppe, 1966, *Naturwissenschaften* **23**, 611.
- Paletta, E. and Hk. Müller-Buschbaum, 1968, *J. Inorg. Nucl. Chem.* **30**, 1425.
- Parks, T.C. and D.J.M. Bevan, 1973, *Rev. Chim. Mineral.* **10**, 15.
- Pausch, H. and Hk. Müller-Buschbaum, 1972, *Z. Naturforsch.*, **B 27**, 888.
- Perez y Jorba, M., 1962, *Ann. Chim. (Paris)* **7**, 511.
- Perez y Jorba, M., H. Mondange, R. Collongues, 1961, *Bull. Soc. Chim. Fr.* **28**, 79.
- Pokrovskii, A.N., V.K. Rybakov and V.K. Trunov, 1969, *Russ. J. Inorg. Chem.* **14**, 1233.
- Polyanskaya, T.M., S.V. Borisov, N.V. Belov, 1971, *Soviet Phys. Crystallogr.* **15**, 636.
- Queyroux, F., 1963, *Bull. Soc. Fr. Mineral. Crystallogr.* **86**, 295.
- Queyroux, F., 1964, *C.R. Acad. Sci., Paris, Ser. C* **259**, 1527.
- Queyroux, F., M. Huber and R. Collongues, 1970, *C.R. Acad. Sci., Paris, Ser. C* **270**, 806.
- Rabenaou, A. and P. Eckerlin, 1958, *Acta Crystallogr.* **11**, 304.
- Radzewitz, H., 1966, *KFK-433*.
- Rau, R.C., 1966, *Acta Crystallogr.* **20**, 716.
- Reid, A.F., A.D. Wadsley and M.J. Sienko, 1968, *Inorg. Chem.* **7**, 112.
- Rode, E.Y. and V.N. Karpov, 1966, *Inorg. Mater.* **2**, 587.
- Roether, U., 1967, Ph.D. Thesis, University of Freiberg.
- Roititi, S. and V. Longo, 1972, *Ceramurgia* **2**, 97.
- Rooksby, H.P. and E.A.D. White, 1963, *Acta Crystallogr.* **16**, 888.
- Rooksby, H.P. and E.A.D. White, 1964, *J. Amer. Ceram. Soc.* **47**, 94.
- Rooymans, C.J.M., 1961, *Z. Anorg. Allg. Chem.* **313**, 234.
- Rossell, H.J., 1976, to be published.
- Roth, R.S., 1956, *J. Res. Nat. Bur. Stand.* **56**, 17.
- Roth, R.S., 1964, *Progress in the Science and Technology of Rare Earths*, Vol. 1, (Pergamon, Oxford) pp. 167-202.
- Quezel-Ambrunaz, S., F. Bertaut and G. Buisson, 1964, *Compt. Rend.* **258**, 3025.
- Ruh, R., 1968, *Proc. 2nd Intern. Conf. Therm. Anal. - 1968*, (Pub. 1969) **2**, 851.
- Sibieude, F., G. Schiffmacher and P. Caro, 1978, *J. Solid State Chem.* **23**, 361.
- Rouanet, A., 1971, *Rev. Int. Htes Temp. Réfr.*, **8**, 161.
- Rouanet, A., J. Coutures and M. Foex, 1972, *J. Solid State Chem.* **4**, 219.
- Ruddlesden, S.N. and P. Popper, 1957, *Acta Crystallogr.* **10**, 538.
- Ruddlesden, S.N. and P. Popper, 1958, *Acta Crystallogr.* **11**, 54.
- Rüdorff, W. and G. Valet, 1953, *Z. Anorg. Allg. Chem.* **271**, 257.
- Ruh, R., 1967, American Ceramic Society Meeting.
- Salmon, R., H. Baudry, J. Grannec and G. Le Flem, 1974, *Rev. Chim. Mineral.* **11**, 71.
- Salmon, R. and G. Le Flem, 1972, *C.R. Acad. Sci., Paris, Ser. C* **274**, 292.
- Scheunemann, K. and Hk. Müller-Buschbaum, 1975, *J. Inorg. Nucl. Chem.* **37**, 1879.
- Schneider, S.J. and R.S. Roth, 1960, *J. Res. Nat. Bur. Stand.* **A64**, 317.
- Schneider, S.J., J.L. Waring and R.E. Tressler, 1965, *J. Res. Nat. Bur. Stand.* **69A**, 245.
- Schnering, H.G. and P. Bleckmann, 1968, *Z. Naturwiss.* **55**, 342.
- Schwarz, H., 1963a, *Z. Anorg. Allg. Chem.* **322**, 15.
- Schwarz, H., 1963b, *Z. Anorg. Allg. Chem.* **322**, 1.
- Schwarz, H. and D. Bommert, 1964, *Z. Naturforsch.*, **B 19**, 955.
- Seeger, K. and R. Hoppe, 1969, *Z. Anorg. Allg. Chem.* **365**, 22.
- Shannon, R.D. and C.T. Prewitt, 1969, *Acta Crystallogr.* **B25**, 925.
- Shannon, R.D., D.B. Rogers and C.T. Prewitt, 1971, *Inorg. Chem.* **10**, 713.
- Shannon, R.D. and A.W. Sleight, 1968, *Inorg. Chem.* **7**, 1649.
- Shaplygin, I.S. and V.B. Lazarev, 1973, *Mater. Res. Bull.* **8**, 761.
- Shoemaker, C.B., 1973, *Z. Kristallogr.* **137**, 225.
- Sibieude, F., 1973, *J. Solid State Chem.* **7**, 7.
- Sibieude, F. and M.G. Chaudron, 1970, *C.R. Acad. Sci., Paris, Ser. C* **271**, 130.
- Sibieude, F. and M. Foex, 1975, *J. Nucl. Mater.* **56**, 229.
- Sibieude, F., D. Hernandez and M. Foex, 1974, *C.R. Acad. Sci., Paris, Ser. C* **278**, 1279.
- Sleight, A.W., 1968, *Inorg. Chem.* **7**, 1704.
- Sleight, A.W., 1968, *Mater. Res. Bull.* **3**, 699.
- Spiridonov, F.M. and L.N. Komissarova, 1970, *Russ. J. Inorg. Chem.* **15**, 445.
- Spiridonov, F.M., L.N. Komissarova, A.G. Kocharov and V.I. Spitsyn, 1969, *Russ. J. Inorg. Chem.* **14**, 1332.
- Spiridonov, F.M., L.N. Popova and R. Ya. Popil'skii, 1970, *J. Solid State Chem.* **2**, 430.
- Spiridonov, F.M., V.A. Stepanov, L.N. Komissarova and V.I. Spitsyn, 1968, *J. Less-Common Metals* **14**, 435.
- Spitsyn, V.I., I.A. Murav'eva, L.M. Kovba and I.I. Korchak, 1969, *Russ. J. Inorg. Chem.* **14**, 759.
- Stadlbauer, E., U. Wichmann, U. Lott and C. Keller, 1974, *J. Solid State Chem.* **10**, 341.
- Steele, B.C.H., 1972, *Electrical conductivity in ionic solids*, in: Roberts, L.E.J., ed., *M.T.P.*

- Steele, B.C.H. (cont.)
International Review of Science, Inorganic Chemistry Series One, Vol. 10, Solid State Chemistry (Butterworths, London) p. 117.
- Steele, B.C.H., 1976, High temperature fuel-cells and electrolyzers, in: Electrode Processes in Solid State Ionics, Proceedings of NATO Advanced Study Institute, 1975, to be published.
- Steele, B.C.H. and G.J. Dudley, 1975, Mass transport in ionic solids, in: Roberts, L.E.J., ed., MTP International Review of Science, Inorganic Chemistry Series Two, Vol. 10, Solid State Chemistry (Butterworths, London) p. 181.
- Strickler, D.W. and W.G. Carlson, 1963, Westinghouse Research Lab. Paper 63-143-267-P2.
- Strickler, D.W. and W.G. Carlson, 1964, Westinghouse Research Lab. Scientific Paper 64-918-273.
- Stubican, V.S., 1964, J. Amer. Ceram. Soc. **47**, 55.
- Stubican, V.S. and R. Roy, 1963, Z. Kristallogr. **119**, 90.
- Summerville, E., 1973, Ph. D. Thesis, The Flinders University of South Australia.
- Sych, A.M. and V.G. Klenus, 1973, Inorg. Mater. **9**, 1081.
- Takahashi, T., 1972, Solid electrolyte fuel cells (theoretics and experiments), in: Hladik, J., ed. Physics of Electrolytes, Vol. 2, (Academic Press, London) pp. 989-1049.
- Tanguy, B., M. Vlasse and J. Portier, 1973, Rev. Chim. Mineral. **10**, 63.
- Templeton, D.H., 1957, Acta Crystallogr. **10**, 788.
- Thorner, M.R., 1969, Ph.D. Thesis, University of Western Australia.
- Thorner, M.R. and D.J.M. Bevan, 1970, J. Solid State Chem. **1**, 536.
- Thorner, M.R., D.J.M. Bevan and J. Graham, 1968, Acta Crystallogr. **B24**, 1183.
- Thorner, M.R., D.J.M. Bevan and E. Summerville, 1970, J. Solid State Chem. **1**, 545.
- Tilloca, G., M. Perez y Jorba and F. Queyroux, 1970, C.R. Acad. Sci., Paris, Ser. C **271**, 134.
- Trömel, M. and J. Hauck, 1969, Z. Anorg. Allg. Chem. **368**, 248.
- Trunov, V.K., G.I. Tyushevskaya and N.S. Afonskii, 1968, Russ. J. Inorg. Chem. **13**, 491.
- Tuller, H.L. and A.S. Nowick, 1975, J. Electrochem. Soc. **122**, 255.
- Vinson, J-M. and J-P. Faurie, 1973, C.R. Acad. Sci., Paris, Ser. C **276**, 1183.
- Vladimirova, Z.A., V.K. Trunov and L.N. Komissarova, 1970, Russ. J. Inorg. Chem. **15**, 1491.
- Von Dreele, R.B., L. Eyring, A.L. Bowman and J.L. Yarnell, 1975, Acta Crystallogr. **B31**, 971.
- Waring, J.L. and S.J. Schneider, 1965, J. Res. Nat. Bur. Stand. **A69**, 255.
- Warsaw, I. and R. Roy, 1964, Progress in the Science and Technology of the Rare Earths, Vol. 1, (Pergamon, Oxford) pp. 203-221.
- Whinfrey, C.G., D.W. Eckart and A. Tauber, 1960, J. Amer. Chem. Soc. **82**, 2695.
- Whitfield, H.J., D. Roman and A.R. Palmer, 1966, J. Inorg. Nucl. Chem. **28**, 2817.
- Willer, B. and M. Daire, 1968, C.R. Acad. Sci., Paris, Ser. C **267**, 1482.
- Wolf, L. and H. Schwab, 1964, J. Prakt. Chem. **4**, 293.
- Wolten, G.M., 1967, Acta Crystallogr. **23**, 939.
- Wolten, G.M. and A.B. Chase, 1967, Amer. Mineral. **52**, 1536.
- Worrell, W.L. and J. Hladik, 1972, Thermodynamic equilibrium diagrams, in: Hladik, J., ed., Physics of Electrolytes, Vol. 2, (Academic Press, London) pp. 747-798.
- Wyart, J., P.V. Klevtsov, L.Y. Kharchenko and T.M. Polyanskaya, 1970, Bull. Soc. Fr. Mineral. Cristallogr. **93**, 536.
- Wyckoff, W.G., 1964, Crystal structures (John Wiley and Sons, New York) Vol. 2, p. 534.
- Wyckoff, W.G., 1965a, Crystal structures (John Wiley and Sons, New York) Vol. 3, pp. 19-21.
- Wyckoff, W.G., 1965b, Crystal structures (John Wiley and Sons, New York) Vol. 3, pp. 15-18.
- Zachariasen, W.H., 1951, Acta Crystallogr. **4**, 231.
- Zintl, E. and U. Croatto, 1939, Z. Anorg. Allg. Chem. **242**, 79.
- Zintl, E. and W. Morawietz, 1940, Z. Anorg. Allg. Chem. **245**, 26.

References to section 6

- Allpress, J.G. and H.J. Rossell, 1978, to be published, private communication.
- Rossell, H.J., 1978, to be published, private communication.
- Summerville, E., J. Drennan and D.J.M. Bevan, 1978, J. de Phys., to be published.

Wichmann, U., 1974, Phase conversion and phase equilibrium of uranium-rare earth mixed oxides, KFK -1924, Kernforschungszent Karlsruhe, Karlsruhe Germany.

Chapter 29

PEROVSKITES AND GARNETS*

C.P. KHATTAK

Crystal Systems Inc. Shetland Industrial Park, P.O. Box 1057, Salem,
 Massachusetts 01970, USA

and

F.F.Y. WANG

Department of Materials Science, State University of New York, Stony Brook,
 New York 11794, USA

Contents

1. Introduction	527
2. Perovskites	528
2.1. Preparation	528
2.2. Crystal chemistry	534
2.3. Crystal structure	537
2.4. Phase transition	552
2.5. Magnetic properties	553
2.6. Electrical properties	558
2.7. Optical properties	561
2.8. Catalytic properties	562
3. Garnets	563
3.1. Crystal structure	563
3.2. Crystal chemistry	564
3.3. Phase equilibria	566
3.4. Preparation	566
3.5. Magnetic properties	569
3.6. Optical properties	579
3.7. Thermal properties	590
3.8. Elastic properties	597
References	601

	coefficients for the electric-dipole rotation
	a_f = face centered cell constant
	A_L = temperature coefficient of lattice
	a_0 = cubic pseudocell constant
	a_0 = lattice constant at 296K
	$a_{ortho}, b_{ortho}, c_{ortho}$ = cell constants of the distorted perovskite
	a_p = primitive rhombohedral cell constant
	B_{ijk} = magnetoelastic energy tensor
	$B(x)$ = Brillouin function (Morrish, 1965)
	C = specific heat
	c = free-space velocity of light
	C_{11}, C_{12}, C_{44} = elastic constants
	C_L = lattice specific heat
	C_M = magnetic specific heat
	C_N = nuclear specific heat
	C_v = specific heat in garnet
	D = crystal field tensor of the ion
	D = dispersion constant

Symbols

A	= elastic anisotropy
a	= cubic lattice constant of garnet
A, B, C	= frequency-dependent

*By acceptance of this article, the publisher and/or recipient acknowledges the U.S. Government's right to retain a nonexclusive, royalty-free license in and to any copyright covering this paper.

- d_0 = lattice spacing in the unstrained film
 E_a, E_d, E_c = probability of an ion at a-, d-, and c-sites, respectively
 f = constant; multiplying factor
 F_k, F_0 = anisotropy energy
 \mathbf{g} = g -tensor of the ion
 g = splitting factor
 $G(\kappa_0/\kappa_0^b)$ = crystal complexity factor
 $g_{N,i}$ = nuclear spin factor
 $G(T)$ = moderating function
 \mathbf{H} = applied external magnetic field
 H_A = anisotropy field
 $\mathbf{H}_a, \mathbf{H}_d, \mathbf{H}_c$ = Fields acting at a-, d-, and c-sites, respectively
 H_{int}^c = phase boundary between the antiferromagnetic and the paramagnetic phase
 H_M = magnetic Hamiltonian
 H_{ME} = linear magnetoelastic energy
 $H_{N,i}$ = field at the nucleus
 I = transmitted light intensity
 I_0 = incident light intensity
 I, b, c, d = mean thermal expansion coefficient
 I_i = nuclear spin
 J_a, J_d, J_c = the intrasublattice exchange constants
 K_1 = first-order magnetocrystalline anisotropy constants
 K_2 = second-order magnetocrystalline anisotropy constants
 k_B = Boltzmann constant
 K_C, K_A, K_D = least square parameters indicating the cation contributions to the lattice constant from the c-, a-, and d-site, respectively.
 $\langle M \rangle$ = average atomic mass of an atom in the garnet crystal in grams
 $\mathbf{M}_a, \mathbf{M}_d, \mathbf{M}_0$ = Moduli of the sublattice magnetizations
 $\mathbf{M}_d(T), \mathbf{M}_a(T), \mathbf{M}_c(T)$ = sublattice magnetization of the d-, a-, and c-sites, respectively
 $M_{\text{Fe}(d)}, M_{\text{Fe}(a)}, M_{\text{Re}}$ = algebraic sublattice magnetizations
 $\mathbf{M}(T)$ = net magnetic moment of the garnet
 $M(T)$ = saturation magnetization of the rare earth iron garnet
 $M_{\text{YIG}}(T)$ = saturation magnetization of YIG
 n = mean infrared refractive index
 n = total magnetic moment
 $\langle n \rangle$ = average refractive index
 N_a, N_d, N_c = the number of atoms per unit volume for a-, d-, and c-sites, respectively
 n_a, n_d, n_c = magnetic moment at a-, d-, and c-sites, respectively
 N_{aa}, N_{ad}, N_{ac}
 N_{da}, N_{dd}, N_{dc}
 N_{ca}, N_{cd}, N_{cc} } molecular field coefficients
 $P_{O_2}(\log P_{O_2})$ = oxygen partial pressure
 R = figure of merit
 R = gas constant
 R = single-surface reflection loss at normal incident
 R_A, R_B, R_O = respective ionic radii
 $\langle r_C \rangle, \langle r_A \rangle, \langle r_D \rangle$ = mean effective radius of C-, A-, and D-sites respectively
 S = spin of the ion
 T = temperature
 t = thickness in centimeters
 t = tolerance factor (defined by Goldschmidt)
 $T(-10^5(1/T))$ = incongruent melting point
 T_N = Neel temperature
 $\langle V \rangle$ = average velocity of sound in the Debye approximation
 V_0 = average velocity of sound in the Oliver and Slack approximation
 $\langle V_0 \rangle$ = average volume in

	cubic angstroms		representations of the
W_{Eu}	= masses of the Eu ion		transverse optical
W_{RE}	= masses of the rare		modes
	earth	(γ)	= average Gruneisen con-
	α = optical absorption		stant
	coefficient	γ_{Fe}, γ_{Re}	= gyromagnetic ratios
$\alpha_1, \alpha_2, \alpha_3$	= direction cosines of M	Γ_T	= sound attenuation
	with respect to the		(dB/ μ sec)
	crystal axes	Δa	= lattice constant in the
α_F (dispersive)	= dispersive contribution		temperature range 296-
	to the Faraday effect in		1400K
	iron garnets	Δd^\perp	= difference between the
α_F (nondispersive)	= nondispersive contri-		lattice spacing in the
	bution to the Faraday		strained and in the un-
	effect in iron garnets		strained condition
	α_r = angle between edges,	ϵ^\perp	= strain perpendicular to
	face centered cell		the surface
α_i, α_j	= direction cosines of	ϵ_{kl}	= strain components in
	magnetization with		Love's notation
	respect to the crystal	θ_D	= Debye temperature
	axes	κ_0	= thermal conductivity
α_p	= angle between edges,	λ	= wavelength
	primitive rhombohedral	$\lambda_{(100)}, \lambda_{(111)}$	= saturation magnet-
	cell		striction constants
β_N	= nuclear magneton	μ_B	= Bohr magneton
Γ	= sound attenuation	ρ	= density
	(dB/cm)	Ω	= angular frequency of
Γ	= total irreducible rep-		the sound wave

1. Introduction

The extensive research devoted to the physics and chemistry of solids during the last quarter of a century has led to great advances in the understanding of the properties of solids in general. One area of very active research has been mixed oxide systems. These have been of particular interest because of their stability and the fact that a wide range of properties can be obtained by substitution of one ion for another. Two of the most extensively studied groups of compounds are the perovskites and garnets.

Ever since the discovery of the ferroelectric properties of barium titanate, perovskite compounds of the type ABO_3 have been widely studied. They now constitute a large group of materials of great importance in solid state physics and chemistry. For example, the electrical conductivity of perovskites varies over many orders of magnitude. Many such as $BaTiO_3$ and $SrTiO_3$ are noted for their high resistivities, which makes them useful as dielectric materials, while others such as $CaMoO_3$ and $LaTiO_3$ are fairly good conductors or semiconductors. Strontium-doped $LaCrO_3$ is currently a possible candidate for high

temperature electrodes. A novel property recently reported is the insulator-metal transition in Sr-doped LaVO_3 . Lead zirconate-lead titanate solid solutions have been used in solid state devices because of their piezoelectric properties. Various perovskites have been utilized for their optical properties such as electro-optic effect, coloration by light, application in laser host materials, etc. In addition to these applications, certain perovskite oxides have catalytic properties comparable to those of platinum in the oxidation of carbon monoxide and hydrocarbons. This is of obvious significance in the area of automobile emission control. The catalytic properties have also been utilized for making ethanol sensors (Obayaski et al., 1976).

The discovery of ferrimagnetism in yttrium iron garnet has attracted attention to the use of these materials for microwave device applications. To date garnets are the most useful materials in the microwave industry because of their magnetization, linewidth, Curie temperature and g -factor properties. With the advent of solid-state lasers, yttrium aluminum garnet was soon found to be an excellent laser host material for room temperature and high power applications.

Current research on weakly ferromagnetic materials, such as garnets and orthoferrites, for magnetic bubble domain devices has stimulated further interest in the magnetic properties of these compounds. These devices will be used for integrated circuit memory and charged coupled devices in the next generation of computer memory technology.

2. Perovskites

2.1. Preparation

The perovskite structure is a close-packed lattice with the general formula ABX_3 . Almost all the known rare earth perovskites are oxides with the rare earth ion occupying the A sites and the present discussion will hence be restricted to ABO_3 type compounds. Since most of the rare earth ions are stable only in the trivalent state the valence relationship is $\text{A}^{3+}\text{B}^{3+}\text{O}_3$. It is much easier to obtain the compounds in polycrystalline than in single crystal form; however in some instances crystals have been prepared for special applications.

2.1.1. Powder synthesis

Many of the perovskite compounds can be prepared by high-temperature solid-state reaction of binary oxides or peroxides. However, some of these tend to be refractory and hence unreactive. Others have a tendency to hydrate or oxidize and are inconvenient to use. Therefore, it is preferable to use carbonates, oxalates, or other easily decomposable compounds, assuming they can be obtained with suitable purity. These materials are usually in the form of fine powders and decompose in the initial stages of the reaction so that faster reaction rates are obtained. In some cases fine powders may be obtained by

evaporation of solutions. The rare earth raw materials are generally sesquioxides. Since solid state reactions often do not proceed to completion on the first firing, repeated regrinding and reheating is usually necessary. The reaction is conveniently followed by weight loss measurements and by X-ray analysis. The reaction is generally carried out in alumina, zirconia or platinum crucibles which are fairly inert towards these compounds. However, if necessary, reaction of the crucible is avoided by placing the reactants on top of compacts of the same material.

In a typical preparation of LaCoO_3 powder, an equimolar mixture of the appropriate oxalates was decomposed by slow heating to 600°C . The resultant material was pressed into pellets and fired at 1000 to 1200°C for two days. Repeated grinding and firing was necessary to eliminate the unreacted material (Racah and Goodenough, 1967).

If one of the constituent materials is volatile, special precautions need to be taken. Problems of this nature are frequently encountered in the synthesis of lead-containing perovskites due to the volatility of lead oxide. Under these circumstances the reaction is carried out in a lead oxide atmosphere, by using excess lead oxide, or in a closed system such as an evacuated silica tube.

In some instances the valence state of an ion may be different in the final compound from that in an available raw material. For example, in LaVO_3 the vanadium is in the trivalent state whereas it is in a pentavalent state in V_2O_5 . Thus LaVO_3 was synthesized by reacting La_2O_3 and V_2O_5 in a vacuum of 10^{-4} mm (Shin-ike et al., 1976). In the case of LaNiO_3 , the compound was prepared by reacting the appropriate oxalates in oxygen (Goodenough and Racah, 1965).

In general, conditions which are ideal for the formation of one compound may be unsuitable for another similar material. Hence the proper equilibrium conditions for the synthesis of each compound under study must be determined.

2.1.2. *Crystal growth*

Although single crystals of some perovskite compounds have been grown in large sizes, those containing rare earths have generally been rather small. This may be because they have high melting points and suitable fluxes are not known. Furthermore, most of the rare earth perovskites undergo phase transitions at elevated temperatures which present problems in the preparation of single crystals by many of the usual techniques.

A majority of the rare earth perovskites have been grown from a fluxed melt. The most commonly used fluxes are lead oxide and lead fluoride. Boron oxide is generally added to increase the solubility. Single crystals are grown by heating the solute and flux to sufficiently high temperatures followed by either slow cooling or evaporation of the flux. A problem commonly encountered in the use of such a technique is the entrapment of lead into the perovskite lattice. It has been found that the growth of LaCrO_3 crystals by evaporation of a $\text{PbF}_2\text{-B}_2\text{O}_3$

TABLE 29.1.
Crystal growth details for some of the rare earth perovskite oxides.

Crystal	Technique ^a	Flux	Temp. range (°C)	Cooling rate (°C/h)	Approximate dimensions (mm)	References
LaAlO ₃ (Mn)	EV	Pb ₇ O ₂ F ₁₀	1200	—	3 × 3 × 0.4	Tsushima (1966)
LaAlO ₃	SC	PbO–PbF ₂	1200–800	1.5–2	10	Zonn and Jaffe (1968)
LaAlO ₃ (¹⁷ O)	EV	PbO–PbF ₂	1280	—	3	Garton et al. (1972)
LaAlO ₃	SC	PbO–PbF ₂ –V ₂ O ₅	1300–980	0.5	11 × 9 × 6	Kjems et al. (1973a)
LaCoO ₃	EV	PbO–PbF ₂	1250	—	2 × 1 × 1	Wanklyn (1972)
LaCrO ₃	EV	PbF ₂ –B ₂ O ₃	1240	—	5 × 4 × 4	Wanklyn (1969)
(La, Pb)MnO ₃	SC	PbF ₂ –PbO	1250	1	—	Morrish et al. (1969)
(La, Pb)MnO ₃	SC	PbF ₂ –PbO	1150	—	1–5	Janes and Bodnar (1971)
La _{0.69} Pb _{0.31} MnO ₃	SC	PbO–B ₂ O ₃	1010–850	50	5	Vogel and Fleming (1975)
LaVO ₃	SC	from melt	1280	5	—	Rogers et al. (1966)
Ba(La _{0.5} Ta _{0.5})O ₃	SC	BaF ₂	—	—	0.5	Galasso et al. (1966)
Ba(Gd _{0.5} Ta _{0.5})O ₃	SC	BaF ₂	—	—	0.5	Galasso et al. (1966)
Ba(Lu _{0.5} Ta _{0.5})O ₃	SC	BaF ₂	—	—	0.5	Galasso et al. (1966)
BaLaLiWO ₆	CZG	—	—	—	5–10 mm/hr	Brixner (1974)
BaLaLiMoO ₆	HPS	—	—	—	—	Brixner (1974)
CeAlO ₃	SC	KF	1300–840	4–5	0.05	Zonn (1965)
PrAlO ₃	SC	PbO–PbF ₂	1285–960	3.5	3	Garton and Wanklyn (1967)
PrAlO ₃	SC	PbO–PbF ₂	1300–800	4.5	5	Zonn and Jaffe (1968)
PrAlO ₃	SC	PbO–PbF ₂ –B ₂ O ₃	1300–950	0.5	20 × 20 × 10	Birgeneau et al. (1974)
(Pr, Pb)MnO ₃	SC	PbO–PbF ₂	1150	—	5	Janes and Bodner (1971)
NdAlO ₃	SC	PbO–PbF ₂	1300–800	4.5	5	Zonn and Jaffe (1968)
NdAlO ₃	SC	PbO–PbF ₂	1280–910	0.7	7	Garton and Wanklyn (1967)
(Nd, Pb)MnO ₃	SC	PbO–PbF ₂	1150	—	5	Holmes et al. (1968)
TbAlO ₃	SC	PbO–PbF ₂ –B ₂ O ₃	1300–900	2	—	Wanklyn (1969)
TbAlO ₃	SC	PbO–PbF ₂ –B ₂ O ₃	1280–950	2.5	3 × 2 × 1.5	Wanklyn (1969)
TbAlO ₃	(1967) SC	Bi ₂ O ₃ –B ₂ O ₃ –Tb ₂ O ₇	1315–815	2	3.5 × 2.5 × 2	Wanklyn (1969)
SmAlO ₃	SC	PbO–PbF ₂	1290–960	2.3	3	Garton and Wanklyn (1967)
SmAlO ₃	SC	PbO–PbF ₂	1200–800	1.5	10	Zonn and Jaffe (1968)
SmFeO ₃	SC	PbO–PbF ₂	1280–900	—	—	Schieber (1964)

(Sm, Tb)FeO ₃	SC	PbO-PbF ₂ -B ₂ O ₃	1300-900	0.5	15	Van Uitert et al. (1970a)
(Sm _{0.55} Tb _{0.45})FeO ₃	HEG	PbO-B ₂ O ₃	990-875	2-20	1	Shick and Nielsen (1971)
Sm _{0.55} Tb _{0.45} FeO ₃	SC/EV	PbO-PbF ₂ -B ₂ O ₃	1300-970	0.5	-	Quon et al. (1971)
Sm _{0.55} Tb _{0.45} FeO ₃	SC	PbO-PbF ₂ -B ₂ O ₃	1280-950	1.25	10 × 10 plate	Nakada et al. (1972)
(Sm, Dy)FeO ₃	SC	PbO-PbF ₂ -B ₂ O ₃	1300-900	0.5	-	Pierce et al. (1969)
EuAlO ₃	SC	PbO-PbF ₂ -B ₂ O ₃ -MoO ₃	1295-900	1	2	Wanklyn et al. (1975)
EuFeO ₃	SC	PbO	1250-1000	6	5 × 5 × 1	Drofenik et al. (1973)
GdAlO ₃	SC	PbO-PbF ₂ -B ₂ O ₃	1290-800	2	6	Wanklyn (1969)
GdAlO ₃	ACRT	PbO-PbF ₂ -B ₂ O ₃	1300-900	0.3-0.6	35 × 30 × 25	Scheel and Schulz-Dubois (1971); Scheel (1972)
GdMnO ₃	SC	PbF ₂	1280-900	1	3 × 3 × 2	Wanklyn (1972)
TbAlO ₃	EV	PbO-PbF ₂	1207	-	3	Garton and Wanklyn (1967)
TbAlO ₃	SC	PbO-PbF ₂ -B ₂ O ₃ -MoO ₃	1295-900	1-2	4.5 × 2.5 × 2	Wanklyn et al. (1975)
TbFeO ₃	HEG	PbO-B ₂ O ₃	990-875	2-20	1	Schick and Nielsen (1971)
TbFeO ₃ (Cr)	Ev	PbF ₂ -B ₂ O ₃	1300	-	5	Van Uitert et al. (1970b)
DyAlO ₃	EV	PbO	1260	-	3	Garton and Wanklyn (1967)
DyAlO ₃	EV	PbO-PbF ₂ -B ₂ O ₃	1220	-	7 × 3 × 2	Wanklyn (1969)
DyAlO ₃	HPS	NaOH	1200	-	-	Dernier and Maines (1971)
DyAlO ₃	SC	PbO-PbF ₂	1290	-	-	Flicstein and Schieber (1973)
DyAlO ₃	SC	PbO-PbO ₂ -B ₂ O ₃ -MoO ₃	1245-900	1-2	3.5 × 2 × 1.5	Wanklyn et al. (1975)
DyFeO ₃	SC	PbO-PbF ₂ -B ₂ O ₃ -MoO ₃	1240-900	1-1.5	-	Wanklyn et al. (1975)
HoAlO ₃	HPS	NaOH	1200	-	-	Dernier and Maines (1971)
HoAlO ₃	SC	PbO-PbF ₂ -B ₂ O ₃ -MoO ₃	1290-900	3	4 × 2 × 1.5	Wanklyn et al. (1975)
HoFeO ₃ (Cr)	SC	PbO-PbF ₂ -B ₂ O ₃	1300-900	1	5	Van Uitert et al. (1970b)
ErAlO ₃	HPS	NaOH	1200	-	-	Dernier and Maines (1971)
ErAlO ₃	SC	PbF ₂ -PbO-B ₂ O ₃ -MoO ₃	1290-900	1-1.3	2	Wanklyn et al. (1975)
ErMnO ₃	SC	PbF ₂ -PbO-B ₂ O ₃	1280-900	1	-	Wanklyn (1972)
TmAlO ₃	HPS	NaOH	1200	-	-	Dernier and Maines (1971)
TmFeO ₃	HYG	KOH	385-390	-	-	Kolb and Laudise (1971)
TmFeO ₃	SC	Bi ₂ O ₃	1300-950	0.5-1	3 × 12	Gendelev and Titova (1971)
YbAlO ₃	HPS	NaOH	1200	-	-	Dernier and Maines (1971)
YbCrO ₃	EV	PbF ₂ -B ₂ O ₃ -PbO ₂	1260	-	3 × 3 × 2	Wanklyn (1972)
YbFeO ₃	SC/EV	PbO-PbF ₂ -B ₂ O ₃	1300-950	0.5	-	Quon et al. (1971)
YbFeO ₃	HEG	PbO-B ₂ O ₃	900-875	2-20	1	Shick and Nielsen (1971)

TABLE 29.1 (Cont.).
Crystal growth details for some of the rare earth perovskite oxides.

Crystal	Technique ^a	Flux	Temp. range (°C)	Cooling rate (°C/h)	Approximate dimensions (mm)	References
YbFeO ₃	SC	PbF ₂ -PbO-B ₂ O ₃	1300-1100	3	12 × 9	Damen and Robertson (1972)
LuAlO ₃	HPS	NaOH	1200	-	-	Dernier and Maines (1971)
LuCrO ₃	EV	PbF ₂ -PbO ₂ -B ₂ O ₃	1260	-	3 × 2 × 2	Wanklyn (1972)
LuMnO ₃	SC	Bi ₂ O ₃	1200	50-100	1	Yakel et al. (1963)
RAIO ₃	SC	PbO	1300-850	30	-	Remeika (1956)
RAIO ₃	SC	Pb ₂ OF ₂	1260-1000	3	6 × 6 × 3	Linares (1962)
RAIO ₃	SC	PbO-PbF ₂ -B ₂ O ₃	1290-800	2	3-6	Wanklyn (1969)
RAIO ₃	SC	Bi ₂ O ₃ -B ₂ O ₃	1315-815	2	3-6	Wanklyn (1969)
RCoO ₃	SC	PbO	1300-850	30	1	Remeika (1956)
RCrO ₃	SC	Bi ₂ O ₃	1300-850	30	-	Remeika (1956)
RCrO ₃	EV	PbF ₂ -B ₂ O ₃	1240	-	5	Wanklyn (1969)
RCrO ₃	EV	PbF ₂ -Bi ₂ O ₃	1230	-	-	Rao et al. (1971)
RFeO ₃	SC	PbO	1300-850	30	-	Remeika (1956)
RFeO ₃	SC	PbO-B ₂ O ₃	1300-950	2	10 × 5 × 2	Remeika and Kometani (1968)

RFeO ₃	HYG	KOH	375	-	10	Kolb et al. (1968)
RFeO ₃	SC	PbO-PbF ₂ -B ₂ O ₃	1290-850	2	5	Wanklyn (1969)
RFeO ₃	SC	PbO-PbF ₂ -B ₂ O ₃	1300-850	2-4	10	Giess et al. (1970)
RFeO ₃	SC	PbO-PbF ₂ -B ₂ O ₃	1300-950	0.5-1	18	Gendelew and Titova (1971)
RFeO ₃	LPE/SC	PbO-B ₂ O ₃	1150-1100	2-20	-	Shick and Nielsen (1971)
RFeO ₃	SC	PbO-B ₂ O ₃	1300-1000	2	5 × 5 × 5	I. Mikami (1973)
						I. Mikami et al. (1973)
RFeO ₃	SC	PbO-PbF ₂ -B ₂ O ₃	1280-950	1.25-5	-	Akaba (1974)
RFeO ₃ (Bi)	SC	PbO-Bi ₂ O ₃ -B ₂ O ₃	1300-950	1-4	10	Remeika et al. (1969)
RFeO ₃ (Ni, Cr, Mn)	EV	PbO-PbF ₂ -B ₂ O ₃	1300	-	-	Van Uiter et al. (1970b)
RFeO ₃ (Ni, Cr, Mn)	SC	PbO-PbF ₂ -B ₂ O ₃	900	-	-	Van Uiter et al. (1970b)
RGaO ₃	SC	PbO	1300-850	30	-	Remeika (1956)
RGaO ₃	HPS	NaOH	1000	-	-	Marezio et al. (1966)
RGaO ₃	HPS	NaOH	1000	-	-	Marezio et al. (1968)
RGaO ₃	SC	PbO-B ₂ O ₃	1300	1-5	-	Marezio et al. (1968)
RMnO ₃	SC	Bi ₂ O ₃	1400-1000	-	plate	Bertaut et al. (1963)
RMnO ₃	EV	Bi ₂ O ₃	1450	-	plate	Bertaut et al. (1963)
R _{2/3} Pb _{1/3} MnO ₃	SC	Pb ₂ OF ₂	1150	-	5	Janes and Bodnar (1971)
RScO ₃	SC	PbO	1300-850	30	-	Remeika (1956)

^aAbbreviations used: ACRT - Accelerated Crucible Rotation Technique, CZG - Czochralski Growth, EV - Evaporation, HEG - Homo-epitaxial Growth, HPS - High-pressure Solution Growth, HYG - Hydrothermal Growth, LPE - Liquid Phase Epitaxy.

flux at 1250°C, resulted in the incorporation of about 7 atomic percent of lead in the compound (Khattak, 1974).

In a fluxed solution there are generally a number of constituents. Under these circumstances the possibility of a competing phase forming instead of the perovskite phase must be considered. For example, it has been found that for RAlO_3 (R = Eu to Er) the garnet phase, $\text{R}_3\text{Al}_5\text{O}_{12}$, has an increasing tendency to form as the radius of the rare earth ion decreases (Wanklyn et al., 1975). Flicstein and Schieber (1973) found that the ratio of $\text{Dy}_2\text{O}_3 : \text{Al}_2\text{O}_3 : \text{PbF}_2$ was decisive in the formation of the perovskite, garnet or oxyfluoride phase.

The problems associated with flux growth have been overcome by the growth from the melt as in the case of LaVO_3 (Rogers et al., 1966). Another method developed recently is the accelerated crucible rotation technique (ACRT) which greatly reduces the problems of diffusion and homogenization in conventional fluxed melts (Scheel, 1972). In other cases high pressure has been utilized for growth of the perovskite phase. Another method developed for orthoferrites for use in bubble domain devices involves the growth of thin films of these compounds. Shick and Nielsen (1971) have utilized the liquid phase homoepitaxial growth technique for this purpose.

Some excellent reviews of single crystal growth techniques have been given by Laudise (1970), Goodenough et al. (1972), Wanklyn (1972), Elwell and Scheel (1975). Details of single crystal growth of a number of rare earth perovskites are given in table 29.1.

2.2. Crystal chemistry

The perovskite family of compounds is one of the most widely studied groups of materials and some of the earliest concepts of modern crystal chemistry were developed in the study of these compounds. The group derives its name from the atomic arrangement first found in the rare mineral perovskite, CaTiO_3 . The structure was originally thought to be cubic but the true symmetry was later shown to be orthorhombic (Megaw, 1946). However, the name "perovskite" was retained for the structure type. The truly cubic structure is referred to as "ideal perovskite", and has a unit cell edge of about 4 Å containing one ABO_3 formula unit. In this structure the B ion is in octahedral coordination and the A cation in twelfold coordination with the oxygen ions. The simple cubic structure is shown in fig. 29.1a. Alternatively, the A cation may be thought of as being in the body center position and the B cation at the corners, in which case oxygens would occupy the center of the edges of the cube, as shown in fig. 29.1b. The basic building blocks of the perovskite structure are the oxygen octahedra. When these octahedra share corners cubic stacking is obtained, while the sharing of faces leads to hexagonal stacking. Thus the prerequisites for a perovskite structure are corner-shared octahedra containing a small B cation in octahedral coordination with a relatively large A cation in the interstices of the framework of octahedra. The stability of the structure arises mainly from the electrostatic (Madelung) energy, so that the relative sizes of the A and

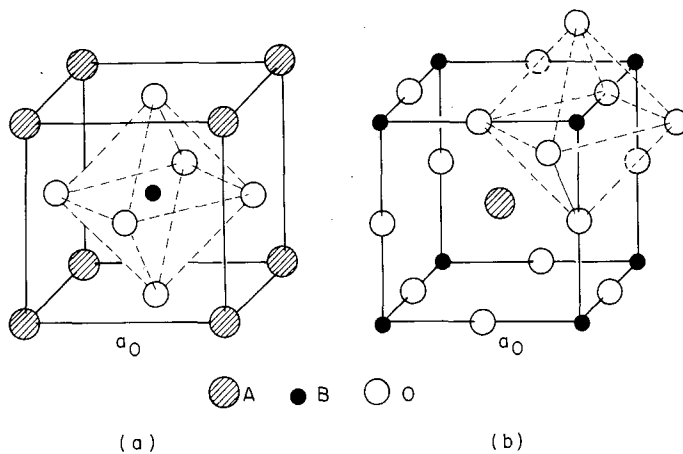


Fig. 29.1. Two methods of representation of an ideal perovskite structure. The octahedral symmetry of the B ions is shown.

B cations are important. In order to have contact between the ions, $(R_A + R_O)$ should equal $\sqrt{2}(R_B + R_O)$, where $(R_A, R_B$ and $R_O)$ are the respective ionic radii. Goldschmidt (1926) defined a tolerance factor, t , to define the limits of stability of the structure:

$$t = (R_A + R_O) / \sqrt{2}(R_B + R_O). \quad (29.1)$$

The perovskite structure is stable within the range $0.75 < t < 1.00$ with t lying between 0.8 and 0.9 in most cases. The necessity for octahedral coordination sets a lower limit of 0.51 \AA on the size of the B cation in oxide systems, since an ion smaller than this does not achieve optimum B–O separation and stabilizes a structure with lower coordination. The tolerance factor and the minimum size of the B ion set a lower bound on the size of the A cation of 0.90 \AA .

An alternative way of viewing the perovskite structure is as a close-packing of oxygen anions, one quarter of which have been replaced by a large A cation, or as a close-packing of ordered AO_3 layers as illustrated in fig. 29.2. The A cation may be thought of as lying at the corners of the basal plane of a hexagonal cell with oxygens at the edge-centers and the face-centered position. Close-packed stacking of these layers leads to the formation of one octahedron of oxygens for each AO_3 unit.

In the rare earth perovskite oxides, the rare earth ion, R, is a relatively large ion and is hence generally the A ion in the ABO_3 structure. Most of the examples in the literature are RBO_3 type compounds but compounds of the type ARO_3 are also known and some examples of these are listed later. In some instances the rare earth ion may substitute for some fraction of the A or B ions leading to the formation of systems of the type $(\text{R}, \text{A})\text{BO}_3$ or $\text{A}(\text{R}, \text{B})\text{O}_3$ respectively.

Early exploratory studies (Wood, 1951; Roy, 1954; Keith and Roy, 1954; Yakel, 1955; Roth, 1957) involved a search for perovskite phases in a number of

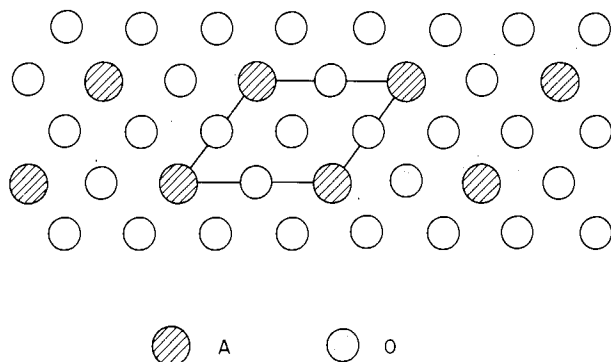


Fig. 29.2. Picture of an AO_3 layer. Closed packing stacking of these layers leads to the formation of one octahedron of oxygens for each Ao_3 unit.

metal oxide systems. Later, more systematic investigations were carried out in a series of compounds in which one of the cations was kept the same and the other varied (Brous et al., 1953; Geller and Wood, 1956; Geller and Bala, 1956; Gilleo, 1957; Koehler and Wollan, 1957; Geller 1957a; Yakel et al., 1963; Eibschütz, 1965). Meanwhile the correlation of the relative ionic radii (Geller, 1957b) and covalent character (Dalziel, 1959) with the crystallography of perovskite compounds was studied. Recently a number of studies have treated perovskite oxides in terms of the basic building blocks of the structure. Some of these studies have discussed perovskite compounds in terms of the displacement parameters from an idealized model (Megaw, 1968a) and changes in the shape and size of the octahedra (Megaw, 1968b, 1968c; Marezio et al., 1970; Glazer, 1972). Review articles dealing with these factors aimed at an understanding of the perovskite structure (Megaw, 1972; Megaw and Darlington, 1975) are of particular interest. Fukunaga and Fujita (1973) have developed a relation between the ionic radii and cell volumes in perovskite compounds by using values for over 200 oxides. This equation of state is useful in predicting the molar volume of a perovskite obtained from a particular combination of elements. Sakhnenko et al. (1972) have developed a method of calculating the interatomic distance in crystals, based on the idea of deformation of the unstressed lengths of cation-anion bonds. These procedures were adopted by Fesenko and Geguzina (1973) to compare the calculated mean unit cell size of 675 compounds with the experimentally observed value. They found that agreement was within 1% in 646 of these compounds. McCarthy and Greedan (1975) and Greedan et al. (1975) have suggested guidelines to predict new phases of compounds containing Eu. Glazer (1975) has described simple ways of determining the symmetry of perovskite structure, using trial models based on tilting of rigid octahedra.

Crystallographic details for some of the rare earth perovskites are listed in table 29.2. Wherever possible, the data are taken from the same source for a particular series of compounds such as manganites, vanadites, etc. Structural

details of other perovskites can be found in the literature (Galasso, 1969; Goodenough and Longo, 1970; Müller and Roy, 1974).

2.3. Crystal structure

Although many of the crystal chemistry concepts developed in the early days can be understood in terms of the ideal cubic structure, investigations in the past two decades have shown a variety of deviations from cubic symmetry, especially in rare earth perovskite oxides. Even though distortions from the simple cubic structure are very frequently observed, such compounds nevertheless exhibit a strong pseudocubic nature. In many previous studies the distortions were very small and the true symmetry was not determined at that time. In such cases the descriptions of the structure were given in terms of a pseudocell. The discussion of perovskite systems in the literature involves many assumptions, revisions, redeterminations and controversies, some of which have not been resolved to date. Even though the distorted structure may exist at room temperature it may transform to the ideal perovskite structure at high temperature. This transition may proceed in several stages via other distorted phases. Deviations from the ideal perovskite structure may occur as a simple distortion of the primitive unit cell, or an enlargement of the primitive cell, or a combination of both.

The space group of the simple cubic structure is $Pm\bar{3}m-O_h^1$ with atoms in the following positions (fig. 29.1): A in 1(b) sites at $(\frac{1}{2}, \frac{1}{2}, \frac{1}{2})$; B in 1(a) sites at $(0, 0, 0)$ and O in 3(d) sites at $(\frac{1}{2}, 0, 0)$. There is one formula unit per unit cell. An example of such an arrangement is provided by EuTiO_3 . This compound was first reported by Brous et al. (1953) and recently studied by McCarthy and Greedan (1975).

A modification of the simple perovskite structure is obtained when two types of B ions with suitably different ionization and size are incorporated. In the case of equiatomic proportions of the two types, the general formula of the perovskite is now $A(B_{0.5}B'_{0.5})O_3$ or $A_2BB'O_6$. It was postulated (Galasso et al., 1959) that an ordered distribution of the two types of B ions along alternate (111) planes is most probable when a large difference exists in either their charges or ionic radii. A completely ordered structure of such a perovskite is shown in fig. 29.3. It can be seen that the unit cell is doubled along all three axes, compared to a primitive unit cell. In the ordered structure the oxygens are slightly shifted towards the more highly charged cation but the octahedral symmetry of the B and B' cations is retained (Steward and Rooksby, 1951; Cox et al., 1967; Khattak et al., 1973, 1975, 1976). The symmetry now becomes face-centered cubic and the space group $Fm\bar{3}m-O_h^5$ with A in 8(c) sites at $(\frac{1}{4}, \frac{1}{4}, \frac{1}{4})$; B in 4(a) sites at $(0, 0, 0)$; B' in 4(b) sites at $(\frac{1}{2}, \frac{1}{2}, \frac{1}{2})$; and O in 24(e) sites at $(\frac{1}{4}, 0, 0)$. There are four formula units of $A_2BB'O_6$ per unit cell.

Distortions from the ideal ABO_3 cubic symmetry occur frequently and structures with tetragonal, orthorhombic, rhombohedral, monoclinic and triclinic symmetry are known. The number of compounds reported to have tetragonal,

TABLE 29.2.
Crystallographic properties of some rare earth perovskite oxides.

Compound	Sym. ^a	a (Å)	b (Å)	c (Å)	Angle	Space group	Remarks	References
LaAlO ₃	R	5.357			$\alpha = 60^{\circ}06'$	R $\bar{3}m$		Geller and Bala (1956)
	R	3.790			$\alpha = 90^{\circ}05'$	R $\bar{3}m$		
	H	5.365		13.11		R3m		
	C	3.818				Pm3m	T = 650°C, cubic T > 435°C	
CeAlO ₃	R	3.716			$\alpha = 90^{\circ}12'$	R $\bar{3}c$		Derighetti et al. (1965); Rango et al. (1966)
	R	5.327			$\alpha = 60^{\circ}15'$	Pm3m	T > 489°C	
PrAlO ₃	R	5.327			$\alpha = 60^{\circ}22'$	R $\bar{3}m$		Kjems et al. (1973a) Roth (1957) Kim (1968) Geller and Bala (1956) Burbank (1970) Birgeneau et al. (1974) Burbank (1970) Birgeneau et al. (1974) Burbank (1970)
	R	7.539			$\alpha = 90^{\circ}21'$	F32/c	T = 239 K	
	R	3.76			$\alpha = 90.25^{\circ}$	R $\bar{3}c$	205 < T < 1320 K	
	O	5.347	7.481	5.322		I112/m	T = 172 K	
	O	5.335	7.477	5.317		I $\bar{1}$	151 < T < 205 K	
	M	3.74	3.74	3.79		D $_{4h}^{18}$	T = 135 K T = 4.2 K, almost tetragonal	
NdAlO ₃	R	5.286			$\beta = 60^{\circ}25'$	R $\bar{3}m$		Birgeneau et al. (1974) Geller and Bala (1956)
	R	3.750			$\beta = 90^{\circ}40'$	R3m		
	O	5.285	5.290	7.473		Pbmm		
	O	5.2912	5.2904	7.4740		Pbmm		
SmAlO ₃	R	5.316			$\alpha = 60^{\circ}19'$	R $\bar{3}m$		Geller and Bala (1956) Dernier and Maines (1971) Geller (1957a)
	R	3.768			$\alpha = 90^{\circ}16'$	R $\bar{3}m$	High pressure preparation T = 850°C, rhombohedral T > 800°C	
	O	5.271	5.292	7.458		Pbmm		
	O	5.267	5.294	7.459		Pbmm		
EuAlO ₃	O	5.247	5.304	7.447		Pbmm		Geller and Bala (1956) Dernier and Maines (1971)
	O	5.250	5.302	7.447		Pbmm	High pressure preparation	
GdAlO ₃	O	5.247	5.304	7.447		Pbmm		Geller and Bala (1956) Dernier and Maines (1971)
	O	5.250	5.302	7.447		Pbmm	High pressure preparation	

TbAlO ₃	O	5.22	5.28	7.41	Pbnn	High pressure preparation	Garton and Wanklyn (1967)
	O	5.2317	5.3097	7.4196	Pbnn		
DyAlO ₃	O	5.23	5.31	7.40	Pbnn	High pressure preparation	Dernier and Maines (1971)
	O	5.2053	5.3172	7.3950	Pbnn		Gilleo (1956)
HoAlO ₃	O	5.18	5.33	7.36	Pbnn	High pressure preparation	Dernier and Maines (1971)
	O	5.1811	5.3229	7.3741	Pbnn		Schneider et al. (1961)
ErAlO ₃	O	5.16	5.32	7.33	Pbnn	High pressure preparation	Dernier and Maines (1971)
	O	5.1595	5.3271	7.3539	Pbnn		Schneider et al. (1961)
TmAlO ₃	O	5.15	5.33	7.29	Pbnn	High pressure preparation	Dernier and Maines (1971)
	O	5.1435	5.3277	7.3335	Pbnn		Schneider et al. (1961)
YbAlO ₃	O	5.12	5.33	7.31	Pbnn	High pressure preparation	Dernier and Maines (1971)
	O	5.1251	5.3310	7.3146	Pbnn		Garton and Wanklyn (1967)
LuAlO ₃	O	5.1012	5.3317	7.3000	Pbnn	High pressure preparation	Dernier and Maines (1971)
YAlO ₃	O	5.179	5.329	7.370	Pbnn	High pressure preparation	Dernier and Maines (1971)
LaScO ₃	O	5.678	5.787	8.098	Pbnn		Geller and Wood (1956)
CeScO ₃	O					No lattice parameter given	Geller (1957a)
PrScO ₃	O	5.615	5.776	8.027	Pbnn		Keith and Roy (1954)
NdScO ₃	O	5.574	5.771	7.998	Pbnn		Geller (1957a)
SmScO ₃	O	5.53	5.76	7.95	Pbnn		Geller (1957a)
EuScO ₃	O	5.502	5.752	7.954	Pbnn		Schneider et al. (1961)
GdScO ₃	O	5.487	5.756	7.925	Pbnn		Faucher and Caro (1975)
DyScO ₃	O	5.43	5.71	7.89	Pbnn		Geller (1957a)
HoScO ₃	O	5.42	5.71	7.87	Pbnn		Schneider et al. (1961)
YScO ₃	O	5.431	5.712	7.894	Pbnn		Schneider et al. (1961)
SmTiO ₃	O	5.468	5.665	7.737	Pbnn		Geller (1957a)
EuTiO ₃	C	3.904			Pm3m		McCarthy et al. (1969)
							McCarthy and Greedan (1975)

TABLE 29.2 (Cont.).
Crystallographic properties of some rare earth perovskite oxides.

Compound	Sym. ^a	a(Å)	b(Å)	c(Å)	Angle	Space group	Remarks	References
GdTiO ₃	O	5.407	5.667	7.692		Pbnm		McCarthy et al. (1969)
TbTiO ₃	O	5.388	5.648	7.676		Pbnm		McCarthy et al. (1969)
DyTiO ₃	O	5.361	5.659	7.647		Pbnm		McCarthy et al. (1969)
HoTiO ₃	O	5.339	5.665	7.626		Pbnm		McCarthy et al. (1969)
ErTiO ₃	O	5.340	5.665	7.624		Pbnm		McCarthy et al. (1969)
TmTiO ₃	O	5.318	5.657	7.613		Pbnm		McCarthy et al. (1969)
YbTiO ₃	O	5.306	5.647	7.607		Pbnm		McCarthy et al. (1969)
LuTiO ₃	O	5.293	5.633	7.598		Pbnm		McCarthy et al. (1969)
YTiO ₃	O	5.274	5.633	7.580		Pbnm		McCarthy et al. (1969)
LaVO ₃	T	5.535		7.830		Pbnm		McCarthy et al. (1974)
CeVO ₃	T	5.519		7.809		Pbnm		McCarthy et al. (1974)
PrVO ₃	O	5.472	5.529	7.774		Pbnm		McCarthy et al. (1974)
NdVO ₃	O	5.451	5.575	7.740		Pbnm		McCarthy et al. (1974)
SmVO ₃	O	5.394	5.581	7.684		Pbnm		McCarthy et al. (1974)
EuVO ₃	O	5.362	5.599	7.651		Pbnm		McCarthy et al. (1974)
GdVO ₃	O	5.342	5.604	7.637		Pbnm		McCarthy et al. (1974)
TbVO ₃	O	5.325	5.606	7.614		Pbnm		McCarthy et al. (1974)
DyVO ₃	O	5.299	5.594	7.593		Pbnm		McCarthy et al. (1974)
HoVO ₃	O	5.276	5.592	7.576		Pbnm		McCarthy et al. (1974)
ErVO ₃	O	5.256	5.581	7.559		Pbnm		McCarthy et al. (1974)
TmVO ₃	O	5.237	5.573	7.545		Pbnm		McCarthy et al. (1974)
YbVO ₃	O	5.223	5.564	7.534		Pbnm		McCarthy et al. (1974)
LuVO ₃	O	5.214	5.561	7.530		Pbnm		McCarthy et al. (1974)
YVO ₃	O	5.274	5.590	7.574		Pbnm		McCarthy et al. (1974)
LaCrO ₃	O	5.477	5.514	7.755		Pbnm		McCarthy et al. (1974)
	H	5.51		13.34			T = 550 K, rhombohedral 550 < T < 1300 K T = 1500 K	Geller (1957a)
LaCrO ₃	C	3.92						Ruiz et al. (1967)
LaCrO ₃	O	5.515	5.479	7.753		Pbnm		Quezel-Ambrunaz and Mareschal (1963)

CeCrO ₃	O	5.475	5.475	7.740	Pbnm	Quezel-Ambrunaz and Mareschal (1963)
PrCrO ₃	O	5.448	5.479	7.718	Pbnm	Quezel-Ambrunaz and Mareschal (1963)
NdCrO ₃	O	5.425	5.478	7.694	Pbnm	Quezel-Ambrunaz and Mareschal (1963)
SmCrO ₃	O	5.367	5.508	7.643	Pbnm	Quezel-Ambrunaz and Mareschal (1963)
EuCrO ₃	O	5.340	5.515	7.622	Pbnm	Quezel-Ambrunaz and Mareschal (1963)
GdCrO ₃	O	5.312	5.525	7.606	Pbnm	Quezel-Ambrunaz and Mareschal (1963)
TbCrO ₃	O	5.291	5.618	7.576	Pbnm	Quezel-Ambrunaz and Mareschal (1963)
DyCrO ₃	O	5.263	5.520	7.552	Pbnm	Quezel-Ambrunaz and Mareschal (1963)
HoCrO ₃	O	5.243	5.519	7.538	Pbnm	Quezel-Ambrunaz and Mareschal (1963)
ErCrO ₃	O	5.223	5.516	7.519	Pbnm	Quezel-Ambrunaz and Mareschal (1963)
TmCrO ₃	O	5.209	5.508	7.500	Pbnm	Quezel-Ambrunaz and Mareschal (1963)
YbCrO ₃	O	5.195	5.510	7.490	Pbnm	Quezel-Ambrunaz and Mareschal (1963)
LuCrO ₃	O	5.176	5.497	7.475	Pbnm	Quezel-Ambrunaz and Mareschal (1963)
YCrO ₃	O	5.241	5.521	7.532	Pbnm	Quezel-Ambrunaz and Mareschal (1963)
LaMnO ₃	O	5.536	5.726	7.697	Pbnm	Voorhoeve et al. (1975b)
CeMnO ₃	O	5.537	5.557	7.812	Pbnm	Quezel-Ambrunaz (1968)
PrMnO ₃	O	5.545	5.787	7.575	Pbnm	Quezel-Ambrunaz (1968)
NdMnO ₃	O	5.380	5.854	7.557	Pbnm	Quezel-Ambrunaz (1968)
SmMnO ₃	O	5.359	5.843	7.482	Pbnm	Quezel-Ambrunaz (1968)
EuMnO ₃	O	5.338	5.842	7.453	Pbnm	Quezel-Ambrunaz (1968)
GdMnO ₃	O	5.313	5.853	7.432	Pbnm	Quezel-Ambrunaz (1968)
TbMnO ₃	O	5.297	5.831	7.403	Pbnm	Quezel-Ambrunaz (1968)

2%Mn is as Mn⁴⁺

TABLE 29.2 (Cont.).

Compound	Sym. ^a	a (Å)	b (Å)	c (Å)	Angle	Space group	Remarks	References
DyMnO ₃	O	5.275	5.828	7.375		Pbnn		Quezel-Ambrunaz (1968)
HoMnO ₃	O	5.27	5.84	7.36		Pbnn	High pressure and high temperature preparation	Waintal et al. (1966)
ErMnO ₃	O	5.26	5.84	7.35			High pressure preparation	Waintal and Chenavas (1967)
TmMnO ₃	O	5.24	5.82	7.335			High pressure preparation	Waintal and Chenavas (1967)
YbMnO ₃	O	5.23	5.81	7.32			High pressure preparation	Waintal and Chenavas (1967)
LuMnO ₃	O	5.22	5.80	7.30			High pressure preparation	Waintal and Chenavas (1967)
YMnO ₃	O	5.205	5.79	7.31			High pressure preparation	Waintal and Chenavas (1967)
LaFeO ₃	O	5.556	5.565	7.862		Pbnn	High pressure preparation	Waintal and Chenavas (1967)
CeFeO ₃	O	5.541	5.577	7.809			Rhombohedral above 980°C	Geller and Wood (1956); Dälziel (1959)
PrFeO ₃	O	5.482	5.578	7.786		Pbnn		Robbins et al. (1969)
NdFeO ₃	O	5.453	5.584	7.768		Pbnn		Marezio et al. (1970)
SmFeO ₃	O	5.400	5.597	7.711		Pbnn		Marezio et al. (1970)
EuFeO ₃	O	5.372	5.606	7.685		Pbnn		Marezio et al. (1970)
GdFeO ₃	O	5.349	5.611	7.669		Pbnn		Marezio et al. (1970)
TbFeO ₃	O	5.326	5.602	7.635		Pbnn		Marezio et al. (1970)
DyFeO ₃	O	5.302	5.598	7.623		Pbnn		Eibschutz (1965)
HoFeO ₃	O	5.278	5.591	7.602		Pbnn		Eibschutz (1965)
ErFeO ₃	O	5.263	5.582	7.591		Pbnn		Eibschutz (1965)
TmFeO ₃	O	5.251	5.576	7.584		Pbnn		Eibschutz (1965)
YbFeO ₃	O	5.233	5.557	7.570		Pbnn		Eibschutz (1965)
LuFeO ₃	O	5.213	5.547	7.765		Pbnn		Eibschutz (1965)
YFeO ₃	O	5.283	5.592	7.603		Pbnn		Eibschutz (1965)
LaCoO ₃	R	5.436				R $\bar{3}c$	T < 375°C;	Wold et al. (1957); Raccach and Goodenough (1967);

	R	5.52		$\alpha = 60^{\circ}0'$	R $\bar{3}$	$T = 937^{\circ}\text{C}$	Raccach and Goodenough (1967)
LaCoO _{2.75}	M	5.4	5.42	7.48			Sis et al. (1973)
PrCoO ₃	O	5.331	5.373	7.587			Bertant and Forrat (1956)
NdCoO ₃	O	5.345	5.345	7.560	Pbnm	High pressure preparation	Demazeau et al. (1974)
SmCoO ₃	O	5.294	5.352	7.504	Pbnm	High pressure preparation	Demazeau et al. (1974)
EuCoO ₃	O	5.261	5.369	7.488	Pbnm	High pressure preparation	Demazeau et al. (1974)
GdCoO ₃	O	5.228	5.387	7.465	Pbnm	High pressure preparation	Demazeau et al. (1974)
TbCoO ₃	O	5.209	5.402	7.425	Pbnm	High pressure preparation	Demazeau et al. (1974)
DyCoO ₃	O	5.180	5.417	7.407	Pbnm	High pressure preparation	Demazeau et al. (1974)
HoCoO ₃	O	5.147	5.417	7.375	Pbnm	High pressure preparation	Demazeau et al. (1974)
ErCoO ₃	O	5.122	5.421	7.357	Pbnm	High pressure preparation	Demazeau et al. (1974)
TmCoO ₃	O	5.104	5.417	7.325	Pbnm	High pressure preparation	Demazeau et al. (1974)
YbCoO ₃	O	5.086	5.419	7.310	Pbnm	High pressure preparation	Demazeau et al. (1974)
LuCoO ₃	O	5.065	5.418	7.290	Pbnm	High pressure preparation	Demazeau et al. (1974)
YCoO ₃	O	5.137	5.418	7.366	Pbnm	High pressure preparation	Demazeau et al. (1974)
LaNiO ₃	R	5.461			R $\bar{3}m$		Demazeau et al. (1974)
	R	7.676			R $\bar{3}m$		Wold et al. (1957)
LaGaO ₃	O	5.519	5.494	7.770	Pbnm	High pressure preparation	Geller et al. (1974)
	R	5.544			R $\bar{3}m$		Geller et al. (1974)
						$T = 900^{\circ}\text{C}$, rhombohedral	Geller (1957a)
						$T > 875^{\circ}\text{C}$	Geller et al. (1974)
CeGaO ₃	R	3.933			R $\bar{3}m$		Geller et al. (1974)
	T	5.490		7.749		Predicted	Geller et al. (1974)

TABLE 29.2 (Cont.).

Compound	Sym. ^a	a(Å)	b(Å)	c(Å)	Angle	Space group	Remarks	References
PrGaO ₃	O	5.458	5.490	7.733		Pbnm		Marezio et al. (1968)
	O	5.460	5.490	7.726		Pbnm		Geller et al. (1974)
NdGaO ₃	O	5.431	5.499	7.710		Pbnm		Marezio et al. (1968)
	O	5.427	5.500	7.705		Pbnm		Geller et al. (1974)
SmGaO ₃	O	5.369	5.520	7.650		Pbnm	High pressure preparation	Marezio et al. (1968)
	O	5.377	5.513	7.654		Pbnm	Quenched from molten state	Geller et al. (1974)
EuGaO ₃	O	5.351	5.528	7.628		Pbnm	High pressure preparation	Marezio et al. (1968)
	O	5.351	5.528	7.628		Pbnm	Quenched from molten state	Geller et al. (1974)
GdGaO ₃	O	5.322	5.537	7.606		Pbnm	High pressure preparation	Marezio et al. (1968)
	O	5.325	5.535	7.607		Pbnm	Quenched from molten state	Geller et al. (1974)
TbGaO ₃	O	5.307	5.531	7.578		Pbnm	High pressure preparation	Marezio et al. (1968)
	O	5.307	5.528	7.577		Pbnm	Quenched from molten state	Geller et al. (1974)
DyGaO ₃	O	5.282	5.534	7.556		Pbnm	High pressure preparation	Marezio et al. (1968)
	O	5.821	5.533	7.555		Pbnm	Quenched from molten state	Geller et al. (1974)
HoGaO ₃	O	5.251	5.231	7.536		Pbnm	High pressure preparation	Marezio et al. (1968)
	O	5.256	5.530	7.536		Pbnm	Quenched from molten state	Geller et al. (1974)
ErGaO ₃	O	5.239	5.527	7.522		Pbnm	High pressure preparation	Marezio et al. (1968)
	O	5.237	5.522	7.517		Pbnm	Quenched from molten state	Geller et al. (1974)

TmGaO ₃	O	5.224	5.515	7.505	Pbmm	High pressure preparation	Marezio et al. (1968)
YbGaO ₃	O	5.208	5.510	7.490	Pbmm	High pressure preparation	Marezio et al. (1968)
LuGaO ₃	O	5.188	5.505	7.484	Pbmm	High pressure preparation	Marezio et al. (1968)
YGaO ₃	O	5.257	5.536	7.533	Pbmm	High pressure preparation	Marezio et al. (1968)
LaYO ₃	O	6.09	5.885	8.505	Pbmm	High pressure preparation	Coutures and Foex (1974)
	M	14.54	3.73	9.10		$T = 1600^{\circ}\text{C};$ $1550 < T < 1750^{\circ}\text{C}$	Coutures and Foex (1974)
	H	3.91		6.245		$T = 1860^{\circ}\text{C};$ $1750 < T < 1975^{\circ}\text{C}$	Coutures and Foex (1974)
	C	4.31				$T = 2050^{\circ}\text{C};$ $1975 < T < 2225^{\circ}\text{C}$	Coutures and Foex (1974)
EuZrO ₃	C	4.18			Pm3m		Shafer (1965)
EuNbO ₃	C	4.008			Pm3m		McCarthy and Greedan (1975)
LaRhO ₃	O	5.524	5.679	7.900	Pbmm	High pressure preparation	Wold et al. (1957)
PrRhO ₃	O	5.4143	5.7473	7.8026	Pbmm		Shannon (1970)
NdRhO ₃	O	5.402	5.772	7.816	Pbmm	High pressure preparation	Wold et al. (1963)
	O	5.3778	5.7551	7.7745	Pbmm		Shannon (1970)
SmRhO ₃	O	5.3211	5.7613	7.7083	Pbmm	High pressure preparation	Shannon (1970)
EuRhO ₃	O	5.2985	5.7607	7.6802	Pbmm	High pressure preparation	Shannon (1970)
GdRhO ₃	O	5.2774	5.7605	7.6584	Pbmm	High pressure preparation	Shannon (1970)
TbRhO ₃	O	5.2541	5.7492	7.6226	Pbmm	High pressure preparation	Shannon (1970)

TABLE 29.2 (Cont.).

Compound	Sym. ^a	a (Å)	b (Å)	c (Å)	Angle	Space group	Remarks	References
DyRhO ₃	O	5.2449	5.7314	7.6002		Pbnm	High pressure preparation	Shannon (1970)
HoRhO ₃	O	5.2299	5.7257	7.5823		Pbnm	High pressure preparation	Shannon (1970)
ErRhO ₃	O	5.2160	5.7117	7.5610		Pbnm	High pressure preparation	Shannon (1970)
TmRhO ₃	O	5.2028	5.6974	7.5428		Pbnm	High pressure preparation	Shannon (1970)
LuRhO ₃	O	5.1861	5.6700	7.5125		Pbnm	High pressure preparation	Shannon (1970)
LaInO ₃	O	5.723	5.914	8.207				Roth (1957)
NdInO ₃	O	5.627	5.891	8.121				Roth (1957)
SmInO ₃	O	5.589	5.886	8.082				Roth (1957)
EuInO ₃	O	5.567	5.835	8.078			High pressure preparation	Shannon (1967)
GdInO ₃	O	5.548	5.842	8.071			High pressure preparation	Shannon (1967)
DyInO ₃	O	5.519	5.751	8.041			High pressure preparation	Shannon (1967)
YInO ₃	O	5.500	5.787	8.053			High pressure preparation	Shannon (1967)
LaHoO ₃	O	5.884	6.094	8.508			High pressure preparation	Shannon (1967)
LaErO ₃	O	5.85	8.43	6.07			High pressure preparation	Berndt et al. (1975)
LaTmO ₃	O	5.85	8.42	6.06			High pressure preparation	Schneider and Roth (1960)
CeTmO ₃	O	5.828	6.035	8.405			High pressure preparation	Schneider and Roth (1960)
LaYbO ₃	O	5.82	8.37	6.02		Pbn2 ₁		Berndt et al. (1975) Schneider and Roth (1960); Muller-Buschbaum and Teske (1968)
	C	4.325				Pm3m	T = 2080°C	Traverse et al. (1968)

CeYbO ₃	O	5.806	6.009	8.373							Berndt et al. (1975)
PrYbO ₃	O	5.776	5.995	8.368							Berndt et al. (1975)
LaLuO ₃	O	5.832	6.013	8.387							Berndt et al. (1975)
CeLuO ₃	O	5.793	5.997	8.344							Berndt et al. (1975)
PrLuO ₃	O	5.768	5.991	8.340							Berndt et al. (1975)
NdLuO ₃	O	5.737	5.974	8.311							Berndt et al. (1975)
EuUO ₃	O	6.020	6.165	8.616							Berndt et al. (1976)
EuNpO ₃	O	6.001	6.150	8.579							Berndt et al. (1976)
La _{0.8} Nd _{0.2} MnO ₃	H	5.506		13.317							Voorhoeve et al. (1975b)
La _{0.8} Rb _{0.2} MnO ₃	H	5.541		13.415							Voorhoeve et al. (1975b)
La _{0.95} K _{0.05} MnO ₃	O	5.538	5.521	7.789							Voorhoeve et al. (1975b)
La _{0.90} K _{0.10} MnO ₃	H	5.524		13.374							Voorhoeve et al. (1975b)
La _{0.8} K _{0.2} MnO ₃	H	5.519		13.381							Voorhoeve et al. (1975b)
La _{0.7} K _{0.3} MnO ₃	H	5.511		13.376							Voorhoeve et al. (1975b)
La _{0.6} K _{0.4} MnO ₃	H	5.511		13.380							Voorhoeve et al. (1975b)
La _{0.86} Sr _{0.16} CrO ₃	O	5.515	5.479	7.753							Meadowcroft (1968)
La _{0.3} K _{0.5} TiO ₃	C	3.914									Roy (1954)
Ce _{0.5} K _{0.5} TiO ₃	C	3.90									Roy (1954)
Nd _{0.5} K _{0.5} TiO ₃	C	3.874									Roy (1954)
La _{0.9} Bi _{0.1} CrO ₃	O	5.47	5.50	7.75							Iwahashi and Iida (1965)
La _{0.5} Sr _{0.5} CoO ₃	C	7.754									Yakel (1955); Gai and Rao (1975)
Eu _{0.80} NbO ₃	C	3.988									Fayolle et al. (1975)
Eu _{0.90} NbO ₃	C	3.994									Fayolle et al. (1975)
La _{0.69} Pb _{0.31} MnO ₃	R	3.893									Vogel and Fleming (1975)
Eu ₂ EuTaO ₆	C	8.309							$\alpha = 90^\circ 11'$		Sato et al. (1975)
Eu ₂ CaWO ₆	C	8.18									Shafer (1965)
Eu ₂ SrWO ₆	C	8.21									Shafer (1965)
La ₂ MgIrO ₆	O	5.59	5.59	7.91							Blasse (1965)
La ₂ CoIrO ₆	O	5.60	5.60	7.92							Blasse (1965)
La ₂ CuIrO ₆	M	5.80	5.60	7.72					$\gamma = 86^\circ 56'$		Blasse (1965)
BaLaLiWO ₆	C	8.032									Brixner (1974)
BaLaNaWO ₆	C	8.273									Brixner (1974)
BaLaKWO ₆	C	8.512									Brixner (1974)
SrLaLiWO ₆	C	7.908									Brixner (1974)
BaLaLiMoO ₆	C	8.0119									Brixner (1974)

TABLE 29.2 (Cont.).

Compound	Sym. ^a	a (Å)	b (Å)	c (Å)	Angle	Space group	Remarks	References
Nd _{0.95} Ca _{0.05} Fe _{0.95} Sn _{0.05} O ₃	O	5.470	5.608	7.792				Lyubutin and Vishnyakov (1973)
Nd _{0.90} Ca _{0.10} Fe _{0.90} Sn _{0.10} O ₃	O	5.476	5.614	7.804				Lyubutin and Vishnyakov (1973)
Nd _{0.85} Ca _{0.15} Fe _{0.85} Sn _{0.15} O ₃	O	5.484	5.618	7.812				Lyubutin and Vishnyakov (1973)
Nd _{0.80} Ca _{0.20} Fe _{0.80} Sn _{0.20} O ₃	O	5.490	5.624	7.828				Lyubutin and Vishnyakov (1973)
Nd _{0.75} Ca _{0.25} Fe _{0.75} Sn _{0.25} O ₃	O	5.500	5.628	7.836				Lyubutin and Vishnyakov (1973)
Nd _{0.70} Ca _{0.30} Fe _{0.70} Sn _{0.30} O ₃	O	5.504	5.634	7.844				Lyubutin and Vishnyakov (1973)
BaCeO ₃	O	6.212	6.235	8.781		Pbnm		Jacobson et al. (1972)
BaPrO ₃	O	6.181	6.214	8.722		Pbnm		Jacobson et al. (1972)
BaTbO ₃	R	6.046			$\alpha = 60^\circ 22'$	R $\bar{3}c$		Jacobson et al. (1972)
	R	8.573			$\alpha = 90^\circ 17'$	R $\bar{3}c$		Jacobson et al. (1972)
SrCeO ₃	O	6.094	6.132	8.638				Solov'eva and Gavrish (1974)
Ba ₂ DyTaO ₆	C	8.454				Fm $\bar{3}m$		Galasso et al. (1966)
Ba ₂ HoTaO ₆	C	8.442				Fm $\bar{3}m$		Galasso et al. (1966)
Ba ₂ ErTaO ₆	C	8.423				Fm $\bar{3}m$		Galasso et al. (1966)
Ba ₂ TmTaO ₆	C	8.406				Fm $\bar{3}m$		Galasso et al. (1966)
Ba ₂ YbTaO ₆	C	8.390				Fm $\bar{3}m$		Galasso et al. (1966)
Ba ₂ LuTaO ₆	C	8.372				Fm $\bar{3}m$		Galasso et al. (1966)
Ba ₂ YTaO ₆	C	8.433				Fm $\bar{3}m$		Galasso et al. (1966)
Ba ₂ LaNbO ₆	T	8.607		8.690				Galasso and Darby (1963)
Ba ₂ NdNbO ₆	C	8.540				Fm $\bar{3}m$		Galasso and Darby (1963)
Ba ₂ SmNbO ₆	C	8.518				Fm $\bar{3}m$		Galasso and Darby (1963)
Ba ₂ EuNbO ₆	C	8.507				Fm $\bar{3}m$		Galasso and Darby (1963)
Ba ₂ GdNbO ₆	C	8.496				Fm $\bar{3}m$		Galasso and Darby (1963)
Ba ₂ DyNbO ₆	C	8.437				Fm $\bar{3}m$		Galasso and Darby (1963)

Ba ₂ HoNbO ₆	C	8.434	Fm3m	Galasso and Darby (1963)
Ba ₂ ErNbO ₆	C	8.427	Fm3m	Galasso and Darby (1963)
Ba ₂ TmNbO ₆	C	8.408	Fm3m	Galasso and Darby (1963)
Ba ₂ YbNbO ₆	C	8.374	Fm3m	Galasso and Darby (1963)
Ba ₂ LuNbO ₆	C	8.364	Fm3m	Galasso and Darby (1963)
Ba ₂ LaPaO ₆	C	8.885	Fm3m	Keller (1965)
Ba ₂ CePaO ₆	C	8.800	Fm3m	Keller (1965)
Ba ₂ PPrPaO ₆	C	8.862	Fm3m	Keller (1965)
Ba ₂ NdPaO ₆	C	8.840	Fm3m	Keller (1965)
Ba ₂ SmPaO ₆	C	8.792	Fm3m	Keller (1965)
Ba ₂ EuPaO ₆	C	8.783	Fm3m	Keller (1965)
Ba ₂ GdPaO ₆	C	8.774	Fm3m	Keller (1965)
Ba ₂ TbPaO ₆	C	8.753	Fm3m	Keller (1965)
Ba ₂ DyPaO ₆	C	8.740	Fm3m	Keller (1965)
Ba ₂ HoPaO ₆	C	8.730	Fm3m	Keller (1965)
Ba ₂ ErPaO ₆	C	8.716	Fm3m	Keller (1965)
Ba ₂ TmPaO ₆	C	8.692	Fm3m	Keller (1965)
Ba ₂ YbPaO ₆	C	8.678	Fm3m	Keller (1965)
Ba ₂ LuPaO ₆	C	8.666	Fm3m	Keller (1965)
Ba ₂ YPaO ₆	C	8.718	Fm3m	Keller (1965)
Ba ₂ CeUO ₆	C	8.87	Fm3m	Awasthi et al. (1967)
Ba ₂ NdUO ₆	C	8.76	Fm3m	Awasthi et al. (1967)
Ba ₂ SmUO ₆	C	8.76	Fm3m	Awasthi et al. (1967)
Ba ₂ EuUO ₆	C	8.68	Fm3m	Awasthi et al. (1967)
Ba ₂ GdUO ₆	C	8.66	Fm3m	Awasthi et al. (1967)
Ba ₂ DyUO ₆	C	8.65	Fm3m	Awasthi et al. (1967)
Ba ₂ HoUO ₆	C	8.65	Fm3m	Awasthi et al. (1967)
Ba ₂ YbUO ₆	C	8.60	Fm3m	Awasthi et al. (1967)
Ba ₂ LuUO ₆	C	8.57	Fm3m	Awasthi et al. (1967)
Pb(Li _{0.25} La _{0.25} W _{0.5})O ₃	C	4.020		Viskov et al. (1966)
Ba(La _{0.5} Ta _{0.5})O ₃	O	8.611		Galasso et al. (1966)
Ba(Gd _{0.5} Ta _{0.5})O ₃	T	8.487		Galasso et al. (1966)
		8.639		
		8.764		
		8.513		

^aAbbreviations used for symmetry: C – Cubic, H – Hexagonal, M – Monoclinic, O – Orthorhombic, R – Rhombohedral, T – Tetragonal.

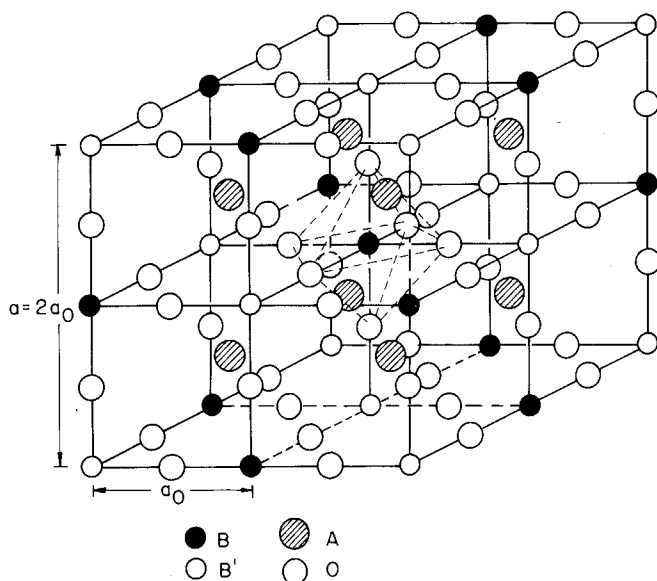


Fig. 29.3. Ordered perovskite structure, $A_2BB'O_6$. The octahedral symmetry of B and B' ions is retained.

monoclinic or triclinic structures is few and detailed structural characterizations have not been carried out in most of these cases. On the other hand, examples of the orthorhombic and rhombohedral structures are numerous.

In the rare earth perovskites, compounds with an orthorhombic distortion are the most common. This structure was first observed in a single crystal of $GdFeO_3$ (Geller, 1956) and later by Coppens and Eibschütz (1965) and is hence sometimes typified as the $GdFeO_3$ structure. The cell constants of the distorted perovskite are related to the cubic pseudocell, a_0 , as follows:

$$a_{\text{ortho}} \approx b_{\text{ortho}} \approx \sqrt{2} a_0 \quad \text{and} \quad c_{\text{ortho}} \approx 2a_0.$$

In many early publications this cell was indexed in terms of a monoclinic pseudocell with $a = b \approx c \approx a_0$ and $\beta \approx 90^\circ$ to emphasize the distortion from the ideal perovskite cell. The true orthorhombic space group $Pbnm-D_{2h}^{16}$ has four formula units per unit cell with atoms in the following positions: A in 4(c) sites at $\pm(x, y, \frac{1}{4}, \frac{1}{2} - x, \frac{1}{2} + y, \frac{1}{4})$; B in 4(b) sites at $(\frac{1}{2}, 0, 0; \frac{1}{2}, 0, \frac{1}{2}; 0, \frac{1}{2}, 0; 0, \frac{1}{2}, \frac{1}{2})$ and O in 8(d) sites at $\pm(x, y, z; \frac{1}{2} - x, \frac{1}{2} + y, \frac{1}{2} - z; \bar{x}, \bar{y}, \frac{1}{2} + z; \frac{1}{2} + x, \frac{1}{2} - y, \bar{z})$ and 4(c) sites. This distorted perovskite form, shown in fig. 29.4, is obtained by tilting of the oxygen octahedra in such a way that the A atoms are displaced along $\langle 1\bar{1}0 \rangle$ pseudocubic directions, or $\langle 010 \rangle$ directions in the orthorhombic cell (Glazer, 1975).

The $Pbnm$ space group is a centric one. In some materials, such as $LaYbO_3$, non-centric symmetry has been found, described by the space group $Pbn2_1-C_{2v}^9$ (Müller-Buschbaum and Teske, 1968). However, the deviations from the centric structure are very small.

An interesting feature of the RBO_3 type compounds with an orthorhombic

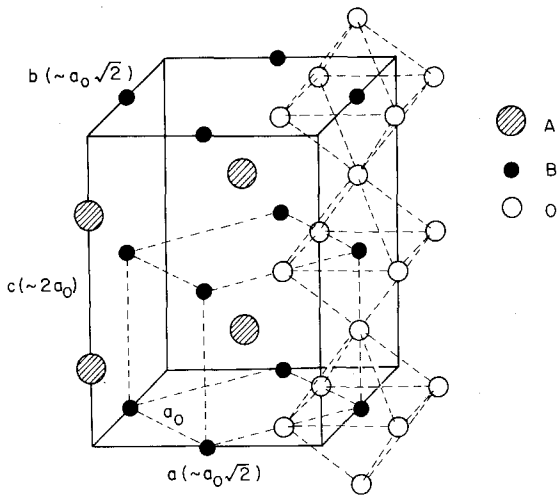


Fig. 29.4. Orthorhombic distortion of the perovskite structure. The relationship to the ideal structure is shown.

structure is the variation of the cell parameters with the rare earth ionic radius. It has been found that while the lattice parameters a and c , and volume of the cell, V , decrease smoothly with the radius of the rare earth ion, the lattice parameter b increases and sometimes goes through a maximum. Such behavior has been reported for RAlO_3 (Dernier and Maines, 1971), RTiO_3 (McCarthy et al., 1969), RVO_3 (McCarthy et al., 1974), RCrO_3 (Quezel-Ambrunaz and Mareschal, 1963), RMnO_3 (McCarthy et al., 1973), RFeO_3 (Eibschütz, 1965), RCoO_3 (Demazeau et al., 1974) and RGaO_3 (Geller et al., 1974).

In early work, rhombohedral distortions were considered in terms of deviations from the primitive cell, a_0 , so that a rhombohedral cell was specified with one formula unit per cell. Subsequent investigations showed that in many cases the anions were displaced so as to require a larger unit cell, and a face-centered rhombohedral cell containing eight formula units with a cell size $a_f \approx 2a_0$ and $\alpha \approx 90^\circ$ was used. Another way of describing such a rhombohedral cell is with a primitive cell containing two formula units with cell edge $a_p \approx \sqrt{2}a_0$ and $\alpha \approx 60^\circ$. The relations (Geller and Bala, 1956) between the face-centered and primitive rhombohedral cells are as follows:

$$a_p = \frac{1}{2}a_f[2(1 + \cos \alpha_f)]^{1/2}, \quad \cos \alpha_p = \frac{1}{2}(3 \cos \alpha_f + 1)/(\cos \alpha_f + 1) \quad (29.2,3)$$

or

$$a_f = a_p(3 - 2 \cos \alpha_p)^{1/2}, \quad \cos \alpha_f = (2 \cos \alpha_p - 1)/(3 - 2 \cos \alpha_p). \quad (29.4,5)$$

Figure 29.5a shows the primitive rhombohedral cell and its relation to the ideal cubic structure. Figure 29.5b indicates how the primitive unit cell is derived from the face-centered rhombohedral cell. Megaw and Darlington (1975) have discussed the geometrical and structural relationship between the various space groups in such distorted perovskites.

The rhombohedral structure is sometimes typified as the LaAlO_3 structure.

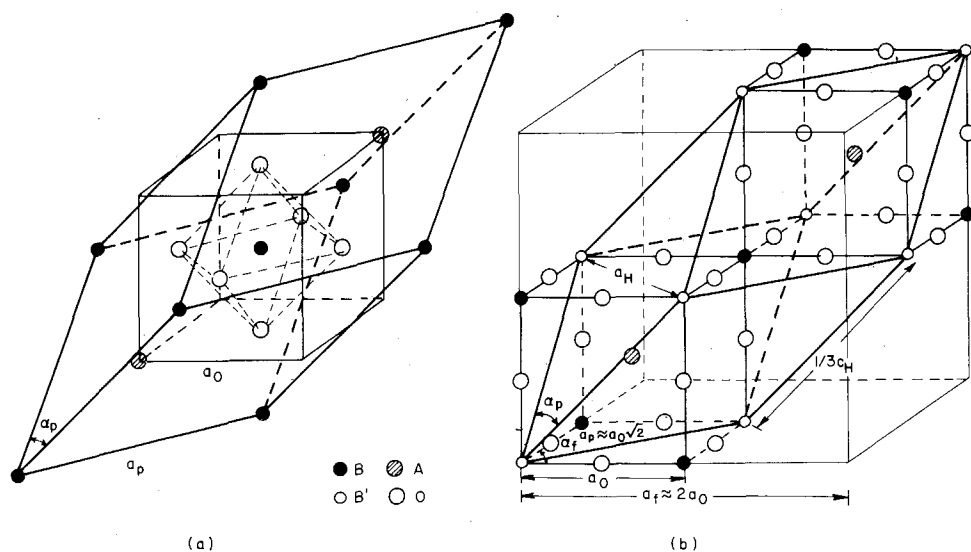


Fig. 29.5. Two methods of representation of the rhombohedral distortion of the perovskite structure. (a) The primitive cell and its relationship to the ideal cell is shown. (b) The face-centered cell and the primitive cell are also shown.

Although in early investigations LaAlO_3 was described as monoclinic (Ruggiero and Ferro, 1955) and tetragonal (Bertaut and Forrat, 1956) it was finally established to have a rhombohedral structure (Geller and Bala, 1956). However, they described it with the space group $R\bar{3}m-D_{3d}^5$. It was later found to have $R\bar{3}c-D_{3d}^5$ symmetry (Derighetti et al., 1965; Rango et al., 1966), and this assignment was confirmed by detailed neutron scattering data (Kjems et al., 1973a).

2.4. Phase transition

A very common feature of the distorted perovskites is the readiness with which they undergo phase transformations as a function of temperature. An example of this is provided by LaAlO_3 , which undergoes a transition to a cubic phase at 489°C (Geller and Bala, 1956). The rhombohedral structure is retained to liquid helium temperature (Granicher et al., 1957; Kiro et al., 1963; Müller et al., 1968).

Rhombohedral PrAlO_3 undergoes a series of transformations and has been the subject of a detailed study. On heating this compound exhibits a transition to a cubic phase at 1320 K similar to that observed in LaAlO_3 . On cooling it undergoes a first order transition to an orthorhombic phase at 205 K, followed by a second order transition at 151 K (Cohen et al., 1969). The 151 K transition has been investigated by X-ray studies (Burbank, 1970), neutron scattering techniques (Kjems et al., 1973b), Raman scattering and fluorescence (Harley et al., 1973), and EPR (Cohen et al., 1974) measurements.

Another interesting example of a rhombohedral perovskite is LaCoO_3 . This was first described in terms of the space group $R\bar{3}m-D_{3d}^5$ (Wold et al., 1957) but later established to have $R\bar{3}c-D_{3d}^6$ symmetry (Raccah and Goodenough, 1967). On heating it transforms to another rhombohedral phase at 375°C with the space group $R\bar{3}$. In the low temperature phase all the Co ions are in the low spin state whereas in the high temperature phase there is ordering of the low spin and high spin Co ions in adjacent (111) planes. At 937°C LaCoO_3 undergoes a transition to another rhombohedral phase, the space group $R\bar{3}$ being retained, but the rhombohedral angle, α , changing from 60.4° to 60.0° . In this phase the geometry is apparently quite cubic but the symmetry is rhombohedral as the ions are shifted from their ideal positions. The transition at 937°C is described according to a localized electron \rightleftharpoons collective electron model (Raccah and Goodenough, 1967).

2.5. Magnetic properties

In the ideal cubic perovskite structure, each oxygen is shared by two B cations, forming a B–O–B angle of 180° . Such a configuration is generally highly favorable for superexchange interactions between magnetic B cations. This exchange is usually negative and therefore results in antiparallel coupling of nearest-neighbor magnetic moments. This may be viewed as a two-sublattice structure, one with spin-up and the other with spin-down moments, and a magnetic structure of this type is designated a G-type structure. Thus in a simple perovskite containing paramagnetic B ions, the sequence of moments from one (111) layer to the next can be represented as $\dots B(\uparrow)B(\downarrow)B(\uparrow)B(\downarrow)\dots$ and the structure is antiferromagnetic. Goodenough (1968) and Kanamori (1959) have discussed the strength and sign of the 180° and 90° superexchange interactions.

When the ions on the two sublattices have different moments, as in $A_2BB'O_6$ perovskites, other spin arrangements are possible. If B' is a diamagnetic ion, the B ions are usually aligned antiferromagnetically in the following sequence $\dots B(\uparrow)B'(\downarrow)B(\uparrow)B'(\downarrow)\dots$ (Blasse, 1965; Cox et al., 1967; Khattak et al., 1976). Here the most important exchange mechanism is believed to be a longer range superexchange interaction through two oxygens of the type B–O–B'–O–B or B–O–O–B. The B–B separation is now considerably more than the 4 \AA , separation found in the ideal perovskites, and there are both 90° and 180° configurations. These interactions are by no means insignificant; for example, the Néel temperature of $\text{Sr}_2\text{NiMoO}_6$ is 71.5 K (Nomura and Nakagawa, 1966).

If both B and B' are paramagnetic ions, the linear B–O–B' interaction is expected to predominate once again, which for negative exchange results in the sequence $\dots B(\uparrow)B'(\downarrow)B(\uparrow)B'(\downarrow)\dots$. An arrangement like this results in a simple ferrimagnetic structure. However, if longer range interactions between B ions alone are of comparable strength, more complex structures can result, for example when B' is the Re^{6+} ion (Khattak et al., 1973, 1975).

The above discussion applies to cubic perovskites with non-magnetic A ions. In ABO_3 perovskites of this type the simplicity of the arrangement makes theoretical calculations more amenable. For ordered perovskites the longer

range interactions complicate the situation somewhat. However, most of the rare earth perovskites have distorted variants of the cubic structure and, in some cases, the displacements from ideal positions may be very substantial. Under these circumstances such simple arguments are no longer valid. Furthermore, a distinction should be made according to the number and type of magnetic ions, viz. (i) magnetic ions on the A sites (for example, rare earth aluminates), (ii) transition magnetic ions on B sites (for example, LaMnO_3 , YCrO_3), and (iii) magnetic ions on both sites (for example, HoFeO_3 , ErCrO_3). Even more complicated magnetic interactions occur when some of the A or B or both ions are replaced by others.

The rare earth perovskites are usually treated in terms of a two-sublattice model with a rare earth ion on the A site and a transition metal ion on the B site. Early neutron diffraction studies (Koehler et al., 1960) indicated that there was little interaction between the two sublattices. This is also suggested by the respective ordering temperatures: for example, in the orthoferrites the iron lattice orders around 700 K and the rare earth lattice only at a few degrees kelvin. An advantage of the low ordering temperature of the rare earth sublattice is that studies can be made well above T_N without much effect from the thermal vibrations of the lattice.

Magnetic structures have been derived as representations in the appropriate magnetic space group (analogous to the crystallographic space group which describes the crystal structure) by the introduction of an "antisymmetry" element. This new element may be thought of as a normal symmetry element combined with a time- (or current-) reversal operator. With the use of this operator the 32 crystalline classes are increased to 90 magnetic classes and the 230 space groups to 1651 magnetic groups. Reviews of this representation theory have been given by Belov et al. (1957), Donnay et al. (1958), Opechowski and Guccione (1965), Bertaut (1968), and Yamaguchi and Tsushima (1973).

Using this approach for the space group Pbnm eight possible magnetic groups are obtained. For each of the space groups, if one operates on the magnetic moment represented as a vector quantity a variety of magnetic modes can be derived as shown in table 29.3. The notation for the positions of the moments is that of Cox (1972) as shown in fig. 29.6. These simple structures can be combined to give a variety of noncollinear structures, and it is possible for reorientation of the magnetic moments to occur at intermediate temperatures. The magnetic structures of some of the rare earth perovskites reported in the literature are given in table 29.4.

In the series RAIO_3 the Al ion is a diamagnetic ion and the only magnetic contribution is from the rare earth ion. Magnetic susceptibility data below 4 K for this series of compounds have been reported by Cashion et al. (1968a; 1968b), and shows that the Gd, Tb and Dy compounds order whereas the Er and Ho compounds show no ordering down to 1.5 K. The phenomenon of metamagnetism, in which a ferromagnetic component is induced in an antiferromagnet by the application of a field, usually described as a "spin flip", has been observed in TbAlO_3 (Mareschal et al., 1968; Bertaut, 1972). Depending on the direction of the

TABLE 29.3.
Magnetic modes for 4(a) and 4(c) sites allowed by symmetry in the family of magnetic space groups derived from the crystallographic group Pbnm (see fig. 29.6).

	A sites or 4(a) sites			B sites or 4(b) sites			
	x	y	z	x	y	z	
Pbnm	A	G	C	-	-	C'	Γ_{1g}
Pbn'm'	F	C	G	F'	C'	-	Γ_{2g}
Pb'nm'	C	F	A	C'	F'	-	Γ_{3g}
Pb'n'm	G	A	F	-	-	F'	Γ_{4g}
Pb'n'm'	-	-	-	G'	A'	-	Γ_{1u}
Pb'nm	-	-	-	-	-	A'	Γ_{2u}
Pbn'm	-	-	-	-	-	G'	Γ_{3u}
Pbnm'	-	-	-	A'	G'	-	Γ_{4u}

applied field this can result in a single or a double ordering transition (Holmes et al., 1968).

The orthochromites are an example of a transition metal ion on the B site. The chromium sublattice in this series orders between 282 K (for LaCrO₃) and 112 K (for LuCrO₃), whereas the rare earth sublattice ordering, if any, occurs below 17 K. Some very complex structures are observed, as for example in TbCrO₃, in which the Tb sublattice undergoes ordering at 4 K and transforms to a different structure at 3.05 K. The coupling between the two sublattices has been investigated by Pataud and Sivardi re (1970a,b).

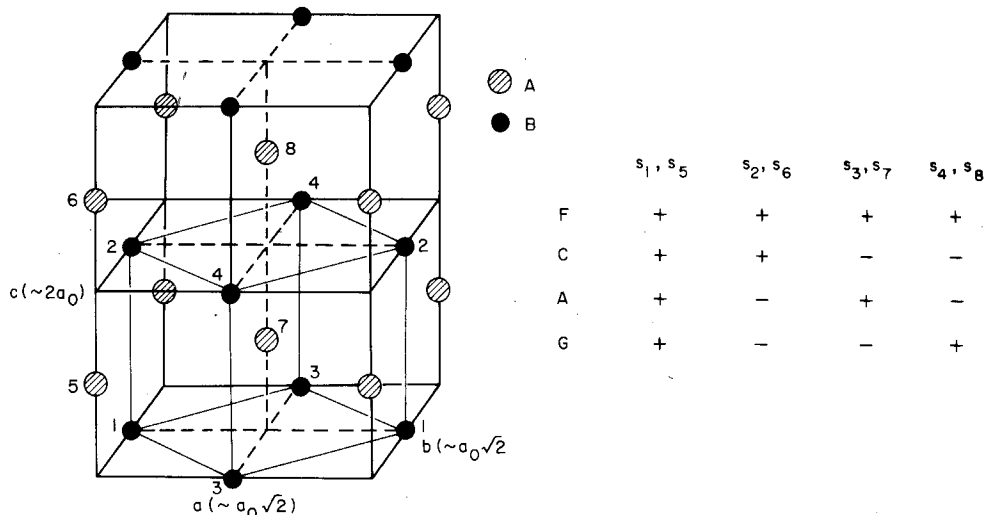


Fig. 29.6. Magnetic structures in orthorhombic perovskite-type compounds.

TABLE 29.4.

Magnetic structures and transition temperatures^a of some rare earth perovskite oxides (see fig. 29.6). The numbers enclosed in parentheses are for the rare earth ion.

Compound	T_N (K)	Magnetic str.	Moment (μ_B)	References
SmAlO ₃	(1.3)			Combarieu et al. (1968)
GdAlO ₃	(3.69)	G(Gd)		Cashion et al. (1968a)
TbAlO ₃	(4)	G, A(Tb)	(8.25)	Mareschal et al. (1968)
DyAlO ₃	(3.42)	F	(7.0)	Herpin and Meriel (1964)
	(3.525)	G, A(Dy)	(8.8)	Holmes et al. (1971b); Bidaux and Meriel (1968)
LaCrO ₃	282	G(Cr)	2.45	Bertaut et al. (1966)
PrCrO ₃	239	G(Cr)	2.46	Bertaut et al. (1966)
	(74.2)	F(Pr)	(0.5)	
NdCrO ₃	224	G(Cr)	2.55	Bertaut et al. (1966)
	(10)	C(Nd)	(1.3)	Bertaut & Mareschal (1967)
SmCrO ₃	192	G(Cr)		Bertaut et al. (1966)
EuCrO ₃	181	G(Cr)		Bertaut et al. (1966)
TbCrO ₃	158	G(Cr)	2.85	Bertaut et al. (1966);
	(4)	F, C(Tb)		Bertaut et al. (1967a);
	(3.05)	complex (Tb)	(8.6)	Mareschal et al. (1968)
DyCrO ₃	146	G(Cr)	2.76	Bertaut & Mareschal (1968)
	(2.16)	complex (Dy)	(9.6)	
HoCrO ₃	141	G(Cr)	2.94	Bertaut et al. (1966)
	(12)	C, F(Ho)	(7.0)	
ErCrO ₃	133	G(Cr)	2.90	Bertaut et al. (1966);
	(16.8)	C(Er)	(5.2)	Bertaut & Mareschal (1967)
TmCrO ₃	124	G(Cr)	2.58	Bertaut et al. (1966)
	(>4)	F(Tm)	(0.8)	
YbCrO ₃	118	G(Cr)	2.80	Bertaut et al. (1966)
LuCrO ₃	112	G(Cr)	2.51	Bertaut et al. (1966)
YCrO ₃	141	G(Cr)	2.96	Bertaut et al. (1966)
LaFeO ₃	750	G(Fe)	4.6	Koehler & Wollan (1957)
PrFeO ₃	711	G(Fe)		Treves (1965); Pinto and Shaked (1972)
NdFeO ₃	760	G(Fe)	4.57	Koehler et al. (1960)
TbFeO ₃	681	G(Fe)	4.8	Bertaut et al. (1967b)
	(8.4)	C, F(Tb)		
	(3.1)	A, G(Tb)		
DyFeO ₃	648	G(Fe)		Treves (1965);
	(3.7)	G, A(Dy)	(9.2)	Gorodetsky et al. (1968) Berton & Sharon (1968)
HoFeO ₃	700	G(Fe)	4.60	Koehler et al. (1960)
	(6.5)	C, F(Ho)	(7.5)	
ErFeO ₃	620	G, F(Fe)	4.62	Koehler et al. (1960)
	(4.3)	C(Er)	(5.8)	Gorodetsky et al. (1973) Vigneron (1976)
TmFeO ₃	630	G(Fe)	-	Treves (1965); Leake et al. (1968)
Sm _{1-x} Dy _x FeO ₃ (0 ≤ x ≤ 1)		G(Fe)		Pierce et al. (1969)
LaMnO ₃	100	A(Mn)	3.9	Wollan and Koehler (1955); Koehler and Wollan (1957)

TABLE 29.4 (Cont.).

Compound	T_N (K)	Magnetic str.	Moment (μ_B)	References
PrMnO ₃	91	A(Mn)	1.8	Quezel-Ambrunaz (1968)
NdMnO ₃	85	A(Mn)	1.7	Quezel-Ambrunaz (1968)
LaErO ₃	(2.4)	complex(Er)	(6.3)	Moreau et al. (1968)
BaTbO ₃	(37)	G(Tb)	(7.99)	Toefield et al. (1972)
TbCoO ₃	(3.31)	A, G(Tb)	(8.0)	Mareschal et al. (1968)
TbVO ₃		C, F(Tb)	(7.6)	Mareschal et al. (1968)
EuTiO ₃	(5.3)	G(Eu)	(7)	McGuire et al. (1966)
La(Mn _{1-x} Cr _x)O ₃				
0 ≤ x < 0.15		A		Bents (1957)
0.15 ≤ x < 0.60		complex		
0.60 ≤ x ≤ 1.00		G		

^aA compilation of the transition temperatures has been reported by Connolly and Copenhaver (1972).

The rare earth orthoferrites are one of the most widely studied series of compounds because of their possible application as technological magnetic materials (Koehler and Wollan, 1957; Treves, 1965; White, 1969; Moskvin and Sinitsyn, 1973a, 1973b; Yamaguchi, 1974). These compounds show a weak spontaneous moment which is attributed to a slight canting of the iron moments which are otherwise antiferromagnetically aligned in a G-type array (Treves, 1962). The iron moments align so that the direction of easy magnetization is along the *a* or *c* axis of the orthorhombic cell (Bozorth et al., 1958). The weak ferromagnetic moment of 0.03–0.07 μ_B /mole led to these materials being considered for bubble logic and memory devices (Van Uitert et al., 1970a; Antonov et al., 1973; Bobeck, 1975). The large anisotropy field and low saturation magnetic field results in flat, square magnetization curves for these compounds (Mikami et al., 1973). The strongest interaction in the orthoferrites is the antiferromagnetic coupling of the iron moments which is reflected in the high Néel temperatures of around 700 K. The weak ferromagnetic component is aligned along the *c* axis at high temperatures (Sherwood et al., 1959). On cooling the iron moments may undergo a reorientation to a preferred alignment along *a* axis. This transition has been the subject of extensive study during recent years (Gyorgy et al., 1968; Gorodetsky et al., 1968; Pinto et al., 1971; Bidaux et al., 1974; Yamaguchi, 1974; Shapiro et al., 1974; Nikolaev and Rusakov, 1976). For some time there was uncertainty about whether this reorientation of moments was continuous or discontinuous. Recently torque measurements (Gyorgy et al., 1968) have indicated that the moments undergo orientation in a continuous manner. Finally, on cooling below 10 K the rare earth ion sublattice orders (TbFeO₃, DyFeO₃, HoFeO₃, ErFeO₃).

The rare earth manganites show very interesting magnetic properties. It is difficult to obtain the Mn ions as Mn³⁺ alone since there is usually some contamination by Mn⁴⁺. When part of the rare earth sites are substituted by a divalent ion, a corresponding number of Mn⁴⁺ are created on Mn³⁺ sites to

maintain stoichiometry. Compounds containing mostly Mn^{3+} or Mn^{4+} ions show antiferromagnetic behavior. However in the range of 25–35% Mn^{4+} content ferromagnetic behavior has been reported (Jonker and Van Santen, 1950; Jonker, 1956). These studies indicated that there was a weak magnetic interaction between Mn^{3+} ions, a negative interaction between Mn^{4+} ions and a strong positive interaction between Mn^{3+} and Mn^{4+} ions. Neutron diffraction studies (Wollan and Koehler, 1955; Koehler and Wollan, 1957) confirmed this, and additional support was provided by a model based on semicovalent exchange by Goodenough (1955). In previous studies it was assumed that the cations are ionically bound based on the overlap of the atomic orbitals of the cations and anions. The semicovalent exchange theory considers the overlap of the empty cation orbitals with the full orbitals of neighboring anions, thereby giving a covalent nature to the binding. The degree of covalency depends upon the relative stability of these orbitals. Similar behavior was found for the combination Co^{3+} and Co^{4+} , but the Cr and Fe compounds were found to be antiferromagnetic (Jonker and Van Santen, 1953). Substitution of two kinds of transition elements in the B sites and the effect on magnetic properties has also been studied (Holmes et al., 1971; Rao et al., 1975).

Just as the presence of Mn^{4+} in $(\text{La}, \text{Sr})\text{MnO}_3$ leads to deviations from simple behavior, the existence of low spin and high spin Co causes complicated behavior in the RCoO_3 compounds. The difference in energy of the trivalent diamagnetic ($S = 0$) low spin state, Co^{III} , and trivalent cobalt ($S = 2$) high spin state, Co^{3+} , is only 0.08 eV (Reccah and Goodenough, 1967). Magnetic susceptibility data for LaCoO_3 showed three regions viz. a low temperature and a high temperature region in which $1/\chi$ vs T was linear but with different slopes, and an intermediate region where $1/\chi$ was essentially independent of temperature (Heikes et al., 1964; Bhide et al., 1972). This has been explained as due to the existence of the predominantly low spin Co^{III} state at low temperatures, and a partial transformation to Co^{3+} up to about 200 K. Above this temperature Co^{3+} and Co^{III} transform to Co^{II} and Co^{4+} pairs. The behavior of LaCoO_3 has been reported extensively in the literature (Jonker and Van Santen, 1953; Goodenough, 1958; Heikes et al., 1964; Goodenough and Raccach, 1965; Naiman et al., 1965; Jonker, 1966; Menyuk et al., 1967; Bhide et al., 1972; Bari, 1972).

Europium titanate, EuTiO_3 , is an example of a rare earth perovskite in which the Eu ion is in the divalent state. From magnetic measurements it was reported that EuTiO_3 is one of the few antiferromagnetic materials with a positive Curie-Weiss constant (McGuire et al., 1966). This was attributed to a 180° superexchange showing a positive value of the exchange integral for next nearest neighbors.

2.6. Electrical properties

Just as the magnetic properties of rare earth perovskites exhibit very diverse behavior, the electrical conductivities also show wide variations. Some compounds have been utilized for their dielectric properties, others show

metallic conductivity, but a majority are semiconductors. Large changes in conductivity have been observed as a result of ionic substitutions. The conductivity behavior is also influenced by structural or magnetic transformations.

The electrical behavior of a material is dependent on the outermost electrons, which may be localized at specific atomic sites or may be collective. Since localized electrons may carry a spontaneous moment, there is a strong correlation between the electrical and magnetic properties of perovskites. Rare earth perovskites with transition metal ions show widely differing electrical properties. For example, LaNiO_3 , which contains Ni in the low spin state Ni^{III} , and LaTiO_3 exhibit collective d-electron behavior, showing a metallic conductivity and Pauli paramagnetism (Goodenough and Racciah, 1965; Ganguly and Rao, 1973).

The orthochromites have been studied by Ruiz et al. (1967) and Rao et al. (1971). The former authors found LaCrO_3 to be a semiconductor with an activation energy of 0.6 eV, while the latter reported a value of 0.22 eV. It is possible that the 0.6 eV figure is related to impurities or native defects. For the heavier rare earth chromites there seem to be two regions of conductivity. In the low temperature region the activation energy increases along the rare earth series (from 0.27 eV for Dy to 0.37 eV for Yb) while the high temperature region is characterized by a value of about 0.23 eV. The mechanism of conduction is attributed to the presence of high mobility Cr^{4+} ions giving rise to p-type extrinsic conduction. The decrease of conductivity in the heavier rare earth compounds may be related to a decrease in the covalency of the Cr-O bond and an increased covalency of the R-O bond. This is similar to the arguments suggested by Goodenough (1966).

In the RMnO_3 series, the electrical behavior of LaMnO_3 has been studied in some detail (Jonker, 1966). He found an abrupt change in conductivity as well as in the magnetic susceptibility as a function of temperature near 450°C (Jonker, 1956). This electrical behavior is explained by Goodenough (1966) on the basis of arguments advanced for orthochromites, namely that the charge carriers are holes hopping amongst localized levels.

In the case of orthoferrites, although the magnetic properties have been studied extensively very little data on their transport properties exist (Jonker 1954; Subba Rao et al., 1971). Here again, as for the RCrO_3 and RMnO_3 series, the conduction mechanism is p-type semiconduction associated with localized d-electrons.

Lanthanum cobaltite, LaCoO_3 , has been reported to have very interesting electrical conductivity behavior (Heikes et al., 1964; Goodenough and Racciah, 1965; Racciah and Goodenough, 1967; Bhide et al., 1972). The material behaves like a semiconductor up to about 125°C. At higher temperatures, $125 < T < 650^\circ\text{C}$, the conductivity increases much more rapidly and later $650 < T < 937^\circ\text{C}$ goes through a broad, flat maximum. Above 937°C it shows metallic behavior. At low temperatures the Co ions are essentially in the low spin Co^{III} state. As the temperature is increased there is coexistence of this and the high spin paramagnetic Co^{3+} state. As the temperature is increased further, the Co^{3+} and Co^{III} ion

pairs transform to Co^{2+} and Co^{IV} pairs. Thus with increasing temperature the fraction of Co^{3+} decreases and disappears around 937°C when only long range order is present, resulting in a first order transition. Along with the spin behavior, the outer electrons also show a transition from localized to a collective behavior. LaCoO_3 is one of the few materials which shows a localized-collective electron transition.

The electrical properties of LaVO_3 have been studied by Rogers et al. (1966), Dougier and Casalot (1970) and Sayer et al. (1975). The material behaves as a semiconductor with an activation energy of 0.12 eV. The d-electrons are considered localized but the low activation energy indicates that the covalent mixing of the orbitals is close to inducing localized-collective electron behavior.

The rare earth perovskites described above contain a trivalent transition metal ion, and the majority are semiconductors. Addition of suitable ions may force part of the transition ion into a higher oxidation state so as to maintain charge neutrality, thereby greatly modifying the conductivity behavior. One of the first such systems to be studied was $\text{La}_{1-x}\text{M}_x\text{MnO}_3$, where M is Ba, Ca or Sr (Van Santen and Jonker, 1950). The introduction of a divalent ion can be formulated as $\text{La}_{1-x}^{3+}\text{M}_x^{2+}\text{Mn}_{1-x}^{3+}\text{Mn}_x^{4+}\text{O}_3$. For example, if M is Sr and $x = 0$, all the Mn ions are in the Mn^{3+} state and occupy equivalent sites, the spin moments are ordered antiferromagnetically below 150 K and the compound exhibits semiconducting properties. An increase in x results in the creation of Mn^{4+} holes, thereby increasing the conductivity. A change in activation energy is observed at the magnetic disorder temperature. For $0.2 < x < 0.4$ the system becomes ferromagnetic and shows a metal-semiconductor transformation (Parker, 1975). The cobaltites show similar behavior. In the case of $\text{La}_{1-x}\text{Sr}_x\text{CoO}_3$ and $\text{Nd}_{1-x}\text{Sr}_x\text{CoO}_3$ the conduction is metallic at room temperature for $x = 0.4$ and 0.23 respectively (Ohbayashi et al., 1974). As already discussed the activation energy for LaVO_3 is very low and following substitution of Sr corresponding to $x = 0.225$ on the La site, the material undergoes a semiconductor-metal transition (Dougier and Hagenmuller, 1975). In the case of $\text{La}_{1-x}\text{Sr}_x\text{CrO}_3$ an increase in conductivity is also seen with increasing Sr content (Meadowcroft, 1969). In all the above examples an increase in conductivity is seen with the addition of Sr; however, for $\text{La}_{1-x}\text{Sr}_x\text{NiO}_3$ a decrease in conductivity is observed (Obayashi and Kudo, 1975). This is because in these compounds the charge neutrality is maintained by the creation of oxygen vacancies rather than Ni^{4+} ions.

Substitution in the B site by another transition metal cation has been studied by Rao et al. (1975). For $\text{LaNi}_{1-x}\text{Co}_x\text{O}_3$ the behavior is metallic for $x = 0.50$, similar to that of LaNiO_3 . This is attributed to the presence of low spin Co^{III} . When $x > 0.50$ the compound is a semiconductor, with the behavior resembling that of LaCoO_3 for $x > 0.90$. In the case of $\text{LaNi}_{1-x}\text{Fe}_x\text{O}_3$ a metallic-semiconductor transition occurs at $x = 0.2$.

The addition of rare earths to dielectric materials has been studied for a long time. Rare earth dopants in BaTiO_3 have been reported to lower the resistivity (Saburi, 1959), while La-doped BaZrO_3 showed an increase in resistivity by several orders of magnitude (Koenig and Jaffe, 1964). The former was attributed

to the formation of Ti^{3+} ions whereas in the latter case the hole concentration was lowered.

2.7. Optical properties

Although the optical absorption and fluorescence spectra of rare earth compounds has been studied for a long time only recently has a correlation with the magnetic properties been studied. The rare earth perovskites are of particular interest since the effect of magnetic ordering of the transition metal ion in the B site can be studied in addition to that of the rare earth ion. Since the difference in ordering temperatures of the two types of ions is large there is little interaction. The absorption spectra either for the host ion or after introduction of a nominal 1% concentration "probe" into a diamagnetic lattice can be studied. In the former case of magnetically concentrated systems a broad spectrum is obtained (with linewidths typically $0.5-5\text{ cm}^{-1}$), while in the latter a sharp spectrum is obtained (linewidths about 0.1 cm^{-1}). A study of the absorption spectra from a rare earth ion is by no means trivial as a typical spectrum may contain at least 100 absorption lines with perhaps only as many as ten sharp enough to display structure related to magnetic effects.

Consider idealized behavior of single ion absorption spectra in a simple two sublattice antiferromagnet. At high temperatures a single absorption line is observed but on cooling below T_N the effective internal field produces a Zeeman splitting of both ground and excited doublet states. This means that as many as four lines are observed in the absorption spectrum below T_N . The appearance of these lines is related to the ordering of the moments. The existence of an external field below T_N may remove the sublattice degeneracy resulting in the appearance of additional splitting. When the external field is larger than that required for a spin-flip or spin-flop certain lines disappear, while others appear in the absorption spectrum (Leask, 1968).

In the rare earth perovskite, RBO_3 type compounds the materials whose optical properties have been explored are those in which B is Al, Gd, Cr, or Fe. Generally the bulk properties are determined by the B ion. When this is a transition metal ion the material tends to be opaque, otherwise transparent. This is associated with the localized 3d electrons of the transition metal ion (Allen 1975). The orthoaluminates and orthogallates are transparent throughout the visible region except for the areas where absorption lines due to the crystal field transitions of the rare earth ion are present (Merker and Herrington, 1964). For example, a triplet structure associated with the Tb^{3+} transitions in $TbAlO_3$ has been reported by Hüfner et al. (1968).

Amongst the RBO_3 compounds containing a transition metal B ion most of the optical work has been done on the orthoferrites. In typical examples of this type optical studies have been made on $ErFeO_3$ (Wood et al., 1969) and $TmFeO_3$ (Malozemoff, 1971). In addition to the absorption lines due to the rare earth ions, broad bands related to the crystal field absorption of the Fe^{3+} ion are present. Another optical property studied for the orthoferrites is the polar Kerr effect

(Wood and Remeika, 1967; Kahn et al., 1969). This is associated with the rotation of plane polarized light incident on a crystal due to the interaction with the magnetic moments present in the material.

The behavior of the orthochromites is similar to that of the orthoferrites but with additional spectra associated with Cr^{3+} . Recent optical data on orthochromites has been reported and discussed by Courths et al. (1970), Tsushima et al. (1970), Meltzer (1970) and Sugano et al. (1971).

2.8. Catalytic properties

The area of catalysis has recently received renewed attention because of possible applications in solving environmental problems. Precious metals have been found useful for the oxidation of CO to CO_2 , but are not effective in the reduction of NO. The possibility of using perovskite type catalysts seems promising since it was reported that LaCoO_3 , LaMnO_3 and their substituted derivatives have interesting catalytic properties in regard to application in fuel cell electrodes (Meadowcroft, 1970) and in the oxidation reduction reactions involved in the control of automotive exhaust emissions (Libby, 1971; Voorhoeve et al., 1972, 1973).

The catalytic properties of RBO_3 type compounds are related to the spin and valence state of the transition metal ion, B (Prakash et al., 1974). These authors have studied the oxidation of CO to CO_2 over rare earth cobaltites and found that NdCoO_3 and HoCoO_3 showed the highest catalytic activity, which is related to the higher activation energy of these compounds (~ 0.3 eV) compared to others in the series (~ 0.1 eV). Sorenson et al. (1974) have studied the reduction of NO over LaCoO_3 and attributed it to the creation of oxygen defects which leave the catalyst in a reduced state.

Since Prakash et al. (1974) found a correlation between the fraction of high spin Co^{3+} present and the catalytic activity, attempts were made by Voorhoeve et al. (1975a) to alter this ratio by substituting a divalent ion. It was found that partial substitution of La by a divalent ion in LaCoO_3 and LaCrO_3 reduced the activity of the compound. However, in the case of LaMnO_3 and LaFeO_3 the catalytic activity was enhanced. Thus efforts were concentrated on the system $\text{La}_{1-x}\text{M}_x\text{MnO}_3$ where M is Pb or Sr. Amongst these two series it was reported that the Sr containing compounds were more stable and catalytically more active than the Pb containing compounds (Gallagher et al., 1974). This was attributed to migration of lead to the surface and deactivation of the catalytic action (Gallagher et al., 1975a). The perovskite systems $\text{La}_{1-x}\text{M}_x\text{MnO}_3$ where M is K, Na, Rb or Ce have also been studied (Voorhoeve et al., 1975b; Johnson et al., 1976).

In order for the catalyst to be effective both in oxidation as well as reduction reactions, it should equilibrate with the exhaust gases without being degraded or mechanically altered. A potential advantage of the oxide systems is the ability to form mixed valence states which are fairly stable under a given set of oxidizing or reducing conditions. The compound can then adjust to these by minor

changes in the stoichiometry and valency states of the cations. Another advantage is their resistance to poisoning. Platinum, the catalyst presently being used for automobile exhaust emission control, is deactivated or poisoned in the presence of lead (Dwyer, 1972). $\text{La}_{0.7}\text{Pb}_{0.3}\text{MnO}_3$ is also deactivated by the migration of lead to the surface when it is heated. However, $\text{La}_{0.7}\text{Sr}_{0.3}\text{MnO}_3$ does not have this problem, although it is poisoned by SO_2 . An addition of as little as 200 ppm platinum imparted significant resistance to poisoning by SO_2 (Gallagher et al., 1975b).

The only ordered perovskite which has been studied for catalytic activity is Ba_2COWO_6 . This has been found to be comparable to the manganese based, rare earth perovskite, but it is easily poisoned in the presence of SO_2 (Voorhoeve et al., 1974).

3. Garnets

3.1. Crystal structure

The determination of garnet structure was first made on natural garnet minerals nearly fifty years ago (Menzer, 1926). Structural refinements were carried out on synthetic YIG crystals (Geller and Gillco, 1957; Batt and Post, 1962; Euler and Bruce, 1965). The symmetry of the single crystal X-ray photograph is $\text{O}_h - m\bar{3}m$. The following types of reflections are present:

$$\begin{aligned} (hkl), & \quad h + k + l = 2n \\ (hk0), & \quad h = 2n \quad \text{and} \quad k = 2n \\ (hkl), & \quad l = 2n \quad \text{and} \quad 2h + 1 = 4n. \end{aligned}$$

Therefore, the most probable space group for garnets is established to be the cubic group $\text{O}_h^{10} - 1a\bar{3}d$.

Garnets have the general chemical formula of $\{\text{C}_3\}[\text{A}_2](\text{D}_3)\text{O}_{12}$, where O denotes the oxygen atom or ion, and C, A, and D denote cations. There are eight formula molecules per unit cell. Therefore, there are 96 *h*-sites which are occupied by oxygens. The point symmetry of the *h*-site is $\bar{1}$. The cation sites in the garnet structure are classified into three types of sites. They are:

(1) Tetrahedral sites: Each tetrahedral or *d*-site is surrounded by 4 *h*-sites to form a tetrahedron. There are 24 *d*-sites in each unit cell. Each *d*-site has the point symmetry group of $\bar{4}(\text{S}_4)$.

(2) Octahedral sites: Each octahedral or *a*-site is surrounded by 6 *h*-sites to form an octahedron. There are 16 *a*-sites in each unit cell of garnet. Each *a*-site has the point group of $\bar{3}(\text{S}_6)$.

(3) Dodecahedral sites: Each dodecahedral or *c*-site is surrounded by 8 *h*-sites to form a triangular dodecahedron. A triangular dodecahedron is a polyhedron which has 12 faces with each face a triangle. There are 24 *c*-sites in each unit cell of garnet. Each *c*-site has the point group of $222(\text{D}_2)$.

Each *d*-site is surrounded by four *d*-sites, four *a*-sites, and six *c*-sites. Each

a-site is surrounded by eight *a*-sites at the corners of a body-centered cube. It is also surrounded by six *d*-sites and six *c*-sites. Each *c*-site is surrounded by four *c*-sites, four *a*-sites, and six *d*-sites. Each *c*-site is translated one fourth of the lattice constant distance from its corresponding *d*-site.

The garnet structure has a high percentage of its polyhedra which share edges. Each tetrahedron shares two edges with triangular dodecahedra, and each octahedron shares six edges with triangular dodecahedra. The triangular dodecahedron has three types of shared polyhedral edges. Each triangular dodecahedron shares two edges with tetrahedra, four edges with octahedra, and four edges with other triangular dodecahedra. Tetrahedra share only corners, i.e., oxygens, with octahedra. A more detailed summary of the information on the crystal structure of garnet appeared elsewhere (Wang, 1973).

3.2. Crystal chemistry

There exists a detailed review of the crystal chemistry of garnets (Geller, 1967). In the following, only a few general features relating to the rare earth ions in garnets will be discussed.

The primary consideration of the occupancy of polyhedral sites by cations is the ionic size. The ionic radius increases with the coordination number (C.N.). A table of effective ionic radii in sites was compiled (Shannon and Prewitt, 1969). In table 29.5 are listed the known examples of rare earth ions occupying the

TABLE 29.5.
Examples of rare earth ions at the *c*-sites (C.N. = 8).

Ion	Ionic radius (°A)	Example
Eu ²⁺	1.25	None reported
La ³⁺	1.18	None reported
Pr ³⁺	1.14	None reported
Nd ³⁺	1.12	None reported
Sm ³⁺	1.09	Fe-, Ga-garnets
Eu ³⁺	1.07	Fe-, Ga-garnets
Gd ³⁺	1.06	Al-, Fe-, Ga-garnets
Tb ³⁺	1.04	Al-, Fe-, Ga-garnets
Dy ³⁺	1.03	Al-, Fe-, Ga-garnets
Ho ³⁺	1.02	Al-, Fe-, Ga-garnets
Y ³⁺	1.015	Al-, Fe-, Ga-garnets
Er ³⁺	1.00	Al-, Fe-, Ga-garnets
Pr ⁴⁺	0.99	None reported
Tm ³⁺	0.99	Al-, Fe-, Ga-garnets
Yb ³⁺	0.98	Al-, Fe-, Ga-garnets
Lu ³⁺	0.97	Al-, Fe-, Ga-garnets
Sc ³⁺	0.87	

TABLE 29.6.
Examples of rare earth ions at the *a*-sites (C.N. = 6)

Ion	Ionic radius (°A)	Example	Reference
Pr ³⁺	1.013		
Nd ³⁺	0.995		
Sm ³⁺	0.964		
Tb ³⁺	0.923		
Dy ³⁺	0.912	Ge-garnets	(Mill', 1965a)
Ho ³⁺	0.901	Ge-garnets	(Mill', 1965a)
Y ³⁺	0.892	Ge-garnets	(Mill', 1965a)
Er ³⁺	0.890	Ge-garnets	(Mill', 1965a)
Tm ³⁺	0.869	Ge-garnets	(Mill', 1965a)
Yb ³⁺	0.858	Ge-garnets	(Mill', 1965a)
Lu ³⁺	0.848	Ge-garnets	(Mill', 1965a)
Pr ⁴⁺	0.78		
Tb ⁴⁺	0.76		
Sc ³⁺	0.730	Ge-garnets	(Tauber et al., 1961)

c-sites, or the triangular dodecahedral sites in garnets. The examples refer to the site occupancy as a major constituent by the rare earth ions. In table 29.6 are listed the examples of rare earth ions occupying the *a*-sites, or the octahedral sites. Rare earth ions have not been found to exist in the *d*-site, or the tetrahedral site. It is apparent that the small size of the tetrahedral site precludes the large sized rare earth ions.

Garnets have the crystal structure: cubic ($O_h^{10} - 1a3d$). As a first approximation the cubic lattice constant of garnet, *a*, can be considered as the linear sum of contributions from the triangular dodecahedral (*c*)-sites, the octahedral (*a*-) sites, and the tetrahedral (*d*-) sites (Wang, 1973).

$$a = K_C \langle r_C \rangle + K_A \langle r_A \rangle + K_D \langle r_D \rangle \quad (29.6)$$

where $\langle r_C \rangle$, $\langle r_A \rangle$, and $\langle r_D \rangle$ are the mean effective radius of *c*-site, *a*-site, and *d*-site cation, respectively, and K_C , K_A , and K_D are the least square parameters indicating the cation contributions to the lattice constant from the *c*-, *a*-, and *d*-sites, respectively. Effective radius values (Shannon and Prewitt, 1969) for the corresponding coordination number (C.N.) and lattice constants of various garnets (germanium garnets, aluminum garnets, iron garnets, gallium garnets: Geller, 1967; silicon garnets: Novak and Gibbs, 1971) were used to calculate the least squares parameters K_C , K_A , and K_D in eq. (29.6) (table 29.7). Values for silicate garnets are derived from the least square values given by Novak and Gibbs (1971). Values for the germanate garnets are also listed in several groups in table 29.7.

TABLE 29.7.

Least square parameters in eq. (29.11) for the cation contributions to lattice constants of various garnets (Wang 1973).

{C}	Cations			Number of data	Parameter		
	[A]	(D)			K_C	K_A	K_D
Ca	Cations exclusive of rare earth	Ge		13	1.89	1.81	22.60
Ca	Rare earths only	Ge		7	1.75	2.00	22.60
Ca	Cations including rare earths	Ge		20	1.85	1.87	22.60
Sr	Cations exclusive of rare earth	Ge		3	2.02	1.64	22.60
Sr	Rare earths only	Ge		7	1.83	1.95	22.60
Sr	Cations including rare earths	Ge		10	1.79	2.02	22.60
Cd	Cations exclusive of rare earth	Ge		9	1.99	1.70	22.60
Rare earths only	Al	Al		16	2.25	1.29	23.18
Rare earths only	Fe	Fe		35	2.06	1.94	18.45
Rare earths only	Ga	Ga		24	-0.32	5.75	19.23
Cations exclusive or rare earths	Cations exclusive of rare earths	Si		56	1.61	1.89	34.77

3.3. Phase equilibria

Garnets have been synthesized in hundreds of varieties, but there are only a limited number of phase equilibria studies available in the systems which contain garnets. In the systems containing the iron garnets, the foremost example is the Y_2O_3 - Fe_2O_3 system. The combined effects of oxygen partial pressure and multi-valencies of Fe convert this system into a ternary system of FeO - Fe_2O_3 - $YFeO_3$ (Van Hook, 1961,1962a). Yttrium iron garnet (YIG) is an incongruent melting compound. Its incongruent melting point is related to the oxygen partial pressure (Van Hook, 1963b).

$$\log p_{O_2} (\text{atm}) = -10^5(1/T). \quad (29.7)$$

3.4. Preparation

3.4.1. Ceramic synthesis

(i) *Oxide method*: Polycrystalline garnets are prepared from the solid state reactions between the constituent oxides. This is the method most easily used and is applicable to all types of garnets. Reaction kinetics vary with the physical states and the impurity levels of the oxide raw materials.

(ii) *Decomposition method*: This method seeks an intimate mix of oxides by the thermal decomposition of mixed components. Preferably, these components are

soluble in common liquid solvents, and they can be mixed in liquid form. For example, iron can be in the form of ferric ammonium sulfate $\text{Fe}(\text{NH}_4)(\text{SO}_4)_2 \cdot 12\text{H}_2\text{O}$, and aluminum can be in the form of aluminum ammonium sulfate $\text{Al}(\text{NH}_4)(\text{SO}_4)_2 \cdot 12\text{H}_2\text{O}$. Yttrium and rare earths can be in the form of chlorides or carbonates. Chlorides of yttrium or rare earths are readily available, but they are deliquescent. Carbonates are therefore to be preferred. This decomposition method is definitely an improvement over the oxide method. It works even in the case of some components which are not soluble. Thermal decomposition produces active sites in the decomposed products. These active sites promote the reactions of formation. The disadvantage lies, however, in the contamination of the reaction residues due to incomplete decomposition reactions.

(iii) *Chemical precipitation method*: In this method, the mixed cations are precipitated out of solution by suitable agents (usually, hydroxide); it produces very intimate mixing when conditions are perfect. The thermal decomposition process is then employed following the filtration of the precipitates. This method is limited in actual applications. Disadvantages include the limits placed on the types of cations, the difficulty and inefficiency of the filtration process, and the expenses of extra reagents required. These last two points reduce the industrial importance of this method.

(iv) *Conventional sintering*: The oxide mix, obtained by any of the above three methods, is pressed into sample shapes which are called green bodies. Green bodies are then sintered in air or in controlled atmospheres.

(v) *Pressure sintering (Hot-press)*: In this method, the oxide mix is simultaneously pressed and heated to an elevated temperature. For instance, Gd-doped GdIG powders of particle size $0.2 \mu\text{m}$ were cold-pressed at room temperature and 2000 kg/cm^2 to 50% theoretical density. The cold-pressed powder compacts were then transferred into alumina dies. Fine-sized alumina powder was used as the pressure transmitting medium. The die assembly was evacuated to about 0.1 Torr, and it was then hot-pressed at $900\text{--}1300^\circ\text{C}$ and $300\text{--}1000 \text{ kg/cm}^2$ for 1–20 h (Coeure et al., 1969). At a hot-pressing operation of 3 h at 1175°C and 1000 kg/cm^2 , the GdIG samples had an average grain size of $3 \mu\text{m}$. Hot-pressing shortens the total processing time and the time at elevated temperatures as compared with conventional sintering processes. The shortening of process time decreases the formation of second phase in the garnet, and it affords better control of grain size in the samples. Grain size can vary from $2 \mu\text{m}$ at 1050°C for 1 h to $20 \mu\text{m}$ at higher temperatures ($> 1250^\circ\text{C}$) and longer times (> 8 h). An improved control of grain size can also be achieved by hot-pressing to $1 \mu\text{m}$ and by annealing at 1400°C to achieve the desired grain size of $10 \mu\text{m}$ (Patton, 1970). Higher porosity is the result of hot-pressing plus annealing.

3.4.2. Single crystal methods

Several recent books describe the growth methods of single crystals extensively (Brice, 1965; Laudise, 1970; Laudise et al., 1971). The methods which

produced garnet crystals successfully include the following:

- (i) *Flux growth method*: Fluxes, such as PbO (Remeika, 1956), PbO-PbF₂ (Nielsen, 1960), PbO-B₂O₃ (Giess, 1962), BaO-B₂O₃ (Linares, 1962b), PbO-PbF₂-B₂O₃ (VanUitert et al., 1965), and PbO-Bi₂O₃ (Esponzoza and Geller, 1964), were used successfully. Gradient method (Laudise et al., 1962) was also employed to improve the crystal yield.
- (ii) *Czochralski growth method*: Iron garnets, being incongruently melting compounds, cannot be grown by the Czochralski method. Aluminum and gallium garnets can be grown by this method readily.
- (iii) *Hydrothermal growth method*: This method is possible to grow garnet crystals, but requires careful adjustment of growth conditions (Kolb and Laudise, 1971).

3.4.3. Epitaxial garnet films

- (i) *Sputtering methods*: Several sputtering methods can be used to grow garnet films (Sawatzky and Kay, 1968). One is the rf reactive sputtering. The other is the dc inert gas sputtering. The third method is the dc reactive sputtering. Currently, the sputtering technique cannot produce high quality epitaxial garnet films.
- (ii) *Chemical vapor deposition method*: The chemical vapor deposition (CVD) process can produce epitaxial garnet film of acceptable quality (Robinson et al., 1971). But a great deal of improvement in the process is still required.
- (iii) *Liquid phase epitaxy methods*: An extension of the flux grown method evolves into the liquid phase epitaxy (LPE) method. Currently, the LPE method produces the best quality garnet films. In this process, the liquid, which consists of flux and garnet, is made to be in contact with the substrate, and the epitaxial garnet film deposits onto the substrate. Most methods employed PbO-B₂O₃ as flux (Blank and Nielsen, 1972). Before insertion into the melt, the substrates, properly etched and cleaned, are held immediately above the melt surface to equilibrate in a region where the temperature is within 1°C of the melt. The substrates are rotated in a horizontal plane at 100–200 rpm during the epitaxial film growth which takes place with 5 to 15°C of supercooling (Gilss et al., 1972). To terminate growth, the substrates are withdrawn from the melt and held immediately above the melt surface rotating at 200–1000 rpm to remove flux adhering to the film. Finally, the wafers are withdrawn from the furnace at a maximum rate of 12 cm/min to prevent thermal shock cracking (Hewitt et al., 1973). Alternate to the horizontal rotation method, a vertical substrate dipping method produces epitaxial garnet film of good quality (Tolksdorf, 1975). The film quality is indicated by the effective lattice misfit, Δa . Below 0.02 Å can be readily achieved by the above LPE method.

In epitaxy, there are three major causes of stress in the film. One is the lattice misfit. The other is the mismatch in the thermal expansions. The third cause is the concentration or impurity effect. The last effect is now reintroduced into the garnet film to achieve the increase in its magnetic uniaxial anisotropy. The ion

implantation method is used to achieve this effect (Wolfe et al., 1973; Hu and Giess, 1975).

Direct measurement of stress and strain in epitaxial YIG films on YAG was made with an X-ray diffraction technique (Zeyfang, 1970; Klokholm et al., 1972). It employs the planes parallel to the film surface for diffraction. The strain perpendicular to the surface ϵ^\perp is given by

$$\epsilon^\perp = (\Delta d^\perp)/d_0^\perp, \quad (29.8)$$

where d_0^\perp is the lattice spacing in the unstrained film, and Δd^\perp is the difference between the lattice spacing in the strained and in the unstrained condition. It was found that ϵ^\perp is -2.1×10^{-3} . The strain parallel to the film surface ϵ^\parallel is calculated to be 2.5×10^{-3} , using a Poisson's ratio of 0.29 (Spencer et al., 1963). Using a Young's modulus E of 2.0×10^{12} dyn/cm² for YIG, a tensile stress of about 6.5×10^9 dyn/cm² parallel to the surface was found at room temperature in a film deposited at 1225°C.

There are other methods of direct stress measurement for films, such as deflection measuring techniques with the traveling microscope (Weiss and Smith, 1962), and the electrobalance (Klokholm, 1969). These methods are limited to the measurement of a one-dimensional state of stress. The stress on a macroscopic scale was a priori assumed to be isotropic. A modified Ligtienberg reflective Moire method (Chiang et al., 1971) measures the two-dimensional state of stress in films. The method consists of projecting a grating onto the film surface which acts as a mirror. The distortion in the grating image due to the bending of the film plate is obtained through the Moire fringes which result from the superpositions of the distorted and reference gratings. The principal stresses can be obtained from the measured moments. This method enables a stress measurement on every point of the film surface. It is a method which can be easily adopted to stress measurements in garnet films on garnet substances.

3.5. Magnetic properties

3.5.1. Magnetization

There are extensive reviews of magnetic garnets (for example, Geller, 1966; Von Aulock, 1965). This article is limited to the magnetic properties of garnets as pertaining to their material properties. Magnetic garnets, such as YIG and RIG, were the first garnets found to be ferrimagnetic (Pauthenet, 1956, 1957, 1958). Néel theory of ferrimagnetism (Néel, 1948), as applied to the garnet structure, considers the sublattices of the a-site and the c-site cations to be ferromagnetically coupled. The d-site cation sublattice is considered to be antiferromagnetically coupled to the a-site sublattice. The net magnetic moment of the garnet is given by

$$\mathbf{M}(T) = \mathbf{M}_d(T) - \mathbf{M}_a(T) - \mathbf{M}_c(T) \quad (29.8)$$

where $\mathbf{M}_d(T)$, $\mathbf{M}_a(T)$, and $\mathbf{M}_c(T)$ are the sublattice magnetizations of the d-site, a-site, and c-site, respectively. When a magnetic cation, such as Gd³⁺, is used to

substitute for the nonmagnetic Y^{3+} ions on the c-site, at a ratio greater than 0.4, there is a temperature at which $M(T) = 0$. This temperature is called the compensation temperature, T_{comp} . Above T_{comp} , the c-site sub-lattice contribution diminishes, and the $M(T)$ curve tends to approach that of YIG. The T_{comp} value is a good indicator of the cation distribution in the garnet, dependent on the heat treatment, preparation condition, and chemical composition.

Magnetic properties of the garnets reveal a great deal about the rare earth ions. First there is a separation of grouping between the lighter rare earth ions, such as La, Pr, Sm, and Eu (Geller et al., 1963²), and the other heavier rare earth ions. Second, some of the rare earth ions in the magnetic garnets have their magnetic spins canted with respect to a preferred spin direction. In DyIG, ErIG, and YbIG, the rare earth spins were found to tilt away from the $\langle 111 \rangle$ easy axis in the $\{110\}$ planes (Pickart et al., 1970). In HoIG, the Fe ions at the d-site have their moments along the $\langle 111 \rangle$ axis, and the Fe ions at the a-site have their moments along the $\langle \bar{1}\bar{1}\bar{1} \rangle$ axis. The Ho ions at the c-site have a double conical arrangement about this axis, and their resultant moment is along the $\langle \bar{1}\bar{1}\bar{1} \rangle$ direction (Herpin et al., 1960; Allain et al., 1966). The spin canting of rare earth ions adds to the complexity, for the spin canting angle can change with temperature and composition. Third, the mixed rare earth garnets, in which more than one kind of rare earth ions exist, show that rare earth ions behaved differently in the presence of other rare earth ions. For example, one finds a magnetic moment of 1.6 and 1.8 Bohr magnetons per Pr^{3+} and Nd^{3+} substituted in LuIG, as compared with 0.8 and 1.0 Bohr magnetons per Pr^{3+} and Nd^{3+} substituted in YIG (Perel and Schieber, 1962).

3.5.2. Molecular field theory

The Néel theory of antiferromagnetism (a molecular field treatment for three sublattices of the garnet structure), as applied to ferrimagnetism (Néel, 1948), shows that the fields acting at a-, d-, and c-sites, respectively, are

$$\begin{aligned} H_a &= H - N_{aa}M_a - N_{ad}M_d - N_{ac}M_c, \\ H_d &= H - N_{da}M_a - N_{dd}M_d - N_{dc}M_c, \\ H_c &= H - N_{ca}M_a - N_{cd}M_d - N_{cc}M_c, \end{aligned} \quad (29.9)$$

where the molecular field coefficients $N_{ad} = N_{da}$, $N_{ac} = N_{ca}$, $N_{cd} = N_{dc}$, and the applied magnetic field field is H . The moduli of the sublattice magnetizations are given by

$$|M_a| = N_a g \mu_B J_a B(x_a), \quad |M_d| = N_d g \mu_B J_d B(x_d), \quad |M_c| = N_c g \mu_B J_c B(x_c) \quad (29.10)$$

where

$$x_i = J_i g \mu_B |H_i| / kT, \quad i = a, d, \text{ or } c \quad (29.11)$$

and where N_a , N_d , and N_c are the numbers of atoms per unit volume for a-, d-, and c-sites, respectively, J_a , J_d , and J_c are the intrasublattice exchange constants,

g is the splitting factor, μ_B is the Bohr magneton, and $B(x)$ is the Brillouin function (Morrish, 1965). The canting of the rare earth ion can be included in this treatment by considering all magnetic moments in vectors. Magnetism equations (29.9)–(29.11) are implicit functions of M ; namely, M exists on both sides of the same equation. The simultaneous sets of three equations for three sublattices make them infinitely more difficult to solve, even with computers. Therefore, there is no thought of further subdividing each crystallographic site into sublattices of Bravais lattices.

In YIG where the c-site ions are nonmagnetic, the picture is simplified into two sublattices, namely, the d- and a-sublattices. A spin wave study of YIG produces exchange constants $J_{ad} = J_{da} = 4.8 \times 10^{-15}$ erg, $J_{aa} = 1.1 \times 10^{-15}$ erg, and $J_{dd} = 2.1 \times 10^{-15}$ erg (Douglass, 1960).

In $\{Y_3\}[R_xFe_{2-x}](Q_yRe_{3-y})O_{12}$, where R and Q are nonmagnetic ions, such as In, Ga, and Al, the molecular field coefficients were found to be (Dionne, 1970)

$$\begin{aligned} N_{dd} &= -30.4(1 - 0.43x), & N_{aa} &= -65.0(1 - 0.42y) \\ N_{ad} &= 97.0(1 - 0.125x - 0.127y) \text{ mole/cm}^3 \end{aligned} \quad (29.12)$$

for $x \leq 0.70$ and $y \leq 1.95$. The values x and y are related to k_a and k_d , which represent the fraction of nonmagnetic ions in the respective sublattice. Thus, the molecular field coefficients are linearly related to k_a and k_d . For substitutions in one sublattice, the coefficient of the opposite sublattice is reduced in magnitude while its own coefficient remains unchanged. For substitutions in either sublattice, the intersublattice coefficient N_{ad} is reduced. Geller (Geller et al., 1964b) found that the concept of canting (Yafet and Kittel, 1952) can be used to interpret the magnetizations of substituted YIG. When substitutions are made in one sublattice, random canting takes place in the opposite one. The amount of canting in a given sublattice appears to be directly related to a change in its molecular field coefficient. Since $|N_{dd}| < |N_{aa}|$ initially, canting would be expected to occur earlier in the d-site in accord with experiment. An extension of this approach (Brandle and Blank, 1976) produced the list of molecular field coefficients for rare earth iron garnets, as shown in table 29.9. The multiplying factor f is given by the equation.

$$M(T) = fM_{YIG}(T). \quad (29.13)$$

This is due to great similarity between the saturation magnetization of the rare earth iron garnet, $M(T)$ and the saturation magnetization of YIG, $M_{YIG}(T)$. Only in the case of Eu, the multiplying factor of needs to be a function of temperature. This approach (Dionne, 1970) relies on the best fit of experimental magnetization data, and it has some inherent disadvantages. It depends on a large amount of experimental data and consistencies among the data. It has a degree of arbitrariness which lacks suitable explanation. The results of this approach, however, relate the magnetic data directly to the cation distribution in the garnet.

Another approach (Gilleo, 1960) uses the statistics of interactions to relate the magnetic data with the cation distributions. For the garnet $\{R_3\}[M_yFe_{2-y}]$

TABLE 29.8.
Melting points of rare earth garnets.

Compound	Melting points (°C)	Reference
Y ₃ Fe ₅ O ₁₂ (YIG)	1495 ± 7 in CO ₂ (P _{O₂} = 1.3 Torr)	(Van Hook, 1962a)
(incongruent)	1555 ± 3 in air	(Van Hook, 1962a)
	1582 ± 5 in O ₂	(Van Hook, 1962a)
	1350 ± 50 in CO ₂	(Van Hook, 1962b)
Gd ₃ Fe ₅ O ₁₂ (GdIG)	1495 ± 7 in air	(Van Hook, 1962b)
(incongruent)	1550 ± 10 in O ₂	(Van Hook, 1962b)
Y ₃ Al ₅ O ₁₂ (YAG)	1970	(Warsaw and Roy, 1959)
(congruent)	1980	(Van Hook, 1963a)
Nd ₃ Ga ₅ O ₁₂ (NdGG)	1515	(Brandle and Valentino, 1972)
Sm ₃ Ga ₅ O ₁₂ (SmGG)	1620	(Brandle and Valentino, 1972)
Gd ₃ Ga ₅ O ₁₂ (GdGG)	1690	(Brandle and Valentino, 1972)
Tb ₃ Ga ₅ O ₁₂ (TbGG)	1715	(Brandle and Valentino, 1972)
Dy ₃ Ga ₅ O ₁₂ (DyGG)	1730	(Brandle and Valentino, 1972)
Ho ₃ Ga ₅ O ₁₂ (HoGG)	1750	(Brandle and Valentino, 1972)
Er ₃ Ga ₅ O ₁₂ (ErGG)	1760	(Brandle and Valentino, 1972)

(M₂Fe₃₋₂)O₁₂ where R is magnetic and M is nonmagnetic, the total magnetic moment can be estimated to be, in Bohr magnetons

$$|n| = |n_c - n_d + n_a|$$

$$= \{3M_c[1 - E_c(k_d)]\} - \{3M_d(1 - k_d)[1 - E_d(k_a)] - 2M_a(1 - k_a)[1 - E_a(k_d)]\}, \quad (29.14)$$

where E_i is the probability of an ion at i -site to be linked with at most one of the magnetic ions.

$$E_c = 4k_d^3 - 3k_d^4, \quad E_a = 6k_d^5 - 5k_d^6, \quad E_d = 4k_a^3 - 3k_a^4. \quad (29.15)$$

This approach does not take into account spin canting. It also fails to include the temperature dependence, but it allows a simple check between the magnetic moment and the cation distribution. Therefore, with either of these two approaches, one can obtain a picture of cation distribution in the garnets from their magnetization data. Magnetization data can be readily obtained in comparison to either X-ray or neutron diffractions, which are usually employed to gain cation distribution information. Because many cations can enter into the garnet structure, and many garnets are magnetic, this approach is a very useful one.

3.5.3. Magnetocrystalline anisotropy

The magnetization \mathbf{M} in a ferrimagnetic material is always bound to a certain preferred crystallographic direction, which is the easy axis. Anisotropy energy F_k is required to turn \mathbf{M} from the easy axis direction to any other direction. Phenomenologically, this magnetocrystalline anisotropy can be described, to a

second approximation, for cubic crystals as

$$F_k = F_0 + K_1(\alpha_1^2\alpha_2^2\alpha_3^2 + \alpha_3^2\alpha_1^2) + K_2\alpha_1^2\alpha_2^2\alpha_3^2 + \dots \quad (29.16)$$

The coordinate axis coincide with the crystal axes, and α_1 , α_2 , and α_3 are the direction cosines of M with respect to the crystal axes. The constants K_1 and K_2 are the first-order and the second-order magnetocrystalline anisotropy constants, respectively. For the purpose of energy minimization, the F_0 term can be neglected. The constants K_1 and K_2 are used to represent the magnetocrystalline anisotropy in the crystal.

The magnetocrystalline anisotropy is a direct measure of the contributions from individual cations in the lattice. The success of the single ion model of the anisotropy theory (Yoshida and Tachiki, 1957; Wolf, 1957), as applied to the ferrites and garnets, makes the anisotropy constants very useful.

A list of magnetocrystalline anisotropy constants of several garnets is shown in table 29.10. There are several general features about them. First, the rare earth ions make a huge contribution to the magnetocrystalline anisotropy constants. Tb ion has the most significant effect, and TbIG has the largest anisotropy constants. Second, K_1 and K_2 are phenomenological constants. Consequently, the neglect of K_2 , or its inclusion, makes a significant difference in the values of K_1 and K_2 . Third, the temperature dependence of K_1 or K_2 is generally a monotonic varying function. Si^{4+} -doped YIG shows a maximum in the temperature dependence of K_1 which has been attributed to the onset of a relaxation process (Van Groenou et al., 1967).

3.5.4. Growth-induced noncubic anisotropy

Whenever multiple types of cations occupy the same crystallographic sites in the garnets, noncubic uniaxial magnetic anisotropy was found to exist. Although

TABLE 29.9.
Molecular field coefficients for rare earth iron garnets
(Brandle and Blank, 1976).

	g	N_{ac}	N_{dc}	N_{cc}	Mult.	J
Sm	0.000	0.00	0.00	0.00	0.94	0.0
Eu	0.000	0.00	0.00	0.00	0.518	0.0
Gd	2.000	-3.44	6.00	0.00	1.000	3.5
Tb	1.500	-1.80	3.40	0.00	1.000	6.0
Dy	1.333	-3.35	3.95	0.10	1.000	7.5
Ho	1.25	-0.75	1.50	0.25	1.000	8.0
Er	1.20	-0.75	1.25	0.00	1.000	7.5
Tm	1.17	-1.00	8.00	0.00	0.760	6.0
Yb	1.144	-1.70	2.00	0.00	0.967	3.5
Lu	0.000	0.00	0.00	0.00	0.862	0.0
Y	0.000	0.00	0.00	0.00	1.000	0.0

*Mult. = $0.000645T + 0.4538$, for $T \geq 100$ K.

TABLE 29.10.
Magnetocrystalline anisotropy constants of garnets.

Formula	(K)	$K_1 \times 10^{-3}$ (erg/cm ³)	K_2	Reference
YIG	4	-24.8	-	
	100	-20.2	-	
	200	-11.0	-	
	300	-5	-	(Von Aulork, 1965)
	78	-22.4	-	(Iida, 1967)
Y ₃ Sc _{0.4} Fe _{4.6} O ₁₂	4	-14.5	-	
	100	-12.0	-	
	200	-6.0	-	
	300	-1.8	-	(Pearson, 1962)
Y ₃ Sc _{0.9} Fe _{4.1} O ₁₂	4	-6.0	-	
	100	-4.0	-	
	200	-1.5	-	
	300	-0.3	-	(Pearson, 1962)
SmIG	100	-8.0 × 10 ¹	-	
	200	-8.0	-	
	300	-2.0	-	(Pearson, 1962)
EuIG	78	-12 × 10 ²	-	(Iida, 1967)
	170	-1.95 × 10 ¹	0.9 × 10 ⁴	
	190	-1.6 × 10 ¹	0.48 × 10 ⁴	
	210	-0.9 × 10 ¹	0.23 × 10 ⁴	
GdIG	230	-0.7 × 10 ¹	0	(Miyadai, 1960)
	4	-26.8	-	
	100	-21.0	-	
	200	-13.2	-	
	300	-6.0	-	(Rodrigue et al., 1960)
TbIG	78	-30	-	(Iida, 1967)
	80	-760.0	-7.6 × 10 ⁶	
	100	-295.0	-	
	200	~-20.0	-	
	300	~-5.0	-	(Pearson, 1962)
DyIG	78	≥1000	-	(Iida, 1967)
	80	-970.0	+214 × 10 ³	
	100	-400.0	-	
	200	~-20.0	-	
DyIG	300	~-5.0	-	(Pearson, 1962)
	78	-980	-	(Iida, 1967)
HoIG	4	~-12 × 10 ³	-	
	80	-800.0	-270 × 10 ³	
	100	-250.0	-	
	200	~-5.0	-	
	300	~-5.0	-	(Pearson, 1962)
ErIG	78	-800	-	(Iida, 1967)
	100	-2.1 × 10 ¹	-	
	200	-1.05 × 10 ¹	-	
TmIG	300	-5.5	-	(Pearson, 1962)
	78	-22	-	(Iida, 1967)
TmIG	77	-2.1 × 10 ²	10 ⁵	

TABLE 29.10 (Cont.).

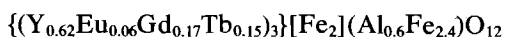
Formula	(K)	$K_1 \times 10^{-3}$ (erg/cm ³)	K_2	Reference
YbIG	100	-1.3×10^2	—	(Miyadai, 1960)
	200	-0.3×10^2	—	
	300	-1.1×10^1	~0	
	100	-3×10^1	—	(Pearson, 1962)
	200	-1.4×10^1	—	
	300	-7	—	
	4	-62×10^2	68×10^2	
	30	-45×10^1	20×10^1	
	78	-38	—	

the presence of rare earth ions is not the necessary condition (Akselrad and Callen, 1971), the existence of such a noncubic anisotropy with the magnetic garnets containing mixed rare earth ions is most interesting. For it demonstrates most dramatically that rare earth ions, notwithstanding with their many similarities, are distinctly different from each other.

There are six inequivalent c-sites in the garnet structure. The site notation in terms of the orientation of local axes of the c-site is listed in table 29.11, following that used by Rosencwaig et al. (1971b). When the magnetic rare earth iron garnets are grown from the melt, either by the flux method or by the liquid phase epitaxy method, the rare earth ions apparently show different crystallographic site preferences according to the substrate crystal orientation and the different rare earth ions.

There are six types of facet cuts which yield useful uniaxial garnet platelets (Bobeck et al., 1971). Type I cut is perpendicular to the $\langle 111 \rangle$ axis which is nearly normal to the $\{211\}$ facets. This $\langle 111 \rangle$ direction is the easy axis emergent from the junction of, and $19^\circ 28'$ off of, the normal to the three $\{211\}$ facets. Type II cut is perpendicular to the $\langle 111 \rangle$ axis contained in a $\{211\}$ facet. The easy axis of the type II cut is also the $\langle 111 \rangle$ axis. Type III cut is perpendicular to the easy axis $\langle 100 \rangle$ in the $\{110\}$ facet. Types IV, V, VI cuts have their easy axis directions in $\langle 110 \rangle$. Type VI cut is for the $\{211\}$ faceted crystal, and Type IV and V cuts are for $\{110\}$ facet crystals.

Representative noncubic anisotropy results can be shown in the case of the garnet



where the measured cubic anisotropy K , of the type III cut of the garnet was found to be -3300 erg/cm³ (Rosencwaig et al., 1971a). The type III cut has the easy axis in $\langle 100 \rangle$, the medium axis in $\langle 110 \rangle_1$, and the hard axis in $\langle 110 \rangle_{11}$ (LeCraw et al., 1971). Its average noncubic, uniaxial, growth-induced, anisotropy was found to be 0 in the easy axis, 7100 erg/cm³ in the medium axis, and 9200 erg/cm³ in the hard axis. A different cut from the $\{211\}$ facet of the same crystal has an easy axis in the $(\bar{1}10)$ plane containing the

$\langle 11\bar{1} \rangle$ and $\langle 112 \rangle$ axes, and at an angle of 52° from $\langle 11\bar{1} \rangle$ toward the $\langle 112 \rangle$ axis. The hard axis lies in this plane, normal to the easy axis. The intermediate axis is the $\langle \bar{1}10 \rangle$ direction. The cubic anisotropy was found to be -3100 erg/cm^3 for this cut. Its noncubic anisotropy was 0 in the easy axis, 1200 erg/cm^3 in the medium axis, and 8000 erg/cm^3 in the hard axis. The noncubic anisotropy can be eliminated by annealing at temperatures above 1200°C . It was found that the cubic anisotropies are nearly the same for all samples and in good agreement with the total anisotropy measured in the same samples after elimination of the noncubic anisotropy by annealing. The magnitude of noncubic anisotropy varies from sample to sample. This variation is significantly greater than can be attributed to experimental uncertainty. It suggests that the growth conditions may be the deciding factor in this variance.

The origin of the uniaxial anisotropy is uncertain, but there are many theories about it. Early explanations of the strains induced during growth are found wanting (Lefever et al., 1965). The current theories include the growth-induced pair-ordering model, the site-reference model, the dipolar mechanism, and the local symmetry distortion model.

The growth-induced pair ordering model (Rosencwaig and Tabor, 1971) proposes that the noncubic anisotropy arises from the presence of a small amount of growth-induced short-range pair ordering which occurs during crystallization. This pair ordering is a result of preferential cation pair-bond directions with respect to the crystal growth facets. There are two mechanisms for this model. One involves the c-site rare earth ions and the d-site iron ions. The other involves the c-site rare earth ions and the d-site iron ions. In applying this model to $\{\text{Eu}_2\text{Er}_1\}[\text{Fe}_2](\text{Fe}_{2.4}\text{Ga}_{0.6})\text{O}_{12}$ (Rosencwaig and Tabor, 1971), less than 1% preferential pair ordering, i.e., $\langle 100 \rangle$ in the first mechanism and $\langle 210 \rangle$ in the second mechanism, can account for the observed noncubic anisotropy.

The site preference model (Callen, 1971a,b) explains the noncubic anisotropy in terms of the preferential occupation, by one of the multiple types of rare earth ions, of particular c-sites. There are two nearest-neighbor tetrahedral sites for each c-site. The next closest neighbors are the octahedral sites. The second-nearest tetrahedral neighbors are sources of the observed noncubic anisotropy, according to Callen (1971a). A combination of pair ordering and site preference is another form of the site preference model (Rosencwaig et al., 1971b). In this version, the nearest tetrahedral and the nearest octahedral neighbors lead to a uniaxial anisotropy under both growth facets. Inclusion of the next-nearest tetrahedral neighbors results in the observed orthorhombic anisotropies. The site selectivity for rare earth ions in garnets was confirmed by the spin resonance spectra. They demonstrated facet-related site selectivity for Nd^{3+} and Yb^{3+} ions in flux-grown YAG (Wolfe et al., 1971). In table 29.12, the average populations of X_1 , X_2 , Y_1 , and Y_2 sites are taken as unity, and the populations of Z_1 and Z_2 sites are presented relative to this average. Under a $\{211\}$ facet, a Z_1 site is 2.3 times as likely and a Z_2 site is 3.5 times as likely as any X or Y site are to be occupied by Nd ions. Equal population of the Z_1 and Z_2 sites would imply uniaxial anisotropy. The orthorhombic anisotropy implies that the Z_1-Z_2 population

TABLE 29.11.
Orientation of local axes of the dodecahedra, or c-,
sites (D^2 Symmetry) (Rosencwaig et al., 1971b).

Site	Axes			Site equivalence	
	<i>a</i>	<i>b</i>	<i>c</i>	{110} facet	{211} facet
X ₁	01 $\bar{1}$	011	100	X	X ₁
X ₂	011	0 $\bar{1}$ 1	100	X	X ₂
Y ₁	$\bar{1}$ 01	101	010	X	X ₁
Y ₂	101	10 $\bar{1}$	010	X	X ₂
Z ₁	1 $\bar{1}$ 0	110	001	Z ₁	Z ₁
Z ₂	110	$\bar{1}$ 10	001	Z ₂	Z ₂

difference is as important as the Z - (X, Y) difference. The site population ratios vary approximately exponentially with Δr , where Δr is the excess of the ionic radius of the rare earth ion over Y^{3+} .

The dipolar mechanism (Sturge, 1972), applied to a garnet containing only Gd^{3+} and Fe^{3+} as magnetic ions, together with the site selectivity on the c-site sublattice, accounts well for the uniaxial term in the growth-induced anisotropy of $\{Y_2Gd\}[Fe_{2.2}Al_{0.8}O]_{12}$. This model requires the calculation of the dipolar and crystal field contributions to the noncubic anisotropy. The rhombic term in the anisotropy cannot be attributed solely to the dipolar mechanism and is attributed to a contribution from the Fe^{3+} sublattices.

The local symmetry distortion model (Akselrad and Callen, 1971) is based on the distortion of the local symmetry around the tetrahedral d-site, caused by referential ordering among their tetrahedral (or other) neighbors. This model is especially useful when the rare earth-based mechanism cannot be operative. In mixed rare earth garnets, a distortion of tetrahedral symmetry can be caused by ordering of dodecahedral site ions. This local symmetry distortion is the cause of noncubic anisotropy.

3.5.5. Magnetostriction

The interaction between magnetization and strain produces a lattice deformation in a magnetized body. When the specimen is magnetized to saturation, the saturation magnetostrictions along the $\langle 100 \rangle$ and $\langle 111 \rangle$ directions are denoted by $\lambda_{\langle 100 \rangle}$ and $\lambda_{\langle 111 \rangle}$, respectively. These linear magnetostrictions arise from the strain-dependence of the magnetic anisotropy. The magnetoelastic energy tensor B_{ijkl} is given by (White and Phillips, 1968)

$$H_{ME} = \sum_{ijkl} B_{ijkl} \alpha_i \alpha_j \epsilon_{kl} \quad (29.17)$$

where α_i 's are the direction cosines of the magnetization (considered to lie along an external magnetic field) with respect to the crystal axes, and the ϵ_{kl} are the

strain components in Love's notation. Keeping terms up to second degree in spin operators, the magnetic Hamiltonian can be written as

$$H_M = \beta \mathbf{H} \cdot \mathbf{g} \cdot \mathbf{S} + \mathbf{S} \cdot \mathbf{D} \cdot \mathbf{S} + H_{\text{elast}} \quad (29.18)$$

where \mathbf{g} and \mathbf{D} are the g -tensor and the crystal-field tensor of the ion, respectively, \mathbf{H} is the applied external magnetic field in the case of a paramagnet or the molecular field in the case of the magnetically ordered crystal, and \mathbf{S} is the spin of the ion. The magnetoelastic energy linear in the strains is

$$\begin{aligned} H_{ME} &= \sum_{kl} (\partial H_M / \partial \epsilon_{kl}) \epsilon_l \\ &= \sum_{\sigma} \sum_{ijkl} \beta (\partial g_{ij}^{\sigma} / \partial \epsilon_{kl})_0 H_i^{\sigma} S_j \epsilon_{kl} + \sum_{\sigma} \sum_{ijkl} (\partial D_{ij}^{\sigma} / \partial \epsilon_{kl})_0 S_i S_j \epsilon_{kl} \end{aligned} \quad (29.19)$$

where the derivatives evaluated at equilibrium are the magnetoelastic constants and the summation is over all σ sites. For a cubic crystal, eq. (29.17) can be written as

$$\begin{aligned} H_{ME} &= B_1 [\alpha_1^2 - \frac{1}{3}] \epsilon_{xx} + (\alpha_2^2 - \frac{1}{3}) \epsilon_{yy} + (\alpha_3^2 - \frac{1}{3}) \epsilon_{zz} \\ &\quad + B_2 [\alpha_1 \alpha_2 \epsilon_{xy} + \alpha_2 \alpha_3 \epsilon_{yz} + \alpha_3 \alpha_1 \epsilon_{zx}] \end{aligned} \quad (29.20)$$

The magnetoelastic energy tensor B_{ijkl} is reduced to two independent magnetoelastic constants $B_1 (= B_{11} - B_{12})$ and $B_2 (= 2B_{44})$, which are related to the saturation magnetostriction constants $\lambda_{(100)}$ and $\lambda_{(111)}$ by

$$B_1 = -(3/2) \lambda_{(100)} (c_{11} - c_{12}), \quad B_2 = -3 \lambda_{(111)} c_{44}. \quad (29.21)$$

If the directional cosines of the linear dilation are β_1 , β_2 , and β_3 with respect to the crystal axes, the dilation is related to magnetostriction constants by

$$\begin{aligned} \delta l / l &= \lambda_0(T, H) + \frac{3}{2} \lambda_{(100)}(T, H) [\alpha_1^2 \beta_1^2 + \alpha_2^2 \beta_2^2 + \alpha_3^2 \beta_3^2 - \frac{1}{3}] \\ &\quad + 3 \lambda_{(111)}(T, H) [\alpha_1 \alpha_2 \beta_1 \beta_2 + \alpha_2 \alpha_3 \beta_2 \beta_3 + \alpha_3 \alpha_1 \beta_3 \beta_1] + \dots \end{aligned} \quad (29.22)$$

The origins of the magnetoelastic constants have been discussed in several reviews (Kanamori, 1963; Comstock, 1965; Jones, 1966; Callen, 1968). Fundamentally, they are the indicators of the changes in crystal field due to strains. Experimentally, they are determined with certain degrees of arbitrariness. Consequently, they have significant variances in values determined by either the strain gauge method or the parallel pump method of the resonance technique. This does not take into account the reduction of symmetry by the presence of the magnetization or strain vector, which adds to the complexities. Phenomenologically, the magnetoelastic constants, or the linear magnetostriction constants as shown in table 29.13, are algebraically additive over all sublattices of the garnet structure. The similarity between them and the sublattice magnetization is very real, and there is also a compensation temperature from the competition of sublattice magnetostrictions. The additive property of magnetostriction is exemplified by the linear dependence of magnetostriction or

TABLE 29.12.
Relative populations of impurity ions in dodecahedral sites of YAG
(Wolfe et al., 1971).

Impurity (approx. %)	at. Facet	Relative population ([X] ≈ [Y] ≈ 1)		Accuracy (%)
		[Z ₁]	[Z ₂]	
3%Nd	{110}	0.65	0.60	10
3%Nd	{211}	2.30	3.50	10
1%Yb	{110}	1.18	1.12	5
1%Yb	{211}	0.93	0.91	7
3%Nd (annealed)	{211}	1.15	1.30	15

rare earth iron garnets on the rare earth concentration (Clark et al., 1968). The difference between the magnetostrictions of YIG and ReIG denotes the rare earth contribution to magnetostriction, which is related to the rare earth magnetization. For GdIG, the results showed

$$\frac{\lambda_{(100)}(\text{GdIG}, 77) - \lambda_{(100)}(\text{YIG}, 77)}{\lambda_{(100)}(\text{GdIG}, 4.2) - \lambda_{(100)}(\text{YIG}, 4.2)} = 0.63 \quad \frac{M(\text{GdIG}, 77) - M(\text{YIG}, 77)}{M(\text{GdIG}, 4.2) - M(\text{YIG}, 4.2)} = 0.60$$

$$\frac{\lambda_{(100)}(\text{GdIG}, 296) - \lambda_{(100)}(\text{YIG}, 296)}{\lambda_{(100)}(\text{GdIG}, 4.2) - \lambda_{(100)}(\text{YIG}, 4.2)} = 0.19 \quad \frac{M(\text{GdIG}, 296) - M(\text{YIG}, 296)}{M(\text{GdIG}, 4.2) - M(\text{YIG}, 4.2)} = 0.18.$$

Also, as shown in table 29.14, the doping of 1.8%Mn in YIG changed the $\lambda_{(100)}$ from -1.4×10^{-6} erg/cm³ for YIG to $+9.0 \times 10^{-6}$ erg/cm³ at 300 K. The λ values are therefore very sensitive to the impurity ions. Present quantum mechanical theory (Callen and Callen, 1963, 1965) fits experimental results in the garnet systems very well. The magnetostriction allows a better understanding of the strain dependence of the crystal field surrounding a single ion. Moreover, garnets have useful technical acoustic properties. Magnetoacoustic, or magnetoelastic, interactions in the magnetic garnets require a knowledge of their magnetostrictions. Therefore, it is an important property which needs to be investigated more thoroughly.

3.6. Optical properties

Synthetic garnets have excellent optical properties. Aluminum garnets are excellent crystal hosts and they are useful as solid state laser materials. Iron garnets have interesting infrared properties. The magnetic optical effects in iron garnets are not only useful in devices, but also provide fundamental information about the materials themselves. Finally, silicon-doped iron garnets have pho-

TABLE 29.13.
Magnetoelastic constants of garnets.

Garnet		B_1	B_2		Reference
YIG	0 K	+6	+29	(cm ⁻¹ /molecule)	(Andres and Luthi, 1963)
	4.2 K	7.2	41	(erg/cm ³ × 10 ⁻⁶)	(Nielsen et al., 1965)
	20.4 K	5.2	23	(erg/cm ³ × 10 ⁻⁶)	(Nielsen et al., 1965)
	78 K	2.3	8.2	(erg/cm ³ × 10 ⁻⁶)	(Nielsen et al., 1965)
	293 K	3.5	6.9	(erg/cm ³ × 10 ⁻⁶)	(Bartel, 1969)
	300 K	+11	+20	(cm ⁻¹ /molecule)	(Andres and Luthi, 1963)
EuIG	4 K	-650	-110	(cm ⁻¹ /molecule)	(Nielsen et al., 1965)
	4.2 K	272	45	(erg/cm ³ × 10 ⁻⁶)	(Nielsen et al., 1965)
	77 K	-500	-53	(cm ⁻¹ /molecule)	(Iida, 1963)
	78 K	227	22	(erg/cm ³ × 10 ⁻⁶)	(Nielsen et al., 1965)
	300 K	-120	-10	(cm ⁻¹ /molecule)	(Iida, 1963)
GdIG	4.2 K	-39	+22	(cm ⁻¹ /molecule)	(Phillips and White, 1966)
	77 K	-23	+29	(cm ⁻¹ /molecule)	(Jones, 1966)
	300 K	~0	+17	(cm ⁻¹ /molecule)	(Jones, 1966)
TbIG	77 K	-3200	-360	(cm ⁻¹ /molecule)	(Iida, 1963)
	300 K	-69	+18	(cm ⁻¹ /molecule)	(Iida, 1963)
Yb _{0.1} Y _{0.9} IG	4 K	-41	+34	(cm ⁻¹ /molecule)	(Jones, 1966)
	77 K	-6	+24	(cm ⁻¹ /molecule)	(Jones, 1966)
DyIG		$B^{12}(\text{cm}^{-1})$	$B^{12}(\text{cm}^{-1})$		(Clark et al., 1966)
	0 K	2900	1090		
HoIG	0 K	1930	430		
ErIG	0 K	-870	590		

toinduced effects which increase the potentiality of these materials in solid-state devices.

3.6.1. Crystal field effect

The garnet structure, as discussed extensively in section 29.3.1, can accommodate a great variety of cations. It is, therefore, an excellent crystal host which can be employed to study the crystal field effects on various cations. The crystal field analysis provides much detailed information about the electronic structure of the cation, and it enables the determination of crystal field parameters for the garnet crystals. The parameters are usually fitted to experimental optical or magnetic data or both. There are still large overall errors in these parameters but they enable us to understand the magnetic anisotropy and optical spectroscopy of the garnet crystals. In recent years, there have been many crystal field studies in rare earth garnets, and they were reviewed and compared in a paper by Wolf (1964), where the principal results are summarized. There are a number of general conclusions, stated by Wolf, which are listed here.

(1) Crystal fields are generally large (~500 cm⁻¹): about an order of magnitude larger than the iron-rare earth exchange.

(2) The local symmetry is far from cubic.

(3) The effect of neighbors other than the eight nearest O^{2-} ions on the crystal field is appreciable.

(4) The second degree terms are extremely sensitive to small changes or uncertainties in structure. This rules out the possibility of extrapolating these parameters from one compound to another (e.g., from a gallium garnet to an iron garnet).

(5) The sixth degree terms in the crystal field are not negligible.

The magnetic anisotropy in the rare earth garnets can be understood by the g -factor values. The agreement between experiments and theoretical calculations is very good, as shown in table 29.15. As discussed, there are six nonequivalent c -sites in the garnet structure. The g -factor axes, as oriented relative to the cubic crystal axes, follow the convention that the g_z direction is along the c axis, as listed in table 29.11. The g_x direction can be either the a axis or the b axis, and the selection is arbitrary. The g -factor values, as shown in table 29.15, are very anisotropic, and the g_x and g_z values are negative in sign.

3.6.2. Magneto-optical effects

Magneto-optical effects are useful in unraveling the electronic structure of atomic, molecular, and solid state systems. There are many types of magneto-optical effects, which have been discussed in several reviews (Pershan, 1967; Freiser, 1968; Dillon, 1968; Suits, 1972). Iron garnets were found to exhibit much Faraday rotation (Dillon, 1958). The present discussion is confined to the Faraday rotation effect. In the near infrared, there are at least two contributions to the Faraday effect in the iron garnets (Krinshick and Chetkin, 1962). The first part is nondispersive and due to ferrimagnetic resonance. It is given for $ReIG$ by

TABLE 29.15.
The g -factors of garnets.

		$ g_x $	$ g_y $	$ g_z $	g_x	g_y	g_z
Y(Dy)AG	(calc.)	0.9	0.5	17.5 ^a			
	(expt.)	0.7	0.4	17.7 ^b			
	(calc.)	11.3	1.9	7.4 ^a			
Y(Dy)GAG	(expt.)	10.8	1.2	7.0 ^c			
	(calc.)	5.1	3.9	10.8 ^d	-5.1	+3.9	-10.8 ^d
	(expt.)	4.0	10.6	4.0 ^c	-4.0	+10.6	-4.0 ^c
ErGAG	(calc.)	4.3 ± 0.3	4.3 ± 0.3	11.3 ± 0.3 ^d	-8.2	±3.4	-7.2 ^d
	(expt.)	8.29	3.47	7.27 ^d			

^aGrünberg et al. (1969); ^bBall et al. (1963); ^cWolf et al. (1962); ^dOrlich and Hübner (1969); ^eCrosswhite and Moos (1967).

the formula

$$\alpha_{\text{F (nondispersive)}} = \left[\frac{2\pi\langle n \rangle}{c} \right] [\gamma_{\text{Fe}}(M_{\text{Fe(d)}} - M_{\text{Fe(a)}}) - \gamma_{\text{Re}}M_{\text{Re}}] \quad (29.23)$$

where $M_{\text{Fe(d)}}$, $M_{\text{Fe(a)}}$ and M_{Re} are the algebraic sublattice magnetizations; (d) and (a) in the subscripts of M_{Fe} denote the d-site and the a-site, respectively; γ_{Fe} and γ_{Re} are gyromagnetic ratios; $\langle n \rangle$ is the average refractive index; and c is the free-space velocity of light. The second part is a dispersive contribution associated with the allowed electric dipole transitions of Fe^{3+} , which give rise to strong absorption in the visible region. It is given by the expression for the ReIG

$$\alpha_{\text{F (dispersive)}} = -A(\omega)M_{\text{Fe(a)}} + B(\omega)M_{\text{Fe(d)}} - C(\omega)M_{\text{Re}} \quad (29.24)$$

where the A , B , and C are the frequency-dependent coefficients for the electric-dipole rotation. The coefficients for YIG, GdIG, and TbIG are listed in table 29.16 (Cooper et al., 1968; Crossley et al., 1969). All the electric-dipole (dispersive) parameters are negative, implying positive rotations from an ion whose moment is antiparallel to the light direction. The octahedral Fe^{3+} gives a much larger contribution than the tetrahedral Fe^{3+} in YIG and GdIG leading to the resultant positive rotations.

Faraday rotation does not depend on frequency for $\lambda > 6 \mu\text{m}$. In TbIG, α changes sign at the compensation point. At $T = 110 \text{ K}$, α undergoes a second change in sign and increases with further decrease in temperature (Chetkin and Shalygin, 1968). This second change in the sign of α was also observed in $\text{Y}_{0.5}\text{Dy}_{0.5}\text{IG}$ in the region of 50 K. At a wavelength greater than $4 \mu\text{m}$, the α of $\text{Bi}_{0.24}\text{Ca}_{2.76}\text{Fe}_{3.62}\text{V}_{1.38}\text{O}_{12}$ (Chetkin and Shalygin, 1968) is positive and independent of λ . The α is $16^\circ/\text{cm}$. In the visible region, the α value is negative.

There are various mechanisms operating in different parts of the spectrum (Dillon, 1968). The magneto-optical effects can arise from:

(1) Spin-orbit splitting of Fe^{3+} ion allowed transitions in the visible or above. These may be charge transfer transitions or allowed single-ion transitions.

TABLE 29.16.
Coefficients for nondispersive and dispersive contributions^a to the Faraday rotations of YIG, GdIG, and TbIG at $1.15 \mu\text{m}$.

Nondispersive	Fe^{3+}	Gd^{3+}	Tb^{3+}
$(2\pi\langle n \rangle/c)\gamma$	9.15	9.15	6.86
Dispersive	A	B	C
YIG	-40.3 ± 1.7	-21.4 ± 1.2	-
GdIG	-42.4 ± 1.8	-27.1 ± 1.3	-1.0 ± 0.2
TbIG	-9.0 ± 15.0	-10.0 ± 11.0	-84.4 ± 2.5

^aFrom Cooper et al. (1968) and Crossley et al. (1969).

- (2) Exchange splitting of rare earth sharp-line transitions.
- (3) Exchange or spin-orbit splittings of rare earth allowed transitions.
- (4) Ferromagnetic resonance and exchange resonances correspond to the response of whole sublattices to external magnetic fields.

Faraday rotations were studied in $\{\text{Bi}_{3-2x}\text{Ca}_{2x}\}[\text{Fe}_2](\text{Fe}_{3-x}\text{V}_x)\text{O}_{12}$ where the V substitutes for tetrahedral Fe leading to a magnetically compensated ferrimagnetic composition at $x = 1.0$ (Buhrer, 1969). Ultraviolet measurements of the complex polar-Kerr effect (rotation and ellipticity) were reported between 1.7 and 5.64 eV for YIG, EuIG, ErIG, and Ga-substituted EuIG (Kahn et al., 1969a,b). Charge transfer transitions at about 4 and 5 eV, associated with Fe(a) and Fe(d), respectively, are found to be responsible for the principal ultraviolet magneto-optical spectra.

3.6.3. Photomagnetic effect

The photomagnetic effect induces a change in magnetic properties through the influence of photons, whereas the magneto-optic effects, such as Faraday rotation, etc., cause the light propagation to be influenced by the magnetization distribution. The photomagnetic effect was first observed in Si-substituted YIG (Teale and Temple, 1967). Changes in crystalline anisotropy were found in YIG:Si, and they depend on the angle between the light polarization and the crystal axes (R.F. Pearson et al., 1968). At 77 K, a single crystal picture frame YIG:Si_{0.05} had its initial permeability of 6 changed to 4 after the light irradiation, and a polycrystalline toroid YIG:Si_{0.005} had its initial permeability of 120 changed to 20 after exposure to the light at an intensity of about 10^{-2} W/cm² (Enz et al., 1969). The light also influences the switching behavior of Si-doped YIG. After irradiation with light, YIG:Si has an extremely square hysteresis loop. When a step field is applied there is a certain period of time during which no flux is switched irreversibly. The level of this delay depends on the amplitude of the applied step field. After this delay, the YIG:Si switches in the normal way. At 4.2 and 77 K these changes are permanent; at 200 K the effects disappear after the termination of light (Holtwijk et al., 1970).

A saturating field was applied along [100] of a (001) polished plate of YIG:Si_{0.03}. Since [100] is a symmetry direction of the cubic crystal, the anisotropy contributes no torque. After 50 sec of illumination with intense white light, linearly polarized with E along [100], the axis of polarization is rotated to [110]. A torque appears and increases rapidly to a value of 1.2×10^4 dyn·cm/cm³. After 150 sec, the polarization axis rotates to [110]. Over the next 100 sec the torque decreases to a large negative value. This type of photoinduced anisotropy implies that there is an anisotropy in the absorption of light by a single set of crystallographic sites. This is a photoinduced dichroism (Dillon et al., 1970). For a crystal plate thickness of 0.011 cm, the dichroism was found to be at 1.5 K

$$\frac{2\Delta I_{(111)}}{I} = 0.035 \quad \text{and} \quad \frac{2\Delta I_{(100)}}{I} = 0.007$$

where I is the light transmitted.

The above photoinduced effects at relatively high levels of Si are reversible. The photoinduced effect at low Si content, i.e., 0.01 to 0.017 Si per YIG formula, is irreversible and does not depend on the polarization of light. A (110) plate of YIG:Si_{0.017} at 4.2 K shows a change in its cubic magneto-crystalline anisotropy after irradiation of light. The contribution of the Fe²⁺ ions to the crystal anisotropy is large, is of opposite sign to K_{YIG} , and increases rapidly with decreasing temperatures. Light irradiation decreases the absolute value of $K_{\text{Fe}^{2+}}$ at 77 K and increases the value at 4.2 K. The percent at 77 K decreases with Si content. Samples doped with Ca instead of Si, and so containing Fe⁴⁺, showed no changes under the same condition. It appears that there are near and far sites for Fe²⁺ in YIG:Si and their relative proportion is influenced by irradiation. At each temperature, the experiment detects only those sites whose relaxation is of the order of ω^{-1} . Consequently, the Fe²⁺ detected at 77 K must be in a substantially different local environment than that observed at 4.2 K (Flanders et al., 1971). Each site has its own easy axis (one of the four $\langle 111 \rangle$ cubic directions) and when the population balance among sites is upset, a uniaxial anisotropy appears. Polarized light can create an imbalance because its coupling to the pancake-like Fe²⁺ wave function is different for differently oriented sites. Using a crystal field theory, it was found that a 5–10% population imbalance between different oriented sites is expected for light polarized along the $\langle 110 \rangle$ direction (Allen et al., 1971). Irreversible photoinduced changes in optical absorption of YIG:Si⁴⁺ and YIG:Ca²⁺ were found in the near infrared region (Gyorgy et al., 1971).

3.6.4. Infrared spectra

Ferrimagnetic garnets, namely the iron garnets, are transparent within the infrared region. The infrared spectra of RIG for various rare earth cations are listed in table 29.17 (McDevitt, 1969). Similarly, the infrared spectra of RAG and RGaG are listed in tables 29.18 and 29.19, respectively. The total irreducible representations of the transverse optical modes are

$$\Gamma = 3A_{1g} + 5A_{2g} + 8E_g + 14F_{1g} + 14F_{2g} + 5A_{1u} + 5A_{2u} + 10E_u + 18F_{1u} + 16F_{2u} \quad (29.25)$$

The factor-group analysis predicts a total of 98 lattice-vibration modes; however, the character table for the point group O_h shows that the translation operations are of symmetry species F_{1u} only. One acoustic mode will also be found in this species and will be infrared-inactive. Therefore, this analysis predicts seventeen infrared-active lattice modes. In table 29.17, ten frequencies were listed for the RIG series. Twelve frequencies were listed for the RGaG series (table 29.19), and fifteen frequencies were listed for the RAG series (table 29.18). They suggest that the powder-transmission method does not yield all of the infrared-active modes.

All of the rare earth garnets have a set of three bands in the 800–600 cm^{-1} region. These bands are isolated by a high-transmission maximum from other

TABLE 29.17.
Infrared lattice frequencies of $R_3Fe_5O_{12}$ garnets^a.

R =	Sm	Eu	Gd	Dy	Ho	Y	Er	Tm	Yb	Lu
	630 cm ⁻¹	635 cm ⁻¹	638 cm ⁻¹	647 cm ⁻¹	655 cm ⁻¹	655 cm ⁻¹	656 cm ⁻¹	658 cm ⁻¹	658 cm ⁻¹	655 cm ⁻¹
	580*	588*	590*	597*	600*	605*	606*	607*	612*	616*
	550	553	555	562	565	566	567	568	568	570
	426	427	435	-	-	-	-	-	-	-
	373	373	379	380	-	381	-	-	-	-
	352	358	361	365	386	369	370	371	374	383
	326	326	326	330	330	338	328	329	331	333
	311	309	307	309	308	318	305	303	305	306
	252	252	254	255	255	269	254	251	253	254
	214	214	213	215	213	227	212	208	211	211
	-	-	-	-	-	144	-	-	-	-
	115	115	112	111	107	110	110	108	108	106
	110	109	107	108	(108)	-	(107)	(106)	(106)	-

^aAfter McDevitt (1969).

spectral features. One other general characteristic shows a strong absorption band in the region 470–370 cm⁻¹.

The yttrium garnets have a number of distinctive features that set them apart from the rest of the rare earth garnets in each series. The frequencies for YAG at 378, 332, 292, 220 cm⁻¹ are higher than the other frequencies in the RAG series (table 29.18). In the low frequency region the 93 cm⁻¹ band is missing from the

TABLE 29.18.
Infrared lattice frequencies of $R_3Al_5O_{12}$ garnets^a.

R =	Dy	Ho	Y	Er	Tm	Yb
	785 cm ⁻¹	788 cm ⁻¹	789 cm ⁻¹	795 cm ⁻¹	800 cm ⁻¹	805 cm ⁻¹
	723*	727*	726*	733*	737*	742*
	690	695	698	698	700	709
	560	563	569	566	570	569
	510	511	512	515	518	516
	455	468	465	460	463	468
	432	438	436	436	440	439
	388	395	398	397	397	397
	-	389	390	388	-	-
	370	371	378	370	371	372
	323	324	332	323	323	322
	280	282	292	279	279	278
	208	206	220	206	201	202
	-	-	178	-	-	-
	168	169	166	168	167	165
	128	126	122	127	126	125
	94	93	-	93	92	92

^aAfter McDevitt (1969).

TABLE 29.19.
Infrared lattice frequencies of $R_3Ga_5O_{12}$ garnets^a.

R =	Sm	Eu	Gd	Dy	Ho	Y	Er	Tm	Yb	Lu
	665 cm ⁻¹	609 cm ⁻¹	673 cm ⁻¹	681 cm ⁻¹	684 cm ⁻¹	688 cm ⁻¹	691 cm ⁻¹	697 cm ⁻¹	700 cm ⁻¹	704 cm ⁻¹
	604	608*	612*	620*	623*	627*	630*	636*	639*	640*
	573	575	578	587	589	590	592	596	595	600
	461	464	469	476	474	476	480	485	483	490
	384	384	388	388	390	393	385	392	387	392
	324	324	322	322	323	340	322	323	320	322
	246	246	246	249	251	257	249	251	251	251
	222	222	222	220	221	234	222	220	219	221
	145	145	145	145	144	147	144	144	143	141
	119	119	118	117	116	114	116	115	113	113
	113	111	111	111	111	—	110	108	108	107
	(88)	(88)	(88)	(88)	(86)	—	(86)	(84)	(84)	(84)

^aAfter McDevitt (1969).

YAG spectrum. Similarly, the frequencies for YGaG at 393, 340, 257, 234 cm⁻¹ are higher than others in the series (table 29.19). In the low frequency region, the 110 and 86 cm⁻¹ bands are missing. In the case of YIG, the 338, 318, 259, 227 cm⁻¹ are higher than others, the 144 cm⁻¹ band is nonexistent in others, and the 107 cm⁻¹ band is missing in the YIG spectrum (table 29.17). From the optical spectra, the energy levels of the ground state multiplets of trivalent rare earth ions in garnets can be determined and are listed in table 29.20 (Oliver et al., 1969a).

3.6.5. Optical absorption

The optical absorption coefficient α can be determined by the equation

$$I = I_0(1 - R)^2 \exp(-\alpha t) \quad (29.26)$$

where I is the transmitted light intensity, I_0 the incident light intensity, R the single-surface reflection loss at normal incidence, and t is the thickness in centimeters. The α values are useful technical quantities and are also excellent monitors of the purity of samples. For example, in an undoped YIG, the α values are about 0.03 cm⁻¹ in the infrared region between 2250 and 8350 cm⁻¹. With a 0.13 at.% Si addition, the α value changes to 6 cm⁻¹ in the region between 5800 and 9100 cm⁻¹ (LeCraw et al., 1965).

The optical absorption of YAG was studied in the region from 10 to 55 000 cm⁻¹ (Slack et al., 1969). No lattice absorption peaks were observed in YAG for wave number less than 80 cm⁻¹ (Milward, 1967). The wave number $\bar{\nu}$ region between 0 and 860 cm⁻¹ is labeled as the one-phonon region where the absorption of one photon generates one phonon. The α values in this region are all fairly high and then decrease rapidly for $\bar{\nu} > 860$ cm⁻¹ (Slack et al., 1969).

The absorption peaks at $\bar{\nu} = 700, 729, 792$ cm⁻¹ are components of the $\bar{\nu}_3$ vibration of the AlO₄ molecular group. These $\bar{\nu}_3$ peaks shift to about 600 cm⁻¹ in

TABLE 29.20.
Energy levels of the ground state multiplet of trivalent rare earth ions in garnets^a.

Ion	Host crystal	Multiplet	No. of levels	Wave number (cm ⁻¹)	Ref.
Gd ³⁺	GdAG	⁸ S ₀	1	0	(b)
Gd ³⁺	GdGaG	⁸ S ₀	1	0	(b)
Tb ³⁺	TbAG	⁷ F ₆	13	0; 4	(c)
Tb ³⁺	YAG	⁷ F ₆	13	0; 5; 61; 70; 116; 207; 270; 432; 443	(d)
Tb ³⁺	TbGaG	⁷ F ₆	13	unknown	—
Tb ³⁺	YGaG	⁷ F ₆	13	unknown	—
Tb ³⁺	YIG	⁷ F ₆	13	0; 6; 38; 40; 55; 55	(e)
Dy ³⁺	DAG	⁶ H _{15/2}	8	0; 70; 116; 197; 256	(f)
Dy ³⁺	YAG	⁶ H _{15/2}	8	0; 59; 101; 175; 233; (474); (517); 860	(g, h)
Dy ³⁺	DyGaG	⁶ H _{15/2}	8	0; 20; 71	(g, h)
Dy ³⁺	YGaG	⁶ H _{15/2}	8	0; 20; 71; 118; 149; (466); 527; 579	(g)
Ho ³⁺	HoAG	⁵ I ₈	17	0; 36; 42; 54; 63	(i)
Ho ³⁺	YAG	⁵ I ₈	17	unknown	—
Ho ³⁺	HoGaG	⁵ I ₈	17	0; 5; 27; 30; 39; 44	(j, k)
Ho ³⁺	YGaG	⁵ I ₈	17	unknown	—
Er ³⁺	ErAG	⁴ I _{15/2}	8	0; 27; 58; 79; 423; 436; 530; 574	(l)
Er ³⁺	ErGaG	⁴ I _{15/2}	8	0; 46; 56; 76	(m)
Er ³⁺	YGaG	⁴ I _{15/2}	8	0; 44; 49; 76; 422; 430; 490; 527	(n)
Tm ³⁺	TmAG	³ H ₆	13	0; 35	(i, o)
Tm ³⁺	YAG	³ H ₆	13	0; 28; 43; 270; 490	(p, q)
Tm ³⁺	TmGaG	³ H ₆	13	0; 63; 85; 113; 123; 184	(o, q)
Tm ³⁺	YGaG	³ H ₆	13	0; 64; 87; 99; 188	(q, r)
Yb ³⁺	YbAG	² F _{7/2}	4	0; 618; 701; 766	(s)
Yb ³⁺	YbGaG	² F _{7/2}	4	0; 546; 599; 624	(s)

^aOliver et al. (1969a); ^bDieke and Crosswhite (1963); ^cCooke et al. (1967); ^dKoningstein (1964); ^eKnight and Huber (1968); ^fKoningstein and Ng (1969); ^gGrunberg et al. (1967); ^hVeyssie and Dreyfus (1967); ⁱMilward (1967); ^jSievers and Tinkham (1963); ^kOnn et al. (1967a); ^lHellwege et al. (1966); ^mDreyfus et al. (1965); ⁿCrosswhite and Moos (1967); ^oBierig and Rimai (1965); ^pKoningstein (1966); ^qJ.J. Pearson et al. (1968); ^rBuchanan et al. (1969); ^sBuchanan et al. (1967).

YGaG and YIG, caused by GaO₄ and FeO₄ groups and the larger sizes and masses of Ga and Fe.

The very lowest wave number mode is at $\bar{\nu} = 123 \text{ cm}^{-1}$ in YAG. In DyAG, HoAG, and ErAG where the rare earth ion substitutes for Y, this mode shifts to 95 cm^{-1} . It further shifts to 85 cm^{-1} for ErGaG and YbGaG. This lowest mode in YAG is probably an external mode of the whole lattice, involving the Y and Al ions.

The region between 860 and 2400 cm^{-1} is believed to be caused by multi-phonon processes in which one photon generates two or more phonons. The α values for the two-phonon processes are about 10^{-2} times as large as the one-phonon processes, and the three-phonon processes give α values about 10^{-4} times as large.

The two phonon processes produce an absorption peak in YAG at 1450 cm^{-1} which is just about $2\bar{\nu}_3$. The three-phonon processes produce the peak at 2120 cm^{-1} , which is nearly equal to $3\bar{\nu}_3$ of the AlO_4 vibration, and it is an intrinsic feature of YAG and is not caused by trace impurities. The $2\bar{\nu}_3$ and $3\bar{\nu}_3$ peaks of FeO_4 groups in YIG occur at 1200 and ~ 1700 cm^{-1} (Cockayne, 1966; Wood and Remeika, 1967).

The range between 30 000 and 52 000 cm^{-1} appears to depend on the purity or the growing conditions of the crystal or both. The α values vary from sample to sample. They do not depend on the stoichiometry of the melt.

The far-infrared lattice absorption bands in garnets at ~ 4 K are listed in table 29.21 (Oliver et al., 1969b). Three types of excitations occur in ReIG. The first is the splitting of the ground Kramers doublet by the exchange field; the second is a transition to a higher crystal field level as split by the exchange field; and the third is a collective mode in which the entire Fe and rare earth sublattices undergo a mutual precession (Tinkham, 1962). The far-infrared magnetic resonance results for YbIG, as extrapolated to 0 K, show a ferrimagnetic resonance at 3.00 ± 0.05 cm^{-1} with a linewidth of < 0.2 cm^{-1} ; an exchange resonance at 13.65 ± 0.05 cm^{-1} with a linewidth of < 0.38 cm^{-1} ; two single Yb ion resonances at 23.2 ± 0.1 cm^{-1} with a linewidth of 0.5 cm^{-1} and at 27.0 ± 0.1 cm^{-1} with a linewidth of 0.5 cm^{-1} ; and a Yb-Yb combination resonance at 26.3 ± 0.1 cm^{-1} with a linewidth of 0.5 cm^{-1} (Richards, 1963).

The optical absorption bands of Cr^{3+} , Fe^{3+} , OH^- , impurities in garnets are

TABLE 29.21.
Far-infrared lattice absorption bands^a in garnets at ~ 4 K.

Garnet	$\bar{\nu}_1(\text{cm}^{-1})$	$\bar{\nu}_2(\text{cm}^{-1})$	Ref.
$\text{Y}_3\text{Al}_5\text{O}_{12}$ (YAG)	12.30	148	(b)
$\text{Dy}_3\text{Al}_5\text{O}_{12}$ (DAG)	94.2 ± 0.4	—	(c)
$\text{Ho}_3\text{Al}_5\text{O}_{12}$ (HoAG)	94.5 ± 0.4	—	(c)
$\text{Er}_3\text{Al}_5\text{O}_{12}$ (ErAG)	96.0 ± 2.0	109 ± 3.0	(d)
$\text{Tm}_3\text{Al}_5\text{O}_{12}$ (TmAG)	87.0	—	(c)
$\text{Yb}_3\text{Al}_5\text{O}_{12}$ (YbAG)	90.0 ± 0.8	—	(e)
$\text{Lu}_3\text{Al}_5\text{O}_{12}$ (LuAG)	88.0 ± 1.0	106.5 ± 0.5	(e)
$\text{Ho}_3\text{Ga}_6\text{O}_{12}$ (HoGaG)	86.0 ± 1.0	111 ± 2.0	(d)
$\text{Er}_3\text{Ga}_6\text{O}_{12}$ (ErGaG)	86.0 ± 1.0	114 ± 3.0	(d)
$\text{Yb}_3\text{Ga}_6\text{O}_{12}$ (YbGaG)	85.0 ± 1.0	111 ± 3.0	(d)
$\text{Sm}_3\text{Fe}_5\text{O}_{12}$ (SmIG)	83.0 ± 2.0	—	(d)
$\text{Ho}_3\text{Fe}_5\text{O}_{12}$ (HoIG)	81.6 ± 0.9	98 ± 2.0	(d)

^aFrom Oliver et al. (1969b); ^bSlack et al. (1969); ^cMilward (1967); ^dSievers and Tinkham (1963); ^eOliver et al. (1969b).

TABLE 29.22.
Optical absorption bands of Cr, Fe, OH impurities in garnets^a.

Impurity	Garnet	Wave number of absorption band maximum (cm ⁻¹)	Ref.
Cr ³⁺	YAG	17 000; 23 000	(b)
Cr ³⁺	YGaG	17 000; 22 500	(b)
Fe ³⁺ (a-site)	YIG	10 200; 11 100; 14 280	(c)
Fe ³⁺ (d-site)	YIG	16 400	(c)
Fe ³⁺ (a-site)	YGaG	23 000; 23 870; 24 270	(c)
Fe ³⁺ (d-site)	YGaG	20 410; 21 050; 26 300; 26 670	(c)
OH ⁻	YIG	3571	(d)

^aFrom Oliver et al. (1969a); ^bWood et al. (1963); ^cWood and Remeika (1967); ^dKolb et al. (1967).

listed in table 29.22 (Oliver et al., 1969a). Impurities are dependent on crystal growing conditions. Hydrothermal YIG contain an appreciable concentration of the OH group which absorbs radiation in a line spectrum extending from 2500 to 3700 cm⁻¹ in the infrared. YIG crystals grown from D₂O solution have the OD isotope stretching frequency from 2200 to 2700 cm⁻¹ with one-to-one correspondence with the OH lines at $\bar{\nu}_{OH} = 1.3 \bar{\nu}_{OD}$. The very broad line at 2930 cm⁻¹ is associated with a site containing the Na⁺ ion.

A Ga-doped YIG crystal contains two lines at 3442 and 3419 cm⁻¹. In undoped YIG, two lines at 3578 and 3568 cm⁻¹ disappear with Ga substitution. They may be due to OH groups in the vicinity of a vacancy in the tetrahedral site.

The OH absorption spectrum is different for different seed orientations, with some individual lines present in crystals of (100) seeds, and missing from crystals of (111) or (211) seeds. The absolute intensity of the strongest OH lines is the least for growth on (111) while the growth on (100), (110), and (211) shows increasing amounts in that order (Wood et al., 1968).

The refractive index of single crystal YIG over the wavelength range 1–6 μm was measured by the minimum deviation method (Johnson and Walton, 1965). The mean refractive indices of YIG as a function of wavelength are listed in table 29.23. The dispersion curve agrees with the mean index results for YIG to within 0.2% by a set of constants $f_1 = 3.739$, $\lambda_1 = 0.28 \mu\text{m}$, $f_2 = 0.79$, $\lambda_2 = 10.0 \mu\text{m}$ as applied to a dispersion curve equation of the form

$$n^2 = 1 + \sum_{i=1,2} \frac{f_i \lambda^2}{\lambda^2 - \lambda_i^2} \quad (29.27)$$

3.7. Thermal properties

3.7.1. Thermal conductivity

The thermal conductivities of garnet crystals, as a group, have been extensively investigated. Studies were made on YIG (Luthi, 1962; Friedberg and

TABLE 29.23.
Mean infrared refractive index of YIG^a.

$\lambda(\mu\text{m})$	n	$\lambda(\mu\text{m})$	n	$\lambda(\mu\text{m})$	n
1.4	2.209	2.5	2.177	4.5	2.134
1.6	2.200	3.0	2.168	5.0	2.118
1.8	2.194	3.5	2.158	5.5	2.103
2.0	2.188	4.0	2.148		

^aJohnson and Walton (1965).

Harris, 1963; Douglass, 1963; Oliver and Slack, 1966; Rives et al., 1966), on YAG (Oliver and Slack, 1966; Klein and Croft, 1967), on YGaG (Holland, 1968), and on DAG (Landau and Dixon, 1970). Theoretical studies were also made on YIG (Bhandari and Verma, 1966; Joshi and Sinha, 1966). These garnet crystals have a thermal conductivity κ of about 0.07 to 0.10 W/cm K at 300 K and reach a κ maximum of 1 to 5 W/cm K near 20 K. The similarity in κ among the garnets, both synthetic and natural, provides a study case of the effect of crystal structure on κ . In the rare earth doped garnet crystals, the κ data can reveal the phonon scattering by the rare earth ions. A detailed discussion of the thermal conductivity of garnets has been presented in an extensive article (Slack and Oliver, 1971), which readers are advised to consult for κ data of garnet crystals.

Briefly, the κ results of garnets can be summarized as follows. All garnets are nonmetallic. They have no free electrons to carry heat, and thus heat transport is predominantly via the phonons. From the Debye temperature, θ_D , obtained in other studies, the κ vs. T experimental curve can be extrapolated to give an experimental value of κ_0 at $T = \theta_D$. This value can be calculated by the equation

$$\kappa_0 = 1.43 \times 10^{-8} \langle M \rangle \langle V_0 \rangle^{1/3} \theta_D^2 \text{ W/cm K} \quad (29.28)$$

where $\langle M \rangle$ is the average atomic mass of an atom in the garnet crystal in grams, and $\langle V_0 \rangle$ is the average volume in cubic angstroms, occupied by one atom of the solid. The ratio κ_0/κ'_0 is called the crystal complexity factor G (Oliver and Slack, 1966). The values of κ_0 , κ'_0 , and G , for several garnets are listed in table 29.24 (Slack and Oliver, 1971). The crystal complexity factor G varies from 0.080 to 0.114 for these garnets, with an average value of 0.09 ± 0.01 . The factor G for the natural garnet, i.e., grossularite [essentially $(\text{Mg}, \text{Fe}, \text{Mn})_3\text{Al}_2\text{Si}_3\text{O}_{12}$] agrees with other synthetic garnets. The ferrimagnetic YIG agrees with other nonmagnetic garnets in their G factors. Therefore, the crystal complexity factor G can be considered as a characteristic feature of the garnet structure, with an average value of 0.09 ± 0.01 .

The theory of the effect of crystal structure on κ is still in a very rudimentary state. It is generally observed that the larger the number of optical branches in the phonon spectrum, the lower the thermal conductivity. In garnets, there are 80 atoms in the primitive unit cells, and there are 97 optical modes at the zone center (Hurrell et al., 1968). The combination of infrared and Raman studies has

TABLE 29.24.
Thermal conductivity values at θ_D for garnet crystals^a.

Crystal	Debye temperature θ (K)	Thermal conductivity (W/cm K)		
		κ_0	κ'_0	G
Grossularite	770	0.043	0.418	0.103
YAG	750	0.042	0.527	0.080
GdAlG	640	0.045	0.521	0.086
LuAlG	620	0.043	0.515	0.083
YGaG	585	0.046	0.447	0.103
GdGaG	520	0.051	0.446	0.114
YbGaG	520	0.039	0.464	0.084
YIG	565	0.038	0.384	0.099

^aFrom Slack and Oliver (1971).

at most found 42 of the 97 optical unknowns. A phonon of energy $k_B T$ at $T = 300$ K has an energy in wave number of 209 cm^{-1} , it is an optical phonon in YAG, and it has a very small or nearly zero propagation velocity. It contributes very little to the thermal conduction in the crystal.

The presence of the low-lying optical modes in YAG and their absences in Al_2O_3 caused the absence and presence of the Umklapp processes in κ data. The characteristic of Umklapp processes is the exponential rise in κ with decreasing temperature. Umklapp processes require that the wave vectors of the three interacting acoustic phonons combine to equal a wave vector of the reciprocal lattice. The wave vectors of the reciprocal lattice are very small in garnets because of the large size of its unit cell. The phonons of relatively low wave vector and low energy can undergo Umklapp processes in garnet. The critical phonon energy is that of the acoustic phonons at the zone boundary. The κ of YAG rises with decreasing temperature with a dependence of $\exp(\theta/bT)$, where b is about 2 and θ is 177 K. This dependence agrees with the observed data.

If the only mechanism which limits the mean free path of the phonon is the boundary scattering, then κ should be proportional to the sample size (Thacher, 1967). At 3 K, the experimental ratio of κ to the sample diameter d of YAG had a temperature dependence of $T^{2.5}$ (Slack and Oliver, 1971).

Phonon scattering produced by the low-lying electronic levels of the rare earth ions in garnets reduces the κ below that of the corresponding non-magnetic garnet. The data on DAG show no anomaly in and through it Neel point T_N of 2.54 K. If there is a magnon contribution to κ near T_N of DAG, it is less than 10% of the lattice κ , and may be zero (Slack and Oliver, 1971). This is in disagreement with the report of a minimum in κ at T_N (Landau and Dixon, 1970). The κ of some magnetic garnets, such as those of Tb, Dy, Ho, Er, and Tm, is suppressed by a one-phonon resonance scattering process for those phonons

whose energies are equal to the energy difference between two electronic levels. The effectiveness of this magnetic scattering is largest for Dy and decreases in the series, Dy, Tb, Tm, Er, and Ho. Its temperature dependence is closely related to the thermally determined population differences between the two levels involved in the transition (Slack and Oliver, 1971).

3.7.2. Specific heat

Specific heat in garnets has been analyzed theoretically (Harris and Meyer, 1962). It can be expressed by

$$C_v = C_L + C_M + C_N \quad (29.29)$$

where C_L , C_M , and C_N refer to the contribution to the total specific heat, C_v , from the lattice, from the interactions between unpaired electrons of the ions (magnetic), and from the electron-nuclear spin interactions (nuclear), respectively. The lattice specific heat, C_L , follows the well-known T^3 law at low temperatures where the ratio θ/T may be taken to be infinite for all practical purposes, and θ is the Debye temperature

$$C_L = RA_L T^3 \quad (29.30)$$

where R is the gas constant. An interpolation scheme to calculate the C_L of ReIG from the C_L of EuIG is found to be more successful in the case of the scaling factor being the $\frac{3}{2}$ power of the ratio of masses of rare earth ion to Eu ion than in the case of the scaling factor being the ratio of the molecular weights of the two garnets. The former case is given by

$$C_L(\text{RIG}) = (W_{\text{RE}}/W_{\text{Eu}})^{3/2} C_L(\text{EuIG}) \quad (29.31)$$

where W_{RE} and W_{Eu} are the masses of the rare earth ion and Eu ion, respectively (Henderson et al., 1969). A list of the lattice specific heat temperature coefficients, A_L , for several RIG and YIG is given in table 29.25.

TABLE 29.25.
Specific heat temperature coefficients for several
ReIG.

	Temperature coefficients ^a	
	Lattice A_L	Nuclear A_N
YIG	0.53×10^{-4}	
SmIG	0.75×10^{-4}	$2.6 \pm 0.4 \times 10^{-3}$
EuIG	0.75×10^{-4}	$9.07 \pm 0.1 \times 10^{-3}$
GdIG	0.75×10^{-4}	
TmIG	0.93×10^{-4}	$0.78 \pm 0.04 \times 10^{-3}$
YbIG	0.96×10^{-4}	$1.6 \pm 0.3 \times 10^{-3}$
LuIG	0.98×10^{-4}	0.82×10^{-3}

^aHenderson et al. (1969).

The nuclear specific heat, C_N , has a T^{-2} dependence given by

$$C_N = RA_N T^{-2} = RT^{-2} 6 \sum_i \frac{1}{3} I_i (I_i + 1) (\Delta_i / k_B)^2 \quad (29.32)$$

for $\Delta_i < k_B T$, where the summation is over the different isotopes and where

$$\Delta_i = g_{N,i} \beta_N H_{N,i} \quad (29.33)$$

is the separation between successive nuclear levels. I_i is the nuclear spin, $g_{N,i}$ is the nuclear splitting factor, β_N is the nuclear magnetron, and $H_{N,i}$ is the field at the nucleus. The C_N of Fe^{57} above 0.4 K is negligible because of the small splitting $\Delta(\text{Fe}^{57})/k_B \approx 3 \times 10^{-3}$ K, and because of the low abundance of this isotope, 2.5%. Therefore, only the C_N of the rare earth ions needs to be considered in RIG. A list of nuclear specific heat temperature coefficients, A_N , for several RIG is also given in table 29.25.

For the magnetic iron garnets, there is a magnetic contribution, C_M , to the specific heats. The magnetic specific heat of YIG, EuIG, and TmIG can be attributed entirely to the acoustical spin-wave modes, since their optical modes have too high an energy to be populated at low temperatures (Harris, 1963). For YbIG and SmIG, the C_M is dominated by the contributions from the low-lying optical modes with energy $E_j(k)$ corresponding to the 12 inequivalent c-sites in the unit cell.

For the acoustic spin-wave modes, the temperature dependence of C_M follows mainly the $T^{3/2}$ relationship coupled with a moderating function $G(T)$

$$C_M = (0.113/4)R(k_B T/D)^{3/2} G(T) \quad (29.34)$$

where D is the dispersion constant which is a linear combination of the exchange integrals in the garnet. The moderating function $G(T)$ can be either calculated or experimentally curve-fitted. One calculated expression of $G(T)$ is (Harris, 1963)

$$G(T) = \{1 + 1.47(k_B T/D)[(5E + F)/D]\} \\ \times [k_B T - 1.6g\beta M][k_B T - g\beta H_A][k_B T]^{-2} \quad (29.35)$$

where H_A is the anisotropy field. For YIG, the C_M data, calculated from eqs. (29.34) and (29.35), using the values $E = 5 \text{ cm}^{-1}$, $F = 0$, and $D = 30 \text{ cm}^{-1}$, and the C_L data, calculated from eq. (29.36) with $A_L = 0.557 \times 10^{-4}$ can be subtracted from the total specific heat, C_v . The remaining part can be empirically fitted by a linear expression (Onn et al., 1967b)

$$C_r = (C_v - C_L - C_M) = R \times 10^{-4} \times 1.11T \quad (29.36)$$

An alternate expression for $G(T)$ is (Henderson et al., 1969)

$$G(T) = \exp(-0.45x) \quad (29.37)$$

where

$$x = g\beta H_i / k_B T \quad (29.38)$$

for YIG, the residual part of C_v after the subtraction of C_L and C_M where C_M is calculated from eqs. (29.34), (29.37), and (29.38), is, within the error limit, a linear function of temperature. The linear temperature coefficient ϵ was found to be $(6.4 \pm 1.5) \times 10^{-5} R$ at $H = 0$ and $(9.0 \pm 2) \times 10^{-5} R$ for $H > 4$ kOe. At 1 K and at 4 K, this linear residual part accounts for $\sim 35\%$ and $\sim 6\%$, respectively, of the total specific heat (Henderson et al., 1969).

In EuIG, the nuclear specific heat, C_N , must be included. The linear residual part had a temperature coefficient of $(0.23 \pm 0.03) \times 10^{-3} R$, and it is $\sim 15\%$ of C_v above 2 K, but becomes negligible below 1.2 K (Henderson et al., 1969). The C_v data of TmIG behave approximately the same as for EuIG and YIG. Their analysis is hampered by the uncertainty on the value of D for TmIG. No evidence of a Tm^{3+} optical level becoming populated at temperatures below 4.5 K was found in the C_v data.

In SmIG, where the optical spin-wave modes dominate, the C_M data can be fitted by the expression

$$C_M = \frac{R}{6}(E/k_B T)^2 \exp(-E/k_B T) \quad (29.39)$$

with $E = 38 \pm 3$ K (Henderson et al., 1969). The same situation obtains for YbIG, but here agreement between data and calculation is not very good (Henderson et al., 1969).

Specific heat measurement is an effective method of obtaining the Debye temperature, θ_D , but it is affected by impurities in the samples. In the case of YIG where many samples were used by different workers, the θ_D , as obtained from the C_v data, varies from 572 to 538 K. A list of the Debye temperatures of several garnets is given in table 29.26, with some of the θ_D values obtained from elastic constant measurements (Oliver et al., 1969a).

Dysprosium aluminum garnet (DAG) is an interesting compound which resembles closely a two-lattice Ising antiferromagnet (Ball et al., 1964). The Dy^{3+} ions have an extremely anisotropic g factor with $g_z \approx 18$ and $g_x \approx g_y \approx 0$. DAG is a highly anisotropic antiferromagnet with moments $S' = \frac{1}{2}$ which point along the $\pm x$, $\pm y$, and $\pm z$ axes. In a magnetic field along a $\langle 111 \rangle$ axis, the x , y , and z sublattices become equivalent. Below 1.66 K, the specific heat of DAG undergoes a first-order transition in applied fields, and above 1.66 K, the transition has a continuous, but finite derivative, in the observed thermodynamic functions (Keen et al., 1966). Close to T_N (2.53 K), the phase boundary between the antiferromagnetic and the paramagnetic phases can be accurately fitted to the data by the expression:

$$H_{int}^c = A[1 - (T/T_N)]^n \quad (29.40)$$

with $n = 0.50 \pm 0.02$ as predicted by theory (Fisher, 1960), $A = 6.52$ kOe, and $T_N = 2.53 \pm 0.01$ K.

The specific heat results of DAG can best be fitted by the equation

$$C = A'(T - T_N)^{-\alpha} + B' \quad (29.41)$$

TABLE 29.26.
Debye temperatures of garnets^{a,b}.

Crystal	$\langle M \rangle$ (g)	θ_D (K)	Method	Ref.
YAG	29.68	750	C_{ij}	(c,d)
Fe ₃ Al ₂ Si ₃ O ₁₂ (Almandite)	23.80	745	C_{ij}	(e)
TbAG	40.22	670	C_{ij}	(f)
TmAG	41.76	620	C_{ij}	(f)
YGaG	40.37	585	C_{ij}	(c)
YIG	36.90	572	C_p	(g)
YIG	36.90	565	C_{ij}	(h)
EuIG	43.36	495	C_{ij}	(h)
LuIG	49.81	458	C_v	(g)
NdGaG	48.67	380	C_v	(i)
YdGaG	52.99	380	C_v	(i)

^aThe terms used: M = average mass of an atom of the crystal, θ_D = Debye temperature, C_{ij} denotes the determination of θ from room temperature elastic constants and C_p , C_v denote the determination of θ from specific heat measurement at low temperatures. ^bFrom Oliver et al. (1969a); ^cSpencer et al. (1963); ^dAlton and Barlow (1967); ^eSoga (1967); ^fOliver et al. (1969a); ^gHarris and Meyer (1962); ^hBateman (1966); ⁱOnn et al. (1967b).

with $\alpha = 0.31 \pm 0.02$ (Keen et al., 1967).

The lambda transition of DAG can also be indicated by the thermal expansion data. For $|1 - (T/T_N)| < 0.1$, the thermal expansion data are consistent with a logarithmic singularity when $T < T_N$ and with a power law behavior for $T > T_N$ (Phillip et al., 1969).

3.7.3. Thermal expansion

Lattice constants of YAG, YGaG, GdGaG, GdIG, and YIG were measured in the temperature range 296–1400 K (Geller et al., 1969). The data were fitted to the expression

$$(\Delta a)/a_0 = I + bT + \frac{1}{2}cT^2 + dT^{-1} \quad (29.42)$$

where a_0 was the lattice constant at 296 K. The polynomial parameters I , b , c , and d for these garnets are listed in table 29.27. Below the Curie temperature of both YIG and GdIG, there is a slight concavity of $(\Delta a/a_0)$ vs. T , while above T_c , $(\Delta a/a_0)$ vs. T is straight for both garnets. The parameters listed in table 29.27 are very sensitive to the observed α values. They are simply empirical parameters used to fix the data.

Dilatometry studies of YAG crystals (Gupta and Valentich, 1971) show good agreement with lattice parameter measurements of YAG powders (Croft, 1965; Geller et al., 1969). Dilatometric data on a polycrystalline YAG sample with about 5% porosity show lowering of thermal expansion. From room temperature

TABLE 29.27.

Polynomial parameters for the mean thermal expansion coefficients of several garnets (Gelber et al., 1969).

	$I(\times 10^{-3})$	$b(\times 10^{-9})$	$c(\times 10^{-9})$	$d(\times 10^{-1})$	a_0 at 296 K(Å)	Temperature range (K)
YAG	-2.968	8.192	0.994	1.535	12.008	296-1401
YGaG	-0.747	4.692	4.519	-2.545	12.274	296-1309
GdGaG	-2.201	7.084	2.457	-0.034	12.375	296-1402
GdIG	-8.580	21.335	-14.422	8.564	12.471	296-553
	-3.012	10.177	-	-	12.471	553-1273
YIG	-11.258	25.661	-17.810	13.155	12.376	296-553
	-3.117	10.496	-	-	12.375	553-1398

to 1673 K, the linear thermal expansion coefficients are $8.9 \times 10^{-6}/\text{K}$ and $8.0 \times 10^{-6}/\text{K}$ for single crystal and polycrystalline YAG, respectively. Change in density, from 4.38 g/cm^3 to 4.35 g/cm^3 , of the polycrystalline sample showed no differences in its expansion.

3.8. Elastic properties

3.8.1. Elastic constants

The elastic constants of EuIG, YIG, GdIG, GeGaG, YGaG, and YAG are tabulated in table 29.28. Two natural silicate garnets are also included in table

TABLE 29.28.
Elastic constants of several garnets.

	C_{11} ($\times 10^{11}$)	C_{12} dyn/cm ²)	C_{44}	Elastic anisotropy $A = \frac{2C_{44}}{C_{11} - C_{12}}$	Density (g/cm ³)	Refs. ^a
EuIG	25.10	10.70	7.62	1.051	6.28	1
YIG	26.80	11.06	7.66	0.973	5.17	1
	26.90	10.77	7.64	0.947	5.17	2
GdIG	27.31	12.50	7.41	1.0007		3
GdGaG						
[001]	28.57	11.49	9.02	1.0562	7.085	4
[110]	28.59	10.53	9.03	1.0574	7.085	4
$\bar{1}\bar{1}0$	28.51	10.47	9.02	1.0574	7.085	4
YGaG	29.03	11.73	9.547	1.10	5.79	5
YAG	33.32	11.07	11.50	1.03	4.55	5
Si-garnet 1	30.73	10.97	9.52		4.247	6
Si-garnet 2	30.48	11.23	9.44		4.183	6

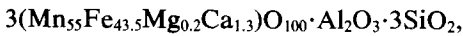
^a1. Bateman (1966); 2. Clark and Strakna (1961); 3. Comstock et al. (1966); 4. Graham and Chang (1970); 5. Spencer et al. (1963); 6. Varma (1960).

TABLE 29.29.
Longitudinal and shear velocities of several garnets.

	Longitudinal velocity $v_1 (\times 10^5 \text{ cm/s})$			Shear velocity $v_s (\times 10^5 \text{ cm/s})$			Ref. ^a
EuIG	W[110],	P[110]	6.375	W[110],	P[1 $\bar{1}$ 0]	3.385	
				W[110],	P[001]	3.484	1
YIG	W[110],	P[110]	7.172	W[110],	P[1 $\bar{1}$ 0]	3.902	
	W[100]	7.209					
	W[110]	7.153		W[110]	3.843		2
GdIG		6.50			3.39		3
GdGaG	W[001]	6.399		W[001]	3.469		
	W[110]	6.402		W[110]	3.470		
	W[1 $\bar{1}$ 0]	6.394		W[1 $\bar{1}$ 0]	3.467		4
YGaG	W[001]	7.080		W[001]	4.0601		
	W[110]	7.1914		W[110],	P[001]	4.0614	
				W[110],	P[1 $\bar{1}$ 0]	3.8655	5
YAG	W[001]	8.5630		W[001]	5.0293		
	W[110]	8.6016		W[110],	P[001]	5.0274	
				W[110],	P[1 $\bar{1}$ 0]	4.9438	5
Si-garnet 1 ^b	W[100],	P[100]	8.51	W[100],	P[100]	4.74	
	W[100],	P[110]	8.47				6
Si-garnet 2 ^b	W[100],	P[100]	8.54	W[100],	P[100]	4.75	
	W[100],	P[110]	8.51				6

^aThe key to the reference numbers is given in table 29.28. ^bThe chemical formulas are Si-garnet -13 $(\text{Mn}_{55}\text{Fe}_{43.5}\text{Mg}_{0.2}\text{Ca}_{1.3})\text{O}_{100}\cdot\text{Al}_2\text{O}_3\cdot 3\text{SiO}_2$; Si-garnet -23 $(\text{Fe}_{81}\text{Mg}_{14}\text{Mn}_1\text{Ca}_4)\text{O}_{100}\cdot\text{Al}_2\text{O}_3\cdot 3\text{SiO}_2$.

29.28. They are designated Si-garnet 1,



and Si-garnet 2,

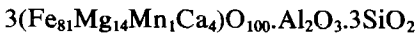


TABLE 29.30.
Microhardness of YIG, YGaG, and YAG (Gendeleev and Shcherbak, 1966).

	Mean microhardness of faces (kg/mm^2)		Error in measuring microhardness of faces (kg/mm^2)		Mean microhardness of crystal H_M	Class of hardness H_0
	(110)	(211)	(110)	(211)		
YIG	1210	1240	35	50	1230	7.5
YGaG	1450	1520	45	75	1490	8.0
YAG	1900	1650	50	85	1730	8.4

(Varma, 1960). The elastic constants increase in the order of EuIG, YIG, GdIG, GdIG, GdGaG, YGaG, Si-garnets 1 and 2, and YAG. Elastic anisotropy is defined for the garnet structure as

$$A = 2C_{44}/(C_{11} - C_{12}). \quad (29.43)$$

From the A values listed in table 29.28, GdIG with an A of 1.0007 has the lowest anisotropy, YGaG with an A of 1.10 has the highest anisotropy. Most of the listed A values in table 29.28 lie within $\pm 5\%$ of isotropy.

The longitudinal and shear velocities of several garnets are listed in table 29.29. Longitudinal velocities fall within the range $6.3\text{--}8.6 \times 10^5$ cm/sec, and shear velocities fall within the range $3.3\text{--}5.0 \times 10^5$ cm/sec.

The temperature dependences of the elastic constants of YAG are found to be negative (Alton and Barlow, 1967). Based on the elastic constants at 25°C C_{11} for YAG is 1.0127 times greater than at 150 K, C_{44} is 1.010 times greater, and C_{12} is 1.007 times greater at 150 K. The isotropy factor A is found to decrease from 1.033 at 300 K to 1.027 at 150 K. As a comparison, the temperature dependences of elastic compliances of natural silicate garnets are found to be positive for s_{11} and s_{44} , and negative for s_{12} (Reddy and Bhimasenacha, 1964). The s_{11} value is 3.84×10^{13} cm²/dyn at 93 K, 3.95×10^{13} at 323 K, and 4.17×10^{13} at 573 K. The s_{12} value is -1.17×10^{13} cm²/dyn at 93 K, -1.14×10^{13} at 323 K, and -1.09×10^{13} at 573 K. The s_{44} value is 2.45×10^{13} , 2.42×10^{13} , and 2.62×10^{13} cm²/dyn for 93, 323, and 573 K, respectively. The temperature gradient of s_{11} varies from 0.00025 at 93 K to 0.0006 at 323 K, and to 0.0012 at 573 K. The $(\Delta s_{12}/\Delta T)$ varies from -0.000125 at 93 K to -0.0002 at 323 K, and to -0.0004 at 573 K. The $(\Delta s_{44}/\Delta T)$ varies from 0.00075 at 93 K to 0.0018 at 323 K, and to 0.0016 at 573 K.

Microhardness values of YIG, YGaG, and YAG are listed in table 29.30 (Gendelev and Shcherbak, 1966). The values are more refined than the previously reported 1500 kg/mm² for YIG (Courtel et al., 1962). On {110} faces, the microhardness is maximum in $\langle 100 \rangle$ and minimum in $\langle 111 \rangle$. On the (110) face of YIG, M.H. $\langle 100 \rangle = 1340$ kg/mm², M.H. $\langle 111 \rangle = 1210$ kg/mm², and M.H. $\langle 100 \rangle >$ M.H. $\langle 110 \rangle >$ M.H. $\langle 111 \rangle$ (Gendelev and Shcherbak, 1966). On {211} faces the maximum M.H. direction is $\langle 110 \rangle$; the M.H. values fall in the directions $\langle 311 \rangle$ and $\langle 210 \rangle$. On the (211) face of YIG, M.H. $\langle 110 \rangle = 1320$ kg/mm², and M.H. $\langle 111 \rangle = 1230$ kg/mm². Replacement of Fe by Ga, and especially by Al, increases microhardness in all directions of the (110) plane. In YAG, {110} faces predominate markedly over {211}, and also prove to be harder. YIG and YGaG {211} faces are harder than {110} faces.

3.8.2. Ultrasonic attenuation

The observed sound attenuations at room temperature were theoretically related with the measured thermal properties of several insulating crystals (Woodruff and Ehrenreich, 1961). The theory applies for the limit of $\omega\tau \ll 1$, where ω is the angular frequency of the sound wave, and τ is the relaxation time of thermal phonons. The sound attenuation Γ in decibels per centimeter is given

by

$$\Gamma = 3.68(\langle\gamma\rangle^2\Omega^2\kappa T/\rho\langle v\rangle^5) \quad (29.44)$$

where $\langle\gamma\rangle$ is the average Gruneisen constant, which depends on the mode and polarization of the sound wave, κ is the thermal conductivity, ρ is the density, Ω is the angular frequency of the sound wave, and $\langle v\rangle$ is the average velocity of sound in the Debye approximation. From the work of Oliver and Slack (1966), a figure of merit R can be obtained from eq. (29.44):

$$R = (\kappa_0/\kappa'_0)(300/\theta)^2(V_0)^{-1/3}. \quad (29.45)$$

The sound attenuation Γ in decibels per centimeter can be expressed in terms of Γ_T in decibels per microsecond by the equation (Oliver et al., 1969a)

$$\Gamma_T = \Gamma \times v \times 10^{-5} \quad (29.46)$$

The sound attenuations, sound velocities, Debye temperatures, and figures of merit for several garnets are listed in table 29.31 (Oliver et al., 1969a). The data for other crystals are also included in table 29.31 for comparison.

TABLE 29.31.
Sound attenuations, Sound velocities, Debye temperatures and acoustic figures of merit of garnets^a.

	Sound attenuation		Sound velocity $v(10^5 \text{ cm/s})$	Debye temp. $\theta_D(\text{K})$	Acoustic figure of merit $R(1/\text{\AA})$
	$\Gamma_\theta(\text{dB/cm})$	$\Gamma_T(\text{dB}/\mu\text{s})$			
Ge	30(l)	14.7	4.96	395	0.22
	9(s)	3.2	3.56		
Si	10(l)	8.5	8.47	674	0.086
	3(s)	1.6	5.42		
SiO ₂	3(l)	2.2	7.2	469	0.06
	2.1(s)	1.2	5.75		
MgO	0.44(s)	0.3	6.50	949	0.013
			17.5(l)		
Diamond			12.8(s)	1900	0.013
			10.6		
TiO ₂	0.6(l)	0.6	5.38	758	0.0068
	0.37(s)	0.2	11.03		
Al ₂ O ₃	0.2(l)	0.2	6.78	950	0.0073
	0.5(s)	0.34	7.2		
LiNbO ₃	0.4(l)	0.29	7.2	785	0.004
Bi _{1/2} GeO ₂₀	1.5(s)	0.3	1.65	240	0.05
MgAl ₂ O ₄	0.4(l)	0.34	8.71	900	0.0083
	0.1(s)	0.07	6.63		
YAG	0.3(l)	0.26	8.56	750	0.006
	0.15(s)	0.075	5.03		
YGaG	0.37(l)	0.26	7.08	585	0.016
	0.2(s)	0.08	4.06		
YIG	0.34(s)	0.165	4.14	540	0.013
			7.31(l)		
TbAlG			4.15(s)	620	0.004
TmAlG			4.14(s)	620	0.004

^aFrom Oliver et al. (1969a).

Acknowledgments

It is a pleasure to thank Dr. David E. Cox for helpful discussions and cooperation throughout the course of this work.

References

- Akaba, R., 1974, *J. Crystal Growth* **24/25**, 537.
 Akselrad, A. and H.B. Callen, 1971, *Appl. Phys. Lett.* **19**, 464.
 Allain, Y., M. Bichara and A. Herpin, 1966, *J. Appl. Phys.* **37**, 1316.
 Allen, J.W., 1975, Optical Properties of Magnetic Oxides, in: Craik, D.J., ed., *Magnetic Oxides, Part 1* (John Wiley and Sons, New York) p. 349.
 Allen, R., J.F. Dillon, Jr., E.M. Gyorgy and J.P. Remeika, 1971, *J. Appl. Phys.* **42**, 1447.
 Alton, W.J. and A.J. Barlow, 1967, *J. Appl. Phys.* **38**, 3023.
 Andres, K. and B. Luthi, 1963, *J. Phys. Chem. Solids*, **24**, 584.
 Antonov, A.V., A.M. Balbashov, V.A. Baltinskii and A.Ya. Chervonenkis, 1973, *Soviet Phys.-Solid State* **14**, 1649.
 Awasthi, S.K., D.M. Chackraburttty and V.K. Tondon, 1967, *J. Inorg. Nucl. Chem.* **29**, 1225.
 Bari, R.A., 1972, *AIP Conf. Proc. No. 5*, 290.
 Ball, M., M.T. Hutchings, M.J.M. Leask and W.P. Wolf, 1963, *Proc. Conf. Low Temp Phys.*, 8th, 1962 (Butterworth, London) p. 248.
 Bartel, L.C., 1969, *J. Appl. Phys.* **40**, 661.
 Bateman, T.B., 1966, *J. Appl. Phys.* **37**, 2194.
 Batt, A. and B. Post, 1962, *Acta Crystallogr.* **15**, 1268.
 Bents, U.H., 1957, *Phys. Rev.* **106**, 225.
 Below, N.V., N.N. Neronova and T.S. Smirnova, 1957, *Soviet Phys.-Crystallogr.* **2**, 311.
 Berndt, U., D. Maier and C. Keller, 1975, *J. Solid State Chem.* **13**, 131.
 Berndt, U., R. Tanamas and C. Keller, 1976, *J. Solid State Chem.* **17**, 113.
 Bertaut, E.F., 1968, *Acta Crystallogr.* **A24**, 217.
 Bertaut, E.F., 1972, *Ann. Phys. (Paris)* **7**, 203.
 Bertaut, E.F. and F. Forrat, 1956, *J. Phys. Radium* **17**, 129.
 Bertaut, E.F., F. Forrat and P. Fang, 1963, *C. R. Acad. Sci., Paris* **256**, 1958.
 Bertaut, E.F., G. Bassi, G. Buisson, P. Bulet, J. Chappert, A. Delapalme, J. Mareschal, G. Rault, R. Aleonard, R. Pauthenet and J.P. Rebouillat, 1966, *J. Appl. Phys.* **37**, 1038.
 Bertaut, E.F. and J. Mareschal, 1967, *Solid State Commun.* **5**, 93.
 Bertaut, E.F., J. Mareschal and G.F. DeVries, 1967a, *J. Phys. Chem. Solids* **28**, 2143.
 Bertaut, E.F., J. Chappert, J. Mareschal, J.P. Rebouillat and J. Siviardière, 1967b, *Solid State Commun.* **5**, 293.
 Bertaut, E.F. and J. Mareschal, 1968, *J. Phys. (Paris)* **29**, 67.
 Ball, M., W.P. Wolf, and A.F.G. Wyatt, 1964, *J. Appl. Phys.* **35**, 937.
 Brice, J.C., 1965, *The Growth of Crystals from the Melt (Selected Topics in Solid State Physics, Vol. 5)* Wiley, New York.
 Berton, A. and B. Sharon, 1968, *J. Appl. Phys.* **39**, 1367.
 Bhandari, C.M. and G.S. Verma, 1966, *Phys. Rev.* **152**, 731.
 Bhide, V.G., D.S. Rajoria, G. Rama Rao and C.N.R. Rao, 1972, *Phys. Rev.* **B6**, 1021.
 Bhide, V.G., D.S. Rajoria, C.N.R. Rao, G. Rama Rao and V.G. Jadhao, 1975, *Phys. Rev.* **B12**, 2832.
 Bidaux, R. and P. Mériel, 1968, *J. Phys. (Paris)* **29**, 220.
 Bidaux, R., J.E. Bouree and J. Hammann, 1974, *J. Phys. Chem. Solids* **35**, 1645.
 Bierig, R.W. and L. Rimai, 1965, *J. Appl. Phys.* **36**, 1199.
 Birgeneau, R.J., J.K. Kjems, G. Shirane and L.G. Van Uitert, 1974, *Phys. Rev.* **B10**, 2512.
 Blank, S.L. and J.W. Nielsen, 1972, *J. Crystal Growth* **17**, 302.
 Blasse, G., 1965a, *Phillips Research Report* **20**, 327.
 Blasse, G., 1965b, *J. Inorg. Nucl. Chem.* **27**, 993.
 Bobeck, A.M., 1975, Magnetic Bubbles, in: Craik, D.J., ed., *Magnetic Oxides, Part 2* (John Wiley and Sons, New York) p. 743.
 Bobeck, A.H., D.H. Smith, E.G. Spencer, L.G. Van Uitert and E.M. Walters, 1971, *IEEE Trans. Magn.* **7**, 461.
 Bozorth, R.M., V. Kramer and J.P. Remeika, 1958, *Phys. Rev. Lett.* **1**, 3.
 Brandle, C.D. and A.J. Valentino, 1972, *J. Crystal Growth* **12**, 3.
 Brandle, C.D. and S.L. Blank, 1976, *IEEE Trans. Magn.* **12**, 14.
 Brixner, L.H., 1974, *Mater. Res. Bull.* **9**, 1041.
 Brous, J., I. Fankuchen and E. Banks, 1953, *Acta Crystallogr.* **6**, 67.
 Buchanan, R.A., K.A. Wickersheim, J.J. Pearson and G.F. Hermann, 1967, *Phys. Rev.* **159**, 245.
 Buchanan, R.A., J.J. Pearson and G.F. Hermann, 1969, *Solid State Commun.* **7**, 195.
 Buhner, C.F., 1969, *J. Appl. Phys.* **40**, 4500.
 Burbank, R.D., 1970, *J. Appl. Crystallogr.* **3**, 112.
 Callen, E.R., 1968, *J. Appl. Phys.* **39**, 519.
 Callen, E.R. and H.B. Callen, 1963, *Phys. Rev.* **129**, 578.
 Callen, E.R. and H.B. Callen, 1965, *Phys. Rev.* **139**, A455.
 Callen, H.B., 1971a, *Appl. Phys. Lett.* **18**, 311.
 Callen, H.B., 1971b, *Mater. Res. Bull.* **7**, 931.
 Cashion, J.D., A.H. Cooke, J.F.B. Hawkes, M.J.M. Leask, T.L. Thorp and M.R. Wells, 1968a, *J. Appl. Phys.* **39**, 1360.

- Cashion, J.D., A.H. Cooke, M.J.M. Leaske, T.L. Thorp and M.R. Wells, 1968b, *J. Mater. Sci.* **3**, 402.
- Chetkin, M.V. and A.N. Shalygin, 1968, *J. Appl. Phys.* **39**, 561.
- Chiang, F.R., C.S. Faber and F.F.Y. Wang, 1971, *J. Appl. Phys.* **42**, 1422.
- Clark, A.E. and R.E. Strakna, 1961, *J. Appl. Phys.* **32**, 1172.
- Clark, A.E., B.F. DeSavage, N. Tsuya and S. Kawakami 1966, *J. Appl. Phys.* **37**, 1324.
- Clark, A.E., J.J. Rhyne and E.R. Callen, 1968, *J. Appl. Phys.* **39**, 573.
- Cockayne, B., 1966, *J. Amer. Ceram. Soc.* **49**, 204.
- Coeuré, P., F. Forrat and J.-C. Gay, 1969, *IEEE Trans. Magn.* **5**, 898.
- Cohen, E., L.A. Risberg, W.A. Nordland, R.D. Burbank, R.C. Sherwood and L.G. Van Uitert, 1969, *Phys. Rev.* **186**, 476.
- Cohen, E., M.D. Sturge, R.J. Birgeneau, E.I. Blount, L.G. Van Uitert and J.K. Kjems, 1974, *Phys. Rev. Lett.* **32**, 232.
- Combarieu, A., J. Mareschal, J. Michel, J. Peyrard and J. Sivardière, 1968, *C.R. Acad. Sci., Paris* **267**, 1169.
- Comstock, R.L., 1965, *Proc. IEEE* **53**, 1508.
- Comstock, R.L., J.J. Raymond, W.G. Nilsen and J.P. Remeika, 1966, *Appl. Phys. Lett.* **9**, 274.
- Connolly, T.F. and E.D. Copenhaver, 1972, *Bibliography of Magnetic Materials and Tabulation of Magnetic Transition Temperatures, Solid State Literature Guides, Vol. 5 (IFI/Plenum Press, New York)*.
- Cooke, A.H., T.L. Thorp and M.R. Wells, 1967, *Proc. Phys. Soc., London* **92**, 400.
- Cooper, R.W., W.A. Crossley, J.L. Page and R.F. Pearson, 1968, *J. Appl. Phys.* **39**, 565.
- Coppens, P. and M. Eibschütz, 1965, *Acta Crystallogr.* **19**, 524.
- Courths, R., S. Hüfner and J. Pelzl, 1970, *Solid State Commun.* **8**, 1163.
- Coutures, J. and M. Foex, 1974, *J. Solid State Chem.* **11**, 294.
- Cox, D.E., 1972, *IEEE Trans. Mang.* **8**, 161.
- Cox, D.E., G. Shirane and B.C. Frazer, 1967, *J. Appl. Phys.* **38**, 1459.
- Croft, W.J., 1965, *Amer. Mineral.* **50**, 1634.
- Crossley, W.A., R.W. Cooper, J.L. Page and R.P. Van Staple, 1969, *J. Appl. Phys.* **40**, 1497.
- Crosswhite, H.M. and H.W. Moos, 1967, *Optical Properties of Ions in Crystals (Wiley-Interscience, New York)* p. 3.
- Dalziel, J.A.W., 1959, *J. Chem. Soc., London* **1959**, 1993.
- Damen, J.P.M. and J.M. Robertson, 1972, *J. Crystal Growth* **16**, 50.
- Demazeau, G., M. Pouchard and P. Hagenmuller, 1974, *J. Solid State Chem.* **9**, 202.
- Derighetti, B., J.E. Drumheller, F. Laves, K.A. Müller and F. Waldner, 1965, *Acta Crystallogr.* **18**, 557.
- Dernier, P.D. and R.G. Maines, 1971, *Mater. Res. Bull.* **6**, 433.
- Dieke, G.H. and H.M. Crosswhite, 1963, *Appl. Opt.* **2**, 675.
- Dillon, J.F., Jr., 1958, *J. Appl. Phys.* **29**, 539.
- Dillon, J.F., Jr., 1968, *J. Appl. Phys.* **39**, 922.
- Dionne, G.F., 1970, *J. Appl. Phys.* **41**, 2264.
- Donnay, G., J.M. Hastings, 1958, *Phys. Rev.* **112**, 1917.
- Dougier, P. and A. Casalot, 1970, *J. Solid State Chem.* **2**, 396.
- Dougier, P. and P. Hagenmuller, 1975, *J. Solid State Chem.* **15**, 158.
- Douglass, R.L., 1960, *Phys. Rev.* **120**, 1612.
- Douglass, R.L., 1963, *Phys. Rev.* **129**, 1132.
- Dreyfus, B., J. Verdone and M. Veyssie, 1965, *J. Phys. Chem. Solids* **26**, 107.
- Drofenik, M., D. Kolar and L. Golic, 1973, *J. Crystal Growth* **20**, 75.
- Dwyer, F.G., 1972, *Catalysis Rev.* **6**, 261.
- Eibschütz, M., 1965, *Acta Crystallogr.* **19**, 337.
- Elwell, D. and H.J. Scheel, 1975, *Crystal Growth from High Temperature Solutions (Academic Press, New York)*.
- Enz, U., W. Lems, R. Metselaar, P.J. Rignierse and R.W. Teale, 1969, *IEEE Trans. Magn.* **5**, 467.
- Espinosa, G.P. and S. Geller, 1964, *J. Appl. Phys.* **35**, 2551.
- Euler, F. and J.A. Bruce, 1965, *Acta Crystallogr.* **19**, 971.
- Faucher, M. and P. Caro, 1975, *Mater. Res. Bull.* **10**, 1.
- Fayolle, J., F. Studer, G. Desgardin and B. Raveau, 1975, *J. Solid State Chem.* **13**, 57.
- Fesenko, E.G. and G.A. Geguzina, 1973, *Soviet Phys.-Crystallogr.* **18**, 336.
- Fisher, M.E., 1960, *Proc. Roy. Soc., Ser. A* **254**, 66.
- Flanders, P.J., C.D. Graham, Jr., J.F. Dillon, Jr., E.M. Gyorgy and J.P. Remeika, 1971, *J. Appl. Phys.* **42**, 1443.
- Flicstein, J. and M. Schieber, 1973, *J. Crystal Growth* **18**, 265.
- Freiser, M.J., 1966, *IEEE Trans. Magn.* **5**, 152.
- Friedberg, S.A. and E.D. Harris, 1963, *Proc. Int. Conf. Low Temp. Phys.*, 8th, 1962, p. 302.
- Fukanaga, O. and T. Fujita, 1973, *J. Solid State Chem.* **8**, 331.
- Gai, P.L. and C.N.R. Rao, 1975, *Mater. Res. Bull.* **10**, 787.
- Galasso, F.S., 1969, *Structure, Properties and Preparation of Perovskite-type Compounds (Pergamon Press, New York)*.
- Galasso, F.S., L. Katz and R. Ward, 1959, *J. Amer. Chem. Soc.* **81**, 820.
- Galasso, F.S. and W. Darby, 1963, *J. Phys. Chem.* **66**, 131.
- Galasso, F.S., G.K. Layden and D.E. Flinchbaugh, 1966, *J. Chem. Phys.* **44**, 2703.
- Gallagher, P.K., D.W. Johnson, Jr. and F. Schrey, 1974, *Mater. Res. Bull.* **9**, 1345.
- Gallagher, P.K., D.W. Johnson, Jr., J.P. Remeika, F. Schrey, L.E. Trimble, E.M. Vogel and R.J.H. Voorhoeve, 1975a, *Mater. Res. Bull.* **10**, 529.
- Gallagher, P.K., D.W. Johnson, Jr., E.M. Vogel and F. Schrey, 1975b, *Mater. Res. Bull.* **10**, 623.
- Courtel, R., H. Makram and G. Pigeat, 1962, Compt. Rend. 254, 4447.**
- Dillon, J.F., Jr., E.M. Gyorgy and J.P. Remeika, 1970, J. Appl. Phys. 41, 1211.**

- Ganguly, P. and C.N.R. Rao, 1973, *Mater. Res. Bull.* **8**, 405.
- Garton, G. and B.M. Wanklyn, 1967, *J. Crystal Growth* **1**, 164.
- Garton, G., B.F. Hann, B.M. Wanklyn and S.H. Smith, 1972, *J. Crystal Growth* **12**, 66.
- Geller, S., 1956, *J. Chem. Phys.* **24**, 1236.
- Geller, S., 1957a, *Acta Crystallogr.* **10**, 243.
- Geller, S., 1957b, *Acta Crystallogr.* **10**, 248.
- Geller, S., 1966, *J. Appl. Phys.* **37**, 1408.
- Geller, S., 1967, *Z. Kristallogr., Kristaggeometrie, Kristallphys., Kristallchem.* **325**, 1.
- Geller, S. and V.B. Bala, 1956, *Acta Crystallogr.* **9**, 1019.
- Geller, S. and E.A. Wood, 1956, *Acta Crystallogr.* **9**, 563.
- Geller, S. and M.A. Gilleo, 1957, *J. Phys. Chem. Solids* **3**, 30.
- Geller, S., H.J. Williams, R.C. Sherwood, J.P. Remeika and G.P. Espinosa, 1963, *Phys. Rev.* **131**, 1080.
- Geller, S., H.J. Williams, G.P. Espinosa and R.C. Sherwood, 1964, *Bell Syst. Tech. J.* **43**, 565.
- Geller, S., G.P. Espinosa and P.D. Crandall, 1969, *J. Appl. Crystallogr.* **2**, 86.
- Geller, S., P.J. Curlander and G.F. Fuse, 1974, *Mater. Res. Bull.* **9**, 637.
- Gendeleev, S.S. and N.G. Shcherbak, 1966, *Soviet Phys.-Crystallogr.* **10**, 592.
- Gendeleev, S.S. and A.G. Titova, 1971, *Bull. Acad. Sci., USSR, Phys. Ser.* **6**, 1131.
- Giess, E.A., 1962, *J. Amer. Ceram. Soc.* **45**, 53.
- Giess, E.A., D.C. Cronemeyer, L.L. Rosier and J.D. Kuptsis, 1970, *Mater. Res. Bull.* **5**, 495.
- Giess, E.A., J.D. Kuptsis and E.A.D. White, 1972, *J. Crystal Growth* **16**, 36.
- Gilleo, M.A., 1956, *J. Chem. Phys.* **24**, 1239.
- Gilleo, M.A., 1957, *Acta Crystallogr.* **10**, 161.
- Gilleo, M.A., 1960, *J. Phys. Chem. Solids* **13**, 33.
- Glazer, A.M., 1972, *Acta Crystallogr.* **B28**, 3384.
- Glazer, A.M., 1975, *Acta Crystallogr.* **A31**, 756.
- Goldschmidt, V.M., 1926, *Skrifter Norske Videnskaps-Akad. Oslo, I. Mat.-Naturv. Kl.*, No. 8.
- Goodenough, J.B., 1955, *Phys. Rev.* **100**, 564.
- Goodenough, J.B., 1958, *J. Phys. Chem. Solids* **6**, 287.
- Goodenough, J.B., 1966, *J. Appl. Phys.* **37**, 1415.
- Goodenough, J.B., 1968, *Magnetism and the Chemical Bond* (John Wiley and Sons, New York) pp. 165-184.
- Goodenough, J.B. and P.M. Racciah, 1965, *J. Appl. Phys.* **36**, 1031.
- Goodenough, J.B. and J.M. Longo, 1970, in *Magnetic and Other Properties of Oxides and Related Compounds* Hellwege, K.H., ed., Landolt-Bornstein, Vol. 4 (Springer-Verlag, New York) p. 126.
- Goodenough, J.B., J.A. Kafalas and J.M. Longo, 1972, *High Pressure Synthesis*, in: Hagemuller, P., ed., *Preparative Methods in Solid State Chemistry* (Academic Press, New York) p. 2.
- Gorodetsky, G., B. Sharon and S. Shtrikman, 1968, *J. Appl. Phys.* **39**, 1371.
- Gorodetsky, G., R.M. Hoenreich, I. Yaeger, H. Pinto, G. Shachar and H. Shaked, 1973, *Phys. Rev.* **B8**, 3398.
- Graham, L.J. and R. Chang, 1970, *J. Appl. Phys.* **41**, 2247.
- Granicher, H., K. Hubner and K.A. Müller, 1957, *Helv. Phys. Acta* **30**, 480.
- Greedan, J.E., G.J. McCarthy and C. Sipe, 1975, *Inorg. Chem.* **14**, 775.
- Grünberg, P., K.H. Hellwege and S. Hüfner, 1967, *Phys. Kondens. Mater.* **6**, 95.
- Grünberg, P., S. Hüfner, E. Orlich and J. Schmitt, 1969, *J. Appl. Phys.* **40**, 1501.
- Gupta, T.K. and J. Valentich, 1971, *J. Amer. Ceram. Soc.* **54**, 355.
- Gyorgy, E.M., J.T. Krause, R.C. Le Craw, L.R. Testardi and L.G. Van Uitert, 1967, *J. Appl. Phys.* **38**, 1226.
- Gyorgy, E.M., J.P. Remeika and F.B. Hagedorn, 1968, *J. Appl. Phys.* **39**, 1369.
- Gyorgy, E.M., J.F. Dillon, Jr. and J.P. Remeika, 1971, *J. Appl. Phys.* **42**, 1454.
- Harley, R.T., W. Hayes, A.M. Perry and S.R.P. Smith, 1973, *J. Phys. C: Solid State* **6**, 2382.
- Harris, A.B., 1963, *Phys. Rev.* **132**, 2398.
- Harris, A.B. and H. Meyer, 1962, *Phys. Rev.* **127**, 101.
- Heikes, R.R., R.C. Miller and R. Mazelsky, 1964, *Physica* **30**, 1600.
- Hellwege, K.H., S. Hüfner, M. Schinkman and H. Schmidt, 1966, *Phys. Kondens. Mater.* **4**, 396.
- Henderson, A.J., Jr., D.G. Onn, H. Meyer and J.P. Remeika, 1969, *Phys. Rev.* **185**, 1218.
- Herpin, A., W.C. Koehler and P. Meriel, 1960, *C.R. Acad. Sci. Paris* **251**, 1359.
- Herpin, A. and P. Meriel, 1964, *C.R. Acad. Sci. Paris* **259**, 2416.
- Hewitt, B.S., R.D. Pierce, S.L. Blank and S. Knight, 1973, *IEEE Trans. Magn.* **9**, 366.
- Holland, M.G., 1968, *IEEE Trans. Sonics Ultrason.* **15**, 18.
- Holmes, L., R. Sherwood and L.G. Van Uitert, 1968, *J. Appl. Phys.* **39**, 1373.
- Holmes, L., L.G. Van Uitert and R. Hecker, 1971a, *J. Appl. Phys.* **42**, 657.
- Holmes, L., L.G. Van Uitert and G.W. Hull, 1971b, *Solid State Commun.* **9**, 1373.
- Holtwijk, T., W. Lems, A.G.H. Verhulst and U. Enz, 1970, *IEEE Trans. Magn.* **6**, 853.
- Hu, H.L. and E.A. Geiss, 1975, *IEEE Trans. Magn.* **11**, 1085.
- Hüfner, S., L. Holmes, F. Varsanyi and L.G. Van Uitert, 1968, *Phys. Rev.* **171**, 507.
- Hurrell, J.P., S.P.S. Porto, I.F. Chang, S.S. Mitra and R.P. Bauman, 1968, *Phys. Rev.* **173**, 851.
- Iida, S., 1963, *Phys. Lett.* **6**, 165.
- Iida, S., 1967, *J. Phys. Soc. Japan* **22**, 1201.
- Iwahashi, K. and S. Iida, 1965, *J. Phys. Soc. Japan* **20**, 1526.

- Jacobson, A.J., B.C. Toefield and B.E.F. Fender, 1972, *Acta Crystallogr.* **B28**, 956.
- Janes, D.L. and R.E. Bodnar, 1971, *J. Appl. Phys.* **42**, 1500.
- Johnson, B. and A.K. Walton, 1965, *Brit. J. Appl. Phys.* **16**, 475.
- Johnson, D.W., Jr., P.K. Gallagher, F. Schrey and W.W. Rhodes, 1976, *Amer. Ceram. Soc. Bull.* **55**, 520.
- Jones, R.V., 1966, *IEEE Trans. Sonics Ultrason.* **13**, 86.
- Jonker, G.H., 1954, *Physica* **20**, 1118.
- Jonker, G.H., 1956, *Physica* **22**, 707.
- Jonker, G.H., 1966, *J. Appl. Phys.* **37**, 1424.
- Jonker, G.H. and J.H. Van Santen, 1950, *Physica* **16**, 337.
- Jonker, G.H. and J.H. Van Santen, 1953, *Physica* **19**, 120.
- Joshi, A.W. and K.P. Sinha, 1966, *Proc. Phys. Soc., London* **88**, 685.
- Kahn, F.J., P.S. Pershan and J.P. Remeika, 1969a, *J. Appl. Phys.* **40**, 1508.
- Kahn, F.J., P.S. Pershan and J.P. Remeika, 1969b, *Phys. Rev.* **186**, 891.
- Kanamori, J., 1959, *J. Phys. Chem. Solids* **10**, 87.
- Kanamori, J., 1963, *Anisotropy and Magnetostriction of Ferromagnetic and Antiferromagnetic Materials*, Rado, G.T. and H. Suhl, eds., *Magnetism*, Vol. 1 (Academic Press, New York) p. 217.
- Keen, B.E., D.P. Landau, B. Schneider and W.P. Wolf, 1966, *J. Appl. Phys.* **37**, 1120.
- Keith, M.L. and R. Roy, 1954, *Amer. Mineral.* **39**, 1.
- Keller, C., 1965, *J. Inorg. Nucl. Chem.* **27**, 321.
- Khattak, C.P., D.E. Cox and F.F.Y. Wang, 1973, *AIP Conf. Proc. No. 10*, 674.
- Khattak, C.P., 1974, unpublished research.
- Khattak, C.P., D.E. Cox and F.F.Y. Wang, 1975, *J. Solid State Chem.* **13**, 77.
- Khattak, C.P., D.E. Cox and F.F.Y. Wang, 1976, *J. Solid State Chem.* **17**, 323.
- Kim, Y.S., 1968, *Acta Crystallogr.* **B24**, 295.
- Kiro, D., W. Low and A. Zuzman, 1963, in: *Low, W., ed., Paramagnetic Resonance*, Vol. 1 (Academic Press, New York) p. 44.
- Kjems, J.K., G. Shirane, K.A. Müller and H.J. Scheel, 1973a, *Phys. Rev.* **B8**, 1119.
- Kjems, J.K., G. Shirane, R.J. Birgeneau and L.G. Van Uitert, 1973b, *Phys. Rev. Lett.* **31**, 1300.
- Klein, P.H. and W.J. Croft, 1967, *J. Appl. Phys.* **38**, 1603.
- Klokhohm, E., 1969, *Rev. Sci. Instrum.* **40**, 1054.
- Klokhohm, E., J.W. Matthews, A.F. Mayadas and J. Angilello, 1972, *AIP Conf. Proc. No. 5*, Part 1, 105.
- Knight, W.D. and D.L. Huber, 1968, *J. Appl. Phys.* **39**, 1069.
- Koehler, W.C. and E.O. Wollan, 1957, *J. Phys. Chem. Solids* **2**, 100.
- Koehler, W.C., E.O. Wollan and M.K. Wilkinson, 1960, *Phys. Rev.* **118**, 58.
- Koenig, J. and B. Jaffe, 1964, *J. Amer. Ceram. Soc.* **47**, 87.
- Kolb, E.D. and R.A. Laudise, 1971, *J. Appl. Phys.* **42**, 1552.
- Kolb, E.D., D.L. Wood, E.G. Spencer and R.A. Laudise, 1967, *J. Appl. Phys.* **38**, 1027.
- Kolb, E.D., D.L. Wood and R.A. Laudise, 1968, *J. Appl. Phys.* **39**, 1362.
- Koningstein, J.A., 1964, *Phys. Rev.* **136A**, 717.
- Koningstein, J.A., 1966, *Theor. Chim. Acta* **5**, 327.
- Koningstein, J.A. and T. Ng, 1969, *Solid State Commun.* **7**, 351.
- Krinchik, G.S. and M.V. Chetkin, 1962, *Soviet Phys.-JETP* **14**, 485.
- Landau, D.P. and G.S. Dixon, 1970, *Bull. Amer. Phys. Soc.* [2] **15**, 1381.
- Laudise, R.A., 1970, *The Growth of Single Crystals* (Prentice Hall, New Jersey).
- Laudise, R.A., R.C. Linares and E.F. Dearborn, 1962, *J. Appl. Phys.* **33**, 1362.
- Laudise, R.A., J.R. Carruthers and K.A. Jackson, 1971, In *Annual Review of Materials Science*, Huggins, R.A., R.H. Bube and R.W. Robers eds., (Annual Review, California) Vol. 1, p. 253.
- Leake, J.A., G. Shirane and J.P. Remeika, 1968, *Solid State Commun.* **6**, 15.
- Leask, M.J.M., 1968, *J. Appl. Phys.* **39**, 908.
- Le Craw, R.C., D.L. Wood, J.F. Dillon, Jr. and J.P. Remeika, 1965, *Appl. Phys. Lett.* **7**, 27.
- Le Craw, R.C., R. Wolfe, A.H. Bobeck, R.D. Pierce and L.G. Van Uitert, 1971, *J. Appl. Phys.* **42**, 1641.
- Lefever, R.A., K.A. Wickersheim and A.B. Chase, 1965, *J. Phys. Chem. Solids* **26**, 1529.
- Libby, W.F., 1971, *Science* **171**, 499.
- Linares, R.C., 1962a, *J. Appl. Phys.* **33**, 1747.
- Linares, R.C., 1962b, *J. Amer. Ceram. Soc.* **45**, 307.
- Lüthi, B., 1962, *J. Phys. Chem. Solids* **23**, 35.
- Lyubutin, I.S. and Yu. S. Vishnyakov, 1973, *Soviet Phys.-Crystallogr.* **17**, 847.
- Malozemoff, A.P., 1971, *J. Phys. Chem. Solids* **32**, 1669.
- Mareschal, J., J. Sivardière and G.F. DeVries, 1968, *J. Appl. Phys.* **39**, 1364.
- Marezio, M., J.P. Remeika and P.D. Dernier, 1966, *Mater. Res. Bull.* **1**, 247.
- Marezio, M., J.P. Remeika and P.D. Dernier, 1968, *Inorg. Chem.* **7**, 1337.
- Marezio, M., J.P. Remeika and P.D. Dernier, 1970, *Acta Crystallogr.* **B26**, 2008.
- McCarthy, G.J. and J.E. Greedan, 1975, *Inorg. Chem.* **14**, 772.
- McCarthy, G.J., W.B. White and R. Roy, 1969, *Mater. Res. Bull.* **4**, 251.
- McCarthy, G.J., P.V. Gallagher and C. Sipe, 1973, *Mater. Res. Bull.* **8**, 1277.
- McCarthy, G.J., C.A. Sipe and K.E. McIlvried, 1974, *Mater. Res. Bull.* **9**, 1279.
- McDevitt, N.T., 1969, *J. Opt. Soc. Amer.* **59**, 1240.
- McGuire, T.R., M.W. Shafer and R.J. Joenk, 1966, *J. Appl. Phys.* **37**, 981.
- Meadcroft, D.B., 1968, *Energy Conversion* **8**, 185.

Keen, B.E., D.P. Landau and W.P. Wolf, 1967, J. Appl. Phys. 38, 967.

- Meadowcroft, D.B., 1969, *Brit. J. Appl. Phys. (J. Phys. D) Ser. 2*, **2**, 1225.
- Meadowcroft, D.B., 1970, *Nature* **226**, 847.
- Megaw, H.D., 1946, *Proc. Phys. Soc.* **58**, 133, 326.
- Megaw, H.D., 1968a, *Acta Crystallogr.* **A24**, 583.
- Megaw, H.D., 1968b, *Acta Crystallogr.* **A24**, 589.
- Megaw, H.D., 1968c, *Acta Crystallogr.* **B24**, 149.
- Megaw, H.D., 1972, *J. Phys., Paris* **33**, Suppl. C2, 1.
- Megaw, H.D. and C.N.W. Darlington, 1975, *Acta Crystallogr.* **A31**, 161.
- Meltzer, R.S., 1970, *Phys. Rev.* **B2**, 2398.
- Menyuk, N., K. Dwight and P.M. Raccah, 1967, *J. Phys. Chem. Solids* **28**, 549.
- Merker, L. and K.D. Herrington, 1964, *Appl. Opt.* **3**, 1311.
- Mikami, I., 1973, *J. Phys. Soc. Japan* **34**, 338.
- Mikami, I., M. Hirano and G. Kamoshita, 1973, *Jap. J. Appl. Phys.* **12**, 557.
- Mill', B.V., 1965, *Dokl. Akad. Nauk SSSR* **165**, 555.
- Milward, R.C., 1967, *Phys. Lett.* **A25**, 19.
- Miyadai, T., 1960, *J. Phys. Soc. Japan* **15**, 2205.
- Moreau, J.M., J. Mareschal and E.F. Bertaut, 1968, *Solid State Commun.* **6**, 751.
- Morrish, A.H., 1965, *The Physical Principles of Magnetism* (John Wiley and Sons, New York) p. 500.
- Morrish, A.H., B.J. Evans, J.A. Eaton and L.K. Leung, 1969, *Can. J. Phys.* **47**, 2691.
- Moskvin, A.S. and E.V. Sinitsyn, 1973a, *Soviet Phys.-Solid State* **14**, 2198.
- Moskvin, A.S. and E.V. Sinitsyn, 1973b, *Soviet Phys.-Solid State* **14**, 2363.
- Müller, O. and R. Roy, 1974, in: *Crystal Chemistry of Non-metallic Materials*, R. Roy ed., No. 4 (Springer-Verlag, New York) p. 153.
- Muller, K.A., W. Berlinger and F. Waldner, 1968, *Phys. Rev. Lett.* **21**, 814.
- Muller-Buschbaum, H.K. and C. Teske, 1968, *J. Inorg. Nucl. Chem. Lett.* **4**, 151.
- Naiman, C.S., B. DiBartolo, A. Linz and R. Santoro, 1965, *J. Appl. Phys.* **36**, 879.
- Nakada, I., R. Akaba and T. Yanase, 1972, *Jap. J. Appl. Phys.* **11**, 1583.
- Néel, L., 1948, *Ann. Phys. (Paris)* **3**, 137.
- Nielsen, J.W., 1960, *J. Appl. Phys.* **31**, 515.
- Nikolaev, V.I. and V.S. Rusakov, 1976, *Soviet Phys.-Crystallogr.* **20**, 519.
- Nilsen, W.G., R.L. Comstock and L.R. Walker, 1965, *Phys. Rev.* **139**, A472.
- Nomura, S. and T. Nakagawa, 1966, *J. Phys. Soc. Jap.* **21**, 1068.
- Novak, G.A. and G.V. Gibbs, 1971, *Amer. Mineral.* **56**, 791.
- Obayashi, H. and T. Kudo, 1975, *Jap. J. Appl. Phys.* **14**, 330.
- Obayashi, H., Y. Sakurai and T. Gejo, 1976, *J. Solid State Chem.* **17**, 299.
- Obayashi, H., T. Kudo and T. Gejo, 1974, *Jap. J. Appl. Phys.* **13**, 1.
- Oliver, D.W. and G.A. Slack, 1966, *J. Appl. Phys.* **37**, 1542.
- Oliver, D.W., G.A. Slack and J.D. Young, 1969a, 1st Semiannual Report, Air Force Mater. Lab. Contract No. F33615-69-C-1286, Proj. No. 7371, June 1969, S-69-1103, General Electric R. & D. Center.
- Oliver, D.W., G.A. Slack and J.D. Young, 1969b, 2nd Semiannual Report, Air Force Mater. Lab. Contract No. F33615-69-C-1286, Proj. No. 7371, December 1969, S-69-1176, General Electric R. & D. Center.
- Onn, D.G., J.P. Remeika, H. Meyer and A.J. Henderson, Jr., 1967, *J. Appl. Phys.* **38**, 1023.
- Opechowski, W. and R. Guccione, 1965, *Magnetic Symmetry*, in Rado, G.T. and H. Shull eds., *Magnetism, Vol. II A* (Academic Press, New York) p. 105.
- Orlich, E. and S. Hüfner, 1969, *J. Appl. Phys.* **40**, 1503.
- Parker, R., 1975, *Electrical Transport Properties*, in: Craik, D.J. ed., *Magnetic Oxides, Part I* (John Wiley and Sons, New York) p. 421.
- Pataud, P. and J. Sivardière, 1970a, *J. Phys., Paris* **31**, 803.
- Pataud, P. and J. Sivardière, 1970b, *J. Phys., Paris* **31**, 1017.
- Patton, C.E., 1970, *J. Appl. Phys.* **41**, 1637.
- Pierce, R.D., R. Wolfe and L.G. Van Uitert, 1969, *J. Appl. Phys.* **40**, 1241.
- Pauthenet, R., 1956, *C.R. Acad. Sci., Paris* **242**, 1859.
- Pauthenet, R., 1957, Thesis, Grenoble, France.
- Pauthenet, R., 1958, *J. Appl. Phys.* **29**, 253.
- Pearson, J.J., G.F. Herrmann and R.A. Buchanan, 1968, *J. Appl. Phys.* **39**, 980.
- Pearson, R.F., 1962, *J. Appl. Phys.* **33**, 1236.
- Pearson, R.F., A.D. Annis and P. Kompfner, 1968, *Phys. Rev. Lett.* **21**, 1805.
- Perel, J. and M. Schieber, 1962, *Jap. J. Appl. Phys.* **1**, 243.
- Pershan, P.S., 1967, *J. Appl. Phys.* **38**, 1482.
- Philp, J.W., R. Gonono and E.D. Adams, 1969, *J. Appl. Phys.* **40**, 1275.
- Phillips, T.G. and R.L. White, 1966, *Phys. Rev. Lett.* **16**, 650.
- Phillips, T.G. and R.L. White, 1967, *Phys. Rev.* **160**, 316.
- Pickart, S.J., H.A. Alperin and A.E. Clark, 1970, *J. Appl. Phys.* **41**, 1192.
- Pinto, H. and H. Shaked, 1972, *Solid State Commun.* **10**, 663.
- Pinto, H., G. Shachar, H. Shaked and S. Shtrikman, 1971, *Phys. Rev.* **B3**, 3861.
- Prakash, O., P. Ganguly, G. Rama Rao, C.N.R. Rao, D.S. Rajoria and V.G. Bhide, 1974, *Mater. Res. Bull.* **9**, 1173.
- Quezel-Ambrunaz, S., 1968, *Bull. Soc. France Mineral. Crystallogr.* **91**, 339.
- Quezel-Ambrunaz, S. and M. Mareschal, 1963, *Bull. Soc. France Mineral. Crystallogr.* **86**, 204.
- Quon, H.H., A. Potvin and S.D. Entwistle, 1971, *Mater. Res. Bull.* **6**, 1175.
- Raccah, P.M. and J.B. Goodenough, 1967, *Phys. Rev.* **155**, 932.
- Rango, C., G. Tsoucaris and C. Zelwer, 1966,

Menzer, G., 1926, Z. Kristallogr. **63**, 157.

- Acta Crystallogr. **20**, 590.
- Rao, C.N.R., O. Prakash and G. Ganguly, 1975, *J. Solid State Chem.* **15**, 186.
- Reddy, P.J. and J. Bhimasenacha, 1964, *Acta Crystallogr.* **17**, 31.
- Remeika, J.P., 1956, *J. Amer. Ceram. Soc.* **78**, 4259.
- Remeika, J.P. and T.Y. Kometani, 1968, *Mater. Res. Bull.* **3**, 895.
- Remeika, J.P., E.M. Gyorgy and D.L. Wood, 1969, *Mater. Res. Bull.* **4**, 51.
- Richards, P.L., 1963, *J. Appl. Phys.* **34**, 1237.
- Rives, J.E., G.S. Dixon and D. Walton, 1966, *J. Appl. Phys.* **40**, 1555.
- Robbins, M.G.K. Wertheim, A. Menth and R.C. Sherwood, 1969, *J. Phys. Chem. Solids* **30**, 1823.
- Robinson, M., A.H. Bobeck and J.W. Nielsen, 1971, *IEEE Trans. Magn.* **7**, 464.
- Rodrigue, G.P., H. Meyer and R.V. Jones, 1960, *J. Appl. Phys.* **31**, 376S.
- Rogers, D.B., A. Ferretti, D.H. Ridgley, R.J. Arnott and J.B. Goodenough, 1966, *J. Appl. Phys.* **37**, 1431.
- Roth, R.S., 1957, *J. Res., Natl. Bur. Stds.* **58**, 75.
- Rosencwaig, A. and W.J. Tabor, 1971, *J. Appl. Phys.* **42**, 1643.
- Rosencwaig, A., W.J. Tabor and R.D. Pierce, 1971, *Phys. Rev. Lett.* **26**, 775.
- Roy, R., 1954, *J. Amer. Ceram. Soc.* **37**, 581.
- Ruggiero, A. and R. Ferro, 1955, *Gazz. Chim. Ital.* **85**, 892.
- Ruiz, J.S., A.M. Anthony and M. Foëx, 1967, *C.R. Acad. Sci., Paris* **264**, 1271.
- Saburi, O., 1959, *J. Phys. Soc. Japan* **14**, 1159.
- Sakhnenko, V.P., E.F. Fesenko, A.T. Shuvaev, E.T. Shuvaeva and G.A. Geguzina, 1972, *Soviet Phys.-Crystallogr.* **17**, 268.
- Sato, K., G. Adachi and J. Shiokawa, 1975, *Mater. Res. Bull.* **10**, 113.
- Sawatzky, E. and E. Kay, 1968, *J. Appl. Phys.* **39**, 4700.
- Sayer, M., R. Chen, R. Fletcher and A. Mansingh, 1975, *J. Phys. C: Solid State Phys.* **8**, 2059.
- Scheel, H.J., 1972, *J. Crystal Growth* **13/14**, 560.
- Scheel, H.J. and E.O. Schulz-Dubois, 1971, *J. Crystal Growth* **8**, 304.
- Schieber, M., 1964, *J. Amer. Ceram. Soc.* **47**, 537.
- Schneidger, S.J. and R.S. Roth, 1960, *J. Amer. Ceram. Soc.* **43**, 115.
- Schneider, S.J., R.S. Roth and J.L. Waring, 1961, *J. Res. Natl. Bur. Stds.* **65A**, 345.
- Shafer, M.W., 1965, *J. Appl. Phys.* **36**, 1145.
- Shannon, R.D., 1967, *Inorg. Chem.* **6**, 1474.
- Shannon, R.D., 1970, *Acta Crystallogr.* **B26**, 447.
- Shannon, R.D. and C.T. Prewitt, 1969, *Acta Crystallogr.* **B25**, 925.
- Shapiro, S.M., J.D. Axe and J.P. Remeika, 1974, *Phys. Rev.* **B10**, 2014.
- Sherwood, R.C., J.P. Remeika and H.J. Williams, 1959, *J. Appl. Phys.* **30**, 217.
- Shick, L.K. and J.W. Nielsen, 1971, *J. Appl. Phys.* **42**, 1554.
- Shin-ike, T., T. Sakai, G. Adachi and J. Shiokawa, 1976, *Mater. Res. Bull.* **11**, 249.
- Sievers, A.J. and M. Tinkham, 1963, *Phys. Rev.* **189**, 1935.
- Sis, L.B., G.P. Wirtz and S.C. Sorenson, 1973, *J. Appl. Phys.* **44**, 5553.
- Slack, G.A. and D.W. Oliver, 1971, *Phys. Rev.* **B4**, 592.
- Slack, G.A., D.W. Oliver, R.M. Chrenko and S. Roberts, 1969, *Phys. Rev.* **177**, 1308.
- Soga, N., 1967, *J. Geophys. Res.* **72**, 4227.
- Solov'eva, A.E. and A.M. Gavrish, 1974, *Inorg. Mater.* **10**, 1336.
- Sorenson, S.C., J.A. Wronkiewicz, L.B. Sis and G.P. Wirtz, 1974, *Amer. Ceram. Soc. Bull.* **53**, 446.
- Spencer, E.G., R.T. Denton, T.B. Bateman, W.B. Snow and L.G. Van Uitert, 1963, *J. Appl. Phys.* **34**, 3059.
- Steward, E.G. and H.P. Rooksby, 1951, *Acta Crystallogr.* **4**, 503.
- Sturge, M.D., 1972, *AIP Conf. Proc. No. 5*, Part 1, 205.
- Sugano, S., K. Aoyagi and K. Tsushima, 1971, *J. Phys. Soc. Japan* **31**, 706.
- Suits, J.C., 1972, *IEEE Trans. Magn.* **8**, 95.
- Tauber, A., C.G. Whinfrey and E. Banks, 1961, *J. Phys. Chem. Solids* **21**, 25.
- Teale, R.W. and D.W. Temple, 1967, *Phys. Rev. Lett.* **19**, 904.
- Thacher, P.D., 1967, *Phys. Rev.* **156**, 975.
- Tinkham, M., 1962, *J. Appl. Phys.* **33**, 1248.
- Toefield, B.C., A.J. Jacobson and B.E.F. Fender, 1972, *J. Phys. C: Solid State Phys.* **5**, 2887.
- Tolksdorf, W., 1975, *IEEE Trans. Magn.* **11**, 1074.
- Traverse, J.J., J. Coutures and M. Foëx, 1968, *C.R. Acad. Sci., Paris* **267**, 391.
- Treves, D., 1962, *Phys. Rev.* **125**, 1843.
- Treves, D., 1965, *J. Appl. Phys.* **36**, 1033.
- Tsushima, K., 1966, *J. Appl. Phys.* **37**, 443.
- Tsushima, K., K. Aoyagi and S. Sugano, 1970, *J. Appl. Phys.* **41**, 1238.
- Van Groenou, A.B., J.L. Page and R.F. Pearson, 1967, *J. Phys. Chem. Solids* **28**, 1017.
- Van Hook, H.J., 1961, *J. Amer. Ceram. Soc.* **44**, 208.
- Van Hook, H.J., 1962a, *J. Amer. Ceram. Soc.* **45**, 162.
- Van Hook, H.J., 1962b, *J. Amer. Ceram. Soc.* **45**, 369.
- Van Hook, H.J., 1963a, *J. Amer. Ceram. Soc.* **46**, 121.
- Van Hook, H.J., 1963b, *J. Amer. Ceram. Soc.* **46**, 248.
- Van Santen, J.H. and G.H. Jonker, 1950, *Physica* **16**, 599.
- Van Uitert, L.G., W.H. Grodkiewicz and E.F. Dearborn, 1965, *J. Amer. Ceram. Soc.* **48**, 105.
- Van Uitert, L.G., R.C. Sherwood, E.M. Gyorgy and W.H. Grodkiewicz, 1970a, *Appl. Phys. Lett.* **16**, 84.
- Rao, C.N.R., G.V. Subba Rao and B.M. Wanklyn, 1971, *J. Phys. Chem. Solids* **32**, 345.

- Van Uitert, L.G., R.C. Sherwood, W.A. Bonner, W.H. Grodkiewicz, L. Pictroski and G. Zydzik, 1970b, *Mater. Res. Bull.* **5**, 153.
- Varma, R.K., 1960, *J. Geophys. Res.* **65**, 757.
- Veyssic, M. and B. Dreyfus, 1967, *J. Phys. Chem. Solids* **28**, 499.
- Vigneron, F., 1976, *J. Phys.*, Paris **37**, 103.
- Viskov, A.S., Yu.N. Venevtsev, G.S. Zhdanov and L.D. Onikienko, 1966, *Soviet Phys.-Crystallogr.* **10**, 720.
- Vogel, E.M. and J.W. Fleming, 1975, *J. Crystal Growth* **29**, 234.
- von Aulock, W.H. ed.; 1965, *Handbook of Microwave Ferrite Materials* (Academic Press, New York).
- Voorhoeve, R.J.H., J.P. Remeika, P.E. Freeland and B.T. Matthais, 1972, *Science* **177**, 353.
- Voorhoeve, R.J.H., J.P. Remeika and D.W. Johnson, Jr., 1973, *Science* **180**, 62.
- Voorhoeve, R.J.H., L.E. Trimble and C.P. Khattak, 1974, *Mater. Res. Bull.* **9**, 655.
- Voorhoeve, R.J.H., J.P. Remeika and L.E. Trimble, 1975a, Talk presented at Academy of Sciences, New York, to be published in *Ann. of New York Acad. Sci.* (in press).
- Voorhoeve, R.J.H., J.P. Remeika, L.E. Trimble, A.S. Cooper, F.J. Salvo and P.K. Gallagher, 1975b, *J. Solid State Chem.* **14**, 395.
- Waintal, A. and J. Chenavas, 1967, *Mater. Res. Bull.* **2**, 819.
- Waintal, A., J.J. Capponi and E.F. Bertaut, 1966, *Solid State Commun.* **4**, 125.
- Wang, F.F.Y., 1973, *Physical and Chemical Properties of Garnets in: Harman, H., ed., Treatise on Materials Science and Technology, Vol. 2* (Academic Press, New York) p. 279.
- Wanklyn, B.M., 1969, *J. Crystal Growth* **5**, 323.
- Wanklyn, B.M., 1972, *J. Mater. Sci.* **7**, 813.
- Wanklyn, B.M., D. Midgley and B.K. Tanner, 1975, *J. Crystal Growth* **29**, 281.
- Weiss, G.P. and D.O. Smith., 1962, *J. Appl. Phys.* **33**, 1166S.
- White, R.L., 1969, *J. Appl. Phys.* **40**, 1061.
- White, R.L. and T.G. Phillips, 1969, *J. Appl. Phys.* **39**, 579.
- Wold, A., B. Post and E. Banks, 1957, *J. Amer. Ceram. Soc.* **79**, 6365.
- Wold, A., R.J. Arnett and W.J. Croft, 1963, *Inorg. Chem.* **2**, 972.
- Wolf, W.P., 1957, *Phys. Rev.* **108**, 1152.
- Wolf, W.P., 1964, *Proc. Int. Conf. Magnetism*, p. 555.
- Wolf, W.P., M. Ball, M.T. Hutchings, M.J.M. Leask and A.F.G. Wyatt, 1962, *J. Phys. Soc. Japan* **17**, Suppl. B-1, 443.
- Wolfe, R., M.D. Sturge, F.R. Merritt and L.G. Van Uitert, 1971, *Phys. Rev. Lett.* **26**, 1570.
- Wolfe, R., J.C. North and Y.P. Lai, 1973, *Appl. Phys. Lett.* **22**, 683.
- Wollan, E.O. and W.C. Koehler, 1955, *Phys. Rev.* **100**, 545.
- Wood, D.L. and J.P. Remeika, 1967, *J. Appl. Phys.* **38**, 1038.
- Wood, D.L., J. Ferguson, K. Knox and J.F. Dillon, Jr., 1963, *J. Chem. Phys.* **39**, 890.
- Wood, D.L., E.D. Kolb and J.P. Remeika, 1968, *J. Appl. Phys.* **39**, 1139.
- Wood, D.L., L.M. Holmes and J.P. Remeika, 1969, *Phys. Rev.* **185**, 689.
- Wood, E.A., 1951, *Acta Crystallogr.* **4**, 353.
- Woodruff, W.O. and H. Ehrenreich, 1961, *Phys. Rev.* **123**, 1553.
- Yafet, Y. and C. Kittel, 1952, *Phys. Rev.* **87**, 290.
- Yakel, Jr., H.L., 1955, *Acta Crystallogr.* **8**, 394.
- Yakel, H.L., W.C. Koehler, E.F. Bertaut and E.F. Forrat, 1963, *Acta Crystallogr.* **16**, 957.
- Yamaguchi, T., 1974, *J. Phys. Chem. Solids* **35**, 479.
- Yamaguchi, T. and K. Tsushima, 1973, *Phys. Rev.* **B8**, 5187.
- Yoshida, K. and M. Tachiki, 1957, *Progr. Theor. Phys.* **17**, 331.
- Zeyfang, R., 1970, *J. Appl. Phys.* **41**, 3718.
- Zonn, Z.N., 1965, *Inorganic Mater.* **1**, 1034.
- Zonn, Z.N. and V.A. Joffe, 1968, *Growth of Crystals* **6A**, 112.

Warshaw, I. and R. Roy, 1959, J. Am. Ceram. Soc. 42, 434.

Chapter 30

RARE EARTH MOLYBDATES (VI)

L.H. BRIXNER and J.R. BARKLEY

Central Research and Development Department, E.I. Dupont de Nemours
 & Co., Wilmington, Delaware 19898, USA

W. JEITSCHKO

Institut für Anorganische und Analytische Chemie, Justus-Liebig Universität,
 Giessen, F.R. Germany

Contents

1. Chemistry and crystal growth	610
1.1. Introduction	610
1.2. The R_2O_3 - MoO_3 phase diagram	610
2. Crystal chemistry, phase transitions and crystallographic aspects	624
2.1. Composition $R_2(MoO_4)_3$	624
2.2. Crystal structures of other R molybdates	632
3. Physical properties	633
3.1. General	633
3.2. Electrical properties	636
3.3. Elastic	639
3.4. Optical	642
3.5. Magnetic	645
3.6. Domain walls	645
3.7. Crystal defects	650
References	652

Symbols

R = Rare earth atom
 β = Phase of a particular structure type

Φ = Vacant A sites
 α = Phase of a particular structure type
 β' = Phase of a particular structure type
 γ = Phase of a particular structure type
 π = Amorphous phase
 T_C = Curie temperature
 P_s = Polarization
 C_{66}^E = Elastic constant
 ω_M = Frequency
 χ_{12} = Shear strain
 χ_s = Spontaneous shear strain
 E_0 = Threshold field
 τ_0 = Critical threshold stress
 d_{31} = Piezoelectric constant
 k_3 = Electromechanical coupling coefficient
 Δn_{ab} = Refractive index change
 p_{66} = Photoelastic constants
 λ = Wavelength
 μ_B = Magnetic moments
 v = Wall velocity
 μ_τ = Wall mobility
 μ_E = Wall mobility
 τ_0 = Threshold stress

1. Chemistry and crystal growth (L.H. Brixner)

1.1. Introduction

Although the rare earths as such, particularly in the form of their oxides, were known since as early as the late 18th century, it was not until over 100 years later when the first molybdates of these elements were described by Hitchcock (1895). Specifically he prepared such compounds as $\text{Nd}_2(\text{MoO}_4)_3$ or $\text{Nd}_2\text{O}_3 \cdot 3\text{MoO}_3$, which represents one of the more important stoichiometries of rare earth molybdates. Very few, if any, publications appeared in the literature thereafter until Borchardt and Bierstedt (1966) prepared certain members of the $\text{R}_2(\text{MoO}_4)_3$ series in the orthorhombic form and recognized they were ferroelectric. This finding sparked considerable interest in these compounds and practically all important preparative, structural and physical studies on the $\text{R}_2(\text{MoO}_4)_3$ compositions were conducted in the past ten years. In addition to the two most common types of rare earth molybdates, R_2MoO_6 and $\text{R}_2(\text{MoO}_4)_3$ (Megumi et al., 1974) described $\text{R}_2\text{Mo}_4\text{O}_{15}$ and $\text{R}_2\text{Mo}_6\text{O}_{21}$ compounds. The physical properties of these materials are less interesting and will only be discussed in context with the $\text{R}_2\text{O}_3/\text{MoO}_3$ phase equilibrium. In their phase diagram (Megumi et al., 1974) did not include the R_6MoO_6 composition, which was prepared by McCarthy (1974). Since this compound has a fluoride structure whose X-ray pattern closely resembles that of C-type Gd_2O_3 , one can easily miss this composition on the Gd-rich side of the phase diagram. Finally, molybdates with the rare earth in unusual valence states such as the scheelite type EuMoO_4 with divalent europium were described by McCarthy (1971).

1.2. The $\text{R}_2\text{O}_3\text{-MoO}_3$ phase diagram

The phase equilibria are discussed for the $\text{Gd}_2\text{O}_3/\text{MoO}_3$ case according to Megumi et al. (1974). With 7f electrons, Gd represents the center of the rare earth series and should be fairly representative, although deviations due to changes in cohesive energy and ionic radius can be expected on either side of the $\text{Gd}_2\text{O}_3/\text{MoO}_3$ system.

Starting with the MoO_3 rich side, we first have the compound $\text{Gd}_2\text{O}_3 \cdot 6\text{MoO}_3$, whose structure is not known. The next compound is $\text{Gd}_2\text{O}_3 \cdot 4\text{MoO}_3$ which also has not yet been characterized structurally. This part of the phase diagram, from 0 to 25 mole% Gd_2O_3 , is summarized in fig. 30.1. The balance of the phase diagram showing the $\text{Gd}_2\text{O}_3 \cdot 3\text{MoO}_3$ and $\text{Gd}_2\text{O}_3 \cdot \text{MoO}_3$ phases is represented in fig. 30.2. As indicated in the previous section, the composition Gd_6MoO_6 should be added to complete the phase diagram.

One can see that this part of the phase diagram is considerably simpler than the MoO_3 rich side. It shows the two congruently melting compounds, $\text{Gd}_2\text{O}_3 \cdot 3\text{MoO}_3$ and $\text{Gd}_2\text{O}_3 \cdot \text{MoO}_3$. Perhaps the most important feature established by Megumi et al. (1974) is the fact that there is essentially no phase width for $\text{Gd}_2\text{O}_3 \cdot 3\text{MoO}_3$ and only the precisely stoichiometric compound exists, a fact rather significant for single crystal growth.

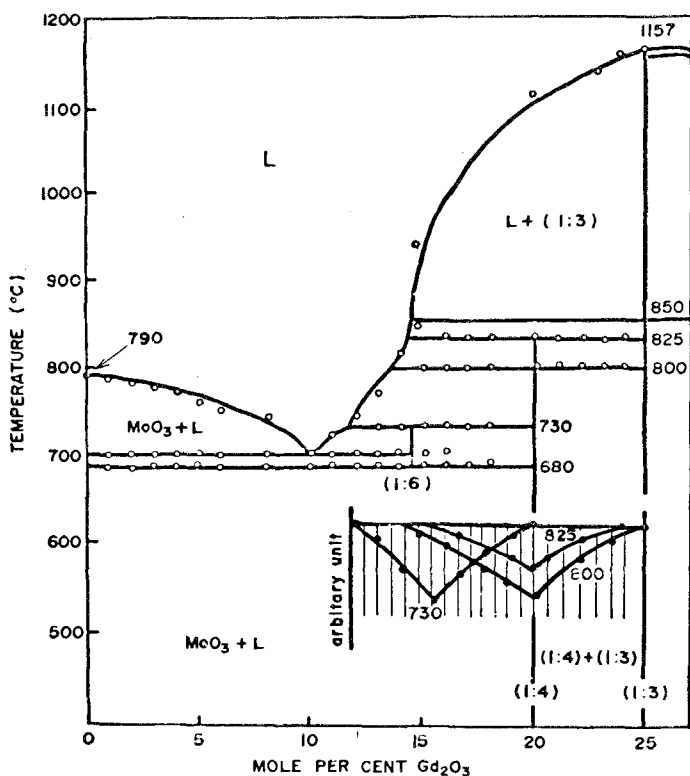


Fig. 30.1. Equilibrium diagram of the region 0–25 mole % Gd_2O_3 ; \circ DTA measured liquidus and solidus temperature, \bullet DTA halt maxima of the reactions at 730°C, 800°C and 825°C, plotted vs. composition.

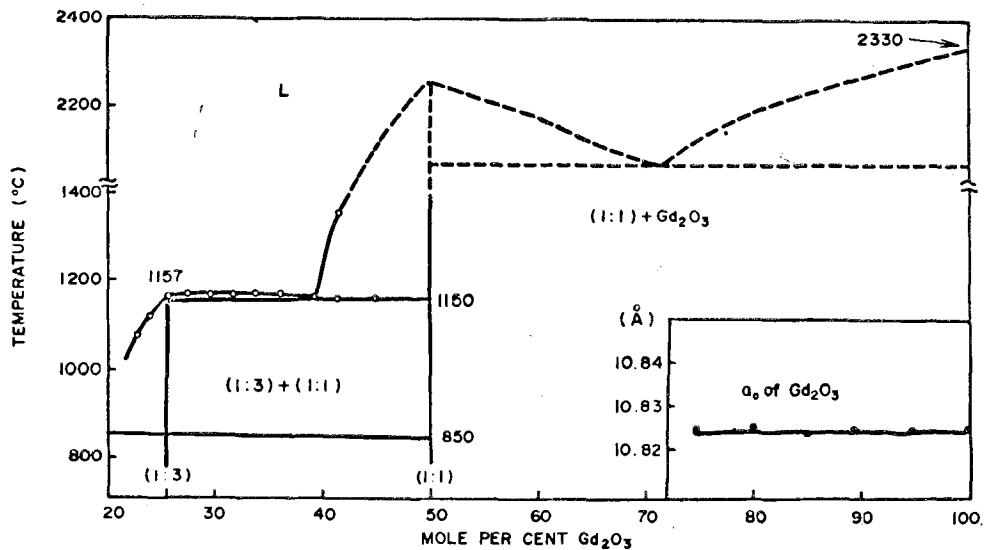


Fig. 30.2. High-temperature equilibrium diagram of the region 25–100 mole % Gd_2O_3 ; \circ DTA measured liquidus, \bullet lattice constants of Gd_2O_3 vs. composition.

TABLE 30.1.
X-ray diffraction data for $Gd_2O_3 \cdot 6MoO_3$ and $Gd_2O_3 \cdot 4MoO_3$.

$Gd_2O_3 \cdot 6MoO_3$		$Gd_2O_3 \cdot 4MoO_3$		$Gd_2O_3 \cdot 6MoO_3$		$Gd_2O_3 \cdot 4MoO_3$	
$d(\text{\AA})$	I	$d(\text{\AA})$	I	$d(\text{\AA})$	I	$d(\text{\AA})$	I
5.477	7	5.824	30	3.731	9	3.437	42
5.333	20	5.384	8	3.696	11	3.321	81
4.818	100	5.242	30	3.567	52	3.282	100
4.729	21	5.035	8	3.526	27	3.211	50
4.548	10	4.436	42	3.364	27	3.184	50
4.215	25	4.149	16	3.331	31	3.097	52
4.101	28	4.001	33	2.929	11	3.025	49
3.953	16	3.743	34	2.891	10	2.928	24
3.899	9	3.616	83	2.852	11	2.744	22
3.839	18	3.587	7	2.829	14	2.720	32

1.2.1. $Gd_2O_3 \cdot 6MoO_3$

Very little is known about this compound beyond the data given by Megumi et al. (1974). They did observe some single crystals in samples annealed at 720°C and then quenched to room temperature. Megumi et al. (1974) assume the structure to be orthorhombic and for identification purposes, their d -values are given in table 30.1.

1.2.2. $Gd_2O_3 \cdot 4MoO_3$

As with the previous compound, almost nothing is known about this composition. Its d -values are listed in table 30.1 together with $Gd_2O_3 \cdot 6MoO_3$.

1.2.3. $R_2O_3 \cdot 3MoO_3$

The molybdates of the rare earths formulated $R_2(MoO_4)_3$ are most important and are known for all R's as well as Y and Sc. They are discussed here in greatest detail. Because of the closely related electronic structures and the small variations in ionic size, most rare earth oxo-metallates such as the niobates $RNbO_4$ (Keller, 1962), the vanadates RVO_4 (Brixner and Abramson, 1965), the stannates $R_2Sn_2O_7$ (Whinfrey et al., 1960), and the titanates $R_2Ti_2O_7$ (Brixner, 1964) exhibit only one prototype structure at room temperature; however, the $R_2(MoO_4)_3$ -type molybdates crystallize in four different structural arrangements. If one includes the temperature-dependent polymorphic modifications and thermodynamically metastable compositions, no less than eight different structures are known to exist for these compounds between room temperature and their respective melting points. This is indeed a fascinating body of rare earth compounds, unique in the protean display of structures as well as physical properties.

Starting with $\text{La}_2(\text{MoO}_4)_3$, we have two structures between the melting point and room temperature. When grown from the melt, the compound crystallizes in the space group $I4_1/a$ of an undistorted scheelite with the parameters listed in table 30.2. This structure can be frozen in, therefore suggesting that the phase transition at 848°C is sluggish and diffusion controlled. The fact that β - $\text{La}_2(\text{MoO}_4)_3$ crystallizes in a scheelite structure indicates that a better formulation for this compound might be $\text{La}_{2/3}\Phi_{1/3}\text{MoO}_4$ to show the relationship to the common ABO_4 -type scheelite where A normally is a bivalent ion such as in CaWO_4 .

Valence compensation in the lanthanum molybdate scheelite is achieved through $\frac{1}{3}$ vacancies in the A sites (indicated as Φ). In fact, it is the ordering of these

TABLE 30.2.

Lattice parameters, space groups, transition temperatures, and melting points of the $\text{R}_2(\text{MoO}_4)_3$ -type rare earth molybdates.

R	Form	$T(^{\circ}\text{C})$	m.p. ($^{\circ}\text{C}$)	$a(\text{\AA})$	$b(\text{\AA})$	$c(\text{\AA})$	$\beta(\text{deg})$	Space group
La	α	848	—	17.006	11.952	16.093	108.44	$C2/c$
	β	—	1024	5.365	—	11.945	—	$I4_1/a$
Ce	—	None	1035	16.902	11.842	15.984	108.58	$C2/c$
Pr	α	987 to β	1045	16.849	11.778	15.914	108.50	$C2/c$
	β	—	—	7.444	—	10.901	—	$P\bar{4}_2/m$
	β'	235 to β	—	10.526	10.578	10.901	—	$Pba2$
Nd	α	961 to β	1081	16.788	11.719	15.849	108.54	$C2/c$
	β	—	—	7.423	—	10.854	—	$P\bar{4}_2/m$
	β'	225 to β	—	10.497	10.543	10.854	—	$Pba2$
Sm	α	910 to β	1122	7.562	11.509	11.557	108.98	$C2/c$
	β	—	—	7.380	—	10.769	—	$P\bar{4}_2/m$
	β'	197 to β	—	10.435	10.472	10.769	—	$Pba2$
Eu	α	881 to β	1144	7.554	11.459	11.497	109.08	$C2/c$
	β	—	—	7.363	—	10.727	—	$P\bar{4}_2/m$
	β'	180 to β	—	10.411	10.444	10.727	—	$Pba2$
Gd	α	857 to β	1171	7.575	11.436	11.424	109.28	$C2/c$
	β	—	—	7.347	—	10.701	—	$P\bar{4}_2/m$
	β'	159 to β	—	10.388	10.419	10.701	—	$Pba2$
Tb	α	835 to β	1172	7.529	11.379	11.401	109.21	$C2/c$
	β	—	—	7.321	—	10.653	—	$P\bar{4}_2/m$
	β'	160 to β'	—	10.352	10.381	10.653	—	$Pba2$
Dy	α	805 to β	1222	7.514	11.344	11.364	109.31	$C2/c$
	β	1030 to γ	—	7.303	—	10.615	—	$P\bar{4}_2/m$
	β'	145 to β	—	10.327	10.351	10.615	—	$Pba2$
	γ	—	—	6.69	—	—	—	Cubic
Ho	β	853 to γ	1245	7.287	—	10.578	—	$P\bar{4}_2/m$
	β'	121 to β	—	10.304	10.324	10.578	—	$Pba2$
	γ	—	—	9.921	13.656	9.867	—	$Pnca$
Er	α	None	1320	9.936	13.515	9.827	—	$Pnca$
Tm	α	None	1390	9.909	13.445	9.782	—	$Pnca$
Yb	α	None	1421	9.864	13.411	9.759	—	$Pnca$
Lu	α	None	1445	9.828	13.389	9.734	—	$Pnca$

vacancies which is responsible for the structural transition into a monoclinic distortion at lower temperatures and we thus have an order-disorder transition at 848°C. For $Ce_2(MoO_4)_3$ the disordered scheelite was not observed, although we expect it to be thermodynamically stable at high temperature. Lattice parameters and melting point for $Ce_2(MoO_4)_3$ are also given in table 30.2. With $Pr_2(MoO_4)_3$, we begin the most interesting region of the rare earth molybdates not only because of the structural complexity but mainly because the next eight rare earth compounds (excluding Pm) exhibit the phenomena of ferroelectricity and ferroelasticity discussed in section 3.3. β - $Pr_2(MoO_4)_3$ melts congruently at 1045°C and has a phase transformation at 987°C. It is only within this narrow temperature range of 58°C that the tetragonal structure, space group $P\bar{4}2_1m$ is thermodynamically stable. However, the transformation is sluggish and diffusion controlled and therefore the high-temperature phase can be quenched in. As we can see in table 30.2 and fig. 30.3, this transformation temperature decreases as one proceeds to the smaller rare earth ions. Obviously the kinetics for the

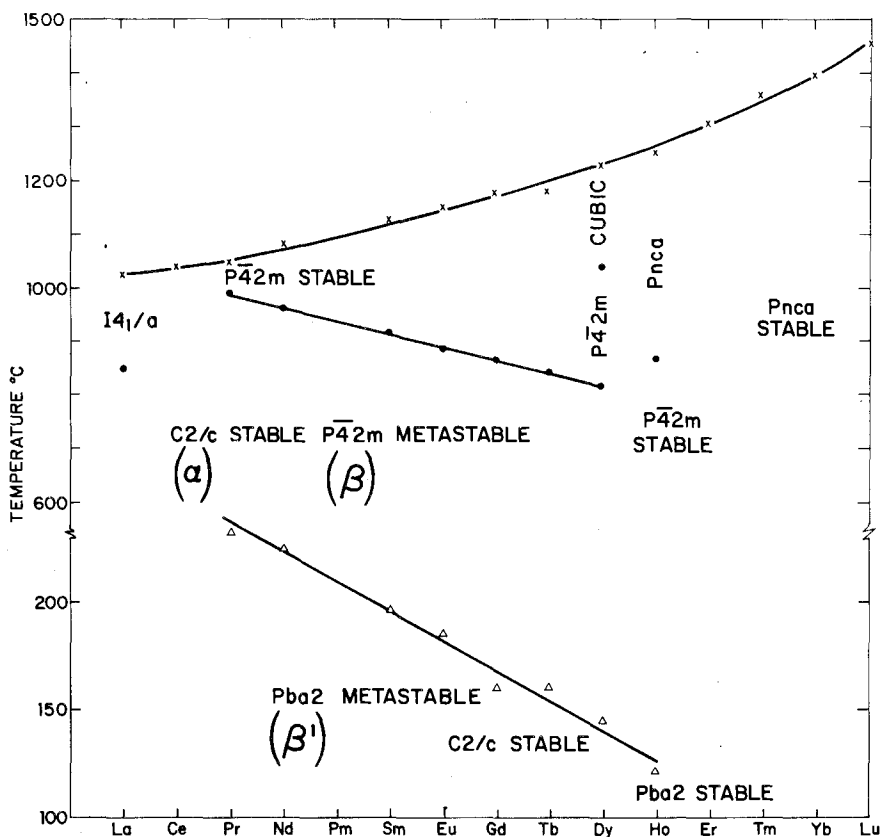


Fig. 30.3. Phase relationships of the $R_2(MoO_4)_3$ -type rare earth molybdates.

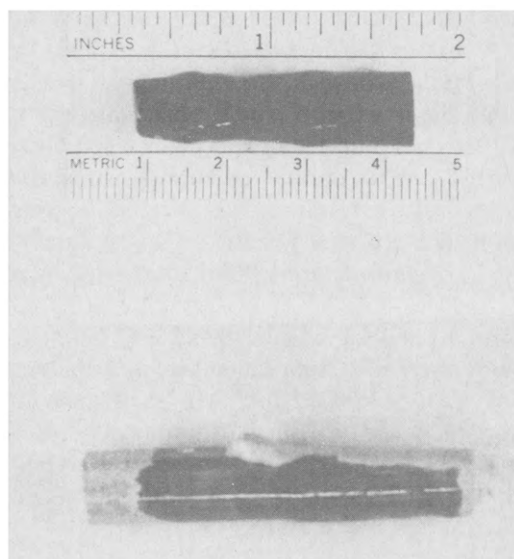


Fig. 30.4. $\text{Nd}_2(\text{MoO}_4)_3$ (top) and $\text{Pr}_2(\text{MoO}_4)_3$ crystals.

transformation to the thermodynamically stable low-temperature α structure are more favorable at the higher transformation temperature, and we believe that this is the reason why $\text{Pr}_2(\text{MoO}_4)_3$ and $\text{Nd}_2(\text{MoO}_4)_3$ have only recently been added to the list of ferroelectric rare earth molybdates by Brixner et al. (1971). To exemplify the difficulties with the α/β transformation for $\text{Pr}_2(\text{MoO}_4)_3$, we show in fig. 30.4 a typical crystal exhibiting some α phase despite rapid quenching. It is contrasted with a single crystal of $\text{Nd}_2(\text{MoO}_4)_3$ where the retention of essentially all β structure is possible. Structurally this noncentric $\bar{4}2m$ type is of great importance as it constitutes the parent phase from which all eight ferroelectric molybdates are derived. The high (β) and low (β') temperature phases of these structures are discussed in section 2. If the thermodynamically metastable β - $\text{Pr}_2(\text{MoO}_4)_3$ is further cooled below 987 to 225°C, it undergoes a second transformation leading to the lower symmetry ferroelastic-ferroelectric orthorhombic $\text{Pba}2$ structure. This structure is, of course, still thermodynamically metastable. Since it is derived from the high-temperature β structure, this type is designated as β' . This sequence of transformations from the stable high-temperature β structure to the metastable β and β' forms is the same for the next five rare earth ions and will therefore not be discussed again. The phase relationships with regard to temperature can best be seen in fig. 30.3. The reason for the increase in melting points of these compounds is the decrease in cell volume giving rise to increased cohesive energy. The thermodynamically stable, high-density, low-temperature α form of $\text{Pr}_2(\text{MoO}_4)_3$ is still isostructural with that of α - $\text{La}_2(\text{MoO}_4)_3$ which has already been discussed. Except for different melting and transformation temperatures, which can be obtained from fig. 30.3 and table 30.2, everything stated about $\text{Pr}_2(\text{MoO}_4)_3$ is

TABLE 30.3.
 X-ray powder pattern for α -Gd₂(MoO₄)₃.

<i>h</i>	<i>k</i>	<i>l</i>	<i>d</i> _{obs}	<i>d</i> _{calc}	<i>I</i> _{obs}	<i>I</i> _{calc}	<i>h</i>	<i>k</i>	<i>l</i>	<i>d</i> _{obs}	<i>d</i> _{calc}	<i>I</i> _{obs}	<i>I</i> _{calc}
1	1	0	6.047	{6.063}	26	{10	1	1	3	-	2.770	-	<1
1	2	-1		{6.059}		{15	1	1	-4				
0	2	0	5.705	5.718	2	2	0	4	1	-	2.764	-	<1
0	0	2	5.384	5.391	19	22	2	2	1	2.723	{2.726}	8	{6
0	2	1	5.045	5.052	18	16	2	2	-3		{2.723}		{3
1	1	1	4.741	{4.747}	8	{<1	0	0	4	-	2.696	-	<1
1	1	-2		{4.742}		{1	1	3	2				
0	2	2	-	3.923	-	1	1	3	-3	2.673	{2.672}	7	{6
2	0	0	3.562	{3.575}	36	{2	2	0	2		2.608		2.609
2	0	-2		{3.572}		{6	2	0	-4	2.605	2.605	14	15
1	1	2		{3.564}		{17	0	4	-2	2.526	2.526	3	3
1	1	-3		{3.560}		{17	3	1	-1	2.447	{2.450}	1	{1
1	3	0		{3.364}		{5	3	1	-2		{2.449}		{<1
1	3	-1	3.361	{3.363}	5	1	0	2	4	-	2.438	-	<1
2	2	-1	3.158	3.158	100	100	2	2	2	-	2.374	-	<1
1	3	1	3.074	{3.070}	7	{<1	2	2	-4	-	2.371	-	<1
1	3	-2		{3.077}		{<1	3	1	0				
0	2	3	3.043	3.043	84	79	3	1	-3	2.333	{2.331}	2	{<1
2	2	0	-	3.031	-	<1	1	3	3		{2.285}		2
2	2	-2	-	3.029	-	<1	1	3	-4	2.281	{2.284}	2	
0	4	0	2.858	2.859	27	27	2	4	-1		{2.282}		{<1

true also for Nd₂(MoO₄)₃. While the high-temperature structure stays the same for Sm₂(MoO₄)₃, we now have a new structure for the α form. This phase is isostructural with Eu₂(WO₄)₃ for which the complete structure has been determined by Templeton and Zalkin (1963). To demonstrate this relationship, intensity calculations were carried out for α -Gd₂(MoO₄)₃ using the published positional parameters of Eu₂(WO₄)₃. The good agreement between the calculated intensities and the powder intensities is indicated in table 30.3. The density of α -Sm₂(MoO₄)₃ is 5.450 g/ml⁻¹ and that of β' -Sm₂(MoO₄)₃ is 4.405 g/ml⁻¹. This density difference is unusually large, reaching almost 25%. It suggests that the β' -structure is rather open and the application of pressure may cause it to collapse. A pressure experiment showed that the $\beta \rightarrow \alpha$ transformation for Gd₂(MoO₄)₃ occurs some 300°C below the ambient transformation point of 855°C. Application of higher pressures and lower temperatures finally led to yet another structural modification called π -GMO[Gd₂(MoO₄)₃]. This form of Gd₂(MoO₄)₃ is amorphous, and experimental details have been given by Brixner (1972). The β' structure collapses under the influence of high pressure, but a complete structural rearrangement is impossible because of the slow kinetics at room temperature resulting in an amorphous structural disarray intermediate between the α and β' structures. The effect of hydrostatic pressure on the β'/β phase transition has been studied by Shirokov et al. (1972). These authors find that as little as 3 kbar raise the Curie temperature from 160°C to almost 240°C.

TABLE 30.4.
X-ray diffraction data for $Gd_2O_3 \cdot 3MoO_3$.

<i>I</i>	<i>d</i> (Å)	<i>I</i>	<i>d</i> (Å)
30	10.699	100	3.478
60	6.059	100	3.293
80	5.349	100	3.284
20	5.207	30	3.209
90	4.679	100	3.031
20	4.326	95	2.941
5	4.269	90	2.804
100	3.729	80	2.799
100	3.677	20	2.674
90	3.566		

In connection with this change of transition temperature via pressure, it is also interesting to refer to the work by Dem'yanov and Shchedrin (1973) who found that neutron irradiation can raise the β'/β phase transition by as much as 200 K permanently. $Eu_2(MoO_4)_3$, $Gd_2(MoO_4)_3$ and $Tb_2(MoO_4)_3$ exhibit exactly the same structural transformations as did $Sm_2(MoO_4)_3$ and detailed numbers can again be extracted from table 30.2 and fig. 30.3. For purposes of identification, the first 19 lines of the β' - $Gd_2(MoO_4)_3$ X-ray diagram are given in table 30.4. Recently, Naussau et al. (1971) mentioned yet another structural modification of Eu, Gd, Tb and Dy-molybdate called γ -phase. We have also observed such a phase for $Tb_2(MoO_4)_3$ but obtained it only upon crystallization from a super-cooled melt and never upon heating of the β phase to the melting point. We therefore believe this to be yet another metastable phase. It appears to be of cubic symmetry. If one looks at the phase relationship diagram in fig. 30.3 and the lattice parameters in table 30.2, it would appear that $Dy_2(MoO_4)_3$ is the easiest compound to grow since its β/α transformation is the lowest and its orthorhombic distortion ($b - a$) the least. And yet $Dy_2(MoO_4)_3$ cannot be obtained as a sound single crystalline boule at all. The reason for this is yet another phase transformation at 1030°C which is disruptive. This means that the volume change associated with the structural transition is so large that the boule will invariably break up. We succeeded in freezing in this δ -phase and tentatively identified it as cubic with a cell edge of 6.96 Å. After this experience, we set out to establish the material which exhibits the lowest β/α transformation and the least $b - a$ distortion which can be grown without this disruptive phase transition. This information is summarized in table 30.5. One can see that as little as 3 Å³ in cell size or 0.001 Å difference in ionic radius determines whether a transition occurs or not. Although not precisely at this transition point, the compound $GdDy(MoO_4)_3$ does grow with greatest ease and has been obtained free of any α phase and thus not exhibiting any laser light scattering. Such a crystal is shown in figs. 30.5 and 30.6. $Ho_2(MoO_4)_3$ constitutes yet another special case. Contrary to Nassau (1971), we were unable to produce an α phase of
et. al.

TABLE 30.5.
Lattice parameters and β/δ transition temperature for some Pba2-type solid solutions.

Composition	$a(\text{\AA})$	$b(\text{\AA})$	$c(\text{\AA})$	$V(\text{\AA}^3)$	$IR(\text{\AA})$	$T_{\beta/\delta}$ ($^{\circ}\text{C}$)	Sound boule
$\text{Dy}_2(\text{MoO}_4)_3$	10.3271	10.3513	10.6145	1134.68	0.912	1030	No
$\text{DyTb}(\text{MoO}_4)_3$	10.3374	10.3631	10.6339	1139.18	0.918	1114	No
$\text{Dy}_{1.4}\text{Gd}_{0.6}(\text{MoO}_4)_3$	10.3377	10.3628	10.6303	1138.79	0.920	1143	No
$\text{Dy}_{0.4}\text{Tb}_{1.6}(\text{MoO}_4)_3$	10.3457	10.3738	10.6460	1142.57	0.921	No	Yes
$\text{Dy}_{1.2}\text{Gd}_{0.3}(\text{MoO}_4)_3$	10.3490	10.3749	10.6433	1142.78	0.922	No	Yes
$\text{DyGd}(\text{MoO}_4)_3$	10.3582	10.3837	10.6564	1146.16	0.925	No	Yes

$\text{Ho}_2(\text{MoO}_4)_3$ at all, and we believe the β' and β structures to be the only thermodynamically stable ones of all the ferroelectric rare earth molybdates. But a new structural complication enters the picture: $\gamma\text{-Ho}_2(\text{MoO}_4)_3$. This structure is orthorhombic, space group Pnca and has been determined by Abrahams (1966) for $\text{Sc}_2(\text{WO}_4)_3$. The transition from β to $\gamma\text{-Ho}_2(\text{MoO}_4)_3$ at 853°C is again disruptive, and no sound boules of β or $\beta'\text{-Ho}_2(\text{MoO}_4)_3$ can be obtained. In addition to this problem, $\text{Ho}_2(\text{MoO}_4)_3$ tends to hydrate at room temperature causing further difficulties. The remaining rare earth molybdates of Er, Tm, Yb and Lu also form hydrates and crystallize only in the Pnca structure without any phase transitions. We have determined their cell dimensions but only in the case of $\text{Lu}_2(\text{MoO}_4)_3$ was this done on a pure single crystal which gave no additional diffraction lines outside the Pnca structure. The other compounds did contain small quantities of the hydrate, and the lattice parameters therefore have to be taken with some reservations. The cell volumes as a function of the best reported ionic radii by Shannon and Prewitt (1969) for the ferroelectric Pba2 compositions are shown in fig. 30.7. In order to get a perfect straight-line relationship, the ionic radius for Pr^{+3} in eight-fold coordination had to be corrected from 0.997 to 0.991 \AA .

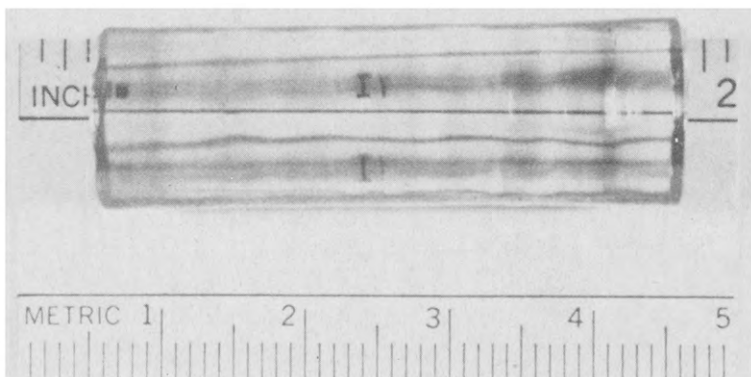


Fig. 30.5. $\text{GdDy}(\text{MoO}_4)_3$ single crystal viewed sideways.

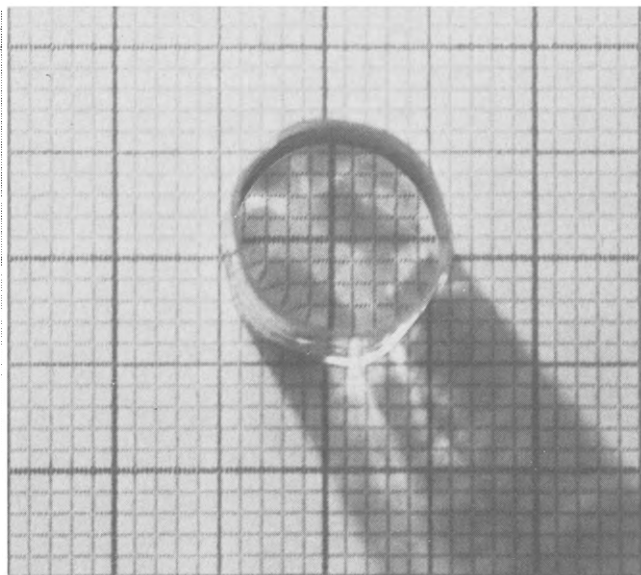


Fig. 30.6. $\text{GdDy}(\text{MoO}_4)_3$ single crystal viewed along growth axis.

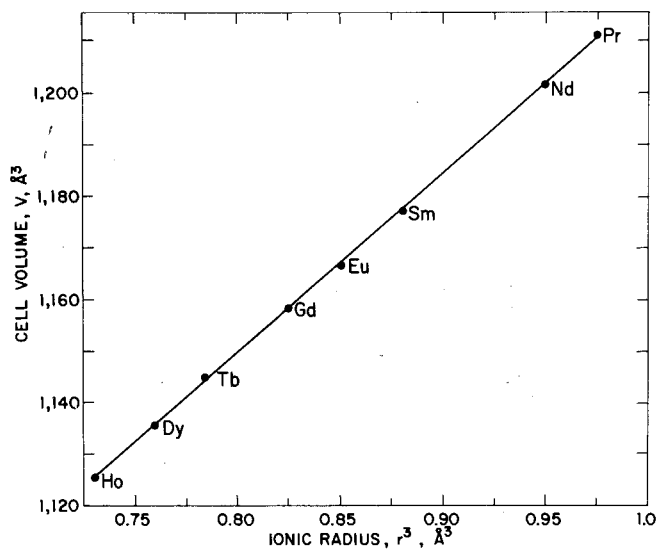


Fig. 30.7. r^3 vs. cell volume for the ferroelectric β' -type $\text{R}_2(\text{MoO}_4)_3$ molybdates.

1.2.3.1. *Single crystal growth of $R_2O_3 \cdot 3MoO_3$ compounds*

Since other species, such as, for instance, the Ln_2MoO_6 compounds exist in the Ln_2O_3 - MoO_3 phase diagram, extreme care must be taken in preparing feed material of high purity and precise stoichiometry. In a solid state reaction where one component sublimates at 770°C and the other melts above 2000°C , this is not easy. The constituent components were the rare earth oxides of at least 99.99% purity obtained from the Kerr-McGee Company, and Climax Molybdenum Co. Ammonium molybdate $(NH_4)_6Mo_7O_{24} \cdot 4H_2O$ was used as a precursor for high purity MoO_3 . The rare earth oxides were fired at 1000°C in air or oxygen for at least 5 to 8 h to ensure the removal of all volatile matter such as H_2O , CO_2 , etc. They were subsequently kept in the desiccator. MoO_3 was prepared by first heating the ammonium salt to 300°C for 10 to 14 h, subsequently raising the temperature to 600°C for another 10 to 14 h. This procedure yielded a highly crystalline pale-yellow MoO_3 . The constituent components were weighed to the nearest mg, mixed for at least 30 min on a "WIG-L-BUG", and fired at 600°C for 10-14 h. After the mixture was ground and refired 1 to 2 h at 600°C , the temperature was raised to 900°C for 2-4 h. Any weight loss occurring during the firing operations was carefully made up with MoO_3 . All colorless rare earth oxides yielded pure-white powders of the corresponding molybdates.

Single crystals were grown by the Czochralski technique, using a 20 kVA "Ecco" high frequency generator as a power source. The working coil was 3 inch OD 8 turns fabricated from flattened $\frac{1}{4}$ inch Cu tubing. The crucible was of 60 mil thick iridium $1\frac{1}{2}$ inch high and $1\frac{1}{2}$ inch wide. Typical growth rates for approximately $\frac{1}{2}$ inch diameter crystals were 0.5 to 0.8 cm/h. Seed rotational speeds varied from 80 to 120 rpm.

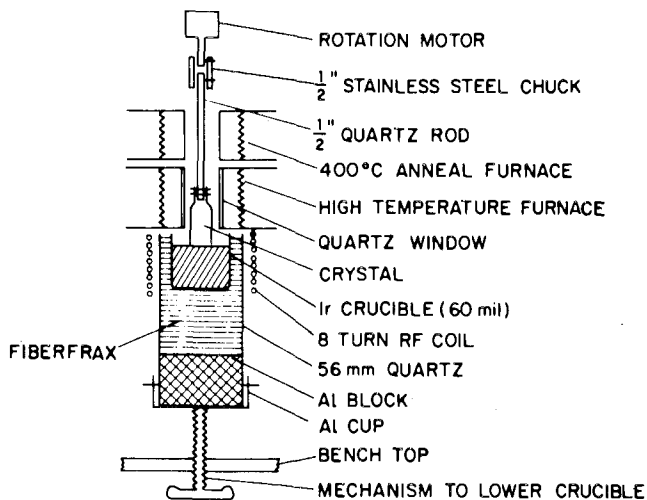


Fig. 30.8. Set-up for Czochralski growth of $R_2(MoO_4)_3$ single crystals.

A problem commonly encountered during growth of these crystals is expansion of the melt upon freezing, which severely distorts the container and often renders it useless after only a few runs. This can be greatly minimized by providing a mechanism which permits the melt to directionally freeze at the end of a run. As can be seen in fig. 30.8, a feed screw lowers the crucible in such a position that the top of the melt is hot while the bottom freezes. There is still slight bulging towards the sides but as many as 50 crystal growth runs could be carried out in the same container without excessive distortion of the crucible if this was done. Repeated melting and freezing during the initial charging of the container is also eliminated if a large quartz funnel is used to continuously feed the powder to the melt until the proper level is obtained. As some of the high-temperature structures (e.g. Pr and Nd) are only stable in a very narrow temperature range, crystal growth had to be carried out in the presence of an afterheater held at the right temperature. This is schematically shown in fig. 30.8. The purpose of the second heater is to allow rapid quenching of the crystal to about 400°C and slow cooling from there. $\text{Lu}_2(\text{MoO}_4)_3$ melted at approximately 1450°C and crystal growth was carried out under 200 psi argon pressure. This greatly reduced but did not eliminate completely the significant vaporization of MoO_3 observed under ambient conditions. MoO_3 losses start becoming noticeable with the Ho compound.

$\text{Gd}_2(\text{MoO}_4)_3$ was most extensively studied. With a melting point of 1171°C and a β/α transformation temperature of 857°C, we have a reasonably broad stability range of 314°C and $\text{Gd}_2\text{O}_3 \cdot 3\text{MoO}_3$ crystals can be grown without an afterheater. However, such crystals will contain small uniformly distributed quantities of α phase giving rise to strong nonspecular scatter of a laser beam passed through the crystal. This type of defect was termed "dispersed inclusions" by Borchardt (1968). Another serious problem, called "axial inclusions" or "feathers" by Borchardt (1968) has also been quantitatively characterized. These defects are Gd_2MoO_6 as first evidenced by a microprobe traverse across such an inclusion. The relative shifts of the Gd and Mo concentrations come close to the calculated amounts for the differences in $\text{Gd}_2(\text{MoO}_4)_3$ and Gd_2MoO_6 . Later on we also succeeded in characterizing this inclusion by X-rays as Gd_2MoO_6 . Its elimination requires the establishment of a flat temperature profile at the crystal/liquid interface. This is achievable in the range of 80 to 120 rpm rotation of the crystal. One other problem is inclusion of metallic particles giving rise to strong specular scatter of a laser beam passed through the crystal. This is observed when either Pt or Pt/Rh containers are used. Epstein (1970) did observe such inclusions and assumed them to be Pt. An electron microprobe analysis of a thin single crystalline slice containing such particles clearly characterized them as metallic Pt as can be seen in fig. 30.9. The use of Ir containers eliminates this problem as neither Ir nor IrO_2 appears soluble in detectable quantities in the melt. We have grown $\text{Gd}_2(\text{MoO}_4)_3$ on [100], [001] and [110] oriented seeds, obtaining the best results with the latter orientation. This is probably due to the fact that the domain walls entering the crystal on cooling through the Curie temperature at 159°C come in along the boule axis, thereby causing the least amount of stress which can give rise to cracking of boules.

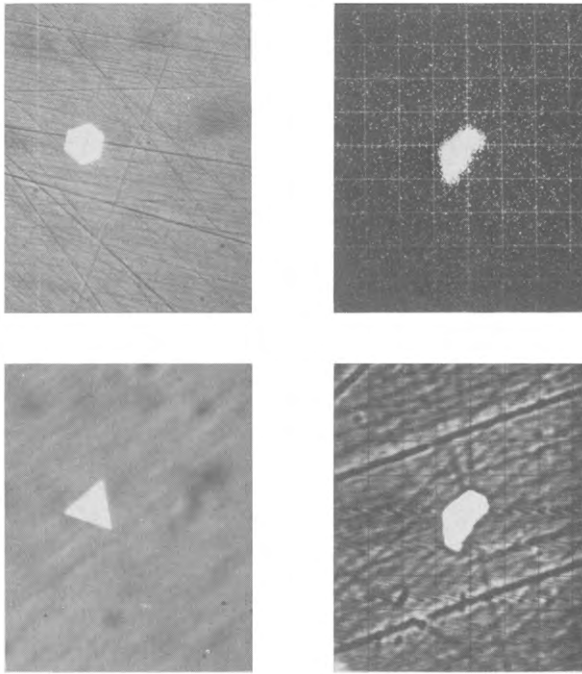


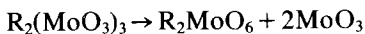
Fig. 30.9. Pt inclusions in $Gd_2(MoO_4)_3$. Left: optical micrographs. Right: top, Pt electron image; bottom: Pt X-ray image.

Combining all this information for the growth of high quality $Gd_2(MoO_4)_3$, the following is suggested.

- (1) Prepare quality feed from high purity constituent components. For ultra-high quality, it will further help to use previously grown and thereby purified material.
- (2) Grow on [110] seed from $1\frac{1}{2}$ " diameter Ir pot at speeds not exceeding 0.8 cm/h and a rotation rate of the crystal of 100 rpm.
- (3) Keep crystal diameter under $\frac{1}{2}$ inch and above β/α transition throughout growth process; subsequently quench rapidly to 400°C.
- (4) Cool at 40°C/h or less with a slight temperature gradient from top to bottom of crystals, so walls will enter in the same way.

1.2.4. The $R_2O_3 \cdot MoO_3$ compounds

As became apparent through the discussion of the metastability of the ferroelectric parent phase, crystal growth of these materials does pose very specific problems. In addition to the possible inclusion of α phase, one must also be concerned about precise stoichiometry. Specific problems are the R_2MoO_6 -type compounds which are related to the previously discussed materials via the equation



The first R_2MeO_6 -type compound where $Me = W$ and $R = Yb$ was probably synthesized by Cleve (1902) and the first molybdate (La_2MoO_6) by Sillen (1943).

According to Sillen (1943), the structure of La_2MoO_6 can best be described as consisting of La_2O_2 and MoO_4 layers. An La_2O_2 layer has in its center a flat square oxygen network in whose interstices the La ions alternately occupy one or the other side. Thus, it is the same arrangement which has been reported for oxyhalides such as LaOCl and LaOBr . The space group is $\bar{I}42m$, constituting noncentric symmetry similar to the β structure of the ferroelectric $\text{R}_2(\text{MoO}_4)_3$ compounds. Ce_2MoO_6 , first reported by Brixner et al. (1972), constitutes an exception in the series of tetragonal R_2MoO_6 compounds. We chose to prepare it by a symproportionation according to



in sealed quartz ampoules. The compound is black, semiconducting, and of different structure than La_2MoO_6 . It crystallizes in a cubic symmetry similar to CaF_2 , suggesting that all R_2MoO_6 compounds may be derived from this prototype by way of ordering and distortion with the three metal ions distributed over the Ca sites and the oxygens in the F position. The fact that Ce_2MoO_6 is the only R_2MoO_6 -type molybdate which is not an insulator suggests that one has a distribution of variable valence states for the Ce ions and pentavalent Mo such as in $\text{Ce}^{+3}\text{Ce}^{+4}\text{Mo}^{+5}\text{O}_6$. Pr_2MoO_6 crystallizes in $\bar{I}42m$ symmetry, and its parameters are listed in table 30.6. This same structure was obtained for Nd_2MoO_6 and Sm_2MoO_6 . The latter compound could also be obtained in a monoclinic form, if prepared at low temperatures. This brings us to the new structure of all remaining rare earth molybdates of the type R_2MoO_6 , starting with Eu_2MoO_6 . Blasse (1966) had given a suggested cell for these compounds

TABLE 30.6.
Lattice parameters and space groups for the Ln_2MoO_6 compounds.

Ln	$a(\text{\AA})$	$b(\text{\AA})$	$c(\text{\AA})$	$\beta(\text{deg})$	Space group
La	4.093	—	16.017	—	$\bar{I}42m$
Ce	5.578	—	—	—	$\text{Fm}3m^*$
Pr	4.030	—	15.852	—	$\bar{I}42m$
Nd	4.005	—	15.813	—	$\bar{I}42m$
Sm	3.965	—	15.686	—	$\bar{I}42m$
	16.628	15.791	5.470	108.28	$\text{C}2/c$
Eu	16.558	15.735	5.439	108.16	$\text{C}2/c$
Gd	16.514	15.678	5.425	108.33	$\text{C}2/c$
Tb	16.462	15.626	5.396	108.35	$\text{C}2/c$
Dy	16.542	15.573	5.371	109.72	$\text{C}2/c$
Ho	16.469	15.516	5.349	109.60	$\text{C}2/c$
Er	16.412	15.479	5.328	109.53	$\text{C}2/c$
Tm	16.266	15.419	5.310	108.57	$\text{C}2/c$
Yb	16.240	15.387	5.290	108.66	$\text{C}2/c$
Lu	16.211	15.346	5.274	108.80	$\text{C}2/c$

*Subcell?

based on a distortion of Sillen's tetragonal La_2MoO_6 . The data were not based on single crystals, and we were completely unable to index our Guinier data using Blasse's (1966) parameters. We therefore attempted to grow single crystals of Gd_2MoO_6 even though the compound melts near 2000°C . We were able to obtain single crystals of a Bi-substituted Gd molybdate of the type $\text{Ge}_{1.7}\text{Bi}_{0.3}\text{MoO}_6$. This allowed us to establish the space group $\text{C}2/c$ ($\text{C}c$ was ruled out by a negative second harmonic generation test) with $a = 16.62 \text{ \AA}$, $b = 11.23 \text{ \AA}$, $c = 5.45 \text{ \AA}$ and $\beta = 108.6^\circ$. One can also use a body-centered cell to describe this structure. There is an obvious relationship to the tetragonal cell of the large rare earth molybdates:

$$a_M \sim \sqrt{2} \times a_T, \quad b_M \sim \sqrt{2} \times a_T, \quad c_M \sim c_T,$$

Sm_2MoO_6 is the link between these two structures as it was obtained in both forms. The transition from tetragonal to monoclinic is not merely a distortion because the tetragonal form is readily obtained at room temperature by air quenching. Thus the transition is slow and involves some rearrangement of atoms. The monoclinic modifications are denser, and high pressure should convert the tetragonal to the monoclinic form. This was possible at 65 kbar with Nd_2MoO_6 , although the indexing of the film was not perfect. The parameters for Gd_2MoO_6 are listed in table 30.6. For the remaining R_2MoO_6 -type rare earth molybdates, the structural situation is simple as they all crystallize in the $\text{C}2/c$ type. Parameters for Tb_2MoO_6 , Dy_2MoO_6 , Ho_2MoO_6 , Er_2MoO_6 , Tm_2MoO_6 , Yb_2MoO_6 and Lu_2MoO_6 are listed in table 30.6. Compared to the complexity of structures for the $\text{R}_2(\text{MoO}_4)_3$ compounds, we certainly have a more "normal" situation with regard to structural types for these R_2MoO_6 compositions.

2. Crystal chemistry, phase transitions, and crystallographic aspects (W. Jeitschko)

The crystal structures of most compounds treated in the previous section are known. They will be discussed and compared here with the emphasis on the differences among the individual structural types. The structural and crystallographic aspects of the displacive phase transition between β and β' - $\text{Gd}_2(\text{MoO}_4)_3$ will be treated in more detail, since they are the basis for the interesting physical properties to be discussed in the final section.

2.1. Composition $\text{R}_2(\text{MoO}_4)_3$

The crystal structures of this composition belong to three basically different structural families with a total of six well characterized structural types: a) defect scheelite structures which can be disordered (1), or ordered of $\text{La}_2(\text{MoO}_4)_3$ type (2) or $\text{Eu}_2(\text{WO}_4)_3$ type (3); b) β - $\text{Gd}_2(\text{MoO}_4)_3$ above (4) and below (5) its displacive phase transition; and c) the $\text{Sc}_2(\text{WO}_4)_3$ type (6) structure. For γ - $\text{Dy}_2(\text{MoO}_4)_3$ a seventh structure was tentatively identified by Brixner (1973) as

cubic. Finally amorphous π - $\text{Gd}_2(\text{MoO}_4)_3$ obtained by "crushing" β - $\text{Gd}_2(\text{MoO}_4)_3$ under high pressure can be counted as an eight modification.

The main differences of the three structural families are in the oxygen coordination of the R ions which decreases from eight in the defect scheelites, over seven in β - and β' - $\text{Gd}_2(\text{MoO}_4)_3$ to six in the $\text{Sc}_2(\text{WO}_4)_3$ type compounds. The Mo atom is always tetrahedrally coordinated by oxygen although octahedral coordination of Mo is known for other compositions.

2.1.1. Defect scheelites $\text{R}_2(\text{MoO}_4)_3$

The $\text{La}_2(\text{MoO}_4)_3$ type structure (Jeitschko, 1973) which occurs for $\text{R} = \text{La}, \text{Ce}, \text{Pr}, \text{Nd}$, and the $\text{Eu}_2(\text{WO}_4)_3$ type structure (Templeton and Zalkin, 1963) found for the molybdates with $\text{R} = \text{Sm}, \text{Eu}, \text{Gd}, \text{Tb}, \text{Dy}$, are best described as derived from scheelite, CaWO_4 . The formula $\text{R}_2(\text{MoO}_4)_3$ can be expressed as $\text{R}_{2/3}\phi_{1/3}\text{MoO}_4$ where ϕ stands for vacant sites. The ordered arrangement of vacancies and R atoms on the Ca site of scheelite gives rise to the superstructures which are shown in fig. 30.10. The main differences between the $\text{La}_2(\text{MoO}_4)_3$ and the $\text{Eu}_2(\text{WO}_4)_3$ type structure is the arrangement of the R atoms and the vacancies. Atomic positions in $\text{La}_2(\text{MoO}_4)_3$ deviate only little from those in scheelite. Considerable distortions from an ideal scheelite arrangement occur in $\text{Eu}_2(\text{WO}_4)_3$. They may, however, be due to the tendency of W for higher coordination (for compositions which occur for both, molybdates and tungstates, it is sometimes observed that W is in octahedral and Mo in tetrahedral coordination) and therefore the distortions may not be present in a molybdate with $\text{Eu}_2(\text{WO}_4)_3$ type structure. To answer the question of why the $\text{La}_2(\text{MoO}_4)_3$ type structure occurs for the big R elements and the $\text{Eu}_2(\text{WO}_4)_3$ type structure for the smaller ones, an accurate structure refinement for a $\text{R}_2(\text{MoO}_4)_3$ compound with $\text{Eu}_2(\text{WO}_4)_3$ type structure would be needed.

Compounds with a superstructure due to an ordering process usually have an order-disorder transition at higher temperatures. As discussed above, such a transition was found for $\text{La}_2(\text{MoO}_4)_3$ about 200°C below the melting point. In $\text{Ce}_2(\text{MoO}_4)_3$ this transition was not observed probably because of insufficient quenching. In the remaining $\text{R}_2(\text{MoO}_4)_3$ compounds the defect scheelite structure is thermodynamically not stable at all at high temperatures and therefore the order-disorder transition does not need to occur. The relatively high speed of the order-disorder transition in $\text{La}_2(\text{MoO}_4)_3$ is easily rationalized since the La positions and vacant sites are interconnected and furthermore at high temperatures the MoO_4 tetrahedra can be easily displaced from their ideal positions.

2.1.2. β - and β' - $\text{Gd}_2(\text{MoO}_4)_3$

The primary crystallization product of $\text{R}_2(\text{MoO}_4)_3$ compounds ($\text{R} = \text{Pr}$ to Ho) has the β - $\text{Gd}_2(\text{MoO}_4)_3$ type structure. As discussed above, this structure becomes thermodynamically metastable for most compositions a few hundred $^\circ\text{C}$ below the melting point. Nevertheless it is kinetically very stable at lower temperatures and undergoes a displacive phase transition to the ferroelastic-

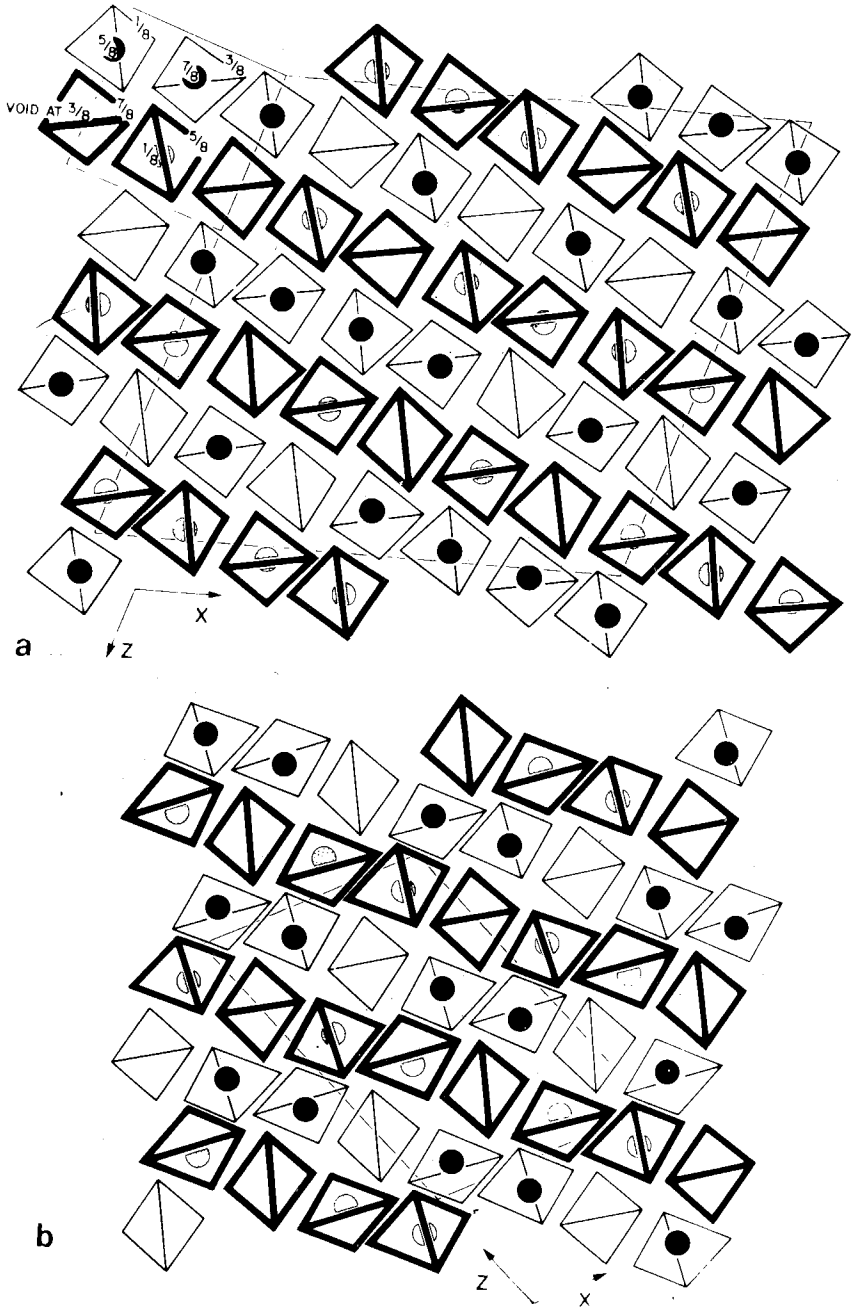


Fig. 30.10. Crystal structures of (a) $\text{La}_2(\text{MoO}_4)_3$ and (b) $\text{Eu}_2(\text{WO}_4)_3$. Projections are along the c axis of the scheelite subcell, which is outlined in the upper left-hand corner of the $\text{La}_2(\text{MoO}_4)_3$ structure. Black dots and dotted circles represent La atoms above and below the MoO_4 tetrahedra. The Mo atoms within the tetrahedra are not shown. (From Jeitschko (1973) by courtesy of Acta Crystallogr.)

ferroelectric β' - $\text{Gd}_2(\text{MoO}_4)_3$ type structure. This latter transition which occurs between 121 (R = Ho) and 235°C (R = Pr) is the basis for the unique properties of these compounds.

The crystal structure of β' - $\text{Gd}_2(\text{MoO}_4)_3$ was solved independently in two laboratories from twinned (Keve et al., 1971) and single crystals (Jeitschko, 1970, 1972). At high temperature the structure is tetragonal with space group $\text{P}\bar{4}2_1\text{m}$. Below the transition temperature it is orthorhombic, space group $\text{Pba}2$. The c axis remains practically the same during the phase transition, while the orthorhombic a and b axis are about $\sqrt{2}$ times larger than the tetragonal a axis (fig. 30.11a). The c axis which is nonpolar in the tetragonal form becomes polar in the

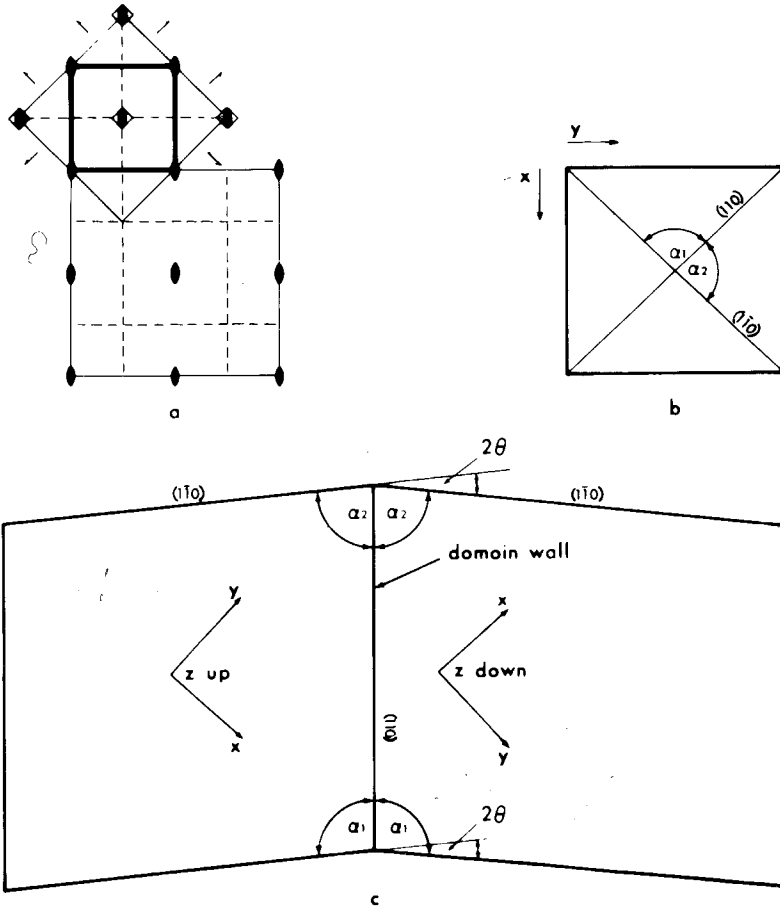


Fig. 30.11. (a) Relation of unit cells of $\beta(\text{P}\bar{4}2_1\text{m})$ and $\beta'(\text{Pba}2)\text{Gd}_2(\text{MoO}_4)_3$. (b) Definition of angles α_1 and α_2 . (c) Schematic drawing of a single crystal of ferroic $\text{Gd}_2(\text{MoO}_4)_3$ with two domains. The $\{110\}$ planes are cleavage planes and domain walls. The shear angle $\theta = \alpha_1 - \alpha_2$ is the angle between the x direction of one domain and the y direction of the other (From Jeitschko (1972) by courtesy of Acta Crystallogr.)

orthorhombic form. This is the basis for the ferroelectric property: the structure can be switched from one orientation state to the other by an electric field along the c axis. During switching the orthorhombic a and b axes interchange and the c axis inverts. Since the orthorhombic b axis is slightly larger than the a axis, the crystals can be switched also by a compressional stress applied along the b axis. The property was termed *ferroelasticity* by Aizu (1970). The shear angle is a function of the difference between the lengths of the a and b axes (figs. 30.11b, c).

As is usually the case with a displacive phase transition, the crystal structure of the high-temperature (β) form (Jeitschko, 1973) comes close to the average of the (two) different orientation states of the low-temperature (β') form. In both forms the Gd atoms are seven-coordinated and the Mo atoms tetrahedrally coordinated by oxygen atoms. The oxygen atoms have either two or three near metal neighbors (fig. 30.12). The positional differences between the β and β'

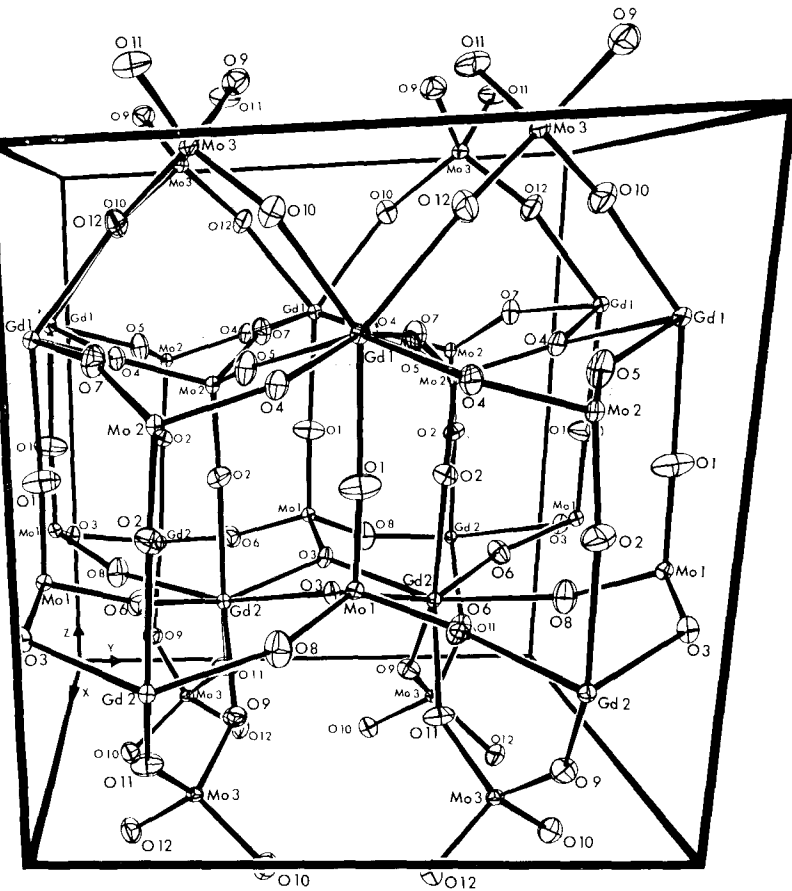


Fig. 30.12. Crystal structure of β' - $\text{Gd}_2(\text{MoO}_4)_3$. It can be seen that most metal atoms are located in the symmetry-related layers at $z \sim 0.3$ and $z \sim 0.7$ respectively.

form are small ($\sim 0.1 \text{ \AA}$) for all atoms except for some of the oxygen atoms of certain MoO_4 tetrahedra. Thus the transition from the prototypic (β) to the ferroic (β') phase of $\text{Gd}_2(\text{MoO}_4)_3$ can be described as the condensation of an oscillatory motion of these MoO_4 tetrahedra. This motion can be seen in the elongated shape of the thermal ellipsoids of some oxygen atoms in the high temperature structure (fig. 30.13).

In the low temperature form the MoO_4 tetrahedra are locked in at either one or the other extreme position in a long-range ordered manner. During ferroelectric (or ferroelastic) switching some MoO_4 groups rotate from one position to the other. The atomic displacements are largest ($\sim 0.7 \text{ \AA}$) for the oxygen atoms of the switching MoO_4 tetrahedra. The metal atoms move only by about 0.1 \AA . The motions occur primarily in the xy plane of the structure. Along the polar z direction the displacements are small and furthermore species (Gd^{3+} , MoO_4^{2-}) with the same charge move mainly against each other in such a way that the change in spontaneous polarisation is small. Thus β' - $\text{Gd}_2(\text{MoO}_4)_3$ is well described as a canted antiferroelectric.

Since the β to β' phase transition results in a doubling of the primitive cell of the structure, additional (superstructure) reflections occur in the diffraction patterns of the low temperature form. These reflections provide the key to the understanding of the phase transition. Their intensities, angular widths and energies were studied as a function of temperature both above and below the transition temperature (Axe et al., 1971; Jeitschko, 1972; Dorner et al., 1972). The results show that upon heating the temperature-dependent physical properties like spontaneous polarisation, shear angle, and birefringence along the c axis (Cummins, 1970) can be accounted for by gradual shifts in atomic positions toward the high-temperature structure. There is, however, a discontinuity at the transition temperature and in that sense the transition is of first order. The behavior of the structure above the transition temperature is a good example for the soft mode model for displacive phase transitions. Thus, the square of the soft-mode frequency varies linearly with temperature over a wide temperature range. The phase transition, however, occurs about 10°C above the temperature at which the frequency extrapolates to zero. In the temperature range just above the transition temperature the mode is also heavily damped. Thus, the phase transition has also some character of a positional order-disorder transition.

The β' - $\text{Gd}_2(\text{MoO}_4)_3$ space group, $\text{Pba}2$, is a *allgemeine* subgroup of $\text{P}\bar{4}2_1\text{m}$, the space group of β - $\text{Gd}_2(\text{MoO}_4)_3$. Therefore translations as well as other symmetry operations are lost during the β to β' transition. The reduction in point group symmetry ($\text{P}\bar{4}2_1\text{m}$ to $\text{Cmm}2$) permits the formation of twin domains while the loss of translational operation ($\text{Cmm}2$ to $\text{Pba}2$) allows the occurrence of antiphase domains (Jeitschko and Wondratschek, 1974; Wondratschek and Jeitschko, 1976). The ferroelastic-ferroelectric twin domains are of course readily distinguished through their physical (e.g. optical) properties. Antiphase domains are more difficult to observe since they have exactly the same lattice orientation. They are revealed best through the mismatch at their boundary (APB) which results in a higher chemical etching rate at the boundary. The APB's form closed

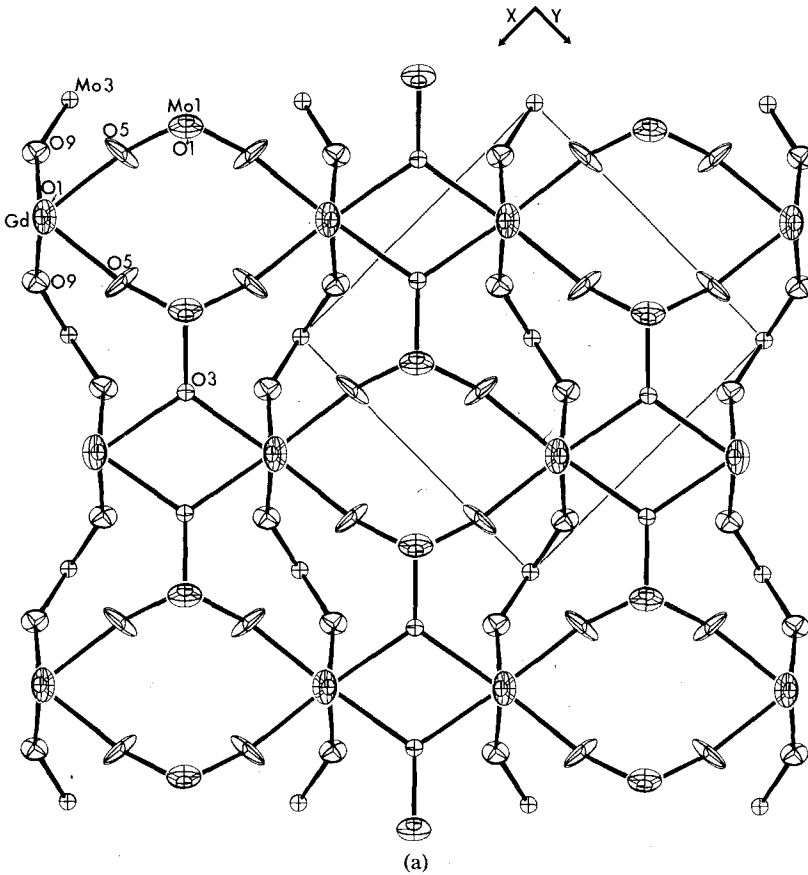


Fig. 30.13.

loops or terminate on dislocations, external surfaces, or on ferroelectric domain (i.e. twin) walls. They are generated and annihilated by moving domain walls (Barkley and Jeitschko, 1973). On the atomic scale, domain walls correspond to a mismatch in the orientation of MoO_4 tetrahedra in one *or* the other plane perpendicular to the c axis, while APB's correspond to a mismatch in *both* planes of the structure (fig. 30.14).

2.1.3. Molybdates with $\text{Sc}_2(\text{WO}_4)_3$ type structure and amorphous $\text{R}_2(\text{MoO}_4)_3$ compounds

The $\text{Sc}_2(\text{WO}_4)_3$ type structure (Abrahams and Bernstein, 1966) occurs for $\text{R}_2(\text{MoO}_4)_3$ compounds with the small R elements from Ho to Lu. In this structure, which has also been described for $\text{Al}_2(\text{WO}_4)_3$ by Craig and Stephenson (1968), RO_6 octahedra are linked via all corners to MoO_4 tetrahedra. The MoO_4 tetrahedra share their corners with four RO_6 octahedra. In this way a very open three-dimensional framework is formed.

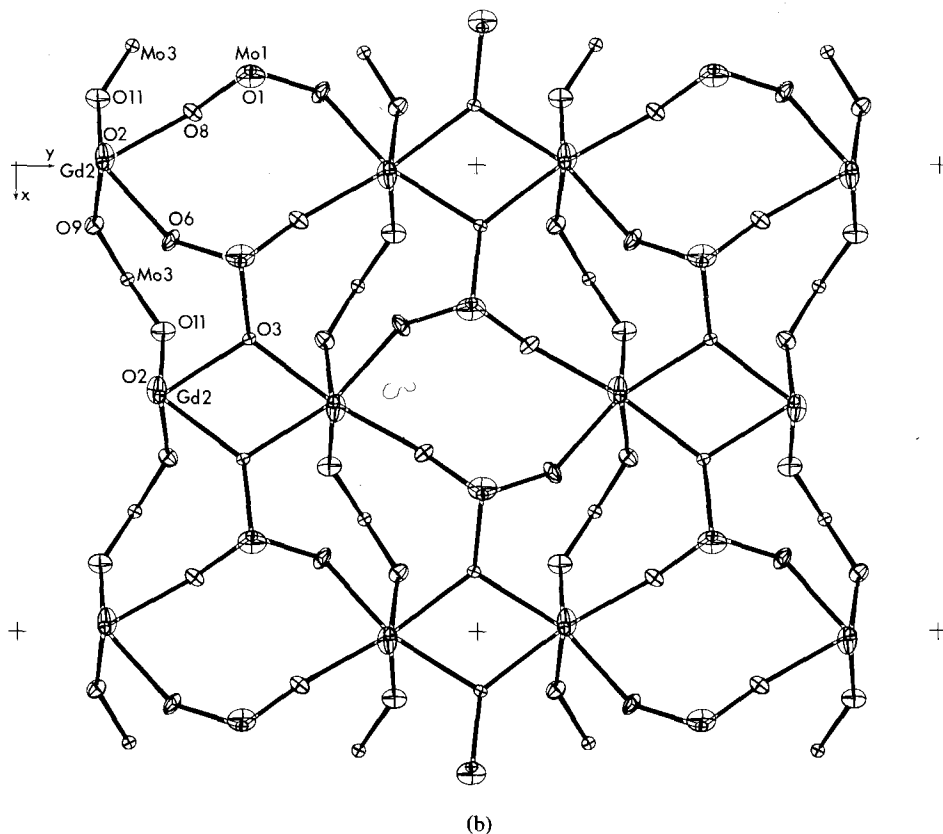


Fig. 30.13. Comparison of the partial structures at $z \sim 0.3$ of (a) β - and (b) β' - $\text{Gd}_2(\text{MoO}_4)_3$. Thermal ellipsoids are plotted at the 50% probability limit. (From Jeitschko (1972) by courtesy of Acta Crystallogr.)

In the previously discussed $\text{R}_2(\text{MoO}_4)_3$ structures the R element is 8-coordinated (defect-scheelites) or 7-coordinated (β - $\text{Gd}_2[\text{MoO}_4]_3$ type compounds). Correspondingly one third of the oxygen atoms is 3-coordinated in the defect scheelite molybdates, and only one sixth of the oxygen atoms are 3-coordinated (always to two R and one Mo) in β - $\text{Gd}_2(\text{MoO}_4)_3$. The remaining oxygen atoms are always coordinated to one R and one Mo. Finally in the $\text{Sc}_2(\text{WO}_4)_3$ type compounds with 6-coordination for R, all oxygens have coordination number 2. Thus, in going from the large to the small R elements the coordination numbers decrease and the volume per formula unit increases in steps from the defect-scheelites over the β - $\text{Gd}_2(\text{MoO}_4)_3$ type to the $\text{Sc}_2(\text{WO}_4)_3$ type compounds. As would be expected, for compositions where two of these basic structure types are found, the lower coordinated structure is always the high temperature form.

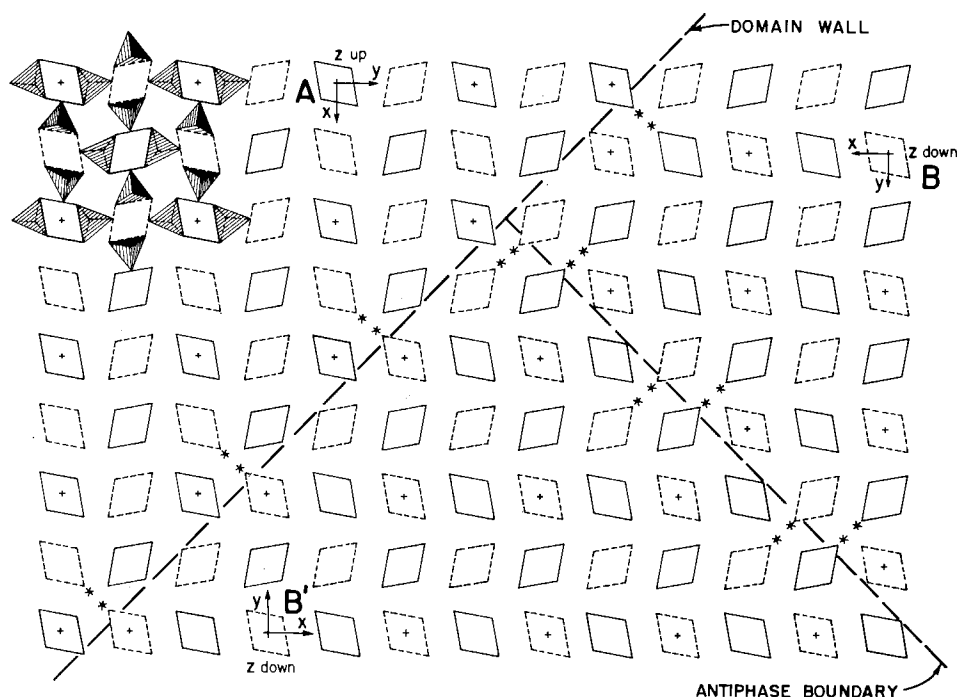


Fig. 30.14. Schematic representation of the β' - $\text{Gd}_2(\text{MoO}_4)_3$ structure. Diamonds drawn with solid and broken lines represent MoO_4 tetrahedra at two different levels in space. The axis system A, B and B' show the crystal in three different orientation states. States B and B' are parallel (their axis systems are drawn antiparallel in the x and y directions, however, they are parallel through the internal symmetry of the structure) but have a translational mismatch at the antiphase boundary. State A is of opposite polarity. (From Barkley and Jeitschko (1973) by courtesy of J. Appl. Phys.)

Brixner et al. (1971) have shown that the β - $\text{Gd}_2(\text{MoO}_4)_3$ structure collapses under high pressure to form the higher coordinated $\text{Eu}_2(\text{WO}_4)_3$ type structure. If the temperature is low (e.g. 25°C) the compound formed is amorphous (Brixner, 1972). A corresponding behaviour can be expected for the molybdates with $\text{Sc}_2(\text{WO}_4)_3$ type structure. In this way the β - $\text{Gd}_2(\text{MoO}_4)_3$ type structure could be obtained for the small R elements. Application of high pressure at moderate temperatures should again yield amorphous products.

2.2. Crystal structures of other R molybdates

Although many more R molybdates with different compositions are described in the literature, few are structurally well characterized. Of the compositions R_2MoO_6 the compounds with R from La to Sm crystallize with the La_2MoO_6 type structure. This structure was determined a long time ago by Sillén and Lundborg (1943) and oxygen positions were only assigned from crystal chemical considerations. It is best described as a layer structure with alternating sheets of

RO_6 octahedra and MoO_4 tetrahedra. The MoO_4 tetrahedra share their corners with RO_6 octahedra of the adjacent sheets above and below. These oxygen atoms are therefore coordinated by one R and one Mo atom. The remaining oxygens belong to the RO_6 layers and are coordinated by four R atoms. The structure of the remaining R_2MoO_6 compounds is probably similar to the structures of Bi_2MoO_6 (Zemann, 1956; van den Elzen and Rieck, 1973) and Bi_2WO_6 (Wolfe et al., 1969) with distorted octahedral oxygen coordination for both R and Mo. In this structure the MoO_6 octahedra share four corners, thus again forming sheets of composition MoO_4 which are interleaved by sheets of composition R_2O_2 . For Sm_2MoO_6 which crystallizes with both structural types, the high temperature structure (La_2MoO_6 type) is again the structure with the lower coordination numbers, as was discussed above for compositions $\text{R}_2(\text{MoO}_4)_3$.

EuMoO_4 is reported to crystallize with a scheelite type structure (McCarthy, 1971; Banks and Nemiroff, 1974) and magnetic measurements show that at least most, if not all Mo is in the hexa-valent state (Hubert, 1975). Compounds where Mo has an oxidation number of less than 6 and the large number of mixed molybdates like $\text{CsR}(\text{MoO}_4)_2$ (Klevtsova et al., 1972) or $\text{K}_3\text{R}(\text{MoO}_4)_4$ (Klevtsov et al., 1975) are outside the scope of the present article.

3. Physical properties (J.R. Barkley)

3.1. General

The most interesting physical properties of the described compounds are found in the β - $\text{R}_2(\text{MoO}_4)_3$ compositions which exhibit the $\bar{4}2m$ to $mm2$, i.e. β to β' , phase transition.

When cooled through the Curie temperature, T_c , the equivalent $[110]$ and $[\bar{1}\bar{1}0]$ axes of the tetragonal phase become the a and b axes of the orthorhombic phase (fig. 30.11). Since these two orthorhombic axes are unequal, the crystal changes shape by a small but significant amount as illustrated in fig. 30.15a and 30.15b. Usually a crystal in the β' phase exhibits several domains which interface along domain walls as shown in fig. 30.15c and 30.15d.

These domains are crystallographically related to each other by the $\bar{4}$ symmetry operation of the β -phase that was lost in the transition. The c -axis reversal across a domain wall is important because the β' phase is polar along c . Thus, the polarization P_s is reversed in adjacent domains.

When an electric field is applied to reverse P_s , the crystal responds by nucleating domain walls along edges. These walls then move sideways to reverse P_s . The hysteresis loop shown in fig. 30.16 relating polarization and applied electric field is characteristic of all ferroelectrics and of the β' phase of $\text{R}_2(\text{MoO}_4)_3$ as recognized by Borchardt and Bierstedt (1967).

The β - $\text{R}_2(\text{MoO}_4)_3$ compositions are unusual ferroelectrics however, in that the temperature dependence of the dielectric permittivity ϵ is not Curie-Weiss type

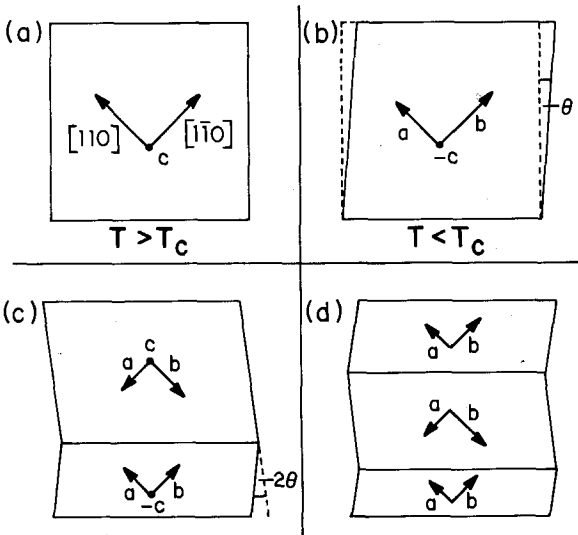


Fig. 30.15. Change in crystal shape observed upon cooling through the $\bar{4}2m$ to $mm2$ transition in β - $R_2(\text{MoO}_4)_3$. For β - $\text{Gd}_2(\text{MoO}_4)_3$ at room temperature, the shear angle $\theta = 10'20''$ and $T_c = 159^\circ\text{C}$.

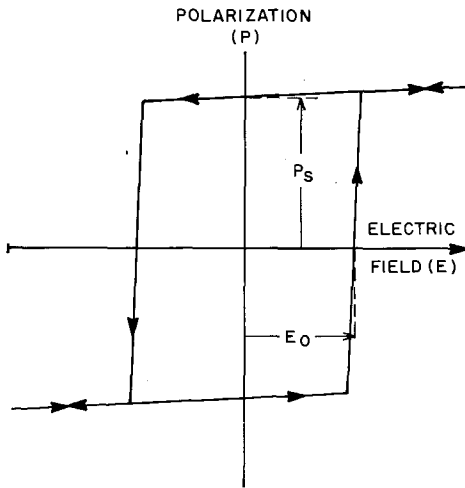


Fig. 30.16. The ferroelectric hysteresis loop relating applied electric field and polarization, both along $[001]$ for β - $R_2(\text{MoO}_4)_3$.

above the Curie temperature. Instead it is certain elastic constants that exhibit large changes when approaching the transition temperature. Cross et al. (1968) observed very little temperature dependence in the small, clamped electric permittivity ϵ_3 of β - $\text{Gd}_2(\text{MoO}_4)_3$ and a strong temperature dependence in the elastic constant C_{66}^E with an anomaly at T_c . They were led to the conclusion that the spontaneous polarization was an incidental but necessary consequence of the

piezoelectric coupling to the shear strain of the β' -phase relative to the β -phase.

Since then, Pytte (1970), Levanyuk and Sinnikov (1970) and Aizu (1971) suggested independently that the β - β' structural change is fundamentally connected with a doubly degenerate soft mode at the Brillouin-zone edge in the β -phase which leads to the doubling of the unit cell.

Direct confirmation of this model was provided by the inelastic neutron-diffraction experiments on β - $\text{Tb}_2(\text{MoO}_4)_3$ of Dorner et al. (1972). They observed for $T > 159^\circ\text{C}$, the frequency ω_M of a doubly degenerate mode at $M(\frac{1}{2}, \frac{1}{2}, 0)$ follows a Curie-Weiss law $\omega_M^2 = A(T - T_c)$ with $A = 0.0165 \text{ meV}^2/^\circ\text{C}$ and $T_c = 149^\circ\text{C}$. Their examination of this soft mode showed that the primary order parameter, which necessarily shows large fluctuations near T_c , has no macroscopic polarization, but is instead antipolar. The "freezing in" of this antiferroelectric static displacement however, couples to the shear strain χ_{12} which in turn produces the polarization by piezoelectric coupling. They show that observed temperature dependences of P_s and χ_s are proportional to the square of this order parameter. Other studies have also supported or at least have been consistent with this description of the transition; for example, Raman scattering by Fleury (1970) and Ganguly et al. (1975); infrared absorption data of Petzelt et al. (1971) and Dvorak (1971); the temperature dependence of the elastic constants by Epstein et al. (1970), Hochli (1972), Courdille et al. (1973, 1975), Chizhikov et al. (1971), and the lattice dynamics calculations of Boyer and Hardy (1972, 1973).

The importance of the "elastic" properties of the β - $\text{R}_2(\text{MoO}_4)_3$ compositions has stimulated definition of a phenomenon called "ferroelasticity" a term coined by Aizu (1969).

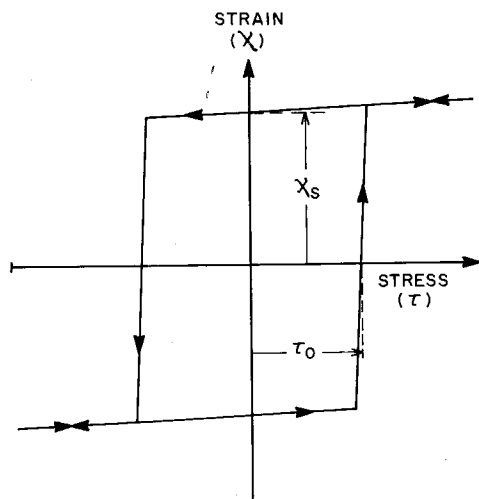


Fig. 30.17. The ferroelastic hysteresis loop relating applied stress and strain, both in the (001) plane, for β' - $\text{R}_2(\text{MoO}_4)_3$.

A material is said to be ferroelastic if it has two or more stable orientational states in the absence of mechanical stress and if it can be reproducibly transformed from one to another of these states by the application of mechanical stress. (Further discussions of ferroelastic behavior can be found in Aizu (1971b, 1974), Abrahams et al. (1971a,b), Sapriel (1974), Toledano (1974), Janovec (1976).) A ferro-elastic "hysteresis loop" analogous to the ferroelectric loop is also observed in β - $R_2(\text{MoO}_4)_3$ as shown in fig. 30.17 (see Kumada, 1969, 1970). The β' -phase of $R_2(\text{MoO}_4)_3$ is called a coupled ferroelectric/ferroelastic which means that polarization reversal necessarily accompanies the strain reversal and vice-versa. Ferroelasticity, like ferroelectricity, is a structure dependent property and is directly inferrable from the point group symmetry change $\bar{4}2m$ to $mm2$ at the transition as described in Aizu's (1969) paper.

The hysteresis loops of fig. 30.16 and 30.17 improperly imply that the switching process for strain or polarization reversal is instantaneous and complete once the threshold field, E_0 or stress τ_0 is exceeded. This switching occurs by domain wall nucleation and movement which is not particularly fast for the β' -molybdates. Much of the "applied" research on these materials concerns this switching process as summarized in ch. 30 section 3.6.

3.2. Electrical properties

As already discussed, the polarization-field relationship is given by the hysteresis loop of fig. 30.16. The temperature dependence of P_s for $\text{Gd}_2(\text{MoO}_4)_3$ as

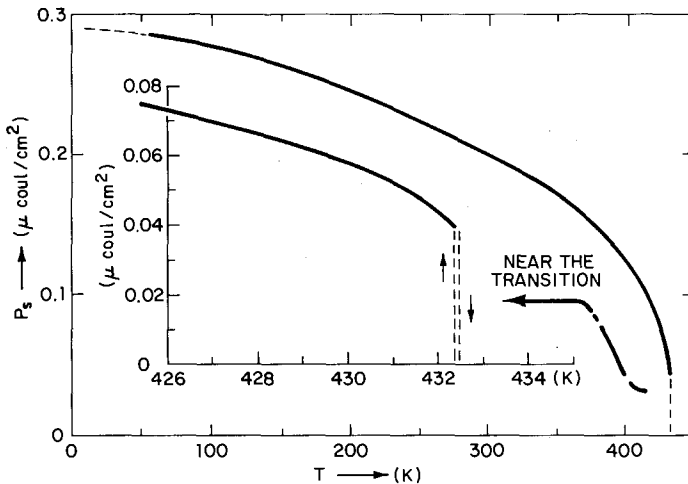


Fig. 30.18. Spontaneous polarization as a function of temperature in β - $\text{Gd}_2(\text{MoO}_4)_3$ single crystal. Above 75 K, P_s is deduced from low-frequency (0.01 Hz) isothermal loops. Below 75 K, P_s is measured from pyroelectric charge and discharge of single-domain samples (Sawaguchi and Cross, 1973).

measured by Sawaguchi and Cross (1973) is shown in fig. 30.18, and agrees with similar data of Aizu et al. (1969) and Cummins (1970). The first order nature of the transition is evident in the marked jump in P_s at the transition. Both Sawaguchi and Cross (1973) and Kumada (1974) observed that the β to β' transition could be forced by applying an electric field to a crystal held slightly above T_c , i.e., in the β phase. In this case double hysteresis loops are observed, further evidence of the first order nature of the transition.

Room temperature values for P_s for selected β' - $R_2(\text{MoO}_4)_3$ compositions are given in table 30.7. The measured value for $\text{Gd}_2(\text{MoO}_4)_3$ agrees reasonably well with values estimated by Keve et al. (1971) and Jeitschko (1972), whereby P_s is due almost entirely to the MoO_4 group rearrangement and the Gd^{3+} ions play no essential role.

The pyroelectric properties of $\text{Gd}_2(\text{MoO}_4)_3$ were measured by Ullman et al. (1972 and 1975). They found that $\text{Gd}_2(\text{MoO}_4)_3$ single crystals operated close to T_c have figures of merit for pyroelectric responsivity comparable to presently utilized pyroelectric detector materials, e.g. Triglycine Sulfate. However, when operating near T_c , they encountered hard-to-control spurious domain nucleation due to small thermal gradients caused by the thermal signal being detected, even though a large biasing field was used to attempt to maintain a single domain state. (Also see Nakamura et al. (1971b) and Kumada (1973) for other field effects near T_c and Shirokov^{et al.}(1972) and Midorikawa et al. (1974) for hydrostatic pressure effects on T_c .)

Both β and β' phases of $R_2(\text{MoO}_4)_3$ are piezoelectric. The temperature dependence of the piezoelectric constants d_{31} and d_{33} as measured by Scheiding et al. (1973) is given in fig. 30.19. At room temperature, $d_{31} \doteq -1.5 \times 10^{-12}$ m/V and $d_{33} \doteq 0.5 \times 10^{-12}$ m/V.

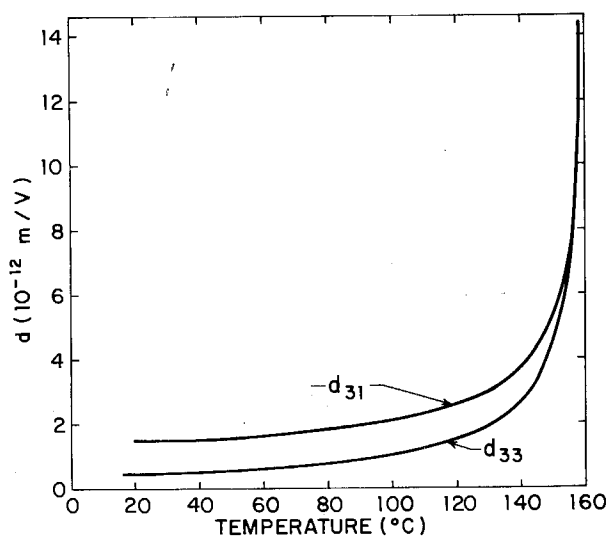


Fig. 30.19. Temperature dependence of the piezoelectric coupling constants d_{31} and d_{33} for β' - $\text{Gd}_2(\text{MoO}_4)_3$ (Scheiding et al., 1973).

TABLE 30.7.
Room temperature properties of selected β - $R_2(\text{MoO}_4)_3$ compositions.

Composition	Lattice constants (<i>l</i>)			T_c (β - β') (°C)	χ_{ab}^a (10^{-3})	P_s (10^{-2} C/m ²)	Wall mobility			Optical ^b	
	<i>a</i> (Å)	<i>b</i> (Å)	<i>c</i> (Å)				μ_E (10^{-6} m ² /V s)	μ_r (10^{-6} m ² /N s)	n_a	Δn_{ab} (10^{-4})	
Pr ₂ (MoO ₄) ₃	10.5255	10.5782	10.9013	235.0 [1]	2.497	—	—	—	—	2.20 [5]	1.9
Nd ₂ (MoO ₄) ₃	10.4966	10.5426	10.8544	244.9 [1]	2.186	—	—	—	—	1.75 [5]	2.7
Sm ₂ (MoO ₄) ₃	10.4352	10.4718	10.7687	197.2 [1]	1.751	>0.24 [3]	—	—	—	—	—
Eu ₂ (MoO ₄) ₃	10.4109	10.4436	10.7269	180.5 [1]	1.568	0.14 [3]	—	—	—	—	—
Gd ₂ (MoO ₄) ₃	10.3881	10.4194	10.7007	159.5 [1]	1.504	0.21 [3]	—	2.1 [6]	3.2	1.85 [7]	4.08
GdTb(MoO ₄) ₃	10.3688	10.3982	10.6766	~162 [8]	1.416	—	—	2.1 [6]	3.1	—	—
GdDy(MoO ₄) ₃	10.3582	10.3837	10.6564	155. [2]	1.229	0.19 [5]	—	1.2 [6]	1.8	1.84 [5]	4.1
Tb ₂ (MoO ₄) ₃	10.3518	10.3807	10.6531	160. [2]	1.394	0.18 [3]	—	2.2 [6]	2.9	1.89 [5]	3.7
Dy ₂ (MoO ₄) ₃	10.3271	10.3513	10.6145	145. [2]	1.170	—	—	—	—	—	—
Gd _{1.3} Ho _{0.7} (MoO ₄) ₃	10.3593	10.3831	10.6606	153.3 [8]	1.147	—	—	0.66 [5]	—	—	—
Ho ₂ (MoO ₄) ₃	10.3038	10.3244	10.5783	121.0 [1]	0.999	—	—	—	—	—	—

^a $\chi_{ab} = (b - a)/(b + a)$ (*l*). ^b Refractive indices given for $\lambda = 6328$ Å.

References [1] Brixner et al. (1972); [2] Brixner et al. (1971); [3] Borchardt et al. (1967); [4] Sawaguchi and Cress (1973); [5] Barkley, unpublished; [6] Flippin (1975); [7] Kumada (1972); [8] Brixner, unpublished.

These values are somewhat lower than Kumada's (1969) earlier measurements. The electromechanical coupling coefficient k_3 was measured by Cummins (1970) to be about 4% at room temperature increasing to about 22% near T_c .

The presence of domain walls significantly influences the resonant behavior of a crystal. Often a particular crystal shape will promote a multidomain state. This frustrates excitation of whole crystal resonances because the sign or sense of the piezoelectric distortion is reversed in opposing domains. A domain wall moving into a previously single domain crystal has the same effect as reversing the [001] field direction in the crystal behind the wall. Thus, the region behind the wall is distorting out of phase relative to the rest of the crystal and unless the wall(s) is (are) judiciously placed relative to nodes, (see Newnham et al. (1975)) crystal resonances are frustrated.

3.3. Elastic

The thermal expansion of $Gd_2(MoO_4)_3$ has been measured by Newnham et al. (1969) and Cummings (1970) by X-ray powder and dilatometric methods respectively. However, by X-ray study of a $Gd_2(MoO_4)_3$ single crystal by Kobayashi et al. (1972) is most recent and thorough. Their data on the temperature dependence of the lattice constants and lattice volume are given in fig. 30.20. The first order nature of the transition is seen as a small discontinuous change in lattice constant with a thermal hysteresis of about $3.5^\circ C$ as seen in fig. 30.21.

The spontaneous lattice strains χ_1 , χ_2 , and χ_3 along the a -, b -, and c -axes and the pure shear χ_{12} in the (001) plane are presented in fig. 30.22 (Kobayashi et al., 1972).

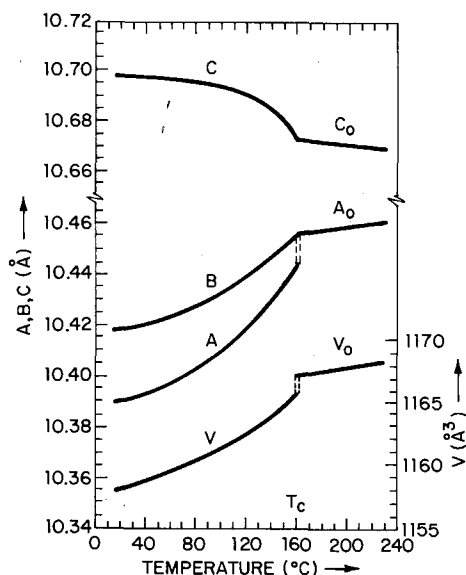


Fig. 30.20. Temperature dependence of the α -, β -, and c -lattice parameters, and the lattice volume V of β - $Gd_2(MoO_4)_3$ (Kobayashi et al., 1972).

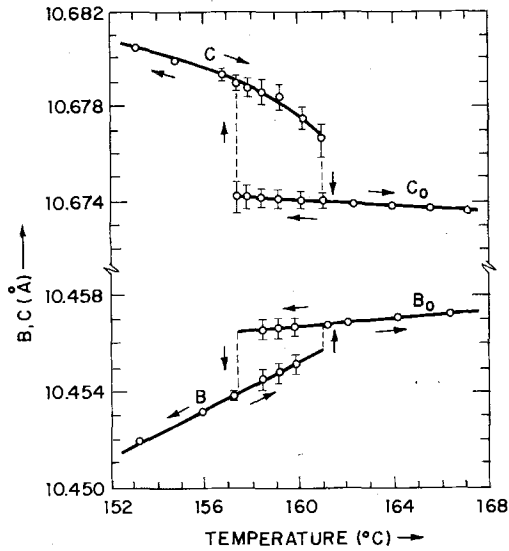


Fig. 30.21. Temperature dependence of the b - and c -parameters of $\text{Gd}_2(\text{MoO}_4)_3$ in the neighbourhood of the Curie temperature (Kobayashi et al., 1972).

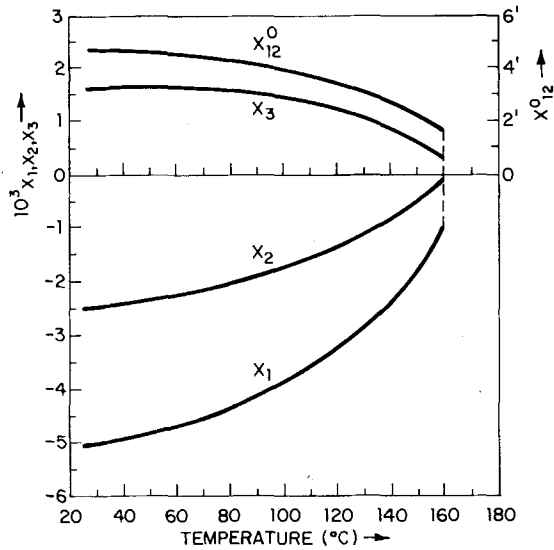


Fig. 30.22. Spontaneous lattice strains χ_1 , χ_2 , and χ_3 along the a -, b -, and c -axes of β' - $\text{Gd}_2(\text{MoO}_4)_3$ as a function of temperature. The pure shear χ_{12} in a plane perpendicular to the c -axis is also indicated (Kobayashi et al., 1972).

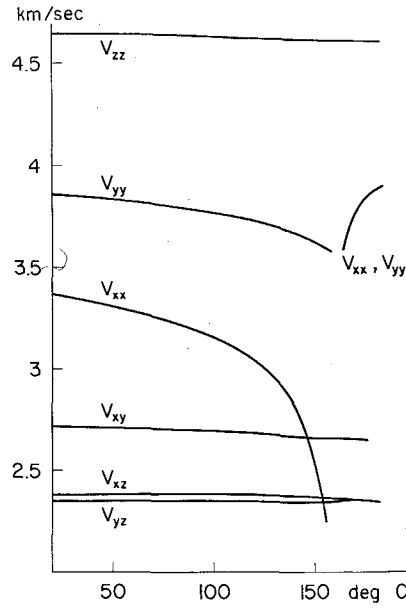


Fig. 30.23. Sound velocities in $\beta\text{-Gd}_2(\text{MoO}_4)_3$. Curves are labeled by propagation axis and polarization axis, xy denotes the axis bisecting x and y. Data taken at zero electric field (Höchli, 1972).

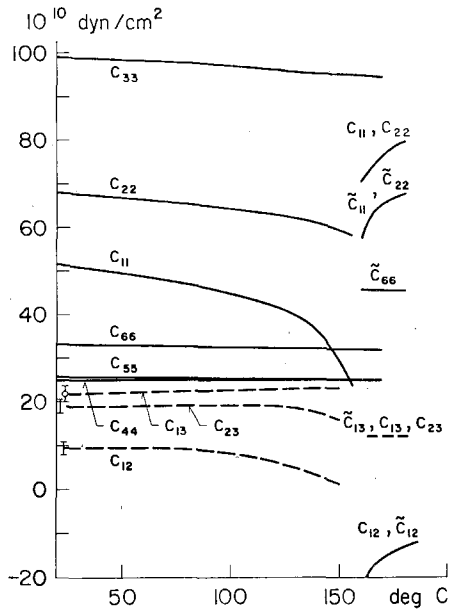


Fig. 30.24. Temperature dependence of the elastic constants in $\text{Gd}_2(\text{MoO}_4)_3$. The \tilde{C} notation refers to the tetragonal axes that are rotated 45° around $[001]$ relative to the orthorhombic (β') axes (Höchli, 1972).

The spontaneous strain (χ_{12})_s may be reversed, as discussed earlier, with fig. 30.17, by applying a compressional stress along the orthorhombic *b*-axis. At very small applied stress, the crystal responds with a small elastic deformation until the critical threshold stress (τ_0) is exceeded at which time domain walls nucleate and move until the region subjected to the stress has been "switched" to the opposite strain state. Decreasing this applied stress to zero leaves the crystal in the "positive", χ_s spontaneous strain state.

Domain wall behavior during this switching process has attracted interest because most device applications in some way involve domain wall movement to modulate electromagnetic or acoustic energy. Domain wall dynamics will be discussed in section 3.6.

Hochli (1972) measured the temperature dependence of sound velocities in $\text{Gd}_2(\text{MoO}_4)_3$ as shown in fig. 30.23 and the elastic constants given in fig. 30.24 and table 30.8. The softening of the lattice at the β - β' transition is obvious from these data.

TABLE 30.8.
Elastic constants in gadolinium molybdate^a.

Temp. (°C)	C_{11}	C_{22}	C_{33}	C_{44}	C_{55}	C_{66}
22	51.6	67.6	98.2	25.1	25.8	33.4
60	49.7	66.2	97.8	25.0	25.7	33.1
100	46.9	64.9	97.2	24.9	25.6	32.5
140	41.5	62.4	96.7	24.7	25.5	31.9
159	32.9	59.5	96.2	24.7	24.8	31.6
160	70.5	70.5	96.0	24.7	24.7	31.6
180	77.0	77.0	95.0	24.7	24.7	31.6

^aTable kindly provided by Höchli in private communication (1972).

3.4. Optical

β - $\text{R}_2(\text{MoO}_4)_3$ boules can be grown that have excellent optical quality. However growth conditions which promote precipitation of other phases such as α - $\text{R}_2(\text{MoO}_4)_3$ or R_2MoO_6 must be carefully avoided as described in section 3.1. When present, these second phases introduce optical scattering that is easily observed under laser illumination. Optical scattering is also caused by degradation of (001) surfaces in a moist atmosphere or from fingerprints. Under these conditions, small, shallow etch pits slowly develop where dislocations exit these surfaces. This problem is eliminated when (001) surfaces are coated with chemically stable thin films of indium or tin oxide which are often used as transparent electrodes.

$\text{Gd}_2(\text{MoO}_4)_3$ is transparent between ~ 2000 and $28\,000\text{ cm}^{-1}$. Other β - $\text{R}_2(\text{MoO}_4)_3$ materials exhibit colors typical of rare earth ions in a highly asymmetric site. UV

excited fluorescence was observed by Borchardt (1965), Δ and Bagdasarov et al. (1971). Borchardt saw laser action at room temperature in $\text{Gd}_2(\text{MoO}_4)_3 + (\sim 3 \text{ wt\% Nd}^{3+})$ crystals in the wavelength range 1.045 to 1.09 μm .

The Raman spectra of the $\beta\text{-R}_2(\text{MoO}_4)_3$ compositions is discussed by Scott (1974) and Shepherd (1971) in addition to those references given in section 3.1.

$\beta'\text{-R}_2(\text{MoO}_4)_3$ single crystals are optically positive and biaxial (Smith and Burns, 1969). The optic axes are in the (100) plane with the acute bisetrix along [001]. The wavelength dependence of the refractive index is given in fig. 30.25 for several $\text{R}_2(\text{MoO}_4)_3$ compositions.

The temperature dependence of Δn_{ab} measured by Smith and Burns (1969) and Cummins (1970) follows approximately the temperature dependence of P_s and χ_s shown in fig. 30.18 and 30.22. But Nakamura et al. (1971) and Kumada (1972) pointed out that in an applied field or stress both the polarization and strain of a single domain crystal are observed to increase, but the birefringence decreases as shown in fig. 30.26. The observed field dependence of the birefringence in the β' phase has the same sign and approximately the same magnitude as that observed in the β -phase. The spontaneous birefringence is thus not caused by the internal field produced by P_s , but rather is directly caused by the ion displacements within a unit cell (as described by the order parameter discussed in section 3.1) which only incidentally causes the macroscopic strain and polarization.* Further discussion and measurements of electrooptic properties of β -

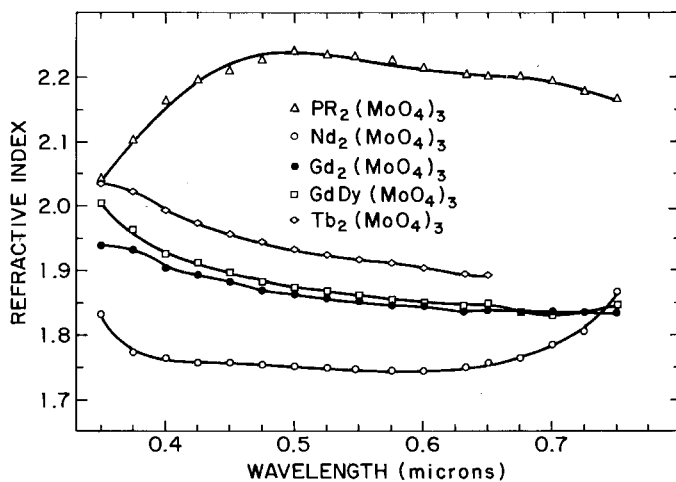


Fig. 30.25. Index of refraction versus wavelength for several $\beta'\text{-R}_2(\text{MoO}_4)_3$ single crystal compositions.

*W. Jeitschko and W. Bindloss (private communication) have pointed out that the ion positions *within* a unit cell in $\beta'\text{-R}_2(\text{MoO}_4)_3$ would provide the orthorhombic symmetry (and presumably the birefringence) even if the a - and b -lattice constants were equal. The large rotation of certain molybdate groups cooling through T_c forces a and b to become unequal which, of course, is the macroscopic strain χ_s . This χ_s in turn causes P_s through piezoelectric coupling.

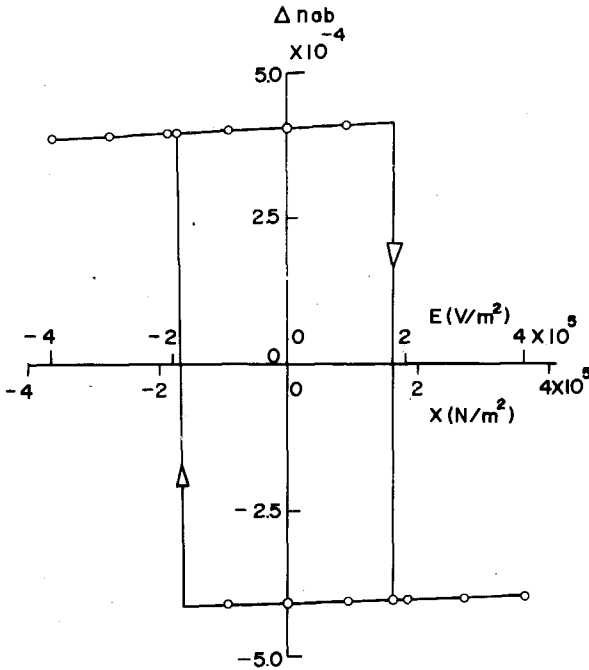


Fig. 30.26. Birefringence Δn_{ab} versus applied field and stress for β' - $\text{Gd}_2(\text{MoO}_4)_3$ at room temperature (Kumada, 1972).

$\text{R}_2(\text{MoO}_4)_3$ can be found in Miller et al. (1971) and Fousek and Konak (1972).

The scattering of light by acoustic waves in single and multidomain crystals of β' - $\text{Gd}_2(\text{MoO}_4)_3$ has been studied by Esayan et al. (1974). They determined all 12 independent photoelastic constants and found the constant p_{66} of opposite sign relative to p_{11} , p_{22} , p_{12} and p_{21} . Thus both electrooptic and elasto-optic constants associated with the shear deformation about [001] appear to be negative.

The domain structure in β' - $\text{R}_2(\text{MoO}_4)_3$ single crystals is readily visible when viewed along [001] between crossed polarizers. Mutually orthogonal conoscopic figures are observed in opposed domains, see Kumada (1972). This means that the optic plane rotates about [001] by 90° as a domain wall moves across the crystal. Therefore, a (001) polished plate prepared with a thickness that provides a quarter wave retardation in one domain (about 0.033 cm for $\text{Gd}_2(\text{MoO}_4)_3$ at $\lambda = 5500 \text{ \AA}$) will have a negative quarter wave retardation in the opposing domain. Incident light directed along [001] and linearly polarized along (110) will exit one domain with right circular polarization and the opposing domain with left circular polarization. A crystal observed through a circular polarizer, alternately blocks or transmits the light upon repeated switching. This property of highly transparent β' - $\text{Gd}_2(\text{MoO}_4)_3$ has stimulated proposals for novel device applications throughout the world. For further discussion of several device applications for β' - $\text{R}_2(\text{MoO}_4)_3$ materials see Smith and Burns (1969), Kumada (1969, 1972) and Barkley et al. (1972).

3.5. Magnetic

Both β -Gd₂(MoO₄)₃ and β -Tb₂(MoO₄)₃ are paramagnetic at room temperature with moments 7.98 μ_B and 9.65 μ_B respectively (Keve et al., 1970). They also found that both compositions remain paramagnetic down to 1.4 K. Fisher et al. (1975) have found that these compositions become antiferromagnetic below 0.3 K and \sim 2 K respectively.

An extensive investigation of the low temperature magnetothermodynamics of β '-Gd₂(MoO₄)₃ and β '-Tb₂(MoO₄)₃ is presented in a series of papers; (Fisher et al., 1972; Hornung et al., 1972; Brodale et al., 1972; Fisher et al., 1973; and Fisher et al., 1975).

3.6. Domain walls

Many domain walls can exist simultaneously in a crystal, as shown in the photograph of fig. 30.27 taken with transmitted light in a polarizing microscope. Although various wall configurations are shown in the figure, walls develop primarily along two orthogonal crystallographic planes (110) and ($\bar{1}10$).

The simplest type of wall is planar and extends across the whole crystal, as sketched in fig. 30.15c and 30.15d. When two orthogonal plane walls are driven into each other with an applied field or stress, the strain that develops at their intersection fractures the crystal. These intersections are avoided when only parallel walls switch a crystal.

Some mention of the importance of the crystal shape seems desirable. The shape of a crystal influences the overall strain pattern and thus the wall configurations that form easiest in that crystal. Domain walls tend to nucleate easily along crystal edges that are not (110) surfaces. Fig. 30.28a shows a crystal shape which promotes formation of two sets of orthogonal walls which readily move in away from the edges. A circular (001) plate may do likewise and attempts to switch it with field or stress will eventually force two perpendicular walls against each other to fracture the crystal.

A crystal shape improved to sustain a greater number of switching cycles has at least 2-edges parallel to (110) planes as shown in fig. 30.28b.

A further refinement to provide a crystal of a potentially long lifetime is to trap a single wall as shown in fig. 30.29. A crystal of this configuration with indium oxide electrodes, has sustained $>10^9$ switching cycles successfully (Barkley et al., 1972).

Crystals mounted in this way can be used to investigate the field and stress dependence of the planar wall velocity.

Kumada et al. (1970) observed that the "sideways" velocity of domain walls driven by electric field increased linearly with fields applied along [001]. Walls may also be driven with shear stress in the (001) plane. Reversing either stress or field direction reverses the direction of wall movement. Flippen (1975) has found that stress and electric field effects on wall velocity are additive following the expression

$$v = \mu_\tau(\tau - \tau') + \mu_E(E - E_0); \quad \tau > \tau_0 \text{ and } E > E_0,$$

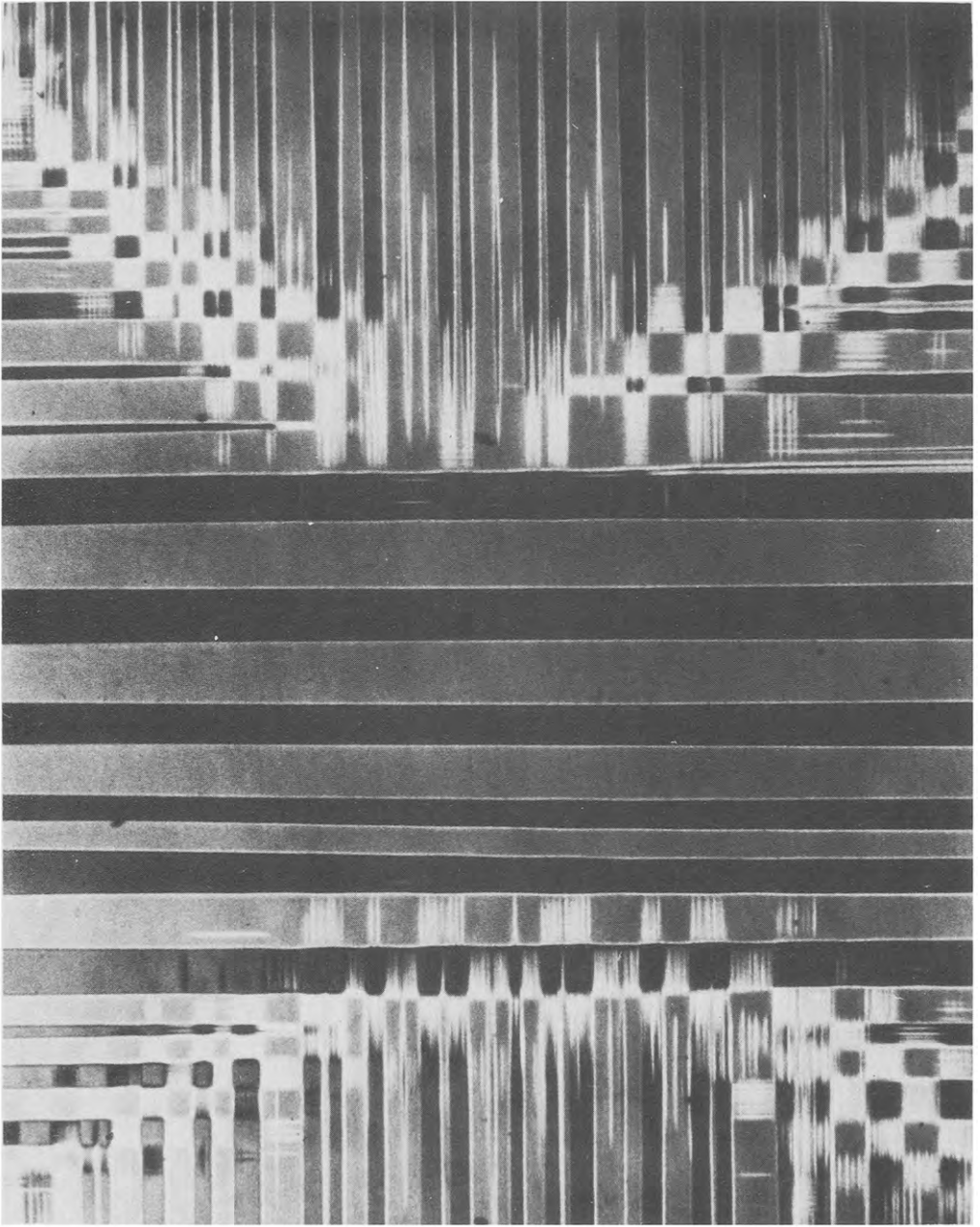


Fig. 30.27. Domain walls observed in a circular (001) plate of β' - $\text{Gd}_2(\text{MoO}_4)_3$ after cooling through T_c .

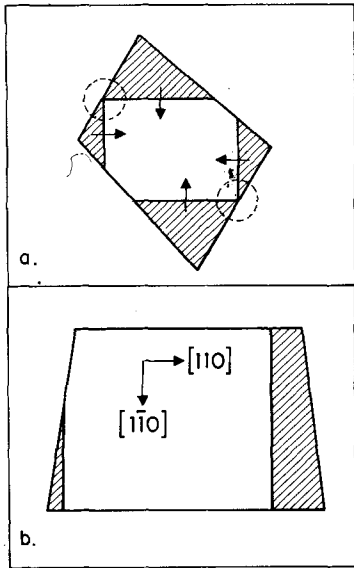


Fig. 30.28. The shape of (001) plates can promote destructive wall intersections (circled in (a)) during switching with field or stress. A crystal shaped to avoid wall intersections as in (b), will promote switching with only parallel walls.

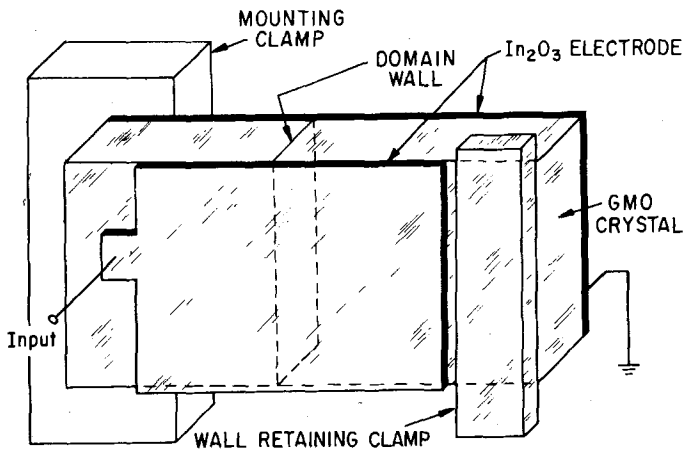


Fig. 30.29. Design for mounting and electroding GMO crystals to suppress nucleation and growth of unwanted domains. A single domain wall permanently retained in the crystal is used to switch the region between the clamps (Barkley et al., 1972).

where the mobilities μ_τ and μ_E are given in table 30.6 for various $R_2(\text{MoO}_4)_3$ compositions τ' and E' are "offset" values that appear to be more sensitive to composition and "character" of the electrode-crystal interface than to internal crystal defects (Barkley, unpublished). The threshold stress τ_0 and field E_0 are those required to initiate wall movement and are sample dependent varying with defect density, second phase concentration, electroding conditions, residual strain, etc.; see Barkely et al. (1972) and Kumada (1973). Under the best conditions and best samples, E_0 values as low as 100–200 volts/cm have been observed. The wall mobilities are fairly insensitive to most of these factors, and depend primarily on the sample composition. The wall mobilities are also temperature independent (Kumada, 1970) up to about 80°C at which temperature the mobility increases and crystals tend to form many domains rather than move a single wall in response to the applied field.

Flippen (1975) also observed that the electric field just sufficient to balance an oppositely directed mechanical stress was independent of the compositions tested, i.e., $\text{Gd}_2(\text{MoO}_4)_3$, $\text{Tb}_2(\text{MoO}_4)_3$, $\text{GdDy}(\text{MoO}_4)_3$ and $\text{GdTb}(\text{MoO}_4)_3$. These compositions have different field and stress mobilities, and the fact that these results are composition independent may suggest that the domain wall velocity is determined primarily by structure factors.

Work along this line has been done by Bornarel (1975) in KH_2PO_4 where he describes domain wall movement in terms of a succession of small steps, jogs or twinning dislocations that move rapidly along the surface of a domain wall. The passage of each step translates the wall a small distance, presumably a lattice spacing. Thus at high domain wall velocities, this step velocity may already approach the speed of sound in these materials. Perhaps a phonon-drag mechanism such as described in Frost and Ashby (1971), may be operative in which under certain conditions a linear relationship exists between the velocity of the (twinning) dislocations along the surface of the wall and the driving force on these dislocations. A useful starting point to interpret the observed domain wall behavior may be to consider the energy loss to the lattice during the rapid rotation of the molybdate groups as a twinning dislocation moves during wall movement.

Normally domain walls in the $R_2(\text{MoO}_4)_3$ materials tend to remain planar, but certain conditions can occur, deliberately or otherwise, which can bend them. In fact, fig. 30.27 shows slightly bent (110) walls that form very thin blade-like domains, similar to those observed by Bornarel (1975) in KH_2PO_4 and Kursten et al. (1973) in $\text{Gd}_2(\text{MoO}_4)_3$. Wall configurations involving these "blade" domains can be nucleated and moved controllably with strong field or stress gradients in the crystals (Barkley – unpublished results). The tips of blade domains move parallel their length at field mobilities between $1\text{--}3 \times 10^{-4} \text{ m}^2/(\text{V sec})$, much higher than the mobility for sideways motion of planar walls.

Another interesting wall configuration that appears to be metastable is called a zigzag wall by Flippen and Haas (1973) and is shown in fig. 30.30. This zigzag (zz) wall appears to be made up of ordinary planar walls which have been bent out of their usual (110) planes (which are vertical and normal to the plane of the figure). These bent walls intersect tangentially at the zz tips.

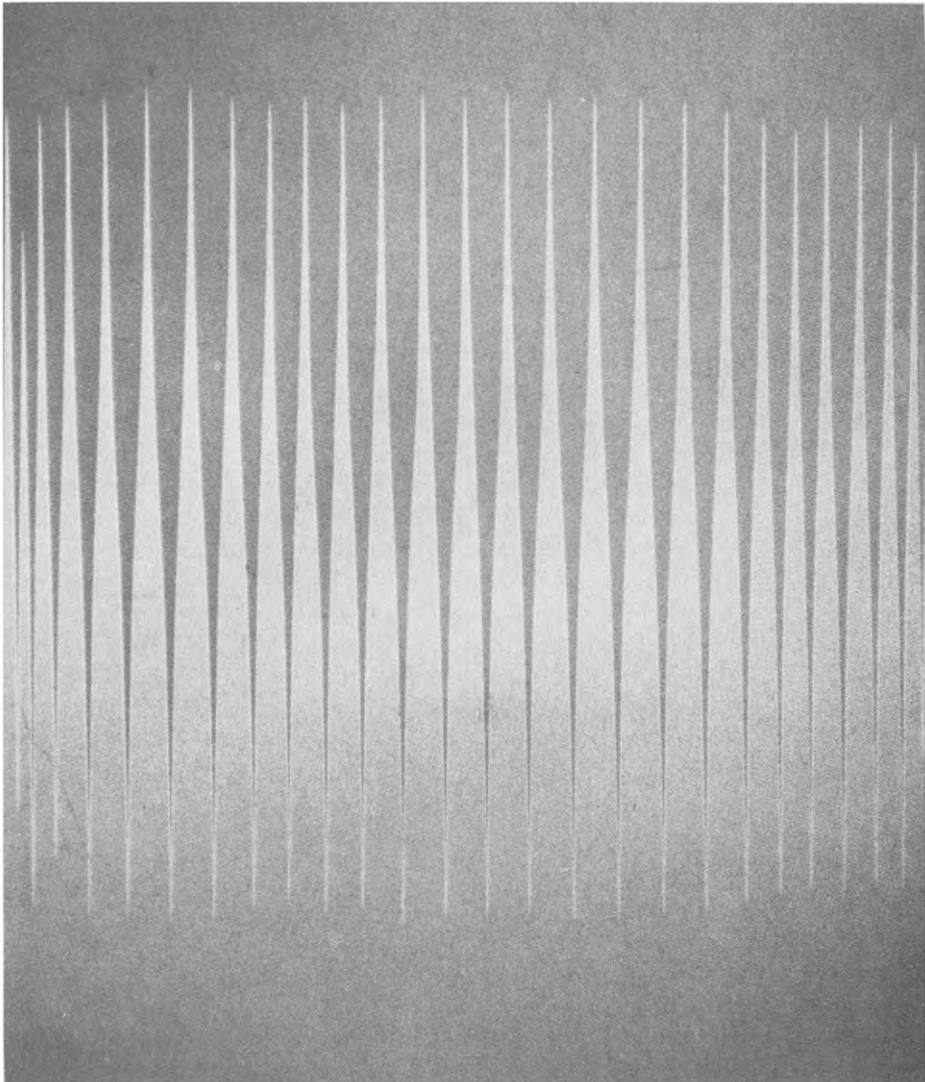


Fig. 30.30. Photograph of a zigzag domain wall in β' - $\text{Gd}_2(\text{MoO}_4)_3$ viewed between crossed polarizers in transmitted light.

Under field or stress, the zz wall moves sideways, i.e., vertically in fig. 30.30, while retaining essentially the same shape. Individual tips remain in the same (110) planes as the zz wall moves across the crystal. The observed zz wall mobility is 20 to 30 times higher than the planar wall mobility.

Individual tips of this zz can be extended if an electric field is applied immediately over the tip. Such tips have been observed to move at about 10^2 m/sec, i.e., about 10% of the velocity of sound. This is much faster than the observed net velocities of the whole zigzag wall. (This observation suggests that

if twinning dislocation motion is a reasonable description of domain wall movement, then these dislocations must be moving at least 10% the sound velocity in these blade tips.)

The actual width of domain walls in β' - $\text{Gd}_2(\text{MoO}_4)_3$ has been the subject of several articles. Domain Walls in ferroelastics would tend to be thicker than strain-free domain walls found in ferroelectrics. This thicker wall reduces the strain energy in the wall. Direct observations of a wall in a polarizing microscope suggests a wall thickness of a few microns (Shepherd and Barkley, 1972) but this observation is complicated by refraction and diffraction of the transmitted light in the region of the wall. Observation of the diffraction pattern from a wall in a (001) plate having a halfwave retardation suggested a wall thickness of $1.3 \mu\text{m}$ (Suzuki, 1972). Shepherd and Barkley (1972) using Raman scattering from the distorted material in a moving wall estimated a wall thickness greater than $\sim 0.8 \mu\text{m}$. However, antiphase boundaries which were discovered later (Barkley and Jeitschko, 1973 and Meleshina et al., 1974), could also have contributed to the observed Raman signal. thus the estimate of $0.8 \mu\text{m}$ from the Raman data could very well be high.

Berg-Barrett X-ray data (Bindloss and Moore, unpublished) suggest a planar wall thickness of less than $1 \mu\text{m}$. Kittel (1972) estimated a wall thickness in β' - $\text{Gd}_2(\text{MoO}_4)_3$ of $\sim 0.4 \mu\text{m}$ from the free energy difference between β and β' phases as derived from the specific heat data of Fouskova (1969).*

A second estimate of the wall thickness was made by Haas and Jaep (1974) by considering the material in the wall as elastically strained β' -phase. Their estimated thickness is $\sim 0.8 \mu\text{m}$. However, the energy per unit surface area of the wall in Kittel's model was estimated to be $\sim 100 \text{ ergs/cm}^2$ as compared with Haas and Jaep's 0.1 erg/cm^2 . It would seem that future experiments on wall energies will differentiate between these estimates, a factor of 10^3 apart.

Thus, at this time, the evidence seems to indicate a wall thickness $\leq 1 \mu\text{m}$, which is indeed much thicker than the pure ferroelectric domain walls which are commonly thought of as a few lattice dimensions thick (Cohen, 1951).

3.7. Crystal defects

Crystal defects impede domain wall movement by increasing E_0 and τ_0 , the minimum field and stress needed to initiate motion. For this reason, studies of chemically etched surfaces of $\text{Gd}_2(\text{MoO}_4)_3$ have been done to investigate the nature of these defects. Kashiwada and Kishino (1974) have used chemical etchants and X-ray transmission topography to identify flat helical dislocations and flat closed loop dislocations that have axes parallel [110] directions. Although these authors did not report on the interaction of these defects with

*Later specific heat data by Cheung and Ullman (1974) also agrees with Fouskova's transition entropy estimate $\sim 0.22 \text{ cal/mole K}$. T_c is observed to increase linearly with hydrostatic pressure at the rate $\delta T_c / \delta p = 29.5 \pm 0.3 \text{ deg/kbar}$ (Shirokov, ^{et al.} 1972). Their estimate of the transition entropy $\Delta s = 0.17 \text{ cal/mole deg}$ also agrees reasonably well with Fouskova's.

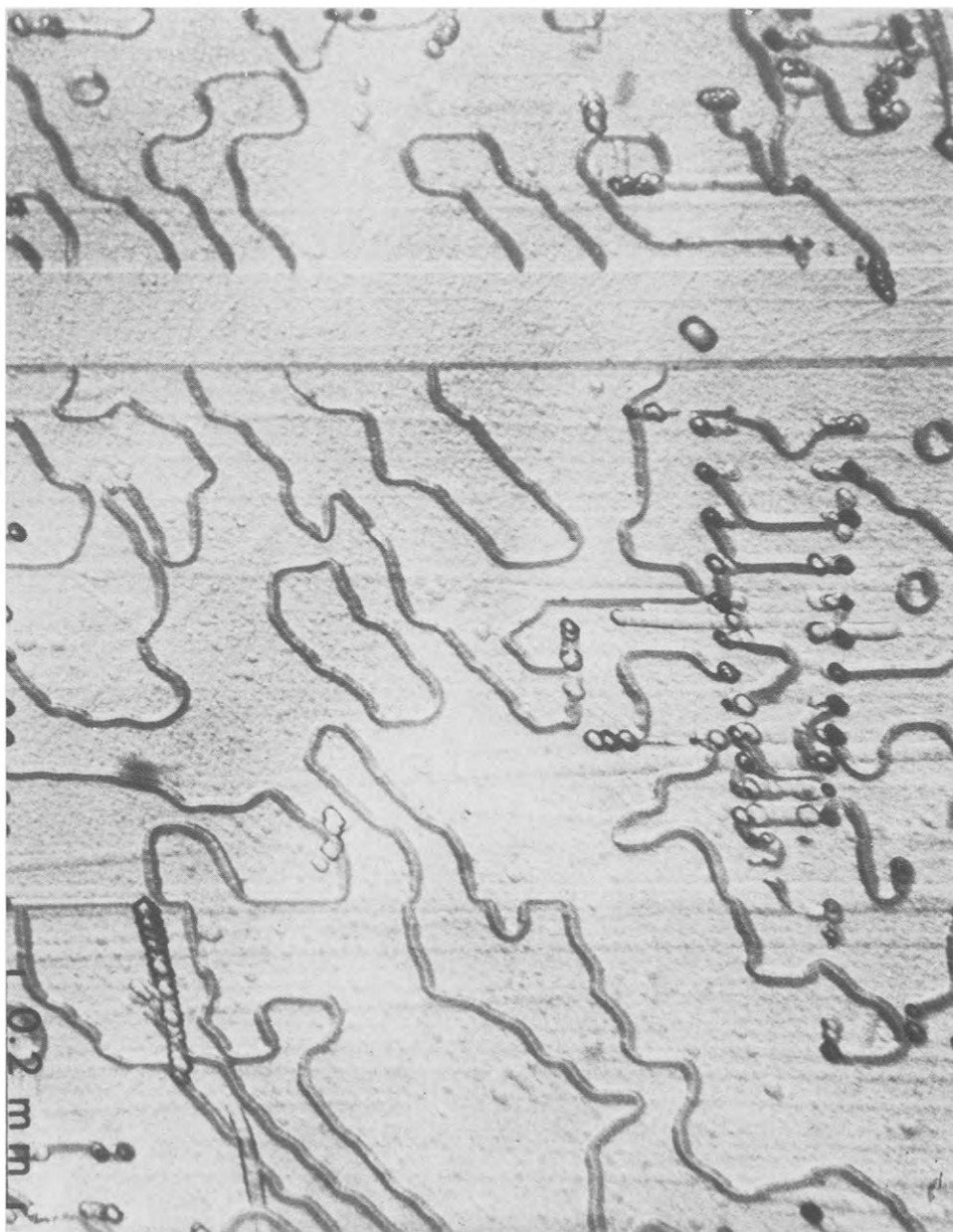


Fig. 30.31. Photomicrograph on an etched (001) surface of $Gd_2(MoO_4)_3$ taken in reflected light. Trench-like etch pits develop along APB's in the negatively charged surfaces but not in the positively charged surface in the reverse domain. This is a typical distribution of antiphase boundaries in crystals cooled through T_C when very little domain wall movement occurs (Barkley and Jeitschko, 1973).

domain walls, our own work (unpublished) shows that E_0 is significantly increased by factors of 1.5 to 3, as a wall attempts to move through an array of these defects. Kumada (1973) uses deliberately induced defects to provide a well-defined threshold field which is advantageous in certain device applications.

Antiphase boundries have been observed in the β' phase by several methods. Barkley and Jeitschko (1973) found that dilute HCl (~5%) formed trench-like etch pits along antiphase boundries, as shown in fig. 30.31. These boundries were rearranged, annihilated and created by domain wall movement or by heating above the Curie temperature. Other researchers have also seen these boundries (Bohm and Kursten, 1973; Meleshina et al., 1974; Capelle and Malgrange, 1973; Yamaoto et al., 1974) with etching and/or X-ray topography or electron microscopy techniques.

The β' - $R_2(\text{MoO}_4)_3$ compositions have been and probably will continue to be a rich source of interesting phenomena related to coupled electrical, elastic and optical properties, which are fortuitously available at room temperature or above in high quality crystals readily grown.

References

- Abrahams, S.C. and J.L. Bernstein, 1966, *J. Chem. Phys.* **45**, 2745.
 Abrahams, S.C. and E.T. Keve, 1971a, *Ferroelectrics* **2**, No. 2, 129.
 Abrahams, S.C., 1971b, *Mat. Res. Bull.* **6**, No. 10, 831.
 Aizu, K., 1969, *J. Phys. Soc. Jap.* **27**, No. 2, 387.
 Aizu, K., A. Kumada, H. Yumoto and S. Ashida, 1969, *J. Phys. Soc. Jap.* **27**, 511.
 Aizu, K., 1971a, *J. Phys. Soc. Jap.* **31**, No. 3, 802.
 Aizu, K., 1971b, *J. Phys. Chem. Solids* **32**, 1959.
 Aizu, K., 1974, *J. Phys. Soc. Jap.* **36**, 1273.
 Axe, J.D. and G. Shirane, 1970, *Phys. Rev.* **B1**, 342.
 Axe, J.D., B. Dorner, and G. Shirane, 1971, *Phys. Rev. Lett.* **26**, 519.
 Bagdasarov, Kh.S., G.A. Bogomolova, A.A. Kaminskii, A.M. Prokhorov, and T.M. Prokhortseva, 1971, *Sov. Phys. - Doklady* **16**, No. 3, 216.
 Banks, E. and M. Nemiroff, 1974, *Inorg. Chem.* **13**, 2715.
 Barkley, J.R., L.H. Brixner, E.M. Hogan, and R.K. Waring, Jr., 1972, *Ferroelectrics* **3**, 191.
 Barkley, J.R. and W. Jeitschko, 1973, *J. Appl. Phys.*, **44**, 938.
 Blasse, G., 1966, *J. Inorg. Nucl. Chem.* **28**, 1488.
 Bohm, J. and H.D. Kürsten, 1973, *Phys. Status Solidi (a)* **19**, 179.
 Borchardt, H.J., 1965, *J. Chem. Phys.* **42**, No. 11, 3743.
 Borchardt, H.J., P.E. Bierstedt, 1966, *Appl. Phys. Lett.* **8**, No. 2, 50.
 Borchardt, H.J. and P.E. Bierstedt, 1967, *J. Appl. Phys.* **38**, No. 5, 2057.
 Borchardt, H.J., 1968, Abstract No. 105, p. 265, *Electrochem. Soc. Spring Meeting, Boston*.
 Bornarel, J., 1975, *Ferroelectrics* **9**, 197.
 Boyer, L.L. and J.R. Hardy, 1972, *Solid State Commun.* **11**, 555.
 Boyer, L.L. and J.R. Hardy, 1973, *Phys. Rev.* **B8**, 2205.
 Brixner L.H., 1964, *Inorg. Chem.* **3**, 1065.
 Brixner, L.H. and E. Abramson, 1965, *J. Electrochem. Soc.* **112**, 70.
 Brixner, L.H., P.E. Bierstedt and A.W. Sleight, 1971, *Mat. Res. Bull.* **6**, 545.
 Brixner, L.H., 1972, *Mater. Res. Bull.* **7**, 879.
 Brixner, L.H., A.W. Sleight and M.S. Lcicis, 1972, *J. Solid State Chem.* **5**, 186.
 Brixner, L.H., 1973, *Rev. Chim. Miner.* **10**, 47.
 Brodale, G.E., R.A. Fisher, E.W. Hornung and W.F. Giauque, 1972, *J. Chem. Phys.* **56**, 6118.
 Capelle, B. and C. Malgrange, 1973, *Phys. Status Solidi (a)* **20**, K5.
 Cheung, K.M. and F.G. Ullman, 1974, *Phys. Rev.* **B10**, No. 11, 4760.
 Chizhikov, S.I., N.G. Sorokin, B.I. Ostrovskii and V.A. Meleshina, 1971, *Sov. Phys.-JETP Lett.* **14**, 336.
 Cleve, A., 1902, *Z. anorg. allgem. Chem.* **32**, 129.
 Cohen, M.H., 1951, *Phys. Rev.* **84**, 369.
 Courdille, J.M. and J. Dumas, 1973, *Phys. Rev.* **B8**, No. 8, 1129.
 Courdille, J.M., R. Deroche and J. Dumas, 1975, *J. Phys. (Paris)* **36**, 891.
 Craig, D.C. and N.C. Stephenson, 1968, *Acta Crystallogr.* **B24**, 1250.
 Cross, L.E., A. Fousková and S.E. Cummins, 1968, *Phys. Rev. Lett.* **21**, No. 12, 812.
 Cummins, S.E., 1970, *Ferroelectrics* **1**, 11.
 Dem'yanov, V.V. and M.I. Shchedrin, 1973, *Sov. Phys.-Solid State* **14**, No. 10, 2620.
 Aizu K., 1970, *Phys. Rev.* **B2**, 754.

- Dorner, B., J.D. Axe and G. Shirane, 1972, *Phys. Rev.* **B6**, No. 5, 1950.
- Dvorak, V., 1971, *Phys. Status Solidi (b)* **46**, 763.
- Elzen, van den, A.F. and G.D. Rieck, 1973, *Acta Crystallogr.* **B29**, 2436.
- Epstein, D.J., W.V. Herrick and R.F. Turek, 1970, *Solid State Commun.* **8**, 1491.
- Epstein, D.J., 1970, Technical Report AFAL-TR-70-172.
- Esayan, S. Kh., Kh. S. Bagdasarov, V.V. Lemanov, T.M. Polkhovskaya and L.A. Shuvalov, 1974, *Sov. Phys.-Solid State* **16**, No. 1, 85.
- Fisher, R.A., E.W. Hornung, G.E. Brodale and W.F. Giaque, 1972, *J. Chem. Phys.* **56**, 193.
- Fisher, R.A., E.W. Hornung, G.E. Brodale and W.F. Giaque, 1973, *J. Chem. Phys.* **59**, 5798.
- Fisher, R.A., E.W. Hornung, G.E. Brodale and W.F. Giaque, 1975, *J. Chem. Phys.* **63**, 1295.
- Fleury, P.A., 1970, *Solid State Commun.* **8**, 601.
- Fleury, P.A., 1971, *Acoust. Soc. Amer.* **49**, No. 3, 1041.
- Flippen, R.B., 1975, *J. Appl. Phys.* **46**, No. 3, 1068.
- Flippen, R.B. and C.W. Haas, 1973, *Solid State Commun.* **13**, 1207.
- Fousek, J. and C. Konak, 1972, *Czechoslovak J. Phys.* **B22**, 995.
- Fousková, A., 1969, *J. Phys. Soc. Jap.* **27**, 1699.
- Frost, H.J. and M.F. Ashby, 1971, *J. Appl. Phys.* **42**, No. 13, 5273.
- Ganguly, B.N., F.G. Ullman, R.D. Kirby and J.R. Hardy, 1975, *Solid State Commun.* **17**, 533.
- Haas, C.W. and W.F. Jaep, 1974, *Phys. Lett.* **49A**, No. 1, 77.
- Hitchcock, F.R.M., 1895, *J. Amer. Chem. Soc.* **17**, 522.
- Höchli, U.T., 1972, *Phys. Rev.* **B6**, No. 5, 1814.
- Hornung, E.W., G.E. Brodale, R.A. Fisher and W.F. Giaque, 1972, *J. Chem. Phys.* **56**, 5007.
- Hubert, P.H., 1975, *Bull. Soc. Chim. Fr.* p. 161.
- Janovec, V., 1976, *Ferroelectrics* **12**, 43.
- Jeitschko, W., 1970, *Naturwiss.* **57**, 544.
- Jeitschko, W., 1972, *Acta Crystallogr.* **B28**, 60.
- Jeitschko, W., 1973, *Acta Crystallogr.* **B29**, 2074.
- Jeitschko, W. and H. Wondratschek, 1974, *Fortsch. Mineral.* **52**, Beiheft 2, 30.
- Kashiwada, Y. and S. Kishino, 1974, *Jap. J. Appl. Phys.* **13**, No. 2, 223.
- Keller, C., 1962, *Z. anorg. allgem. Chem.* **318**, 89.
- Keve, E.T., S.C. Abrahams, K. Nassau and A.M. Glass, 1970, *Solid State Commun.* **8**, 1517.
- Keve, E.T., S.C. Abrahams and J.L. Bernstein, 1971, *J. Chem. Phys.* **54**, 3185.
- Kittel, C., 1972, *Solid State Commun.* **10**, 119.
- Klevtsova, R.F., V.A. Vinokurov and P.V. Klevtsov, 1972, *Sov. Phys.-Crystallogr.* **17**, 240.
- Klevtsov, P.V., L.P. Kozeeva, V.I. Protasova, L. Yu. Kharchenko, L.A. Glinskaya, R.F. Klevtsova and V.V. Bakakin 1975, *Sov. Phys.-Crystallogr.* **20**, 31.
- Kobayashi, J., Y. Sato and T. Nakamura, 1972, *Phys. Status Solidi (a)* **14**, 259.
- Kumada, A., 1969, *Phys. Letters* **30A**, No. 3, 186.
- Kumada, A., 1970, *J. Jap. Soc. Appl. Phys. Suppl.* **39**, 258.
- Kumada, A., 1972, *Ferroelectrics* **3**, 115.
- Kumada, A., 1973a, *J. Phys. Soc. Jap.* **35**, 941.
- Kumada, A., 1973b, *IEEE Trans. Electr. Devices* **ED-20**, No. 10, 866.
- Kumada, A., 1974, *Ferroelectrics* **7**, 145.
- Kürsten, H.D., J. Bohm, C. Scheiding and H. Blumberg, 1973, *Kristall und Technik* **8**, 303.
- Levanyuk, A.P. and D.G. Sannikov, 1970, *Fiz. Tverd. Tela.* **12**, 2997.
- McCarthy, G.J., 1973, *Mater. Res. Bull.* **6**, 31.
- McCarthy, G.J., 1974, private communication to Megumi et al.
- Megumi, K., H. Yumoto, S. Ashida, S. Akiyama and Y. Furuhashi, 1974, *Mat. Res. Bull.* **9**, 391.
- Meleshina, V.A., V.L. Indenbom, Kh. S. Bagdasarov and T.M. Polkhovskaya, 1974, *Sov. Phys. Crystallogr.* **18**, No. 6, 764.
- Midorikawa, M., Y. Ishibashi and Y. Takagi, 1974, *J. Phys. Soc. Jap.* **37**, No. 6, 1583.
- Miller, R.C., W.A. Nordland and K. Nassau, 1971, *Ferroelectrics* **2**, 97.
- Nakamura, T., T. Kondo and A. Kumada, 1971a, *Phys. Lett.* **36A**, No. 2, 141.
- Nakamura, T., T. Kondo and A. Kumada, 1971b, *Solid State Commun.* **9**, 2265.
- Nassau, K., H.J. Levinstein and G.M. Loiacono, 1965, *J. Phys. Chem. Solids* **26**, 1805.
- Nassau, K., J.W. Shiever and E.T. Keve, 1971, *J. Solid State Chem.* **3**, 411.
- Newnham, R.E., H.A. McKinstry, C.W. Gregg and W.R. Stitt, 1969, *Phys. Status Solidi* **32**, K49.
- Newnham, R.E., C.S. Miller, L.E. Cross, T.W. Cline, 1975, *Phys. Status Solidi (a)* **32**(1), 69.
- Petzelt, J., 1971a, *Solid State Commun.* **9**, 1485.
- Petzelt, J. and V. Dvorak, 1971b, *Phys. Status Solidi (b)* **46**, 413.
- Pytte, E., 1970, *Solid State Commun.* **8**, 2101.
- Sapriel, J., 1975, *Phys. Rev.* **B12**, 5128.
- Sawaguchi, E. and L.E. Cross, 1973, *J. Appl. Phys.* **44**, No. 6, 2541.
- Scheiding, C., G. Schmidt and H.D. Kürsten, 1973, *Krist. Tech.* **8**, 311.
- Scott, J.F., 1974, *Rev. Mod. Phys.* **46**, No. 1, 83.
- Shannon, R.D. and C.T. Prewitt, 1969, *Acta Crystallogr.* **B25**, 925.
- Shepherd, I., 1971, *Solid State Commun.* **9**, 1857.
- Shepherd, I. and J.R. Barkley, 1972, *Solid State Commun.* **10**, 123.
- Shirokov, A.M., V.P. Mylov, A.I. Baranov and T.M. Prokhortseva, 1972, *Sov. Phys.-Solid State* **13**, No. 10, 2610.
- Sillén, L.G. and K. Lundborg, 1943, *Z. anorg. allgem. Chem.* **252**, 2.
- Smith, A.W. and G. Burns, 1969, *Phys. Lett.* **28A**, No. 7, 501.

- Suzuki, K., 1972, *Solid State Commun.* **11**, 937.
- Templeton, D.H. and A. Zalkin, 1963, *Acta Crystallogr.* **16**, 762.
- Toledano, J.C., 1974, *Ann. des Tekcommunications* **29**, No. 7/8, 249.
- Ullman, F.G., B.N. Ganguly and J.R. Zeidler, 1972, *J. Electronic Materials* **1**, No. 3, 425.
- Ullman, F.G., K.M. Cheung, G.A. Rakes and B.N. Ganguly, 1975, *Ferroelectrics* **9**, 63.
- Whinfrey C.G., D.W. Eckart and A. Tauber, 1960, *J. Amer. Chem. Soc.* **82**, 2695.
- Wolfe, R.W. and R.E. Newnham, 1969, *Solid State Commun.* **7**, 1797.
- Wondratschek, H. and W. Jeitschko, 1976, *Acta Crystallogr.* **A32**, 664.
- Yamamoto, N., K. Yagi and G. Honjo, 1974, *Phil. Mag.* **30**, (5), 1161.
- Zemann, J., 1956, *Heidelb. Beitr. Mineral. Petrogr.* **5**, 139.

SUBJECT INDEX

- absorption spectra
 nature of transitions, 175
 R^{3+} -ions, 176
 R^{2+} -ions, 184
- 2-acetamidohexafluoro-2-propanol complex, 268
- acetate complex, 262
 stability constants, 241
 thermodynamics, 243
- acetylacetone complex, 266, 267
 emission spectra, 252
 structures, 225, 230, 231, 232
- adiabatic transitions, 151
- adogen, 108
- age dating - Sm, Nd, 64
- Ahrland's parameter δ_A , 136
- alamine, 108
- aliquat, 108
- alkoxides, 267, 278, 279
- allyl complex, 285, 286
- amalgam extraction (Sm, Eu, Yb), 85
- amine extractants, 105, 107
- angular overlap model, 160
- anion-exchange
 extractants, 104
- anisotropic complexes, 149
- anti-base, 134
- antiferromagnetic
 coupling, 163
- antimonides, 155-156
- antipyrène complexes, 265
 magnetic
 susceptibility, 254
 structure, 225, 235
- aqua ions, 122, 126, 138, 151, 239-240, 255
- atomic units, 115, 129
- band intensities, 123, 164
- bastnaesite, 83, 84
- Beer-Lambert law, 188
- benzoylacetone complex
 structures, 232
- benzylethylenediaminetriacetate, N' -, 97
- bis(2-aminoethyl)ethertetraacetate, 96
- bisethoxydithiophosphinate complexes, 279
- 1,2-bis(pyridine-2-aldimino)ethane complexes, 237, 238, 275
- branching ratios
 radiative, 196-197
- bromide complex, 246
- carbonyl, 288
- catalytic properties
 perovskites, 562
- cathodoluminescence, 164
- cation-exchange
 extractants, 103
- cerite, 83
- cerium
 acetylacetone
 (Ce(IV)), 232
 cyclooctatetraene
 structures, 286
 fluoro complex
 structure, 257
 hexanitrate complex, 239
 pentanitrate complex, 237
 pyridine-2,6-dicarboxylate, 277
 TPPO-nitrate (Ce(IV))
 structure, 237
 TTA structure, 230
- cerium anomaly
 geochemical, 17
- cerium metal, 159
- cerium oxidation (to CeO_2 , Ce(IV)), 84, 85
- Ce_2O_3
 thermodynamic
 properties, 368
- $CeO_{1.818}$
 heterogeneous
 reactions, 377
- CeO_x
 oxygen diffusion in, 379, 381
 phase diagram, 353, 354
 structure, 342, 343, 355
 thermodynamic
 properties, 370, 372
- $CeO_{2.8}$
 phase diagram, 354
 structure, 342, 343, 355
- CeO_2
 single crystal growth, 384
- Ce(IV) and Th(IV)
 removal of, 86
- cerium(III) spectra, 126, 145, 165
- chalkophilic elements, 133
- chloride complex
 absorption spectra, 245, 246, 248
 emission spectra, 253
 ESR, 256
 infrared and Raman
 spectra, 258
 magnetic
 susceptibility, 254
- chromatography, 87, 89, 93, 103
- chromium(III) kinetics, 122
- citrate, 95
- citric acid, 89
- collective effects, 163
- concentration-gradient
 elution, 89
- conditional oxidation
 state, 147, 154, 158, 162
- configuration
 interaction, 185
- coordination number, 116, 120, 121, 123, 124, 148, 149
 three, 201, 221

- coordination number (*contd.*)
 four, 222
 five, 223
 six, 221, 224–225
 seven, 226–229
 eight, 229–232
 nine, 125, 161, 234–237
 ten, 237–238
 twelve, 239
 Coulomb interaction, 185
 covalency, 216–217
 cross-linkage, 91, 95
 crystal chemistry
 garnets, 554
 molybdates, 624–652
 crystal growth
 oxides, 382, 384
 crystal structures
 garnets, 563
 hydrides, 303–307
 mixed oxides, 452
 molybdates, 624
 oxides, 342
 perovskite, 535, 545
 crystal types, 116
 cyanate complex, 257, 259
 cyclooctatetraene
 complex, 286–288
 with cyclopentadiene, 288
 cyclopentadiene complexes
 adducts, 283
 alkyl and aryl
 groups, 284–286
 allyl, 285
 cyclooctatetraene, 288
 di, 282
 di- and mono-halides, 283,
 284
 tris-, 281–282
 cyclopropyleneurea, 266

 diamides, 265
 1,2-diaminobutanetetra-
 acetate, 97
 2,3-diaminobutanetetra-
 acetate, 97
 diaminocyclohexanetetra-
 acetate, 91
 dibenzoylmethane
 complex, 220
 structure, 228
 di-2,2-dimethylhexyl
 phosphoric acid, 107
 dielectric constant, 130
 diethylenetriamine, 244, 272,
 274
 diethylenetriaminepenta-
 acetate, 96
 di-2-ethylhexyl phosphoric
 acid, 107
 diffusion
 of hydrogen in
 hydrides, 324, 325
 of oxygen in rare earth
 oxides, 378
 of oxygen in CeO_{2-x} , 379
 of oxygen in $\text{Pr}_7\text{O}_{12±δ}$, 379
 of oxygen in CeO_{2-x} , 380
 dimethylacetamide, 265
 dimethylformamide
 adducts, structure, 231,
 236
 2,6-dimethyl-4-pyrone
 complexes, 225
 dimethylsulfoxide
 complexes, 220, 269, 270
 adducts with
 $\text{R}(\text{DPM})_3$, 228–229
 structures, 235, 237, 238
 3,3-dimethyl-thietane-1-oxide
 adduct with
 $\text{Lu}(\text{DPM})_3$, 228
 di-n-amyI phosphoric
 acid, 106
 di-n-octyl phosphoric
 acid, 106
 dioxides
 electrical properties, 387
 magnetic properties, 390
 mechanical
 properties, 394
 optical properties, 391
 structural
 properties, 342ff
 structure, 350–351
 thermodynamic
 properties, 370
 diphenylsulfoxide
 complexes, 270
 dipicolinate complexes, 277
 structures, 235
 dipivaloylmethane
 complexes, 218, 220, 267
 structures, 225–229, 231–
 233
 terbium emission, 251
 2,2'-dipyridyl
 complexes, 272, 273
 structure, 237
 2,2'-dipyridyl-1,1'-dioxide
 complexes, 269, 270
 displacement
 chromatography, 93
 distribution coefficients, 93,
 105
 dithiocarbamate
 complexes, 118, 149, 152,
 279, 280
 dysprosium
 coordination number 7,
 228
 DPM structure, 228
 NTA structure, 220, 231
 Dy_2O_3
 heterogeneous
 reaction, 317
 structure, 346, 347
 thermodynamic
 properties, 368

 EDTA complexes, 119, 237
 Mössbauer, 254, 277
 stability constants, 241
 thermodynamic data, 242–
 243
 effective operators, 185, 186
 Einstein coefficient, 189
 elastic properties
 garnets, 597
 electrical properties
 higher oxides, 387
 lower oxides, 385, 386
 perovskites, 558
 sesquioxides, 385
 electric dipole operator, 188,
 189, 196
 electron configuration, 127,
 138, 142, 155
 electroneutrality, 128
 electronic properties
 hydrides, 319–323
 electron microscopy, 361,
 362, 363
 electron transfer band, 147,
 148, 165
 electron transfer
 process, 189
 elements
 inner-transition, 82
 elevated temperature
 separation chemistry, 90

- elution chromatography
 anion, 89
 cation, 87
 concentration-gradient, 88
 pH-gradient, 88
- elution sequences, 90, 91, 100, 101, 102, 103
- elutions with
 DTPA, 102
 EDTA, 98
 HEDTA, 100
 NTA, 103
- energy level schemes, 185
- energy transfer, 163
- $\text{ErO}_{1.489}$, 349
- Er_2O_3
 heterogeneous
 reactions, 377
 oxygen diffusion in, 378
 structure, 346, 347
 thermodynamic
 properties, 368
- erbium
 coordination number
 6, 224, 225
 dimethylsulfoxide, 235
 DPM structure, 225
 thiocyanate complex, 224, 259
- erbium(III) spectra, 159, 161, 165
- ESCA, 153
- esters
 orthophosphate, 105, 106
- ethylenediamine
 complexes, 244, 272, 274
- ethylenediaminedimalonate, 96
- ethylenediaminedi-succinate, 90
- ethylenediaminetetra-acetate, 90
- ethylenediaminetriacetate
 N' -benzyl-, 97
 N' -hydroxyethyl-, 100
 N' -methyl-, 97
- ethyleneglycolbis(2-aminoethyl)ethertetra-acetate, 96
- ethyleneurea
 complexes, 264
- ethyl sulfates, 235, 256
- EuO
 occurrence, 340
- single crystal growth, 384
- thermodynamic
 properties, 370
- Eu_3O_4
 occurrence, 340
 thermodynamic
 properties, 370
- $\text{EuO}_{1.45}$, 349
- Eu_2O_3
 polymorphism, 341
 single crystal growth, 384
 thermodynamic
 properties, 368
 vaporization
 characteristics, 371
- europium
 acetylacetone
 adducts, 231
 benzoylacetone, 231, 232
 coordination number 3,
 221
 CPL, 253
 cyclopentadiene
 (Eu(II)), 282
 dipivaloylmethane
 adducts, 228, 231, 232,
 233
 EDTA spectra, 249
 energy levels, 250, 251
 hexafluoroacetylacetone,
 230
 malonic acid, 236
 Mössbauer, 254, 277
 picoline-N-oxide emission
 spectrum, 252
 TTA, 232, 267
- europium anomaly
 geochemical, 6, 15, 32,
 52-55
 as O_2 barometer, 54
 effects of oxygen
 pressure, 54, 55
 experimental studies, 53
- europium reduction (to
 Eu^{2+}), 85
- europium(III) spectra, 125,
 148, 149, 164
- euxenite, 83, 84
- excited state relaxation, 196
- extractions with HDEHP and
 HEHP, 103, 104
- facam complex, 236
- fergusonite, 83, 84
- fluorescing states,
 R^{3+} (aqua), 174, 195-196
- fluorites, 116, 146, 150, 158
 mixed oxides, 489
 oxides, 352
- fluoro complexes, 257
- fod complex, 231, 267
- fractional crystallization and
 precipitation, 86
- fractional parentage, 155
- Franck-Condon
 principle, 112, 150
- free-ion energy levels, 187-
 188
- g -value, 174
- $\text{GdO}_{1.495}$, 349
- Gd_2O_3
 structure, 344, 345
 thermodynamic
 properties, 368
 vaporization
 characteristics, 371
- gadolinite, 83, 84
- gadolinium
 1,2-bis(pyridine-2-
 aldimino)ethane
 structure, 237, 238
 coordination number
 6, 225
 2,6-dimethyl-4-pyrone, 225
 TTA (mass spectra), 267
- garnets
 crystal chemistry, 554-556
 crystal structure, 563
 elastic properties, 597
 magnetic properties, 569,
 579
 growth-induced noncubic
 anisotropy, 573-577
 magnetization, 569, 570
 magnetocrystalline
 anisotropy, 572-575
 magnetostriction, 577-
 579, 581
 molecular field
 theory, 570-572
 optical properties, 579-
 590
 crystal field effect, 580,
 582
 infrared spectra, 585-
 587

- garnets (*contd.*)
 magneto-optical
 effects, 582-584
 optical adsorption, 587-590
 photomagnetic
 effect, 584, 585
 phase equilibria, 566
 preparation
 ceramic synthesis, 566, 567
 epitaxial films, 568, 569
 single crystal
 methods, 567, 568
 thermal properties
 specific heat, 593-596
 thermal
 conductivity, 590-593
 thermal expansion, 596
 gaseous molecules, 112, 121, 164
 geochemical partitioning of
 lanthanides
 amphibole, 37
 apatite, 48, 51, 52
 distribution
 coefficients, 45, 47-52
 equations for, 45
 experiments, 48-52
 feldspar, 19, 32, 34, 35, 48
 fractional
 crystallization, 24, 27, 45, 46, 47, 56, 59, 60
 garnet, 28-29, 37, 40, 41, 42, 48, 51
 models for, 7, 44-47, 55-63
 natural system distribution
 coefficients, 46-47
 olivine, 11, 19, 25, 37, 40, 41
 perovskite, 7
 phenocryst-matrix
 distribution, 48, 49
 pyroxene, 19, 37, 38, 40, 41, 42, 48, 51
 spinel, 37
 surface-equilibrium
 model, 60
 synthetic mineral
 studies, 48-49
 temperature effects, 49-50
 geochemistry
 lanthanides, 2
- Sc, 2
 Y, 2
 geosynclines, 11, 12, 24
 glasses, 164
 glycolate, 88
 glycolate complexes, 262
 stability constants, 241
 structures, 231, 235
 thermodynamic data, 242-244
 gradient elution, 88
 halide anions, 130, 133, 149
 halide complexes (*see*
 bromide, etc.), 257-258
 hard and soft anti-bases and
 bases, 134
 Hartree-Fock methods, 187
 heat of atomization, 136, 159
 height equivalent to a
 theoretical plate, 94
 HETP, 94
 hexafluoroacetylacetone
 complexes, 266
 ligand exchange, 255
 structures, 230, 231
 hexahalide complexes, 121, 148, 149
 hexamethylphosphoramide
 complexes, 260, 269, 270
 higher oxides, 352
 Ho_2O_3
 heterogeneous
 reaction, 377
 structure, 346, 347
 thermodynamic
 properties, 368
 holmium
 acetylacetone
 structure, 231, 232
 coordination number
 7, 228
 dibenzoylmethane
 structure, 228
 dipivaloylmethane, 231, 232
 nitrate complex
 structure, 238
 tropolone, 230
 Hund's rules, 114, 123
 hydration energy, 129, 136
 hydration difference
 parameter, 131, 134
 hydration number, 201
 hydrides
 crystal structures, 303-307
 diffusion of H in, 324, 325
 electronic properties, 319-323
 inelastic neutron scattering
 in, 325, 326
 kinetics of formation, 323
 reaction
 mechanisms, 323
 magnetic properties, 315-319
 Mössbauer
 spectroscopy, 328, 329
 phase relations, 301-303
 La-H system, 304
 Nd-H system, 304
 Ce-H system, 305
 positron annihilation in, 327
 rare earth alloy
 hydrides, 329-333
 specific heat measurements
 in, 327, 328
 thermodynamic
 properties, 307-315
 dihydrides, 308-312
 specific heat, 314, 315
 trihydrides, 312-314
 hydrogen electrode, 129
 hydrolysis constants, 214
 hydroxides of trivalent
 lanthanons, 86
 hydroxyethylethylenedi-
 aminetriacetate, 91
 hydroxyisobutyrate, 88
 hypersensitive
 transitions, 164, 194
 hypersensitivity, 247
 hysteresis
 in oxide systems, 364
 in TbO_x , 365
 icosahedral
 chromophore, 121
 IMDA, 276
 stability constants with
 EDTA, 241
 structure, 277
 thermodynamic data with
 EDTA, 242-244
 indene complexes, 286
 inert support materials, 103

- inner sphere
 complexes, 239, 244
 inner-transition elements, 82
 iodo complexes, 247
 ion-exchange processes, 86
 intensity
 infrared absorption, 194
 interelectronic
 repulsion, 141
 intermediate coupling, 174, 191
 intermediate oxides
 electrical properties, 387
 magnetic properties, 390
 optical properties, 391
 oxygen diffusion, 379
 structural
 properties, 342ff
 thermodynamic
 properties, 368, 370
 ionic radii, 82, 213, 343
 ionization energy, 128, 131, 132, 146, 153
 isomerism, 214
 isomorphic series, 82
 iron cyanide
 complexes, 150, 151
 Judd-Ofelt theory, 189-190
 parameters, conversion
 relationships, 193
 Katzin effect, 125
 kinetics
 of hydride formation, 323
 of oxide reactions, 376
 lactate, 88
 Landé parameter γ_{nl} , 140, 161
 $\text{LaO}_{1.5}$
 structure, 342, 343, 349
 $\text{La}_2\text{O}_{2.998}$, 349
 La_2O_3
 thermodynamic
 properties, 368
 vaporization
 characteristics, 371
 lanthanide abundances, 3-5
 alkali basalts, 24, 27, 39
 anorthosites, 34-36
 basalts, 19, 25
 carbonates, 9, 12, 13, 14
 chondrites, 3, 4, 5
 clays, 10, 12, 13
 continental basalts, 26-30
 earth's crust, 14
 eclogite, 42
 granite, 32-34
 igneous rocks, 19-21
 Japanese basalts, 24, 25
 kimberlite, 29, 30, 40, 41
 komatiite, 25
 KREEP, 30-31
 layered intrusions, 43
 lunar highlands, 30-31
 lunar mare basalts, 22, 23
 minerals, 35
 North American shales, 5, 8
 ocean floor basalts, 16-19, 21-22
 ocean island basalts, 23-26
 ophiolites, 26
 peridotites, 25, 37, 38, 39, 41
 precambrian rocks, 15, 62, 63
 rhyolites, 20
 sandstones, 9, 11, 12, 13, 14
 sea water, 17-19
 sedimentary rocks, 8, 11
 shales, 8, 9
 sun, 3
 tholeiitic basalts, 20, 21, 24, 25, 28
 ultramafic rocks, 37, 38, 39, 40-41
 volcanic rocks, 19, 26-30
 lanthanides
 commercial uses, 71-74
 formation of, 3
 origin of, 3
 lanthanide(II) compounds, 132, 149, 156, 162
 lanthanide(IV)
 compounds, 131, 149, 152
 lanthanide mineral
 resources, 65-71
 allanite, 66-67
 apatite, 67
 assessment, 74-76
 bastnaesite, 68
 fluorite, 68
 monazite, 68-69
 perovskite, 69
 sphene, 69
 xenotime, 69
 zircon, 69
 lanthanum
 coordination number 5, 223
 dimethyl sulfoxide
 structure, 237
 dipyriddy structure, 237
 EDTA structure, 219, 237
 ^{139}La NMR, 255
 pyridine-*N*-oxide
 structure, 231, 234
 lasers, 164
 lattice parameters, 339
 C-type sesquioxides, 342ff
 fluorite dioxides, 342ff
 levels (*J*), 141, 156, 160
 life-time, excited state
 medium effects, 198
 non-radiative, 198
 radiative, 196
 ligand exchange
 kinetics, 255, 275
 liquid-liquid ion-exchange
 chromatography, 103
 lithophilic elements, 133
 lone-pairs, 119
 loparite, 83, 84
 lower oxides
 electrical properties, 385
 magnetic properties, 388
 optical properties, 392
 stable phases in, 340
 luminescence, 147, 163
 $\text{LuO}_{1.485}$, 349
 Lu_2O_3 , 346, 347
 heterogeneous
 reactions, 377
 thermodynamic
 properties, 368
 lutetium
 coordination number 4, 222
 coordination number 7, 228
 DMSO structure, 220, 235
 dipivaloylmethane
 adduct, 228, 229
 hydration, 255
 Madelung potential, 130
 magnetic dipole
 operator, 188, 191

- magnetic properties
 garnets, 569
 higher oxides, 390
 hydrides, 315-319
 lower oxides, 388
 magnetic structures, 390
 sesquioxides, 389
 magnetic susceptibility
 of complexes, 254
 malonic acid
 complexes, 235, 236
 manganese(II) spectra, 160, 163
 mass transport in REO, 376, 377
 mechanical properties
 oxides, 393
 mechanisms of reaction
 in hydrides, 323
 metallic lanthanides, 154
 metals
 tarnishing of, 381
 methanol-water-HNO₃
 systems, 89, 90
 3-methyl-1,2-diaminobutane-
 tetraacetate, 98
 4-methyl-1,2-diaminopentane-
 tetraacetate, 98
 methylethylenediamine-
 triacetate, *N'*-, 97
 mixed oxides, 116, 148, 152, 161
 mixed oxides, compounds
 and structures in
 rare-earth oxide-M₂O
 systems, 452
 rare-earth oxide-MO
 systems, 460, 468-486
 rare-earth oxide-M₂O₃
 systems, 486
 rare-earth oxide-MO₂
 systems, 486, 487, 489, 494, 496, 498
 rare-earth oxide-M₂O₃
 systems, 501, 502
 rare-earth oxide-MO₃
 systems, 495
 mixed oxides, electrical properties of
 rare-earth sesquioxides-
 cerium dioxide, 442, 443, 444
 rare-earth sesquioxides-
 thorium dioxide, 442, 443, 444
 rare-earth sesquioxides-
 zirconium dioxide, 442, 443, 444
 rare-earth sesquioxides-
 zirconium dioxide, 442, 443, 444
 mixed oxides, phase equilibria in
 pseudobinary systems
 rare-earth dioxides-rare-earth
 sesquioxides, 421-426
 rare-earth sesquioxides-
 cerium dioxide, 421-426
 rare-earth sesquioxides-
 hafnium
 dioxide, 426-439
 rare-earth sesquioxides-
 praseodymium
 oxides, 421, 422
 rare-earth sesquioxides-
 rare-earth
 sesquioxides, 403-415
 rare-earth sesquioxides-
 thorium dioxide, 417-421, 486-487
 rare-earth sesquioxides-
 tin dioxide, 440
 rare-earth sesquioxides-
 titanium dioxide, 440, 441
 rare-earth sesquioxides-
 zirconium
 dioxide, 426, 439
 pseudoternary systems
 rare-earth sesquioxides-
 rare-earth sesquioxides,
 403-415
 ternary systems
 uranium-cerium-
 oxygen, 451, 452
 uranium-rare-earth
 metal-oxygen, 444-452
 mixed oxides, structure types
 in
 A-type rare-earth
 sesquioxide, 403, 486, 487
 aeschynite, 485, 486
 α -LiFeO₂, 452, 453, 454, 455, 456
 α -Li₂Eu₃O₈, 479, 484
 α -NaFeO₂, 452, 453, 455, 456
 B-type rare-earth
 sesquioxide, 403, 484
 baddeleyite, 502
 BaZnF₄, 466-468
 β -LiEuO₂, 454, 455, 456, 457
 β -LiFeO₂, 454, 456-468
 β -Li₂Eu₃O₈, 478, 479, 482, 483, 484
 β -Zr₄₈Sc₁₄O₁₁₇, 495
 C-type rare-earth
 sesquioxide, 403
 CaFe₂O₄, 468-486
 CaTa₂O₆, 485, 486
 γ -Zr₁₀Sc₁₀O₂₆, 490, 491, 494
 δ -Zr₃Sc₄O₁₂, 490, 491, 494
 diaspore, 457, 458
 euxenite, 486
 fergusonite, 511, 513, 515
 fluorite, 489, 502, 516, 518
 HoMn₂O₅, 480, 485
 K₂NiF₄, 461
 LiEu₃O₄, 473, 475, 484
 LiSrLaO₃, 476, 481, 484
 Li₈SnO₆, 458
 monazite, 514, 515
 NaCl, 452
 NaHF₂, 457
 perovskite, 458-468
 pyrochlore, 496
 Ruddlesden-Popper
 phases, 458-466
 R₃ReO₈, 516, 517
 R₂WO₆, 495, 516, 517
 scheelite, 511, 512, 515
 Sr₃Ti₂O₇, 465
 tysonite, 507, 511
 UY₆O₁₂, 489
 vernier, 507, 508
 warwickite, 473
 weberite, 501
 wolframite, 513, 514, 516
 woltenite, 514
 Y₂BeO₄, 475, 477
 Y₂TiO₅, 475, 478, 480
 Y₇O₆F₉, 507, 508
 zircon, 514, 515
 mixed-valence
 compounds, 150
 molecular orbitals, 119, 123, 161
 molybdates
 β , β' R₂(MoO₄)₃
 birefringence in, 644

- molybdates (*contd.*)
 change in crystal shape, 634
 domain walls, 645
 electrical properties, 636
 ferroelastic hysteresis, 635
 hysteresis, 634
 index of refraction, 643
 magnetic properties, 645
 physical properties, 638
 piezoelectric properties, 637
 sound velocities in, 641
 spontaneous lattice strains, 640
 structural relationships, 627, 630
 structure of β' , 628, 631
 transition, 633, 634
 crystal chemistry, 624–652
 β and β' - $\text{Gd}_2(\text{MoO}_4)_3$, 625–631
 compounds with $\text{Sc}_2(\text{WO}_4)_3$ -type structure, 632, 633
 defect sheelites
 $\text{R}_2(\text{MoO}_4)_3$, 625, 626
 $\text{R}_2(\text{MoO}_4)_3$, 624
 elastic properties
 $\text{Gd}_2(\text{MoO}_4)_3$, 639, 640
 phase diagrams, 610–624
 Gd_2O_3 - MoO_3 , 610, 611
 Gd_2O_3 - 4MoO_3 , 612
 Gd_2O_3 - 6MoO_3 , 612
 R_2O_3 - MoO_3 , 610, 611
 R_2O_3 - 3MoO_3 , 612–622
 phase transitions, 614, 633
 $\text{R}_2(\text{MoO}_4)_3$
 crystal defects, 650–652
 crystal structures, 626
 domain walls, 645–650
 elastic constants, 641, 642
 electrical properties, 636
 magnetic properties, 645
 optical properties, 642
 R_2O_3 - $x\text{MO}_3$
 cell volume ($x = 3$), 619
 lattice parameters ($x = 1$), 610, 623
 lattice parameters ($x = 3$), 613, 618
 single crystal growth ($x = 3$), 620
 X-ray data from $\text{Gd}_2(\text{MoO}_4)_3$, 616, 617
 monazite, 84
 monoacidic orthophosphate esters, 105, 106
 monoacidic phosphonate esters, 106, 107
 monoxides, 340
 Mössbauer spectroscopy hydrides, 328, 329
 Mott transition, 159
 multiphonon processes, 198

 1,8-naphthyridine complexes, 273–274
 Nd_2O_3
 oxygen diffusions in, 378
 polymorphic transformation, 352
 structure, 344, 345, 349
 thermodynamic properties, 368
 vaporization characteristics, 371
 neodymium acetylacetonate structure, 231
 bromate hydrate structure, 219, 235
 COT complex structure, 288
 dimethylsulfoxide, 220
 IMDA structure, 277
 malonate structure, 235, 236
 methylcyclopentadiene structure, 282
 thiodiacetate structure, 235
 TTA structure, 230, 231
 neodymium(III) spectra, 125, 159
 nephelauxetic effect, 156, 160, 162, 187
 neutral phosphorus (extraction) agents, 105, 106
 neutron scattering in hydrides, 325, 326
 nickel(II) complexes, 118
 nitrate complexes, 237, 238, 260
 nitrilotriacetate, 91, 95
 nitrite complexes, 260
 non-radiative, 197, 200
 nonstoichiometry, 116
 in oxides, 349, 355, 359
 NTA complexes, 220, 231

 optical electronegativity, 149
 optical properties
 binary oxides, 391
 garnets, 579
 perovskites, 561
 ore treatment, 83, 84
 organolanthanide chemistry, 121, 148, 161
 orthite, 83, 84
 ortho-phenanthroline complexes, 231, 266, 272, 273
 oscillator strength, 188
 outer-sphere complexes, 239, 244
 oxalate complexes, 231, 235
 oxidation–reduction reactions
 hydrated electron, 204
 OH-radical, 204
 potentials, standard, 203
 oxidation states, 84, 118, 152, 153
 oxides
 lattice parameter, 339
 structure and bonding, 117, 126, 148
 thermodynamic properties, 368–370
 oxydiacetate complexes, 262
 stability constants, 241
 structures, 235
 thermodynamic data, 242–244

 paramagnetism, 113
 Pearson's dual principle, 134
 perchlorate coordinated, 260
 perovskites
 catalytic properties, 562
 crystal chemistry, 534–537
 crystal structure, 117, 458, 537
 complex, 547–549

- perovskites (*contd.*)
 electronic
 configuration, 151
 ideal, 535
 ordered, 550
 orthorhombic
 distortion, 551, 552
 RAR₃O₇, 538-539
 RCoO₃, 542-543
 RCrO₃, 540, 541
 RFeO₃, 542
 RGaO₃, 543-545
 RInO₃, 546
 RMnO₃, 541, 542
 RNbO₃, 545
 RNiO₃, 543
 RNpO₃, 547
 RR'O₃, 546, 547
 RRhO₃, 545, 546
 RScO₃, 539
 RTrO₃, 539, 540
 RUO₃, 547
 RVO₃, 540
 RYO₃, 545
 RZrO₃, 545
 electrical properties, 558
 magnetic ordering, 553
 magnetic space
 groups, 554, 555
 magnetic
 structures, 556
 optical properties, 561
 phase relationships, 413
 phase transition, 552
 preparation, 528
 crystal growth, 529-534
 powder synthesis, 528
 phase diagram
 hydrides, 301-307
 mixed oxides, 403-452
 molybdates, 610
 oxides, 354, 357, 364
 phase equilibria
 garnets, 566
 phase reactions in rare earth
 oxides
 enthalpy of, 372
 hysteresis, 365
 kinetics, 374, 377
 mechanisms, 378
 tarnishing of metals, 381
 phase relationships
 hydrides, 301-305
 phase transitions
 molybdates, 614, 633
 phenomenological baricenter
 polynomial, 142
 photo-electron spectra, 153
 physical metal, 157
 plate tectonics, 10, 27
 Pm₂O₃
 structure, 344, 345
 thermodynamic
 properties, 368
 polarizability, 134
 polyether complexes, 268
 polymorphism
 higher oxides, 362
 sesquioxides, 340
 porphyrin complexes, 275
 PrO_x
 heterogeneous
 reactions, 377
 isobars, 358
 phase diagram, 356, 357
 structure, 342, 343, 359-363
 thermodynamic
 properties, 370
 Pr₂O₃
 polymorphism in, 341
 structure, 342
 thermodynamic
 properties, 368, 373
 Pr₇O₁₂
 oxygen diffusion in, 378-380
 structure of, 343, 359
 PrO₂₋₈
 crystal growth, 384
 lattice images, 361, 362
 phase diagram, 356, 357
 representative
 isobars, 358
 structure, 342, 343, 359
 praseodymium
 coordination number
 7, 228
 DPM structure, 228, 232
 facam structure, 236
 fod structure, 231
 NTA structure, 220
 terpyridyl structure, 235
 TTA structure, 230
 propanediamine
 complexes, 274
 1,2-propylenediaminetetra-
 acetate, 97
 pseudohalide complexes (*see*
 cyanate, etc.), 258-259
 pseudophase behavior, 365
 pseudoquadrupolar hyper-
 sensitive transitions, 164
 pulse radiolysis
 aqueous solution, 189-190, 204
 pyridine
 adduct with
 Eu(DPM)₃, 231-233
 pyridine-*N*-oxide, 231, 234, 269, 270
 pyrochlore
 structure of, 117, 496
 quaternary ammonium
 ions, 108
 quinuclidine
 adduct with
 Eu(DPM)₃, 228
 RO
 occurrence of, 340
 R_nO_{2n-2}
 color, 342ff
 crystal radius, 343ff
 homologous series in
 CeO_{2-x}, 342ff, 354
 homologous series in
 PrO_{2-x}, 342ff, 357
 homologous series in
 TbO_{2-x}, 342ff, 363, 364
 lattice parameters, 342ff
 lattice type, 342ff
 projected unit cells, 360
 pseudocell, 343ff
 relative volume, 343ff
 symmetry, 342ff
 unit cell, 343ff
 vacancies per unit
 cell, 343ff
 Racah parameters *E*¹ and
*E*³, 143
 radiative relaxation, 196
 radii of atoms and ions, 115, 130
 rare earths
 minerals, 83
 occurrence of, 82, 83
 resin cross-linkage, 91, 95
 Russell-Saunders
 coupling, 140, 155
 Rydberg defect, 140

- salting out, 105
- samarium
- cyclopentadienide (Sm(II)), 283
 - cyclopentadienide structure, 282
 - indene structure, 286
 - TTA, mass spectrum, 267
- samarium neodymium, 64
- samarium sulfide, 56
- samarite, 83
- Sc₂O₃
- heterogeneous reactions, 377
 - structure, 346, 347
 - thermodynamic properties, 368
- scandium
- acetylacetone structure, 225
 - coordination number 3, 221
 - coordination number 6, 225
 - coordination number 8, 218, 234
 - covalency, 218
 - cyclopentadiene structure, 282
 - ethylenediamine complexes, 272
 - hydration, 255
 - relationship to other rare earths, 218-219
 - ⁴⁵scandium NMR, 256
 - tropolone, 226, 231
- Schiff base complexes, 276, 277, 278
- selection rules
- electric dipole transitions, 190
 - magnetic dipole transitions, 191
- separation factors, 88, 90, 94, 99, 101, 104, 106
- sesquioxides
- boiling point, 368
 - ΔG_{298}° , 368
 - ΔH_{298}° , 368
 - electrical properties, 385
 - freezing point, 368
 - high temperature forms, 341, 348
 - lattice parameters, 339
 - magnetic properties, 389
 - magnetic structures, 390
 - mechanical properties, 393
 - melting points, 341
 - nonstoichiometry, 349
 - optical properties, 392
 - polymorphism, 340
 - properties, 342ff
 - S₂₉₈^o, 368
 - structure
 - A-type, 349-351
 - B-type, 350, 351
 - C-type, 350, 351
 - thermal properties, 393
 - thermodynamic properties, 368
 - transition temperatures, 341
 - transitions, 348
 - vaporization characteristics, 371
- sieve effects, 91
- simultaneous excitation, 163
- sintering oxides, 384
- Slater integrals, 185
- SmO
- thermodynamic properties, 370
- Sm₂O₃
- oxygen diffusion in, 378
 - single crystal growth, 384
 - structure, 344, 345
 - thermodynamic properties, 368
 - vaporization characteristics, 371
- solvent extraction, 104
- specific heat
- garnets, 593-596
 - measurements in hydrides, 327, 328
- spectra
- absorption, 245-249
 - charge transfer, 246
 - circular dichroism, 249
 - circularly polarized luminescence, 253
 - emission, 250-253
 - ESR, 256
 - intra 4f, 247-249
 - Mössbauer, 253-254
 - NMR, 255-257
 - spin-orbit coupling, 140, 161
 - spin-orbit interaction, 186
 - spin-pairing energy theory refined, 144, 165
 - spin-pairing parameter *D*, 144
 - spin quantum number *S*, 113, 118
 - stability constant sequences, 97
 - standard oxidation potential *E*^o, 129, 133, 138, 152
 - support materials, 103
 - system difference, 145
- TALSPEAK process, 107
- Tb₂O₃
- thermodynamic properties, 368
- TbO_x
- heterogeneous reactions, 377
 - hysteresis, 364-366
 - phase diagram, 363, 364
 - structure, 344, 345, 346, 347, 363
 - thermodynamic properties, 370, 374
- TbO_{1.83}
- single crystal growth, 384
- TbO_{2-δ}
- lattice image, 263
 - phase diagram, 364
 - structure, 344
- terbium
- acetylacetone emission, 251
 - CPL, 253
 - DPM emission gas phase, 251
 - energy levels, 251
 - TTA mass spectrum, 267
 - terms (*S*, *L*), 141, 144
 - terpyridyl complexes, 235, 266, 272, 273
 - tetrad effect, 147
 - tetramethylmalonamide complexes, 263
 - tetramethylurea complexes, 263, 264, 265
 - thenoyltrifluoroacetone complexes mass spectra, 267
 - structures, 230, 231, 232

- thermal conductivity
garnets, 590–593
- thermal expansion
garnets, 596
- thermal properties
oxides, 393
- thermodynamic data
complexes, 242–244
hydrides, 307–315
oxides, 366–374
- thermodynamic properties of
rare earth oxides
CeO_x system, 372
 ΔG vs. T , 367
 ΔG_f° vs. T , 367
 ΔG vs. T , PrO_x, 373
 ΔG vs. T , TbO_x, 374
 ΔH vs. x for CeO_x, 372
dioxides, 370
fields of stability, PrO_x,
373
fields of stability, TbO_x,
374
high temperature, CeO₂,
372
hydrides, 307–315
intermediate oxides, 370
intermediate phases, 370
sesquioxides, 368
vaporization, 371
- thiocyanate complexes, 108,
224, 258–259
- thiodiacetic acid complex
structure, 235
- thio- β -diketone complexes,
280
- thioxane oxide
complexes, 269, 271
- Th⁴⁺ and Ce⁴⁺
removal of, 86
- thulium chalcogenides, 156
Tm₂O₃
- heterogeneous
reactions, 377
structure, 346, 347
thermodynamic
properties, 368
- tramex process, 107
- transition probability
spontaneous, 184
- β , β' , β'' -triaminotriethyl-
amine complexes, 275
- triethylenetetramine
complexes, 272, 274
- trimethylsilylamine
complexes, 221, 223
- triphenylarsine oxide
complexes, 269, 271
- triphenylphosphine oxide
complexes, 223, 231, 266,
267, 269, 271
- tropolone complexes, 226,
234
- unusual oxidation states
production, 204
- uranium compounds, 128,
150, 444–452
- uranyl ion, 147, 149, 165
- urea complexes, 263, 264,
265
- vanadates, 127, 164
- vaporization characteristics
 C_p vs. T , Y₂O₃, 372
 ΔH vs. T , Y₂O₃, 372
sesquioxides, 371
- vertical transitions, 151
- water-miscible solvents, 89
- X α model, 119
- xenotime, 83, 84
- X-ray spectra, 119, 153, 158
- YbO_{1.495}, 349
- Yb₂O₃
thermodynamic
properties, 368
- Yb₂O₃
structure, 346, 347
- YO
occurrence, 340
- YO_{1.4991}, 349
- Y₂O₃
heterogenous
reactions, 377
single crystal growth, 384
structure, 346, 347
thermodynamic
properties, 368
vaporization
characteristics, 371
- ytterbium
acetylacetone, 228
coordination number 7,
288
cyclopentadiene
(Yb(II)), 282
dimethyl sulfoxide, 235,
238
methylcyclopentadiene
chloride structure, 284
- ytterbium(III) spectra, 148,
162, 163
- yttrium
acetylacetone, 231, 232
antipyrene, 225
benzoylacetone, 228
comparison with
lanthanides, 215
coordination number 6,
225
coordination number 7,
228
hexafluoroacetyl-
acetone, 230, 231
yttrocerite, 83